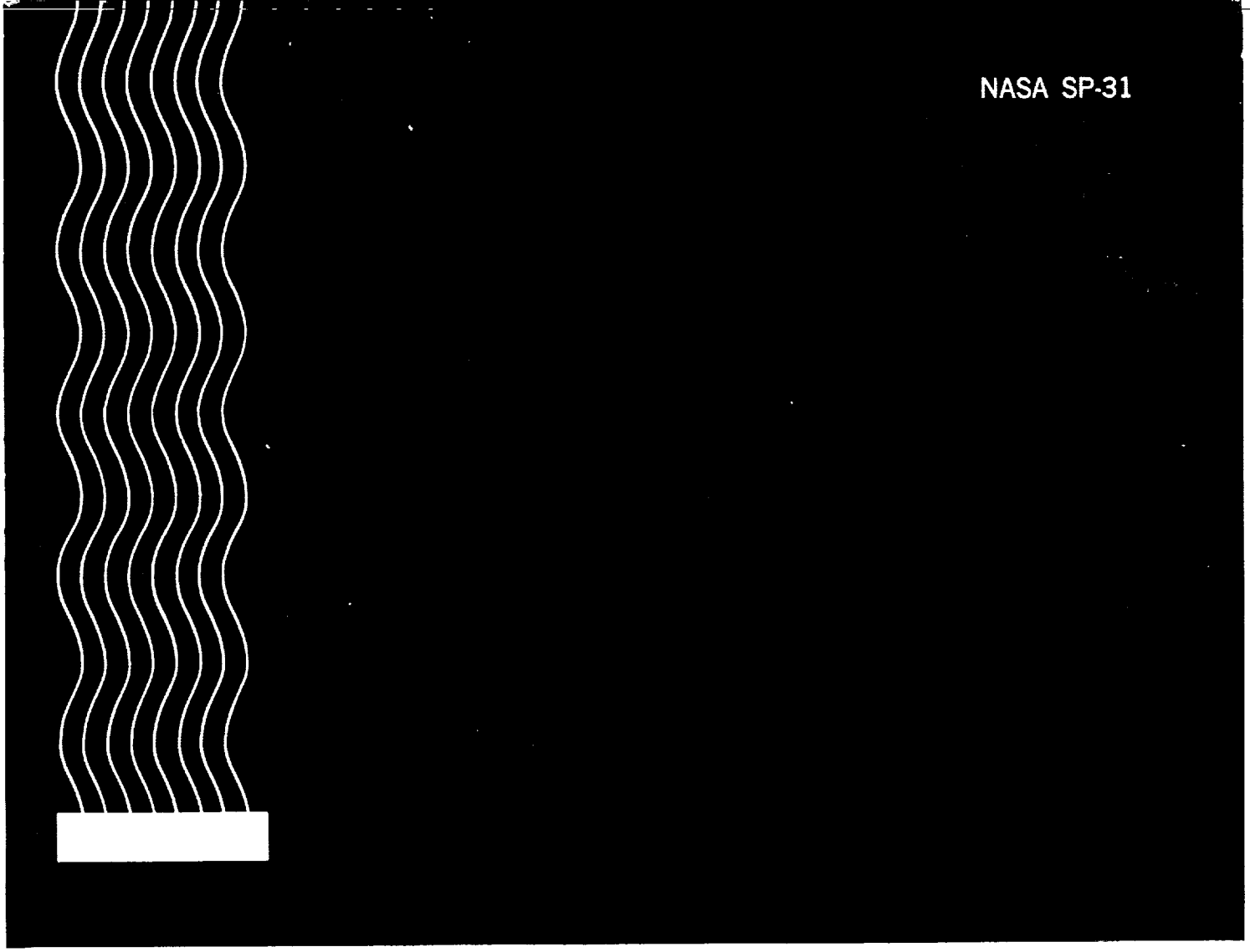

NASA SP-31

MEASUREMENT *of* THERMAL RADIATION PROPERTIES *of* SOLIDS

NATIONAL AERONAUTICS AND SPACE ADMINISTRATION

NASA SP-31

MEASUREMENT *of* THERMAL RADIATION PROPERTIES *of* SOLIDS

A SYMPOSIUM HELD AT DAYTON, OHIO, SEPTEMBER 5, 6, 7, 1962

SPONSORED BY Aeronautical Systems Division, USAF
National Bureau of Standards
National Aeronautics and Space Administration

EDITED BY JOSEPH C. RICHMOND
National Bureau of Standards

Office of Scientific and Technical Information 1963
NATIONAL AERONAUTICS AND SPACE ADMINISTRATION
Washington, D.C.

For sale by the Superintendent of Documents, U.S. Government Printing Office
Washington, D.C., 20402 - Price $3.50 (Paper Cover)

FOREWORD

The Symposium on Measurement of Thermal Radiation Properties of Solids was sponsored jointly by the Aeronautical Systems Division, U.S. Air Force; the National Bureau of Standards; and the National Aeronautics and Space Administration.

James J. Gangler, NASA Headquarters, was general chairman. Robert A. Winn, Physics Laboratory, Aeronautical Systems Division, was program chairman, assisted by Herman Schwartz, of the NASA Lewis Research Center, and Joseph C. Richmond, National Bureau of Standards.

Housekeeping details were handled by the University of Dayton on a contract basis, with C. Robert Andrews, of the University of Dayton Research Center, as chairman of Arrangements.

CONTENTS

SESSION IV—MEASUREMENTS AT MODERATELY HIGH TEMPERATURES (450° TO 1400° K)

PREFACE

This volume contains the proceedings of the Symposium on Measurement of Thermal Radiation Properties of Solids held in Dayton, Ohio, September 5, 6 and 7, 1962. The very great increase in interest in and need for data on the thermal radiation properties of solids as a consequence of the national space program prompted the Aeronautical Systems Division of the U.S. Air Force, the National Bureau of Standards, and the National Aeronautics and Space Administration to join in sponsoring the Symposium.

The overall objectives of the Symposium were to afford (1) an opportunity for workers in the field to describe the equipment and procedures currently in use for measuring thermal radiation properties of solids, (2) an opportunity for constructive criticism of the material presented, and (3) an open forum for discussion of mutual problems.

It was also the hope of the sponsors that the published proceedings of the Symposium would serve as a valuable reference on measurement techniques for evaluating thermal radiation properties of solids, particularly for those with limited experience in the field.

Because of the strong dependence of emitted flux upon temperature, the Program Committee thought it advisable to devote the first session to a discussion of the problems of temperature measurement. All of the papers in Session I were presented at the request of and upon topics suggested by the Committee. Because of time and space limitations, it was impossible to consider all temperature measurement problems that might arise—the objective was rather to call to the attention of the reader some of the problems that might be encountered, and to provide references that might provide solutions.

The four remaining sessions were devoted to discussions of measurement techniques in each of four temperature ranges: Session II on measurements at low temperatures (0° to 200° K); Session III on measurements at satellite temperatures (200° to 450° K); Session IV on measurements at moderately high temperatures (450° to 1400° K); and Session V on measurements at high temperatures (above 1400° K). The dividing lines between sessions were arbitrarily selected on the basis that, to some extent at least, different measurement techniques are employed in the different temperature ranges.

A recognized authority in the field was invited to present the first paper in each session. It was intended to cover the need for and applications of thermal radiation data within that temperature range. These invited papers were presented in full, and were not preprinted or discussed. All of the remaining papers in each session were submitted in response to the general request for papers. The response was so enthusiastic that it soon became apparent that only a fraction of the submitted papers could be presented within the available time. Selection of the papers for presentation at each session was made by the Session Chairman and Program Committee on the basis of (1) presenting as many different experimental techniques as possible and (2) having different laboratories present papers, where possible, rather than having several papers from the same laboratory. Those papers not selected for full presentation were presented by title only.

All submitted papers to be presented were preprinted, and the preprints were sent to all advance registrants. Each author was requested to present only a 10-minute summary of his paper, and at least 15 minutes was reserved for oral discussion of each paper. Advance registrants were also invited to submit prepared discussions. The oral discussion was recorded, edited, and included in these proceedings following the paper being discussed Unfortunately, part of the oral discussion of Session III was lost due to malfunctioning of the recording equipment.

In these proceedings the submitted papers

for each session are published in alphabetical order by senior author, and no distinction is made between those that were presented and those that were presented by title only.

Each paper was reviewed technically by the Session Chairman and then by the Editor. Any technical discrepancies noted were called to the attention of the author for correction. An attempt was made to see that uniform nomenclature was used throughout, and that confusing or misleading statements were clarified. Otherwise, no attempt was made to interfere with an author's individual style. Primary responsibility for the technical accuracy of statements made must reside with the author of each paper.

It is believed that these proceedings will serve as a valuable reference in the field of measurement of thermal radiation properties of solids.

JOSEPH C. RICHMOND
Editor.

SESSION I

TEMPERATURE MEASUREMENTS

Chairman: WILLIAM N. HARRISON

1—PITFALLS IN THERMAL EMISSION STUDIES

BY WILLIAM N. HARRISON

NATIONAL BUREAU OF STANDARDS, WASHINGTON, D.C.

Attention is called to several pitfalls that often beset investigators who make thermal emittance studies. The pitfalls mentioned include the following: (1) conflicting meanings of several frequently used terms as found in the literature, each meaning having authoritative sponsorship; (2) incomplete and hence potentially misleading descriptions of specimens on which reported data are based; (3) reference to emissivity or remittance as a property of a surface rather than a volume property (influenced by the surface); (4) occasional omission of diffuse reflection from analyses of the optical properties of inhomogeneous bodies; (5) failure to observe the restrictions upon conditions that are required for validity of basic equations; (6) uncertainties as to the effective temperature, peculiar to specimens having low absorption indices; and (7) lack of suitable physical standards. Several suggestions are made for avoiding or minimizing the consequences of the pitfalls discussed.

The recent surge of demand for information on the thermal emission and absorption characteristics of materials, and the sparse supply of pertinent knowledge, have already confronted people in numerous laboratories with the problem of initiating experimental work in an unfamiliar field. In a transition of this type there are always potential pitfalls, and this field of study has its full share. There are several sources of possible error or confusion that repeatedly come to the fore in studies of thermal emission and absorption, and it is not obvious to what extent they may vitiate the reliability of experimental findings or otherwise retard the quest for dependable information.

THE LANGUAGE HANDICAP

One of the first obstacles encountered is created by the occurrence of nonsystematic and sometimes conflicting terminology in the literature. Even such a frequently used word as "emittance" is subject to conflicting definitions, for each of which impressive authority can be cited. Experience with this obstacle to communication forces attention on the urgency of the need for terminology that is consistent, not only with respect to definitions of specific terms, but also in the use of word forms which by their structure convey maximum information, especially through systematic use of suffixes. A prime example of the systematic naming of properties involves reserving the ending "ivity" for properties that characterize a *material* (such as emissivity, reflectivity, resistivity, and expansivity) and avoiding this suffix when referring to a property of a *specimen*, which would change with its size or shape. The extra, self-contained communicative potency of this system of nomenclature is illustrated in the familiar distinction between electrical *resistance*, which for any uniform wire is directly proportional to its length, and the *resistivity* of the material used to fabricate the wire, which is a characteristic property. Adherence to this system requires that "emissivity" and "reflectivity" likewise be reserved to designate characteristic constants of a material, rather than being used to denote measured values that would change with the dimensions or surface finish of the specimen.

"Emissivity" under this system is a special case of "emittance", just as "reflectivity" is a special case of "reflectance" and "resistivity" of "resistance."

Some persons may make a point of the fact that the units in which electrical resistance is expressed are not identical with those in which resistivity is expressed, whereas the units for emittance and emissivity are the same, both being dimensionless ratios. This fact illustrates the difficulty of evolving a perfect system of nomenclature, but any apparent deviation from system in this case seems rather superficial, since for both pairs of terms the "ivity" ending is reserved to name a characteristic of the material, and the "ance" ending is used for a property of a specimen that may depend upon its size, shape, and surface condition. The same nonidentity of units applies to *expansion* and *expansivity*, and the same overriding basis of validity of the two terms applies also.

The countersystematic and often conflicting word usages that have developed over the decades originated mostly within separate groups of investigators, engaged in different, though related, areas of study. The development of a homogeneous system of nomenclature will require cooperative effort among a number of technical and scientific organizations that have sponsored mutually incompatible definitions. When such a project is undertaken it is to be hoped that the governing principle of agreement will be to achieve the greatest possible systemization, with the attendant extra communicative potency of the adopted terms. This objective would be advanced by recognition of the distinction between two categories of attributes of materials, known respectively as *intensive* and *extensive*. Given a specimen of homogeneous material, no one questions that a different quantity of the same material under the same conditions would have a correspondingly different volume, inertia, or heat capacity (extensive attributes) nor that such characteristics as specific gravity, temperature, and emissivity (intensive attributes), on the other hand, are independent of the quantity of material. Additional examples are listed in table 1–I. A nomenclature that is compatible with this distinction can be conducive to clear thinking and lucid communication. It is noteworthy that the American Standards Association recommends the use of a specific type face (italic capitals) for letter symbols pertaining to thermodynamic properties (ref. 1).

TABLE 1–I. *Types of Attributes (Examples)*

Extensive:	Intensive:
Volume	Temperature
Mass	Density
Length	Resistivity
Inertia	Reflectivity
Heat capacity	Emissivity

Unless and until agreement on a consistent terminology is reached, we can reduce the jeopardy of verbal pitfalls if we stay alert to the discrepancies in some of the current nomenclature. Likewise we can improve the probability that our own communications will be lucid by choosing and using the most systematic nomenclature available. Specific recommendations concerning definitions will be found in subsequent papers in this book. It is sufficient here to point out the need for unification and systemization of nomenclature in this area of research, and call attention to certain principles of systemization, the universal adoption of which would sharply reduce existing discrepancies.

INCOMPLETE SPECIMEN DESCRIPTIONS

Another obstacle to interpretation of some published results arises from the incompleteness of descriptions of specimens on which data are reported. For example, the material constituting a specimen may be identified only in general terms, such as "oxidized stainless steel." Reported thermal emittance values for such loosely defined specimens are of questionable significance, not only because the alloy is inadequately identified, but also because the thickness of the oxide coating on the alloy is not stated. The thermal emittance of such a composite specimen usually changes drastically with increase in the oxide thickness during the early stages of oxidation; nevertheless, prolonged treatment may be required for accumulation of a layer of oxide thick enough so that additional thickness does not measurably affect the thermal emittance.

Careful scrutiny of the descriptions of specimens used for thermal emittance measurements is often necessary for a reliable evaluation of

the results. By the same token, authors can enhance the value of reports by strict attention to accurate and complete specimen descriptions and by considering the bearing of this information upon possible conclusions from the data.

THE ROLE OF SURFACES IN THERMAL EMISSION

The literature contains numerous references to the thermal emittance, or emissivity, as a property of a *surface*. This useage may have originated in reporting determinations of the emissivities of metals, which have extremely high coefficients of extinction except at certain wavelengths that are too short to affect the reported determinations significantly. The thickness of metal required to yield the highest rate of emission that the material can achieve, and to block significant transmission of the radiant energy, is so small that it may be thought of in a macroscopic sense as a surface layer. It is beyond the scope of these comments to elaborate on the fact that the phenomena comprised by the mechanism of reflection at the surface of a solid or liquid take place, in part, at finite distances from the actual surface plane. For the purpose of this discussion it is considered that these distances are negligible, and that a reflecting surface has virtually zero thickness. In this context, a surface cannot emit but can only reflect some fraction of the radiant flux that impinges upon it.

Thermal emission, as distinguished from reflection, is rigorously a volume phenomenon. To visualize the vast difference in the roles of bulk material and surface one has only to think of a pot of clear molten glass in process of manufacture. Luminous radiant energy reaches the eye of a viewer by radiation directly from its original source element, in the interior of the hot glass, a substantial content of such energy being emitted by elements of volume that are much farther below the surface than the total thickness of most laboratory specimens. The surface of the molten glass reflects part of the incident energy, thus performing a function which is basically the same as for the surface of any other kind of specimen.

In a specimen of solid or liquid material having a continuous, smooth surface (not necessarily flat), the role of the surface, as it affects thermal emission from the specimen, may be compared to that of a clear glass chimney around an open flame used for illumination; the chimney reflects a certain fraction of the luminous energy impinging upon it from the interior, and passes the remainder (neglecting the slight absorption).

Any very small, finite unit of volume within the surface boundaries of a solid specimen may be arbitrarily chosen as the counterpart of the flame. The absorption, scattering, and reflection by the atmosphere within the chimney correspond to similar phenomena that occur within the solid specimen, between the chosen source-volume and the surface. In the solid specimen, regardless of the material composing it, the thermal energy initially radiated from any such interior unit of volume has the spectral distribution of flux that characterizes a blackbody at the same temperature. To function as a perfect radiator or blackbody, the specimen, in addition to being opaque, would be required to transmit the internally radiated energy to the surface without spectral modification and to provide completely unhindered egress for radiant energy reaching the surface at any angle from the interior; however, no specimen of real material will fully meet these requirements. The real specimens that most closely approach blackbody radiation are made up of discrete particles dispersed in the same medium that surrounds the specimen, usually air. This structure reduces reflection at the surface of the specimen to a minimum, but it cannot completely eliminate solid-to-air or comparable interfaces at the surface of the specimen; here reflection occurs, in amounts and spectral distributions that are governed by the respective indices of refraction of the two media. It follows that the surface geometry of the specimen plays a vital part in determining the thermal emission properties of the specimen. This fact explains why it is necessary that a specimen have specified surface characteristics (in addition to being completely opaque) in order for its thermal emittance to be characteristic of the material, appropriate to be designated "emissivity." The most convenient and practical specification of surface geometry is that it be "optically flat." The powerful influence of surface contours provides a practicable

means of modifying the thermal emittance of a specimen; treatments such as etching or sandblasting may greatly increase thermal emittance.

In summary of the role of surface, the following salient facts merit emphasis: (a) whether smooth or rough, a surface or interface as such does not emit, but can only reflect, (b) variation in thickness of the specimen may grossly affect its transmittance, and have a correspondingly large effect upon its thermal emittance. Hence, although the surface of a specimen plays a key role, the practice of referring to the thermal emittance of a *surface* is neither accurate nor conducive to lucidity.

INHOMOGENEITY AND DIFFUSE REFLECTION

The class of materials that gives rise to diffuse reflection is so important, and the fraction of incident radiation that these materials reflect diffusely is often so large, that the phenomenon is worthy of special emphasis. The earlier literature of thermal emission studies, including some excellent descriptions of the basic principles, often touched lightly or not at all upon this vitally important factor. A number of dissertations on the interdependence of emission, transmission and reflection, and the controlling role of extinction coefficient and refractive index [1] were fully applicable only to optically homogeneous materials, since the only aspect of reflection to be considered was the specular reflection at the surface of the specimen, no mention being made of internal scattering and the resulting diffuse reflection, although the latter may greatly exceed the specular reflection in the case of heterogeneous specimens.

In the class of materials typified by opaque, fire-polished ceramics, the occluded particles are often effectively submerged, so that the specular reflectance at the surface is controlled by the refractive index of the medium in which they are dispersed. The specular reflectance of such materials for radiant flux impinging at angles within 45° of the normal typically approximates 4 to 5%. The dispersed particles scatter the internal radiant energy most effectively when their refractive index differs widely from that of the medium in which they are distributed, and when the latter absorbs very slightly. If these conditions are met, and if the size of the dispersed particles is optimal for a given interval of wavelengths, 80% or more of externally incident radiant flux may be internally scattered by reflection from outer and inner surfaces of the dispersed particles as well as by the related refraction, and ultimately returned outward through the surface. In brief outline, such is the nature and extent of the diffuse reflection that has sometimes been omitted from otherwise thorough discussions of emission, transmission, and reflection phenomena. If this omission were not taken into account, it is apparent that the calculation of emittance by subtracting the sum of (specular) reflectance and transmittance from unity could be grossly erroneous.

[1] Or dielectric constant and magnetic permeability, if the alternative approach is used.

RESTRICTIVE CONDITIONS FOR APPLICATION OF BASIC EQUATIONS

The following basic equation is usually one of the first few given in an elementary treatise on the subject:

$$E+R+T=1 \tag{1}$$

where

E emittance
R reflectance
T transmittance of a specimen

It is also true that

$$E=A \tag{2}$$

where A signifies the absorptance.

Well known and elementary as these equations are, certain restrictive conditions must be met in their use if valid results are to be obtained. Thus, if the sum of two of the characteristic quantities is subtracted from unity to establish the third by difference, it is necessary that the geometric and spectral conditions be compatible for all three. For example, if emittance normal to the surface is to be computed from known values of reflectance and transmittance, validity requires that the known values pertain to uniformly diffused illumination and normal viewing or the optical equivalent, normal illumination and hemispherical

viewing. The avoidance of pitfalls in this area calls for careful attention to these restrictive conditions, and to maintaining the clear distinction between (a) the ratio to which each letter-symbol in equation (1) applies, and (b) the rate of flow of energy (power) to which each symbol in equation (3) applies.

Even though all the symbols in equations (1) and (2) pertain to ratios, there is a distinction among them that merits attention: namely, the denominator in the ratio of fluxes which determines E (and only E) has an absolute upper limit for a specimen at any given temperature. When numerical values of flux are substituted into the equations, this peculiarity may be an important factor to consider in maintaining a valid equality. For example, if heat transfer by conduction and convection, or either one, is effective in the environment of a specimen, the temperature of the specimen may be stabilized at a level far removed from that at which it would stabilize through radiant transfer alone. In this case the rate at which radiant energy is reflected and the rate at which it is transmitted may also be at much different levels than would prevail if stabilization at the same temperature were accomplished without conduction or convection. If heat transfer is effected solely by radiation, the condition required for the specimen to emit and absorb at full flux capacity within each wavelength increment, for the temperature at which the rates of absorption and emission are balanced, is that the incident radiant energy have the flux density and spectral distribution of blackbody radiation for the temperature of the specimen. Under this condition the flux reflected and transmitted by the specimen would be limited in an absolute sense as a result of the required limitation on incident flux. But this condition is seldom encountered in practice; rather, when all heat transfer to and from the specimen is by radiation and absorption, temperature stability is usually achieved, if at all, by absorption within one predominant wavelength interval and emission of equal power within another predominant wavelength interval. A familiar example of this condition involves absorption of solar energy by a given object, balanced by emission of radiant energy mostly at other wavelengths, the spectral distribution of the emitted energy being controlled by the comparatively low temperature of the specimen.

To avoid confusion when discussing rates of energy flow rather than ratios, it is desirable to use symbols that are easily distinguished from those in equations (1) and (2); thus,

$$\epsilon+\rho+\tau=\omega \tag{3}$$

where, for any spectral distribution of radiant energy,

ϵ rate at which radiant energy is emitted by the specimen

ρ rate at which radiant energy is reflected from the specimen

τ rate at which radiant energy is transmitted through the specimen

ω rate at which radiant energy is impinging upon the specimen

The two conditions that must be met for equation (3) to be valid are (a) that all heat transfer to and from the specimen be by radiation, and (b) that the specimen be allowed to adjust to the temperature at which it absorbs and emits energy at the same rate regardless of wavelength distributions.

TEMPERATURE PROBLEMS

Optical and radiation pyrometers, which are widely available, can be used to make temperature measurements that are accurate enough for most purposes when the object being observed is (a) hot enough to be incandescent (in the case of optical pyrometers), and (b) completely enclosed within walls that are at the same temperature. In practice, the errors introduced by slight temperature gradients, and by the peephole in the wall of the enclosure often are acceptably small. Under these conditions the thermal emittance of the object being observed has no important bearing upon the temperature determination because the total radiant flux leaving its surface and affecting the detector has the characteristics of blackbody radiation, although a part of it may be reflected by and a part transmitted through the observed object.

If the observed object is heated under other conditions, such as from the reverse side only, or internally by passing an electric current through it, and is radiating into surroundings which are at a lower temperature, appropriate

692-146 O—63——2

information regarding the thermal emission properties of the object is required to permit calibration of the pyrometer for accurate temperature readings.

This situation gives rise to the familiar need of investigators to know the thermal emittance of a specimen in order to determine its temperature or to know its temperature in order to determine its thermal emittance. Specific procedures for alleviating this difficulty are described in subsequent papers.

The final item in this brief review of some frequently encountered pitfalls is one that has received relatively little attention in the literature. Many materials of interest become completely nontransmitting only at substantial thicknesses, and an appreciable temperature gradient within the partially transmitting layer is usually present in determinations of thermal emission properties. It follows that part of the energy radiated from a specimen is emitted by, and is transmitted as radiant energy directly from, elements of the specimen that are located at various levels below the surface, which are at differing temperatures. The fraction of total energy emitted from a specimen that is radiated directly from subsurface elements decreases exponentially with distance below the surface.

A consideration of the effective temperature of the specimen may be useful in this connection. This temperature would lie between the surface temperature and that of the farthest subsurface level of the specimen from which a significant fraction of the radiated energy could escape absorption and reflection, and hence contribute directly to the total radiant energy emitted by the specimen. A rigorous calculation of the effect would include not only the variation in this contribution to observable flux with distance of the emitting element below the surface, but also the wavelength dependency of the maximum depth below the surface from which such contributions can be made.

A complete solution of this problem would be quite complex. However, there are large categories of specimens for which the problem is not serious. Materials having a high thermal conductivity and high extinction coefficient, as typified by metals, usually present no difficulty on this score; some electrical nonconductors with high extinction coefficients likewise induce no serious errors from this source.

Fortunately, there is a self-compensating feature of this phenomenon which is effective in a vacuum. It is best explained by reference to figure 1-1, which is taken from a paper by Jonathan Klein (ref. 2). The thickness values in this figure should be thought of in terms of optical rather than absolute thickness. The level at which the curved line representing temperature gradient joins the broken straight line indicates the maximum depth from which energy can be radiated directly out through the surface of the specimen at a significant rate. At shallower depths the gradient, which is indicated by the slope of the line relative to the normal, steadily diminishes toward the surface. Since the contribution to total radiant flux from the specimen diminishes exponentially with the depth of the source element, reaching virtual zero at the junction of the curved and straight lines, it is apparent that the greater part of the radiant flux from the specimen is affected much less by the temperature gradient

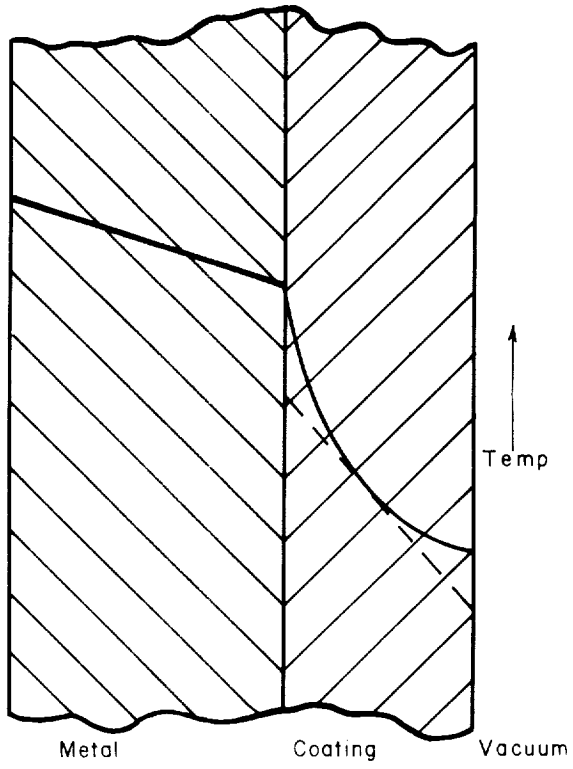

FIGURE 1-1.—Temperature gradients through a thin coating to a vacuum.

than would be the case if the gradient represented by the broken straight line were maintained to the extreme outer surface. This automatic reduction of temperature gradient near the surface may make the extra trouble and expense of working in vacuum well worthwhile.

CONCLUDING REMARKS

One of the major difficulties in making reliable measurements of thermal emittance, over the wide range of conditions for which there is need for data, is the lack of suitable standards. This lack has been remedied in part as a result of work done under sponsorship of the Air Force at the National Bureau of Standards. Several working standards have been carefully measured at NBS for spectral emittance over the range of 1 to 15μ in wavelength, and 800° to 1400° K in temperature. There are three types of materials used for these standard specimens, one type each for high, low, and intermediate thermal emittance. They may be purchased from the Building Research Division of the National Bureau of Standards.

In conclusion, it is evident from the foregoing discussion that the determination of temperature and temperature gradients is an integral part of the measurement of thermal emission properties and phenomena. It is fitting therefore that the first session of the symposium be devoted mainly to the principles and techniques of temperature measurement.

REFERENCES

1. Anon.: Letter Symbols for Heat and Thermodynamics. ASA Y10.4–1957, item VI, Am. Soc. Mech. Eng., c. 1957, p. 4.
2. KLEIN, JONATHAN D.: Radiation Heat Transfer to and from Ceramic Coatings on Metals. Am. Ceramic Soc. Bull., vol. 40, no. 6, June 1961.

DISCUSSION

SCHWARTZ, NASA: What do you think the chances are that the conflicting definitions and nonsystematic terminology mentioned in your discussion can be recitified?

HARRISON: The correction of this bad situation depends first upon the willingness of the several responsible scientific and technical societies and other interested agencies to agree upon the use of an effective, meaningful system of nomenclature, and furthermore, upon the willingness of each interested group to yield in favor of the adopted system in cases of nonconforming definitions. It is not an easy task, technically or psychologically. But I believe that the people involved will recognize the really urgent need of having a scientific language that permits unambiguous communication, and hence will be willing to make the necessary effort, and to yield when necessary for the common good. To get the required support for a successful program it is important that the initiative in this movement be taken by representatives of organizations having sufficient prestige to insure cooperation.

Regarding the conflicting definitions of *emittance* that were previously mentioned, the terminology we are now sponsoring, which currently has wide acceptance, may be illustrated in this way: If a highly absorbing, optically flat substrate is covered uniformly with increasing thicknesses of a highly reflecting, radiation-scattering coating, a plot of reflectance against thickness will show that at low thicknesses of the coating the reflectance rises steeply with increase in thickness. The rate of rise in reflectance becomes progressively less steep with continued increases in coating thickness and utimately becomes effectively zero as the reflectance curve asymptotically approaches the maximum possible reflectance value for the coating material. In practice, it is considered that the asymptote has been virtually reached when further increase in coating thickness yields no measurable rise in reflectance. At all points along this curve where the slope is dependent upon the coating thickness, the reflecting and emitting characteristics of the specimen are referred to in terms of the "ance" ending. The maximum reflectance of which the coating material is capable, as represented by the asymptote, is a characteristic of the coating material, and is designated by a term having an "ivity" ending, namely *reflectivity*. Since there is no transmission, the *emissivity* of the coating is obtained by subtracting the reflectivity from unity.

The objection may be raised that this system of nomenclature is not currently followed by some organizations of national importance, including the Optical Society of America. It is true that the current practice of certain groups conflicts with this system; however, this state of affairs appears to have come about by the failure, so far, of responsible organizations to follow the principles of nomenclature advocated by some of their own most authoritative members. For example, Chairman of the Committee on Colorimetry of the Optical Society of America, Dr. L. A. Jones, published a paper in 1937 in the Journal of the

Optical Society of America (vol. 27, 1937, p. 207) in which he tabulated terms in different columns according to whether they were names of (1) a process, (2) a property of a body, or (3) a property of a material, listing *reflectance* and *reflectivity* under the appropriate headings for conformity with the system we are advocating. Furthermore, in the Symposium on Temperature (Its Measurement and Control in Science and Industry) held under the sponsorship of the American Institute of Physics, the proceedings of which were published in 1941 (Reinhold Pub. Corp., New York), Prof. A. G. Worthing made a strong case for a systematic distinction between the "ance" and the "ivity" endings. In addition, the Report on Letter Symbols for Heat and Thermodynamics, published by the American Standards Association in 1943 (ASA Z10.4—1943), contained a statement of adherence to this principle of nomenclature. The omission of this statement from a later edition did not reflect a change from the stated policy, but rather the decision that the statement was outside the scope of a report on letter symbols. It is evident that the use of the system of terminology that reserves specific suffixes for the names of specific types of properties has long been advocated, and has impressive authoritative backing.

A recent evidence of this fact is to be found in a suggestion by Dr. Deane B. Judd, past president of the Optical Society of America and current editor of the Journal of the Optical Society. He has proposed that a new term which he coined be adopted, and be assigned one of the conflicting definitions now assigned to *emittance*. The new term he suggests is "emissance." Some individuals have expressed apprehension at the thought of still another term being added to the existing long list, but this objection seems minor in comparison with the major confusion resulting from the current incompatibility of different meanings assigned to the same word; Dr. Judd has made a constructive suggestion that merits careful consideration, along with other possible solutions. Wherever the chips fall, our hope is that all important groups, national and international, will look broadly at the nomenclature problem, will get together and agree upon principles of systemization, and will each be prepared to yield on definitions of terms that conflict with the adopted system.

Within the space industry, as represented by the authors at this symposium, we are speaking the same language. Papers presented herein show that an overwhelming majority of authors use emittance and reflectance as properties of a specimen, while emissivity and reflectivity are reserved for characteristics of a material.

2—TEMPERATURE MEASUREMENTS BELOW 1000° K

BY JOHN L. RIDDLE

NATIONAL BUREAU OF STANDARDS, WASHINGTON, D.C.

ABSTRACT [1]

The thermodynamic temperature scale, now defined by assigning the value 273.16 to the triple point of water, is the scale to which all temperatures are ultimately referable. However, temperature measurements are usually made on a "practical" scale, rather than directly on the thermodynamic scale, because such measurements are both more precise and more feasible in terms of cost and time. Practical scales in use today are based on measurements directly on the thermodynamic scale and are as close to a thermodynamic scale as knowledge permitted when they were established.

Values on the International Practical Kelvin Scale (IPKS) are, by definition, equal to the corresponding values on the International Practical Temperature Scale (IPTS) plus 273.15 degrees. The IPTS is realized from −182.97° C (90.18° K) to 630.5° C (903.65° K) by means of platinum resistance thermometers which meet certain requirements of purity and construction and which have been calibrated at four defining fixed points to determine the four coefficients in the specified formula, $R_t = R_0 [1 + At + Bt^2 + Ct^3 (t-100)]$, where, by definition $C=0$ for $t>0$. The four defining fixed points and their assigned values of temperature are the triple point of water (+0.01° C), and the normal boiling points of oxygen (−182.97° C), water (100° C), and sulfur (444.6° C). Because of difficulties in realizing a reproducible equilibrium at the sulfur point it was recommended in 1960 that the freezing point of zinc (419.505° C) be used in place of the sulfur point.

A given platinum thermometer, suitable for use as a defining standard and carefully handled, will repeat within a few ten-thousandths of a degree. Two such thermometers which have been calibrated on the IPTS at different national laboratories can be expected to differ less than 0.003° C at temperatures below 500° C. Since the IPTS was established, improved gas thermometer measurements on the thermodynamic scale have indicated at least the order of magnitude of the differences between the IPTS and the thermodynamic scale over most of the range from −183° C to 630° C. These differences appear to be less that ±0.1° C.

Below the lower limit of the IPTS (−182.97° C or 90.18° K) the NBS–55 scale, which extends down to 10° K, may be used. Calibration on this scale is obtained by comparison with a small group of reference platinum-resistance thermometers maintained at the National Bureau of Standards. Thermometers calibrated at different times may be expected to agree with each other within ±0.001° K and to agree with the thermodynamic scale within ±0.02° K between about 19° K and 90° K. From 19° K down to 10° K these uncertainties increase by about a factor of five.

It is expected that in 1966 the IPTS will be altered by extending the defined range covered by platinum resistance thermometers, both downward to about −253° C, where the IPTS does not now exist, and upward to 1063° C, where the IPTS is now limited by the reproducibility of the platinum-platinum rhodium thermocouple. It is further expected that nearly all values of temperature will be altered to bring them into closer agreement with values on the thermodynamic scale as determined by recent gas thermometer measurements.

---

[1] EDITOR'S NOTE: *This long abstract of his remarks on temperature measurements below 1000° K was prepared by Mr. Riddle as a substitute for the complete text of his paper which is not available for inclusion in these Proceedings.*

DISCUSSION

J. C. RICHMOND: You have discussed a large number of developments concerning platinum-resistance thermometers and I wonder if we have missed an opportunity by not using them for all of our temperature measurements. In particular, has anything been done to reduce the size of platinum-resistance thermometers?

RIDDLE: Small platinum-resistance thermometers available in this country are approximately 5½ mm in diameter and 60 mm long. I understand that smaller thermometers are available in Russia, but I am not sure of their availability in this country. In addition, there are several other difficulties concerning the use of platinum-resistance thermometers rather than thermocouples. One is the time response which for modern-day platinum-resistance thermometers is of the order of 5 or 6 sec. A second difficulty is the amount of money involved, namely, if one desires to make measurements to an accuracy of the order of a thousandth of a degree, a $4,000 bridge is required. In addition, each platinum-resistance thermometer when calibrated costs approximately $800. For most people this is discouraging when considered relative to the use of thermocouples.

3—THERMOCOUPLE AND RADIATION THERMOMETRY ABOVE 900° K[1]

BY HENRY J. KOSTKOWSKI AND GEORGE W. BURNS

NATIONAL BUREAU OF STANDARDS, WASHINGTON, D.C.

This paper reviews the principles of thermocouple and radiation thermometry above 900° K, the present day precision and accuracy, and the commercial instruments currently available. The International Practical Temperature Scale and the Thermodynamic Kelvin Temperature Scale are briefly described. With regard to thermocouples, the presentation is confined to the more generally accepted base, noble, and refractory metal types. Characteristics such as temperature range, stability, and environmental limitations will be emphasized. The optical pyrometry section includes a discussion of emittance corrections, recommendations for using visual optical pyrometers, and the status of photoelectric optical pyrometers. Finally, two-color, three-color, and total-radiation pyrometers are discussed, primarily to show that, in spite of the recent interest in these instruments, they are not generally as suitable for measuring temperature as optical (single-color) pyrometers.

In determining the thermal radiation properties of solids, it is usually necessary to measure the temperature of the solid or the temperature difference between the solid and a blackbody. These measurements often have to be the order of ten times more accurate than the accuracy required in the radiation properties. As a consequence, it is desirable that those working on thermal radiation properties of solids have a basic, up-to-date knowledge of the field of temperature measurements.

The instruments available for accurate thermometry above 900° K are primarily thermocouples and optical pyrometers. The purpose of this paper is to review the principles of thermocouple and radiation thermometry, the present day precision and accuracy, and the commercial instruments currently available. In order to discuss accuracy, meaningfully, it will also be necessary to consider the temperature scales in use today. With regard to thermocouples, the review will be confined to the more generally accepted base, noble, and refractory metal types. Characteristics such as temperature range, stability, and environmental limitations will be emphasized. The optical pyrometry section will include a discussion of emittance corrections, recommendations for using visual optical pyrometers, and the status of photoelectic optical pyrometers. Finally, two-color, three-color, and total-radiation pyrometers will be discussed, primarily to show that, in spite of the recent interest in these instruments, they are not generally as suitable for measuring temperature as optical (single-color) pyrometers.

[1] This paper is largely an updating (ref. 1) or condensation (ref. 2) of sections of two previous publications.

TEMPERATURE SCALES

There are two major temperature scales in use today. These are the Thermodynamic Kelvin Temperature Scale (TKTS) (ref. 3) and the International Practical Temperature Scale (IPTS) (ref. 4).

Thermodynamic Kelvin Temperature Scale

A thermodynamic scale since it is derived from the second law of thermodynamics is

independent of the properties of any substance (ref. 5). However, in order to define such a scale uniquely, it is necessary to select (or define) a number for the temperature of some one thermal state or for a temperature interval between two states. The triple point of water was adopted (refs. 3 and 4) in 1954 by the General Conference on Weights and Measures as the fundamental fixed point on the thermodynamic scale and assigned the temperature 273.16° K. This thermodynamic scale is called the Thermodynamic Kelvin Temperature Scale and temperatures on this scale are designated degrees Kelvin or simply °K. It is considered the fundamental scale to which all temperature measurements should ultimately be referable.

Thermodynamic temperatures can be realized with a gas thermometer. At high temperatures, where a gas thermometer becomes impractical, radiation from a blackbody together with the Planck radiation equation can be used. In general, thermodynamic temperatures can be obtained from experimental measurements of the quantities in any equation arising from the second law of thermodynamics or the equilibrium theory of statistical mechanics.

International Practical Temperature Scale

Accurate measurements on the TKTS are very difficult, and, therefore, a practical scale called the International Temperature Scale was adopted by 31 nations in 1927 and revised in 1948. In 1960, its name was changed to the International Practical Temperature Scale (IPTS). This scale was designed to provide a means for specifying any temperature more conveniently and precisely than is possible on a thermodynamic scale. In addition, the scale was intended to be as close to the thermodynamic scale as existing knowledge and technique permitted.

The IPTS is based on six fixed points (oxygen, triple point of water, steam, sulfur, silver, and gold) and methods for interpolating between these points. Temperatures on this scale are designated degrees Celsius or simply °C (Int. 1948). From 630.5° C (Int. 1948) to the gold point, defined as 1063° C (Int. 1948),[2] temperatures are interpolated by means of a quadratic equation relating temperature to the electromotive force of a standard thermocouple of platinum vs platinum-10% rhodium when one junction is at 0° C and the other is at the temperature being measured. Above the gold point, the IPTS is defined in terms of the Planck equation and the ratio of the spectral radiance of a blackbody at the temperature to be measured to the spectral radiance of a blackbody at the gold point. The instrument normally used to realize the scale in this range is the disappearing filament optical pyrometer.

For details on the definition of or recommendations for realizing the International Practical Temperature Scale, one should consult the official text (ref. 6) or its translation by Stimson (ref. 4).

Accuracy of Realizing the Temperature Scale

The concept of accuracy refers to how well a particular value agrees with the correct value. However, except in a situation where a material standard defines a unit of measurement, such as the meter bar previous to 1960, the correct value is not known and the accuracy of a particular result can never be exactly determined. An experimenter can make an estimate of the constant or systematic errors of a measurement, and this information is certainly useful. Since such estimates are a matter of judgement, they vary greatly from one individual to another, and an objective interpretation on the meaning of the errors is even more difficult if not impossible to make.

There is a manner of obtaining an estimate of accuracy (ref. 2), at least for temperature measurements, which does not possess these limitations. Various national standards laboratories throughout the world independently attempt to realize the TKTS and the IPTS. Moreover, many of these laboratories are continually trying to improve their realization of the scales, and differences among the laboratories are probably the best indications available of how well the scales are being realized. Therefore, a very useful measure of the accuracy of how well the TKTS or the IPTS has been realized is the standard deviation of the population consisting of the means of the population of the temperature determinations performed in each of the national

[2] In this paper, unless stated otherwise, all temperatures will be given on the IPTS. Therefore, for simplicity, (Int. 1948) will be omitted.

TABLE 3–I.—*Estimated Accuracy* [a] *and Precision* [b] *in ° C of Temperature Scales as of 1962*

Temperature, ° C (Int. 1948)	Estimated accuracy of realizing International Practical Temperature Scale of 1948	Estimated precision of thermometers used to realize International Practical Temperature Scale of 1948	Estimated accuracy of realizing Thermodynamic Temperature Scale of 1954 (refs. 7 and 2)	Reported differences Therm. 1954 minus Int. 1948 (refs. 7 and 2)
630.5	[c] 0.02 .2	[c] 0.002 .1	0.3	+0.2
960.8 (Silver Point)	.2	.1	.4	+.5 +1.1
1063 (Gold Point)	[d] .2 .4	[d] .1 .3	.4	+.7 +1.5
2000	2	1	2	[e] +3
4000	10	3	10	[e] +10

[a] Accuracy here means estimated standard deviation of the mean of determinations from each laboratory in which attempts have been made to realize either the international or the thermodynamic temperature scales about the mean of all laboratories.

[b] Precision of a thermometer means the estimated standard deviation of the determinations of any laboratory (using one thermometer) about the mean of the determinations in the same laboratory.

[c] The first of the two entries (0.02) refers to a standard platinum resistance thermometer and the second (0.002) to a standard thermocouple.

[d] The two entries are standard thermocouple and visual optical pyrometer, respectively.

[e] These values are calculated using 1064.5° C for the gold point and 1.4388 cm deg for the second radiation constant, C_2.

laboratories. In practice numerical results are usually not available from all the national laboratories, and therefore only a sample or estimated standard deviation can be determined. Of course, any constant systematic error that exists in all the national laboratories is not revealed in this manner. But neither would it be accounted for in any other manner. Thus it is believed that the above standard or sample standard deviation is the best available estimate of the accuracy of realizing the TKTS or IPTS, and this is how accuracy is defined in this paper. Similarly, precision is defined as the estimated standard deviation of the determination of any laboratory about the mean of the determinations in the same laboratory.

Table 3–I gives the estimated accuracy of realizing the TKTS and the IPTS, the estimated precision of the thermometers used in realizing the IPTS, and reported differences between the two scales. Thermodynamic temperatures at and below the gold point have been obtained by gas thermometry and above the gold point by visual optical pyrometry. The table represents the best that can be done in temperature measurements as of 1962, and it should be emphasized that the accuracy of any temperature measurement can be no better than the accuracy of the scale to which it refers.

The precision and accuracy of realizing the TKTS and the IPTS above 900° K may improve significantly during the next few years as a result of the development of more accurate gas thermometers (refs. 7 and 8), photoelectric pyrometers (refs. 9 to 11), and high temperature platinum resistance thermometers (ref. 12). The latter two thermometers should also be useful for general laboratory use. Mr. Riddle has presented details on a high temperature resistance thermometer at this symposium, and photoelectric pyrometers will be discussed in the Optical Pyrometry Section of this paper.

THERMOCOUPLES

The theory and use of thermocouples to determine temperature are well established. Three fundamental laws governing thermoelectric circuits have been formulated and are supported by a wealth of experimental evidence. They are often combined in the statement:

"The algebraic sum of the thermoelectromotive forces generated in any given circuit containing any number of dissimilar homogeneous metals is a function only of the temperature of the junctions" (ref. 13). One of the major limitations in the use of thermocouples for high precision temperature measurements arises from the fact that unwanted emfs are generated in inhomogeneous thermoele-

ments passing through temperature gradients. When selecting thermocouple materials, care should be taken to obtain as homogeneous material as possible and to have the material in a well annealed state.

An important aspect in any temperature measuring problem using a thermocouple is bringing the measuring junction of the thermocouple to the same temperature as the object or environment whose temperature is to be determined. Such a condition can be approached if care is taken to minimize conduction and radiation losses (refs. 14 and 15). Also, there must be sufficient electrical insulation between thermoelements of the thermocouple so that emf determinations will be a true indication of the temperature of the measuring junction. Often in practice the experimenter may have geometrical or environmental limitations which make it impossible to exercise all the precautions necessary for good thermometry. However, usually the effects resulting from a lack of ideal conditions can be evaluated and accounted for to some extent. The proper use and testing of thermocouples are described in great detail in the literature (refs. 16 to 18).

In selecting a thermocouple for a particular application, one must consider a number of factors. Among these are the environment and temperature range in which the thermocouple is to be used, the stability which can be expected of the thermocouple in this range, the thermoelectric characteristics of the thermocouple, and perhaps the cost of the thermocouple materials. For temperatures below 1200° C inexpensive base metal thermocouples find wide application. At higher temperatures, to 1800° C, it is necessary to use thermocouples made of noble metals, metals which are more or less indifferent to their environment. At still higher temperatures, refractory metal thermocouples are required. These thermocouples are characterized by the high melting points of their constituents. All of these thermocouples may be used with some success at lower temperatures. They should be used at temperatures above their recommended range only in special situations, and then with the understanding that performance may be impaired.

Over the years a wide variety of thermocouples have been used for various temperature measuring situations. Some types have been found superior to others and have come into common use. In what follows the characteristics of the more common thermocouples will be described.

Base Metal Thermocouples (less than 1200° C)

For temperatures up to 1200° C base metal thermocouples having nickel as the major alloying component are used extensively in industry for measuring and controlling temperature. Examples are the Chromel P vs Alumel thermocouple, the Geminol–P vs Geminol–N thermocouple, and the Kanthal+ vs Kanthal− thermocouple. They are inexpensive, have a high thermoelectromotive force, and are reasonably oxidation resistant. These thermocouples are considered to be reproducible to about 0.5° C when used for short periods of time and not used above 900° C. Dahl (ref. 19) showed that a Chromel P vs Alumel thermocouple could be used in air at 1000° C for 1000 hours with a maximum change in calibration of only 5°. At 1200° C, however, a Chromel P vs Alumel thermocouple failed after 200 hours, its calibration change being 12° at the time of failure. Potts and McElroy (ref. 20), in more recent work, have conducted extensive tests to 1000° C on nickel-base thermocouples. These tests include studies on homogeneity, cold working, annealing, oxidation, metallography, and stability.

The maximum recommended operating temperature for nickel-base thermocouples is about 1250° C. Refractories such as porcelain, magnesia, or alumina appear adequate for electrical insulation of nickel-base thermocouples throughout their useful temperature range. The use of a sheathed or swaged thermocouple assembly may appreciably extend the useful life and increase the reliability of these thermocouples in applications where corrosive atmospheres become a problem. Care should be taken to remove carbonaceous materials from insulating and protecting materials before thermocouple assembly, since nickel-base thermocouples may undergo large calibration changes at high temperatures in the presence of such materials. In addition, the use of nickel-chromium alloys under marginally oxidizing conditions should be avoided. Studies by Sibley (ref. 21) show the effect of heating a Chromel P vs Alumel thermo-

couple under such conditions. Relatively large changes (88° F[3] negative drift) were observed in the thermocouple calibration after heating for 280 hours in a marginally oxidizing atmosphere at 2000° F (1093° C). The change was attributed to preferential oxidation of chromium in the Chromel P leg. Sibley also pointed out that marginally oxidizing conditions conducive to preferential oxidation can develop within protecting tubes through contamination or even through stagnation of air. Therefore, the use of large diameter protecting tubes is recommended to permit free circulation of air. However, recently, a special grade of Chromel P alloy which is more resistant to preferential oxidation when subjected to marginally oxidizing conditions has been developed (ref. 21).

Noble Metal Thermocouples (less than 1800° C)

When cost is not a major problem, and it should not be except in situations where large numbers of thermocouples are used, the generally more stable noble metal thermocouples are preferred over the base metal types. A noble metal thermocouple which has thermoelectric characteristics similar to the nickel-base thermocouples has been developed recently (ref. 22). This thermocouple is called Platinel. Tests by the manufacturer show that the temperature-emf curves of the Platinel and Chromel P vs Alumel thermocouples agree within 2% up to 1200° C. Under certain conditions, the Platinal thermocouple has proven to be more stable than nickel-base thermocouples. Stability tests in an oxidizing atmosphere of wet steam and carbon dioxide gas at 1200° C showed the Platinel thermocouple to be superior in performance to a Chromel P vs Alumel thermocouple of the same wire size. Data are also reported by the manufacturer for stability of the Platinel thermocouple in air. After about 1000 hours in air at 1300° C a Platinel thermocouple showed a maximum shift in calibration of only 3°. Platinel thermocouples are currently being studied at NBS by Freeze and Davis. In one test a Platinel thermocouple was electrically heated in air at about 1200° C. From time to time it was checked against a reference thermocouple for changes in calibration. After a total of 1000 hours at 1200° C a shift in calibration equivalent to only 4° at 1200° C was observed. Details on this work by Freeze and Davis should be available in a future ASD technical report.

Another noble metal thermocouple has been developed recently for use in combustion-type atmospheres. The thermocouple has pure palladium for one leg and a platinum–15% iridium alloy for the other. This thermocouple develops roughly three-fourths the electromotive force of a Chromel P vs Alumel thermocouple at 1100° C. Work by Ihnat (ref. 23) showed palladium vs platinum–15% iridium thermocouples were reliable to within ±0.5% when used in an oxidizing atmosphere for periods as long as 400 hours in the 1000° to 1250° C temperature range. Ihnat recommended that the palladium vs platinum–15% iridium thermocouple not be used in a hydrogen atmosphere and that welded junctions be formed under protection of an inert atmosphere. Also, the annealing procedure (refs. 24 and 25) for the thermocouple appears to be important if good stability is to be obtained. Reference tables for the palladium vs platinum–15% iridium thermocouple have been prepared at NBS by Freeze, Caldwell, and Davis (ref. 26).

The most accurate temperature measurements in the range from 630.5° C to about 1300° C, are made with the platinum vs platinum–10% rhodium thermocouple and the platinum vs platinum–13% rhodium thermocouple. These thermocouples are used widely in laboratory applications for reference standards and for precise experimental work. In fact, since the platinum vs platinum–10% rhodium thermocouple is used as the interpolating instrument on the International Practical Temperature Scale of 1948 in the range 630.5° to 1063° C (ref. 4), all other instruments used to measure temperature on the IPTS in this range must ultimately be compared with this thermocouple in some manner. The electromotive force of the platinum vs platinum–13% rhodium thermocouple is slightly higher than the plat-

[3] There are no Fahrenheit units defined on either the International or Thermodynamic Scales. Nevertheless, they are still occasionally used in practice. When temperatures in the literature are given in Fahrenheit units, we have retained the usage in this paper with the approximate Celsius units on the IPTS also given. For this purpose we have defined ° F = 9/5 × ° C (Int. 1948) + 32.

inum vs platinum–10% rhodium thermocouple, about 10% at 1300° C. Otherwise, for all practical purposes, the two can be considered similar in performance.

With carefully handled, well annealed (ref. 27), reference-grade platinum and platinum-rhodium wires, it is possible to obtain a precision with platinum vs platinum-rhodium thermocouples of 0.1° for short periods of time at least up to 1100° C. Thermoelements ranging from 30 to 60 inches in length can be cut randomly from 100 foot lengths of such platinum and platinum–10% rhodium wire, drawn from the same lot, and the calibration of thermocouples fabricated from these wires will seldom differ from the average of all the thermocouples by more than a few tenths of a deg at the gold point (1063° C). With wire of this quality, and in special situations where the temperature gradients along the wires can be expected to be the same from one determination to another, precision of better than 0.1° is possible. Platinum vs platinum–10% rhodium thermocouples are tested at the freezing points of gold (1063° C) and silver (960.8° C) and at 630.5° C and 419.5° C during a primary calibration (ref. 16) at NBS. The uncertainties at each point do not exceed the equivalent of 0.2° C. Well annealed platinum vs platinum–10% rhodium thermocouples fabricated from unused wire are expected to repeat from determination to determination at any of these points to within the equivalent of a few hundredths of a degree.

Platinum vs platinum–10% or–13% rhodium thermocouples are reliable to within ¼% up to 1300° C if used in a clean oxidizing atmosphere and not used for extended periods above 1300° C. High purity alumina is recommended for insulation and protection of these thermocouples when they are to be used for extended periods of time above 1000° C. Though recommended for use in oxidizing atmospheres, recent work (refs. 28 and 29) indicates that they can be used with some reliability in vacuum, neutral, and even reducing atmospheres if precautions are taken to eliminate sources of possible contamination.

Experience indicates that the electromotive force of platinum vs platinum-10% or –13% rhodium thermocouples tends to decrease with time at a given temperature and depth of immersion. The changes are thought to be due to (a) rhodium migration, (b) preferential volatilization or oxidation in the alloy wire, and (c) chemical contamination. Rhodium migration (refs. 29 to 32) is the transfer of rhodium from the alloy wire to the pure platinum wire. It results in instability by decreasing the electromotive force of the thermocouple. Though not fully understood, the process is believed to progress more rapidly in situations where the measuring junction of the thermocouple is used in a region of sharp temperature gradient. Several investigators (refs. 29, 33 to 35) have reported that either platinum or rhodium may be preferentially removed from the alloy wire by volatilization or oxidation. The extent of this effect appears to depend strongly on the temperature and conditions under which the alloy wire is heated. In any event, the effect does not seem to cause any serious problems for temperatures up to 1300° C if the thermocouples are mounted in twin-bore insulating tubes and not used in a rapidly moving oxidizing atmosphere. In most practical applications, chemical contamination of the thermocouple from the surrounding environment is probably the principal factor that limits the useful life of platinum vs platinum-rhodium thermocouples used in the range 630.5° to 1300° C. Common causes and effects of chemical contamination on platinum vs platinum-rhodium thermocouples can be found in the literature (refs. 36 and 37).

For precise temperature measurements in the range 1300° to 1750° C thermocouples utilizing pure platinum as one thermoelement are declining in use in favor of thermocouples employing platiuum-rhodium alloys in both legs. Using an alloy in both legs increases the mechanical strength of the thermocouple at high temperatures and appears to reduce the effects of chemical contamination and rhodium migration. Ehringer (ref. 38) studied the behavior of platinum and platinum-rhodium alloy wires when heated for periods of time in air and hydrogen. He heated the wires in the presence of various refractory oxides such as alumina and silica. In this work alloys of platinum-rhodium were shown to be much less susceptible to changes in calibration than pure platinum.

Metcalfe (ref. 32) showed that a platinum-1% rhodium vs platinum–13% rhodium thermocouple was more stable in a vacuum at 1510° C than a platinum vs platinum–13% rhodium therocouple. The improved behavior was attributed to a reduction in the effects of rhodium migration and chemical contamination. Recent studies have been made by Walker, Ewing, and Miller at the Naval Research Laboratory on the instability of noble metal thermocouples in the range 1000° to 1700° C. Effects of various grades of alumina sheathing on the thermoelectric characteristic of platinum and platinum-rhodium alloys in oxidizing and neutral atmospheres were investigated. They found that the platinum-rhodium alloys were more stable than pure platinum when used in similar environments at high temperatures. A paper covering this work should appear in the literature within a few months.

Three platinum-rhodium alloy combinations have gained general acceptance. These are the platinum–5% rhodium vs platinum–20% rhodium, platinum–6% rhodium vs platinum–30% rhodium, and platinum–20% rhodium vs platinum–40% rhodium thermocouples. The platinum–5% rhodium vs platinum–20% rhodium and platinum–6% rhodium vs platinum–30% rhodium thermocouples have nearly the same thermoelectric characteristics in the range 1300° to 1750° C. Their thermoelectric powers at 1600° C are 10 μv/° C and 11 μv/° C, respectively. The platinum–20% rhodium vs platinum–40% rhodium thermocouple has a thermoelectric power of only 4.5 μv/° C at 1600° C. However, Jewell, Knowles, and Lord (ref. 39) have studied this thermocouple and recommend it for use in the 1700° to 1850° C temperature range. Wire manufacturers in this country have standardized on the platinum–6% rhodium vs platinum–30% rhodium thermocouple. Reference tables are being prepared at NBS for this thermocouple, and reference tables for the platinum–6% rhodium vs platinum–30% rhodium thermocouple have appeared recently in a paper by Obrowski and Prinz (ref. 40). Though no long term stability experiments have been conducted at NBS, excellent stability for short periods of time has been observed with this thermocouple at temperatures up to 1650° C.

Recrystallized alumina has been used successfully for insulation and protection of platinum-rhodium alloys. However, at temperatures approaching 1800° C errors introduced by insufficient electrical insulation between thermo-elements should not be overlooked. Also, caution should be exercised in the use of alumina as an insulating material in the presence of carbonaceous materials at temperatures above 1600° C (ref. 41). Though it is usually recommended that platinum-rhodium alloy combinations be used in oxidixing atmospheres, intermittent use in vacuum, neutral, and hydrogen atmosphere appears possible. Except in cases where these thermocouples can be used in an exceptionally clean environment, protection by high purity alumina will most likely extend their useful life.

Refractory Metal Thermocouples

Increased demands from high temperature technology in the past ten years have led to accelerated programs in the search for thermocouples capable of reliable temperature measurements above the range of platinum-rhodium types. Though the properties of numerous combinations have been explored, only a few displayed promise and have been developed to any extent. Sanders (ref. 42) gives an extensive review of the many thermocouples that have been tried above 1800° C. The two high-temperature thermocouple systems receiving the most attention at present are the tungsten-rhenium and iridium-rhodium systems. Only refractory metal thermocouples of these two systems will be discussed in this paper.

The tungsten vs rhenium and tungsten vs tungsten–26% rhenium thermocouples have been the most widely investigated in the tungsten-rhenium system. Of these two, the tungsten vs tungsten–26% rhenium appears to offer the most promise in terms of high temperature capabilities and accuracy. A gradual decrease in the thermoelectric power of the tungsten vs rhenium thermocouple with increasing temperature limits its use for most practical applications to temperatures below 2200° C. The tungsten vs tungsten–26% rhenium thermocouple has been reported as having a high thermoelectric power up to at least 2800° C and has shown excellent stability

at temperatures as high as 2200° C. In recent work by Lachman (ref. 43) a tungsten vs tungsten–26% rhenium thermocouple was heated for 100 hours at 4000° F (2204° C) in argon and showed a maximum change in calibration of 12° F. Lachman claimed that similar stability could be expected in a hydrogen atmosphere.

As a result of the increasing use of high temperature thermocouples and with improvements in the quality and availability of refractory metal wires, the NBS has initiated a project to investigate the thermoelectric properties of the more promising refractory metal materials. High temperature testing facilities (ref. 44) have been developed at NBS and Thomas is preparing reference tables for the tungsten vs rhenium thermocouple. Thermocouples, made from tungsten wire of different lots obtained from three different commercial sources, and rhenium wires, from different lots from a single commercial source, have been tested in the range 1000° to 2000° C in a helium atmosphere. The maximum deviation for any thermocouple in the group from the average of all the thermocouples is about 20° at 2000° C. Though no long term stability tests on the tungsten vs rhenium thermocouple have been made at NBS, the thermocouple has, in general, proved to be stable for short periods of time at temperatures up to at least 2000° C in a purified helium atmosphere.

A major limitation in thermocouples employing pure tungsten as one thermoelement is the extreme brittleness of the tungsten in the recrystallized state. Handling of tungsten wire after it has been heated above about 1200° C, requires utmost care. The fact that the tungsten–26% rhenium alloy is still ductile at room temperature after being heated for extended periods above its recrystallization temperature suggests the possibility of obtaining a more useful high temperature thermocouple with improved mechanical properties by using tungsten-rhenium alloys in both legs. In a recent test at NBS a tungsten–3% rhenium alloy wire was heated for 1 hour at 2000° C in a purified helium atmosphere. After this treatment it could be bent into a hairpin shape.

For reliable use at high temperatures, tungsten vs rhenium and tungsten vs tungsten–26% rhenium thermocouples require a protective atmosphere free of oxidizing gases. Exposure to air above 1000° C will result in immediate failure of these thermocouples. All traces of water and carbonaceous materials should be removed from insulating and protecting parts before assembling these thermocouples. The behavior of tungsten vs rhenium and tungsten vs tungsten–26% rhenium thermocouples in vacuum (refs. 45 and 46) hydrogen (refs. 47 and 48) neutral (ref. 43) and carbon (refs. 41 and 49) atmospheres has been studied, and the literature should be consulted for details.

Alumina appears satisfactory for electric insulation of these thermocouples up to about 1800° C. Above this range there are no completely satisfactory materials available today. In some cases, satisfactory results have been obtained with beryllia and thoria. Heath (ref. 41) and Sanders (ref. 42) have reviewed the merits and limitations of these and other high temperature refractory oxides.

Thermocouples of the iridium-rhodium system are of particular interest because they show promise as being useful in oxidizing atmospheres above the range of platinum-rhodium types. One proven refractory thermocouple of this type is the iridium vs rhodium–40% iridium thermocouple. It has been calibrated and used to 2100° C in a neutral atmosphere with a maximum uncertainty of 7°. Only minor changes in the calibration of this thermocouple have been reported after 50 hours at 2000° C in an atmosphere containing 2% oxygen. The thermocouple failed after 12 hours in air at 2000° C, but was relatively stable during its lifetime. Moreover, the use of a protective sheath will prolong its life in air (ref. 42). Kuether and Lachman (ref. 45) have studied the behavior of the iridium vs rhodium–40% iridium thermocouple in vacuum at temperatures up to 2600° F (1427° C). They found a shift in calibration equivalent to 21° F at 2000° F (1093° C) after heating an iridium vs rhodium–40% iridium thermocouple in a vacuum for a period of 20 hours at 2600° F (1427° C).

Caldwell and Blackburn at NBS have been working on a program to establish reference tables for several alloy combinations of iridium-

rhodium against iridium. An iridium blackbody inductively heated in a high precentage helium atmosphere is being used in this work. Tables have been prepared for the iridium vs rhodium–40% iridium thermocouple in the range 0° to 2100° C (ref. 50). Eight thermocouples fabricated from three different lots of wire from the same manufacturer were tested and the data used to construct the reference table. The maximum deviation of any of the eight thermocouples from the reference table was about 10° at 2000° C. They were able to use beryllia and thoria for electrical insulation but empirically determined corrections were necessary above 1800° C.

Homogeneous iridium vs rhodium–40% iridium thermocouples are available commercially and they are sufficiently ductile to permit bending on a quarter-inch radius. The major limitations in using this thermocouple are its high cost and relatively low thermoelectric power (5.5 μv/° C at 1300° C and 6.5 μv/° C at 2100° C).

The greatest problem in the reliable use of thermocouples above about 2100° or 2200° C is the lack of satisfactory materials for protection and electrical insulation. The seriousness of insufficient electrical insulation at high temperature is illustrated in a recent report by McGurty and Kuhlman (ref. 51). Due to lack of adequate insulating and protecting materials the use of bare thermocouples is mandatory at present if reliable temperature measurements are to be made at these high temperatures.

A summary of the temperature range, emf, thermoelectric power, and stability of the thermocouples discussed in this paper is given in table 3-II. The numbers are estimates

TABLE 3–II.—*Estimated stability for the more reliable high temperature thermocouples*

Thermocouple	Atmosphere	Approximate electromotive force at temperature indicated, millivolts	Thermoelectric power at temperature indicated, μv/° C	Temperature, °C (Int. 1948)	Estimated change in calibration after being at temperature for time indicated, deg.	
					10 hr	1000 hr
Chromel vs Alumel	Oxidizing	41	39	1000	0.5	5.0
		49	36	1200	2.0	[a] F
Palladium vs platinum-15% iridium	Oxidizing	38	43	1200	0.5	5.0
Platinel+ vs Platinel	Oxidizing	48	32	1200	0.5	3.0
Platinum vs platinum-10% or 13% rhodium	Oxidizing	11 or 12	12 or 13	1100	<0.1	2.0
		15 or 17	12 or 14	1500	1.0	--------
Platinum–6% rhodium vs platinum–30% rhodium	Oxidizing	12	11	1700	4.0	--------
Platinum–5% rhodium vs platinum–20% rhodium	Oxidizing	12	10	1700	4.0	--------
Platinum–20% rhodium vs platinum–40% rhodium	Oxidizing	5	5	1800	6.0	--------
Tungsten vs rhenium	Inert	28	7	2000	10.0	--------
Tungsten vs tungsten–26% rhenium	Inert	37	14	2200	10.0	--------
Iridium vs rhodium–40% iridium	Inert or slightly oxidizing	11	7	2000	10.0	--------

[a] F means the thermocouple would fail before the time indicated.

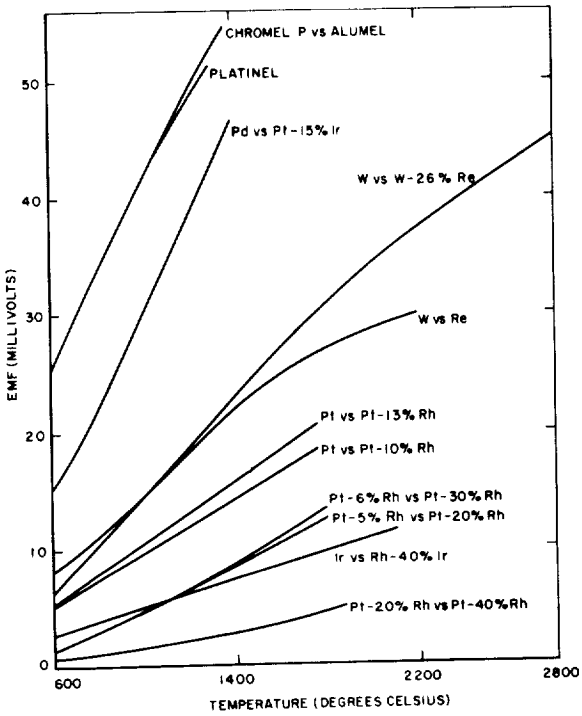

FIGURE 3-1.—EMF plotted against temperature for the more commonly used high temperature thermocouples, reference junction at 0° C.

based on data found in the literature and on experience at NBS. Also, temperature-emf curves for the thermocouples are given in figure 3-1. The curves cover the range of available calibration data, but it is not necessarily recommended that the thermocouple be used over the entire range.

OPTICAL PYROMETERS

When a thermocouple is undesirable because it disturbs the system significantly or unreliable because the temperature is too high, an optical pyrometer should be considered for determining the temperature. Moreover, because the IPTS above 1063° C is defined in terms of radiation, even thermocouples must be ultimately calibrated with a radiation thermometer above this temperature.

The radiation thermometry part of this paper will be organized differently and have significantly fewer references than the thermocouple part. This is due primarily to two reasons. First, there are a large number of thermocouples useful in different environments and temperature ranges while the optical pyrometer is the only radiation device recommended for temperature determinations. Second, one of the present authors was a co-author of a recent monograph on optical pyrometry (ref. 2) from which this review paper draws heavily. It was not thought worthwhile or necessary to repeat details of general pyrometry theory or methods, so only the results considered particularly appropriate for people at this symposium are repeated or summarized.

The measurement of temperature by optical pyrometry is based on the fact that the spectral radiance of a body depends on its temperature. For a blackbody, the spectral radiance is related to the temperature by the well-established Planck radiation equation (for units and notation, see ref. 2):

$$N_{b\lambda}(T)=\frac{C_1\lambda^{-5/\pi}}{e^{C_2/\lambda T}-1} \tag{1}$$

where C_1 and C_2 are constants, λ is the wavelength, and T is the temperature expressed in degrees Kelvin.[4] When the object is not a blackbody, the fractional reduction in spectral radiance, for the same temperature, is given by the spectral emittance, $\epsilon_\lambda(T)$, and the spectral radiance becomes

$$N_\lambda(T)=\epsilon_\lambda(T)N_{b\lambda}(T) \tag{2}$$

In this case, in order to determine the temperature of the object by optical pyrometry, it is necessary to determine not only the spectral radiance but also the spectral emittance. This need for spectral emmittance is probably the major problem in determining temperatures by optical pyrometry. This is particularly discouraging for the people at this symposium because the temperature is needed to determine the spectral emittance and the spectral emittance to determine the temperature (with optical pyrometry). On the other hand, this clearly emphasizes the importance of spectral emittance data and the contributions that can be made in this field.

As a result of the above-mentioned paradox with temperature and spectral emittance, most

[4] This temperature can be expressed on the TKTS or the IPTS. In the latter case, which is usually preferred, the temperature is equal to $t_{Int}+T_o$ where $T_o=273.15°$.

spectral emittance studies utilizing optical pyrometry to obtain the temperature require a blackbody (spectral emittance equal to one). Nevertheless, it is possible to use a non-blackbody whose spectral emittance has been determined previously; and, in addition, optical pyrometers are often checked or calibrated with non-blackbody sources. Therefore, problems inherent in determining the temperature of non-blackbody as well as blackbody sources will be discussed in this paper.

Temperature Determinations With Optical Pyrometers

Optical pyrometers are instruments which determine the spectral radiance, at a particular wavelength, of a radiating object. The determination is usually expressed as the temperature of a blackbody which has the same spectral radiance at this wavelength. Such a temperature is called the brightness and, in general, is a function of wavelength. Mathematically, it is defined by the equation

$$N_{\lambda'}(T)=\epsilon_{\lambda'}(T)N_{b\lambda'}(T)=N_{b\lambda'}(T'_B) \qquad (3)$$

where T'_B is the brightness temperature at wavelength λ'. If the object being sighted on is a blackbody, the brightness temperature is the actual temperature and, of course, is then independent of wavelength.

In order to obtain the temperature of a non-blackbody from an optical pyrometer determination, the spectral emittance at the wavelength associated with the pyrometer is required. The temperature can be obtained from equation (3) or more explicitly from [5]

$$\epsilon_{\lambda'}(t)=\frac{e^{\frac{C_2}{\lambda'(t+T_0)}}-1}{e^{\frac{C_2}{\lambda'(t'_B+T_0)}}-1} \qquad (4)$$

where $t+T_0=T$ and $t'_B+T_0=T'_B$, t is the temperature, and t'_B is the brightness temperature (at wavelength λ') in °C (Int. 1948), $\epsilon_{\lambda'}(t)$ is the spectral emittance at λ' and t, $C_2=1.438$ cm deg, and $T_0=273.15$ deg. Usually, the Wien radiation equation is an adequate approximation [6] for the Planck equation. Then equation (3) can be simplified to

$$\frac{1}{T}=\frac{1}{T'_B}+\frac{\lambda'}{C_2}\ln \epsilon_{\lambda'}(T) \qquad (5)$$

The wavelength λ' is called the mean effective wavelength of the optical pyrometer. The accuracy required for λ' when determining non-blackbody temperatures depends on how rapidly $\epsilon_{\lambda'}$ varies with wavelength. However, the accuracy of the spectral emittance need be only ⅛ to 1/15 the accuracy required in the temperature. For example, in the vicinity of the gold point and at the wavelength of 0.65μ an error of 10% in the spectral emittance results in an error of only 0.65% in temperature. More generally, using Wien's approximation and assuming that the usually small variation of spectral emittance with temperature may be neglected one obtains

$$\frac{dT}{T}=-\frac{\lambda' T}{C_2}\frac{d\epsilon_\lambda}{\epsilon_\lambda} \qquad (6)$$

If an accuracy of $\pm 0.01\mu$ for λ' is adequate, the value 0.65μ can usually be used for visual optical pyrometers manufactured in the United States (as of 1962).

The spectral emittance at 0.65μ has been determined for a number of substances (refs. 52 to 54). In addition, Poland, Green, and Margrave (ref. 55) have published a set of tables, calculated from equation (4), giving the actual temperature as a function of the observed brightness temperature and spectral emittance at 0.65μ.

It is possible, with considerable effort, to determine the mean effective wavelength in visual optical pyrometers considerably better than $\pm 0.01\mu$ (probably about 0.001μ). However, in order to do this, the spectral transmittance of the filters in the optical pyrometer, the relative visibility function of the observer and the color temperature of the source are all required. Instead of determining the visibility function of the observer, a difficult feat, one can probably use a number of observers

[5] In this paper the symbol t designates temperature in °C and T in °K. Though both temperatures are on the ITPS and should be designated t_{int} and T_{int}, for simplicity the subscripts have been omitted.

[6] For a wavelength equal to 0.65μ and $t=4000°$ C the error in using the Wien equation is about 5°. At 3000° C and 0.65μ the error is about 0.5°.

and assume their average is the CIE standard visibility function (ref. 2). This should be adequate because the standard deviation of the mean effective wavelength resulting from differences in the visibility function of observers has been reported (ref. 2) to be about 0.0008μ. If the color temperature of the object is not available from the literature, it can be obtained experimentally by determining the spectral radiance of the object over the spectral bandpass of the pyrometer (approximately 0.62 to 0.75μ). The desired color temperature is the temperature of the blackbody whose spectral radiance curve when multiplied by some constant best fits the observed spectral radiance curve of the source. The actual equations used for calculating the mean effective wavelength with the above data are rather lengthy and will not be given here. The equations as well as their derivations are available in the previously mentioned monograph (ref. 2).

Blackbodies

There are many substances for which the spectral emittance at 0.65μ is not known or not known sufficiently well to obtain an accurate temperature. In this situation, a blackbody must be built into the apparatus. A hollow opaque body containing a small hole can be made to approximate a blackbody extremely well, and sources used as blackbodies are usually of this type. In such bodies, the smaller the area of the hole relative to the area of the walls of the cavity, the higher the emittance or blacker the body. For a particular geometry the blackness of a hollow body also depends on the reflectivity of the inner surface of the cavity including how diffuse or specular it is. A factor often neglected is that the walls of the enclosure should have a uniform temperature. Lack of a uniform temperature can result in a large departure from blackbody conditions. Details for designing blackbodies and for calculating departures from an emittance of one may be found in the literature (refs. 56 to 58).

Intercomparison of Optical Pyrometers

When several optical pyrometers are used in a laboratory, they are often intercompared by using a tungsten strip lamp as a transfer source. These lamps are highly reproducible sources of radiant energy (refs. 2, 59 and 60) and can be calibrated with respect to brightness temperature from 800° to 2300° C with an accuracy only slightly less than the accuracy of realizing the ITPS. In effect, the tungsten strip lamps when used under well defined conditions (orientation, direction of sighting, ambient temperature) serve as a continuous set of fixed points from 800° to 2300° C with a constancy of about 0.5° to 1.0°. One other point must be kept in mind when intercomparing optical pyrometers with tungsten strip lamps. The brightness temperature of a strip lamp is a function of wavelength, and the mean effective wavelengths of commercial optical pyrometers are sometimes different. Therefore, the brightness temperature of a strip lamp as determined with two different pyrometers, even though accurately calibrated, may be different. At 2200° C this difference has been observed to be as high as 5° in commercial optical pyrometers. At 1000° C it is usually less than 1°. For the most accurate optical pyrometer intercomparisons with strip lamps, the mean effective wavelengths of the pyrometers should be obtained and corrections made with the equation (ref. 2)

$$\frac{1}{T'}=\frac{(\lambda'-\lambda)}{\lambda}\left(\frac{1}{T}-\frac{1}{T^c}\right)+\frac{1}{T} \qquad (6)$$

where, again, T and T' are brightness temperatures at wavelength λ and λ', respectively, and T^c is the color temperature of the tungsten lamp.

Another very useful transfer or reference source, that has become available commercially (Mole-Richardson Company, Hollywood, California), is the pyrometric carbon arc. The positive crater of an arc using pure graphite electrodes and operated just below the so-called arc overload current has a brightness temperature of about 3800° K (refs. 61 and 62), reproducible to about 15° K. With appropriate absorbing glass filters, such as those found in optical pyrometers, a carbon arc could also be used at brightness temperatures lower than 3800° K. At the apparent brightness temperature of 1000° K, the reproducibility of such an arc would be about 1°.

Recommendations for Using Optical Pyrometers

When high accuracy is the primary consideration in maintaining or making measurements on the IPTS, a few procedures should be emphasized. Both the small pyrometer lamps in oprical pyrometers and tungsten strip lamps change with use. Therefore, in order to obtain high accuracy a laboratory should use one calibrated strip lamp or optical pyrometer infrequently and compare the strip lamps or pyrometers used regularly to it. For optimum results, the calibration of a visual optical pyrometer should be checked about every 200 hours of use. Great care should be taken concerning the orientation and alignment of the strip lamps; and vacuum strip lamps, which are generally more stable than gas-filled lamps below brightness temperatures (0.65μ) of about 1400° C (ref. 2), should be used whenever possible.

For optimum precision and accuracy in the use of optical pyrometers, laboratories should request NBS to calibrate their pyrometers as a function of pyrometer filament current. The laboratory should then use a standard resistor and sufficiently accurate potentiometer to determine this current. A multiturn smooth-turning rheostat is highly desirable for varying the filament current while making brightness matches. The precision of the matches can often be improved by having the pyrometer mounted rigidly in a comfortable position for a sitting observer. A black cloth thrown over the observer's head and part of the optical pyrometer to shield the observer from any distracting or annoying light is helpful. Observations should always be made from both a dark and bright filament to a match or disappearance and the two results averaged. If one or two individuals primarily use the pyrometer, make sure that their technique of matching or their visibility functions do not give results very different from the average of a larger number (at least 5 or 6) of observers. Blackbodies should be used whenever possible. If blackbodies cannot be used and high accuracy is required, the mean effective wavelengths of the pyrometers should be obtained.

Accuracy and Precision

The precision of visual optical pyrometers is limited by the sensitivity of the human eye. The precision possible by experienced observers using a good instrument under ideal conditions is shown in table 3–I.

The accuracy of brightness temperature determinations with visual optical pyrometers depends on the accuracy with which the IPTS can be realized in the national standards laboratories and how well a visual pyrometer can be calibrated and used relative to this scale. Brightness temperatures can be obtained with an NBS calibrated, commercial, visual pyrometer to about 3° at the gold point, 6° at 2000° C and 40° at 4000° C. Using precisely determined current in the pyrometer lamp as a measure of the brightness temperature the above uncertainties can often be reduced. If one performs his own primary calibration with a carefully designed and constructed pyrometer and with all the precautions taken at a national standards laboratory, it is possible to approach the accuracy listed in column 2 of table 3–I.

Photoelectric Optical Pyrometers

Serious efforts have been underway at a number of national standards laboratories (refs. 9 to 11) for the past five or six years to replace the visual optical pyrometer with a photoelectric optical pyrometer. Since a photomultiplier tube is more sensitive than the eye and can discriminate between smaller differences of radiance, errors in brightness matching and the mean effective wavelength can be reduced significantly. Photoelectric pyrometers developed in the standards laboratories have a precision about ten times greater than that listed for visual pyrometers in table 3–I. Little information is currently available on their accuracy, relative to the IPTS. However, based on the work at NBS, the accuracy realized in the near future is expected to be 2 or 3 times better than that of the visual pyrometer.

Photoelectric pyrometers are now available commercially from the Instrument Development Laboratories, Attleboro, Massachusetts; the Leeds and Northrup Company, Philadelphia, Pennsylvania; and the Pyrometer Instrument Company, Bergenfield, New Jersey. These instruments are reported to have sensitivities varying from 0.5° to that comparable

to the photoelectric pyrometers in the national standards laboratories. Probably of greater significance, in practice, is that these instruments make brightness matches automatically and therefore can be used remotely or to control a source of radiation as well as determine its temperature or brightness temperature.

OTHER TYPE RADIATION THERMOMETERS

Two-Color Pyrometers

Attempts have been made to circumvent the need for spectral emittance corrections when determining temperatures with an optical pyrometer by using a two-color pyrometer (ref. 54). This instrument determines a two-color temperature by measuring the ratio of the spectral radiances at two wavelengths. The two-color temperature is equal to the temperature only if the spectral emittances at the two wavelengths are equal. Unfortunately, spectral emittance usually changes with wavelength. If the change is very small, the two-color temperature will be close to the actual temperature. On the other hand, there are materials (Ag, Cu, Au) for which the spectral emittance changes with wavelength sufficiently fast that the two color temperature differs a factor of two or more from the actual temperature. A detailed analysis of whether a two-color pyrometer or an optical pyrometer determines a more accurate temperature is given by Pyatt (ref. 63). The idea to be emphasized is that a two-color pyrometer is not generally more accurate than an optical pyrometer and some information concerning spectral emittances is needed before the instrument can be used with confidence. Furthermore, two-color pyrometers are inherently less sensitive than optical (single color) pyrometers. For example, when determining the temperature of a blackbody at 2300° K with an optical pyrometer, a change in the spectral radiance at 0.66μ of 1.2% would modify the resulting temperature indication by 2° C. Using a two-color pyrometer a change of 1.2% in spectral radiance at 0.66μ and 1.0% in the opposite direction at 0.56μ would modify the temperature indication by 30° C. Equation (7) is an expression for the sensitivity of a two-color pyrometer when using the Wien approximation

$$\frac{dT}{T} = \frac{\lambda_1\lambda_2 T}{C_2(\lambda_2-\lambda_1)} \frac{d(N_{\lambda_1}/N_{\lambda_2})}{N_{\lambda_1}/N_{\lambda_2}} \tag{7}$$

In general, two-color pyrometers are not recommended for determining temperatures accurately. However, there are applications where one is more interested in the control of temperature than in the measurement of temperature. In such cases, two-color pyrometers may be useful and a variety of such instruments are now available commercially.

Three-Color Pyrometers

During the past few years three-color pyrometers (refs. 64 to 65) have received increasing attention and, at first glance, are very promising as an instrument for obtaining the temperature of an object without having knowledge of its spectral emittance. This is true, however, only if the spectral emittance of the object is exactly linear with respect to wavelength. Proponents of three-color pyrometers claim that since many materials appear to have an approximately linear spectral emittance in the infrared, a three-color *infrared* pyrometer will determine accurate temperatures for these materials. However, what they apparently do not realize is that a slight departure from linearity will result in a large temperature uncertainty. For example, if four different sources of radiation possessed the spectral emittances in figure 3–2 and the temperatures indicated thereon, each would radiate the same between 1.2 and 2.0μ. Thus, one could not distinguish between any of these temperatures by spectral radiance measurements alone, and a three-color pyometer operating in this spectral region would indicate a temperature of 2000° K for all four sources represented by the curves in figure 3–2. Only in the case for which the spectral emittance curve was linear, would this be the correct temperature. A nonlinearity[7] in spectral emittance of 1% would result in a 42° error and a 5% nonlinearity in a 200° error. The accuracy of the best available spectral emittance data probably falls in this range of 1 to 5%. Moreover, to the best of our knowledge, there is no

[7] Nonlinearity in figure 3–2 is defined as the percent deviation of the spectral emittance at 1.6μ from the spectral emittance calculated at 1.6μ for each curve by a linear interpolation between 1.2 and 2.0μ.

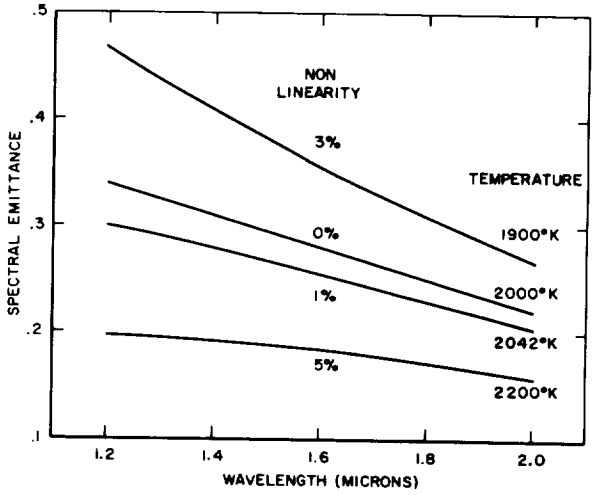

FIGURE 3–2.—Spectral emittance curves and temperatures for four radiation sources which have the same spectral radiance as a function of wavelength from 1.2 to 2.0 μ. A three-color pyrometer operating in this spectral region would indicate a temperature of 2000° K for each of these sources.

theoretical basis for the spectral emittance to be exactly linear. On the other hand when using an optical pyrometer, an error in the spectral emittance at 0.65μ and 2000° K of 1 to 5% would result in a temperature error of only 1.8° to 9°. As a result of the very demanding requirement on spectral emittance linearity, three-color pyrometers are not recommended for (radiation) temperature measurements. To the best of our knowledge, as of 1962, there are no three-color pyrometers available commercially.

Total-Radiation Pyrometers

Total radiation pyrometers are also not very suitable for accurate temperature measurements. Of course, knowledge of an effective emittance for a broad band of wavelengths is necessary, and this must be known more accurately than the spectral emittance for an optical pyrometer. As an example, the total radiance of a blackbody is proportional to the fourth power of temperature while the spectral radiance, say at 0.65μ and 2000° K is proportional to the eleventh power of temperature. In general, the broader the wavelength band of a radiation pyrometer, the greater the problems for determining accurate temperatures. In addition, many of the total-radiation pyrometers require larger targets than optical pyrometers. On the other hand, total-radiation pyrometers can be used to much lower temperatures (ref. 66) and are probably the least expensive radiation pyrometers which have an electrical output suitable for automatic control purposes. Thus they, as the two-color pyrometers, should be considered where control rather than a temperature determination is the primary objective. For those interested in total-radiation pyrometers, a recent book on this subject by Harrison (ref. 67) is recommended.

SUMMARY

Temperature measurements are normally made on the International Practical Temperature Scale and reported in degrees Celsius, i.e., ° C (Int. 1948) or in degrees Kelvin, i.e., ° K (Int. 1948). The latter temperatures are obtained by adding 273.15° to the IPTS Celsius values. Differences between the IPTS when reported in degrees Kelvin and the Thermodynamic Kelvin Temperature Scale above 900° K are usually less than errors in determining the temperature in practice on the IPTS.

Thermocouples are very reliable for making accurate temperature determinations up to at least 1300° C. The use of platinum vs platinum–10% and –13% rhodium thermocouples is recommended in this range when the ultimate in precision and accuracy is desired. From 1300° C to about 1800° C, thermocouples are less reliable due to calibration uncertainties and to increased effects of chemical contamination. In this range thermocouples with a platinum-rhodium alloy in both legs are recommended. Above 1800° C all the previously mentioned difficulties increase and in addition there are no completely satisfactory materials for protection and electrical insulation. Thus, in practice, accurate temperature determinations are very difficult. At present (1962) the more promising thermocouples for use above 1800° C are tungsten vs tungsten–26% rhenium and iridium vs rhodium–40% iridium.

For the determination of temperature of solids by radiation thermometry, an optical (single-color) pyrometer is recommended. For the most accurate temperature determinations a

blackbody and a number of observers (with a visual pyrometer) should be used. If a blackbody cannot be incorporated in the setup, the spectral emittance of the object at the mean effective wavelength of the pyrometer is required. Finally, the calibration of the optical pyrometer should be checked about every 200 hours of use. An infrequently used optical pyrometer or an infrequently used vacuum strip lamp is recommended for this check.

REFERENCES

1. Kostkowski, H. J.: The Accuracy and Precision of Measuring Temperatures Above 1000° K. Proc. of an Int. Sym. on High Temperature Technology, McGraw-Hill Book Co., Inc., 1959, p. 33.
2. Kostkowski, H. J.; and Lee, R. D.: Theory and Methods of Optical Pyrometry. Monograph 41, Nat. Bur. Standards, 1962.
3. Stimson, H. F.: Heat Units and Temperature Scales for Calorimetry. Am. Jour. Pys., vol. 23, 1955, p. 615.
4. Stimson, H. F.: International Practical Temperature Scale of 1948, Text revision of 1960. Monograph 37, Nat. Bur. Standards, 1961; The International Temperature Scale of 1948, Jour. Res., Nat. Bur. Standards, vol. 42, 1949, p. 209.
5. Zemansky, M. W.: Heat and Thermodynamics. McGraw-Hill Book Co., Inc., 1957.
6. Comptes Rendus de la Onizième Conférence Générale des Poides et Mesures, 1960, p. 1.
7. Moser, H.: Review of Recent Determinations of Thermodynamic Temperatures of Fixed Points Above 419° C. Temperature, Its Measurement and Control in Science and Industry (to be published by Reinhold Pub. Corp.).
8. Guildner, L. A.: A National Bureau of Standards Gas Thermometer. Temperature, Its Measurement and Control in Science and Industry (to be published by Reinhold Pub. Corp.).
9. Lee, R. D.: The NBS Photoelectric Pyrometer of 1961. Temperature, Its Measurement and Control in Science and Industry (to be published by Reinhold Pub. Corp.).
10. Middlehurst, J.; and Jones, T. P.: A Precision Photoelectric Optical Pyrometer. Temperature, Its Measurement and Control in Science and Industry (to be published by Reinhold Pub. Corp.).
11. Kandyba, V. V.; and Kovalevskii, V. A.: A Photoelectric Spectropyrometer of High Precision. Doklady Akad. Nauk (U.S.S.R.), vol. 108, 1956, p. 633.
12. Evans, J. P.; and Burns, G. W.: A Study of Stability of High Temperature Platinum Resistance Thermometers. Temperature, Its Measurement and Control in Science and Industry, vol. 3, pt. 1, Reinhold Pub. Corp., 1962, p. 313.
13. Roeser, W. F.: Thermoelectric Thermometry. Temperature, Its Measurement and Control in Science and Industry, Reinhold Pub. Corp., 1941.
14. Thomas, A. R.; Schurin, B.; and Morris, J. C.: Temperature Error Associated with Imbedded Thermocouples. Rev. Sci. Instr., vol. 29, 1958, p. 1045.
15. Pease, R. S.: The Measurement of Specimen Temperature in a High Temperature X-ray Powder Camera. Jour. Sci. Inst., vol. 32, 1955, p. 476.
16. Roeser, W. F.; and Lonberger, S. T.: Methods of Testing Thermocouples and Thermocouple Materials. Nat. Bur. Standards, Circular 590, 1958.
17. Finch, D. I.: General Principles of Thermoelectric Thermometry. Leeds and Northrup Co., Tech. Pub. ENS2(1), 1962, p. 1161.
18. Baker, H. D.; Ryder, E. A.; and Baker, N. H.: Temperature Measurement in Engineering. Vols. 1 and 2, John Wiley & Sons, Inc., 1961.
19. Dahl, A. I.: The Stability of Base Metal Thermocouples in Air From 800° to 2200° F. Temperature, Its Measurement and Control in Science and Industry Reinhold Pub. Corp., 1941.
20. Potts, J. F.; and McElroy, D. L.: Thermocouple Research to 1000° C.—Final Report November 1, 1957, through June 30, 1959. ORNL 2773, Oak Ridge Nat. Lab.
21. Sibley, F. S.: Effect of Environment on the Stability of Chromel-Alumel Thermocouples. High-Temperature Thermometry Seminar, Oak Ridge Nat. Lab., Oct. 1-2, 1959, TID 7586 (pt. 1), p. 16.
22. Accinno, D. J.; and Schneider, J. F.: Platinel—A Noble Metal Thermocouple To Replace Chromel-Alumel. Engelhard Industries, Inc., Tech. Bull., vol. 1, 1960, p. 53.
23. Ihnat, M. E.: A Jet Engine Thermocouple System for Measuring Temperatures up to 2300° F. WADC TR 57-744, Astia Doc. No. 203393.

24. Clark, R. B.; and Hagel, W. C.: High-Output Noble-Metal Thermocouples and Matching Lead Wire. High-Temperature Thermometry Seminar, Oak Ridge Nat. Lab., Oct. 1–2, 1959, TID 7586 (pt. 1), p. 37.
25. Caldwell, F. R.: Thermocouple Materials. Nat. Bur. Standards, Monograph 40, 1962.
26. Freeze, R. D.; Caldwell, F. R.; and Davis, E. R.: Reference Tables for the Palladium vs Platinum-15% Iridium Thermocouple. ASD-TDR-62-525.
27. Corruccini, R. J.: Annealing of Platinum for Thermometry. Jour. Res., Nat. Bur. Standards, vol. 47, RP 2232, 1951, p. 94.
28. Bennett, H. E.: The Contamination of Platinum Metal Thermocouples. Platinum Metals Rev., vol. 5, no. 4, 1961.
29. McQuillan, M. K.: Some Observations on the Behavior of Platinum/Platinum-Rhodium Thermocouples at High Temperatures. Jour. Sci. Instr., vol. 26, 1949, p. 329.
30. Mortlock, A. J.: Error in Temperature Measurement Due to the Interdiffusion at the Hot Junction of a Thermocouple. Jour. Sci. Instr., vol. 35, 1958, p. 283.
31. Darling, A. S.: Rhodium-Platinum Alloys. Platinum Metals Rev., vol. 5, no. 2, 1961.
32. Metcalfe, A. G.: The Use of Platinum Thermocouples in Vacuo at High Temperatures. Brit. Jour. Appl. Phys., vol. 1, 1950, p. 256.
33. Svec, H. J.: Behavior of Platinum/Platinum-Rhodium Thermocouples at High Temperatures. Jour. Sci. Instr., vol. 29, 1952, p. 100.
34. Jewell, R. C.; and Knowles, E. G.: Behavior of Platinum/Platinum-Rhodium Thermocouples at High Temperatures. Jour. Sci. Instr., vol. 28, 1951, p. 353.
35. Powell, A. R.: Behavoir of the Platinum Metals at High Temperatures. Platinum Metals Rev., vol. 2, no. 3, 1958.
36. A Symposium on the Contamination of Platinum Thermocouples. Jour. of the Iron and Steel Inst., vol. 155, 1947, p. 213.
37. Bennett, H. E.: The Care of Platinum Thermocouples. Platinum Metals Rev., vol. 2, No. 4, 1958.
38. Ehringer, H.: Über die lebensdauer von pt-rh termoelementen. Metall. 8, 1954, p. 596.
39. Jewell, R. C.; Knowles, E. G.; and Land, T.: High Temperature Thermocouple. Metal Ind. (London), vol. 87, 1955, p. 217.
40. Obrowski, W.; and Prinz, W.: Neu bestimmte grundwerte fürdie thermopaarkombination pt30%rh–pt6%rh. Archiv für das Eisenhuttenwesen, vol. 33, 1962, p. 1.
41. Heath, J. H.: High Temperature Thermocouples-part 1, Report to United Kingdom Atomic Energy Authority. AEEW-R 141, 1960.
42. Sanders, V. D.: Review of High Temperature Immersion Thermal Sensing Devices for In-Flight Engine Control. Rev. Sci. Instr., vol. 29, 1958, p. 917.
43. Lachman, J. C.: New Developments in Tungsten/Tungsten-Rhenium Thermocouples. Presented at the Instrument Society of America 16th National Conference, Los Angeles, California, Sept. 11, 1961.
44. Thomas, D. B.: A Furnace for Thermocouple Calibrations to 2200° C. Jour. Res., Nat. Bur. Standards, 66C, 1962, p. 255.
45. Kuether, F. W.; and Lachman, J. C.: How Reliable Are the Two New High-Temperature Thermocouples in Vacuum? ISA Jour., vol. 7, 1960, p. 66.
46. Sims, C. T.; Gaines, G. B.; and Jaffee, R. I.: Refractory-Metal Thermocouples Containing Rhenium. Rev. Sci. Instr., vol. 30, 1959, p. 112.
47. Lachman, J. C.; and Kuether, F. W.: Stability of Rhenium/Tungsten Thermocouples in Hydrogen Atmospheres. ISA Jour., vol. 7, 1960, p. 67.
48. Lachman, J. C.; and McGurty, J. A.: Thermocouples for 5000° F Using Rhenium Alloys. Presented at the Electrochemical Society on Rhenium, Chicago, May 4, 1960.
49. Nadler, M. R.; and Kempter, C. P.: Thermocouples for Use in Carbon Atmospheres. Rev. Sci. Instr., vol. 32, 1961, p. 43.
50. Blackburn, G. F.; and Caldwell, F. R.: Reference Tables for 40 Percent Iridium-60 Percent Rhodium Versus Iridium Thermocouples. Jour. Res., Nat. Bur. Standards, 66C, 1962, p. 1.
51. McGurty, J. A.; and Kuhlman, W. C.: Tungsten/Tungsten-Rhenium Thermocouple Research and Development. Presented at SAE National Aeronautic Meeting and Production Engineering Forum, New York, Apr. 6, 1962.
52. Worthing, A. G.: Temperature Radiation Emissivities and Emittances. Temperature, Its Measurement and Control in Science and Industry, Reinhold Pub. Corp., 1941, p. 1164.

53. GUBAREFF, G. G.; JANSSEN, J. E.; and TORBORG, R. H.: Thermal Radiation Properties Survey. Minneapolis-Honeywell Regulator Co., Minneapolis, 1960.
54. Temperature, Its Measurement and Control in Science and Industry. Vol. 3, Reinhold Pub. Corp., Parts 1 and 2, 1962. (Part 3 to be published.)
55. POLAND, D. E.; GREEN, J. W.; and MARGRAVE, J. L.: Corrected Optical Pyrometer Readings. Nat. Bur. Standards, Monograph 30, 1961.
56. DEVOS, J. C.: Evaluation of the Quality of a Blackbody. Physica, vol. 20, 1954, p. 669.
57. VOLLMER, J.: Study of the Effective Thermal Emittance of Cylindrical Cavities. Jour. Opt. Soc. Am., vol. 47, 1957, p. 926.
58. GOUFFÉ, A.: Corrections d'ouverture des corps-noirs artificiels compte tunu des diffusions multiples internes. Revue d'optique, vol. 24, 1945, p. 1.
59. BARBER, C. R.: Factors Affecting the Reproducibility of Brightness of Tungsten Strip Lamps for Pyrometer Standardization. Jour. Sci. Instr., vol. 23, 1946, p. 238.
60. LOVEJOY, D. R.: Accuracy of Optical Pyrometry in the Range 800° C to 4000° C. Canadian Jour. Phys., vol. 36, 1958, p. 1397.
61. MACPHERSON, H. G.: The Carbon Arcs as a Radiation Standard. Temperature, Its Measurement and Control in Science and Industry, Reinhold Pub. Corp., 1941, p. 1141.
62. NULL, M. R.; and LOZIER, W. W.: The Carbon Arc as a Radiation Standard. Temperature, Its Measurement and Control in Science and Industry (to be published by Reinhold Pub. Corp.).
63. PYATT, E. C.: Some Consideration of the Errors of Brightness and Two Color Types of Spectral Radiation Pyrometer. Brit. Jour. Appl. Phys., vol. 5, 1954, p. 264.
64. BRENDEN, B. B.; and NEWKIRK, H. W.: A Multicolor Pyrometer. AEC Res. and Dev. Rep. HW-57162, Rev. Office of Tech. Ser., Dept. of Commerce, Washington 25, D.C., 1958.
65. HORNBECK, G. A.: A High-Speed Ratio Pyrometer. Temperature, Its Measurement and Control in Science and Industry, vol. 3, pt. 2, Reinhold Pub. Corp., 1962.
66. MAGISON, E. C.; and MELLENTIN, K.: The Thermopile in Industrial Radiation Pyrometry. Temperature, Its Measurement and Control in Science and Industry, vol. 3, pt. 2, Reinhold Pub. Corp., 1962.
67. HARRISON, T. R.: Radiation Pyrometry and Its Underlying Principles of Radiant Heat Transfer. John Wiley & Sons, Inc., 1960.

DISCUSSION

QUESTION: Do you know if any work is being done on the determination of fixed points above 1500° C?

KOSTKOWSKI: A considerable amount of such work was done many years ago and can be found in the literature. I am not aware of any recent publications in this field, though I understand that work on such fixed points is being planned in Dr. Franklin's Division at National Bureau of Standards. In addition, I would like to emphasize that a calibrated tungsten strip lamp can be used as an accurate reproducible fixed point of spectral radiance at 0.65 micron from 800 ° to 2300 ° C. Similarly, the positive crater of an arc with pure graphite electrodes, which is now available commercially, can be used as such a fixed point at 3527 ° C.

SESSION II

MEASUREMENTS AT LOW TEMPERATURES (0° TO 200° K)

Chairman: DR. ROBERT J. CORRUCCINI

4—THERMAL RADIATION PROPERTIES OF SOLIDS AT LOW TEMPERATURES

BY ROBERT J. CORRUCCINI

NATIONAL BUREAU OF STANDARDS, BOULDER, COLORADO

This paper provides introductory remarks for the symposium session on thermal radiation properties of solids in the range 0°–200° K. A qualitative description is given of that part of the theory that is unique to low temperatures, after which experimental methods appropriate to low temperatures and present applications of low temperature data are sketched.

This subject has its origins in the invention of the Dewar vessel before the turn of the century. The importance of the silvering in minimizing the exchange of radiant heat across the vacuum barrier was fully appreciated, and the comparative merits of various reflective coatings were known at an early date.

A theory of the reflective behavior of metals existed from almost the same period. This was the free-electron theory of Drude, according to which the electron fluid is accelerated by the electric field of the radiation with negligible phase lag and is damped by collisions with the lattice. At long wavelengths, i.e. such that the frequency of the radiation is much less than the mean collision rate of an electron in the metal, the familiar Hagen-Rubens formula results (ref. 1),

$$A=1-R=2(\nu/\sigma_0{}^{1/2})$$

in which σ_0 is the d-c electrical conductivity in esu, and A and R are the normal spectral absorptivity and reflectivity, respectively, at frequency ν. This formula ought to apply in the far infrared, the wavelength region occupied by thermal radiation from sources well below ambient temperature.

It also became known in some of the earliest experiments performed at the temperatures of liquid hydrogen (20° K) and helium (4° K) that the electrical conductivities of some metals increase by as much as two decades over the room temperature values. (This increase has since been pushed to as much as four decades with modern metal purification techniques.) The fact that the Hagen-Rubens relation predicts corresponding large decreases in the absorptivity at these low temperatures does not seem to have excited much interest in this early period.

Modern interest may be said to have originated with an observation by H. London (ref. 2) in 1940 that the microwave resistivity of tin at low temperatures was much higher than the d-c resistivity. London attributed this to the mean free path of the conduction electrons becoming large at low temperatures compared to the depth of penetration of the electromagnetic wave. As a consequence, the microwave absorption is determined mainly by the scattering of the electrons by the surface of the metal rather than in the body of the metal, i.e., the bulk resistivity no longer controls the absorptivity. This was the first recognition of the anomalous skin effect, a uniquely low temperature phenomenon. It was subsequently explored at microwave frequencies by Pippard and by Chambers (ref. 3) and in the infrared by Ramanathan (ref. 4) and Biondi (ref. 5). In this same period a theory was developed and refined (ref. 6 to 10). The magnitude of the

effect may be illustrated by pointing out that, whereas for a high-purity copper having a conductivity near absolute zero one thousand times as great as its conductivity at room temperature, the classical absorptivity at a wavelength of a few microns is of the order of 10^{-5}, the value calculated from anomalous skin effect theory and the best experimental results are both several hundred times greater.[1]

The theory of the anomalous skin effect contains a parameter to take into account the nature of the reflection of electrons at the surface, i.e. whether specular, diffuse, or intermediate. Comparison with experiment has overwhelmingly favored the assumption of diffuse reflection of electrons, and Pippard has commented (ref. 15) "The assumption of specular reflection of electrons . . . is indeed theoretically improbable, for irregularities on an atomic scale are sufficient to cause large-angle diffraction of the de Broglie waves". Nevertheless a recent experiment of a new kind by Rayne (ref. 16) has suggested the opposite conclusion and has injected new uncertainty into this question.

The theory has been extended by Holstein to include the effects of electron scattering by a phonon-generating process (ref. 17) and by Motulevich, Gurzhi, and others to include electron-electron scattering (ref. 18). Also we may note that optical absorption at low temperatures is a useful tool for investigating electronic band structure in metals and alloys (ref. 19).

The above theoretical developments have provided a stimulus to experimentation which has been supplemented in the past decade by the rapid growth of cryogenic technology and particularly by the advent of large-scale uses of liquid hydrogen. Hydrogen has a low heat of vaporization. Consequently if the liquid is to be retained, the use of highly efficient thermal insulation is indicated. The first large vessels for liquid hydrogen were metallic Dewars with intermediate radiation shields cooled by liquid nitrogen. The total hemispherical absorptances of many technical surfaces for room temperature radiation were measured in order to provide data for the engineering of such vessels (ref. 20 to 23). Most of these measurements were made at the boiling point of nitrogen (78° K) because of experimental difficulties in working at the boiling point of hydrogen.

With the more recent development of improved bulk insulations, the low temperature radiation properties declined in interest for a time, but now with the growth of space technology come new problems which again involve them, for example, the possible use in space of uninsulated tanks for liquid oxygen or hydrogen, radiative heat balance of vehicles in the cold, outer reaches of the solar system, and radiation absorptances of the condensing surfaces of cryopumps.

Let me now indicate the measurement techniques that have been used at low temperatures.

The most complete description of the optical properties in terms of classical electromagnetic theory is obtained by determining the refractive index and the extinction coefficient as a function of frequency and temperature. (The normal reflectivity and absorptivity can be readily calculated from these parameters but the reverse is not true.) These quantities can be calculated from the changes on reflection of the amplitudes and phase of radiation components for which the electric vector is parallel and perpendicular, respectively, to the plane of incidence (ref. 1). Various low temperature measurements of this kind have been described (ref. 24 to 27).

For studies of the anomalous skin effect or of electronic band structure direct measurement of normal spectral absorptivity is sufficient. A calorimetric technique is used in which the temperature rise of the specimen is measured by a sensitive thermometer (ref. 4, 5, and 16). The power absorption is determined by reestablishing the same temperature rise by a calibrated electric heater in the absence of radiation. Almost all measurements of this or the preceding kind have been made at wavelengths shorter than 15μ.

Radiative heat transfer across the vacuum barrier of a Dewar depends upon the total

[1] We may note in passing that the optical and near-infrared absorption by a superconductor is indistinguishable experimentally from that of the same metal in the normal state at the same temperature (refs. 4 and 11 to 13) inasmuch as the energies of the incident photons greatly exceed the energy gap between the superconducting and normal states (ref. 14).

hemispherical emittance of each surface and its absorptance for the spectrum of radiation being received from the other. In cryogenic applications the temperature difference between the two surfaces is usually large, and hence, only the emittance of the warmer surface and the absorptance of the colder surface are important. The latter is readily measured calorimetrically in an apparatus simulating a Dewar in which nonradiative heat transfer has been made negligible by careful design and in which the warmer surface (the enclosing one) is either black, or very large, or both black and large (ref. 20 to 22). From volumetric measurement of the rate of evaporation of the cryogenic liquid in the Dewar and knowledge of the heat of vaporization and the area, the desired absorptance can be calculated. Such absorptances have often been loosely referred to as emissivities. In order to compute them from the experimental data for nonplanar configurations it is necessary to know whether the reflections of the radiation are specular or diffuse. In general, this is not known; the assumption made depends on the author's taste, and consequently the results are to some extent arbitrary. Unfortunately, measurements of this type which yield total hemispherical properties at a fixed temperature are of little interpretive value.

Few measurements have been made of emittances of surfaces at cryogenic temperatures and most of the absorptance measurements have been made with room temperature radiation, 75% of the energy of which is at wavelengths shorter than 20 microns. (Weber has proposed a spectrophotometric technique for measuring the infrared spectral emittance at low temperatures in references 28 and 29 but apparently did not put it to experimental test. A calorimetric method for total emittance is described by R. P. Caren in paper 6.) Thus, little is known of the behavior at longer wavelengths. A remarkable exception is a measurement by Hulburt and Jones (ref. 30) of the (approximately) normal absorptance of a graphite coating at 3.7° K for radiation from a source at 9° to 17° K. A superconducting bolometer having a sensitivity of 3×10^{-12} watt was used. For such radiation, lying mostly at wavelengths between 0.1 and 1 mm, the absorptance of the carbon was only 2 to 4%.

Finally, there may be mentioned direct measurement of the parameter α_s/ϵ that determines the rediative heat balance and hence the temperatures of objects exposed to solar radiation in space. Here α_s is the normal absorptance for solar radiation and ϵ is the total hemispherical emittance of the surface at its own equilibrium temperature. Measurement of the equilibrium temperature of a sample surface which is exposed to an appropriate flux from an arc source while itself radiating thermally to a cryogenic sink suffices to determine this ratio (ref. 31). Such an experiment, if carried out at cryogenic temperatures, would simulate the radiative heat balance of an object in space beyond the orbit of Mars, since it is only at such distances from the sun that cryogenic surface temperatures are possible for an unshaded object.

In all of the foregoing experimental techniques the condition of the surface is an extremely important parameter. While it is obvious enough that metallic surfaces for optical experiments should be clean, it has not always been appreciated that mechanical polishing of a metal to achieve a visually bright surface may cold-work and hence increase the resistivity of a thin but critically important surface layer. In order to realize the characteristics of the bulk metal and to achieve minimum absorptivity in the infrared, such distorted surface material must be removed by nonmechanical methods such as etching or electropolishing.

What experimental difficulties in the foregoing methods are unique to cryogenic temperatures? Two kinds come to mind: (1) Low emissivity surfaces may become fouled by condensation of vapors such as water, outgassed from warm regions of the apparatus. At the lowest temperatures even desorbed air or hydrogen outgassed from metals may cause such fouling. Maintenance of a clean system and a high vacuum (say 10^{-6} mm Hg or better) is necessary to prevent this. (2) In calorimetric methods, extraneous heat leaks via supporting members, thermocouple wires, residual gas, etc. must be made small relative to the radiation heat transfer to be measured. This is more difficult at cryogenic temperatures

than elsewhere because, while the thermal conductivities of alloys, plastics, glassy materials, and gases all decrease as the temperature decreases (ref. 32 and 33), thermal radiation decreases much more rapidly. In fact, the thermal conductivities of pure metals *increase* with decreasing temperature until they reach maxima at various low temperatures (ref. 33). Thus, for example, it is especially difficult to suppress heat conduction if there are electrical leads or thermocouple wires of copper. More detailed consideration of problems of this kind can be found in recent books on experimental techniques at cryogenic temperatures (ref. 32–35).

While we have been concerned up to this point with surface properties, it is worth noting that the infrared transmission of certain nonmetallic powders and fibers used in cryogenic bulk insulations is of considerable practical importance inasmuch as a substantial portion of the heat transfer through such materials is by means of thermal radiation. Examples of such materials are silica aerogel, perlite, and glass fiber. Analysis of the transmission of radiation is complicated by its dependence on particle or fiber size. This subject has been reviewed in detail by Cline and Kropschot (ref. 36).

In the areas of research that have been described, our present knowledge is confined mainly to the visible and near infrared regions out to 10 or 15 μ. The far infrared has been avoided for various reasons such as experimental difficulty, the relative insignificance in most practical situations of radiative heat transfer in this region, and the assumption from classical theory that the reflectivities of metals are devoid of unusual features in this region. Nevertheless, the mere fact that it represents a relatively unknown realm should attract a few hardy explorers. It is to be hoped that they will be rewarded with some interesting discoveries.

REFERENCES

1. Givens, M. P.: Optical Properties of Metals. Solid State Phys., vol. 6, 1958, pp. 313–352.
2. London, H.: The High-Frequency Resistance of Super Conducting Tin. Proc. Roy. Soc., vol. 176, Nov. 1940, pp. 522–533.
3. Pippard, A. B.: Metallic Conduction at High Frequencies and Low Temperatures. Advances in Electronics and Electron Physics, 6, Academic Press, 1954, pp. 1–45.
4. Ramanathan, K. G.: Infra-Red Absorption by Metals at Low Temperatures. Proc. Phys. Soc., vol. 65 no. 390A, July 1952, pp. 533–540.
5. Biondi, M. A.: Optical Absorption of Copper and Silver at 4.2° K. Phys. Rev., vol. 102, no. 4, May 1956, pp. 964–965.
6. Reuter, G. E. H.; and Sondheimer, E. H.: The Theory of the Anomalous Skin Effect in Metals. Proc. Roy. Soc. vol. 195, no. 1042, Dec. 1948, pp. 336–364.
7. Holstein, T.: Optical and Infrared Reflectivity of Metals at Low Temperatures. Phys. Rev., vol. 88, no. 6, Dec. 1952, pp. 1427–1428.
8. Dingle, R. B.: The Anomalous Skin Effect and the Reflectivity of Metals, Part I. Physica, vol. 19, no. 4, Apr. 1952, pp. 311–347; Part II. Comparison Between Theoretical and Experimental Optical Properties. Physica, vol. 19, no. 4, Apr. 1953, pp. 348–364; Part III. General Theory of Low Frequency and Optical Behavior. Physica, vol. 19, no. 8, Aug. 1953, pp. 729–736; Part IV. Theoretical Optical Properties of Thin Metallic Films. Physica, vol. 19, no. 12, Dec. 1953, pp. 1187–1199.
9. Wolfe, R.: Theory of the Reflectivity of Metals. Pt. 2, vol. 68, no. 422A, Feb. 1955, pp. 121–127.
10. Collins, J. G.: The Theory of the Anomalous Skin Effect in Metals for Obliquely Incident Radiation. Appl. Sci. Res., Sect. B, vol. 7, no. 1, 1958, pp. 1–40.
11. Daunt, J. G.; Keeley, T. C.; and Mendelssohn, K.: Adsorption of Infra-Red Light in Supraconductors. Phil. Mag., vol. 23, Feb. 1957, pp. 264–271.
12. Hirschlaff, E.: The Optical Reflectivity of Metals in the Supraconducting State. Proc. Camb. Phil. Soc. (London), vol. 33, pt. 1, 1937, pp. 140–144.
13. McCrum, N. G.; and Shiffman, C. A.: The Optical Constants of Tin Below the Superconducting Transition Temperature. Proc. Phys. Soc. (London), 67, pt. 4, no. 412A, Apr. 1954, pp. 386–388.

14. Biondi, M. A.; Forrester, A. T.; Garfunkel, M. P.; and Satterwaite, C. B.: Experimental Evidence for an Energy Gap in Superconductors. Rev. Mod. Phys., vol. 30, no. 4, Oct. 1958, pp. 1109–1136.
15. Pippard, A. B.: Experimental Analysis of Electronic Structure of Metals. Reports on Progress in Physics, vol. 23, 1960, pp. 176–266.
16. Rayne, J. A.: Temperature Dependence of the Absorptivity of Copper in the Near Infrared. Phys. Rev. Let., vol. 3, no. 11, Dec. 1959, pp. 512–514. For a different experiment suggesting the same conclusion see Cline, D.: Infrared Wavelength Dependence of the Total Absorptivity of Electroplated Silver. J. Appl. Phys., vol. 33, no. 7, July 1962, pp. 2310–2311.
17. Holstein, T.: Optical and Infrared Volume Absorptivity of Metals. Phys. Rev., vol. 96, no. 2, Oct. 1954, pp. 535–536.
18. Motulevich, G. P.: On the Connection Between the Optical Constants of Metals and Their Microscopic Characteristics. Soviet Phys. JETP, vol. 37(10), no. 6, June 1960, pp. 1249–1251.
19. Rayne, J. A.: Optical Properties of Metals. The Fermi Surface, W. A. Harrison and M. B. Webb, eds., John Wiley & Sons, Inc., 1960, pp. 266–278.
20. Zimmerman, F. J.: Total Emissivities and Absorptivities of Some Commercial Surfaces at Room and Liquid-Nitrogen Temperatures. J. Appl. Phys., vol. 26, no. 12, Dec. 1955, pp. 1483–1488.
21. Ziegler, W. T.; and Cheung, H.: Advances in Cryogenic Engineering. Plenum Press, 1956, p. 100.
22. Fulk, M. M.; and Reynolds, M. M.: Emissivities of Metallic Surfaces at 76° K. J. Appl. Phys., vol. 28, no. 12, 1957, pp. 1464–1467.
23. Scott, R. B.: Cryogenic Engineering. D. van Nostrand Co., Inc., 1959, pp. 147–153, 346–348.
24. Roberts, S.: Optical Properties of Nickel and Tungsten and Their Interpretation According to Drude's Formula. Phys. Rev., vol. 114, no. 1, Apr. 1959, pp. 104–115.
25. Alekseevskii, N. E.; and Potapov, E. V.: Calorimetric Method of Determining the Optical Constants of Metals in the Infrared Region at Low Temperatures. Soviet Physics, JETP, vol. 6, no. 1, Jan. 1958, pp. 220–222.
26. Shklyarevskii, I. N.; Avdeenko, A. A.; and Padalka, V. D.: Measurements of the Optical Constants of Antimony in the Infrared Region of the Spectrum at Temperature of 290° and 110° K. Optics and Spectroscopy, vol. 6, no. 4, Apr. 1959, pp. 336–338.
27. Padalka, V. G.; and Shklyarevskii, I. N.: A Method for Making Low-Temperature Measurements of the Optical Constants of Metals. Optics and Spectroscopy, vol. 9, no. 1, July 1960, pp. 63–64.
28. Weber, D.: Spectral Emissivity of Solids in the Infrared at Low Temperatures. Jour. Optical Soc. America, vol. 49, no. 8, Aug. 1959, pp. 815–820.
29. Hulbert, J. A.; and Jones, G. O.: The Superconducting Bolometer as a Detector of Thermal Radiation from Low-Temperature Sources. Phys. Soc. London Proc., vol. 68, pt. 11, no. 431B, Nov. 1955, pp. 801–804.
30. Gordon, G. D.: Measurement of Ratio of Absorptivity of Sunlight to Thermal Emissivity. Rev. Sci. Instr., vol. 31, no. 11, Nov. 1960, pp. 1204–1208.
31. Scott, R. B.: op. cit. Chaps. IX and X.
32. Powell, R. L.; and Blanpied, W. A.: Thermal Conductivity of Metals and Alloys at Low Temperatures, NBS Circular 556, 1954.
33. White, G. K.: Experimental Techniques in Low-Temperature Physics. Oxford, 1959.
34. Hoare, F. E.; Jackson, L. C.; and Kurti, N., eds.: Experimental Cryophysics, Butterworths, London, 1961.
35. Cline, D.; and Kropschot, R. H.: The Thermal Properties of Powder Insulators in the Temperature Range 300°–4° K in Radiative Transfer from Solid Materials, H. H. Blau and H. Fischer, eds., MacMillan Co., 1959.

5—SPACE CHAMBER EMITTANCE MEASUREMENTS

BY C. P. BUTLER AND R. J. JENKINS

U.S. NAVAL RADIOLOGICAL DEFENSE LABORATORY, SAN FRANCISCO, CALIFORNIA

A method for evaluating the total effective emittance of an evacuated space chamber, without recourse to optical techniques, is described. The chamber emittance can be evaluated from the temperature decay and heat capacity of a blackened disk of pure metal suspended by fine wires in the center of a hollow walled chamber cooled by liquid nitrogen. Shutters admit a beam of radiant energy from an image furnace to heat the disc. Experimental results are given for a black space chamber in which materials may be tested from +200° C to −140° C.

Considerable attention is being focused on the simulation of conditions in outer space by means of temperature-controlled, evacuated chambers. The objective of these designs is to provide means for measuring the behavior of spacecraft materials under the conditions encountered outside the earth's atmosphere.

One of the most important considerations in simulating the space environment is the problem associated with the thermal balance between the object and the walls of the chamber. Since the pressures are kept very low, the sole method of heat transfer is by thermal radiation. In space within the solar system, the respective wavelengths at which this energy is absorbed and reradiated vary widely. The wavelength of maximum radiation at 300° K, for example, is approximately 20 times that of the sun. Chamber walls must be at very low temperatures and have an emittance of 1.0 from at least 0.3 to 100 microns to simulate the thermal radiation environment in space. Over this wavelength range, very little is known about black coatings which can be applied to metal surfaces.

Engineering practices have reached a stage where large chambers can be maintained at the low pressures and temperatures corresponding to conditions well above the earth's atmosphere. Less well known is how to simulate the emittance of space on the inner surface of the chambers. While paints and metal dyes are available which appear black, there remains the question of the effective chamber emittance at low temperatures, e.g., when surrounded with liquid nitrogen. If the wall of a space chamber is really black at 77° K, and test specimens are cooled to near this temperature, appreciable energy transfer takes place at wavelengths of 100 microns or more, well beyond the range of conventional spectrometers. Estimates of emittance based on measurements at shorter wavelengths are always open to question.

Since the reflectance of space is zero, any departure from a perfectly black-walled chamber introduces reflections which are difficult to assess, especially when low-temperature optical properties are required.

Three conditions for optimizing the effective emittance of a space chamber are: first, to make the chamber large in comparison to the size of the object under test; second, to incorporate geometrical wall forms to increase the number of reflections; and, third, to coat the inner walls of the chamber with a high emittance material. These three conditions taken together determine the effective emittance of the chamber. This paper describes how the emittance of a space simulating chamber such as this can be measured without recourse to conventional optical techniques. The method

692-146 O—63——4

shows that the emittance of the chamber as a whole can be found from the temperature decay and heat capacity of a pure metal.

THEORY

For the measurement of the total hemispherical emittance of materials, consider an evacuated space simulating chamber with walls at a uniform temperature T_c, and a specimen at a temperature $T_s (T_s < T_c)$ suspended by fine thermocouple wires near the center of the chamber. If the thermal conductivity of the specimen is high enough so that there is no internal temperature gradient and if the thermal conductance of the residual gases and of the thermocouple wires is negligible, then the rate of temperature decay $\dot{T}$ is given by

$$\dot{T} = \frac{\epsilon^* A\sigma(T_s^4 - T_c^4)}{mc} \tag{1}$$

where A is the total radiating area of the specimen, σ the Stefan Boltzmann constant, m the mass of the specimen, c its specific heat capacity at T_s, and ϵ^* is the measured effective emittance of the specimen.

ϵ^* is a complicated function of the actual emittance of the sample surface, ϵ_s, and of the effective emittance of the chamber, ϵ_c, where ϵ_c includes the effect of the chamber geometry as well as the emittance of each increment of wall surface. Then ϵ^* is

$$\epsilon^* = f(\epsilon_s, \epsilon_c) \tag{2}$$

This function must include the changes in the spectral emittance and reflectance of the sample as it cools and is only solvable exactly in the special case where $\epsilon_c = 1$ and T_c^4 is negligible with respect to T_s^4.

From the definition of emittance, namely the ratio of the energy radiated from the surface to that radiated from a Planckian blackbody at the same temperature, it follows that if ϵ^* is measured and found to be 1.0, $f(\epsilon_c, \epsilon_s)$ must be of such a form that $\epsilon_c = \epsilon_s = 1.0$. Furthermore, if ϵ^* is found to be less than 1.0, then, at least for grey bodies, ϵ_c and $\epsilon_s > \epsilon^*$. In the latter case, only minimum values can be given for ϵ_s and ϵ_c.

Experimentally, then, if a black specimen is suspended in a chamber with walls at a temperature lower than that of the specimen and ϵ^* is calculated to be 1.0, from the measured parameters,

$$\epsilon^* = \frac{\dot{T}mc}{A\sigma(T_s^4 - T_c^4)} \tag{3}$$

then the chamber is optically black to specimens at this temperature and may be used to simulate space. If ϵ^* is not equal to 1.0, the chamber may or may not be black, and further considerations are necessary.

Consider a chamber which has an effective number of internal reflections (N) before the energy is reflected back to the specimen and whose walls have a particular hemispherical emittance ϵ_w. To the approximation that the walls can be considered grey, i.e., that the emittance is independent of the wavelength, the fraction of the radiated energy reflected back upon the specimen in such a chamber is $(1-\epsilon_w)^N$ and the effective emittance of the chamber is then $1-(1-\epsilon_w)^N$. Consider a specimen with a surface identical to the wall surface suspended in the chamber so that $e_s = \epsilon_w$ and $T_s^4 \gg T_c^4$.

Since ϵ^* is a minimum value for ϵ_s and ϵ_c, it is clear that

$$\epsilon_c \geqq 1-(1-\epsilon^*)^N \tag{4}$$

If the chamber is large compared to the dimensions of the specimen, it is not difficult to make N equal to at least 3 for example. If the measured value of ϵ^* can be made as high as 0.90, then $\epsilon_c = 1-(1-0.9)^3 = 0.999$. The emittance of the chamber is proven equal to that of a space environment and $\epsilon_\Lambda = \epsilon^*$.

EXPERIMENTAL DESIGN

A schematic drawing of the space simulating chamber designed for this work is shown in Figure 5-1.

A disk of pure metal, about 2 cm in diameter and 1 mm thick, is suspended in a chamber, one end of which terminates in a cone while the other is closed by a shutter whose inner face is grooved. The disk is blackened after the thermocouple wires, each 0.005 inch in diameter, are peened into 6-mil holes drilled in the edge of the disk. These wires pass out through three insulated holes in the chamber to spring-loaded clips which facilitate centering the disk in the center of the chamber.

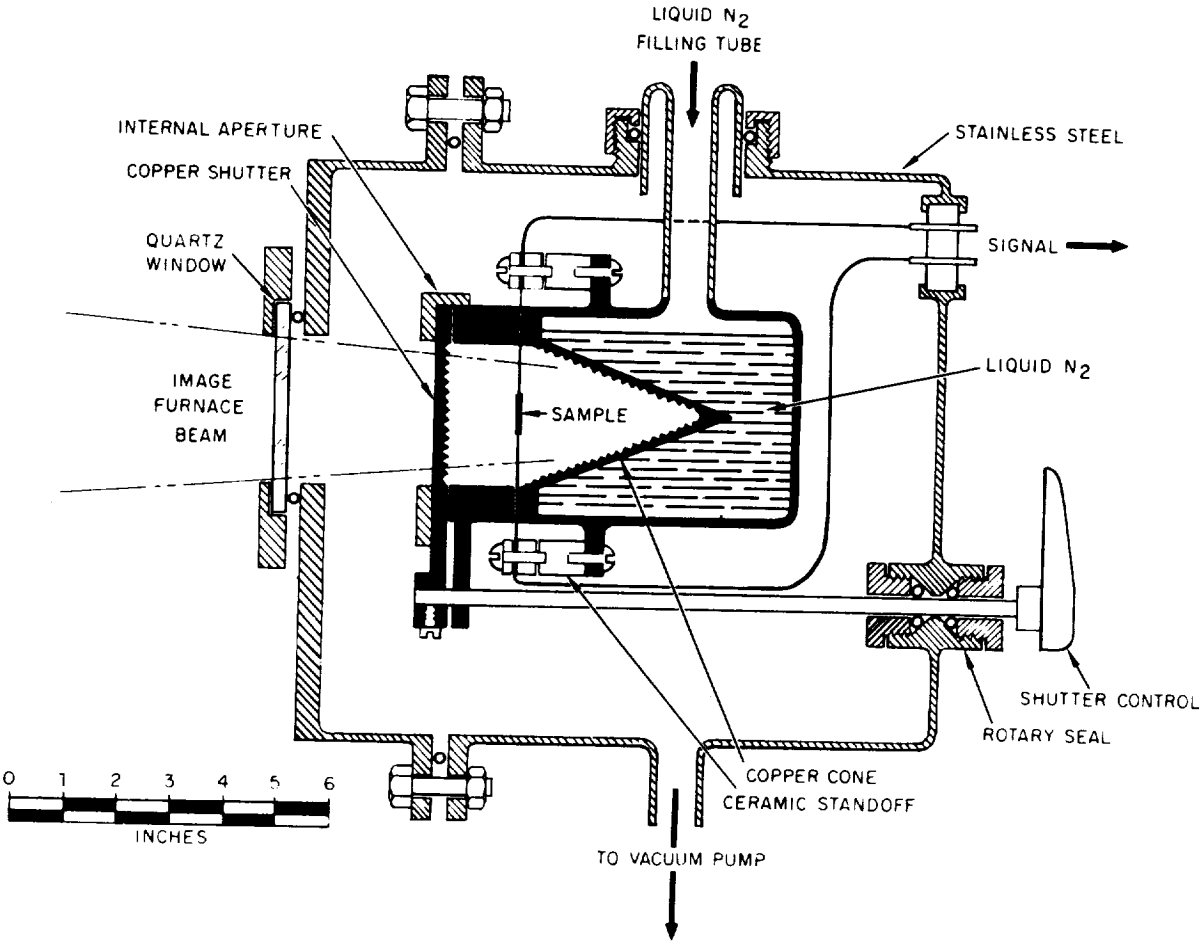

FIGURE 5–1.—Schematic drawing of the space simulating chamber.

Because of the experimental difficulties involved, the chamber and the disk were not coated with the same material. Platinum black was used for the disk, because it was believed to be black over a wide wavelength range, its mass is negligible in relation to the mass of the disk, and it can be readily formed on small disks of copper and silver. It is considerably more difficult to form on large irregular surfaces, so that the inner walls of the chamber were coated with Parson's black lacquer. Each layer of lacquer was baked in air at 160° C for several hours before assembly.

The chamber is cooled by liquid nitrogen added through a stainless steel filling tube held in the outer chamber by an O-ring seal. Both the chamber and the shutter are made from oxygen-free high-conductivity copper for uniformity of the wall temperature. Not shown in the diagram is a covered channel of copper into which the shutter fits when closed so that it will be at the same temperature as the rest of the chamber. A thermocouple is attached to the shutter so that its temperature can be monitored during the runs. It was found to be at the wall temperature, even when the temperature of the radiating disk was as high as 500° K. The outside of the walls of the chamber and the outside of the shutter were polished bright, i.e., to give a low emittance, so that minimum heat transfer occurs to the outer chamber. For the same reason stainless steel was used for the filling tube to minimize heat transfer to the nitrogen. In practice, it was found that the nitrogen consumption was less than ½ liter an hour after

the inner chamber was cooled. The outer chamber remains at ambient temperature.

The specimen is heated by the radiation from an arc image furnace. The furnace is a Brankert projector, employing a 9-mm positive and an 8-mm negative copper-coated cored carbon to form a "blown" arc. The arc operates at 70 amperes and 40 volts. This is an arc whose tail flame is spread more or less uniformly back onto the crater of the positive carbon crater by means of a strong magnetic field. A copper aperature, 4 inches in diameter was made to cover the outer portion of the elliptical mirror, thus providing an irradiance of 0.90 cal cm^{-2} sec^{-1}, which was sufficient to heat any specimen so far tested to 500° K. Stopping the aperture has the further advantage of increasing the f/ratio to 8, which is much easier to handle than lower values.

The arc radiation is admitted to the first chamber through a quartz window and to the second chamber by opening the copper shutter manually through a vacuum flange fitting in the outer chamber. There is no window in the inner chamber. When the temperature of the specimen has reached a given level, the arc radiation is cut off by a shutter not shown on the drawing, then the inner copper shutter is closed, and the disk allowed to cool.

The temperature of the disk is measured by a pre-amplifier digital voltmeter combination (Hewlett-Packard 412A preamplifier, 425CR digital voltmeter) with an overall accuracy measured to be better than 1%. Readings are printed out on a digital printer at intervals selected by the digital counter controller acting as a digital clock. The line frequency was used as a standard, and the timing error is completely negligible over the long time intervals used. The slope of the temperature-time change curve is obtained by subtracting the temperature at one time from that at an earlier time. Since the subtraction of two nearly equal numbers is an inherently inaccurate process, it is necessary to use time intervals as long as several hundred seconds at the lower temperature ranges to obtain acceptably accurate slopes. Several readings of slope are taken at each temperature to reduce the error of ± 1 in the last place common to all digital voltmeters.

RESULTS

The results obtained by recording cooling curves on platinum blacked disks of copper and silver are shown in figure 5–2. The variations around the value of 1.00 are believed due to experimental deviations in the temperature decay curves.

After is was shown that the chamber was black, a copper disk was coated with Parson's black and its emittance measured. It was

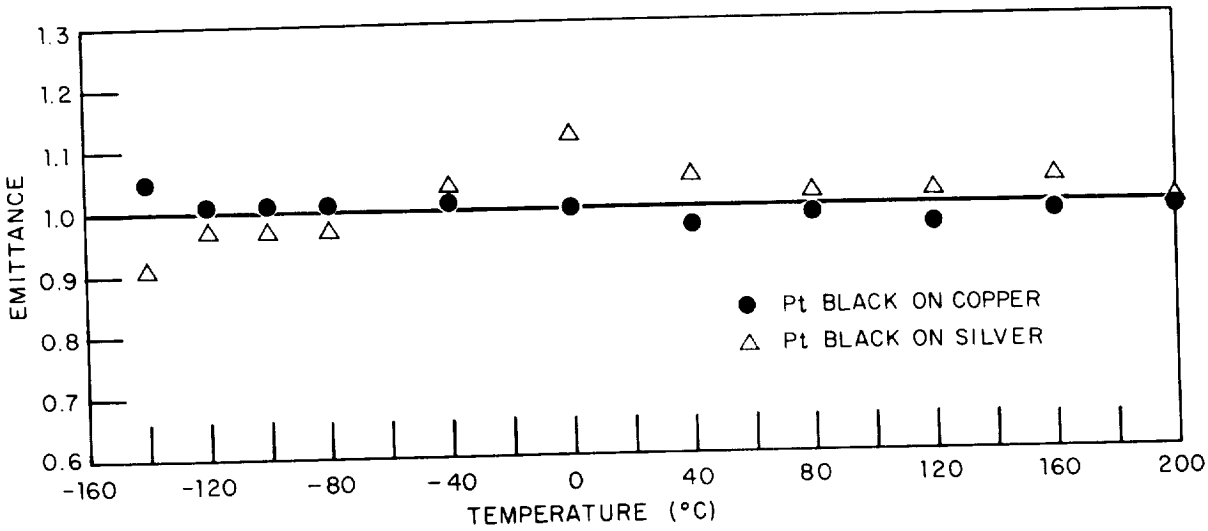

FIGURE 5–2.—Data obtained on platinum blacked disks of copper and silver.

found to be less than 0.90. Since the data shown in figure 5–2 proves that ϵ_c for this chamber is 1.0, then there must be several internal reflections in the chamber, so that ϵ_c by equation (4) is again 1.0. This confirms the original design considerations for achieving a black chamber.

It was also shown that platinum black is black to at least −140° C.

CONCLUSIONS

The techniques reported here are capable of demonstrating that a chamber is optically black over a wide temperature range without recourse to optical measurements. The same techniques can be used on any space-simulating chamber, although care must be used when extrapolations to chambers of other shapes and sizes are made.

DISCUSSION

ZISSIS, Institute for Defense Analyses: It seems that if you are using the multiple reflection method in the chamber to give a high emissivity, instead of Parson's black, you might want to use a black paint whose reflectance would be specular. Parson's black is rather diffuse even for the little bit of reflectance it has. There is a paint, Sicon black, which is an enamel that has a measured emissivity of about 0.93 and the 6 or 7% reflectance is highly specular. If this is really a major contributor to giving you the emissivity of one then this should help you attain it even more precisely.

BUTLER: Thank you, I did not know about that paint.

GORDON, Radio Corporation of America: I would like to know how you measure the intensity of the solar flux on the sample? How do you know it is 1 calorie?

BUTLER: How do we know the beam irradiance or the solar flux? The standard receivers for measuring the irradiance of the arc are either gold or silver disks coated with platinum black. The use of two standards with different decay rates provides a double check. We rely on the published values of specific heat as a function of temperature for these standards. I don't think I need to go through the equation; you understand that. The whole question is, can you make a piece of polished metal optically black over a wide wavelength range. I hope you recognize that the data we are reporting peaks at approximately 15 microns. We are confident that platinum black is indeed black to well beyond this wavelength, including the visible spectrum.

LEIGH, AVCO: I see that you are the first author to mention the fact that we need to know the specific heat as a function of temperature in the heat exchange equation. Some of the previous papers seem to regard this as a constant, and this may not be universally true, especially at very low temperatures. I wonder if you would give us your comments on this fact.

BUTLER: Yes, I am glad you asked that question. We get the specific heat as a function of temperature from the American Institute of Physics Handbook for the pure metals. Someone asked about coatings. We cannot determine the emittance of any coasting unless we know the specific heat of the button as a function of temperature. We ask contractors to supply their coatings on a substrate like Armco iron or a pure metal. In the Metals Handbook, there is an abundance of data on Armco iron. Someone asked about Inconel. It is difficult to use a material like this because we do not have good specific heat values. You cannot use data from the ASME Handbook on Metals Properties. For example, all aluminum alloys are given a single value of 0.23. This is adequate for a rough value, but we must know the specific heat as a function of temperature. That is why we use pure metals for calibration standards and prefer them for substrates for coatings.

GORDON: I would like to comment on that last question by mentioning a technique which we haven't actually tried, but which appears workable. Take a sample, run through and measure the rate of change of temperature. After that determination, coat it with something like Parson's black with a known emissivity. Then, determine the specific heat with a second run and from the first run determine the emittance.

BUTLER: Yes, this is fine, the only difficulty is that Parson's black is not good above 100° or 200°. You always get into difficulty with this problem. We do, however, have another technique at our laboratory in which we use a xenon flash lamp to determine the specific heat of thin samples over a very wide temperature range. This requires a knowledge of the absorptivity for the radiation from the flash lamp and has not been fully exploited as yet. There is one thing we neglect in all coatings work; we neglect the specific heat of the coating. I do not know how you measure this, particularly when coatings are very thin. But when the mass of the coating is, for example, 1% of the mass of the specimen, we neglect it.

CORRUCCINI, NBS: This can be risky with organic coatings because they have large specific heats at low temperatures compared to metals or alloys. Thus, to get the best results one may need to account for them even though they are thin.

6—CRYOGENIC EMITTANCE MEASUREMENTS

BY R. P. CAREN

LOCKHEED MISSILES & SPACE COMPANY, PALO ALTO, CALIFORNIA

In the past a few measurements (ref. 1, 2) have been made of the emissivities of materials at low temperatures. The measurements have been made at a few fixed temperatures, usually 77° K, and almost no measurements exist below 77° K. The present apparatus has been designed so that measurements can be made from a temperature as high as 300° K down to 20° K. The measurements are made calorimetrically by measuring the temperature decay of the sample during given time intervals. In these measurements the specific heat, mass, and surface area of the sample must be known in order to compute the emissivity. There are several important design features that must be incorporated into the apparatus. First, the sample must be almost totally thermally isolated from its surroundings. Second, the sample should have a very high ratio of surface area to heat capacity. Third, provision must be made for accurately monitoring the temperature of the sample in a manner compatible with the second provision.

APPARATUS DESIGN PRINCIPLES

Radiation from the sample-chamber walls to the sample and reflection of sample radiation back to the sample by the sample chamber is prevented by surrounding the sample by gold black walls at liquid helium temperature (4.2° K). The liquid helium temperature walls of the chamber also act as cryopumping surfaces which keep the sample chamber pressure below 10^{-10} mm Hg, thus reducing residual thermal conduction. To monitor the sample temperature, the thermometry is placed in a copper block which is connected to the sample by means of a gold 2·1 atomic % cobalt vs constantan thermocouple. A gold cobalt vs constantan thermocouple is used because it has a high thermoelectric output below 100° K, and both elements have low thermal conductivity at low temperatures. The amplified output of this thermocouple is used to drive electronic circuitry which controls the copper block temperature by varying the current through a heater mounted in the block. The sample and the copper block are maintained to within about 10^{-3}° K of one another by means of this electronic circuit. This 10^{-3}° K temperature control allows the sample temperature to be known accurately from measurement of the copper block temperature. Maintaining the block and sample temperature to within 10^{-3}° K of one another also minimizes thermal conduction from the block to the sample via the differential thermocouple.

APPARATUS

The basic cryostat system is shown in figure 6–1. The sample chamber (1) is surrounded by liquid helium in the space (2). To minimize liquid helium boil-off, the liquid helium is contained in a superinsulated dewar (3) whose outer wall is in a liquid nitrogen bath (4). To further reduce liquid helium boil-off, a heat exchanger (6) consisting of "copper wool" is placed in the neck of the helium dewar. This heat exchanger uses the helium gas which boils off to cool the neck of the dewar, thus intercepting the heat energy conducted down the neck of the helium dewar and the sample chamber support tube (7). The sample assembly is supported by nylon studs which are screwed into copper rods (9) fastened to the sample chamber. The copper plate (10) acts both as a cryopumping surface for molecules coming down the support tube and as a radiation shield for radiation coming from the higher temperature regions up the support tube.

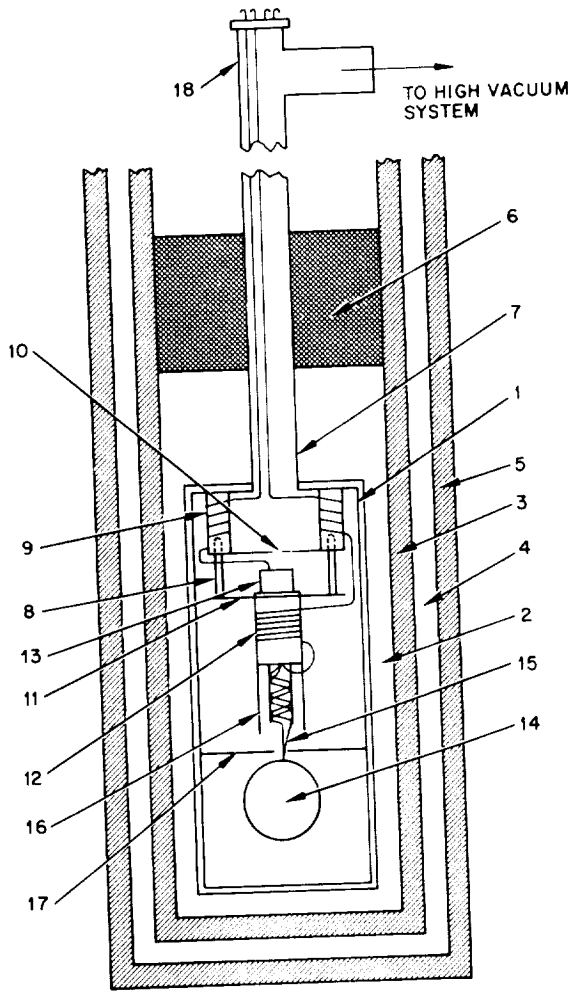

FIGURE 6-1.—Cryostat system.

The copper plate (11) acts as a support for the copper block (12) and the Honeywell Series II germanium resistance thermometer which is used to monitor the block temperature in the temperature range from 100° K to 10° K. For temperatures above 100° K, a copper vs constantan thermocouple is used to monitor the block temperature. The sample (14) is suspended by the 3-mil gold cobalt vs constantan differential thermocouple (15). This thermocouple is wrapped around two glass fibers and surrounded by a radiation shield (16) which is fastened to the copper block. The walls of the sample chamber plus the copper plate (17) form the sample chamber proper. The walls of the sample chamber proper are coated with gold black to minimize the reflectance of radiation from the sample. The resistance thermometer, differential thermocouple, thermocouple, and heater leads are brought out of the vacuum space through the multiterminal hermetic seal (18).

To eliminate conduction from the higher temperature regions to the block-sample system, the leads are placed in thermal contact with the copper rods (9) by wrapping them around the rods and coating them with glyptal. The differential thermocouple leads are further placed in thermal contact with the copper block, thus placing the block junction of this thermocouple at the block temperature. Since the leads are placed in contact with the helium bath via the copper rods (9) before their contact with the copper black, they act as a 10^{-2} to 10^{-1} watt heat leak.

The normal state of the system is for the copper block to cool to the helium temperature. The heater coil is then used to drive the block to higher temperatures. This system, therefore, can be used to control the block temperature. The time constant of this thermal system is much less than the decay time constant of the sample. Thus, the block system can be controlled to the sample temperature. The heater control system is similar to that used by West et al. (ref. 3) for their adiabatic calorimetry work. In the present system the output of the differential thermocouple is fed into a Keithley Model 149 millimicrovoltmeter which is used to drive a Leeds and Northrup AZAR-H recorder and a transistorized current controller which is used to regulate the heater current. The minimum dE/dT for the gold-cobalt vs constantan thermocouple occurs at 10° K and is about 6μv/° K. The Keithley millimocrovoltmeter is sensitive to 10^{-2} μv and thus gives a temperature control of about 10^{-3}° K.

EXPERIMENTAL ACCURACY

The major sources of error in the present emittance apparatus are the various nonradiative

thermal losses by the sample. The thermal loss mechanisms are as follows:

- Thermal conduction from the copper block to the sample through the differential thermocouple
- Radiation fin effect losses from the thermocouple leads
- Thermal conduction from the sample to the sample container walls by residual gas conduction

Table 6–I below lists the magnitude of these thermal leaks together with the total radiation from a representative sample. It is assumed in the calculation of the sample radiation that the sample has a total surface area of 10^1 cm^2 and an ϵ of 10^{-2}. The radiation fin effect is calculated from the data of Lieblein (ref. 3). The fin effect radiation is calculated on the basis of an unshielded thermocouple; with the shielding used in the apparatus, this radiation is reduced by an order of magnitude. The differential thermocouple is a gold-cobalt vs. constantan pair of wires 3 mils in diameter by 10 cm long connecting the copper block and the sample. The data of Powel et al. (ref. 4) is used for the thermal conductivity of the gold-cobalt wire. The residual conductivity is calculated from the equation of Knudsen (see, for example, Scott, ref. 6). Note that it follows from the tabulated data that at 10° K a 20% error in emissivity is expected. At 20° K and above the experimental error is only 3% or less. The above errors are calculated assuming no heat generation due to sample vibration; actually this mechanism will produce heat inputs to the sample which are significant below 30° K unless special precautions are taken to isolate the apparatus from vibration.

TABLE 6–I.—*Total radiation from a representative sample and magnitude of thermal leaks*

Temp., ° K	Total sample radiation, watts	Radiation fin effect, watts	Residual gas conduction (10^{-10} mm Hg), watts	Differential thermocouple conductivity, watts	Radiation fin effect (shield in place), watts
10	5.6×10^{-9}	1.3×10^{-9}	4×10^{-10}	4×10^{-10}	1.3×10^{-10}
20	9.0×10^{-8}	2.0×10^{-8}	1×10^{-9}	7×10^{-10}	2.0×10^{-9}
40	1.4×10^{-6}	3.4×10^{-7}	2×10^{-9}	1.3×10^{-9}	3.4×10^{-8}
60	7.3×10^{-6}	1.8×10^{-6}	3.5×10^{-9}	1.7×10^{-9}	1.8×10^{-7}

REFERENCES

1. FULK, M.; and REYNOLDS, M. M.: Emissivities of Metallic Surfaces at 76° K. Jour. Appl. Phys., vol. 28, no. 12, Dec. 1957, pp. 1464–1467.
2. CAMPELL, D. A.; and SCHULTE, H. A.: Measurement of Emissivity at Low Temperatures. Chrysler Corporation Missile Operations Tech. Rept. MT–R2J (Contract DA-20-018-ORD-14440 Final Progress Report), Nov. 20, 1957. (ASTIA AD–151931).
3. WEST, E. D.; and GINNINGS, D. C.: Automatic Temperature Regulation and Recording in Precision Adiabatic Calorimetry. Rev. Sci. Instr., vol. 28, no. 12, pp. 1070–1074.
4. LIEBLEIN, SEYMOUR: Analysis of Temperature Distribution and Radiant Heat Transfer Along a Rectangular Fin of Constant Thickness. NASA TN D–196, 1959.
5. POWELL, R. L.; BUNCH, M. D.; and GIBSON, E. F.: Low-Temperature Transport Properties of Commercial Metals and Alloys. III. Gold-Cobalt. Jour. Appl. Phys., vol. 31, no. 3, Mar. 1960, pp. 504–505.
6. SCOTT, R. D.: Cryogenic Engineering. D. Van Nostrand Co., Inc., 1960, p. 146.

DISCUSSION

SHAW, Optics Technology: How did you attach the thermocouples to your samples?

CAREN: The thermocouples were spot welded to the samples.

SHAW: How thick were the samples?

CAREN: One mil. We used 3-mil wire. The whole point is that you don't really have to worry about having absolutely perfect thermal contact with the sample. The reason is simply this: the important thing is keeping the temperature difference between the ends of the thermocouple wires within 0.01 to 0.001° because that is what determines how much heat is conducted through the thermocouple. If you have an error of a few hundredths of a degree because you don't have perfect thermal contact with the sample, it simply means that at the end of the decay, you are a couple hundredths of a degree off. But it doesn't mean that your data are going to be off too far.

BARSY, Armstrong Cork Co.: I wonder if you would comment in more detail on the radiation shield that was used on the differential thermocouple, particularly with reference to spacing and the surface finish on the shield.

CAREN: The shield was copper; copper was used because with its high conductivity there will not be much of a thermal gradient down the shield. The surface was chemically cleaned. Insofar as the size is concerned the differential thermocouple was mounted on some approximately 8-mil, Pyrex fibers across a space of about a quarter of an inch, and the shield coming down is on the order of ⅜ inch in diameter and about 1 inch long.

BROWN, Martin-Marietta: We have a problem in determining the EMF outputs of thermocouples at low temperatures corresponding to the relative temperature. How do you calibrate your particular thermocouples?

CAREN: Are you talking of the differential thermocouple?

BROWN: No, the actual end of the couple. How did you determine that you had 35° K? How did you determine that you had an EMF output corresponding to 35° K?

CAREN: The temperature of this block is what I measured to determine the temperature of the sample. It was measured using a copper constantan thermocouple and the copper constantan wires were tempered to the sample temperature by wrapping them around the copper and then fastening down the bead. I think if you temper the thing properly there isn't very much of a problem.

BROWN: What I am interested in is the EMF output of a thermocouple in the range between 4° and 20° K. What do you use for calibrating standards?

CAREN: I was using, to measure the EMF, a K-3 potentiometer.

BROWN: How do you determine that a certain EMF is equal to a certain temperature?

CAREN: The data I am using for the thermocouple output is the Bureau of Standards data which Dr. Corruccini put out on copper constantan and gold-cobalt.

BROWN: Do you use a liquid helium point and a liquid hydrogen point and extrapolate between these two points?

CORRUCCINI, N.B.S: Did you just take our published tables and assume that your thermocouple would match those tables or, as Mr. Brown is suggesting, did you make some kind of a spot calibration that would give you an idea of the deviations from our tables?

CAREN: No, this is rough work and the only thing I did check was nitrogen temperature; just on the thermocouple to see if we were close. That is about all.

CORRUCCINI: You used gold-cobalt versus constantan for your differential thermocouple?

CAREN: Actually, since I planned to go down only to 30° I started using gold-cobalt vs copper because at that temperature I didn't need to think about using the constantan. But when I try to push to lower temperatures I definitely will have to use constantan because of the conductivity of the copper.

CORRUCCINI: I see; I was going by the remark in the published paper. I was going to say that we are more interested now in the combinations using Chromel. We think that gold-cobalt versus Chromel probably is one of the best combinations that could be used here. It has the feature that you desire in your differential thermocouple of low thermal conductivity in both legs, and in addition it has an appreciably higher de/dt than gold-cobalt vs constantan. In case anyone is interested, we hope to put out a reference table for this thermocouple some time in the next year.

TOBEY, Arthur D. Little: Would you care to comment regarding the applicability of this method to coatings?

CAREN: Do you mean metal samples with coatings on them? I can't see any reason why they couldn't be used. It would just be a question of what temperatures you can go down to because you have to remember that you are going to have a fairly large thermal mass. Probably if you're only interested in going to nitrogen temperature or something like that, the method would be perfectly applicable.

BECKETT, NBS: I have a question with regard to the temperature measurements. I believe that you are using a single thermocouple which measures a temperature at a small region on the surface of your sample. Your results, however, are dependent upon the temperature distribution throughout the sample as well as the temperature at a point. How large is the temperature variation throughout the sample?

CAREN: Well, of course, the temperature variation throughout the sample has not been measured but there are two things that have to be kept in mind. In the first place, the rate of cooling is quite slow; in other words, these runs take on the order of 5 hours. If you were cooling quite rapidly, you might get cold spots near the location of the thermocouple because you have a lot of radiating surface. But cooling slowly

you would expect, especially using a copper sample, fairly isothermal conditions throughout the sample.

BECKETT: May I comment? This type of technique is common throughout precision calorimetry wherever they use radiation shields. This is probably justifiable as you have indicated but I have often wondered just how large are the gradients in the thin metal shield, of which your sample is typical, and I am raising the question as to whether or not we are really justified in making such assumptions.

CAREN: Well, I did do some calculations, the accuracy of which I cannot specify today, but at one time I was interested in knowing how long it would take for the thermocouple to come into equilibrium with the sample after the sample temperature was changed. I did my calculations on the assumption of a copper thermocouple wire 1° different from the sample. I found to my surprise that equilibrium is reached in a very short length of time. In the analysis you have several Fourier components. All the higher Fourier components damp out very rapidly, just like heating one end of a bar, and even the long-wave-length Fourier component damps out very quickly. I did this calculation for a 3-mil wire. In the case of the sample discussed in my paper, equilibrium would be faster because while the sample is thinner, it is also more extended.

7—AN APPARATUS FOR MEASURING TOTAL HEMISPHERICAL EMITTANCE BETWEEN AMBIENT AND LIQUID NITROGEN TEMPERATURES

BY G. L. HAURY

AERONAUTICAL SYSTEMS DIVISION, WRIGHT-PATTERSON AIR FORCE BASE, OHIO

An apparatus was designed, fabricated, and calibrated for measuring the mean total hemispherical emittance of solid materials in the temperature range between ambient and liquid nitrogen temperatures. The apparatus is a modified version of an Arthur D. Little design and is particularly adapted for accommodating large, flat samples instead of cylindrical ones. A description of the apparatus together with appropriate operational details are presented in addition to some preliminary data on copper and three samples of aluminum foil. The accuracy of the apparatus, based on these data, has been determined to be within $\pm 2.5\%$.

EXPERIMENTAL APPARATUS

The design of the apparatus was based on one designed and used by Arthur D. Little Co. (ref. 1). The apparatus described in this report is quite similar with the exception of some minor modifications, one of which is the ability of the apparatus to accommodate larger sample surface areas. In figure 7–1, the lines venting vessels (1) and (2) are made of ⅝-inch diameter 0.020 inch wall type 304 stainless steel tubing so as to have minimum heat conduction.

Vessels (1) and (2) are fabricated from ⅛-inch sheet copper and the seams silver soldered. After fabrication, both of these vessels were bright-dipped such that the copper surfaces were clean and oxide-free. Vessel (1) is inserted into vessel (2), the stainless steel tube of vessel (1) being inserted through a copper bushing in the upper portion of guard vessel (2). A layer of insulation consisting of eight aluminum shields alternately separated by means of fiber glass cloth is attached to the top and sides of guard vessel (2) in order to minimize boil off. The spacing between the

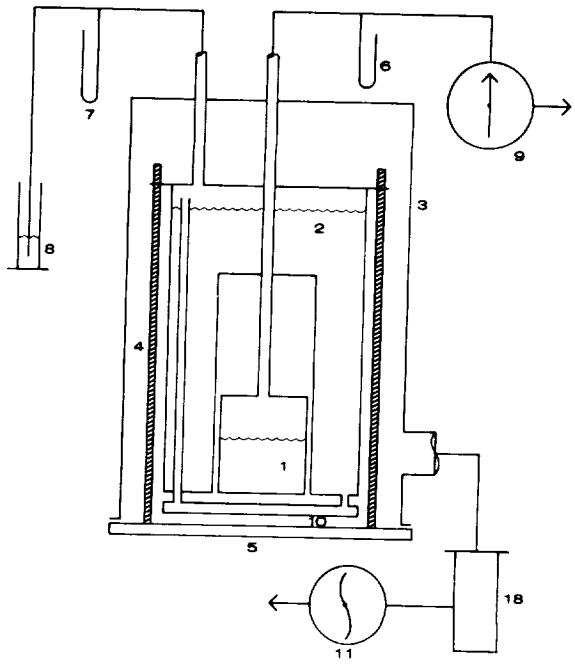

FIGURE 7–1.—Cross-sectional drawing of the total hemispherical emittance equipment.

outside of the measuring vessel and the inner surface of the guard vessel is $\frac{3}{16}$ inch.

Four tubular plastic spacers are inserted between the vessels at 90° apart to assure proper spacing of the walls and to prevent any metal to metal contacts. The guard and measuring vessel assembly are suspended above the copper hot plate (5) by means of four $\frac{3}{8}$-inch stainless steel tie rods (4) spaced 90° apart. The upper ends of the tie rods are insulated from the copper guard vessel (2) by means of nylon inserts. The upper ends are threaded for several inches so that the assembly can be raised or lowered to adjust the spacing between the hot and cold surfaces. The vent tubes from vessels (1) and (2) pass through rubber O-ring seals at the top of bell jar (3) to make vacuum tight seals. The lower flange of the bell jar (3) is sealed to the copper plate (5) by a flat neoprene rubber gasket about 1 inch wide. Pump down of bell jar (3) is acheived with a 1½-inch mechanical fore pump (11) and a 4-inch oil diffusion pump (18). The boil off from the guarded measuring vessel (1) is measured with a wet-test meter (9). A positive pressure of about 2 inches of water is maintained above the liquid in the guard vessel (2) by means of bubbler (8) so that the liquid nitrogen temperature in (2) is slightly positive with respect to liquid nitrogen temperature in (1). This assures that there is no condensation of nitrogen vapors in vessel (1) or in vent tube from (1). Each determination required two specimens of the same material, one 4¾ inches in diameter attached to the measuring vessel (1), and the other 8 inches in diameter, attached to the hot plate (5).

CALIBRATION OF APPARATUS

Prior to the runs that were made for the purpose of accumulating data, the apparatus was calibrated to determine any extraneous heat leaks which would appear as "boil off" from measuring vessel (1). This was accomplished by suspending the flat hollow copper plate (10) approximately ¼ inch below the measuring vessel (1). The plate was filled with liquid nitrogen from vessel (2) as shown. The cold plate, with its exposed surfaces insulated, is shown in figure 7–2 prior to final assembly. Except for negligible side effects, the measuring vessel was completely guarded, and the heat leak to the measuring vessel was found to be 0.044 watt.

ACCURACY OF APPARATUS

A Nichrome electric heater was attached to the bottom of the measuring vessel and covered with aluminum foil. When three different electrical energy inputs of 0.066 watt, 0.254 watt and 0.037 watt were applied to the heater, the recovery as boil off from the measuring vessel was 96.0%, 99.0% and 97.6%, respectively. The accuracy of the apparatus, considering that the heat flux concerned reaches the bottom surface of the measuring vessel, is within ±2.5%.

TEST RESULTS

The mean total hemispherical emittances of the materials that have been run in the apparatus thus far are listed in table 7–I. These emittances were obtained by applying equation (1) for the radiant heat flux between two parallel plates of equal surface area of the same material.

TABLE 7–I.—*Mean Total Hemispherical Emittances*

Sample	Temperature range		Mean ϵ
	Hot face, ° K	Cold face, ° K	
Mechanically polished copper.	294	80	0. 022
Aluminum foil, Reynolds 0.001 in. thick.	275	87	. 060
Aluminum foil, Alcoa 0.0005 in. thick.	285	82	. 055
Aluminum foil, Alcoa 0.00024 in. thick.	277	86	. 065

The plates were placed ¼ inch apart with the pressure in the system being 10^{-4} mm Hg or less.

$$W=\frac{\epsilon}{2-\epsilon}\cdot A\sigma(T_2^4-T_1^4) \qquad (1)$$

where (ref. 2):

W radiant heat

ϵ total hemispherical emittance between temperatures T_2 and T_1 of either surface, on the assumption that $\epsilon=\epsilon_1=\epsilon_2$

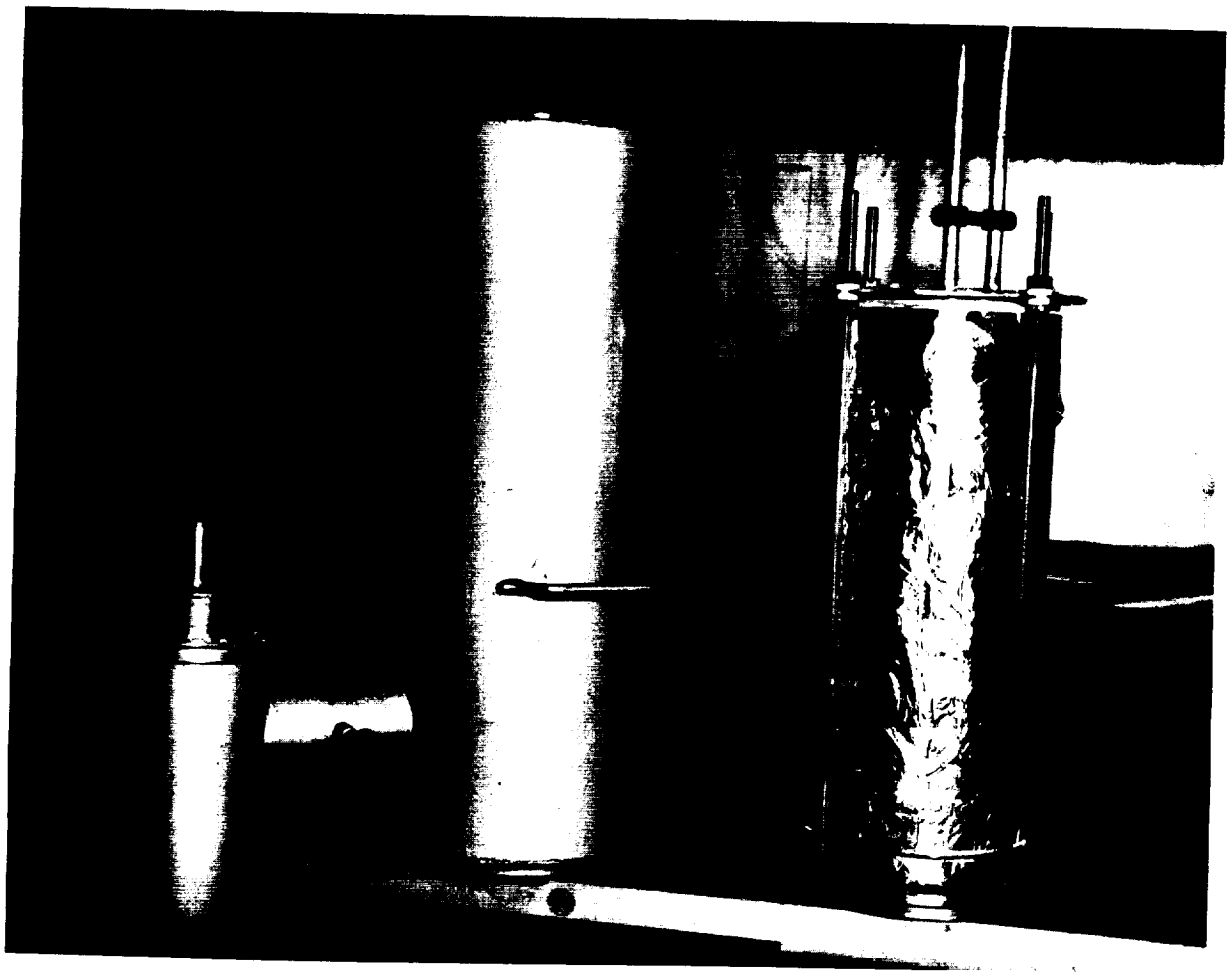

FIGURE 7-2.—Bell jar, guard, and measuring vessel, with cold plate attached.

A surface of cold plate
σ Stefan-Boltzmann constant in proper units
T_2 temperature of hot plate
T_1 temperature of cold plate.

Table 7–II are data on two Corning ceramic materials.

CORRECTIONS

It was assumed that half the heat flux entering the annular space between the guard and measuring vessels (area of opening was 20 sq cm) was absorbed by the measuring vessel. This flux was subtracted from the total flux before data were reduced. A correction was also made for residual boil off which displaced the evaporated liquid. The residual boil off was calculated to be 0.54% of the total boil off when using liquid nitrogen.

TABLE 7–II.—*Mean Total Hemispherical Emittances of Corning Glass Company Ceramic Material*

Sample	Temperature range		Mean ϵ
	Hot face, ° K	Cold face, ° K	
Pyroceram 9606	289	256	0. 89
	236	207	. 85
	177	153	. 82
	292	154	. 79
	288	143	. 80
	247	117	. 80
Multiform 7941	297	161	. 72
	289	153	. 74

CONCLUSIONS

(1) The accuracy of the apparatus when corrections are made for heat leaks is ±2.5% as determined by calibration with a known electrical heat input.

(2) The apparatus is adequate for the measurement of the mean total hemispherical emittance of flat surfaces between 290° K and 80° K.

(3) Measurements made thus far have been in reasonable agreement with those reported in the literature (ref. 3).

REFERENCES

1. Black, I. A.; Fowle, A. A.; and Glaser, P. E.: Development of High-Efficiency Insulation. Article D–1, Advances in Cryogenic Engineering, Plenum Press, Inc., New York, 1959, p. 181.
2. Scott, R. B.: Cryogenic Engineering. D. Van Nostrand Co., Inc., New York, 1959, pp. 147–148.
3. Black, I. A.; and Glaser, P. E.: Progress Report on Development of High-Efficiency Insulation. Article A–3, Advances in Cryogenic Engineering, Plenum Press, Inc., New York, 1960, p. 32.

DISCUSSION

Corruccini, NBS: Your formula for computing the results with the factor ε/(2-ε) contains the assumption that the emittances of the warm and cold surfaces are equal. This is not necessarily a good assumption for these widely different temperatures.

Haury, A.S.D.: It is actually what we call mean emissivity and is an average. It is really not the true emissivity of either surface.

Touloukian, Purdue Univ.: Yesterday and this morning whenever data were reported, there were some specifications. In this case the thickness of the samples was specified, but no other information was given. Why is the thickness of the aluminum sheet important in regard to the emissivity?

Haury: The only purpose of that was to identify samples. There was no meaning here as far as thickness is concerned. I don't think it has any bearing on the measurement. It was simply to distinguish among three different samples of foil of different thicknesses.

Touloukian: But it would have been more informative to know what Pyroceram 9606 and 9608 is. If space can be devoted I would prefer to have some information other than the thickness of the material.

Haury: The thickness of the plate was measured as ⅛ inch.

Touloukian: This is irrelevant as far as emissivity is concerned. Something about the identity of the material should be mentioned. Will the next sample of Pyroceram 9606 be the same? Did you try various samples?

Haury: No, sir; we checked only one sample of each material.

Touloukian: Can I use these data for the next batch of Pyroceram 9606 I order?

Haury: Yes.

Corruccini: I noticed in your apparatus drawing showing the calibrating cold plate in place that there was quite a gap through which radiation could enter from the edges. Although the shape factor for it is rather small, this radiation comes from a high temperature. How sure are you that this edge radiation is not influencing the calibration with the cold plate?

Haury: Well, during the calibration we used an aluminum foil around the cold plate and brought it up to about ¼ inch or so from the bottom of the guard vessel. We made some calculations based on the solid angle and it would be negligible, I think.

Beckett, NBS: I would like to comment on the point that was raised by Professor Touloukian. I think it is very important from the broader, long-range viewpoint that whenever a physical property is measured, the sample must be adequately characterized. This means more than specifying its chemical composition. The physical state of the sample is invariably involved, particularly with complex substances such as Pyroceram. The state of the material is very important when you try to extrapolate or to correlate this measurement with something else. We have a lot of effort being devoted to measurement of various properties throughout the country now. And one of the big difficulties with those who use the information, or who collect, correlate, and evaluate this information, is being able to relate the measurements on one sample by one experimental group with those being made by another. Unless we do have well-characterized samples this is not possible.

Abbot, Naval Radiological Defense Lab.: I notice you have various wattages of heat inputs to the heater plate here. Have you assumed that all this is radiated to the sample?

Haury: I am glad you brought up that point. I failed to mention the calibration by the electrical heat input. There was a Nichrome heater fixed to the bottom of the measuring vessel, and it was assumed that all the heat went into the liquid nitrogen in that case, because the heater was covered with an aluminum foil shield. In that calibration run, in one case we had 99.5% of the heat out as boil off, and at a low heat flux we had around 97% recovery.

8—ERRORS OF THE CALORIMETRIC METHOD OF TOTAL EMITTANCE MEASUREMENT

BY K. E. NELSON AND J. T. BEVANS

SPACE TECHNOLOGY LABORATORIES, INC., REDONDO BEACH, CALIFORNIA

A commonly used technique for total hemispherical emittance measurements is the calorimetric method wherein the net loss from a sample within a known radiation environment is related to the total hemispherical emittance of the sample material. The total error of this method is greatly dependent upon the experimental system, techniques, and procedures utilized. However, there are basic minimal errors which are inherent in the calorimetric method and are primarily dependent upon the ratio of the sample temperature and that of the environment. This paper discusses these minimal errors in quantitative terms and the other contributions to the total error in more general terms.

The analysis of the calorimetric method is developed from the basic heat balance of the sample, the analytic expression for the radiation cooling and the linear expression for the factors contributing to the total error. The assumption is made that the experimental system has been designed to minimize or eliminate system errors, e.g., inter-reflections between sample and surrounds. From the analysis, quantitative results are presented for the sample temperature, the surrounds temperature, the sample absorptance, and the non-equilibrium contributions to the total error.

The results indicate care and attention must be given to the design, construction, and operation of a calorimetric instrument. Even with proper precautions, serious errors can result in operation at sample temperatures below 250° K.

The restrictions imposed upon the thermal radiation properties required for the thermal design and analysis of spacecraft are becoming increasingly severe in terms of the variety of materials which must be considered, the range of temperatures over which the properties are required and the accuracy of the measurements. Of the different methods available for measuring the several types of necessary thermal radiation properties, the calorimetric method of total emittance measurement is one of the important experimental techniques. The apparent simplicity of the necessary equipment and instrumentation, combined with the apparent inherent accuracy, makes this method very attractive to an experimenter. Furthermore, the calorimetric method is the simplest one available for directly measuring the hemispherical emittance of a material. For these reasons, in many laboratories the calorimetric method is rapidly developing into a standard procedure for total emittance measurements.

Experimental results obtained with the calorimetric method and reported in the literature have indicated that the procedure does not necessarily yield values which are consistent between different experimenters and with theory. Discrepancies between experimenters can be largely attributed to sample material differences. Although theoretical predictions and experimental results may not correspond exactly in magnitude, experiment should follow the trend predicted by theory. Figure 8–1, extracted from results given in a recent article (ref. 3), illustrates this descrepancy between theory and experiment. An important application of the calorimetric method is the measurement of total emittance at material temperatures ranging from ambient (~300° K) to cryogenic (10–80° K). The interest for operation of the calorimetric system at temperatures approaching the cryogenic region plus the above anomalies existing at temperatures above 200° K are sufficient incentive for investigating the method in greater detail.

The most direct and obvious procedure for examining the calorimetric method is by a study of the errors involved in the expression

692–146 O—63——5

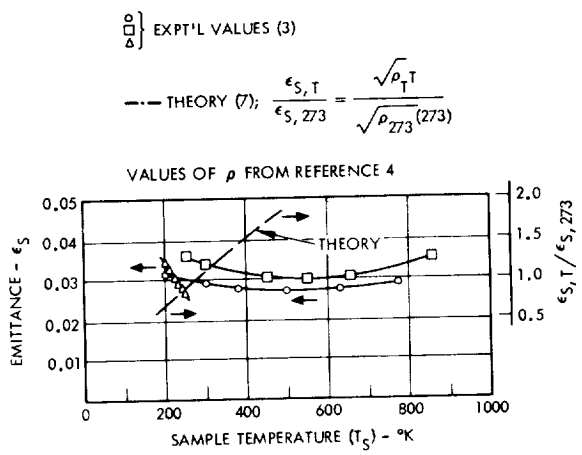

FIGURE 8-1.—Pure electropolished copper emittance data of reference 3 compared to theoretical prediction.

used to compute the value of emittance. This approach assumes certain basic instrument design conditions have been satisfied: the walls of the enclosure have been made as non-reflective as possible to the energy emitted by the sample; and the sample has been placed geometrically within the enclosure in a manner that eliminates or minimizes the reflection of energy emitted by the sample back on to itself. These conditions are usually maintained and should be applicable to all experimental systems.

The purpose of the paper is to describe the errors of the calorimetric method within the restrictions given above. Certain of the contributions to the total error which will be enumerated will be dependent upon the particular system chosen by the experimenter. Conversely, other contributions will be inherent in the calorimetric method and limits or bounds to these will be given.

ANALYSIS

Nomenclature

A	area, cm²; A_s=primary sample emitting area; A_x=sample edge emitting area; A_w=area of support or lead wire
C_1, C_2	first and second radiation constants, respectively
$E(\lambda T)$	monochromatic emissive power of an ideal radiator, watts/cm² -μ
M	molecular weight
P	pressure, mm Hg
T	absolute temperature, °K; T_s=sample temperature; T_0=surrounds; Tg=vacuum gage temperature
$\dot{T}$	derivative of temperature with respect to time, °K/hr; $\dot{T}_s = \dot{T}$ for the sample
V	volume, cm³
c	specific heat, watts/gm
d	density, gm/cm³
k	thermal conductivity, watts/cm² °K/cm; k_w=thermal conductivity of support or lead wire
l	length, cm; l_w=length of lead or support wire
q	heat flow, watts; q_e=electrical equivalent heat flow; q_l=heat loss or leakage; q_{cg}=heat loss by conduction through the residual air within the evacuated enclosure; q_{cw}=heat loss by conduction from the support or leads
t	effective thickness of sample, cm; $t = V/A_s$
w	mass of sample, gm
α	absorptance; α_s=primary sample area absorptance to surrounds radiation; α_x=sample edge area absorptance to surrounds radiation; $\Delta\alpha_s = \epsilon_s - \alpha_s$, equation (2)
γ	ratio of specific heats; $\gamma = 1.41$ assumed in equation (13)
Δ	difference between two quantities
δ	error difference between actual and measured (or calculated) quantity
$[\delta\epsilon_s]^I$	total emittance error contribution from an error in sample temperature measurement; figure 8-2
$[\delta\epsilon_s]^{II}$	total emittance error contribution from the internal energy emitted by the sample; figure 8-3
$[\delta\epsilon_s]^{III}$	total emittance error contribution from the conduction loss by a single support or lead wire; figure 8-4
$[\delta\epsilon_s]^{IV}$	total emittance error contribution from conduction through the residual gas within the evacuated enclosure; figure 8-5
$[\delta\epsilon_s]^V$	maximum possible total emittance error contribution from the assumption $\alpha_s = \epsilon_s$ for idealized materials; figure 8-6
ϵ	total hemispherical emittance; ϵ_s=primary sample area emittance; ϵ_x=sample edge area emittance; ϵ_λ=monochromatic emittance; $\epsilon_{s,T}$=sample emittance at temperature T
λ	wavelength, microns; λ_c=wavelength of change from a monochromatic emittance (ϵ_λ) of unity to zero
ρ	volume resistivity, ohm-cm
σ	Stefan-Boltzmann constant

General

The primary assumptions of the analysis were given in the Introduction. The calorimetric method may be used in two ways: transient and steady state. In the transient procedure, all or part of the energy emitted by the

sample is obtained from the internal heat capacity of the sample. The steady state technique monitors the heat supplied to the sample under conditions of thermodynamic equilibrium with its surrounds. The two methods are particular forms of the more general heat balance expression for the sample:

$$\epsilon_s A_s \sigma T_s^4 + \epsilon_x A_x \sigma T_s^4 - \alpha_s A_s \sigma T_0^4 - \alpha_x A_x \sigma T_0^4 = -wc\dot{T}_s + q_e + q_l \quad (1)$$

A frequent assumption utilized in reducing the complexity of the above equation is that the emittance (ϵ) is equal to the absorptance. Since this is an assumption, the validity can be examined by substituting:

$$\alpha_s = \epsilon_s + \Delta\alpha_s \quad (2)$$

Using this in equation (1) and collecting terms yields:

$$\epsilon_s A_s(\sigma T_s^4 - \sigma T_0^4) + \epsilon_x A_x(\sigma T_s^4 - \sigma T_0^4) = \Delta\alpha_s A_s \sigma T_0^4 + \Delta\alpha_x \sigma T_0^4 - wc\dot{T}_s + q_e + q_l \quad (3)$$

Assuming the contributions to the total error to be consistent rather than random, i.e., additive in a linear manner, the total error can be expressed as:

$$\frac{\delta\epsilon_s}{\epsilon_s} = \left[\frac{\delta\epsilon_s}{\epsilon_s}\right]_c + \left[\frac{\delta\epsilon_s}{\epsilon_s}\right]_q + \left[\frac{\delta\epsilon_s}{\epsilon_s}\right]_{n-g} + \left[\frac{\delta\epsilon_s}{\epsilon_s}\right]_x \quad (4)$$

where

$$\left[\frac{\delta\epsilon_s}{\epsilon_s}\right]_c = \left[\frac{\delta A_s}{A_s}\right] + 4\left(\frac{T_s^4}{T_s^4 - T_0^4}\right)\left(\frac{\delta T_s}{T_s}\right) + 4\left(\frac{T_0^4}{T_s^4 - T_0^4}\right)\left(\frac{\delta T_0}{T_0}\right) \quad (5)$$

$$\left[\frac{\delta\epsilon_s}{\epsilon_s}\right]_q = \left\{\frac{1}{\epsilon_s A_s \sigma(T_s^4 - T_0^4)}\right\} \left\{(wc\dot{T})\frac{\delta\dot{T}}{\dot{T}} + (wc\dot{T})\frac{\delta wc}{wc} + q_e\frac{\delta q_e}{q_e} + q_l\frac{\delta q_l}{q_l}\right\} \quad (6)$$

$$\left[\frac{\delta\epsilon_s}{\epsilon_s}\right]_{n-g} = \left\{\left(\frac{\Delta\alpha_s}{\epsilon_s}\right)\left(\frac{T_0^4}{T_s^4 - T_0^4}\right)\right\} \left\{4\frac{\delta T_0}{T_0} + \frac{\delta A_s}{A_s} + \frac{\delta(\Delta\alpha_s)}{\Delta\alpha_s}\right\} \quad (7)$$

$$\left[\frac{\delta\epsilon_s}{\epsilon_s}\right]_x = \left(\frac{\epsilon_x A_x}{\epsilon_s A_s}\right)\left\{\frac{\delta\epsilon_x}{\epsilon_x} + \frac{\delta A_x}{A_x} + 4\left(\frac{T_s^4}{T_s^4 - T_0^4}\right)\frac{\delta T_s}{T_s} + 4\left(\frac{T_0^4}{T_s^4 - T_0^4}\right)\frac{\delta T_0}{T_0} + \left(\frac{\Delta\alpha_x}{\epsilon_x}\right)\left(\frac{T_0^4}{T_s^4 - T_0^4}\right)\left[4\frac{\delta T_0}{T_0} + \frac{\delta A_x}{A_x} + \frac{\delta(\Delta\alpha_x)}{\Delta\alpha_x}\right]\right\} \quad (8)$$

The various terms in equation (4) can be designated for future convenience: the conventional error, equation (5); the heat measurement error, equation (6); the non-gray error, equation (7); and the edge effect error, equation (8). The last three total error contributions may be made independent of the sample emittance (ϵ_s) by multiplying both sides of the equation by ϵ_s, whereas the first contribution, equation (5), is dependent upon ϵ_s. Therefore, the conventional error term is a percentage contributor to the total percentage error, but the remaining three terms contribute increments to the uncertainty in ϵ_s.

Conventional Error, Equation (5)

This equation represents the errors involved in measuring the basic physical quantities of an emittance sample: sample area, sample temperature, and surrounds temperature. Each of these quantities is subject to different degrees of accuracy but the most important is the temperature of the sample. For a fixed sample size and surrounds, i.e., a given experimental system, only the sample temperature varies. The magnitude of this error is shown in figure 8–2 for several values of the quantity $\delta T_s/T_s$, i.e., temperature error, as a function of the ratio of sample to surrounds temperature.

The Heat Measurement Error, Equation (6)

The energy emitted by the sample must be obtained from either the internal energy of the sample or from an externally supplied source (e.g., an electrical heater). If the internal heat capacity is utilized, the calorimetric method is generally considered to be operated in the transient mode and $wc\dot{T}$ terms of equation (6) are included. When the steady state method of operation is used, the transient terms ($wc\dot{T}$) are assumed to be zero or negligible and all of the energy emitted by the sample is supplied by the

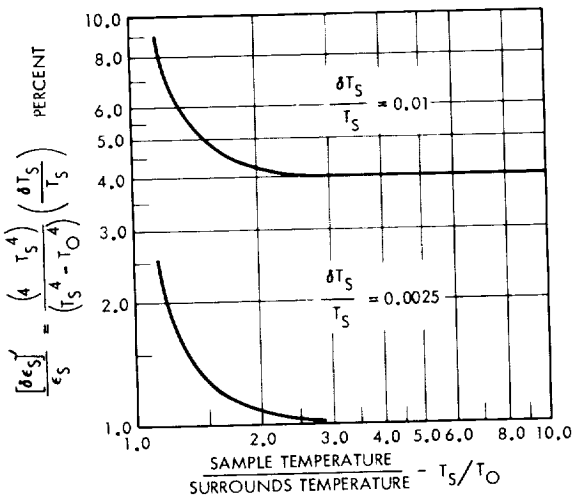

FIGURE 8–2.—Contribution to the total error from an error in sample temperature measurement.

term q_e. The neglect of the transient term in steady state operation can be a serious source of error under certain conditions, as will be shown. Consequently, the error contribution for this term is present in both modes of operation.

The heat measurement error is independent of the emittance (ϵ_s) of the sample and is a numerical error; i.e., ϵ_s can be cancelled from both sides of equation (6). When this is done, the heat measurement error can be considered only as $\delta\epsilon_s$. With this in mind, the first term of equation (6) can be written as:

$$\frac{wc\dot{T}}{A_s\sigma(T_s^4-T_0^4)}\frac{\delta\dot{T}}{\dot{T}}=\frac{(wc)}{A_s\sigma(T_s^4-T_0^4)}(\delta\dot{T}) \quad (9)$$

For a specific sample, the ratio of mass to area can be characterized by a thickness (t) and by selecting specific materials, equation (9) may be computed as a function of the following variable:

$$\frac{dct}{2\sigma(T_s^4-T_0^4)} \quad (10)$$

Figure 8–3 shows the contribution to the total error for aluminum and copper samples as a function of the sample temperature. The surrounds temperature (T_0) was taken to be that corresponding to liquid nitrogen and liquid helium, and the sample was assumed to be a planar sample with a volume to emitting area ratio of $\frac{1}{2}t$. For other sample geometries, the volume to emitting area should be used to modify the values shown in figure 8–3. The specific heat (c) of the two materials as a function of sample temperature were obtained from reference 5.

The error contribution resulting in an error in the heat capacity of the sample is pertinent to the transient method of operation. Similarly, the heat supplied to the sample (q_e) pertains to the steady state procedure. The final term in equation (6) affects both methods since it is the heat loss error term. Energy losses by conduction along the thermocouple, power and support leads and conduction through the residual gas in the system should be considered.

For a single thermocouple wire, support, electrical lead, etc., the conduction loss can be written as (radiation effect neglected):

$$q_{cw}=\frac{k_w A_w}{l_w}(T_s-T_w) \quad (11)$$

or

$$q_{cw}=\frac{k_w A_w}{l_w}\Delta T \quad (12)$$

Equation (12) must be multiplied by

$$A_s[\sigma(T_s^4-T_0^4)]^{-1}$$

to obtain an estimate of the conduction loss from a single wire relative to the sample-emitted energy. This estimate is shown in figure 8–4 for three common thermocouple materials.

Generally, the assumption is made that convection losses from a sample are negligible if the system pressure is less than 10^{-4} or 10^{-5} mm Hg. The heat loss by conduction at low pressures is dependent upon such system parameters as enclosure dimensions, method of securing the low pressure, sample size, etc. An estimate of the heat conduction from a sample was made with the expression given by Scott (ref. 6) assuming accommodation coefficients of unity and an enclosure area large, relative to the sample area:

$$q_{ca}=0.2426\frac{(\gamma+1)}{(\gamma-1)}\left(\frac{P}{\sqrt{MT_g}}\right)(T_s-T_0) \quad (13)$$

The pressure (P) was evaluated at 300° K (gage temperature Tg), the molecular weight (M) was assumed to be 28.8 at all pressures,

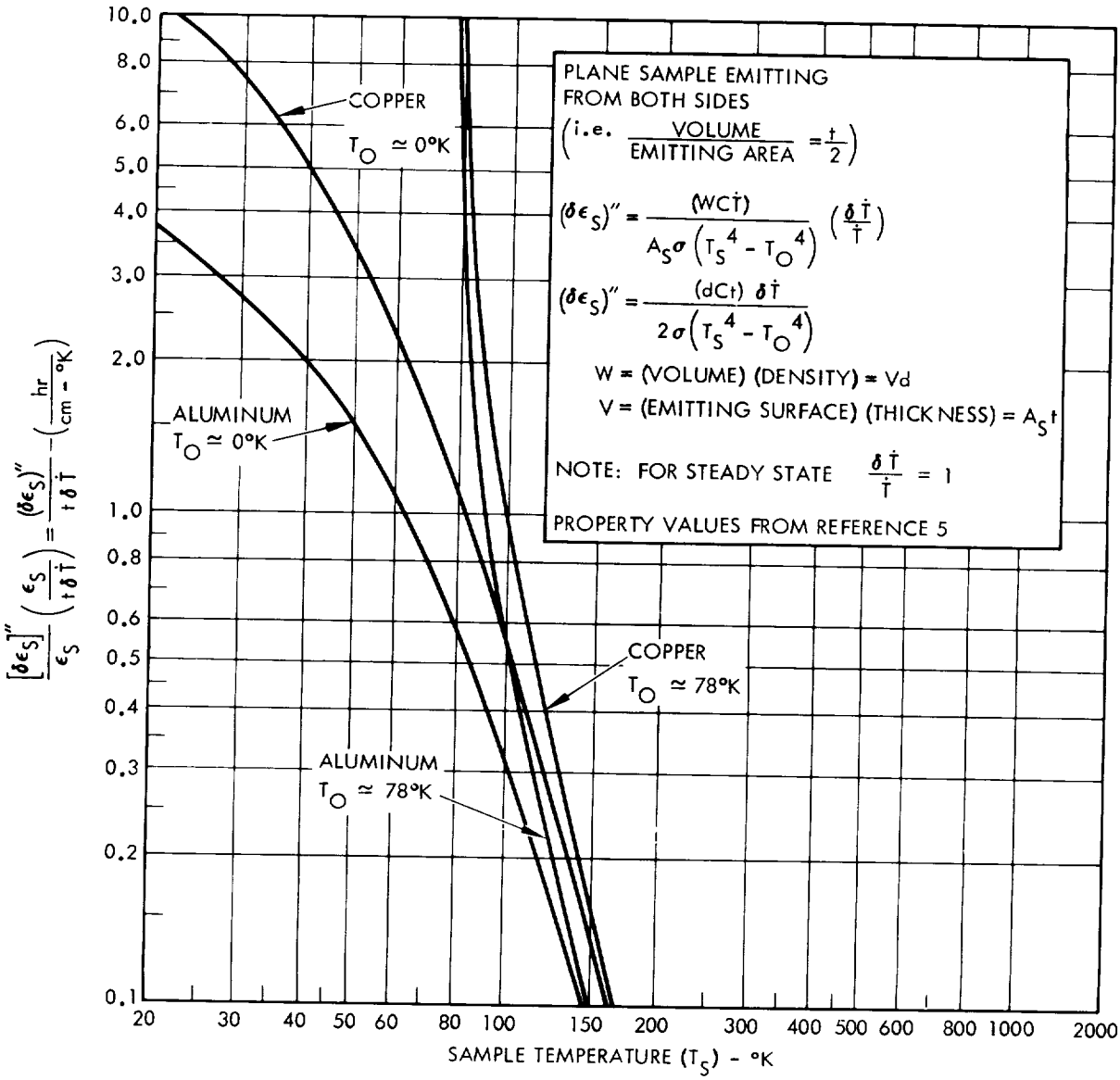

FIGURE 8–3.—Error contribution for internal energy emitted by sample.

and value of the ratio of specific heats (γ) was taken as 1.41. If the conduction through the air is neglected, the error in the heat loss (q_l) is given by equation (13):

$$q_l = q_{ca} \tag{14}$$

Consequently, the contribution to the total error is equation (13) multiplied by $[\sigma(T_s^4 - T_0^4)]^{-1}$. In figure 8–5, the calculation of the error resulting from neglect of this loss is given as:

$$\frac{(\delta\epsilon_s)^{IV}}{P} = \frac{q_{ca}}{P\sigma(T_s^4 - T_0^4)} \tag{15}$$

The Non-Gray Error, Equation (7)

The most frequent assumption made in the calorimetric method, steady state, or transient modes is that the emittance of the sample is equal to its absorptance. The emittance is related to the energy spectrum of the sample, whereas, the absorptance depends upon the radiosity of the surrounds and the absorptance of the sample to this surrounds radiation. Since the surrounds are generally at a low

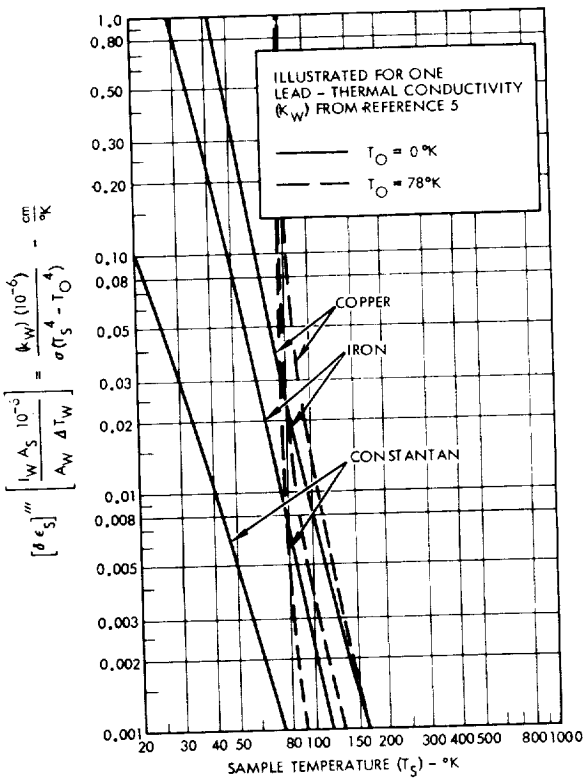

FIGURE 8-4.—Error contribution from lead conduction loss.

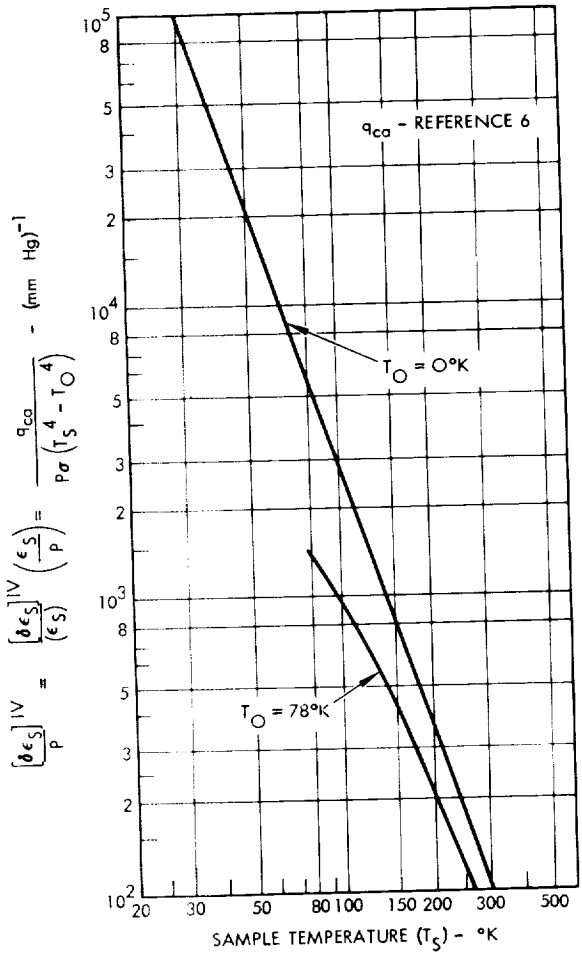

FIGURE 8-5.—Error contribution from conduction through the residual air in the evacuated enclosure.

temperature, the spectral absorptance of the sample must be known or assumed at very long wavelengths (30 microns and greater). Very little is known about the spectral characteristics of materials at these wavelengths, and only for pure polished metals does theory and limited experiment provide adequate assurance that this assumption is reasonable. Should an ideal metal sample become contaminated with an oxide, this assumption could become an invalid one.

Equation (7) is for the total non-gray error, but the most important term is the last one:

$$\left[\frac{(T_0^4)}{(T_s^4-T_0^4)}\right]\left[\frac{\delta(\Delta\alpha_s)}{\epsilon_s}\right] \tag{16}$$

As with the heat measurement error, this error contribution can be expressed as an increment to $\delta\epsilon_s$ but the evaluation is more readily performed with emittance of the sample (ϵ_s) included. To determine this portion of the non-gray error, two extreme cases of the spectral properties of a surface are used: (1) $\epsilon_\lambda=\alpha_\lambda=1$, $0\leq\lambda\leq\lambda_c$; $\epsilon_\lambda=\alpha_\lambda=0$, $\lambda\geq\lambda_c$ and (2) $\epsilon_\lambda=\alpha_\lambda=0$, $0\leq\lambda\leq\lambda_c$; $\epsilon_\lambda=\alpha_\lambda=1$, $\lambda_c\geq\lambda$. The expressions for $\delta\epsilon_s/\epsilon_s$ for the last term in equation (7), under the assumption $\alpha_s=\epsilon_s$ are:

Case 1:

$$\left[\frac{\delta\epsilon_s}{\epsilon_s}\right]^V=\left(\frac{T_0^4}{T_s^4-T_0^4}\right)\frac{\int_{\lambda_c T_0}^{\lambda_c T_s}\frac{E(\lambda T)}{\sigma T^5}\,d(\lambda T)}{\int_0^{\lambda_c T_s}\frac{E(\lambda T)}{\sigma T^5}\,d(\lambda T)} \tag{17}$$

Case 2:

$$\left[\frac{\delta\epsilon_s}{\epsilon_s}\right]^V=\left(\frac{T_0^4}{T_s^4-T_0^4}\right)\frac{\int_{\lambda_c T_0}^{\lambda_c T_s}\frac{E(\lambda T)}{\sigma T^5}\,d(\lambda T)}{\int_{\lambda_c T_s}^{\infty}\frac{E(\lambda T)}{\sigma T^5}\,d(\lambda T)} \tag{18}$$

where:

$$\frac{E(\lambda T)}{\sigma T^5}=\frac{C_1}{(\lambda T)^5[\exp.\,(C_2/\lambda T)-1]} \tag{19}$$

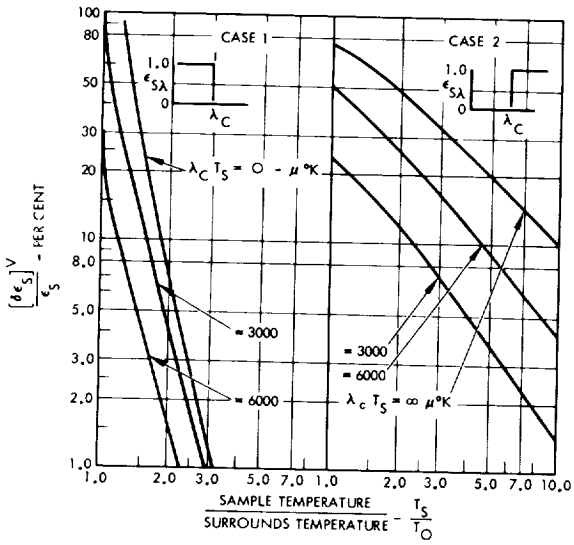

FIGURE 8–6.—Error contribution from an idealized non-grey sample.

Equation (19) is the non-dimensional form of Planck's equation and was tabulated by Dunkle (ref. 1). The maximum values of $\delta\epsilon_s/\epsilon_s$ can be obtained from equations (17) and (18) and will be found to occur at $\lambda_c T_s = 0$ and $\lambda_c T_s = \infty$ respectively. The magnitudes of the error contribution obtained from equations (17) and (18) are shown in figure 8–6.

The results given in figure 8–6 are applicable to either calorimetric or radiometric measurements of the sample emittance. These results differ from those given by Edwards and Nelson (ref. 2), since they maximized only for $\Delta\alpha$. Figure 8–6 is a more general approach since the maximum value of either expression is obtained at small or large values of $\lambda_c T_s$ rather than at the value of $\lambda_c T_s \approx 2900$ found by Edwards and Nelson.

The Edge-Effect Error, Equation (8)

The expression for the error resulting from neglect of the edge of a sample is given in equation (8). Examination of this relation will show that it contains each of the errors in the total sample emittance error (eq. (5), (6), and (7)) but in terms of the unknown edge emittance. The important multiplying factor in this error contribution is the ratio of edge area to sample area and this error can only be minimized by reducing this ratio. A sphere has an edge to emitting surface area ratio of zero except for connectors or assembly joints. Other geometries will have finite edge areas and, hence, this term must be included.

SUMMATION

The various error contributions given by equations (5), (6), (7), and (8) have been treated in the preceding discussions. For the conventional error, equation (5), the error from an incorrect temperature measurement was described (fig. 8–2); the heat measurement error, equation (6), was expressed as a lead conduction loss (fig. 8–4), an error contribution from the assumption of steady state (fig. 8–3), and an air-conduction loss (fig. 8–5); the assumption of sample emittance equal to the sample absorptance was given by equation (7), and one term of this error was described (fig. 8–6); and the neglect of edge losses, equation (8), was discussed briefly. For equations (5) through (8), certain terms were selected for elaboration, and, of these, the neglect of the internal energy under the steady state assumption (eq. (10), fig. 8–3), the air conduction loss (eq. (15), fig. 5) and the non-gray error contribution (eq. (17) and (18), fig. 8–6) are not generally considered in the literature. The sample temperature measurement error, the lead wire loss and the remaining terms of equations (5) and (6) are almost always considered. The edge-effect error contribution, equation (8), is frequently neglected. Thus, the important error contributions are those which have been ignored in the past.

The magnitude and importance of the error contributions usually considered cannot be understated. Figures 8–2 and 8–4 exemplify this. For example, an error in sample temperature measurement of 0.25° K will cause an error contribution of approximately 3% for 78° K surrounds (liquid nitrogen) as the sample temperature approaches 90° K; but under the same surrounds and sample temperatures, this error is over 10% for a sample temperature uncertainty of 1° K. The heat loss by conduction from a single wire is similarly important. In figure 8–4, the wire conduction loss is related to the parameter:

$$\frac{A_s l_w}{A_w \Delta T_w} \times 10^{-6}$$

This quantity has a value of unity for the conditions of:

$A_s = 10$ cm^2

$A_w = \frac{10^{-4}\pi}{4}$ (approx., 0.01-cm or 0.004-inch diameter wire)

$l_w = 7.8$ cm

$\Delta T = 1$.

Hence, neglect of this loss can cause an error of approximately 0.01 in ϵ_s at a sample temperature of 80–100° K for an iron lead and 0.05 for a copper lead; these values increase by a factor of 10, if the sample temperature is reduced to 50° K. In terms of percentage error, these contributions can easily represent an error of 10 to 100% for a polished metal sample. If the temperature of the surrounds is that of liquid nitrogen (78° K), the error is significantly larger. The lead loss could essentially be eliminated, if a super-conducting material were used for the leads. However, this would apply to sample temperatures below 18° K and the other contributions to the total error would make such a measurement impractical. These error contributions would be increased for liquid nitrogen surrounds. Emphasis should be made of the fact that this is for a temperature difference of only 1° K in a 7.8-cm wire length and can be considered to represent the uncertainty in temperature when correcting for lead losses.

The edge effect error, equation (8), is dependent upon the sample geometry selected and the manner of fabricating the sample. A spherical sample will minimize this error contribution, but this geometry will require a significant time for cooling to the desired temperature. In addition, a spherical sample is not as convenient experimentally as other geometries. If various materials are to be measured, each surface requires a new sample sphere or the same sphere must be reused. Applying coatings upon the same spherical sample can be difficult since many electrochemical coatings are not compatible with any arbitrary material. Several spherical sample holders necessitate calibration of each holder in terms of specific heat, thermal conductivity, area, heat loss, etc. An alternative is a thin disk or rectangular foil sample composed of the desired material with or without a coating. The edge effect error contribution must now be considered. Its magnitude may become significant since equation (8) contains all the terms in equations (5) and (7) but for the properties of the sample edge and sample temperature. By making the ratio of sample edge to sample emission area small, the multiplier of all terms in equation (8) can be minimized. This ratio is not small for a disk sample since the total sample thickness must include an internal heat source and/or other instrumentation.

A disk geometry for a sample is not easily adapted to a transient measurement for the restriction on edge to sample area requires the sample to be thin, but this condition is not compatible with the need for accurate knowledge of the internal heat capacity (wc). If coated samples are used, the coating may be a significant but unknown fraction of the total sample heat capacity. This indefiniteness would be reflected in an increase in the heat capacity error contributions of equation (6).

The foregoing discussion indicates the design and construction of a calorimetric method is a series of accuracy compromises. Instrumentation, lead losses, edge area, sample size, sample geometry, etc., must all be considered together. The error contributions given in figures 8–3, 8–5, and 8–6 can be placed in a different category; they are error contributions in the calorimetric system that are difficult to eliminate. The neglected internal heat capacity of a steady state measurement or the uncertainty in the quantity $\delta \dot{T}$ of a transient measurement can be a very difficult error factor. For a sample 1 mm thick and an uncertainty in the temperature transient of 1° K/hr, the increment in ϵ_s is approximately 0.1 with a sample temperature of 90° K and liquid nitrogen cooled surrounds. For a polished metal sample, this represents an error contribution in excess of 100%. If the sample temperature is restricted to a minimum of say 200° K, the error contribution can be held within a tolerable limit.

The importance of a high vacuum is demonstrated by the curves given in figure 8–5. If a pressure of 10^{-4} mm Hg is used, an error increment of 0.10 is introduced in the measure-

ment at a sample temperature of approximately 100° K. If a lower sample temperature is required, the vacuum must be correspondingly greater, 10^{-6} to 10^{-8} mm Hg, for the same value of error increment.

The portion of the non-gray error presented in figure 8–6 is an upper limit obtained by idealizing the spectral properties of a material. Practical examples of such extreme properties are difficult to find for little is known about the spectral properties of materials at long wavelengths ($\alpha > 30$ microns). It is one of the basic problems of the calorimetric method since the method is generally considered the easiest technique for measuring practical thermal radiation properties at these wavelengths. However, an example of case 1 could be a metal surface coated with SiO_2–SiO. Such a coating corresponds to quartz, and quartz begins to become transparent in the wavelength region of 40–50 microns. Since an apparent incentive to using the calorimetric method for emittance measurements is the accuracy attained with metal samples, it is disturbing to note that case 2 would correspond to a "perfect" metal sample with a coating or oxide film which becomes opaque at very large wavelengths. An example of case 2 might be a silicon sample with a vacuum deposit of aluminum on the back surface, e.g., a material transparent to approximately 20–30 microns and opaque beyond this wavelength. Practically, few materials will correspond to these idealizations but the possible magnitude of this error contribution should not be overlooked. For example, in liquid nitrogen surrounds a sample at a temperature of 200 °K can be in error by several per cent for case 1 or an order of magnitude larger for case 2. Use of liquid helium surrounds will decrease this error for the same sample temperature.

With the exception of equation (5), the error contributions can be described in terms of either an increment to the total error or as a percentage error in the quantity ϵ_s. The latter concept is most often used and is the one normally reported. The increment in the error is a useful approach to the problem of errors since the increments are independent of the value of emittance (ϵ_s), and they act as lower limit to the accuracy of emittance. Thus, an increment of 0.01 may not be significant if ϵ_s equals 0.9, but it is very important if an emittance of 0.05 or less is to be measured.

CONCLUSIONS

The design, construction and operation of a calorimetric emittance measuring instrument requires care and attention. The calorimetric method is not, in itself, the quick solution to emittance measurements at low temperatures. In all but one of the error contributions discussed (gaseous conduction loss, figure 8–5), liquid helium or hydrogen cooled surrounds will reduce the total error. The use of liquid nitrogen cooled surrounds probably limits operation to a sample temperature of 200 °K. The colder surrounds will allow measurements to be made at sample temperatures down to about 100 °K.

REFERENCES

1. Dunkle, R. V.: Thermal Radiation Tables and Applications, Trans. Am. Soc. Mech. Engrs. 76: 549, 1954.
2. Edwards, D. K., and Nelson, K. E.: Maximum Error in Total Emissivity Measurements due to Non-Greyness of Samples American Rocket Soc. Jour. 31: 1021, 1961.
3. Gaumer, et al: Calorimetric Determinations of Thermal Radiation Characteristics, Progress in International Research on Thermodynamic and Transport Properties, p. 575, American Soc. Mech. Engrs., Academic Press, 1962.
4. Gray, D. E., ed.: American Institute of Physics Handbook, McGraw-Hill, 1957, pp. 4–13.
5. Johnson, V. J., ed.: A Compendium of the Properties of Materials at Low Temperature (Phase I), Part I. Properties of Solids, National Bureau of Standards Cryogenic Engineering Laboratory, WADD Technical Report 60–56, Contract No. AF 33(316)–58–4, Project No. 7360, October 1960.
6 Scott, R. B.: Cryogenic Engineering, Van Nostrand Co., 1959, pp. 145–6.
7. Snyder, N. W.: "Radiation in Metals", Trans. Am. Soc. Mech. Engrs. 76: 541, 1954.

DISCUSSION

CORRUCCINI: Thank you very much Mr. Bevans. I think a careful error analysis of this kind is extremely valuable as a guide to experimentalists who may overlook or perhaps make only very rough estimates of some of these things that you have discussed.

L. MCKELLAR, Lockheed: May I have the first slide please? These are more in the way of comments than anything else. One thing on which Dr. Corruccini might comment is the expression you have there, the Hagen-Rubens expression, the theoretical expression. I believe that approaching 200° K or lower this really is no longer applicable, and the curve has less of a slope. I think to the left of 300° K probably it is closely applicable. I'm not sure about this, perhaps Dr. Corruccini can comment.

But more directly, in our paper of last winter, we pointed out that we did not believe the increase in emittance shown at temperatures below around 400° K, 500° K because we felt, as Mr. Bevans pointed out, that this may have been due to gaseous conduction. Because of that we instituted a look into gaseous conduction. Unless I'm mistaken one of the equations we evaluated was the one that Mr. Bevans showed, and I think this depends on an assumption of a Maxwellian velocity distribution for the gases remaining in the chamber. I believe this is the assumption usually made and is normal in calorimetric techniques. But having a large temperature ratio from wall to sample, the distribution is not Maxwellian. How important the departure from the Maxwellian is, it is hard to assess. Consequently, I would advise that what we really want is a criterion for pressure at which we could neglect gaseous conduction. I think the general approach that Dr. Gordon showed—taking the maximum possible energy of the molecules leaving the chamber wall and the maximum possible energy of the molecules leaving the sample and finding the difference—would give a useful criterion because it certainly gives an upper limit which is really what we want.

BEVANS: I should turn this over to Dr. Corruccini. I cannot argue whether the theory is good below 200° K or not. Obviously the dotted line went a little bit below it. Around 273° K, spectral data compare well with the Hagen-Rubens relations, but this theory is usually the upper limit in reflectance. If the data are above that in reflectance or below that in emittance, one begins to worry about the instruments. I think that it is useful at least from the point of view of establishing trend. We purposely avoided citing the reference specifically on the slide as we felt that it is only important to look at the trend. Also, we tried to avoid any comment about magnitude.

CORRUCCINI: I think the point that Mr. Bevans was making with the slide is qualitatively valid. Although one hardly expects quantitative agreement between theory and experiment, one does expect agreement as to the *sign* of the temperature dependence.

BEVANS: As for your other question about the use of Knudsen's equation, we got the expression from Scott, and I have to admit that I have not looked at the original reference. I can see at least one individual in the audience who probably could answer the question about whether that equation is valid or not. I do agree that a balance of kinetic energy is a much better one since it forms an upper bound. In a similar manner, the non-gray error mentioned in your question, forms an upper bound. This is the maximum error one could anticipate. The practical aspects of this non-gray error analysis are open to question because of the idealizations that have been made. The only thing they do, as far as we are concerned, is wave a red flag at us.

TOULOUKIAN, Purdue Univ.: Referring to your first slide comparing experimental data with theory, I believe the sole purpose of this is to give the theoretical bounds rather than a comparison of experiment with theory. The theoretical predictions may not be compared with observed data since the theory is for an ideal model, and the experiment is on a real sample. The knowledge of the theoretical bounds is useful. In our own work, we use this criterion as a tool, at least to screen data that fall above it.

BEVANS: This does raise a point. You omit data that fall above the values predicted from the Hagen-Rubens relation. The question was raised this morning as to whether the simple Hagen-Rubens relation is a good approximation in the cryogenic region. I think that possibly it is even open to some question in the temperature region that I used. I don't know as I haven't looked at it carefully.

GAUMER, Lockheed: Since Dr. Caren was making cryogenic emittance measurements he has looked into it, and to the very best of our knowledge the Hagen-Rubens relationship is completely inapplicable in the cryogenic area. I would certainly not use that as an upper or lower bound for anything.

BEVANS: Which way does it lie, Dr. Gaumer?

GAUMER: I do not know which way it lies, but it is very involved with the anomalous skin effect, and you cannot justify a treatment of that kind at the wavelengths that we are discussing.

BEVANS: Well, the slide showed temperature roughly above 200° K.

GAUMER: I understand that, and I agree with the slide. But we are now slanting the discussion to cryogenic regions which are the region where you have the possibility of serious errors in calorimetric determinations.

BEVANS: I open the question even to above 200° K.

GAUMER: We don't know; we don't dare use the balance.

BLACKMON, Air Force Calibration Lab.: I was wondering, Dr. Corruccini, if you had any experience with air bubbles being formed on the surface of metals, say, possibly, when liquid nitrogen is poured right up against the surface of the metal. This came up when we were trying to cool lead sulfide detectors by pouring liquid nitrogen directly on them. By dropping thermocouples right at the surface we found a difference of 25° K from the liquid nitrogen temperature which is 77° K. By looking with a microscope we found that

there were air bubbles right on the surface. I wonder if this is something that might exist with other metals, that a tremendous error might arise from assuming that the surface temperature is the same as that of the liquid nitrogen. Have you any experience in that area?

CORRUCCINI: If you have a large heat flux from the solid to the liquid, you can have a substantial film ΔT. I hope this was the situation with you as I wouldn't be able to explain it otherwise.

BLACKMON: Would you say that this is something that might exist with other metals? The only way to get the temperature down was to push a thin aluminum rod down in the liquid nitrogen and let the aluminum rod touch the sample. By conduction, the heat went from the detector up the aluminum rod, and we were able to reduce the temperature considerably.

CORRUCCINI: Essentially you are adding more heat transfer surface area in that way. Such surface heat transfer is more a property of the fluid than of the solid, and it depends entirely on the heat flux that you are delivering across the interface. Was the metal in good thermal contact with the exterior through a solid support or something of that sort?

BLACKMON: Around this specimen was vacuum, and we could only assume that it was these air bubbles that were preventing the specimen from getting down to the temperature of liquid nitrogen. I was wondering if it might be expected, with copper or any other material, that you will never get the surface down that close even though you pour the liquid nitrogen right up against the surface.

CORRUCCINI: Was there active boiling?

BLACKMON: Yes, and it was allowed to settle for over an hour.

CORRUCCINI: But were these bubbles stationary on the surface?

BLACKMON: Yes, right against the surface. You could see them with a microscope.

CORRUCCINI: In that case, I don't know what your trouble was unless your temperature measurements were way off. If it were actively boiling, it would just be the film ΔT; if not, then I don't know.

GAUMER: I would like to comment again on this heat loss by residual gas conductive losses. I think the applicability of the Knudsen equation is at least questionable. We are looking into this, and it turns out to be rather abstruse theoretically and a difficult problem in that respect. But, practically, it is never a difficult problem. It is a very simple thing to do. You make a run at 10^{-4}, you make another run at 10^{-5}, 10^{-6} and so on. When you get the same apparent emittance at successively lower pressures, it seems physically obvious that you cannot have a pressure-dependent loss term. Now, we have done this, and we find that below 10^{-6} for sample temperatures around 200° K there is no change in apparent emittance, which tells us, regardless of what the theory is explaining the mechanism, pressure is not having an important effect on the apparatus.

BEVANS: Yes, but Dr. Caren of your group does need his low pressures because of the level of the heat fluxes involved at these low temperatures.

GAUMER: That is true, but he has 10^{-10} using liquid helium. You are quite right; we require a very low pressure there.

SESSION III

MEASUREMENTS AT SATELLITE TEMPERATURES (200° to 450°K)

Chairman: GERHARD B. HELLER

9—REQUIREMENTS FOR EMITTANCE MEASUREMENTS OF THERMAL CONTROL SURFACES OF SPACECRAFT

BY GERHARD B. HELLER

NASA GEORGE C. MARSHALL SPACE FLIGHT CENTER, HUNTSVILLE, ALABAMA

This paper is an introduction to the discussion of measuring techniques for the emittance of spacecraft surfaces. It discusses the required physical properties and their ranges for the thermal design of spacecraft. The parameters affecting thermal equilibrium are discussed; the emittances of the spacecraft surfaces in various wavelength regions are important physical properties for the thermal design. The various types and properties of radiative fluxes to and from the spacecraft are summarized. From this, the required ranges are derived for the determination of emittance and transparency of surfaces. Requirements are given for one type of surface important to the Manned Lunar Landing Project.

The design of the first U.S. satellite, Explorer I, required the study of a new problem, which is now generally known under the term, "thermal design" (ref. 1, 2, 3, 4, 5, and 6). Without a thorough analysis of all thermal aspects, the temperatures may fall anywhere within the range of 200° to 500° K and may also fluctuate in the whole range. This range exceeds by far the tolerances of instruments and batteries. By proper design this range can be narrowed to a band of ±30° C or, in some cases, to ±15° C by passive control. A closer temperature control can be obtained by various degrees of active or semi-active controls. Parameters affecting the thermal design fall into three classes:

(1) mechanical design parameters, such as size, geometrical shape, component arrangement, etc.

(2) physical properties, such as thermal conductivity, thermal emittance, contact resistance, outgassing, etc., and the dependence of these properties on the effects of the space environment.

(3) orbital characteristics, attitude of the spacecraft and position relative to the sun, depending on day and hour of launching.

Control of the on-board temperatures can be achieved passively by selecting the time of launching, emittance of the surface materials, and attitude of the space vehicle. The surface emittances and the time variation of these emittances due to the space environment are the most important parameters, once the time of launching and the attitude are determined. The same is true for active control systems which utilize variable control surface.

Prior to 1957, a comparatively small research effort went into the thermal emittance analysis and into the measuring techniques for determining emittances in the visible and IR (infrared) spectral regions for this purpose. The advent of the first satellites brought an increased interest in this subject. However, the excellent record of Explorer I, which was kept at 21° ± 20° C throughout the battery life of three months (ref. 3 and 4) seemed to indicate that there is no problem, or that all the problems had been solved. Consequently, temperature-measurement sensors were eliminated from subsequent Explorer satellites because of limitations in the available telemetry channels. However, due to the failure of Explorer III after 43 days and similar occurrences in other spacecraft, it was found necessary to measure temperature in all succeeding spacecraft. These early experiences are interesting if we compare them with the present efforts. Now, thermal design is a well-established and recognized part of every space vehicle effort. The necessity for flight testing

TABLE 9–I.—*Types of Radiation Affecting Thermal Equilibrium of Surface of Spacecraft*

Type of radiation	Approximate wavelength range (λ), μ	Blackbody Temperature °K	λ of maximum Spectral Intensity at (μ)	Other characteristics
Direct solar	0.2 to 3	6000	0.48	Collimated within 8-sec. arc circularly polarized.
Earth-albedo; Lunar-albedo.	0.2 to 3*	6000	0.48	Hemispherically diffuse radiation, high contents of polarized light.
IR radiation from surface of earth.	3 to 30	288 (mean value)	10	Hemispherically diffuse radiation.
IR radiation from atmosphere.	3.5 to 35	250 (mean value)	11.5	Hemispherically diffuse radiation.
IR radiation from surface of space vehicle.	3 to 30	Typical value 288	10	Depends on surface material.
IR radiation from surface of moon.	10 to 100	120	24	Very likely hemispherically diffuse radiation.
	2 to 20	400	7	
Solar UV; Solar X-ray; Van Allen radiation; Cosmic radiation.	0.1 to 0.2			This is not important for the heat flux balance, but affects design surfaces.
X-rays; γ-rays, neutrons from nuclear devices on board.				Effects on both the thermal flux equilibrium and on damage to thermal design surfaces.

*It is generally assumed that the spectral distribution of the albedo (reflectance of earth and similar bodies) is such that the reflected radiant flux has the same spectral distribution as that incident from the sun. It is not known how accurate this assumption is in the whole solar spectrum.

of temperature sensors is generally accepted. The purpose is twofold: (1) monitoring (to determine the effectiveness of the thermal design), and (2) testing of specially prepared sensors (to investigate the effect of the space environment on new control surfaces). It is gratifying to know that enough high quality work is being performed to justify a symposium on the laboratory measuring techniques for determining emittance. Earlier discussions of requirements are given in references 2, 4, 5, 6, 7, 8, and 9.

Table 9–I summarizes the types of radiation that interact with the space vehicle surface and that have a decisive effect on its thermal equilibrium. From this list of the radiative environment we can determine the requirements for measurements and for the simulation of the space environment in the laboratory. (See also references 6 and 10.)

The physical quantity we intend to determine is the emittance of the surface materials in all spectral ranges of electromagnetic waves in the solar spectrum and the IR spectrum. In computing thermal balance for spacecraft it is necessary to consider the radiation properties of many components; these properties are determined only partly by the internal constitution of the materials. Another important factor is the surface texture, and when the outer layer of material on any component transmits significantly the emittance of the substrate contributes to that of the whole unit. The information needed is the emittances of the bodies as used, for consideration in conjunction with actual flux magnitudes. Summaries of some theoretical and experimental results are given in references 8, 9, 11, 12, and 13.

There is an unfortunate confusion in the area of the nomenclature. However, some excellent work on standardization has been done by NBS (ref. 14). Figure 9–1 describes a typical situation for a spacecraft. The spacecraft radiates energy in the IR spectrum and absorbs electromagnetic energy in the UV (ultraviolet), visible, and near-IR from the sun, and the longwave-IR radiation from the earth and the atmosphere. The albedo (reflectance) of the earth and similar bodies provides some reinforcement of direct solar radiation. For

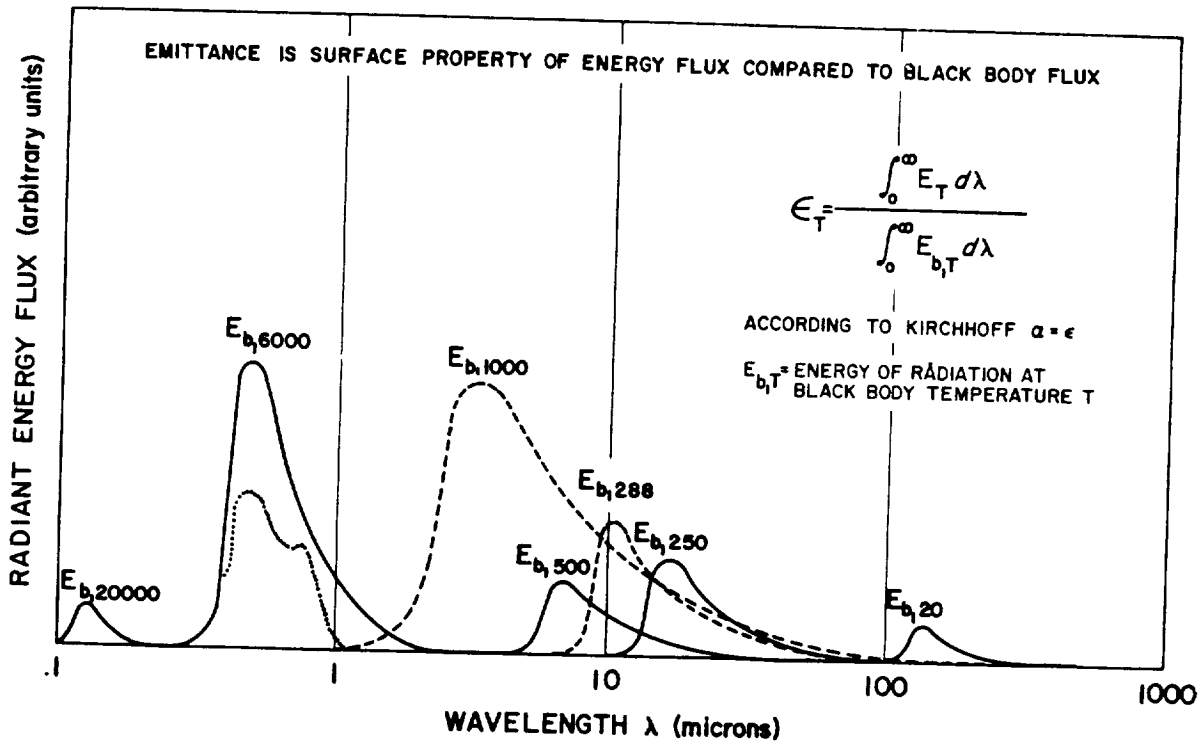

FIGURE 9–1.—Typical blackbody energy fluxes of spacecraft radiation environment.

components of nuclear systems we can expect that the spacecraft will also emit energy in the near infrared and visible spectrum. In all cases, we deal with the same physical phenomenon. According to Kirchhoff's law, we have the general relationship (ref. 15)

$$\alpha = \epsilon \text{ or } \alpha/\epsilon = 1 \tag{1}$$

which applies for all types of specimens. The conventional definition is being used for α and ϵ by referring them to a blackbody flux at a given temperature. Figure 9–1 shows schematic spectral distributions of the blackbody fluxes in various temperature regions significant for spacecraft. The dotted line under the $E_{b,6000}$ curve shows the fraction of blackbody flux that might be absorbed by the spacecraft in this spectral region. The emittance or absorptance is a dimensionless number given by the ratio of the integrated energy fluxes.

$$\epsilon_T = \alpha_T = \frac{\int_0^\infty E_T d\lambda}{\int_0^\infty E_{b,T} d\lambda} \tag{2}$$

where

E_T spectral radiative flux of specimen, at temperature T

$E_{b,T}$ spectral radiative flux of blackbody at temperature T

λ wavelength.

For each of the blackbody flux curves (fig. 9–1) the total emittance values needed may be computed with equation (2). The integral from zero to infinity of the blackbody flux curves should be used only for specific blackbody temperatures. This is indicated by the index T in equation (2). According to equation (1), emittance and absorptance values of a specimen are identical at any wavelength or summed for all wavelengths. Ratios of various emittances (or absorptances) should not be used without indication of the respective temperatures for which they apply.

It should also be pointed out that for some systems, the energy emitted via radio antennas, which covers emittance in another portion of the electromagnetic spectrum, is not negligible

in the energy household of the spacecraft. For some materials, especially those with mirror-type surfaces, the important quantity is the reflectance ρ. We know that according to energy considerations we have for opaque bodies

$$\rho = 1 - \epsilon \tag{3}$$

which means that for opaque bodies the quantity ϵ is sufficient to define the radiative properties. For measuring procedures in the laboratory, the following well-established symbols are used (ref. 15):

ρ reflectance
ϵ emittance
α absorptance

These quantities are all ratios. Reflectance and absorptance are fractions of incident flux. Emittance is always a fraction of the radiative flux of a blackbody at the specimen temperature; hence, for equations (1) and (3) to be valid, ρ and α must also represent fractions of the same blackbody flux. All three quantities can be used to describe the radiation property of a material and can be converted from one to the other by equations (1) and (3). It is arbitrary which one we use; however, it would simplify matters if we convert all values to one of the three. I would propose using only the emittance for the definition of the physical properties, and indicating the applicable temperature by subscripts, such as ϵ_{1000}, ϵ_{288}, ϵ_{300}, etc.

The often-used symbols ϵ_s or α_s for emittance or absorptance of bodies for radiation in the solar spectrum requires a better definition of the solar spectrum used for the computation. Standardization would be highly desirable.

It is generally assumed that satellite temperatures depend on the ratio of emittances $\epsilon_s/\epsilon_{300}$ which is identical with α_s/α_{300}. It should be pointed out that this ratio must be used in conjunction with actual flux of incident solar energy and allowances made for frequent changes in flux of both incident and emitted energy accompanying changing temperatures in outer layers of the satellite. The mean temperatures of several spacecraft having the same α_s/α_{300} ratio can be quite different. From the types of radiation listed in Table 9–I, we can derive the requirements for simulation in the laboratory.

The spectral emittance is needed as a function of angle of incidence i, temperature T, the amount p, and angle θ of polarization of incident radiation.

In the case of IR radiation, spectral emittance is needed because effective temperatures have to be considered in the range from cryogenic temperatures to white-hot surfaces. In the latter case the whole range of radiation from visible to IR is required. A much neglected area is the spectral range from 15 to 100 microns and above. The equilibrium temperature of a space vehicle in a low earth orbit, but shielded from the sun, is about 200° K. At this temperature, 75% of the IR radiation is emitted above 15 microns. Extrapolated values of the spectral emittance are likely to be in error. If values considerably above 15 microns are not available, total emittance values for a number of typical temperatures may be more meaningful. The following temperatures are suggested as typical for the surfaces of spacecraft materials in equilibrium with the space environment: 150°, 200°, . . . 450°, 500° K. For interplanetary probes close to the sun or to the outer planets these limits will have to be extended. Both total normal and total hemispherical emittances are needed. Measurements such as these are directly applicable to the analysis of thermal design parameters, and supplement the spectral emittance measurements.

For materials that are transparent, or partially transparent, it is necessary to measure both emittance and transmittance of each layer of a multilayer system, e.g., optically coated glass slides over solar cells. We need for each layer spectral emittance and spectral transmittance, as functions of angle of incidence i, temperature T, the amount p, and angle θ of polarization of incident radiation.

Experimental techniques for measuring emittances of space vehicle surfaces are of interest in considering thermal radiation properties of materials in the range of satellite temperatures (refs. 16, 17, 18, 19, 20, 21, and 22). Instruments for such measurement are well known to investigators in this field under the following descriptive terms: portable field instrument,

calorimeter, specular integrating hemisphere, Hohlraum, total normal emissometer, and reflectometer.

A paper by Neel and Robinson (ref. 22) describes measuring techniques and results of a space experiment that was flown on the S–16, also known as the OSO (Orbital Solar Observatory).

Laboratory techniques allow us to determine the emittance of well-defined surfaces. We can subject these to various types of simulated environments and study the effect on the emittance. The space experiment shows us how good our assumptions were. This type of experiment is very important for the development of thermal design surfaces for space application. Until now, this type of experiment has been neglected. However, more emphasis is now being placed by various organizations within NASA on thermal sensor experiments. Two examples are a follow-up experiment on the OSO and a set of sensors on a Saturn vehicle.

One point that cannot be overemphasized is the importance of a complete description of the surfaces of materials that are to be measured. Results depend very strongly on the prior history and preparation of a surface. It is necessary to know whether the sample in the laboratory is the sane as the surface on the spacecraft.

The emittance requirements for space vehicles employed in the Manned Lunar Landing Project are particularly for surfaces on the upper stages of the Saturn systems and the Apollo systems. The emphasis for both applications is on solar reflectors with low emittance in the solar spectrum range and high emittance in the IR spectrum range around 10 microns. Requirements can be summarized as follows:

(1) easy applicability
(2) little or no change due to aerodynamic heating and other atmospheric effects, and to vehicle vibration, etc.—thorough laboratory and flight testing required
(3) little or no change due to the space environment, such as UV, other radiation, thermal effects (especially thermal cycling), micrometeoroids, etc.—thorough laboratory and flight test program required
(4) low weight
(5) low cost

The radiation properties of a coating on a metallic substrate and compatible with the other requirements should be

ϵ_s as low as possible (0.2)
ϵ_{300} as high as possible (0.8)
τ_s may be from 0 to 1 (if it is >0, the underlying metal surface should be polished)
τ_{300} to be 0

In most cases, "white" coatings are considered to be opaque in both the solar and IR spectrum. From this list it should be apparent that opaqueness is required only for the IR and that a "transparent" coating on a polished metal fulfills the same requirement as a "white" coating. If the environmental effects during the boosting phase or the space environment cannot be eliminated, it is necessary to determine exactly the expected changes. These changes have to be reproducible and have to be known within close tolerances.

REFERENCES

1. Heller, G.: The Explorer—The Explorer Story and the Temperature Control of the Satellite Package. Jour. of the Franklin Institute, vol. 6, Dec. 1958, p. 89.
2. Heller, G.: Thermal Problems of Satellites. Materials in Space Environment. Proc. of the Fifth Sagamore Ordnance Materials Res. Conf. (issued by Syracuse University Research Institute), MET 597–596, Sept. 1958, pp. 89–126.
3. Heller, G.: Problems Concerning the Thermal Design of Explorer Satellites. IRE Trans. Mil. Elec., vol. MIL–4, no. 98, 1960.
4. Heller, G.: Thermal Control of the Explorer Satellites. ARS Jour., 1960, p. 344.
5. Jones, B. P.; and Heller, G. (Marshall Space Flight Center, NASA): Thermal Problems of the Saturn Payloads on the Moon. MNN–M–RP–4–60, July 1960.
6. Heller, G.: Thermal Environment and Control of Space Vehicles. Handbook of Astronautical Engineering (H. H. Koelle, ed.), McGraw-Hill Book Co., Inc., 1961.
7. Heller, G.: Introduction to Contractors Conference on Emissivities and Thermal Problems. Langley Research Center, NASA, Sept. 1960.

8. SCHOCKEN, K.: The Emission and Reflection of Radiation by Metals. Proc. Sym. on Radiative Transfer from Solid Materials (H. H. Blau, Jr. and H. Fischer, ed.), The Macmillan Co., 1962.
9. Research Projects Division (Marshall Space Flight Center): Optical Properties of Satellite Materials—The Theory of Optical and Infrared Properties of Metals. NASA TN D–1523, Mar. 1963.
10. JOHNSON, F. S.: Satellite Environment Handbook. Stanford Univ. Press, 1961.
11. RICHMOND, J. C.: Coatings for Space Vehicles. First Sym. Surface Effects on Spacecraft Materials (F. J. Clauss, ed.) John Wiley & Sons, Inc., 1960.
12. MERRILL, R.; SNODDY, W. C.; and SCHOCKEN, K.: The Results of Emittance Measurements Made in Relation to the Thermal Design of Explorer Spacecraft. NASA TN D–1116, May 1962.
13. GOETZEL, C. G.; and SINGLETARY, J. B.: Space Materials Handbook. Lockheed Missile & Space Company (AF Contract AF 04(647)–673), 1962.
14. HARRISON, W. N.; et al: Standardization of Thermal Emittance Measurements. Nat. Bur. Standards-WADC TR 59–510, Part I (Mar. 1960), Part II (Feb. 1961), Part III (Mar. 1962).
15. FORSYTH, W. E. (ed.): Measurement of Radiant Energy. McGraw-Hill Book Co., 1937.
16. FUSSELL, W. B.; TRIOLO, J. J.; and JEROZAL, F. A.: Paper 12. Portable Integrating Sphere for Monitoring the Reflectance of Spacecraft Coatings *in* Measurement of Thermal Radiation Properties of Solids (J. C. Richmond, ed.) NASA SP–31, 1963.
17. Op. cit. JANSSEN, J. E.; and TORBORG, R. H.: Paper 18. Measurement of Spectral Reflectance Using an Integrating Hemisphere.
18. Op. cit. BRANDENBERG, W. M.: Paper 10. The Reflectivity of Solids at Grazing Angles.
19. Op. cit. GORDON, G. D.; and LONDON, A.: Paper 16. Emittance Measurements at Satellite Temperatures.
20. Op. cit. STREED, E. R.; MCKELLAR, L. A.; ROLLING, R., Jr.; and SMITH, C. A.: Paper 25. Errors Associated with Hohlraum Radiation Characteristics Determinations.
21. Op. cit. ZERLAUT, GENE A.: Paper 29. An Apparatus for the Measurement of the Total Normal Emittance of Surfaces at Satellite Temperatures.
22. Op. cit. NEEL, CARR B.; and ROBINSON, GILBERT G.: Paper 20. Measurement of Thermal-Radiation Properties of Temperature-Control Surfaces in Space.

10—THE REFLECTIVITY OF SOLIDS AT GRAZING ANGLES

BY W. M. BRANDENBERG

GENERAL DYNAMICS/ASTRONAUTICS, SAN DIEGO, CALIFORNIA

An integrating sphere reflectometer for reflectivity measurements of imperfectly diffused samples as a function of angle of incidence from 15° to 88° is described. The measurements extend over a wavelength region from 0.19 to 2.65 μ. The performance of the integrating sphere is tested against theory and an error analysis is included.

The reflectivity of a surface is defined as the ratio of the reflected to the incident flux. It depends on the surface material, the wavelength of the incident radiation, and the angle the incident rays make with the normal to the surface. There are in principle two ways of measuring the reflectivity of an imperfectly diffuse surface (fig.10–1).

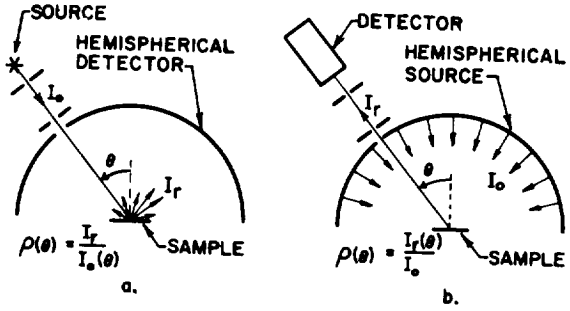

FIGURE 10–1.—Reflectometers: a—unidirectional, and b—diffuse illumination.

1. A collimated beam of monochromatic radiation is incident on the sample surface at an angle θ to the normal of the surface. The sample is placed at the center of a hemispherical detector of uniform sensitivity. The ratio of the reflected flux as measured by the detector to the total incident flux is equal to the reflectivity of the sample at the angle θ.

2. The sample is placed at the center of a hemispherical source of uniform brightness. The reflected flux is measured by an unidirectional detector making an angle θ with the normal to the sample-surface. The ratio of the reflected to the incident flux is again equal to the reflectivity of the surface at the angle θ.

It can be shown, using Helmholtz's reciprocity theorem (ref. 1), that the reflectivity measured by the two arrangements is the same.

As early as 1899, Paschen devised a hemispherical collector for diffuse reflection measurements. Since it was impractical to build a detector of uniform sensitivity, he replaced the detector by a polished and silvered hemisphere. The sample and the detector are placed next to one another at the origin of the hemispherical mirror which focuses the radiation reflected from the sample onto the detector (fig.10–2a). Many modifications of

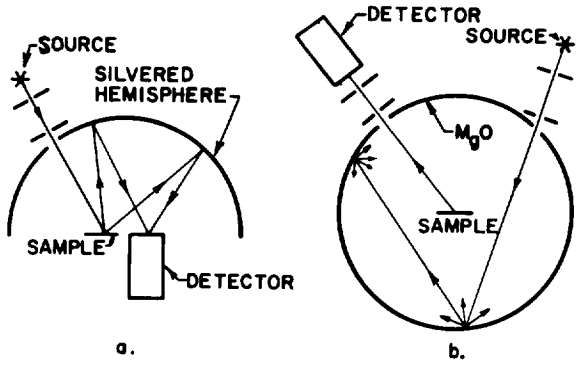

FIGURE 10–2.—Reflectometers: a—mirror and b—integrating sphere.

these so-called reflectometers have appeared over the years (ref. 2 and 3); some of them are built for varying angle of incidence. However, no one has ever completely solved the

problem of how to calibrate these reflectometers over the whole angular region.

A hemispherical source of uniform brightness is obtained by the use of an integrating sphere (fig. 10–2b). Integrating spheres have long been used in various ways in the photometry of light sources (Ulbrichtische Kugel). Such a sphere is usually made of two hemispherical metal caps which are coated inside with magnesium oxide (MgO). The application of the sphere to diffused reflection measurements is based on the assumption that the MgO coating reflects radiation according to Lambert's cosine law. As shown in fig. 10–2b, a collimated beam of radiation is directed through a port onto the wall of the sphere where it is diffusely reflected. The individual rays will again be diffusely reflected so that uniform radiation density inside the sphere and uniform brightness over the surface of the sphere results. For uniform illumination the sample may be placed anywhere within or on the surface of the sphere. For angular reflectivity measurements it is most convenient to place the sample at the origin of the sphere. If the sample is made to turn around its normal as well as around an axis perpendicular to the plane of incidence, reflectivity measurements for all directions of incidence are possible. Such an integrating sphere reflectometer is described in the next section.

INTEGRATING SPHERE REFLECTOMETER

Experimental Arrangement

The experimental equipment consists of a tungsten or ultraviolet lamp as a source, an integrating sphere, a double-beam spectrometer covering the wavelength region from 0.19 to 2.65μ, a phototube or lead sulfide detector, a chopper, a low-frequency amplifier, and a recorder (fig. 10–3). The mount holding the sample at the center of the sphere is in the form of a half cylinder. It turns around the vertical diameter of the sphere. The back of the holder is covered with MgO. The filament of the tungsten source or the arc of the ultraviolet lamp is focused, by a quartz lens, onto the back of the sample holder from which the radiation is diffusely reflected. Due to the cylindrical shape of the holder, the radiation

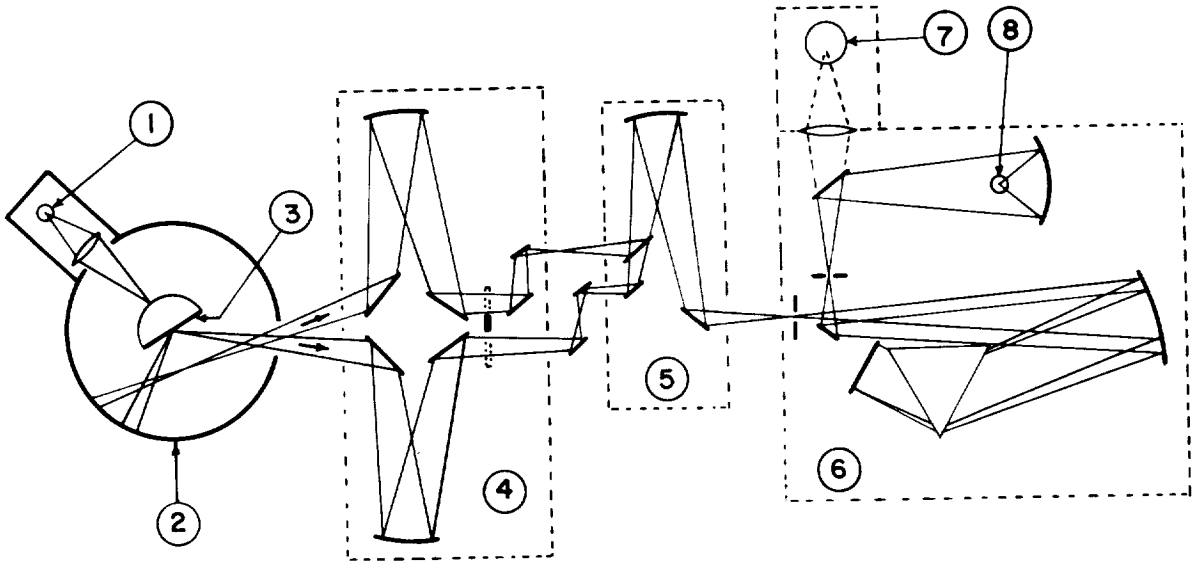

1. TUNGSTEN OR U.V. SOURCE
2. INTEGRATING SPHERE
3. SAMPLE
4. SOURCE - OPTICS
5. BEAM COMBINER
6. MONOCHROMATOR
7. PHOTOTUBE
8. LEAD SULFIDE DETECTOR

FIGURE 10–3.— Optical schematic of integrating sphere reflectometer.

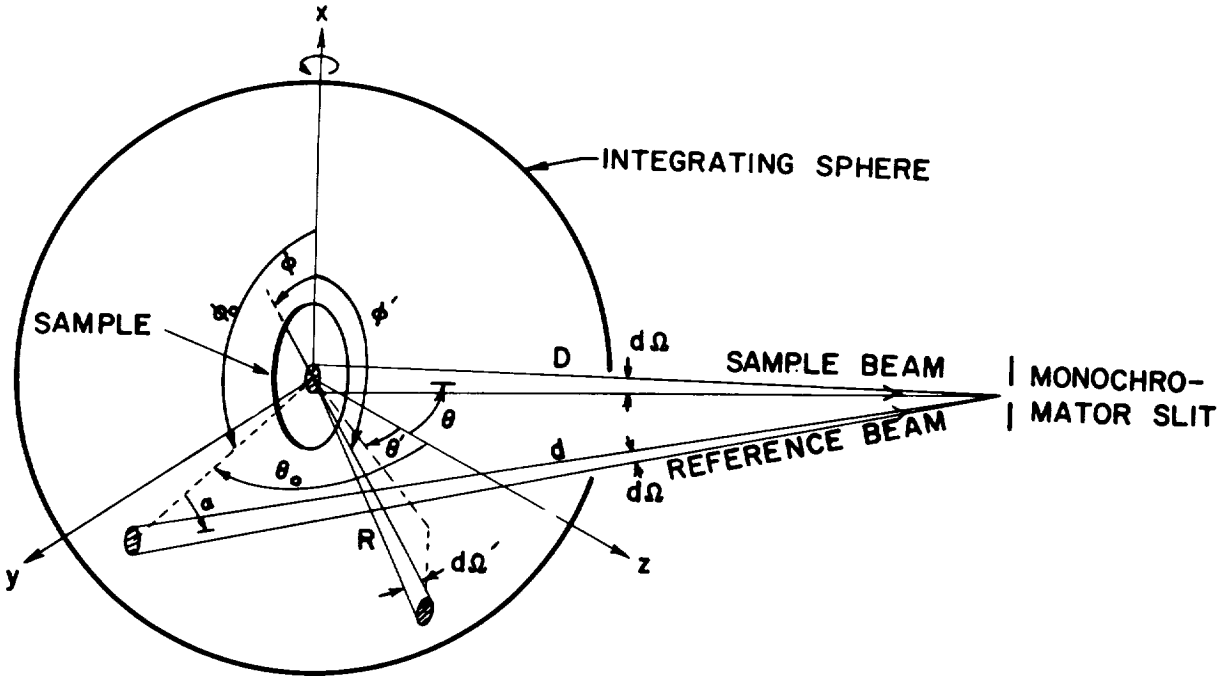

FIGURE 10-4.—Beam geometry of integrating sphere reflectometer.

from the source is always scattered from the same point within the sphere as the sample is turned through the polar angles from 0° to 90°. To allow measurements over the azimuthal angles, the sample can be turned around its normal axis. The spectrometer is a double-beam instrument. The two beams have the entrance slit and the optics of the spectrometer in common so that both the reference and the sample beam subtend the same solid angle at the detector. The wall of the integrating sphere serves as the reference. The chopped signals, as received by the detectors, are amplified and the ratio of the two signals is displayed on the recorder. The recorder shows the flux ratio of sample to reference beam which, as will be shown, is equal to the reflectivity of the sample.

Theory

The geometry of the beams is described in a rectangular coordinate system with its origin at the center of the sphere, figure 10-4. The x-axis lies in the plane of the sample surface and coincides with the rotation axis of the sample holder. The sample lies in the xy-plane so that the z-axis is normal to the sample surface. The reference beam and the beam reflected from the sample lie in the yz-plane. Let θ be the polar angle of incidence measured from the z-axis and ϕ the azimuthal angle of incidence as measured from some arbitrary reference line on the sample. Similarly, the points on the sphere surface are described by (R, θ', ϕ') where R is the radius of the sphere. The energy radiated from a unit area per unit time per unit wavelength into solid angle $d\Omega$ is called the monochromatic surface brightness

$$B_\lambda d\Omega = \frac{dE d\Omega}{dA dt d\lambda} \qquad (\text{ergs-sec}^{-1}\text{-cm}^{-3}\text{-sr}). \quad (1)$$

The monochromatic intensity incident per unit sample area (A_s) from an area dA at (R, θ', ϕ') of the integrating sphere wall is

$$dI_{\lambda i} = \frac{dE_i}{dA_s dt d\lambda} = B'_\lambda(\theta', \phi') \cos\theta' d\Omega' \qquad (\text{ergs-sec}^{-1}\text{-cm}^{-3}\text{-sr}) \quad (2)$$

where

$B'_\lambda(\theta', \phi')$ = brightness of the sphere wall at (R, θ', ϕ') normal to the wall

$d\Omega' = \frac{dA}{R^2}$ = solid angle subtended by dA at the sample (sr).

The monochromatic intensity reflected by the sample and incident per unit detector area (A_D) at (D, θ, ϕ) is given by

$$dI_{\lambda r}=\frac{dE_r}{dA_D dt d\lambda}=B_\lambda(\theta,\phi)d\Omega \quad (\text{ergs-sec}^{-1}\text{-cm}^{-3}\text{-sr}) \quad (3)$$

where

$B_\lambda(\theta, \phi)$ = brightness of the sample in the direction (θ, ϕ)

$d\Omega = dA_s \cos\theta/D^2$ = solid angle subtended by the sample area dA_s at the detector (sr).

The monochromatic intensity of the reference beam incident on the detector from an area dA at (R, θ_0',ϕ_0') of the sphere wall is

$$dI_{\lambda 0}=\frac{dE_0}{dA_D dt d\lambda}=B'_{\lambda_0}(\theta_0',\phi_0',\alpha)d\Omega \quad (\text{ergs-sec}^{-1}\text{-cm}^{-3}\text{-sr}) \quad (4)$$

where

$B'_{\lambda_0}(\theta_0', \phi_0', \alpha)$ = brightness of the sphere wall at the point (R, θ_0', ϕ_0') in the direction α of the reference beam

$d\Omega = dA \cos\alpha/d^2$ = solid angle subtended by the reference area at the detector (sr)

α = angle between reference beam and normal to the wall at (R, θ_0', ϕ_0').

Use has been made of the fact that the solid angles of the reference and sample beam are the same. The reflectivity of the sample as measured by the detector and displayed on the recorder is, according to equations (3) and (4), equal to

$$\rho_{\lambda m}=\frac{dI_{\lambda r}}{dI_{\lambda 0}}=\frac{B_\lambda(\theta,\phi)}{B'_{\lambda_0}(\theta_0',\phi_0',\alpha)}. \quad (5)$$

Equation (5) gives the true reflectivity of the sample for all angles only when the wall brightness B_0' is uniform over the hemisphere subtending the sample and if the radiation of the wall is completely diffuse. When this is not the case the measured reflectivity is in error. The error depends on whether the sample is specular or diffuse or partly specular and partly diffuse.

Specular Sample

A specular sample reflects radiation in such a way that the angle of reflection is equal to the angle of incidence. Therefore, for a specular sample the reflectivity is given by the ratio of the sample brightness to the wall brightness

$$\rho_{\lambda s}=\frac{B_\lambda(\theta,\phi)}{B'_\lambda(\theta',\phi')} \qquad (\theta=\theta',\phi=\phi'). \quad (6)$$

Substituting from equation (5) for the sample brightness gives

$$\rho_{\lambda s}=\rho_{\lambda m}\frac{B'_{\lambda_0}(\theta_0',\phi_0',\alpha)}{B'_\lambda(\theta',\phi')}=\rho_{\lambda m}\gamma_\lambda. \quad (7)$$

The monochromatic brightness ratio γ_λ describes the brightness distribution over the integrating sphere. Obviously, if the brightness distribution is completely uniform the brightness ratio is equal to one for all angles and the true reflectivity of the sample is equal to the measured reflectivity. The brightness ratio was measured at $\lambda=0.546\ \mu$ with a silvered mirror as a sample (fig. 10–5). In the horizontal plane, which

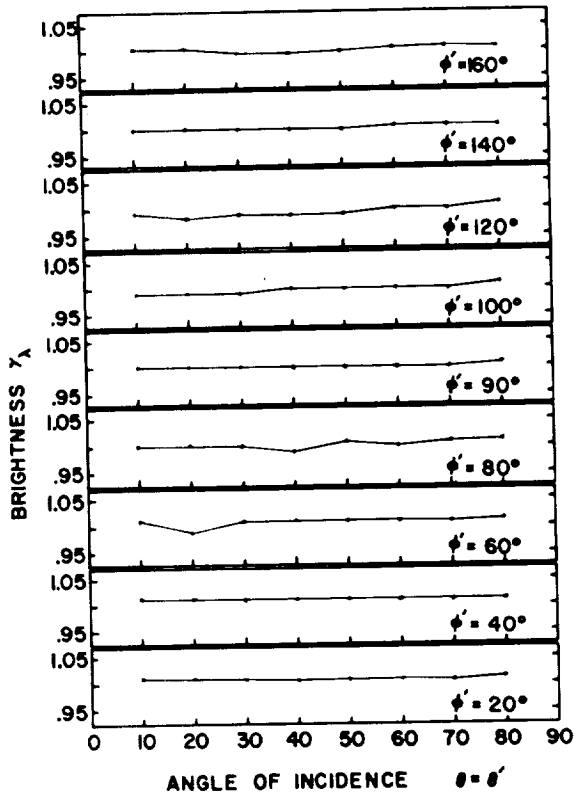

Figure 10–5.—Brightness ratio plotted against angular position.

is the plane of incidence for specular samples, it did not vary by more than 2%.

Diffuse Sample

A sample is diffuse if the incident radiation is reflected according to Lambert's cosine law. Namely, the brightness of a diffuse sample is the same when viewed from different angles.

The intensity, averaged over the hemisphere, which is incident on the sample, is according to equation (2)

$$(I_{\lambda i})_{\text{av.}}=\frac{\int_0 dI_{\lambda i}}{\int_0 \cos\theta' d\Omega'}=\frac{1}{\pi}\int_0 B'_\lambda(\theta',\phi')\cos\theta' d\Omega' \tag{8}$$

where the integration is over the hemisphere subtending the sample. Using equations (3), (5), and (8), the true reflectivity of a diffuse sample is given by

$$\rho_{\lambda D}=\frac{dI_{\lambda r}}{(I_{\lambda i})_{\text{av.}}d\Omega}=\frac{\pi B_\lambda(\theta,\phi)}{\int_0 B'_\lambda(\theta',\phi')\cos\theta' d\Omega'}$$

$$=\rho_{\lambda m}\frac{\pi}{\int_0 \frac{1}{\gamma_\lambda}\cos\theta' d\Omega'} \tag{9}$$

Again, it is evident from equation (9) that the true reflectivity is equal to the measured reflectivity if the brightness ratio is equal to one for all angles. The factor

$$\pi\cdot\left(\int\frac{1}{\gamma_\lambda}\cos\theta' d\Omega'\right)^{-1}$$

may be calculated for each angle of incidence using the brightness ratio given in figure 10–5. It varies by less than 0.5% from one for all angles of incidence.

Imperfectly Diffuse Samples

Equations (7) and (9) allow the calculation of the true reflectivity from the measured reflectivity for specular and diffuse samples once the brightness ratio of the integrating sphere is known. Obviously no formula can be given for the true reflectivity of imperfectly diffuse samples. However, the error e_{id} involved in measuring the reflectivity of an imperfectly diffuse sample is less than the error obtained for a specular sample and greater than the error obtained for a diffuse sample.

$$1-\frac{\int_0\frac{1}{\gamma_\lambda}\cos\theta' d\Omega'}{\pi}<e_{id}<1-\frac{1}{\gamma_\lambda}. \tag{10}$$

According to figure 10–5 this error is less than 2% but greater than 0.5%.

Polarization Effects

Due to the mirror surfaces in the monochromator, both beams are slightly polarized when they reach the detector. Since the beams travel through the same path, they are polarized by the same amount. However, a specular or imperfectly diffuse sample will cause an additional polarization of the sample beam, which introduces an error to the recorded reflectivity. The error due to polarization by the spectrometer can be shown to be

$$e_\lambda=\left(\frac{1}{1+\beta}\right)\left(\frac{\rho_{\lambda\perp}+\beta\rho_{\lambda\parallel}}{\rho_\lambda}\right)-1 \tag{11}$$

where $1-\beta$ is fractional polarization due to the spectrometer, β is the ratio of the intensity parallel to the plane of incidence to the intensity perpendicular to the plane of incidence, $\rho_{\lambda\perp}$ is the monochromatic reflectivity of the sample for the perpendicular component, $\rho_{\lambda\parallel}$ is the monochromatic reflectivity of the sample for the parallel component, and $\rho_\lambda=(\rho_{\lambda\perp}+\rho_{\lambda\parallel})$ is the monochromatic reflectivity of the sample.

For $\beta=0$ (total polarization), the error is equal to $e_\lambda=\rho_{\lambda\perp}\rho_\lambda^{-1}-1$ and for $\beta=1$ (no polarization) the error is equal to zero as expected. The fractional polarization of the beam by the spectrometer used in this experiment (Perkin-Elmer Model 13) is shown in figure 10–6. The polarization has a maximum at 0.8μ. Figure 10–7 shows the error introduced by this polarization for a glass surface and a silvered mirror. For a dielectric the error is a maximum at the polarizing angle ($\tan\theta=n$). At this angle, the error is independent of the properties of the dielectric and is simply a function of the fractional polarization

$$e_\lambda=\frac{1-\beta}{1+\beta}\qquad(\tan\theta=n). \tag{12}$$

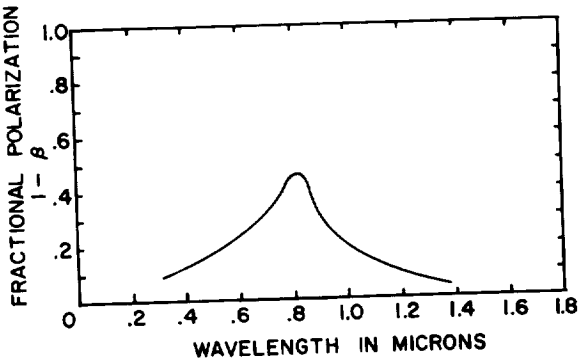

FIGURE 10–6.—Fractional polarization plotted against wavelength.

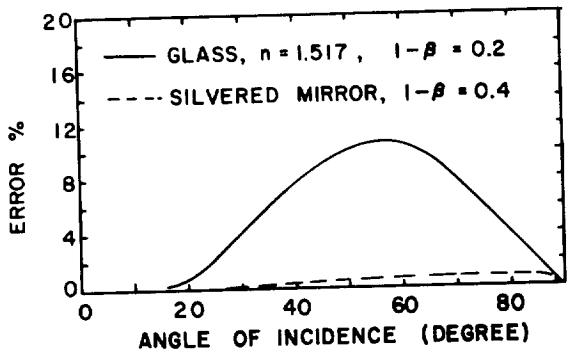

FIGURE 10–7.—Influence of angle of incidence on error due to polarization by spectrometer.

Therefore, the error might be considerable if the fractional polarization is large. According to this analysis, a polarizer is needed for accurate angular reflectivity measurements in the wavelength region where $\beta<1$. A Nicol prism may be placed in front of the monochromator to determine the reflectivity in the parallel and perpendicular polarizing component separately. The total reflectivity is then equal to the mean value of the parallel and perpendicular component.

EFFECT OF EXIT PORT

The reflectivity determination can also be affected by the presence of the exit port on the sphere, because the sample which is viewing the hemisphere subtending it sees the exit port as a black hole. The illumination of the sample is diminished by the presence of this hole. For a diffuse sample the error introduced to the reflectivity by the exit port is easily obtained by equation (9):

$$e_\lambda = 1 - \frac{\int_0 \gamma_\lambda^{-1} \cos\theta' d\Omega'}{\pi} \qquad (13)$$

where the integration is taken over the hemisphere subtending the sample, and γ_λ^{-1}, the inverse monochromatic brightness ratio, is zero over the entrance port. For a sphere diameter of 8 inches and a porthole diameter of 1 inch the error at 0.546μ is 1.6%. For specular or almost-specular samples, this error is negligible if the specular component of the sample beam is not directed through the porthole. This implies that the reflectivity of specular samples cannot be measured for angles of incidence smaller than 15°. However, this is not a serious defect of the sphere since the reflectivity for any sample stays approximately constant between 0° and 15°.

RESULTS

A check on the performance of the sphere was obtained by comparing the measured angular reflectivity of a black glass sample to the values obtained from electromagnetic theory (fig. 10–8). Black glass was used to eliminate reflection from the second surface; its index of refraction was $n=1.517$ at 0.546μ. The reflectivities represented by the solid lines were calculated from the Fresnel equations

$$\rho_\lambda = \frac{1}{2}(\rho_{\lambda\perp} + \rho_{\lambda\parallel}) = \frac{1}{2}\left\{\left[\frac{\cos\theta - (n^2 - \sin^2\theta)^{\frac{1}{2}}}{\cos\theta + (n^2 - \sin^2\theta)^{\frac{1}{2}}}\right] + \left[\frac{n^2\cos\theta - (n^2 - \sin^2\theta)^{\frac{1}{2}}}{n^2\cos\theta + (n^2 - \sin^2\theta)^{\frac{1}{2}}}\right]^2\right\}. \qquad (14)$$

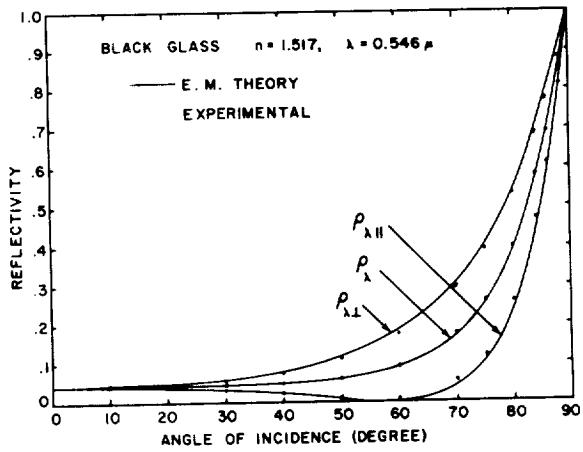

FIGURE 10–8.—Effect of angle of incidence on reflectivity of glass.

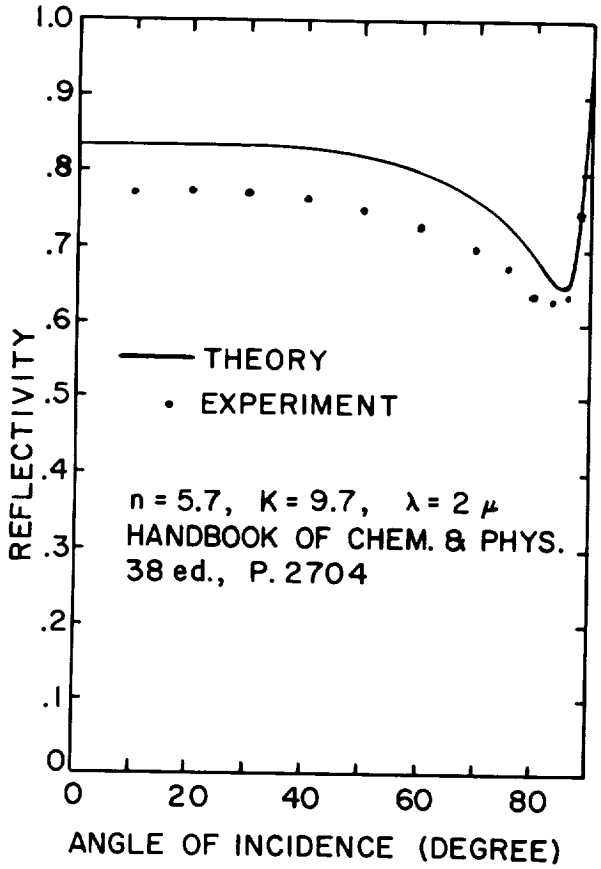

FIGURE 10–9.—Effect of angle of incidence on reflectivity of platinum.

For the total reflectivity, experiment and theory agree within 0.5%, whereas, for the parallel and perpendicular reflectivities, they differ slightly. This is due to insufficient polarization. At the time these measurements were made, a Nicol prism was not available, and ordinary polarizing glass was used instead. In effect, the parallel reflectivity was mixed with some of the perpendicular reflectivity raising its value and vice versa for the perpendicular reflectivity.

Next, the reflectivity of a platinum mirror was measured at 2-μ wavelength and compared to theory (fig. 10–9). The reflectivity of an absorbing media is given by (ref. 4)

$$\rho_\lambda = \frac{1}{2}\left[\frac{\left(n-\frac{1}{\cos\theta}\right)^2+K^2}{\left(n+\frac{1}{\cos\theta}\right)^2+K^2}+\frac{(n-\cos\theta)^2+K^2}{(n+\cos\theta)^2+K^2}\right] \quad (15)$$

where K is the extinction coefficient describing the decay of the electromagnetic wave in the media. The experimental values are consistently lower than the predicted values by up to 5%. This was also observed by Edwards and Gier (ref. 5). A final analysis of the platinum layer, which was obtained by evaporation, showed an abundance of 87% platinum, 10% iron, and 3% tungsten. The decrease in reflectivity may be a result of these impurities in the platinum.

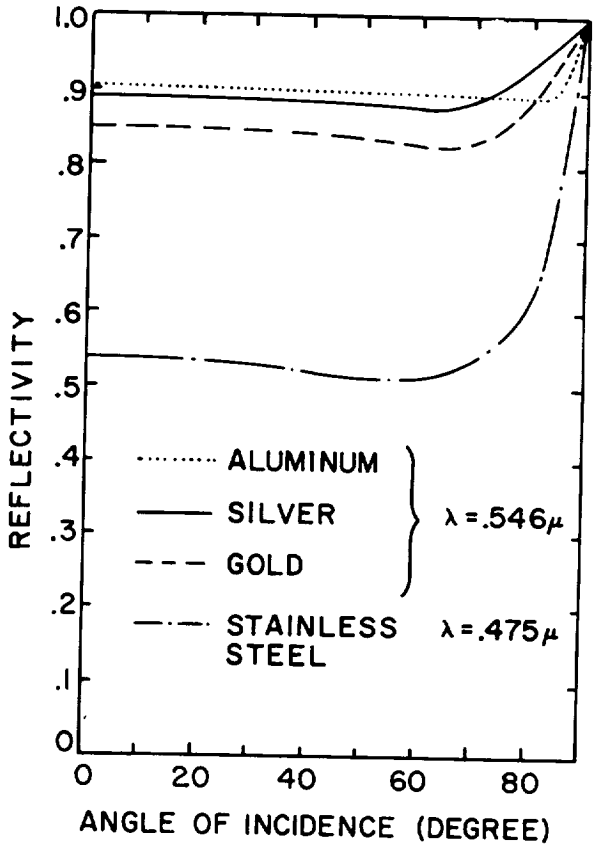

FIGURE 10–10.—Effect of angle of incidence on reflectivity of some metals.

Figure 10–10 shows the angular reflectivities of various metals measured with the described integrating sphere-reflectometer.

CONCLUSION

The unique feature of this integrating sphere reflectometer is its ability to measure reflectivity at grazing angles (minimum angle be-

tween beam and sample plane is 2°). The specifications of the instrument are:

Angles of incidence = 15° to 88°
Wavelength range = 0.19 to 2.65μ
Accuracy = better than 2%

ACKNOWLEDGMENT

I would like to express my thanks to Dr. J. T. Neu for his many helpful suggestions during the development of the instrument and to R. E. Gillson for his careful data taking.

REFERENCES

1. McNicholas, H. J.: Equipment for Routine Spectral Transmission and Reflection Measurements. NBS Jour. Res., vol. 1, no. 5, Nov. 1928, pp. 793–857.
2. Dunkle, R. V.; and Gier, J. T.: Report Div. Army Eng. Corps, 31, 1955.
3. White, J. U.: USAF Tech. Rep. No. 6511–4, Air Mat. Command, 1951.
4. Jenkins, A.: Fundamentals of Optics. McGraw-Hill Book Co., 2nd ed., 1950.
5. Edwards, D. K.; Gier, J. T., et al: Integrating Sphere for Imperfectly Diffuse Samples. Jour. Opt. Soc. of America, vol. 51, no. 11, Nov. 1961, pp. 1279–1288.

DISCUSSION

Gaumer, Lockheed Missiles and Space Company: The use of the apparatus for other than grazing angle measurements would be of interest. It would also be of interest to know what source is used to enable measurements down to 0.19μ. Other similar spheres apparently are limited to 0.25 or 0.3μ.

It looks like a Gier-Dunkle integrating sphere on a model 112 Perkin-Elmer instead of single beam.

Brandenberg: The source was a hydrogen arc lamp. The equipment is suitable for reflectance measurements at angles of incidence from 15° to 88° from the normal. The integrating sphere is of our own manufacture and is attached to a Model 13 Perkin-Elmer spectrometer.

11—A DYNAMIC THERMAL VACUUM TECHNIQUE FOR MEASURING THE SOLAR ABSORPTION AND THERMAL EMITTANCE OF SPACECRAFT COATINGS

BY W. B. FUSSELL AND J. J. TRIOLO

NASA GODDARD SPACE FLIGHT CENTER, GREENBELT, MARYLAND

AND JOHN H. HENNIGER

AMERICAN RESEARCH AND MANUFACTURING CORPORATION, ROCKVILLE, MARYLAND

Equipment has been set up for measuring the solar absorptance and thermal emittance of spacecraft coatings by a dynamic thermal vacuum technique. The apparatus and the method used are modeled closely on that described by G. D. Gordon. The apparatus consists of: (1), a high vacuum chamber with inner walls cooled by liquid nitrogen; (2), a powerful carbon arc lamp.

In operation a test sample coated with the material under investigation is suspended in the vacuum chamber facing a window in the chamber wall. A thermocouple in the test sample enables its temperature to be recorded. The sample is illuminated by the arc lamp and its rise in temperature recorded to above ambient temperature. The arc lamp is then turned off, and the temperature drop in the sample is recorded. While the arc lamp is on, its intensity of illumination is measured.

From the sample temperature-time data and the intensity of the arc lamp, the solar absorptance and thermal emittance can be computed to within $\pm 7\%$.

INTRODUCTION

As shown by Hass, Drummeter, and Schach (ref. 1), the solar absorptance ($\bar{\alpha}$) and the thermal emittance ($\bar{\epsilon}$) of spacecraft coatings are of fundamental importance in determining the equilibrium temperature of a satellite in space. This is because the input term in the radiation balance equation of a satellite is proportional to the solar absorptance and the output term is proportional to the thermal emittance. (There are several other factors, such as the solar illumination intensity, the satellite orientation, etc., which enter into the radiation equation, of course.)

There are a number of different methods of measuring $\bar{\alpha}$ and $\bar{\epsilon}$. One way of classifying these methods is by the type and variety of data obtained. Optical methods measure $\bar{\alpha}$ and $\bar{\epsilon}$ by the radiation reflected from or emitted by materials; this radiation may be either spectrally resolved or integrated. Thermal methods measure $\bar{\alpha}$ and $\bar{\epsilon}$ by the temperature or rate of change of temperature of materials. Optical methods require the elimination of, or the control of, background radiation. Thermal methods require, in addition, the evacuation to a high vacuum of the chamber surrounding the sample of the material being measured. Also, to obtain $\bar{\alpha}$ values by thermal methods, a light source whose spectral distribution is similar to that of the sun ("solar simulator") is necessary, plus instrumentation for measuring the intensity of the light from the solar simulator.

The different methods for measuring $\bar{\alpha}$ and $\bar{\epsilon}$, then, are classified as follows:

A. Optical Methods
   1. Reflectance Measurements
      a. Spectrally Resolved
         (1) 0.3–2.5 μ, for $\bar{\alpha}$
         (2) 5–35 μ, for $\bar{\epsilon}$

b. Integrated
(1) Light Source × Detector Resistance must match solar spectrum approx., for $\bar{\epsilon}$
(2) Light Source × Detector Response must match 300° K blackbody approx., for $\bar{\epsilon}$

2. Emitted Radiation Measurements, for $\bar{\epsilon}$ only
a. Spectrally Resolved
(1) 5–35 μ
b. Integrated

B. Thermal Methods
1. Equilibrium Measurements
a. With Electrical Heating for $\bar{\epsilon}$
b. With Solar Simulator as Heater, for $\bar{\alpha}$, $\bar{\epsilon}$
c. With Solar Simulator, for $\bar{\alpha}$ (Water Calorimeter)
2. Dynamic Measurements
a. With Solar Simulator as Heater, for $\bar{\alpha}$ and $\bar{\epsilon}$
b. Adiabatic Cooling, for $\bar{\epsilon}$

It is now appropriate to run through the above outline in sequence and to describe in detail the instrumentation available for each method, its advantages and disadvantages, and the accuracy and validity, from the thermal design viewpoint, of the data obtained.

A1a(1), Spectrally Resolved Reflectance Measurements from 0.3 to 2.5 μ, for $\bar{\alpha}$

This wavelength region contains 95.3% of the sun's energy (ref. 2); there is 1.2% below 0.3μ and 3.4% above 2.5μ. Total reflectance measurements can be made to a precision of $\pm$0.5% absolute (that is, for example, a reading of 11% reflectance lies between 11.5 and 10.5%) with a Beckman DK–2 spectrophotometer with an integrating sphere reflectance attachment, for example. However, the integrating sphere is most accurate when the test sample reflectance is near that of the reflectance standard used, and, furthermore, when the polar reflectance patterns are similar (ref. 3). Thus, a specular sample should be measured with a specular standard and a diffuse sample with a diffuse standard. If the test sample is neither perfectly diffuse nor perfectly specular, but falls somewhere in between, it may be difficult to obtain a reflectance standard having a similar polar reflectance pattern. In this case, the accuracy of the measurement may be questionable since the average number of reflections undergone by light reflected from the test sample before it reaches the detector, may not be equal to the average number of reflectances undergone by light reflected from the reflectance standard. If the interior coating of the sphere possessed a reflectance of 100%, this difference in the average number of reflections would be unimportant, since it is the light absorbed at each reflection which produces a difference between measurements otherwise equal but having a different average number of reflections. The highest reflectance obtainable for a sphere coating at present is about 98% (in the visible) with a thick (several millimeters) coating of magnesium oxide, and so there is a possibility of error in reflectance measurements with an integrating sphere on materials having both a diffuse and specular component of reflectance. Unfortunately, there is not at present a good theoretical treatment of the integrating sphere when used with materials of this type, so that the magnitude of the error for these materials is difficult to estimate.

Since solar illumination will usually strike the exterior surface of a satellite at both normal and non-normal incidence, it is important to know the variation of the solar absorptance of a material with angle of incidence. If the optical constants, n and k (n being the index of refraction and k the extinction coefficient), of the material are known at a reasonable number of wavelengths in the 0.3–2.5μ range, then Fresnel's equations (ref. 4) enable its solar absorptance to be computed at any angle of incidence. It is also possible to compute the solar absorptance of a material at a given angle of incidence from its total reflectance spectrum obtained experimentally. Although the conventional integrating-sphere reflectometer gives the total reflectance for normal (or near-normal) illumination only (a quantity called the "normal total reflectance"), a modified design of integrating sphere has been made[1] which allows total reflectance to be measured at angles of incidence from 10 deg to 80 deg.

[1] By Gier and Dunkle, Thermal Instruments, Los Angeles 66, Calif.

Mathematically expressed, the procedure for computing the solar absorptance of a given material from its total reflectance spectrum at a given angle of incidence is:

$$\bar{\alpha}(\theta)=1-\bar{\rho}(\theta), \tag{1}$$

$$\bar{\rho}(\theta)=\frac{\int_{\lambda=0.3\mu}^{\lambda=2.5\mu} R_\lambda(\theta)H_\lambda d\lambda}{\int_{\lambda=0.3\mu}^{\lambda=2.5\mu} H_\lambda d\lambda}, \tag{2}$$

where

$\bar{\alpha}(\theta)$ solar absorptance at angle of incidence θ
$R_\lambda(\theta)$ total reflectance at wavelength λ at θ
H_λ solar extra-terrestrial spectrum[2]
$\bar{\rho}(\theta)$ solar reflectance at θ.

In practice, the integrals in equation (2) are approximated by discrete summations.

An experienced technician can measure the total normal reflectance spectrum of a sample through the solar region on a conventional recording, integrating sphere spectroreflectometer and compute its normal solar absorptance in approximately 2 hours, using manual read-off and data reduction techniques. Digital readout and computer data integration would reduce this time drastically.

A1a(2), Spectrally Resolved Reflectance Measurements From 5 to 35μ, for $\bar{\epsilon}$

This wavelength interval contains 91.0% of the energy of a 300° K blackbody, 1.3% of its energy being radiated at shorter wavelengths, and 7.7% at longer wavelengths (using for C_2, the second radiation constant in Planck's function, the value 1.438 cm-°K). Total reflectance measurements can be made in this region by a hohlraum (heated oven) attachment to an infrared spectrophotometer,[2] or by a Coblentz hemispherical mirror attachment to an infrared spectrophotometer.[3] The heated oven has two openings, one of which allows the insertion of a water-cooled sample holder which keeps the sample at a reasonable temperature (100° F), even though the oven may be very hot (1100° C). The other opening allows the infrared spectrophotometer to view either the interior wall of the oven, or the sample. It thus acts as the radiation source for the spectrophotometer. The Coblentz hemisphere is really an approximation to an ellipsoidal mirror and is based on the light-collecting properties of such a mirror, all light reflected from a sample placed at one focus of the ellipsoid being collected by the mirror and brought to a focus at the conjugate focus of the mirror. Thus, an infrared detector placed at the conjugate focus will respond to the reflected light from the sample; if the field-of-view of the detector is wide enough to encompass a complete hemisphere, then the detector will measure the sample total reflectance (provided also the detector has uniform spatial sensitivity).

The hohlraum oven can be used to make either absolute or relative total reflectance measurements. The interior wall of the oven is approximately an isothermal blackbody and provides in this manner an absolute standard of radiation (the fundamental requirement here is that the wall of the oven be at least spatially uniform in the sense of having a uniform brightness—at each wavelength of measurement—when viewed from any direction) against which the reflected light from the sample can be compared. It is also possible to use the hohlraum oven for relative reflectance measurements by making two runs, one giving the sample reflectance relative to the oven, the other giving the reflectance of a standard whose absolute reflectance is known relative to the oven.

By the principle of reciprocity (ref. 5), it can be shown that the total reflectance of a material illuminated at a given angle of incidence, as measured by an integrating sphere or collecting mirror, is equal to the total reflectance of the material under conditions of uniform diffuse illumination, the reflected light now being viewed by a detector at an angle equal to the given angle of incidence. The essence of the proof of this statement is the reciprocity of the transfer function, denoted by $\tau(\theta, \theta')$, which describes the amount of light incident at an angle, θ (from a small element of solid angle dw), which is scattered into a small element of solid

[2] For example, a Perkin-Elmer model 13 infrared spectrophotometer in conjunction with a Perkin-Elmer model 205 diffuse reflectance attachment.

[3] Such as a Beckman hemisphere reflectance attachment used with a Beckman IR-7 infrared spectrophotometer.

angle about the angle of reflection, θ (for simplicity, the transfer function is assumed not to depend on the azimuthal angle, ψ; the proof still holds even if τ is a function of ψ). The principle of reciprocity is that

$$\tau(\theta, \theta') = \tau(\theta', \theta).$$

The measurement procedures and the data reduction procedures for computing the total hemispherical emittance and the total normal emittance of a material are expressed concisely by the following equations:

$$\bar{\epsilon}_H(T) = \bar{\alpha}_H(T), \tag{3}$$

$$\bar{\alpha}_H(T) = 1 - \bar{\rho}_H(T), \tag{4}$$

$$\bar{\rho}_H(T) = \frac{\int_{\lambda=5\mu}^{\lambda=35\mu} \int_{\theta=0}^{\theta=\pi/2} \rho(\theta, \lambda) 2\pi \sin\theta \cos\theta d\theta J_\lambda(T) d\lambda}{\int_{\lambda=5\mu}^{\lambda=35\mu} \int_{\theta=0}^{\theta=\pi/2} 2\pi \sin\theta \cos\theta d\theta J_\lambda(T) d\lambda} \tag{5}$$

$$\bar{\epsilon}_N(T) = \bar{\alpha}_N(T), \tag{6}$$

$$\bar{\alpha}_N(T) = 1 - \bar{\rho}_N(T), \tag{7}$$

$$\bar{\rho}_N(T) = \frac{\int_{\lambda=5\mu}^{\lambda=35\mu} \rho_N(\lambda) J_\lambda(T) d\lambda}{\int_{\lambda=5\mu}^{\lambda=35\mu} J_\lambda(T) d\lambda} \tag{8}$$

where

$\bar{\epsilon}_H(T)$ total hemispherical emittance at temperature T° A,

$\bar{\alpha}_H(T)$ total absorptance for completely diffuse blackbody radiation at temperature T (by Kirchoff's law of radiation, $\bar{\epsilon}_H(T)$ and $\bar{\alpha}_H(T)$ are equal) (ref. 6),

$\bar{\rho}_H(T)$ total reflectance for completely diffuse blackbody radiation at temperature T°,

$\rho(\theta, \lambda)$ total reflectance for illumination of wavelength λ incident at angle θ,

$J_\lambda(T)$ Planck blackbody function for the total radiation of a blackbody per unit area, and per unit wavelength interval at T and λ:

$$J_\lambda = C_1' \left[\lambda^5 \exp\left(\frac{C_2}{\lambda T}\right) - 1\right]^{-1},$$

$C_1' = 1.191 \times 10^{-5}$ erg-cm^2-sec^{-1},

$C_2 = 1.439$ cm-°K,

$\epsilon_N(T)$ total normal emittance at T,

$\bar{\alpha}_N(T)$ total absorptance for normally incident blackbody radiation at temperature T ($\bar{\alpha}_N(T) = \bar{\epsilon}_N(T)$ by Kirchoff's law of radiation, as noted above),

$\bar{\rho}_N(T)$ total reflectance for normally incident blackbody radiation at temperature T.

In the actual computation, of course, the integrals in equations (5) and (8) are replaced by discrete summations. In the hohlraum reflectometer and the Coblentz-hemisphere reflectometer described above, the quantity measured is $\rho(0, \lambda)$, the total reflectance at wavelength λ for normally incident radiation. A variable angle of incidence hohlraum can be obtained commercially, however, and allows values of $\rho(\theta, \lambda)$ to be obtained over the range from $\theta = 20°$ to $\theta = 70°$.

If experimental data on $\rho(\theta, \lambda)$ is lacking and only data for $\rho(0, \lambda)$ is available, the integration indicated in equation (5) with respect to θ can be carried out by using the theoretical variation of $\rho(\theta, \lambda)$ with θ. Details of this procedure are given in Jakob's excellent work on heat transfer (ref. 7). The process consists, basically, of assuming the material in question to be an isotropic substance whose optical constants are known and which has a smooth flat surface. In this case Fresnel's equations (ref. 4) can be used—as mentioned previously—to calculate the reflectance $\rho(\theta, \lambda)$ for any θ at any λ for which the optical constants are known. Since smooth surfaces are required by the theory, this excludes roughened and diffusely reflecting surfaces. Jakob presents tables and graphs (ref. 8) giving the ratio of total hemispherical emissivity to total normal emissivity as a function of total normal emissivity for electrical conductors and insulators. By means of these data, values of total normal emittance obtained from optical measurements can be converted to total hemispherical emittance, the quantity of interest for thermal design purposes.

An experienced technician using a conventional infrared recording spectrophotometer, attached to a hohlraum as described above for its radiation source, can measure the total reflectance spectrum of a sample over the thermal region and read off and reduce the data manu-

ally to a total normal emittance value in approximately a day or a day-and-a-half.

A1b(1), Integrated (Non-Spectrally Resolved) Reflectance Measurements Over the Solar Spectrum, for $\bar{\alpha}$

If a light source and a detector combination can be found whose combined response function matches the solar spectrum approximately (such a device should not be difficult to construct), then this source-detector combination could be used with an integrating sphere or collecting mirror total reflectometer to give solar absorptance values for materials directly. For many common spacecraft coatings (e.g., aluminum, gold, silver, black and white paints) the spectral match between the light source-detector response function and the solar spectrum need not be particularly close on a high-resolution basis. The important thing is that the average absorptance for the light source-detector spectrum should be close to the average absorptance for the solar spectrum. That is,

$$\bar{\alpha}=\frac{\int_{\lambda=0.3\mu}^{\lambda=2.5\mu}\alpha_\lambda H_\lambda d\lambda}{\int_{\lambda=0.3\mu}^{\lambda=2.5\mu}H_\lambda d\lambda}, \tag{9}$$

the solar absorptance, should be approximately equal to

$$\bar{\alpha}'=\frac{\int_{\lambda=0.3\mu}^{\lambda=2.5\mu}\alpha_\lambda s_\lambda d\lambda}{\int_{\lambda=0.3\mu}^{\lambda=2.5\mu}s_\lambda d\lambda} \tag{10}$$

the average absorptance for the light source detector spectrum, where

α_λ absorptance at λ,
s_λ source-detector spectral intensity at λ.

Practically, it seems that an incandescent lamp with a suitable filter and a flat thermal detector such as a bolometer or thermopile might work. Possibly an incandescent lamp in conjunction with a phototube having an S–1 response would be acceptable. It was found (report being prepared by Triolo) that a carbon arc with rare-earth-cored carbons is a good solar simulator in the above sense.

A1b(2), Integrated Reflectance Measurements Over the Thermal (300° K) Spectrum, for $\bar{\epsilon}$

If a radiation source-detector combination can be found whose combined response function matches the spectrum of a 300° K blackbody approximately, then this source-detector combination could be used with a collecting mirror total reflectometer to give thermal emittance values for materials directly. The hohlraum reflectometer used in conjunction with a flat thermal detector would obviously need filtering if operated in its normal temperature range (800–1000° C).

It is possible that chopped blackbody radiation at 50–100° C above ambient temperature, if efficiently collected by suitable optics (at least f/2, say), would provide sufficient power to measure thermal emittance with a thermopile in the above manner. (This assumes a thermopile with a responsivity of 0.1 volt/watt, a receiver area of 1 mm^2, and a minimum output of 10 microvolts.)

A2a, Spectrally Resolved Emitted Radiation Measurements From 5 to 35μ, for $\bar{\epsilon}$

The thermal radiant power emitted by a 300° K blackbody into an infrared spectrophotometer whose field of view it fills can be calculated. If the effective aperture of the spectrophotometer is f/2 or better and if the radiation detector is a typical thermal detector, then a bandwidth of 1 wave-number at 600 wave numbers (17μ) should provide an output of the order of 10 mv (neglecting absorption in the spectrophotometer and in the air). It should be possible, therefore, to measure the emitted radiation of materials at ambient temperature directly in this region, provided suitable cooled shields are used to lower the surrounding background radiation. A simpler approach is to heat the sample of material under investigation to several hundred degrees above ambient temperature.

A2b, Integrated Emitted Radiation Measurements, for $\bar{\epsilon}$

The measurement problems are simplified in this case, compared with those of the preceding section (A2a), since spectral resolution is not required. Commercial radiometers are available [4] which will measure the emittance of materials to within 0.03 absolute, if the tem-

perature of the material is accurately known.[4]

B1a, Equilibrium Thermal Measurement With Electrical Heating, for $\bar{\alpha}$

If a sample of the material under consideration is placed in a vacuum chamber which is then evacuated at 10^{-4} mm of Hg or better, the sample can lose heat only by radiation to the walls of the chamber or by conduction through attached lead wires. If the walls of the vacuum chamber are essentially black and isothermal, and if electrical heating leads are attached to an internally mounted heating element in the sample, then the sample emittance can be calculated if the wall temperature, sample temperature, sample surface area, electric power input to the sample, and the lead losses, are known. Materials of low emittance require samples of large surface area to produce a sufficiently large ratio of radiative heat transfer to conductive heat transfer through the leads.

B1b, Equilibrium Thermal Measurements With Solar Simulator as Heater, for $\bar{\alpha}/\bar{\epsilon}$

A sample of material suspended in a vacuum chamber evacuated to at least 10^{-4} mm of Hg, and illuminated by a solar simulator of known intensity of illumination, will reach an equilibrium temperature, T_2, given by the following equation:

$$T_2^4=\left(\frac{\bar{\alpha}}{\bar{\epsilon}}\right)\left(\frac{I}{\sigma}\right)\left(\frac{A_p}{A_s}\right)+T_1^4 \qquad (11)$$

where

$\bar{\alpha}$ average solar absorptance of the illuminated area of the sample (this will depend on the shape of the sample, that is, whether it is plane, spherical, cylindrical, etc., and on the direction of illumination with respect to the axes of symmetry of the sample)

ϵ average thermal emittance of the sample

I intensity of illumination of the solar simulator, that is, its total radiant power per unit area

σ Stefan-Boltzmann constant, 5.67×10^{-12} watts-cm^{-2}-°K^{-4}

A_p projected area of the sample as viewed in the direction of illumination

A_s total surface area of the sample

T_1 temperature in degrees Kelvin of the walls of the vacuum chamber.

[4] For example, the Barnes Engineering Co. R-4DT industrial radiometer.

It should be noted that the walls of the vacuum chamber are assumed to be black (for thermal radiation) and isothermal. (The ratio of A_p/A_s is 1/2 for a plane figure illuminated normally, 1/4 for a sphere, $\frac{1}{2}\left(1+\frac{L}{R}\right)^{-1}$ for a cylinder illuminated on its axis (L is the length, etc.)

If the sample has a thermocouple attached to it to measure T_2, and thermocouples are also attached to the interior walls of the vacuum chamber to measure T_1, and if a calibrated thermal radiation detector is used to measure the intensity of illumination from the solar simulator at the samples, I, measurement of the physical dimensions of the sample provides values for A_p and A_s, and all quantities are known in equation (11) except $\bar{\alpha}/\bar{\epsilon}$, which can therefore be solved for. (For example, if $\bar{\alpha}/\bar{\epsilon}=1$, $T_1=0$, $I=0.1397$ watt cm^{-2} (the solar constant), then $T_2=60.3°$ C or $333.5°$ K for a flat plate illuminated normally.) Lead losses have been neglected in equation (11).

B1c, Equilibrium Thermal Measurements With a Solar Simulator as Heater, Conductive Transfer Predominant, for $\bar{\alpha}$

In this type of measurement no vacuum chamber is necessary. Radiation from a powerful solar simulator is allowed to illuminate a portion of the upper surface of a water-cooled, cylindrical hollow chamber. If the illuminated area is coated with a material whose solar absorptance is to be measured, then measurement of:

(1) the average radiant intensity of the solar simulator across the test surface
(2) the input and output temperatures of the cooling water
(3) the rate of flow of the cooling water
(4) the area of the test surface illuminated

allows the solar absorptance of the test material to be computed. This method requires a sufficiently rapid flow of water to restrict the rise in output temperature of the cooling water to a value that is capable of precise measurement (say, 10° to 20° C) but that is not so large that radiative heat transfer or air conduction dissipates a significant portion of the input power absorbed by the illuminated test surface.

B2a, Dynamic Thermal Measurements With a Solar Simulator as Heater, for $\bar{\alpha}$ and $\bar{\epsilon}$

A test sample coated with the material under investigation is suspended in a vacuum chamber evacuated to below 10^{-4} mm Hg. The vacuum chamber has cooled black walls (liquid-nitrogen cooling is desirable) except for a small port covered by a quartz window. The temperature of the test sample and the wall temperature are continuously monitored during the measurement process. The sample is first heated to 20° to 40° C above ambient temperature by the illumination of a solar simulator, incident upon the sample through the quartz window. The solar simulator is then turned off, and the sample is allowed to cool to 20° to 70° C below ambient temperature. The radiant intensity of the solar simulator, at the sample, is continuously monitored during the heat-up phase of this procedure. The rate of change of sample temperature with time, dT/dt, is obtained from the recorded curve of temperature as a function of time. The rate of change values are then plotted as ordinate against T^4 as abscissa. If the solar simulator intensity and the wall temperature of the vacuum chamber remained approximately constant during the measurements, the data when plotted in this manner will fall on two parallel straight lines. All heat-up data will fall on (or near) one line, the cool-down data will fall on the other line. If the thermal emittance of the material being measured is independent of its temperature, and if the specific heat of the sample is also independent of temperature, then, as Gordon has shown (ref. 9), the equation connecting dT/dt and T^4 during heat-up is

$$mc\frac{dT}{dt}=A_p\bar{\alpha}I+P-A_s\bar{\epsilon}\sigma T^4, \tag{12}$$

where all the quantities have been previously defined except

m mass of sample
c specific heat of the sample per unit mass
P incident thermal radiation (from the walls of the vacuum chamber and the quartz window).

During cool-down, the solar simulator is turned off and so equation (12) reduces to

$$mc\frac{dT}{dt}=P'-A_s\bar{\epsilon}\sigma T^4, \tag{13}$$

where P' is the incident thermal radiation for the cool-down. It is seen from equations (12) and (13), then, that dT/dt plotted as ordinate against T^4 as abscissa, produces two straight lines as follows:

Heat-up (solar simulator on):

(a) Slope of line

$$s_H=\frac{A_s\sigma}{mc}\bar{\epsilon}, \tag{14}$$

(b) Intercept with x-axis

$$\left(\frac{dT}{dt}=0\right),\ i_H=\frac{A_p\bar{\alpha}I+P}{A_s\bar{\epsilon}\sigma}; \tag{15}$$

Cool-down (solar simulator off):

(a) Slope of line,

$$s_c=\frac{-A_s\sigma}{mc}\bar{\epsilon}, \tag{16}$$

(b) Intercept with x-axis

$$\left(\frac{dT}{dt}=0\right),\ i_c=\frac{P'}{A_s\bar{\epsilon}\sigma}. \tag{17}$$

It is seen, therefore, that the slope of both lines is proportional to $\bar{\epsilon}$, and that—if $P'=P$—the difference in the intercepts, i_H-i_c, is proportional to $\bar{\alpha}/\bar{\epsilon}$. Thus both $\bar{\alpha}$ and $\bar{\epsilon}$ can be found by this method.

The advantage of this method, compared with equilibrium methods, is that measurements can be made more rapidly, since equilibrium need not actually be achieved. Furthermore, since the values of $\bar{\epsilon}$ obtained by this method are based on the slope of a line relating dT/dt to T^4, rather than its position in the x-y plane, constant heat losses or heat inputs do not affect the measurements. Also, since the walls of the vacuum chamber are cooled, the incident thermal radiation is small compared with the solar simulator radiation, and uncertainties as to wall temperature or thermal radiation from the quartz window do not affect the measured value of $\bar{\alpha}/\bar{\epsilon}$ too greatly.

Two technicians are required to operate the equipment used for measuring $\bar{\alpha}$ and $\bar{\epsilon}$ by the above method at GSFC, one to operate the

solar simulator (a carbon arc lamp with rare-earth cored carbons), the other to operate the vacuum chamber and temperature recorder. About 2–3 days are required for each complete measurement of the $\bar{\alpha}$ and $\bar{\epsilon}$ values of a material. This includes time required to pump down the vacuum chamber, and time required to reduce the temperature data.

B2b, Dynamic Thermal Measurements With Adiabatic Cooling for $\bar{\epsilon}$

This method is similar to B2a but in this case the light source need not be a solar simulator since it is used solely to heat the test sample to a temperature somewhat *above* the temperature at which the thermal emittance value is desired. Furthermore, the intensity of the light source is not measured, and the walls of the vacuum chamber need only be cooled to a temperature appreciably *less* than the temperature at which $\bar{\epsilon}$ is desired. A description of this method is given by Butler and Inn (ref. 10).

DESCRIPTION OF PRESENT EQUIPMENT SET UP AT GODDARD SPACE FLIGHT CENTER FOR MEASURING $\bar{\alpha}$ AND $\bar{\epsilon}$ OF SPACECRAFT COATINGS BY TRANSIENT THERMAL VACUUM TECHNIQUES (WITH A SOLAR SIMULATOR)

There are five main components (all commercially available) of the apparatus:

(1) the vacuum system
(2) the solar simulator
(3) the liquid nitrogen cooled shroud which goes inside (1)
(4) the temperature recorder
(5) the solar simulator intensity measuring equipment.

The vacuum system (1) is a High Vacuum Equipment Corporation C0018 (18-inch diameter) bell jar evaporator. This system (without the liquid nitrogen cooled shroud) has an ultimate vacuum of approximately 5×10^{-7} mm of Hg. The bell jar is stainless steel with two 5-inch diameter quartz sight ports, as can be seen in figure 11–1 (only one port is used for the measurements, however).

The solar simulator (2) is a Strong Electric Company "UHI" automatic reflector arc lamp, type 91013–1W/0, which operates at about 60 volts and 175 amp input to the lamp

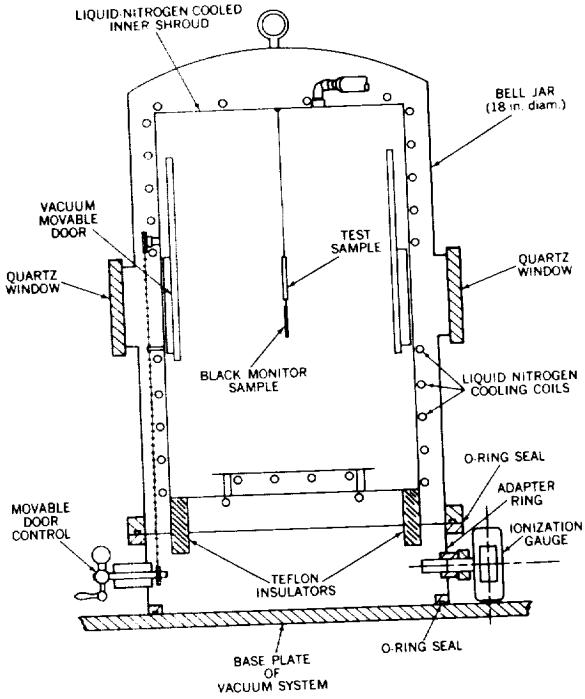

FIGURE 11–1.—Cross-section view of the cooled shroud and vacuum-system bell jar.

itself. The arc lamp uses 13.6-mm cored carbons for both the positive and negative carbons. The negative carbon is copper shielded. It will operate automatically for about 45 min on one positive carbon.

The liquid nitrogen cooled shroud (3) was also designed and made by the High Vacuum Equipment Corporation. It is 15 inches in diameter and 24 inches high and is designed, as figure 11–1 shows, to fit inside the bell jar of the vacuum system, except for the base of the shroud, the "adaptor ring", which rests on the baseplate of the vacuum system and which supports the bell jar. The shroud is made of nickel-plated copper, and has two circular 5-inch diameter ports, one of which has a cover which is externally moveable through a chain attached to a rotary crank handle in the adaptor ring. The shaft of the crank handle penetrates the adaptor ring through a vacuum seal fitting. The other port has a cover which can be moved, but has no external handle. The upper portion of the shroud opens up about a vertical hinge like a "clam-shell" for the insertion of test samples. The adaptor ring also contains the liquid nitrogen feedthroughs, the thermocouple

feedthroughs, and the vacuum seal for the ionization gauge. The adaptor ring serves the purpose of lifting the base of the shroud so that it does not obstruct the upward movement of the high-vacuum valve—located in the baseplate—of the vacuum system. The adaptor ring is joined, at its bottom, to the baseplate, by an O-ring seal. The top of the adaptor ring is also joined by an O-ring seal to the bottom of the bell jar.

The temperature recorder is a Minneapolis-Honeywell Universal model 15 Electronik multipoint recorder, with a temperature range of -200 to $+100°$ C. It records a temperature every 2 sec, and, since there are 8 channels, data points are recorded 16 seconds apart for any particular channel.

The solar simulator intensity measuring equipment (5) consists of an Eppley Laboratory pyrheliometer, 50 junction, as the detector, and a Hewlett-Packard microvoltmeter model 425A to indicate the detector output.

The liquid nitrogen feeding mechanism is also important and includes a 50-liter Dewar flask with a transfer tube driven by dry nitrogen.

The light from the solar simulator is collimated by a quartz lens, plano-convex, 6 inches in diameter and having a focal length of 23 inches. This lens collimates the light from the solar simulator to within 12 deg. (This is due to the fact that light from both the positive carbon crater and the tail flame is utilized. The tailflame is 2–3 inches in length.) In use, the carbon arc lamp is placed so that the arc gap is located 95 inches from the test sample, which is suspended in the center of the shroud (3).

A motor-driven chopper is placed between the collimating lens and the vacuum chamber. Since the light intensity at the sample is too high—about 2 solar constants—when the carbon arc lamp is operating at its level of maximum stability, the chopper is required to reduce the light intensity at the sample to the desirable level of one solar constant while allowing the carbon arc lamp to operate at its optimum output level. The chopper has interchangeable blades which attenuate the light beam by different proportions.

The test samples used with the equipment are made in a sandwich form. Two copper plates, 2 inches square by $\frac{1}{32}$ inch thick, are accurately cemented together with a 5-mil copper-constantan thermocouple centered between them (figure 11–2). The plates are held

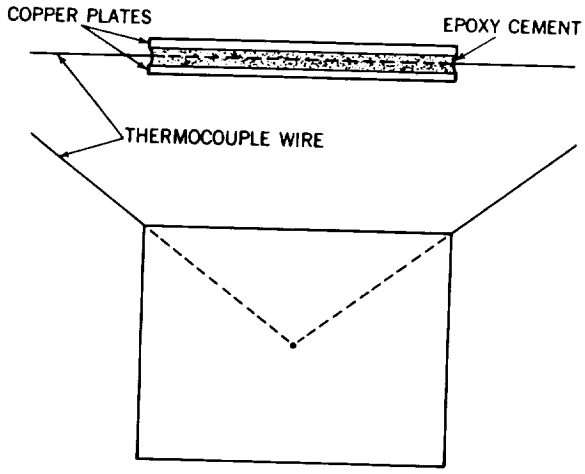

FIGURE 11–2.—Test sample thermocouple configuration.

in place by a jig to keep the thermocouple in position and to line up the square edges of the plates. An epoxy cement is used to bind the two halves of the test sample together. The thermocouple junction is forced into good thermal contact with both copper plates by mechanical pressure; the epoxy cement locks the thermocouple in place and maintains the good thermal contact. A mold release compound, PVA,[5] is used to prevent the cement from adhering to the jig. This mold release compound, unlike grease, leaves no residue to prevent the test coating from adhering to the copper substrate. At this point the coating to be measured is applied to the copper sandwich. Coating after assembly prevents the high-emittance epoxy from remaining uncoated and producing a large error for low-emittance coatings (like polished or evaporated metals). In addition, when evaporated metal coatings are to be measured, the coating is allowed to extend onto the thermocouple leads also. This has the effect of reducing the error due to heat loss through the leads. If the coating has a high emittance, the enamel is stripped off the

[5] Polyvinyl alcohol made by Gilbert Plastics.

thermocouple leads, leaving 3 inches of bare thermocouple wire, which has an emittance of less than 0.1. The sample assembly is suspended by means of its thermocouple leads from the top of the shroud, as shown in figure 11–3. The leads are led into the vacuum

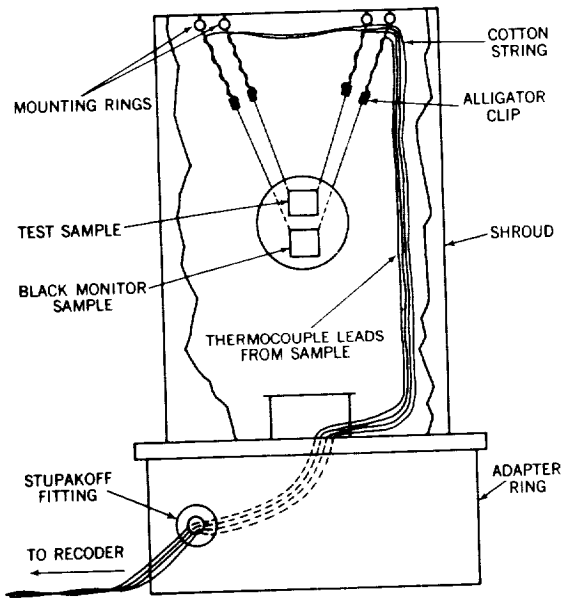

FIGURE 11–3.—Sample suspension technique and thermocouple vacuum feed-throughs.

system by means of a Stupakoff fitting which is located in the adaptor ring, as previously mentioned. Thus the thermocouple wires are a continuous stretch of one metal only from the recorder terminals to the sample, the Stupakoff fitting having an equal number of copper and constantan lead-throughs. In this way stray thermal voltages, due to unequal temperature gradients between junctions of dissimilar metals, are avoided.

OPERATING PROCEDURE FOR OBTAINING THERMAL EMITTANCE MEASUREMENTS WITH THE GODDARD SPACE FLIGHT CENTER THERMAL VACUUM CHAMBER (FIGURES 11–4 AND 11–5)

The test samples are mounted in the shroud and, by adjusting the leads, are centered in the sight port. A small battery-powered incandescent light is placed at the arc crater position and is collimated to illuminate the samples. This enables the sample to be positioned so that its entire frontal area is illuminated. The wires are held in place by two alligator clips which are suspended from the top of the shroud interior by two lengths of cotton string (figure 11–3).

Next, the chamber is closed and pump-down is started. When the pressure is below 10^{-4} mm of Hg, liquid nitrogen is circulated through the shroud, the recorder is turned on, and shroud temperature is monitored. The system is ready for operation when the shroud has dropped in temperature to about $-190°$ C and its temperature is stable. (At equilibrium, the shroud is uniform in temperature to within $\pm 5°$ C.) At this point the pressure is normally in the low 10^{-6} range. To reduce the errors due to heat loss from the sample caused by gas conduction, the measurement procedure is not started until about one hour later, when the pressure has reached the low 10^{-7} range (the ultimate vacuum of the GSFC system is 2×10^{-7} mm of Hg, which is reached in 2½ hours).

The movable door in the shroud is now closed so that the arc can be turned on—and adjusted after it has warmed up—without being seen by the test sample prematurely. When the intensity is steady as determined by the pyrheliometer (figure 11–6), the movable door is opened and the heat-up data recorded. After the sample has traversed the desired temperature range, the movable door is closed and the arc lamp is shut down. The door remains closed until the arc carbons stop glowing. (The door is also closed during a heat-up run if the carbon arc lamp acts up and the intensity begins to wander.) For coatings which have a high $\bar{\alpha}/\bar{\epsilon}$ ratio, the motor-driven chopper is employed to reduce the illumination from the arc lamp which strikes the sample, and thus to bring the sample equilibrium temperature down to a value within the range of the recorder.

After the movable door is closed and the test sample is no longer illuminated by the carbon arc lamp, the sample starts to cool down. The sample temperature is also recorded during this cool-down process. The heat-up and subsequent cool-down cycle is repeated several times to increase the amount of data available and to improve the accuracy of the $\bar{\alpha}$ and $\bar{\epsilon}$ values derived from these data by averaging a number of measurements of $\bar{\alpha}$ and $\bar{\epsilon}$.

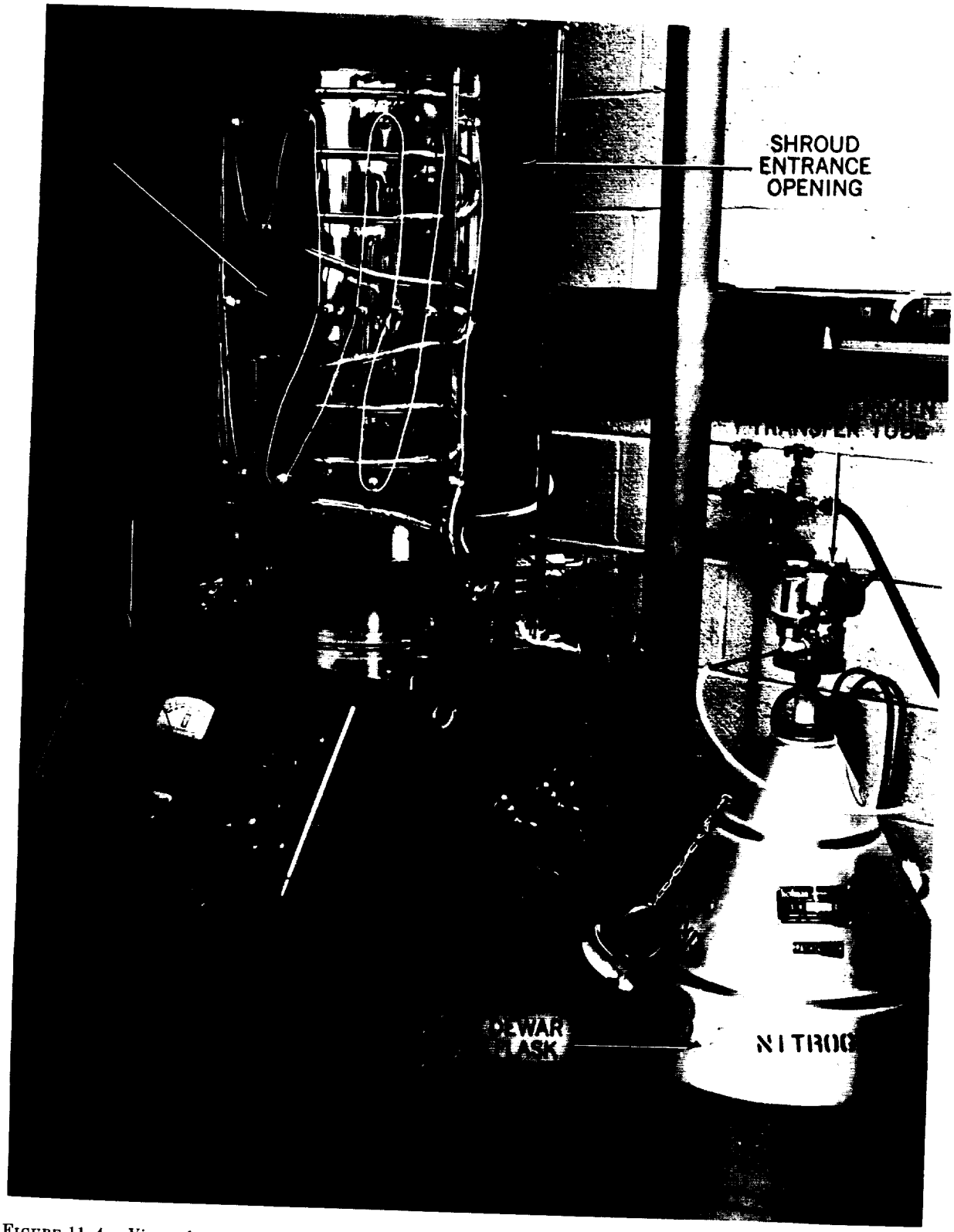

FIGURE 11–4.—View of the vacuum system and cooled shroud. Shroud is in the "open" position. Movable door is also open.

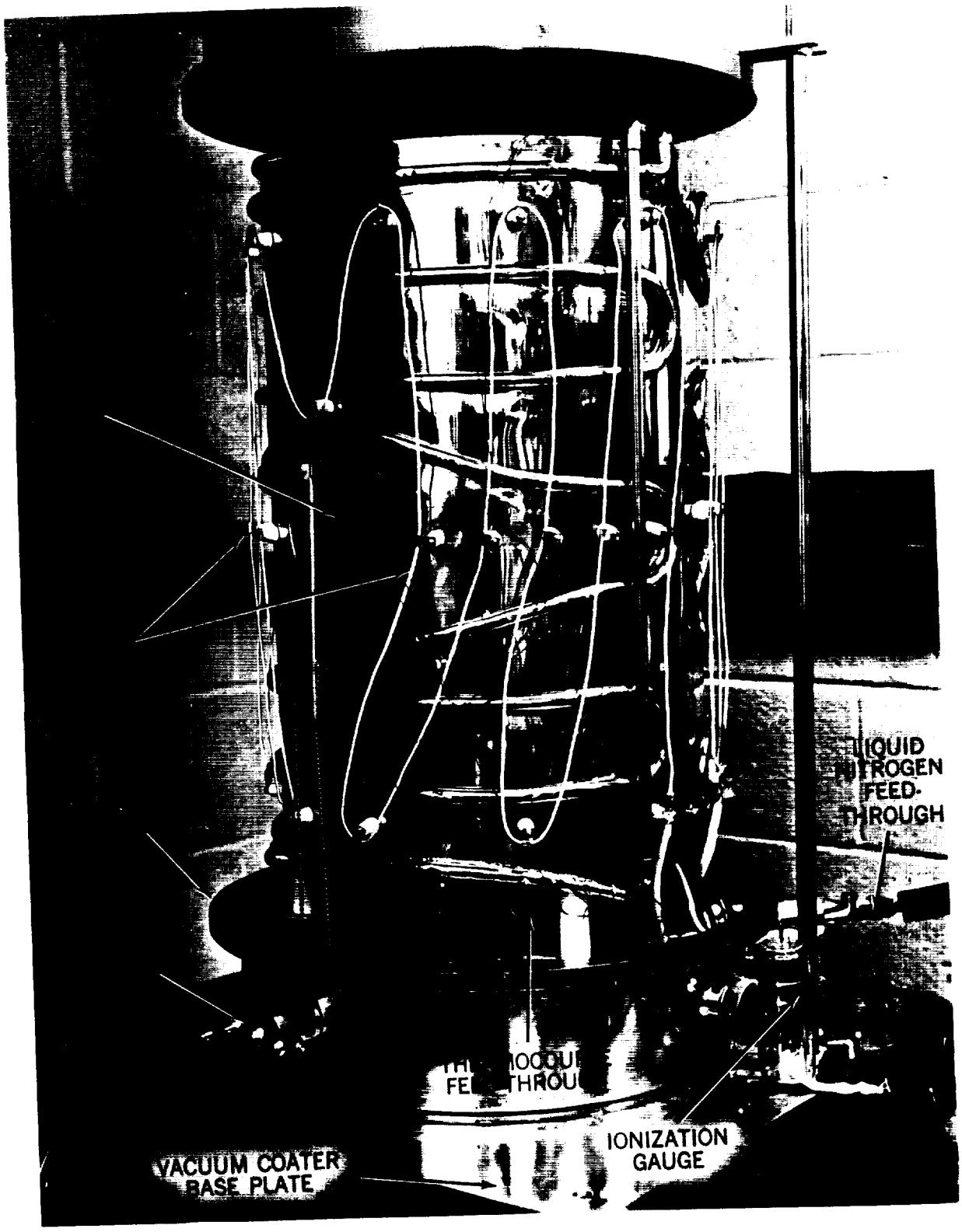

FIGURE 11–5.—Cooled shroud detail view, showing thermocouple leads and feed-throughs.

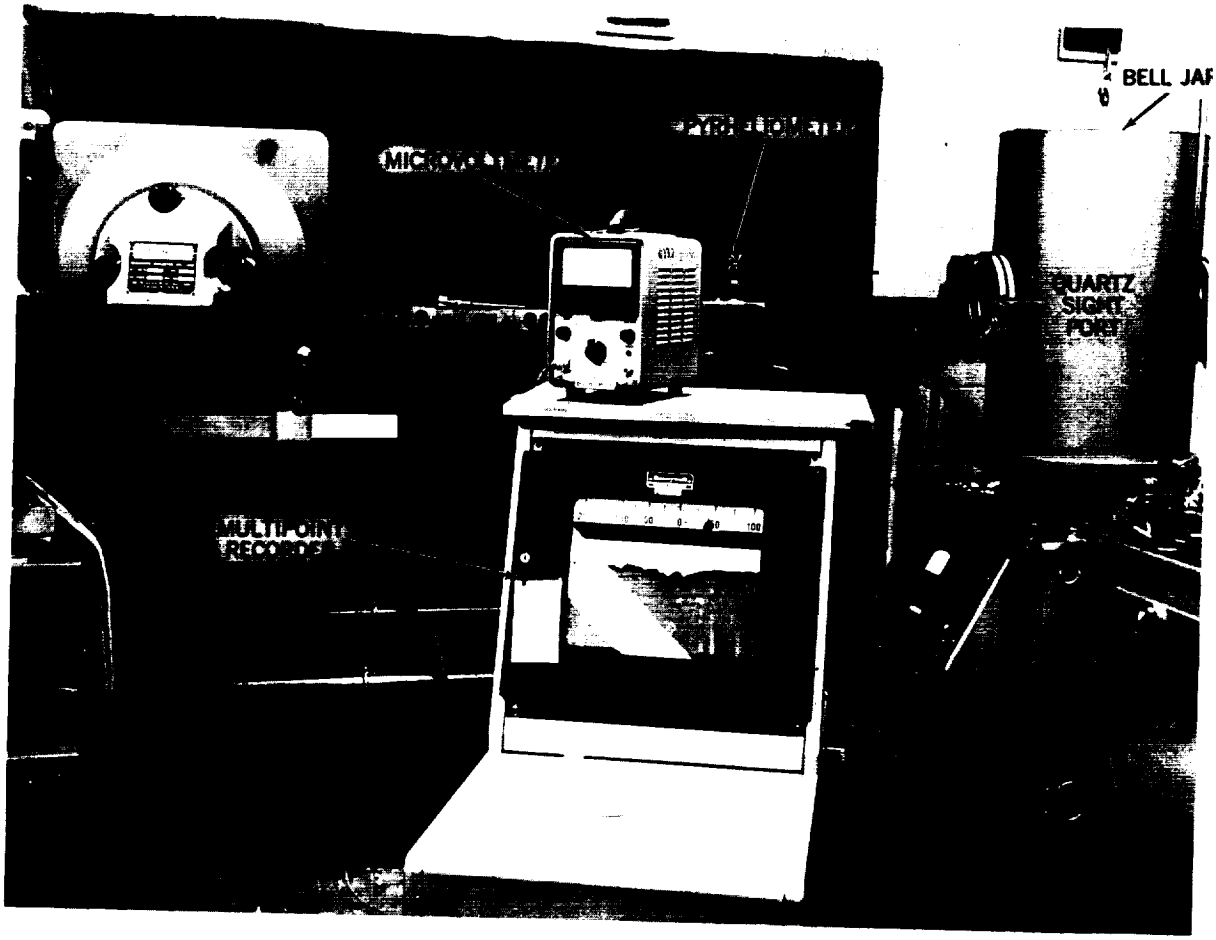

FIGURE 11-6.—View of the complete thermal vacuum setup, showing solar simulator (carbon arc), light-intensity measuring equipment, and multichannel temperature recorder. Bell jar is in the operating position.

THE MAJOR ERRORS AFFECTING THE ACCURACY OF $\bar{\alpha}$ AND $\bar{\epsilon}$ VALUES OBTAINED BY TRANSIENT THERMAL VACUUM TECHNIQUES

There are two types of errors to be considered: random errors and systematic errors.

The random errors are the major limitation of the accuracy of the measurements made with the present equipment. Most of the systematic errors can be computed and corrected for as is shown below. However, random errors in the temperature and light intensity measurements cannot be corrected for, but the magnitude of these errors can be estimated. The fractional errors due to random errors were calculated to be as follows:

(1) for thermal emittance values

$$\frac{\Delta\bar{\epsilon}}{\bar{\epsilon}}=\pm 0.070,$$

(2) for solar absorptance values

$$\frac{\Delta\bar{\alpha}}{\bar{\alpha}}=\pm 0.075,$$

(3) for $\bar{\alpha}/\bar{\epsilon}$ values

$$\frac{\Delta\left(\frac{\bar{\alpha}}{\bar{\epsilon}}\right)}{\left(\frac{\bar{\alpha}}{\bar{\epsilon}}\right)}=\pm 0.028.$$

FIGURE 11-7.—Solar simulator detail view, showing quartz collimating lens and positive and negative carbons.

These fractional errors can be reduced by taking the average of several measurements, or by improving the instrumental accuracies (reduced noise, for example) and the read-off accuracies. The assumptions made in calculating the fractional errors above are:

(1) $\sigma T^4 >> \sigma T_0^4$ (that is, sample equilibrium temperature, with *no* illumination) is much lower than ambient temperature.
(2) Measurements for $\bar{\alpha}/\bar{\epsilon}$ are made near the sample equilibrium temperature *with* illumination.
(3) The error in time measurement is negligible.
(4) The spectral match of the solar simulator with the solar spectrum is perfect.

The systematic errors are due to the following causes:

(1) thermal conduction losses through the leads
(2) variation in thermal emittance with temperature
(3) variation of specific heat of the substrate (copper) with temperature
(4) heat loss due to gas conduction
(5) temperature gradients within the test sample.

Each of these sources of error is now examined in detail:

Heat Loss Due to Thermal Conduction Through the Leads

Gordon (ref. 9) gives the following equations for the heat flow through a lead wire:

$$q=\pi\left[\frac{K\sigma\bar{\epsilon}_w D^3(T^5-5T_0^4T+4T_0^5)}{10}\right]^{1/2}, \quad (18)$$

where

q heat flow through the lead wire
K thermal conductivity of the wire
$\bar{\epsilon}_w$ thermal emittance of the wire
D diameter of the wire
T the sample temperature
T_0 the temperature of the wall of the vacuum chamber.

The derivation of this equation has been worked out by Gordon (private communication), also. It starts from the fundamental differential equation describing the heat flow.

$$K\frac{d^2\theta}{dx}\pi r_w^2=\bar{\epsilon}_w\sigma(\theta^4-T_0^4)2\pi r_w, \quad (19)$$

where new symbols are

θ temperature along the wire
r_w radius of the wire
x distance along the wire measured from the sample.

Then, by one integration, Gordon proceeds efficiently to equation (18). The wire is assumed to be semi-infinite, of isothermal cross-section so that the temperature is only a function of x; the heat flow is assumed to be steady-state. The boundary condition at $x=\infty$ is $T=T_0$ and $d\theta/dx=0$.

Gordon (ref. 9) further compares the heat flow through the lead wire with the radiative heat flow from the sample. He gives an upper bound for the fractional error in $\bar{\epsilon}$, the thermal emittance of the test sample, as

$$\frac{\pi}{A_s\bar{\epsilon}}\left[\frac{Ke_wD^3}{10\sigma T^3}\right]^{1/2}\geq E, \quad (20)$$

where

E fractional error in $\bar{\epsilon}$,
A_s surface area of the test sample.

A typical numerical example for a low emittance sample is:

K 0.97 cal-sec^{-1}-cm^{-1}-°K^{-1} (copper at 300° K)
$\bar{\epsilon}_w$ 0.04 (copper, 300° K)
D 0.005 in.=0.0127 cm
T 300° K
σ 5.67×10^{-5} erg-cm^{-2}-sec^{-1}-°K^{-4}
A_s 54.8 cm^2 (2 in.×2 in.×1/16 in.)
$\bar{\epsilon}$ 0.02 (vacuum-deposited gold).

Inserting these values in equation (20) gives an upper bound for the fractional error in $\bar{\epsilon}$ due to lead losses of 0.04. (The lead loss for the constantan lead of the copper-constantan thermocouple is negligible compared with the lead loss for the copper lead, due to the much lower relative thermal conductivity of constantan compared to copper.) (The fractional error in $\bar{\epsilon}$ is defined as $\Delta\bar{\epsilon}/\bar{\epsilon}$, where $\Delta\bar{\epsilon}$ is the absolute error in $\bar{\epsilon}$.) For samples possessing a higher thermal emittance, the fractional lead loss error given by equation (20) will be proportionately less, of course.

The Variation of Thermal Emittance With Temperature (Applies to Metals Only)

Jakob has shown that the thermal emittance of polished metals varies with the temperature. This is due to two factors: (1) The variation in the spectral emittance with wavelength, which is of the form

$$\epsilon_\lambda=0.476\left(\frac{r_e}{\lambda}\right)^{1/2}-0.148\,\frac{r_e}{\lambda}, \qquad (21)$$

where

ϵ_λ spectral emittance at wavelength λ
r_e electrical resistivity (cgs units)
(equation (21) holds for $0<r_e/\lambda<0.5$);

the variation in the electrical resistivity with temperature. For pure metals (ref. 12) the resistivity is approximately proportional to the absolute temperature. Considering equation (21), it is obvious that as the temperature increases and the maximum of the Planck blackbody spectrum shifts towards shorter wavelengths in accordance with Wien's law (ref. 13), the emittance will increase. Integration of equation (21) over the blackbody spectrum to obtain the total thermal emittance at a temperature of T° absolute yields

$$\bar{\epsilon}=0.751(r_eT)^{1/2}-0.396\,r_eT, \qquad (22)$$

where $\bar{\epsilon}$ is the thermal emittance, as always (equation (22) holds for $0<r_eT<0.2$).

For the region of interest, that is, for measurements of the thermal emittance of metals near ambient (300° K) temperature, a typical value of r_eT is 7.5×10^{-4} (cgs), for gold.

To consider the effect of the variation of the thermal emittance with temperature on the measured value of $\bar{\epsilon}$ computed from the slope—or tangent, if not a straight line—of the curve of dT/dt, plotted as a function of T^4, it is desirable to repeat equation (12) for the heat-up curve of the sample,

$$mc\,\frac{dT}{dt}=A_p\bar{\alpha}I+P-A_s\bar{\epsilon}\sigma T^4. \qquad (23)$$

Let

$$\frac{dT}{dt}=y,$$

$$T^4=x,$$

$$mc=c',$$

$$A_s\sigma=\sigma'.$$

Using these substitutions, equation (12) reduces to

$$c'y=A_p\bar{\alpha}I+P-\sigma'\bar{\epsilon}x. \qquad (24)$$

The tangent to the curve at the point (y, x) is $dy/dx\equiv y'$, and

$$c'y'=-\sigma'\bar{\epsilon}-\sigma'\bar{\epsilon}'x, \qquad (25)$$

where

$$\bar{\epsilon}'\equiv\frac{d\bar{\epsilon}}{dx}.$$

To evaluate $\bar{\epsilon}'$ in terms of $d\bar{\epsilon}/dT$ and dT/dx, since

$$\frac{d\bar{\epsilon}}{dx}=\frac{d\bar{\epsilon}}{dT}\cdot\frac{dT}{dx},$$

it is necessary to return to equation (22). This equation reduces to

$$\bar{\epsilon}=0.751(r_eT)^{1/2} \qquad (26)$$

for metals near ambient temperature. Equation (26) may be written in the form

$$\bar{\epsilon}=\bar{\epsilon}_0\frac{T}{T_0} \tag{27}$$

since—as mentioned above—

$$r_e\approx r_{e0}\frac{T}{T_0}, \tag{28}$$

where

$\bar{\epsilon}_0$ value of $\bar{\epsilon}$ at temperature T_0,
r_{e0} the value of r_e at T_0.

By equation (27), therefore,

$$\frac{d\bar{\epsilon}}{dT}=\frac{\bar{\epsilon}_0}{T_0} \tag{29}$$

and so it is found that

$$-c'y'=\frac{5}{4}\sigma'\bar{\epsilon} \tag{30}$$

or

$$\bar{\epsilon}=-\frac{4}{5}\left(\frac{c'y'}{\sigma'}\right). \tag{31}$$

On the other hand, assuming that $\bar{\epsilon}$ is not a function of T leads to the result

$$\bar{\epsilon}=-\left(\frac{c'y'}{\sigma'}\right). \tag{32}$$

Thus the value of $\bar{\epsilon}$ obtained by equation (32) must be multiplied by 4/5 to correct for the variation of $\bar{\epsilon}$ with T, if the sample coating is a pure metal. (Obviously the correction factor depends on the exponent of the power of T which best describes the variation of $\bar{\epsilon}$ with T for the material under investigation, even if it is not a pure metal.)

The Variation of Sample Specific Heat (Copper) With Temperature

The specific heat of copper varies quite rapidly with temperature from 0° K to about 300° K (ref. 14). From 300° K to higher temperatures, it increases linearly at a rate of roughly 0.01 cal-gm^{-1} °K^{-1} per 370° K. At 300° K the specific heat of copper is approximately 0.093 cal-gm^{-1} °K^{-1}.

If both c' and $\bar{\epsilon}$ are considered as functions of T in equation (13) above, then upon differentiating y with respect to x, it is found that

$$y\left(\frac{dc'}{dx}\right)+\left(\frac{dy}{dx}\right)c'=-\sigma'\bar{\epsilon}-\sigma'\left(\frac{d\bar{\epsilon}}{dx}\right)x,$$

or

$$y\left(\frac{dc'}{dx}\right)+\left(\frac{dy}{dx}\right)c'=-\frac{5}{4}\sigma'\bar{\epsilon}, \tag{33}$$

where some of the substitutions of the preceding section have been employed. Assume next that P' in equation (13) can be neglected and substitute the resulting value of y into equation (33) above to get

$$-\frac{\sigma'\bar{\epsilon}x}{c'}\left(\frac{dc'}{dx}\right)+c'\left(\frac{dy}{dx}\right)=-\frac{5}{4}\sigma'\bar{\epsilon}.$$

Therefore, solving for $\bar{\epsilon}$ leads to the result

$$\bar{\epsilon}=\frac{-c'\left(\frac{dy}{dx}\right)}{\sigma'\left[\frac{5}{4}-\left(\frac{x}{c}\cdot\frac{dc}{dx}\right)\right]}. \tag{34}$$

For the linear portion of the curve giving the specific heat of copper as a function of temperature, it is found that $(x/c')(dc/dx)=0.022$, approximately. This is much less than 5/4 and so the variation of specific heat of copper with temperature is insignificant above 300° K, but begins to be significant below 200° K.

Heat Losses Due to Thermal Conduction Through the Residual Gas in the Vacuum Chamber

The fractional error in $\bar{\alpha}/\bar{\epsilon}$, E, due to thermal conduction through the gas in the vacuum chamber is given by Gordon (ref. 9) as

$$E<\left(\frac{3}{2}\right)\frac{K(T-T_0)\nu}{\bar{\epsilon}\sigma(T^4-T_0^4)}<\left(\frac{3}{2}\right)\frac{K\nu}{\bar{\epsilon}\sigma T^3}, \tag{35}$$

where

K Boltzmann constant, 1.38×10^{-16} erg-deg^{-1}
ν number of molecules that impinge on unit area of the sample in unit time (about 1.3×10^{23} cm^{-1} sec^{-1} for air at STP)
T_0 temperature of the wall of the vacuum chamber, °K
T sample temperature,

and it is assumed that the average energy

transfer per molecule is not greater than $(3/2)K(T-T_0)$. This error is negligible at pressures in the 10^{-7} range, even with emittances as low as 0.01, for temperatures above 100° K. Even at very low temperatures near 100° K, the proportional error for an emittance of 0.01, and a pressure of 2×10^{-7} mm of Hg, will be only about 0.012.

DATA REDUCTION PROCEDURES

As mentioned in Section B2 of the Introduction, the values of $\bar{\epsilon}$ and $\bar{\alpha}/\bar{\epsilon}$ can be calculated by use of equations (14), (15), (16), and (17), so that (symbols defined in Section B2 a)

$$s_H=s_c=\frac{-\sigma A_s\bar{\epsilon}}{mc}$$

and

$$i_H-i_c=\frac{A_p\bar{\alpha}I+P}{\sigma A_s\bar{\epsilon}}-\frac{P'}{\sigma A_s\bar{\epsilon}}.$$

If it is assumed that errors mentioned in the preceding section have been corrected for, or found negligible, and if it is further assumed that $P=P'$ (that is, that the absorbed thermal power from the surroundings, specifically *excluding* the radiation from the solar simulator, is equal for both the heat-up and cool-down phases of the measurement), then

$$\bar{\epsilon}=\frac{-s_cmc}{A_s\sigma}=\frac{-s_Hmc}{A_s\sigma} \tag{36}$$

and

$$\frac{\bar{\alpha}}{\bar{\epsilon}}=(i_H-i_c)\frac{\sigma A_s}{IA_p}. \tag{37}$$

Note that if dT/dt is plotted against σT^4 instead of T^4 as abscissa, then the σ drops out of the above equations (36) and (37).

The data are recorded in the form of temperature as a function of time by the multipoint recorder. The intensity of the solar simulator is measured by the pyrheliometer and the microvoltmeter. A smooth curve is run through the temperature-time data so that the "noise" can be eliminated, the slope (or tangent) is read from this curve at desired intervals. Ship's curves are very useful for the curvefitting process. The time interval chosen varies inversely with the rate of temperature change, for instance, this interval near equilibrium (dT/dt very small) is as long as 640 seconds for samples coated with vacuum evaporated metals of low emittance.

Tables of σT^4 in watts/cm^2 are employed, the values of T running from 0° K to 600° K in 0.1° intervals, and are found to expedite the calculations. The tables can easily be run off on an IBM digital computer such as the 7090. Since the heat-up and cool-down lines, on the graph of dT/dt vs. σT^4, are usually parallel (if the surroundings remain at a constant temperature, the lines are parallel), the emittance can be calculated from either line; the cool-down line, however, has more data points (since dT/dt is less in absolute value for the cool-down curve than it is for the heat-up curve) and hence is more reliable for this reason.

After uncorrected values of $\bar{\epsilon}$ and $\bar{\alpha}$ have been obtained in this manner, the four systematic errors listed are calculated and the appropriate corrections made.

The table presents the results of some measurements which have been made by the Thermal Systems Branch at GSFC. The results of both optical and thermal vacuum measurements are given. Conversion factors for converting total normal emittance (from optical measurements) to total hemispherical emittance (from thermal vacuum measurements), and vice versa, are given in Jakob's text on heat transfer (ref. 8). For very low emittance metal coatings, for example, the ratio of total normal to total hemispherical emittance is about 1.3. For dielectrics having a total normal emittance of 0.9, the ratio is 0.935.

Figure 11–8 shows a typical plot of dT/dt versus σT^4 for carbon black silicone base paint.

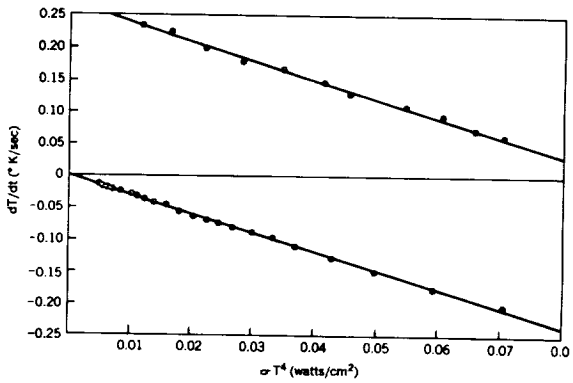

FIGURE 11–8.—Graph showing typical data for derivative of temperature with respect to time (dT/dt) as ordinate plotted against σT^4 as abscissa (σ=the Stefan-Boltzmann constant), for carbon black in silicone vehicle paint.

TABLE 11–I.—*Comparison of Values of Solar Absorptance and Thermal Emittance, Obtained by Both Optical and Thermal Vacuum Measurements, for Four Common Spacecraft Coatings (Vacuum-deposited metals and paint)*

Coating	(1) $\left(\frac{\bar{\alpha}}{\bar{\epsilon}}\right)_H$	(2) $\bar{\epsilon}_{\nu_c}$	(3) $\bar{\epsilon}_{NC}$	(4) $\bar{\epsilon}_{NM}$	(5) $\bar{\alpha}_c$	(6) $\bar{\alpha}_{DK}$
Evaporated gold	9. 2	0. 0239	0. 015	----	0. 183	0. 200
Aluminized Mylar*	2. 68	. 0618	. 037	0. 035	. 129	. 131
Evaporated aluminum	4. 02	. 0424	. 026	. 022	. 17	. 156
Carbon black paint, silicon vehicle	1. 18	. 817	. 872	. 907	. 964	. 956

(1) $\left(\frac{\bar{\alpha}}{\bar{\epsilon}}\right)_H$ = ratio of solar absorptance to total hemispherical emittance (for T = 300° K).
(2) $\bar{\epsilon}_{\nu_c}$ = uncorrected total hemispherical emittance, as measured thermally.
(3) $\bar{\epsilon}_{NC}$ = corrected total normal emittance, calculated from thermally measured total hemispherical emittance.
(4) $\bar{\epsilon}_{NM}$ = total normal emittance, measured optically (should be close to value of (3)).
(5) $\bar{\alpha}_c$ = solar absorptance calculated from thermal measurements with a carbon arc solar simulator.
(6) $\bar{\alpha}_{DK}$ = solar absorptance, from optical measurements (should be close to value of (5)).
*With scribed lines 2–3 mils thick forming ¼-in. squares of evaporated aluminum.

Some evaluation of the system can be made by making note of the parallel lines and the cool-down intercept of the abscissa (near zero).

CONCLUSIONS

The accuracy of the measured $\bar{\alpha}/\bar{\epsilon}$ ratio is probably less than that predicted, since the spectral match of the solar simulator (carbon arc lamp) with the solar spectrum is not exact. (A project for future investigation will be to measure the spectral distribution of the carbon arc as a function of the current and intensity.)

The accuracy of the thermal emittance measurement is especially good for low emittance materials—compared with the accuracy of the optical and thermal equilibrium methods of measuring $\bar{\epsilon}$ for these materials—and therefore this type of measurement fills a need even though it consumes more man-hours of labor than the optical method by a factor of perhaps 2, since one thermal vacuum measurement requires about 6 man-days.

All the emittance data in table 11–I are within the accuracy predicted. The accuracy can be improved by increasing the accuracy of temperature measurement; probably this can be effected by using a manually balanced potentiometer bridge to measure the thermocouple voltages.

FUTURE IMPROVEMENTS AND MODIFICATIONS TO THE PRESENT EQUIPMENT

Improvements and modifications planned for the near future are:

(1) a multisample holder which will permit more than one set of measurements for each pump-down of the vacuum system.

(2) a digital computer program which will allow a good deal of the data reduction process described to be done by a computer. It is estimated that this computer program will reduce the number of man-days consumed in data reduction for each measurement from 3 to 0.5. Initially the data will be acquired from the multipoint recorder chart and reproduced on punched cards suitable for one of the GSFC IBM 7090 digital computers. Eventually, it is planned to digitalize the output of the multipoint recorder and then feed this digital output directly to a computer.

(3) an oil-free vacuum system. This vacuum system will eliminate the possibility of oil from the diffusion pump backstreaming onto the test sample. At present backstreaming is prevented by continuously running liquid nitrogen through the shroud and baffle; however, when the

liquid nitrogen is not used, test samples quickly (less than 1 day) become contaminated with oil. The oil-free vacuum system will employ a conventional mechanical forepump coupled with a Welch No. 1377A Turbo-Molecular pump which works on the molecular-drag principle (ref. 15). This type of pump uses no oil except for lubrication, but probably a cooled baffle or trap will also be useful here. The oil-free vacuum system will also eliminate the possibility of a diffusion pump "boiling over" due to failure of the cooling water.

REFERENCES

1. Hass, G.; Drummeter, L. F.; and Schach, M.: Temperature Stabilization of Highly Reflecting Spherical Satellites. Jour. Optical Soc. America, vol. 49, no. 9, Sept. 1959, pp. 918–924.
2. Johnson, F. S.: The Solar Constant. Jour. Meteorol., vol. 11, no. 6, Dec. 1954, pp. 431–439.
3. Jacquez, J. A.; and Kuppenheim, H. F.: Theory of the Integrating Sphere. Jour. Optical Soc. America, vol. 45, no. 6, June 1955, pp. 460–470.
4. Jenkins, F. A.; and White, H. E.: Fundamentals of Optics. 3d ed., McGraw-Hill, 1957, pp. 531, 208, 429, and 434.
5. Ibid. p. 208.
6. Ibid. p. 429 ff.
7. Jakob, M.: Heat Transfer. John Wiley & Sons, Inc., 1949, vol. 1, pp. 41–52.
8. Ibid. p. 52.
9. Gordon, G. D.: Measurement of Ratio of Absorptivity of Sunlight to Thermal Emissivity. Rev. Sci. Instr., vol. 31, no. 11, Nov. 1960, pp. 1204–1208.
10. Butler, C. P.; and Inn, E. C. V.: The Total Hemispherical Emissivity of Metals. U.S. Naval Radiological Defense Laboratory, Tech. Rep. USNRDL-TR-327, May 1959.
11. Jakob, op. cit., p. 51.
12. Jakob, op. cit., p. 45.
13. Jenkins and White, op. cit., p. 434.
14. Goldsmith, A.; Waterman, T. E.; and Hirschhorn, H. J.: Thermophysical Properties of Solid Materials. Elements (Melting Temperature Above 1000° F). Rev. Ed., Armour Res. Found. WADC Tech. Rep. 58–476, vol. 1, Aug. 1960.
15. Becker, W.: Uber Eine Neue Molekularpumpe. Advances in Vacuum Science and Technology, (E. Thomas, ed.), Proc. 1st Internat. Congress on Vacuum Techniques, Namur, Belgium, June 1958. Pergamon Press, 1960, vol. 1, pp. 173–176.

DISCUSSION

G. F. Vanderschmidt, Lion Research Corporation: Without going too deeply into the difference between this paper and the one submitted by me with Gaumer and Hohnstreiter, I would like to point out a few differences in approach. Our paper describes two instruments, one of which is used for measuring the far infrared emittance of the surface. This instrument is unique and the Fossell, Triolo, and Jerozal approach cannot be used for this purpose.

The second instrument described in our paper is a reflectometer, very similar in application to that described by Fussell, Triolo, and Jerozal but somewhat different in constructional details. The most important difference in out reflectometer design is that it permits measurement in the ultraviolet out to 2537Å. The region at 2537Å is of particular interest since deterioration of coated surfaces almost always first appears as an increase in absorption in this region of the spectrum.

12—PORTABLE INTEGRATING SPHERE FOR MONITORING REFLECTANCE OF SPACECRAFT COATINGS

BY W. B. FUSSELL AND J. J. TRIOLO

NASA GODDARD SPACE FLIGHT CENTER, GREENBELT, MARYLAND

AND F. A. JEROZAL

CONTINENTAL TECHNICAL SERVICE, INCORPORATED, SILVER SPRING, MARYLAND

In the thermal design of spacecraft, the input term in the radiation balance equation for a space vehicle in free space—removed from significant earth radiation—is directly proportional to the solar absorptivity of the illuminated portion of the vehicle. For opaque spacecraft coatings, incident solar radiation which is not absorbed must be reflected; thus, the solar absorptivity of such coatings can be computed from spectrally resolved total reflectance measurements. The solar absorptivities of spacecraft coatings in common use can be estimated to within approximately $\pm 20\%$ or better by using total reflectance data at wavelengths between 0.27 and 1.65μ.

An integrating sphere is the most convenient device for measuring the total reflectance of opaque coatings of different degrees of curvature, specularity, and diffusivity. A portable single-beam, 6-inch diameter integrating sphere reflectometer has been designed and fabricated at the GSFC and has been extensively used to detect changes in the solar absorptivity of spacecraft coatings due to environmental testing, ageing, or contamination. The interior of the sphere is coated with six coats of a barium sulfate powder (USP), mixed with 0.2% sodium (carboxymethl) cellulose as binder, over a machined (nonpolished) aluminum surface. This coating has a reflectance of 0.93 at 0.4μ, 0.96 at 0.6μ, and 0.96 at 0.8μ, assuming it to be equal to the coating of Middleton and Sanders. This type of coating was employed because of its much greater durability, compared to magnesium oxide.

The sphere has provision for the insertion of standard 2 x 2-inch square interference filters for spectral resolution. Commercially available photomultiplier tubes as detectors are used and a commercially available amplifier with a large D'Arsonval-type meter as the output indicator. It was necessary to employ an ultra-stabilized (better than 0.01% regulation for both line and load) power supply for the light source of the integrating sphere to obtain satisfactory stability. It was also necessary to "age" the lamps used in the light source for about 1 hour to ensure stability; in addition, a magnetic-type voltage regulator was used in the power line to the photomultiplier power supply and output amplifier. Short-term fluctuations under these conditions were found to be less than $\pm 0.5\%$, and long-term drift was less than 8% per day.

The optic axis of the light source was displaced by 7½° from the sphere radius through the center of the sample port; since the diameter of the light port is ¾ inch, this allows specular (and diffuse) surfaces having radii of curvature greater than 3 inches to be measured without an abnormal and uncorrectable amount of light lost out the light source port. Experimental tests with the sphere on specular, gold-plated, cylindrical shells of radii 3.5, 6.5, 12.5, 18.5, and 24.5 inches showed no significant geometrical effect on sphere efficiency. Using the formula given by Jacquez and Kuppenheim for a "perfect" sphere, and the substitution method, it was estimated that the maximum absolute error for the sphere is 4.4% at 0.4μ, 7.2% at 0.6μ, 6.5% at 0.8μ, and 5.3% at 1.0μ; these data are for a standard having 100% reflectance, a

692-146 O—63——8

sample having 0% reflectance, and a sphere coating of barium sulfate paint.

The Importance of Total Reflectance Measurements on Coatings in the Thermal Design of Spacecraft

In the thermal design of spacecraft (ref. 1) the input term in the radiation balance equation for a space vehicle in free space—removed from significant earth radiation—is directly proportional to the average solar absorptance of the illuminated portion of the vehicle. The output term in the radiation balance equation—neglecting internally generated power—is directly proportional to the average thermal emittance of the total exterior surface of the space vehicle. To this approximation, therefore, its equilibrium temperature is proportional to $(\bar{\alpha}/\bar{\epsilon})^{0.25}$, where $\bar{\alpha}$=average solar absorptance, and $\bar{\epsilon}$=average thermal emittance. In a space vehicle whose outer surface is composed of several materials, $\bar{\alpha}$ is computed by summing up individual terms for each material illuminated by the sun. Each term is the product of its solar absorptance (which will in general depend on the angle of incidence of the sun's rays on each element of surface) multiplied by the fraction of the total projected area normal to the direction of illumination which the material occupies.

It is thus highly desirable to be able to measure at least the normal solar absorptance of small areas of a space vehicle's surface. For opaque spacecraft coatings, incident solar radiation which is not absorbed must be reflected. The solar absorptance of such coatings can, therefore, be computed from spectrally resolved total reflectance measurements. (When a solar simulator—a terrestrial light source whose spectral distribution matches that of the sun from the thermal design point of view—is available, a total reflectometer can be devised which will yield the solar absorptance from non-spectrally resolved data. This is a project of great merit.)

Although it is desirable to obtain a complete curve of the total reflectance of a given coating as a function of wavelength from at least 0.3 to 2.5 μ, suitable assumptions about—or prior knowledge of—the general nature of the absorptance spectrum often make data at a few selected wavelengths very helpful and enable an approximate estimate of the solar absorptance to be made from such data. In most cases the coating material is known, and the problem is one of detecting small changes in the solar absorptance due to "contamination", that is, to surface deterioration caused by handling, corrosion, tarnishing, or environmental testing.

Metal surfaces are usually more sensitive to contamination and surface condition than paints. This is partly due to their low absorptance when clean, vacuum-deposited, surfaces are measured. For example, the solar absorptances of some common metals are: (1) aluminum, $\bar{\alpha}$=7.78%; (2) gold, $\bar{\alpha}$=19.25%; (3) silver, $\bar{\alpha}$=4.9%; and (4) rhodium, $\bar{\alpha}$=18.25% (ref. 2). It is especially important, therefore, that metallic spacecraft coatings be checked frequently for increased values of solar absorptance due to surface deterioration. It is of interest at this point to note that 80% of the absorbed solar energy lies between 0.27 and 0.89 μ for silver, and between 0.41 and 1.13 μ for aluminum. In both cases, 10% of the absorbed energy occurs at shorter wavelengths than the short wave limits, and another 10% occurs at longer wavelengths than the long wave limits. For a perfect black paint, the 80% limits—as defined above—are 0.41 and 1.65 μ. It is believed that measurements of absorptance between the 80% limits for any coating should enable the solar absorptance of the coating to be estimated to better than 20% of its true value. Figure 12–1 presents the absorptance spectra of the four metals mentioned: aluminum, gold, silver, and rhodium. The data are those given by Dr. Hass of ERDL, Fort Belvoir, in the AIP Handbook. Silver and aluminum represent the opposite extremes with respect to the wavelengths of the dominant regions of absorption. For comparison, the solar extra-terrestrial spectrum, derived from Johnson's data (ref. 3) is displayed in figure 12–2. Figures 12–3 and 12–4 present the average absorptances for aluminum, gold, silver, and rhodium, multiplied by the percentage of solar energy increments for small bandwidths, starting (except for silver, where 0.25 μ, is the initial point) at 0.30 μ and running out past 5 μ and integrated from a nominal λ=0 to

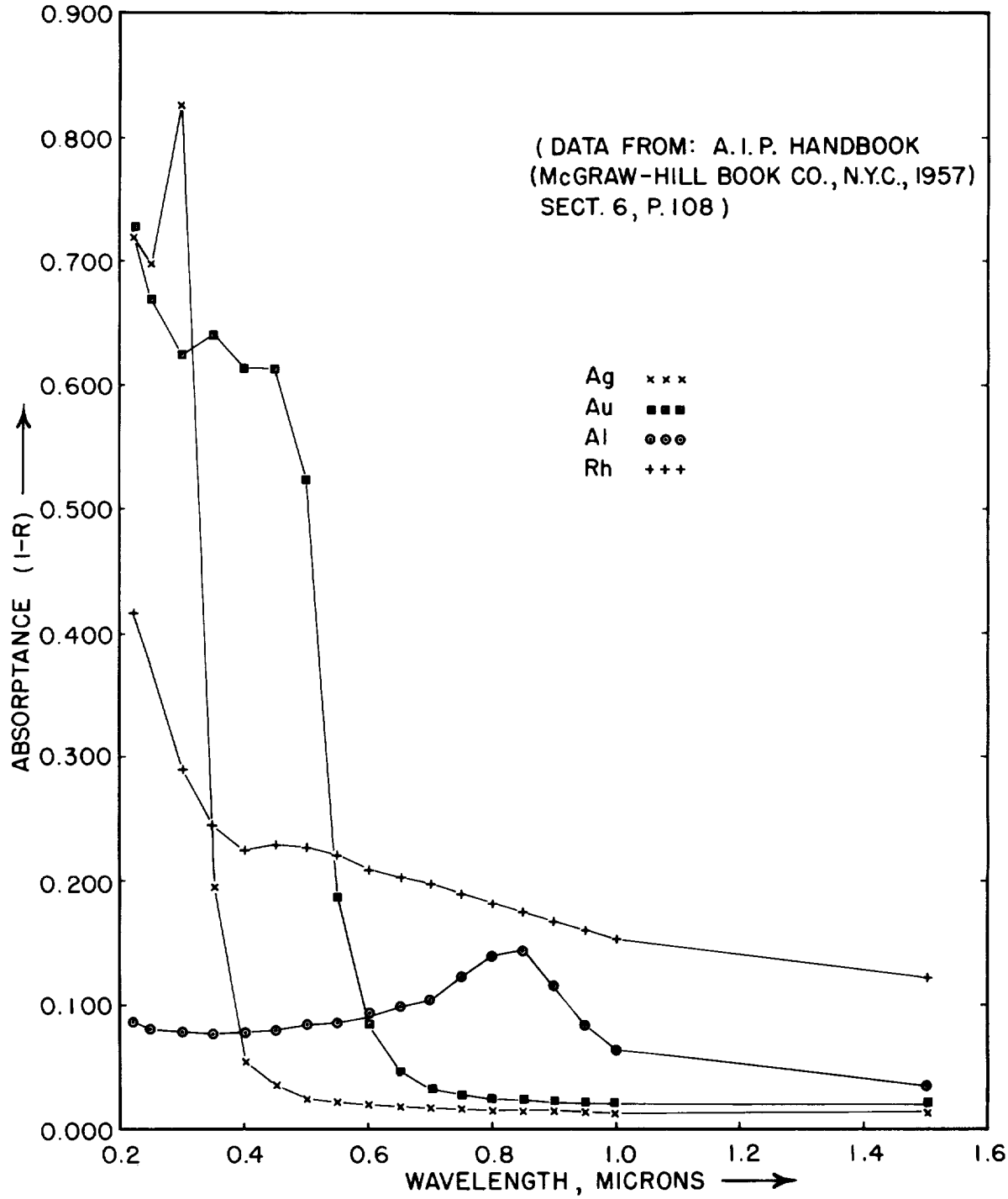

FIGURE 12-1.—Absorptance plotted against wavelength for aluminum, silver, gold, and rhodium.

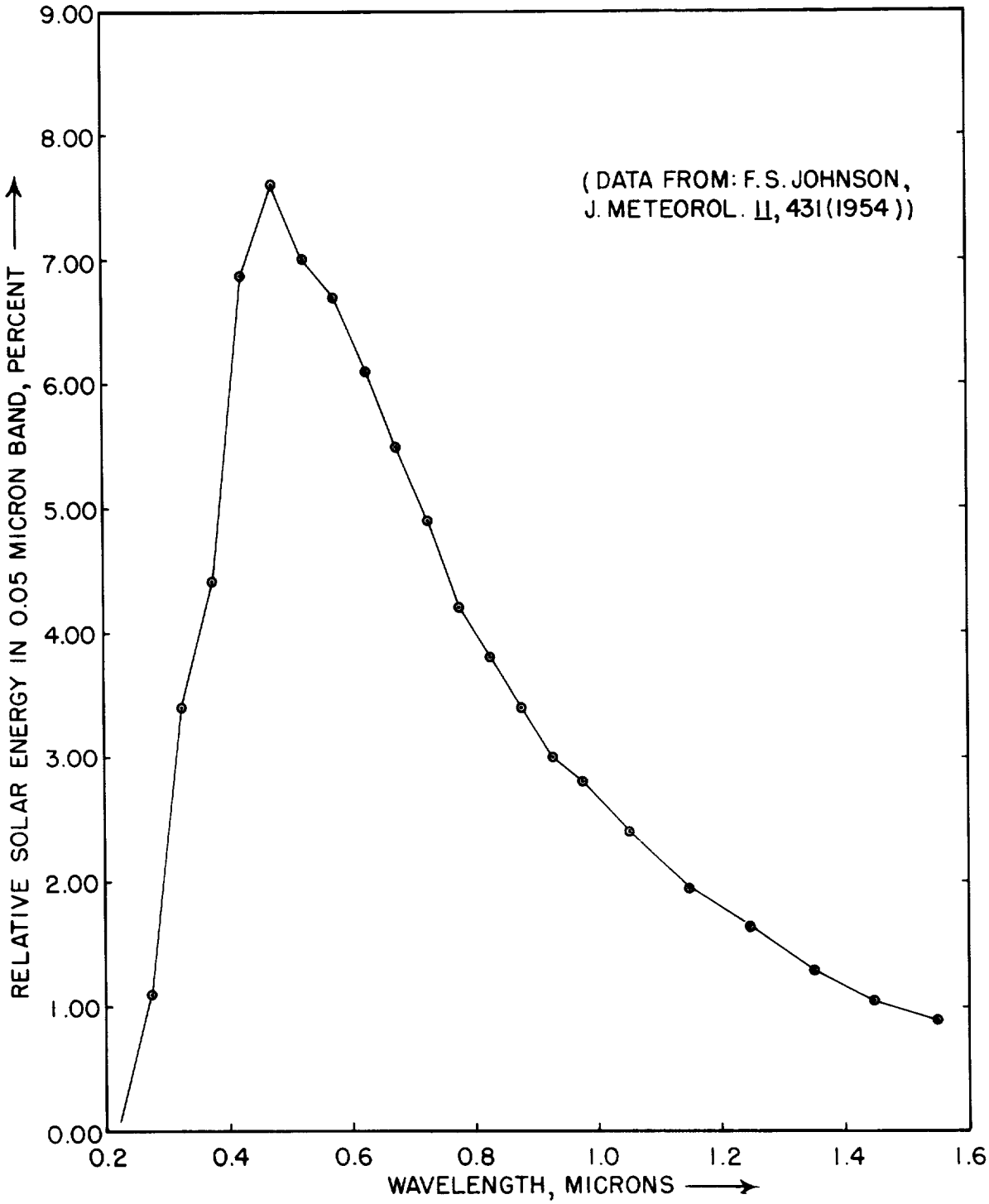

FIGURE 12-2.—Extra-terrestrial solar spectrum plotted against wavelength.

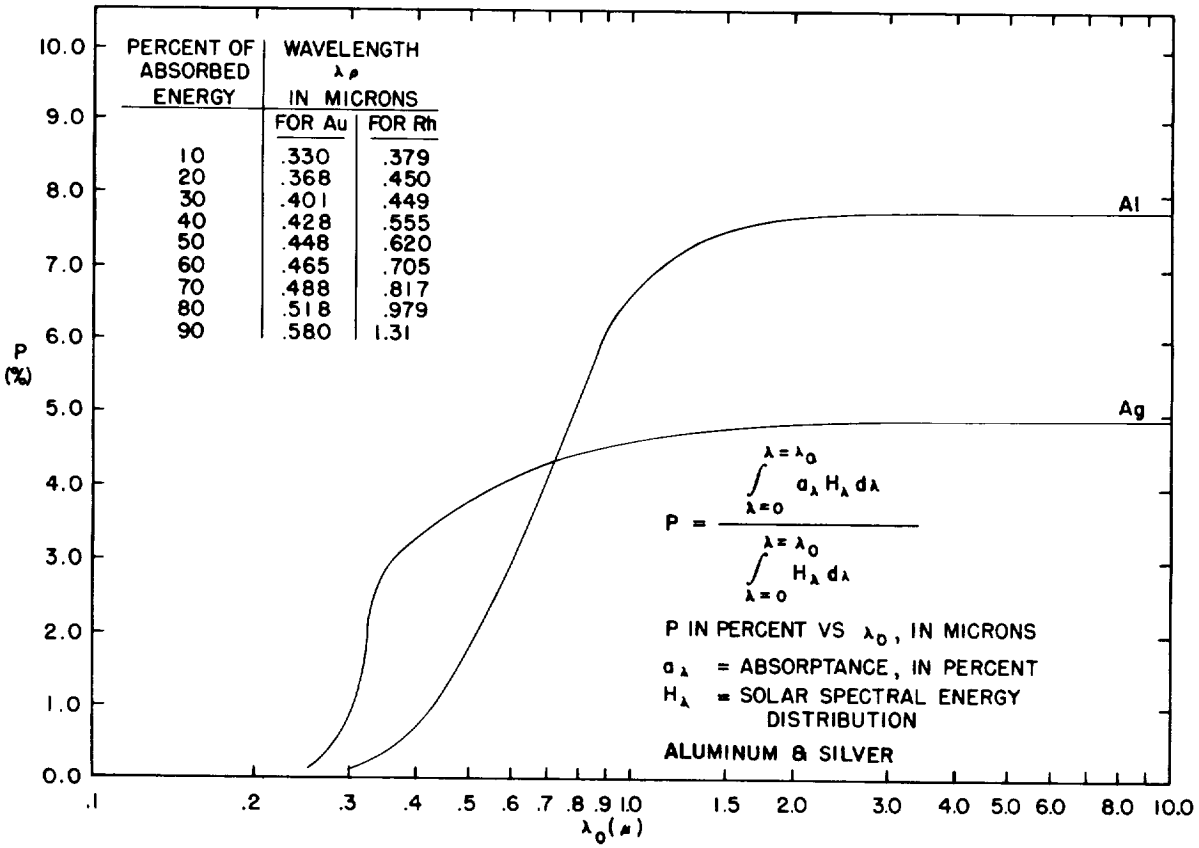

FIGURE 12-3.—Percentage of absorbed solar energy from a nominal $\lambda=0$ to $\lambda=\lambda_0$ plotted against λ_0 (wavelength) for aluminum and silver.

$\lambda=\lambda_0$ vs λ_0, the wavelength. These data give a good picture of the dominant wavelength interval within which the major portion of the sun's energy is absorbed by each of these metals.

Description of the Integrating Sphere Coatings Monitor and Its Purpose

Spacecraft surfaces often have various degrees of curvature and surface roughness. An integrating sphere is a convenient device for measuring the total reflectance of such surfaces, since it collects nearly all the reflected light, independently of whether the light is diffusely or specularly reflected and, also, independently of the radii of curvature of the surfaces, provided the radii are larger than a certain minimum radius which is set by the geometry of the sphere.

Figure 12-5 presents a cross-section view of a portable, 8-lb, 6-inch diameter, single-beam, integrating sphere fabricated recently at GSFC for monitoring the solar absorptance of spacecraft coatings. The interior of the sphere is coated with the barium sulfate paint described by Middleton and Sanders (ref. 4).

As figure 12-5 shows, light from the lamp goes through the small aperture (apertures available ranging in size from 1/16-inch to 3/8-inch diameter). (A collector lens between the lamp and the aperture would be desirable here to increase the amount of light collected from the lamp.) The aperture is focused by the glass lens onto the sample which is pressed close to the exterior of the sample port. Light reflected from the sample is collected by the sphere (in diffusely reflecting materials, a small fraction of the light is lost out the light source port) and produces uniform illumination on the inner wall of the sphere which is viewed by the photomultiplier detector. There is a slot in the light source housing into which standard 2 x 2-inch square interference—or other—filters can be inserted. The lamp used in the light

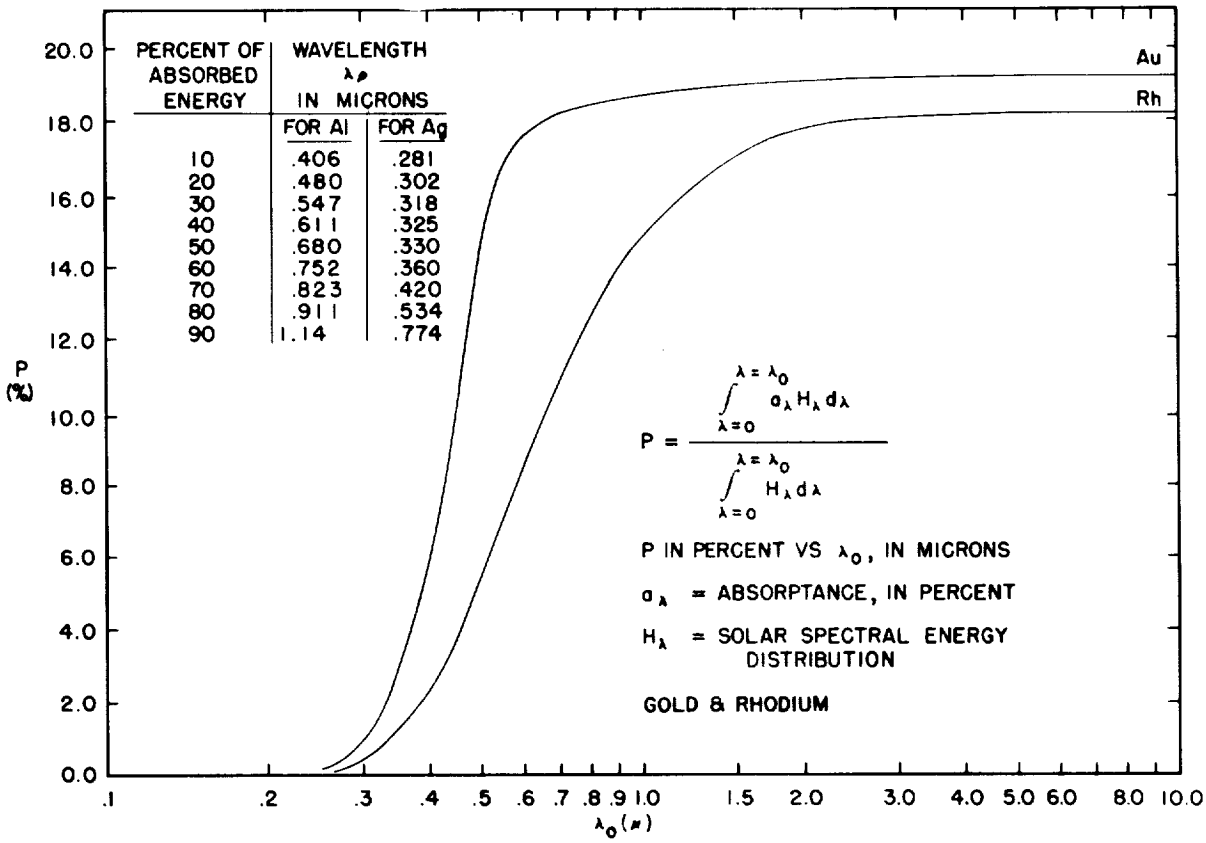

FIGURE 12-4.—Percentage of absorbed solar energy from a nominal $\lambda=0$ to $\lambda=\lambda_0$ plotted against λ_0 (wavelength) for gold and rhodium.

source is a General Electric No. 1493 microscope illuminator lamp. This is rated at 6.5 volts and 2.75 amperes. It has been found [1] that the luminous intensity of a new lamp is not steady; however, if the lamp is aged for an hour at its rated voltage and current, it becomes stable thereafter. Satisfactory stability of the light output from the lamp can be achieved only with an ultra-stabilized power supply for the lamp.

It can easily be shown that the light output from the lamp (considered as a grey body) over a narrow wavelength interval is a very sensitive function of the temperature. For example, for a lamp having a color temperature of 2800° K, the radiant output at a wavelength of 5000 A varies as the equivalent of the 10th power of the temperature, that is,

$$\frac{J_\lambda(T+\Delta T)}{J_\lambda(T)} = 1+\frac{\Delta T}{T}\frac{C_2}{\lambda T} = 1+10\frac{\Delta T}{T}$$

where

J_λ radiant output per unit wavelength interval and unit surface area
T absolute temperature of the lamp, °K
C_2 1.438 cm-°K
λ wavelength cm.

After some experimentation, a Harrison Laboratories model 808 AX power supply was found satisfactory. This is a chopper-stabilized, regulated power supply which regulates to better than 0.01% (or 1 millivolt) for both line and load.[1] The photomultiplier tube, its housing, and its associated amplifier, power supply,

[1] Jerozal, F. A.: Report on Coatings Monitor. NASA Goddard Space Flight Center in-house report, I 633-62-6, April 1962.

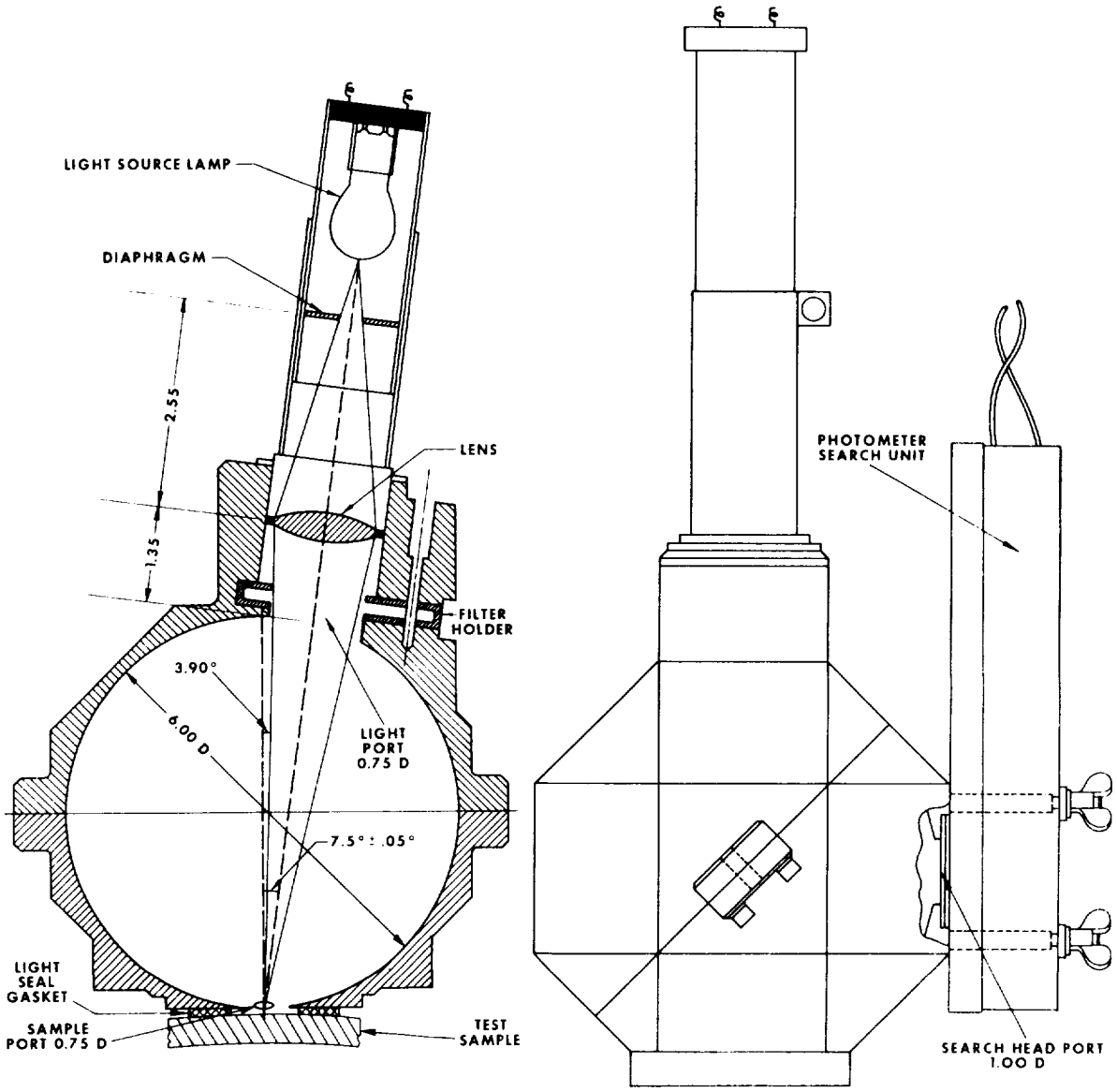

FIGURE 12–5.—Cross-section view of integrating sphere. All dimensions in inches.

and output indicating meters are part of a Photovolt Corporation model 520–M photometer. Photomultiplier tubes having S–1, S–4, S–5, and S–11 spectral sensitivity cathodes are available as accessories for this equipment. It was also found necessary to use a Sola model CV–1 constant voltage transformer (500 va-115 volts) in the power line for the 520–M photometer obtained from Allied Radio Corporation. This is a harmonic-free, static magnetic type of voltage regulator.[1] The 520–M has a small, internal magnetic regulator, but this proved insufficient to provide adequate stability. Combined with the ultrastable light source power supply, the model CV–1 magnetic voltage regulator used as described above gave a highly stable output. Short-term fluctuations were less than $\pm 0.5\%$, and long-term drift was less than 8% per day.

Figure 12–6 displays the complete integrating sphere coatings monitor apparatus. The integrating sphere is at the left; attached to

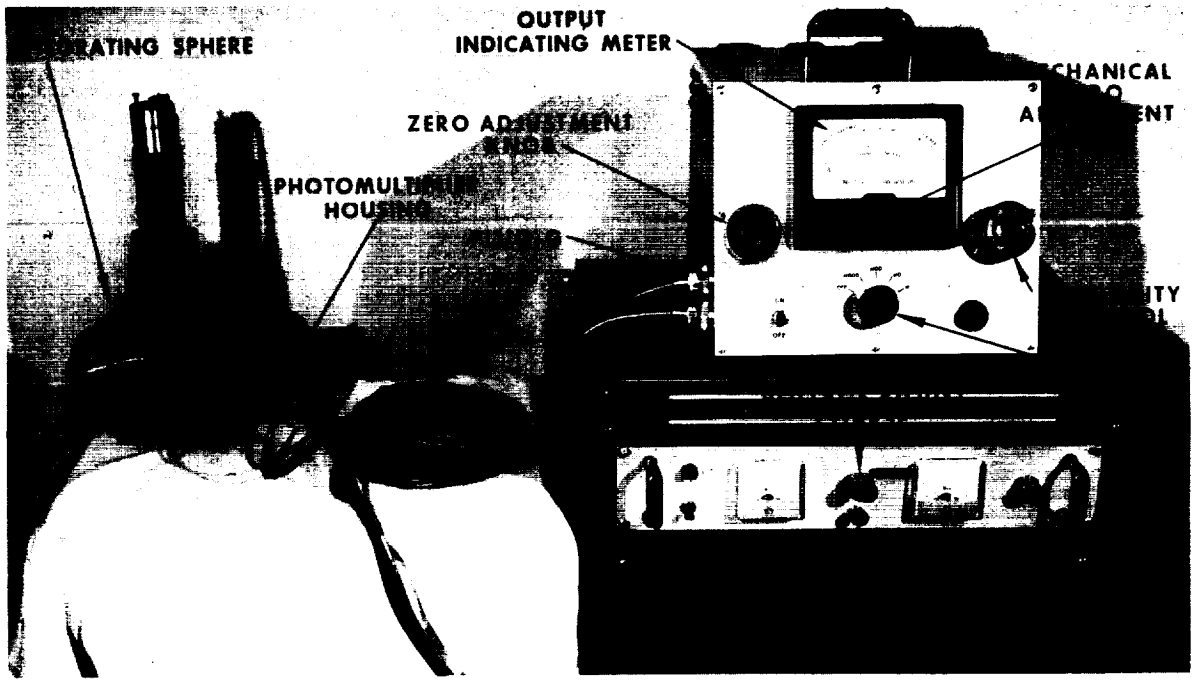

FIGURE 12–6.—Reflectance monitor panel components.

the right side of the sphere is the photomultiplier housing. On top of the power supply console, at right, is the Photovolt photometer amplifier, showing the large meter which indicates the light level striking the photomultiplier tube. (The photometer has provision for attaching a recorder. As yet, however, a recorder has not been used with this equipment.) Figure 12–7 shows the rear stowage compartments of the power supply console with the integrating sphere and output indicators in position. The total weight of the integrating sphere with the detector housing and light source attached is about 8 lb.

The operating procedure for the sphere [1] is briefly as follows:

1. The lamp and the photomultiplier supply are turned on and the equipment allowed to warm up for ½ hour
2. An opaque blank is put in the filter slot and the output meter checked for zero on all ranges. (The sample port, of course, must also be blocked off during this check.)
3. With the high voltage off the photomultiplier dynodes to avoid damage to the

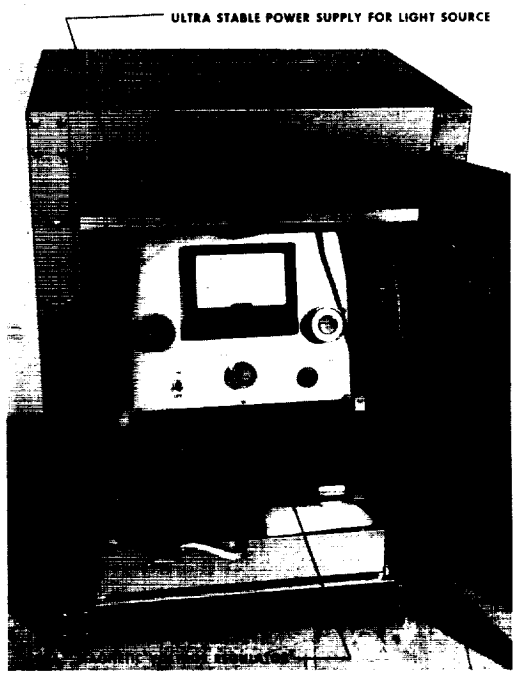

FIGURE 12–7.—Reflectance monitor stowage compartment.

[1] See footnote on p. 108.

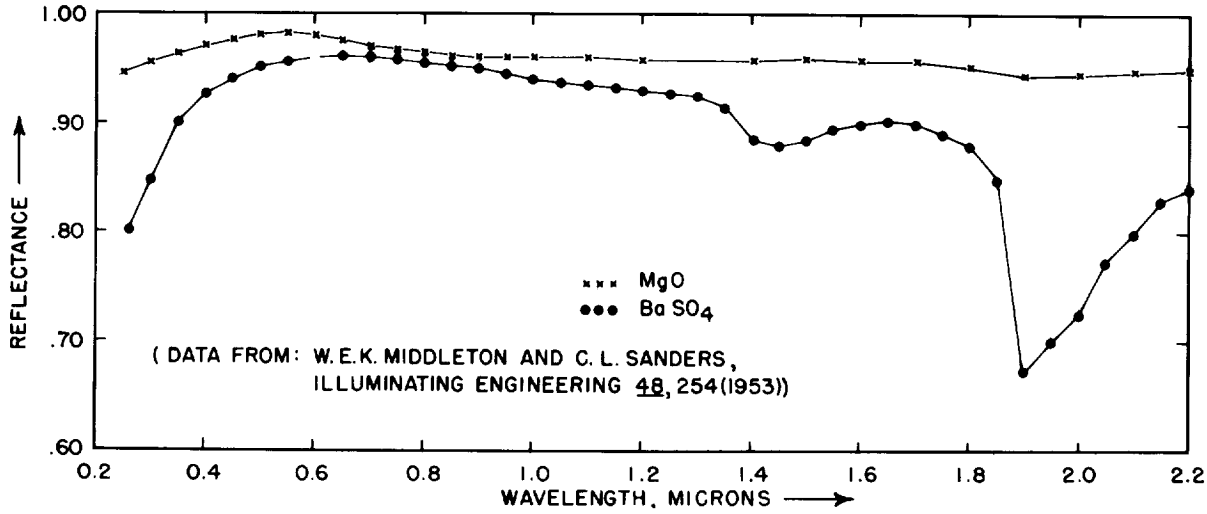

FIGURE 12-8.—Reflectance of magnesium oxide and barium sulfate—0.1% sodium (carboxymethyl) cellulose as binder—plotted against wavelength.

photomultiplier by excessive current, due to stray light leaking into the sphere through the sample port, a known standard of specular reflectance—for example, vacuum deposited gold or aluminum on glass—is placed over the sample port if the test sample is also specular, or nearly so. If the test sample is highly diffuse, a reference sample coated with a thick layer (at least 6 mm) of magnesium oxide smoke should be used. The substrate of the sample should be a polished metal surface to secure a reflectance near that given in the literature for magnesium oxide (ref. 5).

4. After the reflectance standard is securely pressed against the light seal gasket so that no stray light enters the sphere—and is pressed firmly enough so that the surface of the standard is within at least ⅛ inch of the sample port—the photomultiplier voltage is turned on, and the sensitivity of the output meter is adjusted until the meter reads a convenient value—for example, 80—near the high end of the scale. The reading for the standard is recorded, and the high voltage to the photomultiplier is turned off again.
5. The reflectance standard is now removed from the sample port and the test sample placed over the sample port. The photomultiplier voltage is turned on, and the meter reading recorded. The ratio of the sample reading to the standard reading, multiplied by the absolute reflectance of the standard, gives the absolute reflectance of the sample.

This method of measuring reflectance is known as the substitution method, and is distinguished from the comparison method which requires an additional port in the sphere for the reflectance standard.

Evaluation of the Errors of the Integrating Sphere

To evaluate critically the errors in the integrating sphere, it is necessary to consider the following:

1. diameter of sphere, $d_s = 6.00$ *inches*
2. diameter of the sample port, $d_p = 0.75$ *inch*
3. diameter of the light port, $d_L = 0.75$ *inch*
4. diameter of the detector port, $d_o = 1.00$ *inch*
5. diameter of aperture stop in light source as imaged on sample port, $d_{AI} = 0.36$ *inch* (for 0.125-inch diameter aperture)
6. angular displacement of optic axis of light source from radius through center of sample port, $\theta_L = 7.5$ deg
7. reflectance of sphere coating varies with wavelength as shown in figure 12-8, $R_s = 0.95$ at 0.5μ, and a flat maximum of 0.96 extends from 0.6 to 0.7μ

8. goniometric reflection characteristics and absolute reflectance values of sample and reference; that is, roughly, whether the sample and reference are diffusely or specularly reflecting.

A definitive treatment of the theory of the integrating sphere has been given by Jacquez and Kuppenheim (ref. 6). Their formula for the reflectance ratio of a "perfect" sphere (that is, a sphere in which the test samples, the reflectance standards, and the detector surface, are curved so as to match perfectly the inner surface of the spheres over their appropriate apertures) is as follows:

$$\frac{B_S}{B_{ST}}=\frac{R_S}{R_{ST}}\left[1-\frac{\frac{(R_{ST}-R_S)C}{S}}{1-\frac{R\cdot D}{S}-\frac{R_S\cdot C}{S}}\right] \quad (1)$$

where

B_S=total light flux passing into detector port when test sample is over sample port
B_{ST}=total light flux passing into detector port reflectance standard is over sample port
R_S=reflectance of test sample
R_{ST}=reflectance of reflectance standard
R=reflectance of interior of the integrating sphere
A=spherical area of entrance port
B=spherical area of photocell port
C=spherical area of sample port
S=total internal area of sphere, $4\pi R^2$
D=S–A–B–C.

Strictly considered, this formula is not correct for computing the error in measurements with flat samples, as Jacquez and Kuppenheim (ref. 6) show; however, the formula does indicate the approximate value of the error and is less complex than the correct expression, which is

$$\frac{B_S}{B_{ST}}=\frac{R_S}{R_{ST}}\left[1-\frac{\frac{(R_{ST}-R_S)R\cdot D'\cdot C}{S\pi}}{1-\frac{R\cdot D}{S}-\frac{R_S\cdot R\cdot D'\cdot C}{S\pi}}\right] \quad (2)$$

where

$$D'=\int_D \frac{(\rho-L\cos\theta)(L-\rho\cos\theta)}{(\rho^3+L^2-2_\rho L\cos\theta)}\,da \quad (3)$$

and

ρ=radius of sphere.
L=distance from center of sphere to center of sample.
da=element of surface area.

It can be seen from equation (1) that, for given C, D, S, and R, with R_S and R_{ST} as variables, the maximum value of the error occurs for R_S=0 and R_{ST}=1.00. Evaluating C/S and D/S as indicated for the dimensions given yields

$$\frac{C}{S}=0.0039,$$

$$\frac{D}{S}=0.985.$$

Equation (1) thus reduces to

$$\frac{B_S}{B_{ST}}=\frac{R_S}{R_{ST}}\left[1-\frac{0.0039(R_{ST}-R_S)}{1-0.985R-0.0039R_S}\right] \quad (4)$$

Equation (4) was applied to the following cases:

1. aluminum standard, gold sample, 0.35 to 0.90μ wavelength
2. gold standard, aluminum sample, 0.35 to 0.90μ wavelength
3. 100% reflectance standard, black paint (carbon black pigment in a silicone vehicle) sample
4. 100% reflectance standard, white paint (zinc sulfide pigment in a silicone vehicle) sample
5. 100% reflectance standard, 0% reflectance sample.

The results are displayed in figure 12–9. (In calculating the points shown, the sphere wall reflectance was taken from the data presented in figure 12–8.) It is seen that the maximum proportional error occurs with the 100% reflectance standard and the 0% reflectance sample, for which the error is only 7% at 6000 A. It should be particularly noted that equation (1) applies only to perfectly diffuse samples and standards. If the sample is specular and the standard is diffuse, then

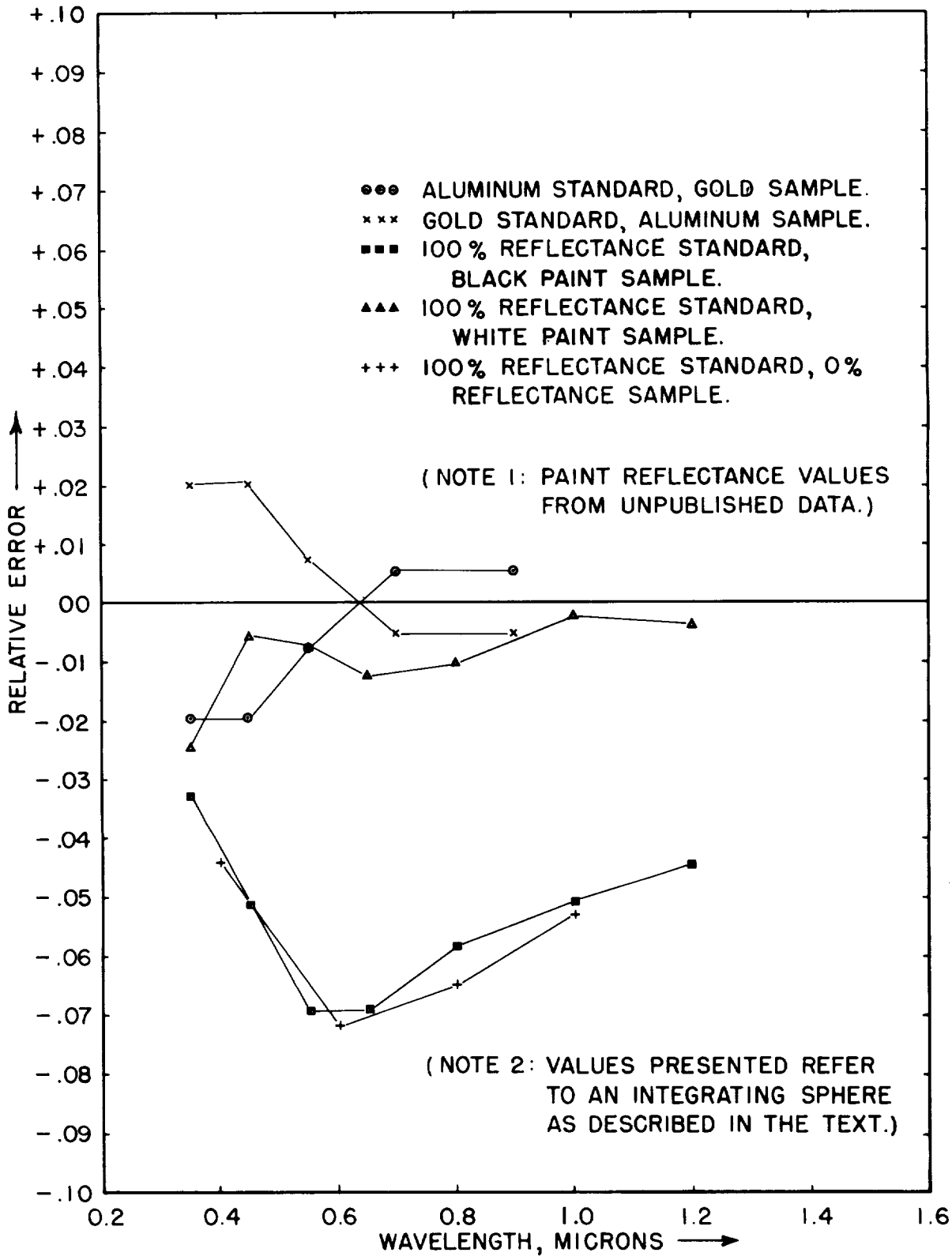

FIGURE 12-9.—Proportional errors of a perfect integrating sphere for several standard sample combinations.

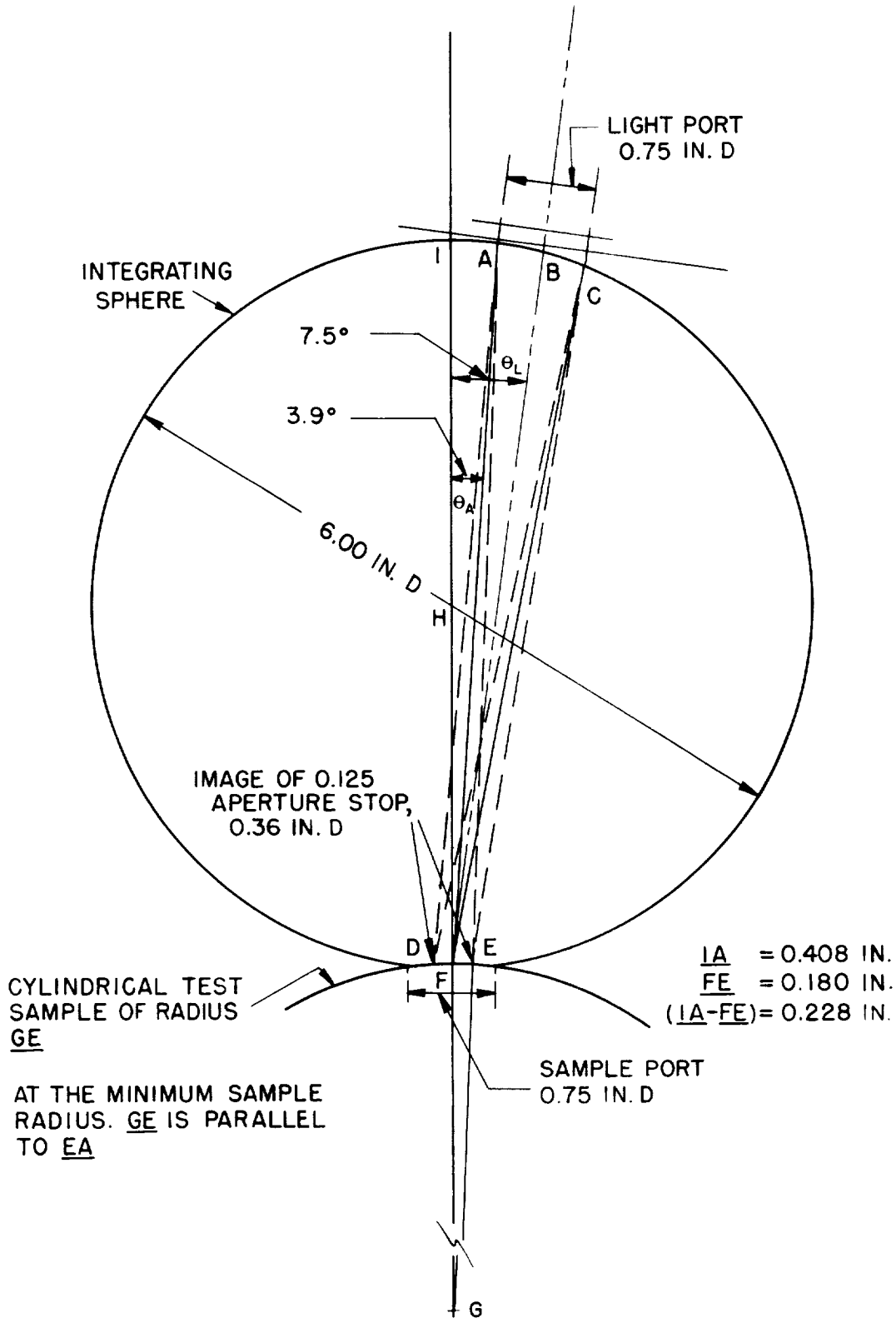

FIGURE 12–10.—Sphere geometry and minimum radius of sample curvature.

$$\frac{B_S}{B_{ST}} \approx \frac{R \cdot R_S}{R_{ST}} \tag{5}$$

approximately. If both sample and standard are specular, then $B_S/B_{ST} \approx R_S/R_{ST}$ is in the diffuse case. It is felt that the mathematical expression for the flux ratio of standard to sample for the specular case should lead to results similar to those calculated from equation (1).

The minimum radius of sample curvature which the integrating sphere will measure accurately depends on three factors. These factors have been given above as follows, by item numbers as previously listed:

6. displacement of optic axis of light source from radius through center of sample port, $\theta_L = 7.5$ deg
3. diameter of light port, $d_L = 0.75$ *inch*
5. diameter of aperture stop as imaged at sample port, $d_{AI} = 0.36$ *inch* (for a 0.125-inch diameter aperture).

Figure 12–10 shows the appropriate geometry to be considered in calculating the minimum radius of sample curvature. At the minimum radius of curvature, a ray from the left-hand edge of the light port, A, strikes the sample at the right-hand side of the aperture stop image, E, *normally*. (Actually, only the *effective* light port diameter should be used. This is the diameter of the area of the lens illuminated by the lamp. The size of this illuminated area—in turn—depends on the diameter of the aperture stop, the size of the lamp filament, the aperture-filament and lens-aperture distances, and the relative aperture of a collector lens, if one is used. For the optical system used in the present integrating sphere, a 0.125-inch diameter aperture would illuminate about half the diameter of the lens.) Since the ray AE does strike the sample normally, this means that the reflected ray *coincides* with AE and that the radius from G to E, GE, is parallel to AE. Using the geometrical relationship between the sides of the approximately similar triangles GEF and GAI, it is found that

$$\frac{GE}{FE} = \frac{GA}{IA}$$

or,

$$GE = \frac{FE(GE + AE)}{IA}$$

or,

$$GE = \frac{FE \cdot AE}{IA - FE}. \tag{6}$$

Using the dimensions given in figure 12–10, equation (6) becomes

$$GE = \frac{0.180 \times 6.00}{0.228}$$

or,

$$GE = 4.74 \text{ inches}.$$

However, as noted, the full diameter of the light port is not utilized with the 0.125-inch aperture, and, taking 0.375 inch as the approximate effective diameter of the light port, the minimum sample radius of curvature for this situation is found in the same manner to be

$$EG' = 2.60 \text{ inches}.$$

To check this calculation, gold-plated cylindrical shells having radii of 3.5, 6.5, 12.5, 18.5, and 24.5 inches were made up and their reflectance measured with the integrating sphere. The results showed no apparent trend from large to small radii and a variation from the sample mean of $\pm 1.75\%$, which could quite possibly be due to variation in reflectance of the gold plating from sample to sample.

CONCLUSIONS

It is concluded that the present integrating sphere reflectometer described is moderately satisfactory for checking the solar absorptance of spacecraft coatings. Desirable future modifications are:

1. a collector lens between the lamp and the aperture stop to increase the light gathering efficiency of the optical system
2. a more stable photomultiplier power supply and amplifier
3. the use of an output recorder
4. an exact analysis of the efficiency of an integrating sphere when used with non-perfectly-diffuse samples and standards
5. quartz optics to extend the ultraviolet range
6. attachment of a lightweight monochromator to provide continuous wavelength coverage.

REFERENCES

1. HASS, G.; DRUMMETER, L. F., JR.; and SCHACH, M.: Temperature Stabilization of Highly Reflecting Spherical Satellites. Jour. Optical Soc. America, vol. 49, no. 9, Sept. 1959, pp. 918–924.
2. Computed from data in the *A.I.P. Handbook*. McGraw-Hill Book Company, Inc., 1957, Section 6, p. 108.
3. JOHNSON, F. S.: The Solar Constant. Jour. Meteorology, vol. 11, no. 6, Dec. 1954, pp. 431–439.
4. MIDDLETON, W. E. K.; and SANDERS, C. L.: An Improved Sphere Paint. Illuminating Eng., vol. 48, no. 5, May 1953, pp. 254–256.
5. MIDDLETON, W. E. K.; and SANDERS, C. L.: The Absolute Spectral Diffuse Reflectance of Magnesium Oxide. Jour. Optical Soc. America, vol. 41, no. 6, June 1951, pp. 419–424.
6. JACQUEZ, J. A.; and KUPPENHEIM, H. F.: Theory of Integrating Sphere. Jour. Optical Soc. America, vol. 45, no. 6, June 1955, pp. 460–470.

13—INSPECTION TOOLS FOR MEASUREMENT OF THE RADIATION PROPERTIES OF SATELLITE TEMPERATURE CONTROL SURFACES

BY R. E. GAUMER AND G. F. HOHNSTREITER

LOCKHEED MISSILES & SPACE COMPANY, PALO ALTO, CALIFORNIA

AND G. F. VANDERSCHMIDT

LION RESEARCH CORPORATION, CAMBRIDGE, MASSACHUSETTS

Most satellite vehicles rely on passive thermal control to maintain the operating temperature of the vehicle. Specially designed paints and other surface treatments are used to maintain an exact balance between heat inputs, such as insolation, and the amount of energy emitted by the satellite surface by radiation at the satellite's operating temperature. The satellite's operating temperature is generally near room temperature. As a consequence, in manufacturing the temperature control surfaces of satellites, solar absorptivity α_s and room temperature emittance ϵ must be accurately controlled. Since weathering and handling of the satellite in the prelaunch environment may change these quantities, the satellite temperature control surfaces should also be given a prelaunch check to assure that values of α and ϵ are still within specification.

This paper describes the development of semiportable equipment for making measurements of the emittance ϵ of a room temperature surface and the spectral absorptivity α_λ of a surface over the solar range. The equipment is designed for use on the production line and at missile launch sites. The equipment is to be used as part of a reliability and quality assurance program.

Although advanced models of the inspection device may prove to provide a basic method for determining surface emittance and reflectance directly, the scope of this report covers only the ability to provide comparative readings.

PHYSICAL PRINCIPLE OF OPERATION AND ANALYSIS

As will be described later, the emissometer head consists basically of a cooled and evacuated chamber with an 8-junction bismuth-silver thermopile so mounted that one side sees only the cooled platen, while the front surface is irradiated by the sample whose emittance is to be measured. A schematic diagram of this arrangement is shown in figure 13–1.

In order to calculate the sample emittance, a consideration of the energy interchange must be made on the basis of temperatures, emittances, and view factors within the emissometer head. Due to the rapidly converging series found in the calculation of the radiation interchange between the head elements, the heat

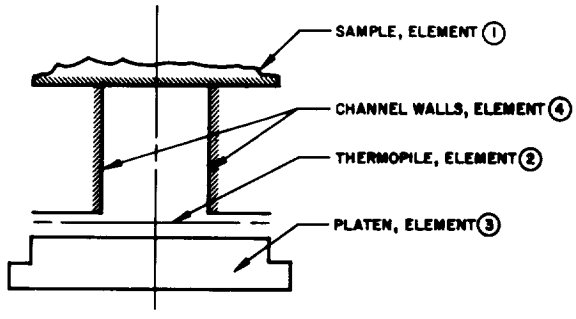

FIGURE 13–1.—Schematic arrangement of emissometer head elements.

balance to the thermopile may be approximated by the following steady-state equation

$$q_{12}-q_{24}-q_{23}+q_{142}=0 \qquad (1)$$

where the subscripts refer to the emissometer elements. The thermopile temperature is deduced from this equation as

$$T_2^4=\frac{\epsilon_1 F_{21} T_1^4+\epsilon_4 F_{24} T_4^4+\epsilon_3 F_{23} T_3^4+(1-\epsilon_4) F_{42}\epsilon_1 F_{14} T_1^4}{\epsilon_1 F_{21}+\epsilon_4 F_{24}+\epsilon_3 F_{23}+(1-\epsilon_4) F_{42}\epsilon_1 F_{14}} \qquad (2)$$

where T refers to temperature, ϵ to emittance, and F to view factor, and the subscripts correspond to the emissometer elements. The solution of this equation was solved parametrically by an IBM 7090 computer and the results are presented graphically in figures 13–2, –3, –4, and –5.

Effect of Sample Temperature and Ambient Air Temperature Deviations on Emittance Determinations

Figure 13–2 shows the effect of varying sample temperature on the detector temperature. The curves show a nonlinear increase in output with increasing sample temperature and a maximum deviation in output for the higher values of emittance. This case was evaluated with a channel emittance of 0.05 which is used in the standard model inspection devices due to the increase in output and decrease in zero signal provided with a highly reflective channel coating. The highly reflective channel also minimizes any instrument error due to specularity differences between samples, and provides emittance values which are more nearly hemispherical than normal. For this case, the thermopile temperature rises 13.5° F over the full-scale emittance range for a normal sample temperature of 530° R.

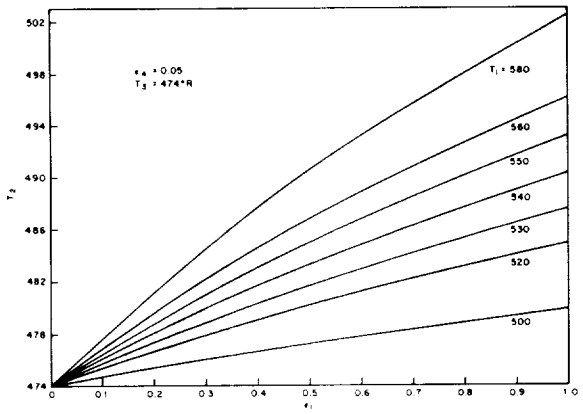

FIGURE 13–2.—Thermopile sensing element temperature as a function of sample emittance, showing effect of sample temperature.

Figure 13–3 shows the results of figure 13–2 plotted as a normalized output against sample emittance, which is directly comparable to emissometer output. This graph gives the degree of the output curve change for three widely differing sample temperatures. As seen from the graph, the degree of change is quite small indeed. Thus, a single output scale is possible when the samples are all at any reasonable temperature level, although compensation must be made if the samples are not at the same temperature. This compensation is made through using data such as are presented in figure 13–2.

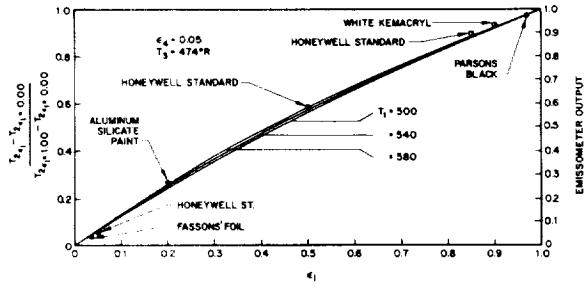

FIGURE 13–3.—Emissometer output and normalized temperature ratio as a function of sample emittance, showing effect of sample temperature.

Also plotted in figure 13–3 are seven experimental data points, using the ordinate directly as emissometer output. Although the points do not fall exactly on the line for the given surface temperature, they do confirm the shape of the curve and allow compensation to be made for surface temperature based on theoretical results.

Figure 13–4 gives the change of thermopile output due to changes in platen temperature. The platen temperature is affected by ambient air temperature changes via the cooling water supply. Of course, this depends on the efficiency of the Peltier cooling unit at a given temperature differential of operation. Thus,

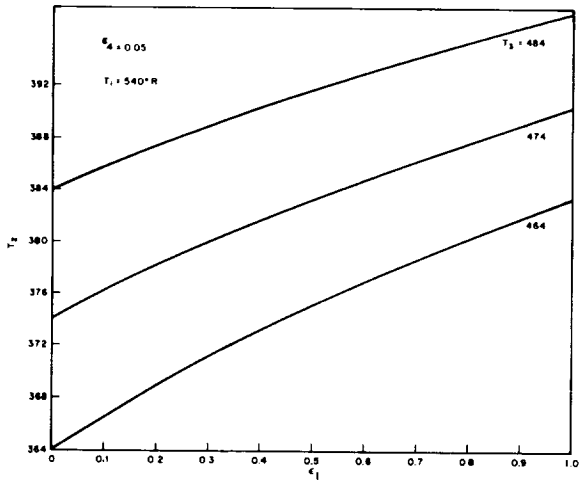

FIGURE 13–4.—Thermopile sensing element temperature as a function of sample emittance, showing effect of platen temperature.

a necessary question to be answered is "How much do ambient air temperature changes affect the shape of the output curve, and thus the accuracy of the instrument?" This question can be answered by figure 13–5 in which the data of figure 13–4 are presented as surface emittance vs. normalized output which corresponds to emissometer output. As can be seen from the graph, little difference is observed when the platen temperature is constant anywhere within a 20° F temperature differential. It is assumed that the platen temperature differential of 20° F more than covers the ambient air differential of 40° F for which the emissometer is to be utilized.

Description of Apparatus

An emissometer head based on this theory is shown in figure 13–6 in cross section. The surface 3 is a copper platen cooled by a thermoelectric element. The hot surface of the

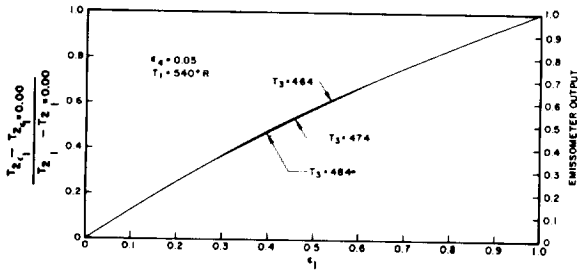

FIGURE 13–5.—Emissometer output and normalized temperature ratio as a function of sample emittance, showing effect of platen temperature.

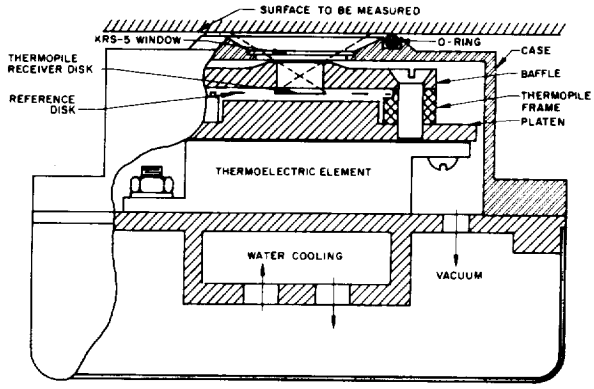

FIGURE 13–6.—Cross section of emissometer head (¾×).

thermoelectric element is kept at room temperature by a small water-cooled cavity behind the element. The platen surface is finished in Parson's flat optical black. The platen supports an Eppley Laboratory, Incorporated 8-junction bismuth-silver thermopile with a ⅜-inch-diameter receiver disk. The receiver disk of the thermopile is the surface 2 in the above analysis. It is finished in carbon black.

A baffle maintained at the platen temperature is placed over the thermopile and prevents the thermopile from seeing any radiation except the radiation from the surface to be measured (dotted lines). The inner surface of the baffle is finished in Parson's flat optical black. The hole through which radiation passes may be finished in either a highly reflecting material to improve the coupling between the thermopile receiver and test surface, or may be coated with Parson's flat optical black. In the former case, the measurement is more nearly of total hemispherical emissivity and in the latter case, more nearly of normal emissivity.

The reference junctions of the thermopile are eight small receiver disks located around the main receiver disk. These reference junctions are maintained at the platen temperature by radiant interchange with the platen and baffle plate.

The construction is housed in a stainless-steel case with an infrared transparent window. The window material, KRS–5, is almost completely non-absorbent between 3 and 30 μ where the largest part of room temperature blackbody radiations exist. The case is evacuated to between 1 and 10 μ Hg by a small two-stage mechanical pump. A felt seal is

used to define the distance between the head and surface to be measured.

The head can easily be held in the hand. The aperture diameter of 1.0 inch permits measurement of small surfaces. A 15-ft umbilical consisting of a rubber vacuum hose, two rubber water lines, two lines for supply of the thermoelectric element current, and two lines for measuring the signal from the thermopile connects the head to the console (figure 13–7).

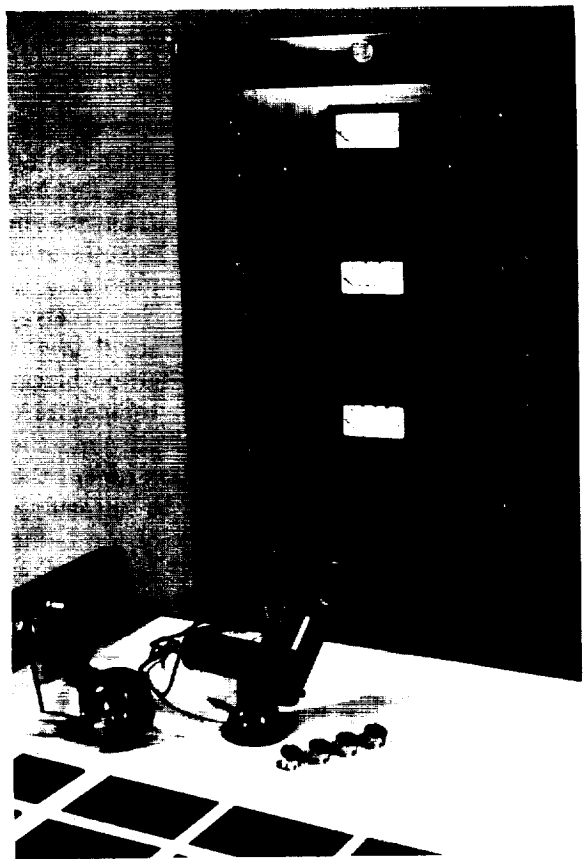

FIGURE 13–7.—Emissometer inspection device console showing emissometer head, hemispherical reflectometer head, filters, and test thermal control surfaces.

The console contains a power supply for operating the thermoelectric element (approximately 0–1 volt DC at 20 amp), a vacuum pump for continuous evacuation of the head to keep the window from frosting and to eliminate gaseous conduction, and an amplifier for reading out the thermopile signal. Thermoelectric element cooling water may be supplied from house lines or may be supplied by a circulator which cools the water by means of a radiation fan heat exchanger. An interlock is provided which shuts off the thermoelectric cooler supply unless the water is flowing.

When a highly reflecting surface is used as the sample surface, a signal of about 0.15 millivolt is observed, indicating an apparent difference in temperature between sample and reference junctions. This zero signal is due to energy reaching the receiver disk from sources other than the sample surface. This signal may be removed by a variable bucking voltage applied in series to the thermopile ("low standare set"). The gain of the amplifier ("high standard set") used to measure the thermopile voltage may be adjusted to provide full-scale indication when a high emissivity surface is used as the sample. A typical output is 1.0 millivolt for a Parson's black standard with emittance of about 0.97.

Emissometer Procedure

In practice, a Fasson's foil standard ($\epsilon=0.03$) and a Parson's black standard ($\epsilon=0.97$) maintained at the same temperature as the object to be measured are used to calibrate the instrument. The low standard adjustment is set to provide an output meter indication of 0.03 when the Fasson's foil standard is in place and the high-standard adjustment is set to provide an output meter indication of 0.97 when a Parson's black standard is in place. The head is then placed on the object to be measured and the emittance can be read directly from the dial of the instrument. As a check, a sample of the finish being measured, carefully maintained and recently measured in the laboratory, is measured by the emissometer and the reading compared with that of the test object.

Emissometer Accuracy, Reproducibility, and Drift

The accuracy of the emissometer is defined as the ability of the instrument to determine surface emittances within a given tolerance range. This accuracy is determined by calibrating the instrument to two known emittance values; 0.03 (Fasson's foil) and 0.97 (Parson's black) and then using the instrument to determine the emittance values of at least four additional surfaces whose emittances have previously been determined by calorimetric meth-

ods. The difference in readings between the actual values and the emissometer values is defined as the emittance measurement uncertainty and serves to give an emittance tolerance for the emissometer in a given range. Typical tolerances which the standard-model emissometer is capable of meeting are as follows:

Emittance Range	*Measurement Accuracy*
$0<\epsilon<0.1$	± 0.015
$0.1<\epsilon<0.2$	± 0.030
$0.2<\epsilon<0.5$	± 0.030
$0.5<\epsilon<0.8$	± 0.040
$0.8<\epsilon<1.0$	± 0.050

As has been shown, the emissometer accuracy is directly proportional to the temperature differential between the thermal control surface to be tested and the standards used to calibrate the instrument. As determined experimentally, the effects of the temperature difference are 4% error per °C in the instrument reading for a high-emittance sample. To eliminate this known source of error, a surface-temperature thermometer will be used to establish the existing temperature differential. If possible, the standard will be brought to the thermal control surface temperature; but, if this is not possible, reference will be made to a temperature correction graph for the proper correction factor. This graph is to be prepared from existing data, part of which is shown in figures 13–2 and –3, which cover the effect of sample temperature changes from 40° F to 120° F at 5° F intervals, and the emittance range of 0 to 1 divided into 25 intervals.

The reproducibility of the emissometer was determined by taking five emittance readings on seven samples and allowing 10 minutes to elapse between readings on a particular surface. The reproducibility is expressed as the maximum spread of values thus obtained. Typical values of reproducibility which the standard-model emissometer is capable of meeting are as follows:

Emittance Range	*Measurement Reproducibility*
$0<\epsilon<0.1$	± 0.015
$0.1<\epsilon<0.5$	± 0.020
$0.5<\epsilon<1.0$	± 0.030

The tolerances of accuracy and reproducibility are shown graphically in figure 13–8 together with the measured values obtained with the experimental model inspection device.

The drift of the emissometer, as determined experimentally, does not exceed $\pm 2\%$ of the high emittance standard (Parson's black) reading, nor does it exceed $\pm 1\%$ of full-scale meter reading for the low emittance standard (Fassons' foil) reading over a 1-hour period without adjustment of instrument settings.

REFLECTOMETER PHYSICAL THEORY OF OPERATION

Two types of reflectometers have been tested. The first ("hemispherical instrument") is useful for comparison work. The second ("spherical instrument") is used for the purpose of reducing surface specular effects and, in addition, for handling smaller samples than can be handled on the hemispherical instrument. In both cases, emphasis is placed on the ability to obtain an ultraviolet absorption of surfaces, since an increase in ultraviolet absorptivity of the surface is the most sensitive indication of surface deterioration.

Absorption measurements are made by measuring the reflectance of the sample. In the case of the hemispherical instrument, a beam of light from a lamp is projected onto the surface to be measured. As much of the reflected light as possible is collected by a hemispherical shell placed over the object to be tested. The shell is coated on the inside with a highly diffuse reflecting coating such as magnesium oxide or a more durable coating of flat-white silicate paint which directs the reflected light through a filter to a photocell cathode. The photocurrent from the cell is taken as a measure of the reflected light at the filter pass wavelength. The method is very simple and permits rapid comparison of surfaces with a standard sample of the same surface carefully maintained and checked by a laboratory spectrophotometer. The method does not provide absolute measurements of reflectance, however, since the system is much more efficient in collecting light from diffuse reflectors than from specular reflectors. Since degradation of surface does not generally involve changes in the specularity of the reflected radiation, the instrument may be used as a comparison tool whenever a standard

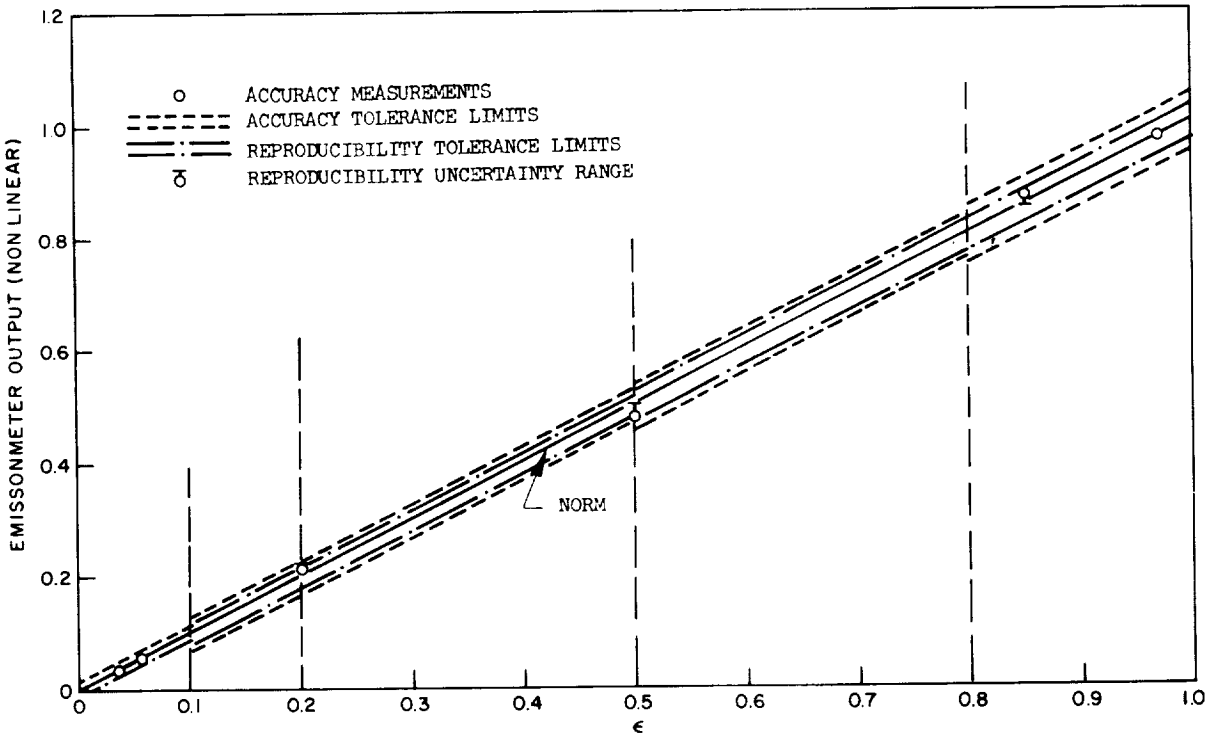

FIGURE 13-8.—Accuracy and reproducibility tolerance limits as a function of sample emittance, showing experimental results.

sample of the surface to be tested is available.

The spherical instrument provides reflectance measurements independent of the specular nature of the surface and permits the measurement of a much smaller (1-inch diameter) area surface. A spherical cavity is coated on the inside with a highly diffuse reflecting material such as magnesium oxide or a more durable coating of flat-white silicate paint. The sample is placed at an aperture at one end of the sphere and is diffusely illuminated by lamps whose output is directed at the wall of the sphere; the lamp output is baffled to prevent direct illumination of the sample. A small aperture at the opposite side of the sphere from the sample permits a lens to form an image of the sample on a photocell cathode blocked by a filter. By comparison of the output from the photocell for the surface to be measured with the output for a surface of known reflectance (e.g., a magnesium oxide standard) the reflectance may be calculated.

Reflectometer Theory and Analysis

An approximate solution to obtain the output of the reflectometer equipped with the spherical diffusing head is as follows: Assume the total energy into the diffusing chamber which can affect the output of the phototube as

$$E=\int I_\lambda d\lambda \tag{3}$$

where the integral is evaluated for the particular filter wavelength range under consideration.

Assume that the energy into the diffusing chamber can be related to the energy falling on the sample I, as follows

$$I_1=R_E F_{\text{sphere-sample}}\, E \tag{4}$$

where

$$F_{\text{sphere-sample}}=\frac{A\text{sample}}{4\pi R^2}=\frac{1}{16}$$

for the given geometry, and RE is the effective reflectance of the spherical head system to the sample including the following effects as well as many other effects peculiar to diffuse spheres (ref. 1):

1. deviations from a perfectly diffuse wall coating
2. light losses at entrance and by lens system

3. interreflections within sphere and absorption by the sphere and sample
4. shadowing by lamp baffles
5. polarization within the enclosure
6. losses and reflections from the lens.

The energy transfer from the sample to the lens aperture is

$$I_2 = F_{\text{sample-lens aperture}}\,\rho_{\text{sample}}\,I_1 \qquad (5)$$

where $F_{\text{sample-lens aperture}}$ is obtained from well-known expressions for the view-factor between two plane circular surfaces with common central normal, and is 0.000960 for the reflectometer geometry.

The output of the photocell is

$$W = KI_2S_{pt}T_lT_f \qquad (6)$$

where

K diaphragm placement constant. ($K=1$ when the photocell sees just the sample area used in the above calculations.)

T_l lens transmittance given by

$$T_l = \int T_{l_\lambda}\,d\lambda \qquad (7)$$

T_f filter transmittance given by

$$T_f = \int T_{f_\lambda}\,d\lambda \qquad (8)$$

S_{pt} phototube sensitivity given by

$$S_{pt} = \int S_{pt_\lambda}\,d\lambda \qquad (9)$$

where the integration for T_l, T_f and S_{pt} is carried out for the particular filter wavelength range under consideration.

Grouping these expressions together gives the photo tube output as

$$W = (K\rho_{\text{sample}}R_gES_{pt}T_lT_f)6\times10^{-5} \qquad (10)$$

From equation (10) it may be estimated that the output of the photocell will be a small number indeed. To check the ability of the instrument to yield sufficient output, a series of experiments was performed with an experimental model. The results gave readings ranging from 29.0 to 0.22 millimicroamperes, which are easily measured with the present reflectometer output system.

Reflectometer Description of Apparatus

Both reflectometers use the same lamp, filter, and photocell system to cover the range from green to ultraviolet (5500 Å to 2537 Å). A low-pressure mercury lamp with a quartz envelope is used as a source. The lamp produces a line spectrum, the most intense component of which is the 2537 Å line. Sufficient intensity is available in the green and blue regions of the spectrum to permit measurements to be made. Corning glass filters permit isolation of the green, blue, and ultraviolet portions of the spectrum. Although it is not possible to isolate the 2537 Å line, a Pyrex filter can be used to eliminate completely the 2537 Å and pass all the remaining lines with only 5% attenuation. By comparing the reflection without filters with reflection with the Pyrex filter in place, the effect of the 2537 Å may be measured by subtraction. The photocell uses an S–5 surface, which permits measurement from about 2200 to 6000 Å.

Figure 13–9 shows the overall sensitivity of

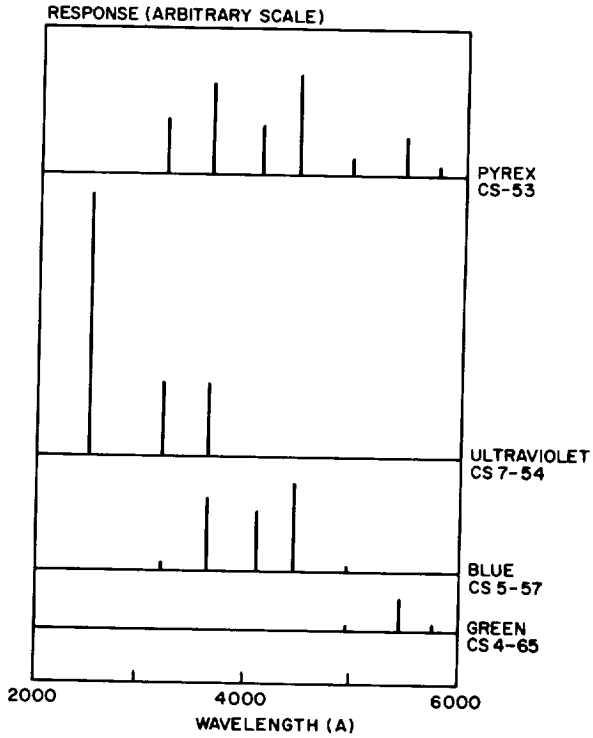

FIGURE 13–9.—Response of lamp-filter-photocell combination. The no-filter response is 5% higher in the Pyrex filter curves and includes the 2537 A response at about double the response shown for the ultraviolet filter case.

the system in arbitrary units, obtained by multiplying the lamp output at each wavelength by the transmission of the Corning filter by the response of the photocell.

The hemispherical reflectometer is shown in figure 13–10. The mercury lamp is placed in the cylindrical housing which projects at 45°

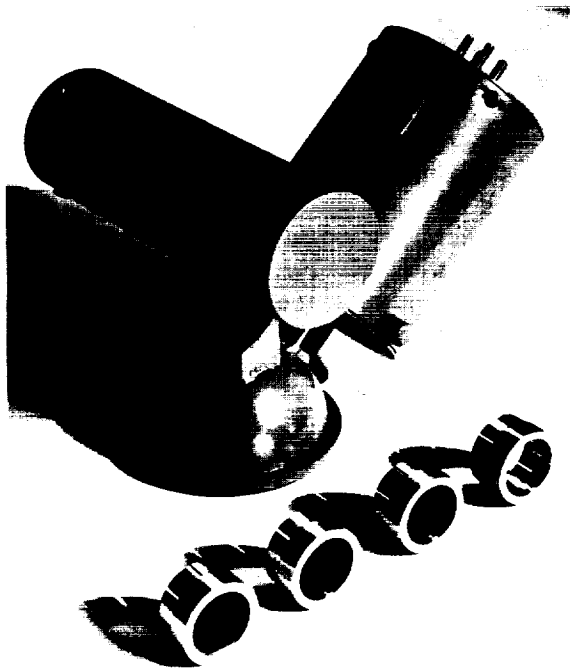

FIGURE 13–10.—Hemispherical reflectometer head with four filters for use with ultraviolet lamp.

from the hemisphere. Two baffles in the tube confine the emergent beam to the plane of the sample. The hemispherical cavity contains a flange with a felt gasket which seals the hemisphere against light leaks. The photocell is placed in the cylinder at the top of the hemisphere. Filters are placed in the path of the light beam by removing the lamp housing.

The spherical reflectometer, modeled after the work of Kortum (ref. 2), is shown in the sketch of figure 13–11. Two low-pressure mercury discharge lamps are used. A quartz lens produces an image of the sample at the stop position; the stop restricts transmission of more than three-fourths of the diameter of the image. Thus, even though the focal plane shifts slightly in passing from green to ultra-

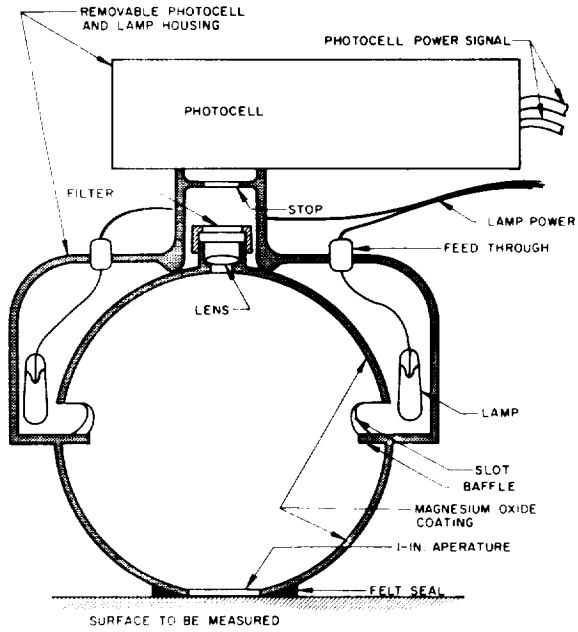

FIGURE 13–11.—Spherical reflectometer (cross section)

violet due to the dispersion of the quartz, only light from the sample reaches the photocell.

Both instruments use a similar readout device. The device is basically a Lion Research Corporation standard electrometer, which permits measurement of photocurrent from about 10^{-10} amp full scale to 10^{-7} amp full scale.

Reflectometer Procedure

When used with the hemispherical head, a negligible amount of light reaches the photocell if a perfectly absorbent flat surface is used as a sample (e.g., if the head is directed into a dark room). The head is placed on the standard sample of the surface to be measured, and the sensitivity increased until a substantial reading is obtained. The head is then placed on the surface to be measured; the same reading will be obtained if the two surfaces are identical.

The spherical head shows a small photocurrent output when used on a perfectly absorbent surface (e.g., directed into a darkened room). This output arises chiefly from stray light scattered into the photocell by the optical system. A zero control is used to remove this unwanted component from the signal.

The readout for the spherical head is calibrated in the following way. A flat-white silicate paint standard of 86% reflectance is placed at the sample position. The sensitivity

of the reflectometer is continuously adjustable to give 86% scale indication with whatever filter is used. A Parson's black standard with reflectance of 5% is then placed at the sample position, and the zero control is adjusted so that the instrument reads 5%. Reflectance of the sample may now be read directly on the output scale. The assumption can be made that the output for any other value of reflectance between these values will be linear, and an output scale can be so designed. However, if serious nonlinearities are present due to the effective reflectance of the spherical head system to the sample (R_E), the problem can be solved by experimentation or analytical solutions of R_E. The experimentation involves further calibration with known standards, which leads to the comparison function of the instrument, as well as utilization of a spectrometer to determine the exact wavelength range for the system with each particular filter utilized.

The reflectometer can be used most accurately for production testing of known thermal control surfaces by utilization of carefully prepared and measured standards for these surfaces. In this manner the reflectometer merely compares the thermal control surface reflectance values with the standard surface values, and thus determines the difference in readings between the surfaces. Based on prior limits, the usability of the thermal control surface is thus determined.

If a surface has no carefully prepared reference sample available, the reflectometer can still be utilized to give reflectance values. In this case, prior experimentation with the spherical diffusing head is necessary to determine the shape of the reflectometer output vs. reflectance curve. This will be incorporated into the instrument dial scale. The reflectance determinations are obtained in much the same manner as the emittance measurements with the emissometer (i.e., by use of high and low standards to calibrate the instrument prior to use).

Hemispherical Head Reflectometer Drift, Sensitivity, and Reproducibility

The drift of the reflectometer, as determined experimentally, was essentially zero for practical usage in the most sensitive readable range over a one-hour period.

The sensitivity of the reflectometer is defined as the ability of the instrument to detect changes of reflectance between two given surfaces in a spectral range compatible to a given lamp-filter combination. The experimental evidence has shown that the reflectometer equipped with the hemispherical head is capable of detecting a ± 0.02 difference in reflectance for any two surfaces of similar specular nature. The spherical head is also capable of detecting this same difference and largely eliminates the specular requirement, as observed in experiments performed on magnesium oxide and Fasson's foil.

The reproducibility of the reflectometer was determined by taking five reflectance readings on seven samples and allowing 10 minutes to elapse between readings on a particular surface. The experimental evidence has shown the reproducibility of the reflectometer to be less than $\pm 2.0\%$ of full-scale reading for the entire reflectance range.

The measurements obtained with the spherical head reflectometer coated with magnesium oxide are shown in table 13-I as phototube current output.

TABLE 13-I.—*Data from Experimental Spherical Head Reflectometer With Magnesium Oxide Coating*

(Values in millimicroamperes)

Filter	No specimen *	Freshly prepared magnesium oxide	Freshly prepared aluminum foil	Parson's black	Skyspar epoxy white paint	Aluminum paint
None	1.8	27.0	29.0	3.4	8.8	20.0
Green	.17	1.2	1.3	.22	1.1	1.0
Blue	.40	4.1	4.5	.52	3.0	3.5
UV	.74	10.0	10.0	1.0	1.7	6.7
Pyrex	.59	7.4	8.0	.86	4.9	5.8

* Zero reading.

CONCLUSIONS AND RECOMMENDATIONS

The device which has been described in this paper appears to fulfill a long-standing need in the aerospace industry. The primary utility of this instrument lies in its capacity to make rapid determinations of the important thermal radiative characteristics of hardware items under manufacturing and launch base conditions. This device may be used as a tool for quality control, field inspection, material acceptance, and a variety of similar industrial applications.

The accuracy of determinations made with this instrument is extremely dependent upon the quality and quantity of reflectance and emittance standards used in conjunction with the measurements. Although some effort has already been expended upon the development of suitable standards, a major integrated effort seems clearly indicated.

There are many indications that more research and development effort on such a device would be profitable in terms of acquisition of an absolute measurement device. If the reflectometer energy source were extended to 1.0 μ the solar reflectance could be determined with greater confidence. The physical principles upon which measurements are based are sufficiently fundamental and directly related to solar absorptance and infrared emittance that absolute determinations of α_s and ϵ may be possible with the apparatus in the near future. At present, however, this inspection device must be regarded as a satisfactory instrument for the practical evaluation of surface thermal radiation parameters with adequate engineering accuracy.

ACKNOWLEDGMENTS

The authors wish to express their appreciation to J. W. Pieper for writing the computer program for equation (2) and to E. Candidus for his experimental and design assistance.

REFERENCES

1. Edwards, D. K.; Nelson, K. E.; Roddick, R. D.; and Gier, J. T.: Basic Studies on the Use and Control of Solar Energy. Annual Report 60–93, National Science Foundation Grant 9505; University of California at Los Angeles.
2. Kortum, Gustav: Kolorimetric-Photometric und Spectrometric, Springer-Verlag, Berlin, 1955, p. 332.

14—CALORIMETRIC DETERMINATION OF INFRARED EMITTANCE AND THE α_s/ϵ RATIO

BY R. E. GAUMER AND J. V. STEWART
LOCKHEED MISSILES & SPACE COMPANY, PALO ALTO, CALIFORNIA

The most important thermal radiation parameter involved in the passive thermal control of spacecraft is the ratio of solar absorptance to infrared emittance—the α_s/ϵ ratio.

Various techniques exist for the determination of the α_s/ϵ ratio of materials; most of them involve a separate determination of α_s and of ϵ. Indeed, most present techniques measure spectral reflectance over the appropriate spectral region and the α_s/ϵ ratio is then calculated. Such calculations are lengthy and arduous but, most importantly, involve a series of assumptions regarding specularity, angular dependence, surface profile, polarization effects, and the like. Our present basic understanding of the physical phenomena is far from complete and, accordingly, it seems wise to develop measurement techniques which require the fewest assumptions in order to convert raw data to meaningful information.

This paper will describe a device which was designed specifically to determine the α_s/ϵ ratio of materials in the room temperature range. The data output is sample equilibrium temperature, which may be directly converted to α_s/ϵ in one simple operation.

DESCRIPTION OF APPARATUS

Figure 14–1 is a simplified schematic diagram of the α_s/ϵ device. A sample, supported by its own thermocouple leads, is suspended inside a blackened copper inner chamber which is cooled by liquid nitrogen and enclosed in a stainless steel outer chamber in which a vacuum of 1×10^{-6} mm Hg or less is maintained. Radiant energy from a solar simulator is split and directed by mirrors through openings at the ends of the inner and outer chambers, thereby irradiating the sample on both sides. The temperature change of the sample is recorded by a millivolt recorder and, from the plot of temperature vs. time, α_s/ϵ and ϵ can be determined. Figures 14–2 and 14–3 are photographs of the general experimental setup.

PRINCIPLE OF OPERATION

The α_s/ϵ device operates on the principle that a body, thermally isolated in a vacuum, will absorb incident radiant energy according to its α for that radiation, and it will emit thermal energy according to its total hemispherical emittance, ϵ. For a given material, α will depend generally upon the spectral distribution of the incident radiation and ϵ will depend upon the temperature of the material. For space applications, one is usually interested in the absorptance of a material for energy with the spectral distribution of the sun. This absorptance is referred to as α_s. If the energy balance is established for a body absorbing and emitting radiant energy in vacuo (i.e., radiant energy absorbed = thermal energy emitted + energy stored) one gets:

$$I\alpha A_1+I_1\alpha_1 A_2=\sigma A\epsilon T^4+mC_p\frac{dT}{dt} \qquad (1)$$

where

- I intensity of incident radiation
- α absorptance of the material for this radiant energy
- A_1 area irradiated
- I_1 incident intensity from sample surroundings, i.e., in this case energy from the liquid nitrogen walls; equal to σT_w^4 ($T_w\simeq80°$ K)
- α_1 absorptance of the sample for radiation from the liquid nitrogen walls; approximately equal to ϵ

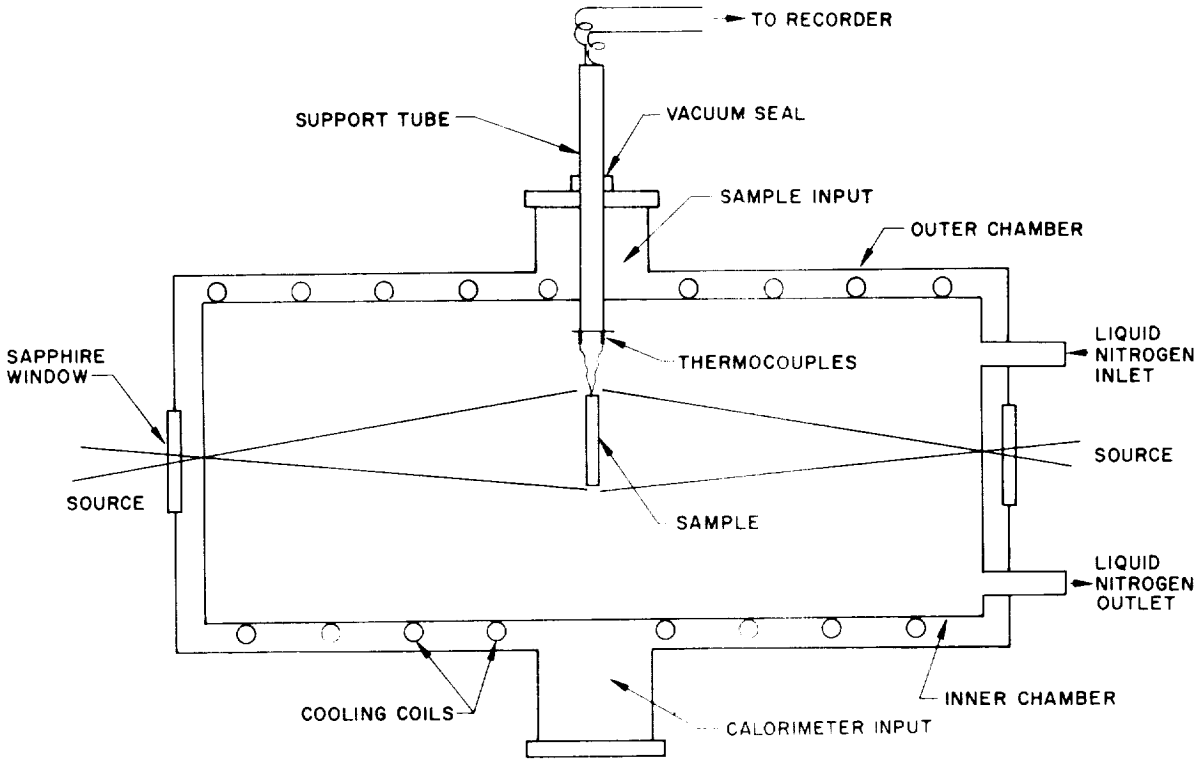

FIGURE 14-1.—Schematic diagram of α_s/ϵ device.

A_2 area of sample seeing liquid nitrogen walls; equal to A
σ Boltzmann constant
A emitting area
ϵ emittance of sample
T sample temperature
m sample mass
C_p specific heat of sample
t time

since $I_1\alpha_1 A_2=\sigma A\epsilon T_w^4$ equation (1) becomes

$$I\alpha A_1=\sigma A\epsilon(T^4-T_w^4)+mC_p\frac{dT}{dt}. \tag{2}$$

Usually $T_w^4 \ll T^4$ and the radiation from the walls is ignored.

The α_s/ϵ ratio is determined by irradiating the sample with energy from a solar simulator and allowing the sample to equilibrate. For this case the energy balance becomes:

$$I\alpha_s A_1=\sigma A_2\epsilon T^4 \tag{3}$$

since $dT/dt=0$ at equilibrium. Thus, the α_s/ϵ ratio is represented by

$$\frac{\alpha_s}{\epsilon}=\left(\sigma\frac{A_2}{A_1}\right)\frac{T^4}{I} \tag{4}$$

The intensity of the incident radiation is determined by a calorimeter, set at the sample position, whose surface has an α_s/ϵ of unity. Thus, I is given by the equation:

$$I=KT_c^4$$

where K is the appropriate constant for the calorimeter, and T_c is the temperature of the calorimeter.

For determinations of α_s/ϵ the sides of both the calorimeter and the sample are made negligibly thin. Thus, the emitting areas and absorbing areas are equal and equation (4) becomes:

$$\alpha_s/\epsilon=\frac{\sigma T^4}{I}$$

where

$$I=\sigma T_c^4$$

thus

$$\frac{\alpha_s}{\epsilon}=\left(\frac{T}{T_c}\right)^4. \tag{5}$$

If, after irradiation, the source is turned off and the sample allowed to cool, the energy balance equation becomes:

$$mC_p\frac{dT}{dt}=\sigma A_2\epsilon T^4. \tag{6}$$

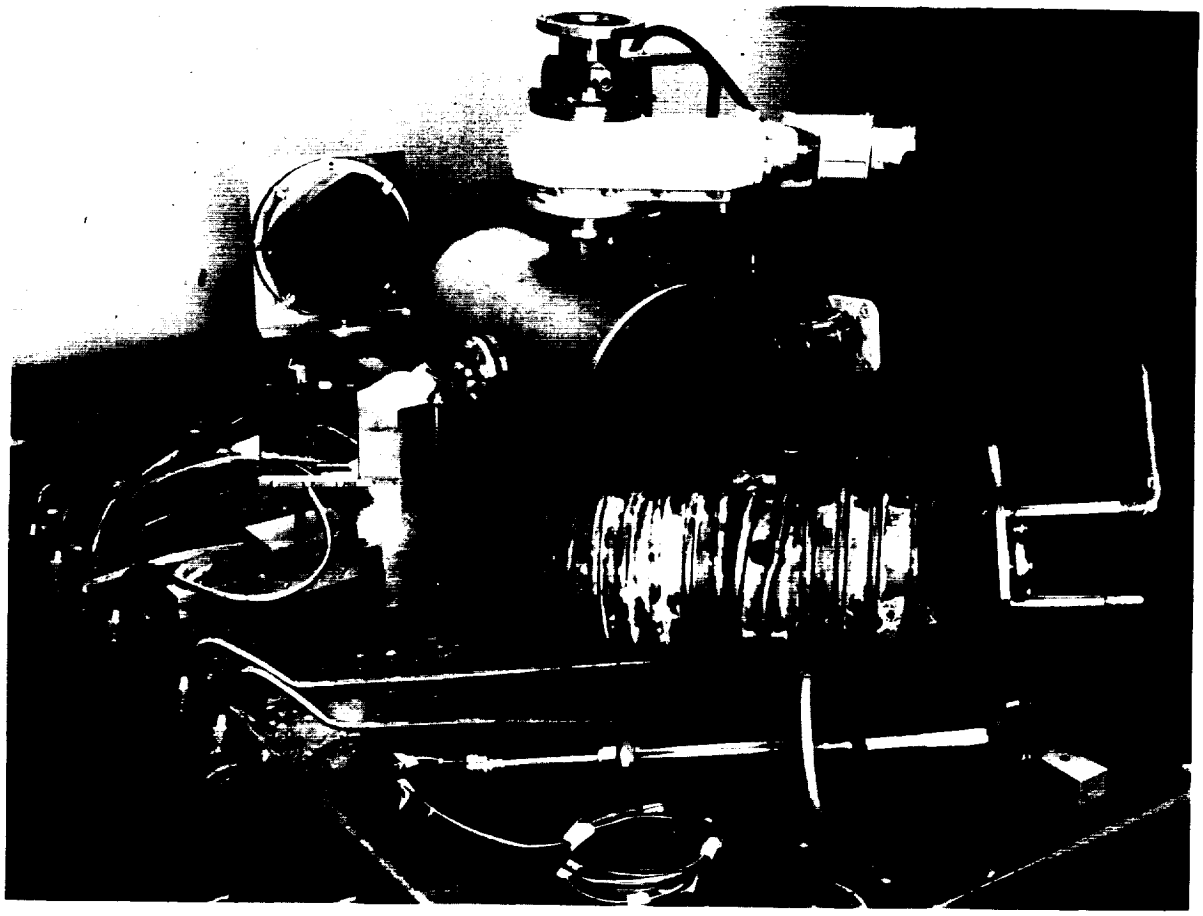

FIGURE 14-2.—Photograph of inner and outer chambers.

If it is assumed that C_p is independent of temperature, the above equation can be integrated to

$$\epsilon=\frac{mC_p}{3\sigma A(t_2-t_1)}\left(\frac{1}{T_1^3}-\frac{1}{T_2^3}\right) \qquad (7)$$

where T_1 is the sample temperature at time t_1 and T_2 is the sample temperature at time T_2. When the temperature decay is recorded with time, then the total hemispherical emittance of the sample can be determined with equation (6) or (7). The use of equation (7) is preferable since equation (6) involves the experimental determination of two quantities $\left(\frac{dT}{dt}\text{ and }T^4\right)$, thereby introducing more possible errors than in equation (7).

ERROR ANALYSIS

General

ERROR IN DETERMINATION OF α_s/ϵ RATIO

Using equation (5)

$$\Delta(\alpha_s/\epsilon)=\frac{4T^3\Delta T}{T_c^4}-\frac{4T^4\Delta T_c}{T_c^5}$$

$$\left|\frac{\Delta(\alpha_s/\epsilon)}{\alpha_s/\epsilon}\right|=4\left|\frac{\Delta T}{T}\right|+4\left|\frac{\Delta T_c}{T_c}\right|.$$

since

$$\Delta T=\pm 2^\circ \text{ K}$$

$$\frac{4\Delta T}{T}=\pm 3\% \text{ at } 300^\circ \text{ K}$$

$$\therefore\left|\frac{\Delta(\alpha_s/\epsilon)}{\alpha_s/\epsilon}\right|\simeq\pm 6\%$$

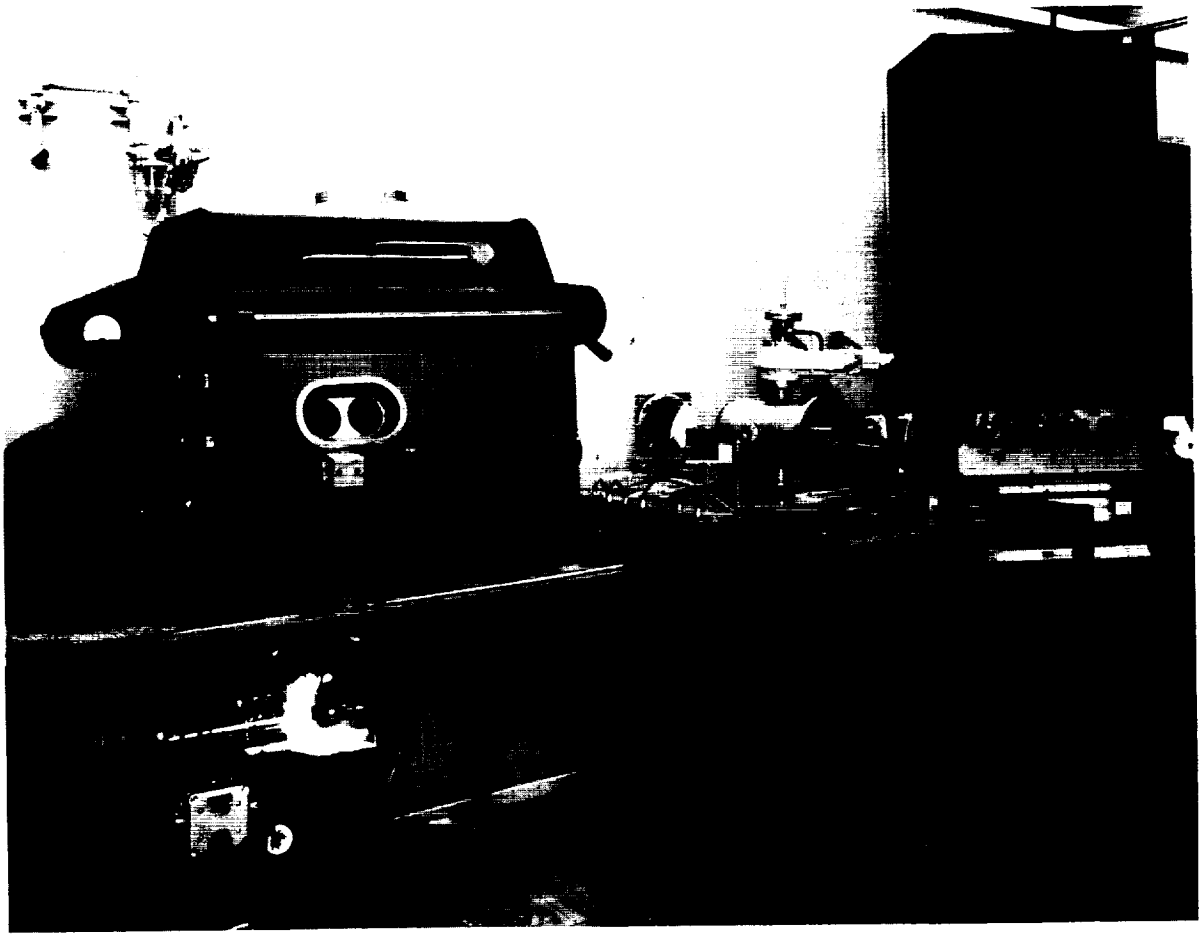

FIGURE 14–3.—General experimental setup.

This is a 6% error without taking into account the variation of the solar simulator from the actual distribution of the sun. The effect of this variation is discussed by Gaumer, Streed, and Vajta (ref. 1).

ERROR IN THE DETERMINATION OF EMITTANCE

Using equation (6) and assuming no error in mC_p, σ, A, and t_2-t_1, then

$$\Delta\epsilon=\left[\frac{mC_p}{3\sigma A(t_2-t_1)}\right]\frac{3\Delta T}{T^4}$$

$$\frac{\Delta\epsilon}{\epsilon}=\frac{3\Delta T}{T}$$

$$\Delta T=\pm 2^\circ \text{ K}$$

$$\therefore\frac{\Delta\epsilon}{\epsilon}=\pm 3\% \text{ at } 200^\circ \text{ K}$$

$$=\pm 2\% \text{ at } 300^\circ \text{ K}$$

$$=\pm 1.5\% \text{ at } 400^\circ \text{ K}$$

It should be noted that unless certain precautions are taken, there will be an error due to specific heat. One reason for this is that when the emittance of coated samples is desired, the coatings will add a certain unknown thermal mass to the sample substrate. Then it is necessary either to calculate the thermal mass due to the coating or to make the sample substrate so massive that the contributions of the coating to the total thermal mass is negligible. Since, for many coatings, the specific heat is not well known, the latter method may be more desirable. It is convenient to use as a sample substrate a substance whose specific heat is very well known and whose thermal capacity per unit volume is relatively high. A substance such as commercially pure copper (99.9%) satisfies all these requirements.

Another error is introduced because specific heat varies with temperature, a fact that was

ignored in the derivation of equation (7). However, if the temperature increment is made small enough, the error due to this effect becomes negligible. For example, the specific heat of copper changes less than 1% for each 10° K change above 280° K and for each 20° K change above 300° K. A 5° K to 10° K increment is used in actual measurements. If greater accuracy is desired, a curve of the dependency of specific heat with temperature can be used in the integration.

Thus, it appears that the only significant uncertainty in emittance is the uncertainty in temperature. For most materials and temperatures this will be true. However, in reality, there are miscellaneous errors, discussed below, which seriously affect the accuracy of this particular device in the measurement of low emittance samples at low temperatures.

Miscellaneous Errors

Neglecting T_w^4

Neglecting T_w^4 will cause less than a 1% error above 253° K and less than 2% error at 213° K, for a wall temperature of 80° K. Since equation (2) requires determination of the slope as well as a T^4 term, another 3% to 4% error cannot be avoided. Thus, it appears that the integrated form is the most accurate for use down to 200° K. As will be seen, the accuracy of the α_s/ϵ device decreases markedly below 225° K and so T_w^4 can be neglected for all cases of interest ($T \geq 225°$ K) without affecting the accuracy of the instrument.

Reflection From the Walls

In the α_s/ϵ device the cold walls are coated with Parson's black paint, which has the properties of being highly absorbing ($\alpha \simeq 0.97$) and nonspecular. This, plus the fact that the view factor of the chamber to the sample is less than 0.06, insures that a negligible amount of energy, which has left the sample, will return to the sample.

Gaseous Conduction

The vacuum chamber is kept at a pressure of 2×10^{-6} mm Hg or less during each run. Calculations of heat transfer due to gaseous conduction assuming free molecular flow and Maxwellian distribution show that gaseous conduction can be considered negligible, above 300° K, for a vacuum of 2×10^{-6} mm Hg. Table 14–I compares the energy radiated by a sample of 0.02 emissivity with the energy lost by gaseous conduction.

Holes in Chamber

The estimated view factor of the sample to the holes in the chamber is less than 0.01. Since the holes are at room temperature, the error associated with the holes in the chamber wall will be less than 1% for all temperatures above 300° K. At 200° K this error rises to 4% and is independent of the emittance of the sample.

Thermocouple Conduction Losses

Conduction losses due to radiation and conduction in a rectangular fin have been reported by S. Lieblein (ref. 2). The results of this report can be used to determine the conduction losses in a thermocouple wire by making an appropriate geometrical transformation. Calculations were made for a 0.013-mm-diameter chromel-alumel thermocouple 2.5 cm long, assuming a thermocouple end temperature of 275° K and an emissivity of 0.2. For a sample temperature of 260° K there is essentially no thermocouple loss, but on either side of this temperature the conduction term becomes significant. At sample temperatures above 260° K there is conductive gain to the sample. Since the thermocouple loss depends upon the junction temperature and the emittances of

Table 14–I.—*Estimate of Error Due to Gaseous Conduction*

T, ° K	Heat radiated by sample, watts/m²	Gaseous conduction poss., watts/m²	% Error
200	1.81	3.79×10^{-2}	2
250	4.43	5.37×10^{-2}	1
300	9.19	6.95×10^{-2}	<1

the thermocouple wires, neither of which is well known and which vary from run to run, the the absolute thermocouple conduction loss is probably not known to better than an order of magnitude. Table 14–II gives an estimate of the possible error for a 0.02 emittance sample.

Table 14–III summarizes the errors in emittance for various emittances and temperatures. Some typical emittance data for different materials are given in Table 14–IV.

CONCLUSIONS

These data indicate that the accuracy of a device designed specifically for room temperature determinations is severely degraded at lower temperatures. In order to determine emittance by this method at lower temperatures, i.e., in the range from 250° K down to 100° K, major design modifications would be necessary.

The extension of applicability of such a device to the high temperature regime (300° K$<T<$1000° K) should be a simple design problem. Work is in progress to produce an instrument capable of accurate measurements in the cryogenic temperature range, but here the experimental difficulties are considerable. The present device works well in emittance determinations but very accurate determinations of α_s/ϵ are dependent upon the development of a satisfactory source of solar radiant energy.

TABLE 14–II.—*Estimate of Error Due to Thermocouple Conduction Loss*

[For 0.02 emittance sample]

T, ° K	Heat radiated by sample, watts	Thermocouple loss, watts	%
200	5.64×10^{-3}	1.8×10^{-3}	32
250	1.38×10^{-2}	1×10^{-4}	1
300	2.86×10^{-2}	1×10^{-3}	4
350	5.39×10^{-2}	2×10^{-3}	4

TABLE 14–III.—*Errors in Emittance for Various Emittances and Temperatures*

° K	Error independent of remittance, %				Error dependent upon emittance, %								
					$\epsilon=0.02$			$\epsilon=0.10$			$\epsilon=0.50$		
	E_w	E_h	E_T	Total	E_g	E_c	Total*	E_g	E_c	Total*	E_g	E_c	Total*
200	2	4	3	9	2	32	43		6	15	—	1	10
250	1	2	3	6	1	1	8		—	6	—	—	6
300	—	—	2	2	—	4	6		1	3	—	—	2
350	—	—	2	2	—	4	6		1	3	—	—	2

*Includes all errors dependent or independent of emissivity.
E_w—error from neglecting temperature of the wall.
E_h—error due to holes in chamber.
E_T—error due to temperature measurements.
E_g—error due to gaseous conduction.
E_c—error due to thermocouple conduction.

TABLE 14–IV.—*Typical Data for Different Materials*

Material	Emittance		
	Reflectance techniques	Total hemispherical apparatus	α/ϵ Device
Parson's black	0.92 ± 0.06	0.971 ± 0.003	0.95 ± 0.04
Polished copper	$.02^{+.05}_{-.01}$	$.028 \pm .002$	$.015 \pm .005$
Rokide C	$.80 \pm .05$	$.835 \pm .003$	$.85 \pm .04$
Aluminum pigment in silicone binder	$.20 \pm .05$	----------	$.21 \pm .01$
White acrylic paint	$.84 \pm .05$	----------	$.84 \pm .04$
Leafing aluminum pigment in acrylic binder	$.33 \pm .05$	----------	$.35 \pm .02$
Non-leafing aluminum pigment in acrylic binder	$.48 \pm .05$	----------	$.49 \pm .02$
Aluminum foil	$.03^{+.05}_{-.02}$	----------	$.03 \pm .01$

Material	α/ϵ Ratio	
	Reflectance techniques	α/ϵ Device
Aluminum foil	1.5–12.0	2.8 ± 1.0
White acrylic paint	$.31 \pm .06$	$.18 \pm .04$
Non-leafing aluminum pigment in acrylic binder	$.92 \pm .08$	$.94 \pm .20$
Leafing aluminum pigment in acrylic binder	$.64 \pm .08$	$.80 \pm .20$

REFERENCES

1. GAUMER, R. E.; STREED, E. R.; and VAJTA, T. F.: Paper 15—Methods for Experimental Determination of the Extra-Terrestrial Solar Absorptance of Spacecraft Materials *in* Measurement of Thermal Radiation Properties of Solids (Joseph C. Richmond, ed.). NASA SP–31, 1963, Table 15–I.
2. LIEBLEIN, S.: Analysis of Temperature Distribution and Radiation Heat Transfer Along a Rectangular Fin of Constant Thickness. NASA TN D–196, Nov. 1959.

15—METHODS FOR EXPERIMENTAL DETERMINATION OF THE EXTRA-TERRESTRIAL SOLAR ABSORPTANCE OF SPACECRAFT MATERIALS

BY R. E. GAUMER, E. R. STREED, and T. F. VAJTA

LOCKHEED MISSILES & SPACE COMPANY, PALO ALTO, CALIFORNIA

Two basic methods of experimentally determining solar absorptance are described Spectral diffuse reflectance and total simulated solar absorptance measurements are compared in terms of accuracy, instrumentation, sample requirements, and data reduction. The use of spectral data during material development to optimize desirable optical characteristics is shown. The need for good solar spectral distribution simulation is emphasized for total absorptance measurements. Typical data obtained by each method are included.

The temperature control of spacecraft is generally accomplished by a radiation heat balance with the space environment. Thermal energy incident on a spacecraft originates from any or all of three sources: direct solar insolation, planetary albedo, and planetary emission. For a near-earth satellite, the relative magnitude of these three sources are in the ratio of approximately 6:2:1, respectively. Both the insolation and albedo are comprised of the solar spectrum; a thorough knowledge of how much of this energy is absorbed by the spacecraft is mandatory if the temperature is to be controlled. Although the literature contains considerable solar absorptance data (refs. 1, 2, 3, and 4), a continuing need for additional measurements exists to develop new materials and to determine values more precisely for space applications.

MEASUREMENT PHILOSOPHY

Generally, two types of solar absorptance (α_s) measurements are made to determine total or spectral values. Spectral data are most useful during development of materials because they can provide significant information regarding optimization of parameters such as thickness, composition, surface roughness, angular dependence, and stability. To obtain the effect of these parameters, a measurement technique must be inherently reproducible. In addition, the technique must provide adequate spectral resolution over the solar radiation spectrum to enable integration of the data with respect to wavelength to obtain a measure of the total solar absorptance. The technique must also be adapted to rapid measurement of easily prepared samples and present the data in a form which can be readily compared in successive measurements or reduced by automatic methods. In essence, the techniques must provide research data in a routine manner.

Total absorptance determinations imply illumination of a surface and the measurement of the amount of energy reflected or absorbed. Simulation of the space environment in terms of pressure, temperature, spectral distribution, and incidence angle are desirable but not absolutely necessary. Because the data are used for design purposes, absolute accuracy is the prime objective. The experimental procedure should be subject to a completely objective evaluation of the total resultant uncertainties. Sample preparation and exposure should realistically duplicate service conditions. The method requires precise instrumentation attachment and measurement accompanied by

692-146 O—63——10

careful data reduction and analysis. Measurements are usually made only on surfaces carefully selected for a particular application.

Both types of measurements are dependent upon accurate knowledge of the extra-terrestrial solar distribution. Data in the ultraviolet and infrared regions are particularly subject to revision as new solar spectral measurements are reported. For instance, values of the fraction of energy in the spectral band from 0.300μ to 0.359μ have discrepancies of 10% regularly and variations as large as 40% have been observed. Although only relatively small amounts of the total energy are in this region, the inherently greater absorptance by most materials makes a 10% uncertainty of significant importance when calculating or predicting spacecraft equilibrium temperatures. Seasonal variations of 3.4% are caused by changes in the earth-sun distance. The extra-terrestrial solar constant, 2.002 cal-cm^{-2}-min^{-1}, has been estimated to be in error by less than 3.0% (ref. 5).

MEASUREMENT PROCEDURES

Spectral Reflectance

The measurement requirements outlined for spectral data essentially dictate the use of a reflectance method. Diffuse reflectance determinations in the spectral range from 0.25 to 2.0μ usually employ an intergrating sphere and a spectrophotometer. A comprehensive review of integrating spheres for determination of reflectance as a function of angle of incidence has been reported by Edwards et al. (ref. 6) for spectral measurements from 0.33 to 2.5μ. No attempt to perform measurements as a function of angle is reported in this paper.

The particular apparatus utilized in this work is the model 14M Cary recording spectrophotometer with a Cary model 1411 diffuse reflectance attachment.[1] The optical system, shown in figure 15–1, employs two lenses and a 45° mirror to direct the non-dispersed radiation from the light source through the bottom sphere port onto the sphere wall. The radiation is diffusely reflected within the sphere to illuminate the sample and reference materials positioned at their respective ports. The radiation

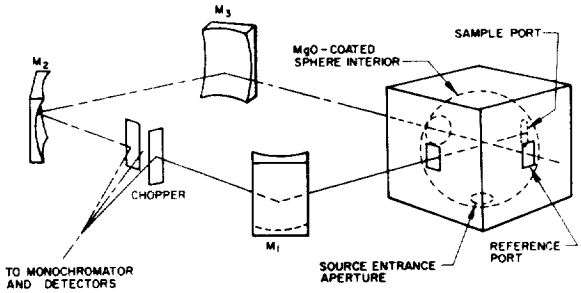

FIGURE 15–1.—Schematic diagram of the integrating sphere and associated optics used for spectral reflectance measurements from 0.27 to 1.8 μ.

reflected from the sample and reference materials passes through the appropriate sphere ports to be chopped and alternately directed into the double monochrometer. The monochromatic radiation is directed to the appropriate detector and the ratio of the resultant individual signals is electronically amplified and presented on a stripchart recorder in terms of reflectance vs. linear wavelength. A 500-watt tungsten projection lamp and a lead sulphide detector are used in the infrared, and a high pressure 100-watt mercury lamp and a 1P28 phototube detector are used in the visible and ultraviolet. Correction for the spectral reflectance of the reference and other optical differences between the two paths can be compensated for by an adjustable electrical cam (multipot) as a function of wavelength, permitting data to be recorded in direct reflectance units. The sample port can be positioned with respect to the sample viewing optical axis to permit measurements including or excluding the specular component of reflectance. Usual measurements include both specular and diffuse reflectance. The sample spectral absorptance is determined from the simple relation for an opaque material, $\rho+\alpha=1$.

There are several possible sources of error, such as stray or scattered radiation, electronic amplifier and recorder noise, nonisotropic sphere radiation distribution, reference material reflectance inaccuracy, and data reduction. Established tests for stray or scattered light, electronic noise, response time, optical alignment, and sphere coating efficiency can be performed to verify that reproducibility of 0.01 transmittance unit can be achieved. The errors due to sphere nonhomogeneities and aperture area (4% of

[1] Applied Physics Corp., Monrovia, Calif.

the total sphere surface) are difficult to assess. Reference 7 reports the error due to sphere inefficiencies for a comparison-type measurement to be approximately 0.01 in total reflectance when the ratio of aperture areas to total sphere area is 0.05. The error was shown to be approximately the same for specular or diffuse samples if the sphere is designed so that no primary incident radiation is reflected through a port on the first reflection from sample or reference. Both reference and sample ports of the 9-cm diameter magnesium oxide (MgO) coated sphere are baffled from the area where incident radiation initially impinges. Undoubtedly the greatest source of error results from the lack of absolute reflectance values or instability of the reference material. Long-term studies and experience with MgO, magnesium carbonate ($MgCO_3$), and vacuum-deposited aluminum have resulted in the choice of aluminum as the most stable, easily handled, and reproducible material. Initial use of $MgCO_3$ was hampered by water vapor absorption and the resultant absorption peaks at 1.39 and 0.85μ. Variation in the reflectance of $MgCO_3$ as measured at LMSC and by others (refs. 8, 9) is shown in figure 15–2. Integration of the maximum and minimum reflectance values shown with respect to the extra-terrestrial solar distribution indicates that an uncertainty of 0.04 could occur in determining α_s of a spectrally flat coating.

Attempts to use MgO as the reference material resulted in the preparation of a new standard almost daily, and even then the reproducibility of freshly prepared coatings indicated approximately 3% variations. The change in reflectance of MgO with ultraviolet exposure time is shown in figure 15–3 (ref. 10). The change in reflectance as a function of time after preparation (varying from 5 minutes to 4 months), also shown in figure 15–3, supplements measurements reported in reference 6. The difference in total α_s for the extreme values shown for MgO would result in an uncertainty of 0.06 for a spectrally flat surface. MgO has the additional disadvantage of being susceptible to damage from shock and handling because of inherently poor adhesion.

The extensive work by Hass (ref. 11) pertinent to the spectral reflectance of vacuum-deposited aluminum has been investigated further by Janssen et al. (ref. 12) as shown in figure 15–4. The relatively good reproduci-

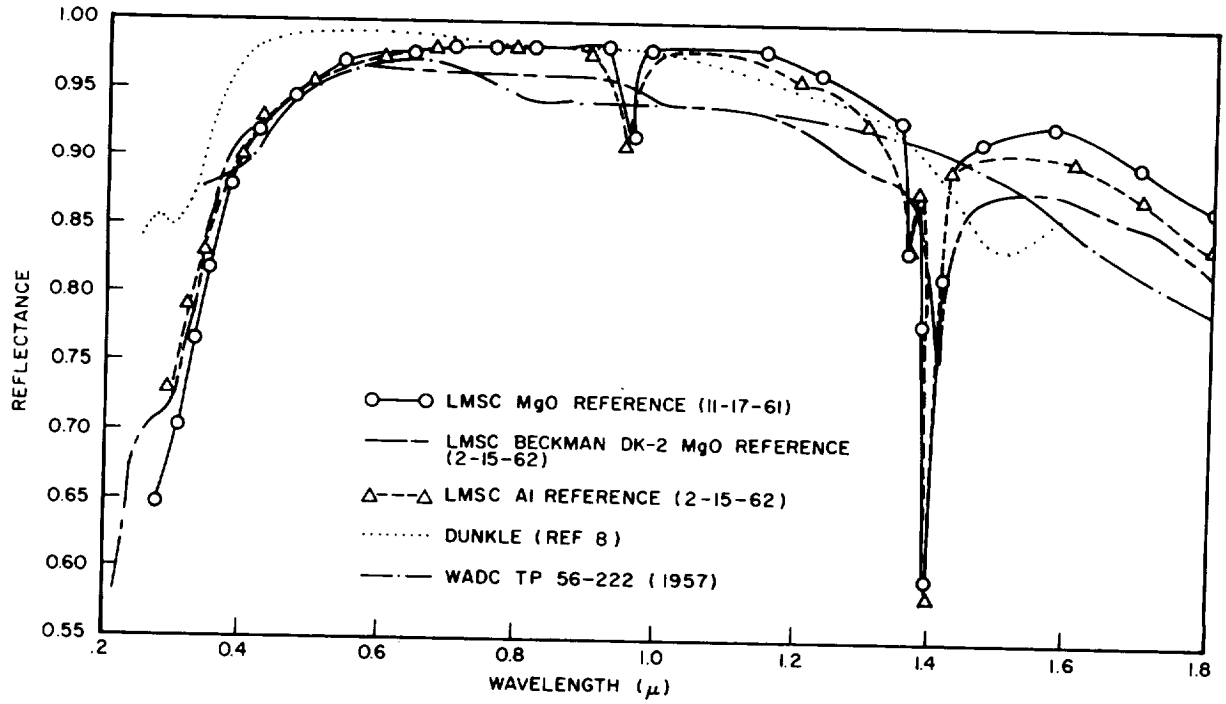

FIGURE 15–2.—The reflectance of magnesium carbonate measured under various conditions by several investigators.

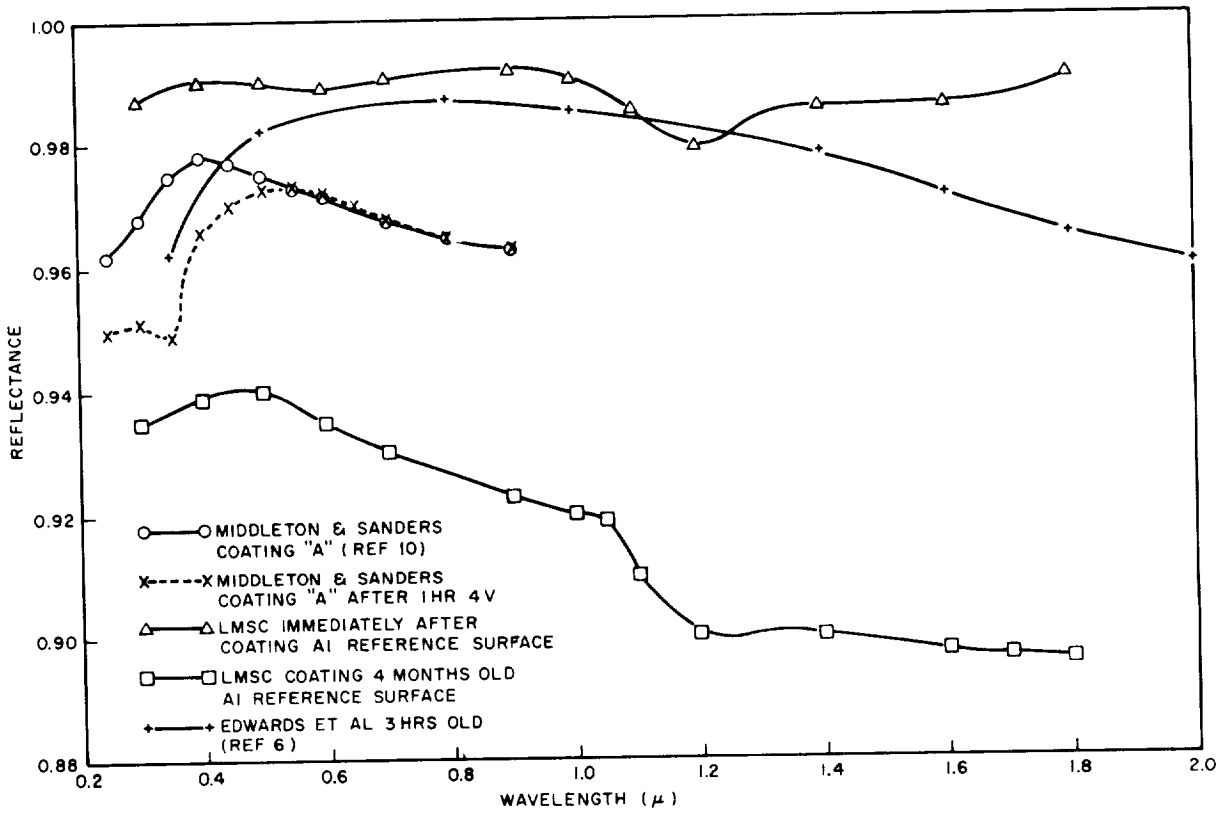

FIGURE 15–3.—The reflectance of magnesium oxide measured under various conditions and by several investigators.

bility and stability above 0.4μ for coated, optically polished glass suggests it as a practical reference material. The reflectance below 0.4μ, shown in figure 15–4, becomes increasingly lower at the shorter wavelengths for coated window polish glass, which presumably would be the poorest surface used as a standard. Integration of the extreme reflectance values shown in figure 15–4 with respect to the extra-terrestrial sun results in an α_s of 0.12 for the window glass and in α_s of 0.08 for the data of Hass.

The solar absorptance is defined by

$$\alpha_s = \frac{\int_0^\infty \alpha_\lambda s_\lambda d\lambda}{\int_0^\infty s_\lambda d\lambda} \tag{1}$$

where α_λ=monochromatic absorptivity, s_λ= monochromatic intensity of solar radiation, and λ=wavelength. Because finite wavelength intervals $\Delta\lambda$ must be selected to specify the intensity, α_s can be approximated by

$$\alpha_s = \frac{\sum_i^n \bar{\alpha}_{\lambda n} s_{\lambda n} \Delta\lambda}{\int_0^\infty s_\lambda d\lambda} \tag{2}$$

where $\bar{\alpha}_{\lambda n}$ is the average monochromatic absorptivity for the mean wavelength λ_n of the particular $\Delta\lambda$. Equation (2) may be written as

$$\alpha_s = \sum_i^n f_n \bar{\alpha}_{\lambda n}$$

and f_n is defined as

$$f_n = \frac{s_{\lambda n}\Delta\lambda}{\int_0^\infty s_\lambda d\lambda}.$$

Thus, f represents the fraction of the solar constant associated with the wavelength interval $\Delta\lambda$. The solar spectrum is divided into equal energy fractions, n, and these fractions are multiplied by $\bar{\alpha}_{\lambda n}$ and summed to give α_s.

The data reduction procedure is performed by manually taking reflectance values directly

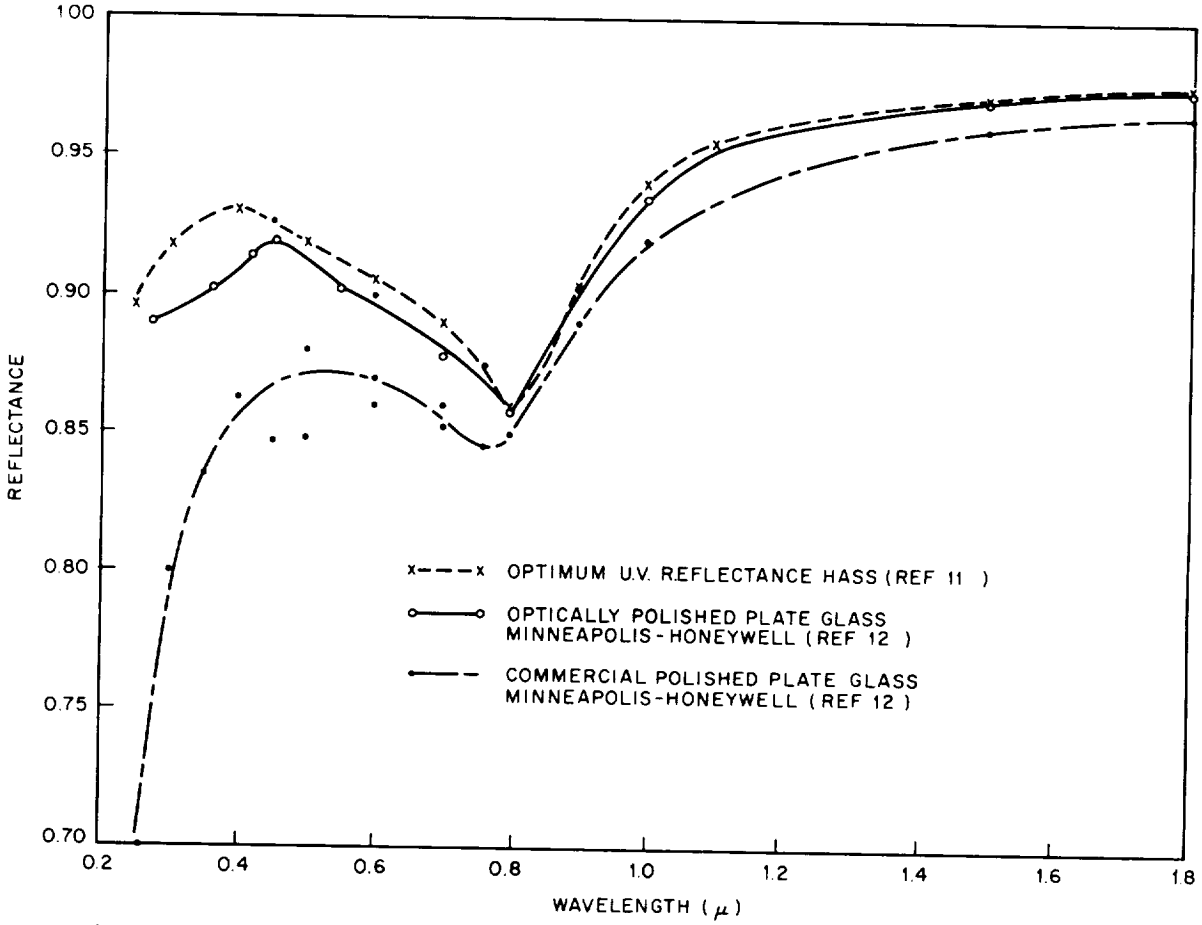

FIGURE 15-4.—The spectral reflectance of vacuum deposited aluminum for several conditions.

from the chart recording. A maximum of 100 points can be taken over the spectral interval from 0.27 to 1.8μ or as few as are necessary to adequately define points of curve inflection. It has been experimentally determined that by judicious selection, 15 to 30 points is sufficient to give values of α_s within 0.5% of those obtained by taking 100 points. The solar spectral energy distribution curve of Johnson (ref. 13) is then numerically integrated with the spectral reflectance as a function of wavelength at these 15 to 30 points on an IBM 7090 computer in 1% energy increments. The resulting value of normal solar reflectance is then subtracted from 1.0 to obtain normal solar absorptance. Because solar energy exists beyond each end of the spectral range measured, 0.35% below 0.27μ and 7.5% above 1.8μ, approximations are routinely programmed to account for this energy as determined from measured reflectance values for wavelengths adjacent to the particular region. When greater accuracy is desired, spectral data obtained from infrared reflectance measurements can be similarly integrated. Total uncertainties in the data reduction procedure are considered to be less than 0.01.

Because of the difficulty in deriving an expression to relate all of the error sources related to the measurement procedures, it is convenient to add the individual errors to obtain a maximum uncertainty as follows:

$$\Delta\rho_s = \Delta I + \Delta E + \Delta R_s + \Delta D$$

where

ΔI = instrumentation errors = 0.01
ΔE = sphere inefficiency = 0.01
ΔR_s = standard material reflectance error = 0.04
ΔD = data reduction error = 0.01

A resultant error in α_s can be calculated by assuming $\Delta\rho_s = \Delta\alpha_s = 0.07$; then for $\alpha_s = 1.0$,

$\Delta\alpha_s/\alpha_s=0.07/1.0$ or a 7% error results. If $\alpha_s=0.1$ then $\Delta\alpha_s/\alpha_s=0.07/0.1$ and a 70% error is indicated. In actual practice, the percentage error is less for the extreme values shown because the instrument zero and 100% can be set accurately, and because the reference material reflectance values are chosen between the possible extreme limits. Uncertainties in knowing the solar constant cannot rightfully be considered a measurement error and the random nature of electronic and data reduction should combine to give an rms error of about ± 0.01.

Absorptance Technique

Another technique exists for the experimental determination of solar absorptance, α_s. The physical principle for this technique is the following: a thin disc of known thermal mass is suspended in an evacuated chamber with blackened cryogenic walls and is uniformly illuminated by a radiation source equivalent to the sun. The sample will equilibrate at a temperature dependent on the α_s/ϵ ratio of the sample surface; when the radiant source is removed the sample temperature will decay as a function of the surface emittance and, having experimentally determined both α_s/ϵ and ϵ, the solar absorptance may be calculated. The physical principles may be analytically represented as

$$P=\frac{A\Omega}{R^2}\int_{\lambda_1}^{\lambda_2} s_\lambda \alpha_\lambda d\lambda \tag{3}$$

P radiant power absorbed by the sample
A sample absorbing area$=2\pi r^2$ (neglecting edges)
R distance between sample and source
Ω solid angle viewed by the sample
s_λ source spectral radiant intensity
α_λ sample spectral absorptance
$\lambda_1;\lambda_2$ wavelength limits (0.3μ to 3.9μ for 1% simulation)

Since A, R, and Ω are all known instrumental parameters, the energy absorbed by the sample may be more simply expressed as

$$I'=c_1\int_{\lambda_1}^{\lambda_2} s_\lambda \alpha_\lambda d\lambda \tag{4}$$

In the case of an equilibrium determination of α_s/ϵ the energy balance becomes

$$I'=c_1\int_{\lambda_1}^{\lambda_2} s_\lambda \alpha_\lambda d\lambda=A\sigma\epsilon_s T_s^4 \tag{5}$$

where

ϵ_s = sample emittance at temperature T_s
T_s = sample equilibrium temperature
σ = Stefan-Boltzmann constant

Performing the indicated integration of the appropriate solar spectral range and lumping instrumental constants,

$$I\alpha_s=c_2\epsilon_s T_s^4 \tag{6}$$

where I = intensity of the source. Thus,

$$\alpha_s/\epsilon_s=c_2\frac{T_s^4}{I}. \tag{7}$$

The techniques for determination of sample emittance ϵ_s have been described in sufficient detail elsewhere (ref. 14). Assuming that ϵ_s has been determined, either from a temperature decay curve or by some other method, the governing relationship is

$$\alpha_s=c_2\frac{\epsilon_s T_s^4}{I}. \tag{8}$$

The samples employed are usually 1 in. to 1½ in. in diameter and are as thin as is compatible with structural requirements to minimize transverse thermal gradients. A thickness of 0.050 in. is common, and, if coatings are being measured, care must be taken to coat the edges as well as the faces of the samples. The sample calorimeter must be sufficiently large with respect to the sample that radiative thermal interchange is largely geometry-independent. A chamber of 6-in. diameter and 10-in. length fulfills this requirement. The calorimeter walls are maintained at about 80° K to ensure negligible heating of the sample by radiation originating at the wall. The walls must be blackened with a material of very high absorptance so that no reflected solar radiation is incident upon the sample. Parson's optical black lacquer, with $\alpha_s=0.99$, may be employed.

The vacuum must be maintained at a level of 10^{-5} mm Hg or less to ensure that all heat transfer is by radiation. Standard vacuum equipment consisting of forepump, diffusion pump, trap, and baffle is adequate. Two sources presently in use are the 800-watt xenon compact arc lamp[2] and 10-mm Ultrex carbon electrodes.[3] Both sources are used in conjunction with an Ashcraft Super-High Lamp Projector.[4]

A front surfaced aluminized mirror 16-in. in diameter collects and directs the energy to an aluminized open wedge. The divided beam is collected and focused into the calorimeter as shown in figure 15–5. Sapphire windows, 1½ in. in diameter, are located at opposite ends of the calorimeter. Sapphire transmits energy over the spectral band from 0.2 to 6.0μ and remains relatively cool because of its good thermal conductivity. A complete description of the apparatus is given in reference 15.

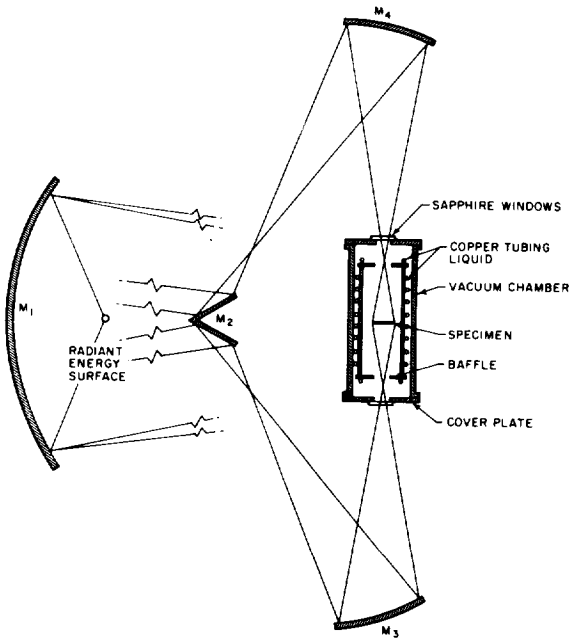

FIGURE 15–5.—Double aperture solar absorptance apparatus.

Sample temperature may be determined by means of 0.005-in. diameter thermocouples. Thermal conductive losses through the thermocouple leads can constitute a significant experimental correction; consequently, it is desirable to minimize thermal conduction by making the A/L ratio as small as is consistent with good thermometry. Temperatures usually are recorded on a strip-chart potentiometer recorder, so that true thermal equilibrium can easily be judged and also to facilitate emittance determinations by graphical reduction of the time-temperature decay curve.

It is instructive to perform an error analysis of solar absorptance determinations by this technique, both in order to estimate experimental accuracy and also to point out problem areas. From the basic relationships of equation (6), it can be shown that

$$\frac{\Delta\alpha_s}{\alpha_s}=4\frac{\Delta T}{T}+\frac{\Delta\epsilon}{\epsilon}-\frac{\Delta I}{I} \tag{9}$$

The emittance ϵ can be determined calorimetrically to within 5% with ease, and to 3% with some difficulty. Intensity determinations in the one solar constant range may be performed with an accuracy of 3–5%. Also contributing to the source uncertainty are intensity variations caused by arc wandering and uneven electrode feeding for carbon arcs and envelope transmission and general degradation with time for the gas filled arc lamps. Short-term fluctuations between 5 and 10% have been experienced and have resulted in sample equilibrium temperature variations of 3 to 5%. The other large uncertainty involves accurate sample temperature measurement. If the intensity employed is 0.14 watt/cm^2, then the calculated equilibrium temperatures are as follows:

α_s/ϵ	T(°C)	ΔT
10	434	5
5	320	3
1	123	2
0.2	−7	2
0.1	−49	2

The probable practical uncertainties in temperature measurement are indicated in the right column. The values shown above indicate approximately 1% accuracy in $\Delta T/T$, thus causing a 4% error in α_s. The maximum uncertainty in the determination of α_s by this procedure is about 14%. With careful experimental procedures, an rms error in α_s of 8% is indicated.

[2] Manufactured by Hanovia Lamp Division of Englehard Hanovia, Inc.

[3] Manufactured by The National Carbon Co.

[4] Manufactured by C. S. Ashcraft Mfg. Co.

Departures of the radiant source from exact duplication of the spectral intensity distribution of the extra-terrestrial sun will cause additional uncertainties. Referring to equation (3), if s_λ and α_λ are known, both s and α_s are completely calculable, since the extra-terrestrial solar spectral distribution is known with relatively good accuracy. Because of the normally greater absorption in the ultraviolet by both organic and metallic materials, the solar simulation source must emit adequate radiation in this spectral region. Two commonly-available sources are specialized carbon arcs and gas-filled arc lamps of xenon and xenon-mercury. Evaluation of these sources can be made by comparing their spectral characteristics with those of the extra-terrestrial sun.

The spectral distribution of the Diamant 1600-watt xenon lamp without reflector (ref. 16), 10-mm diameter Ultrex carbon arc electrodes operated at 155 to 160 amperes,[5] and the terrestrial solar radiation for air mass=1.0 (ref. 5) were normalized and compared with the spectral distribution of the extra-terrestrial sun (ref. 13) and absorptances for these sources were calculated using 2% equal energy intervals over the spectral region shown in figures 15–6, –7, –8, and –9. Values of α_s for each source were

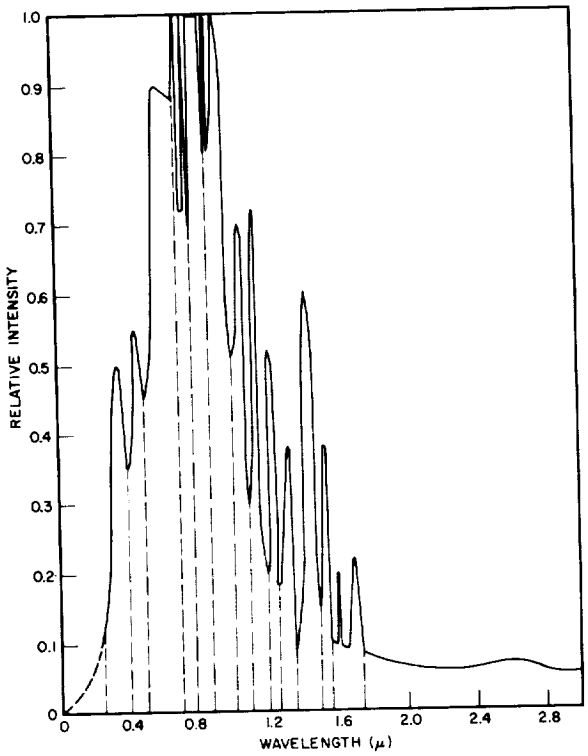

FIGURE 15–6.—Spectral distribution of xenon-diamant 1600-watt lamp without reflector (ref. 16).

[5] According to a private communication from National Carbon Co.

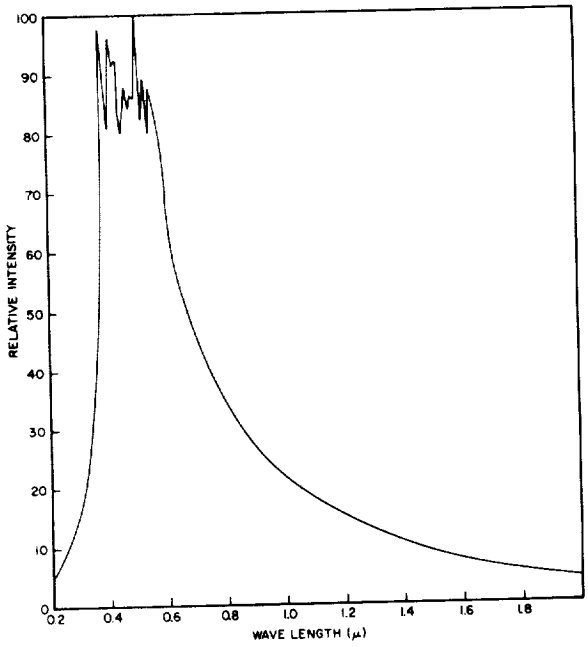

FIGURE 15–7.—Spectral distribution of 10-mm Ultrex carbon electrode.[5]

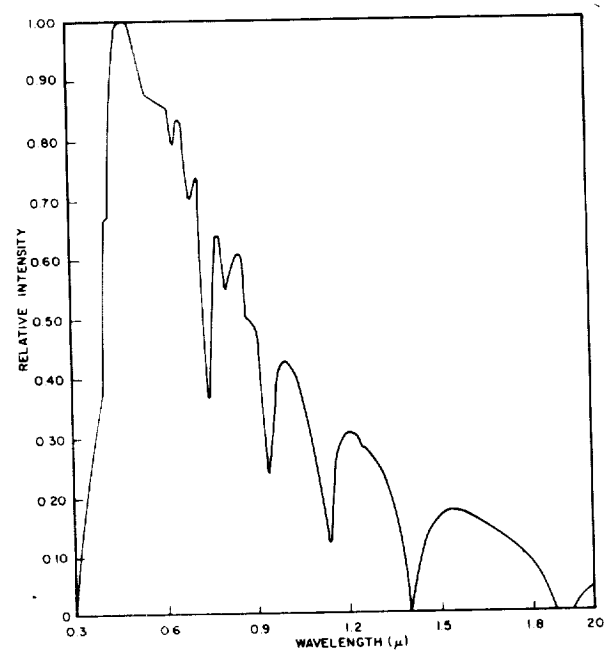

FIGURE 15–8. Spectral distribution of solar irradiance at optical mass=1.0 (ref. 13).

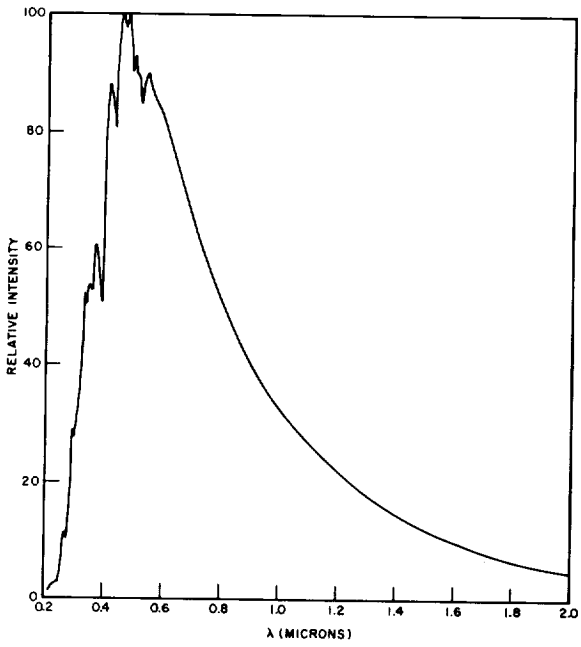

FIGURE 15–9.—Spectral distribution of extraterrestrial solar irradiance (ref. 13).

computed, as described in the data reduction, for a flat absorber, a UV absorber, a flat reflector, and partial solar absorber. Table 15–I lists the computed values for convenient comparison. No significance should be attached to the third decimal number, other than as an indication of the magnitude of differences. The absence of UV radiation in the terrestrial sun is particularly noticeable in the higher visible-reflecting surfaces because of their inherent absorption in this spectral region. Resulting α_s values are, therefore, lower than values obtained for extra-terrestrial conditions. Obviously, the flat black coating values are not susceptible to variations in spectral distribution. The differences in values for aluminum foil apparently results from the xenon lamp peak energy at 0.8μ and the carbon arc energy peaking at about 0.4μ. It is apparent that α_s for coatings with significant spectral variations could readily vary by ± 10 to 15% from the desired extra-terrestrial value, unless corrections for spectral differences are made.

RESULTS

The characteristics of materials which influence the solar absorptance magnitude and stability must be carefully measured and analyzed prior to specification of the material for a particular application. Figure 15–10 shows the

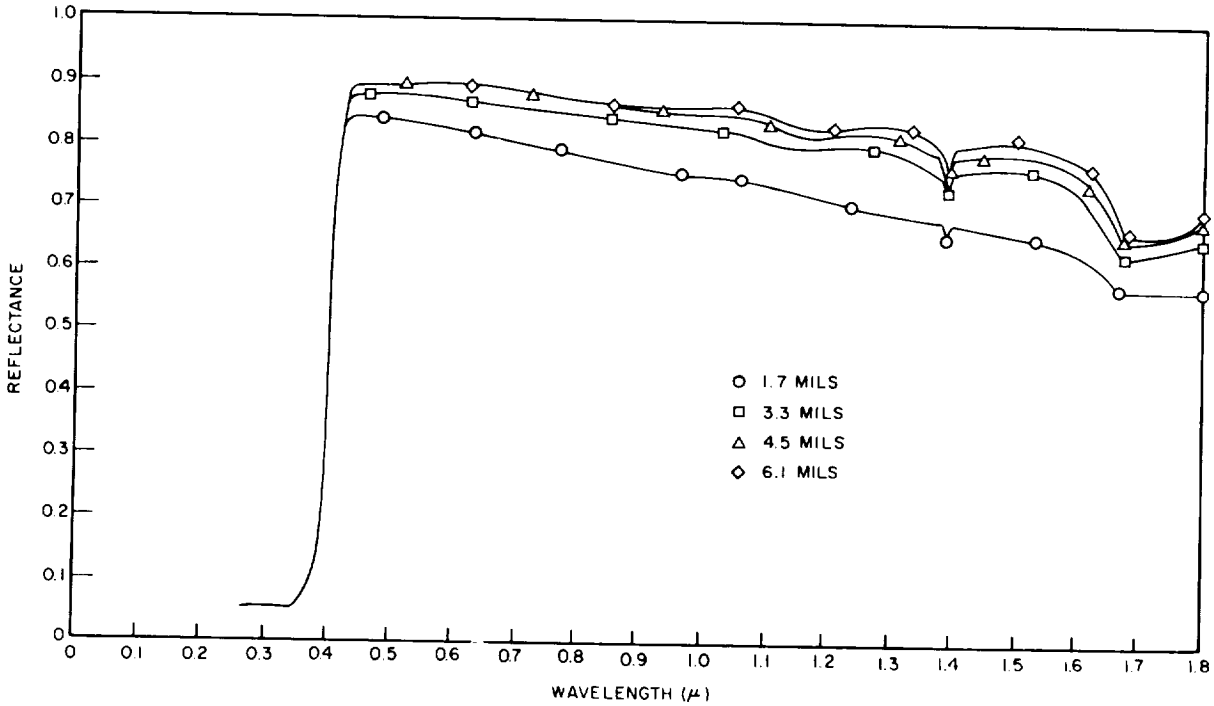

FIGURE 15–10.—The spectral variations in reflectance of an inorganic paint as a function of coating thickness.

TABLE 15–I.—*Calculated Total Solar Absorptance of Four Typical Materials When Irradiated With Sources of Different Spectral Distribution*

Coating	Ultrex carbon	Sea-level sun	Extra-terrestrial sun	Xenon arc lamp
Inorganic white paint	0. 162	0. 139	0. 128	0. 155
Aluminum foil	. 141	. 125	. 127	. 110
Black flat paint	. 983	. 982	. 978	. 977
White acrylic paint	. 281	. 223	. 262	. 297

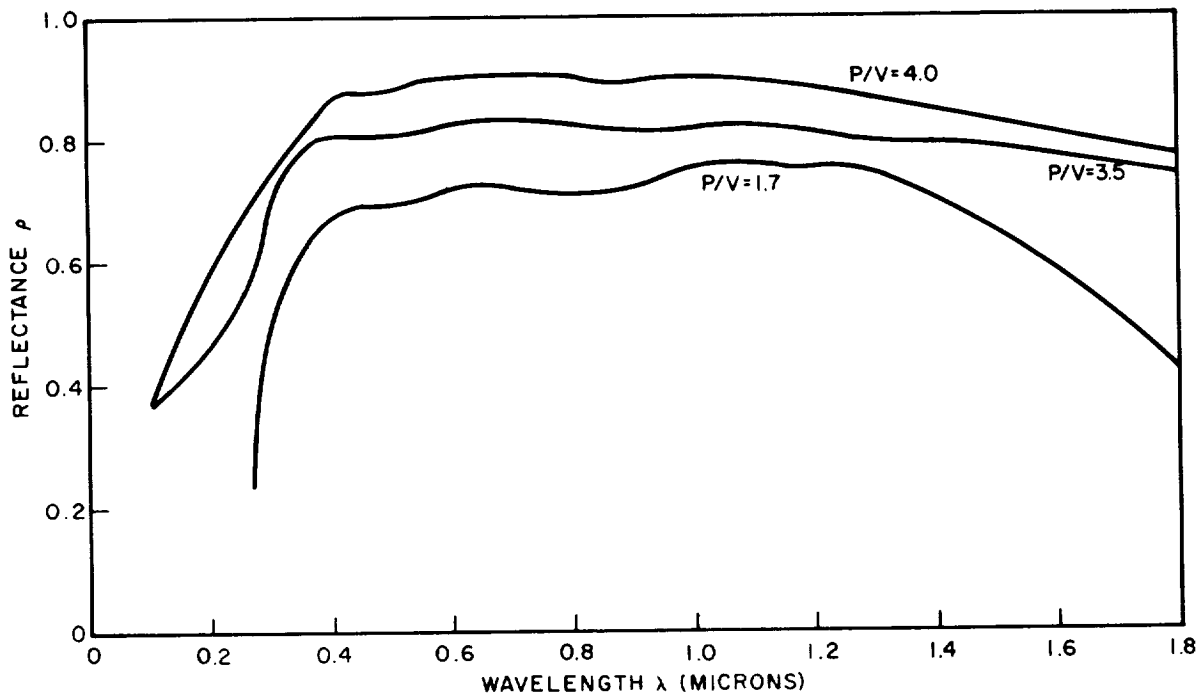

FIGURE 15–11.—The spectral reflectance of a pigmented sodium silicate coating with three different pigment-to vehicle (P/V) ratios.

dependence of spectral reflectance on thickness for a white acrylic coating. A thickness greater than 5.0 mils (0.005 in.) is necessary to ensure achievement of uniformly high visible and near-infrared reflectance. Values of α_s varied from 0.30 to 0.22 for the 1.7- and 6.1-mil thicknesses, respectively.

The optimization of pigment-to-vehicle ratio in the development of a white inorganic coating (ref. 17) is shown in figure 15–11.

The importance of ultraviolet performance to predict the stability of α_s in the space environment must be considered on all exterior coatings. Figure 15–12 illustrates the spectral nature of ultraviolet exposure effects on an epoxy coating and the resultant change in α_s from 0.21 to 0.46 for the equivalent of 500 sun hours.

The role of spectral reflectance measurements in investigations of this type clearly cannot be duplicated by any other existing measurement technique.

Table 15–II presents α_s values for typical thermal control surfaces investigated at LMSC with the described reflectance apparatus.

CONCLUSIONS

The role of spectral reflectance measurements for optimizing solar optical characteristics during material development cannot be duplicated by any other existing measurement technique.

TABLE 15–II.—*The Solar Absorptance (α_s) and Total Hemispherical Emittance (ϵ) at 500° R for Typical Materials Used for Spacecraft Thermal Control*

Material	Identification	α_s	500° R ϵ_H
Flat absorbers			
Rokide "C"	Flame-sprayed chrome oxide	0. 90	0. 85
Platinum black beryllium	Electrolytic deposited	. 94	. 80
Black acrylic paint	Sprayed to 5.0 mils	. 94	. 83
Black silicone paint	Sprayed to 5.0 mils	. 89	. 81
Flat reflectors			
Leafing Al acrylic	Sprayed to 3.0 mils	. 30	. 33
Nonleafing Al acrylic	Sprayed to 5.0 mils	. 44	. 36
Al silicone	Sprayed to 5.0 mils	. 25	. 26
Al silicate	Sprayed to 4.0 mils	. 35	. 37
Solar absorbers			
Aluminum	Polished and degreased	. 39	. 03
Gold over titanium with resin undercoat.	Polished	. 30	. 03
Beryllium	Chemically and mechanically polished	. 44	. 06
Inconel-X foil	Chemical polish	. 62	. 14
Solar reflectors			
Pigmented sodium silicate paint	Sprayed to 5.0 mils	. 14	. 91
Epoxy white paint	Sprayed to 5.0 mils	. 26	. 93
Sapphire	Coated on back side with silver	. 10	. 43
White plastic tape	Pressure-sensitive	. 24	. 89

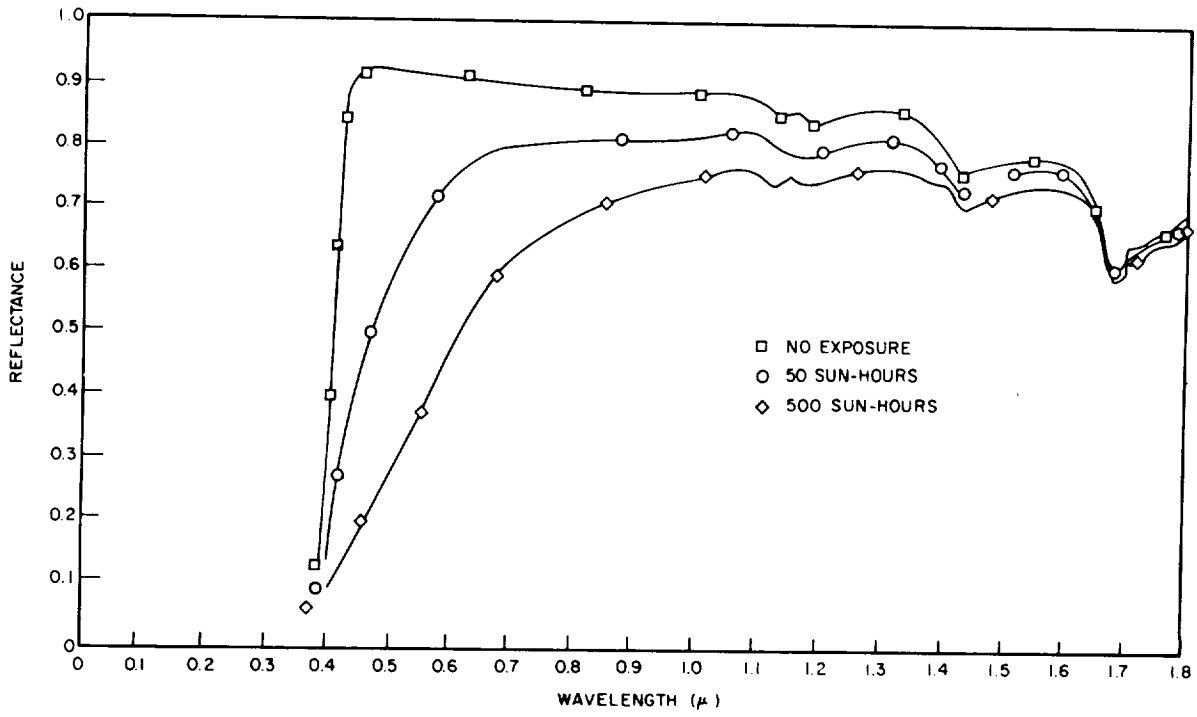

FIGURE 15–12.—The spectral variations in degradation of a white acrylic paint resulting from ultraviolet exposure.

The achievable accuracy compares favorably with absorptance measurement techniques for materials with values of α_s above 0.20. For materials with absorptances less than 0.20, routine absorptance techniques should be inherently more accurate for existing sources. Prior knowledge of the material spectral absorptance and the source spectral intensity can enable further corrections to total absorptance data. The development of improved solar simulation sources and accurate stable reflectance standards is a prerequisite to better measurements.

REFERENCES

1. Gubareff, G. G.; Janssen, J. E.; and Torborg, R. H.: Thermal Radiation Properties Survey. Minneapolis-Honeywell Regulator Co., 1960, p. 245.
2. Handbook of Chemistry and Physics, 31st ed., Chemical Rubber Pub. Co., 1949, p. 2297.
3. Edwards, D. K.; Nelson, K. E.; Roddick, R. D.; and Gier, J. T.: Basic Studies on the Use and Control of Solar Energy. National Science Foundation Grant 9505, Rep. No. 60-93, Oct. 1960.
4. Gaumer, R. E.; and McKellar, L. A.: Thermal Radiation Control Surfaces for Spacecraft. Lockheed Missiles and Space Division, LMSD 704014, Mar. 1961, p. F-1.
5. Handbook of Geophysics, Ref. ed., Macmillan Co., 1960, pp. 15–16.
6. Edwards, D. K.; Gier, J. T.; Nelson, K. E.; and Roddick, R. D.: Integrating Sphere for Imperfectly Diffuse Samples. Jour. Optical Soc. America, vol. 51, 1961, p. 1279.
7. Jacquez, J. A.; and Kuppenheim, H. F.: Theory of the Integrating Sphere. Jour. Optical Soc. America, vol. 45, 1955, p. 460.
8. Dunkle, R. V.: Spectral Reflectance Measurements. First Symposium on Surface Effects on Spacecraft Materials, (F. J. Clauss, ed.), John Wiley & Sons, Inc., 1960, p. 117.
9. Betz, H. T.; Olson, O. H.; Schurin, B. D.; and Morris, J. C.: WADC Tech. Rep. 56-222, Armour Research Foundation, May 1957.
10. Middleton, W. E. K.; and Sanders, C. L.: The Absolute Spectral Diffuse Reflectance of Magnesium Oxide. Jour. Optical Soc. America, vol. 41, 1951, p. 419.
11. Hass, G.: Filmed Surfaces for Reflecting Optics. Jour. Optical Soc. America, vol. 45, 1955, p. 945.
12. Janssen, J. E.; Schmidt, R. N.; and Torborg, R. H.: Emittance Standards. Final Report Subcontract No. 28-866 to LMSC, Honeywell Research Center, Hopkins, Minn. Ser. 37416, Dec. 1961.
13. Johnson, F. S.: The Solar Constant. Jour. of Meteorol., vol. II, Dec. 1954.
14. Gaumer, R. E.; McKellar, L. A.; Streed, E. R.; Frame, K. L.; and Grammer, J. R.: Progress in International Research on Thermodynamic and Transport Properties. Academic Press, Jan. 1962, p. 545.
15. Gaumer, R. E.; and Stewart, J. V.: Calorimetric Determinations of the Infrared Emittance and the α_s/ϵ Ratio. Symp. on Measurement of Thermal Radiation Properties of Solids, Dayton, Ohio, Sept. 1962.
16. Gibson, D. W.; and Weinard, J.: Studies of the Spectral Energy Distribution of Different Light Sources in Connection with Solar Simulation. Proc. IES, 1962, p. 453.
17. Tsukamoto, J.: Inorganic Passive Thermal Control Surfaces. Lockheed Missiles and Space Division, LMSD 3-71-61-15, Oct. 1961.

16—EMITTANCE MEASUREMENTS AT SATELLITE TEMPERATURES

BY G. D. GORDON AND A. LONDON

RCA ASTRO-ELECTRONICS DIVISION, PRINCETON, NEW JERSEY

Measurements of the total hemispherical emittance have been made using calorimetric techniques; both transient and steady state measurements have been used.

The sample, in the form of a thin plate (2 in. x 2 in.), is suspended within a cylinder located inside a vacuum chamber. For transient measurements the cylinder walls are cooled with liquid nitrogen, and the sample is heated with an arc light. When the arc light is turned off, the emittance can be determined from the rate of change of temperature and specific heat of the sample. For the steady state measurements an electrical heater is contained inside the sample, and the emittance is determined from the equilibrium temperature and the electrical power input.

The apparatus was originally designed, and is still used, to measure the ratio of absorptance to emittance. In order to decrease errors due to time variations, the sample time constant was decreased by making the sample as thin as possible; this also minimizes thermal gradients in the sample. The conduction along the supporting wires is minimized by using only the two thermocouple wires (and two power leads when necessary) for support, and minimizing the wire diameter (0.003 in. to 0.010 in.). Conduction through the gas is minimized by maintaining the pressure below 10^{-5} mm. The error due to thermal radiation from the sample reflected by the walls is minimized by having the walls black (emittance greater than 0.9) and by maximizing the area ratio of wall to sample. A quantitative evaluation of each of these errors is presented.

Measurements of emittance have been made for many years, but with the advent of artificial satellites these measurements have received new impetus and direction. In many cases the emittance as a function of angle and wavelength is not required, but only the total hemispherical emittance. Furthermore, the emittance is desired at temperatures, and for special surfaces, in which the total power radiated is quite small. For these purposes, calorimetric techniques have advantages compared to the usual measurement of intensity of the emitted radiation.

For calorimetric measurements, the sample is suspended in a vacuum, so that radiation from the sample is the predominant mode of heat transfer. The amount of power radiated is then determined by either measuring the rate of change of temperature (transient method), or by equating it to electrical power generated in the sample (steady state). Both the transient method (ref. 1–3) and the steady state (ref. 3–7) have been used and described previously. The apparatus and method described in this paper differs primarily in the following: a flat, thin sample is used to reduce the sample time constant; the number and wire diameter of the sample supports are minimized, as this has been shown to be an important source of error; a method is used to extrapolate to the equilibrium temperature, which is useful in speeding up the measurements and increasing the accuracy; and a quantitative evaluation of the errors has been made, which has proved useful in the improvement of the measurements.

APPARATUS

The main apparatus consists of a sample inside a copper cylinder, mounted in a vacuum chamber. The cylinder, with the inside painted black, was 18 in. long and 14 in. in diameter. A 2.5-in.-diameter hole at one end for use with arc light illumination was completely closed when not in use. Outside of the copper cylinder was soldered ¼-in. copper tubing, through which either liquid nitrogen or water was circulated. The cylinder was mounted inside a standard

17-in.-diameter glass bell jar, evacuated by an oil diffusion pump to a pressure below 10^{-5} torr.

The sample was covered externally with the surface to be measured and contained an internal electrical heater. The sample, usually 2 x 2 in., was made as thin as possible to reduce the thermal gradients in the sample and to decrease the time constant; by reducing the ratio of the thermal mass (mc) to the total surface area (A), the sample time constant ($mc/4\epsilon A\sigma T^3$) is decreased, and therefore the total measurement time is reduced.

The heater is made of thin Nichrome wire (0.002 in.) wound on a thin (0.010 in.) square sheet of glass epoxy board. Two opposite sides of the board are notched to hold the wire in position. The heater is eventually sandwiched between two square thin aluminum sheets (0.015 in.), each of which is slightly larger in area than the heater. A copper-constantan thermocouple junction is welded to one of the aluminum sheets, or otherwise placed in good thermal contact. The fine thermocouple wire extends about 4 in. beyond the edge of the aluminum sheet. The conduction of the supports is minimized by using only the two thermocouple leads and two power leads for support, and minimizing the wire diameter. The internal surfaces of the aluminum sheets are covered with a thin, insulating epoxy resin layer to prevent short-circuiting the heater wires. The sheets are then cemented to the heater with additional epoxy cement. The material whose emittance is to be measured is now applied to the sample surface. A paint can be applied directly to the aluminum surfaces; a flexible sheet, such as mylar, can be cemented to it.

MATHEMATICAL BACKGROUND

The rate of change of thermal energy with time, t, in the sample is equal to the power absorbed from the internal electrical heater, P, plus the power from the incident thermal radiation, Q, minus the thermal power radiated from the sample. The heat balance equation is therefore:

$$mc\frac{dT}{dt}=P+Q-\epsilon A\sigma T^4 \tag{1}$$

where the sample has a mass m, specific heat c, temperature T, surface area A, and thermal emittance ϵ (σ is the Stefan-Boltzmann constant).

In the steady state case, with the electrical heater turned off, the sample will reach the cylinder temperature T_c given by

$$Q=\epsilon A\sigma T_c^4. \tag{2}$$

With the electrical heater turned on, another equilibrium temperature T_E is reached given by

$$P+Q=\epsilon A\sigma T_E^4. \tag{3}$$

The desired emittance is then determined by eliminating Q from equations (2) and (3) and solving for ϵ:

$$\epsilon=\frac{P}{A(\sigma T_E^4-\sigma T_c^4)}. \tag{4}$$

The transient analysis can be useful in two respects: to determine the equilibrium temperatures more accurately, and to determine the ratio $\epsilon A/mc$. If A/mc is known, the latter serves as an independent determination of the emittance.

For temperature measurements over a wide range it is useful to plot the temperature derivative dT/dt as a function of σT^4. The equilibrium temperature is then determined from the abscissa intercept, and $\epsilon A/mc$ is determined from the slope of the straight line.

For temperatures close to the equilibrium temperature, the exponential approximation is useful

$$T=T_E+(T_i-T_E)e^{-t/\tau} \tag{5}$$

where τ, the sample time constant is given by

$$\tau\equiv\frac{mc}{4\epsilon A\sigma T_E^3}. \tag{6}$$

If three temperature readings T_1, T_2, and T_3 are taken, evenly spaced in time, with a time interval h, the equilibrium temperature can be directly calculated from

$$T_E=T_2+\frac{(T_2-T_1)(T_3-T_2)}{(T_2-T_1)-(T_3-T_2)}. \tag{7}$$

The time constant can also be determined from these three temperatures as:

$$\tau=\frac{h}{\ln\dfrac{T_2-T_1}{T_3-T_2}}. \tag{8}$$

Once the time constant is known, the ratio $\epsilon A/mc$ can be determined by using equation (6).

SOURCES OF ERROR

The emittance measurement depends on the net heat radiated from the sample to the walls. Some of the major sources of error are caused by heat transfer by other methods. The quantities of heat transferred must be compared to that transferred by the sample, which is:

$$P=\epsilon A(\sigma T_E^4-\sigma T_C^4)=247 \text{ mw} \qquad (9)$$

for a particular sample of low emittance.

The definition of symbols, and the numbers for this example are given in table 16–I.

TABLE 16–I.—*Quantities in a Sample Measurement*

Symbol	Definition	Magnitude
A	Total sample surface area.	9.75 in.^{2}
A_a	Extraneous surface area.	0.3 in.^{2}
A_c	Cylinder area	1100 in.^{2}
D	Supporting wire diameter.	0.005 in.
P	Internal electrical power.	247 mw
T_c	Cylinder temperature	298° K
T_E	Sample equilibrium temperature.	343.5° K
ϵ	Sample emittance	0.11
ϵ_a	Extraneous area emittance.	1
ϵ_c	Internal cylinder emittance.	0.9
ϵ_w	Supporting wire emittance.	0.2
k	Thermal conductivity (copper).	10 w/in.-°K
σ	Stefan Boltzmann constant.	3.657×10^{-11} w/in.^{2}-°K^4

Extraneous Area

Possibly the entire sample is not covered with the surface whose emittance is to be measured. This is especially serious if the emittance to be measured is small, and a few small areas exist with emittances close to unity. In the particular example, this heat is:

$$\epsilon_a A_a(\sigma T_E^4-\sigma T_c^4)=66 \text{ mw} \qquad (10)$$

and was therefore a major source of error.

Conductivity of Wires

Thermal conduction losses through the supports are minimized by suspending the sample from long thin wires. Assuming the wires are infinitely long, of isothermal cross section, and do not radiate back to the sample, the heat flow q from each copper wire is

$$q=\pi\left[\frac{1}{10}k\sigma\epsilon_w D^3(T_E^5-5T_c^4T_E+4T_c^5)\right]^{1/2}$$
$$=2.3 \text{ mw}. \qquad (11)$$

The constantan wire dissipates less heat, due to its lower conductivity, in this case only 0.6 mw. There are three copper wires and one constantan, for a total of 7.5-mw dissipation, which produces a maximum error of 3% in the measured emittance. Due to the uncertainty in the emittance of the wire, it is difficult to make an accurate correction, and therefore the error should be minimized by using small diameter wires.

Extraneous Radiation

If the cylinder walls are not perfectly black, some of the thermal radiation from the sample will be reflected by the walls back to the sample. This will cause the measured emittance ϵ_M to be less than the sample emittance ϵ. An estimate of this error can be obtained from Cristiansen's equation

$$\frac{1}{\epsilon_M}=\frac{1}{\epsilon}+\left(\frac{1}{\epsilon_c}-1\right)\frac{A}{A_c}. \qquad (12)$$

This error can be decreased by increasing either the cylinder emittance or the cylinder area. In the present case, the error is of the order of 0.01% and therefore negligible.

Conductivity of Gas

The vacuum required to eliminate conduction through the gas can be estimated by calculating the number of molecules ν that impinge on the sample per unit time and per unit area. Assuming the average energy transfer cannot be greater than $3/2k(T_E-T_c)$, the fractional error E incurred in ϵ is then

$$E\leq\frac{3}{2}K(T_E-T_c)\nu/\epsilon\sigma(T_E^4-T_c^4)<\frac{3}{2}K\nu/\epsilon\sigma T_E^3 \qquad (13)$$

where K is the Boltzmann constant. By the

kinetic theory of gases (ref. 8), this can be transformed to

$$E<\frac{pc}{2\epsilon\sigma T^4} \tag{14}$$

where p is the gas pressure and c the average molecular speed. For a temperature of $T=300°$ K, this simplifies for air to

$$E<\frac{70p_{\text{torr}}}{\epsilon} \tag{15}$$

where p is measured in torr (mm of Hg). An experimental determination of the equilibrium temperature for various pressures is in agreement with equation (15).

Temperature Measurement

This error includes not only the actual accuracy in the measurement of the temperature at one point, which is usually quite good, but the effect of temperature gradients in the sample, the determination of the average cylinder temperature, and the constancy with time of the latter. In the present example the estimated accuracy in the temperature is of the order of one degree; since the temperature difference is 45°, this produces only a 2 or 3% error in the emittance. Should the need arise, a temperature accuracy of 0.1° is probably readily attainable.

CONCLUSIONS

Calorimetric measurements have been used as a practical means of obtaining the total hemispherical emittance of a sample. The present measurements have an accuracy of 10% for some samples, but the errors increase for measurements of low emittance. The accuracy could probably be substantially increased by reducing certain sources of error. From the analysis an accuracy of 5 to 10% is possible, even for an emittance of 0.05, which would be useful information for spacecraft construction.

REFERENCES

1. Butler, C. P.; and Inn, E. C. Y.: A Method for Measuring Total Hemispherical Emissivity of Metals. *Surface Effects on Spacecraft Materials*, F. J. Clauss, ed., John Wiley & Sons, Inc., 1960, pp. 195–211.
2. Gordon, G. D.: Measurement of Ratio of Absorptivity of Sunlight to Thermal Emissivity. Rev. Sci. Instr., vol. 31, no. 11, Nov. 1960, pp. 1204–1208.
3. Gaumer, R. E.; McKellar, L. A.; Streed, E. R.; Frame, K. L.; and Grammer, J. R.: Calorimetric Determinations of Thermal Radiation Characteristics. *Progress in International Research on Thermodynamic and Transport Properties*, J. F. Masi and D. H. Tsai, eds., Academic Press, 1962, pp. 575–587.
4. Hass, G.; Drummeter, L. F., Jr.; and Schach, M.: Temperature Stabilization of Higher Reflecting Spherical Satellites. Jour. Optical Soc. America, vol. 49, no. 9, Sept. 1959, pp. 918–924.
5. Drummeter, L. F., Jr.; and Goldstein, E.: Vanguard Emittance Studies at NRL. *Surface Effects on Spacecraft Materials*, F. J. Clauss, ed., John Wiley & Sons, Inc., 1960, pp. 152–163.
6. Richmond, J. C.: Some Methods Used at the National Bureau of Standards for Measuring Thermal Emittance at High Temperatures. *Surface Effects on Spacecraft Materials*, F. J. Clauss, ed., John Wiley & Sons, Inc., 1960, pp. 182–194.
7. Shaw, C. C.: Apparatus for the Measurement of Spectral and Total Emittance of Opaque Solids. *Surface Effects on Spacecraft Materials*, F. J. Clauss, ed., John Wiley & Sons, Inc., 1960, pp. 220–246.
8. Jeans, J. H.: *Kinetic Theory of Gases*. University Press (Cambridge), 1952, p. 192.

DISCUSSION

W. B. Fussell, Goddard Space Flight Center: Gordon and London describe a system which is very similar to the Goddard system. The major differences between the Goddard technique and the G & L technique are:

(1) The Goddard technique is designed to yield accurate emittance values for coatings having very low emittances such as vacuum deposited gold and aluminum. The following considerations apply to the measurement of low emittance coatings:

(a) Since time constants are long, and a long time is required for equilibrium to be achieved, transient techniques allow emittance data to be obtained more rapidly,

(b) Since radiative heat transfer is small, conductive heat losses must be minimized for accurate data. This implies eliminating electric power leads by relying on radiant energy to heat up the test sample, coating the thermocouple leads with the coating being measured for a short distance beyond the test sample, and maintaining a vacuum of better than 10^{-6} mm of Hg (the fractional error in emittance for an emittance value in the 0.02 range at a pressure of 10^{-5} mm of Hg is 0.035 at 300° K).

(2) Most low emittance coatings are metallic and, hence, have an emittance which varies approximately proportionally with the absolute temperature. For a data reduction method which determines the emittance from the slope of the curve giving the rate of change of sample temperature as a function of the fourth power of the absolute temperature of the sample, the variation of emittance with temperature requires that the measured value of the slope be multiplied by a correction factor of 0.8.

(3) Thermal emittance values, computed from thermal data, are correlated with thermal emittance values computed from optical data (total reflectance spectra) by employing tables derived from Fresnel's formulae for the variation of reflectance with angle of incidence. The G & L method, as described in the body of their paper, is applicable only for the emittance measurement and has no provision for the measurement of the α/ϵ ratio.

To sum up, I believe that the Goddard technique gives more accurate thermal emittance values for low emittance materials, particularly metals. In addition, the Goddard procedure for correlating optical and thermal emittance data is probably unusual in some respects.

R. E. Gaumer, Lockheed Missiles and Space Company: The absorptance and emittance of the black cylinder wall, as a function or temperature, either are not known or have not been stated. The amount of energy emitted by the wall, in the example given in the paper, is almost certainly an appreciable portion of the total energy exchanged and consequently may not be neglected.

Although it is true that pure theory would lead one to believe that 10^{-5} mm Hg is an adequate vacuum to insure that the predominant mode of heat transfer is radiation, our experience indicates that the requisite vacuum is pronouncedly dependent on the temperature of the sample and container and also upon the relative dimensions of the sample and container.

The thermal mass of the heater and supporting film is apparently not known and, due to the sample geometry employed, may well be an appreciable portion of the total thermal mass.

The probable presence of pronounced thermal gradients within and throughout the sample configuration due to the use of various glues and adhesives is, in my opinion, likely to distort the temperature distribution to such an extent that the temperature measurement at one point by the thermocouple employed is, at best, a crude approximation of the average sample temperature. These gradients due to interfacial impedences are extremely serious in any transient determination, since interfacial impedence may well be the limiting factor of the flow of thermal energy from the heater to the cylinder wall.

Equation (9) appears to be in error since this is an energy balance upon the sample, and the energy received by the sample from the wall is

$$\sigma\epsilon_{wall}\epsilon T^4_{wall}$$

and not

$$\sigma\epsilon T^4_{wall}$$

Our experience has been that an absolute accuracy of 1° K in temperature determinations is extremely difficult when one considers the problems of thermocouple attachment, calibration, standardization, and time variation. An accuracy of 1° K is certainly not readily attainable by conventional techniques. The difficulty here is that the small-diameter thermocouples, which indeed are necessary to minimize extraneous heat losses, must be individually and carefully calibrated.

It is quite disappointing that no data are presented in the paper by which some comparison to the error analysis given may be made.

Although it is stated that the apparatus was designed and is used to measure α/ϵ ratio, the paper contains no discussion of the methods of determination of this ratio. As is pointed out in my paper on this topic, the primary power and usefulness of this technique, as opposed to the several other calorimetric techniques, lies in the very determination of the α/ϵ ratio. Indeed it is in this area that most of the practical problems lie. Many other devices are capable of adequate determinations of emittance by calorimetric techniques.

Despite this criticism, which I hope will be received in the constructive spirit in which it is intended, it seems quite clear that the further development of apparatus such as this will be very useful for practical determinations of the important thermal radiation parameters associated with the thermal radiative control of spacecraft.

692-146 O—63——11

17—HEATED CAVITY REFLECTOMETER MODIFICATIONS

BY R. J. HEMBACH, L. HEMMERDINGER, AND A. J. KATZ

GRUMMAN AIRCRAFT ENGINEERING CORPORATION, BETHPAGE, N.Y.

The heated cavity reflectometer is the most practical device available for thermal reflectance measurements of opaque surfaces. Its application, however, is based upon the reciprocity of incident and reflected radiation. As a result, it is extremely sensitive to any deviations from a true black-body cavity. The greatest errors come from non-uniform temperature, and non-homogeneous field of view. This report describes the modifications to an upright hohlraum reflectometer to correct the errors inherent in its original design. Data taken on the redesigned device are compared with those of the original design, demonstrating the improvements accomplished. The work was performed on a Perkin-Elmer model 205 infrared reflectivity attachment which was used in conjunction with a model 13 infrared ratio recording spectrophotometer of the same make.

Soon after the reflectometer/spectrophotometer equipment went into operation in our laboratory (figure 17–1), it became obvious that the data being generated were of little or no value for our needs. We decided to undertake a reasonably extensive evaluation and modification program. Our goal was to determine the ultimate applicability of the upright heated cavity concept to our requirements in aerospace heat transfer engineering. Keeping in mind the pressing needs for this type of data, we tried, wherever possible, to revise the existing equipment rather than to redesign parts completely which would require long downtime periods.

During the course of this program, the technical staff of the Perkin-Elmer Corporation was consulted on matters pertaining to the optics of the problem. We gratefully acknowledge their valuable contribution to our effort.

At the present time, we are in the process of evaluating the overall effects of our modifications on various categories of surfaces. The results will be published as soon as available.

DESCRIPTION OF ORIGINAL CAVITY

The cavity which was modified is a $5\frac{13}{16}$ inches high nickel cylinder, with inside diameter of $4\frac{1}{2}$ inches. It has a flat nickel base plate and a 165° conical nickel crown. The wall thickness of the cavity is $\frac{1}{4}$ inch. The cavity is supported by three Inconel legs, $\frac{3}{8}$ inch in diameter and $6\frac{3}{4}$ inches long, which are welded to the base. The legs are bolted to the bottom casing of the furnace jacket. A 2-inch diameter viewing port is bored on center in the cavity base. The internal cavity wall is grit blasted and blackened by operating the cavity 2 to 3 days at 1500° F to form a nickel oxide coating. An Inconel tube 7 inches long is welded in the crown of the cavity. The tube is inclined 7° 30′ off the vertical center line of the cavity. The center line of the tube intersects the internal surface of the crown perpendicularly $1\frac{1}{8}$ inches from the cavity center line. The function of the tube is to introduce and locate the specimen to be tested in the cavity. The specimen is carried in a water-cooled sample holder.

The power source for heating the cavity is a cylindrical hump furnace heater element $7\frac{1}{2}$-inch diameter by 10 inches high. The heater is a potted Nichrome resistor-Alundum cement unit rated at 2.5 kw. When installed in the furnace jacket on a 4-inch thick preformed diatomaceous earth block, the heater overlaps the base and crown of the cavity by approximately 2 inches. The remainder of the furnace assembly consists of a top insulating brick 4 inches thick, powdered diatomaceous earth insulation, and three thermocouple probes for cavity-temperature regulation.

The reflectometer is operated in conjunction with a double-beam ratio-recording spectro-

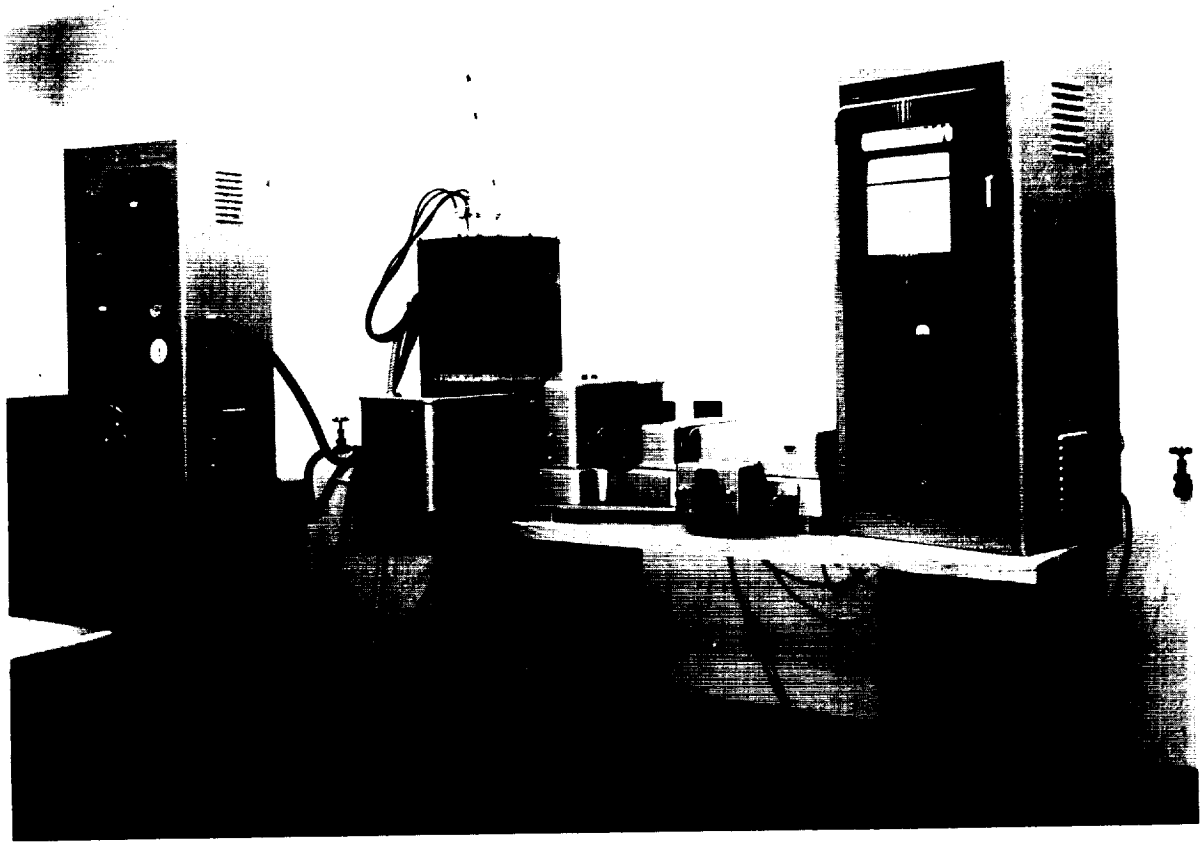

FIGURE 17–1.—Original reflectometer/spectrophotometer installation.

photometer (Perkin-Elmer model 13). It is mounted immediately above double-beam transfer optics (the cavity and transfer optics together with the power supply and controls constitute Perkin-Elmer's model 205 infrared reflectivity attachment). The cavity temperature is maintained at a nominal 1470° F. The transfer optics "see" a 6° diverging bundle of radiant and reflected energy through the viewing port, inclined at an angle of 9°21′ from the vertical centerline of the cavity. The crossover point for the two beams is approximately 2⅜ inches below the viewing port. The 100% line on the ratio recording is obtained with the beams viewing two areas on the crown of the cavity 180° apart. The sample to reference (I/I_o) trace on the same recording is obtained by rotating the entire cavity assembly 90° to place one beam on the sample and the other beam on the crown.

The standard sample holder furnished with the equipment consists of an inner concentric tube specimen cooling assembly and an integral outer jacket which is also water cooled. The sample is maintained at a temperature of 100° F by the cooling water. The complete sample holder assembly is fabricated of stainless steel. The outer cooling jacket makes direct metal-to-metal contact with the Inconel tube when the sample holder is in position in the cavity.

The sample holder is equipped with two interchangeable nose pieces. The 17° angle head holds the specimen at an angle of 18°51′ to the sample beam to produce a diffuse-plus-specular reflectance reading. The flat head holds the specimen at an angle of 1°51′ to the sample beam for measuring the diffuse component only. The angle of incidence of the reference beam with the crown of the cavity remains constant at 1°51′, independent of the sample holder head or the rotational position of the cavity.

The crown angle of incidence being only 1°51′, any specular component from the reference surface is distorted because the reference surface reflects an image of the 2-inch viewing port and the relatively cold area around it. This situation has led to values of reflectance greater than unity. To correct this condition, the manufacturer recently produced a new cavity. The old conical crown has been replaced by a flat plate installed normal to the sample holder tube (at an angle of 7°30′ to the plane of the base). The internal surface of this new top plate is milled with 1/16-inch-deep grooves to form a diamond pattern over the entire crown. The reference beam incident angles for this crown are now 16°51′ for the I/I_0 run and 9°21′ for the 100% line run. We have not purchased one of these new cavities. Instead, special platinum reference surfaces have been installed in our original cavity. These are discussed below.

DESCRIPTION OF CAVITY MODIFICATIONS

The modification program was planned to make all changes as simple as possible, avoiding complete redesign of the equipment wherever feasible. The double-beam ratio-recording operation of the original equipment was maintained, as was the mechanical rotation of the entire cavity assembly 90° for running the I/I_0 and the 100% traces. The double beam feature has the advantage of short data acquisition time. When the cavity and sample are at thermal equilibrium, the time required to record the spectral reflectance of the specimen in the 1.5-μ to 15-μ region is approximately 45 min. This time element is particularly desirable in the laboratory when sorting materials, studying the deterioration of a specimen surface after repeated exposure to detrimental conditions, or when it is necessary to predict rapidly how a surface's emittance will vary with temperature. Although this report does not consider the experimental error possibilities in the spectrophotometer equipment itself, we must point out the distinct advantage of the constant-I_0 (reference signal) condition maintained at the thermocouple detector in ratio recording. A constant I_0 restricts operation to a small portion of the thermocouple's response curve, thus minimizing nonlinearity problems in the detector system.

Within this framework, four major problem areas were selected for special attention:

1. temperature gradients in the cavity
2. oversized viewing port
3. unreliable sample holder design
4. fixed crown angle in the cavity.

To begin our study the internal temperatures in the cavity were mapped prior to modification. Double Chromel-Alumel thermocouples were installed in 23 areas on the cavity. The double thermocouple installation (fig. 17–2) was

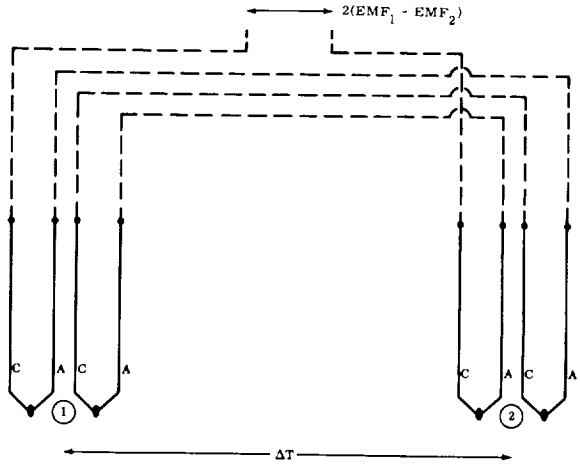

FIGURE 17–2.—Thermocouple installation method.

selected to obtain extreme (0.2%) accuracy in ΔT measurement. The resulting EMFs of the bucking double thermocouple installation were measured with a K–3 Leeds & Northrup potentiometer. The measured gradients were severe; the maximum gradients, observed with the sample holder in place, exceeded 100° F at a cavity temperature of 1470° F.

The initial tests required the development of instrumentation techniques and equipment beyond those in the original device. We found that the best method for fastening the thermocouples to the cavity was to embed the junctions in small drilled holes (0.090-inch dia. and 0.187-inch deep) in the cavity wall and pot them in place with a high-temperature ceramic cement. Small Nichrome ribbon straps spotwelded to the outer cavity proved to be the most suitable method of securing the thermocouple leads. An embrittlement problem with the Alumel leads made it necessary to resort to stainless steel

sheathed thermocouple wire despite the connector problems which this type of wire present.

The embrittlement was noticed during the tear down of the cavity following a sample holder gasket failure. A series of laboratory tests was conducted in a muffle furnace at temperatures ranging from 1200° to 1700° F. The purpose of the tests was to reproduce the Alumel embrittlement condition. The embrittlement was not achieved with the muffle furnace tests. The decision to change to shielded wire was based on the recommendations of the thermocouple manufacturer who had experienced the Alumel embrittlement when the thermocouple wire was exposed to a high-temperature, high-humidity environment.

Although the double thermocouple method for measuring ΔT produced the required accuracy, the initial installation was time consuming to use and limited the experimenter to ΔT readings between fixed areas in the cavity. A thermocouple selector switching circuit was developed to support the modification program. The switching circuit consisted of two 24-position and one 10-position thermocouple switches and three 2-position selector switches. The circuit enables the operator to select ΔT readings between some predetermined area in the cavity and any one of 24 other areas in the cavity. In addition, the circuit allowed the user to switch from the ΔT mode and read the actual temperature at each thermocouple junction.

Three modifications were adopted to correct the temperature gradient condition: auxiliary trimmer heaters were designed and installed, a low-heat-sink sample holder was substituted for the original, and heat shielding was installed in critical areas. Four electrical trimmer heaters were added to support the main 2.5-kw cylindrical heater around the cavity. These consisted of a sample holder tube heater, 500 watts at 5 amp; a crown heater, 1.2 kw at 10 amp; a base and viewing port heater, 1.2 kw at 10 amp; and leg heaters, 150 watts at 5 amp. A separate four-channel power supply was designed and constructed for the auxiliary heaters. Each heater output was controlled by its respective voltage regulator. The circuit was designed so that the power consumed by each heater could be checked at will with a single wattmeter through a switching system. All auxiliary heaters were relay operated in phase with the main heater relay of the original temperature control console.

Fabrication of auxiliary heaters with a long life expectancy proved to be a problem. The main factors governing the design of durable heaters are:

1. careful watt density and coil diameter-to-spacing ratio (interference factor) for the particular resistor element material selected
2. compatability of resistor wire material and the supporting ceramic
3. proper lead-in wire to resistor element cross sectional area ratio and mechanical bond.

For this modification, coiled Nichrome wire was embedded in Alundum furnace cement, and fired at 1900° F. A braided Nichrome lead, carbon arc welded to the resistor to give an area ratio in excess of 7 to 1, was used.

The first heaters fabricated were laced to an air-drying ceramic support. This technique proved to be completely unreliable. Failures occurred at the crown lead in wire-resistor element connection and between two adjacent coils in the viewing port heater section. The construction technique used does not provide means for rigidly supporting the lead in wire-resistor element connection. Coil-to-coil spacing of the resistor element is also not controlled in this method. A green-yellow discoloration of the air-drying ceramic indicated that a chemical reaction between the ceramic and the Nichrome element had taken place, although heater failures directly attributable to this reaction were not observed. Intermediate heaters consisting of shielded Nichrome wire fastened to a glass rock bed exhibited an improved life characteristic and were used in a temporary installation.

The sample holder furnished with the equipment had to be abandoned entirely. When the water-cooled sample holder was in place and at equilibrium conditions, the new auxiliary crown heater could not hold the temperature gradient in the crown area to below 13° F even with a mean cavity temperature of only 872° F One local area at the intersection of the sample holder tube and crown remained at 33° F below the 872° F mean cavity temperature.

A new sample holder was designed to eliminate the large heat sink capacity of the original one. The outer water-cooled jacket which made direct thermal contact with the sample holder tube in the cavity crown was discarded. An insulated triple concentric tube body assembly was fabricated to replace it and to serve as a housing for the water-cooled nose assemblies which were also redesigned. Figure 17–3 shows

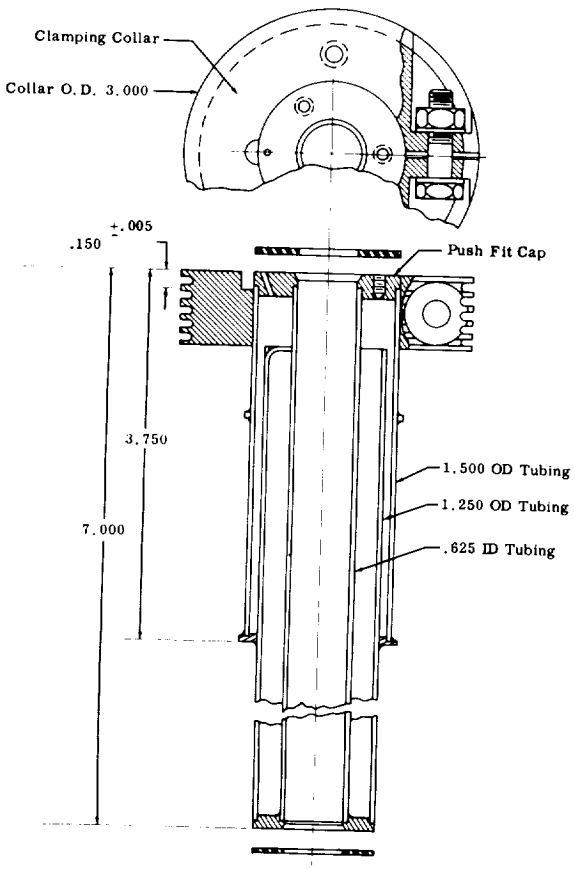

FIGURE 17–3.—Concentric tube sample holder body.

the construction of the body assembly. The tubes which make up the body assembly were ¾, 1¼ and 1½ inches in outside diameter. These and the remaining detail parts in the sample holder area were fabricated from 300 series stainless steel. The volume between the tubes was packed with Celite. The top finned collar clamp was designed to be positioned and locked to control the depth of insertion of the sample into the cavity.

The center concentric delivery and return tube of the original design was replaced by a two tube nose assembly as shown in figures 17–4 and 17–5. Four interchangeable nose assemblies were made to maintain the diffuse plus specular and plain diffuse feature of the original equipment and also to provide a no risk (closed chamber) version for each case. The closed chamber version of the nose assemblies eliminates all gasket requirements. The end of the nose assembly is permanently sealed with a ⅛-inch thick copper plate which is silver brazed in position. The copper plate and the body of the nose assembly are grooved, to route a thermocouple to the rear surface of the specimen. The specimen is set on the copper nose plate with a colloidal silver lubricant and is held in place by the retaining sleeve and retainer nut. The $\frac{3}{16}$-inch tube section of the nose assemblies was wrapped with high-temperature insulating blanket material (Cerefelt) prior to installation in the body assembly.

In the original sample holder, when a specimen was being installed in the angle head, it was necessary to rotate at least one metal surface against the gasket face to establish a water-tight seal. This design arrangement increased the probability of water leakage. One water leakage incident in GAEC's laboratory destroyed the mirrored surfaces of the transfer optics immediately below the cavity, damaged the surface of the specimen which was being tested, and opened up the base heater circuit. The flat-head adaptor of the original equipment does not present the same gasket problem but introduces a new problem. The sliding surfaces in this case are the sample and the retainer nut's shoulder. When working with soft material such as aluminized Mylar, the retainer nut twists and wrinkles the specimen.

The nose assembly of the new sample holder was redesigned to overcome the two difficulties discussed. In this design, the gasket and sample are compressed into a sealed position without a shearing motion. This was accomplished by inverting the specimen retainer nut and adding a new specimen retaining sleeve as shown in figure 17–5. Another unique feature is the manifold connection which permits rapid interchangeability of nose assemblies. The staggered tube lengths prevent the improper installation of the manifold, avoiding the possibility of utilizing the

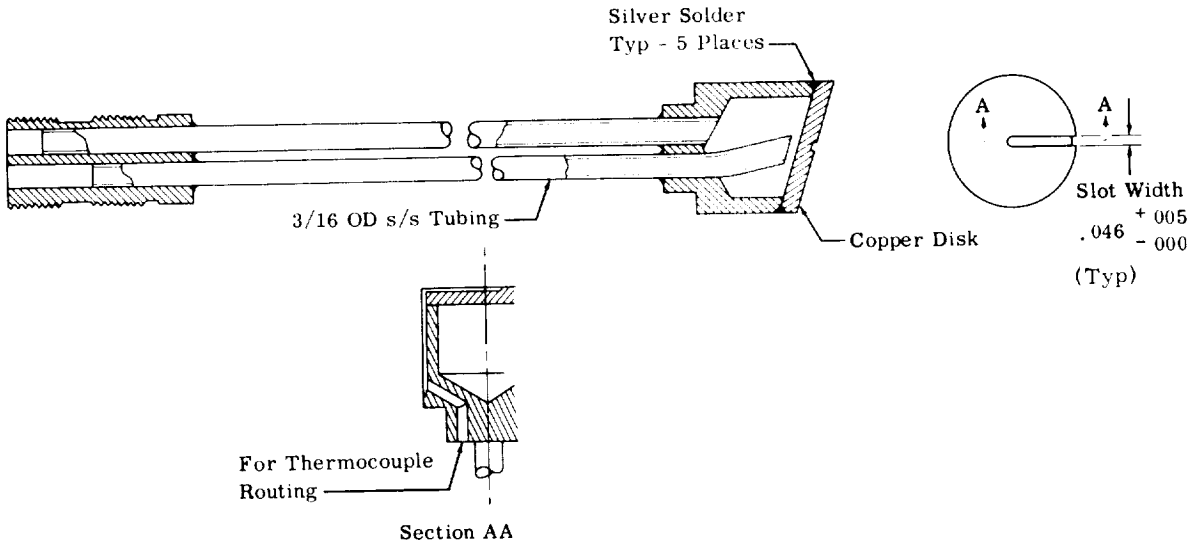

FIGURE 17–4.—Closed chamber angle head.

water supply tube as the drain line. Details of the mainfold connection appear in figure 17–5.

The new nose assemblies were machined at two angles to the plane perpendicular to the sample holder center line. One nose assembly, machined at 1°51′, presents the sample to the optics of the equipment at normal incidence. The other nose assembly, machined at 17°, maintains the 18°51′ incident angle of the original equipment.

To complete the temperature gradient modifications, radiation shielding was installed around the sample holder tube heater, the crown, and the viewing port. All shields were fabricated of 321 stainless steel. Although they have performed satisfactorily, some unevenness in the oxidation coating of the stainless steel was noted. As a result, any hardware to be installed in the cavity in the future will be fabricated of Inconel X. One shield envelops the outer surface of the sample holder tube heater, sliding over the heater and resting on the crown shield. The crown shield covers the entire opening of the main furnace heater enclosing the complete upper surface of the auxiliary crown heater assembly. This shield plus celite insulation replaces the top formed brick in the original furnace. The viewing port

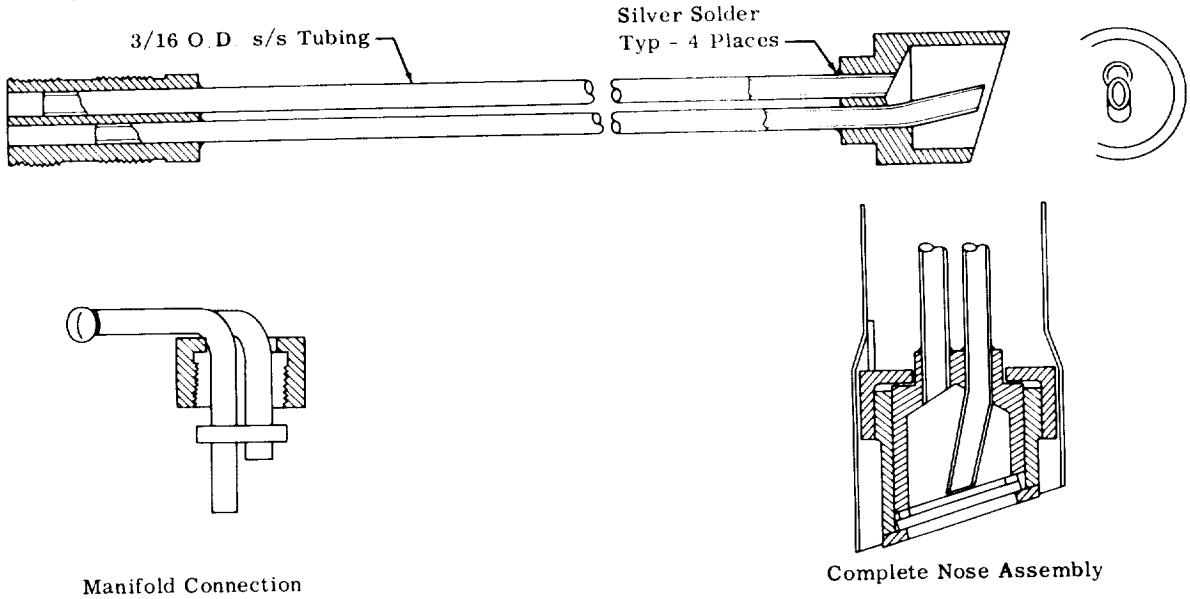

FIGURE 17–5.—Sample holder angle nose assembly.

shield is conical (included angle, 18°42′) and is positioned in the center of the new viewing port insert. The curtain portion of the viewing port insert is sandwiched between the viewing port heater and the conical shield.

The specular reflectance fin was designed to remove the hohlraum fixed crown angle restriction. The fin mounts were so designed that the original double-beam mode would be retained and the makeup of the reference beam could be varied from full diffuse to diffuse plus specular radiation at 18°42′ from the disk's normal. This was accomplished by mounting three 1⅜ inch diameter platinum disks 0.005 inch thick from the crown of the cavity. The disks were spot welded to a 321 stainless steel open support ring. The support ring is attached to a 5/16-inch diameter shaft approximately 1.00 inch long at an angle of 9°21′ to the shaft's centerline. The crown of the cavity was drilled and reamed to accept the shafts. A collar piece, which sets the center of the fin approximately 0.400 inch below the crown of the cavity was fastened to the shaft section that protrudes from the outer cavity wall, and nested in a spotface recess in the outer cavity wall. The center of each shaft was drilled to accept a 5/16-inch o.d. 4-hole ceramic insulator. The insulators serve to route the leads from the double thermocouple installation on the rear surface of the platinum disks (see figs. 17–6 and 17–7). The centers of the disks are located radially 1⅛-inch from the cavity center line and in positions 90°, 180° and 270° from the sample holder assembly. The metal to metal contact area between the shaft and collar and the cavity was coated with a high-temperature silver lubricant.

The added flexibility of the rotating platinum disks allowed the operator to select a normal incidence angle for the reference beam when working with the flathead or diffuse sample holder or any angle of incidence up to 18°42′ for the reference beam when making specular plus diffuse reflectance studies. Rotation of the sample holder and one reference disk (90° from the sample) makes it possible for the sample and disc to view the same point in the cavity although the shape factors are not identical.

FIGURE 17–6.—Specular reflectance fin—front face.

FIGURE 17–7.—Specular reflectance fin—back face.

The theory describing the operation of the specular fin assumes that the hohlraum cavity is an ideal blackbody and that the platinum disk's temperature is identical to the cavity's temperature.

The signal leaving the surface is

$$Q=\rho_P I+\epsilon_P G$$

where ρ_P and ϵ_P are the reflectance and emittance of the platinum, respectively, I is the incident signal from the cavity walls, and G is the emission of a blackbody at the temperature of the platinum. If the cavity is a blackbody, and the platinum is at cavity temperature,

$$I=G$$
$$\rho_P+\epsilon_P=1$$
$$Q=I_{BB}$$

If the platinum is not at cavity temperature, since $\epsilon_P<<1$, the error is relatively small.

Holding the disk at cavity temperature was difficult with the suspended disk system employed. During early tests, the disks were suspended from the cavity crown with fixed ceramic rods. The original sample holder was being used at that time. Under these conditions, heavy radiation from the rear of the fins to the cool neck of the sample holder reduced

the three fin temperatures to 33° below the cavity's side wall temperature of 872° F. A direct conduction path was established from the crown to the disks, and a radiation shield was added to the new sample holder configuration to maintain high disk temperatures.

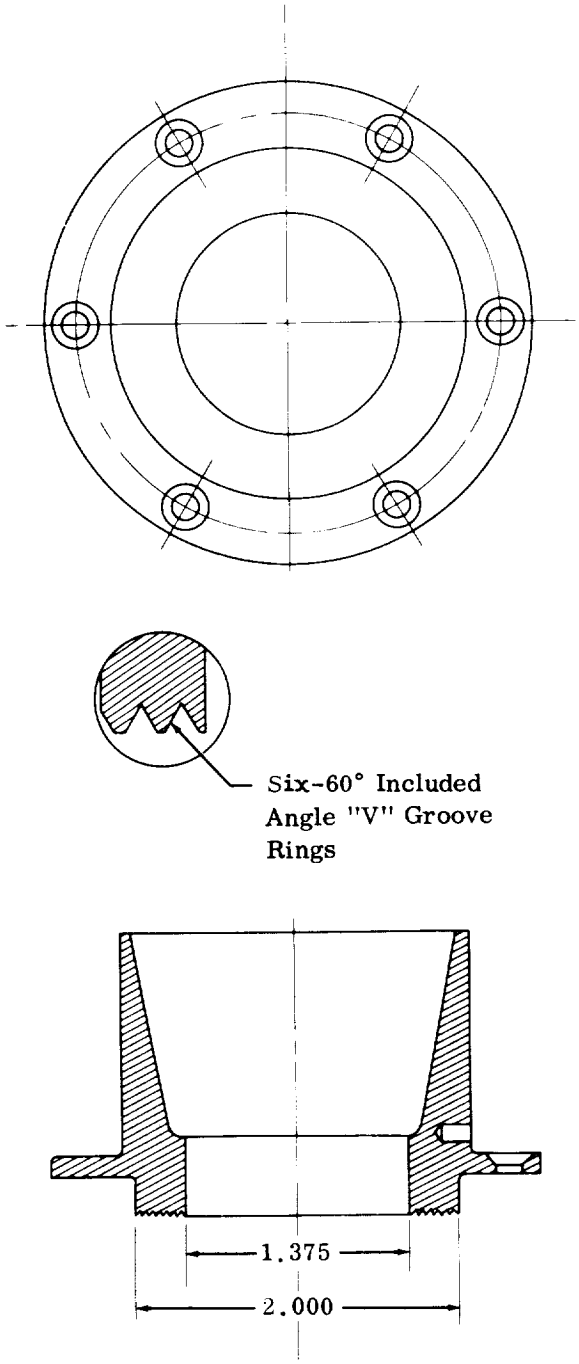

FIGURE 17–8.—Hohlraum guard ring.

The reduction in viewing port diameter was fixed by the geometrical relationship of the cavity and its optics. To determine the minimum possible viewing port diameter, a lamp source was focused on the exit slit of the monochromator as is customary in spectrophotometer alignment. A full-scale layout of the modified cavity (cross-sectional plane through sample holder and one platinum disk) was erected above the transfer optics. Using the green line (5460 Å) Littrow mirror setting, the slit image was focused on the sample and platinum disk's mean plane, 1⅛ inches from the cavity center line on the full-scale layout. Mapping the cross-sectional area of the two beams in the viewing port plane of the cavity indicated that the 2.000-inch viewing port diameter could be reduced to 1.375 inch. A flanged stainless steel viewing port adapter was machined with an integral cylindrical shaped curtain which loosely fitted the bore of the base and viewing port heater unit. The curtain extension was recessed to accept the conical heat shield (fig. 17–8). The surface of the adapter facing into the cavity was machined with a series of 0.050-inch deep concentric "V" grooves.

If the cavity interior were completely isothermal, any specularity in the surface would be unimportant. In reality, however, we must accept some temperature nonumiformity. The effects of temperature gradients are minimized if the interior of the cavity is a diffuse reflector. Since it would have been difficult to machine grooves into the cavity walls without cutting it open, we decided initially to sandblast the inside surfaces with a course grit. After holding the cavity at 1750° F for 24 hours to oxidize it, we noticed that some of the grit had become embedded in the cavity wall and now appeared as white spots on the oxidized surface.

A second attempt was made to roughen the cavity walls. This time we mixed nickel filings with Dutch Boy high-temperature black paint (46H47) and applied it to the surfaces. The filings had been "roasted" and thoroughly cleaned previously. Figure 17–9 pictures the "sand paint finish" which this process produces. The nickel chip paint was applied by brush, cured at 500° F for 1 hour, and fired at 1400° F.

The best subsurface for paint adhesion was rough nickel oxide thoroughly cleaned (alcohol

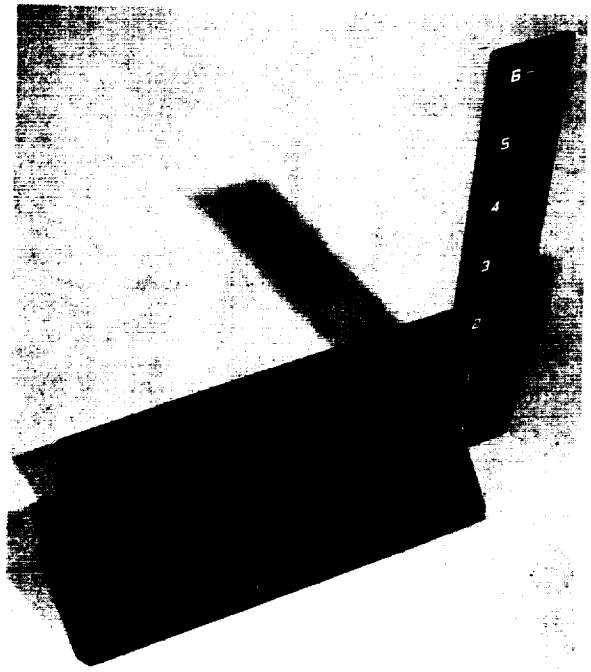

FIGURE 17–9.—Samples of cavity interior finishes.

and degreasing process). Application of the paint to bright nickel, whether rolled, polished, or grit blasted, resulted in peeling after the 1400° F firing process. Applying the paint to the internal walls of the cavity with an airbrush produced the same negative results, despite the rough oxide surface preparation. The reason seemed to be paint runs and an overly heavy coating of the paint. This apparently resulted in the paint failure in the first cavity test. Subsequent applications of the high temperature black paint to the cavity's internal walls by hand brushing produced the desired paint adhesion property.

CONCLUSION

A series of modifications has been made to a commercially-available upright heated-cavity reflectometer. Figure 17–10 compares the device before and after modification. The purpose of the changes was to increase the accuracy and reliability of the device for spectral reflectance measurements of opaque samples. The results appear most encouraging although only preliminary information on the performance of the

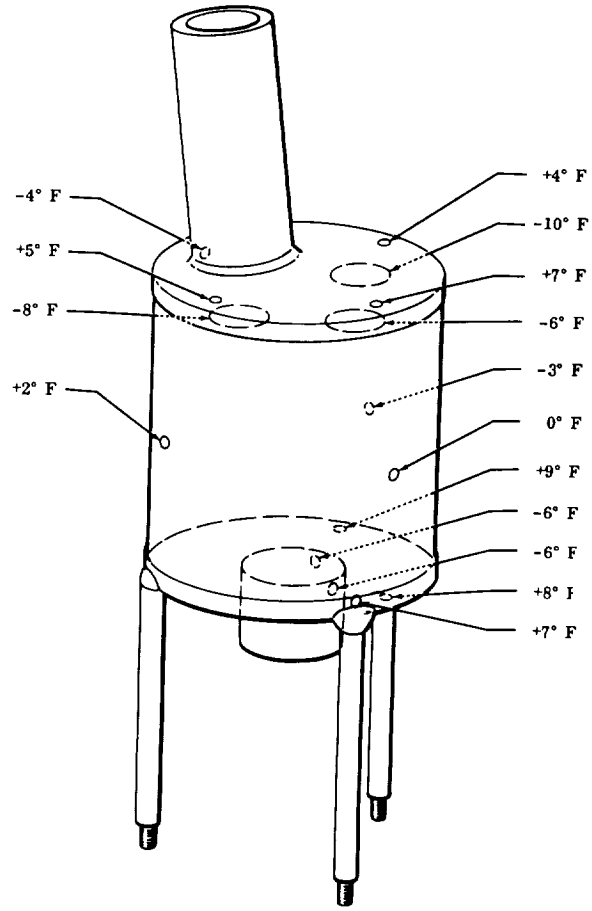

FIGURE 17–10.—Temperature gradients at nominal cavity temperature of 1200° F.

equipment is currently available. Figure 17–11 shows the temperature gradients after modification.

This report describes in detail the modifications which were made. Appendix A shows the computation of the space curves defining the cross point of the traces of the specular components of sample and reference surfaces. We do not suggest that the view factors are equal, only that both surfaces "look" at the same point on the cavity wall. The computation of the improvement gained by the inclusion of the viewing port adapter appears as appendix B.

Final results of the improvements accomplished by these modifications will be published when available.

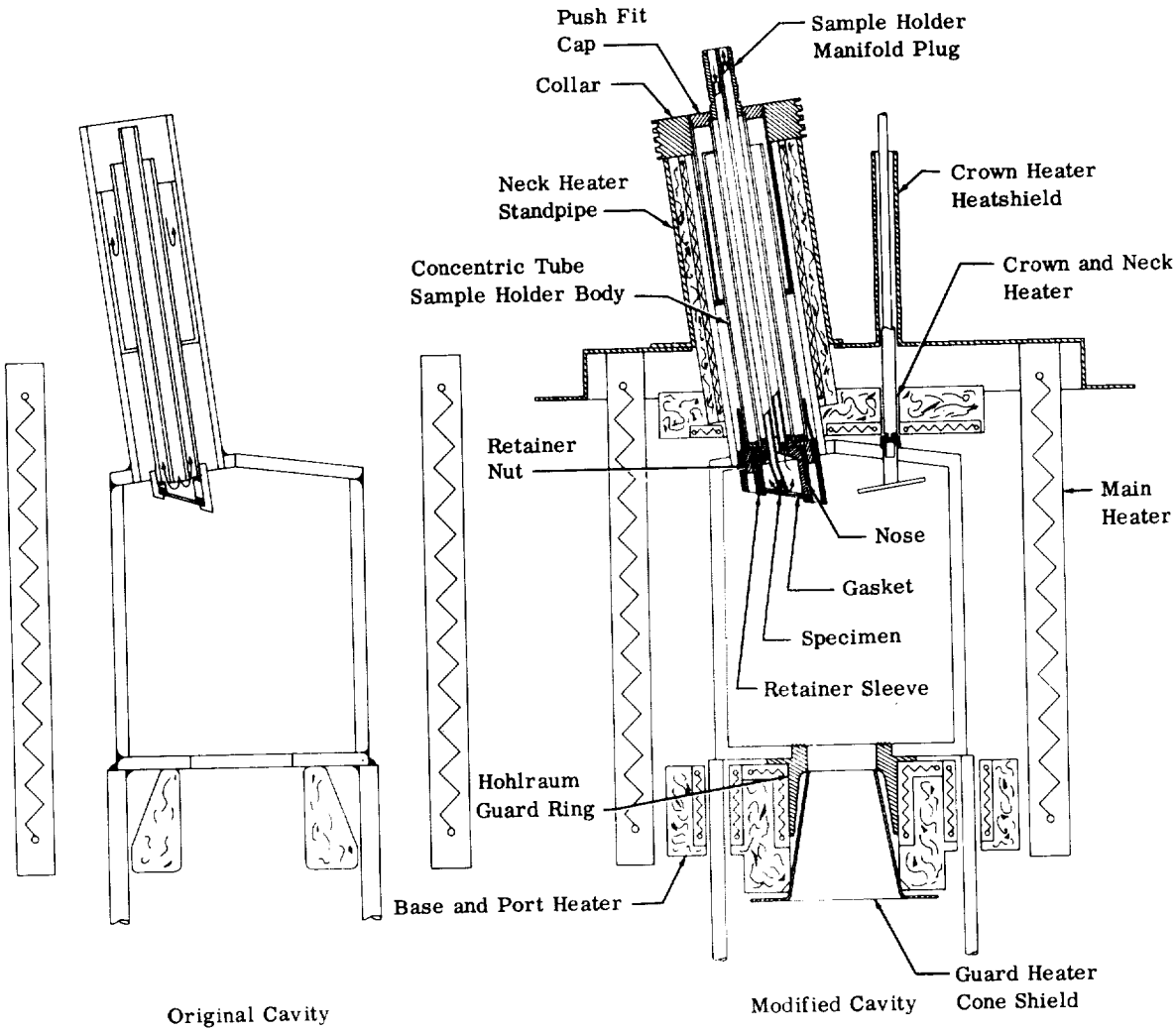

FIGURE 17-11.—Comparison of original and modified installation.

REFERENCES

1. DUNKLE, R. V.; EDWARDS, D. K.; GIER, J. T.; NELSON, K. E.; and RODDICK, R. D.: Heated Cavity Reflectometer for Angular Reflectance Measurements in Progress in International Research on Thermodynamic and Transport Properties (ASME), Academic Press, 1962, pp. 541–562.
2. GIER, JOSEPH T.; DUNKLE, ROBERT V.; and BEVENS, JERRY T.: Measurement of Spectral Reflectivity from 1.0 to 15 microns, Jour. Optical Soc. Am., vol. 44, 1954, pp. 558–562.
3. RIED, CHARLES D.; and MCALISTER, E. D.: Measurement of Spectral Emissivity from 2μ to 15μ. Jour. Optical Soc. Am., vol. 49, 1959, pp. 78–82.

APPENDIX A—ANALYSIS OF THE SPACE CURVES DEFINING THE ORIGIN OF THE SPECULAR COMPONENT ON THE CAVITY WALL

The analysis is based on a single center ray of the energy beam, and the incident-reflected ray relationship is reversed for convenience.

REFERENCE DISK

For axes– choose z axis along disk shaft and zy plane in plane of symmetry of cavity to form righthand system. Origin is in plane of disk.

α, γ	constants determined by geometry
$\overline{N}$	normal to mirror
$\overline{V}$	incident beam (in yz plane)
$\overline{V}'$	reflected beam
$\overline{N}$	$\sin\alpha \sin\phi$, $\sin\alpha \cos\phi$, $\cos\alpha$
$\overline{V}$	0, $-\sin\gamma$, $-\cos\gamma$
ϕ	Rotation about disk or sample holder ℄

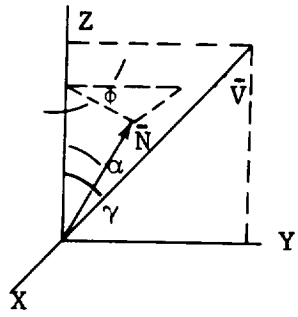

In specular reflection: $\overline{N} \times V = \overline{N} \times V'$

$$\begin{bmatrix} \bar{i}\ (-\sin\alpha\cos\phi\cos\gamma+\cos\alpha\sin\gamma) \\ +\bar{j}\ (\sin\alpha\sin\phi\cos\gamma) \\ +\bar{k}\ (-\sin\alpha\sin\phi\sin\gamma) \end{bmatrix} = \begin{bmatrix} \bar{i}\ (\sin\alpha\cos\phi\ V_k'-\cos\alpha\ V_j') \\ +\bar{j}\ (\cos\alpha\ V_i'-\sin\alpha\sin\phi\ V_k') \\ +\bar{k}\ (\sin\alpha\sin\phi\ V_j'-\sin\alpha\cos\phi\ V_i') \end{bmatrix}$$

Equating components, we find

$$V_j' = \cot\phi V_i' - \sin\gamma$$

$$V_k' = \frac{\cot\alpha}{\sin\phi} V_i' - \cos\gamma \qquad (1)$$

to normalize,

$$V_i'^2 + V_j'^2 + V_k'^2 = 1$$

Hence

$$V_i' = 2\sin\alpha\sin\phi\ (\sin\alpha\cos\phi\sin\gamma + \cos\alpha\cos\gamma) \qquad (2)$$

The equations for the reflected ray are then:

$$\frac{x}{V_i'} = \frac{y}{V_j'} = \frac{z}{V_k'} \qquad (3)$$

Substituting appropriate values of α and γ we obtain

$$\frac{x}{A\sin\phi\cos\phi + B\sin\phi} = \frac{y}{C\cos^2\phi + D\cos\phi + E} = \frac{z}{F\cos\phi + G} \qquad (4)$$

where A, B, C, D, E, F, and G are determined by the constants α and γ. Equation (4) is solved simultaneously with the equation for the cylinder wall,

$$x^2 + (y-a)^2 = r^2 \qquad (5)$$

where a is the radial distance from center of cavity to center of disk and r=cavity internal radius.

When this yields $z > b$, the reflected ray strikes the base of the cylinder and equation (5) must be replaced by

$$z = b \qquad (6)$$

where b=distance from base to center of disk.

SAMPLE DISK

Using primed coordinates to represent the system for the sample, the X', Y', Z' coordinates are skewed with respect to the cylinder and may be transformed to correspond to coordinates of reference disk for convenience.

This involves a rotation about the X' axis of $\beta°$ and a translation of Y' by $a'+a$ where β is the angle between the sample holder axis and axis of cavity. The untransformed equations for the reflected ray are in the form of equation (4) with appropriate constants.

The transformation equations are

$$X' = -x$$

$$Y' = -(y-(a'+a))\cos\beta - z\sin\beta$$

$$Z' = z\cos\beta - (y-(a'+a))\sin\beta$$

The final form of the equation becomes,

$$\frac{x}{A' \sin\phi' \cos\phi' + B' \sin\phi'} = \frac{H_y + J_z}{C' \cos^2\phi' + D' \cos\phi' + E} = \frac{K_y + L_z}{F' \cos\phi' + G'} \tag{7}$$

which is solved simultaneously with equation (5) to determine space curve.

APPENDIX B—ANALYSIS OF THE CHANGE IN THE SHAPE FACTOR OF THE EMITTED BEAMS RESULTING FROM A CHANGE IN THE VIEWING PORT DIAMETER

The geometry of the cavity is shown on the drawing with

$$\beta = 9°21'$$

$$\alpha_1 = 12°30'$$

$$|\bar{r}| = \frac{5.13}{\cos 12°30'} = 5.26$$

$$\frac{\bar{r}}{|\bar{r}|} = 0,\ \sin\alpha_1,\ \cos\alpha_1$$

$$\bar{N}_2 = \sin\beta \sin\phi,\ \sin\beta \cos\phi,\ \cos\beta$$

$$\cos\alpha_2 = \frac{\bar{r}}{|\bar{r}|} \cdot \bar{N}_2 = \sin\alpha_1 \sin\beta \cos\phi + \cos\alpha_1 \cos\beta$$

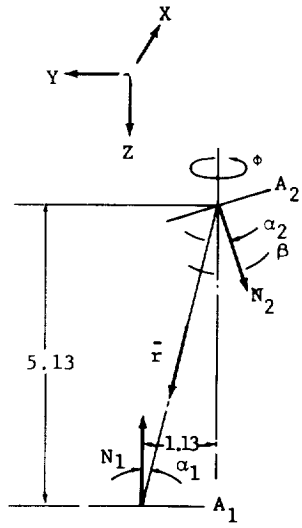

The extremes in α_2 exist for $\phi = 0$, and $\phi = \pi$.

$$\cos\alpha_2|_{\phi=0} = 0.998$$

$$\cos\alpha_2|_{\phi=\pi} = 0.928$$

The view factor represents the fraction of radiation from A_1 which impinges on A_2.

$$F_{21} = \frac{A_1 \cos\alpha_1 \cos\alpha_2}{\pi r^2}$$

The original size of the viewing port, A_1, was π square inches. The size was reduced to 0.473 π square inches.

When $\theta = 0$,

$$\Delta F_{21} = \frac{0.527\pi}{\pi r^2} (0.976)(0.998) = 0.0186$$

When $\theta = \pi$

$$\Delta F_{21} = \frac{0.527\pi}{\pi r^2} (0.976)(0.928) = 0.0173$$

These represent reductions of approximately 50% by virtue of the reduction of viewing port diameter of $\frac{5}{8}$ inch.

APPENDIX C—NEW DATA ON INCREASED HOHLRAUM ACCURACY

Since the release of the main body of this paper, data have been generated which illustrate the increased hohlraum accuracy obtained with the modifications described in the text. Figure 17–12 compares the data generated with the GAEC modified hohlraum cavity to the original Dunkle and Gier data and UCLA data for similar platinum samples. The latter two sets of data were replotted from the curves presented in reference 1. Data from reference 1 were also used in the comparative presentations in figures 17–13 and –14. The comparative studies are for similar samples and not for identical samples; therefore, a discussion of the deviations in data observed in different laboratories is difficult. Nevertheless, by reviewing figures 17–12 to –14, it is seen that agreement in data is very good above 4μ. The 1.5- to 4-μ area covers the sharp low-wavelength side and peak energy area of the 1200° F blackbody curve. This indicates that the slight deviations below 4μ are most probably associated with the temperature gradient condition in the cavity. The modified cavity was designed such that the sample and platinum disks are capable of looking at the same area in the cavity. It is possible that in the initial survey runs the sample and platinum disk rotational settings were not precise and that the sample and disk were not looking exactly at the same zone in the cavity.

Figures 17–15 and –16 are two curves from the thermal radiation properties support program for the Orbiting Astronomical Observatory project at GAEC. The hard-coat sulfuric acid anodized sample was typical of the Martin hard-coat process. The hard-coat thickness was 2 mils. The sample was boiled 75 min in nickel acetate following the sulfuric acid bath. The substrate material was unclad 2014 T6 aluminum.

The substrate for the alodine sample of figure 17–16 was reworked before the alodine treatment was applied. The Alclad coating on the 7075 T6 blank was removed by polishing with rubbing compound. The resulting exposed 7075 T6 surface (mirror finish) was cleaned with MEK and then processed through the prealodine cleaning process. The time-concentration information for the alodine process was one to three minutes immersion in alodine 1200 chromate solution. The treated sample was then rinsed in an acidulated bath for 15 to 30 sec and air dried.

Spectral reflectance measurements data for high-emittance materials were not included in this appendix addition to the paper. Since data generated on materials of this type are subject to sample emission erros, especially at the longer wavelengths, information will not be released until we are sure of the exact surface temperature condition for each sample. Several methods of measuring sample surface temperature of high ϵ materials are now under investigation. When substantial progress is made, a separate report will be prepared and data for high ϵ samples will be published.

The total emittance values tabulated in each figure were obtained from the data for the curve and the IBM program discussed in the body of this paper. Emittances are quoted to 3 significant figures to help show the trend of total emittance with sample temperature. The error we have associated with the data presented is from ± 0.01 to ± 0.02 of the actual observed values. A more precise error estimate will be forthcoming following our error analysis study.

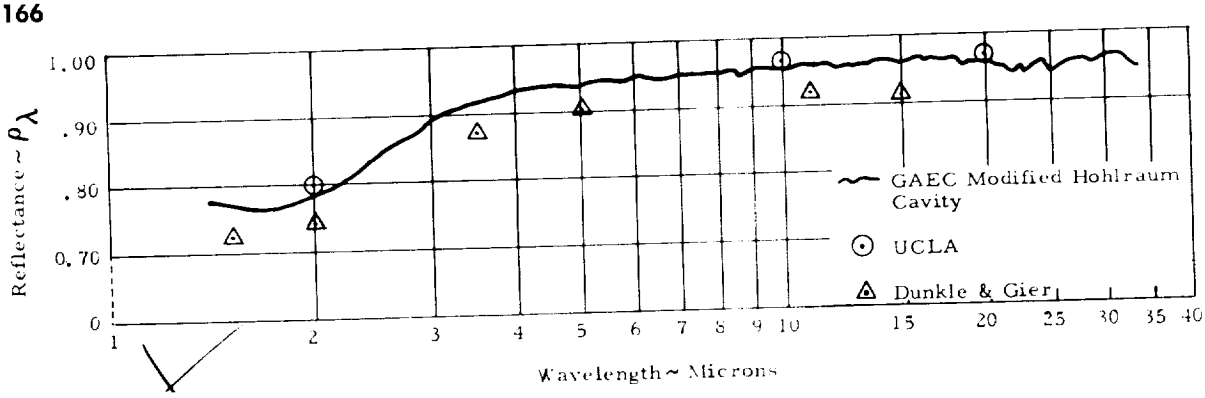

FIGURE 17-12.— Spectral reflectance of platinum foil 0.005 inch thick. Integrated emittance: $\epsilon_{0°F}=0.040$, $\epsilon_{500°F}=0.040$, and $\epsilon_{1000°F}=0.041$.

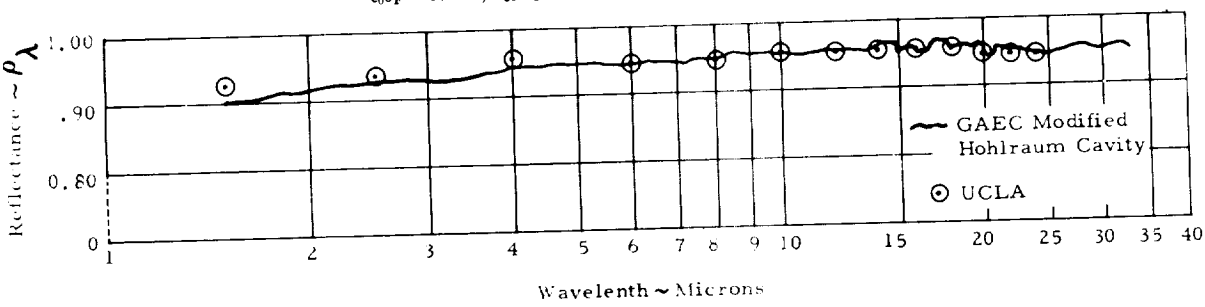

FIGURE 17-13.—Spectral reflectance of vacuum-evaporated 24K gold on fiberglass. Integrated emittance: $\epsilon_{-500°F}=0.042$, $\epsilon_{0°F}=0.043$, $\epsilon_{1000°F}=0.044$, and $\epsilon_{2000°F}=0.045$.

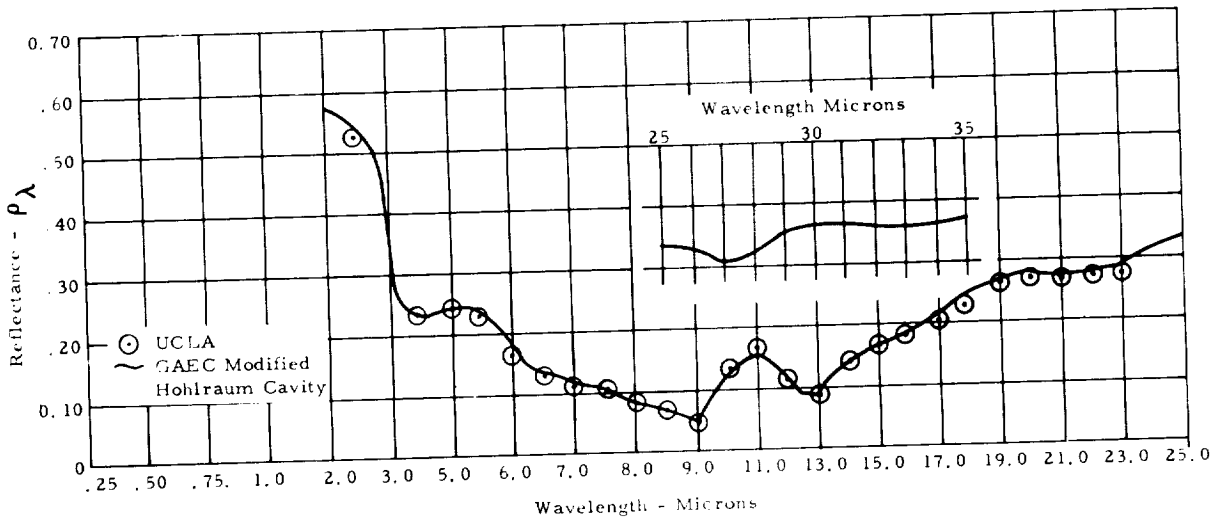

FIGURE 17-14.—Spectral reflectance of white porcelain enamel P-110. Integrated emittance: UCLA--$\epsilon_{1000°F}=0.819$, and $\epsilon_{-1000°F}=0.767$; and GAEC - $\epsilon_{1000°F}=0.828$, and $\epsilon_{-1000°F}=0.769$.

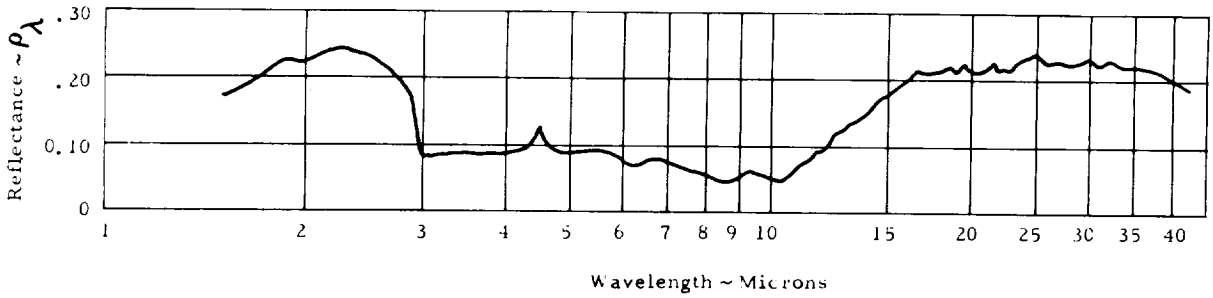

FIGURE 17–15.—Spectral reflectance of hard-coat sulfuric acid anodized aluminum. Integrated emittance: $\epsilon_{-500\,F}=0.830$, $\epsilon_{0^\circ F}=0.842$, $\epsilon_{100^\circ F}=0.863$, and $\epsilon_{200^\circ F}=0.879$.

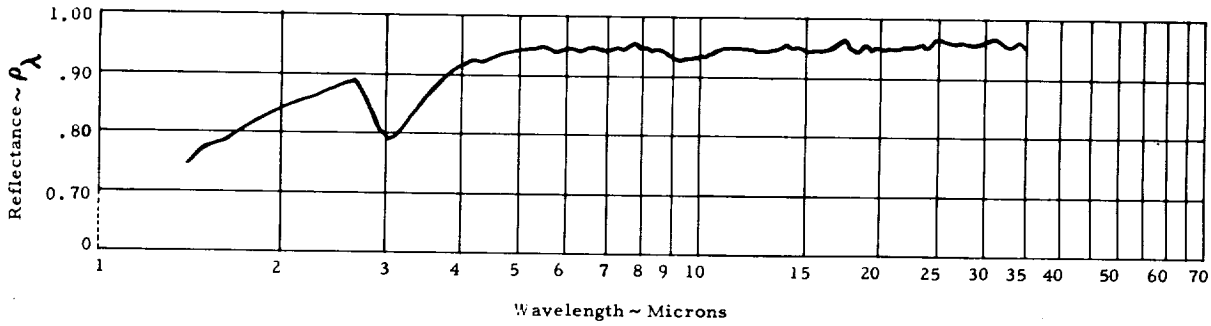

FIGURE 17–16.—Spectral reflectance of Alodined 7075 T6 aluminum Alclad removed by compounding. Integrated emittance: $\epsilon_{-500\,F}=0.051$, $\epsilon_{0^\circ F}=0.052$, $\epsilon_{100^\circ F}=0.054$, and $\epsilon_{200^\circ F}=0.056$.

18—MEASUREMENT OF SPECTRAL REFLECTANCE USING AN INTEGRATING HEMISPHERE

BY J. E. JANSSEN AND R. H. TORBORG

HONEYWELL RESEARCH CENTER, HOPKINS, MINNESOTA

An integrating hemisphere reflectometer is described for measuring the spectral, diffuse reflectance of materials over the range 0.25 to 30 microns in a high vacuum or atmosphere. Specimen temperature can be varied over the range from room temperature to 1350° F or higher. The calibration procedure is presented and the error caused by spherical aberration produced by the hemishpere is discussed. Reflectance measurements on identical specimens are compared with similar measurements made in two other laboratories by different techniques and found to be in good agreement.

The earliest use of a highly specular reflecting hemisphere to collect the scattered energy reflected by a diffuse surface and concentrate the energy on a sensor is attributed to Paschen in 1899 (ref. 1). Coblentz described a similar device in 1913 (ref. 2). More recently Birkebak and Hartnett (ref. 3), and Kozyrev and Vershinin (ref. 4) have published data taken with a highly polished hemispherical reflectometer.

In these devices, a concave, highly polished, glass hemisphere with a highly reflective evaporated metal coating was used to approximate an ellipsoidal mirror. A specimen was located a short distance to one side of the center of the hemisphere and a thermopile was located at a conjugate position. Radiant energy from a suitable source was projected through an aperture in the hemisphere and onto the specimen. The reflected energy was collected by the hemisphere and focused on the thermopile as shown in figure 18–1.

A reference measurement was made by projecting the same energy directly onto the thermopile. The reflectance of the specimen was then equal to the ratio of the two measurements divided by the reflectance of the hemisphere. In order to adapt this technique to spectral measurements and heated specimens, it was necessary to introduce a diffuser at one of the conjugate foci and use an external optical system to focus the energy into a spectrometer (ref. 5) as shown in figure 18–1.

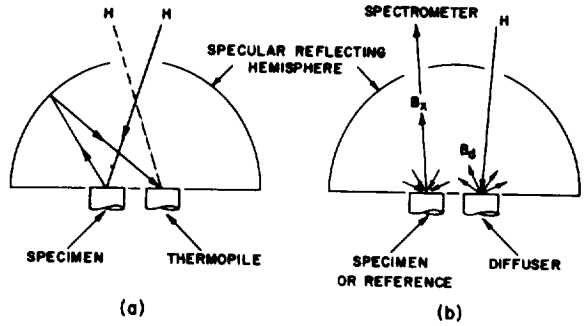

FIGURE 18–1.—Integrating hemisphere reflectometers.

The wide spectral range of interest and the low energy levels required the use of a photomultiplier sensor for the visible region and a vacuum thermocouple for the infrared.

MODIFIED INTEGRATING HEMISPHERE

Figure 18–1(b) shows a schematic of the modified integrating hemisphere. A diffuse reflector (diffuser) was located on a diameter of the hemisphere a short distance to one side of the center, and the specimen was located at a conjugate position. The hemisphere was large enough compared to the distance between the diffuser and specimen so that it approximated an ellipsoid.

The energy from a tungsten lamp, mercury vapor lamp, or globar was projected through an aperture and focused on the diffuser. The energy reflected from the diffuser was recollected by the hemisphere and focused onto the specimen. The diffuser reflected with a good

approximation to Lambert's cosine law, thus irradiating the specimen with a hemispherical distribution of incident energy. Some of the energy was reflected out the exit aperture and some was reflected back to the diffuse reflector. An infinite number of internal reflections between the diffuser and specimen occurred with some energy being reflected out the exit aperture to the spectrometer with each internal reflection.

Derivation of the equation for the reflectance of a specimen can be carried out in two different ways. A ray of energy can be followed through its many internal reflections and it will be found to yield a geometric series for which the sum can be written. Eckert (ref. 6) has pointed out a simple procedure which was originally used by Poljak (ref. 7).

Let B_d be the apparent brightness of the diffuser. (See figure 18–1.) This is made up of the initial reflection of the incident beam of intensity H plus all of the interreflections with the sample or reference. The apparent brightness does not include any energy emitted by the diffuser or sample, however, since this can be eliminated by zeroing the spectrometer with the silts open but the incident beam blanked off. Similarly the brightness of the specimen is given by B_x. Then

$$B_x=\rho_h\rho_x(1-2F)B_d \tag{1}$$

where:

ρ_h reflectance of hemisphere
ρ_x reflectance of specimen
F fraction of energy lost out each aperture

The brightness of the diffuser, B_d, is given by:

$$B_d=\rho_d H+\rho_d\rho_h(1-2F)B_x \tag{2}$$

where ρ_d is the reflectance of the diffuser

Solving for B_x from (1) and (2),

$$B_x=\frac{\rho_x\rho_d\rho_h(1-2F)H}{1-\rho_x\rho_d\rho_h^2(1-2F)^2} \tag{3}$$

If the specimen is replaced with a reference surface, a similar equation can be written,

$$B_r=\frac{\rho_r\rho_d\rho_h(1-2F)H}{1-\rho_r\rho_d\rho_h^2(1-2F)^2} \tag{4}$$

Equations (3) and (4) can then be solved for the ratio of the reflectance of the specimen to that of the reference.

$$\frac{\rho_x}{\rho_r}=\frac{B_x/B_r}{1-Z(1-B_x/B_r)} \tag{5}$$

where:

$$Z=\rho_r\rho_d\rho_h^2(1-2F)^2$$

In deriving equation (5) it was assumed that the diffuser gave a cosine distribution of reflected energy and that the specimen and reference were both either diffuse or specular. If the reference is specular and the specimen is diffuse, equation (1) is valid for the energy which interacts with the diffuser but is not valid for the energy reflected from the reference out the aperture to the spectrometer.

The reason for this is that the energy reflected by a specular surface to the sensor comes from a particular, small area on the hemisphere and the energy lost out the aperture after being reflected by the specular surface does not affect the energy incident on this spot. Consequently if a diffuse specimen is compared with a specular reference the measured brightness ratio must be divided by the loss factor $(1-2F)$ before using equation (5). If a specular sample is compared with a diffuse reference the brightness ratio must be multiplied by the loss factor $(1-2F)$ before using equation (5).

Figure 18–2 is a general plot of equation (5). It is seen that the best measurement accuracy can be achieved if a reference can be chosen with a reflectance approaching that of the sample and the factor Z has a high value.

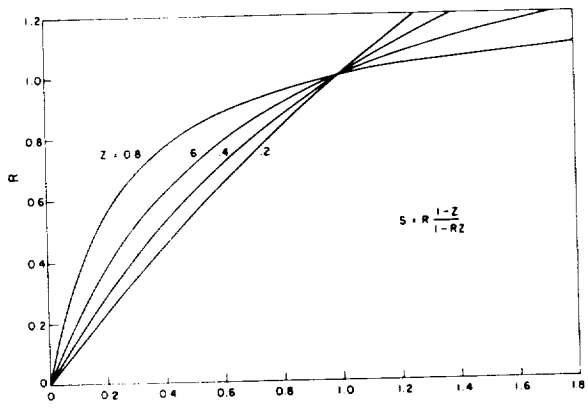

FIGURE 18–2.—Diffuser calibration equation.

APPARATUS

A war surplus bombsight bubble was used as the hemisphere. It was actually slightly more than a hemisphere and had a steel mounting flange attached. The hemisphere was glass, precision ground and polished to approximately 9⅝ in. inside diameter. Two 1-in. diameter holes were drilled in the hemisphere for the entrance and exit apertures and the inside was aluminized by vacuum depositing an opaque coating of high-purity aluminum.

A diffuser of reasonably high reflectance that reflected with a cosine distribution and whose properties were stable in a vacuum at room temperature was required. Aluminum, stainless steel, and brass were investigated. In an effort to assure better scattering of the energy incident on the diffuser, concentric corrugations 0.008 in. deep by 0.040 in. from crest to crest were machined in the surface as shown in figure 18–3. The diffusers were then blasted with coarse silicon carbide and chemically cleaned. Measurements of the spatial distribution of reflected energy showed that aluminum exhibited both the highest reflectance and the best distribution and was therefore selected as the diffuser material.

Energy from a Globar located about 4 in. from the diffuser was projected onto the diffuser at an angle of about 36° from the normal. The reflected energy was measured as a function of angle in a plane perpendicular to the diffuser surface (Plane A, figure 18–3). A Perkin-Elmer model 112 spectrometer was used to make the measurements. The data for 1μ and 8μ are shown in figure 18–3.

With the Globar remaining fixed, the diffuser was then tilted until the spectrometer recorder gave a maximum signal. This occurred with the Globar energy incident at about 26° from the normal and the energy reflected to the spectrometer at 10° from the normal as shown in Plane B, figure 18–3. It was expected that by making measurements of reflected energy at an angle more nearly equal to the angle of incidence, any diffuser specularity would tend to show up.

The data at 1 μ both for the aluminum diffuser and the magnesium carbonate ($MgCO_3$) diffuser are in good agreement with the cosine distribution. At the shorter wavelengths $MgCO_3$ is known to be a good diffuser, and our measurements on $MgCO_3$ were made to check the validity of the experimental setup. At 8 μ, the aluminum diffuser data deviates somewhat from a cosine distribution. The data for 26° incident energy measured in Plane B deviated considerably more. This indicates that the aluminum diffuser is somewhat specular at long wavelengths. It was, therefore, necessary to calibrate the equipment with specimens of known reflectance. This procedure is discussed in the section on calibration.

A turret with eight positions was provided for mounting specimens, diffusers and reference surfaces at the proper location with respect to the center of the hemisphere. The diffuser and specimen were 1⅛-in. diameter and were located at conjugate positions on each side of the center of the hemisphere with a center to center distance of 1¼ in. Ceramic specimen holders with tungsten heating elements were provided at two positions and a chromel-alumel thermocouple welded to a small flat nickel strip was held to each specimen surface with a spring-loaded clip made of tungsten wire. Specimen temperatures were recorded with a Brown recorder. Figure 18–4 shows the hemisphere and turret with the various diffusers, specimen heaters, and a specimen. The heaters were powered by storage batteries and a rheostat was used for control purposes. Water cooling was provided to keep the diffusers at approximately room temperature.

An external nut on the turret tube and means for positive indexing were provided to adjust the location of the specimen and diffuser surfaces with respect to the center of the hemisphere and thus maintain precise optical alignment. The height of the individual surfaces on the turret could be independently adjusted to bring any two or more to the same height and thus make allowance for variation of specimen thickness.

The hemisphere was mounted on the rear end plate of the vacuum chamber and the turret was mounted on a second plate bolted to the rear end plate as shown in figure 18–5. This arrangement made it possible to remove the turret to change specimens without disturbing the hemisphere. A rotary seal consisting of two O-rings lubricated with diffusion pump oil was

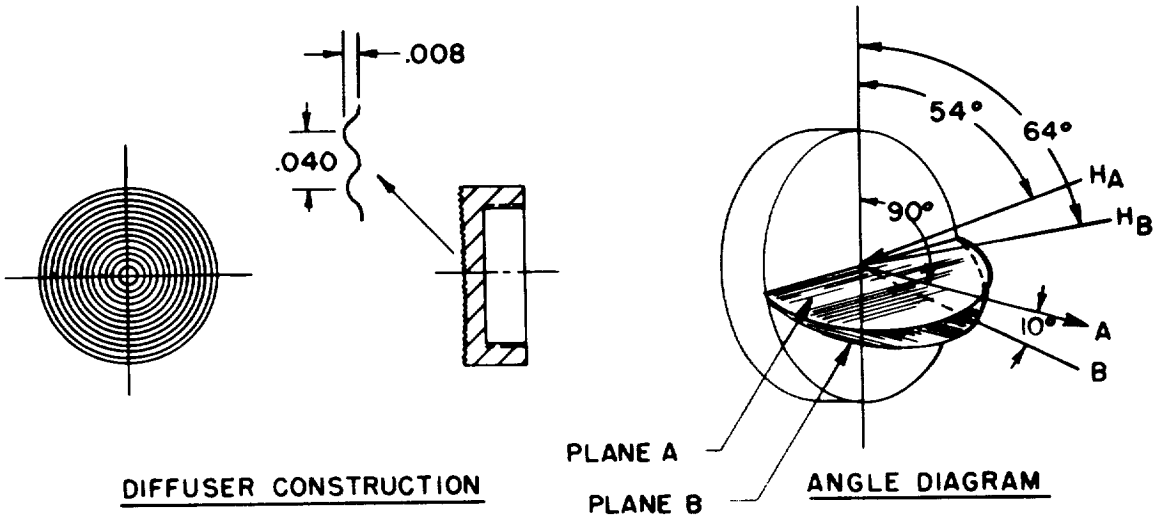

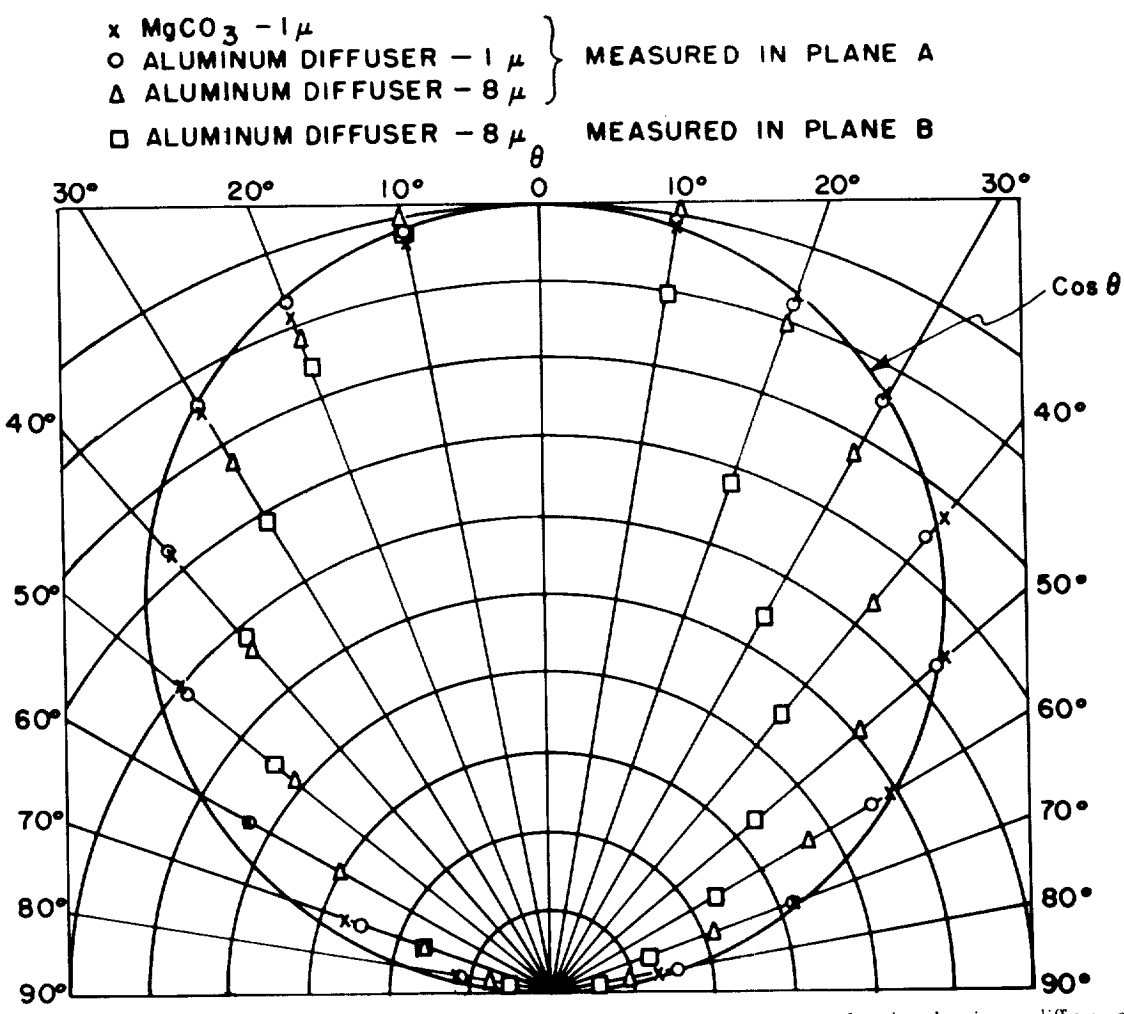

FIGURE 18-3.—Sketch of aluminum diffuser and goniometric reflectance data for the aluminum diffuser and magnesium carbonate.

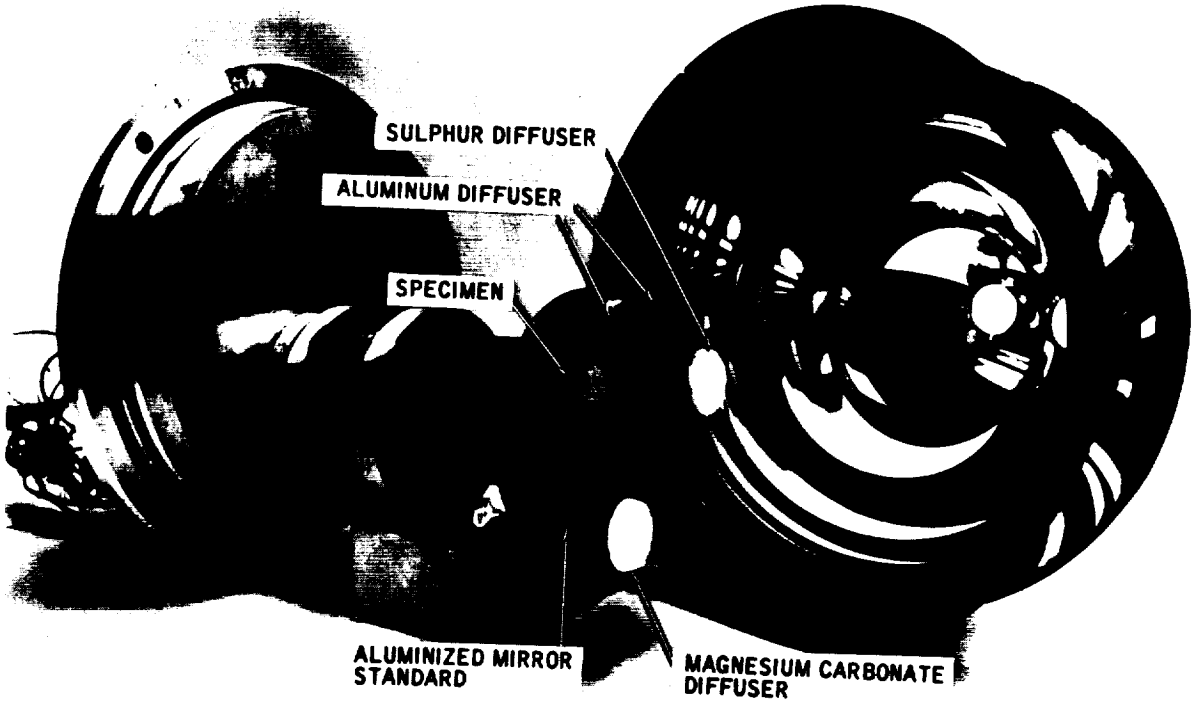

FIGURE 18–4.—Hemisphere and turret.

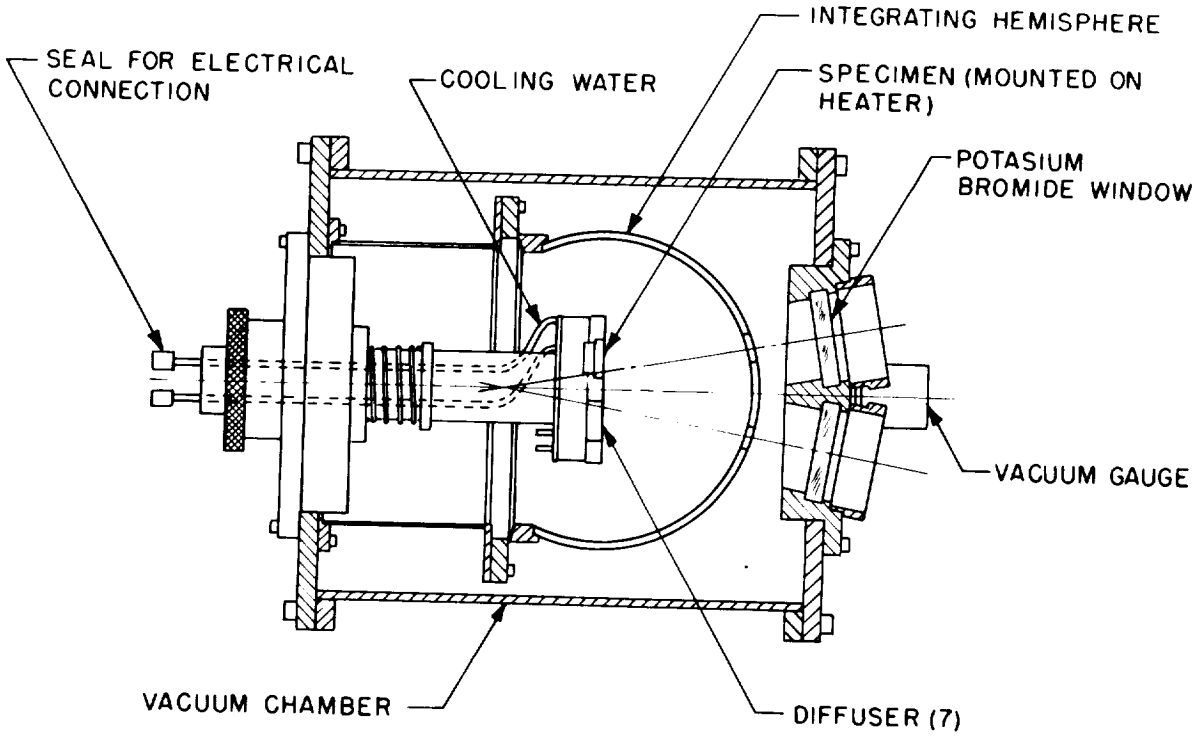

FIGURE 18–5.—Vacuum chamber and hemisphere.

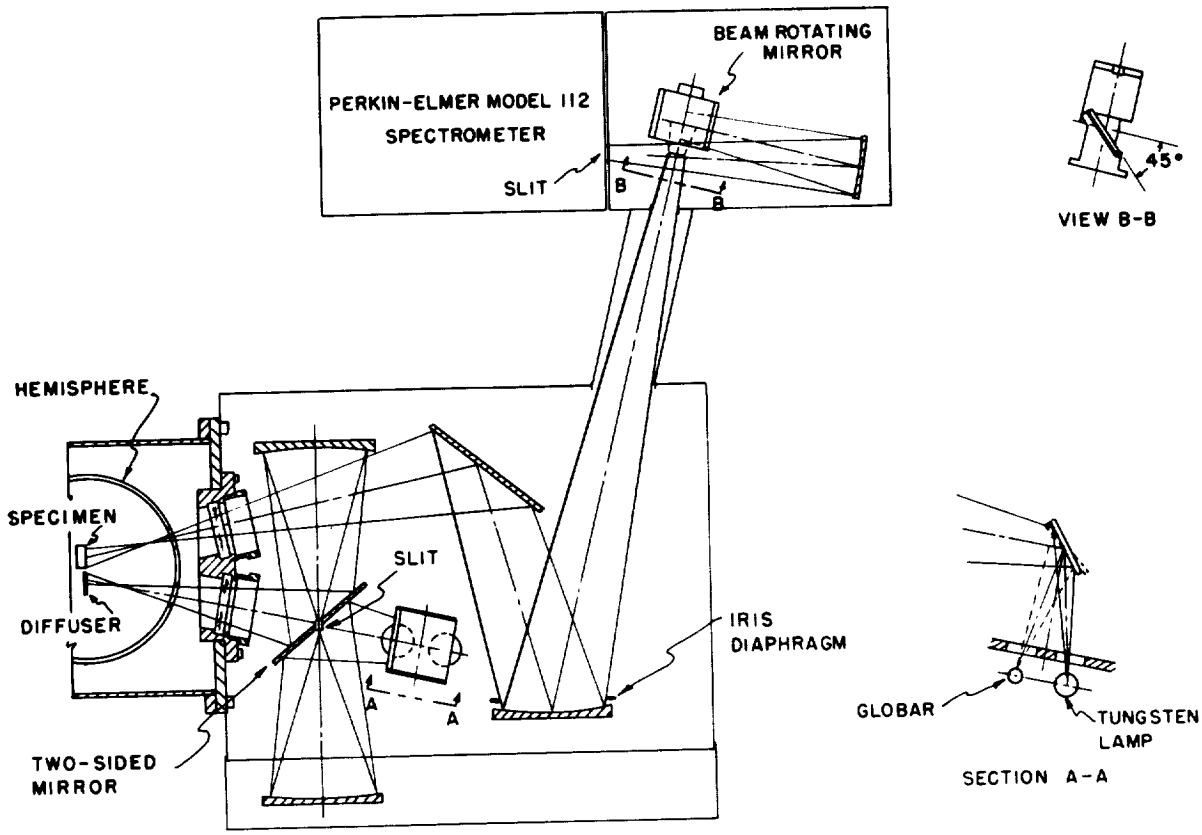

FIGURE 18–6.—Reflectometer optical system.

provided for turret rotation. Two 3-in.-diameter potassium bromide windows were provided in the front end plate, and a heater was provided to keep these windows at a temperature of about 100° F to prevent fogging. The vacuum gage was also mounted in the front end plate. Neoprene O-ring gaskets were used at all joints.

The vacuum chamber, valve, pump, optical system, and associated equipment were mounted on a steel framework which was in turn bolted to the console of the spectrometer. The whole assembly was raised off the floor on screw jacks to achieve and maintain the desired optical alignment.

The optical system is shown in figure 18–6. Since a Globar did not provide enough energy at the short wavelengths, it was necessary to use a tungsten ribbon filament lamp for the visible region. The tungsten lamp was replaced with a mercury vapor lamp for measurements in the UV region. A two-position mirror was incorporated for switching from one source to the other (Section A–A, fig. 18–6). The slit on the entrance system was mounted in a ⅝-in.-diameter brass tube which was cemented in a hole in the middle of the double-sided 45° mirror. This mirror was aluminized on both sides. Two 6-in.-diameter f/1 spherical mirrors were required to produce an image of the source slit on the diffuser. The image was about ⅛ in. wide by ⅝ in. long, and in line with a horizontal line connecting the center of the diffuser and specimen.

Energy reflected from the specimen out the exit aperture was deflected by a plane mirror to a 6-in. f/2.5 spherical mirror; it passed through a beam rotating mirror arrangement (Section B–B, fig. 18–6) and finally was focused by the spectrometer source parabola into the entrance slits of the Perkin-Elmer model 112 spectrometer. Since the images on the diffuser and specimen were horizontal and the spectrometer slits were vertical, it was necessary to incorporate a beam rotating mirror in the optical system. Horizontal in-line images were used

to reduce the effect of spherical abberation. The entire optical system was enclosed in a light-tight housing which was kept dry with a pan of silica gel.

Quartz, sodium chloride, potassium bromide, and cesium iodide prisms were used to cover the spectral range from 0.25 to 30 μ. A 1P21 photomultiplier was used up to about 0.8 μ and a Reeder vacuum thermocouple for the remainder of the spectrum.

CALIBRATION

The integrating hemisphere yields a ratio of the reflectance of a specimen to that of a reference. A material with known reflectance properties is therefore required for the reference. Since the technique makes it possible to compare a diffuse surface with a specular surface, an evaporated film of aluminum on glass was chosen as the primary reference. The normal spectral reflectance of an evaporated film of aluminum on glass was measured by Strong's technique (ref. 8). Three specimens of the aluminized glass were arranged as shown in figure 18–7.

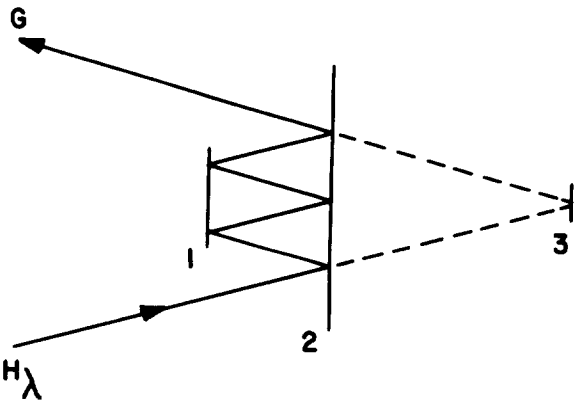

FIGURE 18–7.—Hemisphere reflectance determination.

Surface 2 was located one-third of the distance from surface 1 to 3, and all surfaces were parallel. Surface 2 could be removed, however, so that a beam of energy could be focused on surface 3 at an angle of 10° from the normal. The energy reflected to the spectrometer was then,

$$G_1 = H_\lambda \rho_r \tag{6}$$

When surface 2 was replaced, five reflections occurred between surfaces 1 and 2. The energy reflected to the spectrometer was then:

$$G_5 = H_\lambda \rho_r^5 \tag{7}$$

and the fourth root of the ratio yielded the reflectance of the aluminized glass.

$$\rho_r = \left(\frac{G_5}{G_1}\right)^{\frac{1}{4}} \tag{8}$$

This method gave high sensitivity and tended to reduce measurement errors. It required precise alignment of the mirrored surfaces, however. Alignment was achieved by mounting the three specimens on a common bar. Precise alignment of the aluminized glass specimens was achieved by projecting a beam of light to the specimens from a distance of about 20 ft and at an angle of about 10° to the normal. The reflected beam was focused on a screen also about 20 ft away. The aluminized glass specimens were then aligned so that the images from the 1 and 5 reflection cases were coincident on the screen. The reflectance data are presented in figure 18–8 and are seen to be in good agreement with the data of Hass (ref. 9) and, in the infrared, with the theoretical reflectance calculated from the Hagen-Rubens equations which states that for a pure metal in the infrared region,

$$\rho = 1 - 36.05\sqrt{r/\lambda} \tag{9}$$

where:

r resistivity, 2.828×10^{-6} ohm-cm for commercially pure aluminum at 20° C

λ wavelength, μ

Some trouble was encountered when commercially polished glass was used as a substrate for the aluminum film. It produced a substantially lower reflectance in the visible and UV region due to the roughness of the glass. Polishing the plate glass to optical standards eliminated this scattering loss and brought the data into substantial agreement with that of Hass.

The aluminum film on these specimens was produced at the same time and under the same conditions as the film on the integrating hemisphere and the reference surfaces. The reflectance values were, therefore, used for both

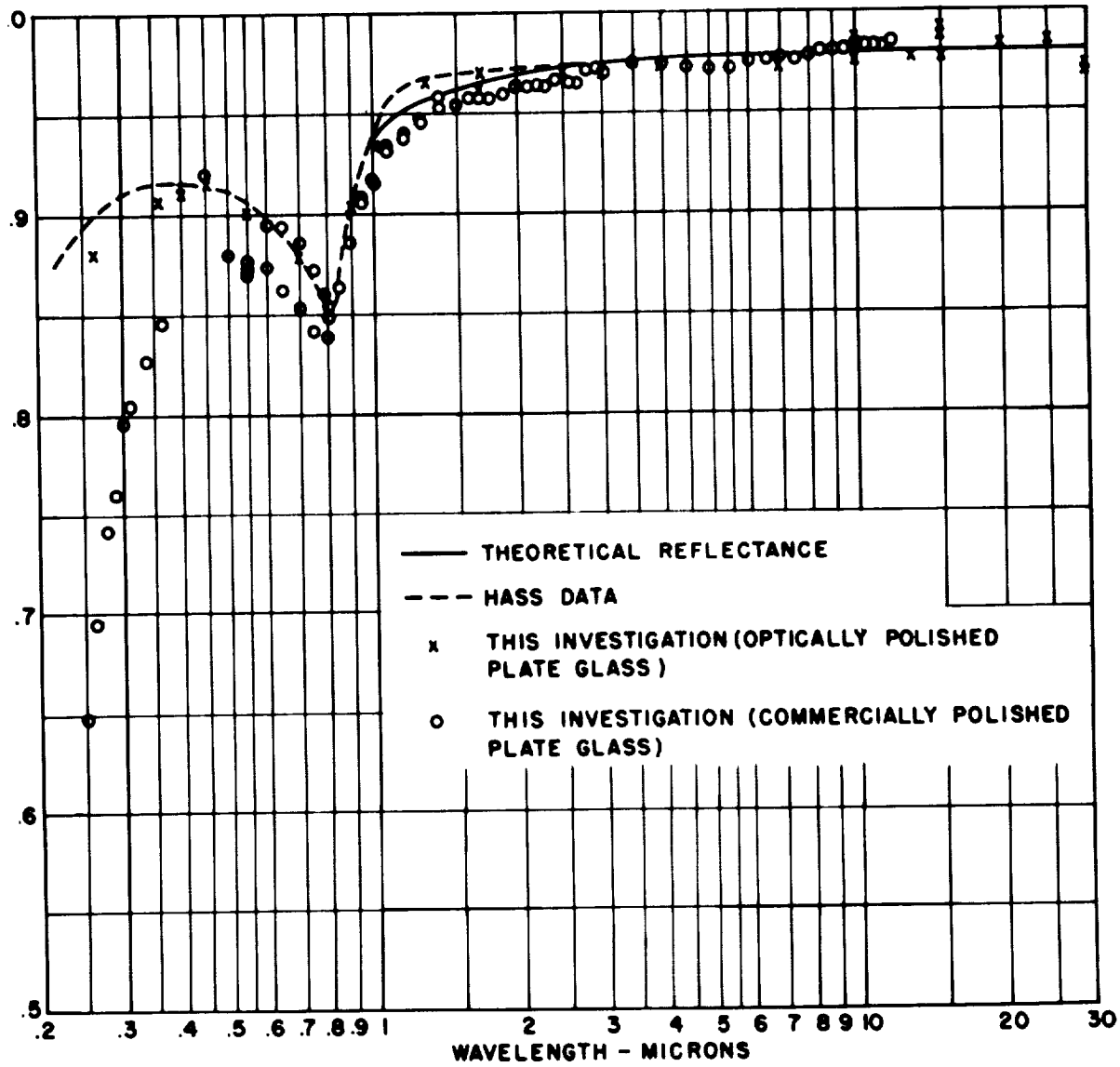

FIGURE 18-8.—Spectral reflectance of evaporated aluminum on glass.

the reference surface and the reflectance of the hemisphere.

The instrument factor, Z, was determined in two ways. Because of diffuser specularity at the longer wavelengths, the most reliable method was found to be a direct measurement of the factor with the aid of a second known reference or standard. This second reference was prepared by mounting a layer of 2mm glass rods across a 1¼-in. diameter glass ring. The rods were then ground and polished until a flat polished surface passing through the longitudinal centerline of the rods was achieved. Every other rod was then removed and an evaporated aluminum film was deposited on the remaining grid. A disk painted with Parson's optical black lacquer was mounted behind the grid. The completed standard then consisted of alternate areas of black spaces which were nonreflective and aluminum film on glass which was highly reflective. The reflective surface covered 50% of the total area and when compared with a fully aluminized reference, the reflectance ratio was 50% at all wavelengths. Equation (5) could then be solved for Z.

The Z factor was also computed from the reflectances of the hemisphere, diffuser and reference and the loss factor. The aluminized glass reference and hemisphere had the same reflectance which was determined as described above. The diffuser reflectance was measured by using two identical diffusers—one as the primary diffuser and one as the specimen. One variable was then eliminated making it possible to write equation (5) in the form:

$$\frac{\rho_d}{\rho_r} = \frac{1+\sqrt{4V(1/D)B_{dd}/B_{dr}(1-1/DB_{dd}/B_{dr})+1}}{2V(1-1/DB_{dd}/B_{dr})} \tag{10}$$

where:
$V=\rho_h{}^4D^2$
$D=1-2F$

The loss factor D=1−2F could be computed from the geometry of the apertures, diffuser, and specimen or reference. If the diffuser established a truly hemispherical distribution of energy reflected from it, the term F was the solid angle which the apertures subtended with respect to the diffuser or specimen. The equation for the solid angle factor between two parallel disks is (ref. 10):

$$F=1/2(x-\sqrt{x^2-4(r_a/r_d)^2}) \tag{11}$$

$$x=1+(s/r_d)^2+(r_a/r_d)^2 \tag{12}$$

where:

r_a=radius of aperture, 0.5 in.
r_d=radius of diffuser, 0.5625 in.
s=distance between diffuser and aperture, 4.678 in.

Therefore,

$$F=0.0111$$

and

$$D=0.978$$

ERRORS

There were several sources of uncertainty in the measurements which made it difficult to calculate the overall error. A major source of uncertainty was introduced by the spherical aberration produced by the hemisphere. This caused energy reflected from a point on the diffuser to be spread out along a line on the specimen as shown in figure 18-9. This line passed through the point of origin and the center of the hemisphere. Subsequent reflections produced increased scattering until some of the energy missed the diffuser or specimen and was lost.

In order to conserve the energy, the magnification of the source optics was chosen such that the energy projected on the diffuser was confined to a band about ⅛ in. wide and ⅝ in. long as shown in figure 18–9. The magnification of the pick-up optics was then chosen such that the spectrometer with wide open slits received the energy from the entire illuminated band on the specimen. Although an energy gradient existed over the length of this band, it was effectively integrated by the sensor in the spectrometer. Analysis showed that the energy loss was negligible with this arrangement.

Scattered radiation produced by the windows in the vacuum chamber also was an unknown source of error. It was possible for energy scattered by surface reflections from the entrance window to fall directly on the specimen without first being reflected by the diffuser. This was particularly troublesome in the case of a specular specimen or the aluminized glass standard. In these cases an appreciable amount of energy could be reflected specularly to the spectrometer without first being diffused by the diffuser. To prevent this, it was necessary to tilt the specimen or standard slightly so that the direct reflection of the entrance window did not enter the spectrometer.

The diffusers produced a third area of uncertainty. The equations assumed a Lambertian distribution of reflected energy. The diffusers were somewhat specular beyond about 2μ, however, and the calculated values for the factor Z gave reflectance values that appeared too high. The Z values measured by the technique described in the section on calibration effectively solved this problem.

Focusing of the diffuser and specimen was critical. The hemisphere had a very shallow depth of field, and it was necessary to locate the surface of the specimen and diffuser within a few thousandths of an inch of a plane passing through the center of the hemisphere. It was found that the turret could be adjusted with the focusing nut to give a maximum signal and the position of the nut could be marked. Locating the proper position for both the specimen measurement and the reference measurement

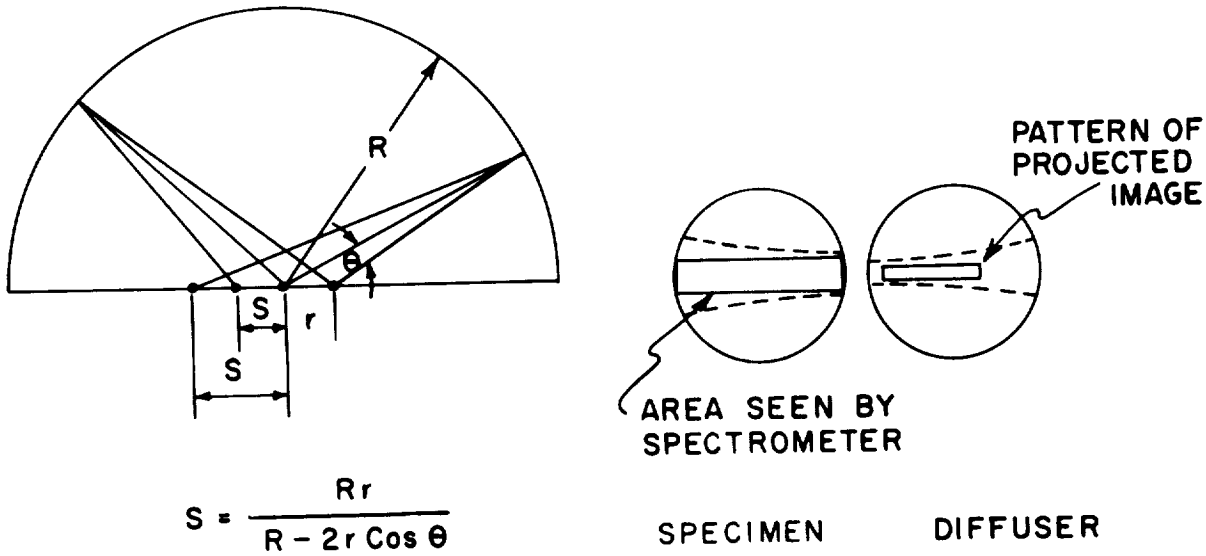

$$S = \frac{Rr}{R - 2r\cos\theta}$$

FIGURE 18-9.—Spherical aberration.

in this way gave 99% or greater reproducibility in most cases. Good reflectors were more critical in this respect than poor reflectors.

The amplifier and sensor noise also were sufficient to limit measurement accuracy at low energy levels where a high amplifier gain was required. This was especially troublesome at the ends of the spectrum when the specimen-to-reference reflectance ratio was small. When the specimen reflectance was only 10% of the reference reflectance (diffuser or aluminized glass standard) the instrument recording error could be 10% of this ratio. Zero drift in the instrument was also annoying at high gains, necessitating repetitive readings to obtain a reproducible zero.

Measurements at 0.8μ were awkward. The spectral response of the photomultiplier dropped off sharply in this region and gave readings of questionable accuracy. On the other hand this represented the lower limit for the thermocouple and required maximum amplifier gain along with maximum noise. Disagreement between the two sensors ranged from zero to more than 25% in a few cases. Although both sensors were used at 0.8μ, the thermocouple data were considered more reliable. In order to get an indication of the overall accuracy, the measurements on several materials were compared with those of other investigators.

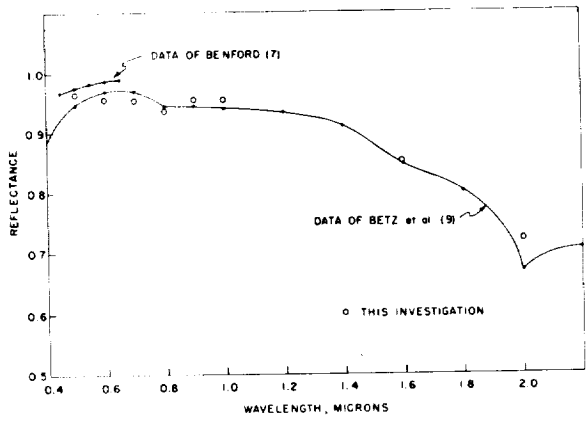

FIGURE 18-10.—Reflectance of magnesium carbonate.

COMPARATIVE DATA

Figure 18-10 shows a comparison of our measurements on freshly scraped magnesium carbonate, with those of Benford (11) and Betz (12). These data agree within 1.5% except for the measurement at 2.0μ. Disagreement here may have been due to the wide spectrometer slits we were forced to use to compensate for spherical aberrations, and the presence of a narrow absorption band at 2.0μ. Our spectral resolution probably was not as good as in the case of Betz's measurements.

Arrangements were also made to have two other laboratories measure the normal spectral reflectance of identical specimens punched from

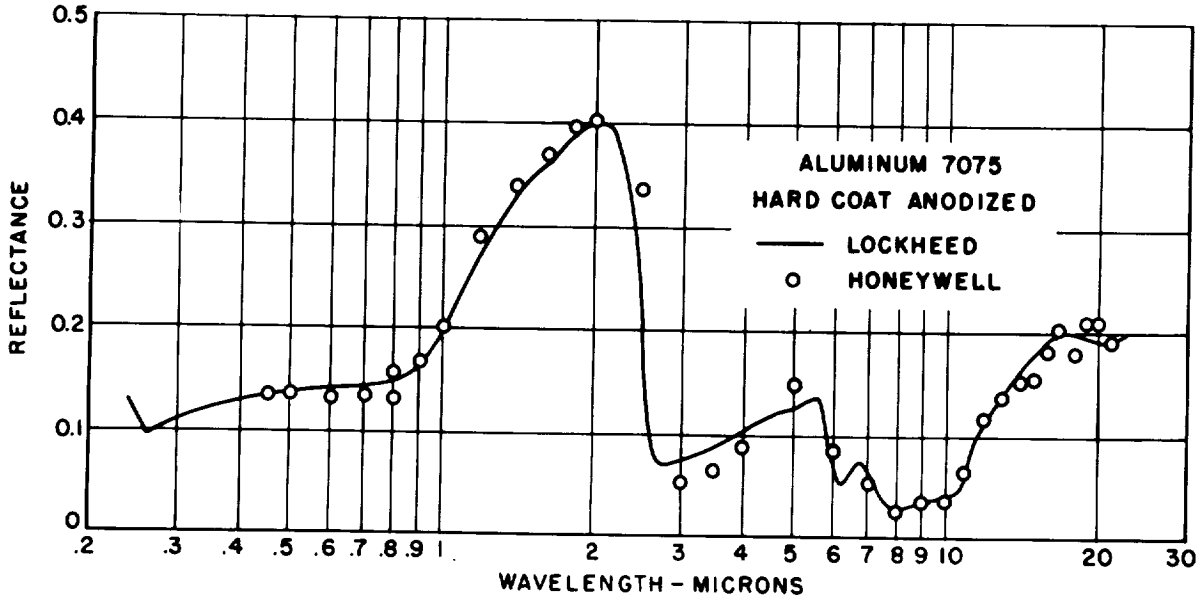

FIGURE 18-11.—Reflectance of hard coat anodized aluminum.

the same coupon of anodized aluminum. The Solar Radiation Laboratory of the University of California measured the reflectance of chromic acid anodized 1075 aluminum and sulphuric acid anodized 7075 aluminum over the spectral range of 0.35 to 3μ. The Thermodynamics Laboratory of Lockheed Missiles and Space Company also measured these specimens over this spectral range as well as a specimen of 7075 anodized by the hard-coat process (low-temperature sulfuric acid). Both of these laboratories used the Cary integrating sphere for measurements in this range. In addition, Lockheed measured the three specimens in the infrared region from 2 to 21μ with a Gier-Dunkle hohlraum reflectometer. These data are compared with data obtained on identical samples with the integrating hemisphere reflectometer in figures 18-11, -12, and -13. The agreement was generally acceptable.

Because of the wide spectrometer slits used with the integrating hemisphere to reduce spherical aberration problems, our measurements did not resolve the interference bands in the chromic acid anodized specimen. Our measurements did give an integrated average which was in agreement with the other data in this region, however.

The spectral range has recently been extended to 0.25μ at the short wavelength end of the spectrum by using a mercury vapor lamp source, and to 30μ at the long wavelength end by using a cesium iodide prism. This prism gives rather poor spectral resolution but it does provide data in the 23- to 30-μ region.

The specimen is mounted on a small heater and is supplied with a thermocouple. Measurements have been made with specimen temperatures ranging from room temperature to 1300° F. Since the spectral reflectance does not change greatly with temperature unless the surface undergoes a physical or chemical change, temperature control is not critical. Elevated specimen temperatures do increase the energy emitted by the specimen, however. It was found that at about 1350° F the emitted energy became so large in the IR region that the spectrometer could no longer be zeroed. Under these conditions it should be possible to use the heated specimens as the energy source and measure it against two different diffuse references. This possibility has not yet been investigated, however.

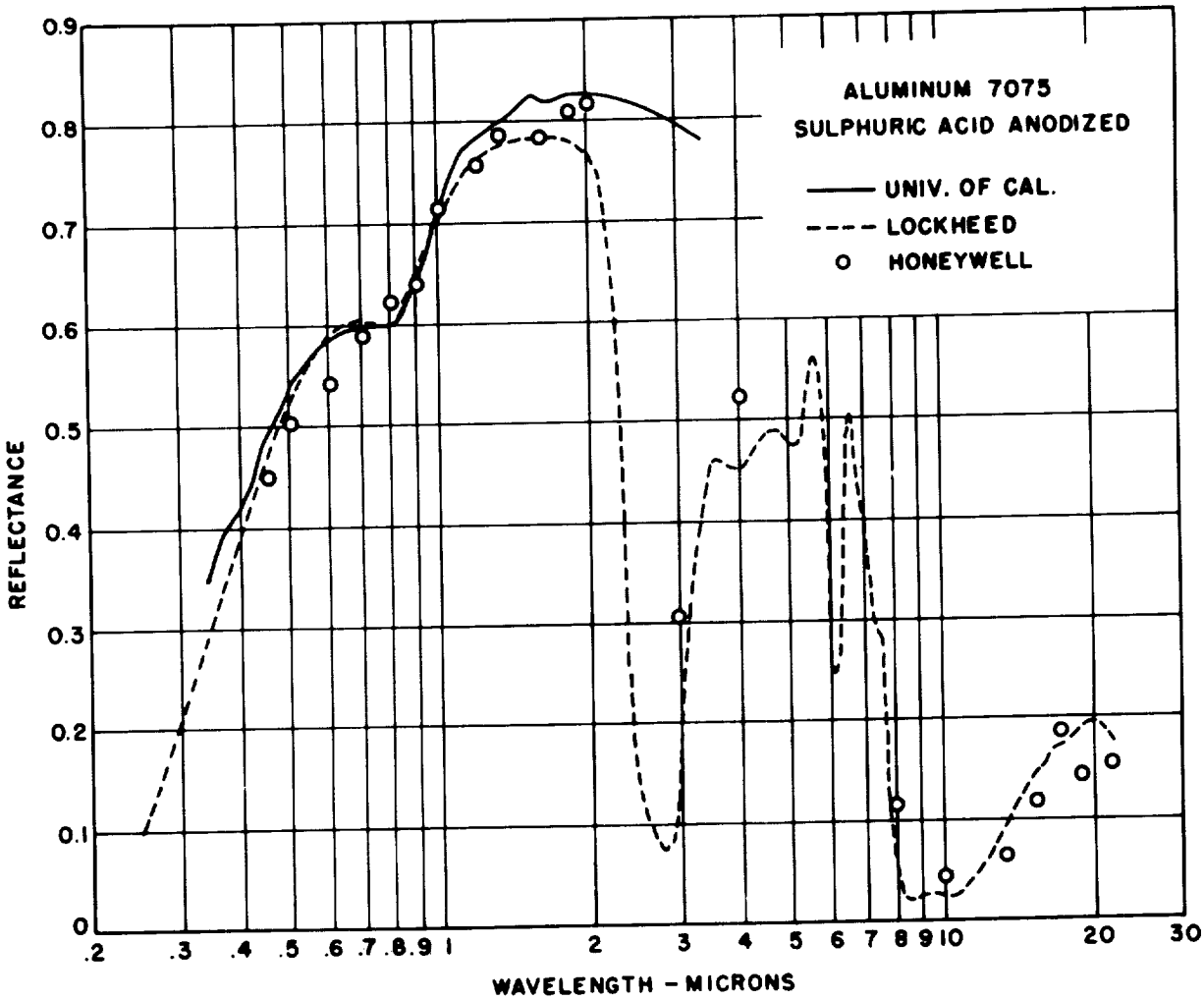

FIGURE 18-12.—Reflectance of sulfuric acid anodized aluminum.

REFERENCES

1. PASCHEN, VON F.: Uber die Vertheilung der Energie im Spectrum des schwarzen Korpers bei neideren Temperaturen. Gesammtsitzung vom 27 Apr. 1899, p. 405–420.
2. COBLENTZ, W. W.: The Diffuse Reflecting Power of Various Substrates. Nat. Bur. Standards Bull., vol. 9, 1913, p. 283.
3. BIRKEBAK, R. C.; and HARTNETT, J. P.: Measurements of the Total Absorptivity for Solar Radiation of Several Engineering Materials. Trans. ASME, vol. 80, no. 2 1958, p. 373.
4. KOZYREV, B. P.; and VERSHININ, O. E.: Determination of Spectral Coefficients of Diffuse Reflection of Infrared Radiation from Blackened Surfaces. Optics and Spectroscopy, vol. VI, no. 4, Apr. 1959, p. 345.
5. JANSSEN, J.; TORBORG, R.; LUCK, J.; and SCHMIDT, R.: Normal Spectral Reflectance of Anodized Coatings on Aluminum, Magnesium, Titanium, and Beryllium. ASD TR 61-147, Sept. 1961.
6. ECKERT, E. R. G.; and DRAKE, R. M., JR.: Heat and Mass Transfer. 2d Ed., McGraw-Hill Book Co., 1959, p. 405.

7. Poljak, G.: Tech Physics U.S.S.R. 1: 555, 1935.
8. Strong: Procedures in Experimental Physics, Prentice Hall Inc.
9. Hass, G.: Filmed Surfaces for Reflecting Optics. Jour. Opt. Soc. Am., vol. 45, no. 11, Nov. 1955, p. 945–952.
10. Hamilton, D. C.; and Morgan, W. R.: Radiant-Interchange Configuration Factors. NACA TN 2836, 1952, p. 32.
11. Anon.: Handbook of Chemistry and Physics. 38th Ed. Chemical Rubber Pub. Co.
12. Betz, Howard T.; Olson, O. Harry; Schuren, Bert D.; and Morris, James C.: Determination of Emissivity and Reflectivity Data on Aircraft Structural Materials. Part II: Technique for Measurement of Total Normal Emissivity, Normal Spectral Emissivity, Solar Absorptivity, and Presentation of Results. WADC TR 56–222. Oct. 1958.

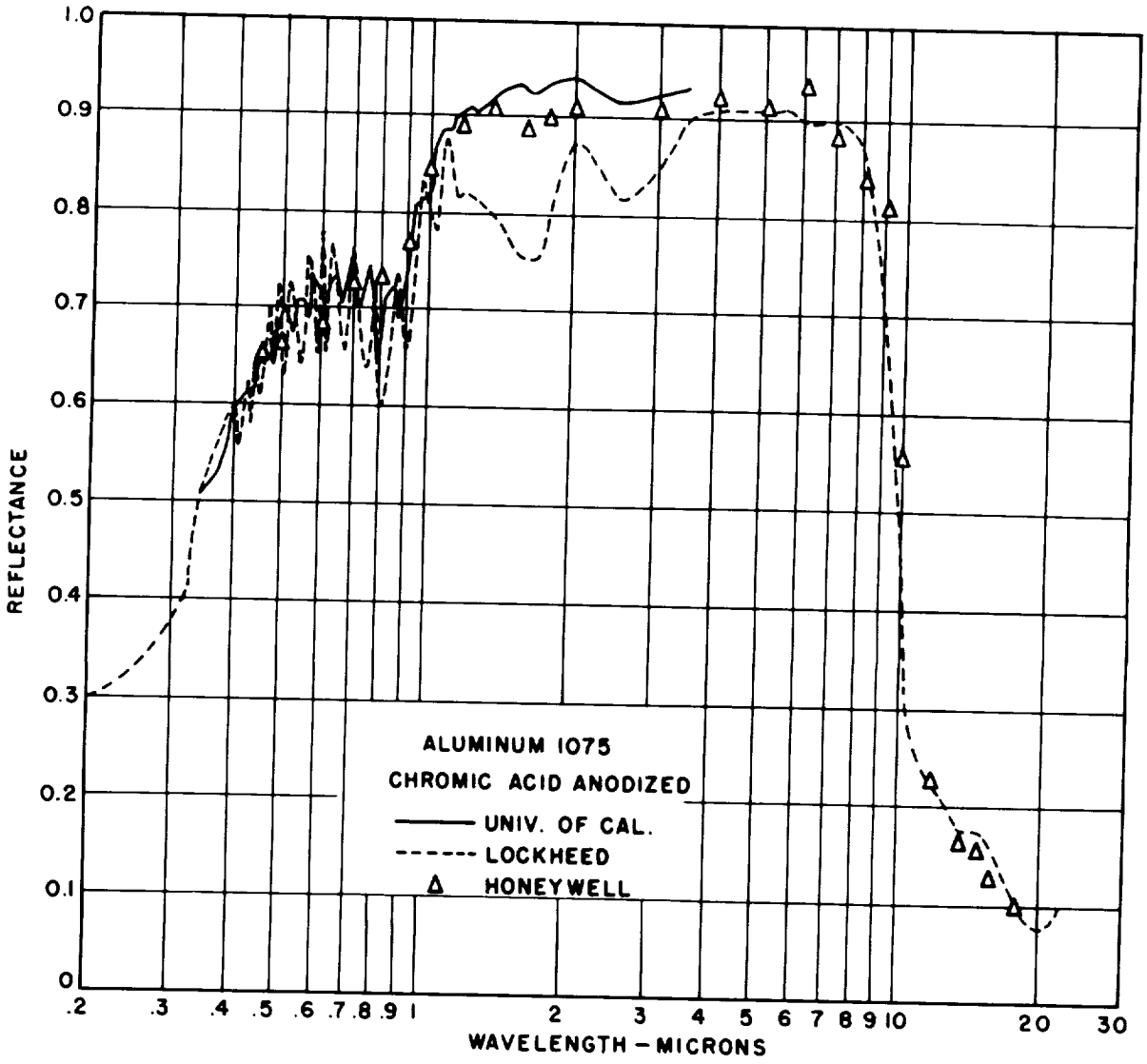

Figure 18–13.—Reflectance of chromic acid anodized aluminum.

DISCUSSION

R. E. GAUMER, LMSC: The paper is well written and describes a very versatile measurement apparatus. The use of a single-beam measuring system has advantages of simpler optical and electronic systems, but requires greater source and electronic stability than the double-beam system. It was not clear how the emitted energy for elevated temperature infrared measurements was compensated for at temperatures below 1300° F. This energy becomes appreciable at the long wavelengths for ambient and room temperature samples if source chopping is not used. The use of a lead sulfide detector for the spectral range from 0.6 to 2.0 μ would alleviate the difficulties ascribed to lack of energy and gain problems.

In normal use the integrating hemisphere gives the diffuse reflectance from a sample illuminated from a source at some angle θ. When used this way the multiple reflections from the hemisphere collect energy over the total solid angle and concentrate it on a suitable detector.

As modified by the authors, the hemisphere is no longer used in this role and is instead used simply to place energy from the total solid angle onto the sample and the reflected energy is detected at near normal angles. As such, it is performing much like a hohlraum, and its results are the same, with some advantages and some serious disadvantages when compared to a hohlraum system.

The disadvantages of the hohlraum are mainly those of sample heating and hohlraum temperature control. The former is generally amenable to correction, and the latter controllable with proper design. In any event absolute error can in general be held to ± 0.02 reflectance units out to 20 to 25μ.

The disadvantages of the hemisphere method as used here is the necessity of reference samples of known materials at all temperatures used. The use of reference materials is always questionable; however, their stability at the elevated temperature interjects still more uncertainty. When information on the absolute reflectance of a reference material which is stable, diffuse, and easily duplicated becomes available, it may be possible to use this method to advantage as a rapid sampling device. However, the absolute data obtained are no more certain than the standards used.

For hot samples the lack of chopped incident energy requires zeroing out sample emission with the amplifier. All other background signals must likewise be "zeroed" out. In general this is satisfactory in operations where the spurious signal is about 5% of the total signal. In this case the spurious signal might approach 90% of the total for a poor reflector. It is obvious that such conditions are intolerable.

19—HEMISPHERIC SPECTRAL REFLECTANCE OF SOLIDS

BY W. E. MARTIN

RCA ASTRO-ELECTRONICS DIVISION, PRINCETON, NEW JERSEY

A knowledge of the capacity of an opaque material to absorb various wavelengths of radiation is important for the space-vehicle designer as an aid to his estimation of design requirements. In general, the basic data needed in this area are not available. Because of the high temperatures involved, it is impractical to make emittance measurements at the shorter wavelengths. Therefore, absorptance is determined indirectly by measuring the spectral reflectance of a material under conditions of diffuse illumination.

Measurements of the spectral reflectance of non-transparent media from 350 to 2500 mμ have been made by irradiating a sample with a hemispherical diffuse source, and measuring the reflected flux at an angle of 45° to the normal.

The diffuse source consists of three coincident hemispheres. An outer hemisphere mounts 96 incandescent lamps pointed radially inward. A second hemisphere shades the base of each lamp and reflects diffusely the radiance of these lamps. The inner hemisphere is a light-diffuser 5 in. in diameter, made from translucent grit-blasted glass. The base plane of the coincident hemispheres is a disk coated with electrolytic aluminum having a reflectance of 0.7 to 0.9 through the spectral range of measurement. The base plane provides a virtual image of the innermost hemisphere. A sample is placed at a port located in the base plane at the origin of the coincident hemispheres, and therefore is irradiated as though it were surrounded by a sphere of uniform wall brightness. An area of the sample (viewed at 45°) is projected into the entrance slit of the monochromator, and the flux received is a measure of the sample reflectance.

The absolute reflectance is determined by the relative radiant intensities from the sample and from a standard reflector. Both a diffuse standard and a specular standard have been used. The diffuse standard is a block of magnesium carbonate ($MgCO_3$) whose surface properties can be repeatedly renewed by scraping. The specular standard is an evaporated aluminum coating on a glass substrate, protected with a magnesium fluoride overcoating. The absolute reflectance of the $MgCO_3$ standard was determined from the literature, and the reflectance of the specular standard was measured on a Cary model 14 spectrophotometer with an accuracy of ±0.5%.

Measurements have demonstrated the capability of the apparatus, and represent significant contributions to the design of particular space vehicles. The measurement program has not been comprehensive, but has been limited to surfaces considered applicable, and with an overall accuracy of about 5 to 10%. The most severe limitation of the equipment has been the necessity of viewing specialized interference-coated specular samples at an angle of 45°. Future plans include measurements at viewing angles near the normal for some materials, since many samples show significant variations in reflectance with angle of view. In addition, the standards of absolute reflectance utilized should be verified by calibrations with NBS standards of diffuse reflectance.

The energy incident on a space vehicle originates primarily from the sun, and secondly from the solar radiation diffusely reflected from the earth and its atmosphere.

Most of this incident energy lies in the short-wavelength region (0.2 to 3.5 μ). There is also long-wavelength incident energy from self-emitted earth radiation (through the atmospheric windows), and from low-temperature radiation from the atmosphere itself.

The surface radiative properties of satellite materials in the near-ultraviolet, the visible, and the infrared spectral regions are important in determining the thermal equilibrium of an

692-146 O—63——13

in-flight space vehicle. This equilibrium is governed primarily by the absorption of incident energy and the re-emmission of this energy at long wavelengths. Therefore, the equilibrium temperature is a function of the physical-optical characteristics of the surface materials used.

Freedom to select those surface properties meeting the exact needs for a particular design requires an investigation of the radiative properties of many materials. The investigation must determine: (1) the absorptance (α_λ) of these materials for the incident solar energy; and (2) the spectral emittance (ϵ_λ) of the materials at low temperatures. Instrumentation has been developed to determine these properties. This report describes the development of instrumentation for the measurment of diffuse spectral reflectance (ρ_λ) of a variety of materials.

REFLECTANCE UNDER CONDITIONS OF DIFFUSE ILLUMINATION AND 45° VIEWING

Instrumentation

The spectral absorptance α_λ for opaque materials is related to the spectral reflectance ρ_λ by the equation $\alpha_\lambda=1-\rho_\lambda$;[1] thus, a knowledge of ρ_λ gives α_λ indirectly. By weighting α_λ with the known solar spectrum (the primary source), the effective solar absorptivity is

$$\alpha=\frac{\int \alpha_\lambda w_\lambda d_\lambda}{\int w_\lambda d_\lambda}.$$

In earlier experiments, goniometry was employed to obtain α_λ. This was a tedious, inaccurate, time-consuming method, since the partial reflectance must be integrated over all angles at each $d\lambda$. To hasten this process, an integrating hemisphere (fig. 19–1) was fabricated.

The device shown in figure 19–1 is an aluminum hemisphere with 96 lamps distributed uniformly over its surface. The illuminated target (specimen surface) is positioned at the center of the hemispheric basal plane. Inserted between the outer hemisphere and the basal plane is an intermediate hemisphere with viewing port. The intermediate hemisphere

[1] The spectral absorptance so computed is that for a direction of incidence equal to the direction of viewing under which ρ_λ was measured.

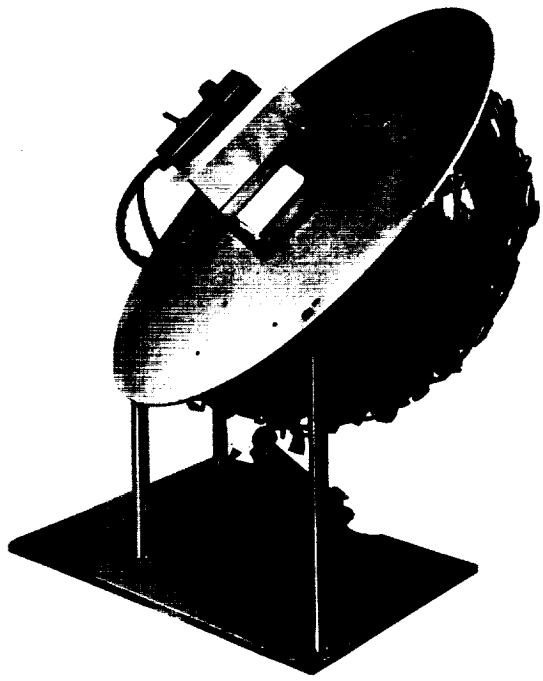

FIGURE 19–1.—Reflectance device.

was instrumented with a lighting-fixture diffusing globe made into an inner coincident hemisphere to yield a uniform wall luminosity. The reflected flux which passes through the monochromator entrance slit, via an arbitrarily placed aperture in the side of the hemisphere wall, is a measure of the total reflectance of the target.

Apparatus

Operation of the reflectance instrumentation is described with reference to figure 19–2. The monochromator entrance slit shown in the lower right-hand corner of the drawing is imaged in object space through the coincident viewing ports by the spherical mirror via the diagonal mirror and the 45° flat mirror, thus forming an entrance pupil at the sample port. The entrance pupil formed allows only radiation that is reflected from a specimen to enter the monochromator entrance slit. Thus, the boundaries of the area subtended by the entrance slit are well defined. If a specimen located at the sample port is characteristically specular, the focus depth of field is sufficiently great to image the slit on the innermost diffusing hemisphere through the reflectance of that

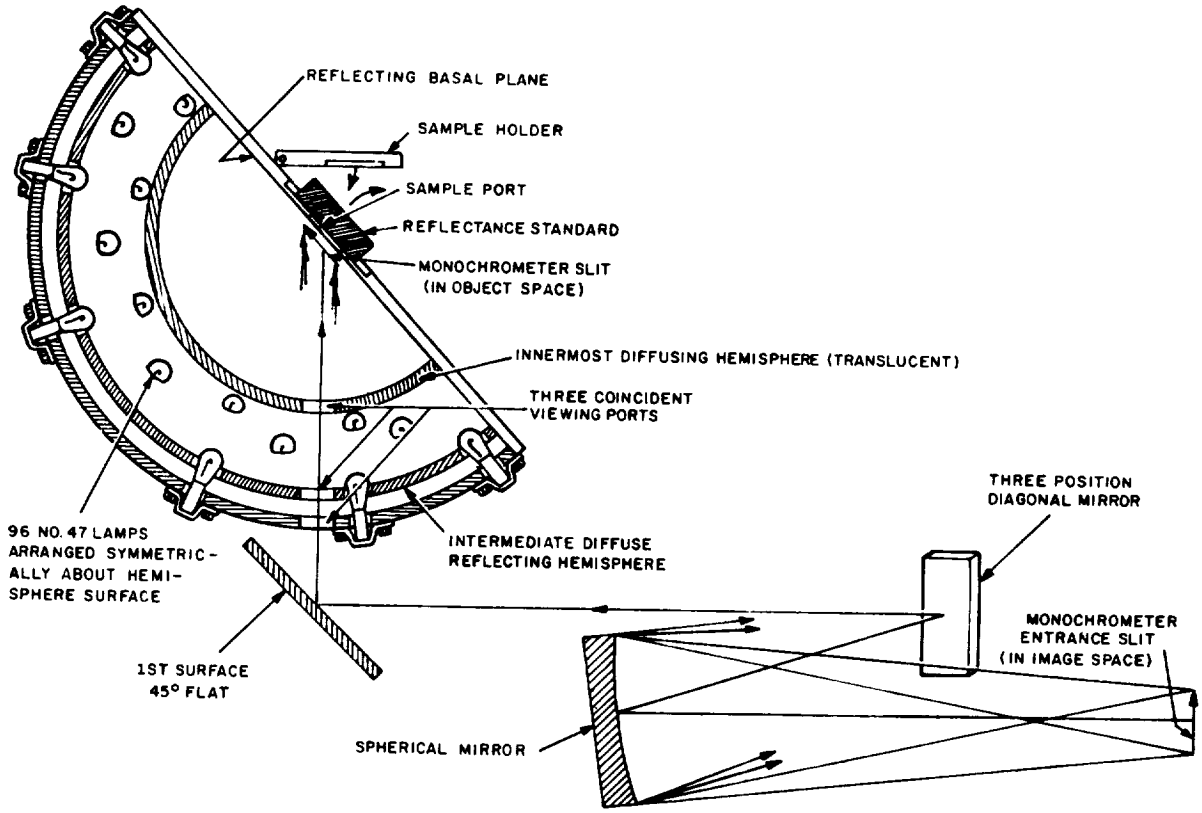

FIGURE 19–2.—Line drawing of reflectance apparatus.

specimen. However, if the specimen is diffuse, then illumination of the specimen is integrated over the 2π solid angle of the hemisphere, and is reflected diffusely into the entrance slit. The equations developed later shown that for equal values of diffuse and specular reflection, an exactly equal flux passes into the entrance slit.

The reflectance device in cross section (fig. 19–2) shows diagrammatically how the 96 lamps are mounted to the outer hemisphere for illumination of the innermost translucent diffusing hemisphere. It should be pointed out that the number of lamps, and their geometrical arrangement, is designed to provide uniform irradiation of the inner hemisphere, and that further uniformity is obtained due to the virtual image of the entire composite structure in the basal plane. This arrangement in effect provides a spherical surface surrounding the specimen with many reflections and re-reflections, and provides a very uniform wall brightness. The wall brightness of the inner hemisphere has been probed without detection of non-uniformity within the sensitivity limits of measurement equipment available.

Figure 19–3 shows an external view of the arrangement described above. The nature of the inner hemisphere initially limited the usable spectral range to between 350 and 1100 mμ. At 350 mμ, the glass substrate becomes opaque; and at 1100 mμ, the diffusing character of the hemisphere cuts off (fig. 19–4) and the hemisphere then becomes transparent, resulting in non-uniformity of wall luminosity.

The characteristic diffusion property of this intermediate hemisphere was extended to 3.0μ by blasting the innermost wall with a 1200-mesh grit resulting in a transmission curve noted by the lower curve of figure 19–4. Thus, the usable range of the instrumentation now extends from 350 to 3000 mμ. By using a standard target, relative reflectance of a specimen is converted into an absolute measurement from the mathematical analysis, as follows:

The action of the integrating hemisphere is best explained by considering an unknown idealized diffuse specimen at P in figure 19–5.

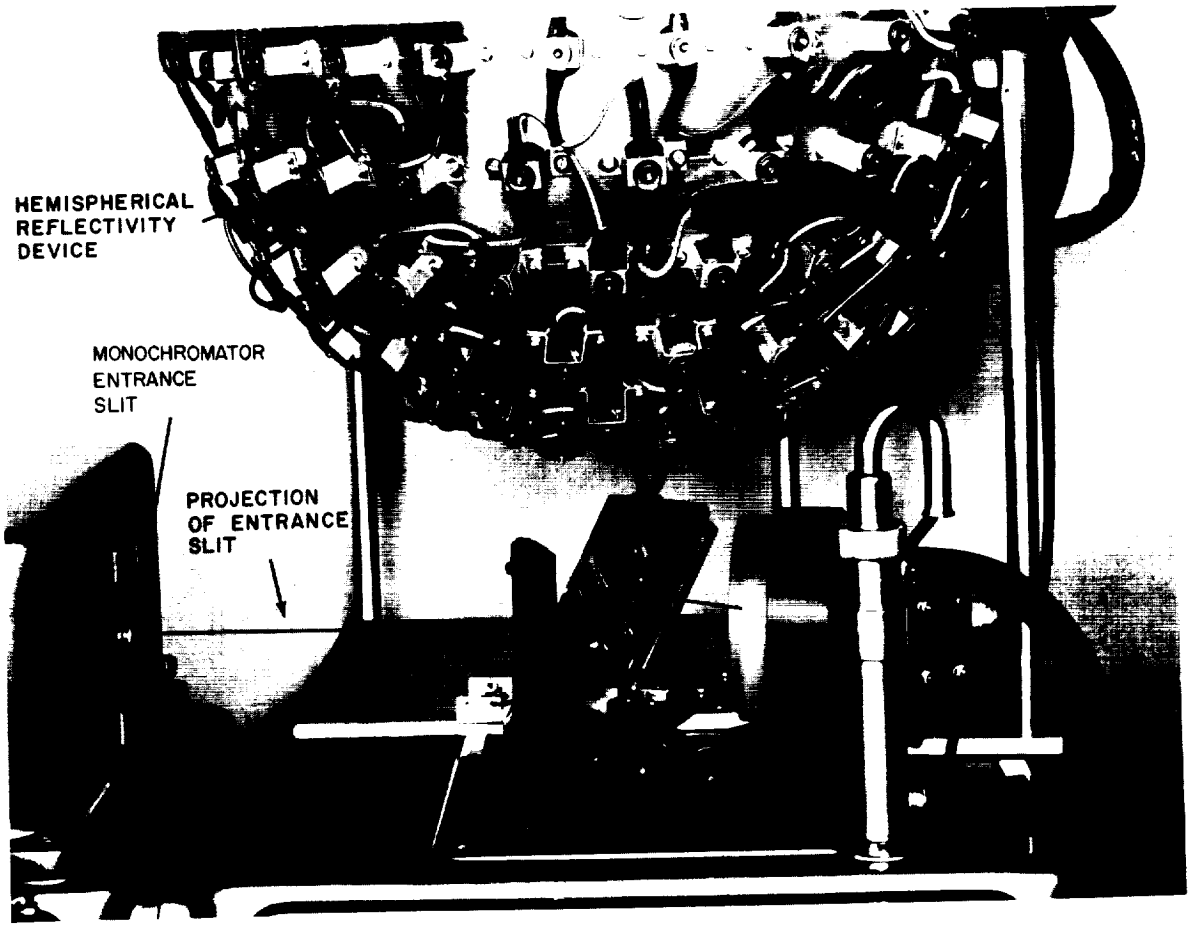

FIGURE 19–3.—Arrangement of reflectance apparatus.

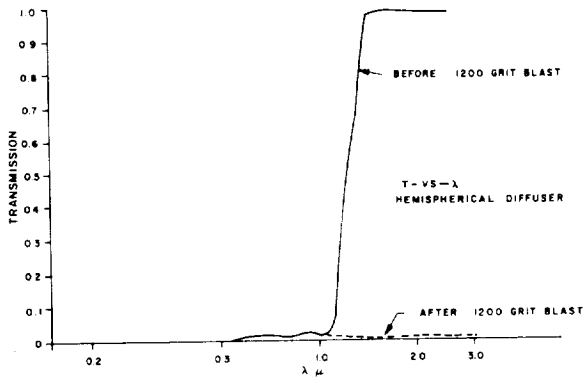

FIGURE 19–4.—Specular transmission of inner hemisphere.

Replace the specimen with an idealized specular reflector, and then compare the radiation for a given $d\lambda$ flux density entering the monochromator entrance slit. The specular reflector is used here as a standard; however, the standard could have been a diffuse surface.

The flux emitted/unit area, or luminosity L, of the hemisphere wall emitted at $d\sigma$ is $L_\sigma d\sigma$. and the intensity

$$I_0 = \frac{L_\sigma d\sigma}{\pi}$$

$$I(\theta) = I_0 \cos\theta = \frac{L_\sigma d\sigma}{\pi} \cos\theta$$

E_p is the flux received/unit area at P.

$$\therefore dE_p = \frac{I_{(\theta)}}{r^2} \cos\psi = \frac{L_\sigma}{\pi r^2} \cos\theta \cos\psi d\sigma$$

$$E_p = \int_L \frac{L_\sigma \cos\psi}{\pi r^2} \cos\theta d\sigma$$

and for a hemisphere $\theta = 0$ because the terminal side of θ is always coincident with the normal.

$$\therefore E_p = \frac{L_\sigma}{\pi r^2} \int_L \cos\psi d\sigma$$

$$\frac{L_\sigma}{\pi r^2} \int_L \cos\psi 2\pi r^2 \sin\psi d\psi$$

$$=2L_\sigma\left[\frac{\sin^2\psi}{2}\right]_0^{\frac{\pi}{2}}=L_\sigma$$

L_p, the flux density leaving $P=\rho_X E_p$

$$\therefore L_p=\rho_X L_\sigma \text{ and } \rho_X=\frac{L_p}{L_\sigma}$$

ρ_X reflectance of unknown diffuse surface
ρ_s reflectance of standard specular surface.

For the specular case where the angle of incidence is equal to the angle of reflection:

$$\rho_s=\frac{L_\rho'}{L_\sigma}$$

assuming all the flux is in the specular direction for the specular standard:

$$\rho_X=\rho_s\frac{L_pL_\sigma}{L_\sigma L_\rho'}=\rho_s\frac{L_p}{L_\rho'}=\rho_s\frac{D_X}{D_S}$$

where D_X is monochromator recorder output deflection for the unknown sample and D_S is that of the standard.

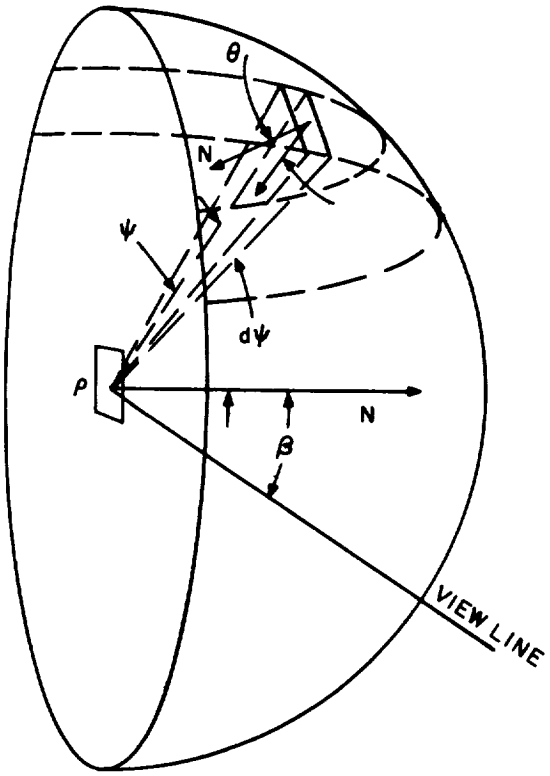

FIGURE 19–5.—Geometrical relationships of the reflectance device.

The derivation in the analysis shows that the total reflectance for a diffuse specimen integrated over a 2π solid angle can be compared exactly to the reflectance of the specular standard if the integrating hemisphere has a uniform wall luminosity. It is immaterial whether the reflectances fall between the limits of being totally diffuse or totally specular, because the system measures the total reflectance of the specimen under test.

To complete the instrumentation, we must determine the absolute spectral reflectance of a material used as a laboratory reflectance standard. One approach to this determination was a literature search for the diffuse spectral reflectance of magnesium carbonate ($MgCO_3$), which is an easily-maintained material obtained commercially in block form. This material can be scraped repeatedly for renewed repeatable surface properties.[2] The other approach is to procure a coated aluminized specular surface of high durability which has been spectrally calibrated by high-precision absolute-reflectance measurement equipment.

Upon consideration of the slight angular dependence function of a diffuse standard, it would appear that the reflectance data on $MgCO_3$ reported in references 1 and 2 can be utilized.

An ideal cosine reflecting surface positioned at P (fig. 19–5) results in an amount of flux (F) depending only on the angular dependence of reflectivity ρ_β entering the monochromator entrance slit at P. Considering the factors dependent on view angle (β), proof is given that flux is constant if ρ_β is constant, since the slit projection length is the variable with β, and the width β is constant. Proof of the constancy of flux is given below by considering the surface at P, an elemental area dA viewed at β_0 (normal incidence), and again at various angles.

$$dF=\frac{\rho_\beta E_p\cos\beta dA}{(\pi r^2)}$$

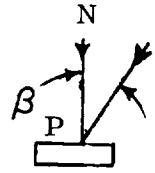

[2] Since the writing of this paper the reflectance has been observed to vary from block to block and even within the same block as material is scraped away.

At various angles of β, the elemental areas maintain the following trigonometric relationships at constant width: where

$$dA_2=\frac{dA_0}{\sin(90°-\beta)}=\frac{dA_0}{\cos\beta}$$

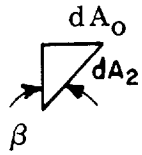

Thus,

$$\frac{dF_{\beta_0}}{dF_{\beta_2}}=\frac{K\rho_{\beta_0}E_\rho dA_0}{K\rho_{\beta_2}E_\rho\cos\beta dA_2}=\frac{\rho_{\beta_0}E_\rho dA_0}{\rho_{\beta_2}E_\rho dA_0}$$

and it is seen that the flux entering the entrance slit is constant, with the exception of the angular dependence of ρ_β, which is relatively constant with angles of incidence as great as 45° (ref. 3).

The conclusion was reached, from geometrical relationships, that it would be necessary to view the sample port at an angle of 45° so that large errors would not be introduced by the fact that the viewing port subtends a large solid angle at normal incidence.

After fabrication of the reflectance device, the angular dependence of reflectance (ρ_β) was measured for two types of materials: a specular standard and a diffuse standard. For the diffuse standard, errors were introduced when the sample was normal to the viewline, because of the solid angle subtended by the viewing port in the inner hemisphere wall, as mentioned above. Therefore, it was impractical to measure precisely the angular dependence of reflectance. The measure of the specular standard dependence on angular reflectance, however, could be made at various view angles, with results indicating no angular dependence of reflectance up to 45°. This is shown by the theoretical Fresnel relations (ref. 4) where

$$\rho_{(\beta)}=\frac{1}{2}[r_p r_p^*+r_s r_s^*] \qquad (1)$$

$$r_p=\frac{\cos\beta_1-\underline{n}\cos\beta_0}{\cos\beta_1+\underline{n}\cos\beta_0}$$

(*denotes complex conjugate).

$$r_s=\frac{\cos\beta_0-\underline{w}\cos\beta_1}{\cos\beta_0+\underline{n}\cos\beta_1}$$

$$\underline{n}=n-jk$$

$$\underline{n}\sin\beta_1=\sin\beta_0$$

Equation (1) is plotted in figure 19–6 for

$$\frac{k}{\underline{u}}=0$$

(low absorption coefficient) and it can be seen that there is no angular dependence of reflectance to at least 45° for high values of ρ_{β_0}.

The reflectance of the first-surface aluminized mirrors used as specular standards was measured by J. F. Hall and Richard J. Walsh of Bausch and Lomb, Incorporated, on a Cary model 14 spectrophotometer to an accuracy of $\pm 0.5\%$ through the spectral range between 200 and 2200 mμ (fig. 19–6). In the experimental measurement of the relectance of the specular standard at 45 degrees, no change in reflectance relative to the reflectance at near-normal incidence could be detected, which agrees with the theoretical consideration presented by equation (1) and figure 19–7. Further, this measurement gives credence to the assumption of uniform wall luminosity for the inner hemisphere.

With the absolute specular and spectral reflectances as reported by Hall and Walsh and a view angle β (45°), a measurement of the total reflectance of $MgCO_3$ was made, utilizing the first-surface aluminized specular mirror as a standard. Figure 19–8 shows the absolute reflectance obtained for $MgCO_3$ in the reflectance device, relative to that reported in references 1 and 2. Figure 19–9 shows this reflectance in more detail.

The maximum error exhibited by the data in figure 19–8 is 7.5% at 1200 mμ and is attributed to the assumptions made concerning the use of

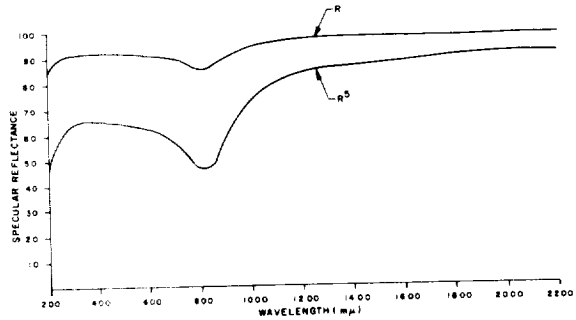

FIGURE 19–6.—Reflectance of aluminized mirror standard. Aluminum plus magnesium fluoride peaked at 608 Å.

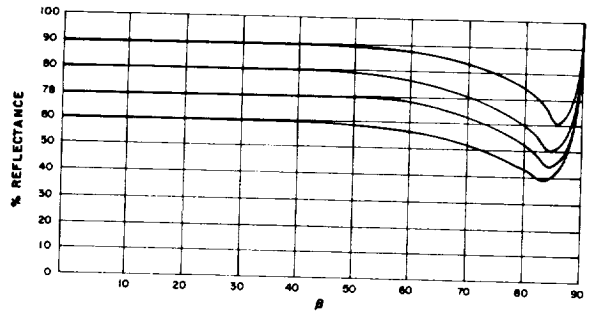

FIGURE 19–7.—Theoretical angular dependence of reflectance for metallic film.

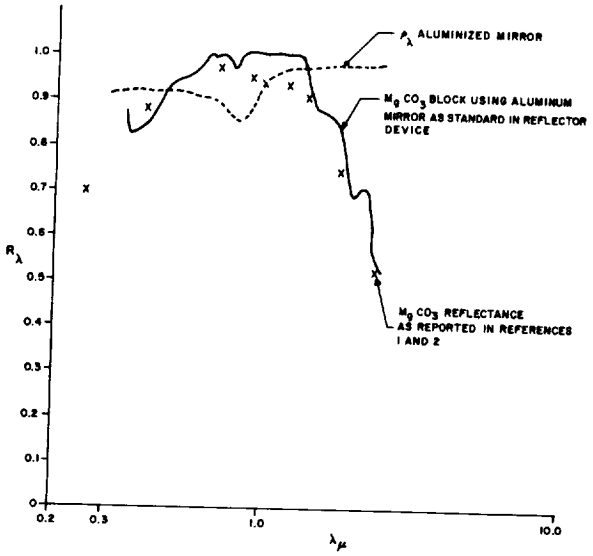

FIGURE 19–8.—Measurement and comparison of magnesium carbonate reflectance.

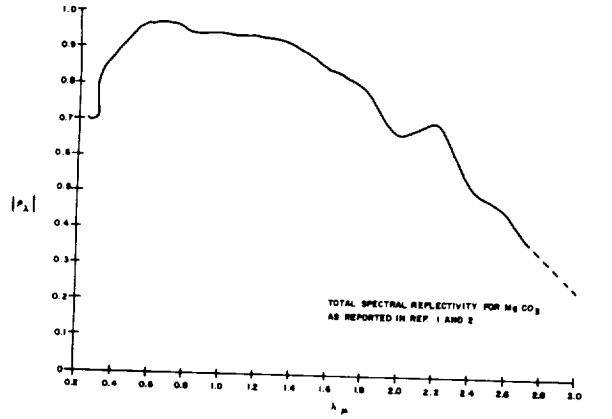

FIGURE 19–9.—Absolute reflectance of magnesium carbonate.

normal-view reflectance data for both specular and diffuse standards at an actual measurement view angle of 45°. In all subsequent data obtained with the hemispherical reflectance device, the reflectance standard used is $MgCO_3$, as reported in references 1 and 2, for the assumption is that angular errors will cancel as long as the view angles for the standard of reflectance and the specimen are the same.

Measurement Procedure

The monochromator is utilized in a single-beam comparison manner as a means for selection of the wavelength (λ) and the resolution ($d\lambda$). Measurements are made point by point through the spectral range of interest in order to obtain as high an accuracy as possible. It is not the purpose of this paper to describe the action of the monochromator in detail; therefore, it is sufficient to say that the output electrical signals are proportional to the radient flux received by the monochromator's detector for the $d\lambda$ and λ chosen, and that the monochromator is a conventional unit widely used by workers in the field.

Briefly, the spectral measurements are made in the following manner, after alignment of the reflectance device.

The wavelength drum of the monochromator is set to a calibration setting for a desired wavelength (λ). The slit width is opened to a desired width defining $d\lambda$. The specimens and holders are removed from the sample port and a zero-radiation recorder-output signal is obtained. A standard of reflectance is then positioned in the viewing port, and the output signal is adjusted by varying the gain of the amplifier for an upscale signal output. The test sample is then positioned at the sample port, and the output signal is recorded. It is usually necessary to readjust the amplifier so that the upscale and downscale output signals fall within fullscale deflection of the recorder. The reflectance of the test specimen is then

$$\rho_{\lambda_x} = \rho_{\lambda_{std}} \frac{D_x - D_0}{D_{std} - D_0}$$

where ρ_{λ_x} is the total reflectance of the specimen, $\rho_{\lambda_{std}}$ is the absolute reflectance of the standard of reflectance within the wavelength band, and D_x, D_o, and D_{std} are the respective recorder deflections.

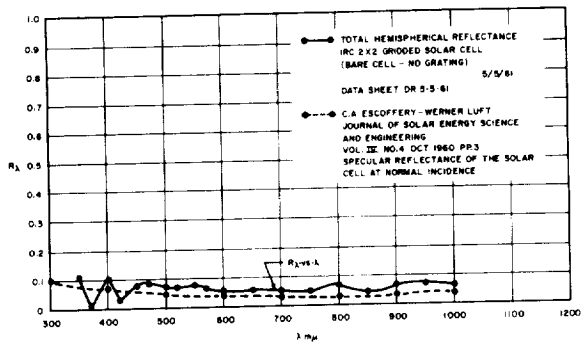

FIGURE 19–10.—Comparison of reflectance measurements for boron-doped silicon cell.

These same measurements are now repeated at other wavelengths until the entire spectral region is covered

Similar methods have been described in the literature by others (ref. 5 and 6).

Results

Performance of the equipment in its present state is best demonstrated by studying figures 19–10, 19–11, and 19–12, which show in graphical form reflectance data obtained for a variety of materials, and correlating them with measurements of other workers. Figure 19–10 demonstrates correlation of low-reflectance material; reflectance data for boron-doped silicon solar cells obtained with the developed instrumentation are compared to published data by Escoffery (ref. 7). Figure 19–11 shows correlation between measurements on a quenched-sulfur diffuse material as reported orally by Dr. Max Kronstein, New York University (ref. 8), and data obtained with RCA Astro-Electronic Division's instrumentation for this same material.

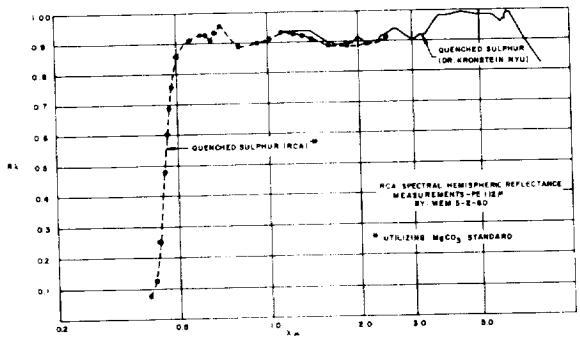

FIGURE 19–11.—Comparison of reflectance for quenched-sulfur material.

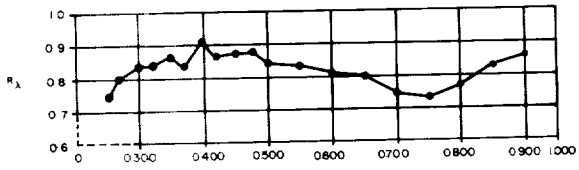

FIGURE 19–12.—Measured data for aluminized reflector at 45° incidence. Magnesium carbonate standard used.

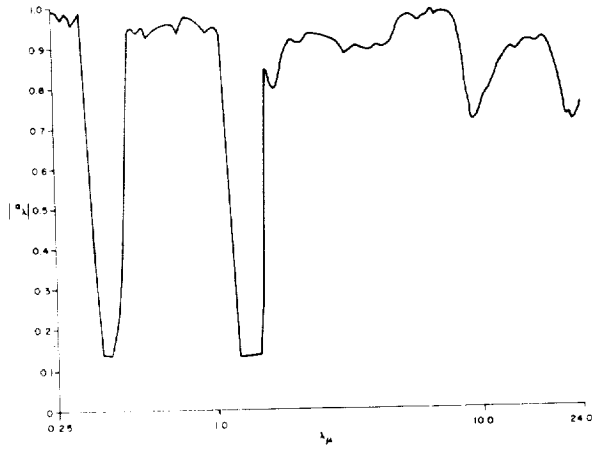

FIGURE 19–13.—Portion of total spectral absorption of solar-cell composite, as determined by reflectance device. IRC 2 by 2 gridded solar cell, blue/red optical coating, Laboratory Inc., filter composite, and RCA data sheets: SR 82561–2 and E92061–2. $\alpha = 0.780$, $\epsilon = 0.861$, and $\alpha/\epsilon = 0.906$.

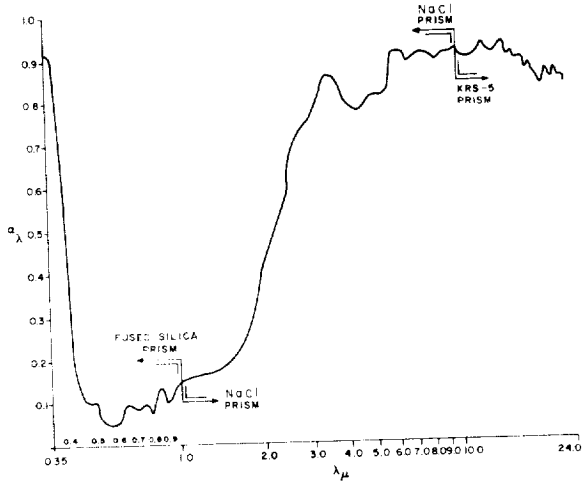

FIGURE 19–14.—Portion of spectral absorption of paint sample as determined by reflectance device.

Figure 19–12 shows data obtained on an aluminized mirror, which correlates quite well with generally accepted data.

Figures 19–13 and –14 show types of data obtained with the developed instrumentation.

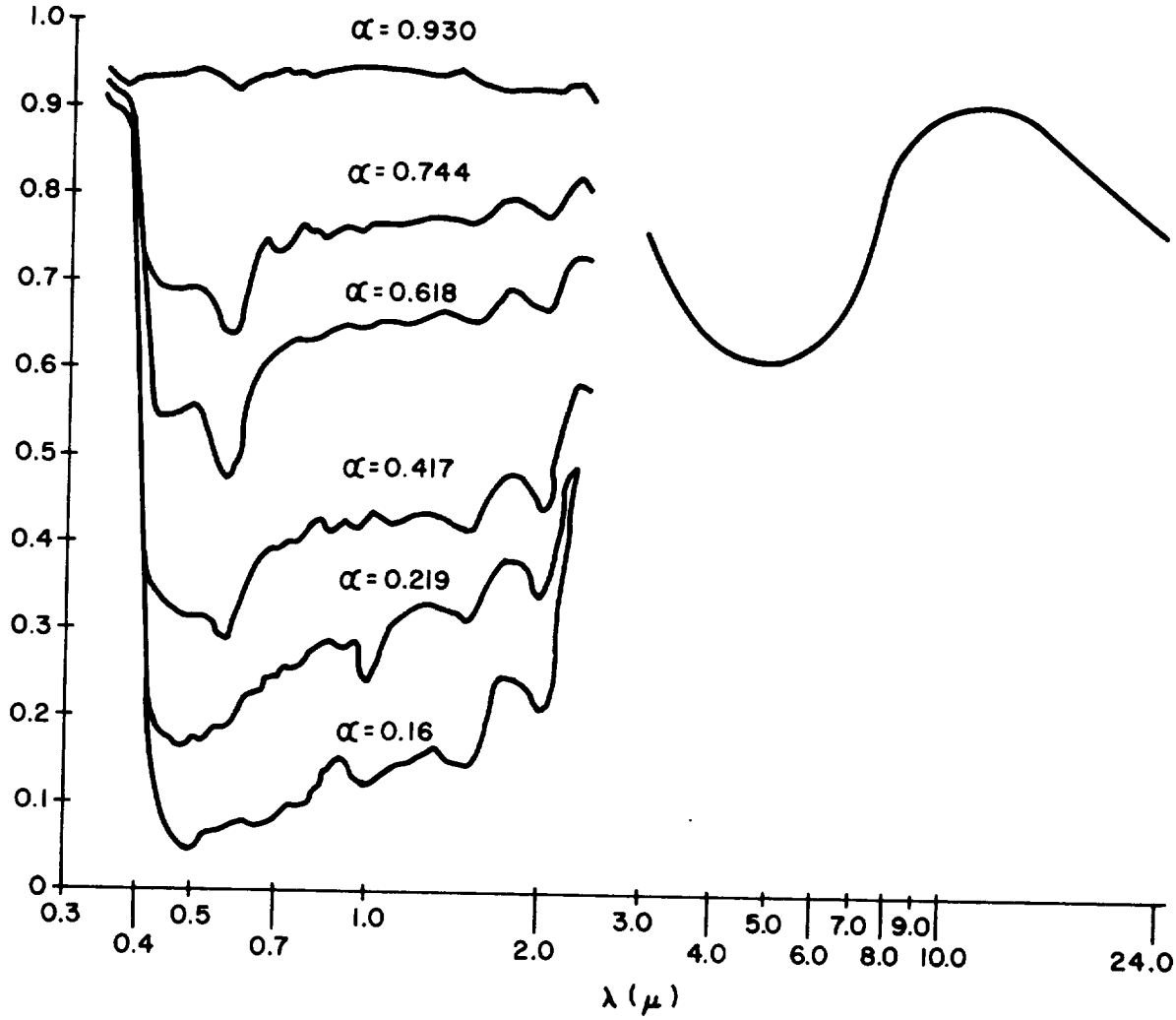

FIGURE 19-15.—Spectral absorption of black and white paint mixture.

Obviously, information above 3.0μ is obtained with different equipment; however, transition from one spectral region and instrumentation to another is accomplished without serious matching problems and indicates good correlation in this regard. Figure 19-15 shows additional measurements made with the developed instrumentation; it shows how α_λ changes with formulations of different parts by weight of a mixture of black and white paint.

RECOMMENDATIONS AND CONCLUSIONS

Extending the spectral range of the diffusing hemisphere to at least 3.0μ by grit blasting with a 1200-mesh grit has been successfully accomplished. Extending the short-wavelength cutoff of the system to at least 200 $m\mu$ requires an exotic hemisphere material, such as quartz or sapphire, which is prohibitively expensive.

The projection of the monochromator entrance slit, as the system is instrumented, is at a view angle of 45°. This angle should be corrected for some materials to an angle of about 10°. For specular interference films, for instance, the path of the rays within the film is significantly increased with increasing incidence angle, which introduces significant errors in measurement. The ray path-length increase was a problem when measuring the total reflectance of solar cells with interference-film glass covers. Here, the problem lies in the measurement of reflectance at high incidence angles

where the spectral tuning of the interference film is designed for normal incidence. Some of the results show high peaks of reflectance developed in the center of band-pass filters. Further, there is an expected spectral shift in cut-on-cutoff wavelengths of about 10% because of the 45° incidence.

The system developed has an accuracy $\gtrsim 7.5\%$. However, further work should be done to obtain a measure of the absolute angular reflectance at various wavelengths for the standards used, and correlations should be obtained of these standards of reflectance with NBS standards of diffuse reflectance.

REFERENCES

1. Betz, Howard T., et al.: Determination of Emissivity and Reflectivity Data on Aircraft Structural Materials. WADC TR 56, pt. II, Oct. 1958, p. 222.
2. Benford, Lloyd, and Schwartz: Jour. Opt. Society of America, vol. 38, no. 5, 1948, p. 995.
3. Dunkle, R. V., et al.: Angular Reflectance Measurement. Second Symposium on Thermophysical Properties, ASME, Jan. 1962, p. 541.
4. Heavens, O. S.: Optical Properties of Thin Solid Films. Butterworth's Scientific Pub., London, 1955.
5. Escoffery, C. A., and Luft, Werner: Optical Characteristics of Silicon Solar Cells and of Coatings for Temperature Control. Jour. Solar Energy, Science, and Eng., vol. IV, no. 4, Oct. 1960, pp. 1–10.
6. McNicholas, H. J.: Absolute Methods in Reflectometry. NBS Jour. Res., vol. 1, no. 1, July 1928, pp. 29–73.
7. McNicholas, H. J.: Equipment for Measuring the Reflectivity and Transmissive Properties of Diffusing Media. NBS Jour. Res., vol. 13, no. 2, Aug. 1934, pp. 211–236.
8. Kronstein, Max: Research and Investigations on Spectral Reflectance and Absorption Characteristics of Camouflage Paint Materials and Natural Objects. ASTIA AD 100058.

20—MEASUREMENT OF THERMAL-RADIATION PROPERTIES OF TEMPERATURE-CONTROL SURFACES IN SPACE

BY CARR B. NEEL AND GILBERT G. ROBINSON

NASA AMES RESEARCH CENTER, MOFFETT FIELD, CALIFORNIA

As part of an investigation of the emittance stability of spacecraft temperature-control coatings, a method was devised for measuring the thermal-radiation characteristics of surfaces during flight in space. The method consists of measuring the temperature history of a number of thermally isolated test surfaces. From the temperature-response curves, the radiation characteristics of the surfaces are deduced by use of a transient thermal analysis.

Such an experiment was included on the S–16 Orbiting Solar Observatory, which was launched March 7, 1962. Based on the measurements made in this experiment, it was concluded that the technique offers a reasonably accurate method of determining the thermal-radiation characteristics of surfaces in space. Comparisons of the flight measurements with values obtained in the laboratory showed an over-all agreement to within less than 10%.

Since the temperature control of space vehicles depends on the thermal-radiation characteristics of the vehicle surfaces, it is important that the radiation properties of the surfaces not change during flight in space. The space environment, however, can cause changes in surface characteristics, leading to inadequate temperature control. As part of an investigation to study the long-term stability of a number of typical temperature-control coatings, an experiment was devised for inclusion in a satellite to measure the radiation properties of surfaces in the space environment. Although the primary purpose of the investigation is to study the emittance stability of surfaces, the purpose of this paper is to describe the technique for measuring these characteristics during flight in space; hence, no discussion of degradation of surface coatings will be presented.

The method consists essentially of measuring the temperature of the surfaces while they are subjected to the various heating sources in space. In the past, as in references 1 and 2, correlations of measured skin temperature on satellites with calculated values have been complicated by the necessity to account for large amounts of conduction and radiation to other parts of the satellite structure. In the present method, the surfaces are thermally isolated to minimize extraneous heat losses. The radiation characteristics of the surfaces are deduced from the temperature measurements.

Six different surfaces were tested in the experiment. A seventh surface, which was designed to remain unchanged in space, was used as a reference. The test equipment was installed on the S–16 Orbiting Solar Observatory, a sun-oriented earth satellite, which was launched March 7, 1962. Temperatures of the surfaces were telemetered from the satellite. Comparisons of the temperatures of the test surfaces with that of the reference surface provide a basis for evaluating changes in the thermal characteristics of the test coatings.

In this paper, the method of obtaining thermal-radiation characteristics from temperature measurements of surfaces in space is discussed. The temperature-measuring technique and the integration of the experiment into the satellite systems are described, and the data-acquisition procedure is touched on briefly. Comparisons are made between the radiation properties obtained from the flight data and those measured in the laboratory prior to flight.

An assessment is made of the flight method of determining the radiation characteristics of surfaces.

SYMBOLS

A area of sensor surface, ft²

c specific heat of sensor disk, Btu/lb-°F

H_a reflected solar radiation from earth incident on sensor surface, average for one revolution of satellite about its axis, Btu/hr-ft²

H_p radiant energy emitted by earth incident on sensor surface, average for one revolution of satellite about its axis, Btu/hr-ft²

H_s direct solar radiation incident on sensor surface, average for one revolution of satellite about its axis, taken as $442/\pi$ Btu/hr-ft²

K heat-exchange constant for sensor mount, Btu/hr-°R⁴

Q_L heat-exchange rate between sensor disk and mounting cup, Btu/hr

T temperature of sensor disk, °R

T_b temperature of base plate, °R (assumed to be same as mounting-cup temperature)

W weight of sensor disk, lb

α_a albedo-radiation absorptance of sensor surface

α_e earth-radiation absorptance of sensor surface

α_s solar-radiation absorptance of sensor surface

ϵ emittance of sensor surface

θ time, hr

σ Stefan-Boltzmann constant, 0.173×10^{-8} Btu/hr-ft²-°R⁴

DESCRIPTION OF MEASURING TECHNIQUE

Experimental Requirements

To assure over-all reliability and accuracy in the technique for determining the radiation characteristics of the test surfaces, the following requirements were set forth at the outset of the experiment:

1. thermally iolated test surfaces
   Thermal isolation minimizes corrections which must be applied to the data as a result of unwanted heat exchanges.
2. thermal mass of test sensors tailored to heating environment
   The sensors must be rapidly responsive yet have high enough thermal lag to permit measurement of the rate of temperature change as the satellite moves into the earth's shadow.
3. stable reference surface
   A surface with stable radiation characteristics under exposure to the space environment provides a basis for detecting any changes in the test surfaces.
4. continuous in-flight calibration of temperature-measuring system
   In-flight calibration permits accurate measurement regardless of drift in the electronic equipment of the measuring system.
5. sensitive telemetry and temperature-measuring systems
   A sensitive system is the final requirement for accuracy in the temperature measurements.

Radiation-Sensor Design

In accordance with the first requirement, the sensors were designed to minimize extraneous heat losses from the test surfaces. Each surface is 1 inch in diameter, and was placed in a mounting cup, as illustrated in figure 20–1. The surfaces were mounted on three small Kel-F supports to minimize the conduction path. Radiant heat losses to the mounting cup were minimized by the use of four radiation shields. All interior surfaces were polished and were coated with gold to further reduce the radiant exchange. Surface temperature is measured by means of a thermistor soldered to the underside of the test disk.

The radiation sensors were arranged in a circular cluster, with the reference surface in the center, as shown in figures 20–2 and 20–3. The design of the reference surface is indicated in figure 20–2. The surface is composed of razor blades stacked together to form a large number of notches which cause multiple reflections and eventual absorption of most of the incident radiation. As a result, the reference surface is essentially a blackbody. Because of the large number of reflections, any change in the emittance of the individual sur-

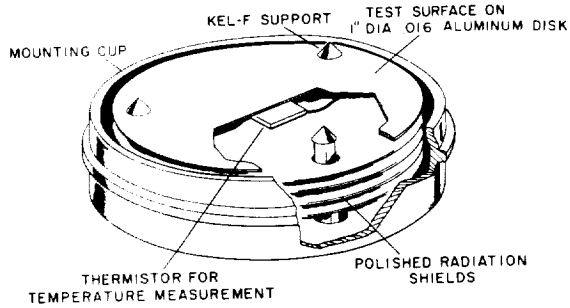

FIGURE 20–1.—Test surfaces.

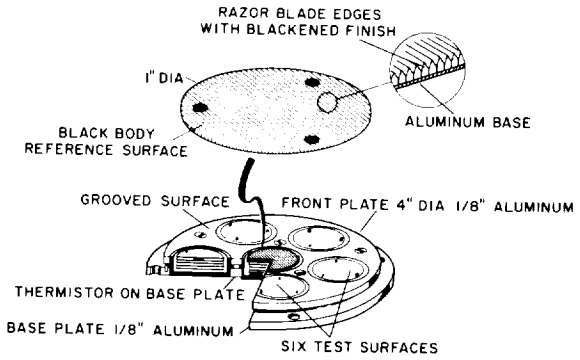

FIGURE 20–2.—Mounting of radiation sensors.

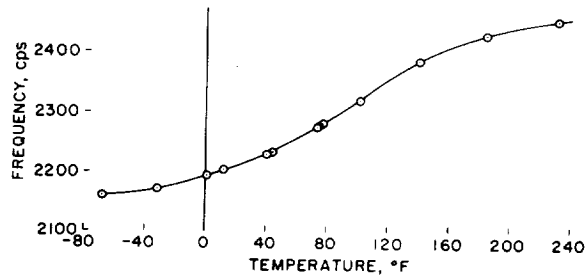

FIGURE 20–4.—Typical calibration curve: surface 7, razor-blade reference.

faces in the notches will have only a very small effect on the over-all emittance or absorptance of the reference surface. To permit correction for heat exchanges between the test surfaces and the sensor mounting cups, the temperature of the base plate is measured with a thermistor. Since the cups are in intimate thermal contact with the base plate, it is assumed the cups are at all times at base-plate temperature.

Temperature-Measuring System

In the measurement of sensor-surface temperature, the thermistors are switched sequentially into a resistance-controlled oscillator, which modulates the frequency of the satellite transmitter. The switching is performed by means of a solid-state switch. The entire electronic package, including the switch, a voltage regulator, and the resistance-controlled oscillator, is shown in figure 20–3. Details of electronic circuitry for the temperature-measuring system are given in the appendix.

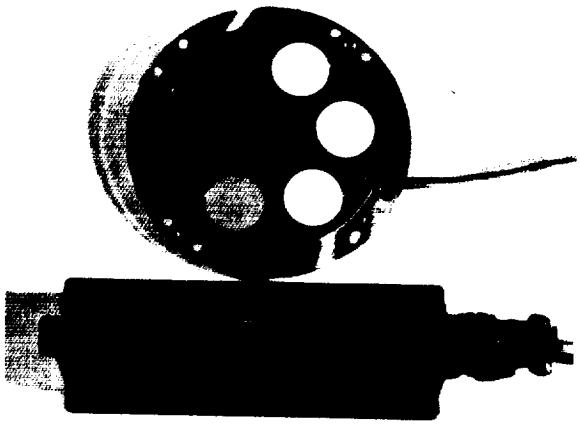

FIGURE 20–3.—Radiation sensor-plate assembly and electronic package.

A typical calibration of the subcarrier frequency as a function of sensor temperature for one of the sensors is shown in figure 20–4. The attenuation of sensitivity at the low and high temperature extremes is caused by limiting resistors in the circuit. The purpose of the limiting resistors is to restrict the frequency range of the resistance-controlled oscillator to prevent interference with other telemetry channels in the event of a short or open circuit in the thermistor wiring.

The thermistor resistances were tailored to provide maximum sensitivity in the range of maximum expected surface temperature for each sensor.

Sensor Heat-Loss Measurements

To provide a basis for correcting the surface-temperature measurements for heat exchange between the surface and mounting cup, measurements were made of the heat-loss characteristics of a number of the sensor assemblies. These tests were performed in a small vacuum chamber. Measurements were made of the heating rate required to maintain various temperature differences between surface and cup for two cup temperatures. Reduction of the heat-exchange data showed that the rate of heat loss or gain can be expressed as follows:

$$Q_L = K(T^4 - T_b^4) \qquad (1)$$

in which the average value of K for nine assemblies was found to be 1.03×10^{-12} Btu/hr-°R^4.

Description of S–16 Satellite

The S–16 Satellite on which the experiment was installed is shown in figure 20–5. The

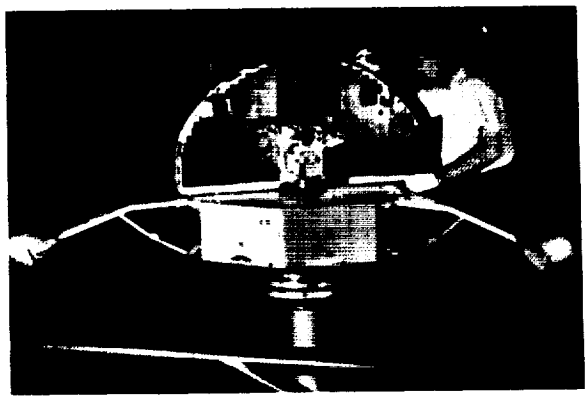

FIGURE 20–5.—S–16 Orbiting Solar Observatory on which emissivity stability experiment was installed.

satellite has two main parts: a lower section, consisting of a nine-sided wheel, which rotates to provide gyroscopic stabilization, and a stabilized semicircular upper section aimed at the sun, containing the experimental equipment for spectroscopic studies of the solar radiation in the short wavelength regime. The stabilized section, or sail, contains solar cells for the electrical generation of power to operate the experimental equipment and the satellite systems. A number of the experiments, including the radiation-sensor plate, are located in the rotating wheel of the satellite. The radiation-sensor plate was mounted on the rim of the wheel, as shown in figure 20–6. In this location, the sensors alternately look at the sun and the earth as the wheel rotates. The rotational speed is 30 rpm, which is sufficiently high that the sensor temperatures do not vary as the wheel rotates.

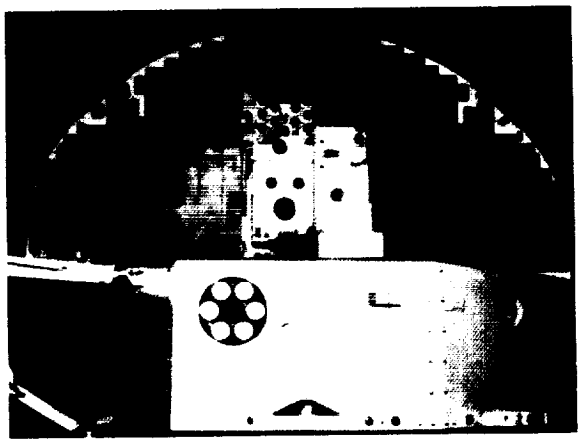

FIGURE 20–6.—Location of sensor plate for emissivity stability experiment.

The satellite was launched into an orbit about 350 statute miles above the earth. The orbit is inclined about 33° with respect to the equator, as illustrated in figure 20–7. The orbital period is 96.15 minutes.

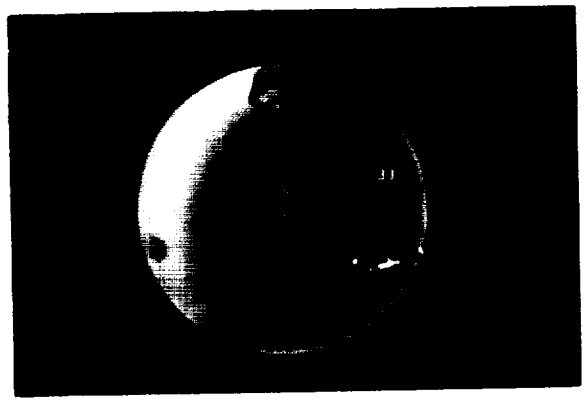

FIGURE 20–7.—Orbit of S–16 satellite.

Data Acquisition

Information from all the experiments on the S–16 satellite except the emissivity stability experiment was accumulated during 90 of the 95 minutes of the satellite orbit. These data were stored on a magnetic-tape recorder on the satellite, which was commanded to play back at the end of the 90-minute period of data acquisition. The command signal was initiated from one of five Minitrack stations located in the north-south picket line along the east coast of the North American continent and the west coast of the South American continent. The command stations include Fort Myers, Florida; Quito, Ecuador; Lima, Peru; Antofagasta, Chile; and Santiago, Chile. Data from the emittance experiment were not accumulated on the tape recorder, but came into the satellite transmitter directly in real time when the transmitter was commanded from the ground stations. This system permitted receipt of about 5 minutes of data for each orbit of the satellite. For a complete picture of the temperature history of the sensors, it was necessary, then, to piece together segments of data from a number of successive orbits.

TABLE 20–I.—*Test Surfaces*

Surface	Solar absorptance, α_s			Surface emittance, ϵ			Flight surface α_s/ϵ,	Source
	Flight surface	Spare surface		Flight surface	Spare surface			
		(a)	(b)		(a)	(b)		
1. TiO_2 in epoxy	0.26	0.23	0.24	0.86	0.86	0.85	0.30	Ames Research Center
2. TiO_2 in silicone	.27	.27	.30	.76	.74	.73	.36	Marshall Space Flight Center
3. White porcelain enamel	.31	.29	.29	.75	.76	.77	.41	Ferro Corporation through Marshall Space Flight Center
4. Aluminum powder in silicone			.24			.26	.92	Goddard Space Flight Center
5. Al-SiO-Ge [c]	.39		.37	.15		.15	2.60	AERDL through Goddard Space Flight Center
6. Al-SiO-Ge-SiO [d]	.52		.46	.18		.21	2.89	AERDL through Goddard Space Flight Center
7. Razor-blade reference [e]		1.0	.99		.92	.93	1.07	Ames Research Center

[a] Measured in November 1960 by LMSC.
[b] Measured in June 1962 by LMSC.
[c] Composition of surface 5: layered construction; stainless-steel substrate, followed by opaque aluminum, 1.1 μ SiO, 110 Å Ge (top layer).
[d] Composition of surface 6: layered construction; stainless-steel substrate, followed by opaque aluminum, 1.1 μ SiO, 200 Å Ge, 500 Å SiO (top layer).
[e] Measured values for spare razor-blade reference surfaces are for two different units.

TEST SURFACES

The Emissivity Stability Experiment is a joint effort of several agencies to measure the stability of typical temperature-control surfaces. A tabulation of the surfaces selected for testing, their radiative characteristics, and the agencies which provided them is presented in table 20–I. The first three surfaces listed are typical of low-temperature surfaces with low solar absorptance and high heat rejection. The fourth surface has an absorptance-to-emittance ratio of about one, with both absorptance and emittance being low, to minimize temperature excursions of a vehicle utilizing this coating as the vehicle passes alternately from sunlight to shadow.

Surfaces 5 and 6 were of layered construction, as described in table 20-I. This system was devised by Dr. Georg Hass of the Army Engineer Research and Development Laboratory, Fort Belvoir, (AERDL) to test the erosion rate of silicon monoxide films. It is expected that the thin germanium layer on surface 5 would be removed by erosion, causing a large decrease in α_s, and a corresponding drop in the surface temperature. Subsequently, the top silicon monoxide film on surface 6 would be removed, followed by the underlayer of germanium, causing a similar decrease in surface temperature. The difference in time between the drop in temperature of surface 5 and that of surface 6 would provide an indication of the lifetime of the 500-Å-thick silicon monoxide film.

With the exception of specimens 5 and 6, absorptance and emittance of the flight surfaces were measured by Lockheed Missiles and Space Company in Palo Alto, California (LMSC). Absorptance values were determined from reflectance measurements in an integrating sphere over the wavelength range from 0.31 to 1.8μ, and emittances were obtained with a hohlraum reflectometer over wavelengths from 2 to 22μ. Values of absorptance and emittance of flight surfaces 5 and 6 were obtained by AERDL, using a similar technique. Also included in this table for comparison are measurements of the absorptance and emittance of the spare sensors at two widely separated times (approximately 1½ years apart). All measurements of the spare sensors were made with basically the same equipment as before by the LMSC. The purpose of these measurements was to determine whether there had been any significant shift in the thermal properties of the surfaces as a result of the extended time period. The table indicates that the radation charac-

teristics remained essentially constant throughout this time, although the absorptance of surface 2 apparently increased about 10%.

No measurements were made of the actual flight disks for surfaces 4 and 7. It is assumed that the values obtained for the spare units apply to the flight surfaces.

RESULTS OF FLIGHT MEASUREMENTS AND ANALYSIS OF DATA

Heating Environment of Test Surfaces

Before the results of the flight measurements are presented, it would be well to consider the heating environment of the test surfaces as the satellite rotates around the earth. The surfaces receive heat primarily from three sources: direct solar radiation, reflected solar radiation from the earth, and direct radiation from the earth. In addition, a small amount of energy is exchanged between the back of the surface and the mounting cup. The equation depicting the heat balance of the test surfaces in this radiation environment is given as follows:

$$H_s A\alpha_s + H_a A\alpha_a + H_p A\alpha_e = \sigma\epsilon A T^4 + Wc\frac{dT}{d\theta} + K(T^4 - T_b^4) \quad (2)$$

The terms on the left side of the equation represent the three primary heat inputs. The first term on the right side represents the heat emitted from the surface. The next term represents the heat stored in the sensor, and the third term, the heat exchanged between the back of the surface and the mounting cup. In the subsequent analysis, the value of albedo-radiation absorptance of the sensor, α_a, was assumed equal to the value of solar-radiation absorptance, α_s. Likewise, the value of earth-radiation absorptance, α_e, was taken equal to the value of surface emittance, ϵ. Accordingly, expressions used in the remainder of the paper will contain only the solar absorptance, α_s, and the surface emittance, ϵ.

Energy from direct solar radiation is constant during the time that the satellite is in the sun. Heating from the reflected sunlight, however, varies with satellite position and aspect. This is, perhaps, the most uncertain of the heating input terms, since the albedo varies with geographical position, cloud cover, and type of terrain beneath the satellite. According to Heller (ref. 1), values between 24 and 54% of the incident solar radiation have been used for the albedo term in temperature considerations. The value of earth, or planetary, radiation is another variable, although the variations are not believed to be as great as for the albedo energy (ref. 3). The basic problem, then, in obtaining α_s and ϵ from the above equation is to obtain correct values of H_s, H_a, and H_p to be used with the measured flight temperatures.

Measured Temperature Histories

The temperature histories for each of the sensors, as derived from the telemetry records, are shown in figure 20–8. Also included for comparison are calculated sensor-temperature variations. The method of calculation is described in a later section. The temperature measurements shown were obtained during only the first 80 orbits of the satellite, which represents about the first five days of the satellite life. These initial orbits of the satellite were analyzed separately, so that comparisons could be made between ground measurements and those in flight before any large amount of surface degradation had taken place. In the case of the two white paints, titanium dioxide in epoxy and titanium dioxide in silicone, however, changes in the surface properties occurred within the first few hours of flight.

All the sensors displayed the same characteristic temperature response as the satellite passed around the earth. Each sensor heated up rapidly as the satellite broke into the sunlight, and its temperature reached a peak shortly after midday. The temperature dropped somewhat as the satellite neared the end of its day; then the sensor cooled quickly as it became enveloped in the shadow again.

Concerning the changes mentioned previously in the white paints, the data obtained for these surfaces are shown in figures 20–8A and 20–8B. The apparent scatter of data, for the most part, is not true scatter, but, rather, is caused by a progressive increase in the sensor temperature-response curve as the satellite lifetime increases. The increase is believed to be due to surface degradation and not to changes in the heating environment. This is

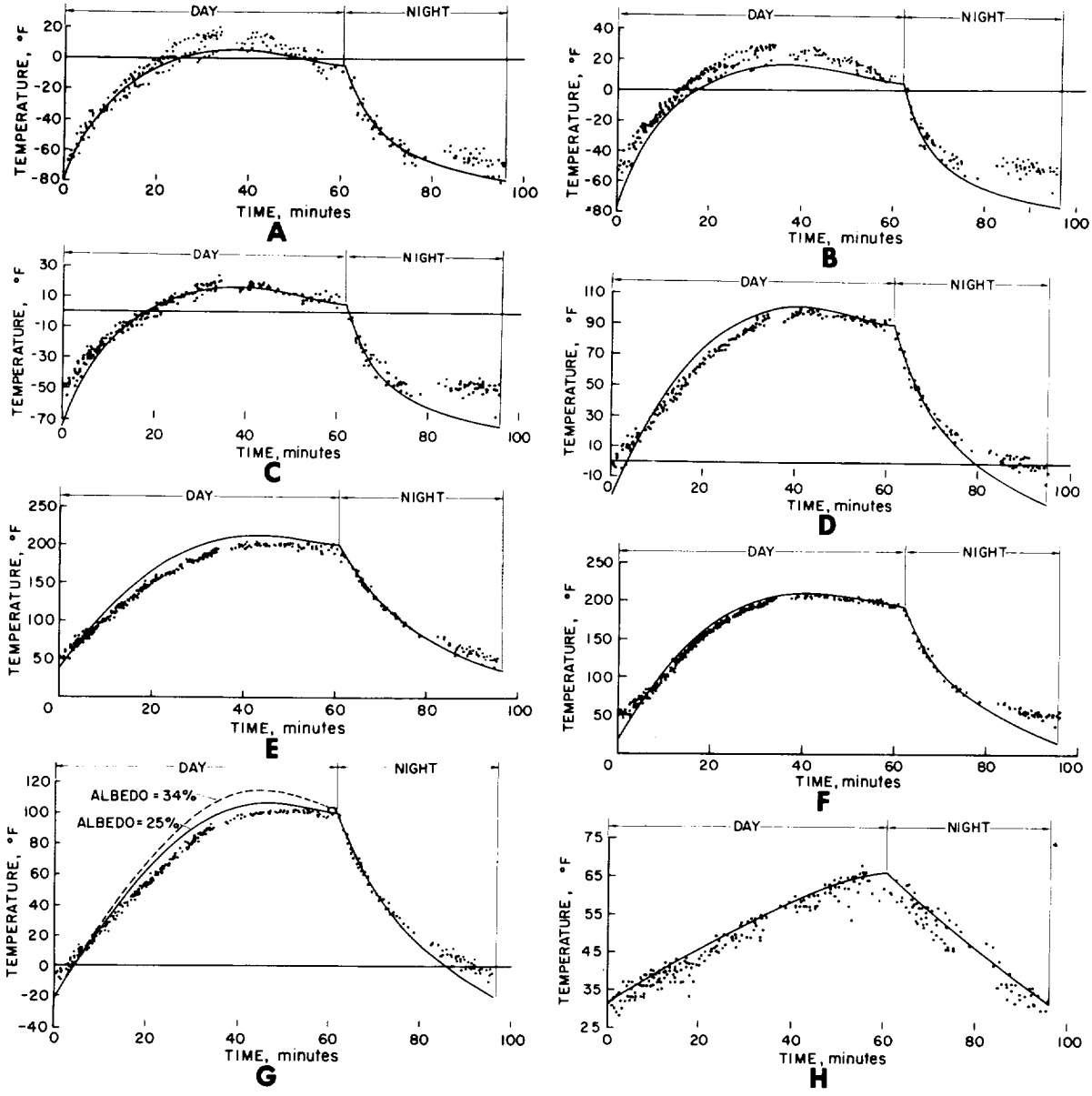

FIGURE 20-8.—Measured and calculated temperature histories.

A.—Surface 1, titanium dioxide in epoxy.

B.—Surface 2, titanium dioxide in silicone.

C.—Surface 3, white porcelain enamel.

D.—Surface 4, aluminum powder in silicone.

E.—Surface 5, aluminum-silicon monoxide-germanium.

F.—Surface 6, aluminum-silicon monoxide-germanium-silicon monoxide.

G.—Surface 7, razor-blade reference.

H.—Base plate.

692-146 O—63——14

concluded from a study of the data for the razor-blade reference surface (fig. 20–8G), which showed no similar change in its temperature response over the same time period. The aluminum-powder paint and the two germanium-silicon monoxide surfaces (fig. 20–8D, –8E, and –8F) likewise exhibited repeatable time-temperature histories, lending further proof that the environment was unchanging.

The base-plate temperature is shown in figure 20–8H. The curve shown in this figure was not calculated, but was faired through the data to provide a basis for correcting the heat exchange between the sensor surfaces and the mounting cups.

Determination of Surface-Radiation Properties

To derive the surface-radiation properties, α_s and ϵ from the flight data, the heat-balance expression (eq. (2)), was rearranged as follows:

$$\frac{\alpha_s}{\epsilon}=\frac{\sigma}{H_s+H_a}\left[T^4-\frac{H_p}{\sigma}+\frac{K}{\sigma A\epsilon}\,(T^4-T_b^4)+\frac{Wc}{\sigma A\epsilon}\,\frac{dT}{d\theta}\right] \tag{3}$$

This equation prevails only during the sunlit portion of the orbit. For analysis of the data, it is desirable to select a position in this part of the orbit in which each of the terms is known with precision. The solar-radiation term H_s is constant while the satellite is in the sunlight, and can be accurately evaluated. The energy received from the reflected sunlight, however, which is represented by the term H_a, is subject to diurnal variations, as well as variations due to satellite orientation. Because of uncertainty as to the exact value to use for albedo, a position should be chosen in the orbit for analysis of data where the reflected sunlight is small, and consequently, the uncertainty in H_a will not greatly influence the result.

Knowledge of the planetary radiation is considerably more precise, although some variations do exist in this value (ref. 3). Heating due to planetary radiation, H_p, is nearly constant throughout the orbit, and, hence, there is little choice as to selection of a point to minimize this term. The remainder of the terms in equation (3) are based on the temperature measurements, and once again, an orbital position should be chosen where the values can be determined most accurately. Such a point would be where the temperatures are relatively high since the measuring system is most sensitive in this temperature region. The last term in the equation involves the rate of temperature change of the sensor, $dT/d\theta$. As is well known, unless the data are very good, the accuracy attendant with measuring slopes generally is not high. Therefore, it is desirable to select a region in the temperature measurements where the slopes are small.

A position in the orbit which satisfies all of these requirements is found in the sunlit region just before day-night transition. At this point, the albedo energy approaches zero because the satellite does not see any of the sunlit side of the earth. Also, the sensor temperatures are near the maximum values, and the rate of temperature change is small. By elimination of the albedo term, H_a, equation (3) can be rewritten as follows:

$$\frac{\alpha_s}{\epsilon}=\frac{\sigma}{H_s}\left[T^4-\frac{H_p}{\sigma}+\frac{K}{\sigma A\epsilon}\,(T^4-T_b^4)+\frac{Wc}{\sigma A\epsilon}\,\frac{dT}{d\theta}\right] \tag{4}$$

This expression was used to derive values of α_s/ϵ from the flight data. The heating-input terms for solar heating, H_s, and planetary heating, H_p, were based on geometrical considerations, as well as the solar constant and the planetary-radiation constant. The work of Altshuler (ref. 4) served as the basis for evaluation of H_p. In the derivations, the solar constant was taken as 442 Btu/hr, sq ft, and the planetary radiation was assumed to be 73 Btu/hr, sq ft. Because of the location of the sensors on the rim of the rotating wheel, the effective solar heating, H_s, is $1/\pi$ times the solar constant, or 141 Btu/hr-ft^2. A more complicated geometrical consideration is involved in the evaluation of H_p, due to proximity of the earth. At the day-night transition, the average integrated value of H_p was computed to be 26.9 Btu/hr-ft^2. Values of surface emittance, ϵ, in the last two terms of equation (4) were obtained as explained in the following.

The emittances of the test surfaces were determined from the measured temperature decay of the sensor after the day-night transition. When the satellite has passed out of the sun's view into the shadow of the earth, there is no heating by direct or reflected solar radiation, and equation (2) can be rearranged and ex-

TABLE 20–II.—*Comparison of Flight and Ground Measurements of Solar-Radiation Absorptance (α_s) and Emittance (ϵ) of Sensor Surface*

Surface	α_s/ϵ		ϵ		α_s	
	Ground	Flight	Ground	Flight	Ground	Flight
1. TiO_2 in epoxy	0.30	0.27	0.86	0.87	0.26	0.24
2. TiO_2 in silicone	.36	.32	.76	.76	.27	.24
3. White porcelain enamel	.41	.32	.75	.75	.31	.24
4. Aluminum powder in silicone	.92	.96	.26	.25	.24	.24
5. Al-SiO-Ge	2.60	3.27	.15	.11	.39	.36
6. Al-SiO-Ge-SiO	2.89	2.75	.18	.17	.52	.47
7. Razor-blade reference	*1.07	.97	*.93	.96	*.99	.94

*Average for the two spare reference surfaces.

pressed as equation (5), which gives the surface emittance.

$$\epsilon=\frac{1}{A(H_p-\sigma T^4)}\left[Wc\frac{dT}{d\theta}+K(T^4-T_b^4)\right] \quad (5)$$

In this expression, the dominant terms are the planetary radiation, H_p, the measured surface temperature, T, and the rate of temperature drop of the surface, $dT/d\theta$. This last term contributes the greatest uncertainty to the measure of emittance.

Once the values of emittance are determined from solution of equation (5), the corresponding values of absorptance, α_s, can be determined from the previously calculated results of α_s/ϵ from equation (4).

Comparison of Ground and Flight Measurements

The flight measurements of α_s/ϵ, ϵ, and α_s, as determined by the procedure outlined above, are compared in table 20–II with the earlier ground measurements.

Comparisons of the ground and flight measurements of α_s/ϵ are the most meaningful, inasmuch as the flight determined values of α_s/ϵ are more accurate than the measurement of ϵ, or the subsequent calculation of α_s. In general, the agreement between ground and flight measurements of α_s/ϵ is good. The largest discrepancy obtained is for surface 5, in which the flight value of α_s/ϵ is about 25% higher than that measured in the ground tests. The data for surface 3 (white porcelain enamel) also show some disagreement, with the flight measurement being about 20% below the ground value.

The flight values of ϵ agree surprisingly well with the ground measurements, in view of the fact that the flight values were derived from the temperature-decay slopes. The only large descrepancy between flight and ground measurements of ϵ is in the value for surface 5. It appears that this discrepancy is the main contributor to the difference in flight and ground measurements of α_s/ϵ, since the absorptance values agree within 10%.

The flight values of α_s, which were obtained by multiplying the measurements of α_s/ϵ by ϵ, also show generally good agreement with the ground measurements. The discrepancy noted previously in α_s/ϵ for surface 3 apparently is due to a difference in the values of absorptance, since the ground and flight measurements of ϵ are in perfect agreement.

In comparing the ground and flight measurements given in table 20–II, it is well to keep in mind the basic differences in the two measuring techniques. The ground values are based on integrated spectral reflectance measurements, with certain corrections applied to make up for areas of incompleteness in the environmental considerations. In the flight technique, on the other hand, the radiation characteristics must be inferred from temperature measurements, while the environmental conditions, of course, are completely appropriate. The good agreement obtained with the two techniques is encouraging.

The close agreement between flight and ground measurements of the radiation characteristics of the two white paints (surfaces 1 and

TABLE 20–III.—*Summary of Probable Errors in Flight Measurements and Effect on the Evaluation of* α_s/ϵ

Term in eq. (4)	Probable error in term			Resulting error in α_s/ϵ, %		
	White Coatings	Aluminum powder and-ref. surf.	SiO-Ge films	White Coatings	Aluminum powder and ref. surf.	SiO-Ge films
T	±5° F	±3° F	±4° F	±9	±3	±3
H_p	±6%	±6%	±6%	±4	∓1	∓0.5
K	±15%	±15%	±15%	±3	±1	±5
$dT/d\theta$	±15° F/hr	±10° F/hr	±20° F/hr	±3	±2	±3

2), however, may be somewhat fortuitous. Since changes in the characteristics were taking place rapidly after start of exposure to the space environment, the initial values were somewhat difficult to establish. Selection of the appropriate level of sensor temperature at the point of day-night transition was guided by knowledge of the shape of the calculated temperature-response curve, and the level of maximum temperature measured during the first orbit. Thus, additional uncertainty is involved in the flight measurements for these surfaces.

Estimation of Measurement Errors

The question of accuracy in determining the flight values of α_s/ϵ was investigated by evaluation of the probable errors in each of the terms in equation (4). A summary of the probable errors and the resulting effect on evaluation of α_s/ϵ is given in table 20–III.

In the table, the surfaces are divided into three general classes, depending on the ratio of α_s/ϵ, and, hence, on the level of maximum temperature. Since temperature is the only term in this table which was actually measured by telemetry from the satellite, a few words concerning this measurement are in order. The estimated accuracy of the frequency bandwidth, as received by the ground stations, is ±1 percent. This results in a temperature measurement accuracy of about ±3° F. Coupled with the probable temperature-calibration errors and with the probable data-reduction errors, the estimated maximum error in temperature measurement is believed to be about ±5° F. The plotted results of the temperature measurements appear to substantiate this estimate. Since there was no evidence of systematic error in measurements, but, rather, random scatter, it is believed that a careful fairing of a curve through the data would result in an error of only 3° or 4° F, as indicated in the table.

The largest error in the determination of α_s/ϵ is caused by uncertainty in the measured temperature for all surfaces except the germanium-silicon-monoxide films. In the case of these films, the largest probable error is caused by possible errors in the heat-loss term K. Since it is not likely that these errors would be cumulative, the maximum probable error for the white coatings is believed to be slightly greater than 10 percent, and somewhat less for the other surfaces. Applying these estimated maximum errors to the flight measurements would not account for the differences observed between the flight and ground measurements for surfaces 3 and 5, as noted previously. No attempt will be made here to resolve these differences.

A similar analysis was made to study the probable errors in the determination of ϵ. The surfaces were again divided into three main groups. The results of the analysis are given in table 20–IV.

As mentioned previously, uncertainties in measuring the temperature decay, $dT/d\theta$, can lead to the greatest error in the determination of ϵ. The generally good agreement between ground and flight measurements of ϵ, however, indicates that the actual errors are small. In the case of surface 5, the probable errors would have to have been cumulative to make the flight value agree with the ground measurement. This does not seem likely, but no explanation for the discrepancy can be given at this time.

TABLE 20–IV.—*Summary of Probable Errors in Flight Measurements and Effect on Evaluation of* ϵ

Term in eq. (5)	Probable error in term			Resulting error in ϵ, %		
	White coatings	Aluminum powder and reference surface	SiO–Ge films	White coatings	Aluminum powder and reference surface	SiO–Ge films
T	$\pm 5°$ F	$\pm 3°$ F	$\pm 4°$ F	∓ 7	∓ 3	∓ 5
H_p	$\pm 6\%$	$\pm 6\%$	$\pm 6\%$	± 3	± 1	± 0.5
K	$\pm 15\%$	$\pm 15\%$	$\pm 15\%$	± 2	∓ 1	∓ 8
$dT/d\theta$	$\pm 70°$ F/hr	$\pm 35°$ F/hr	$\pm 50°$ F/hr	∓ 11	∓ 7	∓ 10

Comparison of Measured and Calculated Temperature Histories

Since the flight values of α_s and ϵ were obtained from the data at one particular location in the orbit (i.e., the day-night transition), it is interesting to compare calculated curves of the sensor-temperature histories based on these values with the experimental measurements throughout the entire orbit. The calculated curves should agree fairly well with the data in the vicinity of the day-night transition, but agreement throughout the remainder of the orbit would depend on the correct selection of values for albedo and planetary radiation.

Temperature histories were calculated for the various sensors by solving equation (2) for the entire orbit. The heating-input terms involving albedo and planetary radiation were obtained from a consideration of the geometrical factors involved. The data of reference 4 served as the basis for evaluating these terms at each orbital position. In these calculations, the solar constant was taken as 442 Btu/hr-ft^2, the intensity of reflected solar flux was assumed to be 110 Btu/hr-ft^2, and the planetary radiation was taken as 73 Btu/hr-ft^2. The value of 110 Btu/hr-ft^2, for the reflected energy represents an albedo of 25%, which is somewhat below the value normally accepted in temperature calculations.

The sensor-temperature-history calculations were performed on an IBM 7090 computer. The longitude, latitude, and altitude position data for each minute in time of the satellite orbit, were taken from the Refined World Map, which is based on satellite tracking data. This information was fed into the computer program for calculating the various values of heating input.

Comparisons of the calculated curves with the measured temperature histories are shown in figure 20–8 for the seven sensors. As expected, the calculated curves agree reasonably well with the data during the period just before day-night transition and immediately following this point. In the remainder of the sunlit part of the orbit, the calculated curves generally lie somewhat higher than the measured temperatures. Better over-all agreement with the measurements could be obtained if a lower value for the albedo were assumed in the calculations. However, such an approach could not be justified without more definitive information on the intensity and angular distribution of the reflected solar flux. An additional calculation was performed for the razor-blade reference surface (figure 20–8G), to illustrate the dependence of the level of the temperature curve on the value of the assumed albedo. In this case, the value chosen was 34%, as recommended in reference 4. It is seen from this curve that the albedo has an important influence insofar as matching the measured temperature history of the sensor is concerned.

During the nighttime part of the orbit, the calculated temperature curve in all cases followed the measurements during the initial part of the temperature decay, but, as the temperature dropped further, the calculated curve fell below the measured values. This disagreement during the latter part of the nighttime cycle could possibly be due to insensitivity (and the accompanying inaccuracy) of the temperature-measuring system at the lower temperatures, caused by the frequency-limiting resistor in the oscillator circuit.

TABLE 20–V.—*Percentage Contribution to Value of α_s/ϵ Made by Temperature, Planetary Radiation, Heat Loss to Base, and Heat Storage in Disk*

Contributing item	Term in eq. (4)	Percentage contribution to value of α_s/ϵ		
		White coatings	Aluminum powder and reference surface	SiO-Ge films
Temperature measurement	T^4	185	120	75
Planetary radiation	H_p/σ	−65	−20	−6
Heat loss to base	$(K/\sigma A\epsilon)(T^4 - T_b^4)$	−17	5	35
Heat storage in disk	$(Wc/\sigma A\epsilon)\ (dT/d\theta)$	−3	−5	−4

Assessment of Flight Technique for Determining Thermal-Radiation Characteristics

Aside from the obvious difficulties involved in any satellite experiment, the temperature-measuring technique appears suitable for determining thermal-radiation characteristics of surfaces. Reasonably accurate measurements can be deduced from the temperature histories, provided the over-all measurement accuracy is within a few degrees Fahrenheit. This method of measurement, of course, produces values of diffuse solar absorptance, and total hemispherical emittance, both of which are sought in ground-measuring techniques. However, no information on the spectral characteristics of the surfaces can be deduced from the flight data.

Several items in the measuring technique could be improved, and several areas of uncertainty in the assumptions could be crystallized by appropriate auxiliary measurements. Continuous measurement of the sensor temperature throughout the orbit, for example, would eliminate the problem of attempting to piece together short segments of the temperature history to reconstruct the entire sensor-temperature-response curve. This is especially important when the surface characteristics are changing with time. Reducing the mass of the sensors to make them more responsive would improve the accuracy in determining α_s/ϵ from the temperature measurements. More accurate knowledge of the earth albedo and planetary radiation would reduce some of the uncertainties involved in this technique.

It is interesting to investigate how improvements in the temperature-measuring system, in the sensor design, and in knowledge of the planetary radiation could lead to more accurate measurements of α_s/ϵ and ϵ. The relative contribution to the measurement of radiation properties of each of the terms in equations (4) and (5) was computed. As before, the surfaces were divided into three main groups, depending on the α_s/ϵ ratio. Table 20–V shows the percentage contribution to the determination of α_s/ϵ of each of the four terms of equation (4).

As would be expected, the surface temperature contributes the greatest percentage to the value of α_s/ϵ for all three types of surface. This stresses the need for accurate temperature measurement. For the white coatings, planetary radiation contributes a large percentage, and the importance of accurate knowledge of this value is obvious.

The heat loss term is relatively small for the white coatings and the aluminum-powder and reference surfaces. However, because of the high surface temperatures involved, the heat-loss term for the silicon-monoxide-germanium films becomes quite large. It is apparent that the heat-loss term could be reduced by better thermal isolation or by designing the equipment so that the base temperature would operate closer to the surface temperature.

In all cases, the transient heat-storage term was sufficiently small to be of little concern.

A breakdown of the items contributing to the value of ϵ shows a similar heavy dependence on the temperature measurement for all three types of surface, as indicated in table 20–VI.

The planetary radiation also contributes a large percentage to the measurement of ϵ

TABLE 20–VI.—*Percentage Contribution to Value of ϵ Made by Temperature, Planetary Radiation, Heat Loss to Base, and Heat Storage in Disk*

Contributing item	Term in eq. (5)	Percentage contribution to value of α_s/ϵ		
		White coatings	Aluminum powder and reference surface	SiO-Ge films
Temperature measurement	σT^4	150	120	109
Planetary radiation	H_p	−50	−20	−9
Heat loss to base	$K(T^4-T_b^4)$	14	−6	−52
Heat storage in disk	$Wc(dT/d\theta)$	86	106	152

for the white coatings. The heat-loss term once again is large for the silicon-monoxide-germanium films, as would be expected. The heat-storage term is a major contributor to the measurement of ϵ. This illustrates the need for accurate determination of the rate of temperature decay. It should be noted that equation (5) consists of two groups of terms multiplied together and hence the sum of the terms in each group must equal 100%. Since there are two groups, the total contribution amounts to 200% for each coating category.

In summary, accurate measurement of the thermal-radiation properties of surfaces by the temperature-measuring technique requires precise measurement of the surface temperature history, good thermal isolation, and accurate knowledge of the amount of planetary radiation.

CONCLUSIONS

An analysis was made of the surface-temperature measurements of a number of test surfaces on a satellite to obtain the thermal-radiation characteristics of various coatings. The results were compared with laboratory measurements based on reflectance techniques, and the values of absorptance and emittance on an over-all average basis differed by less than 10%. It is concluded that the temperature-measuring technique affords a reliable means for deriving the thermal-radiation characteristics, provided the temperature measurements are reasonably accurate.

APPENDIX—DETAILS OF TEMPERATURE-MEASURING CIRCUITRY

The thermistor resistances control the output of a subcarrier oscillator which modulates the satellite transmitter during telemetry of the sensor temperatures. To conserve telemetry channels, all temperatures are transmitted on one frequency channel by means of a solid-state commutator switch. The switch contains ten points, seven of these points are for the thermistors measuring the temperatures of the test surfaces, and one is for the thermistor measuring the base temperature of the sensor mounts for heat-balance correction. The remaining two points are for standard calibrating resistors representing two levels of thermistor temperature.

In addition to the subcarrier resistance-controlled oscillator and the commutator switch, the electronic equipment also contains a voltage regulator which provides a stable voltage source for the oscillator and the switch. A block diagram of the electronic unit is given in figure 20–9, and the circuit diagram is presented in

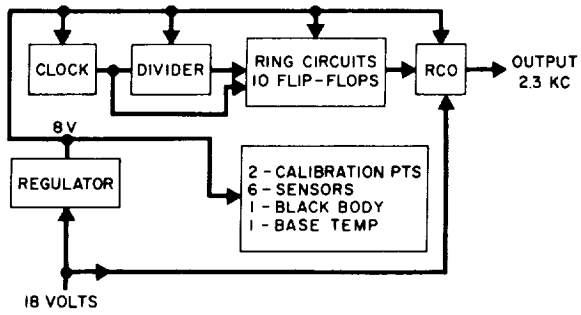

FIGURE 20–9.—Block diagram of emissivity experiment.

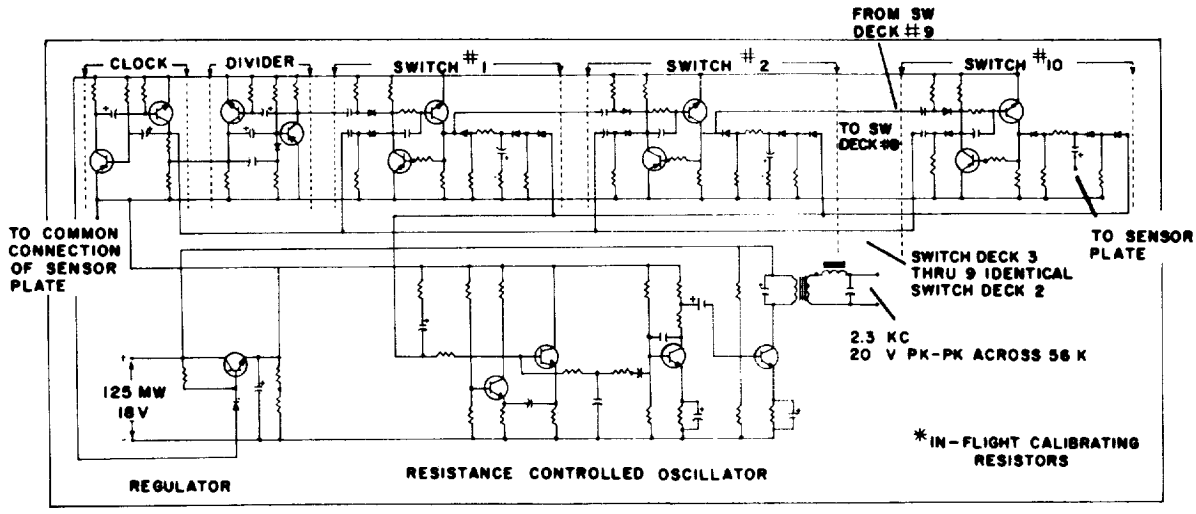

FIGURE 20–10.—Circuit diagram of electronic package.

figure 20–10. Operation of the various components will be described.

10-CHANNEL COMMUTATOR SWITCH

The output of the subcarrier oscillator is controlled by ten flip-flops arranged in a ring circuit. When a flip-flop is on, an impedance containing the thermistor resistance is switched into the controlling position of the subcarrier oscillator, causing a change in frequency. The first flip-flop in the ring is controlled by a divider. Each subsequent flip-flop is controlled by a clock. The divider initiates the ring action by turning on the first flip-flop. The clock applies an "off" pulse to all the flip-flops, and due to the inherent time delay involved in turning off the flip-flop, the action of the flip-flop being turned off causes the succeeding flip-flop to be turned on. This action is repeated until all ten of the flip-flops have come on and have been turned off individually in a prearranged order. The time taken for the complete cycle, about 7 seconds, is controlled by the clock and the divider. A typical flight record, processed from the Minitrack magnetic tape and showing the operation of the 10-channel switch, is figure 20–11.

CLOCK

The clock is an astable multivibrator with a period of ⅓ second. Dissimilar transistors are used so that the transistors are either both on or both off. This scheme was used to conserve power in the other circuits that were not symmetrical (i.e., divider and ring circuits). The output of the clock is differentiated and clipped, leaving only a negative spike. These spikes are applied to all ring circuits and to the divider.

FIGURE 20–11.—Typical flight record showing operation of 10-channel solid-state switch.

DIVIDER

The divider is a triggered astable multivibrator with a nonsymmetrical period of approximately 20 to 1. The long portion of the cycle and "off" period of the transistors is controlled by an RC discharge that is interrupted by negative clock spikes. The twentieth interruption discharges the RC circuit to zero, causing the divider to flip. The short "on" period of the divider is differentiated and clipped to give a positive spike which is fed only to the No. 1 ring circuit. This spike initiates the countdown of the ring circuit.

RING CIRCUITS AND SWITCHES

The bistable ring circuits consume power only when they are on because of the use of dissimilar transistors. These circuits are switched on by a positive spike, and they are turned off by the negative spike coming from the clock. The ring circuit is actually a broken ring, having the No. 1 circuit turned on by the divider. As the No. 1 circuit is turned off, it turns on the No. 2 circuit and so forth around the ring. The switching circuit uses two diodes to give a very high open-circuit resistance. In other respects, it is standard and is closed when the corresponding ring circuit is conducting. One side of each of the switches is tied to a common lead at the subcarrier oscillator, and the other terminals are connected to the sensing thermistors.

RESISTANCE-CONTROLLED OSCILLATOR

The resistance-controlled oscillator is a standard, direct-coupled astable multivibrator that operates well into the saturated mode. Band-limiting resistors are used so that resistances of zero to infinity will give a corresponding shift in the center frequency of 2.3 kc $\pm 7\frac{1}{2}\%$. The output of the oscillator is fed to active and passive filters, which reduce the total harmonic distortion to less than 1%. Some amplitude modulation is present because of the narrow band of the filters. However, this is less than 5%, and is removed in the receiver. The oscillator is stable to less than $\pm 3\%$ over a temperature range of $-10°$ C to $+70°$ C. Since two standard resistors are switched in for calibration, any shift in the oscillator frequency can be accounted for. The oscillator output is fed directly to the transmitter with a modulation index of 1.

VOLTAGE REGULATOR

The regulator operates from the satellite 18-volt supply, and provides an output of 8.6 volts regulated to within $\pm 0.1\%$ for a shift of ± 2 volts in the supply. The regulated voltage is constant over a temperature range of $-10°$ C to $+70°$ C. The power consumption of the regulator is 40 milliwatts during normal operation.

REFERENCES

1. Heller, Gerhard B.: Problems Concerning the Thermal Design of Explorer Satellites. IRE Transactions on Military Electronics, April–July 1960, pp. 98–111.
2. Cohan, H.; and LaBlanc, E. A.: Discoverer Orbital Thermodynamic Design—Predictions and Flight Data Correlation. Spacecraft Thermodynamics Symposium, March 28, 1962. Lockheed Missile and Space Co. Research Laboratories, Palo Alto, Calif.
3. Camack, W. G.: Albedo and Earth Radiation. 1962 Proceedings of Institute of Environmental Sciences.
4. Altshuler, Thomas L.: A Method for Calculating the Thermal Irradiance Upon a Space Vehicle and Determining its Temperature. General Electric Co., T.I.S. Report R60SD386, Aug. 1960.

DISCUSSION

Leonard Eisner, Barnes Engineering Co.: Table 20–II shows reasonable agreement between ground and flight values of α_s/ϵ, except for surfaces 3 and 5. In the latter case, could there have been a temperature effect involved; e.g., a change in the emissivity or in the wavelength cut off of the germanium film associated with a temperature difference of the sample between the ground and flight data?

Neel: A more likely reason for the discrepancy is the angular dependence of the spectral properties of the film.

21—A SIMPLE PHOTOMETER WITH WIDE DYNAMIC RANGE

BY KARL H. NORRIS

U.S. DEPARTMENT OF AGRICULTURE, BELTSVILLE, MARYLAND

A multiplier-type phototube is operated in a constant-anode-current mode with the dynodes supplied with line voltage pulses through a high-voltage control tube. Circuits are given for both half-wave and full-wave operation. A dual-beam system is described for the full-wave circuit, using an optical-beam switch synchronized with the line voltage. A non-linear attenuator corrects the photometer output to give a linear variation with optical density. Beam sorting is accomplished with transistor switches, and a cathode follower provides a low-impedance output. This photometer is shown to have a linear range of greater than 6 logarithmic decades, and a peak-to-peak noise equivalent to an optical-density change of 0.002 at a response time of 0.3 sec for full scale. The performance of the photometer is illustrated with a measurement of the spectral absorption of a piece of wood 1.5-cm thick and a measurement of the sideband rejection of interference filters.

Aborption spectroscopy of highly pigmented and dense light-scattering samples require a photometer of wide dynamic range. Density differences of 4 logarithmic decades or more between regions of high and low absorption are quite common for intact biological tissues. Previous work (ref. 1) has shown the advantage of the multiplier-type phototube in a constant-anode-current mode for this type of measurement. Operating in this mode, the dynode accelerating voltage is normally supplied from a high-voltage d-c supply. This supply need not be regulated, but low ripple is required to obtain low signal noise at high response speed. Batteries can be used, but the current drain is such that a bulky battery pack is required. The high-voltage supply is the main source of failures in this type of circuit so a photometer was developed to operate without the d-c supply.

DESIGN

The constant-anode-current circuit functions equally well on pulsed d-c for the accelerating voltage. The voltage pulses can be provided by a high-voltage transformer, making a simple photometer possible. In its simplest form the photometer consists of a high-voltage transformer, a high-voltage control tube, a multiplier phototube with associated resistors and a low-sensitivity voltmeter. This circuit, as shown in figure 21–1, gives output pulses which vary from 100 volts at high light level to as high as 2000 volts at dark. The output voltage varies exponentially with the reciprocal of the light flux, and a range of greater than seven logarithmic decades is easily obtained with many phototubes. The control tube serves a dual function in this circuit. It controls the magnitude of the voltage pulse to the phototube to keep the anode current constant, and it

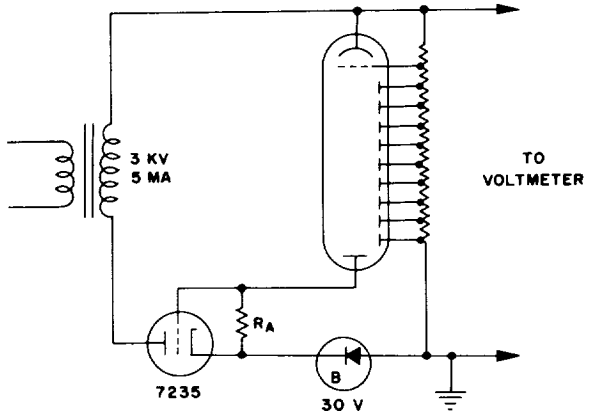

FIGURE 21–1.—Constant-anode-current circuit, using pulsed voltage on the dynodes.

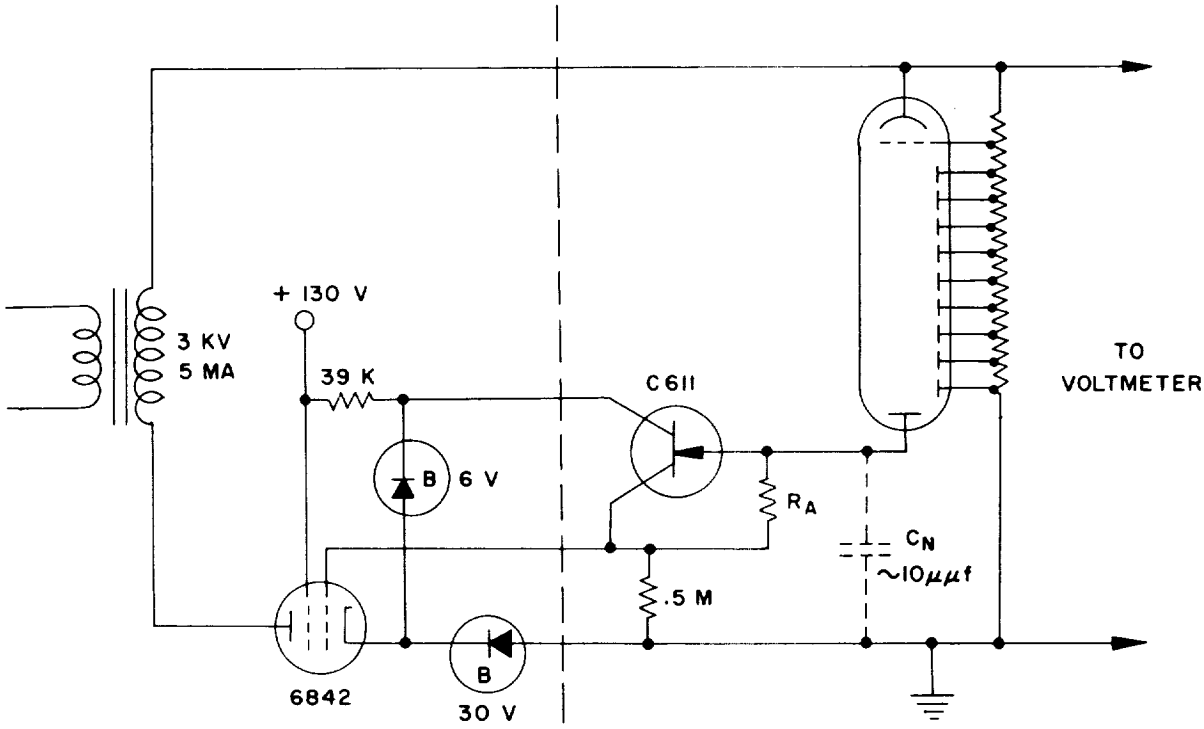

FIGURE 21-2. Improved circuit, using field-effect transistor as impedance converter.

serves as a rectifier to block the reverse cycle of the line voltage. The zener diode provides the positive voltage for the anode of the phototube.

Grid current of the control tube limits the minimum value for the anode current to about 0.5 μ amp. The maximum accelerating voltage is limited by the arc-over voltage of the phototube. An isolation stage between the phototube and the control tube can reduce the grid current limitation and extend the range. A vacuum tube can be used for this isolation stage, but a field-effect transistor offers an advantage. The transistor can be mounted at the phototube socket, minimizing capacitive loading, without adding appreciable heat load. The C611 transistor permits operation at an anode current as low as 0.01 μ amp. The improved circuit, as shown in figure 21-2, incorporates the transistor and uses a high-voltage tetrode as the control tube. This circuit tends to oscillate under certain conditions, but this can be controlled by a small neutralizing capacitor ($C_n \approx 10 \mu\mu f$) between the anode and ground.

Operating the multiplier-phototube with voltage pulses at the line frequency introduces limitations on the frequency of the light source. On the other hand, the frequency selectivity of the photometer can be used to advantage by chopping the light source with a chopper synchronized to the line frequency. This is particularly useful in double-beam systems in which the two beams are alternated at 30 times per second. Alternate photometer-output pulses then represent the separate beams. These output pulses can be sorted with a synchronous switch to charge two capacitors. The voltage difference between these two capacitors represents the difference in light intensity between the two beams. Since the output pulses vary approximately as the logarithm of the light level, the voltage difference between the capacitors varies nearly linearly with the difference in density between the two light signals.

The use of a center-tapped high-voltage transformer and two control tubes provides a photometer which utilizes both the positive and negative swings of the line voltage (fig 21-3). This full-wave circuit is very convenient for use in double-beam systems where the light beams are alternated at 60 times per

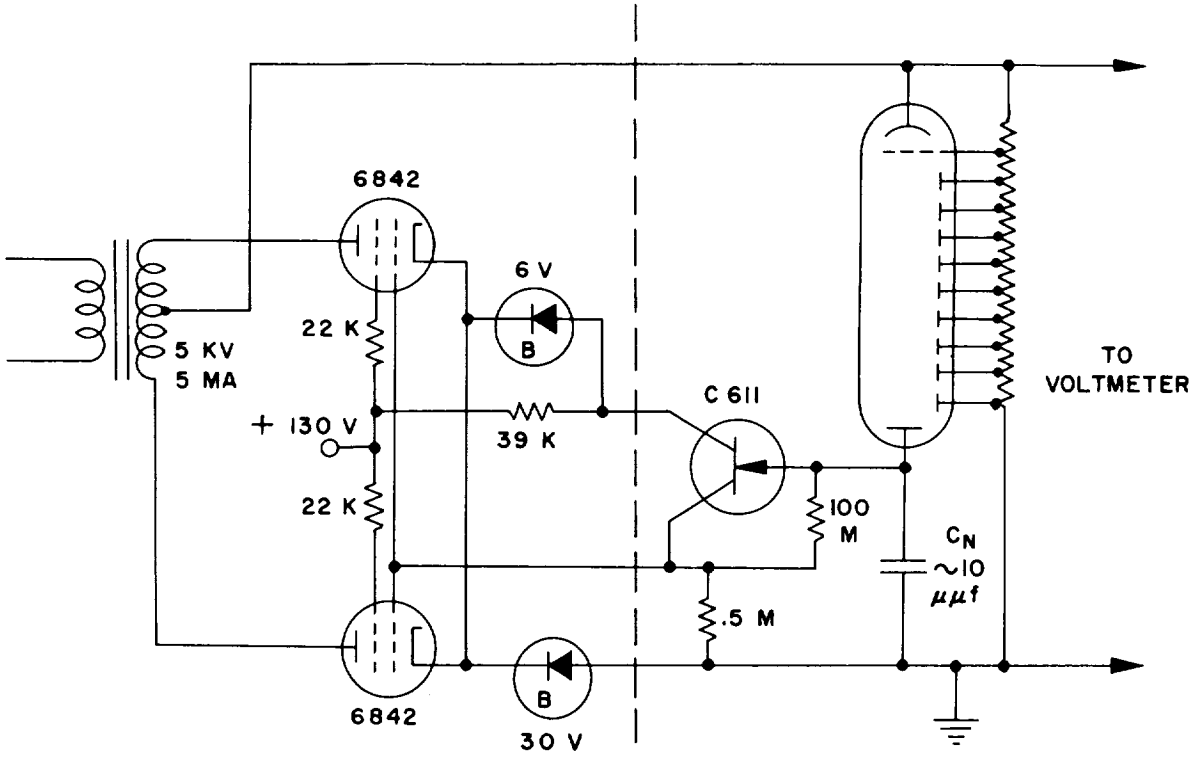

FIGURE 21-3. Full-wave photometer circuit.

second. One of the light beams is synchronized with the positive line pulses and the other with the negative line pulses.

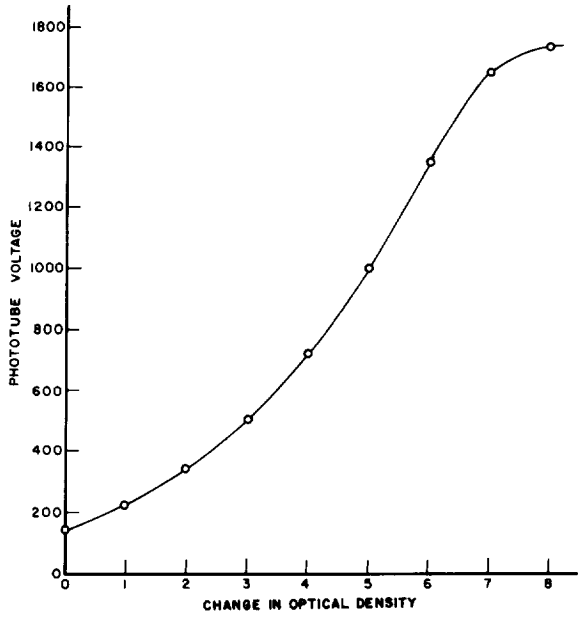

FIGURE 21-4.—Voltage vs. light-level change for circuit of figure 21-3 using 6911 (S1) phototube.

The relationship between the phototube voltage and light level for the full-wave circuit is shown in figure 21-4 for a Du Mont 6911 phototube (S-1 photosurface). The light level is expressed as the change in optical density from an arbitrary zero level of approximately 1×10^{-3} watts. (Optical density $\equiv \log 10\ I_0/I$, where I_0 is the initial intensity and I is the reduced light intensity.) The maximum voltage is limited by the dark current to slightly less than 1800 volts for this tube at a constant anode current of 0.03 μ amp. Over a limited region the relationship between phototube voltage and change in optical density is sufficiently linear for many applications without any further corrections. When needed, an attenuator of adjustable linearity (fig. 21-5) is used. This attenuator with selected zener diodes provides an output voltage which can be adjusted to be linear with change in optical density over a range of at least six decades (fig. 21-6).

The pulse sorting for the full-wave photometer is accomplished with transistor switches triggered by line-voltage pulses using the circuit of figure 21-7. The field-effect transistors are biased to the non-conducting state by the

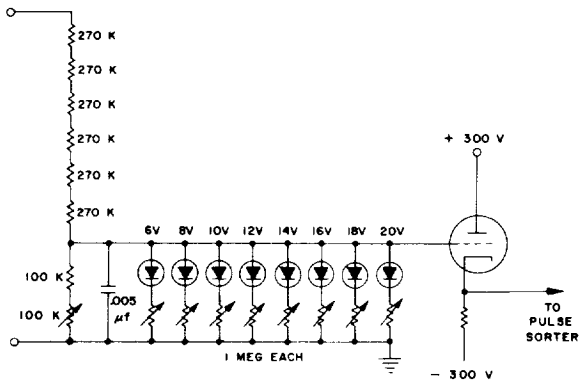

FIGURE 21-5.—Non-linear attenuator.

negative d-c supply regulated to 36 volts by a zener diode. Positive line voltage swings cause one transistor to be turned on, and negative swings cause the other transistor to be turned on. During the on periods the capacitors are charged to the phototube voltage pulse as obtained from the nonlinear attenuator during that period of the cycle. This arrangement requires careful synchronization of three components; the pulse-sorting circuit, the phototube voltage, and optical-beam switch. The pulse-sorting circuit and the photometer are connected to a common supply, so no additional synchronization is required between these two. The most convenient optical-beam switch is a 3600-rpm synchronous motor driving a filter

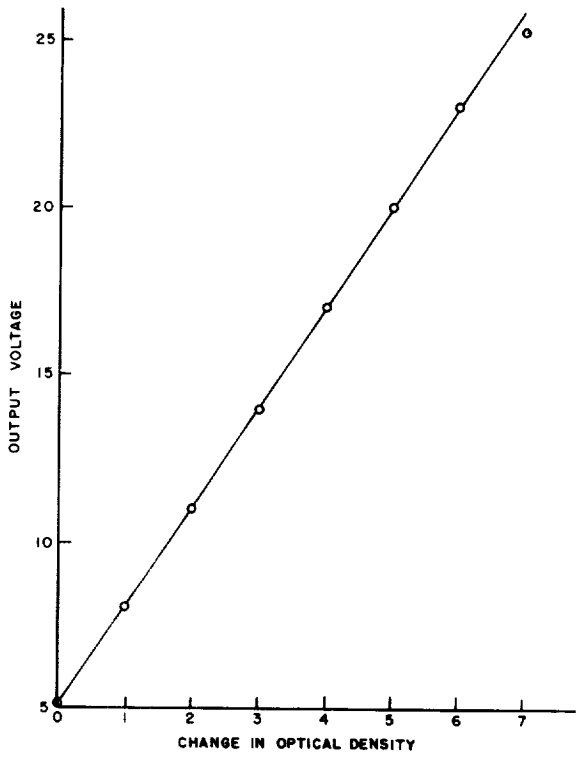

FIGURE 21-6. Voltage vs. light-level change for photometer with logarithmic attenuator.

wheel, rotating sector, or rotating semi-circular mirror. The angular position of the rotating element on the shaft of the motor is determined

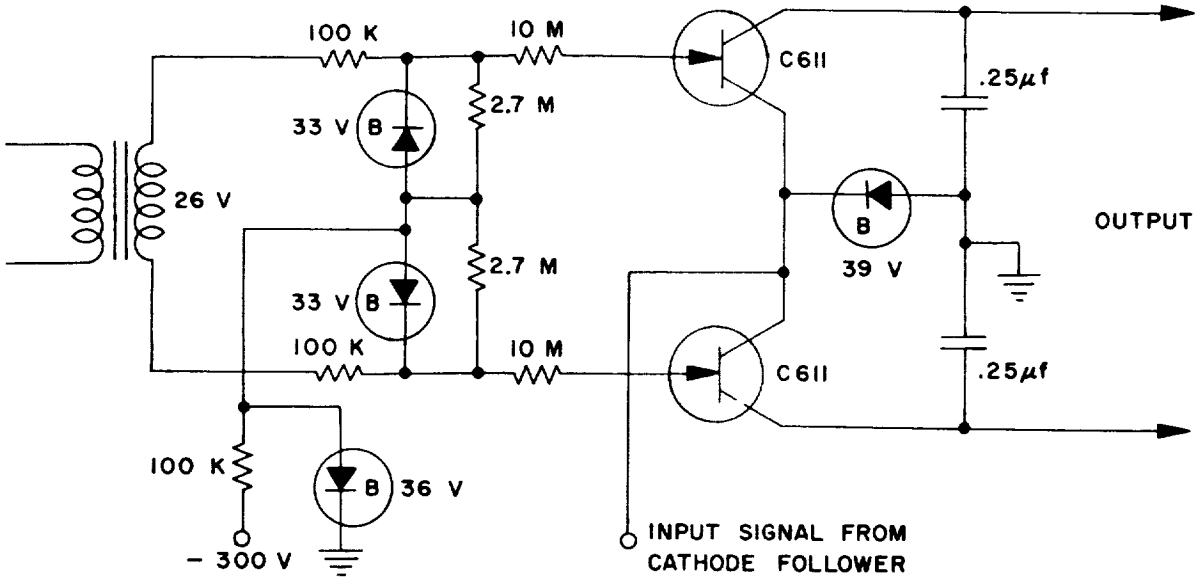

FIGURE 21-7.—Pulse-sorting circuit for the full-wave photometer.

by trial and error to give the proper synchronization with the photometer and pulse sorter. Once this synchronization is established no further adjustment is required. A motor which always locks into synchronization at the same phase position of the line voltage is required.

The difference in voltage appearing across the two capacitors of the pulse-sorting circuit represents the difference in optical density between the two beams of light striking the phototube. This voltage difference is coupled through balanced cathode followers to an electronic recorder of variable sensitivity and response speed. An isolated, variable d-c voltage is introduced in series with the difference voltage to provide a zero offset.

PERFORMANCE

The full-wave photometer has been tested with a Du Mont 6911 and an EMI 9558 phototube. It should work equally well with other multiplier-type phototubes. All the results given in this paper were obtained with a 6911 phototube selected for low equivalent anode-dark-current. The 9558 has a lower equivalent anode-dark-current, giving a greater density range.

The dynamic range of the photometer is demonstrated in figure 21–8, which shows an oscilloscope trace of the photometer output pulses. The central trace shows the voltage obtained when the two beams differ by an optical density of 2.0. The other trace is for two beams differing by an optical density of 6.0 indicating a dynamic range of greater than 6.0.

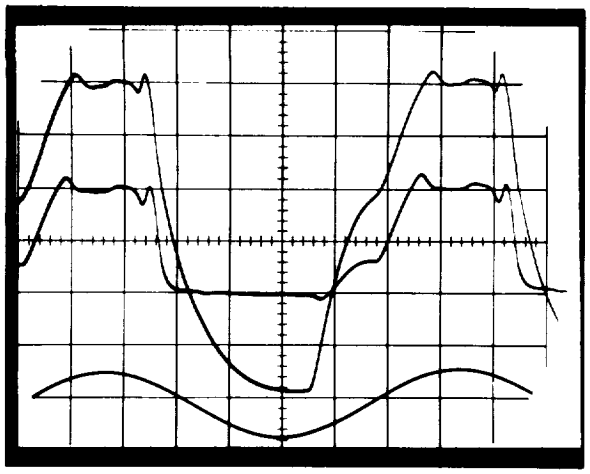

FIGURE 21–8.—Photometer-output voltage. The center trace was obtained with two light beams differing by an optical density of 2.0. The larger trace was obtained with two light beams differing by an optical density of 6.0. The bottom trace is from the line voltage.

The output noise of the photometer was recorded for 3 minutes at two different response speeds (fig. 21–9). The peak-to-peak noise is less than ± 0.001 at maximum response speed and less than ± 0.002 at a response of 5 sec for full-scale travel. Figure 21–10 shows the response to a sudden change in density level at both response speeds. The response of the photometer is faster than that of the recorder, as shown by the response measured with the oscilloscope (fig. 21–11). The photometer gives a full-scale swing in less than 0.1 sec.

Fatigue effects are observed when the light level is changed more than 7 decades. However, the recovery is sufficiently fast that a dynamic range of more than 10 decades was measured, allowing 100 sec for recovery from the maximum light intensity.

The drift of the photometer operating as a dual-beam instrument is less than that equivalent to an optical density change of ± 0.005 per hour. Drift is not likely to be caused by the photometer itself, but by the cathode followers or the zero-offset voltage.

APPLICATIONS

Each of the three versions of this photometer has been used in operating instruments for several months, giving trouble-free performance. The first two circuits are in use on rotating filter-wheel instruments in which two interference filters, rotating at 1800 rpm, serve as fixed wavelength monochromators. The third circuit is used in a double-beam spectrophotometer of the type described by Chance (ref. 2) where two grating monochromators provide separate monochromatic beams. Our spectrophotometer provides for wavelength scanning and recording of absorption differences as distinguished from the point-by-point measurement of the Chance instrument. The wide dynamic range of the full-wave photometer is used to advantage in this spectrophotometer, permitting spectral absorption measurements of dense, light-scattering samples normally considered to be opaque. The spectral absorption

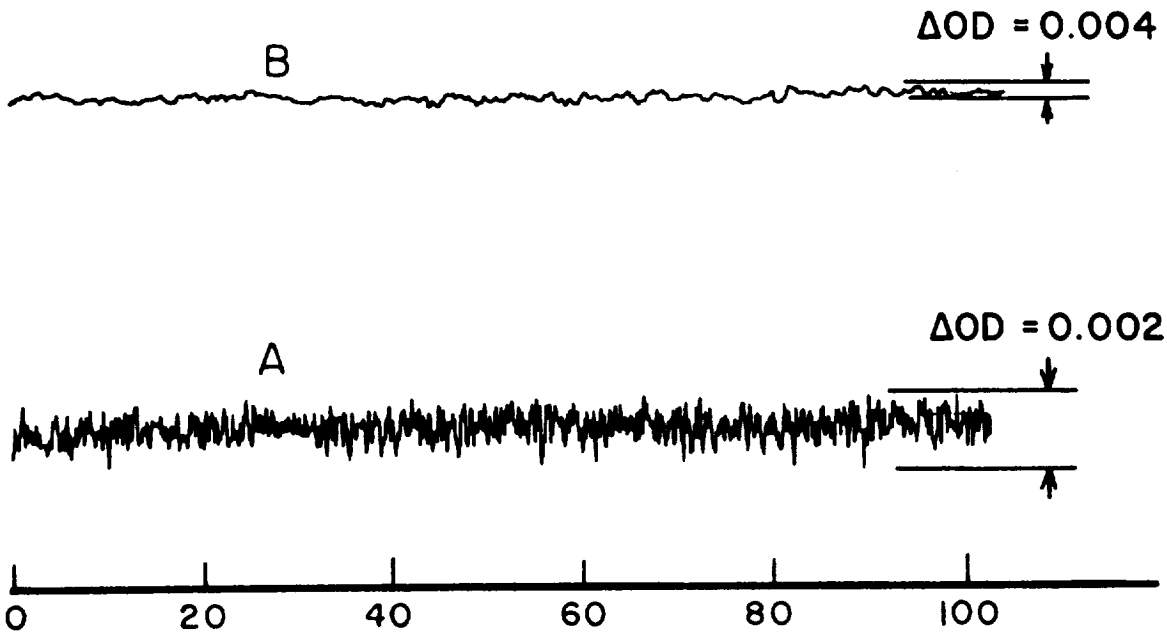

FIGURE 21-9.—Photometer noise: curve A obtained at maximum response speed, curve B obtained at 5.0-second response. ΔOD = change in optical density.

curves of 1.5-cm thick pieces of wood in the 700- to 1000-mμ region are examples (fig. 21-12). Curve A, obtained in a region containing a knot, shows an absorbance greater than 4 for wavelengths below 700 mμ, but an absorbance of only 2 in the 850-mμ region. Well-defined absorption bands are apparent at 920 mμ and 1000 mμ. Both of these bands are undoubtedly overtones of infrared absorption bands. Curve B shows a greater absorbance for the same piece of wood in a region free from knots. The presence of the oil in the knot decreased the scatter loss for curve A, giving lower absorbance. This spectrophotometer is now being used to study pigment changes in a wide range of biological tissues.

The measurement of the spectral properties of filters is another application where the wide-range photometer can be used to advantage. The characteristics of three interference filters

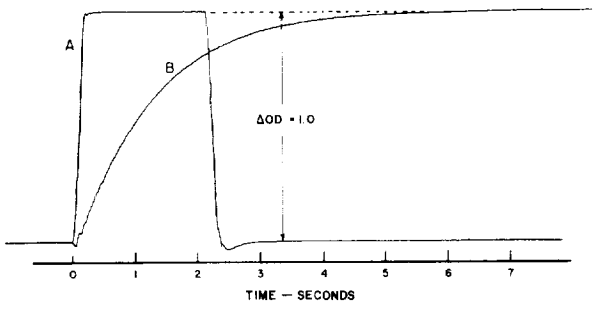

FIGURE 21-10.—Speed of response with recorder: curve A at maximum response speed, curve B at 5.0-second response. ΔOD = change in optical density.

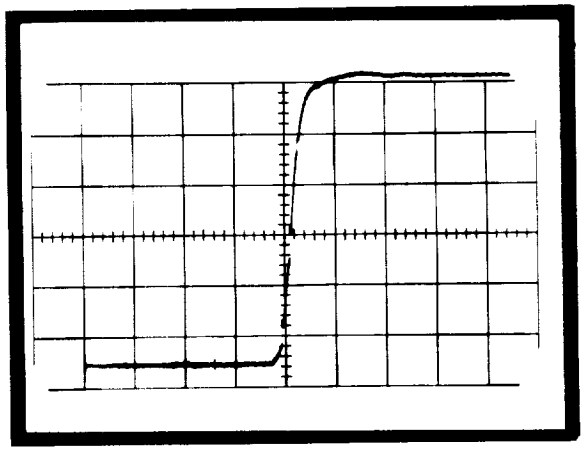

FIGURE 21-11.—Photometer response speed with oscilloscope. Sweep speed = 10 cm/sec.

as shown in figure 21–13 show that filter A has much more of a spike-type transmission band than filters B and C but it also has a long-wavelength transmission band. Filter C has a wider bandwidth and lower transmission at its peak wavelength, but it has a much greater side-band rejection. The sideband rejection of filter C is even greater than shown here. Stray light from the monochromator limits the maximum absorbance.

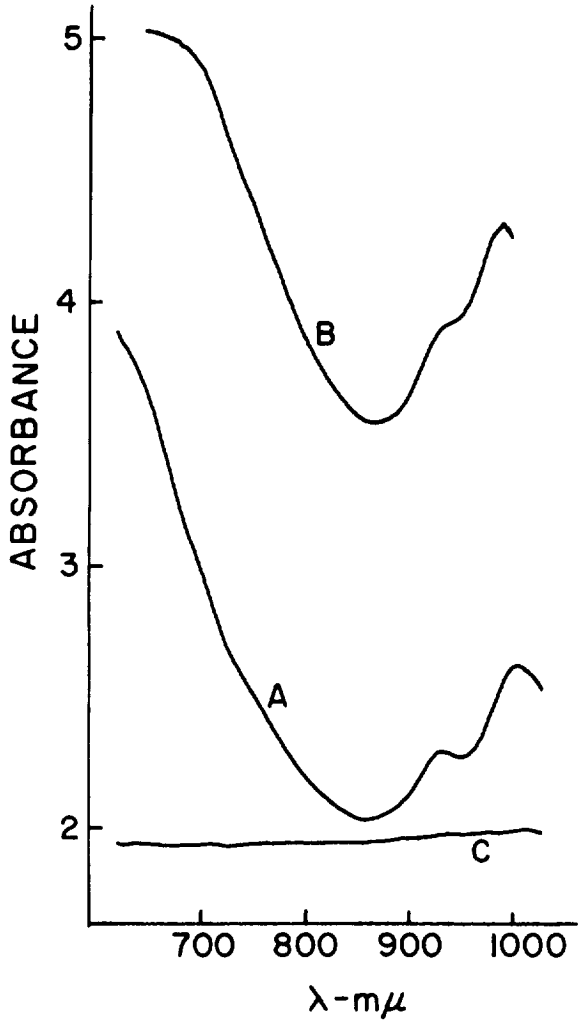

FIGURE 21–12.—Spectral absorption of wood. Curve A is 1.5-cm thick piece of wood containing a knot. Curve B from the same piece of wood in a region without a knot. Curve C, displaced from zero, is the spectral response of the spectrophotometer with no sample; half-bandwidth—30 mμ.

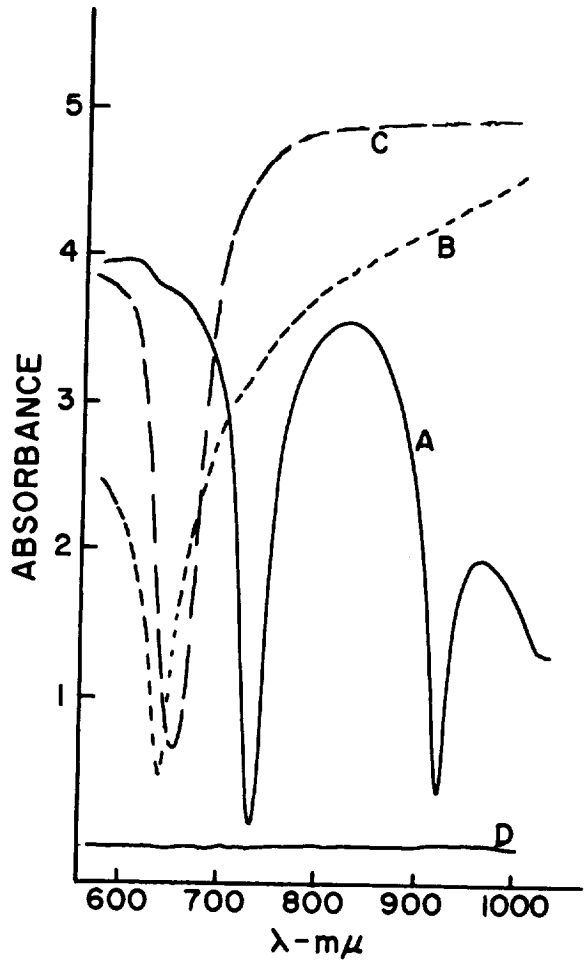

FIGURE 21–13.—Spectral response of interference filters. Curves A, B, and C are from different types of interference filters. Curve D is the spectral response of the spectrophotometer; half-bandwidth—6.7 mμ

REFERENCES

1. NORRIS, K. H.; and BUTLER, W. L.: Techniques for Obtaining Absorption Spectra on Intact Biological Samples. IRE Trans. on Bio-Medical Electronics, vol. BME–8, no. 3, July 1961, pp. 153–159.
2. CHANCE, B.: Rapid and Sensitive Spectrophotometry. I. The Accelerated and Stopped-Flow Methods for the Measurement of the Reaction Kinetics and Spectra of Unstable Compounds in the Visible Region of the Spectrum. Rev. Sci. Instr., vol. 22, no. 8, Aug. 1951, pp. 619–638.

692-146 O—63——15

22—EMISSOMETER, A DEVICE FOR MEASURING TOTAL HEMISPHERICAL EMITTANCE

BY R. SADLER, L. HEMMERDINGER, AND I. RANDO

GRUMMAN AIRCRAFT ENGINEERING CORPORATION, BETHPAGE, NEW YORK

The recent importance of space exploration has created a demand for accurate knowledge of many material properties previously unknown. One area where little data are available is the determination of surface thermal radiation properties at different temperatures. Due to the absence of atmosphere in space, thermal radiation becomes the predominant mode of heat transfer and is especially critical in determining a satellite's thermal balance. For this reason, accurate knowledge of the radiation properties of many newly developed materials is needed to perform a thorough thermal analysis of any spacecraft.

The emissometer described in this paper is a device now being used at Grumman Aircraft Engineering Corporation to measure the total hemispherical emittance of many new materials to be used in the fabrication of the Orbiting Astronomical Observatory (OAO).

DESCRIPTION

The emissometer is based on the principle of a guarded heater and is shown in figure 22–1. It consists of a 2½-in., disk-shaped specimen heater which sits inside of a larger cup-shaped heater or guard, and is thermally insulated from it. The guard provides an isothermal surrounding for the test specimen and its heater so that heat is lost only by radiation from the specimen surface which faces the cold wall in the vacuum chamber (fig. 22–2).

The guard heater cup is constructed of heavy aluminum to prevent temperature gradients along its inside surface, and fiberglass legs support the specimen heater so that conduction errors are minimized. The test specimen, a 2½-in. diameter flat disk, is attached to the heater with a thin layer of silicone grease to insure good thermal contact. The heating elements of the specimen and guard heaters are constructed of stainless steel jacketed Nichrome wire which has a very low resistance change with temperature. Separate power controls to the specimen and guard heaters make independent temperature adjustments possible and allow the heat lost from the specimen surface to be controlled.

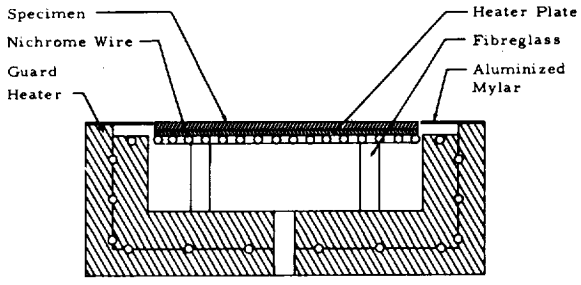

FIGURE 22–1.—Cross section of emissometer.

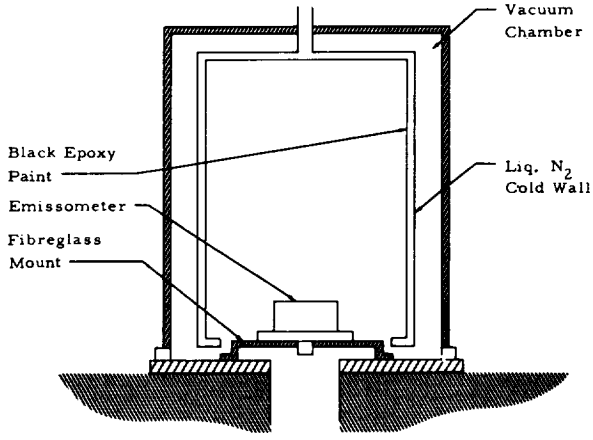

FIGURE 22–2.—Emissometer in bell jar.

All thermopiles and thermocouples are made of calibrated copper and constantan wire to insure adequate sensitivity in the range of test temperatures. Temperature differences between the guard and specimen heater are detected with a 6-junction thermopile which activates a relay system supplying pulses of power to a specimen heater. This system supplies power to the heater when it is colder than the guard, and shuts off just before the heater reaches guard temperature. The early shut-off is in anticipation of system temperature overshoot. In this manner the specimen heater temperature is maintained within 1° F of the guard temperature. The power supplied to the specimen heater is measured only after a steady-state condition is achieved between the guard and its surroundings. The amplitude of each power pulse is computed by measuring the current flow in the heater circuit and the heater resistance. Clocks record the amount of time the power is supplied to the heater, as well as the total duration of the steady-state test period. The average power supplied to the specimen during the steady-state portion of the test is obtained by multiplying the amplitude of the power pulse by the total fraction of time the power was supplied.

Thermocouples placed on the inside surface of the guard and on the back of the specimen heater provide a check on the relay system and allow the specimen temperature to be read. These thermocouples are monitored on a Bristol recording potentiometer so that a permanent record of the specimen and guard temperatures is obtained for each test. All thermocouple, thermopile, and heater leads are wrapped several times within the guard cavity and physically fastened to it to reduce conduction losses through the wires.

OPERATION

The emissometer lends itself readily to the measurement of so-called "space materials" because it can be operated in a vacuum chamber without difficulty. For such applications the assembled emissometer with test specimen is placed in a vacuum chamber equipped with a black epoxy-painted liquid nitrogen cold wall (fig. 22–2). The guard heater power is set to a predetermined value to produce a desired equilibrium temperature and the configuration is allowed to come to equilibrium. The specimen power relay system keeps the specimen heater temperature within 1° F of the guard temperature at all times. When a steady-state condition is attained, all of the power supplied to the specimen heater must be lost as radiation from the specimen surface to the cold wall. Therefore, from an accurate measurement of the power supplied to the specimen heater, the quantity of heat emitted from the test surface to its surroundings can be calculated. A comparison of this quantity with the amount of heat emitted by a "black" surface of the same area determines the hemispherical emittance of the specimen. The emittance (ϵ) is thus calculated knowing the resistance of the specimen heater (R_s), the current supplied to the heater (I_s), the temperature of the specimen surface (T_s), and the temperature of the cold wall (T_w), and assuming no radiation is reflected from the black wall back to the specimen. It is expressed as

$$\epsilon = \frac{I_s^2 R_s}{\sigma(T_s^4 - T_w^4)A_s}$$

DATA

All the data presented were obtained with the emissometer placed in a vacuum chamber evacuated to a pressure of 5×10^{-6}mm of mercury to minimize losses due to atmospheric convection and conduction. The first few tests were conducted with a thermocouple attached to the edge of the specimen surface to determine the magnitude of the temperature drop across the silicone grease interface. These tests indicated that the gradient was negligible. It is suggested, however, that a similarly placed thermocouple be used when the substrate of a test specimen has low thermal conductivity.

The measurements of white porcelain enamel presented in table 22–I, were made during the early development stages of the emissometer and show a shift from the UCLA [1] integrated spectral data plotted in figure 22–3. The data for the porcelain enamel and 2014 T6 anodized aluminum (figure 22–4) were made without automatic temperature control. For these tests the 1° F temperature difference was maintained by manual adjustment which seriously limited the testing time available. The use of

[1] University of California at Los Angeles.

TABLE 22–I.—*Emittance Data on Varius Materials To Be Used in Orbiting Astronomical Observatory*

Sample	Automatic Control	Temp., °R	E.
5-mil Ferro white porcelain enamel on 2014 aluminum		557	0. 714
		465	. 775
		423	. 798
		372	. 682
Alcoa lighting sheet S.I. grade	X	574	. 712
		560	. 785
		467	. 745
		375	. 720
Anodized 2014 T6 aluminum		574	. 595
		513	. 657
		468	. 675
		408	. 582
		352	. 626
Aluminum side of aluminized Mylar		600	. 0466
Gold on fiberglass:			
R, Ω* Condition of Fiberglass			
2 smooth		659	. 0779
2 smooth	X	580	. 0798
2 sandblasted	X	600	. 288
2 smooth, degreased	X	603	. 0616
5 smooth fiberglass	X	599	. 0548
5 smooth fiberglass	X	597	. 0615
1 sandblasted fiberglass	X	610	. 222
1 sandblasted fiberglass	X	610	. 224

* Resistance in ohms used to measure thickness of gold.

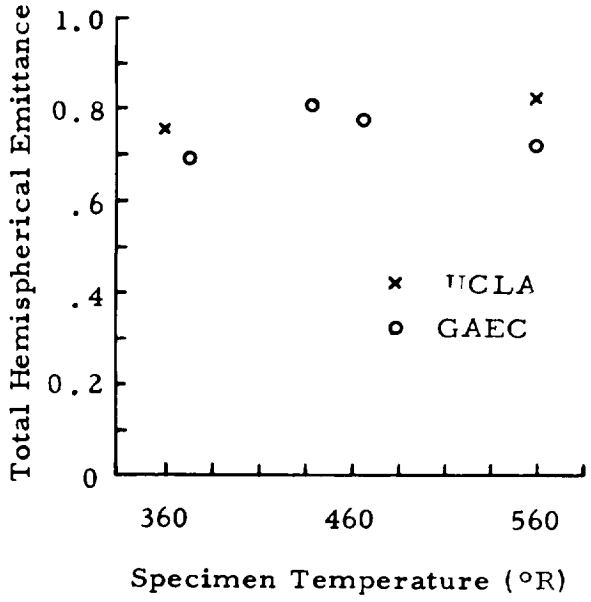

FIGURE 22–3.—Emittance of 5-mil Ferro enamel on 2014 aluminum.

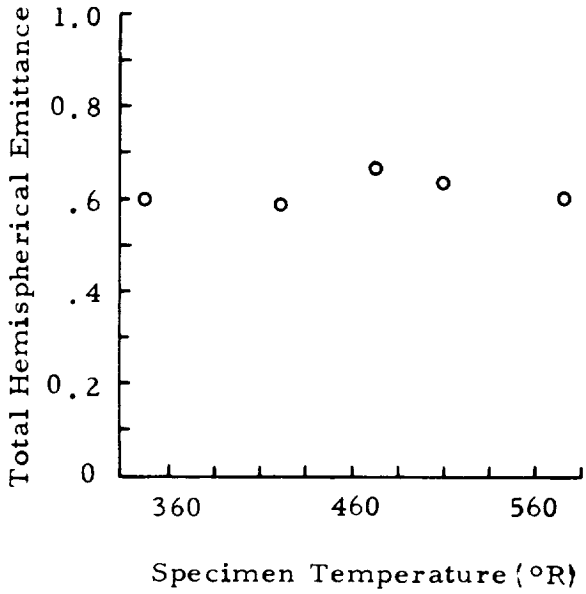

FIGURE 22–4.—Emittance of anodized 2014 T–6 aluminum.

an automatic temperature control has made longer testing times possible with a subsequent improvement in the reproducability of results. A test of S.I. grade Alcoa lighting sheet was made with the automatic temperature control installed and a comparison to UCLA integrated spectral data is shown in figure 22–5.

Measurements of 24-karat gold, vacuum deposited on various fiberglass substrates in various thicknesses have also been made. The emittance values show a large spread due to the condition of the substrate surface (fig. 22–6). Data on other materials are shown in figures 22–7 to –9.

CONCLUSION

In its present state of development, the emissometer system allows one sample per day to be tested. The speed of operation and simplicity of data reduction make the system particularly suitable for production supervision and quality control of thermal radiation coatings. Aside from speed, the system has the advantage of measuring total hemispherical emittance regardless of the spectral characteristics or diffuseness of the test surface. In addition, the measurements are carried out under a simulated space environment so that data are obtained under the actual conditions which prevail in a space vehicle.

The materials already tested and subsequent materials to be tested are for use in the manufacture of the Grumman Aircraft Engineering Corporation Orbiting Astronomical Observatory. The emissometer is playing a large role in the development and quality control of the radiation surfaces making up the thermal control system of this satellite.

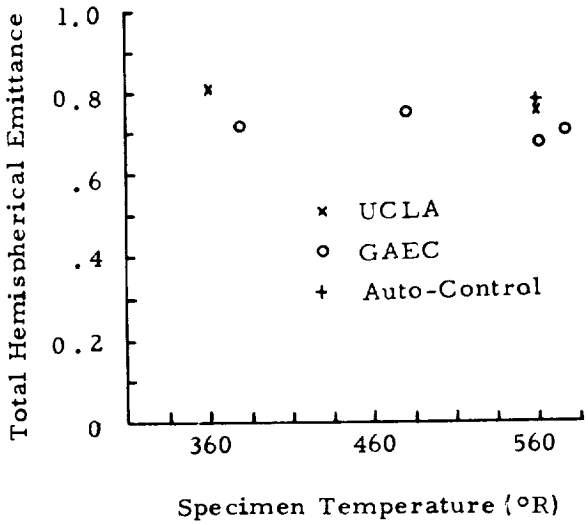

FIGURE 22–5.—Emittance of Alcoa S. I. Alzak.

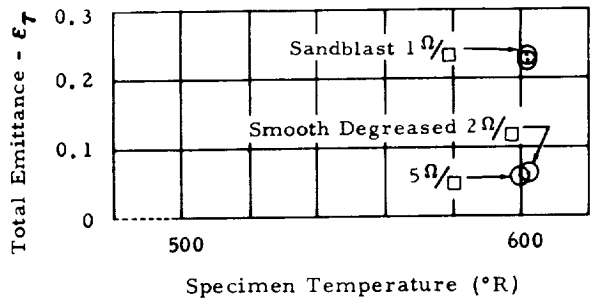

FIGURE 22–6.—Effect of temperature on total emittance of gold on fiberglass.

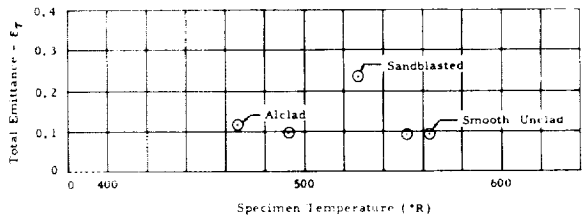

FIGURE 22–7.—Effect of temperature on total emittance of Alodined 7075 T6 aluminum.

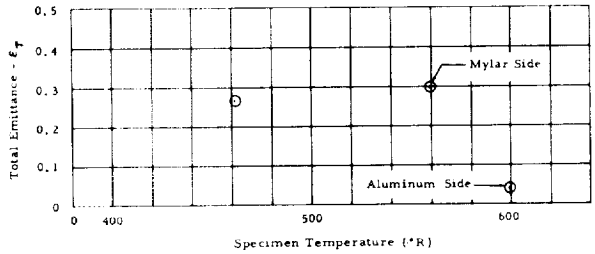

FIGURE 22–8.—Effect of temperature on total emittance of NRC-2 insulation in various configurations.

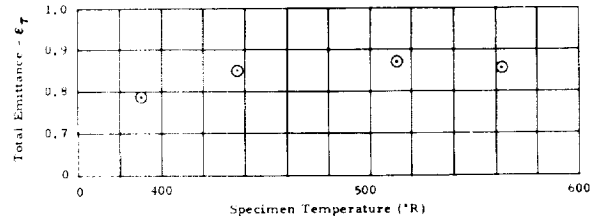

FIGURE 22–9.—Effect of temperature on total emittance of Martin Hardcoat Anodize on 7075 T-6 unclad aluminum.

APPENDIX—ERROR ANALYSIS OF EMISSOMETER

LIST OF SYMBOLS USED

ϵ	Total hemispherical emittance
Q	Heat flow, Btu/hr
σ	Stefan-Boltzmann constant, Btu/hr-ft²-°R⁴
C	Conversion factor=3.414 Btu/hr/watt
T	Absolute temperature, °R
A	Area, ft²
k	Thermal conductivity, Btu/hr-ft²-°R/ft
l	Length, ft
I	Electric current, amp
R	Electric resistance, ohms
Ω	Resistance (used to measure thickness of vapor-deposited gold), ohms

Subscripts

H	Specimen heater
G	Guard heater
s	Specimen
W	Liquid nitrogen cold wall
E	Error introduced by nonisothermal conditions

Notes

The Btu used in all calculations is the mean Btu defined as 1054.8 joules.

The wall temperature used in all calculations is the boiling temperature of nitrogen at 1 atmosphere (140° R).

A vacuum of 5×10^{-6} mm of mercury was maintained during all tests to reduce convection losses to a minimum.

Fiberglass Heater Supports

Dimensions: 0.030 x 0.625 x 0.25 in.

$$\frac{A}{l}=\frac{0.0075}{0.625}=0.012 \text{ in.}$$

$$\frac{A}{l}=0.001 \text{ ft.}$$

$$k \text{ for fiberglass}=0.29 \frac{\text{Btu}}{\text{ft}^2\text{-hr°-R-ft}^{-1}}$$

$$\left(\frac{kA}{l}\right)_{\text{total}} \text{ for 3 legs}=3\times0.29 \frac{\text{Btu}}{\text{hr-ft}^2\text{-°R-ft}^{-1}} \times0.001 \text{ ft}$$

$$=0.0009 \frac{\text{Btu}}{\text{hr-°R}}$$

Thermocouples and Thermopile

Wire diameter=0.01 in.
Cross section=0.0000785 in.²

Length of leads=20 in.; $\frac{A}{l}=0.000003925$ in.

Length of thermopile elements=6 in.;

$$\frac{A}{l}=0.00001308 \text{ in.}$$

Conductance per thermocouple

$$=(k_{\text{copper}}+k_{\text{constantan}})\frac{A}{l}$$

$$=\left(226 \frac{\text{Btu}}{\text{ft}^2\text{-hr-°R-ft}^{-1}}+80 \frac{\text{Btu}}{\text{ft}^2\text{-hr-°R-ft}}\right) \times\frac{3.93}{12} \text{ ft}\times10^{-6}$$

$$=0.000100 \frac{\text{Btu}}{\text{hr-°R}}$$

$$\text{Conductance of thermopile}=3\times25.5 \frac{\text{Btu}}{\text{hr-°R-in.}} \times13.1\times10^{-6} \text{ in.}$$

$$=0.001 \frac{\text{Btu}}{\text{hr-°R}}$$

Conductance of 20-in. copper thermopile leads:

$$=2\times226 \frac{\text{Btu}}{\text{hr-ft}^2 \text{ (°R/ft)}}\times\frac{1 \text{ ft}}{12 \text{ in.}}\times3.93\times10^{-6} \text{ in.}$$

$$=0.000148 \frac{\text{Btu}}{\text{hr-°R}}$$

Total conductance of 2 thermocouples and thermopile

$$=0.00135 \frac{\text{Btu}}{\text{hr-°R}}$$

Conductance of Heater Leads

Wire diameter = 0.023 in.
Cross section area = 0.00049 in.^{2}
Lead length = 20 in.

$$k = 226 \frac{\text{Btu}}{\text{hr-ft}^2\ ^\circ\text{F/ft}}$$

$$\frac{kA}{l} = 18.8 \frac{\text{Btu}}{\text{hr-in.}\ ^\circ\text{R}} \times \frac{0.00049\ \text{in.}^2}{20\ \text{in.}}$$

$$= 0.000461 \frac{\text{Btu}}{\text{hr-}^\circ\text{R}}$$

For 2 leads $\frac{kA}{l} = 0.000922 \frac{\text{Btu}}{\text{hr-}^\circ\text{R}}$

Total Heat Exchange by Conduction

$$\left(\frac{kA}{l}\right)_{\text{tot}} = 0.0009 \frac{\text{Btu}}{\text{hr-}^\circ\text{R}} + 0.00135 \frac{\text{Btu}}{\text{hr-}^\circ\text{R}} + 0.000922 \frac{\text{Btu}}{\text{hr-}^\circ\text{R}}$$

$$= 0.00317 \frac{\text{Btu}}{\text{hr-}^\circ\text{R}} = 0.000930 \frac{\text{watts}}{^\circ\text{R}}$$

For a gradient of 1° F the total heat exchange is 0.000930 watts.

Radiant Heat Exchange Between Specimen Heater and Guard

For a body completely enclosed by another body a good approximation to the net heat exchange is given by:

$Q_{\text{net}} = E_{H\to G}\sigma A_H(T_H^4 - T_G^4)$; and $E_{H\to G} = \dfrac{1}{\frac{1}{\epsilon_H} + \left(\frac{1}{\epsilon_G} - 1\right)\frac{A_H}{A_G}}$

If we consider the rear surface of the specimen heater which sees only the guard, this expression is a good approximation to the net heat flow from the specimen heater to the guard heater due to radiation.

Calculation of Radiation Error and Total Error

$A_H = \pi(1.25\ \text{in.})^2 = 4.90\ \text{in.}^2$

$A_G = (1.375)^2 + (2.75)(0.875) = 13.5\ \text{in.}^2$

$\epsilon_H = 0.05$ (aluminized Mylar); $\epsilon_G = 0.1$ (machined aluminum)

$$E_{H\to G} = \frac{1}{\frac{1}{0.05} + \left(\frac{1}{0.1} - 1\right)\frac{4.90}{13.5}} = \frac{1}{23.27}$$

$$E_{H\to G} = 0.0429$$

$$E_{H\to G}\sigma A_s = \frac{(0.0429)(0.174)(0.0341)}{3.41 \frac{\text{Btu/hr}}{\text{watt}}} \frac{\text{Btu}}{\text{hr-}^\circ\text{R}^4} \times 10^{-8}$$

$$= 0.746 \times 10^{-12} \frac{\text{watt}}{^\circ\text{R}^4}$$

By dividing the quantity $Q_E/\sigma A_s(T_s^4 - T_W^4)$ by the emissivity of the specimen to be tested and multiplying the result by 100, the percentage error due to a temperature difference of 1° F between the heater and guard is obtained.

Temperature Measurement Error

The use of calibrated thermocouple wire reduces the possible temperature error to ±½° F. If we called T_s' the measured temperature and T_s the actual temperature we have:

$$\epsilon_s = \frac{I_s^2 R}{(T_s^4 - T_W^4)A_s},$$

$$\epsilon_s' = \frac{I_s^2 R}{(T_s'^4 - T_W^4)A_s}$$

$$\%\ \text{error} = \frac{\epsilon_s' - \epsilon_s}{\epsilon_s} \times 100 = \left(\frac{\epsilon_s'}{\epsilon_s} - 1\right) + 100$$

$$= \left(\frac{T_s^4 - T_W^4}{T_s'^4 - T_W^4} - 1\right) \times 100$$

TABLE 22-II.—*Temperature Data for Heater and Guard*

T_s (°R)	T_G (°R)	$Q_{H\to G}$ (watts)	Q_E (watts)*	$\frac{Q_E}{A_s\sigma(T_s^4 - T_W^4)}$
560	559	0.000403	0.00133	0.000785
460	459	.000224	.00115	.00144
360	359	.00118	.00105	.00368

*Conduction + radiation.

This quantity is calculated below for temperatures of 560° R, 460° R, and 360° R.

T_s(°R)	T_s'(°R)	$\left(\frac{T_s^4 - T_W^4}{T_s'^4 - T_W^4}\right)$	% Error
560	559	1.01	1
460	459	1.01	1
360	359	1.01	1

From these data we may conclude that an error of 1° F in a temperature reading will cause a 1% error in the emittance calculation for the range of temperatures considered.

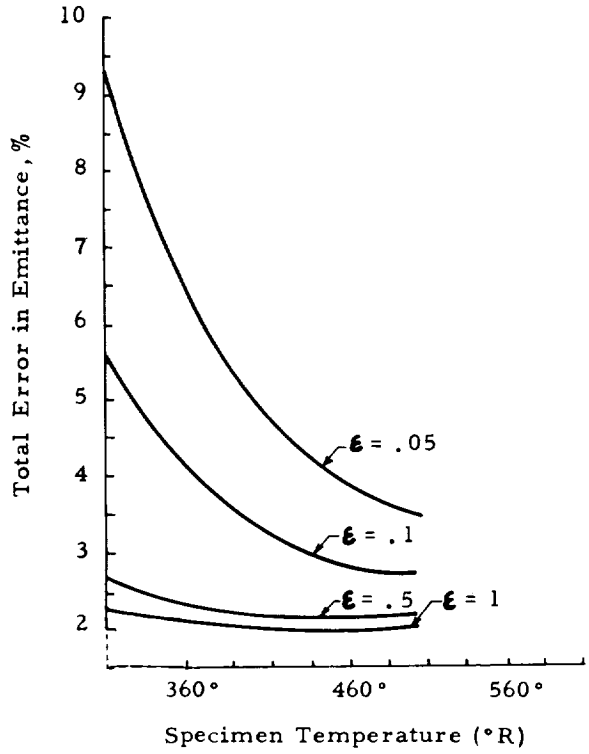

FIGURE 22-10.—Effect of temperature on total percentage of error.

Errors in Power Measurement

The specimen heater resistance is measured accurately to 0.01%, and the resistance of the Nichrome heater element is very insensitive to temperature changes in the range of test temperatures. Therefore, it is assumed that no error is introduced into the emittance calculation from the value used for the specimen heater resistance. The voltage source for the heater is a large storage battery which is frequently checked to ensure its output. It will be assumed therefore that the current flow through the heater remains constant during the test and the only error introduced into the power calculation is due to erroneous amperage readings. The ammeter used in the emissometer system is a dual range (250–500 ma) Weston d-c milliammeter. The instrument sensitivity is ±¼% of full scale so that the maximum error which can be read is ±1.25 ma. The usual current setting for a test is 300 ma so that an error of 0.425% is possible in the current reading which produces an error of $(1.00425)^2 \times 100 = 0.9\%$ in the emittance calculation.

Thus, there is a fixed error of 1.9% due to instrument inaccuracy to which must be added any error due to temperature differences between the specimen heater and the guard heater. The total percent error as a function of specimen temperature is shown in figure 22-10 for specimen emittance of 0.05, 0.10, 0.50 and 1.00. From this figure it is obvious that the error is largest when specimens having low emittance are tested at low temperatures.

23—LOW-TEMPERATURE TOTAL EMITTANCE CALORIMETER

BY R. N. SCHMIDT AND J. E. JANSSEN

HONEYWELL RESEARCH CENTER, HOPKINS, MINNESOTA

Apparatus consisting of an evacuated chamber, liquid nitrogen-cooled thermopile, and sample heater, for measuring total hemispherical emittance in the range $-100°$ to $+200°$F is described. The thermopile is calibrated with the aid of a blackbody, and the emittance of a specimen is computed from the heat balance at the thermopile surface. Hemispherical values are obtained by locating the sample close to the thermopile so that is sees the sample through a solid angle of nearly 2π steradians. A theoretical error analysis indicates a maximum uncertainty of $\pm 3.25\%$, but comparative measurements indicate an experimental error of only $\pm 2\%$.

Radiation property values are becoming increasingly more important with the recent advances in space research. The absence of an atmosphere in space eliminates convection and and conduction as modes of heat transfer and leaves radiation or possibly mass ejection as the only means for the transfer of heat to or from spacecraft. When evaluating the heat radiated from a surface, the total hemispherical emittance of the surface at its temperature is required. Because manned spacecraft will be operated at near room temperature there is a great need for an accurate method of determining total hemispherical emittance at these relatively low temperatures.

APPARATUS

Figure 23–1 shows a schematic of an apparatus which has been used to measure total hemispherical emittance over the temperature range $-100°$ to $+200°$ F with an estimated maximum uncertainty of $\pm 3.25\%$. The design consists of a cooled detector (Brown radiamatic thermopile) in an evacuated cooled enclosure. The sample is held in a heated sample holder suspended from the cover just above the thermopile. The enclosure is evacuated to 10^{-5} mm of Hg or lower to eliminate free convection and gaseous conduction. The walls and bottom of the enclosure, as well as the detector, are cooled with liquid nitrogen to reduce background radiation. The sensor sees only the samples or the walls of the enclosure. The shape factor from sensor to sample is 0.988 leaving 0.012 for the shape factor from sensor to walls. A short collimating tube is employed

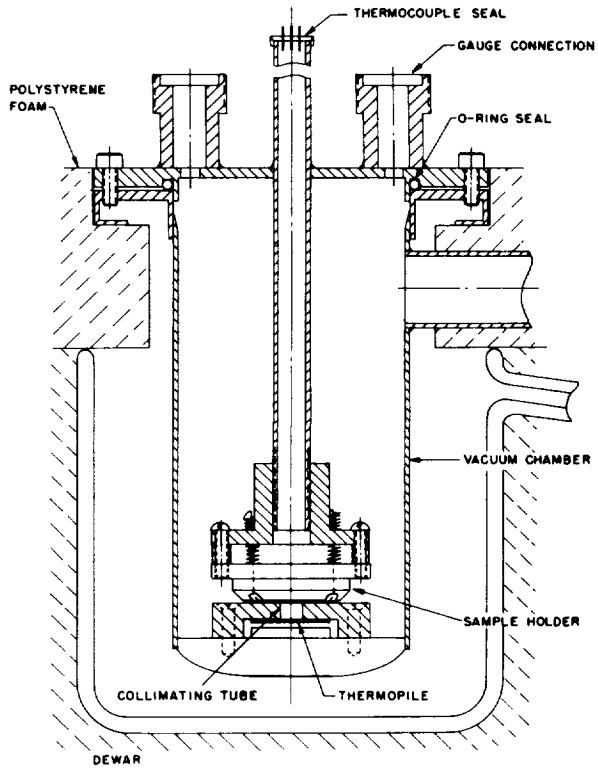

FIGURE 23–1.—Total emittance calorimeter.

between the sample and thermopile to increase the distance between them and yet maintain a high shape factor between the detector and sample. The increased distance is needed to assure no direct contact between the sample and thermopile due to warpage of the thermopile leads, and to decrease the possibility of conduction in the gas layer if the vacuum were to be less than expected.

The collimating tube arrangement facilitates easy installation of the thermopile and provides a heat sink mounting for the thermopile. It also shields the thermopile cold junctions. The collimating tube is made of highly polished copper with a reflectance of 98% in the infrared. Because the reflectance is less than 1.00, a small error is introduced by the collimating tube. This error is discussed in some detail later.

The sample holder is made of copper and contains a resistance heater to maintain the sample at the desired temperature. Three spring clips are used to hold the sample in place. The sample holder is suspended from the cover with a stainless steel tube. Provisions are made for adjusting the sample holder height. This enables the measurement of samples varying in thickness and yet maintaining a high shape factor for all samples. Samples each 1⅛ inch in diameter and approximately ⅛ inch thick are presently used. The samples must be flat and smooth on the back side to assure good thermal contact between the sample and the sampleholder.

Since the measurements are made in a vacuum of about 10^{-6} mmHg the samples must be able to tolerate these conditions at the desired measurement temperatures. Excessive outgassing of a sample produces condensation on the thermopile and an error in the measurement.

The sample surface temperature is measured with two 40-gauge copper-constantan surface thermocouples. The junction of each is soldered to a small piece of copper shim stock. This thin copper plate is held down with the spring clips which are also used to hold the sample (fig. 23–2) in the sample holder. Because the sample holder contained the heater and, therefore, was hotter than the sample, the surface thermocouples were insulated from the sample clips by two thicknesses of fiberglass paper. A

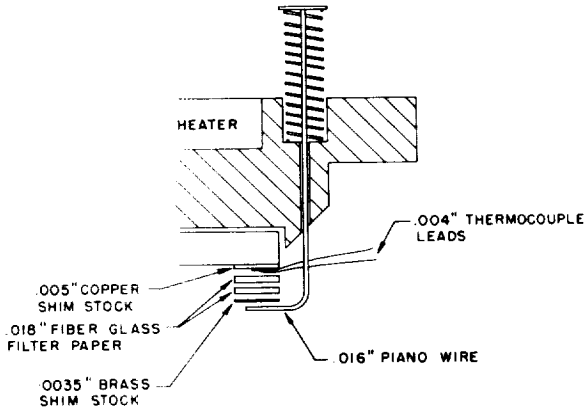

FIGURE 23–2.—Surface thermocouple installation.

piece of polished spring brass shim stock was placed between the sample clip and the fiberglass paper to prevent crushing of the paper and also to reduce the emittance at that point. In order to check the surface temperature measurement, the surface thermocouples were compared to a thermocouple imbedded in a copper sample painted with black paint. They all agreed within 1° F; therefore, it is quite safe to estimate the uncertainty of the sample surface temperature measurement to be within ±1.5°.

The apparatus is calibrated by replacing the sample and sample holder with a blackbody. The blackbody consists of a thick-walled copper tube with a roughened surface coated with Parson's optical black lacquer. A calibration curve was determined by varying the blackbody temperature over the necessary range. Figure 23–3 shows the calibration curve.

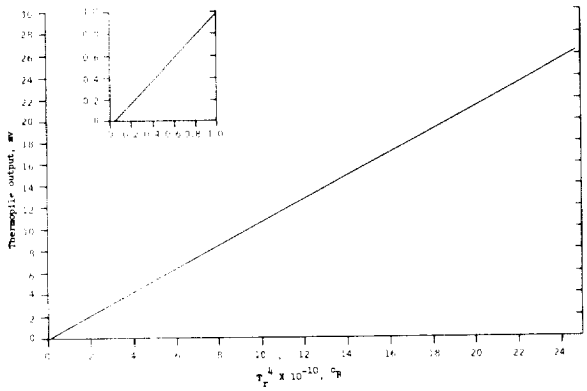

FIGURE 23–3.—Blackbody calibration.

ANALYSIS

The equation for calculating the emittance of the sample is derived from a radiation heat balance for the surface of the sensor. The energy radiated from the specimen to the detector is

$$Q'_{s-d} = \epsilon_s A_s F_{sd} \sigma T_s^4 \quad (1)$$

where:

σ Stefan Boltzmann constant
ϵ_s emittance of sample
A_s area of sample
F_{sd} shape factor from sample to detector
T_s absolute temperature of sample.

Energy radiated from the detector and background to the sample and reflected back to the detector also must be considered. This energy can be estimated by the following equation:

$$Q''_{s-d} = \epsilon_d \rho_s A_s F_{sd} \sigma T_d^4 \quad (2)$$

where:

ϵ_d emittance of detector
T_d absolute temperature of detector
ρ_s reflectance of sample for incident energy from the detector.

This equation assumes that

$$\epsilon_d T_d^4 = \epsilon_b T_b^4$$

where:

ϵ_b emittance of background
T_b absolute temperature of background.

This assumption is very good for the low emittance samples ($\epsilon = 0.10$). However, for a 0.50 emittance sample $\epsilon_d T_d^4 \cong 2\epsilon_b T_b^4$ and for 0.85 emittance samples $\epsilon_d T_d^4 \cong 3\epsilon_b T_b^4$. Nevertheless, this assumption causes less than 0.25% error in the final emittance value. A small amount of background radiation falls directly on the detector, since the sample does not completely fill the hemisphere of space above the detector ($F_{ds} \pm 1$). This energy is estimated by

$$Q_{b-d} = \epsilon_d A_b F_{bd} \sigma T_d^4 \quad (3)$$

where:

A_b area of background seen by detector
F_{bd} shape factor from this area to detector.

This equation also assumes $\epsilon_d T_d^4 = \epsilon_b T_b^4$ which causes less than 0.02% error in the final emittance value for any sample. The energy radiated by the detector is

$$Q = \epsilon_d A_d \sigma T_d^4 \quad (4)$$

One more energy source must be considered: the energy which is emitted from the sample and reflected by the detector back to the sample and then reflected back to the detector. Since the detector is nearly black, only this first re-reflection need be considered. This energy is especially important for the low-emittance samples where the reflec ance of the sample is quite high ($\rho_s \cong 0.90$). Considering the shape factors involved, about one half of the energy reflected by the detector comes back to the detector. The detector is painted with Parson's optical black lacquer, which was measured and found to have an emittance of 0.977; the literature states the emittance to be 0.98. Therefore, we will assume the reflectance of the detector to be 0.02. This energy is handled by multiplying Q'_{s-d} by $(1+0.01\ \rho_s)$. This correction factor is quite small and does not affect the final emittance value appreciably.

Assuming the reciprocity relationship holds,

$$A_s F_{sd} = A_d F_{ds}$$

and

$$A_b F_{bd} = A_d F_{db} = A_d (1 - F_{ds})$$

the net radiation to the detector is

$$\begin{aligned} Q_{net} &= (1+0.01\rho_s) Q'_{s-d} + Q''_{s-d} + Q_{b-d} - Q_d \\ &= (1+0.01\rho_s)\sigma\epsilon_s A_d F_{ds} T_s^4 + \sigma\epsilon_d \rho_s A_d F_{ds} T_d^4 \\ &\quad + \sigma\epsilon_d A_d (1 - F_{ds}) T_d^4 - \sigma\epsilon_d A_d T_d^4 \end{aligned}$$

Rewriting

$$\frac{Q_{net}}{\sigma A_d F_{ds}} = (1+0.01\rho_s)\epsilon_s T_s^4 + \epsilon_d \rho_s T_d^4 - \epsilon_d T_d^4 \quad (5)$$

ρ_s in the second term can be changed by Kirchhoff's law ($\rho_s = 1 - \epsilon_s$) if the temperature of the detector is not greatly different from that of the sample. Also, if the temperature of the sample is considerably higher than that of the detector the second term is orders of magnitude lower than the first and any error due to Kirchhoff's law would be negligible. Kirchhoff's law can be applied directly to the ρ_s in the first term because the energy considered in that term originated from the sample and

was reflected back to the sample by the detector which approximates a grey body. Therefore, the energy would have the same spectral distribution as the sample which makes it applicable to Kirchhoff's law.

$$\frac{Q_{net}}{\sigma A_d F_{ds}} = [1+0.01(1-\epsilon_s)]\epsilon_s T_s^4 - \epsilon_d \epsilon_s T_d^4$$

rewritting

$$\epsilon_s = \frac{Q_{net}/\sigma A_d}{F_{ds}[[1+0.01(1-\epsilon_s)]T_s^4 - \epsilon_d T_d^4]} \quad (6)$$

The numerator of this equation is determined by a blackbody measurement. For a blackbody ($\epsilon=1$)

$$1 = \frac{Q_{net}/\sigma A_d}{F_{dr}(T_r^4 - \epsilon_d T_d^4)} \quad (7)$$

where:
T_r absolute temperature of blackbody
F_{dr} shape factor from detector to blackbody

Combined equations (6) and (7) give

$$\epsilon_s = \frac{F_{dr}(T_r^4 - \epsilon_d T_d^4)}{F_{ds}[[1+0.01(1-\epsilon_s)]T_s^4 - \epsilon_d T_d^4]} \quad (8)$$

The calibration curve (fig. 23–3) was determined by varying the blackbody temperature over the necessary range and plotting the temperature to the fourth power versus the detector voltage output. Then T_r^4 is determined from this curve; T_s is determined by the surface thermocouple; T_d is the thermocouple hot junction temperature and is determined by a thermocouple at the cold junction and the thermopile output. There are ten thermopile junctions; therefore, knowing the output and temperature calibration for the materials making up the thermopile, we can determine the temperature difference between the cold and hot junctions. With T_d, T_r^4, T_s, ϵ_d, and the shape factors for both the blackbody and sample, which were calculated from physical measurements, the sample emittance can be determined from equation (8). First the sample emittance is estimated and put in the denominator of equation (8) and then the sample emittance is calculated. This calculated value can then be put back into the denominator of the right side of the equation and a new estimate of emittance can be calculated. However, if the first estimate is reasonable, the second calculation is unnecessary because the emittance correction term is very small.

RESULTS

The emittance of several known materials was measured to check the procedure. Parsons optical black lacquer gave a value of 0.974 and 0.983 at room temperature which compares favorably with published values of 0.98. The hemispherical emittance of evaporated gold on glass was measured to be 0.018 at room temperature which agrees well with the literature. Total emittance measurements were also made on room temperature emittance standards (ref. 1). The surfaces of the three different standards consisted of two basically different materials. One standard consisted of a highlead glaze on sintered lithium doped nickel oxide, $\epsilon=0.858$, another consisted of evaporated aluminum covering the glaze, $\epsilon=0.027$. The third standard was a combination of the above two; 43% of the glazed nickel oxide surface was covered with evaporated aluminum, $\epsilon=0.515$. The partially covered surface was obtained by evaporating through a screen-type mask of known open area ratio. The emittance of the third standard was also calculated from the emittance of the other two and the known area ratio. The calculated emittance of 0.501 compared favorably with the measured value, which gave a check on the accuracy of the apparatus for the 50% emittance range.

ERRORS

The measurement error can be broken down into two separate parts, random and systematic. The random error is usually determined by measuring samples several times. This was done for several samples and found to be $\pm 2.0\%$.

The systematic error is somewhat difficult to determine precisely. One systematic error is in the surface temperature measurement. Most of the surface temperature measurement error is random and is expressed by the above error. However, there may be a small systemtic error in the temperature measurement due to error in the thermocouple calibration. Extra precaution is taken to eliminate any errors which might have existed in thermocouple

circuits due to dissimilar metals. All the thermocouple leads are changed to copper leads in an isothermal environment and from that point on through switches and the potentiometer all the leads are copper. It is estimated that all of the systematic error in the temperature measurement is due only to the copper-constantan thermocouple calibration error and equal to $\pm \frac{1}{4}\%$.

Another systematic error is due to the variation from a true hemispherical measurement—that is, the deviation from unity of the shape factor between the thermopile and the sample or blackbody and the effect of the collimating tube. Both of these effects accentuate the normal emittance; however, they will have no effect on the emittance value of a sample which emits energy with a cosine distribution since the error is calibrated out with the blackbody. A calculation for an evaporated aluminum surface was made to estimate the error in using the collimating tube. Data for the angular dependence of emittance for the aluminum was taken from Eckert (ref. 2). The calculation assumed the reflectance of the collimating tube to be 98% (the reflectance of polished copper in the infrared) and showed that an error of -1.0% was caused by the collimating tube. However, Eckert's data were taken from reflectance measurements and these measurements were made only in the plane normal to the surface and containing the incident ray. The effect of the variation in reflectance for the hemispherical case is unknown but should be equal to or less than for the normal case. For all metal surfaces aluminum seems to have the largest deviation from the cosine law. Eckert's data also show that the non-metal surface emittance values drop off at the grazing angles where the aluminum increases sharply to several times the average value; therefore, we assume the error calculated for aluminum to be as large as could be expected for any material.

The error caused by the shape factor, being less than 1.0, is assumed to be negligible or contained in the random error for the following reasons. For a metal surface, the random error is smaller than the expressed 2% because the surface temperature measurement is more accurate. There is very little difference between the two surface thermocouples when measuring a metal sample. Therefore, we will assume the error caused by the shape factor, which is less than 1.0%, to be included in the random error for conductors. The shape factor error for non-conductors is negligible because the emittance drops off sharply at the low angles where the loss of radiation from the sample to thermopile would occur. Although this small error is positive and the collimating tube error is also positive for non-conductors, the addition of both is less than the stated 1.0% for the collimating tube error. Therefore, we assume the shape factor error is lumped in with the collimating tube error.

The blackbody calibration error is assumed to be negligible or contained in other errors for the following reasons. In any event the blackbody calibration error (both random and systematic) is small. The random error is very small because the calibration data were taken many times and have very little scatter The systematic error is very small because the blackbody is a hole (aspect ratio of 4) and the hole surface has a high-emittance coating. The emittance of the blackbody was assumed to be 1.0 in the calibration equation. Because the blackbody emittance is less than 1.0 the sample emittance would have a positive error. As stated before for conductors, the collimating tube would cause a negative error, therefore, the combination is less than the collimating tube error. In the case of a non-conductor, we will look at the energy distribution.

As is shown on page 418 of Eckert (ref. 2), the emittance of a hole is 1.0 for the large angles but the hole emittance approaches the emittance of the surface as the angle approaches the grazing angles. As was stated before, the collimating tube and shape factor errors for the non-conductor are positive because the energy distribution drops off at the low angles where the assumed blackbody does not. Therefore, if the true blackbody reference does drop off, this error will be reduced, however, not as much as the blackbody emittance being less than 1.0 will increase the error. Because the collimation tube and shape factor errors are small as expressed before, and are even smaller when the true blackbody distribution is considered, the sum of the blackbody calibration

error, shape factor error and collimating tube error is assumed less than 1.0%.

All other errors are assumed negligible, therefore, the total estimated maximum uncertainty is ±3.25%. The comparative measurements indicate that the real error is about ±2%.

Acknowledgments

The authors wish to acknowledge the support for this work by the U.S. Air Force and Lockheed Aircraft Corporation Missiles and Space Company (Subcontract No. 28–866, Prime Contract No. AFO4(647)–564).

REFERENCES

1. Janssen, J. E.; Schmidt, R. N.; and Torborg, R. H.: Emittance Standards. Final Report, Serial No. 37416, Honeywell Research Center. Hopkins, Minn.
2. Eckert, E. R. G.; and Drake, Jr., Robert M.: Heat and Mass Transfer. McGraw-Hill Book Co., Inc. 1959.

24—SPECTRAL EMITTANCE MEASUREMENTS FROM 40° C TO 200° C

BY DONALD L. STIERWALT

U.S. NAVAL ORDNANCE LABORATORY, CORONA, CALIFORNIA

Instrumentation has been developed for measuring the spectral emittance of both opaque and transparent materials from 40° C to 200° C in the 2 to 25 μ spectral region. The technique consists of measuring the radiation from a heated sample and comparing with that from a blackbody reference source. A Beckman IR-3 spectrophotometer has been modified for this purpose. By programming the IR-3 with a blackbody at the same temperature as the sample, the spectral emittance is read out directly on the recorder chart. With a minor modification, it should be possible to make these measurements at dry ice or liquid nitrogen temperatures, and to make total reflectance measurements over the entire temperature range —196° C to 200° C with a further modification. Spectral emittance measurements have been made on germanium, silicon, cadmium sulfide, Irtran I, Irtran II, and several other transparent and opaque materials. Curves of spectral emittance for a selection of these materials at several temperatures are presented.

In general, when radiation is incident upon an object, part of the radiation is reflected, part is absorbed, and the rest is transmitted. If all of the radiation is absorbed, the object is called a blackbody. The thermal radiation emitted by such an ideal blackbody is given by the Planck equation

$$W_\lambda(T)=C_1\lambda^{-5}\left(\exp\frac{C_2}{\lambda T}-1\right)^{-1} \qquad (1)$$

where

C_1 $2\pi c^2 h$

C_2 $\frac{hc}{k}$

h Planck constant

k Boltzmann constant

c speed of light

This is the spectral emissive power of a blackbody, i.e., the power emitted per unit area per unit wavelength interval.

For a body that is not a perfect absorber, the absorptivity A is defined as the fraction of the incident energy which is absorbed. According to Kirchhoff's law, such a body will emit thermal radiation in the amount

$$W_0(T)=\epsilon W(T) \qquad (2)$$

where where $\epsilon=A$ and $W(T)$ is the thermal radiation of a blackbody at temperature T. The emittance ϵ is the ratio of the thermal emission of a body at a given temperature to that of a blackbody at the same temperature, and is equal to the absorptivity of the body. The equality of the emittance and the absorptivity can be shown to hold at each wavelength so that $\epsilon_\lambda=A_\lambda$. We have, then, for the spectral emissive power from an object

$$W_{o\lambda}(T)=\epsilon_\lambda W_\lambda(T) \qquad (3)$$

In general, the spectral emittance ϵ_λ is a function of both wavelength and temperature.

If we consider a quasi-transparent sample with optically smooth plane parallel sides, in the spectral region where $\kappa/n \ll 1$ the following approximations hold for the reflectance, transmittance, and emittance:

$$R=\frac{r^2[1+\epsilon^{-2\alpha t}(1-2r^2)]}{1-r^4e^{-2\alpha t}} \qquad (4)$$

692-146 O—63——16

$$T=\frac{(1-r^2)^2\epsilon^{-\alpha t}}{1-r^4\epsilon^{-2\alpha t}} \tag{5}$$

$$\epsilon=\frac{(1-r^2)(1-\epsilon^{-\alpha t})}{1-r^2\epsilon^{-\alpha t}} \tag{6}$$

where n is the real part of the complex index of refraction, κ is the imaginary part, i.e., $n^*=n-i\kappa$, $r=\frac{n-1}{n+1}$, $\alpha=\frac{4\pi\kappa}{\lambda}$, the absorption coefficient, and t is the sample thickness. Adding (4), (5) and (6) one can verify that

$$R+T+\epsilon=1 \tag{7}$$

In the case of a nearly transparent sample where $\alpha t \ll 1$, equation (6) reduces to

$$\epsilon=\alpha t \tag{8}$$

Thus one can determine the absorption coefficient from a measurement of ϵ and t.

For an opaque sample $\epsilon=1-R$. Thus emittance measurements provide a method of determining total reflectance at normal incidence. This is especially useful for polished metal surfaces where $R\rightarrow 1.00$, in which case ϵ is a measure of the deviation from a perfect reflector.

INSTRUMENTATION

The spectral emittance of a body is found by measuring its thermal radiation as a function of temperature and wavelength. A Beckman IR 3 spectrophotometer was modified for this purpose. Figure 24-1 is a top view of the optical system of this instrument before modification. The compartments are evacuated, eliminating atmospheric absorptions, and each is lined with copper tubing through which temperature-controlled water is circulated. The sample is heated by conduction from the polished aluminum holder (fig. 24-2). Power to the heaters is controlled by the platinum resistance element which is one arm of a bridge. The temperature of the sample holder is monitored by the copper-constantan thermocouple.

The sample chamber (fig. 24-3) is a copper cone with an apex angle of 15°. The chamber was plated on the inside with iron and then oxidized. The iron oxide surface and geometry

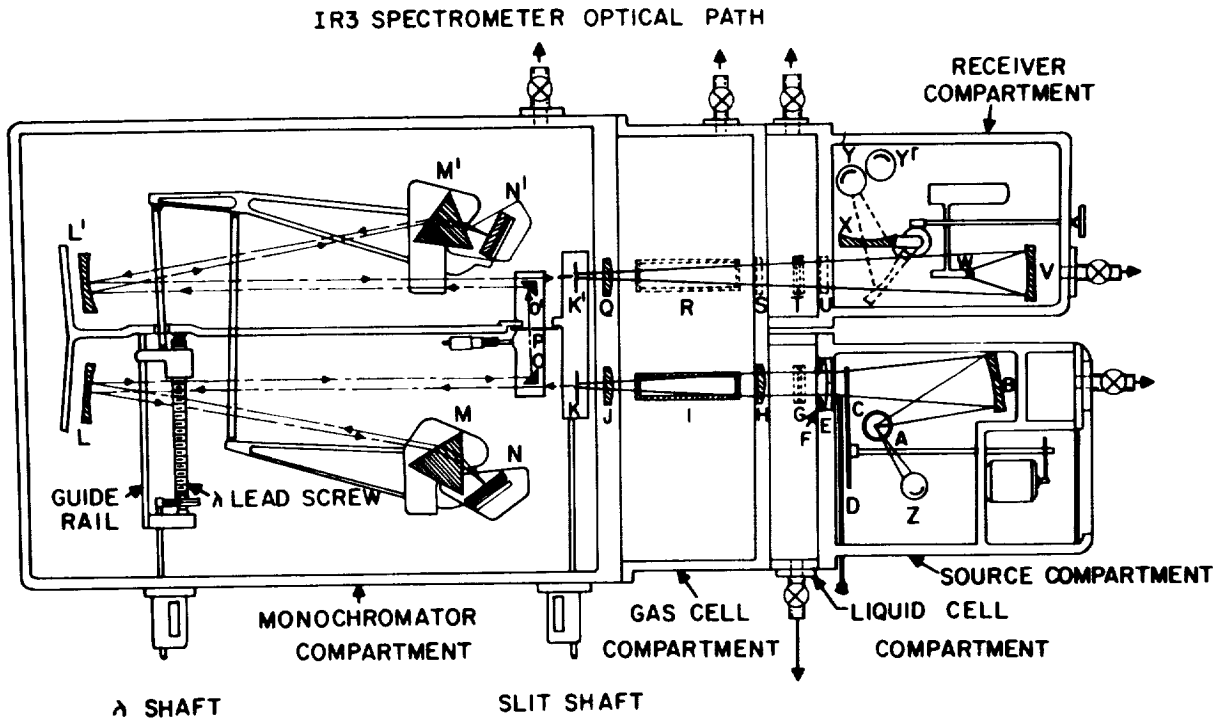

FIGURE 24-1.—Optical path of the Beckman IR-3 spectrometer before modification.

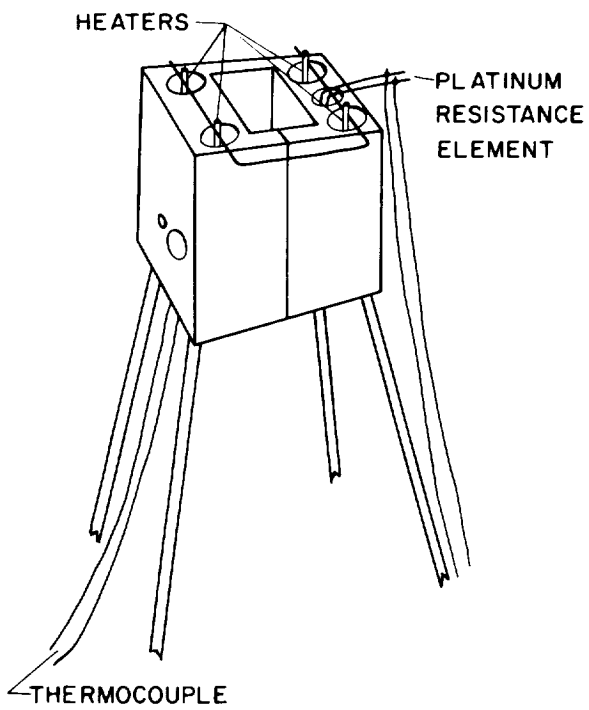

FIGURE 24-2.—Polished aluminum sample holder.

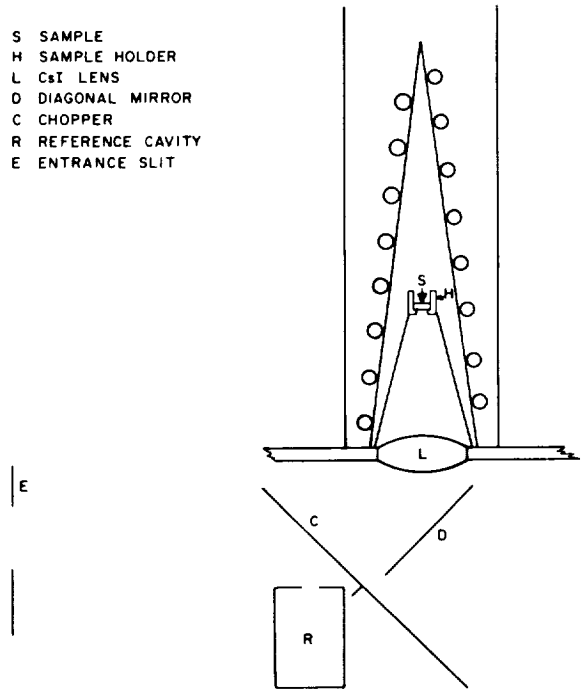

FIGURE 24-3.—Sample chamber.

of the cone make an excellent blackbody. This is necessary in the case of transparent samples in order to prevent radiation from the sample or sample holder being reflected back through the sample and into the monochromator. Copper tubing is soldered to the outside of the cone and the same water which regulates the monochromator temperature is circulated through these coils. The cesium iodide lens, L, and the sample holder are fitted into the gas cell compartment cover. The sample chamber fits onto this cover with an O-ring vacuum seal so that the chamber can be evacuated along with the gas cell compartment. The mirror, D, may be swung aside for making transmission measurements using the Nernst glower source shown in figure 24-1. When the diagonal mirror, D, is in the position shown in the figure, radiation from the sample is focused on the entrance slit of the monochromator. The chopper, C, has a mirror surface, so that the radiation entering the monochromator comes alternately from the sample and from the reference cavity, R. The a-c signal from the detector is proportional to the difference in energy between the sample beam and the reference cavity beam. Adding all sources which contribute to the signal, we have

$$S_s = K[(\epsilon_s W_s + R_s W_m + T_s W_m) R_d T_\ell + (1 - T_\ell) R_d W_m + (1 - R_d) W_m - R_c W_r - (1 - R_c) W_m] \quad (9)$$

where S is the signal voltage, and K is a constant which depends upon the transmittance of the monochromator and the responsivity of the detector. The subscripts s, m, d, ℓ, c, and r refer to the sample, monochromator, diagonal mirror, lens, chopper, and reference cavity. The first term inside the brackets represents the radiation emitted, reflected, and transmitted by the sample. The second term is the radiation from the lens, the third is from the diagonal mirror, the fourth is from the reference cavity and the last is from the chopper. It is assumed that the lens, diagonal mirror, and chopper are at the same temperature as the monochromator. Using equation (7), equation (9) reduces to

$$S_s = K[\epsilon_s R_d T_\ell (W_s - W_m) + R_c (W_m - W_r)] \quad (10)$$

Following the same procedure with the blackbody as the source in place of the sample we find

$$S_{bb} = K[R_d T_\ell (W_{bb} - W_m) + R_c (W_m - W_r)] \quad (11)$$

For the measurements presented here, the reference cavity was maintained at monochromator temperature so that $W_r = W_m$. Solving (10) and (11) for the emittance ϵ we find

$$\epsilon = \frac{S_s}{S_{bb}} \frac{W_{bb} - W_m}{W_s - W_m} \tag{12}$$

In the case where the blackbody is at sample temperature (12) reduces to

$$\epsilon_s = \frac{S_s}{S_{bb}} \tag{13}$$

A block diagram of the apparatus is shown in figure 24–4. The output from the synchronous rectifier is fed to the servo system which varies the slit width, maintaining constant energy to the detector. This slit width information, along with the wavelength, is stored by the tape recorder. By using a blackbody at sample temperature to standardize the slit program we make $S_{bb} = 1$ in equation (13). Then the blackbody is replaced by the sample, the playback from the tape programs the slits and wavelength drive, and the emittance is recorded directly on the chart recorder. Figure 24–5 is an example of the emittance directly recorded for a silicon sample. The blackbody used for standardization was a cavity machined from reactor-grade graphite to

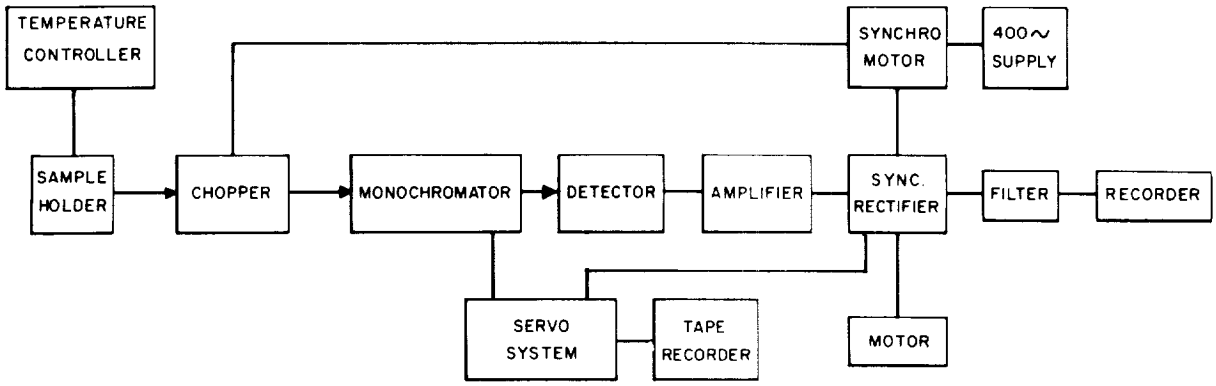

FIGURE 24–4.—Block diagram of apparatus.

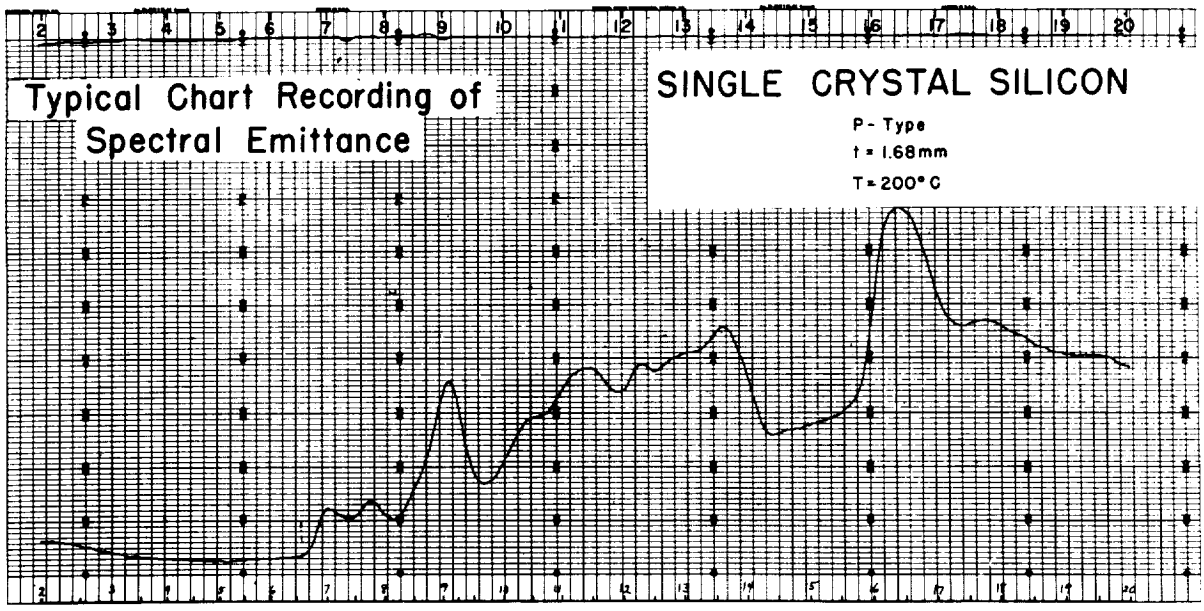

FIGURE 24–5.—Typical chart recording of spectral emittance.

fit the sample holder. Its emittance was compared with a standard blackbody and found to be at least 0.99 from 2 to 25 μ.

For samples with very low emittance the gain of the amplifier can be changed between standardization and playback runs, expanding the emittance scale. An example of this is shown in figures 24-6 and 7. Figure 24-6 shows the emittance of a five-millimeter sample of cadmium sulfide from 2 to 25 μ. In the 2- to 11-μ region, the emittance is so low that much detail is lost. Therefore, this section of the spectrum was scanned with the gain increased by a factor of ten. The result is shown in Figure 24-7 in which several emission bands can be seen.

FUTURE WORK

Examination of equations (9) through (13) reveals that the sample temperature may be above or below monochromator temperature as long as there is a sufficient difference between the two. Therefore, low-temperature emittance measurements can be made by providing a cooled sample holder. For opaque samples this will be relatively easy since no provision must be made for transmitted radiation.

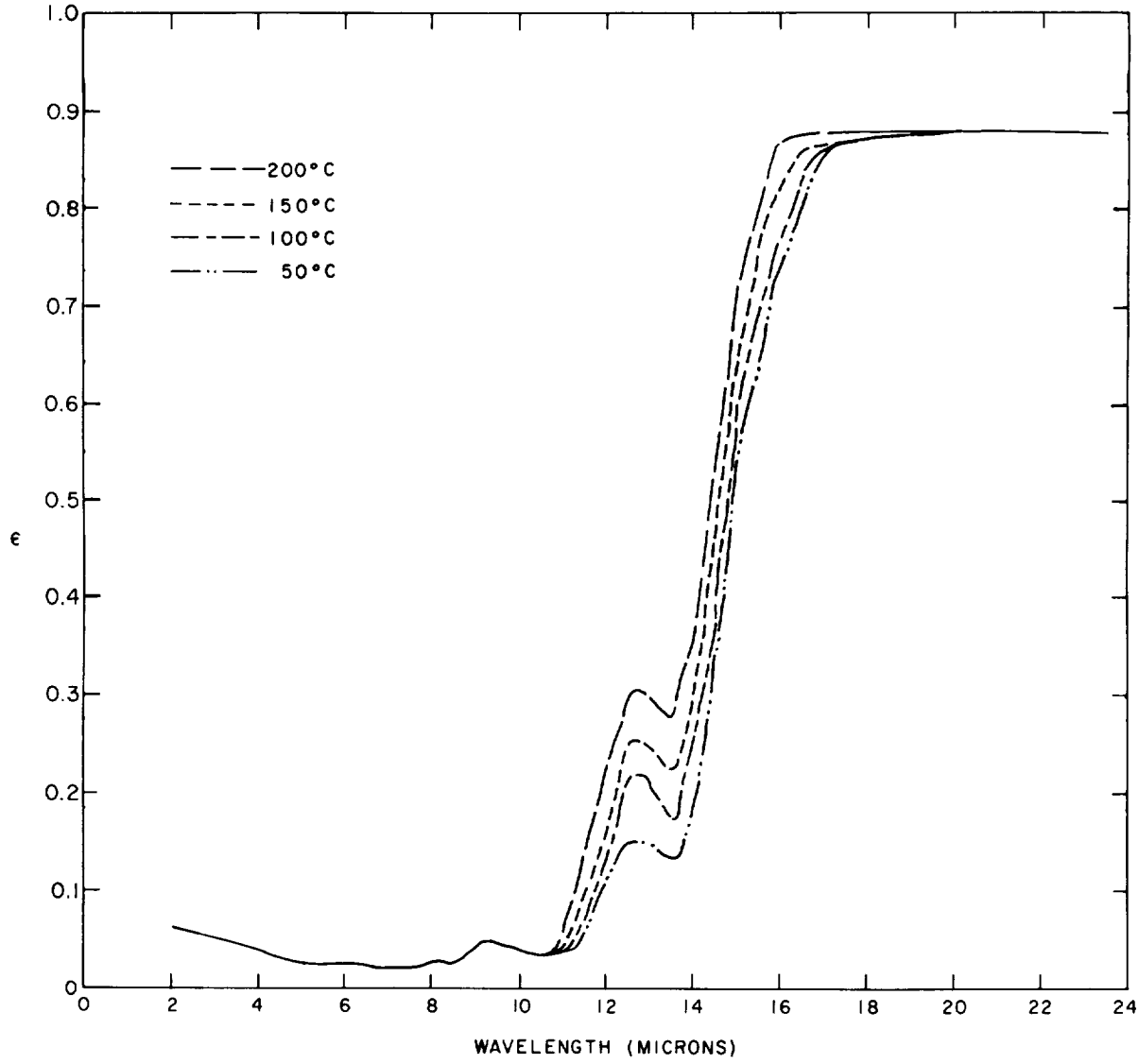

FIGURE 24-6.—Emittance of cadmium sulfide (t = 5.1 mm).

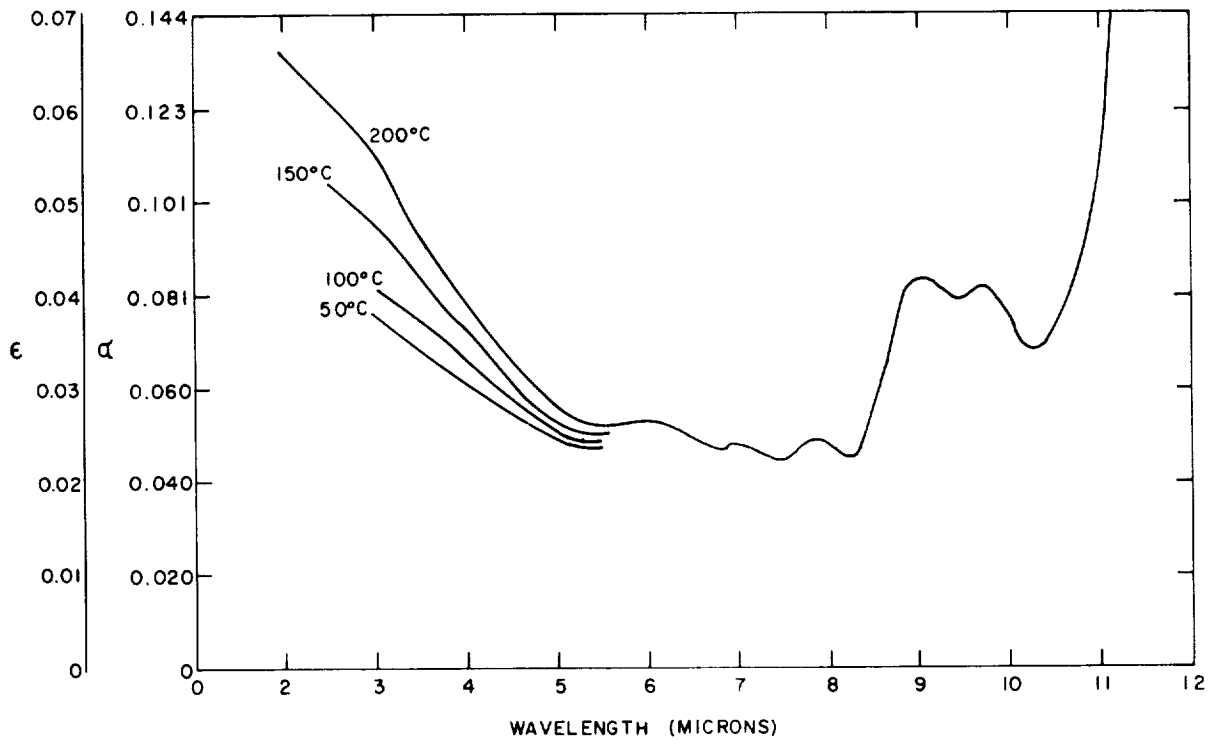

FIGURE 24-7.—Emittance, ϵ, and absorption coefficient, α, of cadmium sulfide ($l=5.1$ mm).

Another planned modification is the use of a cooled photoconductive detector in place of the thermocouple now being used. This will increase both the sensitivity and the spectral resolution available. An interesting possibility is that of maintaining the reference cavity at sample temperature and the blackbody at monochromator temperature. Then the emittance becomes

$$\epsilon_s=\left(1-\frac{S_s}{S_{bb}}\right)\frac{R_c}{R_d T l} \tag{14}$$

If the reflectances of the mirrors R_c and R_d are equal we have

$$\frac{S}{S_{bb}}=1-\epsilon_s T l \tag{15}$$

If a cesium iodide (CsI) plate having the same transmittance as the CsI lens is placed over the reference cavity aperture and maintained at monochromator temperature, this becomes

$$\frac{S_s}{S_{bb}}=1-\epsilon_s \tag{16}$$

In this way we would have a very sensitive measure of emittance where ϵ approaches 1.00.

25—ERRORS ASSOCIATED WITH HOHLRAUM RADIATION CHARACTERISTICS DETERMINATIONS

BY E. R. STREED, L. A. McKELLAR, R. ROLLING, JR., AND C. A. SMITH

LOCKHEED MISSILES & SPACE COMPANY, PALO ALTO, CALIFORNIA

Thermal radiation constitutes the dominant mode of heat transfer for an orbiting satallite. Consequently, prediction of component temperatures necessitates knowledge of the thermal radiation characteristics of vehicle materials (ref. 1). Such data may be obtained through infrared spectral reflectance measurements performed with a hohlraum.

A hohlraum is essentially a heated-cavity reflectometer with walls at uniform temperature. In the device under discussion the cooled sample forms part of one wall. With the exception of the solid angle subtended by the cavity aperture, a cooled sample is irradiated uniformly from hemispherical space. Energy reflected from the sample in a near-normal direction passes out the hohlraum aperture and is compared monochromatically to the radiance of the hohlraum wall. From a reciprocity theorem of Helmholtz (refs. 2, 3), this ratio is equal to the reflectance of the sample for similarly near-normal incident unidirectional irradiation. This quantity will be referred to as near-normal spectral reflectance.

The most obvious advantage of this apparatus is the spectral information gained. A less obvious but very real advantage is that with present, reasonably well-proved reflectance devices, one may perform rapid measurements on specimens of production surfaces with a minimum of sample preparation. These features are particularly useful to a space thermal control materials development program, such as that underway at LMSC (refs. 4, 5, 6). The primary disadvantages are the many sources of error and uncertainty which are to be discussed herein. Certain of these have received attention elsewhere in the literature (refs. 7, 8). The purpose of this paper is to outline a measurement correction procedure and uncertainty analysis applicable to the utilization of hohlraums as primary tools in space material programs.

SYMBOLS

C_2	Plank's second radiation constant (1.438)
E	spectral black body emissive power, watts/cm²μ
F_{nm}	configuration factor of surface n to surface m (fraction of radiation leaving surface n, which is incident on surface m)
J	spectral surface radiance (sum of emitted, reflected, and transmitted radiation flux per unit area per unit wavelength), watts/cm²μ
r	ratio between two detected monochromatic radiant flux densities (ratio-recording spectrophotometer output); apparent near-normal spectral reflectance as reduced directly from reflectometer recording chart.
T	temperature, ° K
α	spectral absorptance
α_H	hemispherical spectral absorptance
α_{HT}	total hemispherical absorptance
Γ	spectral surface irradiance (total radiation incident on a unit area from all directions), watts/cm²μ
ϵ	spectral emittance
ϵ_H	total hemispherical emittance
λ	wavelength (μ)
ρ	spectral reflectance
ρ_N	near-normal spectral reflectance

DESCRIPTION OF APPARATUS

The requirements for a device to determine the infrared spectral characteristics of opaque materials at room temperature were first proposed by Worthing (ref. 9). Implementation of the technique was achieved by Gier et al (ref. 10) to form an integrated system with an infrared spectrophotometer. Additional similar devices (refs. 11, 12) have been adapted to

other equipment and the complete apparatus is now commercially available.

A general view of the equipment is shown in figure 25–1. The original apparatus was designed and constructed by C. C. Shaw (ref. 13). The heated-cavity reflectometer (hohlraum) is mounted above and to the side of the double-beam model 13 Perkin-Elmer spectrophotometer. The sample is located in a water-cooled sample holder flush with the top of the cavity, such that reflected energy from the cavity can be viewed simultaneously with energy emanating from a portion of the cavity housing. The energy is collected by a double-beam optical system and directed into the standard spectrometer optical chopping and transfer system. Auxiliary equipment consists of a water pressure regulator, a water temperature regulator, and automatic temperature controllers for the hohlraum. Data is presented on a strip chart as a function of wavelength for visual perusal before complete reduction.

The hohlraum assembly, shown in figure 25–2, is contained in a double, stainless steel radiation shield to minimize losses to the surroundings and to permit operation of the apparatus without excessive external water cooling. The type 310 stainless steel cavity is ⅜ in. thick, by 8¾ in. high, and 5¼-in. inside diameter. The cavity is mounted concentric to the vertical optical axis and can be rotated 180° to permit viewing of sample or reference area through either optical beam. A temperature of 800° C is maintained within ±5° C with an average electrical power input of 3200 watts. Power is furnished to three main heaters by thermocouple-sensing, magnetic-amplifier controlled, saturable-reactor a-c power supplies. The neck and inner-bottom heaters are manually controlled with variable transformers.

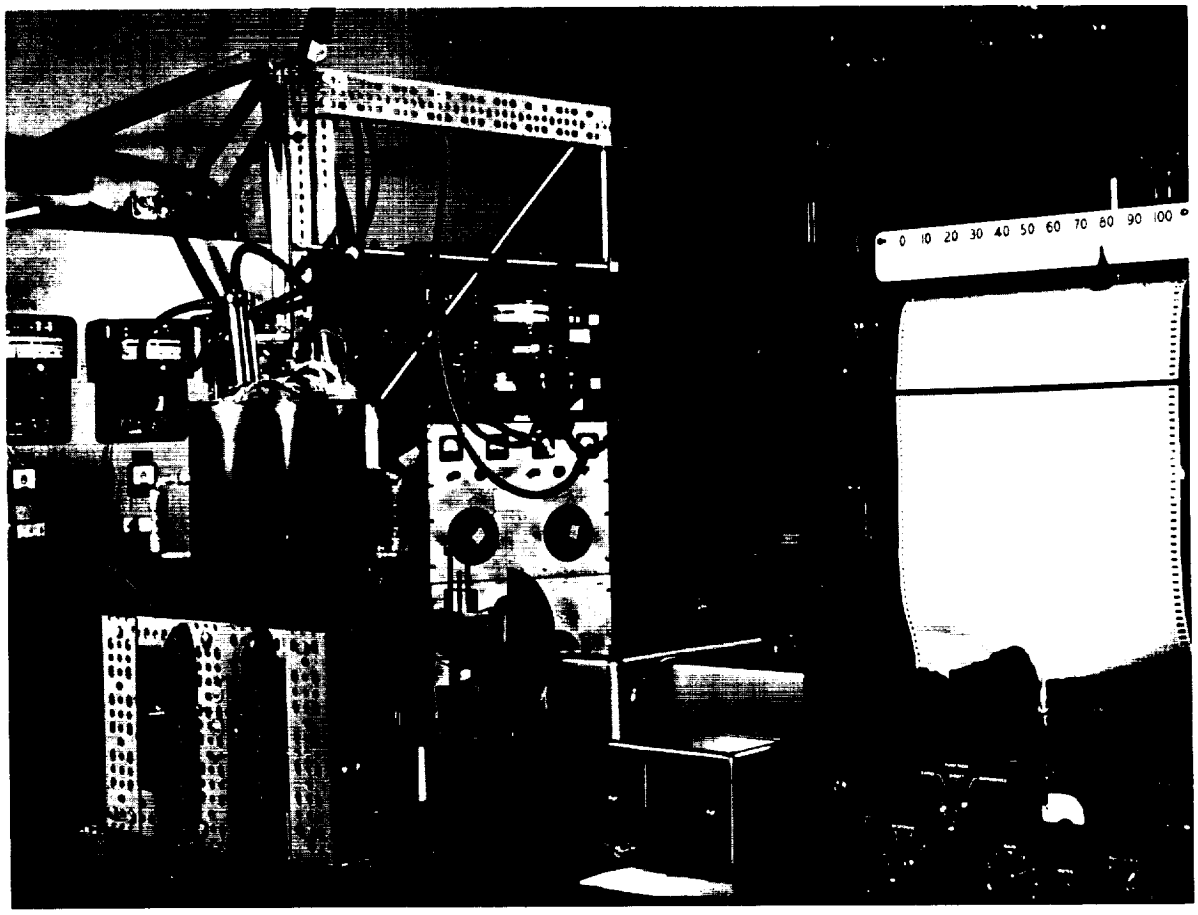

FIGURE 25–1.—Hohlraum and associated equipment.

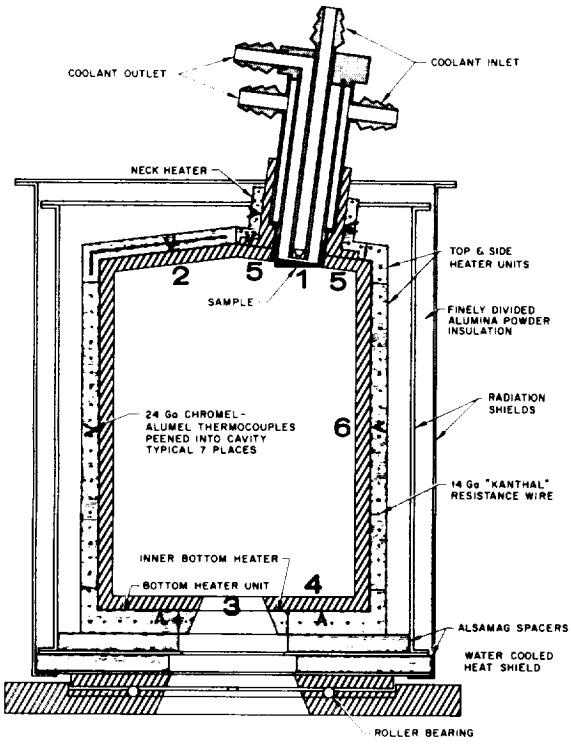

FIGURE 25-2. Hohlraum schematic.

The water-cooled sample holder accepts 1-in. diameter samples. Coated samples are prepared on 0.040- to 0.060-in.-thick aluminum or copper substrates to achieve maximum cooling. Cooling water is adjusted to about 3-lb pressure and can be temperature-controlled with a mixing valve. The sample holder mount inclines the sample-face normal about 4° off of the sample-aperture optical axis to ensure that highly specular samples do not reflect a mirror image of the exit aperture.

The optical schematic shown in figure 25–3 illustrates the split-beam arrangement maintained until the radiation from both beams has been synchronously chopped. Radiation originating from the reference and sample areas is collected by identical spherical mirrors M_1. The radiation is then directed to identical plane mirrors M_2; to identical spherical mirrors M_3; and focused on plane mirror M_4 to form one of the stops in the system. It is then collected and redirected in the horizontal optical axis by spherical mirror M_5 to the standard spectrometer optical transfer system. All spherical optical elements in the system are employed as close to on-axis as possible to reduce coma. Alignment of the system is performed by directing a visible light beam through the external port in the monochromator and into the exit slit. The optics are initially aligned by going through the system backwards and adjusting each mirror for focus and vignetting. A crosshair mounted in a special open holder is inserted in the normal sample area. The optical elements are adjusted until an image of the entrance-slit is properly positioned on the crosshairs. The hohlraum is then rotated 180° and the other optical beam is similarly adjusted for alignment and focus. The final alignment is accomplished by inserting a small tungsten source and diffuser in the sample holder and ensuring that the optical system provides proper focus and illumination of the entrance slit by each beam.

Operational Procedure

After the hohlraum has achieved a uniform temperature, as indicated by optical pyrometer or thermocouple measurements, minor adjustments are made to set the 100% and 0% levels for ratio recording. By rotating the hohlraum 90° from the normal operating position, both optical systems can view heated portions of the cavity roof. By adjusting the detector optical elements, a setting is achieved at which no change in the 100% reference occurs when the I/I_0 or I_0/I ratio is taken. This procedure must be followed throughout the desired spectral range. The instrument zero is obtained at the starting wavelength by adjusting the chopper phasing until an arbitrary but equal minimum signal is recorded when the individual beams are blocked. A measure of cross-talk (electronic over-lapping of one beam on the other) can also be adjusted for a minimum at this time.

Reflectance spectra are obtained after the 100% and a "working" zero level have been determined for the wavelength interval from 1.8 to 22.0 μ (fig. 25–4). The "working" zero level is established by scanning through the spectral range with the sample holder out. This gives a measure of the background and scattered radiation. The instrument is operated with a silt-servo system which controls slit width to provide constant energy for the monochromator reference beam.

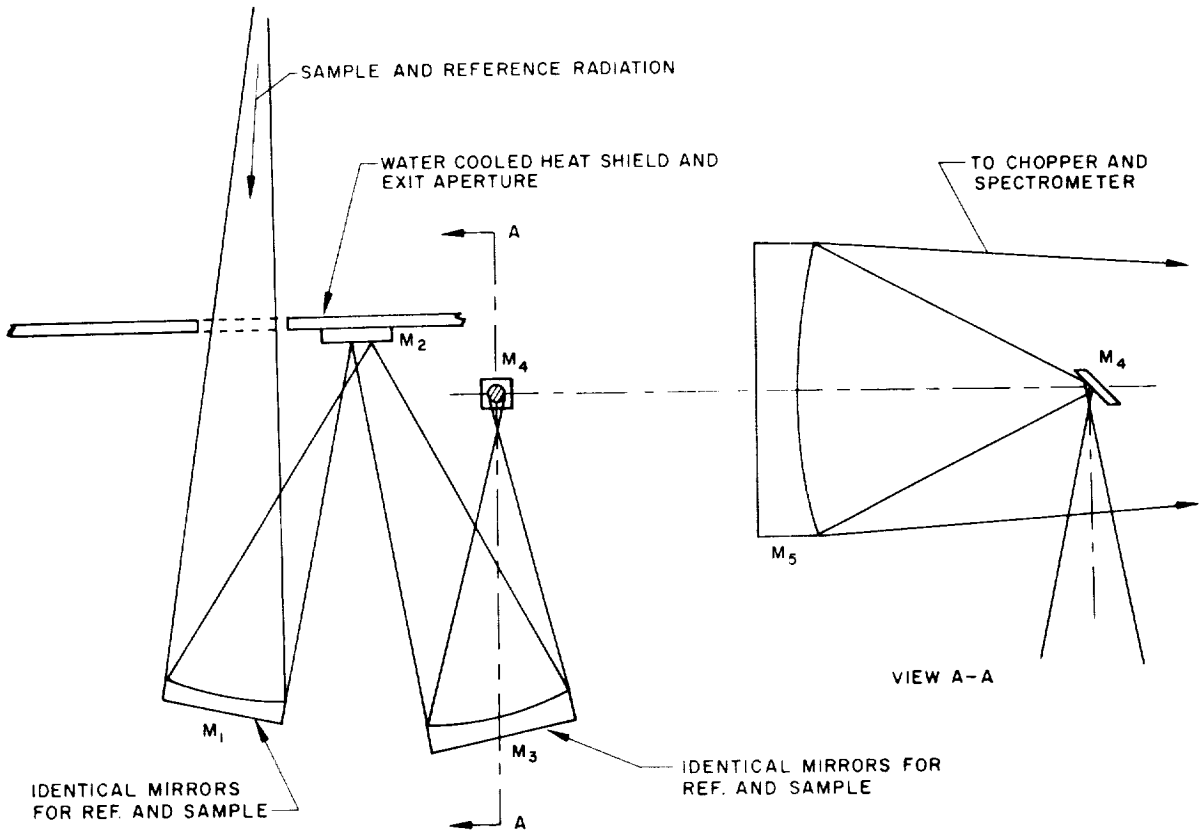

FIGURE 25-3.—Optical system schematic.

Wavelength calibration is accurate to 0.05 μ as performed with water, carbon dioxide, polystyrene, and ammonia absorption data points recommended in reference 13.

Because the largest interest is in ambient temperature emittance determinations, detailed spectra are not particularly desired in the 1.8- to 6.0-μ range. A potassium bromide (KBr) prism is used to provide sufficient spectral resolution and to eliminate prism changing. Therefore, no loss in accuracy is attributed to the use of relatively wide slits and a scanning time of about 7 min to cover the entire range. A response time commensurate with the 2-sec full-scale recorder balance and an amplifier gain with a 1% or less noise value are used.

Data reduction is performed by use of a Gerber variable scale set, with the ends of the scale on the zero and 100% lines of the strip chart (fig. 25–4). Reflectance values are tabulated with corresponding wavelength-drive drum numbers. A maximum of 150 points can be used, but usually fewer than 50 are adequate to define the curve without loss of accuracy. The drum number is converted to wavelength and programmed with the reflectance values for reduction by an IBM 7090 digital computer (reference 4). The computer performs numerical integration, using one hundred points, each of which represents a 1% energy increment of black-body energy for a particular temperature. The integrated value is subtracted from 1.0 to give total normal emittance and is routinely determined for 5 sample temperatures. The entire data reduction process is considered to cause an uncertainty of 0.01 in ρ.

BASIC EQUATIONS

In order to evaluate the effect of wall temperature on radiant interchange within the hohlraum, the cavity surfaces have been broken up into discrete zones, as identified in figure 25–2. Each of these zones will be assumed to have uniform but not necessarily

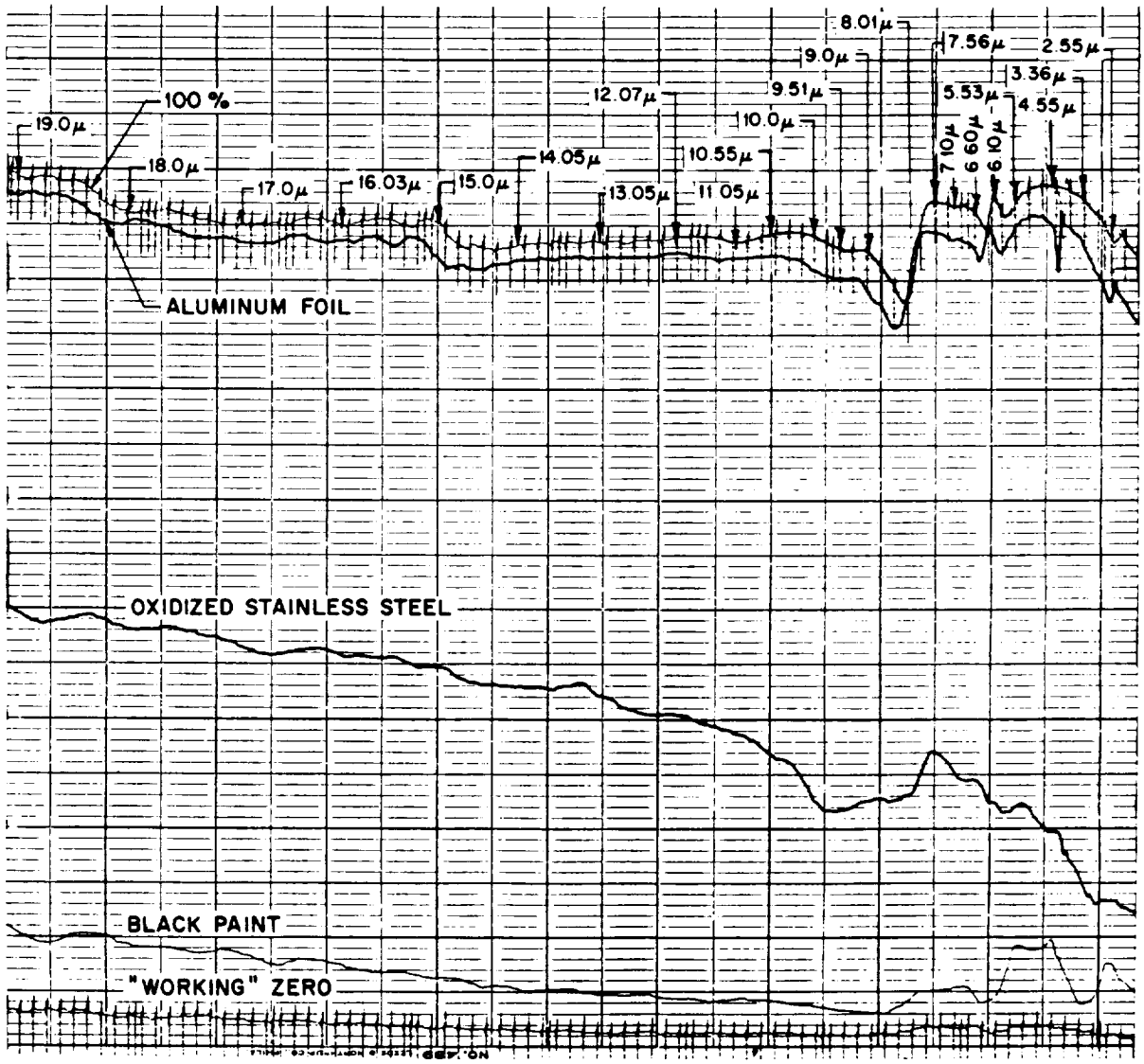

FIGURE 25–4.—Typical hohlraum chart recording.

equal, temperature, irradiation, and radiance. In the following development each term for radiant flux (J, E, Γ) and for radiation characteristic (ρ, ϵ, α) refers to tde spectral value at the measured wavelength.

The spectrophotometer output represents a ratio of two radiant energy intensities. The three ratios measured and recorded in determining the near-normal spectral reflectance of a sample are:

$$r_{100}=100\%\text{ level}=\frac{J_2'-J_c}{J_2''-J_c}$$

$$r_0=\text{zero level}=\frac{J_0-J_c}{J_2-J_c}$$

$$r_1=\text{sample trace}=\frac{J_1-J_c}{J_2-J_c}$$

where J_2' is the radiance of the cavity top viewed by one beam and J_2'' the radiance viewed by the other beam when the cavity is rotated 90° from the sample position. The apparent near-normal spectral reflectance is computed as follows:

$$r=\frac{r_1-r_0}{r_{100}-r_0} \qquad (1)$$

Even though temperature gradients may exist such that $J_2' \neq J_2$ and $J_2'' \neq J_2$, the cavity construction is such that $J_2'' = J_2'$. Using this in Equation (1) gives

$$r = \frac{J_1 - J_0}{J_2 - J_0} = \frac{\rho_{N1}\Gamma_1 + \epsilon_{N1}E_1 - J_0}{J_2 - J_0} \tag{2}$$

If the material specimen being measured is sufficiently thick, in relation to its absorption coefficient, to be "opaque" (for practical purposes less than 1% of incident spectral energy transmitted), then $1 - \rho_{N1} = \alpha_{N1}$. If one then states that $\alpha_{N1} = \epsilon_{N1}$ then the sample reflectance is related to the instrument response r by

$$\rho_{N1} = r\left[\frac{J_2 - J_0}{\Gamma_1 - E_1}\right] + \frac{J_0 - E_1}{\Gamma_1 - E_1} \tag{3}$$

Finally, if the cavity is isothermal, with the exception of the aperture and the sample, and if the aperture and sample are small enough to have negligible effect on cavity-wall radiances then

$$J_2 = \Gamma_1 = E_2$$

and

$$\rho_{N1} = r + (1 - r)\frac{E_1 - E_0}{E_1 - E_2} \tag{4}$$

The second term on the right side of equation (4) corrects for the effect of sample emission on instrument response. In a properly designed and operated hohlraum this is the only significant correction required. Other sources of error are amenable to evaluation; however they will be treated here as uncertainties, since the exact temperature distribution and spectral properties of the hohlraum walls are unknown and thus their effects cannot be applied as corrections to r.

ANALYSIS OF UNCERTAINTIES

The uncertainty in a measured value of ρ may be divided conveniently into that connected with the hohlraum proper and that external to the hohlraum, i.e., found in the optical system, spectrophotometer, and data reduction process.

Uncertainties Associated With Hohlraum Proper

Certain errors are intimately connected with the hohlraum configuration and may be minimized by proper design. Departures from uniform, isotropic sample irradiation are caused by the inevitable departures from isothermal wall conditions, by the presence of the aperture, and by cavity wall specularity.

Attention is called to the term in equation (2) for the sample irradiation, Γ_1. If there were no temperature differences or apertures in the cavity this term would be equal to E_2, the monochromatic emissive power of a black body at T_2. However, such is not the case, and evaluation of Γ_1 requires a summation process over the interior of the cavity. If the hohlraum walls are diffuse and are divided into M surface zones, each of uniform radiosity J_n, then

$$\Gamma_1 = \sum_1^M F_{1n}J_n$$

If equations (1)–(3) are applied to measurements of specular samples, ρ_{N1} must be carefully evaluated. With perfectly specular samples Γ_1 is replaced by J_4, the radiosity of the bottom of the cavity, since the monochrometer sees the mirror image of area 4. Unfortunately, most materials are neither perfectly diffuse nor perfectly specular, and interpretation of $\rho_{N1}\Gamma_1$ in such cases requires information on the directional dependence of sample reflectance in addition to the spatial distribution of energy inside the hohlraum. However, the two limiting conditions of perfectly diffuse and perfectly specular adequately represent the behavior of many engineering materials. Thus, the uncertainty in ρ_N for these two cases will be discussed in the following paragraphs.

An expression for the uncertainty, Δ_T, in measured values of reflectance due to the uncertainty in cavity temperature regulation may be derived from equation (3) as a function of wavelength. However, rather than correct for the effects of nonuniform wall temperature, it is desirable to establish a criterion for wall temperature regulation which will result in a tolerable uncertainty in reflectance. The value of Δ_T obtained for a given wall temperature uncertainty is approximately the same as the change in instrument response effected by a given wall temperature variation. An expression for the effect of wall temperatures on instrument response, r, is derived and plotted as a function of wavelength, for both diffuse and specular samples. In these computations

the cavity walls were assumed to be grey and diffuse, with $\epsilon=0.7$.

It should be noted that this error is affected by the cavity wall radiation characteristics. A black cavity ($\epsilon=1.0$) would incur greater uncertainties with the same temperature differences (ref. 7), but would be easier to maintain at near-isothermal conditions. Conversely, if wall reflectance were increased from 0.3 to 0.7 at 10 μ, the error in spectral reflectance of diffuse samples at 10 μ for a given temperature distribution would be decreased by 10% (see fig. 25-7).

The viewing aperture not only affects the sample and reference area radiances directly, as a source of low-intensity irradiation, but indirectly, through having the same effect on the cavity walls. The indirect effects on reflectance measurement are second order; only the direct effect will be discussed here. This can be shown to cause measured values of reflectance for perfectly diffuse samples to be low by the amount Δ_A, where $\Delta_A=rF_{13}(1-\rho_2)/(1-F_{13})$. With perfectly specular samples, this discrepancy does not occur since no radiation reflected directly through the aperture by the sample comes directly from the aperture. With samples of intermediate specularity this error is difficult to assess; again the directional dependence of reflectance must be known. It is possible to envisage a sample with a reflection distribution function or partial reflectivity such that the error in reflectance would be greater than that for a perfectly diffuse sample.

Wall specularity influences errors due both to wall temperature nonuniformities and to the aperture. While the magnitude of this effect is difficult to assess, it is obvious that it is desirable to have a diffuse inner cavity surface and thus eliminate this source of uncertainty.

The presence of the cooled sample itself disturbs the isotropic nature of the cavity radiation exchange. The greatest effect is that on the radiosity of the reference area (zone 2). If this sample-to-reference area radiation exchange is considered alone, it is found that the net effect on spectral reflectance values will be equal to or less than Δ_I where

$$\Delta_I=r\epsilon_{N1}\rho_2F_{21}$$

If care is not taken in design of both the sample holder and the cavity heaters in the vicinity of the installed holder (zone 5), significant cooling of the adjacent cavity walls will result. Criteria similar to those developed in the next section for temperature gradients apply here. Fortunately, reflectance measurements are less sensitive to departures from isothermal conditions here than in other sections of the cavity wall. The term for the zero-level intensity in equation (3), J_0, should be accurately determinable; the uncertainty in reflectance due to uncertainty in J_0 is given by

$$\Delta_0=[(1-r)/\Gamma_1-E_1)]\Delta J_0$$

Consideration of the methods used to obtain a "working" zero level reveals that the value to be used for J_0 depends upon proper evaluation of the radiance of the laboratory walls in the vicinity of the instrument. For a large enclosure the wall radiance is closely approximated by that of a blackbody at air temperature, unless the "zero" sight directly views a heating duct or other such local hot spot. If care is used to eliminate the possibility of sighting on a hot spot, then the use of $J_0=E_{room\ temp}$ is justified with a possible small error in room temperature evaluation. If room temperature is determined to $\pm 2°$ C then $\Delta J_0=2\times10^{-5}$ watts/cm^2-μ at 20 μ, which gives $\Delta_0=1.9\times10^{-3}$ as an estimate of the magnitude of this term. A wavelength of 20 μ is chosen for this computation since the error in J_0 is greatest at long wavelengths and 20 μ approaches the upper useful limit of the present instrument.

As mentioned, the effect of sample emission is a calculable error which may be applied as a correction to the observed value of reflectance. An expression for this correction is given in equation (4), and shown as a function of wavelength for various sample face temperatures in figure 25–5. A similar expression for the effect of sample emission on instrument response is derived later in equation (6). The evaluation of this effect can have a significant uncertainty itself, Δ_E, due to difficulties encountered in sample temperature measurement. It should be kept in mind that in general the sample has both axial and radial temperature gradients. Although these can be minimized through proper

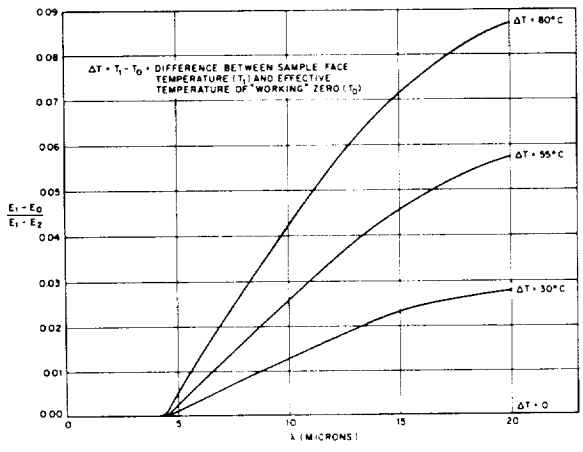

FIGURE 25–5.—Effect of sample emission on reflectance measurements.

sample holder design, the uncertainty in temperature measurement must include both the error in the measurement per se and the range of temperatures found due to these gradients. This problem is covered at greater detail in the discussion of experimental techniques. The resultant uncertainty in the sample emission correction for a uniform surface temperature is given by:

$$\Delta_E = \frac{\partial}{\partial T_1}\left[\frac{(1-r)(E_1-E_0)}{E_1-E_2}\right] = -\frac{(1-r)(E_2-E_0)}{(E_2-E_1)^2}\,\frac{E_1\phi e^{\phi}}{(e^{\phi}-1)}\,\frac{1}{T_1}$$

where

$$\phi = \frac{C_2}{\lambda T_1}$$

Sources of Error External to Hohlraum

The advantage of a complete double-beam system is apparent in attempting to assess the sources of measurement errors and their magnitude. Although the spectrometer may not be operated with maximum utilization of energy because it is adjusted to provide equal energy from both beams on the detector, it is by virtue of this equality that factors such as slit-width variations, chopper-temperature variations, differences in optical systems, and electronic drift are minimized. A measure of the stray and scattered radiation is determined by running a "working" zero with each run. The resulting signal is subtracted from both sample and 100% levels in obtaining reflectance values (eq. (1)).

In spite of the ratio-recording feature there still exists an uncertainty in the absolute value of a result due to changes in optical path conditions and alignment, nonreproducibility of silt width, and amplifier drift. The only way to assess the magnitude of such difficulties is through a comparison of results on standard samples which are run each day. Observations conducted in this laboratory indicate that reproducibility of results is effected to ±0.01 reflectance units due to the above possible variations. This will be taken as an uncertainty in near-normal spectral reflectance:

$$\Delta_s = 0.01$$

Summary of Sources of Error

The preceding discussion will now be summarized. The apparent near-normal reflectance, r, is related to the sample reflectance by equation (5):

$$\rho_{N1} = r + (1-r)\left[\frac{E_1-E_0}{E_1-E_2}\right] + [\Delta_E+\Delta_T+\Delta_A+\Delta_s+\Delta_0+\Delta_1] \quad (5)$$

where the Δ terms are the estimated uncertainties in the absolute value of ρ_N after the sample emission correction has been applied. Following the experimental evaluation of several of these errors, the uncertainty analysis and correction procedure indicated in equation (5) is carried out for measurements performed on three specific samples.

EXPERIMENTAL EVALUATION

A program was undertaken to obtain experimental verification of the magnitude of errors associated with non-uniform hohlraum temperatures and sample emission. To effectively demonstrate these errors, the hohlraum temperatures were varied in several zones and sample temperatures were varied over extremes which exceeded those expected in normal operation.

Three different samples were used to demonstrate the effect of the errors for the full range of sample types normally received by the laboratory. Parson's black paint was chosen to illustrate that sample heating causes significant errors in reflectance determinations for good emitters and that this error can exceed 100% for this material. Fasson foil, a highly

specular aluminum foil, was chosen to clearly illustrate the errors caused by hohlraum temperature variations and also to show that good reflectors exhibit very small effects from sample heating. Oxidized stainless steel was used to illustrate both effects on a sample whose properties lay somewhere between the other two extremes, both in specularity and in reflectance.

Previous experience with these same samples has shown that their optical properties are not affected by exposure to the temperature levels associated with these measurements. However, in order to assure that some small change would not take place during the investigation, all samples were first run at the highest sample temperature, with all subsequent observations made at lower temperature levels.

The Parson's black paint sample was prepared by spraying a ⅛-in. thick, 1-in.-diameter copper disk with two coats of the paint material. This produced a uniform 2-mil coating over the sample. The spraying was accomplished after the sample was instrumented and placed in the water-cooled sample holder, which allowed the measurements to be completed without further handling of the surface.

The Fasson foil sample consisted of a 2-mil thickness of foil attached to a ⅛-in-thick, 1-in.-diameter copper disk, which was then placed in the sample holder. The surface was not cleaned prior to the hot sample runs, so there are bands evident in the data which are caused by the protective coating placed on the aluminum foil by the manufacturer. The surface was cleaned prior to the runs made for evaluation of the effects of hohlraum temperature variation.

The stainless steel sample was a ⅛-in.-thick disk which had been oxidized for several hours at elevated temperatures so that its optical properties would fall between those of the high emitter and reflector. The optical properties of this sample were shown to be stable by repeated runs over long periods of time.

All samples had 36 B & S gage Chromel-Alumel thermocouples mounted on the back surface for sample temperature determinations. The thermocouples were protected from the sample coolant by a very thin rubber sheet and a second copper disk behind the sheet. This arrangement protected the thermocouple junction and the leads so that conduction and convection losses were eliminated and true sample back-surface temperatures were measured. Analytical estimates of the temperature gradient through the sample thickness show that the gradient is highest for the Parson's black sample due to its high absorption and low thermal conductivity. The estimated gradients at the center of the viewed area through the sample thickness were as follows:

- Parson's black: $\Delta T \approx 21^\circ$ C
- stainless steel: $\Delta T \approx 3^\circ$ C
- Fasson foil: $\Delta T \approx 1^\circ$ C

These estimates are based upon an analytical solution for one-dimensional heat transfer through the sample and do not represent actual measurements on the surface in question. Measurements were also conducted to provide some knowledge of the temperature gradient along the radius of the sample. To accomplish this three Chromel-Alumel thermocouples were mounted on the back of the Parson's black specimen and their output recorded as a function of centerline sample temperature. The results of these measurements showed that the radial gradient does not exceed 15° C, which would not affect the reflectance measurement more than 0.015 reflectance units.

The effects of hohlraum temperature variation were determined with the three samples run cold. One of the hohlraum temperature distributions was taken as a base from which the other distributions were varied in order to demonstrate the change in instrument reponse from this base cavity condition. The temperatures used as a reference state were—top, 809° C; side, 828° C; bottom, 814° C—which shows that there was departure from a hohlraum state. Thus, the changes in reponse due to imposed temperature variations should not be interpreted directly as changes from an isothermal condition.

The construction of the cavity is such that it is not possible to change the temperature of a given section uniformly. For example, when the side heater current is reduced the center portion temperature is reduced significantly more than the end sections which continue to receive energy from the top and bottom heater (fig. 25 2). Thus, the change observed in r

for a given section temperature change is not expected to be as large as that predicted by analysis for a change of the entire zone.

Temperatures were measured at the beginning of each run after steady-state conditions were achieved. "Side" temperature is the center of the side wall, "top" refers to the reference area opposite the sample port of the top of the cavity, and "bottom" refers to an area half way between the viewing port and the side wall directly beneath the reference area. These locations were chosen as representative samples of the desired gross area temperatures.

In order to compare the experimental results to analytical predictions it is desirable to return to equation (2) and derive an expression for the change in instrument response with specified non-isothermal conditions and hot samples. From equation (2) the apparent reflectance as indicated by the reflectometer apparatus is

$$r=\frac{J_1-J_0}{J_2-J_0}=\frac{\rho_{N1}+\epsilon_{N1}E_1-J_0}{J_2-J_0}$$

Using the relations $1-\rho_N=\alpha_N$ and $\alpha_N=\epsilon_N$ for monochromatic exchange with opaque materials and defining $\delta=r-\rho_{N1}$ results in equation (2) taking the form

$$\delta=\rho_{N1}\frac{\Gamma_1-J_2}{J_2-J_0}+(1-\rho_{N1})\frac{E_1-E_0}{J_2-J_0} \qquad (6)$$

From the definition of δ it is seen that equation (6) is an expression for the difference between the instrument output and the true reflectance, which shows the effect of non-uniformity in the cavity and sample emission. Of course, when the cavity is uniform, such that $\Gamma_1=J_2$, and the sample is cooled, such that $E_1=E_0$, then $\delta=0$, giving $\rho_{N1}=r$. With the form given in equation (6) it is possible to compare the analytical predictions of changes in instrument response with those observed in the laboratory.

Table 25–I presents a numerical comparison of the observed and predicted change in instrument response for a specific change of temperature distribution in the hohlraum.

The tabulated values were taken from figure 25–6, which presents the observed ratio, r, as a function of wavelength. The predicted values were taken from the results of a network solution for wall radiances with stated temperature

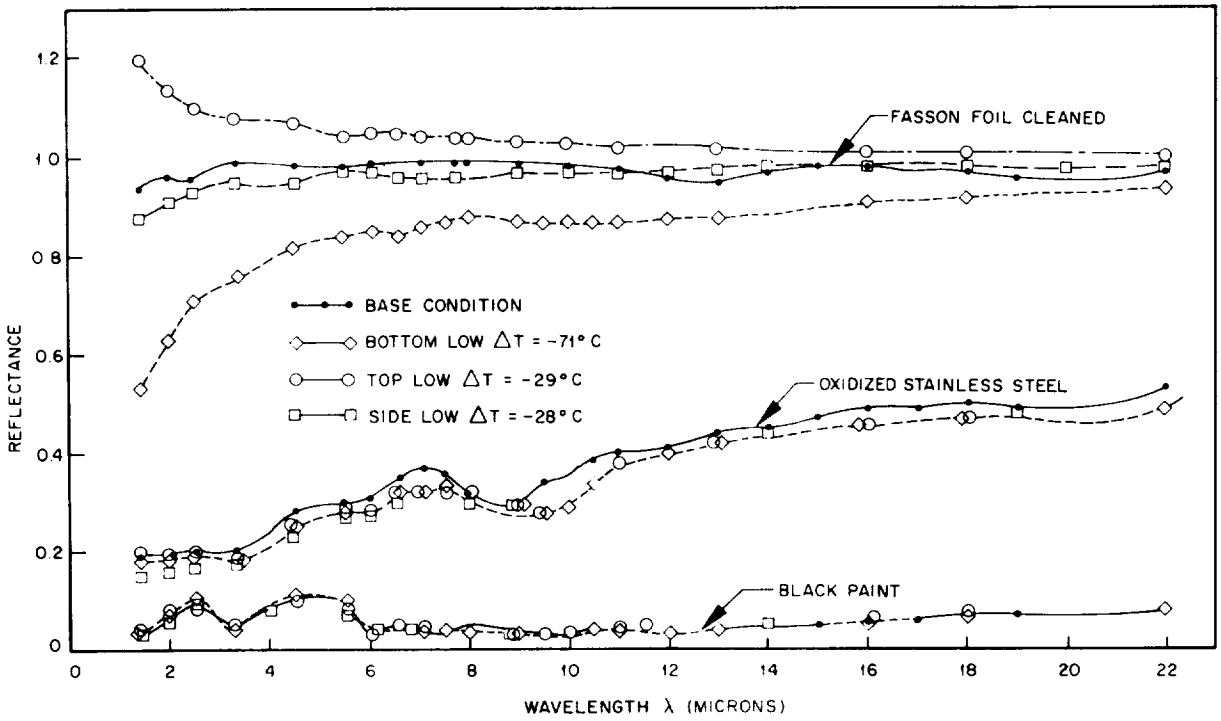

FIGURE 25–6.—Hohlraum data showing effects of nonuniform cavity temperatures.

TABLE 25–I.—*Effects of Cavity Temperature Distribution on Spectral Reflectance Measurements*

Sample Type	λ (μ)	Δρ* Bottom ΔT = −71° C		Δρ* Top ΔT = −29° C		Δρ* Side ΔT = −28° C	
		Exp.	Theo.	Exp.	Theo.	Exp.	Theo.
Black paint	1.46	−0.01	------	+0.01	------	+0.02	------
	2.55	−.02	−0.002	+.02	+0.002	−.01	−0.002
	4.55	−.01	−.001	------	+.001	------	−.001
	6.10	------	−.0005	------	+.001	------	−.001
	10.0	------	−.0002	------	+.0005	------	−.0005
	14.0	−.01	------	------	------	------	------
	17.0	−.01	------	------	------	------	------
Oxidized stainless steel	1.46	------	------	+.01	------	−.04	------
	2.55	−.01	−.003	−.005	+.007	−.04	−.006
	4.55	−.03	−.004	+.01	+.006	−.05	−.005
	6.10	−.04	−.002	+.005	+.005	−.03	−.004
	10.0	−.06	−.002	------	+.005	−.01	−.003
	14.0	−.02	−.001	------	+.004	------	−.003
	17.0	−.03	−.001	------	+.002	------	−.002
Fasson foil	1.46	−.40	------	+.26	------	−.06	------
	2.55	−.24	−.26	+.16	+.225	−.02	------
	4.55	−.17	−.15	+.09	+.14	−.03	------
	6.10	−.13	−.12	+.06	+.11	−.02	------
	10.0	−.11	−.08	+.05	+.085	------	------
	14.0	−.08	−.075	+.045	+.08	------	------
	17.0	−.06	−.070	+.035	+.075	------	------

* Experimental Δρ is not given where a chage in ρ is less than ±0.01 since this is the expected value of instrument error.

levels. The analysis assumed a wall emittance of 0.7 throughout the spectral region of interest. Some of the analytical results are shown in figures 25–7 and –8. The comparison was not

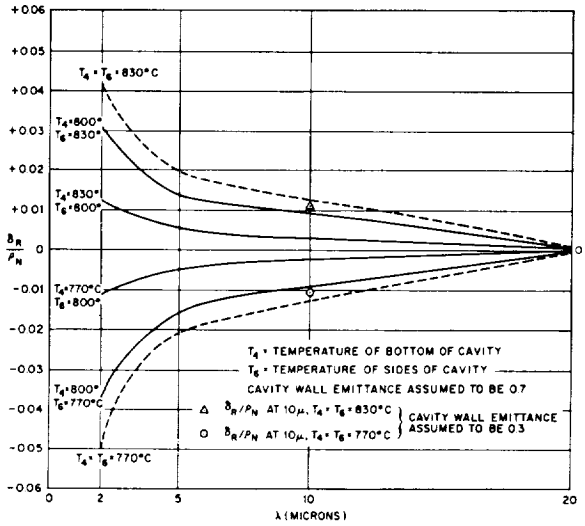

FIGURE 25–7.—Effect of cavity temperature variations on instrument response (perfectly diffuse samples).

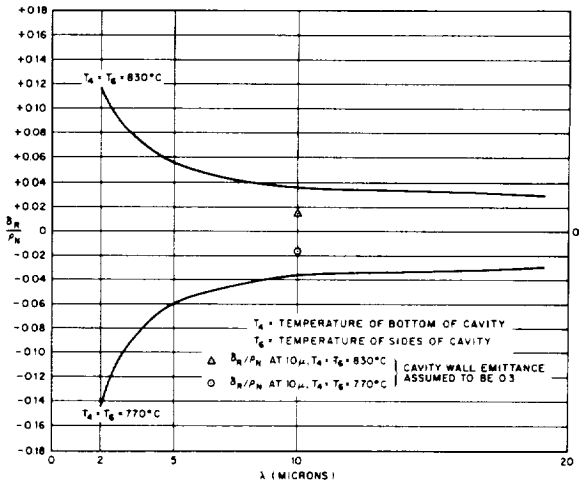

FIGURE 25–8.—Effect of cavity temperature variations on instrument response (perfectly specular sample).

expected to be very good since the temperature of any one region or zone could not be varied uniformly in the actual cavity. In addition there is normally only a ±.01 accuracy in reproducing results for any one value of ρ_{N1}.

Considering the experimental difficulties the comparison in Table 25–I is reasonable.

As was expected, the effects of nonuniform temperature are greatest for high reflectors, and bottom temperature changes are particularly important for the case of specular samples. The close agreement between observed and predicted values for the aluminum was better than expected in view of the large temperature gradient near the viewing port of the cavity. In view of the apparent agreement in Table 25–I, it appears reasonable to use the analytical expression in equation (6) to establish a basis for temperature control. The results, when based upon a hohlraum temperature of 800° C ($r=1.0$, $E_1=E_0$, and $\lambda=2.0$ μ), indicate that temperature uniformity should be maintained to $\pm 2°$ C for $\delta \leqq 0.01$. If such accuracy is not necessary at short wavelengths, then less precise control is required. For example, if an uncertainty of ± 0.01 is desired at wavelengths longer than 4 μ only, then control to $\pm 15°$ C is adequate.

Table 25–II is a comparison of predicted and observed changes in instrument response, Δr, due to sample temperature increases. The experimental data for the table were taken from experimental determinations shown plotted in figure 25–9. In the figure, the values of ΔT are increases in sample temperature above the lowest temperature possible with the present holder. The comparison of observations with predictions for sample emission is good, showing that sample emission corrections can be applied with confidence where sample surface temperature is known.

TABLE 25–II.—*Effects of Sample Temperature on Spectral Reflectance Measurements*

Sample Type	λ (μ)	Δr		Δr	
		Exp.	Theo.	Exp.	Theo.
		$\Delta T=+15°$ C		$\Delta T=+46°$ C	
Black Paint	4. 55	0	-----	0	-----
	6. 10	0	0. 001	. 005	0. 011
	8. 0	. 005	. 002	. 02	. 015
	12. 0	. 01	. 005	. 03	. 030
	16. 0	. 01	. 010	. 04	. 041
	19. 0	. 015	. 013	. 05	. 046
		$\Delta T=+30°$ C		$\Delta T=+78°$ C	
Oxidized stainless steel	4. 55	0	-----	0	-----
	6. 10	0	0. 002	0	0. 004
	8. 10	. 03	. 003	. 02	. 009
	12. 0	. 02	. 008	. 04	. 025
	16. 0	. 02	. 013	. 08	. 033
	19. 0	. 01	. 014	. 08	. 050
		$\Delta T=+15°$ C		$\Delta T=+35°$ C	
Fasson* foil	4. 55	0	-----	0	-----
	6. 10	0	-----	0	-----
	8. 0	0	-----	0	0. 001
	12. 0	0	0. 0006	0	. 002
	16. 0	. 01	. 001	. 01	. 003
	19. 0	. 01	. 0013	. 01	. 003

*Variations observed with Fasson foil were of the same order of magnitude as instrument noise, with only a trend toward increasing ρ observable.

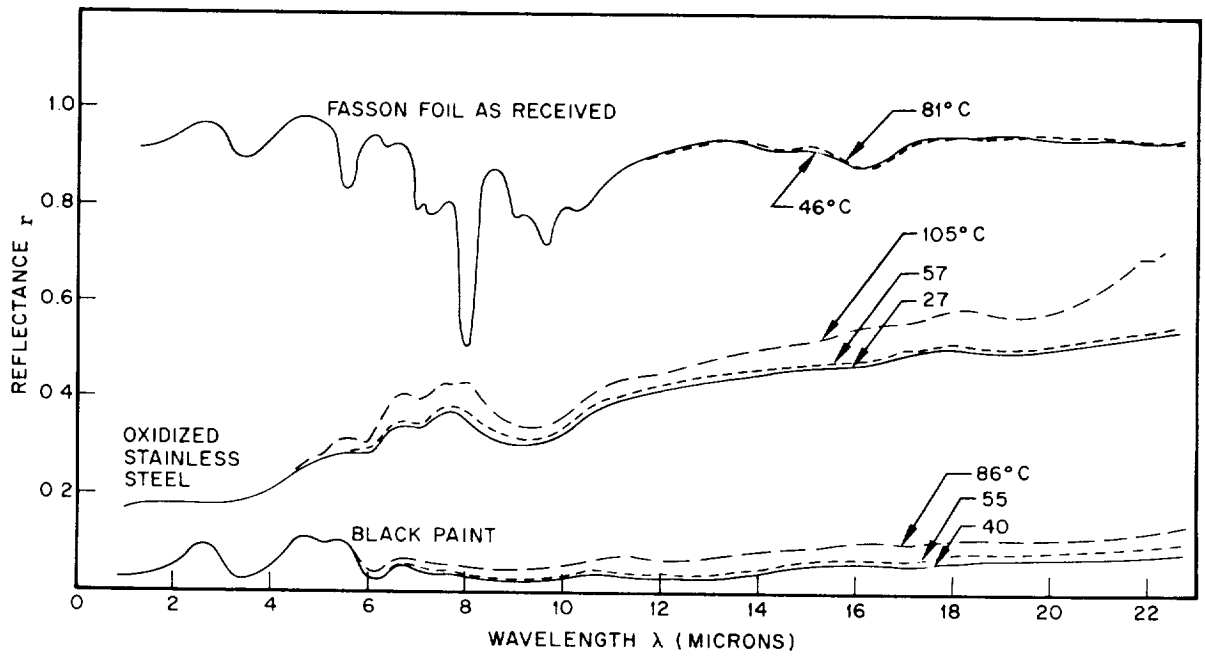

FIGURE 25–9.—Hohlraum data showing effects of sample temperature.

APPLICATION OF ANALYSIS TO HOHLRAUM DATA

The uncertainty analysis and corrections procedure outlined in the previous sections will now be clarified by application to the data obtained in the sample emission runs shown on figure 25–9. The analysis was performed for each material at the lowest sample temperature. The results of the computations are presented in table 25–III.

The first step in the process is to correct r, the indicated reflectance, for sample emission in order to obtain a nominal value of ρ_N. The accuracy of this correction depends upon an estimate of surface temperature, which is inferred from the backface temperature. The

TABLE 25–III.—*Application of Correction and Uncertainty Analysis Procedure to Hohlraum Data*

Material	λ (μ)	r	T_B* (° C)	T_1** (Est.) (° C)	Sample emission correction	ρ_N	$\Delta\rho_N$
Parson's black paint	2	0.05	40	61 ± 10	~0	0.05	±0.01
	5	.10	40	61 ± 10	−0.001	.10	±.01
	10	.02	40	61 ± 10	−.017	.01	±.01
	20	.07	40	61 ± 10	−.032	.04	±.02
Oxidized stainless steel	2	.18	27	30 ± 2	~0	.18	±.01
	5	.27	27	30 ± 2	−.001	.27	±.01
	10	.33	27	30 ± 2	−.003	.33	±.01
	20	.51	27	30 ± 2	−.004	.51	±.01
Fasson aluminum foil (w/ lacquer)	2	.94	46	47 ± 1	~0	.94	±.02
	5	.97	46	47 ± 1	~0	.97	±.01
	10	.80	46	47 ± 1	−.001	.80	±.01
	20	.95	46	47 ± 1	−.001	.95	±.01

*T_B: temperature of back face of sample.
**T_1: temperature of front face of sample.

third column of table 25–III shows the data used in this procedure and indicates the probable temperature error introduced.

For the hohlraum configuration used it is found that the effect of sample-to-reference area radiant interchange will give a maximum uncertainty, $\Delta_I \leq 0.0003$. The uncertainty in evaluation of J_0 by using $J_0 = E_{room\ temp}$ gives $\Delta_0 \leq 0.002$ at the ongest wavelengths, where Δ_0 has its maximum value. The uncertainty Δ_A due to the aperture is also small for the present hohlraum and has the maximum value of $\Delta_A = 0.0003$ for a diffuse reflector. The value of this term can be higher for the oxidized stainless steel due to its specular nature; however, this could not be expressed quantitatively due to the lack of data on the directional dependance of sample reflectance. Δ_I, Δ_0, and Δ_A were not included in the results presented in table 25–III due to their obvious negligible effects.

The remaining uncertainties in equation (5) were evaluated as functions of wavelength to determine $\Delta\rho_N$. In the derivation of the remaining terms, it has been assumed that these terms (Δ_E, Δ_T, Δ_s) are essentially independent since their causes are small perturbations about the ideal condition. In the final summation, it may then be concluded that each error has an equal probability of being within its assigned uncertainty interval. The uncertainty interval of ρ_N, as given by $\pm\Delta\rho_N$, is then best evaluated by taking the root-sum-square of Δ_E, Δ_T, and Δ_s. The probability that the error in any particular measurement of ρ_N will be less than $\Delta\rho_N$ is the same as that associated with the individual errors and their respective uncertainties (Δ_E, Δ_T, Δ_s) (ref. 15).

For the measurements performed on Fasson aluminum foil, the uncertainty due to cavity temperature non-uniformities Δ_T and external instrumentation Δ_s predominated. With oxidized stainless steel, Δ_s was more important. Uncertainty due to sample temperature measurement, Δ_E, was significant only for Parsons black, and then only at long wavelengths. At 20 μ, $\Delta_E \approx \Delta_s$; Δ_s was the only other significant source of uncertainty with Parsons black.

DISCUSSION OF RESULTS

The direct measurement of infrared spectral emittance of coatings and materials at ambient room temperature is impractical because of the small intensity of radiated energy. Therefore, a reflectance method which provides sufficient energy, is reproducible, illuminates the sample diffusely, has a simple sample configuration, and permits rapid sample changing and measurement is desirable.

The hohlraum apparatus meets these requirements. Interpretation and application of the data obtained by the apparatus must be generally tempered with knowledge of the physical principles involved. Data must be corrected for specific operational characteristics of associated optical equipment and for sample emission in some instances. The theoretical analysis and experimental evaluation presented is applicable where the apparatus is used in a routine manner to investigate materials with special optical properties, to screen commercially available materials for optical characteristics classification, and to study changes in optical properties with composition, application, or environmental-exposure variations.

As indicated in the analysis of instrument error and operating procedure, many of the inherent or possible equipment uncertainties are reduced by utilizing the double-beam system with a 100% level and a "working" zero level established at the beginning of each run. Establishing these values for each data chart on which four or five sample values are recorded provides an hourly correction for changes in equipment performance. Additional operational uncertainties are minimized by measuring "working" standards of highly specular reflecting and diffuse absorbing materials at the beginning of each day's operation.

The analysis of uncertainties for the three measured samples shows that the normal spectral reflectance may be obtained to within ± 0.02 reflectance units when sample emission corrections are applied and hohlraum temperatures carefully regulated.

This represents a large percentage error in reflectance for high emitters; however, where a low-temperature emittance is inferred from the reflectance, the error in ϵ_N is of the same order of magnitude as found in radiometric methods. Inferring ϵ_N in the same way for Fasson foil results in a large percentage error in emittance (10 to 30%).

In addition to the uncertainties and errors discussed in the reflectance measurement technique, the directional dependence of the sample must be considered in interpretation of the results for spacecraft design use. The infrared radiation characteristic most often desired for heat transfer calculations is the total hemispherical emittance, while the value obtained from the hohlraum determination is near-normal reflectance. The calculation of near-normal absorptance from this expression is $1-\rho_N=\alpha_N$ for opaque systems. A value for total hemispherical absorption, from which is inferred a value of total hemispherical emittance, must then be obtained. The total hemispherical absorptance is commonly computed through use of the multiplicative factors derived by Eckert for α_{HT}/α_{NT} (ref. 15), which can at best be considered as an approximation. In reference 16, this expression is shown to be as much as 12% in error when compared to experimental values. Detailed knowledge of the directional radiative behavior is required to accurately evaluate ϵ_{HT} from spectral reflectance measurements.

In conclusion, with proper hohlraum design and operation, utilizing the ratio-recording technique and correcting for the effect of sample emission, it is possible to perform rapid measurements of infrared spectral near-normal reflectance with uncertainties of 0.02 reflectance units. Values of total hemispherical emittance may be estimated from these measurements with suitable accuracy for material screening and evaluation purposes. Furthermore, when utilized in an integrated thermal radiation characteristic measurement program, the hohlraum values provide a valuable check on the emittance data obtained with other techniques.

ACKNOWLEDGMENT

The work described in this paper was sponsored by the SSD of the U.S. Air Force Systems Command under Contract No. AF-04(647)-787.

REFERENCES

1. Camack, W. G.; and Edwards, D. K.: Effects of Surface Thermal-Radiation Characteristics on the Temperature Control Problem on Satellites. First Symposium on Surface Effects on Spacecraft Materials, (F. J. Clauss, ed.), John Wiley & Sons, Inc., 1960, pp. 3–54.
2. McNicholas, H. J.: Absolute Methods in Reflectometry. NBS Jour. Res., vol. 1, Oct. 1927.
3. Von Fragstein, C.: Uber de Formulierung des Kirchoffschen Gesetzes und ihre Bedeutung fur ein Zweckmassige Definition von Remissionzahler. Optik, vol. 12, 60, 1955-
4. Gaumer, R. E.; and McKellar, L. A.: Thermal Radiative Control Surfaces for Spacecraft. Lockheed Missiles and Space Div., LMSD 704014, Mar. 1961.
5. Gaumer, R. E.; Clauss, F. J.; Sibert, M. E.; and Shaw, C. C.: Materials Effects in Spacecraft Thermal Control. Lockheed Missiles and Space Div., LMSD-704019, Nov. 1960.
6. McKellar, L. A.: Effects of the Spacecraft Environment on Thermal Control Materials Characteristics. Spacecratt Thermodynamics, (F. J. Clauss, ed.), John Wiley & Sons, 1960, p. 220A.
7. Dunkle, R. V.: Spectral Reflectance Measurements. First Symposium on Surface Effects on Spacecraft Materials (F. J. Clauss, ed.), John Wiley & Sons, Inc., 1960, pp. 117–136.
8. Dunkle, R. V.; Edwards, D. K.; Gier, J. T.; Nelson, K. E.; and Roddick, R. D.: Heated Cavity Reflectometer for Angular Reflectance Measurements. Progress in International Research on Thermodynamic and Transport Properties, (Am. Soc. o Mech. Engineers), Academic Press, 1962, pp. 541–562.
9. Worthing, A. G.: Temperature Radiation Emissivities and Emittances. Temperature, Its Measurement and Control in Science and Industry, vol. 1, Reinhold Pub. Corp., 1941, pp. 1164–1187.
10. Gier, J. T.; Dunkle, R. V.; and Bevans, J. T.: Measurements of Absolute Spectral Reflectivity from 1 to 15 Microns. Jour. Optical Soc. America, vol. 44, no. 7, July 1954.
11. Reid, C. D.; and McAlister, E. D.: Measurement of Spectral Emissivity from 2μ to 15μ. Jour. Optical Soc. America, vol. 49, no. 1, Jan. 1959, pp. 78–82.

12. STARR, W. L.; and STREED, E.: Modification of the Gier Blackbody Reflectometer for Use in the Beckman IR3 Spectrophotometer. Jour. Optical Soc. America, vol. 45, July 1955.
13. SHAW, C. C.: Apparatus for the Measurement of Spectral and Total Emittance of Opaque Solids. Surface Effects on Spacecraft Materials, (F. J. Clauss, ed.), John Wiley & Sons, Inc., 1960, p. 220A.
14. PLYLER, E. K., DANTI, A.; BLAINE, L. R.; and TIDWELL, F. D.: Vibration-Rotation Structure in Absorption Bands for the Calibration of Spectrometers from 2 to 16 Microns. NBS Jour. Res., vol. 64, Jan. 1960.
15. JAKOB, MAX: Heat Transfer, John Wiley & Sons, Inc., 1957.
16. KLINE, S. J.; and MCCLINTOCK, F. A.: Describing Uncertainties in Single Sample Experiments. Mech. Eng., vol. 75, 1953, pp. 3–8.

26—RADIATIVE PROPERTY MEASUREMENTS OF THERMAL CONTROL COATINGS FOR SPACECRAFT

BY M. A. TURNER

MSD/GENERAL ELECTRIC, KING OF PRUSSIA, PENNSYLVANIA

The major problems in establishing the reliability of thermal control coatings in spacecraft are the measurement of their radiative properties–solar absorptance, emittance and transmittance, including their dependence upon angle of incidence—and the prediction of the effect of pre-flight, ascent and orbital environments upon these properties. For high precision each type of coating requires a different measurement approach as well as a tailored procedure for evaluating the environmental effects.

Spectrophotometers which measure reflectance yield the greatest accuracy for materials having reflectances near zero. Surface emission and other extraneous sources degrade the accuracy of the emittance determination for such specimens. However, these instruments yield large discrepancies in determining the values of highly specular surfaces having very low emittance or solar absorptance. The properties of such surfaces are measured with greater precision by calorimetric methods in a model solar simulator.

A set of reference coating samples, a flat absorber, a specular reflector, a solar absorber, a solar reflector, and a couple of intermediate types are employed as a means of "calibrating" the spectrophotometers for routine measurements by comparison with direct calorimetric measurements in a vacuum, and with measurements obtained in other laboratories.

In long-lived vehicles, such as the astrophysical communications and weather satellites, degradation of the radiative properties, usually in the form of darkening of white coats and clear films, comes about principally as a result of pre-flight smudging, solar ultraviolet and long-term Van Allen belt irradiations. The uncertainties in predicting these effects are greatest for surfaces having low values of solar absorptance and emittance or high transmittances.

The reduction of the limits of uncertainty in the predicted radiative properties of surface finishes and coatings applied to long-lived vehicles such as the communications and weather satellites yields greater flexibility in the use of passive temperature control. The requirements for active devices such as thermally sensitive shutters or added battery weight to provide temperature control are reduced.

These limits involve a number of factors of which the more significant usually include:

(a) measurement of radiative properties
(b) formulation and application procedures
(c) pre-flight maintenance of coatings and orbital environments

This assumes that the surfaces are protected by shrouds from thermal degradation during ascent.

Since errors in measurement are significant in all coating evaluations, a method of reducing limits of uncertainty in radiative property measurements is the first concern of this paper. It is partially substantiated by internal experience as well as by the literature (refs. 1, 2, 3). The procedure utilizes:

(a) routine normal reflectance measurements over the solar spectrum and the blackbody emission spectrum at vehicle skin temperature with in-house spectrophotometers—Perkin-Elmer model 205 and Beckman DK1;
(b) preparation of four or more types of stable reference surfaces—black organic enamel, black and white porcelain enamels, siliconized aluminum mirrors, aluminized silicone—for use as bases

of comparison of the spectrophotometric measurements with calorimetric measurements and measurements in other laboratories;

(c) use of calorimetric determinations of radiative properties of the reference samples in a "solar simulator"—liquid nitrogen cooled cold wall vacuum chamber fitted with mercury, (Hg), Hg-argon, Hg-xenon, xenon, or other lamps—as a check of the results from the in-house spectrophotometers; and

(d) check measurements obtained at other laboratories.

Subsequent sections deal with the environmental factors in the order listed.

Finally, the relative importance of the several measurement and environmental factors as applied to different types of surfaces is considered.

SPECTROPHOTOMETRIC MEASUREMENT ERRORS

The spectrophotometric spectral reflectance measurements are reduced to yield integrated values of solar reflectance or reflectance over a blackbody spectrum at the satellite operating temperature. The basic relationship is:

$$\rho = \frac{\int_0^\infty \rho_\lambda S_\lambda d\lambda}{\int_0^\infty S_\lambda d\lambda}$$

where

ρ_λ=spectral reflectance or the dimensionless fraction of the incident source radiation of wavelength λ which is reflected by the given surface.

S_λ=monochromatic source intensity, energy $\times$ area^{-1} $\times$ time^{-1} $\times$ unit wavelength^{-1}, employing the Johnson curve for the solar spectrum or a blackbody spectrum at thermal temperatures.

Subtraction of integrated reflectance from unity yields the desired solar absorptance or emittance.

The evaluation of the spectral reflectance poses the principal problem. The following analyses of errors involved in the integrated reflectances yields the basis for "comparison" with alternative calorimetric techniques. The errors consist of two components—the systematic bases and the random limits of uncertainty. It is noted that the magnitudes of these errors in reflectance affect high values of solar absorptance or emittance (i.e., values over 0.85) by less than 5%. On the other hand, the limit of uncertainty in a nominal value of emittance of 0.05 is +60%±80%

Solar Absorptance

A Beckman DK 1L spectrophotometer, equipped with a magnesium oxide (MgO) coated integrating sphere, yields the spectral reflectance of a surface for monochromatic radiation over the wavelength range of 0.2 to 2.5μ. The signal from the surface is compared with that from a reference MgO surface. The total solar reflectance of the reference MgO surface is assumed to be 0.95. The sources of error in the solar reflectance of the surface in question are summarized as follows:

Source of error	*Magnitude of error*	
	Specular	*Diffuse*
(a) Degradation of reference MgO sample and the internal MgO coating on the integrating sphere.	−0.01 to 0.08	+0.01 to 0.08
(b) Comparison of dissimilar samples with MgO reference.	−0.05 max	−0.01 max
(c) Miscellaneous error overall	+0.005	+0.006
	−0.03±0.01	+0.01 ±0.01

Error (a) may be held to +0.01 by normal maintenance of the reference MgO sample and the internal MgO coating of the Beckman sphere.

Edwards et al. (ref. 1, 3) claim a precision of ±.015 with their spectrophotometric equipment. However, their measurement of reflectance of platinum at 2μ as a function of angle of incidence was biased from the reflectance curve calculated from the fresnel equation by a magnitude of −0.04. Thus, there may be a bias in the solar reflectances obtained with an

integrating sphere greater than ±0.015 for specular samples.

Miscellaneous errors due to direct irradiation of the detector and nonlinearity of detector are suspected.

Emittance

The following errors are inherent in the Perkin-Elmer model 205 hohlraum-monochromator-spectrophotometer:

Source of error	Magnitude of error: Specular	Magnitude of error: Diffuse
(a) Temperature gradient in hohlraum	+0.03±0.03	+0.03±0.03
(b) Exit port (assuming a 1½ in. diameter port and a distance from sample to port of 4 in.).	−0.018±0.018	−0.018±0.005
(c) Emission of sample	nil	negligible
(d) Nonlinearity of detector	+0.01±0.01	unknown
(e) Correction from "normal" measurements to hemispherical reflectances.	±0 to 0.02	±0 to 0.02
(f) Miscellaneous errors due to extraneous sources, optical aberrations, spectral shift of reflected beam overall.	+0.022±0.04	+0.032±0.04

Error (a) was observed by operating the hohlraum at different temperatures and measuring reflectances on the same samples.[1] The integrated values of emittance varied with hohlraum temperature as follows:

Hohlraum temperature, °C.	E at 100° F.
900	0.80
750	.92
400	.94

STANDARD REFERENCE SURFACES FOR COMPARISON OF SPECTROPHOTOMETRIC WITH CALORIMETRIC MEASUREMENTS

The selected reference surfaces are prepared by coating all surfaces—front, back and edges—of ⅞-in. diameter by 0.062 in. thick Al or steel mounting disks. Each mount is fitted with a thermocouple as shown in figure 26–1 prior to coating to permit mounting for calorimetric radiative property determinations. The thermocouple lies in the plane of the disk and is brazed or welded at the center to reduce temperature sensing errors during transient heating or cooling of the sample. The dimension of the disk is selected to permit mounting in the spectrophotometers as well as in a cold-walled solar simulator.

The selection of the standard reference surfaces is based principally on stability against storage, handling, measurement and cleaning treatments as well as suitability as references for different surface types. The flat absorber types are compared with black reference surfaces, e.g., a matte black porcelain enamel. The flat reflectors with specular surfaces are compared with siliconized aluminum mirror references. The solar reflectors are compared with matte white porcelain enamels. The solar collectors are compared with aluminum mirror references.

The calibration procedure—comparing spectrophotometric, calorimetric and outside laboratory measurements of radiative properties of the reference samples—must account for aging by such factors as handling and atmospheric reaction, as well as random errors and systematic biases in measurements. Weighting of the different types of measurement will depend upon the type of surface—flat absorber, solar collector, flat reflector or other—and the degree of randomness and reproductibility of the measurements.

ERRORS IN CALORIMETRIC DETERMINATIONS OF RADIATIVE PROPERTIES

Calorimetric techniques for determining total radiative properties promise to reduce the limits of uncertainty in low values of solar absorptance and emittance as determined by the spectrophotometric measurements. They are adaptable to measurement of total absorptance as a function of angle of incidence.

[1] Unpublished data from C. Foster, MSD, General Electric Co.

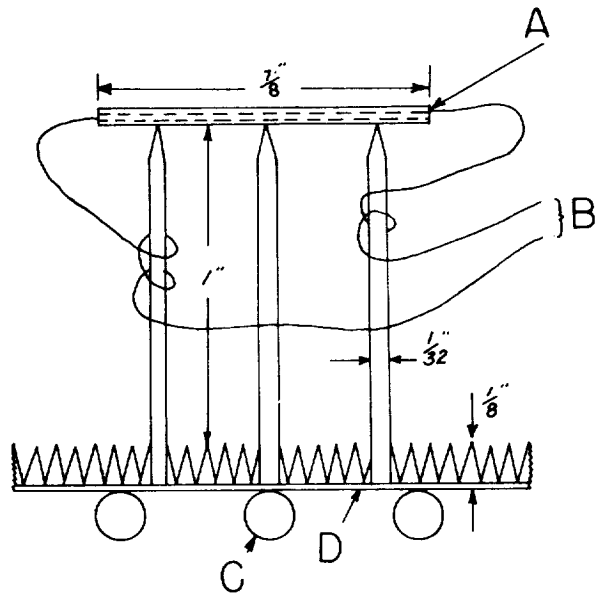

FIGURE 26-1.—Sample mounting in cold-walled chamber.

A—Sample: 2-8 mil coating applied front, back, and edge of ⅞-inch dia. by 1/16-inch thick Al 2024 T3 or steel disk with 15-mil slot through center.
B—Copper-constantan thermocouple, 5-mil dia., inserted with junction brazed at center. Calibrate thermocouple after coating by inserting sample in plastic bag in three baths: distilled water, liquid nitrogen, and boiling water (noting barometric pressure).
C—Liquid nitrogen cooled.
D—3-Point needle mounting grid coated with black pigmented silicone alkyd over washer primer and cured 1 hr at 4° F.

Greater accuracy is achieved in determining emittance than solar absorptance since the radiation sources—*Hg* arc or *Hg*-xenon—do not exactly duplicate the sun spectrally.

Figure 26-2 is a schematic of the apparatus.

The radiation source is a 1000-watt G.E. *A-H6 Hg* vapor lamp with water cooled quartz jacket. The emission spectrum for this lamp is suppled by the Outdoor Lighting Department, General Electric Company. Since a parabolic reflector is employed to yield a collimated beam, the radiation intensity at the sample level decreases with radial positon.

The calorimetric determination of the radiative properties is achieved by comparing heat balances over the individual samples with those over adjacent "standard reference samples."

The transient heat balance is:

$$\alpha A_s Q F_{q-s} = (2A + Ap)\sigma[F_{s-c}\epsilon T^4 - F_{c-s}\alpha_c T_c^4] + M\left[a + \frac{b}{T} + \frac{c}{T^2}\right]\frac{dT}{dt}$$

α	absorptance
A_s	area of sample as viewed by the radiation source, ft$_2$ (the area of one face if in a normal position)
F_{q-s}	geometry factor for source-to-sample
Q	source intensity, Btu/ft^2-hr
A	area of one face of the sample, ft^2
Ap	sample perimeter area, ft^2
σ	Stefan Boltzmann constant, Btu/ft^2-hr-°R^4
T	temperature of the sample, °R
F_{s-c}	geometry factor for sample-to-cold wall
ϵ	emittance of sample (normally identical for all surfaces)
T_c	effective sink temperature, °R
F_{c-s}	geometry factor for sink-to-sample
α_c	absorptance of sample for sink radiation
M	masss of sample, lb
$a,b+c$	sample specific heat coefficients with units to yield Btu/lb-°R
t	time, hr.

The geometry factors—F_{q-s}, F_{s-c}, and F_{c-s}—are normally assumed to be unity if the following precautions are utilized in designing the test apparatus:

(a) The sample is set 3 reflector diameters from the parabolic reflector.
(b) The sample is set 3 sample diameters from the bottom.
(c) The bulk (over 90%) of the lamp energy is collimated, vertically.
(d) The walls are painted black.

The intensity Q and the effective sink temperature T_c are mapped at the sample level by heat balances for a matrix of like black reference samples for which all other parameters together with temperature-time histories are known. The chamber is pumped down to cold equilibrium with the lamp off to yield T_c. The lamp is then turned on and the vacuum maintained until steady-state warm equilibrium is achieved to yield the map of Q values from the resulting temperature-time histories with the black references.

Having mapped Q and T_c, values of α and ϵ may be calculated from heat balances in the steady state for the unknowns by comparing

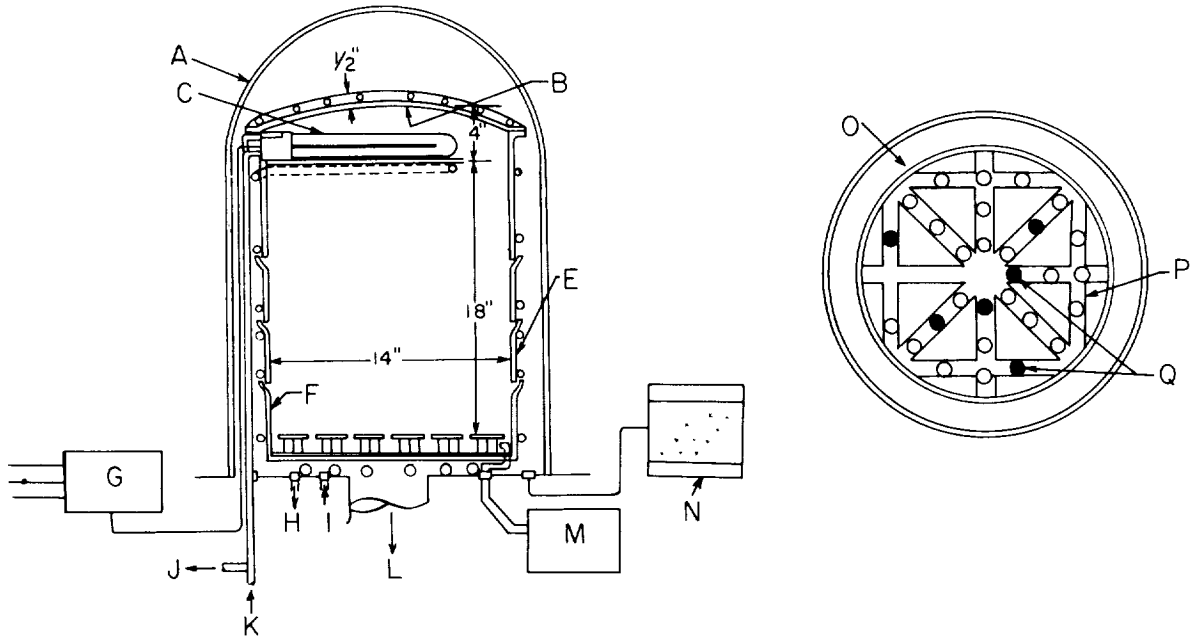

FIGURE 26-2.—Calorimetric determination of ultraviolet degradation of radiative properties.

A—Bell jar.

B—Parabolic aluminum mirror.

C—1000-watt GE A-H6 quartz lamp source. Water-cooled. 0.06-×-1 inch source with 1⅛-inch air-cooled jacket. Radiation output about 600 watts/$4\pi sr$, yielding at the sample level:

radius, inches	*Btu/ft²-hr*
1½	1400
2	1330
3½	970
5	830
5 (60% power)	500

D—Baffle below lamp, top side coated black.

E—Thermocouples:

1. Top of reflector.
2. Bottom of lamp baffle.
3. Bottom of cold wall can.
4. Side of cold wall can.

F—Liquid nitrogen-cooled jacket.

G—Transformer and power control.

H—Nitrogen gas.

I—Nitrogen liquid.

J—Water outlet.

K—Water inlet.

L—To vacuum.

M—Thermocouple vacuum gage.

N—30-Point recorder with 2-sec time constant and up to 1-ft/min chart travel.

O—To measure angular dependence of absorptance mount only one row of samples at desired angles of incidence.

P—Mounting grid.

Q—Black reference samples.

Additional devices—thermopiles, black boxes, collimating baffles—may be employed for transmittance and alternative emittance determinations.

them with the heat balances for the black references.

The technique can be employed to determine the dependence of emittance on temperature by either operating with different source intensities—obtained at different radial positions or by using different power inputs and possibly by interchanging lamps of different outputs—or by studying the transient temperature-time histories during start-up and after shutdown by means of the heat balance equation and its derivative with respect to the parameter T^4.

It should be noted that a study of ultraviolet effects on the radiative properties may be combined with these measurements. In the event that the emittance is affected on the irradiated side only—not expected for high values—, spectrophotometric measurements

may be employed to note the differences between exposed and unexposed surfaces.

By orienting the samples relative to the collimated source, the angular dependence of absorptance can be measured.

The sources of error in calorimetric determinations of solar absorptance and emittance are:

Source of error	Magnitude, % α_s	Magnitude, % ϵ
(a) Variations in source intensity Q (via comparison of temperature-time history of black samples with specimen)	±5	nil
(b) Extrapolation from source spectrum to solar spectrum	±4	nil
(c) Measurement of A_s, A, A_p	±2	±1
(d) Measurement of T	±2	±2
(e) Measurement of M	±1	±1
(f) Knowledge of heat capacity constants a, b and c	±2	±2
(g) Overall	±4	±2

Somewhat wider overall limits may be expected for low values of α_s and ϵ, i.e., less than 0.30.

Of prime concern in calorimetric determinations is the temperature measurement. An error of 1% in temperature measurement is reflected as a 4% error in emittance. When the thermocouple is attached normally with Saureisen cement, the emittance values appear to be in error by +20 to +100% during transient heating and −40 to −10% during transient cooling. On the other hand thermocouple attachment by welding normally yielded an emittance of a Rokide A sample of 0.91±0.02, as equilibrium was approached during the heating and 0.89±0.02 during the cooling transients. Attachment as shown in figure 26-1 would yield greater precision.

Calorimetric measurements may be adapted to orbital tests as in the ARENTS Program (General Dynamics/Astronautics). The data are reduced by comparing temperature-time data telemetered back to earth. In general, this involves transient conditions.

COMPARISON OF ACCURACIES OF MEASUREMENT TECHNIQUES

Case 1: α_s=0.3 and ϵ=0.85

Method of measurement	Magnitudes of limits of uncertainty α_s	ϵ	α_s/ϵ
(a) Internal spectrophotometric	±0.02	±0.04	±0.05
(b) Internal and external (UCLA) spectrophotometric	±.02	±.03	±.04
(c) Internal calorimetric	±.02	±.02	±.03
(d) Internal spectrophotometric and internal calorimetric	±.02	±.01	±.02
(e) Internal and external spectrophotometric and internal calorimetric	±.02	±.01	±.02

Case 2: α_s=0.22 and ϵ=0.85

Method of measurement	Magnitudes of limits of uncertainty α_s	ϵ	α_s/ϵ
(a) Internal spectrophotometric	±0.02	±0.01	±0.022
(b) Internal and external spectrophotometric	±.02	±.01	±.022
(c) Internal calorimetric	±.02	±.004	±.011
(d) Internal spectrophotometric and internal colorimetric	±.01	±.003	±.008

LIMITS OF UNCERTAINTY IN RADIATIVE PROPERTIES IMPOSED BY PRE-FLIGHT COATING MAINTENANCE

Handling, assembly, storage and shipping invariably cause smudging. Restorative measures such as cleaning with detergents, or application of a washable overcoat followed by washing, tends to increase solar absorptance or emittance. This places a premium on hard, durable and washable coating films.

A typical air-dried organic enamel—a Stoner Mudge white base—was coated with Elvanol, dried over night and washed with warm water. As expected, the total solar absorptance in-

creased from 0.31 to 0.33 in the process. On the other hand, a rutile-pigmented silicone alkyd treated in the same manner showed no significant change, i.e., the measured solar absorptance was 0.23 before and 0.22 after treatment.

As a rule of thumb, the reflectance may be expected to decrease by 0 to 5% due to the preflight environment, with normal care in coating maintenance.

LIMITS OF UNCERTAINTY IN RADIATIVE PROPERTIES IMPOSED BY ORBITAL ENVIRONMENTS

The principal factors of concern involve the ultraviolet and charged particle degradations resulting in increased solar absorptance of white coatings. Less marked effects also occur in flat reflectors and solar collector types. Thermal cycling and loss of weight in the vacuum of space have not yielded significant effects in the coating system considered for the −200° to 200° F temperature regime.

All air-dried organic white base enamels show 20–50% increases in solar absorptance after exposure to a hundred or more sun hours of ultra-violet. Organic enamels requiring curing at 300° to 400° F—fully methylated silicones—show much greater stability against further solarization (refs. 5 and 6). Tompkins (ref. 6) and Sibert (ref. 7) point up the high stability of certain inorganics, e.g., zinc oxide pigmented potassium silicates.

Similar results have been found in a cursory examination of the effects of electron irradiation, simulating Van Allen belt exposures for one year, on selected organic coatings. Table 26–I summarizes the results from an exposure of 1.6×10^{10} rads at the surface. The data supports the following observations:

(a) Solar absorptances of air-dried white enamels increased by 80 to 180%.

(b) Curing the paints 1 hour at 400° F almost completely stabilized the silicone alkyd and the methylphenyl silicone against electron degradation although the curing darkened the alkyd severely.

In summary, the following estimates of errors in predicting the degree of changes in solar absorptance of white coatings are proposed:

(a) Changes due to ultraviolet exposure of 200 sun hours.

Type of coating	*Solar absorptance, %*	*Emittance, %*
Organics air-dried	±15	±1
Organics dried at 300° 400° F	±7	nil
Selected inorganics cured at 270° F	±6	nil

(b) Changes due to an exposure of 10^{10} rads of charged particles at the surface (roughly 1 year in a synchronous equatorial orbit).

Type of coating	*Solar absorptance, %*	*Emittance, %*
Organics air-dried	±30	±2
Organics cured at 300°–400° F	±5	nil
Selected inorganics cured at 270° F	unknown	nil

RELATIVE IMPORTANCE OF THE ERRORS IN MEASUREMENT AND IN PREDICTION OF ENVIRONMENTAL EFFECTS

The overall limits of error in predicting solar absorptance after one year in orbit resulting from the various sources is estimated for several types of coatings as follows:

Type of coating	*Measurement errors, %*	*Effects of ultraviolet, %*	*Electrons, %*	*Overall, %*
White base, organic:				
Air dried	±10	±15	±30	20
Cured at 300°–400° F	±10	±7	±5	8
White base, inorganic—cured at 270° F	±10	±6	(?)	8
Flat reflector	±15	±6	(?)	14
Solar reflector	±4	±2	(?)	3
Flat absorber, black	±3	nil	nil	3

TABLE 26-I.—*Electron Radiation Effects on Typical Organic Coatings*

Formulation	Cure	As-received		10^{17} e-cm^{-2} of 60 kev-e^{-1} [a]		10^{16} e-cm^{-2} of 600 kev-e^{-1} [b]	
		α_s	ϵ	α_s	ϵ	α_s	ϵ
Vapor-deposited 1400 AS.0/A1/S.0/A1 disk		0.14	0.04	[c]0.29	[c]0.06	--	----
Vita-Var PV100–26% PVC rutile in silicone alkyd	Air-dried	.22	.88	.52	.89	--	----
	8 hr at 200° F	--	.87	.46	.89	--	----
Aluminized silicone alkyd	Air-dried	.33	--	.34	--	--	----
	1 hr at 250° F	.32	.29	.32	--	0.34	0.31
Zinc sulfide in methyl phenyl silicone	1 hr at 400° F	.30	.91	.32	.91	--	----
Rutile 50% PVC in methyl phenyl silicone	1 hr at 400° F	.24	.82	.23	.78	.24	----
Rutile in silicone alkyd	1 hr at 400° F	.42	.89	.42	--	--	----
Rutile in silicone acrylic	Air-dried	.25	.86	.45	.88	--	--
Rutile in polyurethane	Air-dried	.25	.91	.69	--	--	----

[a] The dosage from 10^{17} e-cm^{-2} of 60 kev-e^{-1} is 1.6×10^{10} rad.
[b] The dosage from 10^{16} e-cm^{-2} of 600 kev-e^{-1} is 4×10^{8} rad.
[c] Significant increases may also have been caused by handling, in addition to the irradiation.

The measurement errors are dominant in predicting the emittances, i.e., the range from $\pm40\%$ for low values to $\pm3\%$ for high values.

CONCLUSIONS

The degree of reliability achieved in calling out coatings for radiative property control in long-lived vehicles in orbit depends principally upon:

(a) Utilization of curing techniques at elevated temperatures to stabilize up to 400° F selected organic and inorganic coating systems against ultraviolet and charged particles effects.

(b) more accurate measurements, to be achieved principally by comparison of calorimetric data with similar values computed from spectrophotometric data.

REFERENCES

1. DUNKLE, ET AL.: Heated Cavity Reflectometer for Angular Reflectance Measurements. ASME Symposium on Progress in International Research in Thermodynamic and Transport Properties, p. 541.
2. GAUMER, ET AL.: Calorimetric Determinations of Thermal Radiation Characteristics. ASME Symposium on Progress in International Research in Thermodynamic and Transport Properties.
3. EDWARDS, ET AL.: Integrating Sphere for Imperfectly Diffuse Samples. Jour. Optical Soc. of America, Oct. 1961.
4. VAN VLIET, R. M., ET AL.: Spectrally Selective Coatings for Temperature Control of Space Probes. WADD TR 60-386, Oct. 1960.
5. GAUMER, CLAUSS, ET AL.: Material Effects in Spacecraft Thermal Control. LMSD 7040 19, Nov. 1960.
6. TOMPKINS, EDWIN H.: Stable White Coatings. ARF 3207-5, Apr. 1962.
7. SIBERT, M. E.: Inorganic Surface Coatings for Space Applications. Symposium Papers, Division of Organic Coatings and Plastics Chemistry, Sept. 1961.

27—LOW-TEMPERATURE EMITTANCE APPARATUS

BY ROBERT W. WARD AND JOHN F. McDONOUGH

NASA LANGLEY RESEARCH CENTER, LANGLEY, VIRGINIA

This paper describes a method of emittance measurement for very thin sheet materials in the temperature range of 273° K to 373° K. A mathematical expression is derived for the emittance of the innermost of two concentric cylinders, and simplifying assumptions are made to reduce this relationship to the usual equation for a heated "wire in vacuo." The error due to the simplification is discussed. The apparatus and instrumentation are described and some results are presented.

The need for a method to accurately measure total hemispherical emittance at satellite temperatures became apparent early in the Echo A–12 project. Echo A–12 is a larger and more rigid version of the successful Echo I passive communication satellite. The rigidity is achieved by using a three-layer laminate, consisting of a sheet of 0.35-mil-thick Mylar sandwiched between two 0.18-mil sheets of aluminum foil. After the compactly folded satellite has been injected into orbit it will be inflated to a sphere, 135 ft in diameter, by internal pressure. This internal pressure will sufficiently stress the laminate to cause a permanent set, resulting in a rigid, self-supporting sphere.

The equilibrium temperature of the inflated satellite must be controlled to a value of about 330° K in order not to exceed the maximum operating temperature of two radio beacons which are attached to the skin of the satellite for tracking purposes.

An analysis of the heat-balance equations of the satellite revealed that the ratio of solar absorptance to thermal emittance α/ϵ would have to be 1.67 to give the desired equilibrium temperature. However, α/ϵ for the surface of the laminate was known to be about 6, which would give an equilibrium temperature of about 453° K. An experimental program was then planned to lower α/ϵ to the desired value by the application of the proper amount of either an organic, epoxy-based paint or an inorganic type of coating referred to as alodine.

In support of the program, it was found that α could be measured routinely and accurately by a reflectance method using a Beckman DK–1 spectrophotometer. The measurement of ϵ, however, required the development of a new apparatus which could measure accurately emittances over a wide range of values and at temperatures from 273° K to 373° K.

The selection of a method to measure these emittances presented two aspects: (1) the low-temperature range with the inherent difficulty of low energy levels which makes the system sensitive to stray ambient energy, and (2) the form of the test material, an extremely thin (but opaque), flexible sheet.

The low-energy problem indicated use of the power-dissipation method, in which a known amount of power is dissipated by radiation from the test sample. The second problem involved finding a suitable configuration which was simple enough mathematically for an easy calculation of the desired emittance and having a shape readily adaptable to the application of a thin sheet. The simple arrangement of two concentric spheres was rejected because of the difficulty in making a flat sheet conform to a spherical surface, which left the only configuration of reasonable simplicity that of two concentric cylinders.

SYMBOLS

A area

F view factor for blackbodies; F_{12} = portion of total radiation from surface 1 incident on surface 2

R radiant flux per unit area; ${}_1R_2$ = flux due to emission of A_1 reflected by A_2
ϵ emittance
ρ reflectance
r radii of cylinders
L length of cylinders
T absolute temperature
δ Stefan-Boltzmann constant
q heat transfer per unit time
F' view factor for graybodies
α solar absorptance

Subscripts:

1 inner cylinder
2 outer cylinder
3 one end of outer cylinder
4 other end of outer cylinder
0 outer cylinder and both ends of outer cylinder
t total
n normal
λ wavelength

RADIATIVE HEAT TRANSFER FROM INNER CYLINDER TO ITS SURROUNDINGS

In the case of two concentric cylinders of length L and radii r_1 and r_2, the net energy transfer between the inner cylinder and its surroundings can be expressed as (ref. 1).

$$q_t = q_{12} + q_{13} + q_{14} \tag{1}$$

where q_t is the total energy transferred between the inner cylinder surface A_1 and the three surfaces that it "sees" A_2, A_3, and A_4 (fig. 27–1). Since radiative heat exchange is proportional to the difference in the fourth powers of the absolute temperatures, each component of q_t can be expressed as

$$q_{12} = \delta A_1 F'_{12}(T_1^4 - T_2^4) \tag{2}$$

$$q_{13} = \delta A_1 F'_{13}(T_1^4 - T_3^4) \tag{3}$$

$$q_{14} = \delta A_1 F'_{14}(T_1^4 - T_4^4) \tag{4}$$

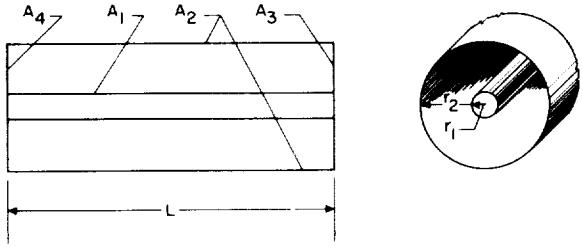

FIGURE 27–1.—Two concentric cylinders.

Since in our apparatus we cool the outer cylinder and the ends to the same temperature, $T_2 = T_3 = T_4 \equiv T_0$, and $q_{13} = q_{14}$ by symmetry, then

$$q_t = \delta A_1 F'_{12}(T_1^4 - T_0^4) + 2\delta A_1 F'_{13}(T_1^4 - T_0^4)$$
$$= \delta(T_1^4 - T_0^4)(A_1 F'_{12} + 2A_1 F'_{13}) \tag{5}$$

Where F'_{12} and F'_{13} are functions of the geometry of the particular configuration and the emittances of the various surfaces. In our case the emittances of the outer cylinder and the ends are made equal, $\epsilon_2 = \epsilon_3 = \epsilon_4 \equiv \epsilon_0$, and it can be shown that (appendix)

$$q_t = \frac{\delta A_1 \epsilon_1 \epsilon_0}{\gamma}(T_1^4 - T_0^4)\left[\frac{2F_{32}\rho_0\Delta + A_3 F_{12}\gamma}{A_3(1 - F_{22}\rho_0)} + \frac{2\Delta}{A_2}\right] \tag{6}$$

from which

$$\epsilon_1 = \frac{\gamma q_t}{\delta A_1 \epsilon_0 (T_1^4 - T_0^4)\left[\frac{2F_{32}\rho_0\Delta + A_3 F_{12}\gamma}{A_3(1 - F_{22}\rho_0)} + \frac{2\Delta}{A_2}\right]} \tag{7}$$

$$\gamma = 1 - F_{22}\rho_0 - F_{34}\rho_0 + F_{22}F_{34}\rho_0^2 - 2F_{23}F_{32}\rho_0^2$$

$$\Delta = A_3 F_{12} F_{23}\rho_0 + A_2 F_{13} - A_2 F_{13} F_{22}\rho_0$$

It is evident that as $\epsilon_0 \to 1.0$ ($\rho_0 \to 0$), then $\gamma \to 1.0$ and $\Delta \to A_2 F_{13}$. Under these conditions:

$$\epsilon_1 = \frac{q_t}{\delta A_1 (T_1^4 - T_0^4)(F_{12} + 2F_{13})} \tag{8}$$

For the view factor F, the following relationship exists (ref. 1),

$$A_1 F_{11} + A_1 F_{12} + A_1 F_{13} + A_1 F_{14} = A_1$$

or

$$F_{11} + F_{12} + F_{13} + F_{14} = 1$$

Since $F_{11} = 0$ and by symmetry $F_{13} = F_{14}$, then

$$F_{12} + 2F_{13} = 1$$

and

$$\epsilon_1 = \frac{q_t}{\delta A_1 (T_1^4 - T_0^4)} \tag{9}$$

In this apparatus the minimum $T_1 = 273°\ K$ while $T_0 = 78°\ K$

$$T_1^4 >> T_2^4$$

$$\epsilon_1 \approx \frac{q_t}{\delta A_1 T_1^4} \tag{10}$$

Equation (10) is the familiar equation for the "wire in vacuo method" used to measure the emittance of materials in wire form at elevated temperatures[2].

If we assume ϵ_0 to be only 0.8 instead of unity, then the error resulting from the use of equation (10) rather than equation (7) is less than 2%. This is calculated by obtaining values for the view factor from reference 3. In the actual apparatus ϵ_0 was made greater than 0.9 by the use of flat black paint.

APPARATUS

The inner cylinder of the previously described configuration, hereafter called the heater rod, was made from a 42-in.-long Inconel tube (fig. 27–2). This tube was ⅝ in. in diameter and had 1/32-in. wall thickness. The tube was heated resistively by a 60-cycle current controlled by an external power supply. The current was measured on a General Electric model P–3 ammeter.

The sample was wrapped tightly on the outside along the full length of the rod, and a 20-in.-long section in the center of the rod was chosen to be the test section. Two small wires were attached to the rod, one at each end of the test section, and were passed along the longitudinal axis of the rod and out the end to a Ballantine true rms voltmeter. This value for the voltage drop across the test section V multiplied by the current reading I gave the value of q_t to be used in equation (10).

To insure that no power was lost from the test section due to heat being conducted along the rod to the colder electrical terminals at the ends, auxiliary guard heaters were used at each end to remove the thermal gradient. These heaters were constructed by winding nichrome wire between two layers of sprayed aluminum oxide. The temperatures of the heaters were controlled independently by external 5-amp Variacs.

The temperature of the rod was monitored at 12 positions along the outside surface by point-contact copper-constantan thermocouples.

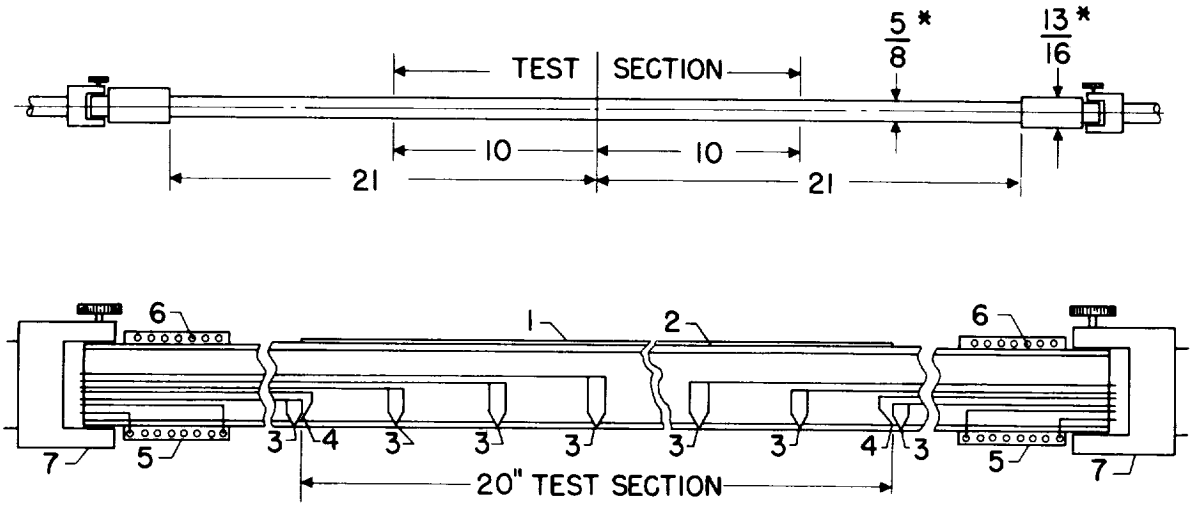

1 - SPECIMEN
2 - HEATER TUBE, 5/8 O.D. 9/16 I.D. INCONEL
3 - THERMOCOUPLES
4 - VOLTAGE LEADS TO MEASURE POWER TO SPECIMEN
5 - GUARD HEATERS
6 - NICROME HEATER WIRE
7 - CURRENT LEADS
* NOT DRAWN TO SCALE

FIGURE 27–2.—Drawing of heater rod.

The leads from the thermocouples were passed along the axis of the rod to the end, and the output of the thermocouples was recorded on a Brown strip chart recording potentiometer. The equilibrium temperature that was made constant across the test section was used for T_1 in equation (10).

The outer cylinder, hereafter called the coolant chamber, was constructed of 0.094-in.-thick, type 304 stainless steel. As can be seen from figure 27–3, the chamber was designed with double walls, the space between them being filled with liquid nitrogen. The joints of the chamber were welded and tested for leaks at a pressure of 30 psi. The leak test was necessary since the chamber had to contain the liquid nitrogen when placed in a vacuum tank.

The radius of the inner wall of the chamber was chosen to be 6 inches. In order to insure that ϵ_0 of equation (7) be as large as possible, the surface of the inner wall was painted with flat black paint.

The heater rod was supported at each end by small rings attached to the coolant chamber. The rings were wrapped with glass tape at points of contact with the rod to minimize the conductive heat transfer, and the arrangement was such that the axis of the rod was concentric with the axis of the chamber.

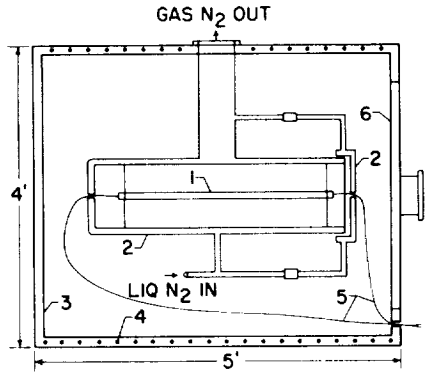

1. SPECIMEN HEATER TUBE
2. COOLANT (LIQUID N_2) CHAMBER
3. VACUUM CHAMBER
4. REFRIGERATION COILS
5. ELECTRICAL LEADS (THERMOCOUPLES, HEATER CURRENT, AND SPECIMEN VOLTAGE)
6. VACUUM CHAMBER DOOR

FIGURE 27–3.—Drawing of heater rod and coolant chamber installed in vacuum tank.

The ends of the chamber were also filled with liquid nitrogen. One end was fixed in place while the other end could be removed to change the sample. The movable end was designed so that when closed there was adequate venting for the chamber during evacuation.

The temperature of the inner wall of the coolant chamber was monitored by two copper-constantan thermocouples attached to the wall and connected to a Brown strip chart recording potentiometer. This temperature was used to insure that T_0 in equation (9) was maintained at 78° K.

The coolant chamber with the sample installed inside was mounted in a 4- by 6-foot vacuum tank (fig. 27–3) which could be evacuated to a pressure of 1×10^{-6} mm of Hg in 1 hour. The pressure was measured on a CEC type GIC–110 ionization vacuum gage. A provision was made in the wall of the tank to allow the coolant chamber to be filled with liquid nitrogen and to let the gaseous nitrogen escape. The power, voltage, and thermocouple leads were passed through special terminals in the wall of the tank. The inner wall of the tank was cooled to about 175° K by circulating liquid ethylene. This additional refrigeration lowered the consumption of liquid nitrogen to about 1 quart per hour when the sample was maintained at its highest temperature, 373° K.

PROCEDURE

With the heater rod out of the coolant chamber and the vacuum tank, the sample was wrapped smoothly about the rod and adhesively bonded. The rod was then replaced in the coolant chamber and the end of the chamber attached. The vacuum tank was sealed and evacuated. After the nitrogen tank had been filled, the rod was cooled to below 273° K by radiation.

The main power supply (see fig. 27–4) was then turned on and the current was increased until the temperature of the rod reached 273° K. After further small adjustments were made in the current to maintain the rod at 273° K, any thermal gradient across the rod was removed by independent adjustment of the Variacs controlling the guard heaters. A reading was then

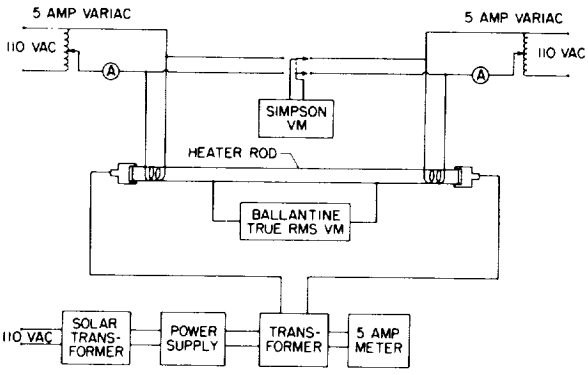

FIGURE 27–4.—Electrical instrumentation system.

taken of the power. The sequence was repeated for rod temperatures 323° K and 373° K. A period of about 5 hours was required for a complete cycle from the time the rod was placed into the vacuum chamber until measurements had been completed at the three temperatures.

RESULTS AND CONCLUSIONS

An error analysis of the instruments revealed that an instrumentation error of 4% could be present in a measurement. When the error due to approximations made in the equations discussed in a previous section is taken into consideration, the overall maximum error of the system is less than 6%.

A comparison was made of the value of emittance measured with this system to that measured by another method. Values of normal spectral reflectance were measured for a sample of the laminate material which had been treated with alodine. These reflectance measurements were made with a Perkin-Elmer 13–U spectrophotometer, using the Gier-Dunkle technique, with the sample at 373° K. The normal spectral emittance $\epsilon_n(\lambda)$ was calculated from Kirchhoff's law. The following equation was numerically integrated to give the total normal emittance ϵ_n of the sample,

$$\epsilon_n = \frac{\int_0^\infty \epsilon_n(\lambda) J(\lambda,T) d\lambda}{\int_0^\infty J(\lambda,T) d\lambda}$$

where $J(\lambda,T)$ is Planck's blackbody distribution function.

The assumption was then made that the sample radiated according to Lambert's law, so that the total normal emittance of the sample was equal to the total hemispherical emittance. The comparison of this value to the measured value at 373° K agreed to within experimental error.

The apparatus has been used to measure more than 150 samples which were painted or treated with alodine. It was determined that the alodine treatment is the more satisfactory method of altering the emittance. The emittance has been correlated to the chemical composition of the alodine and the thickness of the coating. Some typical results for one alodine mixture are shown in figure 27–5.

At present, plans are being made to improve the apparatus by the use of a new design for the heater rod, utilizing d-c operation and indirect heating of the rod. A more accurate and quicker measurement should then be possible.

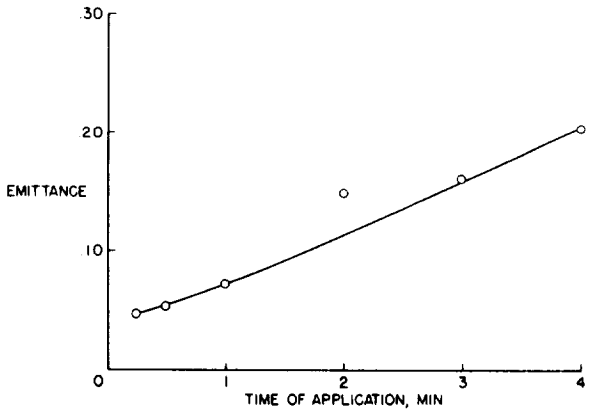

FIGURE 27–5.—Emittance versus time of application for Echo A–12 laminate. Alodine mixture 401. Sample temperature 273° K.

APPENDIX—DERIVATION OF EQUATIONS FOR RADIATIVE HEAT TRANSFER AND VIEW FACTORS FOR TWO CONCENTRIC CYLINDERS (Fig. 27-1) OF LENGTH L AND RADII r_1 AND r_2

Setting up a heat balance, and assuming that $T_2=T_3=T_4=0°$ K and that $\delta T_1^4=1.0$, since view factors are independent of temperature (ref. 1), gives:

1. Flux away from A_1, neglecting self-emission (by reflection)

$$[A_1F_{11}(\epsilon_1+{}_1R_1)+A_1F_{21}\,{}_1R_2+A_1F_{31}\,{}_1R_3+A_1F_{41}\,{}_1R_4]\rho_1=A_1\,{}_1R_1 \quad \text{(A1)}$$

$A_1F_{11}\epsilon_1$ = flux emitted by A_1 and incident on A_1
$A_1F_{11}\,{}_1R_1$ = flux reflected by A_1 and incident on A_1
$A_1F_{21}\,{}_1R_2$ = flux incident on A_1, reflected by A_2
$A_1F_{31}\,{}_1R_3$ = flux incident on A_1, reflected by A_3
$A_1F_{41}\,{}_1R_4$ = flux incident on A_1, reflected by A_4

2. Flux away from A_2 due to emission of A_1

$$(A_1F_{12}\epsilon_1+A_2F_{32}\,{}_1R_3+A_2F_{43}\,{}_1R_4+A_2F_{22}\,{}_1R_2)\rho_2=A_2\,{}_1R_2 \quad \text{(A2)}$$

3. Flux away from A_3 due to emission of A_1

$$(A_1F_{13}\epsilon_1+A_3F_{23}\,{}_1R_2+A_3F_{43}\,{}_1R_4+A_3F_{33}\,{}_1R_3)\rho_3=A_3\,{}_1R_3 \quad \text{(A3)}$$

4. Flux away from A_4 due to emission of A_1

$$(A_1F_{14}\epsilon_1+A_4F_{24}\,{}_1R_2+A_4F_{34}\,{}_1R_3+A_4F_{44}\,{}_1R_4)\rho_4=A_4\,{}_1R_4 \quad \text{(A4)}$$

Equations (3) and (4) are equivalent by symmetry.

To find the view factors F' which take into account greybodies, we remember that δT^4 is set equal to unity and that $[A_m\,{}_nR_m][\epsilon_m/(1-\epsilon_m)]$ is equal to the rate of energy absorption at surface A_m. Then the following relations hold:

$$A_1F'_{12}=A_2\,{}_1R_2\left(\frac{\epsilon_2}{1-\epsilon_2}\right)$$

$$A_1F'_{13}=A_3\,{}_1R_3\left(\frac{\epsilon_3}{1-\epsilon_3}\right)$$

$$A_1F'_{14}=A_4\,{}_1R_4\left(\frac{\epsilon_4}{1-\epsilon_4}\right)$$

$$(A_1F_{21}\,{}_1R_2+2F_{31}\,{}_1R_3)\rho_1=A_1\,{}_1R_1 \quad \text{(A5)}$$

$$F_{11}=0$$
$$F_{31}=F_{41}$$
$${}_1R_3={}_1R_4$$
$$(A_1F_{12}\epsilon_1+2A_2F_{32}\,{}_1R_3+A_2F_{22}\,{}_1R_2)\rho_2=A_2\,{}_1R_2 \quad \text{(A6)}$$

$$F_{32}=F_{42}$$
$${}_1R_3={}_1R_4$$
$$(A_1F_{13}\epsilon_1+A_3F_{23}\,{}_1R_2+A_3F_{34}\,{}_1R_3)\rho_3=A_3\,{}_1R_3 \quad \text{(A7)}$$

$$F_{33}=0$$
$${}_1R_3={}_1R_4$$
$$F_{43}=F_{34}$$

Solving equations (6) and (7) for ${}_1R_2$ and ${}_1R_3$

$$A_1F_{12}\epsilon_1+2A_2F_{32}\,{}_1R_3+A_2F_{22}\,{}_1R_2=\frac{A_2}{\rho_2}\,{}_1R_2$$

$$A_1F_{13}\epsilon_1+A_3F_{23}\,{}_1R_2+A_3F_{34}\,{}_1R_3=\frac{A_3}{\rho_3}\,{}_1R_3$$

$$\left(\frac{A_2}{\rho_2}-A_2F_{22}\right){}_1R_2-2A_2F_{32}\,{}_1R_3=A_1F_{12}\epsilon_1 \quad \text{(A8)}$$

$$-A_3F_{23}\,{}_1R_2+\left(\frac{A_3}{\rho_3}-A_3F_{34}\right){}_1R_3=A_1F_{13}\epsilon_1 \quad \text{(A9)}$$

$$A_3F_{23}\left(\frac{A_2}{\rho_2}-A_2F_{22}\right){}_1R_2-2A_2A_3F_{23}F_{32}\,{}_1R_3=A_1A_3F_{12}F_{23}\epsilon_1 \quad \text{(A10)}$$

$$-A_3F_{23}\left(\frac{A_2}{\rho_2}-A_2F_{22}\right){}_1R_2+\left(\frac{A_2}{\rho_2}-A_2F_{22}\right)\left(\frac{A_3}{\rho_3}-A_3F_{34}\right){}_1R_3=\left(\frac{A_2}{\rho_2}-A_2F_{22}\right)A_1F_{13}\epsilon_1 \quad \text{(A11)}$$

$$\left[\left(\frac{A_2}{\rho_2}-A_2F_{22}\right)\left(\frac{A_3}{\rho_3}-A_3F_{34}\right)-2A_2A_3F_{23}F_{32}\right]{}_1R_3=A_1A_3F_{12}F_{23}\epsilon_1+\left(\frac{A_2}{\rho_2}-A_2F_{22}\right)A_1F_{13}\epsilon_1 \quad \text{(A12)}$$

Let

$$\alpha=\frac{A_2-A_2F_{22}\rho_2}{\rho_2}$$

$$\beta=\frac{A_3-A_3F_{34}\rho_3}{\rho_3}$$

$$\varphi=2A_2A_3F_{23}F_{32}$$

$$\theta=A_1A_3F_{12}F_{23}\epsilon_1$$

$$\psi=A_1F_{13}\epsilon_1$$

Substituting in equation (12)

$$(\alpha\beta-\varphi)\ {}_1R_3=\theta+\alpha\psi$$

$${}_1R_3=\frac{\theta+\alpha\psi}{\alpha\beta-\varphi}$$

Substituting in equation (10)

$$A_3F_{23}\alpha\ {}_1R_2-\varphi\left(\frac{\theta+\alpha\psi}{\alpha\beta-\varphi}\right)=\theta$$

$${}_1R_2=\frac{\varphi\left(\frac{\theta+\alpha\psi}{\alpha\beta-\varphi}\right)+\theta}{A_3F_{23}\alpha}$$

$${}_1R_3=\frac{A_1A_3F_{12}F_{23}\epsilon_1+\frac{A_2}{\rho_0}(1-F_{22}\rho_0)A_1F_{13}\epsilon_1}{\frac{A_2}{\rho_0}(1-F_{22}\rho_0)\frac{A_3}{\rho_0}(1-F_{34}\rho_0)-2A_2A_3F_{23}F_{32}}$$

where $\rho_2=\rho_3=\rho_4=\rho_0$

$${}_1R_3=\frac{A_1\epsilon_1\rho_0(A_3F_{12}F_{23}\rho_0+A_2F_{13}-A_2F_{13}F_{22}\rho_0)}{A_2A_3(1-F_{22}\rho_0-F_{34}\rho_0+F_{22}F_{34}\rho_0^2-2F_{23}F_{32}\rho_0^2)} \tag{A13}$$

Let

$$(A_3F_{12}F_{23}\rho_0+A_2F_{13}-A_2F_{13}F_{22}\rho_0)=\Delta$$

$$(1-F_{22}\rho_0-F_{34}\rho_0+F_{22}F_{34}\rho_0^2-2F_{23}F_{32}\rho_0^2)=\gamma$$

$${}_1R_3=\frac{A_1\epsilon_1\rho_0\Delta}{A_2A_3\gamma} \tag{A14}$$

$${}_1R_2=\frac{\varphi\left(\frac{A_1\epsilon_1\rho_0\Delta}{A_2A_3\gamma}\right)+\theta}{A_3F_{23}\alpha}$$

$$=\frac{2A_2A_3F_{23}F_{32}\left(\frac{A_1\epsilon_1\rho_0\Delta}{A_2A_3\gamma}\right)+A_1A_3F_{12}F_{23}\epsilon_1}{\frac{A_3F_{23}A_2}{\rho_0}(1-F_{22}\rho_0)} \tag{A15}$$

$${}_1R_2=\frac{A_1\epsilon_1\rho_0(2F_{32}\Delta\rho_0+A_3F_{12}\gamma)}{A_2A_3(1-F_{22}\rho_0)\gamma} \tag{A16}$$

$$A_1F'_{12}=A_2\ {}_1R_2\frac{\epsilon_0}{\rho_0}$$

$$A_1F'_{13}=A_{31}R_3\frac{\epsilon_0}{\rho_0}$$

$$\rho_0=1-\epsilon_0$$

$$A_1F'_{12}=A_2\left[\frac{A_1\epsilon_1\rho_0(2F_{32}\rho_0\Delta+A_3F_{12}\gamma)}{A_2A_3(1-F_{22}\rho_0)\gamma}\right]\frac{\epsilon_0}{\rho_0}$$

$$A_1F'_{12}=\frac{A_1\epsilon_1\epsilon_0(2F_{32}\rho_0\Delta+A_3F_{12}\gamma)}{A_3(1-F_{22}\rho_0)\gamma} \tag{A17}$$

$$A_1F'_{13}=A_3\left(\frac{A_1\epsilon_1\rho_0\Delta}{A_2A_3}\right)\frac{\epsilon_0}{\gamma\rho_0}=\frac{A_1\epsilon_1\epsilon_0\Delta}{A_2\gamma} \tag{A18}$$

From equation (1), the heat-transfer equations for radiation from the inner cylinder to its surroundings are

$$q_t=\delta A_1F'_{12}(T_1^4-T_0^4)+2\delta A_1F'_{13}(T_1^4-T_3^4) \tag{A19}$$

which can be expressed as

$$q_t=\delta(T_1^4-T_0^4)\ (A_1F'_{12}+2A_1F'_{13}) \tag{A20}$$

$$T_2=T_3=T_4=T_0$$

$$q_t=\delta(T_1^4-T_0^4)\left[\frac{A_1\epsilon_1\epsilon_0(2F_{32}\rho_0\Delta+A_3F_{12}\gamma)}{A_3(1-F_{22}\rho_0)\gamma}+\frac{2A_1\epsilon_1\epsilon_0\Delta}{A_2\gamma}\right]$$

$$q_t=\frac{\delta A_1\epsilon_1\epsilon_0}{\gamma}(T_1^4-T_0^4)\left[\frac{2F_{32}\rho_0\Delta+A_3F_{12}\gamma}{A_3(1-F_{22}\rho_0)}+\frac{2\Delta}{A_2}\right] \tag{A21}$$

Therefore,

$$\epsilon_1=\frac{\gamma q_t}{\delta A_1\epsilon_0(T_1^4-T_0^4)\left[\frac{2F_{32}\rho_0\Delta+A_3F_{12}\gamma}{A_3(1-F_{22}\rho_0)}+\frac{2\Delta}{A_2}\right]} \tag{A22}$$

These equations are based on the assumption that the test specimen radiates in accordance with Lambert's law and that Kirchhoff's law holds despite the difference in temperature between the test specimen and its surroundings. It is possible that neither of these conditions hold rigorously, but the resulting error should be negligible.

REFERENCES

1. McAdams, William H.: Heat Transmission. Third ed., McGraw-Hill Book Co., Inc., 1954.
2. Worthing, A. G.: Temperature Radiation Emissivities and Emittances. Temperature—Its Measurement and Control in Science and Industry. Reinhold Publ. Corp. (New York), 1941, pp. 1164–1187.
3. Hamilton, D. C.; and Morgan W. R.: Radiant-Interchange Configuration Factors. NACA TN 2836, 1952.

28—A SILICON CELL TRANSMISSIVITY-REFLECTIVITY METER FOR USE WITH SOLAR RADIATION

BY JOHN I. YELLOTT AND LAWRENCE CHAMNESS

YELLOTT SOLAR ENERGY LABORATORY, PHOENIX, ARIZONA

The silicon photovoltaic cell which is now in wide use as a power source for satellites and space vehicles can also be used as the sensitive element in radiometers for measuring the intensity of direct and diffuse solar radiation. This paper describes an adaptation of an inexpensive silicon cell pyrheliometer (Sol-A-Meter) which was originally intended to measure the intensity of the direct solar beam. It has been found that the instrument can also be used to make rapid determinations of the transmittance, τ, and reflectance, ρ, of transparent materials for solar radiation at incident angles from 0° to 80°. The absorptance, α, which cannot be measured directly, can be found from the relationship:

$$\alpha = 1.00 - (\tau + \rho)$$

The limitations imposed by the spectral response of the typical silicon solar cell appear to have little adverse effect upon the accuracy of the results obtained with the Sol-A-Meter, while the strong signal and the instantaneous response of the instrument, combined with its low cost, make it a useful tool for determining solar-optical properties of transparent materials.

The silicon photovoltaic cell was literally rocketed into technical prominence on March 17, 1958, when the first multi-year satellite, Vanguard I, was put into orbit. Today, the signals which still come from Vanguard I have been joined by more powerful voices from its more sophisticated successors such as Telstar, but they all owe their usefulness to the silicon solar cells which convert the sun's radiation directly into electricity. On the earth's surface, power from solar cells is still far too expensive for all but a few specialized applications, but other uses are being found to capitalize on the remarkable properties of these devices. One of the most interesting applications is in the field of solar radiometry.

The earliest publications of the Bell Laboratories team which invented the silicon photovoltaic cell (ref. 1,2) disclosed the fact that the short-circuit current produced by typical cells when exposed to bright sunshine was about 25 ma/cm_2, while the variation of short-circuit current with changing intensity of insolation was essentially linear. At constant insolation, the short-circuit current was found to increase slightly with rising temperature up to a limiting value at about 160° F; beyond this temperature, the current diminished as the internal resistance of the cell increased.

The combination of linear response and small positive temperature-current characteristic indicated that the silicon cell would be useful in the measurement of solar radiation. Accordingly, an investigation was undertaken at the Yellott Solar Energy Laboratory early in 1961 (ref. 3) to determine the suitability of commercially available silicon cells for this purpose. It soon was found that the simple instrument shown diagrammatically in figure 28–1, consisting of a silicon cell shunted by a low resistance in thermal contact with the cell, gave consistent and accurate response to both direct and diffuse solar radiation of varying intensity. Since the measured quantity was the short-circuit current, in terms of the millivolts drop across the shunting resistance, the name "Sol-A-Meter" was coined to describe the device.

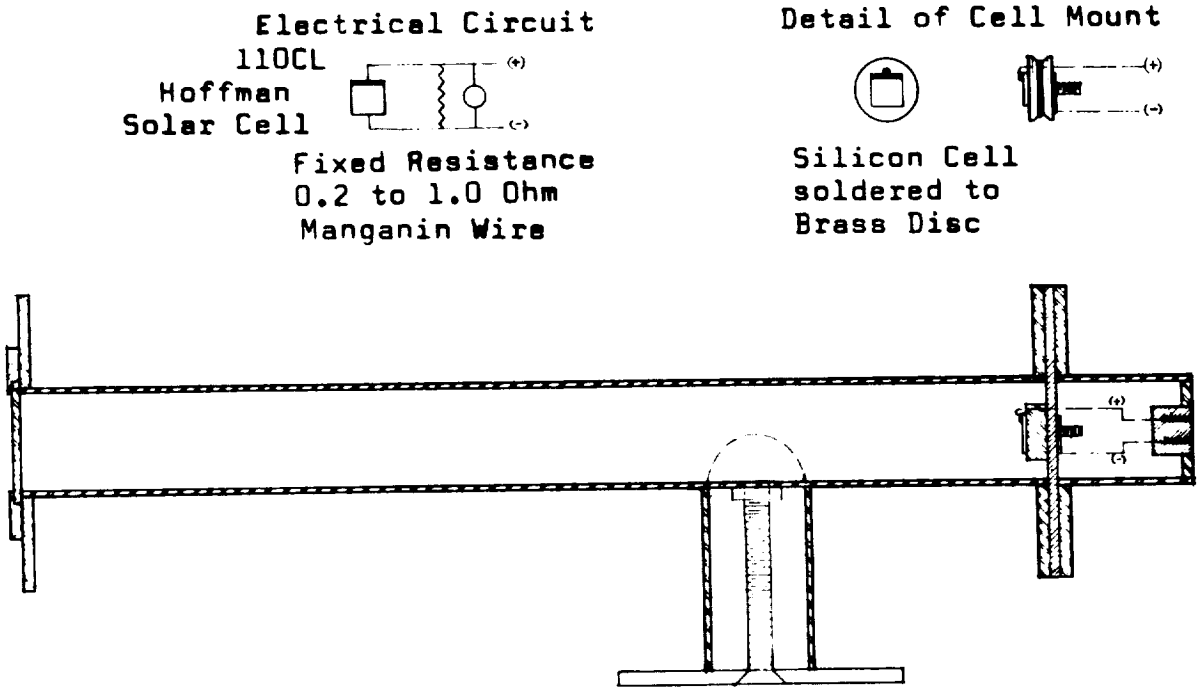

FIGURE 28–1.—Cross-section of normal incidence Sol-A-Meter.

In a much more detailed study of the properties of the Sol-A-Meter, carried out early in 1962, K. Selcuk [1] found that excellent temperature compensation could be obtained by adding a suitable thermistor to the Manganin shunting resistance. He also determined the deviation from the cosine law which takes place at high angles of incidence, and found that the change in spectral distribution of sunlight with changing solar altitude also necessitated careful calibration against a "color-blind" pyrheliometer of the thermopile type, such as the well-known Eppley instrument.

Some months ago, the need arose at our laboratory for quick and accurate determinations of the solar optical properties (transmittance, τ, absorptance, α, and reflectance, ρ) of many different types of glass at incident angles from 0° (normal incidence) to 90° The instrument shown in figure 28–2 was designed for this purpose and when preliminary tests indicated likihood of success, the first prototype was constructed. The present paper presents the results obtained with this instrument for a number of well-known types of glass.

TRANSMITTANCE MEASUREMENTS WITH NORMAL-INCIDENCE PYRHELIOMETERS

A normal incidence Sol-A-Meter (NIS) of the type shown in figure 28–1 was built, with a standard Hoffman type 110 CL silicon cell as the sensitive element. This cell was soldered to the upper surface of a brass disk, and a groove was turned into the side of the disk, to accept a 4.57 in. length of 30-gage Manganin wire which was shunted across the cell's connecting leads. A preliminary check had shown that the cell's short-circuit current in bright sunshine was about 25 ma, and, consequently, a 1-ohm resistance was selected to give a maximum signal of 25 mv.

A calibration test of the instrument using an Eppley pyrheliometer (No. 4003) as the standard, gave the results shown in figure 28–3. The influence of changing spectral distribution of the incident sunlight is demonstrated by the non-linear nature of the curve of millivolts output vs solar intensity in Btu/hr-ft^2. For solar altitudes above 60°, the relationship becomes nearly linear, so most of the tests were made when the sun was high in the sky.

[1] Selcuk, K.; and Yellott, J. I.: Measurement of Direct, Diffuse, and Total Solar Radiation with Silicon Photovoltaic Cells submitted for publication to "Solar Energy", Assoc. for Applied Sol. Eng.

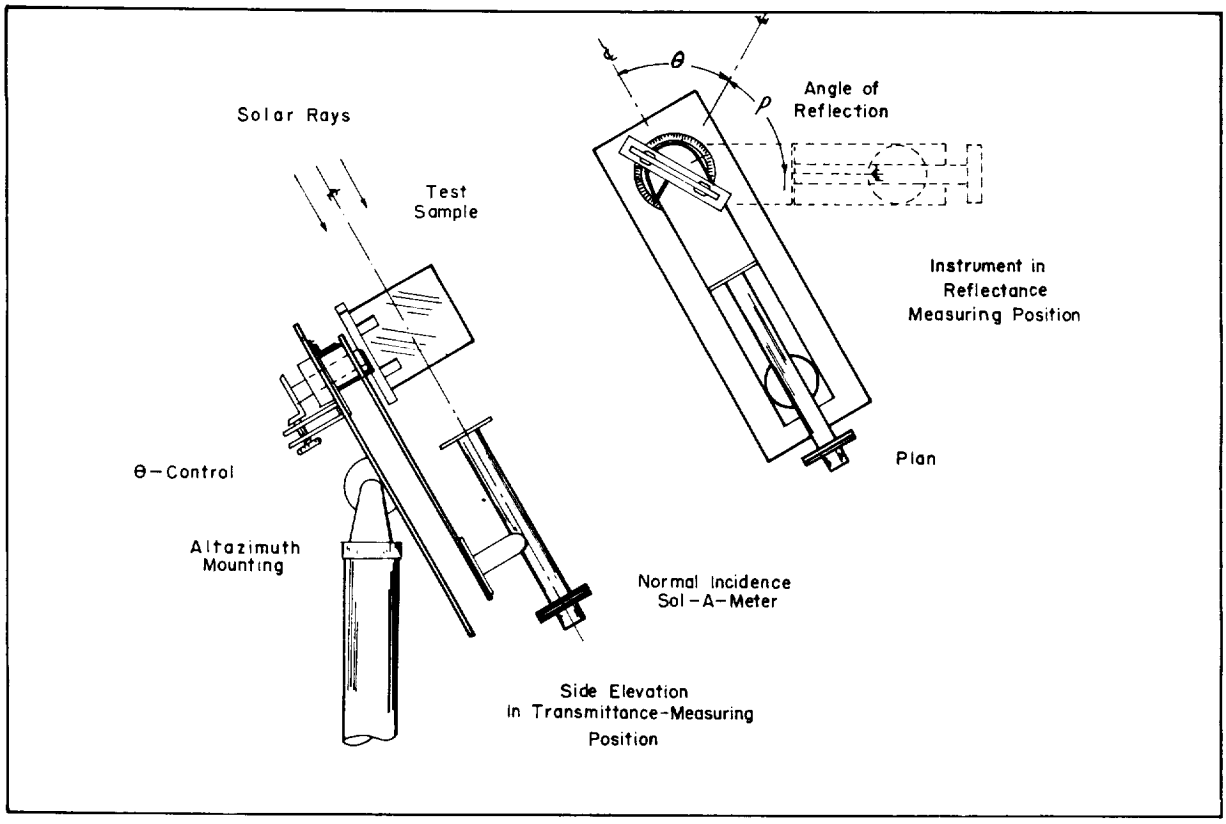

FIGURE 28-2.—Sol-A-Meter adapted to measure transittance and reflectance.

A sun-following mount was constructed in which a sample of glass could be interposed into the solar beam ahead of the pyrheliometer. The sample could be rotated throughout 90° so that the incident angle between the sample and sun's rays could also be varied from 0° to 90°. A graduated dial enabled the incident angle to be adjusted by 1° increments. Either the Eppley pyrheliometer or the NIS could be attached to the mount. When the Eppley instrument was used, its output was connected directly to a 0- to 10-mv Varian strip-chart recorder, since its maximum signal was about 4.6 mv.

The NIS gave signals up to 25 mv, and so its output was connected to the input of a 1,000-ohm potentiometer, and the recorder was connected across the output. The signal, with no glass in the sample holder, could thus be adjusted to give a 100% reading on the recorder. When the glass sample was inserted into the light path, the recorder immediately indicated a reduced signal, which was in fact the percent transmittance of the glass for solar radiation at the existing angle of incidence.

A series of transmittance measurements was made with the Eppley pyrheliometer, and it was found that the time of response was great enough to necessitate continuous monitoring of the solar beam intensity so that the resulting transmittances could be compensated for the minute-by-minute variations in the sun's radiation.

The NIS was then installed on the instrument and the same samples were tested again. It was found that the results were virtually identical in most cases, leading to the conclusion that the spectral sensitivity of the silicon cell was not a serious disadvantage. The response of the silicon cell was so rapid that the entire range of incident angles could be covered in 90 to 120 sec, and the need for monitoring the solar beam was thus eliminated. On a clear day, the variations in direct beam intensity are

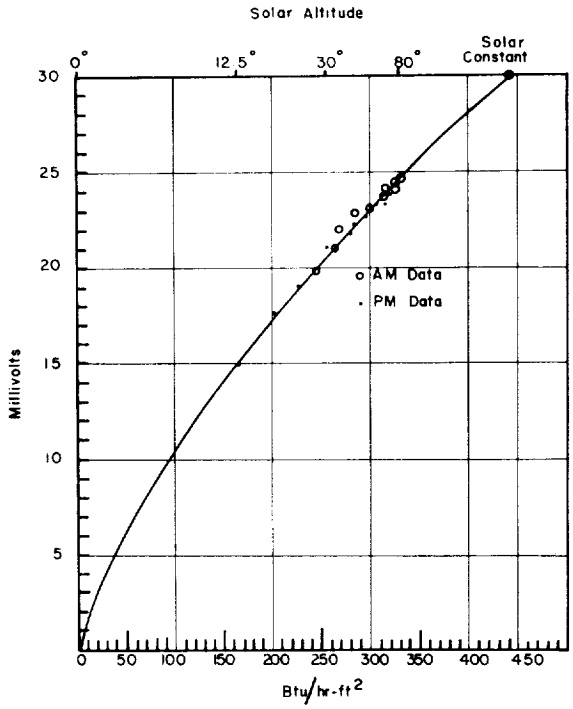

FIGURE 28-3.—Calibration curve for normal incidence Sol-A-Meter.

generally slow enough so that the "no-glass" readings at the beginning and end of a transmittance test are virtually identical.

REFLECTANCE MEASUREMENTS WITH THE NORMAL INCIDENCE SOL-A-METER

After it had been shown that the NIS gave virtually the same values of transmittance as the thermopile-type Eppley pyrheliometer, a new sun-following mount was constructed as shown in figure 28-2. A rotatable arm was provided to carry the Sol-A-Meter so that it could first be lined up with the incoming solar beam to determine the transmittance. It could then be swung around in front of the sample to line up with the angle of reflection. The correct position could be found from the graduated dial by which the incident angle was determined.

As soon as the new instrument was put into operation, it was found that the reflected sunlight could give an adequate signal even for 10° incident angles with heat-absorbing glasses. In addition, the operator could readily look down the tube of the NIS and determine exactly when the reflected beam was lined up correctly with the center-line of the instrument.

The virtually instantaneous response of the silicon cell again proved to be an important asset, because it was possible to determine both transmittance and reflectance over the entire range of incident angles within three minutes. Since the Eppley pyrheliometer had been freed for its proper task of measuring the direct beam intensity, its output could be observed to make sure that there had been no significant change in the sunshine during the brief interval required to make the test.

ABSORBTANCE DETERMINATIONS

Since both the transmittance, τ_θ, and the reflectance, ρ_θ, for any incident angle can now be measured, it is a simple matter to determine the absorbtance, α_θ, for the same angle, since:

$$\tau_\theta + \rho_\theta + \alpha_\theta = 1.000 \qquad (1)$$

The results of tests to measure the solar-optical properties of four of the glasses listed in Table 28 I are also shown in figures 28-4, -5, and -6. The charts show the familiar behavior for the properties in question. Both transmittance and absorbtance must reach zero at $\theta = 90°$, when the reflectance becomes 100%. Transmittance diminishes gradually as the incident angle increases, but absorbtance first increases to a maximum as the length of path through the glass grows longer. At about 60° incident

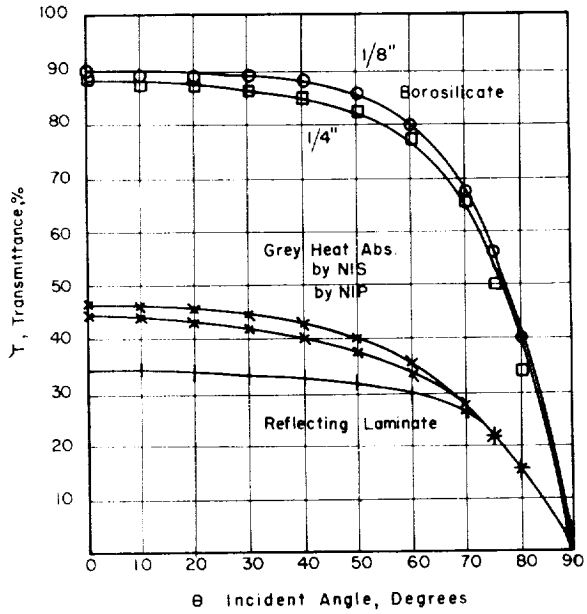

FIGURE 28-4. Transmittance vs incident angle for four typical glasses.

TABLE 28-I.—*Solar-Optical Properties of Six Typical Glasses for Incident Angles from 0° to 90°*

Deg.	Borosilicate						Soda-Lime Plate, ¼ in. Thick		
	⅛ in. Thick			¼ in. Thick					
	τ	ρ	α	τ	ρ	α	τ	ρ	α
0	90	------	----	89. 0	------	----	77. 0	------	----
10	89. 0	7. 0	4. 0	87. 0	6. 5	6. 5	75. 0	6. 0	19. 0
20	89. 0	7. 0	4. 0	87. 0	6. 0	7. 0	75. 0	6. 5	18. 5
30	89. 0	7. 0	4. 0	86. 0	6. 5	7. 5	74. 0	6. 5	19. 5
40	88. 0	8. 0	4. 0	85. 0	7. 0	8. 0	72. 5	7. 0	20. 5
50	86. 0	9. 0	5. 0	82. 5	9. 0	9. 5	70. 0	8. 0	22. 0
60	80. 0	13. 0	7. 0	77. 5	13. 0	9. 5	64. 0	12. 0	24. 0
70	67. 5	24. 0	8. 5	66. 5	24. 0	9. 5	53. 5	22. 0	24. 5
75	56. 0	35. 0	9. 9	50. 5	35. 0	14. 5	44. 0	30. 0	26. 0
80	34. 0	44. 5	11. 5	40. 5	49. 5	10. 0	32. 0	42. 0	26. 0
90	0	100	0	0	100	0	0	100	0

Deg.	Grey-Heat Absorbing			Gold Reflecting Laminate			"12.5%" Heat Absorbing		
	τ	ρ	α	τ	ρ	α	τ	ρ	α
0	46. 3	------	----	28. 0	------	----	42. 0	------	----
10	45. 8	5. 0	49. 2	34. 0	24. 0	42. 0	41. 5	5. 0	53. 5
20	45. 0	5. 0	50. 0	34. 0	24. 0	42. 0	41. 0	5. 0	54. 0
30	44. 0	5. 5	50. 5	33. 5	23. 5	43. 0	40. 0	5. 0	55. 0
40	42. 5	6. 0	51. 5	33. 0	24. 0	43. 0	39. 0	5. 5	55. 5
50	40. 0	7. 0	53. 0	32. 0	26. 0	42. 0	37. 0	7. 0	56. 0
60	35. 0	10. 5	54. 5	30. 0	27. 0	43. 0	34. 0	11. 0	54. 0
70	28. 5	20. 5	51. 0	27. 0	34. 0	39. 0	28. 0	21. 5	50. 5
75	24. 0	24. 0	52. 0	23. 0	39. 0	38. 0	23. 5	31. 0	46. 5
80	----	------	----	----	------	----	----	------	----
90	0	100	0	0	100	0	0	100	0

angle, however, the influence of the rapidly rising reflectance takes over, and the absorbtance also moves rapidly towards zero, along with the transmittance.

The values of the three properties at normal incidence can also be determined by spectrophotometric methods, knowing the probable spectral distribution of the solar intensity. The data usually employed for this purpose are those of Moon (ref. 4) which were calculated at a time when the accepted value of the solar constant was 419 Btu/hr-ft². Today, it is agreed that the more probable value of the solar constant is 441 Btu/hr-ft², or 2.0 Langleys, but the spectral distribution proposed by Moon is still in general use. Comparing the results of tests made with the NIS for $\theta=0°$ with results calculated from Moon's data, it is found that agreement within 2% is usually obtained.

CONCLUSIONS

The silicon cell pyrheliometer can be used with confidence to determine the solar-optical properties of many types of glass over the entire range of incident angles. When the absolute value of the solar radiation intensity is needed, the Sol-A-Meter can give reliable results if it has been calibrated against a thermopile-type instrument to determine the effect of air mass variation, etc. For relative values, which are obtained when the transmittance and reflectance are determined, the spectral limitations of the silicon cell do not appear to impair the usefulness of the device.

The writers would like to express their appreciation to Ronald Clegg and James Wonderly

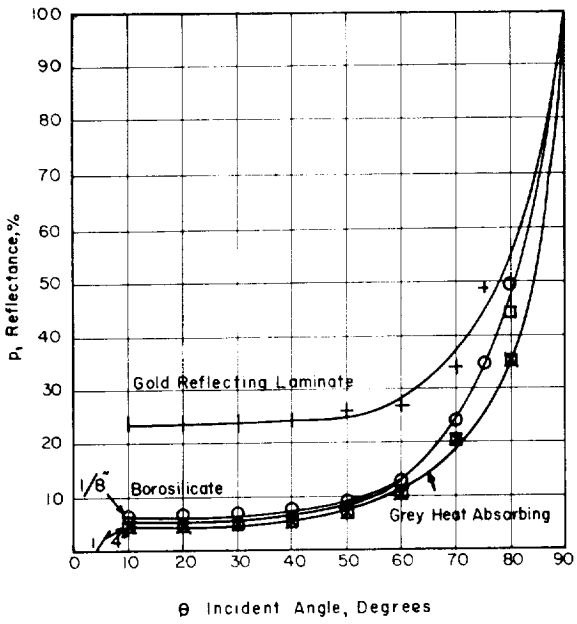

FIGURE 28–5.—Reflectance vs incident angle for the glasses of figure 28–4.

of the Yellott Solar Energy Laboratory staff, who made most of the measurements which are reported here.

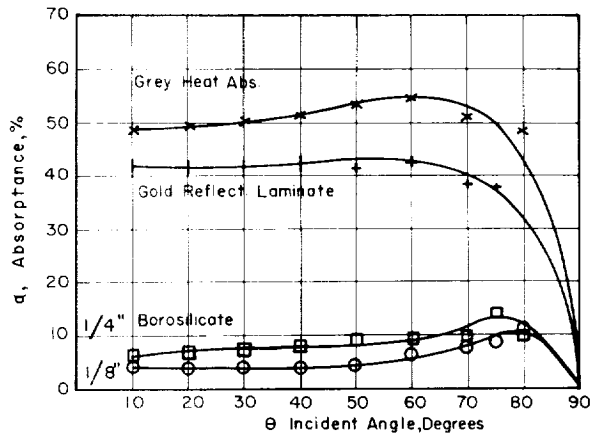

FIGURE 28–6.—Absorbtance vs incident angle for the glasses of figure 28–4.

REFERENCES

1. CHAPIN, D.; FULLER, C.; and PEARSON, G.: A New Silicon p-n Junction Photocell for Converting Solar Radiation into Electrical Power. Jour. App. Phys., vol. 25, 1954, p. 676.
2. PEARSON, G.: Electricity for the Sun. Proc. 1955 World Symposium on App. Solar Energy, Stanford Res. Inst., 1956.
3. YELLOTT, J. I.; KOKOROPOULOS, P.; and FOGLE, T.: Use of Silicon Cells as Pyrheliometers. Sounion Conference, Greek Atomic Energy Commission, Athens, 1961.
4. MOON, PARRY: Proposed Standard Solar Radiation Curves for Engineering Use; Jour. Franklin Inst., vol. 230, Nov. 1940. p. 583,

29—AN APPARATUS FOR THE MEASUREMENT OF THE TOTAL NORMAL EMITTANCE OF SURFACES AT SATELLITE TEMPERATURES[1]

BY GENE A. ZERLAUT[2]

NASA GEORGE C. MARSHALL SPACE FLIGHT CENTER, HUNTSVILLE, ALABAMA

This report discusses the theory, design, and test results achieved with a device that measures total normal emittance of surfaces at temperatures in the 50—100° C range. The blackbody and sample used in the device are housed in a vacuum chamber (1.6×10^{-4} torr). Attached to the vacuum chamber is an evacuated radiometer. For a detector, a well-baffled, 28-junction, iron-constantan, radial thermopile was built. In use, the total emittance is measured as the ratio of the thermoelectric EMF generated by the sample to the thermoelectric EMF generated by the blackbody, at the same temperature and pressure. The thermopile output was determined to be 150 μv per Btu/ft^2-hr at blackbody temperatures of 340° K or greater. The device can be modified for measuring total normal emittance at high temperatures; however, the selectivity of the thermopile receiver, plus lack of sufficient energy at low temperatures, precludes the measurement of emittance at cryogenic temperatures.

The need for thermal radiation data on aerospace engineering materials is becoming increasingly important as vehicle stages and complete vehicles become larger and more complicated. The radiant heat exchange between the surface of hot missile components and their external environment plays an important part in the ultimate surface temperature of the body in question and, therefore, the cooling requirements for the system in general. Likewise, the radiant heat transfer between the surface of an orbiting vehicle and the sun and earth largely determines its equilibrium skin temperature.

The emittance of a surface is a measure of its "radiator efficiency"—its efficiency for dissipating heat by radiation. Therefore, it is necessary that the thermodynamacist and the aerospace design engineer have available to them highly reliable emittance data on aerospace materials.

[1] Subject of a NASA-Marshall Report entitled "An Apparatus for the Measurement of the Total Normal Emittance of Surfaces at Low Temperatures," MTP-P&VE-M-62-4, dated February 23, 1962.

[2] Present affiliation: Armour Research Foundation of Illinois Institute of Technology, Chicago, Illinois.

DEFINITION OF TERMS

The term emittance is taken to mean a property of a sample. It is the ratio of the radiancy of the sample to the radiancy of a blackbody at the same temperature and under the same conditions. On the other hand, emissivity is the limiting case of emittance. It is a fundamental property of a material and is measured as the emittance of an optically smooth, opaque sample of the material. The terms emittance and emissivity are often used interchangeably although not always correctly. However, both will be denoted by the symbol ϵ throughout this paper.

Spectral emittance refers to the ratio of the spectral radiancy (or monochromatic radiancy at a given wavelength) from a body to that of a blackbody at the same temperature, and is denoted by ϵ_λ. Total emittance, ϵ_t, is a measure of the ratio of the radiancy of a sample, as a consequence of its temperature, to the radiancy of a blackbody at the same temperature and includes all wavelengths from zero to infinity. Hemispherical emittance, ϵ_h, refers to the emission in all possible directions, i. e., 2π steradians

for flat, optically smooth surfaces. Normal emittance, ϵ_n, (a special case of directional emittance, ϵ_θ), refers to the emittance normal to the surface (normal refers to the direction of the axial ray of a beam that is encompassed by a small solid angle), and is the ratio of the normal steradiancy of a sample to that of a blackbody at the same temperature.

Therefore, "total normal emittance," "total hemispherical emittance," and "normal spectral emittance" are terms which describe not only a particular thermal radiation property but also denote a specified technique for measurement.

THEORETICAL CONSIDERATIONS

According to Kirchoff's law, for opaque specimens,

$$\epsilon_\lambda = \alpha_\lambda = 1 - R_\lambda \tag{1}$$

where ϵ_λ, α_λ, and R_λ are the spectral emissivity, spectral absorptivity, and spectral reflectivity, respectively. An exact expression of Kirchoff's law may be derived by assuming that a body at temperature T absorbs a fraction ϵ_λ of monochromatic radiation of wavelength λ falling upon it. Then, if $W_{b\lambda}\, d\lambda$ is the power per unit area emitted by a perfect blackbody between the wavelengths λ and $\lambda + d\lambda$, the body in question would emit an amount

$$W_\lambda d_\lambda = \epsilon_\lambda W_{b\lambda} d\lambda \tag{2}$$

Rearrangement of equation (2) provides a exact expression of spectral emissivity defined by

$$\epsilon_\lambda = \frac{W_\lambda d\lambda}{W_{b\lambda} d\lambda} \tag{3}$$

Total emissivity may then be calculated from spectral emissivity according to

$$\epsilon_t = \frac{1}{W_b} \int_0^\infty \epsilon_\lambda W_{b\lambda} d\lambda, \tag{4}$$

where the term $W_{b\lambda} d\lambda$ is the spectral radiancy. $W_{b\lambda} d\lambda$ may be calculated from Planck's total radiation law

$$W_{b\lambda} d\lambda = \frac{C_1}{\lambda^5} \cdot \frac{d\lambda}{e^{C_2/\lambda T} - 1}, \tag{5}$$

where C_1 and C_2 are radiation constants and $d\lambda$ is the wavelength increment over which $W_{b\lambda}$ is computed. Integration of equation (5) over the limits zero to infinity results in the Stefan-Boltzmann law,

$$W_b = \int_0^\infty W_{b\lambda} d\lambda = \frac{C_1}{C_2^4} \cdot \frac{6\pi^4}{90} T^4 = \sigma T^4, \tag{6}$$

where σ is known as the Stefan-Boltzmann constant. From equation (4), it may be seen that

$$W = \epsilon_t \sigma\, T^4, \tag{7}$$

where W is the radiancy of a body having a total emissivity ϵ_t.

The most common method of measuring emittance is the comparison of the heat flux emitted in a normal direction by a sample and by a blackbody at the same temperature and under identical conditions. The ratio of these two fluxes is by definition total normal emittance, ϵ_n.

The radiancy, or heat flux, is measured by use of a radiation detector, e.g., thermocouple, thermopile, or bolometer. For such detectors, the output or thermoelectric EMF is a function of the net radiation exchange between the receiver and its surrounding, i.e., sample or blackbody. Thus, the ratio of the EMFs generated when the detector views first a sample and then a blackbody at the same temperature is a direct measurement of the emittance. This may be shown by considering first the case when the detector views the blackbody:

$$EMF_b = kW_b = k\sigma(T^4 - T_D^4), \tag{8}$$

where k is a factor which includes the detector calibration (output) and the geometrical factor between the detector receiver and the blackbody, and T and T_D are the absolute temperature of the blackbody and the detector, respectively. Next, let us consider the case for the samples:

$$EMF = kW = k\sigma\epsilon_t(T^4 - T_D^4), \tag{9}$$

where ϵ_t is the total emittance of the sample. By solving both equations for k and equating, we obtain

$$k = \frac{EMF_b}{\sigma(T^4 - T_D^4)} = \frac{EMF}{\sigma\epsilon_t(T^4 - T_D^4)} \tag{10}$$

Solving equation (10) for ϵ_t, we obtain

$$\epsilon_t = \frac{EMF}{EMF_b} \tag{11}$$

DESIGN OF THE EMISSOMETER

Since the measurement of total hemispherical emittance of surfaces requires for most methods the accurate determination of several parameters, methods for the direct measurement of total normal emittance received the most attention. It was desired that the device be constructed from equipment and parts on hand and that construction costs be minimized. Furthermore, it was desired that the apparatus be relatively simple to operate and that it require a minimum of up-keep. These requirements precluded the use of complicated and expensive electronic measuring and display equipment. It was also desirable that the measurement of emittance be accomplished under high vacuum.

The methods and devices of Wilkes (ref. 1), Gier and Dunkle (ref. 2), and Gier and Boelter (ref. 3) for measuring total normal emittance were adapted and modified to fit our needs and resources. Although the general emissometer design is taken from Wilkes, the fact that his report does not describe the many problems associated with the measurement of very small *EMF*s necessitated certain changes. These changes and the description of the various problems in measuring the *EMF* are, then, the basis for this paper.

Chamber, Blackbody and Sample Holder

The vacuum chamber (figures 29–1 and –2) serves the dual purpose of permitting both sample and radiometer evacuation during measurements. It is connected to a vacuum system comprised of forepump, diffusion pump and liquid nitrogen baffle, which are capable of maintaining an ultimate chamber pressure of 1×10^{-5} torr. The chamber top is integral with the blackbody or sample holder, whichever is in position. The blackbody is the conical depression type, treated theoretically by Edwards (ref. 4). It is cooled and heated by means of circulating thermostatically controlled

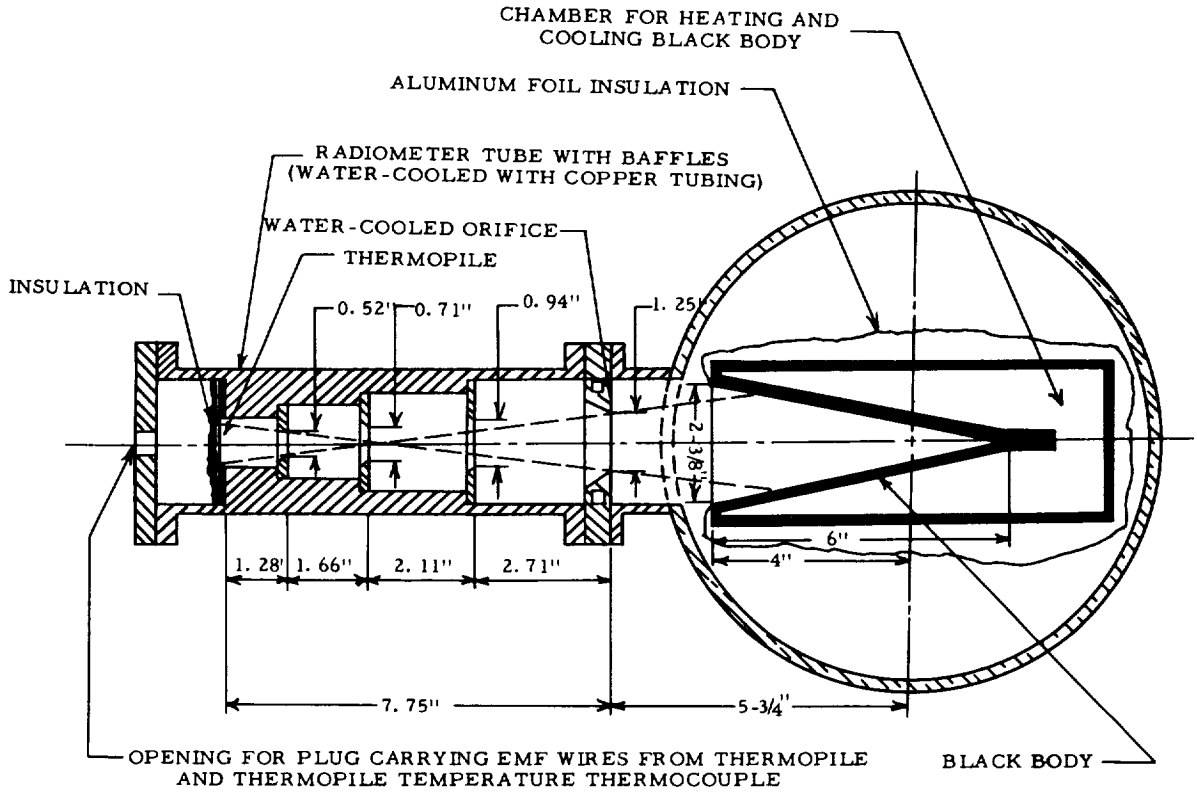

FIGURE 29–1.—Top view section of emissometer with blackbody in position.

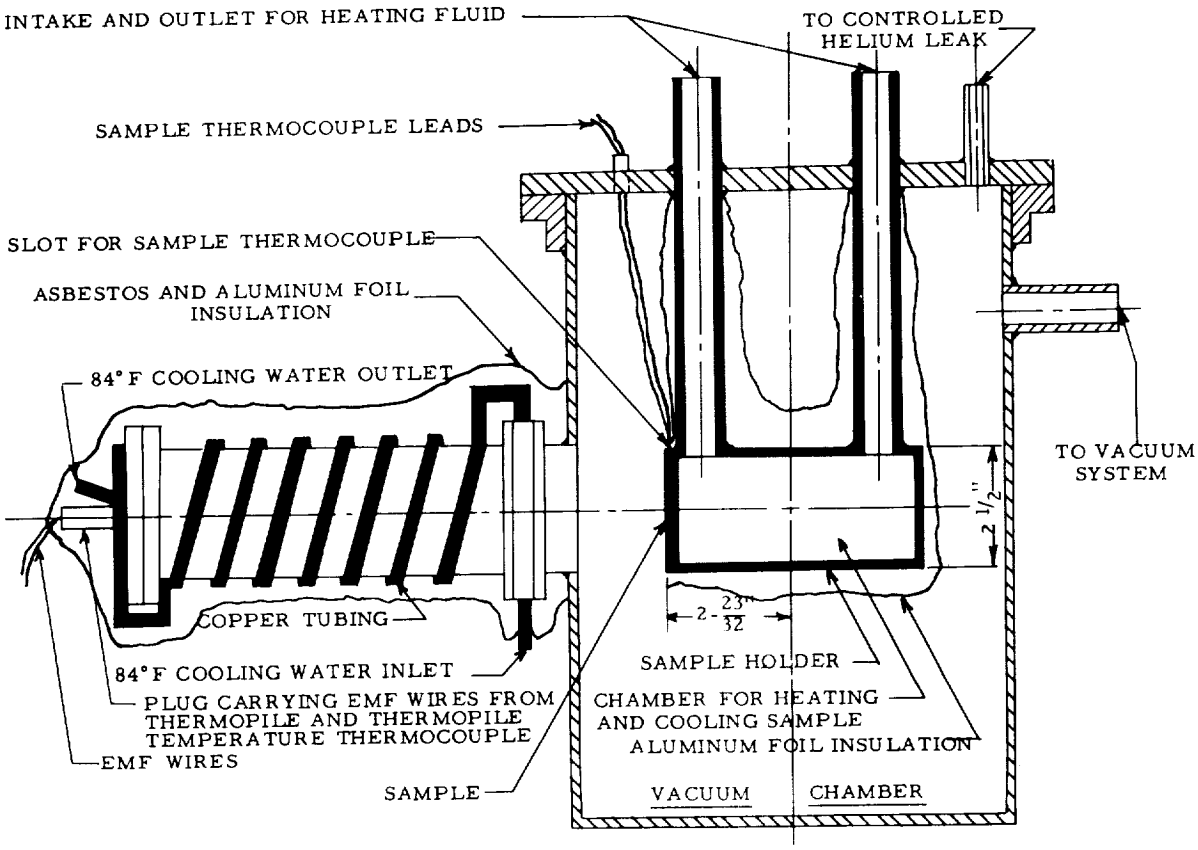

FIGURE 29–2.—Side view and section of emissometer with sample holder in position.

water (see figures 29–1 and –3). The sample holder is constructed on the same principle and is provided with a centered slot for the sample temperature thermocouple (fig. 29–2 and –4).

Radiometer and Thermopile Detector

The radiometer is shown in detail in figure 29–1. It is provided with four radiation baffles whose apertures converge upon the thermopile receiver. Thus, the effective sample area is always the area of the limiting aperture, regardless of the exact distance from the sample or blackbody face to the thermopile receiver. The last or limiting baffle is water cooled in order to prevent transient heating of the radiometer walls due to absorption from the sample or blackbody. In addition, the radiometer tube is constructed with massive seats, permitting easy assembly of the baffles as well as providing a heat sink which stabilizes the temperature of the baffles and thermopile cold junctions. The radiometer tube and endplate are closely wound with square copper tubing through which the water from the water-cooled orifice is circulated. The thermopile and its entire surroundings (except the small solid angle defined by the limiting aperture) are thus maintained at the same temperature. Temperature gradients are further minimized by heavily insulating the entire radiometer with asbestos fiber and aluminum foil (fig. 29–2).

The requirement that the measuring circuitry be simple, plus the design, size and shape limitations posed by the radiometer, restricted the type of thermopile which could be used. Use of a radiation thermocouple would have necessitated the use of amplification and chopping, the principle of one type of bolometer. Ordinarily, a focusing front-surface mirror system is required in addition to amplification.

The thermopile consists of thermocouples in series with hot junctions (as in fig. 29–5) grouped so as to receive a maximum of incident radiation and cold junctions shielded from incident radiation. Their thermoelectric *EMF*'s

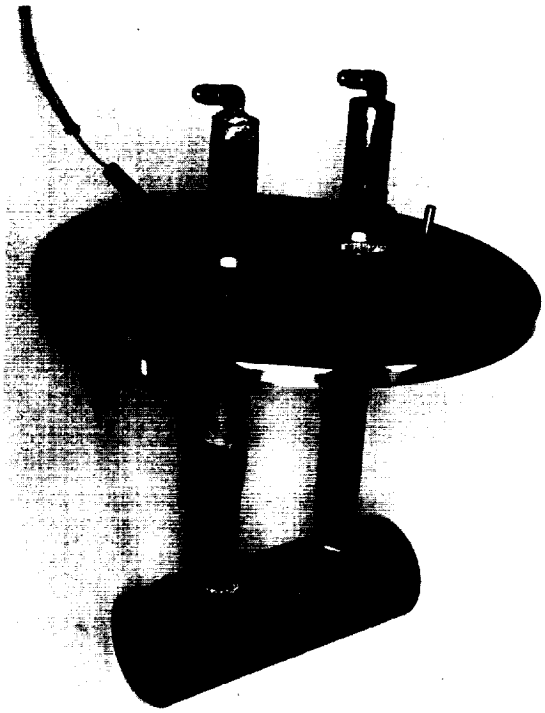

FIGURE 29–3.—Photograph of the blackbody.

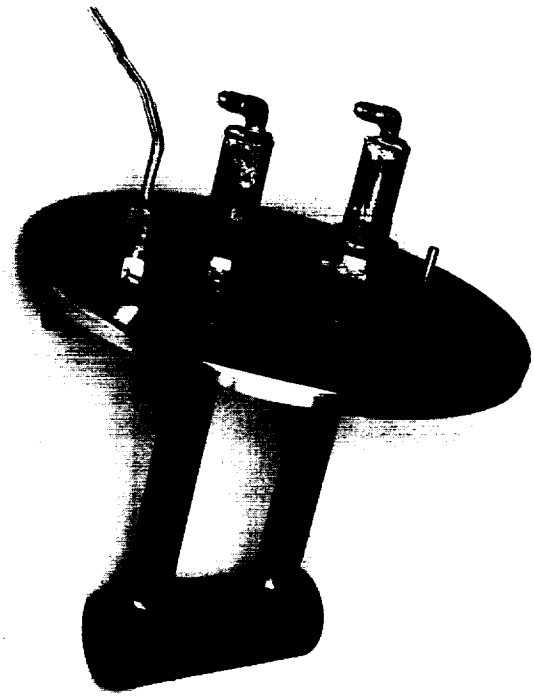

FIGURE 29–4.—Photograph of the sample holder.

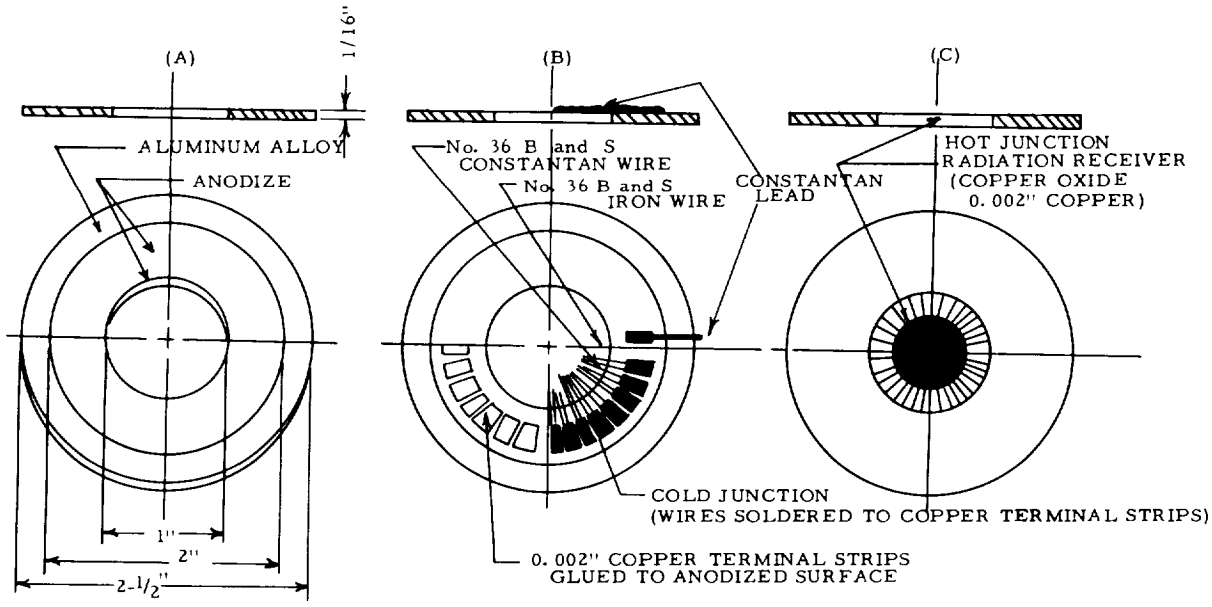

FIGURE 29–5.—Construction of 28-junction iron-constantan radial thermopile.

are additive, eliminating the need for signal amplification. The previously mentioned restrictions necessitated the construction of a senstitive thermopile as opposed to the purchase of a specially designed, custom-built detector.

A total of six thermopiles have been built. The major problems associated with the early "piles" consisted of inadequate heat sinks for the cold junction and extremely inefficient blackbody radiation receivers. Thermopile 4 is pictured (enlarged 1.35×) in figure 29–6 and is the precursor to the thermopile in use. It is a 14-junction iron-constantan thermopile employing No. 28 B and S thermocouple wire. The main difficulty with this thermopile was thought to be the large thermal cross section with resultant loss in thermoelectric *EMF*. A similar thermopile utilizing No. 36 silver-bismuth thermocouples was subsequently constructed. Unfortunately, it was destroyed while blackening the receiver. The bismuth melted at very low temperatures and was extremely brittle and easily broken.

Thermopile 6 is shown in figure 29–5. Like thermopile 4 shown in figure 29–6, it is constructed of iron-constantan wire (No. 36 B&S gauge) and is electrically insulated from the aluminum mounting by an anodized surface. The thermopile mounting is pictured in figure 29–5A with the anodized portion shown as the shaded area. The anodize electrically insulates while maintaining thermal contact with the cold junctions. This thermopile was constructed from 28 thermocouple junctions as shown in figure 29–5B and required tedious manipulations under a stereo-microscope. Each thermocouple was soldered to a 0.002-in.-thick copper terminal strip which was glued in intimate contact to the anodized surface. The receiver is shown in figure 29 5C and was constructed from a 0.002-in.-thick copper strip which had been blackened with copper oxide by the "Ebonol" process. Each hot junction was then individually glued to the receiver. The opposite side of the receiver was then painted with a very thin coat of a highly pigmented carbon black paint.

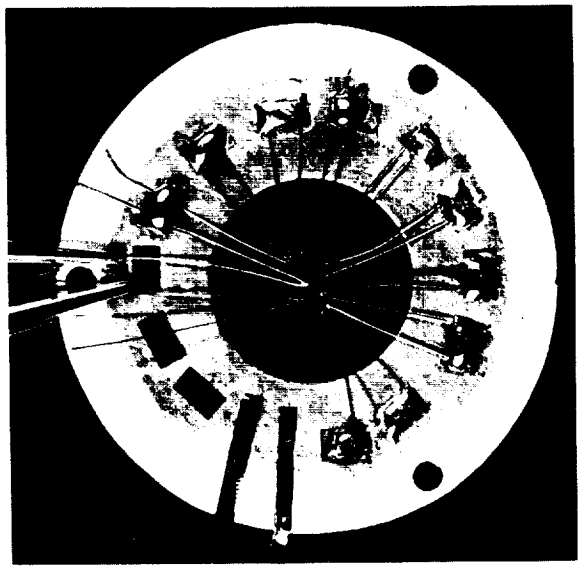

FIGURE 29–6. - Photograph of 14-junction iron-constantan radial thermopile during manufacture (1.35X).

The Assembled Emissometer

The assembled emissometer is shown in figure 29–7. The vacuum chamber was provided with a thermocouple pressure gage and an ionization gage which was placed between the chamber and the liquid nitrogen trap. A NRC thermocouple-ionization control was used to monitor the pressure in the chamber. The pressure was maintained at $1.60+0.05\times10^{-4}$ torr (0.160 ± 0.005 μ) by use of a helium-filled weather balloon and a precision needle valve. The helium was passed through a magnesium perchlorate-filled drying tube.

The blackbody and thermopile temperature thermocouple *EMF*'s were measured with a Leeds & Northrup portable millivolt potentiometer. The thermocouple cold junctions were maintained at 0° C. The thermopile output was measured with a Leeds & Northrup *K*–2 potentiometer, with a Honeywell electronic galvanometer and a reversing switch to balance transient *EMF*'s. All leads, regardless of their length, were closely trimmed and shielded with braided, tinned-copper shielding. In addition, the potentiometer, batteries, electronic galvanometer and reversing switch were all resting on a single sheet of copper to which all shielded leads were grounded at a common point (floating ground). Care was taken to insure against developing ground-loops with the copper groundwire.

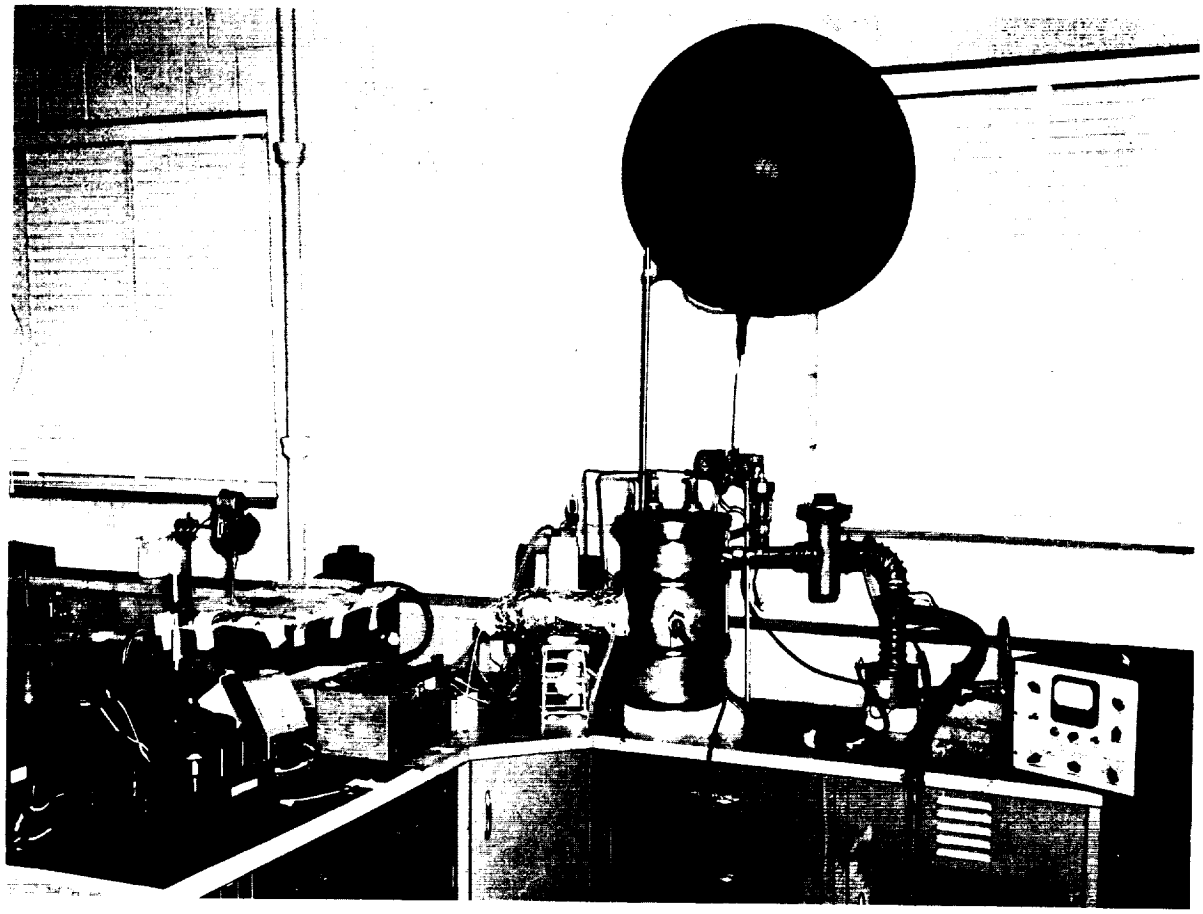

FIGURE 29–7.—Photograph of the entire total normal emissometer assembly.

THERMOPILE CALIBRATION

Since the determination of the reference blackbody *EMF* for each emissivity measurement would be extremely time consuming, a thermopile calibration curve was developed for a thermopile temperature of 84° F and a chamber pressure of $1.60 \pm 0.05 \times 10^{-4}$ torr. This temperature and pressure were found to be most easily reproduced. The thermopile calibration is presented in figure 29–8. The calibration was made by increasing the blackbody temperature from 84° F (with a ΔT of 0° F) to 208° F (with a ΔT of 124° F) and plotting the thermopile output in microvolts against ΔT.

The selective, or spectral, nature of the thermopile receiver determines the degree to which the pile output deviates from a linear response with the net energy transfer between the "pile" and the blackbody. The degree of selectivity can be calculated by performing a relatively simple thermal radiation balance using the calibration curve in figure 29–8.

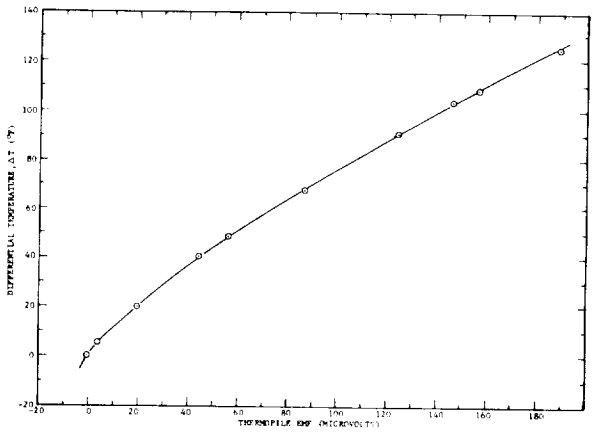

FIGURE 29–8.– Blackbody calibration of the 28-junction thermopile radiometer. Thermopile 6, temperature 84° F, calibration at 1.6 ($\pm$0.05) $\times$ 10^{-4} mm Hg pressure.

If we let

$$k=KF_{RB}$$

(from eq. (8)), the equation becomes

$$V=KF_{RB}\sigma(T^4-T_D^4), \tag{12}$$

where V is the output (EMF) in millivolts, K is the thermopile constant, and F_{RB} is the geometrical factor of the receiver with respect to the blackbody. Since the receiver can see only the blackbody, the effective blackbody (or sample) area is taken as the area of the limiting, water-cooled orifice (fig. 29–1). In this case, the area of the receiver will be regarded as an incremental area, ΔA_R. Figure 29–9 shows the geometrical relationship between the receiver and blackbody. The geometrical factor for radiation exchange between surfaces separated by a nonabsorbing medium is (ref. 5)

$$F_{RB}=\frac{1}{A_R}\frac{1}{\pi}\int_{A_R}\int_{A_B}\frac{\cos\theta_R\cos\theta_B}{S^2}\,dA_R dA_B, \tag{13}$$

where θ_R is the angle between the normal to ΔA_R and the line s connecting it with ΔA_B, and θ_B is the corresponding angle for ΔA_B. Since $\cos\theta_R=\cos\theta_B=l/s$ and $s=\sqrt{r^2+l^2}$ (from fig. 29–9),

$$F_{RB}=\frac{1}{\pi}\int_0^{r_1}\frac{l^2}{r^2+l^2}\,2\pi r dr, \tag{14}$$

Integration of equation (14) results in

$$\begin{aligned}F_{RB}&=\frac{r_1^2}{r_1^2+l^2} \qquad (15)\\ &=(0.625)^2/(0.625)^2+(7.75)^2\\ &=0.00646\\ &=6.46\times10^{-3}\end{aligned}$$

Substituting F_{RB} and solving equation (12) for K, we obtain

$$K=\frac{V_{(mv)}}{6.46\times10^{-3}\sigma(T^4-T_D^4)}. \tag{16}$$

Equation (16) was used to calculate the thermopile output at various temperatures from the values contained in figure 29–8. They are tabulated in table 29–I below:

TABLE 29–I.—*Thermopile Calibration and Selectivity Determination*

I ΔT, °F	II Blackbody T, (° F)	III EMF μ v	IV K, μv/Btu/ft²-hr	V λ Max, μ
124	668	188. 6	152	7. 80
108	652	156. 5	151	8. 00
90	634	124. 3	151	8. 25
67	611	86. 5	151	8. 54
48	592	56. 1	144	8. 81
19	563	20. 0	137	9. 25

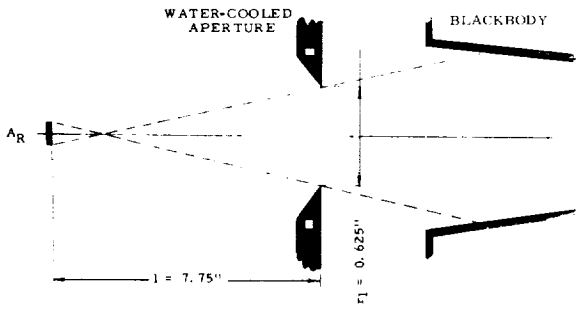

FIGURE 29–9.—Geometrical relationship between the receiver and blackbody.

Column IV in table 29–I gives the thermopile constant in per μv/Btu/ft²-hr for six blackbody temperatures and corresponding EMFs. It will be noted that the constant varies from 137 μ per Btu/ft²-hr to 152 μv per Btu/ft²-hr, indicating that the thermopile is selective in nature. Column V in table 29–I presents the peak wavelength for the blackbody radiation corresponding to the various blackbody temperatures. The blackened thermopile receiver appears to be a flat absorber to about 8.5/μ wavelength after which the receiver coating tends to become somewhat transparent (with the pile possessing

TABLE 29–II.—*Total Normal Emittance of Selected Surfaces*

Material	ϵ_t	T, °K
Gold, electrolytically polished	0.021	360
Aluminum, 1100, polished with MgO and water	.022	370
Copper, sand-blasted	.147	356
Paint, white, aluminized with leafing 3.0-mil Al	.716	363
	.763	320
Paint, white, aluminized with non-leafing 3.0-mil Al	.645	367
	.757	321
Paint, carbon black, *CB*–1*T* 15–10 (2.0 mils)	.760	366
	.761	350
	.763	332
Enamel, porcelain, potassium titanate opacified	.821	355
Enamel, porcelain, potassium titanate opacified, overcoated with phosphate-bonded potassium titanate	.868	358
Paint, white, Anatase, A–31 45	.910	360
Paint, white, Kry-Kote	.880	360

90% of the output to radiation $\geq 9.25\ \mu$ that it had to radiation $\leq 7.8\ \mu$).

DISCUSSION OF RESULTS

Table 29–II presents the total normal emittance of selected surfaces. They were measured by obtaining the "pile" *EMF* when the sample was in place and by dividing the *EMF* for the blackbody at the same temperature by reading from the curve in figure 29–8.

The values obtained for both polished gold and polished 2S aluminum agree closely with the values reported in the literature.

The selective nature of the emittance of both aluminized white paints is indicated by the increase in their emittance with decreasing temperature (longer wavelength). This is opposite to the expected selectivity, if any, which might be presumed from the fact that the reflectance of aluminum increases with longer wavelengths.

The emittance of the carbon black paint, CB–1T–15–10, was measured at three temperatures in order to determine if the anomaly noted above was due to thermopile calibration errors at the lower temperatures. The results indicate that this is not the case since the emittance values are identical at all three temperatures and agree with measurements of thin coatings of pure carbon black paints as reported in the literature.

DISCUSSION OF PROBLEMS

Several major problems arose during the course of the checkout and calibration of the instrument. Most of these problems were simply the result of attempting to measure *EMFs* in the microvolt region. Problems concerned with the choice of thermopile design have already been discussed. However, the sensitivity of the thermopile to pressure changes was quickly realized. While much of the pressure dependence of sensitive thermopiles is due to the attenuation of the radiation by carbon dioxide and water molecules, even small, instantaneous pressure changes caused large, spurious *EMFs*. These effects are thought to be due to transient thermals caused by the adiabatic expansion and contraction of the residual gas in the chamber.

Another problem affecting the thermopile was the breaking of the vacuum at the end of a particular set of measurements. It was found that a rush of air on opening the chamber caused a slight bending of the thermopile receiver and a subsequent short of nearly one-third of the junctions. This problem was corrected by inserting a needle valve into the chamber wall and slowly bleeding in air over a period of several minutes.

Still another thermopile problem concerns minute changes in the 84° F cooling water.

These changes occurred during the on-cycle of the immersion heaters in the constant-temperature water bath and caused considerable error in the *EMF* even though the thermopile temperature thermocouple could detect no temperature change. The problem was not apparent during the summer months when the room temperature and bath temperature were nearly the same. It is thought that the problem is due to the slight change in temperature that occurs in the thermopile surroundings before it is manifested in the thermopile cold-junctions. This situation was partially alleviated by placing insulation between the thermopile rear and the radiometer end-plate. In addition, the use of a well-insulated, large water bath, which can be shut off and which will maintain a constant temperature during the *EMF* measurements, has permitted circumvention of the problem.

Spurious effects not attributable to the thermopile caused a great amount of concern during early calibration attempts. During this period, the *EMF* leads, both from the potentiometer to the reversing switch, and from the switch to the galvanometer, were unshielded. Furthermore, great switch voltages developed both within the potentiometer and the reversing switch. The system was extremely sensitive to shock, movement of clothing (static electricity), and air currents. These effects were eliminated by shielding all leads (including those to the batteries and on the reversing switch) and grounding each lead separately at a common point on a copper sheet, upon which the entire measuring circuit had been placed.

CONCLUSIONS

The total normal emissimeter described in this report possesses excellent precision in the temperature range discussed. Results compare favorably with the literature. It can be modified easily for use at high temperature by designing and constructing a high-temperature blackbody and sample holder. The selective nature of the receiver as well as the lack of energy at low temperature precludes the use of the instrument at sample temperatures below 0° C.

REFERENCES

1. Wilkes, G. B.: Total Normal Emissivities and Solar Absorptivities of Materials. WADC TR 54-42, March 1954.
2. Gier and Dunkle: *in* Giedt, W. H., Principles of Engineering Heat Transfer, D. Van Nostrand Co., Inc., New York, 1957, p. 269.
3. Gier, J. T.; and Boelter, L. M. K.: The Silver-Constantan Plated Thermopile *in* Temperature, Its Measurement and Control in Science and Industry, Reinhold Publishing Corp., New York, 1941, p. 1284.
4. Edwards, D. F.: The Emissivity of a Conical Black Body. Report No. 2144-105-T, The University of Michigan Engineering Research Institute, Ann Arbor, Michigan, November 1956.
5. Giedt, W. H.: op. cit., p. 254.

DISCUSSION

Roger N. Schmidt, Minneapolis-Honeywell Regulator Co.: The technique discussed by Mr. Zerlaut and the one used at Hopkins Research Center have a basic difference in that they do not cover the same area of property measurement. Mr. Zerlaut's paper discusses the measurement of total *normal* emittance which uses a method similar to that used by others for many years. When considering the total energy radiated by a surface, the total *hemispherical* emittance of the surface rather than the total *normal* is required. Total normal measurements are generally easier to make than total hemispherical, and total normal emittance is sometimes required for specific heat transfer calculations. While the method for total hemispherical emittance measurement is simple and straight forward, to our knowledge it has not been previously reported.

The possibility of experimental error in the measurement of normal emittance appears to be greater than in the measurement of total hemispherical emittance. Background radiation can be troublesome when the temperature of the background is nearly the same as the sample temperature and the background shape factor is 100 times larger than the sample shape factor. In the hemispherical technique the shape factor of the surroundings is 1/100 of the shape factor for the samples, and the background is at liquid nitrogen temperature.

The sample surface temperature and blackbody temperature measurement are very critical for emittance measurements. Although Mr. Zerlaut does not discuss

these measurements, it appears from his pictures that he used only one thermocouple in the blackbody and one thermocouple in the sample holder. A sufficient number of thermocouples should be used to assure uniformity in the blackbody and sample surface temperatures. We have used two sample sufrace thermocouples and three blackbody thermocouples.

The emittance calculation procedure presented in Mr. Zerlaut's paper is different from ours in that it assumes a constant correlation coefficient between the thermopile output and the heat flux incident on the thermopile. This potential source of error can be eliminated by adjusting the blackbody temperature to give the same heat flux as the sample as we do in our hemispherical measurements rather than by adjusting blackbody and sample to the same temperature and measuring the ratio of heat fluxes as Mr. Zerlaut does. This can be shown as follows:

The energy transferred by radiation from the sample to the thermopile is,

$$Q_{s-t}=\sigma F_{s-t}\epsilon_s(T_s^4-T_t^4) \tag{1}$$

where:

Q_{s-t}	energy interchange between the sample and thermopile
σ	Steffan Boltzmann constant
F_{s-t}	shape factor of sample to thermopile
ϵ_s	normal emittance of sample
T_s	surface temperature of sample
T_t	temperature of thermopile hot junctions

Because Mr. Zerlaut's calculation equation neglects the energy radiated from the background and thermopile and reflected by the sample to the thermopile, it is neglected here in order to simplify the calculation equation. However, a detailed analysis should be made to show whether this term can be neglected and what error it causes in the final results. This term can be relatively *very* large if the sample is highly reflective because the background temperature is nearly as high as the temperature of the sample. If the background and sample are at the same temperature, all samples will appear to be black!

The blackbody calibration of the thermopile will be used to determine Q_{s-t}. The energy transferred by radiation from the blackbody to the thermopile is,

$$Q_{b-t}=\sigma F_{b-t}\epsilon_b(T^4-T_t^4) \tag{2}$$

where:

Q_{b-t}	energy interchange between the sample and thermopile
F_{b-t}	shape factor of blackbody to thermopile
ϵ_b	emittance of blackbody
T_b	temperature of blackbody

Making the same assumption as Mr. Zerlaut,

$$\epsilon_b=1.0$$
$$F_{b-t}=F_{s-t}$$

and, if the blackbody temperature is adjusted so that the thermopile output is the same for both the sample and the blackbody,

$$Q_{s-t}=Q_{b-t} \tag{3}$$

Equations (1), (2), and (3) can be combined to give:

$$\epsilon_s(T_s^4-T_t^4)=(T_b^4-T_t^4)$$

or

$$\epsilon_s=\frac{(T_b^4-T_t^4)}{(T_s^4-T_t^4)} \tag{4}$$

T_b is the blackbody temperature determined from the blackbody calibration curve from the sample thermopile output. T_s is the sample surface temperature and is determined by thermocouples. T_t is the thermopile hot junction temperature and is determined from the thermopile cold junction temperature and the output of the thermopile. For Mr. Zerlaut's apparatus the hot and cold junctions are nearly the same temperature and therefore the cold-junction temperature could be used in place of the hot junction temperature. This calculation procedure does not assume a constant correlation between the thermopile output and the impinging energy on the thermopile because the thermopile output is the same for the blackbody and sample. The emittance is determined from the respective temperatures. However this equation does assume the thermopile receiving area is non selective (graybody). Mr. Zerlaut states that his blackbody data indicates some thermopile selectivity; however, these data may demonstrate the large error which exists as the sample and blackbody temperature approach the background temperature. If this selectivity does exist for his thermopile coating, there are many other coatings that he could use which are good graybodies in the infrared.

SESSION IV

MEASUREMENTS AT MODERATELY HIGH TEMPERATURES (450° TO 1400° K)

CHAIRMAN: JOSEPH C. RICHMOND

30—THERMAL RADIATION IN SPACE NUCLEAR ELECTRIC POWER SYSTEMS

BY HERMAN SCHWARTZ

NASA LEWIS RESEARCH CENTER, CLEVELAND, OHIO

The heat rejection temperatures for a number of space nuclear electric power plants fall within the temperature range of 450° K to 1400° K. The characteristics of these power-plants and the manner in which thermal radiation properties and surfacings affect their performance are discussed.

Nuclear electric power systems for spacecraft, once developed, would have the unique characteristic of providing a large amount of electrical power for long continuous periods at minimal weight and cost. In terms of their method for power conversion, these systems can be divided into two broad categories, dynamic engines, which convert heat energy into electrical energy by some mechanical means, and static engines, which convert heat energy directly into electrical energy.

The dynamic engine that has been receiving the most consideration is the one which employs a turbine as the energy converter in a Rankine or Brayton cycle. A schematic of a power system which uses a turbine in a Rankine cycle is given in figure 30–1. Thermal energy developed in a nuclear reactor is carried by a liquid metal such as lithium or a eutectic of sodium and potassium to a heat exchanger. On the secondary side of the heat exchanger a liquid metal such as potassium or mercury is brought to a boiling temperature and then vaporized. The vapor imparts energy to the turbine that in turn is mechanically transmitted to the rotor of an electrical generator. Upon leaving the turbine, the vapor enters a direct condensing radiator. Here waste heat is radiated at constant temperature as the vapor is condensed to liquid. A certain amount of subcooling also takse place in the radiator. The liquid is then sent to a pump and the cycle is begun once again.

In the Brayton cycle, figure 30–2, a gas such as helium is employed as the working medium. Heating of the gas within the reactor, rather

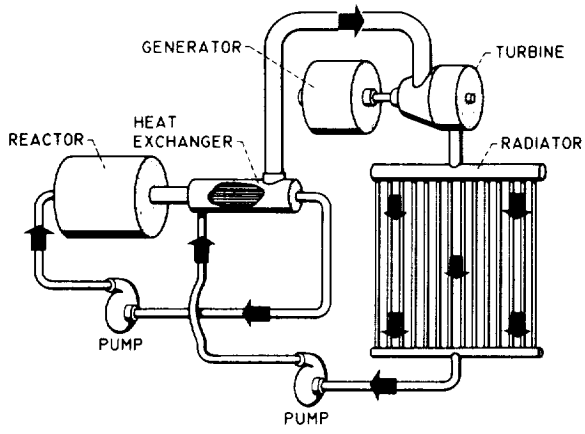

FIGURE 30–1.—Schematic of Rankine cycle space power system.

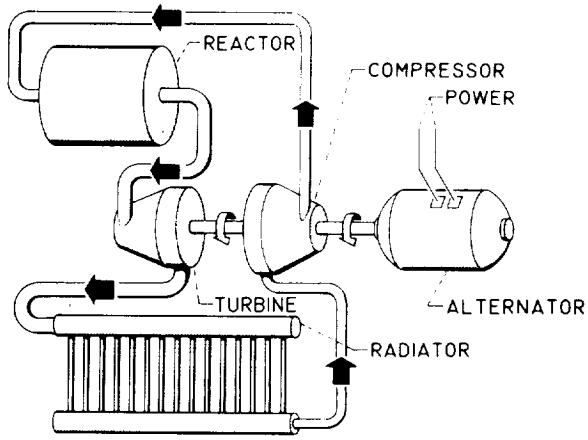

FIGURE 30–2.—Schematic of Brayton cycle space power system.

than from an intermediate heat exchanger, is chosen. The gas then passes through the turbine and the radiator. The radiator is not isothermal as in the Rankine cycle because of the sensible heat loss in the gas. On leaving the radiator, gas pressure is restored by a compressor which is on the same shaft as the turbine and alternator rotor.

Static engines, also known as direct conversion devices, are contenders in the space nuclear electric picture. The thermionic converter is an example of a static engine that has been receiving considerable attention during the past few years. In the thermionic emitter (fig. 30–3) a cathode is heated to a temperature high enough to obtain appreciable electron emission. In a space application, the anode is maintained at approximately half the absolute temperature of the cathode. The role of the cesium is to make the route for the electrons easier when going from emitter to collector. At a megawatt of electrical power literally thousands of such units are required. They are situated in the reactor, the cathode being integral with the surface of the fuel element and the anode being cooled by a liquid metal, such as lithium, which circulates through the reactor. The liquid

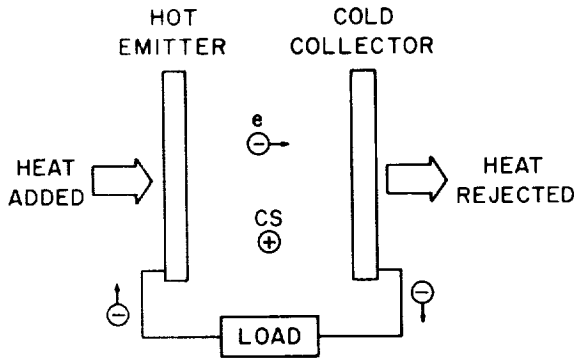

FIGURE 30–3.—Thermionic converter.

metal carries the heat to a radiator; and, because of the sensible heat loss in the fluid, a temperature difference exists across the radiator.

THE RADIATOR IN NUCLEAR ELECTRIC POWER SYSTEMS

A view of the radiator in the Rankine cycle is shown in figure 30–4. Vapor of high quality comes from the turbine and is distributed by a header to the tubes. Within the tubes the vapor is completely condensed, and the liquid is returned to the pump via the exit header. A cross section of the typical tube and fin is also given in figure 30–4. The function of the liner

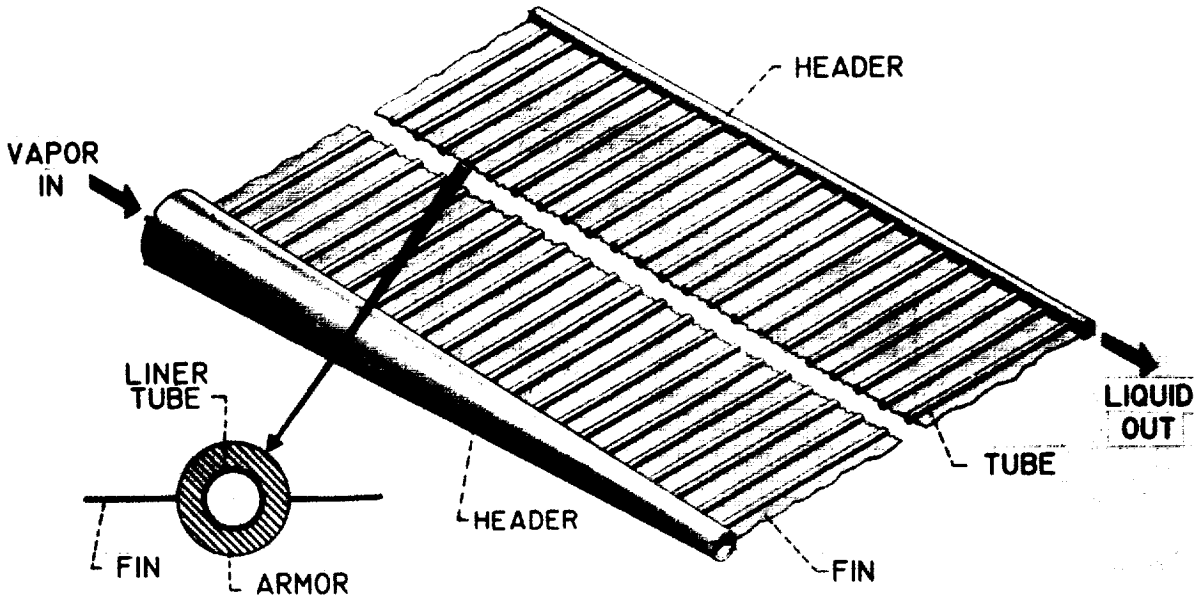

FIGURE 30–4.—Typical fluid radiator.

tube is to contain the condensing liquid metal vapor; the armor that surrounds the tube is selected on the basis of providing protection against tube puncture by micrometeroroids. Finning is employed to minimize the exposed area of the tube, thereby effecting a maximum heat rejection per unit weight of the radiator. To further enhance heat rejection and reduce weight, a high-emittance coating is placed on the surface of the fin and armor.

The radiation heat transfer from the radiator can be simply expressed as

$$Q=2\epsilon_{th}\sigma A_r T_r^4-\alpha_s G A_r \cos\gamma \qquad [1]$$

when A_r is the flat plate area of the radiator; T_r, the radiator temperature; G, the solar constant; and γ, the angle between the incoming radiation and the perpendicular to the flat plate. Solar radiation reflected by the earth and the far infra-red radiation of the earth are neglected in equation (1). Solving for the radiator area

$$A_r=\frac{Q}{2\epsilon_{th}\sigma T_r^4-\alpha_s G\cos\gamma} \qquad [2]$$

where T_r is established from a cycle optimization that minimizes the weight of the system and Q is obtained for a given net electrical power output by a cycle analysis.

In order to minimize A_r, which is proportional to radiator weight, ϵ_{th} should be brought as close to 1 as possible and α_s made to approach zero. For the case in which heat rejection temperatures exceed 1000° F, the $\alpha_s G \cos\gamma$ term becomes negligible and solar absorptance (α_s) need not be considered.

A nuclear turbo-electric powerplant, designated SNAP 8, is presently being developed to produce 30 kw of net electrical power. The condensing temperature of its mercury working fluid is 700° F. The temperature of the fin varies from 700° F at its root to about 550° F at the midline between adjacent tubes. For SNAP 8 there are two types of surfacings under investigation, one having an emittance greater than 0.90, with no firm restriction on absorptance, and the other surfacing having an emittance greater than 0.85, with a solar absorptance less than 0.3. Both are required to show minimum degradation of radiation properties in the space and nuclear environment for a period of 14 months.

In a 1-megawatt turbo-electric system using a Rankine cycle, the radiator is required to operate at a temperature approximating 1300° F. For this temperature level the emittance, and not the solar absorptance, affects the radiator area. The radiator in the 1-megawatt system represents as much as 70% of the total powerplant weight; and from this consideration, it is essential to strive for every small increase in thermal emittance. Related to increasing the emittance is the need for reducing the error band in the emittance measurements. Present methods of measuring emittance are accurate to only ±4% and this uncertainty greatly increases the powerplant weight.

Another important aspect of heat rejection in the nuclear turbo-electric system is keeping the electrical generator and power conditioning equipment from exceeding temperature limits imposed by electrical materials. The electrical components are generally required to operate considerably below the main radiator temperature (~1300° F), and, therefore, separate heat rejection systems are needed. An alternator efficiency of 94%, and transformer and rectifier efficiencies of 99% and 98.5%, figure 30–5, was assumed in plotting to give the percentage increase in radiator area for different limiting component temperatures. The same emittance was used for the main radiator and that for cooling electrical components; the solar ab-

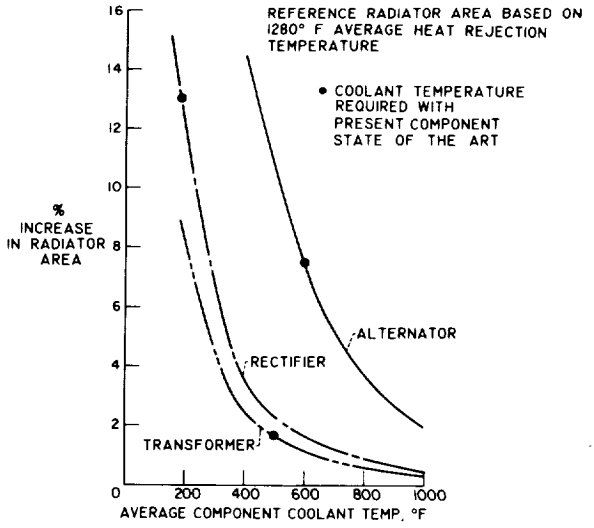

FIGURE 30–5.—Effect of average component coolant temperature on radiator area required for electrical equipment cooling.

sorptance was assumed as zero. These curves emphasize the need for surfacings having high emittance and low solar absorptance in radiators which cool the electrical components.

A 1-megawatt system that employs the Brayton cycle has slightly different surfacing requirements for its main radiator. A high emittance is to be maintained over a wider temperature range and the surfacing must withstand higher temperatures. The surfacing conditions for a 1-megawatt thermionic system is, in many ways, similar to that discussed for the Rankine cycle.

TAILORING OF COATINGS

Over the years there has been considerable activity in measuring emittance properties, but a relatively minor effort has been expended in formulating coatings to give a desired spectral emittance. Lately, interest has developed in tailoring coatings for specific applications. The technique consists of mixing substances or using multilayers of substances whose spectral emittances are known. Illustrating the method, substances A and B have spectral emittances as shown in figure 30–6; upon mixing the substances a compromise of spectral emittance, shown as curve C, may result. By varying the ratio of constituents it is possible to approach a desired spectral curve. In an ideal case, for which the fundamental parameters of scattering and absorption coefficients and indices of refraction were advantageous, it would be possible to approach the maximum spectral values of both substances.

This technique, if successfully developed, will have an important weight effect on nuclear electric power systems. It will satisfy the two main requirements in these systems, the high thermal emittance for the high heat rejection temperatures and the combination high thermal emittance and low solar absorptance for the low heat rejection temperatures.

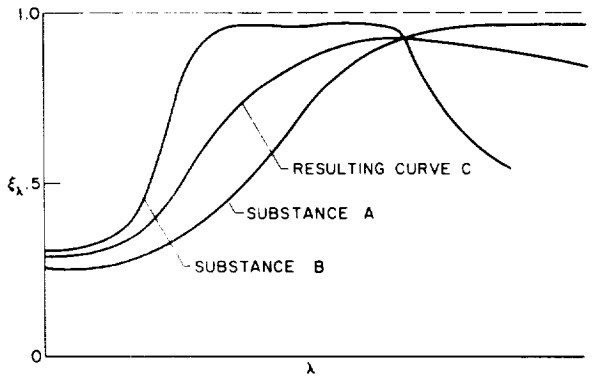

FIGURE 30–6. — Possible effect of mixing two substances with different spectral emittances.

31—TOTAL NORMAL AND TOTAL HEMISPHERICAL EMITTANCE OF POLISHED METALS

BY G. L. ABBOTT

U.S. NAVAL RADIOLOGICAL DEFENSE LABORATORY, SAN FRANCISCO, CALIFORNIA

An apparatus has been designed, built, and tested that will measure the total hemispherical emittance, total normal emittance, normal and hemishperical spectral emittance, angular distribution of radiation and resistivity of metals from 1000° K to their melting points. The flat ribbon sample is resistance heated while held in a mount capable of 230° rotation in a vacuum of 10^{-6} torr. The apparatus and measuring techniques are described and examples of resulting data given.

Radiant heat transfer is especially important at very high temperatures or at the very low pressures encountered in space. The ability of a surface to lose heat by radiation is described by the product of its total hemispherical emittance, the Stefan-Boltzmann constant, and the fourth power of its absolute temperature. There is an increasingly large volume of data presently being accumulated on the total normal emittance of a variety of surfaces. Indiscriminate substitution of these data for those of total hemispherical emittance in heat transfer problems could lead to serious errors. The equating of these two emittance values is permissible only when the angular distribution from the surface obeys Lambert's cosine law. This report describes the techniques whereby one can examine the relationships between these two emittance parameters for various classes of real surfaces.

The reliance that can be put upon high-temperature emittance data in solving heat transfer problems at the present time is not very high for several reasons. Emittance measurements are inherently very difficult to make because high surface temperatures are hard to measure accurately, and at low temperatures background radiation is a problem. The purity level of a given material may vary or the surface may not be entirely free of contamination. The geometry of the surface may vary as a result of different preparation techniques or because of thermal etching or recrystallization. Finally, the differences may simply depend on whether the quantity being measured is total normal or total hemispherical emittance. The seriousness of the situation just described is evident when one looks at the published total emittances reported for the same material as a result of different investigations.

In accordance with the National Bureau of Standards (ref. 1), the radiating properties of surfaces are defined as follows. Emittance is a property of a specimen; it is the ratio of the rate of emission of radiant energy to that of a black body radiator at the same temperature under the same conditions. Emissivity is a fundamental property of a material and is numerically equal to emittance of a specimen of the material that has an optically smooth surface and is sufficiently thick to be opaque. It is further assumed that the surface is free from contamination and the crystalline structure and its defects adjacent to the surface are the same as those of the interior. The emittance and the emissivity can be either normal or hemispherical depending upon whether the comparison with the black surface is of the intensity normal to the surface or of all of the power radiated regardless of angle. They can, also, be either spectral or total depending upon whether the comparison is of the radiation in a narrow spectral band or whether it includes all wave lengths. The

term spectral emittance, used in this report, implies normal spectral emittance.

An expression for the total normal emissivity of metals at moderately low temperatures has been derived by Aschkinass (ref. 2) and Foote (ref. 3). The theoretical formula derived by Foote and corrected according to the latest value of the second radiation constant, (C_2= 1.438, International temperature scale of 1948, reference 4), is

$$\epsilon_n=0.578(\rho T)^{1/2}-0.179(\rho T)+0.044(\rho T)^{3/2}+\ldots \quad (1)$$

where T is the absolute temperature in degrees Kelvin and ρ is the resistivity in ohm-cm. Taking the angular distribution into account, Davisson and Weeks (ref. 5) have derived an expression for the total hemispherical emissivity of metals. With the latest value of C_2, their formula becomes

$$\epsilon_H=0.754(\rho T)^{1/2}-0.635(\rho T)+0.673(\rho T)^{3/2}+\ldots \quad (2)$$

A number of assumptions and approximations must be made before arriving at these equations (ref. 6). At higher temperatures, they become less valid. The object of the research is to develop a technique for making rather exhaustive and precise measurements on a few materials in order to help explain the wide variations in presently published emittance data and the deviations of the actual from the theoretical data.

In comparing the measured emittances with the theoretical emissivity which was discussed above, it is necessary to reconsider the relationships between the two quantities. The emittance is equal to the emissivity when certain conditions are met. (1) The specimen must be opaque. This is not a difficult requirement to meet for metals. (2) The specimen must be free of surface contamination. This can be achieved reasonably well by cleaning and polishing the specimen and performing the measurements in a sufficiently good vacuum or in an inert atmosphere. Even here an adsorbed layer of gas is held at the surface except in the most extreme vacuums. However, it is assumed that this layer is too thin to be of consequence. (3) The crystalline structure and its defects at the surface must be characteristics of the material rather than a product of the surface treatment. This will always be violated to some extent by polishing or rolling. (4) The surface must be optically smooth; once the specimen is adequately polished, it will retain a smooth surface at low temperatures. However, at elevated temperature, recrystallization and thermal etching take place and the specimen appears rough to the eye.

Aside from the difference between emittance and emissivity, variations in measured emittance can be due to variations in the purity of the specimens. Comparisons of the electrical resistivity can serve as a check on this point. Another possible source of variation in the reported emittance values is the difficulty of accurate temperature determinations.

The previous mechanical and thermal history of a bulk metal influences its optical properties, making it very difficult to achieve reproducible conditions for experimentation. Some investigators in this field are studying single crystals in an attempt to overcome this effect. However, they have found that minute imperfections in single crystals also cause variations in their results. Despite these problems, several theoretical ideas that describe these phenomena have been proposed. Unfortunately, they have not yielded mathematical expressions which are consistently in agreement with experiment (ref. 7).

For practical purposes, the most important parameter of radiant heat transfer is the total hemispherical emittance. Since the total normal emittance is the parameter most often measured, it is of interest to investigate the relationship between the two for various classes of materials. By using the techniques and apparatus described in the following paragraphs, the total hemispherical emittance, total normal emittance, normal spectral emittance, and resistivity can be measured.

THEORY OF THE METHOD

The differential equation of heat flow in an electrically heated ribbon of conducting metal is given by

$$I^2R=IE=-A\frac{\partial}{\partial z}\left(K\frac{\partial T}{\partial z}\right)+DAC\frac{\partial T}{\partial t}+\epsilon_H P\sigma T^4-\alpha P\sigma T_0^4$$

where I is the current; R, the resistance per unit length; E, the voltage per unit length; z, the distance along the ribbon; A, the cross sectional area; K, the thermal conductivity; T, the absolute temperature; D, the density; C, the heat capacity; ϵ_H, the total hemispherical emittance; P, the radiating area per unit length; σ, the Stefan-Boltzmann constant; and α, the absorptivity of the ribbon at temperature T for radiation with a relative spectral distribution equal to that of a blackbody at the wall temperature T_0. The terms on the left side of this equation represent the power generated within the ribbon and are equated to the power dissipated by conduction and radiation plus the energy stored. The last term on the right is the power absorbed by the ribbon from its surroundings at temperature T_0. This equation does not include a convective term since a vacuum environment only will be considered. It is also assumed that the walls are non-reflecting. In a steady state condition at the center of a ribbon of sufficient length to establish a uniform temperature region, the energy will be lost by radiation only. Then this equation reduces to

$$I^2R=IE=P\sigma(\epsilon_H T^4-\alpha T_0^4)=\epsilon_H P\sigma(T^4-\frac{\alpha}{\epsilon_H}T_0^4)$$

It is often found that α/ϵ_H is set equal to one, or that the term $\alpha T_0^4/\epsilon_H$ is neglected altogether. The omission of the term will account for an error which is less than 1% when T/T_0 is equal to 3 or greater, but if $T_0=300°$ K an appreciable error may occur when dealing with ribbons at temperatures much less than 1000° K. When $\alpha T_0^4/\epsilon_H$ is taken into account, the problem arises as to what value to attach to α/ϵ_H. One method of reasonable approximation is to consider equation (2). If the radiation from the surroundings at T_0 is assumed to have a blackbody distribution, the absorptance of the ribbon based on the free electron theory of metals at temperature T becomes

$$\alpha=a(\rho T_0)^{1/2}+b(\rho T_0)+c(\rho T_0)^{3/2}+\ldots$$

where ρ is the electrical resistivity while the emittance is

$$\epsilon_H=a(\rho T)^{1/2}+b(\rho T)+c(\rho T)^{3/2}+\ldots$$

from which

$$\frac{\alpha}{\epsilon_H}=\frac{a(\rho T_0)^{1/2}+b(\rho T_0)+\ldots}{a(\rho T)^{1/2}+(b\rho T)+\ldots}$$

$$\frac{\alpha}{\epsilon_H}\approx\left(\frac{T_0}{T}\right)^{1/2}$$

and

$$I^2R=IE=\epsilon_H P\sigma\left[T^4-\left(\frac{T_0}{T}\right)^{1/2}T_0^4\right] \qquad (3)$$

When the voltage per unit length and the current are known, both the resistivity and total hemispherical emittance may be found from equation (3). Thus,

$$\rho=\frac{EA}{I} \qquad (4)$$

and

$$\epsilon_H=\frac{EI}{P\sigma\left[T^4-\left(\frac{T_0}{T}\right)^{1/2}T_0^4\right]} \qquad (5)$$

The total normal emittance may be determined with a thermopile that has been calibrated for blackbody radiation by comparing the normal emissive power of the specimen relative to that of a blackbody at the same temperature. Thus, the total normal emittance is:

$$\epsilon_N=\frac{Bx}{P\frac{\sigma}{\pi}\left[T^4-\left(\frac{T_0}{T}\right)^{1/2}T_0^4\right]} \qquad (6)$$

where B is the thermopile calibration constant and x is the thermopile output voltage.

Now the ratio of total hemispherical to total normal emittance may be arrived at by two methods. First, by the quotient of the emittances from equations (5) and (6) and, second, by measuring the angular distribution of radiation from a plane surface. The ratio by the first method is

$$\frac{\epsilon_H}{\epsilon_N}=\frac{EI}{\pi Bx} \qquad (7)$$

The calculation of this ratio by the latter method is based on the following derivation. The total radiant power emitted into a hemisphere per unit area is

$$H=\epsilon_H\sigma T^4=\int_0^{\pi/2}\epsilon_N\frac{\sigma T^4}{\pi}f(\theta)2\pi\sin\theta\,d\theta \qquad (8)$$

where $\epsilon_N \sigma T^4/\pi$ is the power emitted per unit solid angle normal to the surface, $f(\theta)$ is the ratio of the intensity at angle θ to the normal intensity and $2\pi \sin \theta \, d\theta$ is the differential solid angle. When the assumption is made that the emitting surface is Lambertian, then $f(\theta)=\cos \theta$, but this is not valid in the case of polished metals. The expression for the ratio of total hemispherical to total normal emittance may then be written

$$\frac{\epsilon_H}{\epsilon_N}=2\int_0^{\pi/2} f(\theta) \sin \theta \, d\theta = 2\int_0^1 f(\theta) d \, (\cos \theta)$$

This may be numerically integrated in the form of the sum

$$\frac{\epsilon_H}{\epsilon_N}=2\sum_{n=1}^{S} f(\theta_n) \, (\cos \theta_n - \cos \theta_{n+1}) = \frac{2}{S}\sum_{n=1}^{S} f(\theta_n) \tag{9}$$

where S is the number of equal increments along the cos θ axis between 0 and 1, and the θ are chosen such that the cos θ_n are separated by equal increments of $1/S^n$, and $f(\theta_n)$ is the ratio of the intensity at θ_n to the normal intensity.

Since the interest here is only in relative intensity, no absolute calibration of the detector is necessary as in the case where the detector is used for direct determination of normal emittance.

The spectral emittance at 0.65μ may also be readily determined if the true temperature and brightness temperature of the ribbon are known. On the basis of Wien's law, the following relation is established

$$\epsilon_\lambda \exp \, (-c_2/\lambda T) = \exp \, (-c_2/\lambda T_A)$$

where T is the true temperature of the ribbon and T_A is the brightness temperature. This reduces to

$$\epsilon_\lambda = \exp\left[-2.211\times 10^4 \left(\frac{T-T_A}{TT_A}\right)\right] \tag{10}$$

where $\lambda=0.65\mu$ and $c_2=1.438$. Therefore, the total hemispherical emittance, total normal emittance, spectral emittance, and resistivity of a conducting ribbon may be found if the true temperature, apparent temperature, current, voltage per unit length and angular distribution of emitted energy are known.

EXPERIMENTAL ARRANGEMENT

Figures 31–1 and 31–2 are pictures of the experimental arrangement. The sample under test is in the form of a ribbon 12 in. long, 0.4 in. wide, and 0.005 in. thick. The ribbon is supported vertically in a mount capable of being rotated 230° about the ribbon axis. To account for expansion, a tension adjustment is attached to the lower support arm (which is hinged) and may be adjusted during operation by a rotating vacuum feed-through. This is accomplished by rotating the ribbon mount to align a tongue and groove configuration. The ribbon clamps and exposed supporting structure are force water cooled. Power is delivered to the ribbon by flexible 4/0 copper cable which is spiraled with the Viton A cooling water hoses at the upper and lower supports. Sufficient slack is employed to allow 230° rotation.

The thermopile is the detector from a Minneapolis-Honeywell "Radiomatic" pyrometer and consists of 10 iron-constanton elements with a circular configuration 3 mm in diameter. The thermopile housing is water cooled to give cold junction stablization and blackened within with camphor black to minimize reflections. The radiation enters an aperture which can be adjusted to vary the vertical field of view, and impinges on the detector which is coated with an aqueous solution of lamp black. An electrically operated shutter opens or closes the entrance. The field of view is wider than the ribbon and approximately 0.04–.08 in. along its length. In order to be sure that radiation seen by the thermopile is direct and not spurious reflections or radiation from other internal components, a water cooled plate is mounted behind the ribbon and opposite the thermopile. The blackened surface of the plate (fig. 31–1) has horizontal 30° grooves, $\frac{1}{16}$ in. deep, and forms the total field of view of the thermopile (except for the ribbon).

The temperature and voltage per unit length are determined by attaching fine wires to the ribbon (thermocouple wires for temperature). Two techniques are used for attachment depending on the material. One is the direct welding of 0.005-in. wires to the ribbon; the other consists of drilling 0.005-in. holes in the ribbon and swaging the end of the wire in the hole. The swaging technique results in a nearly

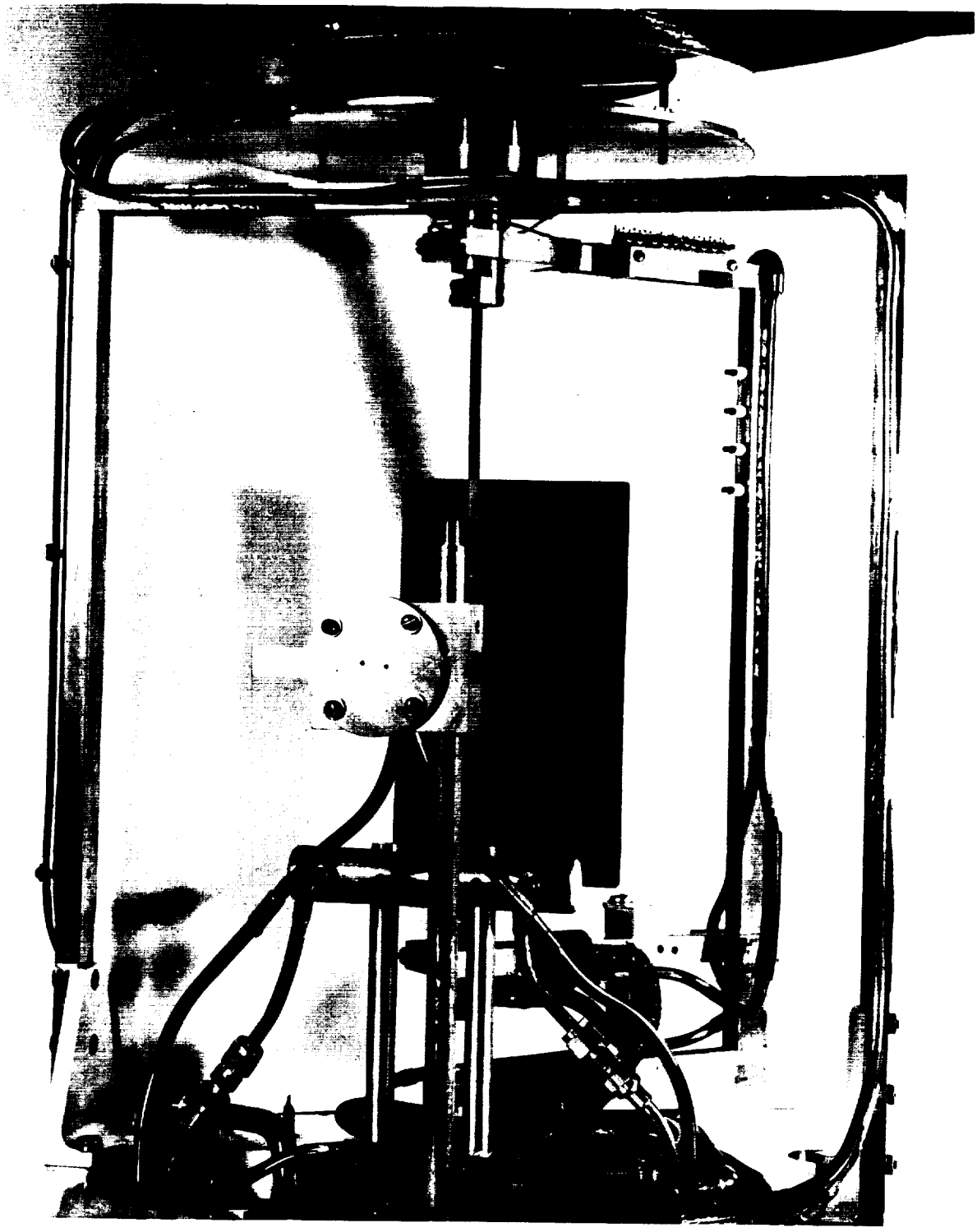

FIGURE 31-1.—Ribbon mount assembly for emittance measurements.

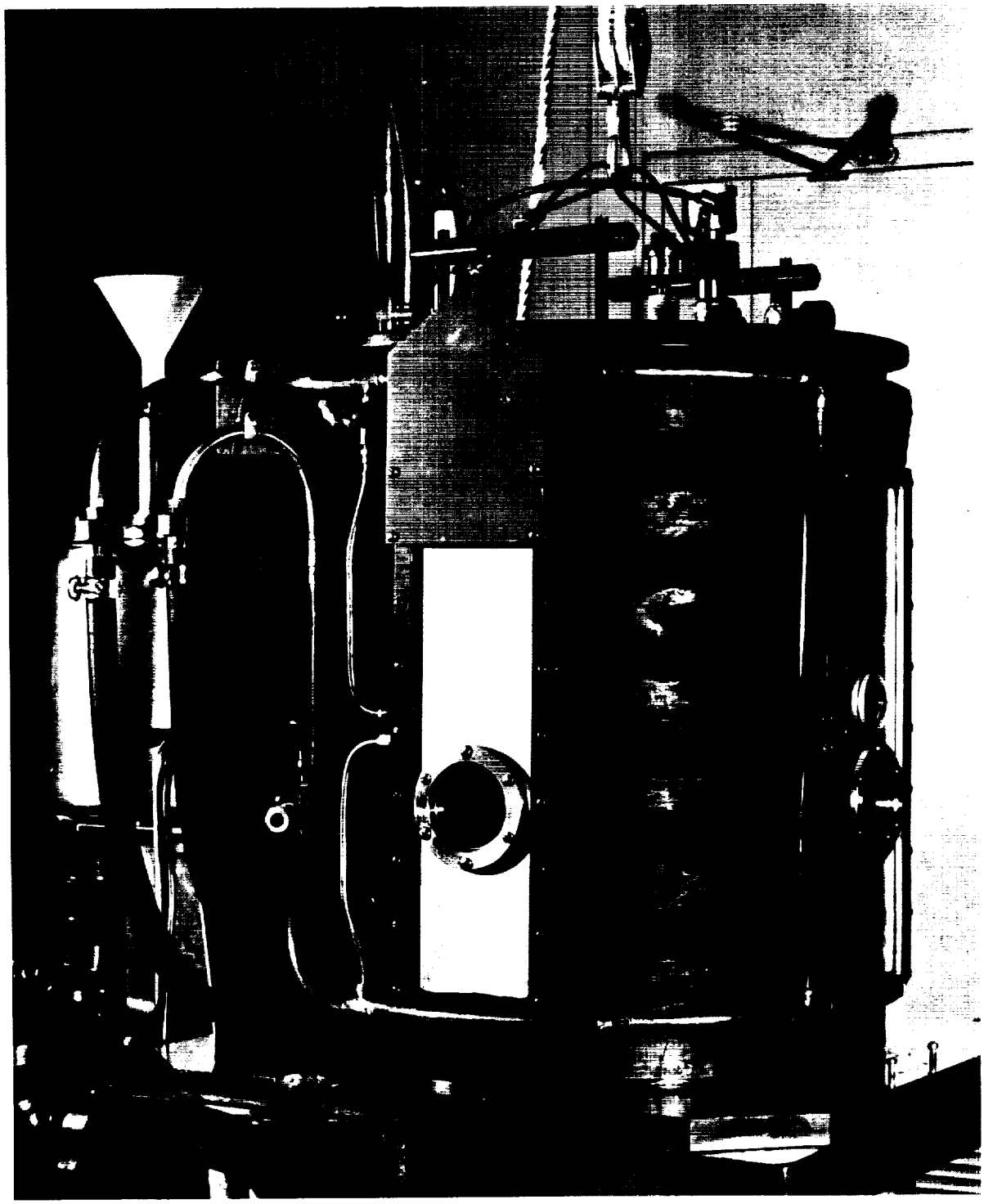

FIGURE 31.2. Water-cooled vacuum chamber enclosing ribbon mount assembly.

massless junction and is generally preferable to welding; however, when the sample has high ductility (platinum, gold, etc.) and the melting points of the sample and attached wires do not differ widely, welding is more satisfactory.

Thermocouples presently being used are Chromel-Alumel, platinum-platinum, 10% rhodium, and tungsten-tungsten, 26% rhenium. In the case of the tungsten wires, welding has been unsuccessful due to the room temperature brittleness of the metal. The tungsten ribbons tested have had 0.005-in. holes drilled successfully by the "Elox" process permitting the tungsten and tungsten, 26% rhenium wires to be easily swaged to a firm fit. The electrical circuit of the thermocouple is completed through the ribbon itself with the wires attached about 0.6-in. apart on a line perpendicular to the a-c heating current flow in order to minimize a-c pickup in the external measuring circuit.

This apparatus is enclosed in a water cooled chamber and maintained at a pressure of about 10^{-6} torr. A liquid nitrogen cooled baffle system is installed between the oil diffusion pump and the chamber to aid in maintaining a good vacuum. Many precautions have been taken to insure a minimum of outgassing as system components become warm due to absorption from the hot ribbon. All internal wiring is either bare or ceramic coated and will withstand red heat without noticeable effect. Water hoses are Viton A (low outgassing) and other components are either metallic or ceramic.

The external electronics consists of a precision potentiometer for temperature determination, a d-c microvoltmeter, and a digital d-c voltmeter to amplify and display the thermopile output (overall accuracy, ±1%). An a-c to d-c converter is used in conjunction with the digital voltmeter to measure the voltage per unit length in the uniform temperature region of the ribbon (measurement accuracy: ±0.25%). The current is determined from the voltage received across a precision shunt as measured with a-c to d-c converter (overall accuracy ±0.5%). The power source is a 10-kw voltage regulated variable a-c power supply. A micro-optical pyrometer is used for brightness temperature measurements. A precision gearing system with dial resolution of 0.1 deg is used to impart angular motion to the ribbon. By using a simple potentiometer circuit, the angular information may be displayed on the digital voltmeter. A digital printer connected to the digital voltmeter for convenience becomes a necessity when physical properties change rapidly with time.

CALIBRATION AND PROCEDURE

The thermopile was calibrated in its normal mode of operation by sensing the power radiated normally by a platinum strip blackened with electrolytically deposited platinum from a chloroplatinic acid solution. The total power radiated per unit area of surface was determined by the voltage gradient and the current through the ribbon. The principal function of the black coating was to produce a diffuse radiating surface whose radiant intensity was proportional to the cosine of the angle of emission with respect to the normal. Under these conditions, the power radiated per unit solid angle normal to the surface is simply equal to the electrical power dissipated divided by π. The angular distribution of the radiation was measured whence the cosine law was followed very closely (fig. 31–3). This demonstrated the reliability of the angular measurement system and the freedom from wall reflections, as well as verifying the assumption of a radiating surface which obeyed Lambert's cosine law. At 973° K, the true temperature as determined with a thermocouple was within 1.0% of the brightness temperature measured by the disappearing filament optical pyrometer. Also, the power temperature obtained by equating the electrical power dissipation and the Stefan-Boltzmann radiation law was within 1% of that indicated by the thermocouple over the range of temperature from 700° K to 1100° K. This was a verification of the blackness of platinum black in this temperature interval. Below 700° K, deviations are probably due to the semi-transparence of the black at long wave lengths. The linearity of the thermopile was checked by plotting the electrical power dissipation versus thermopile output voltage as shown in figure 31–4 up to the maximum temperature at which the black coating was stable. This breakdown occurred just above 1100° K. The total radiant power of a blackened strip at 1100° K is approximately equal to that from a polished platinum strip at 1600° K. The linearity of the thermopile over

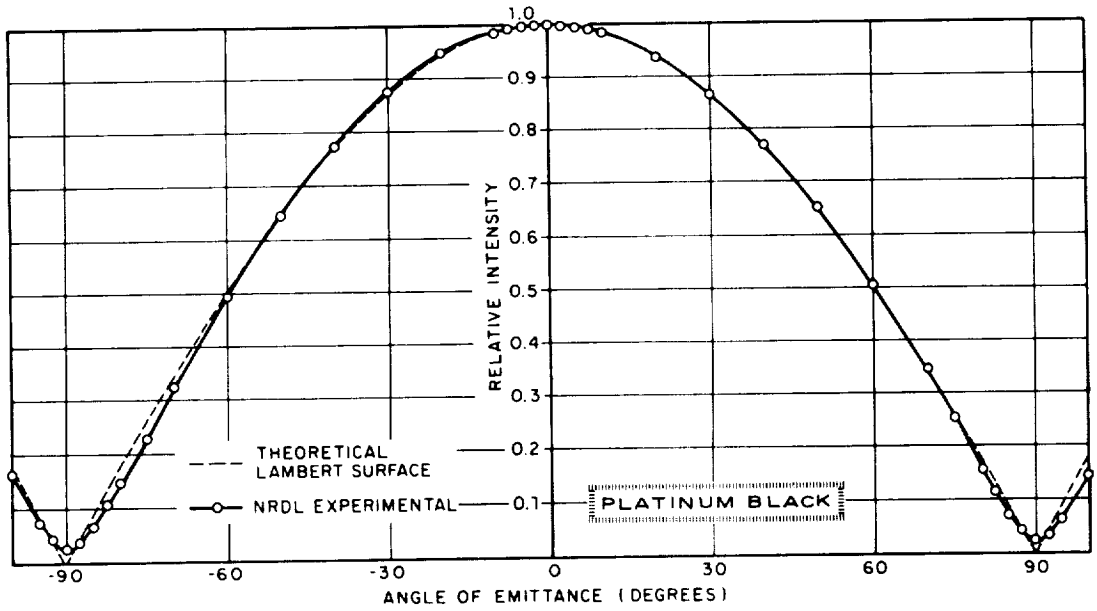

FIGURE 31–3. Flux density relative to normal flux density of a platinum-black surface versus angle of view.

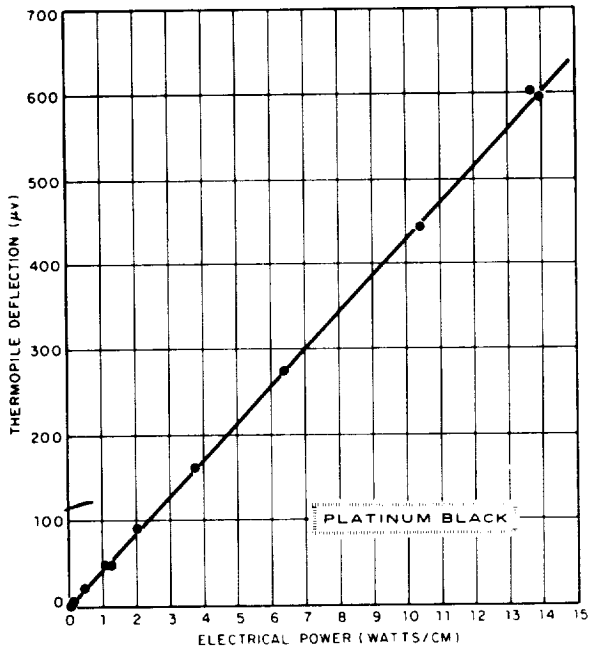

FIGURE 31–4. Thermopile deflection (μv) versus electrical power (watts/cm) in a platinum blackened ribbon.

a wide ribbon temperature interval demonstrated the satisfaction of the requirement for a receiver having a flat spectral absorptivity characteristic.

The disappearing-filament optical pyrometer was capable of measuring the brightness temperature of a spot as small as 0.001 in. in linear dimensions and could detect differences in temperature in the order of 1 or 2 deg. The pyrometer was calibrated against a secondary standard blackbody furnace (emissivity of 0.99) at 1273° K and its linearity was checked by observing a tungsten ribbon filament at a higher temperature on two different pyrometer scales. The estimated accuracy of brightness temperature measurements is better than ±1%. The optical pyrometer has been used to give a more accurate indication of true temperature by observing the difference in temperature between the point of thermocouple contact and its surroundings. Assuming that the spectral emittance of the ribbon is constant over very small temperature changes, this difference may be added to that measured by the thermocouple and has amounted to about 5° C to 10° C depending on the sample involved and the temperature.

For polishing, samples are attached circumferentially on a rotatable drum that can be lowered to the surface of a rotating lap. The axis of the drum and lap intersect at right angles. In this way the lap, which rotates at high speed, contacts the ribbon over a small area; the whole ribbon being polished by rotating the drum slowly. The resulting polish,

using fine aluminum oxide powder, is very specular.

In order to determine the electrical resistivity of the sample as a function of temperature, it is necessary to know the cross sectional area to a reasonable accuracy. There are three ways of determining this area. First, knowing the length and width of the ribbon plus the density, the area may be computed from its measured weight. Second, the area may be computed from direct measurement of its width and thickness. Third, if the electrical resistivity at room temperature is known, the average cross-sectional area between two points on the ribbon may be determined from a measurement of the resistance between these points. In the first case, published values of the density are not adequate for the present purpose since this property is apt to vary significantly depending on the manufacturing technique. With refractory metals (our main emphasis), where powder metallurgy or arc casting are prevalent, the problem is more serious than with platinum, gold, etc. As an example, the density of tungsten varies from 16.5 to 19.3 grams/cc as one goes from the sintered (up to 3000° C) through the swaged to the drawn state. Although the width and length may be measured with fair accuracy, the thickness measurement has not proved to be satisfactory due to slight variations along the ribbon. A micrometer has been found to give thicknesses about 5 to 10% higher than the average cross-sectional area determined by the assumed value of electrical resistivity. The resistivity at room temperature is sensitive to density as well as purity. However, the percentage variation in published values of room temperature resistivity appears to be generally less than the variations in density. In addition, the resistance measured at room temperature is between the voltage probes therefore taking into account dimensional variations resulting in an effective electrical cross sectional area. The latter method has been used up to the present time. Consequently, while the variation of resistance with temperature is completely measurable, the magnitude of the resistivity at any temperature depends on data from other investigations. While emittance properties are of principal concern, a precise determination of the density of the actual specimen being tested should be accomplished in order that a more accurate measure of resistivity could be made simultaneously with emittance.

The total hemispherical emittance is determined from equation (5) and the total normal emittance from equation (6). The total normal emittance also may be determined with equations (5) and (9). The spectral emittance at 0.65 μ is determined from accurate measurements of the true temperature and the brightness temperature in conjunction with equation (10).

RESULTS

To typify the type of information available with this system, some data on platinum are included. Figures 31–5 and 31–6 are graphs of the angular distribution of flux from a platinum ribbon at two different temperatures, plotted against the angle of view (from the normal) and the cosine of the angle of view. In these figures, the cosine of the angle of view equals the relative flux from a Lambert surface. The departure from a Lambert surface of a polished metal can be readily seen. In figure 31–6, the ratio of total hemispherical emittance to total normal emittance can be visualized easily as the area under the experimentally observed curve. The area defined by the straight line segments is equal to unity. Although it is necessary to measure only the distribution in the interval $0 \leq \theta \leq 90°$ to find the ratio, it was found advantageous to use the interval $-90 \leq \theta \leq 90°$ so that the effect of any angular misalignment would be averaged and there would be a check on possible spurious reflections. This ratio is shown as a function of total normal emittance in figure 31–7. The dashed curve is the theoretical ratio obtained from equations (1) and (2). The experimental values of the total hemispherical and total normal emittance are shown in figure 31–8 along with the theoretical curves based on equations (1) and (2). The total normal emittance was obtained by the thermopile deflections and equation (6) and also by dividing the total hemispherical emittance by the ratio obtained from the angular distributions.

Spectral emittance data as determined with the optical pyrometer and thermocouple ac-

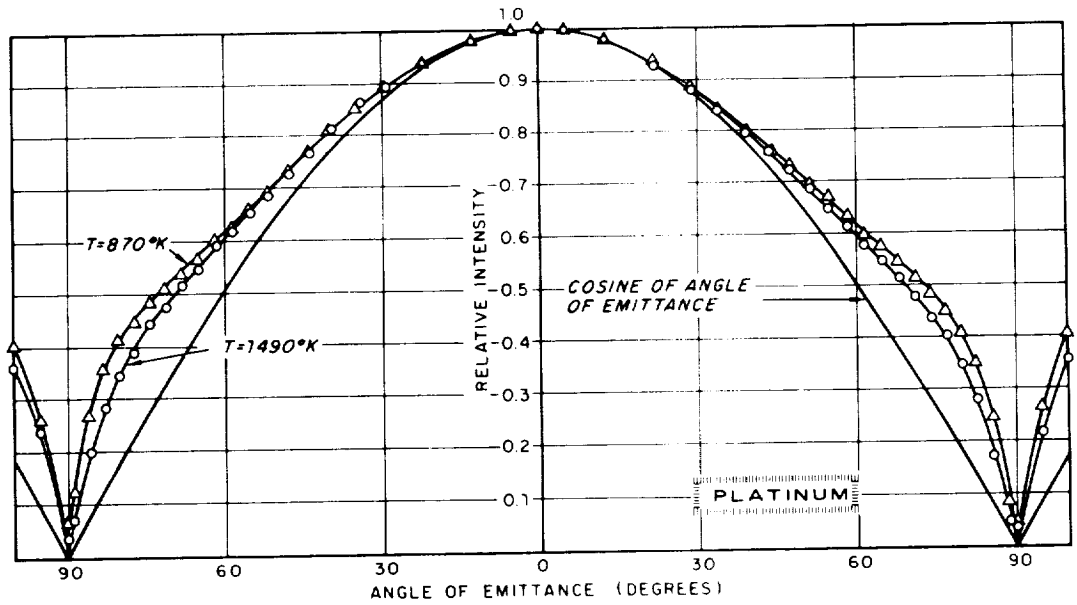

FIGURE 31-5. Flux density relative to normal flux density versus angle of view.

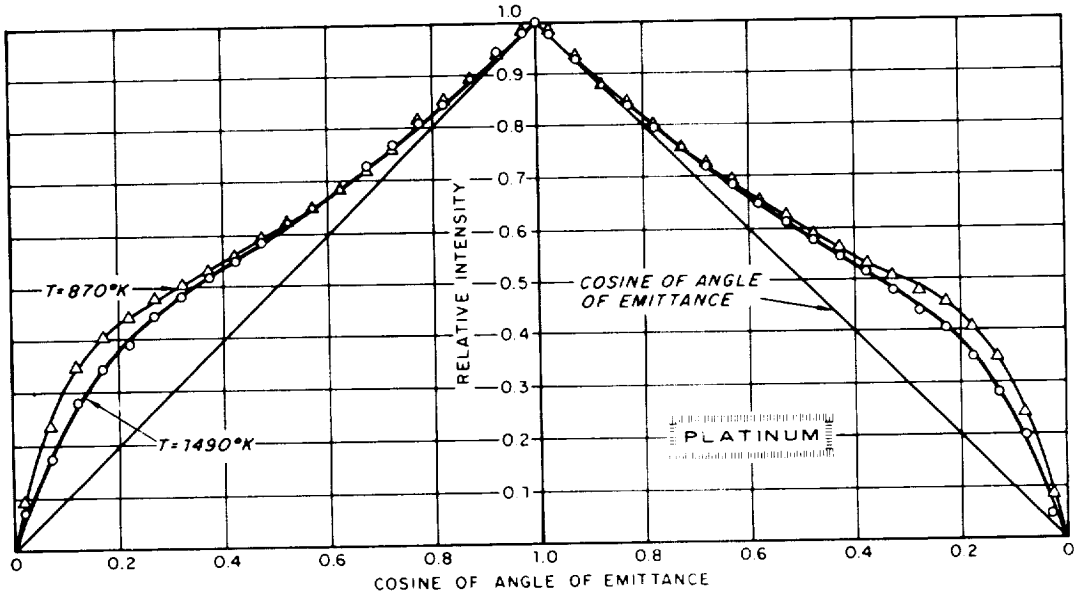

FIGURE 31-6. Flux density relative to normal flux density versus cosine of angle of view.

cording to equation (10) are shown in figure 31-9. The specimen had some surface peculiarities giving rise to the spread seen at the higher temperatures.

These data on platinum were taken on a prototype apparatus which was identical in principle and technique, however slightly different in form. The details of that instrumentation may be found elsewhere (ref. 6). Studies have also been made on molybdenum (ref. 8) and are currently in progress on tantalum, tungsten, niobium, and chromium.

CONCLUSIONS

Instrumentation has been designed, fabricated, and tested for the measurements, over a wide temperature range, of the total hemispherical emittance, total normal emittance, angular

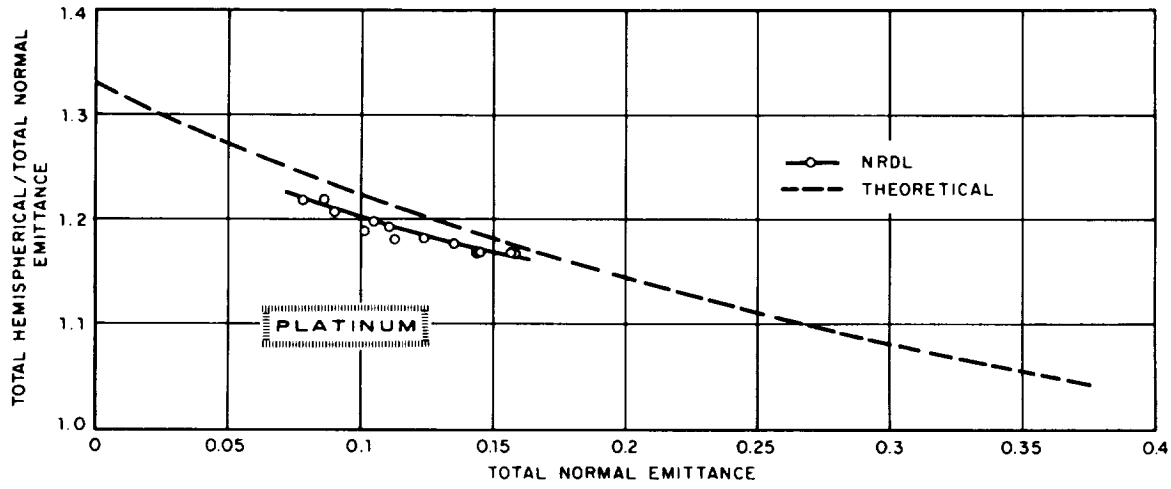

FIGURE 31-7.- Effect of total normal emittance on ratio of total hemispherical to total normal emittance.

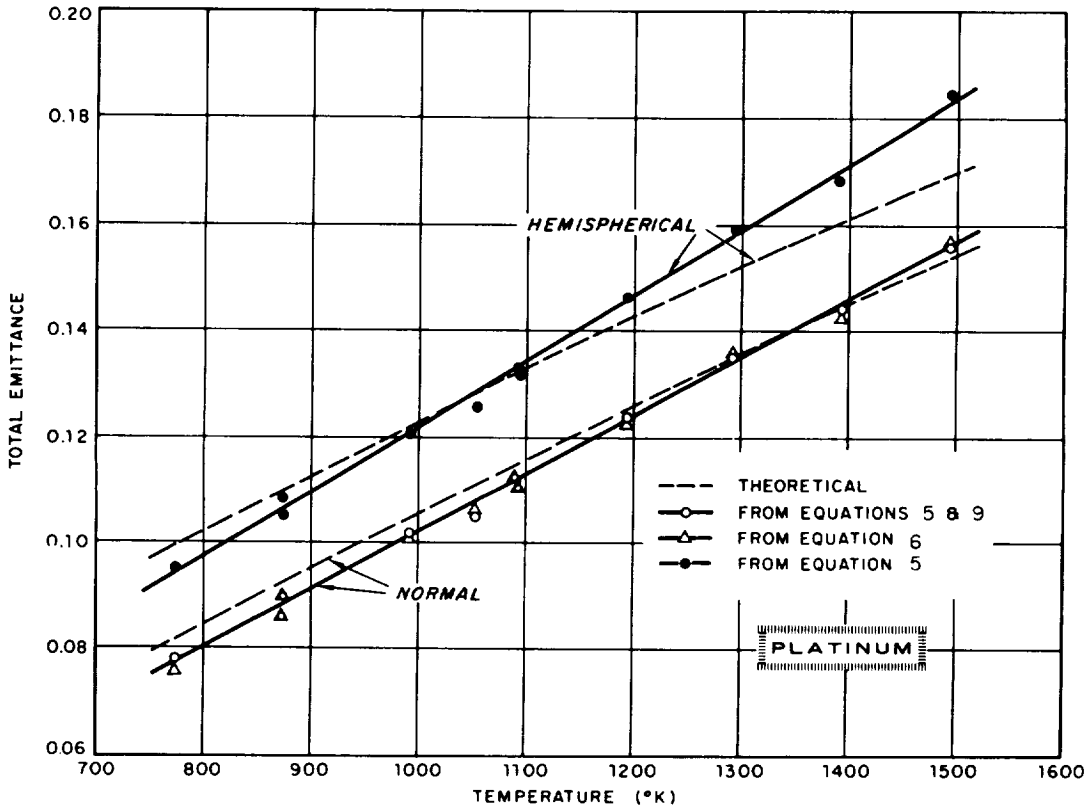

FIGURE 31-8.- Effect of temperature on total hemispherical and total normal emittance.

distribution of total flux, and the spectral emittance at 0.65 microns on a single surface of an electrically heated metallic strip. The estimated overall accuracy of the system is ±5%. The apparatus is capable of studying all metals (available in ribbon form) up to their melting points; however, present temperature determining techniques limit the accuracy above 3000° K.

Plans are currently underway to make spectral measurements from 0.4 microns to 25 microns as a function of angle, temperature,

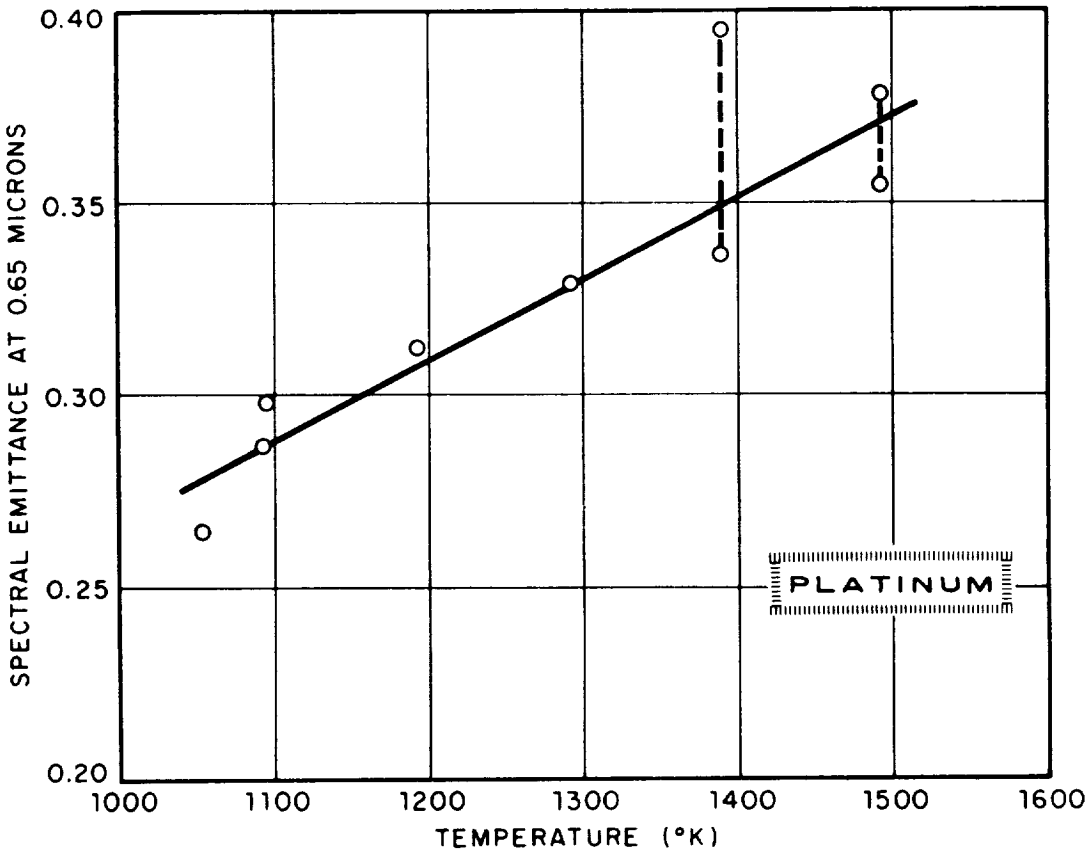

FIGURE 31-9. Effect of absolute temperature on spectral emittance at 0.65 μ.

and plane of polarization. Quartz and potassium bromide optics will be used. The fact that these measurements can be made at the same time as the total emittance measurements demonstrates the versatility of this technique.

The current expanding interest in the optical properties of metals at high temperatures and under various environmental conditions increases the need for a more sophisticated and detailed study on a few materials as well as a general investigation covering a wide range of materials. Both may be readily accomplished with this apparatus.

REFERENCES

1. HARRISON, W. N.; RICHMOND, J. C.; PLYLER, E. K.; STAIR, R.; and SKRAMSTAD, H. K.: Standardization of Thermal Emittance Measurements. WADC Technical Report 59-510, Aug. 1959.
2. ASCHKINASS, E.: Ann. Phys. Lpz., vol. 17, 1905, p. 960.
3. FOOTE, P. D.: Bull. Nat. Bur. Standards, vol. 11, 1914/1915, p. 607.
4. FORSYTHE, W. E.: Smithsonian Physical Tables. 9th ed, Smithsonian Institute, 1954.
5. DAVISSON, C.; and WEEKS, J. R.: Jour. Optical Soc. America, vol. 8, 1924, p. 581.
6. ABBOTT, G. L.; ALVARES, N. J.; and PARKER, W. J.: Total Normal and Total Hemispherical Emittance of Polished Metals. Pt. I, USNRDL, WADD-TR-61-94, 1961.
7. VAN BUEREN, H. G.: Imperfections in Crystals. North-Holland Pub. Co., Amsterdam, 1960, p. 454.
8. ABBOTT, G. L.; ALVARES, N. J.; and PARKER, W. J.: Total Normal and Total Hemispherical Emittance of Polished Metals. Pt. II, USNRDL, WADD TR-61 94, Feb. 1962.

DISCUSSION

J. Richmond, NBS: This paper is now open for discussion, and I would like to start out by asking how you got values at angles up to practically 90°. These are the first data I have seen obtained at such a very narrow grazing angle. Do you have a very wide specimen to get such data?

Abbott: In reality, the width of the ribbon is less than the field of view of the thermopile. Hence, the radiating area seen by the thermopile varies as the cosine of the angle from the normal. A specimen with a Lambert surface would then have a true cosine radiation dependence. The radiation from the 0.005-in. edge at grazing incidence becomes a serious factor only within the last couple of degrees. Edge radiation has virtually no effect on the integration of the angular distribution.

V. J. DeSantis, Space Science Laboratories, General Electric Co.: What quantity of radiation do you think is contributed by losses due to conduction, convection, and changes in area due to thermal expansion?

Abbott: The conduction term in the heat balance equation actually goes to zero since the uniform portion of the ribbon in the middle is being used. In other words, the heat generated is lost only by radiation in the uniform temperature region. That is why a long ribbon is needed. With respect to conduction down the wires, this is small at high temperature due to the rather large amount of power being generated and the small diameter of the wires. There is a slight temperature depression at the point of contact of the thermocouple wires. This is accounted for by observing the area adjacent to the thermocouple contact with an optical pyrometer and then observing the general area of the specimen. If it can be assumed that the spectral emittance is constant over a small temperature difference in the order of 10° C, this observed temperature difference can be added to the thermocouple measurement. We are running at pressures of about 10^{-5} to 10^{-6} torr which are adequate according to studies we made in our laboratory using calorimetric techniques where we varied the pressure and measured the emittance of a blackened sample. The emittance was observed to be constant below a pressure of 10^{-4} torr at a temperature of 74° C indicating that convection losses were insignificant in this pressure range, particularly at higher temperatures since the radiant heat transfer is a function of T^4 compared to some lower power of T for convective or free molecular conduction. The linear expansion due to temperature was not considered in these results.

Dwight Moore, NBS: I believe you have mentioned that the accuracy of the measurement was about 5%. Did that apply to both the normal measurement and the hemispherical measurement? Would the accuracy of the ratio of the two be of about that same magnitude? Also, how did you arrive at that 5%?

Abbott: A 1% error in temperature is approximately a 4% error in emittance, based on T^4. Therefore, 1% error is as low as possible for temperature measurement. The actual angular distribution, itself, I would consider the most accurate. We haven't made any error analysis, but the ratio measurement, being a relative technique not depending really on any absolute number, is probably quite accurate, and we have been able to reproduce it to within about 1%.

In measuring normal emittance, the calibration of the thermopile is probably the least accurate factor, due to thermopile cold junction temperature change. These measurements were made on a system that did not have that blackened background that I showed you. Since then we have made other measurements with a cooled thermopile, but there was some heating of the back wall of the bell jar which at that time did cause some error in the calibration of the thermopile. In other words, these things were thrown in with this 5% that we feel could be lower, but not much.

Moore: Did you have any reflection error from the walls?

Abbott: We did at first, so we had to move the bell jar until the ribbon or supports were not at a conjugate focus. The inside of the bell jar was blackened with black paint. The diameter of the bell jar was 18 in. which is large compared to the sample size, and this minimized the reflection problem. One way to check for these reflections is to plot the angular distribution. There were irregularities on the curve which were eliminated by painting and reorientation of the bell jar.

C. H. Leigh, AVCO Corporation: The deviation from the cosine law seems to be somewhat temperature dependent. Could this be explained by surface changes?

Abbott: It is also explained theoretically. The ratio of equation (2) to equation (1) shows this temperature dependence. The temperature dependence of emittance, either hemispherical or normal, is related to temperature and resistivity as in equations (1) and (2). Surface effects could cause a slight change in the ratio with time at high temperature but they would not be responsible for greater deviation in the cosine law at lower temperature.

Leigh: Were calculations of resistivity and temperature coefficient of resistivity from your measurements?

Abbott: Yes. This was difficult because the thickness of the sample must be known accurately to make accurate measurements of the resistivity. Fortunately, for the emittance measurements, the perimeter is the only thing that is needed, and this can be measured easily. But the thicknesses have been quite a problem. There are several ways of getting at this. Measurements of resistivity as a function of temperature were made, and the errors are large. We have done some recent work on thickness measuring, and we will be able to nail that down a little bit better, we hope.

Richmond: Could it be done by weighing the specimen and using the average weight per unit length?

Abbott: Well, what we have undertaken is density measurements essentially and/or weighing it in and out of water. Unfortunately, the density of, say, tungsten is any where from 16 to 19 specific gravity and the weight of the sample itself is in the order of 7 or 8 grams. The precision of our equipment is such that we haven't been able to get reproducible results measuring density. We do not know why. It just doesn't seem to work out.

W. CLAYTON, Boeing Company: Is it true that your thermopile calibration was based on a platinum black? That is what I understood.

ABBOTT: That is correct.

CLAYTON: Then possibly all your results should be biased on the high side because of temperature measurement and calibration errors. In the first place, an optical reading is compared to a thermocouple reading. A thermocouple attached to the surface will always read low, giving a high value for emittance. I doubt if 10° correction is sufficient. I don't believe that sighting an optical next to the thermocouple and then away from it will pick up the real error in an attached thermocouple. Secondly, you based your decision that platinum was a black reference on a total hemispherical measurement which also has the same error in it. So the error has not been canceled. Your overall accuracy is probably closer to 5 10% with all the answers being biased high because temperature will be low.

ABBOTT: If the platinum black surface were not black, the total hemispherical emittance, as determined with the power balance technique, and the optical pyrometer temperature would not be equal to 1, which it was. If the coincidence occurred whereby the surface was not black and the optical pyrometer error and the thermocouple error were both such as to give a resultant calculated emittance of 1, I would agree with you. However, the pryometer and thermocouple have been independently calibrated. Also, the blackness of platinum black has been verified in independent calorimetric measurements. I should re-emphasize that each thermocouple wire is attached separately to the ribbon, so that the junction is really two junctions in series. The decrease in temperature is readily observed with the optical pyrometer as one approaches the point of contact of the individual wires. Theoretically, one would not expect a sudden increase or decrease in temperature within the last 0.001 in. which can be resolved with the pyrometer. In effect then, we are measuring the temperature of a surface.

32—A SIMPLE TECHNIQUE FOR DETERMINING TOTAL HEMISPHERICAL EMITTANCE BY COMPARING TEMPERATURE DROPS ALONG COATED FINS

BY W. H. ASKWYTH, R. CURRY, AND W. R. LUNDBERG

PRATT & WHITNEY AIRCRAFT DIVISION, UNITED AIRCRAFT CORPORATION, EAST HARTFORD, CONNECTICUT

A simple technique for determining total hemispherical emittance in vacuum is described. The method is based on the principle that if fins which are identical in every respect except emittance are heated at one end to the same temperature, and in the same environment, the temperature drop along the length of the fin is a function of the emittance only. It presents the advantage of extreme simplicity and low cost, making emittance measurement of large numbers of samples quick and inexpensive.

Emittance determinations are based on a comparative technique rather than on an analytical calculation. Several identical fins with coatings of known emittance are heated, at one end, to a given root temperature and the root-to-tip temperature difference, ΔT, is measured for each fin. A correlation of ΔT as a function of emittance may then be obtained for that root temperature. Coatings with unknown emittance may be applied to similar fins, and the ΔT across these fins may be interpreted from the correlation as corresponding to a particular emittance.

For a particular temperature level of interest, a fin can be chosen to give a ΔT which is large enough to measure accurately, yet small enough that it can be assumed that emittance does not vary significantly over the temperature span.

Several aluminum fins had been coated with various coatings of known emittance and heated to approximately the same root temperature. A comparison of the ΔT for each fin to its value of emittance indicated that a good experimental correlation can be obtained even though no effort was made to control the significant parameters carefully. Good agreement is obtained by comparing the correlation to analytical determinations of emittance.

An analysis of the fin parameters needed for particular temperature ranges indicates that this method is practical for temperatures as low as $-100°$ F and at least as high as 1350° F.

Of the many methods used to determine, with reasonably good accuracy, the total hemispherical emittance of materials in vacuum, few, if any, exist which permit rapid emittance testing of coating materials. During the progress of an emittance measuring program at Pratt & Whitney Aircraft (ref. 1), it became increasingly apparent that it would be desirable to develop new methods for rapid testing of a large number of samples. As new coating materials with high emittance were found, it was observed that, in most cases, it would be wise to investigate several variables in the coating composition or procedure which could have a significant effect on emittance.

Therefore, an apparatus was conceived which could be designed and built in a short time, which would be relatively inexpensive except for the cost of the vacuum equipment, and which would permit rapid screening, including set-up time, of large numbers of samples. Test samples to be used with this apparatus can be easily prepared for coating (such as by sandblasting) and when coated, are sufficiently rugged to eliminate the necessity for extreme care in handling, and can be readily instrumented and installed. No elaborate, and, therefore, expensive, electrical or optical systems are necessary, and data taking is simplified to

the degree that highly skilled test-stand personnel are not required.

The method described in this paper for rapid emittance testing is based on the principle that if radiating fins which are identical in every respect except emittance are heated at one end to the same temperature and in the same environment, the root-to-tip temperature differences of the fins (when compared to each other) will depend only on the emittances of the fins.

NOMENCLATURE

Symbols

A	cross-sectional area of fin perpendicular to conducted heat flow	ft^2
$I_a(\Phi)$	$=1/[\Phi(1-\tau_s{}^4)+2\Phi^2]^{1/2}$, integrand of approximate solution of equation (7)	
$I_e(\Phi)$	$=1/[\Phi(1-\tau_s{}^4)+2\Phi^2+2\Phi^3+\Phi^4+\Phi^5/5]^{1/2}$, integrand of exact solution of equation (6)	
k	thermal conductivity of fin material	$B/hr\text{-}ft\text{-}^\circ R$
L	tip to root (total) fin length	ft
L_a	approximate solution for L based on equation (7)	ft
L_e	exact solution for L based on equation (6)	ft
m	$=dT/dx$	$^\circ R/ft$
P	radiating portion of fin perimeter around a section perpendicular to the direction of conducted heat flow	ft
T	$=T(x)$, temperature of fin at distance x from the tip	$^\circ R$
ΔT	$=T_r-T_t$	$^\circ R$
T_r	$=T(L)$, temperature of fin root (at distance L from the tip)	$^\circ R$
T_s	effective temperature of surroundings to which fin is radiating	$^\circ R$
T_t	$=T(0)$, temperature of fin at tip (i.e., at $x=0$)	$^\circ R$
t	half thickness of rectangular fin radiating from both sides	ft
w	width of rectangular fin	ft
x	distance measured from fin tip toward the root	ft
β_a	$=\Lambda_a{}^2=\epsilon\sigma pL_a{}^2T_t{}^3/kA$	
β_e	$=\Lambda_a{}^2=\epsilon\sigma pL_e{}^2T_t{}^3/kA$	
ϵ	total hemispherical emittance of fin surface	
ζ	$=\Phi/(1-\tau_s{}^4)$, temperature parameter	
λ	$=(\epsilon\sigma px^2T_t{}^3/kA)^{1/2}$ fin length parameter	
or	$(\epsilon\sigma x^2T_t{}^3/kt)^{1/2}$ rectangular-fin length parameter	
Λ_a	$=(\epsilon\sigma pL_a{}^2T_t{}^3/kA)^{1/2}$	
Λ_e	$(\epsilon\sigma pL_e{}^2T_t{}^3/kA)^{1/2}$	
σ	0.173×10^{-8} (Stefan-Boltzmann constant)	$Btu/hr\text{-}ft^2\text{-}^\circ R^4$
τ	$=\tau(x)=T(x)/T_t$	
τ_r	$=\tau(L)=T(L)/T_t$	
τ_s	$=T_s/T_t$	
Φ	$=\Phi(x)=(T(x)-T_t)/T_t$	
Φ_r	$=\Phi(L)=(T_r-T_t)/T_t$	

Subscripts

a	approximate value per equation (7)
e	exact value per equation (6)
r	of the fin root
s	of the surrounding environment
t	of the fin tip

DISCUSSION OF METHOD

Analyses of radiating fins (ref. 1, 2, and 3) show that the temperature drop along a radiating fin is a function of a generalized length parameter,

$$(\epsilon\sigma pL^2T_r{}^3)/k_A \text{ or } (\epsilon\sigma L^2T_r{}^3)/k_t$$

root temperature and of sink temperature. Thus, if the thermal conductivity, sink temperature, and geometry of a fin are known, and the fin is heated to a given root temperature, this generalized parameter reduces to a constant times emittance, and the temperature drop along the fin becomes a function of emittance only. Brandt, Irvine, and Eckert (ref. 2) used this principle to determine the emittance of a pure iron wire.

The method discussed herein does not involve an analytical determination of emittance. Instead, it compares the temperature drop along a coated fin of unknown emittance to that of fins with coatings of known emittance. If several fins, of the same geometry and material, are heated to the same root temperature and the emittance of each fin is known, a correlation of the root-to-tip temperature drop, ΔT, as a function of emittance, can be obtained. Figure 32–1 shows an example of such a relationship for a given set of conditions.

A fin with a coating of unknown emittance may then be heated to the same root temperature and the ΔT measured may be interpreted from figure 32–1 as corresponding to a particular value of emittance.

One disadvantage of this technique, as discussed up to this point, is that it requires

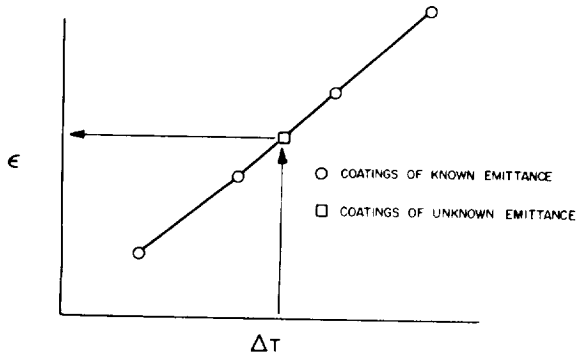

FIGURE 32–1.—Typical calibration curve.

heating each fin to exactly the same root temperature. In practice, this could become very time consuming and thus defeat the purpose of this technique. Therefore, it would be desirable to heat the fins to root temperatures which were only approximately the same. In the appendix it is shown how the fin parameters may be manipulated so that a generalized family of curves emerges in which the parameter β is a function of T_r/T_t and T_s/Tt_t as shown in figures in the appendix.

If the effect of T_r on T_s is made to be negligible, the use of these curves simplifies the data-taking process considerably. It becomes necessary to heat the various test fins to only a reasonably approximate common temperature.

The only term in the generalized parameter β which is not easily measurable and not always known precisely is the thermal conductivity, k, of the fin. However, if all test fins are made from a single sheet of stock (for example, several hundred 2-in. by 2-in. fins can be made from a 4-ft by 8-ft sheet of aluminum), conductivity, like the geometric variables, is constant for all tests.

An indication of the merit of the method under discussion for the measurement of total emittance was obtained at Pratt & Whitney Aircraft while conducting a program concerned with subject matter other than that treated herein. In that program, several 4-in. by 4-in. by 0.040-in. fins of coated aluminum material were heated repeatedly at their roots, the prime objective being to obtain an indication of the quality of the bond between the coating and the substrate when subjected to thermal cycling. Thermocouples were located at the root, in the mid-region, and close to the

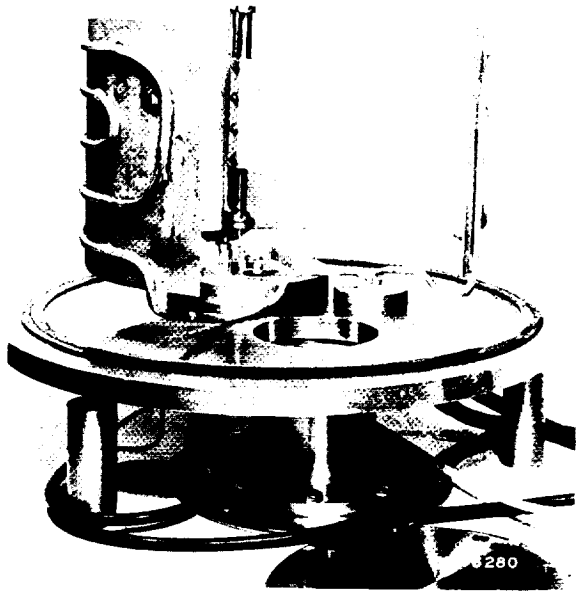

FIGURE 32–2.—Aluminum fin thermal cycling rig.

tip of each fin. In the test setup, the instrumented fin and heating unit were installed in a glass bell jar, with a water-cooled radiation shield placed around the fin in order to prevent overheating of the bell jar. The setup is shown in figure 32–2. The only parameters which were essentially constant for all tests were fin root temperature and the product of thermal conductivity and fin thickness, k_t.

Several nonrepeatable test conditions prevailed which could well affect the relation of the observed test data to true total emittance. A brief discussion of each follows.

The portions of the heater protruding from the heater block were clean and shiny in the early tests but became increasingly oxidized as the test program progressed. A considerable amount of heat was radiated from these portions of the heater since they could be seen to glow moderately. Thus, the heat input to the top and bottom edges of the fins was not consistent from test to test.

The sink temperature was not the same for each test. It is difficult to determine the relative contributions to the effective sink temperature of the water-cooled shield, the glass bell-jar, and the protruding portions of the heater. However, observation of the apparatus (as may be seen in fig. 32–2) would indi-

cate that the water-cooled radiation shield contributes significantly, and perhaps makes the major contribution, to the sink temperature. Water temperature in the shield varied by 30° to 40° F for tests performed in winter from those in summer.

The locations of thermocouples on the fins varied slightly from one fin to another. The thermocouples were placed as follows: one approximately ⅛-in. from the tip and referred to herein as the "tip" thermocouple, a second ¾ in. from the first, and a third midway between these two. No attempt was made to measure the distances precisely. Three possible sources of error could be attributed to minor variations in thermocouple placement: slight variations in effective fin length, resulting in a probably small error; deviation of tip thermocouples from a position in which dT/dx would be equal to zero; and variation in root thermocouple location with respect to the heater block, probably the most significant of the potential sources of error.

Notwithstanding these possible non-repeatable factors, a reasonably good correlation was obtained from the test data. The latter are presented, in figure 32–3, solely for the purpose of illustrating the feasibility of the method under discussion. The solid line in figure 32–3 represents the emittance values which may be calculated using the analysis presented in the appendix. Each set of connected points represents an area of uncertainty for a particular coating. These areas pertain to uncertainty attributable to slight differences in ΔT for thick and thin coatings and to uncertainty as to the proper emittance values to assign to the coating. The latter uncertainty results from two factors: spread in existing emittance data and variation of emittance with temperature (large temperature drops were obtained in these tests).

For each fin subjected to the thermal cycling tests, approximately 15 sets of temperature data for a nominal root temperature of 750° F were taken. However, there was considerable scatter about this 750° F temperature level. Figure 32–4 shows the parameter $\epsilon\sigma L^2/k_t(\beta$, with the temperature term removed) plotted as a function of T_r for all of the points obtained during three typical tests. The fact that each set of points scatters about a horizontal line indicates that it is not necessary to have identical temperature settings for each test.

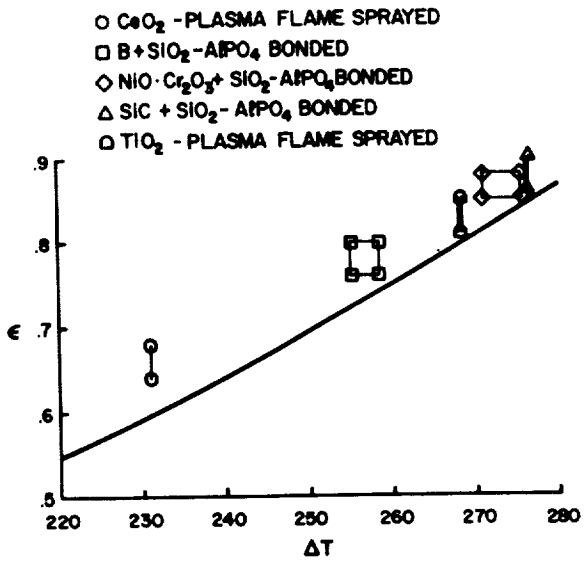

FIGURE 32–3.—Total emittance vs root-to-tip temperature drop. Values of emittance shown are those developed previously by Pratt & Whitney for each of the coatings. $T_r = 750°$ F. $T_s = 50°$ F.

DISCUSSION OF PROPOSED APPARATUS

An apparatus is currently being designed which will eliminate, or minimize, most of the disadvantages of the proposed technique. An existing vacuum system is to be used which consists of a 16-in. diameter, 20 in. high, blackened, and water-cooled metal chamber, with two windows, and a 400-liter/sec., oil-diffusion pump upon which the chamber is mounted. Ordinary refrigerants or liquid nitrogen may be used for cooling in place of water if very low sink temperatures are desired. Pressures less than 1×10^{-6} mm Hg can be reached with this system in less than one hour, with no bake-out required. A 6-in.-diameter instrumentation flange will contain the sample holder, power feed-throughs, radiation heaters, a radiation baffle to prevent heater radiation from reaching the fin portion of the sample, water-cooling for this baffle, and thermocouple feed-throughs. Figure 32–5 is a schematic of a possible sample and heater configuration.

As shown in figure 32–5, the sample is to be heated by radiation heaters. These will be completely enclosed to prevent heater radiation from reaching the chamber walls as well as the fin portion of the sample. This method of

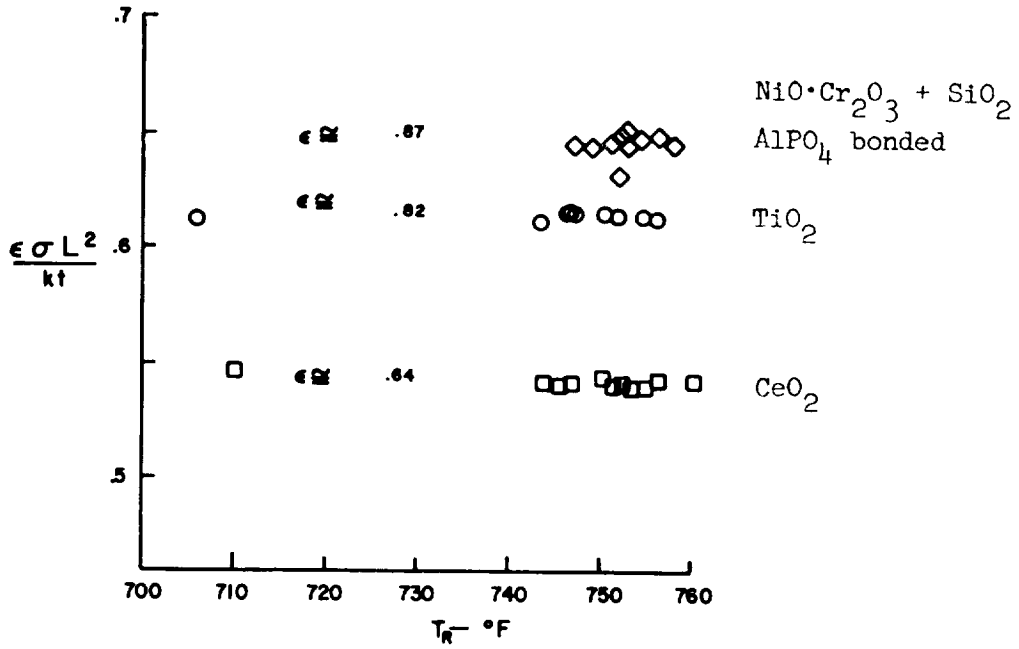

FIGURE 32-4. Emittance factor vs root temperature.

heating the samples was chosen in order to keep the mass of the system as low as possible and thus reduce equilibrium time for each power setting. The sample holder will be removable, and several of these will be made, so that "down-time" on the equipment may be reduced to a minimum by having additional instrumented samples ready for testing as soon as each test is completed. A potentiometer will be used to measure the thermocouple output.

SAMPLE SELECTION

For a temperature level of interest, a sample will be selected based on the following considerations:

(1) The root to tip ΔT must be large enough to measure to a high degree of accuracy and small enough so that emittance does not vary significantly over the length of the fin. Thus, fins would be selected to give temperature drops of the order of 50 to 100° F.

(2) The length must be long enough so that distances (length) between thermocouples may be measured accurately, or so that slight differences in the fin lengths of the samples will have negligible effect on the results.

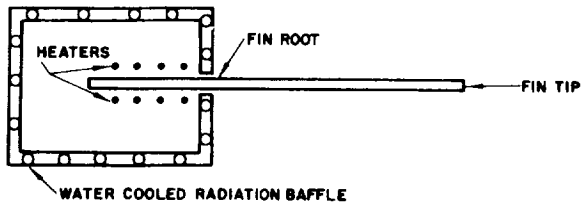

FIGURE 32-5.—Schematic drawing of test fin, heaters, and water-cooled radiation baffle, top view.

(3) The sample must be thick enough so that pre-coating preparation, by sandblasting or chemical etching, for example, may be performed in the same way as would be done on an actual radiator fin. An example of a sample of insufficient thickness would be foils a few mils in thickness. Such thin samples would be more difficult to prepare for coating than would be actual radiator fins.

Figure 32-6 shows how L and $2t$ may be varied for a particular set of temperatures. As shown in this figure, increased thickness may be compensated for by additional length.

(4) The thermal conductivity times total thickness, $2kt$, of the fin must be large relative

692-146 O—63——21

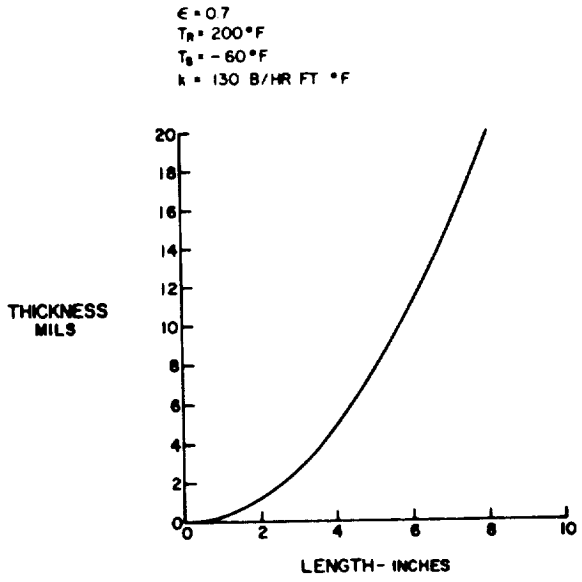

FIGURE 32-6.—Selection of fin length and thickness to give ΔT of 100° F for typical conditions.

to the $2kt$ of the coating to prevent having fins with higher "effective thicknesses" when coating materials with high conductivities are used—such as silicon carbide. This is, perhaps, one of the most significant limitations of this method since only high-conductivity fin materials, or thick fins, may be used. However, for most applications, aluminum, beryllium or copper fins will be used.

Calculations based on these considerations were used for selecting tentative samples to be tested at root temperatures of approximately −100°, +200°, 500°, 800° and 1350° F. The problem of heating a sample by radiation at a higher temperature than 1350° F has not been examined and hence the possibility exists that a modified design may be necessary for tests at higher root temperatures.

APPENDIX—CORRELATION OF ANALYTICALLY DETERMINED TEMPERATURE DISTRIBUTION FOR A RECTANGULAR FIN RADIATING TO A UNIFORM SINK

Examination of an approximate solution of the constant A, p, k, T_s, and ϵ radiating fin problem (fig. 32-7 and ref. 1 and 4) indicated that a desirable mode of presenting the exact temperature distribution solution would be to plot lines of constant τ_s on a chart of $\phi_r/(1-\tau_s^4)$ versus β_r, since ϕ_r and τ_s are computed from measured temperatures. It was possible to estimate that very little spread between the lines of constant τ_s over the range of interest $(0 \leq \tau_s < 1.0)$ would occur and that the spread would be small in the range of ϕ_r of primary interest $(0 < \phi_r < 0.4)$.

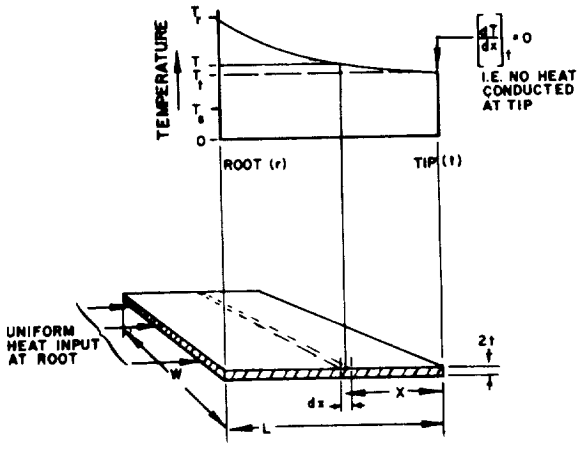

FIGURE 32-7.—Temperature distribution along rectangular fin radiating from both sides.

The temperature distribution results of reference 1 were replotted in the desired form, but were thought to be too uncertain in the desired ranges to justify not recomputing the distributions. The computation presented there was, therefore, undertaken, making use of an integration technique involving an approximate solution in order to avoid appreciable error in the graphical integration employed.

The heat balance on an element of length, dx, assuming one-dimensional heat conduction in the fin, yields the differential equation:

$$d(k_r A\,(dT/dx)) = \epsilon\sigma p(T^4 - T_s^4)dx \qquad (1)$$

(ref. 1 and 3). Letting $m = dT/dx$, $dm/dx = d^2T/dx^2$, and $m = (dT/dm)(dm/dx)$; i.e.,

$$m\,dm/dT = d^2T/dx^2. \qquad (2)$$

Eliminating d^2T/dx^2 between (1) and (2) yields:

$$m\,dm = (\epsilon\sigma p/k_r A)(T^4 - T_s^4)dT \qquad (3)$$

Integrating (3) once with the boundary condition that $m=0$ and $T=T_t$ at the fin tip, i.e., for zero conduction heat flow at the fin tip, yields:

$$dT/dx=(2\epsilon\sigma p/k_A 1)^{1/2}[(T^5-T_t^5)/5-T_s^4(T-T_t)]^{1/2} \quad (4)$$

(cf ref. 1, eq. (9)).

Letting $\phi=(T-T_t)/T_t$,

$\tau_s=T_s/T_t$

and $\lambda^2=\epsilon\sigma p x^2 T_t^3/k_A 1$ (5)

(4) may be written

$$\int_0^{\phi_r}\frac{d\Phi}{[\Phi(1-\tau_s^4)+2\Phi^2+2\Phi^3+\Phi^4+\Phi^5/5]^{1/2}}=2^{1/2}\int_0^{\Lambda_e}d\lambda=2^{1/2}\Lambda_e \quad (6)$$

where integration limits indicate $T=T_t$ at $x=0$. For the region $0<\Phi\ll 1.0$, an approximate analytic solution, Λ_a, may be obtained by neglecting the last three terms in the square bracket. Thus,

$$\int_0^{\phi_r}\frac{d\Phi}{[\Phi(1-\tau_s^4)+2\Phi^2]^{1/2}}=2^{1/2}\int_0^{\Lambda_a}d\lambda=2^{1/2}\Lambda_a \quad (7)$$

Substituting $u=\Phi^{1/2}$, the integral may be readily evaluated anlytically, whence:

$$2^{1/2}\sinh^{-1}[2\Phi_r/(1-\tau_s^4)]^{1/2}=2^{1/2}\Lambda a \quad (8)$$

Subtracting (6) from (7):

$$2^{1/2}(\Lambda_a-\Lambda_e)=\int_0^{\phi_r}(I_a(\Phi)-I_e(\Phi))d\Phi \quad (9)$$

where

$I_a(\Phi)=1/[\Phi(1-\tau_s^4)+2\Phi^2]^{1/2}$

$I_e(\Phi)=1/[\Phi(1-\tau_s^4)+2\Phi^2+2\Phi^3+\Phi^4+\Phi^5/5]^{1/2}$

$2^{1/2}\Lambda_a$ is given by (8).

For $\tau_s^4\to 1.0$, inspection of (8) shows that:

$$\Phi_r\to 0 \text{ for finite } \Lambda_a$$

and inspection of (9) shows that in this circum-

TABLE 32-1. *Analytically Determined Temperature Distribution for a Rectangular Fin Radiatin to a Uniform Sink*

τ_s	ϕ	ζ	β_e	β_a	$\frac{I_a(\phi)-I_e(\phi)}{2^{1/2}}$
0. 0	0. 05	0. 05	0. 09675	0. 09683	0. 00680
	. 10	. 10	. 18729	. 18792	. 01764
	. 20	. 20	. 35144	. 35576	. 04027
	. 40	. 40	. 62263	. 64756	. 07768
	. 60	. 60	. 83421	. 89724	. 01209
	. 80	. 80	1. 00198	1. 11695	. 11653
	1. 00	1. 00	1. 13668	1. 31377	. 12427
0. 6	0. 05	0. 05744	0. 11060	0. 11072	. 00829
	. 10	. 11488	. 21319	. 21404	. 02093
	. 20	. 22977	. 39709	. 40253	. 04634
	. 40	. 45955	. 69567	. 72566	. 08599
	. 60	. 68933	. 92475	. 99864	. 11020
	. 80	. 91911	1. 10424	1. 23659	. 12370
	1. 00	1. 14889	1. 24724	1. 44844	. 13038
0. 8	0. 05	0. 08468	0. 16845	0. 16872	. 01368
	. 10	. 16937	. 30453	. 30617	. 03276
	. 20	. 33875	. 55361	. 56340	. 06639
	. 40	. 67750	. 93728	. 98553	. 11005
	. 60	1. 01620	1. 21862	1. 32941	. 13200

stance: $(L_a - L_e)/L_a \to 0$. Thus, for $\tau_s^4 \to 1.0$, $(\lambda_a - \lambda_e)/\lambda_a \to 0$.

Since inspection of (8) shows that a plot of Λ_a (or β_a) versus $\Phi_r/(1-\tau_s^4)$ is independent of τ_s, and, since $L_e \to L_a$ as $\Phi_r(1-\tau_s) \to 0$ (for any τ_s), it appeared convenient to produce a final general plot of the temperature distribution as $\phi_r/(1-\tau_s^4)$ versus $(\epsilon\sigma p L_e^2 T_f^3)/k_s A = \beta_e$, with lines of constant τ_s. Evaluation of the right-hand side of (9) was done graphically, and the resultant temperature distribution relations are presented in figures 32–8 and –9 and in table 32 I.

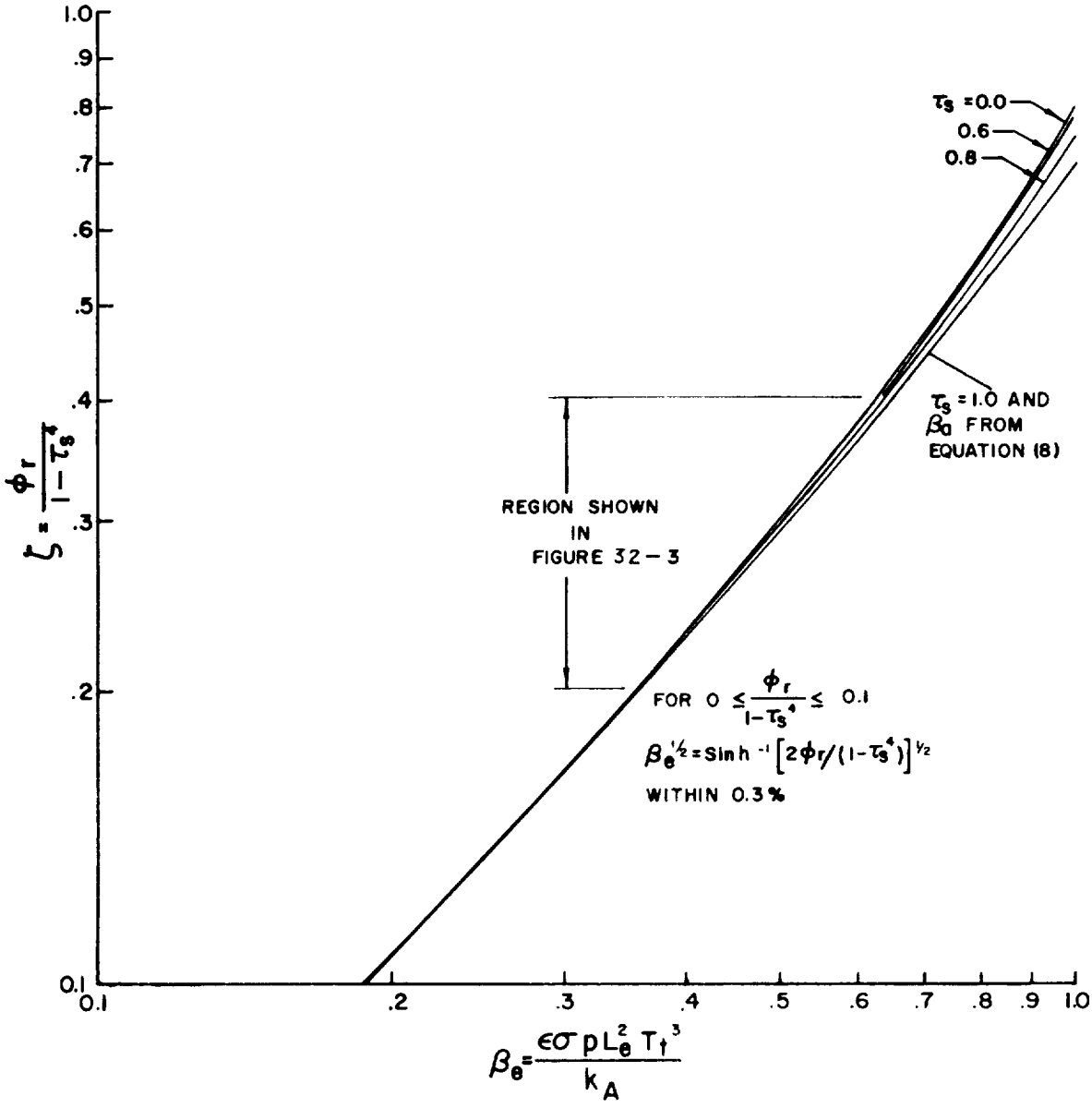

FIGURE 32–8.– Analytically determined temperature distribution for a rectangular fin radiating to a uniform sink.

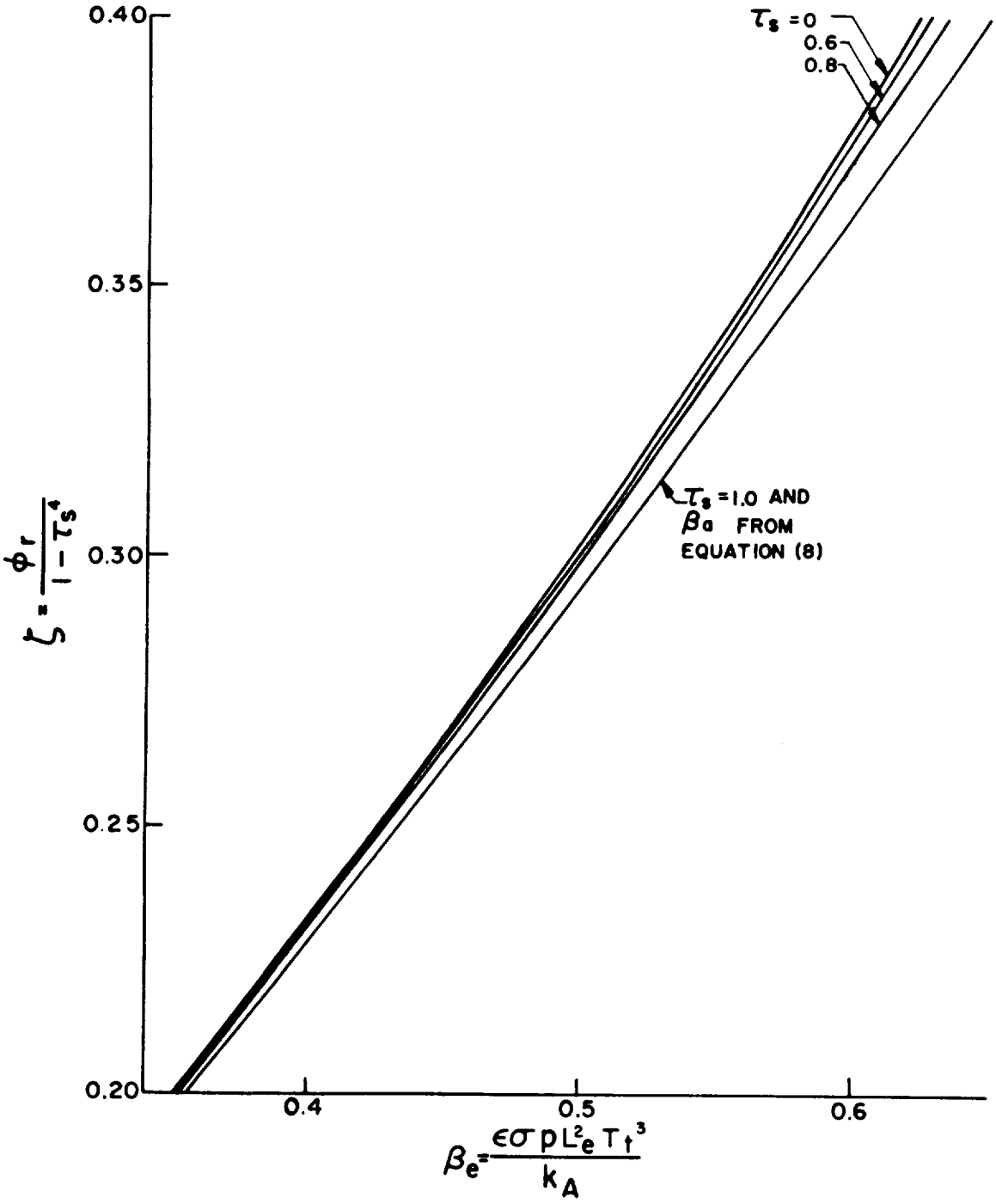

FIGURE 32 9. Analytically determined temperature distribution for a rectangular fin radiating to a uniform sink.

REFERENCES

1. Lieblein, S.: Analysis of Temperature Distribution and Radiant Heat Transfer Along a Rectangular Fin of Constant Thickness. NASA Technical Note D-196.
2. Brandt, J. A.; Irvine, T. F.; and Eckert, E. R. G.: Proceedings of the Heat Transfer and Fluid Mechanics Institute. 1960.
3. Pratt & Whitney Aircraft Co. Reports under NASA Contract NASw-104.
4. Bartas, J. G.; and Sellers, W. H.: Radiation Fin Effectiveness. ASME 59-HT-17.

DISCUSSION

William Clayton, The Boeing Co.: It appears that the method cannot be relied upon to give an accurate emittance value. Several assumptions are required. One is that, in order to make any sense out of the values, constant emittance down the fin must be assumed. It seems to be a slow technique for screening, since about a half an hour total time is required to get a point.

Materials can be screened by simply back heating and measuring total normal emittance. Since high emittance is sought, the results are not much different from total hemispherical emittance, and data can be obtained every minute with every point at a different temperature. Because of its slowness, a calorimetric technique, which is what the method described in this paper is essentially, does not offer advantages for screening. Is there some emittance variation due to temperature or due to variations in the coating and what is the estimated accuracy?

Askwyth: Where emittance is a function of temperature, it usually is not a strong function of temperature over temperature intervals such as 50° to 100° F. This does not result in too great error. Time is involved in making measurements, as I said before, but it is a good vacuum technique and a simple technique that does not require highly skilled testing personnel. Large amounts of data can be taken in this way with very little engineering supervision. The only readings that are required are two temperature readings, so there is little chance of getting bad data with this technique.

Clayton: My point is that I don't see how you can get really good data.

Askwyth: The technique involves comparing one coating with another. When several variations of a given coating are applied to several fins, the one that gives the largest root-to-tip temperature difference is going to have the highest emittance. This would be used in conjunction with another emittance rig in which more accurate data can be obtained. In other words, it is a quick screening process.

Clayton: Was the technique a vacuum technique?

Askwyth: Yes. The time necessary to take a data point is not half an hour per point, but approximately half an hour for the first point. Fifteen minutes would be needed to pump down, then half an hour for the first point, and after that the time necessary for each successive data point would depend on how far apart the temperatures were. Obviously, if a point were taken every 50°, the time needed would not be very long—probably only a few minutes. But in going from 200° F to 1000° F spacing the points several hundred degrees apart the equilibrium time for each point would be longer. Another consideration is the possibility of stacking samples so that multiple samples could be run, and so that the total test time for a group of samples would be considerably reduced. For example, suppose 1×4-in. fins and an 8-in. long heater block were used. Then 8 fins could be stacked and 8 tests conducted simultaneously. One thing that I did not mention during the talk is how we can overcome the necessity of being at the same fin root temperature in each test. The appendix describes an analytical technique which permits us to come to approximately the same root, or tip, temperature. We chose to base our analysis on the tip temperature.

E. R. Streed, Lockheed Missiles and Space Company: Is it possible to distinguish between spectral differences and differences in emittance as a function of thickness of the coating, by this method?

Askwyth: Spectral differences?

Streed: Differences in total emittance are due to the spectral difference as a function of temperature down the rod or as a function of thickness of the coating.

Askwyth: Coating thickness variation is one of the things for which this rig could be used. We could test several thicknesses of a given coating and get a correlation of emittance as a function of thickness. We would coat several fins with different thicknesses of the same material, all at the same time, and note the variation in temperature differences. As I said before, this is one of the purposes for which we had planned this rig.

Streed: One of the advantages of reflectance techniques is that the differences in spectral emittance can be seen. By coating two samples of different thicknesses, it is possible to differentiate between them.

33—A MULTICHAMBER CALORIMETER FOR HIGH-TEMPERATURE EMITTANCE STUDIES

BY A. I. FUNAI

LOCKHEED MISSILES & SPACE COMPANY, PALO ALTO, CALIFORNIA

An eight-chambered vacuum calorimetric apparatus for measuring and evaluating the total hemispherical emittance of high-temperature radiator coatings is described. The method for obtaining emittance values is presented and an error analysis identifies the important parameters. A detailed description of the sample and the sample heating and temperature measuring systems are also given. Preliminary results confirm the suitability of the apparatus for measuring emittances with an accuracy of $\pm 5\%$.

The design of high-temperature radiators for spacecraft calls for materials with suitable thermophysical and structural properties together with a high surface emittance. Certain oxide-coated metals appear to offer a good combination of properties for this purpose, but the behavior of these metal-oxide combinations at elevated temperatures (up to 2000° F) and in the high vacua of space is largely undetermined. A study sponsored by the Aeronautical System Division [1] is presently being conducted at Lockheed Missiles & Space Company to measure the emittances of certain metal-oxide combinations and to evaluate their stability over 30-day periods of time at elevated temperatures in a simulated space-vacuum environment.

For this study, a multichambered calorimeter has been designed and built to permit the simultaneous study of eight separate samples. Total hemispherical emittances, accurate to within $\pm 5\%$ can be determined. Total hemispherical emittance is inferred from an energy balance on an electrically heated sample suspended inside a vacuum chamber with low temperature, low reflectance walls. This paper describes the apparatus and the experimental method by which total hemispherical emittance is measured. The important parameters are identified and the sources of error are discussed and evaluated.

[1] Contract No. AF33(657) 7493, Task No. 73812.

EMITTANCE

Total hemispherical emittance is the quantity of primary concern for selecting radiator coatings for high-temperature service. Other chemical and physical characteristics are of interest mainly because of their influence on the emittance and the mechanical integrity of the coating. For this study, a calorimetric method was judged to be superior to other methods, such as reflectance or radiometric methods, because the test procedure is relatively simple and total hemispherical emittances are obtained directly. The only disadvantage of the method is the requirement for relatively complicated sample construction, which is discussed later.

With the calorimetric method, the sample is suspended inside a vacuum chamber with black, cooled walls (fig. 33–1) and is maintained at the desired temperature level with a measured amount of electrical power. If the vacuum is such that heat transfer by gas conduction and convection can be neglected, the energy balance on the sample at steady state can be written as:

$$P_a = EI = \epsilon_1 A_1 \sigma T_1^4 - R_{12} A_1 \sigma T_1^4 - \alpha_{12} A_1 \sigma T_2^4 + P_e + P_c \quad (1)$$

where:

P_a	total applied power
E	applied voltage to heater element
I	current through heater element
ϵ_1	total hemispherical emittance of sample at temperature T_1
A_1	surface area of sample

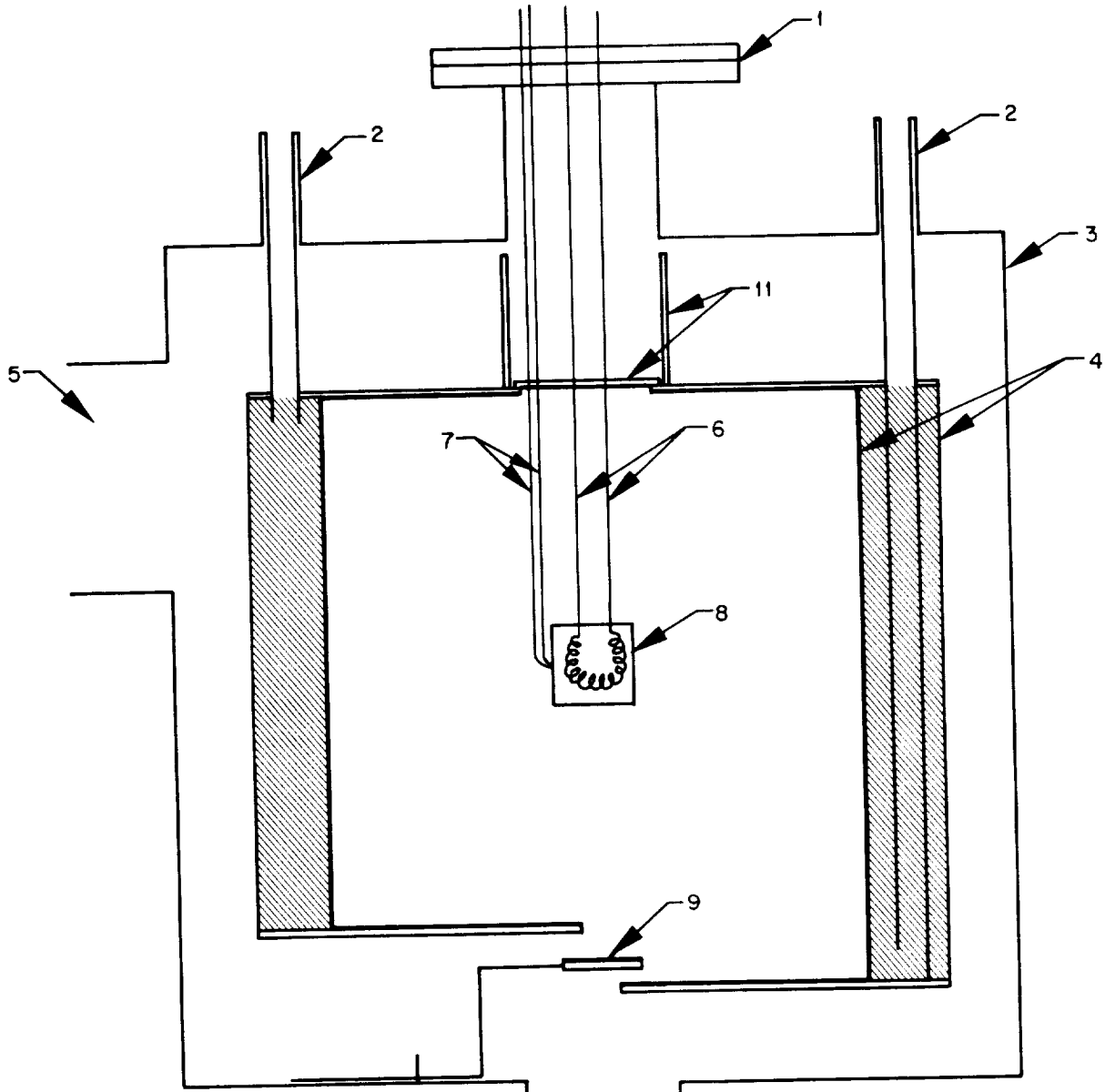

FIGURE 33-1. Total hemispherical emittance test chamber.

σ Stefan-Boltzmann constant
T_1 sample temperature
R_{12} reflection factor to account for the absorption of energy reflected back to the sample by the chamber walls
α_{12} absorption of sample for energy radiated by the chamber walls
T_2 chamber wall temperature
P_c I^2R loss in power leads
P_c conduction loss through power and thermocouple leads

The reflection factor, R_{12}, can be written as:

$$R_{12}=\frac{1}{\left(\frac{\alpha_{21}}{1-\alpha_{21}}\right)\frac{A_2}{A_1\epsilon_1}+1} \tag{2}$$

where α_{21}=absorptance of the chamber walls for energy radiation by the sample and A_2= area of chamber walls.

The value of α_{21} is at least 0.90 and the ratio of A_2/A_1 is 50. Substituting these values into equation (2) yields: $R_{12}\leq 0.002$. Therefore, the second (reflection) term of equation (1) can be disregarded. If the chamber walls are cooled with liquid nitrogen, then the third term of equation (1), which accounts for the energy radiated by the chamber walls and absorbed by the sample, can also be neglected, since T_2^4/T_1^4 is only 3×10^{-4} for $T_2=-320°$ F and $T_1=600°$ F.

With these simplications, the emittance, ϵ_1, can be written as:

$$\epsilon_1=\frac{P}{A_1\sigma T_1^4}=\frac{P_a-P_c-P_c}{A_1\sigma T_1^4} \tag{3}$$

The losses P_c and P_c are calculable within acceptable accuracies from materials properties, lead dimensions, and measured temperatures and currents.

The probable error in ϵ_1, derived from equation (3), is

$$\delta\epsilon_1=\frac{\Delta\epsilon_1}{\epsilon_1}=\left[\left(\frac{\Delta P}{P}\right)^2+\left(\frac{\Delta A_1}{A_1}\right)^2+\left(\frac{A\sigma}{\sigma}\right)^2+\left(\frac{4\Delta T_1}{T_1}\right)^2\right]^{1/2} \tag{4}$$

where

$$\left(\frac{\Delta P}{P}\right)^2=\frac{\Delta P_a^2+\Delta P_c^2+\Delta P_c^2}{(P_a-P_c-P_c)^2} \tag{5}$$

For sample temperatures of 600° F, it has been observed that P_c and P_c are about 2% of P and that their relative magnitudes (with respect to P) decrease as the sample temperature is increased. Although the uncertainties in P_c and P_c are comparatively high, (about 25 and 10%, respectively), their effect on the uncertainty in ϵ_1 is small. Values for the other parameters in equations (4) and (5) are given in table 33–I, together with their estimated probable errors and the resulting values of $\delta\epsilon_1$ for two representative cases: $\epsilon_1=0.80$, $T_1=600°$ F; and $\epsilon_1=0.80$, $T_1=2000°$ F. With equations (4) and (5) and the data in table 33–I, it is readily found that the uncertainty in ϵ_1 is almost entirely determined by the uncertainty in the sample temperature.

The probable errors for T_1 shown in table 33–I are based upon the sum of the squares of the estimated relative errors due to thermocouple inaccuracies, instrument errors, and non-uniformities in sample temperature.

TABLE 33–I. *Representative Data and Probable Errors for Calorimetric Emittance Measurements*

	n	δn	n	δn
T_1, ° F	600	0.010	2000	0.012
A_1, in.^{2}	4.700	0.002	4.700	0.002
σ (watt/in.^{2}-deg^4)	3.657×10^{-11}	negligible	3.657×10^{-11}	negligible
P (watts)	16.70		480.0	
P_a (watts)	17.30	0.005	489.6	0.005
P_c (watts)	0.30	0.25	4.8	0.25
P_c (watts)	0.30	0.10	4.8	0.10
ϵ_1	0.80	0.041	0.80	0.048

APPARATUS

Test Chambers

To study a number of samples within a reasonable length of time, two assemblies of four test chambers each have been built. Thus eight individual samples may be studied simultaneously. Figure 33-2 shows one of these assemblies with its associated vacuum

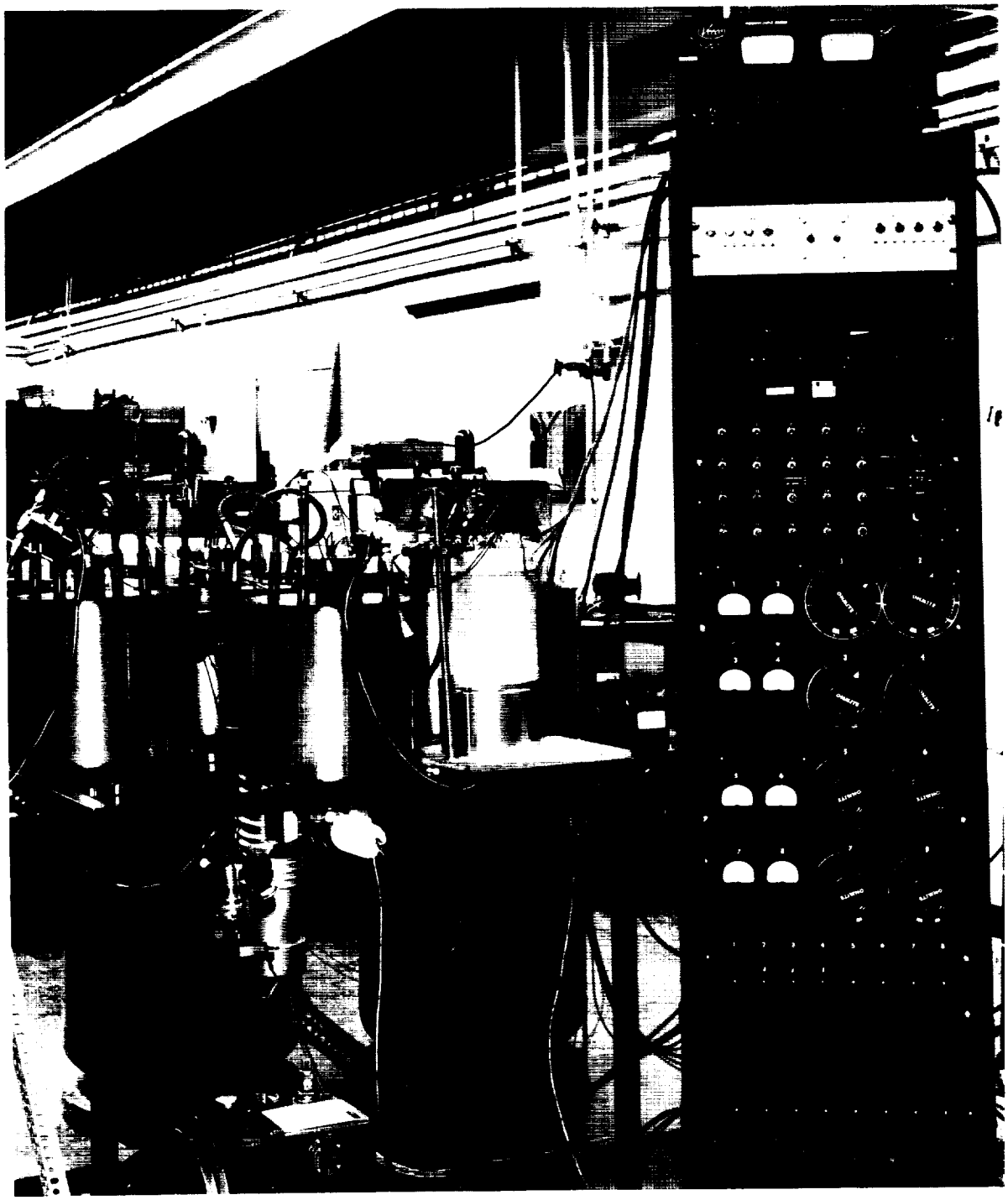

FIGURE 33-2.- Emittance stability test stand.

pumps and the power-control rack at the right. Each of the four stainless-steel vacuum chambers is 11 in. in diameter and 11 in. high. The chambers are connected to a control vacuum manifold by 4-in. diameter steel pipe, and the entire assembly is evacuated by pumps which connect to the lower end of the manifold. On the top of each chamber are the sample-entry-port vacuum flange and the four fill-and-vent tubes for the liquid nitrogen which is used to cool the walls of the inner calorimeter chamber. The bottom plate for each vacuum chamber contains a window and a magnet-operated shutter through which, when the shutter is opened, the bottom of each sample may be viewed as it is tested.

Each inner calorimeter chamber is built in two halves, as shown in figure 33–3. The chambers are made of ⅛ in. thick copper and the cylindrical portion is double-walled to contain the liquid nitrogen. The inner and outer diameters of each chamber are 7 and 9 in., respectively. One half is 7 in. high and the other half is 7¾ in. high. This difference in height leaves a ¾ in. step at the bottom of the chamber to facilitate evacuation by the vacuum system. The chambers hang inside the stainless-steel vacuum jackets by their liquid nitrogen fill and vent tubes, which are brazed to the tops of the pipes shown in figure 33–2. These brazed joints are the only points of contact between the inner chamber and its outer vacuum jacket. The 2 in. diameter hole in the top of each chamber permits the sample to be lowered into the chamber, and when the sample is in position the hole is covered with a copper radiation shield which contains the necessary power-lead and thermocouple-wire feed-throughs. A ½-in.-diameter hole is located in the bottom of the chamber so that the sample may be viewed through the previously mentioned viewing window. This hole is normally shielded by the magnet-operated shutter which swings into the ¾-in. step at the bottom of the chamber.

All of the inner-wall surfaces of the calorimeter chambers and the radiation shields have been sandblasted and coated with Parson's black [2]—an optical black lacquer with a spectrally flat absorptance of 0.98 reported in ref. 1. As a result, these surfaces are highly absorptive and diffusive. After each assembly was completed, the chambers were baked-out for two days, under vacuum, at temperatures up to 350° F.

[2] Manufactured and sold by Thos. Parsons and Sons, Ltd., England.

Vacuum System

Each of the test chamber assemblies has been designed to attain a high vacuum, and a test is not considered satisfactory unless the chamber pressure is 10^{-5} mm Hg or less. Typical pressures in the 10^{-7} mm Hg range have been obtained using a NRC 4-in. oil diffusion pump with a rated pumping speed of 220 liters/sec at 10^{-5} mm Hg. Large pumping areas between the chambers and the central vacuum manifold are provided to utilize the maximum pumping capacity of the pump. The pressure in each assembly is measured with an ionization gauge which is located at the bottom of one of the test chambers.

At pressures of 10^{-5} mm Hg, the mean-free-path of gas or vapor particles in the system is from one to two orders of magnitude larger than the chamber dimensions; consequently the number of particles returning to the sample is determined primarily by the absorptive character and capacity of the chamber walls. Because of the rough texture and low temperature of the chamber walls, particle capture is enhanced both by adsorption and condensation. This factor, combined with a small sample-area to chamber-area ratio, serves to minimize particle return to the sample. The geometry of each four-chambered assembly is such that the samples are also effectly shielded from one another by the cold, outer surface of each chamber. Before each test interval, the chamber walls are desorbed by a high-temperature bakeout.

Sample Design and Instrumentation

Sample

Each sample consists of a hollow cylinder, 1 in. in diameter and length, with 0.060 in. thick walls (fig. 33–4). Samples are machined from rod stock of the base material being studied. The sample cap is attached to the cylinder by means of two hollow pins cut from 0.060-in. tubing (steel or molybdenum) which pass through matching holes drilled through the

FIGURE 33-3. Inner calorimeter chamber for emittance apparatus.

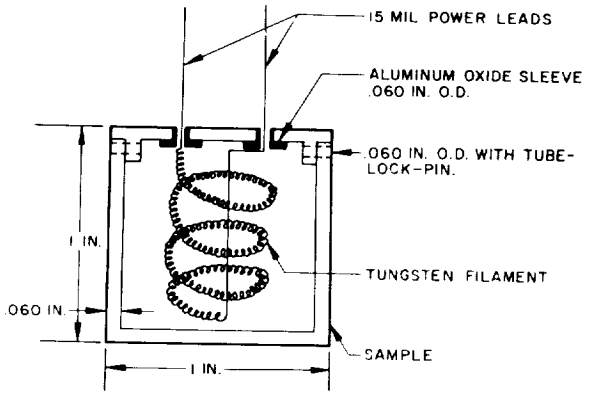

FIGURE 33–4.—Sample and heating elements detail.

cylinder wall and a circular lip on the underside of the cap. Two additional holes (0.060 in.) are drilled through the top of the cap through which pass the power leads (15-mil molybdenum or tungsten). The power leads are sized small enough to minimize heat conduction losses but large enough to support the sample and heater at elevated temperatures. Each lead is electrically insulated from the cap by a short, ceramic sleeve with a 0.10 in. shoulder on one end. A typically instrumented sample is shown in figure 33–5.

SAMPLE HEATER

Samples are heated by passing a measured amount of d-c power through a standard 500-watt or 1000-watt tungsten lamp filament. These filaments are formed in the laboratory on a ½-in. diameter mandrel to produce a coil-on-coil shape which fits inside the sample. An analysis of the approximate operating temperature and corresponding life expectancy of these filaments has been made using data contained in the MIT Tube Laboratory Manual (ref. 2) and based on the following assumptions:

1. that the steady-state energy exchange between the filament and the sample is approximated by:

$$EI=\epsilon_f A_f \sigma T_f^4=\epsilon_1 A_1 \sigma T_1^4+\alpha_f A_f \sigma T_1^4 \qquad (6)$$

where the subscript f signifies the filament characteristics.

2. that $\alpha_f=\epsilon_f$; therefore, equation (6) can be rewritten as:

$$T_f^4 \cong \left(\frac{\epsilon_1 A_1}{\epsilon_1 A_f}+1\right) T_1^4 \qquad (7)$$

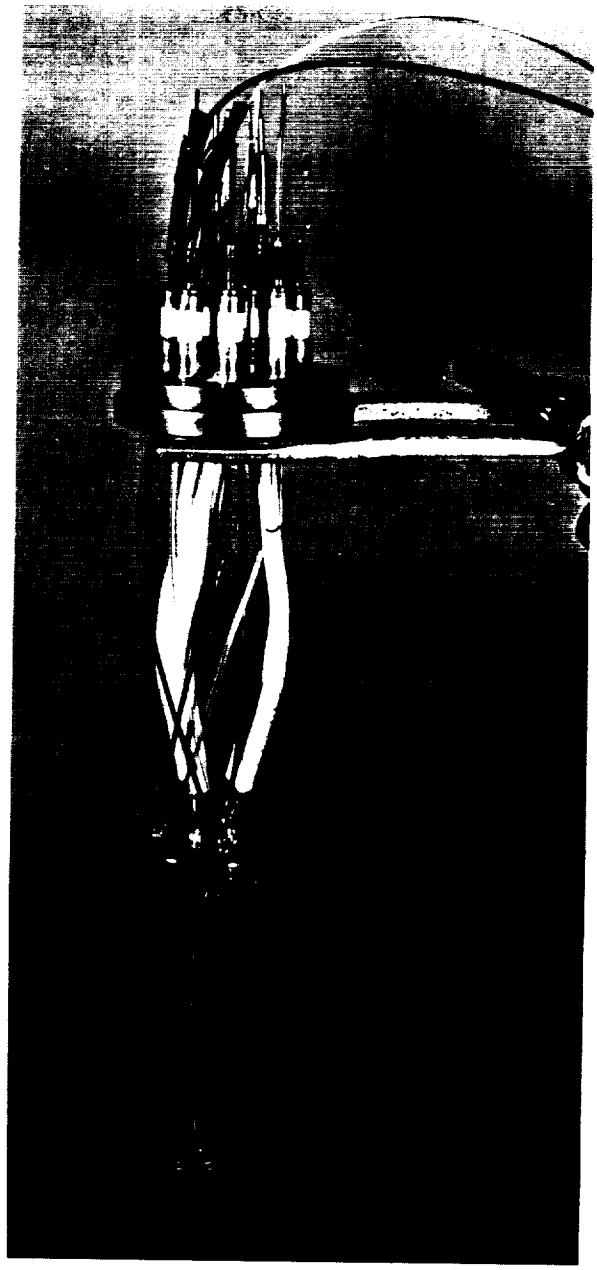

FIGURE 33–5.—Typically instrumented sample.

3. that $\epsilon_f=0.4$ and the effective radiating areas, A_f, of the 500-watt and 1000-watt filaments are 4.0 and 6.0 cm², respectively.

4. that $\epsilon_1=0.90$ and $A_1=30$ cm².

The results of substituting these values into equation (7) are shown in table 33–II. This analysis indicates that the 500-watt filament is satisfactory for maintaining sample temperatures up to 1500° F and that the 1000-watt

TABLE 33-II.—*Estimated Operating Temperatures and Life Expectancies for Sample Heaters*

Sample temperature, (° F)	Approximate Operating Temperature (T_f), ° F		Approximate Life Expectancy [a], hr	
	500-watt Filament	1000-watt Filament	500-watt Filament	1000-watt Filament
1500	3570	3240	60, 000	$>10^6$
1800	4200	3790	150	7, 000
2000	4600	4170	<20	200

[a] Based on normal life expectancy of 1000 hr.

filament should be satisfactory for sample temperatures up to 1800° F. The need for a larger filament is indicated for sample temperatures of 2000° F. Larger diameter and longer filaments have been successfully wound in the laboratory but have not yet been tried.

TEMPERATURE MEASUREMENTS

Sample temperatures are measured with 40-gage thermocouples which are spot-welded or peened to the surface of the metallic substrate of the sample. If the thickness and thermal conductivity coefficient of the coating are known, a correction can be made to the measured temperature to obtain the true surface temperature of the sample. Thermal gradients through ceramic-coated specimens of stainless steel and Inconel of about 1° F/mil at 900° F and 5.4° F/mil at 1800° F have been reported by Richmond and Stewart (ref. 3). The coating thicknesses involved in the present study do not exceed 2 or 3 mils.

All of the thermocouples are calibrated by comparing them with standard thermocouples obtained from NBS. Chromel-Alumel thermocouples are used for measurements up to 1000° F and platinum-platinum/13% rhodium thermocouples are used for measurements from 1000° F to 2000° F. The initial accuracy of the measurements has been determined to be ±2° F at 600° F and ±5° F at 2000° F. Within the 1000° F and 2000° F limits for each type of thermocouple wire, no significant EMF drift has been observed over 240-hr periods.

The reference junction of each thermocouple is maintained in an ice bath and the output voltages are measured with copper extension wires from the ice bath. A schematic of the thermocouple circuit is shown in figure 33-6.

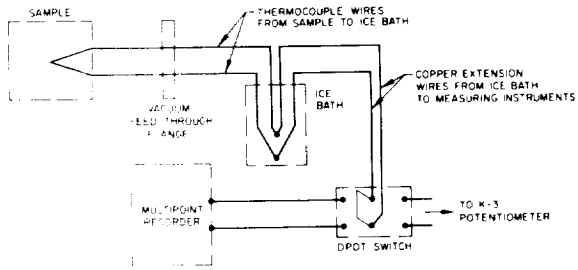

FIGURE 33-6.—Thermocouple circuit schematic.

Normally the voltages are recorded on a Bristol multipoint recorder to indicate temperature stability; however, when an accurate measurement is desired for an emittance determination, the voltages is read with a Leeds & Northrup type K-3 potentiometer.

Sample temperatures can also be checked through the viewing port with either an optical or a two-color recording pyrometer. One such preliminary check on an unoxidized stainless-steel sample at 2000° F indicated that sample temperature variations from the bottom center to the edge were less than 10° F.

POWER MEASUREMENT AND CONTROL

A schematic of one of the eight parallelled power measurement and control circuits is shown in figure 33-7. The d-c power is supplied to the sample heater by a constant-voltage (adjustable), variable load rectifier. The power level is controlled by the output voltage setting on the power supply and by a control rheostat in each circuit which adds or subtracts to the circuit resistance. An ammeter indicates the current in the circuit; however, when an accurate current measurement is desired, the voltage drop across a standard resistor (calibrated manganin shunt) is measured with the K-3 potentiometer. The voltage drop across the sample

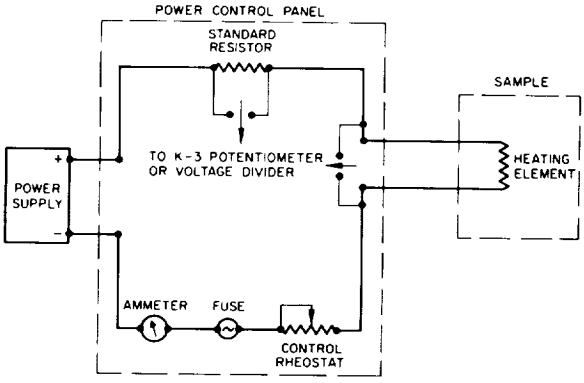

FIGURE 33–7.—Electrical power circuit schematic.

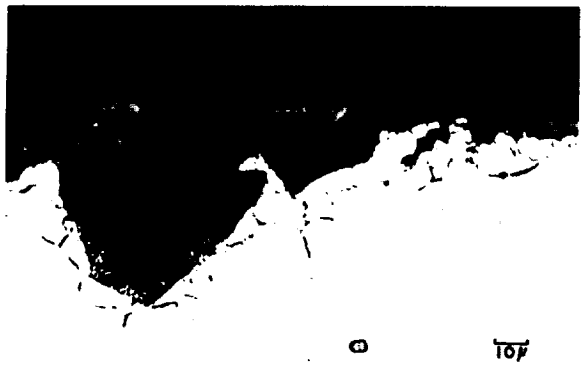

FIGURE 33–8.—Cross-sectional photomicrograph of oxide coating on Inconel X.

heater is usually read from the power lead terminals on the vacuum flange, (upper plate in fig. 5), and the correction, P_e, is made for the I^2R loss from this point to the sample. Heater voltages have been obtained from EMF leads attached to the power leads directly above the sample; however, the added accuracy by this method does not justify the additional effort and risk of electrical failure involved. Heater voltages are also measured with the K 3 potentiometer, usually after being passed through a suitable voltage divider.

To obtain a measure of the heat loss from the sample through the power leads, (P_c), one or more thermocouples are attached to the power leads at measured distances above the sample (fig. 33–5). From these temperatures, an estimate of the temperature gradient just above the sample can be obtained and the corresponding heat loss then calculated. Power lead temperature data are also used for determining the leadwire resistance which is used in the P_e correction term.

RESULTS

To date, 30-day emittance-stability tests have been completed on ten separate samples of oxidized stainless steel and Inconel alloys. Typical emittance values obtained from these samples are shown in table 33–III. No significant change in the emittance of these samples was observed over the 30-day test periods. At present, efforts are being made to characterize the oxide layers on these samples by means of photomicrographs and X-ray diffraction patterns. A photomicrograph of the oxide layer on a sample of Inconel X is shown in figure 33–8.

ACKNOWLEDGMENTS

This study was sponsored by the Aeronautical Systems Division, Air Force Systems Command, Wright-Patterson Air Force Base. Considerable assistance in the design and construction of the test apparatus and in the preparation of this paper has been received from the Thermophysics Research staff under the direction of Dr. R. E. Gaumer.

TABLE 33–III. *Typical Emittance for Oxidized Stainless Steel and Inconel Alloys (30-Day Test)*

Sample	T,° F	ϵ_1
Stainless steel type 304, sandblasted and oxidized at 1800° F for 2 hr	600	0.75
	900	.82
	1200	.87
Stainless steel type 304 ELC, sandblasted and oxidized at 1800° F for 2 hr	600	.70
	900	.81
	1200	.90
Inconel X, sandblasted and oxidized at 1975° F for ½ hr	800	.78
	1500	.86
Inconel 702, sandblasted and oxidized at 1975° F for ½ hr	800	.74
	1500	.83

REFERENCES

1. IGY Instruction Manual, Part VI: Radiation Instruments and Measurements, Pergamon Press, New York, 1958, p. 436.
2. Research Laboratory of Electronics, Tube Laboratory Manual. 2d ed., Massachusetts Institute of Technology, Cambridge.
3. Richmond, J. C.; and Stewart, J. E.: Spectral Emittance of Uncoated and Ceramic-Coated Inconel and Type 321 Stainless Steel, NASA Memo 1-9-59W, April 1959.

DISCUSSION

Richmond: A discussion on this paper has been prepared by T. G. Kollie of the Oak Ridge National Laboratory.

Kollie, Oak Ridge National Lab.: Rather than present the discussion which will be published in the proceedings along with our paper, No. 38, I will ask two questions on this technique, both of which are giving us trouble. Perhaps you have thought about these things and have come up with some answers. You discarded the correction term for area measurement. For example at 1100° C, a first order expansion correction for INOR 8, which is a nickel-molybdenum-chromium-iron alloy, gives about a 2% change in area. Have you done this?

Funai: Are you talking about thermal expansion? Yes, we are correcting for this. We still feel that the sample-temperature error predominates over the sample-area measurement error.

Kollie: Regarding the temperature measurement, in our measurements we have encountered quite a large temperature variation from the top to the bottom of the specimen. We believe this is due partly to our heater design, and I notice that you are having trouble with your heater design. I wonder if this might tend to make the top hotter than the bottom. This was quite severe. We noticed a 60° temperature difference (near 500° C) from the top to the bottom with a very similar specimen to that used in this paper.

Funai: We have not noticed this as we use only one thermocouple because of contractural relationships.

We have suspended samples in a laboratory bell jar and heated them up to various temperatures, usually to red heats and on up to 2000° F, and observed them with a pyrometer. Visually the samples appear fairly uniform. At 2000° F we observed with the optical pyrometer no greater difference from top to bottom of the sample than 10° C which we believe was our reading accuracy with the pyrometer. As I pointed out, the apparatus is so designed that during a 30-day test we can look at the bottom of the sample, and we have noticed no appreciable thermal gradient there. I might mention, however, that we are putting two thermocouples on the sample, one on each side. Using 3-mil Chromel-Alumel and 3-mil platinum-platinum 13% rhodium thermocouples we are finding temperature differences on the order of 1 to 2% of the absolute temperature, so this is a problem. We have calibrated these thermocouples and found them good to within 1% at least, and probably better. The problem is essentially an attachment problem, we think. In fact, we are initiating a subcontract to try to evaluate various attachment techniques and their effects on surface temperature measurements.

Askwyth, Pratt and Whitney Aircraft: We have used a technique very similar to this in making emittance measurements and in running samples for periods of time of 300 to 900 hours, which is roughly comparable to what you are doing. We have used a resistance-heated, hollow-cylindrical sample with a small blackbody hole and an optical pyrometer to measure the temperature of this blackbody hole. We have also used thermocouples, and we found that we have had a serious problem when using platinum-platinum rhodium thermocouples on stainless steel. As an example, in about a dozen of these endurance tests, we sometimes had as much as 18° change in indicated temperature during the first overnight period, and over the next few days the change would sometimes increase to as much as 30° to 40°. I do not know why this is so, but we do have this problem with platinum-platinum rhodium on stainless steel.

Funai: We have not observed this particular problem, but we understand some people have had problems with platinum in the presence of silicon in a reduced oxygen partial pressure or in vacuum. Since many of the oxidation-resistant coatings that are being used or are being developed for the columbium and molybdenum alloys are a silicide-base coating, we are anticipating trouble in this regard, based on what we have been told. We have not run into it directly ourselves. On the stainless steel samples though, we have observed very good temperature stability from both the Chromel-Alumel and the platinum-rhodium thermocouples at sample temperatures of 600° and 900° F.

Askwyth: Have you ever measured temperature distribution along the sample with a high-emittance coating on the sample? You had something in the paper about a 10° maximum temperature difference for noncoated stainless steel samples. I wonder how this would be with a high-emittance surface.

Funai: We have observed the samples in the bell jar, but we have not actually attempted to measure their temperatures with thermocouples.

Askwyth: In your paper I noted that you use a vac-ion pump in one assembly and an oil diffusion pump in the other. In baking out the system using the vac-ion pump do you ever get an outgassing problem with the Parson's black?

Funai: We are no longer using the vac-ion pump because of difficulties we had in initially setting up our

automatic liquid nitrogen feed and shut-off control circuitry. We had some warm pots in the morning on two or three occasions because of no liquid nitrogen. This allowed a considerable transient gas load to be released from the chamber walls which was sufficient to choke off the vac-ion pump. It was then necessary to use a diffusion pump system in order to get the vac-ion pump back in operation. After a couple of these cycles we kept the 4-inch diffusion pump on permanently. I think this problem was independent of the coating on the chamber walls.

ASKWYTH: You said you have a problem with liquid nitrogen cooling when the sample is at 1400 or 1500° F. Why don't you use water cooling? At those temperatures the ratio of the fourth power of the sample temperature to that of typical water temperature is approximately 200 to 1.

FUNAI: For samples operating at 600° F or higher, water-cooled chambers should be just as good as liquid-nitrogen-cooled chambers as far as the emittance determination goes. We are continuing to use liquid nitrogen, however, to improve the vacuum and to reduce the amount of particle return from the chamber walls to the sample.

SCHWARTZ: Mr. Funai, in developmental testing what is the difficulty of going through quite a few samples. You are able to handle four at a time, but what is the problem in actually preparing these samples in cylindrical form?

FUNAI: The instrumentation of the sample?

SCHWARTZ: Not necessarily the instrumentation, but, instead, the application, or the oxidizing of the metal cylinder.

FUNAI: The coatings to the sample?

SCHWARTZ: Yes.

FUNAI: Procurement of rod stock of some of the newer alloys such as the refractory-metal alloys is a little more difficult than for sheet stock. Rod stock is also more expensive. Machining of the samples may be a little more difficult than would be the fabrication of samples from sheet material. None of these disadvantages is prohibitive though. The oxide coatings we have formed on the stainless steel and Inconel samples appear to have the same characteristics—spectral reflectance, coating thickness, chemical composition and visual appearance—as the coatings we obtained on flat disks of sheet stock of these materials. We have found some variations in the appearance of the oxide coating on each sample and between samples, but the same variations were noticed on the disk samples. The oxidation-resistant coatings we have received have been applied both to disks and to the cylindrical samples by commercial suppliers with no apparent difficulty.

GARY GORDON, Radio Corporation of America: What is the advantage of a hollow cylindrical sample versus a thin-plate sample?

FUNAI: Our preference for the hollow cylindrical sample is based primarily on our belief that we can achieve better uniformity of sample temperature with this type of sample than with the thin-plate sample. From the point of view of easier sample preparation and of being able to use sheet material to fabricate the sample rather than machining it from rod stock, the thin-plate sample design seems superior. We have considered using thin-plate samples in the past but have not designed a heater which would keep the sample at a suitably uniform temperature.

692-146 O—63——22

34—INSTRUMENTATION FOR EMITTANCE MEASUREMENTS IN THE 400° TO 1800° F TEMPERATURE RANGE

BY A. GRAVINA, R. BASTIAN, AND J. DYER

REPUBLIC AVIATION CORPORATION, FARMINGDALE, NEW YORK

Equipment is described which was used to measure simultaneously the spectral and total normal emittance of materials in the temperature range from 400° to 1800° F while contained in ambient and vacuum environments. Equipment design, set-up, and experimental procedures are presented. Also included is a description of present activities directed towards the assembly of equipment which will help improve experimental accuracy and also provide for angular emittance measurements in order to obtain more comprehensive data.

The first part of this paper describes an apparatus used to measure the total and spectral normal emittance of materials contained in various environments. The equipment was designed and fabricated as part of a US Air Force-sponsored program oriented towards investigating material emittance behavior under various environmental conditions in the temperature range from 400 to 1800° F.[1] This is followed by a description of present company sponsored activities which includes the assembly of equipment to provide a more comprehensive experimental approach by providing for angular emittance measurements.

The equipment used for the Air Force program is capable of measuring simultaneously the total intensity and spectral distribution of radiant energy emitted by heated specimens in any desired atmosphere including vacuum. The complete system consists essentially of:

a. a single-beam dual-channel radiation measuring instrument which gives total and spectral data simultaneously

b. a test chamber which allows samples to be heated via resistivity to over 2500° F in controlled atmosphere

c. a vacuum system with a pressure capability of 10^{-4} mm Hg or lower in the test chamber

d. a high-temperature reference blackbody functional from 400 to 1800° F

e. auxiliary instrumentation for sample heating and recording of total and spectral data.

DUAL-CHANNEL RADIOMETER

The dual-channel radiometer was vendor fabricated [2] in accordance with Republic Aviation specifications. The instrument consists of a F/5 collecting optical system followed by a Leiss Model 9000 single monochromator for giving spectral data of sample emission and a total radiation channel for measuring total radiation output directly. The dual function is accomplished by time sharing incoming radiation between the two channels with an optical chopper operating such that radiation is interrupted at a rate of 80 times per second (i.e., the chopper generates a carrier frequency of 80 cps) and is continually referenced against an internally contained blackbody whose function is to supply a constant background signal. Both channels utilize thermistor bolometers as detectors.

The optical system installation is shown in figure 34-1. Radiation emitted by the source,

[1] This program was initiated and monitored by the Thermodynamics Section, Thermophysics Branch, Materials Central of ASD under Contract AF33(616)-5925. A complete description is available in the final WADD report, TR 60-102, which covers work done during the period from July 1958 to September 1960.

[2] Barnes Engineering Co., Stamford, Conn.

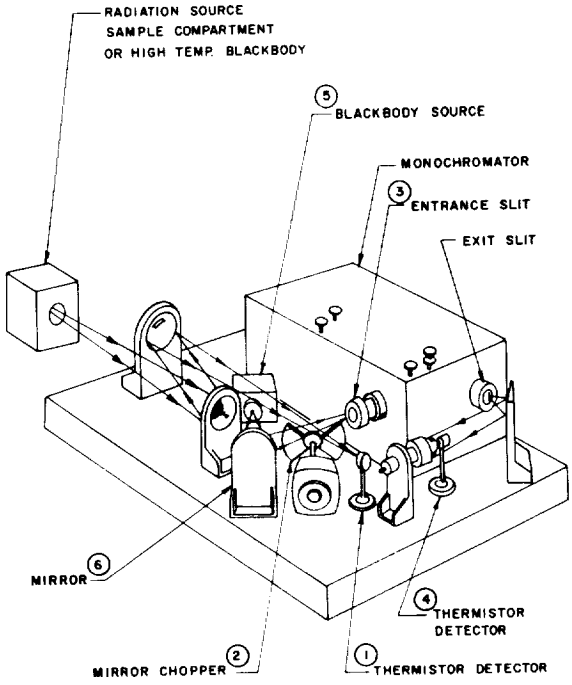

FIGURE 34-1.—Optical system of dual channel radiometer.

which may be either the high-temperature reference blackbody or the sample in its chamber,[3] is focused by a folded mirror system onto the total channel thermistor (1) and by reflection (after the chopper blade has advanced by 90°) from the mirrored chopper (2) onto the entrance slit (3) of the monochromator and thence to the spectral channel thermistor (4) which receives dispersed target radiation.

The mirrored chopper serves to optically chop the target radiation and continuously reference it against radiation from a low-temperature Barnes 1A blackbody (5). Hence, the two detectors yield simultaneously continuous total radiation and the spectrally distributed radiation as determined by the nonochromator scanning. When the optical path to the total channel is blocked by the front surface of the chopper, the rear surface of the chopper, also mirrored, directs radiation from the low-temperature blackbody via the mirror (6) to the total channel detector. Also, when the total channel thermistor receives radiation from the target, low-temperature blackbody radiation is focused onto the monochromator entrance slit as shown in figure 34-1. Thus, the low-temperature blackbody alternately supplies to each thermistor background radiation when target radiation is prevented from reaching that particular thermistor.

The electrical output of each thermistor is an 80-cps sinusoidal wave, the peak to peak value being proportional to the difference in intensity of target and low-temperature blackbody radiation. A preamplifier produces an a-c amplification of 5000 followed by an additional amplification of 1000 by the amplifier section of the Barnes SRA-1A synchronous rectifier-amplifiers. Synchronous rectification of this signal produces a d-c signal which has a magnitude directly proportional to the incident radiation. Each signal drives a pen of a Leeds & Northrup Speedomax X1-X2 recorder.

TEST CHAMBER

The test chamber was designed and fabricated at Republic Aviation. It is viewed from different aspects in figures 34-2 through -5. The chamber is constructed primarily of stainless steel and has a cylindrical configuration 10 in. in diameter and 15 in. in length. The interior is coated with "Zapon" black paint to

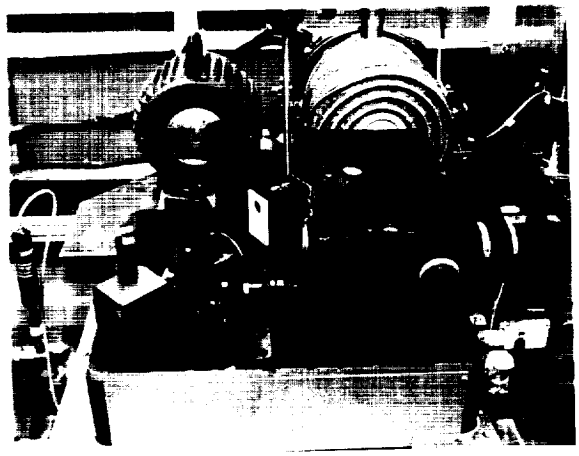

FIGURE 34-2.—Radiometer with RS-8A reference blackbody in source position.

[3] Note that two blackbodies are utilized in the optical system. The high temperature blackbody (400° - 1800° F) functions as a reference radiation source or target when reference curves are recorded. This is replaced by the sample holder when sample radiation is to be determined. The low temperature blackbody (5 in fig. 34-1) functions as a background reference source for both the total and spectral channel. This blackbody is maintained from 100° to 200° F dependent upon sample test temperature.

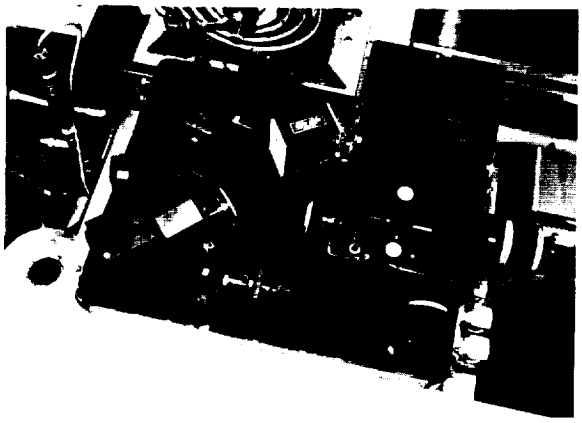

FIGURE 34–3.—Radiometer optical system showing test chamber in source position.

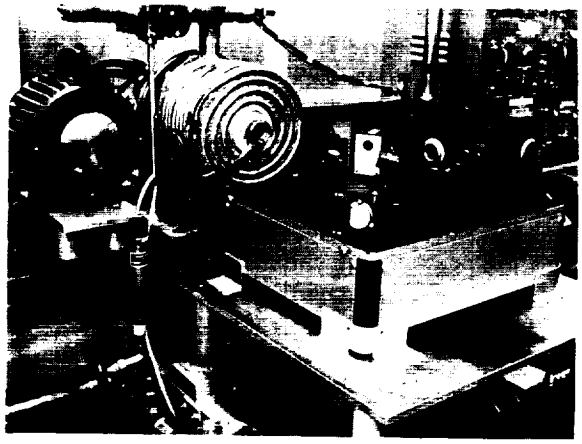

FIGURE 34–4.—Integration of radiometer with blackbody and test chamber.

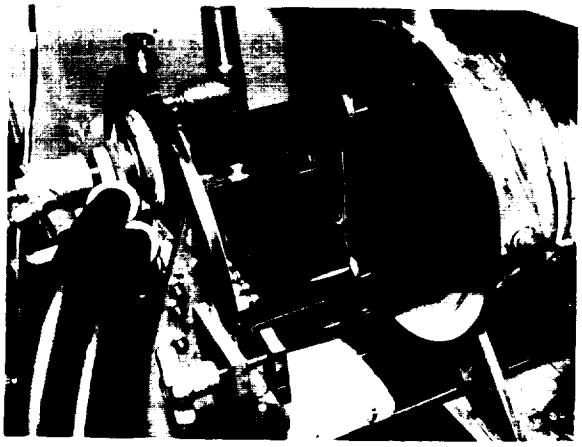

FIGURE 34–5.—Test chamber in open position showing sample positioned between electrodes.

reduce internal reflections. Reference to the figures will illustrate some of the construction details.

From figure 34–2 it is seen that the entire exterior is water-cooled via the copper tubing jacket. The exit port for sample radiation may be seen at the top center portion of figure 34–3. A sodium chloride window is mounted in the port when the chamber is to be evacuated. The knurled knob seen just below the port controls a shutter inside the chamber which is used to cover the window when evacuation takes place, thus protecting it from possible deposition due to sample sublimation. Another port and shutter arrangement (not visible in the figures) is located on the chamber side and is used for observing specimens while under test. A light is mounted inside the chamber to facilitate viewing. The light is turned off when runs are being made.

In figure 34–5 is seen the back plate of the sample holder on which is mounted a pair of water-cooled copper electrodes and a thermocouple gland. Electrical cabling used to supply power to the electrodes is seen in the left foreground. The ends of the electrodes are fitted with copper caps, spring loaded against the specimen to allow expansion due to specimen heating.

A water-cooled copper plate (not shown in fig. 34–5) containing an aperture the same size as that of the high temperature reference blackbody is mounted about ⅛ in. in front of the sample to further prevent back-scattered radiation from entering the field of view of the detector.

The back plate is moved via a drive gear arrangement into the chamber to position a specimen for testing. The dimensions of the electrodes, etc. placed the sample in the focal plane of the collecting mirror of the optical system when the back plate was sealed against the flange of the chamber.

VACUUM SYSTEM

The vacuum system utilized is standard in design and capable of attaining pressures of 10^{-4} to 10^{-5} mm Hg. Test pressures of interest in this program were 5000 and 5–10 μ in addition to atmospheric. The mechanical pump is a Cenco 92003 Type 1 Megavac which acts as fore pump for an all-metal water-cooled Consolidated Electrodynamics Corporation VMF size 44 diffusion pump.

Pressure readings in the 5000-μ range are observed on a Veeco Vacuum Corporation

SP-1S millimeter-range vacuum gage and readout in the 5–10-μ region is achieved on a Consolidated Electrodynaimes Corporation Type 2201-03 Pirani gage.

HIGH-TEMPERATURE REFERENCE BLACKBODY SOURCE

The high-temperature reference blackbody which is used as a source when standard spectral emissive power curves are obtained is a Barnes Engineering RS-8A modified to operate from 400° F to 1800° F. This unit is proportionately temperature controlled to $\pm 0.5\%$ at 1800° F and has an emittance of 0.99 ± 0.01. To equalize the optical path for both sample and reference blackbody when samples are run in other than normal atmospheric conditions, a sodium chloride window is mounted in front of the blackbody. This is not shown in the photographs.

INSTRUMENTATION FOR SAMPLE HEATING AND RECORDING OF TOTAL AND SPECTRAL DATA

Resistive heating of samples is accomplished by stepping up the 110-v a-c line voltage via a 5-kva Variac transformer and utilizing this output to drive a second transformer with a high primary to low secondary turn ratio. The sample is connected directly across the secondary of this transformer. Sample power output is regulated manually via the Variac.

The sample configuration found most suitable for use with this power arrangement was a tensile shaped specimen 6 in. long, $\frac{1}{16}$ in. thick and $\frac{3}{8}$ in. wide in the necked-down portion which is 4.5 in. long; the ends being $\frac{1}{2}$ in. wide. To ascertain whether the sample heating was uniform in the region seen by the radiometer system, an optical pyrometer was used. It was found that the pyrometer filament disappeared over its length when compared to the heated necked-down portion of the sample as a background.

Chromel-Alumel No. 30 gage thermocouples were used to monitor sample temperature. These were welded onto the center of the necked-down portion of the sample directly opposite the portion of the sample viewed by the radiometer. In cases of nonconducting coatings, a small portion of the coating was removed to expose base metal. Sample temperature readout was obtained on a Leeds and Northrup millivolt potentiometer resolvable to within 0.10 mv (± 5° F).

Spectral and total channel signal readouts were simultaneously obtained from a Leeds and Northrup X1—X2 Speedomax recorder.

Spectral scanning was optional with respect to either manual or automatic operation. Automatic scanning was achieved by a synchro transmitter-receiver combination. The synchro transmitter, (Bendix Aviation Corp. model No. 4, type 3H6) was driven by the recorder chart drive motor and in turn actuated a synchro receiver (Bendix Aviation Corp. model No. 4, type 3F) which rotated the monochromator wavelength drive. A scan time of about 4 min. for the wavelength range of about 1 through 12 μ (the effective wavelength distribution of radiation from samples and blackbody in the temperature range of interest) gave sufficient wavelength resolution to satisfy the needs of this program. Since there was no provision for automatic slit programming, constant slits, with the aid of the electronic gain controls, afforded proper recorder pen deflection, at each temperature.

SYSTEM INTEGRATION

The test chamber, high-temperature reference blackbody and the radiometer optical system were integrated most easily into a compact working unit by utilizing a lathe bed. The lathe bed carriage afforded the necessary lateral motion which would permit either the sample or the reference blackbody to be optically aligned with the radiometer (which rested on a table attached rigidly to the lathe bed frame) when each in its turn was acting as the radiation source. Repeated proper alignment of each source was assured by mechanical stops which limited the lateral motion of the lathe bed carriage to the proper position.

Figure 34-2 shows the reference blackbody and test chamber mounted side by side on a platform attached to the lathe bed carriage with the reference blackbody in this instance acting as the source of radiation. Figure 34-3 shows a clearer view of this aspect where now the test chamber is on axis. Motion of the test chamber relative to the vacuum system manifold was

accomplished by using a 4-ft stainless steel bellows coupling.

A schematic of the complete system is shown in figure 34–6.

The sample chamber, because of its complex of water, vacuum, and electrical connections, occupied a fixed position on this platform which was mounted on the ways of the lathe bed. This platform could traverse the lathe bed laterally, and the test chamber had only this one freedom of movement which defined the sample plane. Therefore, the radiometer which contains the Leiss monochromator was positioned relative to the test chamber so as to place the entrance slit of the monochromator (and also the total channel detector) conjugate to the sample plane for proper imaging.

The blackbody was then mounted on the platform adjacent to the test chamber and positioned laterally and vertically to interrupt the optical axis of the radiometer, whereupon it was moved back and forth along the optical axis until maximum output (recorder deflection) was obtained. This was found to occur over a depth of focus of about 2 in. The final position selected was at the midpoint. It was observed that this position was conjugate to an image on the monochromator entrance slit of that portion of the conoid of Sturm which is elongated in the vertical direction, thus maximally overlapping the slit.

Wavelength calibration was achieved by utilizing suitable standards of emission and absorption.

The procedure initially entailed rotating the dispersing prism manually in discrete increments and recording a series of steps representing the levels of spectral normal energies of the corresponding wavelengths. Meanwhile a separate channel recorded the total normal energy. This procedure was employed con-

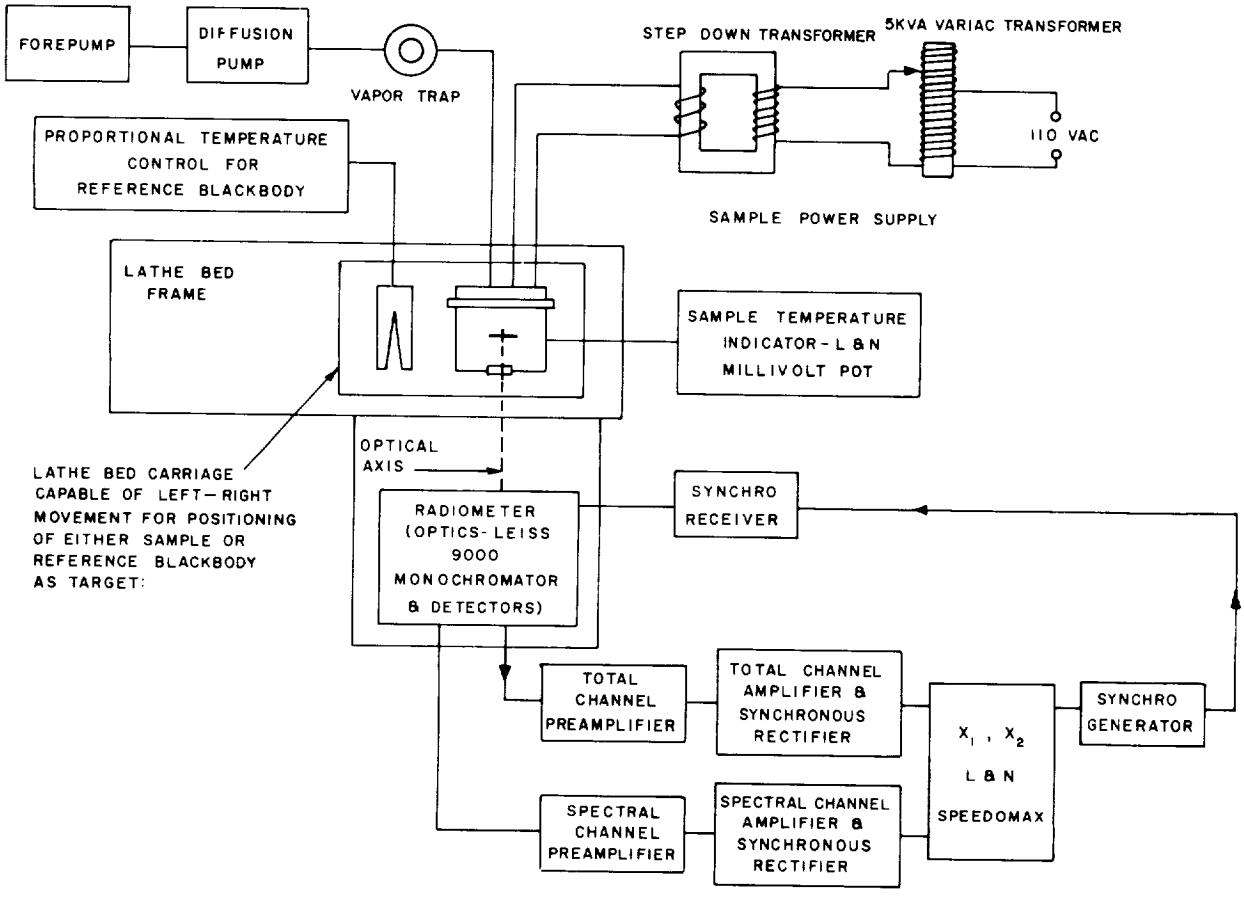

FIGURE 34–6.—Schematic of system.

secutively on the blackbody and the test sample.

Subsequently, after satisfactory system operation was demonstrated, the automatic scanning of the spectrum by means of synchro motors was used to rotate the prism and a continuous spectral emission curve was recorded.

Single-bean operation was employed whereby two consecutive curves corresponding to the blackbody and the sample were obtained. By superimposing the two curves, corresponding spectral points could be compared to obtain a plot of the spectral emittance. Spectral emittances were computed by taking the ratios of sample and blackbody readouts at a given temperature at 0.1-μ intervals or less. Atmospheric absorption bands served as convenient reference indices to aid the superposition process.

CRITIQUE OF MEASUREMENTS

Instrumentation

For total emittance, any disparity in temperature between the sample and blackbody introduces a relative emittance error that is four times the percentage of the disparity. For example, to measure total emittance to within a relative experimental error of $\pm 2\%$ the absolute temperatures must not differ by more than $\pm 0.5\%$. For spectral emittance, the relative error at the wavelength of maximum emission approaches five times the relative temperature error. The minimization of error therefore is directly related to the accuracy with which sample and reference temperatures are matched. This means that the blackbody controller settings must be precise and sample temperature measurements must be scrupulously made. Thermocouples should be calibrated, as should the potentiometers used. Readings must be precise and room-temperature compensation must be maintained on the potentiometer.

Blackbody temperatures were obtained and controlled by the Barnes proportional controller which has a rated accuracy of $\pm 0.5\%$ at 1000° C (1832° F). Readout was obtained on a recording potentiometer accurate to $\pm 0.3\%$.

Sample temperatures were measured with No. 30 Chromel-Alumel thermocouples which are accurate to $\pm 0.75\%$ at 1000° C. Temperatures were read on a potentiometer accurate to $\pm 0.15\%$.

In addition to these inherent instrumentation errors, there were errors due to accuracy limitations in setting and reading the instruments.

Data Reduction

The spectral emission curves plotted by the recorder were subject to data reduction limitations particularly in the regions of atmospheric absorption, where the slopes were very steep, and in regions of low emission where the recorder deflection was minimal (i.e., below 1μ and above 12μ).

It should be noted that, for a blackbody at 1800° F, 96.6% of the total energy is between 1 and 12μ. At 600° F, 82% of the total energy lies between 2 and 12μ, with an additional 7% out to 15μ.

Temperature Gradients

Specimen temperatures were measured with thermocouples welded onto the metal substrate. In a few instances where there were thick ceramic coatings, appreciable thermal gradients were introduced. According to one reference each mil of thickness of ceramic coating produces a 1° F gradient. For a test temperature of 1800° F this would reduce the emittance approximately 0.2% for every mil.

Vacuum Tests

These tests were subject to an error produced by the unequal rates of deterioration of NaCl windows. It was found that the sample chamber cooled the attached window, causing water vapor condensation whereas the blackbody window, which was slightly warmed by the blackbody casing, remained dry. The water condensation fogged the chamber window, lowered its transmittance (especially in the visible and near infrared) and consequently, reduced the emittance value for the test sample a variable amount, depending upon the degree of cloudiness. To alleviate this condition, the windows were repolished when fogging became severe.

Sample

A final point to be made in regard to the test results is that, in general, differences in sample preparation, composition, surface texture, thick-

ness and adhesion can cause appreciable variations in emittance. Furthermore, different heating rates and temperature exposure durations can affect the rate of sample degradation with concomitant modification of the emittance. This implies that sample process control and test history are important experimental parameters when reporting test data.

Total Error

The total root mean square error is estimated to be $\pm 8\%$ for nonvacuum tests and $\pm 10\%$ for vacuum tests.

COMPARATIVE TEST RESULTS

A comparison of results obtained on the RAC apparatus with published values for a number of available materials indicated that the instrument was providing reliable data. Unfortunately, spectral data were scarce on materials available for testing and the comparisons had to be made for total values only. For example, the Rinshed-Mason Company indicated that their Q36K802 paint has a total normal emittance of 0.90 at 1200° F which conformed exactly to the value obtained with the total channel of this instrument. Hanovia reported their liquid gold at 0.047 at 480° F, which value compared favorably with 0.05 at 500° F obtained at RAC. The emittance of stably oxidized Inconel-X was reported to be 0.92 at 1800° F (ref. 1) which value was in excellent agreement with that obtained at RAC. All these measurements were made in an air environment at atmospheric pressure.

SYSTEM MODIFICATION AND ADDITIONS

Features are being incorporated into the RAC facility which provide greater reliability, convenience, and allow for a more comprehensive approach to emittance measurements. Current interest centers about the design and fabrication of a goniometric-type instrument which will permit the measurement of emittance as a function of angle as well as the other significant variables. Angular characteristics of emittance (and reflectance) should be determined experimentally to adequately describe existing materials and to aid in developing new ones with tailored properties. Also, knowledge of the angular function will permit the calculation of integrated quantities more precisely than the approximate methods presently employed. It is only for true cosine emitters that the hemispherical emittances can be deduced accurately from the normal values. For other types of surfaces, ranging from highly polished metals to highly emissive materials, various degrees of approximation (ref. 2) are necessary, since no unified theory exists which treats all types of surfaces adequately.

A chamber is under construction which has provision for rotating the sample relative to a radiometer optical axis in addition to facilities for sample resistive heating in vacuum and controlled atmosphere. A cutaway view is shown in figure 34–7. Sample rotation is achieved by placing the electrodes, which also serve as specimen mounts, on a base plate subassembly capable of rotation relative to the main, stationary, chamber baseplate. Vacuum sealing is effected between the moveable and stationary parts of the baseplate by O-ring seals. All thermocouple and other components relevant to the measurements are brought into the chamber through vacuum-tight glands mounted in the moveable baseplate assembly. The moveable baseplate is capable of rotation through an angle of $\pm 90°$ relative to the optical axis. Rotation is achieved via a precision gear drive and the angular setting is read from a calibrated dial plate as shown. All seams and joints will be nicrobrazed to insure a vacuum-tight assembly.

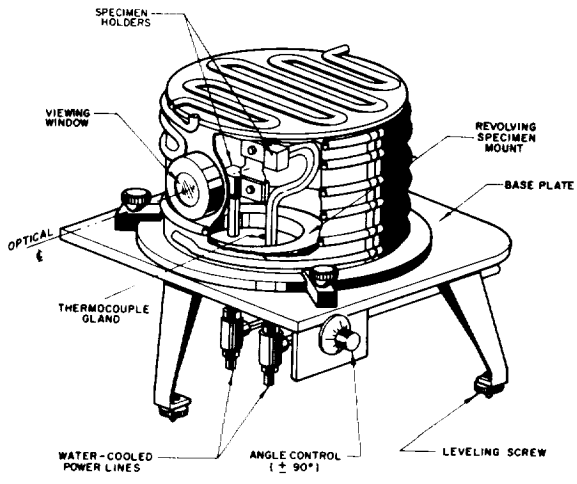

FIGURE 34–7.—Sample test chamber for angular emittance measurements in controlled environments.

Sample-blackbody temperature disparity will be minimized by utilizing the sample power supply and temperature control system shown in figure 34–8. The desired test temperature will be set on the blackbody proportional controller and any disparity between it and the sample temperature is manifested by an error voltage generated by the differential thermocouple. One element to the couple is connected to the blackbody and the other to the sample. The output of the differential thermocouple will activate a null balance recorder in which the error signal is amplified and fed into the three-mode current-adjusting-type controller. This controller, which has rate, reset and proportioning band, will automatically feed the necessary correction signal into a high or low power range load circuit. Each load circuit, of which that shown in figure 34–8 is typical, consists of a magnetic amplifier, saturable core reactor and a stepdown transformer across which the sample is connected. The correction signal is amplified by the magnetic amplifier and the output controls the saturable core reactor impedance such that the line current is adjusted to a value necessary to maintain the sample at the blackbody temperature. One load circuit is applicable for sample power levels ranging from 0.34 to 40 watts whereas the other is operable over the range from 40 to 7500 watts.

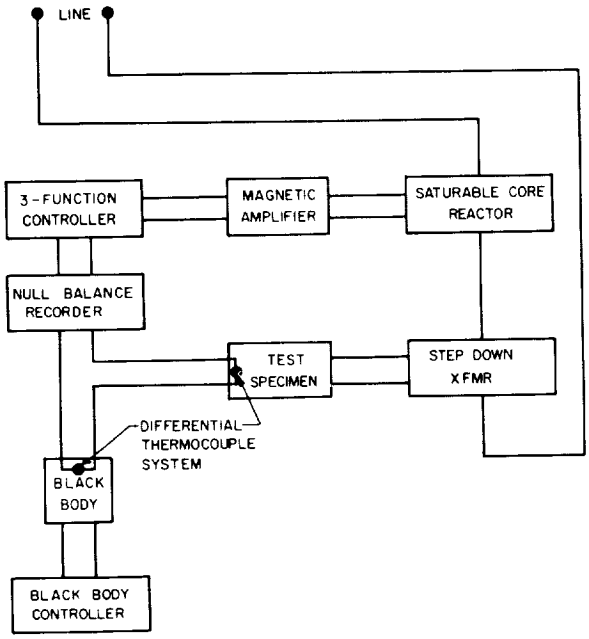

FIGURE 34–8.—Sample power supply and automatic temperature-control system.

The spectrophotometric portion of the apparatus is variable in that two systems, dependent on the particular experiment, may be used. One is the spectral/total radiometer previously described whereas the other is a universal type automatic ratio recording spectrophotometer. The present philosophy is to integrate the systems in an "open" construction type arrangement whereby either optical system may be used in conjunction with the sample chamber-blackbody-temperature control system. This type of integration yields a system prone to modification with a minimum of effort while providing maximum flexibility of operating conditions.

Depending upon the temperature, spectral region and degree of angular rotation, available radiation will impose limits upon angular emittance measurements. The approach anticipated is to sacrifice spectral resolution where necessary to gain photometric precision. In the limiting case total channel rather than spectral channel measurements can be made.

35—METHODS USED TO STUDY THE ABSORPTION, REFLECTION, AND EMISSION OF INORGANIC SALTS ABOVE AND BELOW THE MELTING POINT

BY JACOB GREENBERG

NASA LEWIS RESEARCH CENTER, CLEVELAND, OHIO

In order to investigate the species that exist in fused salts it has been necessary to devise spectroscopic techniques to study these liquids at elevated temperatures. The purpose of this paper is to review some of the methods which are being used in the study of the optical properties of fused salts. A modified Beckman DU spectrophotometer with specially designed quartz cells was used initially to obtain data on these materials in the region extending from the near ultraviolet to the near infrared. Since no container materials are available which will transmit infrared radiation in the full range, withstand high temperatures, and not react with the molten salt themselves, two new methods have been devised to obtain absorption spectra of these systems above and below the melting point. In one method, the salt is supported in the interstices of a fine-mesh platinum screen, and, in the other, the salt is placed on a heated gold reflecting disk.

ABSORPTION SPECTRA

Near Ultraviolet, Visible, Near Infrared

INSTRUMENTATION

This is a relatively convenient range to work in because of the applicability of quartz optics. Figure 35–1 shows the schematic of a Beckman DU spectrophotometer which has been modified to enable us to melt a salt in a quartz cuvette and obtain its absorption spectra. One of the essential requirements in the construction of a high-temperature spectrophotometer is the maintenance and control of a constant, uniform temperature about two optical cells. In order to accomplish this, the two optical cells were embedded in a metal furnace block. This metal block was placed in an insulated mounting which was movable in order to allow for positioning of the cells in the light path. The metal furnace block and insulated mounting were then enclosed in a light-tight aluminum box which had water-cooled spacers at each end. This entire unit, consisting of the light-tight box which contained the furnace and insulated mounting, was put in place of the regular sample containing case of the Beckman DU instrument. To compensate for the elongation of the light path, a quartz magnifying lens and a photomultiplier detector were used.

The problem of thermal radiation is inherent in the use of a high-temperature spectropho-

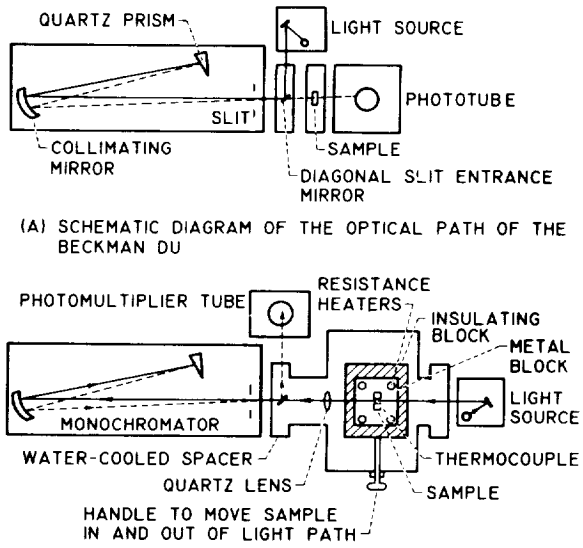

FIGURE 35–1.—Schematic diagrams of high-temperature modification of the Beckman DU.

tometer since the cell itself as well as the block emits radiation. This background radiation can be eliminated from our measurements in the following ways:

(a) special techniques for balancing the dark current
(b) use of filters
(c) monochromatizing after the light beam passes through the sample.

Above a certain temperature, depending upon the metal used (lower for steel than for copper), the first two procedures were not quite sufficient In order to reduce the amount of thermal radiation reaching the phototube, the detecting unit and light source were interchanged. In this case, light passed through the sample first and then entered the monochromator. The optical system of the Beckman monochromator was thus reversed. The photomultiplier tube was not exposed directly to the metal furnace block. The amount of background radiation reaching the detector was substantially reduced. Previous to this modification, 650° C. was the uppermost limit at which spectral data could be recorded. With the instrument modified in this manner the upper limit for recording data is the softening point of the curette. Figure 35–1 shows the schematic of the modified Beckman DU spectrophotometer.

Cells

Three sizes of quartz cell were used. If the melt contained any oxide or hydroxide, the salt would wet the quartz and upon freezing would crack the cell. If the melt was dry the salts would freeze and solidify in a solid detached from the cell walls. The 10-mm cell was made by fusing four quartz optical flats together. To this cell body was attached a tube, 10 mm in inside diameter, which consisted of a graded seal of quartz to Pyrex to facilitate sealing it to a vacuum system. The first item necessary for the construction of the 2-mm cell body was a U-shaped rib of quartz which was 2 mm thick. Two quartz optical flats were then fused onto this rib. To this cell body was attached a tube, 8 mm in diameter, which consisted of a graded seal of quartz to Pyrex. This cell was used in most of the experiments. If the melts were weakly absorbing, the measurements were repeated in 10-mm cells. If the melts were intensely absorbing, the measurements were repeated in capillary cells.

A stainless steel spacer 0.02 mm thick, 42.5 mm long and 10 mm wide was necessary for the construction of the capillary cell. This spacer was sandwiched between two quartz optical flats which were 12 mm wide. The four corners of the two optical flats were fused and the spacer removed. The cell body was then completed by fusing the two longest edges. With nitrogen gas being blown continuously through the tube to make sure that the capillary edge did not close, a quartz tube was fused to each end of the capillary body. Since convection is limited in such a cell, the edges of the cell were made to slope for ease in cleaning. This was done by pulling on the optical flats as each quartz tube was attached. Figure 35–2 shows the schematic diagram of the quartz capillary cell.

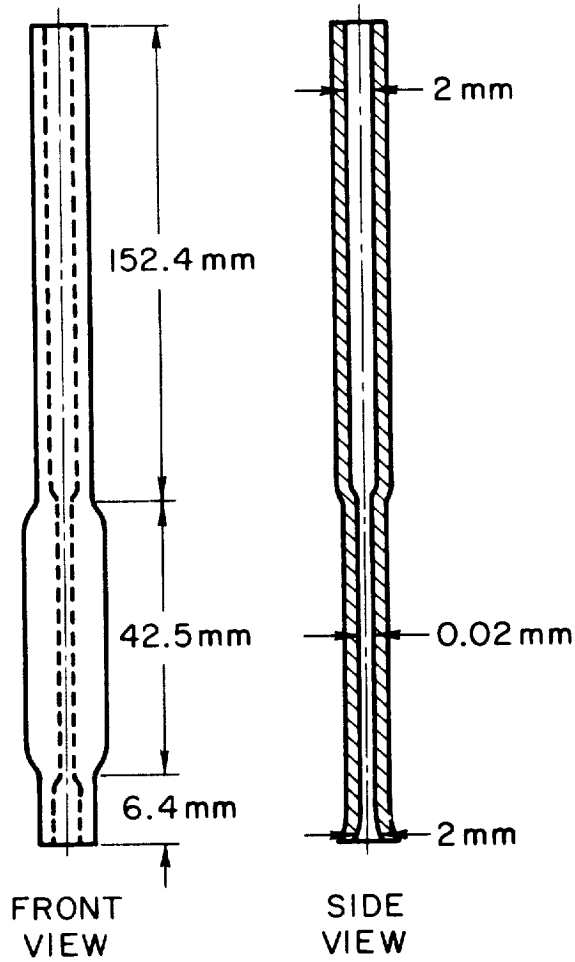

Figure 35-2.—Schematic diagram of quartz capillary cell.

Experimental Results

All the salts were carefully dried. The alkali halides, in particular, required prolonged vacuum drying at gradually increasing temperatures. All chloride and bromide salts were further dried by fusing and washing with the appropriate anhydrous halogen halide. It was necessary to wash molten silver chloride with chlorine gas and then hydrochloric acid to reverse any decomposition which occurred upon melting. With the exception of zinc bromide, the observed spectra divide the wavelength scale into two parts, one of complete transmission and one of complete absorption (ref. 2). The transition between these two regions is sharp. Since the molar extinction coefficients for pure molten salts are of the order of 10^4, in order to resolve some peaks it was necessary to do dilution experiments (ref. 3). Figure 35–3 shows the absorption edges usually observed for pure molten salts.

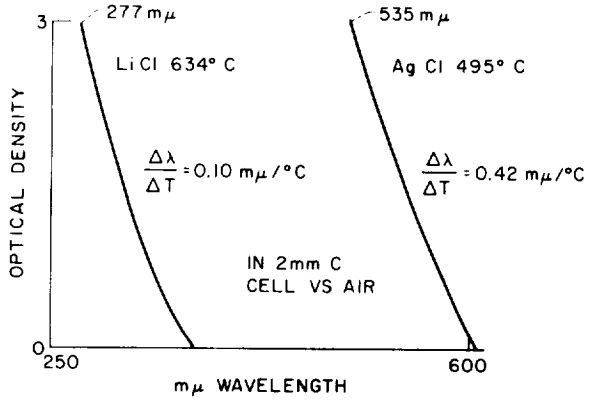

Figure 35–3.—Absorption spectra of pure salts.

These absorption edges for halide salts move to longer wavelengths (lower energies) as the temperature increases. The reason for this is that the absorption mechanism is one of charge transfer from the anion to surrounding cations. This electron transfer is made easier due to collision impact by the cation into the anion sphere as the temperature increases. This explanation of the absorption process applies very well to the eutectic mixture as shown in figure 35–4. When the mechanism of absorption is one in which an electron is ejected from a halogen negative ion, a neutral halogen atom is left behind. The ground state of a halogen atom is a doublet. This doublet was observed in the

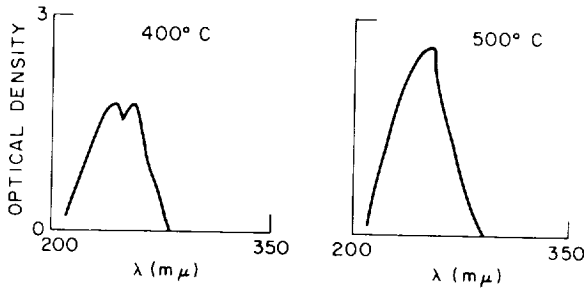

Figure 35–4.—Absorption spectra of 5 mol percent potassium iodide in lithium chloride-potassium chloride.

case of potassium iodide in lithium chloride-potassium chloride (KI in LiCl-KCl) and in lithium bromide-potassium bromide (LiBr-KBr). The peak maxima for the KI doublet in LiCl-KCl at 400° C occur at 250 mμ and 270 mμ. This separation corresponds to an energy of 0.37 ev. The doublet separation for the iodine atom which is larger than for the bromine atom, is reported as being 0.94 ev. (ref. 4). In the molten salt the doublet separation is smaller and cannot be resolved at higher temperatures. This is expected since the ground state is delocalized and therefore dependent upon long-range order. Upon melting, long-range order is destroyed and the energy levels of the ground state are brought closer to those of the excited states. This would account for the broadening of bands observed.

In the case of crystals, a region of continuous absorption indicates that an electron has been promoted to a conduction band or that the series limit of the "exciton levels" has been reached (ref. 5). Since the absorption spectra of alkali halide solutions do not show a region of continuous absorption, it is not likely that the electron moves freely through the liquid but that it is effectively bound to the positive hole which it leaves.

Again, in keeping with this interpretation it is observed that the larger the anion of the halide series (the lower the ionization potential), the lower the energy at which the absorption edge occurs.

In conclusion, spectra due to charge transfer will show definite shifts with temperature. However, if the absorption mechanism is due to inner shell transitions, the bands observed will have lower extinction coefficients and be-

come more intense as the temperature is raised. This is the case for the rare earths.

Infrared

Instrumentation

In order to overcome the materials problem, two new techniques have been devised which allow for the absorption of radiation without the interference of a container (ref. 6).

Platinum Screen Technique.—Figure 35–5 is a schematic of the platinum screen cell used for obtaining data on samples run in air. The screen was 32 mesh with 0.15-mm diameter wire. It was heated directly by passing up to 20 amp alternating current through it without complicating effects. Because of the small thermal mass, the standard cell holder for the Perkin-Elmer model 21 and model 13 was modified and used in the routine way without insulating or cooling problems. In the study of alkali nitrates, it was estimated from density and area considerations that the sample thickness was approximately 0.05-mm (ref. 7). For operating in vacuum, cells have been used which are heated directly or by use of a 2-ohm ceramic-core resistance heater placed on the outside of the platinum screen chamber. A platinum-rhodium thermocouple is attached to the center of the screen. With the screen about 20-mm wide a uniform temperature can be maintained across a 10-mm path at the center. A 32-mesh screen will diminish the intensity of the beams about 50%, and this required that the reference beam be attenuated a similar amount. The use of a single loop of platinum to support a droplet adds the complication of scattering and diffraction effects not observed in the use of the fine-mesh screen.

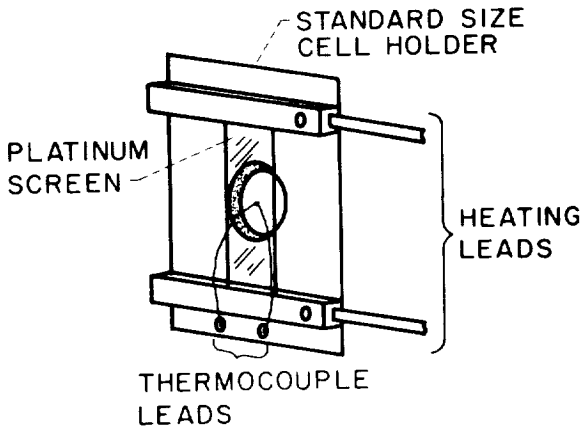

Figure 35–5.—Platinum screen apparatus.

Reflectance Cell.—The reflectance cell technique (ref. 6) was complementary to the platinum screen technique in the sense that it allowed for variations in sample thickness. The optics that were used are from a Perkin-Elmer reflectance attachment for the model 21 spectrophotometer. These optics were designed to deflect the beam perpendicularly to the light source with a minimum loss of intensity. The salts were purified (for the alkali nitrates this meant bubbling with dry nitrogen gas and filtering through Pyrex glass wool) and pipetted onto the gold (50% Au 10% Pt) disk. The window holder was then placed onto the Pyrex cup and the system evacuated if necessary. The cell, which was heated by a 2-ohm resistance heater, was brought to temperature before the salt was pipetted into it. The temperature was controlled by means of a proportional controller.

Results

There is good agreement between the data obtained by the two methods. As with the quartz curettes, if the melts were free of hydrolysis or oxidation products, no material deterioration was noted. In both cases, salts could be allowed to freeze without complicating effects.

In general, it has been observed that the infrared band intensities and position do not change very much in going through the melting point. In accordance with thermodynamic data it can be understood that at 50° C above the melting point, the ground states of the species present are not appreciably disturbed. The variation of frequency with the state of aggregation has been the subject of several investigations. The generalization that has been made is that if there are weaker bonding forces, there will be lower frequencies of oscillation (ref. 8 and 9). Therefore, a shift to lower frequencies would be expected in going from the crystal to the melt to solution. It was observed that in the case of the alkali nitrates and nitrites, in general, the fundamental frequencies shift to lower energies as the temperature is raised. However, no uniform change with temperature

was detected for the combination and overtone bands. However, the shift of the primary O-H frequency in sodium hydroxide can be related to the presence of hydrogen bonding in the melt (ref. 10).

The infrared absorption spectra of sodium nitrite, above and below the melting point, was investigated by the platinum screen technique (ref. 7). At 2μ where there is relatively little absorption in the melt due to the particular species present, there is usually a decrease in the percentage transmission upon freezing. This is primarily due to the formation of dendrites, cracks, and other scattering centers in the solid. Investigation of this portion of the spectrum can be of interest in determining the structure of the solid. In particular, these physical absorption centers will contribute to the emission of the solid sample. Similarly, in the study of liquids, an indication of polymer formation in the melt can be obtained from a study of scattering, in the case of sulfur dissolved in alkali thiocyanates (ref. 11).

EMISSION SPECTRA

In all cases, in order to account for the temperature dependence of absorption peak intensities, emission phenomena must be considered. This is particularly important in the infrared, where $h\nu$ is of the same order of magnitude as kT. We have found that there are, in general, two types of radiation emitted: one corresponding to the general thermal radiation and, superimposed upon this, a specific emission corresponding to the intrinsic absorption bands of the species present. Since the general thermal radiation is a function of mass and the presence of physical absorbing centers, by using smooth samples about 0.1 mm thick it is possible to obtain emission curves which were the mirror image of the absorption curve. Similar work has been reported on such substances as Octoil and butyl phthalate with the highest temperature reached being 175° C (ref. 12). A study of band emissivities showed that the emission intensity of any band increased with temperature in accordance with the equation $N=N_0exp-(E/RT)$. The value of E in most cases agreed with that calculated from the wavelength of the emission band.

REFLECTION SPECTRA

Surface reflectance studies have been made by using the reflectance cell and allowing the salt to freeze. The reflectance of inorganic salts has been observed to be dependent upon the type of bonding present. Silver chloride has been observed to be a very good reflector ($\sim 50\%$ in 2–15μ range). This is interpreted in terms of the multiplicity of electronic states permissible. A study of changes in the reflectance phenomena can be used to indicate changes in chemical constitution. For example, if small alumina spheres are added to silver chloride, a decrease in reflectance can be associated with the presence of compound formation.

When the salts are molten, reflectance from the surface of the liquid is relatively low. However, when the salt freezes, high reflection is observed from the solid surface at positions corresponding to fundamental absorption bands. The reason for this is related to the fact that dissipation of absorbed radiation is greater in the liquid than in the solid lattice. These types of reflection from a solid are known as Restrahlen. This phenomenon has been used to select the positions of the fundamentals as well as to produce relatively monochromatic radiation at specific wavelengths in the infrared.

CONCLUSION

In studies of this nature, the factors of container materials, sources of heat, and instrumentation problems involved with thermal radiation are of prime importance. Once the container problem has been solved, it is necessary to account for the thermal radiation. In the visible region this can be done by allowing only monochromatic light through the sample. In the infrared it has been accomplished by chopping the source beam and not the emitted beam.

Investigations are being continued to collect further information on the melting process and structure of liquids. Since the support of a liquid in the pores of a screen allows maintenance of a liquid sample in any position of the beam, a modification of this cell is now being used to obtain X-ray diffraction data above and below the melting point.

REFERENCES

1. Sundheim, B. R.; and Greenberg, J.: High-Temperature Modification of Beckman DU Spectrometer. Rev. Sci. Inst., vol. 27, no. 9, Sept. 1956, pp. 703–704.
2. Sundheim, B. R.; and Greenberg, J.: Absorption Spectra of Molten Salts. Jour. Chem. Phys., vol. 28, no. 3, Mar. 1958, pp. 439–441.
3. Greenberg, J.; and Sundheim, B. R.: Absorption Spectra in Molten Salt Solutions. Jour. Chem. Phys., vol. 28, no. 5, Nov. 1958, pp. 1029–1032.
4. Mott, N. F.; and Gurney, R. W.: Electronic Processes in Ionic Crystals, Oxford, 1940.
5. Mott, N. F.; and Gurney, R. W.: Electronic Processes in Ionic Crystals. Oxford, 1940, chap. III.
6. Greenberg, J.; and Hallgren, J.: Techniques for Measuring the Infrared Absorption Spectra of Fused Salts. Rev. Sci. Inst., vol. 31, no. 4, April 1960, pp. 444–445.
7. Greenberg, J.; and Hallgren, L. J.: Infrared Absorption Spectra of Alkali Metal Nitrates and Nitrates Above and Below the Melting Point. Jour. Chem. Physics, vol. 33, no. 3, Sept. 1960, pp. 900–902.
8. Hibben, J. H.: The Raman Effect and Its Chemical Applications. Reinhold Publ. Corp., New York, 1939.
9. Williams, D.; and Decherd, L.: The Oscillation Frequencies of Nitrates. Jour. American Chem. Soc., vol. 61, no. 6, June 1939, pp. 1382–1384.
10. Greenberg, J.; and Hallgren, L. J.: Infrared Spectra of NaOH Above and Below the Melting Point. Jour. Chem. Physics, vol. 35, no. 1, July 1961, pp. 180–182.
11. Greenberg, J.; Sundheim, B. R.; and Gruen, D. M.: Solutions of Sulfur in Fused Salts. Jour. Chem. Physics, vol. 29, no. 2, Aug. 1958, p. 461.
12. Kapff, S. F.: Infra-Red Emission Spectra of Hot Liquids. Jour Chem. Physics, vol. 16, May 1948, pp. 446–453.

36—MEASUREMENT OF SPECTRAL NORMAL EMITTANCE OF MATERIALS UNDER SIMULATED SPACECRAFT POWERPLANT OPERATING CONDITIONS

BY R. D. HOUSE, G. J. LYONS, AND W. H. ASKWYTH

PRATT & WHITNEY AIRCRAFT DIVISION, UNITED AIRCRAFT CORPORATION, EAST HARTFORD, CONNECTICUT

An apparatus was designed and constructed to determine spectral normal emittance of materials in an environment closely simulating the vacuum of space. The apparatus is capable of measuring spectral emittance of structural materials or coatings over a wavelength range accounting for the major portion of blackbody energy at the temperature at which these measurements are made. The method used is the same as that used by Larrabee and by DeVos, in which comparison is made of the radiant intensity normal from a specimen tube surface to that of a small "blackbody hole" drilled in the tube wall. The ratio of these intensities, at a given wavelength, is a very close approximation to the spectral normal emittance of the specimen surface. A comparison of the data obtained in the apparatus discussed in this paper to those obtained by Larrabee and by DeVos indicates close agreement. Furthermore, values of total normal emittance obtained by integration of the spectral emittance data compare very well with total hemispherical emittance data measured directly in another apparatus at Pratt & Whitney Aircraft. Several experimental investigations were carried out to substantiate the accuracy of the data. These included evaluation of errors introduced by scattered light from the sodium chloride window, evaluation of errors introduced by scattered white light in the monochromator, and an estimation of the quality of the blackbody hole in the specimen tube.

When spacecraft powerplants were first considered, very little thermal radiation data were available for materials which could be used in such powerplants. Furthermore, most of the existing data had not been obtained in vacuum environments. Therefore, a decision was made at Pratt & Whitney Aircraft to construct an apparatus capable of measuring spectral emittance under conditions which would closely simulate the vacuum of space. At that time a study was made of the techniques used by other experimenters for similar work.

Through consultation with Dr. Wayne B. Nottingham, Professor of Physics at Massachusetts Institute of Technology, and Dr. William L. Trousdale, Assistant Professor of Physics at Trinity College, the decision was made to use the method of Larrabee (ref. 1) and DeVos (ref. 2) for measuring spectral normal emittance.

The method of Larrabee and DeVos for measuring spectral normal emittance is to compare the radiant intensity normal from a specimen tube surface to the radiant intensity from a small blackbody hole drilled in the tube wall. This comparison is made at a series of discrete, narrow wavelength bands. Since both intensities originate from essentially the same temperature, and since the radiation from the hole is essentially the same as that from a blackbody at the tube temperature, the ratio of surface intensity to blackbody hole intensity is a close measure of the spectral normal emittance of the specimen surface.

The specimens used with the apparatus described in this paper were in the form of metal tubes with thin non-metallic coatings on the metal base. The emittances obtained were based on the essentially blackbody radiation from a cavity at the temperature of the metal substrate. This procedure had an engineering advantage for the intended application of the data in that the questions of how much tempera-

692-146 O—63——23

ture drop there was through the coating layer and how opaque the coating layer was did not require separate answers. The data, as reported, give a direct measure of the emissive power of the surface as a function of the substrate metal temperature.

APPARATUS

General Remarks

To determine the spectral emittance of materials under conditions which would closely simulate the vacuum of space and which would permit accurate and meaningful measurements to be made, a test rig was designed and fabricated that would reasonably satisfy the following basic requirements:

(1) Radiation leaving the surface of the specimen should not be reflected to a significant degree back to the specimen by the walls of the test chamber.

(2) The pressure in the chamber should be as low as possible so that adverse effects of the low outer-space pressures on the radiation properties of material surfaces could be simulated to some reasonable degree. (Pressures as low as 10^{-9} mm Hg were attained with this apparatus. All pressures at which data were taken were low enough to make the thermal conductivity of the gas negligible.)

(3) Spectral emittance should be measured over a wavelength band which would account for the major portion of blackbody energy at the temperature at which the measurements were made.

Description of Apparatus

The spectral emittance apparatus, shown in figure 36–1, consists of a test chamber, the equipment for evacuating it, a power supply for

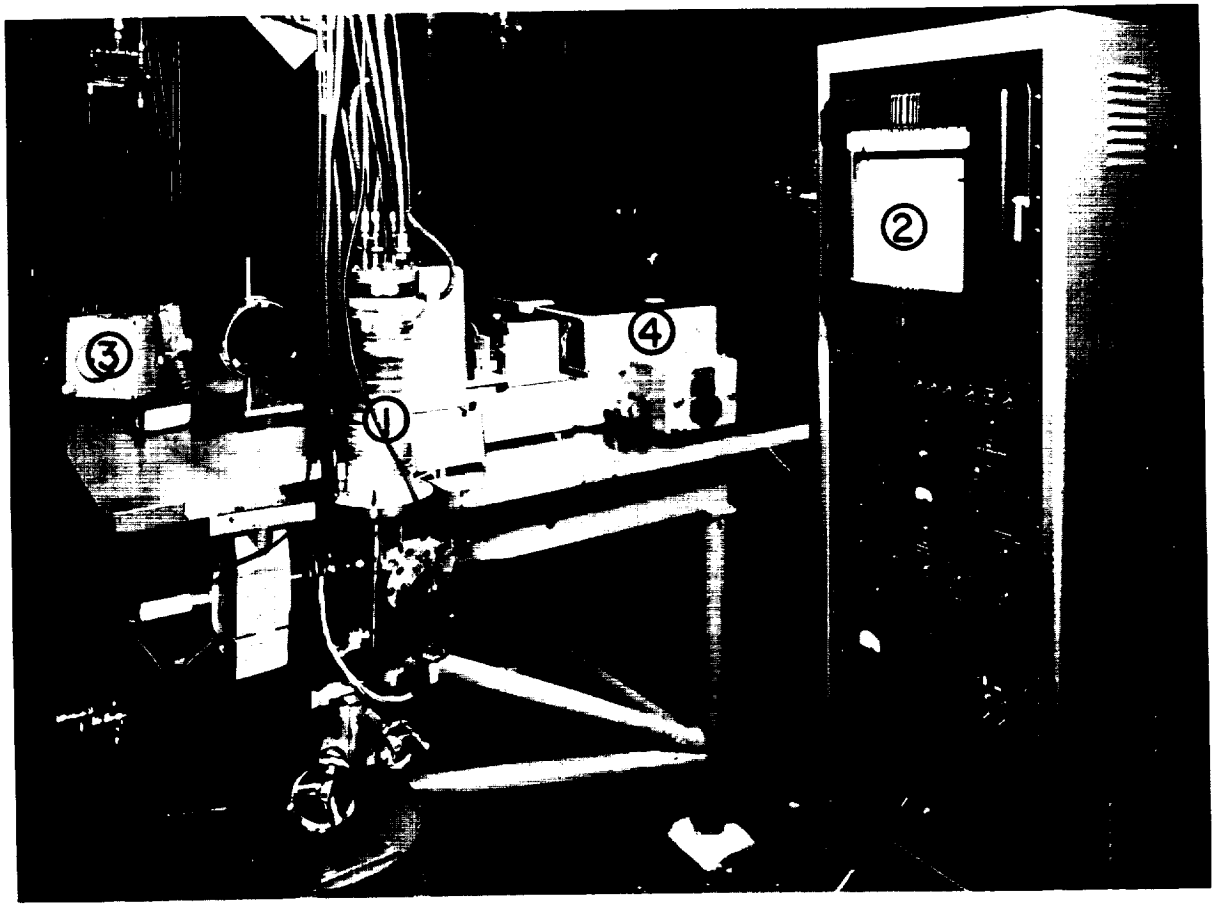

FIGURE 36–1. Spectral emittance apparatus: (1) vacuum chamber, (2) recorder, (3) optical pyrometer, and (4) spectrophotometer.

heating a test specimen in the chamber, the specimen power and temperature measuring instruments, and an infrared spectrophotometer equipped with external optics in order to view the specimen.

The test chamber is a 13-in.-long flanged tube having a 3-in. internal diameter. The inner wall is grooved and blackened to provide a low reflectance surface. The chamber is wrapped with $\frac{3}{16}$-in. diameter copper tubing in order to water-cool the walls, thereby limiting the amount of radiation emitted directly from the walls to the specimen. A 2.5-kw heating element for baking out the chamber during the initial evacuation is wound over the cooling coils.

Cover plates, to cap both ends of the tube, are bolted on, and the joints made vacuum-tight by means of 0.020-in.-diameter gold wire O-rings compressed between the polished flange surfaces. The upper cover plate is equipped with a water-cooled copper electrode assembly to carry heating current to, and also to support, the specimen. In the construction of the support, provision is made for thermal expansion of the specimen. To reduce the amount of energy specularly reflected from the chamber wall to the specimen, the support assembly positions the specimen parallel to the vertical centerline of the chamber, but displaced $\frac{3}{4}$-in. from it. The theoretical considerations for positioning the specimen off-axis are outlined in reference 3. The water-cooled power leads, the potential leads, and the thermocouple wires are secured in and insulated from the top cover plate by means of a commercial "glass" potting compound (Pyroceram). Details of the top cover plate, including the specimen holder, are shown in figure 36–2. The bottom cover plate serves as the connecting point for the evacuating system through a 1-in. inner diameter manifold.

The entire test chamber assembly is mounted on a milling machine table to permit the specimen under test to be positioned at the focal point of the spectrophotometer's optical system.

A viewing port is incorporated in the side of the chamber and consists of an optically plane, sodium chloride window cemented with epoxy resin to a stainless steel flange. The flange is bolted and sealed with a gold O-ring to a mating flange that is welded to a tubular extension from the chamber wall. This viewing port is visible in figure 36–3. A thin, rolling disk shutter made of magnetic steel is installed between the sodium chloride window and the chamber to prevent evaporated specimen material from condensing on the window during those periods when the window is not used. Such deposition of material on the window would introduce an error in the temperature measured with the optical pyrometer. A magnet is used to roll the shutter aside when readings or visual observations are to be made.

The evacuating equipment used for attaining the required low pressures consists of an oil-sealed mechanical pump in conjunction with a liquid-nitrogen cold trap and an ion-gettering pump. The mechanical pump, which has a limiting pressure of 10^{-4} mm Hg, is used during bake-out and the initial pump-down of the system. To attain pressures as low as 10^{-9} mm Hg, the ion-gettering pump is used after completion of the bake-out cycle. The degree of vacuum is measured with a Barard-Alpert ionization gage and also by monitoring the current to the ion-gettering pump.

The specimens tested in this rig are usually in the form of thin-walled circular tubes approximately nine inches long and with 5- or 10-mil wall thickness and an outer diameter of approximately 0.25 in. However, for those metals which could not be obtained in the form of drawn circular tubes, triangular tube specimens are formed by folding 1.1-in.-wide strip stock into isosceles triangles. A triangular specimen formed in this manner has a frontal width (base) of 0.1 in., a vertex angle of approximately 14° and a side of 0.5 in. Since it is difficult to apply a uniform coating to an irregular surface, the use of triangular tubes is limited to the testing of uncoated metals.

A rectangular hole, 0.035 in. wide by 0.076 in. long, is cut in the wall of each specimen tube to provide an integral blackbody radiation source to serve as a reference standard for spectral emittance measurements. The hole also permits optical pyrometer temperature measurements without requiring surface emittance corrections. The two specimen configurations are shown in figure 36–4. When circular tubes are used, the section of the tube wall directly behind the blackbody hole is flattened in such a way that a nonnormal surface is

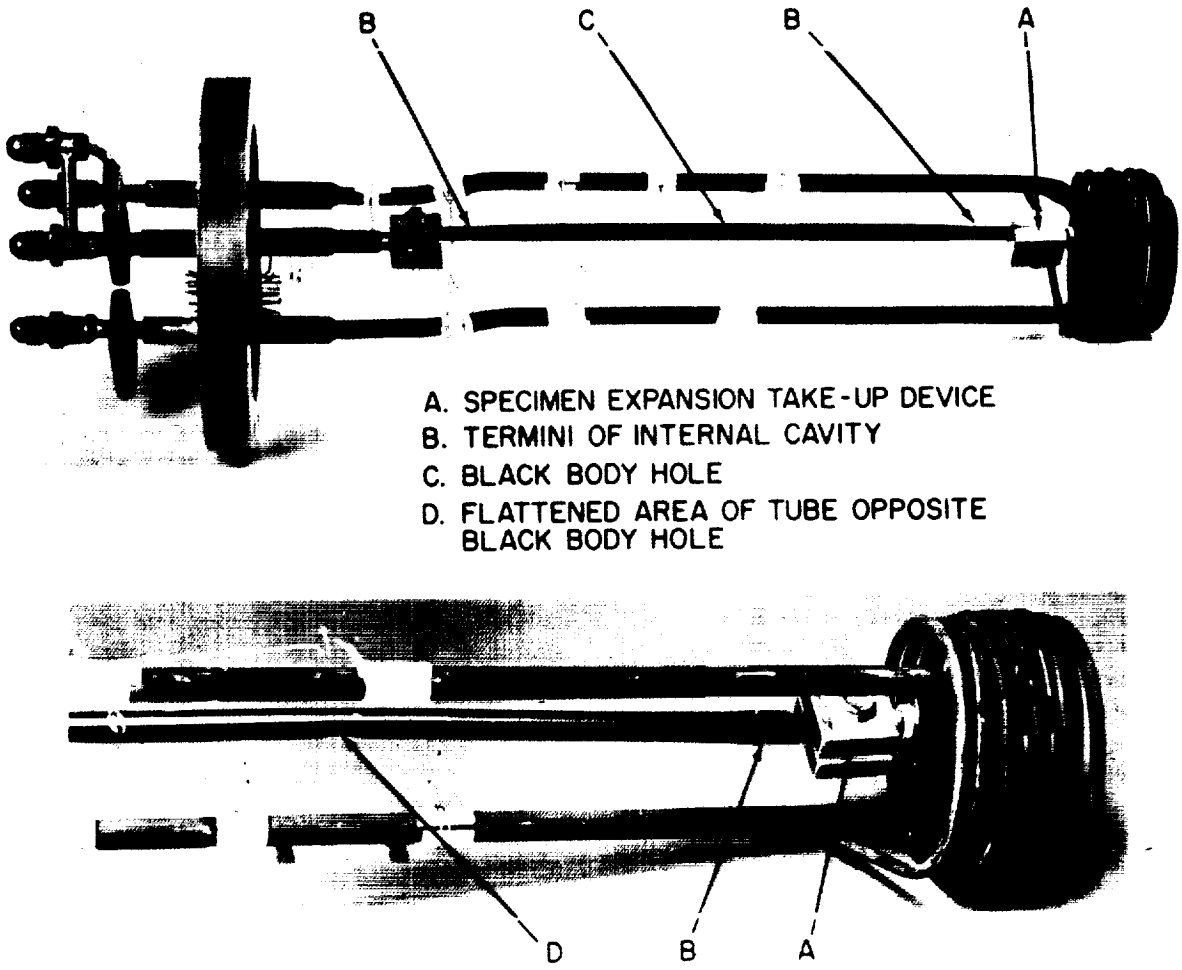

FIGURE 36-2.—Specimen and holder for spectral apparatus.

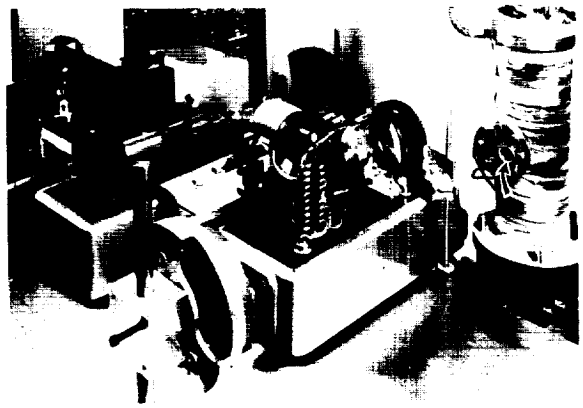

FIGURE 36-3.—Spectrophotometer with cover removed (arrow shows viewing port of vacuum chamber).

presented when viewed through the hole. This is done to ensure that the energy specularly reflected through the hole from this portion of the tube-wall inner surface emanates from other portions of the wall rather than from outside the hole.

The ends of the specimen are flattened and clamped to the upper and lower electrodes after the expansion takeup spring is compressed by an amount equivalent to the maximum amount of thermal expansion expected. The specimen is then electrically heated by its own resistance to the test temperature.

The specimen temperature when 1400° F or above is measured by an optical pyrometer and at lower temperatures by thermocouples. The optical pyrometer is mounted on a hinged bracket attached to the viewing port of the chamber and views the specimen through a plane mirror, as shown in figure 36-5. When

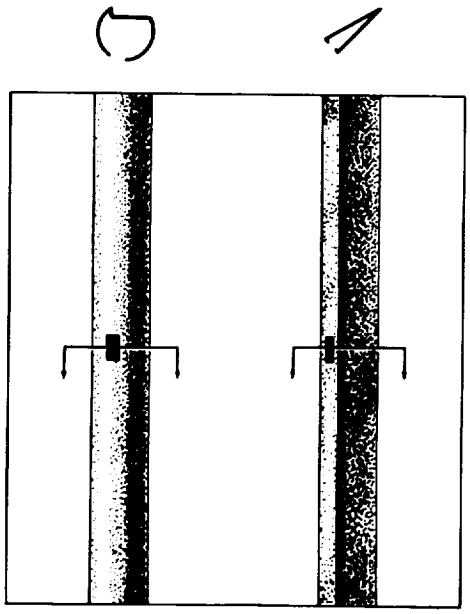

FIGURE 36–4.– Typical circular and triangular tube specimens showing 0.76 by 0.35-inch blackbody holes.

not in use, the optical pyrometer and mirror assembly can be swung clear of the viewing port. The pyrometer is calibrated in place to correct for optical losses at the sodium chloride window and at the mirror.

The outside surface area of the test section of the specimen is determined by using a cathetometer to measure the spacing between the potential leads and a micrometer caliper to measure the mean diameter of a circular tube or the strip width from which a triangular tube is formed.

The optical system for measuring spectral emittance is shown in figures 36–6 and –7 and consists of a modified Perkin-Elmer model 13–U spectrophotometer and added external optics. These external optics, used to direct the radiant energy from the specimen into the optical system of the spectrophotometer, consist of a 6-in. collecting mirror with a 24-in. radius of curvature, labeled as M–2 in figure 36–6, and two diagonal mirrors, labeled as M–1 and MO. To maintain permanent optical alignment, the spectrophotometer and external optics are bolted to a specially designed optical bench. The spectrophotometer wavelength drum has been calibrated over the wavelength range from 0.45 to 15μ by the use of the emission spectra of mercury, sodium, potassium, thorium, and cadmium, and by use of the absorption spectra of water, ammonia, carbon dioxide, and Mylar film.

Several changes currently being made to the apparatus are described in the last section of this paper.

PROCEDURE

In conducting tests in the spectral emittance rig, the tubular specimen is mounted in the electrode fixture of the top cover plate, and the complete assembly is installed in the chamber with the blackbody hole of the specimen aligned with the viewing port in the chamber wall. The evacuating process consists of two stages. First, by using the mechanical oil-sealed pump with a liquid nitrogen trap, the vacuum chamber, ion-gettering pump, and ionization gauge are pumped out while the chamber is baked at a temperature of 350° F to 375° F. This process takes 4 hr. Then, the roughing pump is valved off, and the ion-gettering pump is started. A pressure of 10^{-8} mm Hg is attained in approximately 4 hr. When required, leak-detection is performed with a helium leak-detector.

Spectral emittance data are taken with the dual-beam spectrophotometer operated in the ratio mode; that is, the ratio of measuring beam to reference beam power is directly recorded. Three separate scans over a range of wavelengths are made at each specimen temperature to establish the "100% line," the "emittance line," and the "zero line." The 100% line is established with both beams viewing the radiation from the integral blackbody; the emittance line is established with the measuring beam viewing the radiation from the specimen surface and the reference beam viewing the blackbody; and the zero line is established with the measuring beam blocked off and the reference beam viewing the blackbody. These three scans yield the ratios of measuring-beam power to reference beam power for each "line". From these ratios spectral emittance is calculated at each wavelength using the relationship.

$$\epsilon_{\lambda n}=\frac{(\text{emittance line ratio})-(\text{zero line ratio})}{(100\%\text{ line ratio})-(\text{zero line ratio})}$$

A typical record of the data obtained is shown in figure 36–8. Discussion of the fact that the

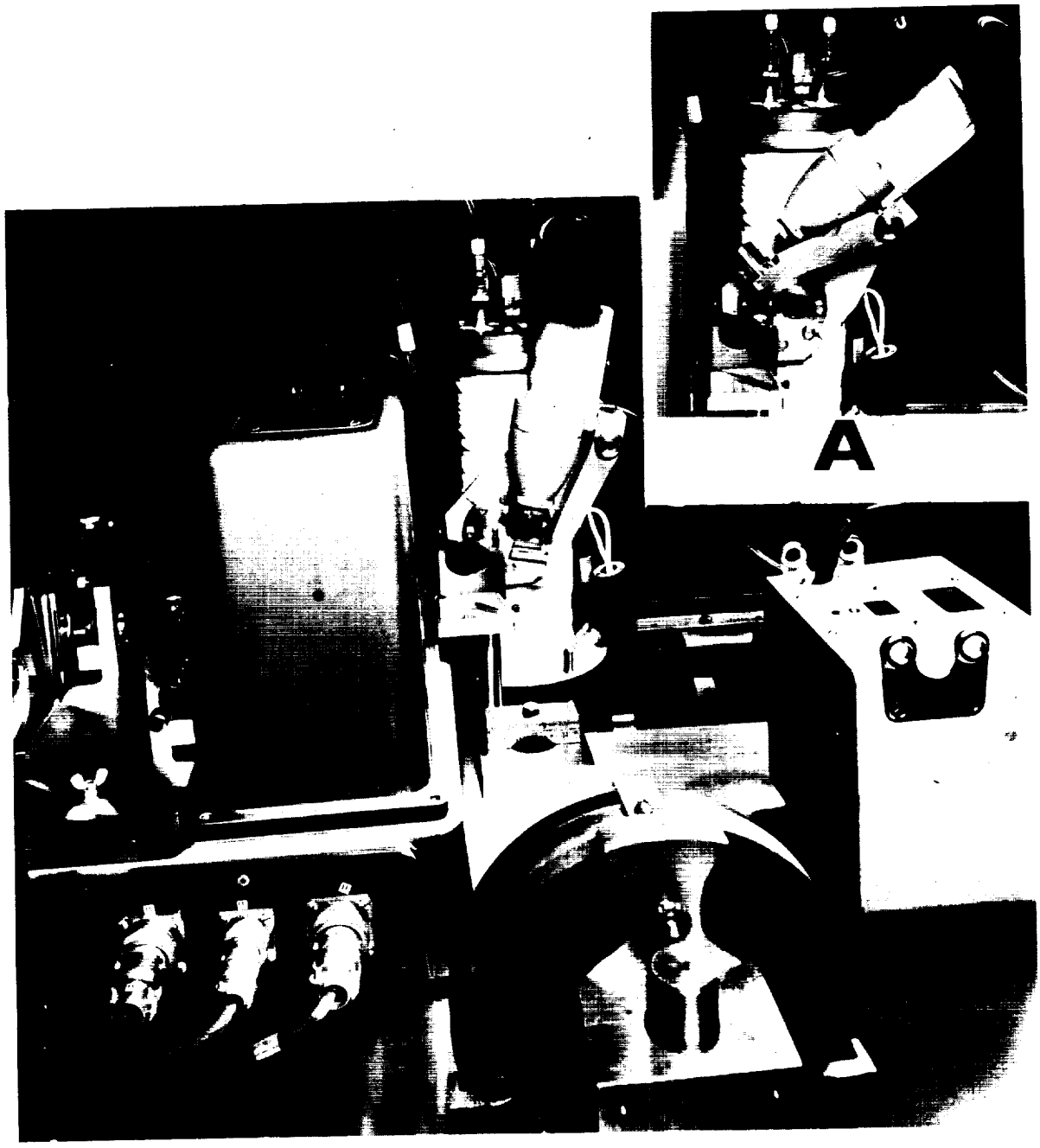

FIGURE 36–5.—Hinged bracket mounting of optical pyrometer in measuring position. (A) Optical pyrometer swung away for spectral emittance measurements.

100%-line ratio is not constant and of the reason for application of the 100% line in the calculation of emittance is presented in reference 4.

When it is desirable to obtain total normal emittance, the spectral normal emittance data are integrated in the following manner.

Total normal emittance may be written as

$$\epsilon_{tn} = \int_{\lambda=0}^{\infty} \epsilon_{\lambda n} \left(\frac{E_{\lambda b}}{\sigma T^4}\right) d\lambda \qquad (1)$$

$$= \int_{\eta=0}^{\infty} \epsilon_{\lambda n} \left(\frac{E_{\lambda b}}{\sigma T^5}\right) T d\lambda$$

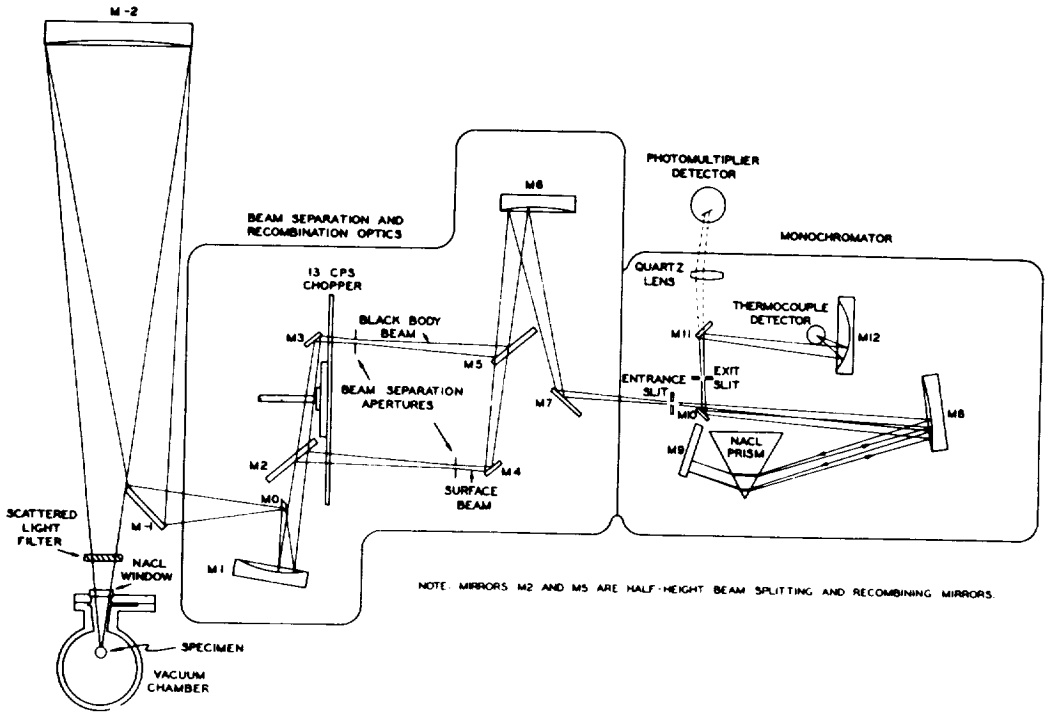

FIGURE 36-6.—Schematic diagram of the optical system of Perkin-Elmer model 13-U infrared spectrophotometer adapted for measurements of spectral emittance.

Since T is constant for each integration, equation (1) may be written

$$\epsilon_{tn}=\int_{n=0}^{\infty}\epsilon_{\lambda n}(\eta)F(\eta)d\eta \qquad (2)$$

where $\eta=\lambda T$

$$F(\eta)=\frac{E_{\lambda b}}{\sigma T^5}=\frac{(C_1/\sigma)(\eta)^{-5}}{e^{C_2/\eta}-1} \qquad (3)$$

$\epsilon_{\lambda\eta}(\eta)=\epsilon_{\lambda n}$ expressed as a function of η.

The expression

$$\int_{\eta_1}^{\eta_2}\epsilon_{\lambda n}(\eta)F(\eta)d\eta$$

is integrated graphically over the range of η corresponding to the wavelength range in which data are obtained, λ_1 to λ_2.

The error incurred from the lack of data over the entire wave-length range from zero to infinity is usually very small, and it may be reduced even further by estimating a correction. For this purpose, it is assumed that (1) the spectral emittance is constant from the longest wave length measured, (λ_2) to infinity, and is equal to the spectral emittance at the longest wavelength measured, and that (2) the spectral emissivity is constant from zero wave length to the shortest wave length measured, (λ_1), and is equal to the spectral emissivity at the shortest wave length measured. The final equation for total normal emittance is then

$$\epsilon_{t\eta}=\epsilon_{\lambda\eta}(\eta_1)\int_0^{\eta_1}F(\eta)d\eta+\int_{\eta_1}^{\eta_2}\epsilon_{\lambda n}(\eta)F(\eta)d\eta+\epsilon_{\lambda n}(\eta_2)\int_{\eta_2}^{\infty}F(\eta)d\eta \qquad (4)$$

The evaluation of the first and last terms can be simplified by using the tables contained in R. V. Dunkle, ASME Transactions 76,549 (1954), where $\int_0^{\eta_1}F(\eta)d\eta$ is written as $E_{b(0-\lambda T)}/\sigma T^4$ and is tabulated as a function of λT.

PRECISION

Possible sources of error in the results were considered to arise either in the measuring instruments, or in the specimen and chamber.

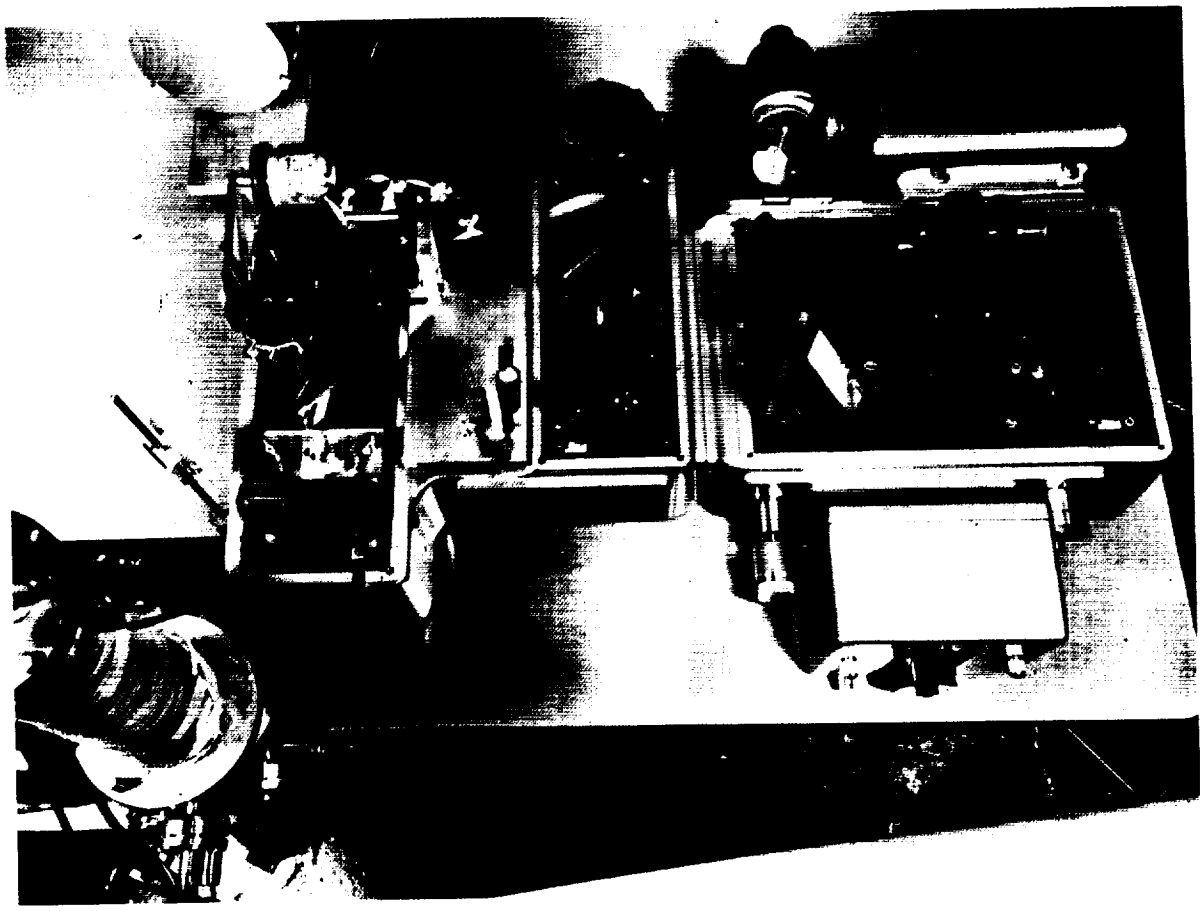

FIGURE 36-7.—Spectral emittance optical system with modified infrared spectrophotometer.

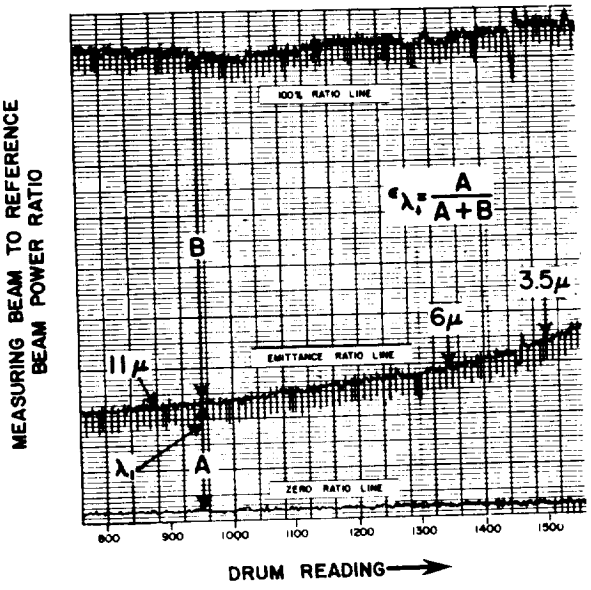

FIGURE 36-8.— Typical spectrophotometer beam power ratio scans (portion of wavelength range).

These are discussed briefly below, and in greater detail in reference 3.

Precision of the Instrumentation Only

Considering the precision of the instrumentation only, it was estimated that the accuracy of the spectral emittance values was in the order of ±2% (RMS). This figure-of-merit is concerned with the precision of the actual recording of the ratio of measuring beam power to reference beam power.

In evaluating the precision of the instrumentation, an investigation was made into the errors originating in the optical system and in the electronic system of the spectrophotometer. The sources of errors investigated included scattered light in the monochromator, imperfections in the optical system before the beam-separating apertures, and detector and amplifier noise, each of which will be considered in the order mentioned.

Scattered White Light in the Monochromator

Early in the program it was observed that the data obtained on the spectral emittance rig when using the lead sulfide detector were obviously erroneous in the wavelength region between 0.67 and 1.15 μ, and at a wavelength of 2.7 μ and beyond. The same phenomenon was observed when using the thermocouple detector at wavelengths shorter than 1.15 μ. The exact point of the departure from the expected curve was a function of the temperature of the specimen.

Figure 36–9 illustrates the discrepancies of the spectral emittance values obtained with the three different detectors. A series of experiments performed to determine the cause of these discrepancies indicated that radiation other than monochromatic radiation was reaching the detectors. The source of this interfering radiation was scattered white light inside the monochromator. To minimize the effect of scattered light components, various optical filters were obtained which would prevent light in the wave bands of peak detector response from entering the monochromator. Scattering of light at other wavelengths had an insignificant effect on the values of spectral emittance. A blue-green glass filter, Corning no. 4303, was used in conjunction with the lead sulfide detector, and a water-filled glass filter, ½ in. thick, was used for both the lead sulfide and thermocouple detectors. Further testing with and without the filters indicated that the filters effectively eliminated the discrepancies in the emittance values.

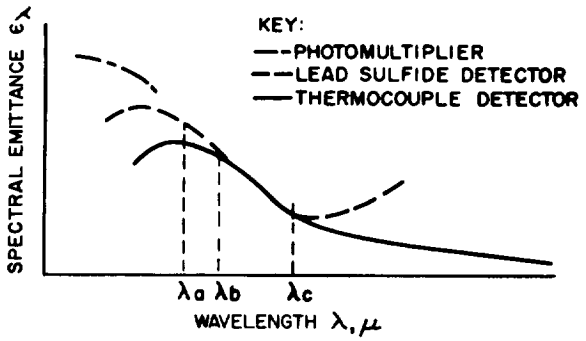

Figure 36–9.- Comparison of spectral emittance data obtained with photomultiplier, lead sulfide, and thermocouple detectors.

Imperfections in the Optical System

Imperfections in the optical system, before the beam-separation apertures, would produce beam intermixing, thereby introducing an error in the spectral emittance measurements obtained. The intermixing of the beams could be caused by improper positioning of the specimen with respect to the optical system so that the beams emanated from other than the desired areas. This was eliminated by careful optical alignment prior to each run.

The intermixing could also result from accumulated aberrations of two of the five reflecting elements before the beam-separation apertures (fig. 36–6). The most notable aberrations were astigmatism of the 6-in. collecting mirror, M–2, which was operated off-axis, and astigmatism, as well as spherical aberration. of the spherical mirror, M–1, which is operated both off-axis and with magnification. The thick viewing window in the vacuum chamber also may introduce spherical aberration. This astigmatism and spherical aberration was overcome by providing a blackbody hole of sufficient size so that the sampling area within the blackbody was well removed from the hole boundary and, in addition, by selecting the location of the sampling area on the surface so that it was sufficiently removed from the blackbody hole.

A third cause for intermixing of the beams could be scattered light resulting from surface imperfections, as well as foreign material, on the vacuum chamber window, and the five reflecting surfaces before the beam-separating apertures.

Since the error due to scattered light could not be eliminated, it was necessary either to compensate for it or to show it to be insignificant. Experiments were conducted to determine the regions of the specimen from which the light that became scattered originated, and to ascertain the percentage of surface energy which was scattered into the blackbody beam during actual emittance measurements. The test results showed that the errors caused by the presence of aberrant and scattered light could be neglected by reason of the size of blackbody hole used, if the salt window was in good optical condition.

Detector and Amplifier Noise

Detectors and amplifier noise was found not to be a problem with the signal levels available when using the subject instruments.

Errors Due to Specimen Configuration and Chamber Design

Sources of error due to specimen configuration and chamber design were considered separately from the instrumentation. Three such sources of error which were considered and evaluated are discussed briefly below.

Reflected Power Within the Chamber

One source of error was reflected power within the chamber, such as the power emitted from the specimen and reflected, first by the chamber walls, then from the specimen, and finally into the "surface beam" entering the spectrophotometer. This was found to be insignificant, provided that the walls of the chamber had high absorptance, and provided that the sample was positioned away from the vertical centerline of the chamber.

Temperature Difference Between Surface and Blackbody

The difference between the surface temperature and the internal temperature of the blackbody was considered by defining the measured results as "effective emittance", a value which was desired for heat transfer calculations.

Nonblackness of Blackbody Hole

The hole in the specimen fell short of behaving as an ideal blackbody. This departure from an emittance of unity could be due to either or both of two factors. The hole area might not be negligibly small in comparison to the internal area of the cavity, resulting in the hole having an emittance less than 1.0 if the internal cavity was at a uniform temperature. By using the analytical method of DeVos (ref. 4), the quality of the blackbody radiation was estimated to be no less than 97.5%.

A second factor could be that the effective temperature of the hole might not necessarily be the same as that of the nearby surface because the heating of the tube was not necessarily uniform. The nonuniform heating resulted both from nonuniform wall thickness and from nonuniform current density attributable to the presence of the hole. As regards the latter effect, the hole caused the current density to be less than normal at both ends of the hole (near the centerline), and greater than normal near all four corners of the hole, as well as along its two sides. This phenomenon was particularly evident during the testing of a high-emittance coating on a stainless steel tube.

Previous tests conducted on tubular specimens made of substrate metals with higher thermal conductivities did not have sufficient temperature perturbation in the vicinity of the blackbody hole to be detected visually. However, the observation during the testing of the stainless steel tube raised the question of the effect of local temperature perturbation on the quality of the blackbody, and therefore, on the accuracy of the emittance data obtained.

The quality, or more correctly effective emittance, of the standard blackbody hole was evaluated by comparing the apparent surface emittance adjacent to the 0.035-in. by 0.070-in. blackbody used in the regular emittance measurements, with the surface emittance near two 0.018-in.-diameter, "ideal," blackbody holes located approximately 0.75 in. above and below the standard hole. By using single-beam optics and extremely accurate alignment, it was possible to use the 0.018-in. holes for this check, although it was not practical to use these small holes for routine measurements employing the dual-beam optics. The effective emittance of the standard blackbody hole was determined as the ratio of the true to the indicated surface emittance, where the true emittance of the surface was taken as that measured at the 0.018-in. holes. The effective emittance of the standard blackbody hole then becomes

$$\epsilon_{\lambda he}=\frac{I_{\lambda h}}{I_{\lambda b}(T_s)} \tag{5}$$

where $I_{\lambda b}(T_s)$ is the intensity of an ideal blackbody at temperature T_s, the temperature of the nearby surface spot and $I_{\lambda h}$ is the actual intensity of the standard hole. For a surface spot near the ideal hole the true spectral normal emittance is:

$$\epsilon_{\lambda s}(T_s)=\frac{I_{\lambda s}(T_s)}{I_{\lambda b}(T_s)} \tag{6}$$

Substituting $I_{\lambda b}$ (T_s) from (6) into (5)

$$\epsilon_{\lambda hc}=\frac{\epsilon_{\lambda s}(T_s)I_{\lambda h}}{I_{\lambda s}(T_s)}$$

where

$\epsilon_{\lambda s}$ true spectral normal emittance of the surface, which is that measured at the small ideal blackbody holes at temperature (T_s)

$I_{\lambda h}$ radiation intensity from the standard blackbody hole.

$I_{\lambda s}$ radiation intensity from the specimen surface near the standard blackbody hole.

These experiments were carried out on both stainless-steel and columbium tubes. High-contrast photographs of these tubes heated to 1600° F are shown in figures 36–10 and –11. It may be noted that temperature perturbation was much less severe in the vicinity of the standard blackbody hole in the case of the columbium tube. Temperature perturbation was negligible for both tubes in the vicinity of the small (0.018-in.) holes. The temperature along the length of the columbium tube was not uniform, apparently due to a taper in the tube wall thickness. As a result of this, the experimental evaluation of the quality of the blackbody hole in the columbium tube was of questionable value, as indicated by the lack of agreement between the surface emittance measured near the two small holes. However, lack of temperature perturbation at the hole made the DeVos calculation applicable. In the case of the stainless-steel tube coated with chromium black, the surface emittances measured at the small holes agreed within 0.1%; therefore, the experimental values of the quality of the standard blackbody hole were considered accurate. The fact that these experimental values were greater than 1.00 (1.04 at 0.6 μ and 1.012 at 2.0 μ) was undoubtedly referable to the significant temperature perturbation in the region of that hole. This investigation demonstrated the desirability of using specimen tubes

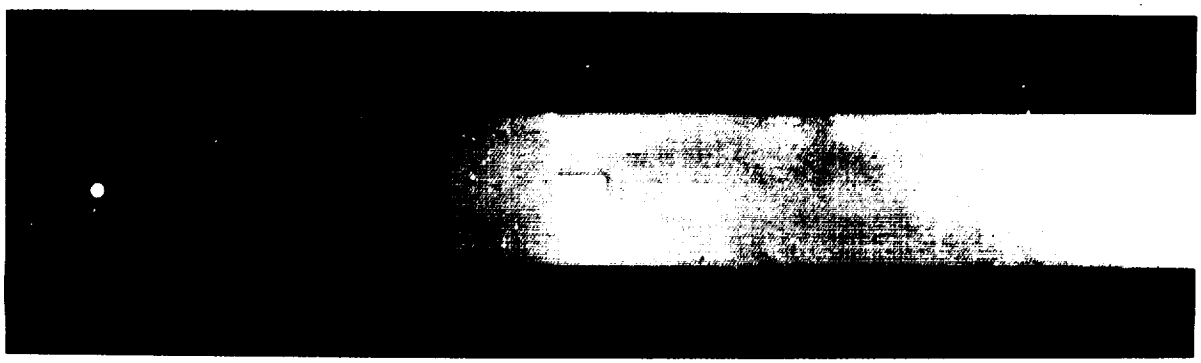

FIGURE 36–10.—Columbium tube with vapor-blasted surface.

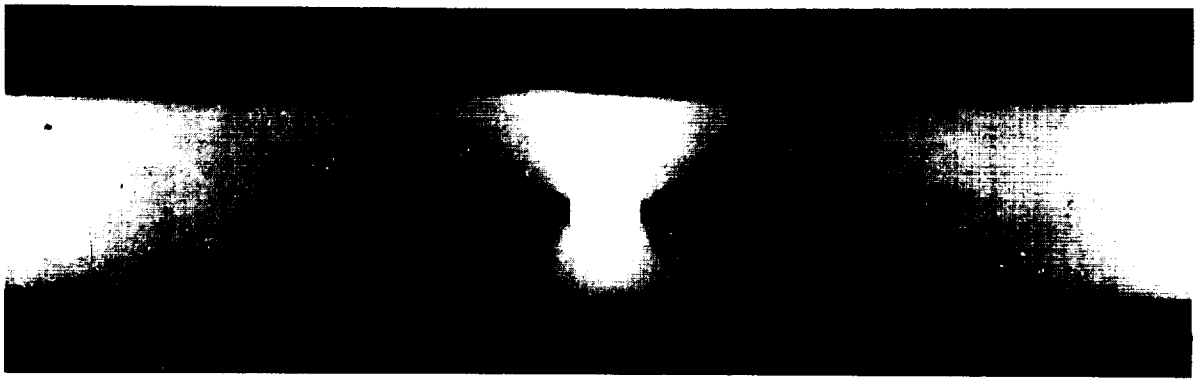

FIGURE 36–11.—Stainless steel tube with chromium black coating.

with high thermal conductance and the necessity of having tubes of uniform wall thickness.

RESULTS AND DISCUSSION

Several materials, including coatings and refractory metals, were tested in the spectral emittance rig. Tungsten was chosen as the most suitable one for checking the validity of the data because of the availability of reliable spectral emittance data for comparison. A wedge-shaped specimen was made of tungsten and used for this purpose.

Exact agreement between the published data and those obtained with this apparatus was not anticipated since emittance is a property of the specimen surface as well as of the material from which the specimen is made. However, results obtained during the checkout running agreed well with the previous data of the other experimenters. As shown in figure 36–12, measurements of spectral normal emittance were taken at temperatures of 1700°, 2110°, and 3090° F in the wavelength region between 0.5 and 12.0μ. In comparing the results of this testing with the results obtained, by DeVos (ref. 1) and Larrabee (ref. 2), it was noted that all of the data showed the spectral emittance to decrease with increasing temperature in the visible wavelength range, and to increase with increasing temperature in the infrared wavelength range. The node at which the constant-temperature lines of spectral emittance cross was noted at approximately the same wave length as shown by DeVos. Figure 36–13 compares

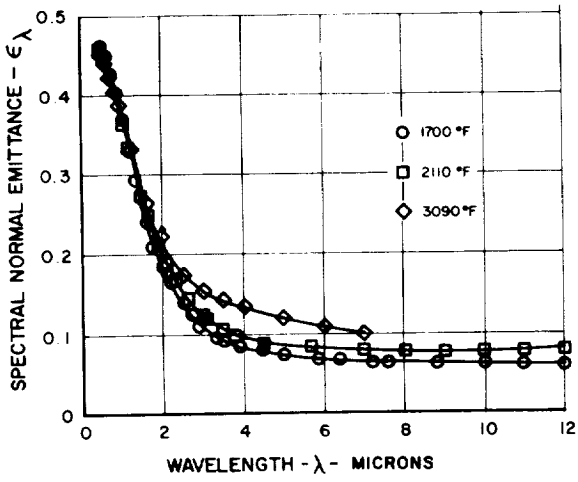

FIGURE 36–12.—Spectral normal emittance of tungsten.

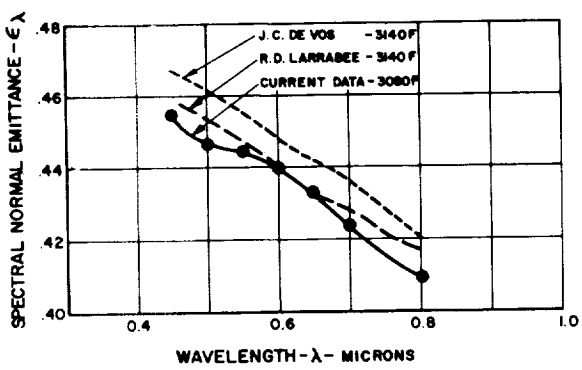

FIGURE 36–13. Comparison of spectral normal emittance of tungsten data.

the results obtained by Larrabee and DeVos to those obtained in the present work in the visible wavelength region.

Values of total normal emittance were obtained by integrating the spectral emittance data by the procedure outlined. These values compare very well with total emittance values obtained directly in another apparatus at Pratt & Whitney Aircraft.

Rig Modifications in Progress

Several changes are currently being made to improve the accuracy of the apparatus and to simplify the test procedure:

(1) The spherical collecting mirror, M–2, has been replaced with a specially designed off-axis ellipsoidal mirror. The new mirror eliminates astigmatism previously encountered due to off-axis operation and thus provides better resolution of the two beams. It is of larger size (8 in.) than the old one (6 in.) but of the same focal length. The larger collecting surface permits greater flexibility of data taking (smaller blackbody hole, lower operating temperature for a given wavelength, or a smaller wavelength band for a given temperature) due to the increased energy available for a given set of conditions.

(2) The method of separating the two beams by means of half-height beam separating mirrors, has been changed. The beams will be separated by a two-hole aperture located at the prime focus of the large collecting mirror, M–2. Two plane diagonal mirrors will then be used to reflect the beams, in slightly different directions, to the small spherical mirror, M–1.

The sample surface beam leaving mirror M–1 will be intercepted by a half-width mirror (replacing the existing M2). The blackbody beam leaving mirror M1 will pass the half-width mirror and will be intercepted by mirror M3. The recombining optics will remain essentially the same.

(3) As a result of the increased amount of energy collected with the large mirror, emittance samples for future testing will have a smaller blackbody hole. This will improve the quality of the blackbody hole.

(4) A new vacuum-chamber cover and sample-holder assembly, which will permit easier alignment of the specimen with reference to the optical system, has been constructed.

REFERENCES

1. Larrabee, R. D.: The Spectral Emissivity and Optical Properties of Tungsten. M.I.T. Res. Lab. Electronics Tech. Rep. 328, May 21, 1957.
2. DeVos, J. C.: A New Determination of the Emissivity of Tungsten Ribbon. Physics, vol. XX, 1954, pp. 690–714.
3. Anon.: Measurement of Spectral and Total Emittance of Materials and Surface Under Simulated Space Conditions. PWA–1863, Pratt & Whitney Aircraft Co., 1960.
4. DeVos, J. C.: Evaluation of the Quality of a Blackbody. Physics, vol. XX, 1954, pp. 669–689.

37—THE MEASUREMENT OF TOTAL NORMAL EMITTANCE OF THREE NUCLEAR REACTOR MATERIALS

BY T. LIMPERIS, D. M. SZELES, AND W. L. WOLFE

UNVERSITY OF MICHIGAN, ANN ARBOR, MICHIGAN

The purpose of this study was to determine the total normal emittance at different temperatures of several materials used in the Enrico Fermi nuclear reactor presently under construction in Monroe, Michigan. These materials are 304 stainless steel, A–7 carbon steel, and borated graphite. The surfaces of these materials exhibit a wide range in degree of (non-uniform) oxidation.

THEORY

Emittance may be defined as the ratio of radiation emitted from a sample surface to that emitted from an ideal radiator or blackbody, both having exactly the same geometrical and temperature conditions. (The emittance of a blackbody is by definition 1.) Total emittance implies that radiation of all wavelengths is being considered, and normal emittance implies that the observation point for detecting the emitted radiation is on an axis normal to the radiating surface. According to the Stefan-Boltzmann law the amount of power per unit area emitted from a material is given by the relationship

$$W=\epsilon\sigma T^4$$

where W is the radiant flux density at the surface, ϵ is the emittance, σ is the Stefan-Boltzmann constant, and T is the absolute temperature in degrees Kelvin (° K).

The radiant flux density at the surface from a blackbody is given by

$$W_b=\sigma T_b^4 \tag{1}$$

The radiant flux density at the surface of a sample material is

$$W_s=\epsilon_s\sigma T_s^4 \tag{2}$$

Expressions (1) and (2) can be used to solve for ϵ_s in two ways: T can be made equal to T_b, the equal temperature method; and W_s can be equated to W_b, the equal flux method. In the equal-temperature method the emittance is finally expressed as

$$\epsilon_s=\frac{W_s}{W_b} \tag{3}$$

while in the equal flux method, it becomes

$$\epsilon_s=\left(\frac{T_b}{T_s}\right)^4 \tag{4}$$

At first glance it appears as though determination of the emittance of a material is an easy task; the experiment is simply arranged so that either the temperatures or radiant fluxes are equal and the ratio of the other quantities are then determined. But the experimenter is troubled immediately by two problems: radiation absorption by the atmosphere and the radiant flux of the environment. The absorption by the atmosphere is a highly complicated function of wavelength and this makes any analytical treatment of it very difficult—if not impossible. Radiation from the surroundings can be accounted for both experimentally and theoretically. The equal temperature method is used.

A radiometer produces an electrical signal which is dependent on the level of radiation incident upon the sensing element. In a vacuum the expression for the linear region of response is given by

$$V_s=aW_s+b \tag{5}$$

or if expressed as a function of temperature

$$V_s=a\epsilon_s\sigma T_s^4+b \tag{6}$$

where V_s is the electrical signal generated, a is

a proportionality constant, and b is the electrical signal induced by the radiant flux from the environment. A plot of this expression (V_s against T^4) is, of course, a straight line with an intercept at b on the V_s coordinate. Emittance can then be determined by first measuring the flux from the sample and then that from the reference blackbody. Plots of V_s against T^4 for the sample, and V_b against T_b^4 are obtained, and effective signal voltages V_s' and V_b' can be found, where V_s' is defined as

$$V_s' = V_s - b = a\epsilon_s \sigma T_s^4 \tag{7}$$

Similarly,

$$V_b' = V_b - b = a\sigma T_b^4 \tag{8}$$

Then by taking the ratio of equations (7) and (8)

$$\frac{V_s'}{V_b'} = \frac{a\epsilon_s \sigma T_s^4}{a\sigma T_b^4} = \epsilon_s \left(\frac{T_s}{T_b}\right)^4$$

By finding V_s' and V_b' at the same temperature (i.e., $T_s = T_b$) the solution for the emittance of the sample is

$$\epsilon_s = \frac{V_s'}{V_b'} \tag{9}$$

In this discussion it was assumed that the emittance is not a function of wavelength. Also, it was assumed that the atmosphere did not affect the measurements. Both of these assumptions must be investigated. The atmosphere may be taken in account as follows: Let $\tau\ (T)$ represent the percentage transmission of total blackbody energy as a function of blackbody temperature. Since a greybody has the same spectral shape as a blackbody but different absolute amplitude, $\tau\ (T)$ also represents the percentage of absorbed greybody radiation as a function of greybody temperature. With this in mind one can then determine ϵ_s from in-atmosphere measurements.

V_s' and V_b' now become

$$V_s' = a\tau(T)\epsilon_s \sigma T_s^4 \tag{10}$$

and

$$V_b' = a\tau(T)\sigma T_b^4 \tag{11}$$

and again the ratio of equations (10) and (11) is

$$\frac{V_s'}{V_b'} = \frac{a\tau(T)\epsilon_s \sigma T_s^4}{a\tau(T)\sigma T_b^4} = \epsilon_s \left(\frac{T_s}{T_b}\right)^4$$

Therefore, $\tau\ (T)$ cancels from the equation, and, with the equal-temperature method, ϵ_s has the same expression as in a vacuum (eq. 9). Careful consideration of spectral dependence of atmospheric absorption indicates that the equal-energy technique would lead to erroneous results since in this method the reference blackbody and sample are at different temperatures; i.e., $\tau\ (T_1)$ in the numerator is different from $\tau\ (T_2)$ in the denominator, where T_1 =sample temperature and T_2=blackbody temperature.

EXPERIMENTAL PROCEDURE

The steps of the experiment can be outlined as follows:

1. Determine if the samples are greybody radiators.
2. Obtain the relationship between signal voltage and temperature for all sample types; do the same for a reference blackbody.
3. Reduce the data to effective signal voltage and compute the emittance.

The following is a more detailed description of these steps.

Greybody Identification

The first step is to determine whether the samples have an emittance that does not change appreciably with wavelength over the spectral region considered and in the temperature range of interest. This is a relatively straightforward problem in spectroscopy and does not require an absolute measurement of power. To accomplish this, a double-pass, double-prism, Leiss monochromator with sodium chloride prisms was used along with the necessary electronics (Perkin-Elmer preamplifier, filter circuits, and thermopile) to observe the monochromatic radiant emittance from 1 to 12 μ, of the samples at three temperatures, 593° K, 753° K and 923° K. The resulting spectral distribution of flux was compared with the spectral distribution of flux from a reference blackbody at the same three temperatures. The peak of the blackbody and sample curves are normalized to unity, and the curve contours are compared. If the samples are greybody radiators the envelopes of the spectral distribution of flux curves should be congruent with the corresponding blackbody curves. This was indeed found to be the case.

The experimental setup used in performing this measurement is shown in figure 37-1. Figure 37-2 is a block diagram of the same

experiment. The wavelength dependence of the radiant flux from one sample at 923° K along with the radiant flux spectra from the reference blackbody at the same temperature is given in figures 37–3 and 37–4. The blackbody curve differs somewhat from the corresponding sample curve in some regions because the measurements were made on different days, and the atmospheric absorption bands change in intensity depending on the ambient temperature, pressure, and relative amount of atmospheric constituents. However, there is little doubt from observing the data that the samples are greybody emitters.

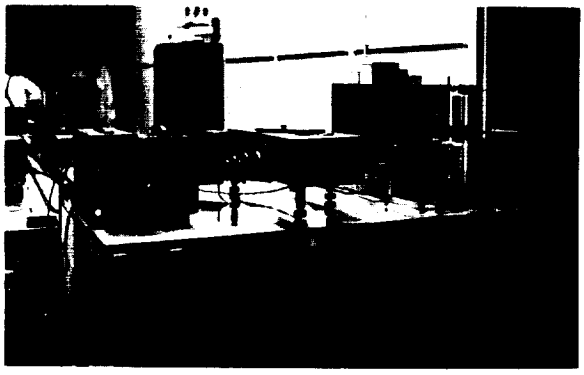

FIGURE 37–1.—Equipment setup for monochromatic studies.

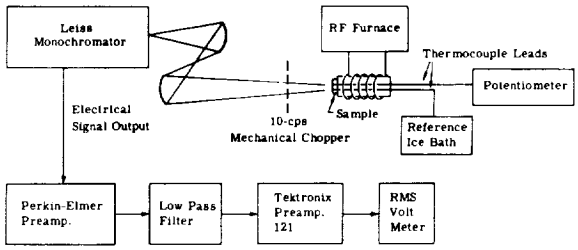

FIGURE 37–2.—Block diagram for monochromatic studies.

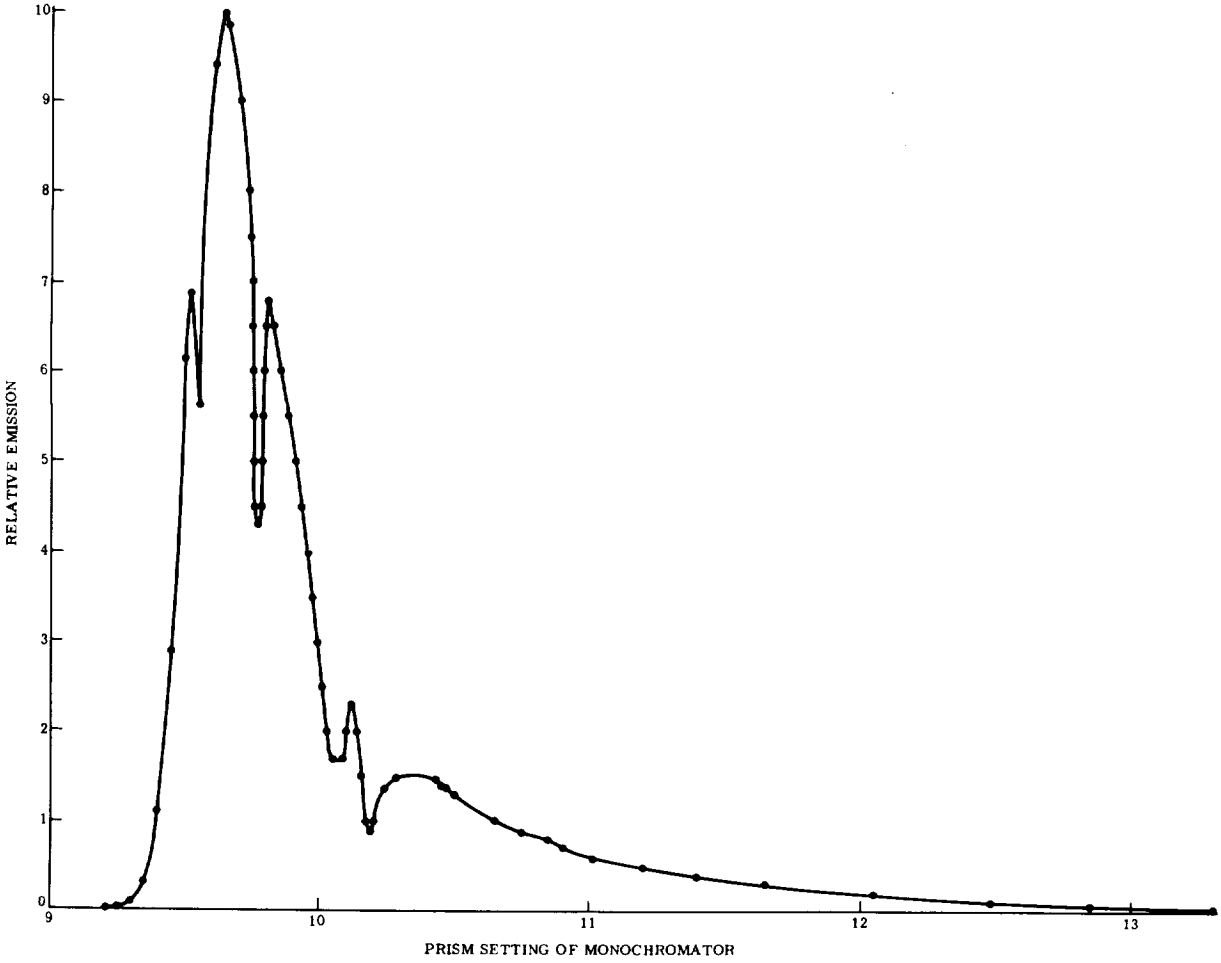

FIGURE 37–3.—Spectral flux distribution of 650° C blackbody.

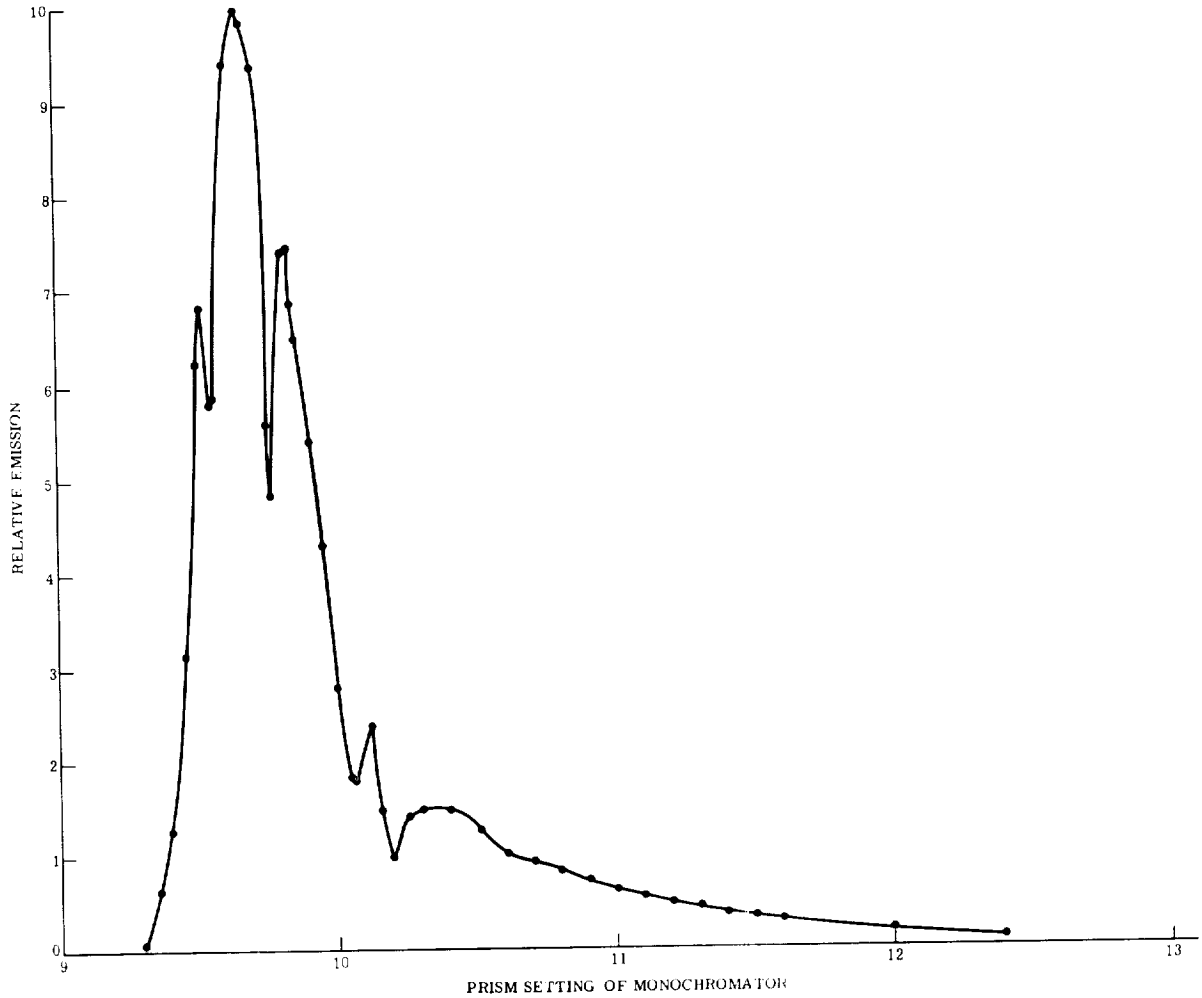

FIGURE 37–4.—Spectral flux distribution of A–7 carbon steel at 650° C (slightly pitted).

Relationship Between Signal Voltage and Temperature

Next it is necessary to establish a comparison measurement of the ratio of fluxes from the samples and an adjustable blackbody, avoiding an absolute measurement of power. To do this a Barnes radiometer is set up and its field of view carefully measured. Then the sample and a blackbody are placed behind a pair of identical baffles, which lie on an axis at right angles to the radiometer optical axis (fig. 37–5 and 37–6). The optical components are then aligned carefully so that the blackbody or the sample appears in the same place in the field depending on the position of the switching mirror. The path lengths from the sample to the radiometer and from the blackbody to the radiometer are the same.

A Barnes R 4 radiometer (ref. 1), shown in figure 37–1 is used to provide a signal voltage dependent upon irradiance level. This radiometer employs 4-in. Cassegrainian optics with a 0.3 by 0.3-mm thermistor detector. It is assumed that the detector has a flat spectral response[1] and that the front-surface mirror optics do little to distort the spectral character of the incident radiation. The optical system is designed to provide some degree of variable focusing from infinity to 25 ft although this is not altogether possible with a Cassegrainian system. For a focus setting of 25 ft the field of view of the radiometer, 25 ft from the sensing head, is determined by scanning in three

[1] This implies that the detector provides a constant output voltage regardless of the spectral content of the radiation as long as the irradiants is constant.

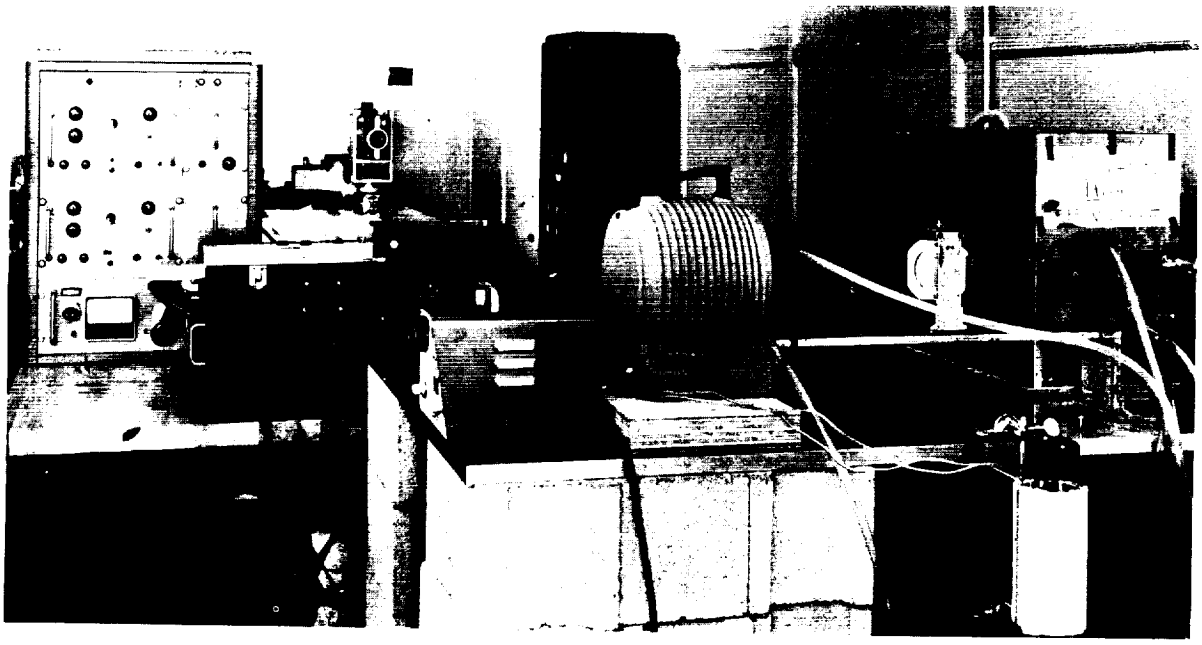

FIGURE 37-5.—Emittance experimental setup.

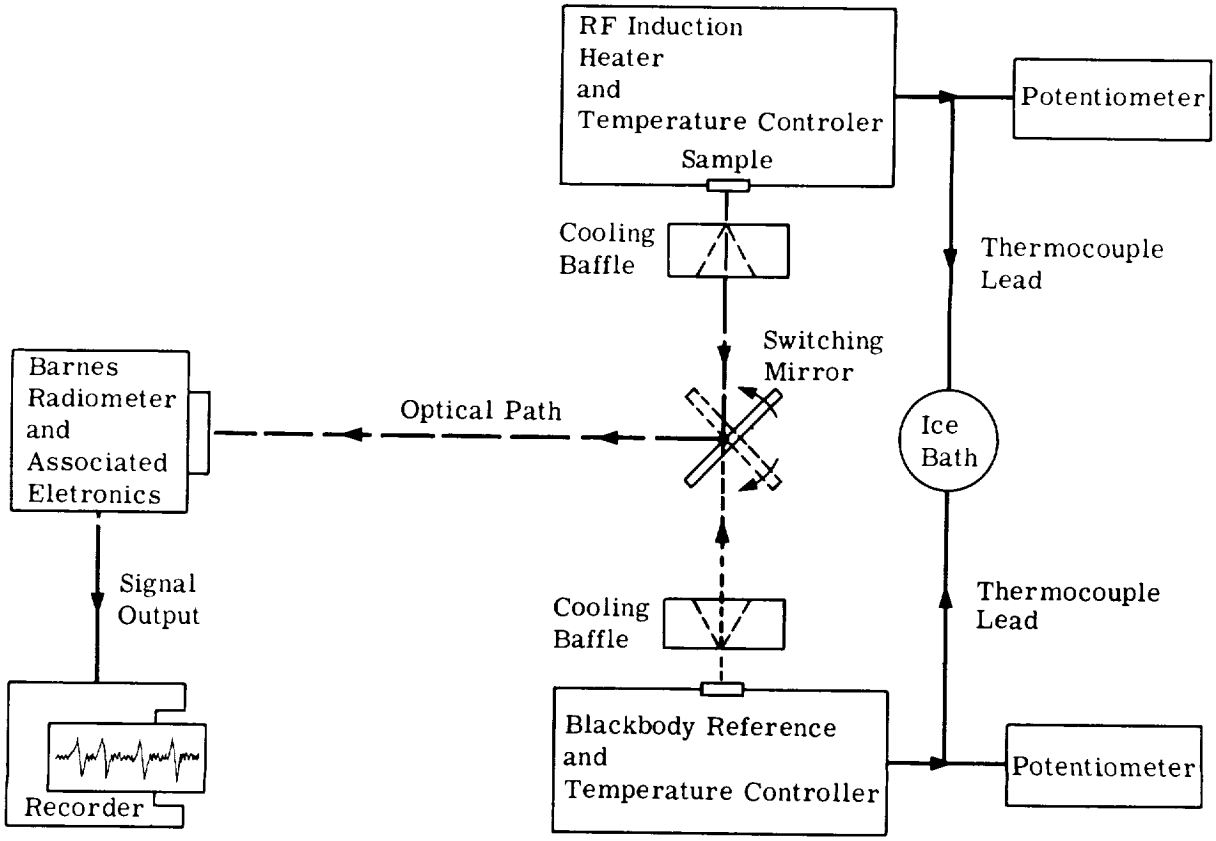

FIGURE 37-6.—Block diagram of experimental setup.

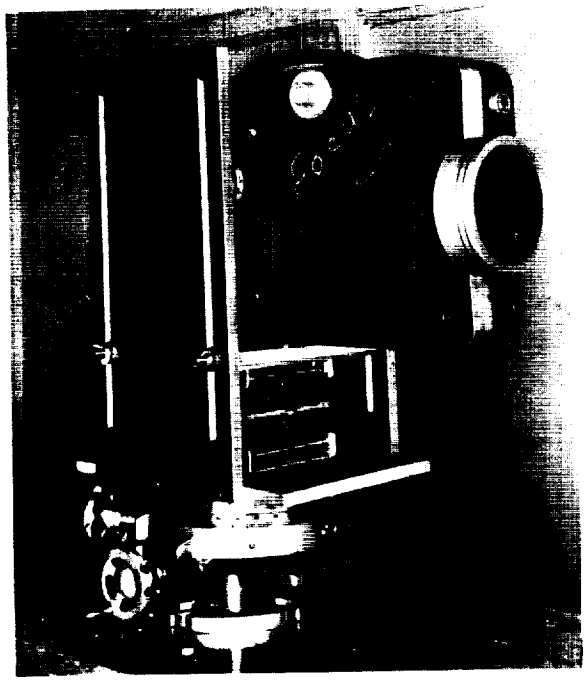

FIGURE 37–7.– Radiometer and mount assembly.

dimensions a variable slit illuminated by a Nernst glower. A map is made in this manner to show the responsitivity of the system as a function of spatial position of the source. Equal relative response lines in the plane 25 ft from the radiometer are concentric squares which are somewhat distorted. The one-half-power points of relative response form a square 2 cm on a side, and for all practical purposes the zero-relative-response points form a square 2.5 cm on a side.

A rigidly mounted switching mirror (fig. 37–8) facilitates switching the field of view of the radiometer from the sample to the reference blackbody. The mirror is a 3-in. front-surfaced aluminized reflector with the axis of rotation lying along the front surface. The mirror assembly is mounted on an aluminum table. Two water-cooled baffles are mounted on the switching assembly. The baffles are cut from 2-in. by 1.5-in. copper waveguide and copper conical sections (1 mm thick) are inserted in the baffles. The largest diameter of the cone is 25 mm and the smallest diameter is 3 mm. The axes, defined by the two cones, are aligned (collinear) and intersect the switching mirror at the axis of rotation (fig. 37–6). With this arrangement the radiometer field of view lies on the 1-in. cone. The cone is cooled to tap-water temperature. The radiometer observes a 3-mm diameter circle on the sample emitting surface, and the same area of the blackbody emitting surface, as well as some of the cold baffle (fig. 37–9). A theodolite is used to align the system optically.

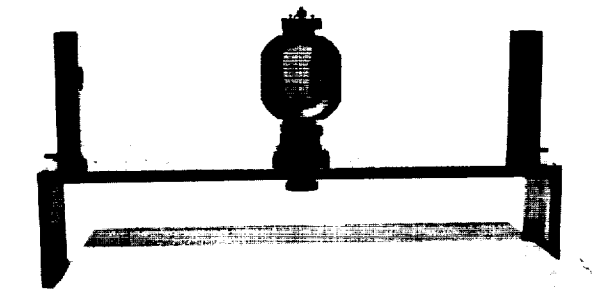

FIGURE 37–8.– Switching mirror assembly.

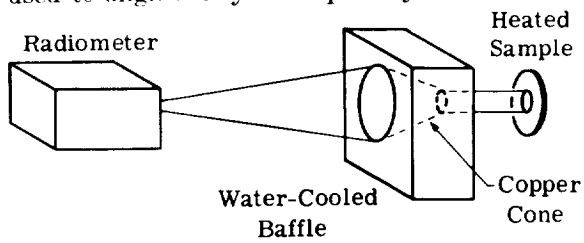

FIGURE 37–9.– Diagram of what the radiometer "sees"

The blackbody is positioned behind one baffle, and the sample with its associated RF furnace is positioned behind the other baffle. A thermocouple is attached to the sample surface by spot welding, and its reference junction is placed in an ice bath. A thermocouple is also provided with the IRI model 101 blackbody to monitor its temperature. The reference junction is placed in the same ice bath as the sample reference junction.

With a Variac connected to the electrical power source of the RF furnace, the temperature of the sample surface can be controlled. Simultaneously the blackbody and sample are raised in temperature while the radiometer is pointed first at one and then at the other by the switching mirror. The signal out of the radiometer is noted for the sample and blackbody as a function of their temperature. Figure 37–10 is an example of the data which depicts the radiometer signal as a function of temperature for 304 stainless steel and the blackbody.

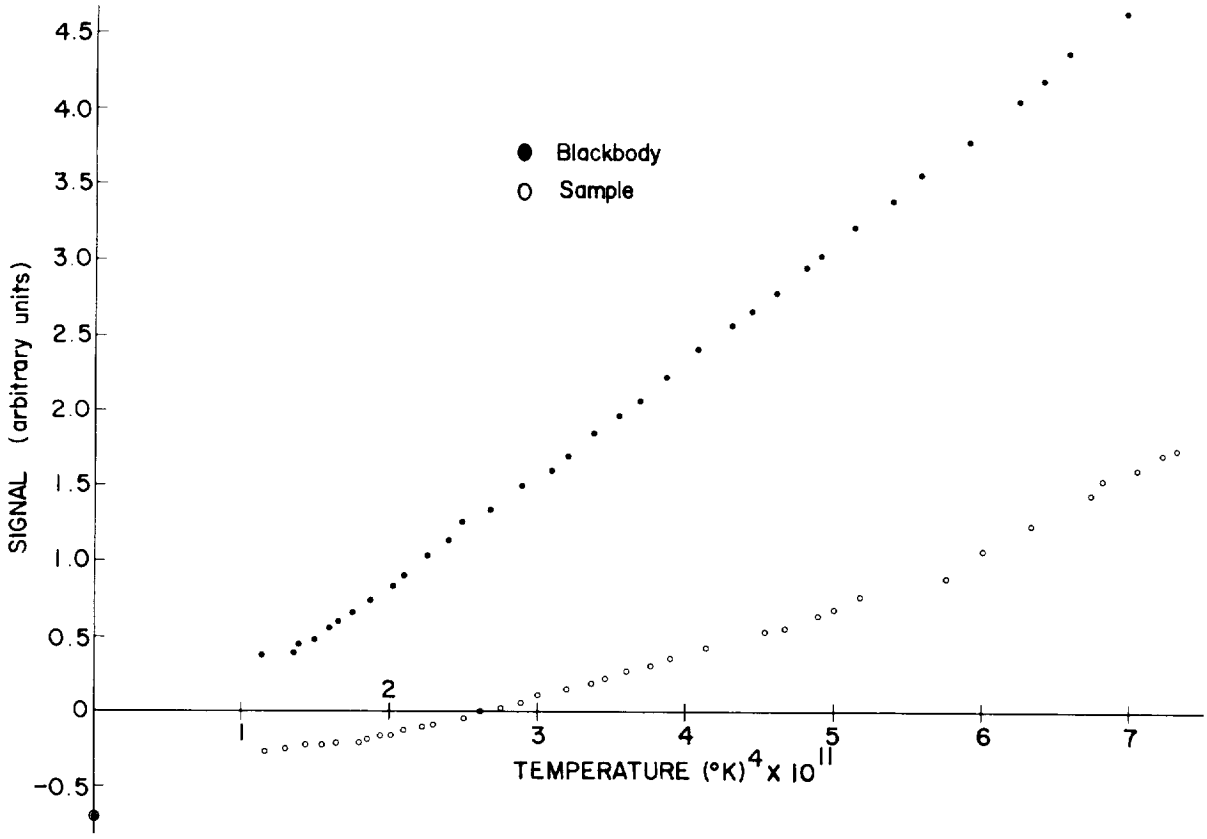

FIGURE 37-10.—304 stainless steel (untreated but slightly pitted) run 2.

Reduction of Data

For each sample run the value of the constant b of equations (7) and (8) is measured. This is necessary since it takes about 2 hours to make an experimental run and conceivably the tap-water temperature and consequently the baffle temperature will change from run to run. The value of b is obtained by placing a metal plate which had been cooled to liquid nitrogen temperature (77° K) behind the baffle and measuring the signal output from the radiometer. With this value of b, V_s' and V_b' can be computed from equations (7) and (8). With these values of V_s' and V_b' and equation (9) the emittance is calculated for the temperatures between 600° K and 950° K in 25° K steps. The data, emittance versus temperature for 304 stainless steel, are shown in figure 37-11.

ESTIMATE OF EXPERIMENTAL ERROR

Taking relative rather than absolute measurements, the total error is kept at a minimum, but there were difficulties in accurately determining the values of V, T and b for the final calculations of ϵ_s. These parameters enter into the problem in the following way:

$$V_s = a\sigma\tau_1\epsilon_s T_s^4 + b_1 \tag{12}$$

and

$$V_b = a\sigma\tau_2\epsilon_b T_b^4 + b_2 \tag{13}$$

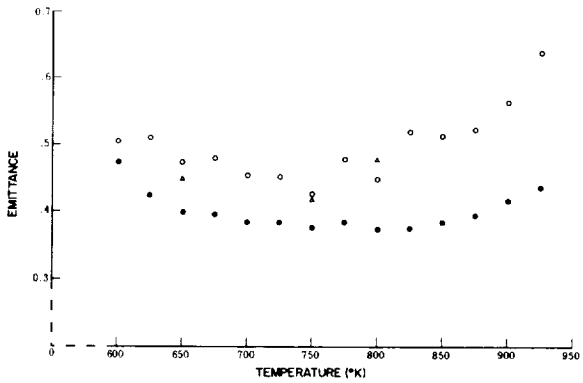

FIGURE 37-11.—Emittance vs. temperature—304 stainless steel (untreated-slightly corroded), runs 1 and 2.

The emittance is obtained by solving for ϵ_s.

$$\epsilon_s = \frac{\tau_2}{\tau_1}\left(\frac{T_b}{T_s}\right)^4 \frac{V_s - b_1}{V_b - b_2}\,\epsilon_b \tag{14}$$

where τ_1 is the percentage transmission by the optical path in front of the sample, similarly τ_2 is for the path in front of the blackbody, b_1 is the value of V_s when the sample is at 0° K, and b_2 is the value of V_b when the blackbody is 0° K.

A good approximation to the fractional error in emissivity is

$$\frac{\Delta\epsilon_s}{\epsilon_s} = \frac{\Delta\tau_2}{\tau_2} - \frac{\Delta\tau_1}{\tau_1} + 4\left(\frac{\Delta T_b}{T_b} - \frac{\Delta T_s}{T_s}\right) + \frac{\Delta\epsilon_b}{\epsilon_b} + \frac{\Delta(V_s - b_1)}{V_s - b_1} - \frac{\Delta(V_b - b_2)}{V_b - b_2} \tag{15}$$

The constants b_1 and b_2 may be expressed as

$$b_1 = a\sigma\tau_1\epsilon_1 T_1^4 + a'\sigma\epsilon'(T_H^4 - T_D^4)$$

and

$$b_2 = a\sigma\tau_2\epsilon_2 T_2^4 + a'\sigma\epsilon'(T_H^4 - T_D^4)$$

where ϵ_1 and ϵ_2 are the emittances of the baffles; T_1 and T_2 are the temperatures of the baffles; T_H and T_D are the temperatures of the radiometer head and the detector, respectively; ϵ' is the effective emittance; and a' is the geometric constant inside the radiometer. When the system is thermostatic, $T_H = T_D$ and the last term of equation (16) is zero. Then

$$b_1 = a\sigma\tau_1\epsilon_1 T_1^4 \tag{16}$$

and

$$b_2 = a\sigma\tau_2\epsilon_2 T_2^4 \tag{17}$$

Since the baffles have been coated with the same flat black enamel, $\epsilon_1 = \epsilon_2$, and since tap water flows through both baffles at a rapid rate, $T_1 = T_2$. Then it can be justifiably stated that $b_1 = b_2$, and the only error in measurement would be in the accuracy of determining the associated signal voltage.

Since b and V are determined in the same manner, V' can be substituted for $V - b$ in equation (15), and

$$\frac{\Delta\epsilon_s}{\epsilon_s} = \frac{\Delta\tau_2}{\tau_2} - \frac{\Delta\tau_1}{\tau_1} + 4\left(\frac{\Delta T_b}{T_b} - \frac{\Delta T_s}{T_s}\right) + \frac{\Delta\epsilon_b}{\epsilon_b} + \frac{\Delta V_s'}{V_s'} - \frac{\Delta V_b'}{V_b'} \tag{18}$$

It can be said that $\tau_2 = \tau_1$ at equal temperatures (T_b and T_s) because the optical paths are nearly the same. With the null method of determining V_s, V_b and b, the uncertainty is the same for each [i.e., $\Delta(V_s - b) = \Delta(V_b - b) = \Delta V$]. Therefore, equation (17) becomes

$$\frac{\Delta\epsilon_s}{\epsilon_s} = 4\,\frac{\Delta T_b - \Delta T_s}{T} + \Delta V\left(\frac{1}{V_s'} - \frac{1}{V_b'}\right) + \frac{\Delta\epsilon_b}{\epsilon_b} \tag{19}$$

The individual terms in this expression are

$$\frac{\Delta T_b}{T} = 0.005$$

$$\frac{\Delta T_s}{T} = 0.01$$

$$\Delta V\left(\frac{1}{V_s'} - \frac{1}{V_b'}\right) = 0.02$$

$$\frac{\Delta\epsilon_b}{\epsilon_b} = 0.001$$

This analysis shows that the maximum error is less than 8%.

The value of $\Delta T_b/T$ was obtained from the manufacturers manual as a realistic error when using a platinum-platinum rhodium thermocouple in this temperature range. The error in ϵ_b was obtained from the same manual. The value of $\Delta T_s/T$ was estimated on the following bases: It is possible to have severe temperature gradients across the 3-mm diameter sample section that the radiometer was viewing. It was assumed, however, that these gradients were small (less than 10° K at 1000° K), since moving the sample around caused no significant changes in radiometer signal. The radiometer is capable of detecting at least 2° K temperature changes on the sample surface. The fractional error in determining the value of signal voltage was estimated as 0.03.

REFERENCES

1. Astheimer, R. W.; and Wormser, E. W.: High-Speed Infrared Radiometers. TD78, Jour. Opt. Soc. Am., vol. 47, 1957, p. 340 *and* A New Instrument for Far Infrared Thermal Photography TD79, Jour. Opt. Soc. Am., vol. 47, 1957, p. 340 (Abstracts only).
2. Instruction Manual, Model 101 Infrared Industries Blackbody, 1962.

38—THE TOTAL HEMISPHERICAL EMITTANCE OF PLATINUM, COLUMBIUM–1% ZIRCONIUM, AND POLISHED AND OXIDIZED INOR–8 IN THE RANGE 100° TO 1200° C

BY D. L. McELROY AND T. G. KOLLIE

OAK RIDGE NATIONAL LABORATORY, OAK RIDGE, TENNESSEE[1]

Equipment was developed for measuring the temperature dependence of the total hemispherical emittance (E_t:T) of metal and alloy strips to 1200°C using direct heating in a constant-temperature, blackbody vacuum chamber. Precise specimen dimensions and thermocouple positioning are requisite to the method and the techniques developed to accomplish these are described. If the systematic errors of this equipment are evaluated, the E_t measurement accuracy is ±2.7% and the reproducibility is ±0.5%. Experimental measurements on platinum (Pt), columbium–1% zirconium (Cb–1% Zr), and Inor–8 strips illustrated effects which cause changes in E_t. Increased E_t:T occurred with increasing surface roughness and oxidation. Results are presented which show the effects of specimen reaction with the measuring environment and specimen-oxide reactions. The electrical resistivity of the specimen was obtained from the data taken in an E_t determination. A change in the electrical resistiveity of Inor–8 occurs between 400° and 600° C and is accompanied by a corresponding change in E_t:T. Finally, the applicability of the method for determining E_t:T on a cylindrical specimen was demonstrated.

The process of radiant heat transfer is of extreme importance in the control of heat flow in high-temperature operations. The total hemispherical emittance (E_t) of the emitting material is a measure of its ability to dissipate heat by radiation and relates the rate of heat transfer to the product of the Stefan-Boltzmann constant and the fourth power of its temperature. Interest in this property arose over the possibility of altering the amount of radiant energy emitted by several components of the Molten Salt Reactor Experiment (nuclear) by controlling the surface properties of Inor–8 within the limits of existing metallurgical specifications. Thus, this research was primarily concerned with developing equipment and techniques to yield data on the temperature dependence of E_t for engineering design usage.

The technique selected for measuring this physical property was a modification of the hot-filament method used by Worthing (ref. 1) which employs a specimen strip heated by an external power source in a constant-temperature, blackbody vacuum chamber. The method requires a measurement of the specimen temperature and the power dissipated in the specimen. These data are used with a steady-state heat balance to calculate E_t of the specimen by the equation

$$E_t = \frac{V \cdot I}{A\sigma(T_s^4 - T_c^4)} \qquad (1)$$

where A is the surface area of the specimen between the voltage taps, σ is the Stefan-Boltzmann constant, T_s is the average specimen temperature, T_c is the average blackbody vacuum chamber temperature, and $V \cdot I$ is the electrical power dissipated over the test section. Specimen heat gains or losses considered in obtaining this equation are the power generation in the specimen, the radiant energy incident upon the specimen, and the radiant energy

[1] Operated for the U.S. Atomic Energy Commission by the Union Carbide Corporation.

emitted by the specimen. Specimen heat gains or losses which are neglected include all the reflected radiant energy, the heat loss by atmospheric convection and conduction, the heat loss by conduction to the input electrodes, and the heat loss by conduction through the thermocouple leads. Modifications of this method have been described by Richmond and Harrison (ref. 2); Abbott, Alvares, and Parker (ref. 3); Dotson (ref. 4); Bradley and Entwistle (ref. 5); Davisson and Weeks (ref. 6); and Forsythe and Watson (ref. 7). These investigators employed different types of specimens, power sources, and temperature sensors to determine the requisite data for calculation of E_t:T of polished, coated, and oxidized metals and alloys. Salient features of these studies are compared in Table 38–I. Two noteworthy features of these studies include the use of two specimen lengths by Bradley and Entwistle (ref. 5) to evaluate the heat loss from the ends of their sample and the formula modification of Abbott, Alvares, and Parker (ref. 3) to account for the power absorbed by the strip from its surrounding, i.e.,

$$E_t = \frac{V \cdot I}{A\sigma[T_s^4 - (T_c/T_s)^{1/2} T_c^4]} \qquad (2)$$

Equation (2) is superior to equation (1) because a first-order approximation, $(T_c/T_s)^{1/2}$, is included for the specimen absorptance/emittance, which is incorrectly set equal to unity in equation (1). For this reason equation (2) was used to calculate E_t in the present study. In addition, the specimen electrical resistivity was calculated from the current flowing in the specimen, the voltage drop along the specimen, and the specimen dimensions.

DETAILED DESCRIPTION OF COMPONENTS

Specimen

The specimen was machined in the form of a sheet tensile-test specimen. The ends of the 10½-in.-long specimen were 1-in. wide and contained ¼-in. holes for power lead attachment and vertical suspension. The central 6-in. portion of the specimen was machined and polished to a width of 0.200 ± 0.0001 in. and a thickness of 0.010 ± 0.0001 in. These tolerances were not used in the initial studies, but were later adopted to achieve uniform specimen temperatures. The first specimens were produced by cold rolling and filing to a uniform web thickness. A hand-polishing technique was used on the initial specimens, which included rough finishing through 4–p metallographic paper, polishing with Linde A and B alumina, and a final polishing with diamond paste. The resulting specimen had a surface finish approaching that of a finished metallographic specimen prior to etching. Since this experiment is particularly sensitive to the specimen surface condition, it is important to specify in detail the preparation procedure. Methods to categorize the surface are being studied.

Temperature Measurement System

A primary measurement in this method is the specimen temperature. For this purpose 0.005-in.-diam $Pt_{90}Rh_{10}$/Pt thermocouples were chosen. This noble metal combination was selected for the following reasons: (1) thermocouples made from given spools of Pt and $Pt_{90}Rh_{10}$ wire exhibit the maximum reproducibility obtainable among the commonly available types of thermocouples; (2) the thermal EMF/temperature relation of this combination is known better in the temperature range of interest than that of any other combination; and (3) this combination is applicable over the desired temperature range and operating environment of this apparatus.

After the specimen was polished, five Pt_{90}-Rh_{10}/Pt thermocouples were attached along its central section. Using a stereomicroscope the specimen was marked at 1-cm intervals and the individual theremocouple wires were welded to the specimen with a modified tweezer welder. The hot junction was made through the specimen and the ends of the wires were separated laterally by about five wire diameters. The 3-in.-long thermocouple wires were welded to other $Pt_{90}Rh_{10}$ and Pt wires when the specimen was placed in the apparatus. The thermocouples extended through vacuum seals made from ½-in drilled-out bolts, epoxy resin, and O-rings to an ice-bath cold junction where twist junctions were made to pure copper wires. Thermocouple readout was effected by Leeds & Northrupp thermal-free switches and an L & N type K 3 potentiometer. Thermal-free solder was used on all switch connections and the switches were insulated with vermiculite to reduce thermal EMSF.

TABLE 38–I. *Hot-Filament Vacuum Method for Determining E_t:T*

Investigator	Materials	Specimen Form	Temperature Range °C	Temperature Sensor	Power Supply	Vacuum, torr	Voltage	Remarks by Investigator
L. E. Dotson	Columbium–1% zirconium coatings.	Sheet, 3 x 0.24 x 0.045 in.	850–1100	Leeds & Northrupp optical hole in specimen.	Rectified a-c 0 to 500-amp, 3% ripple.	1×10^{-5}	Mechanical columbium contact.	Accuracy ±5% at 0.5.
J. C. Richmond W. N. Harrison.	Nickel, type 430 stainless steel, Inconel, type 321 stainless steel.	Sheet, 20 x 0.65 x 0.01–0.2 cm.	200–1000	0.005-in. Chromel-Alumel thermocouple.	Transformed a-c ±1%	2×10^{-5}	10-megohm VTVM via thermocouple.	Good agreement with GE specimens.
G. L. Abbott N. J. Alvares. W. J. Parker.	Platinum	Sheet, 30 x 1 x 0.008 cm.	650–1200	0.005 in. Chromel-Alumel thermocouple M-H Radiomatic.	Transformed a-c ±1%	10^{-4}	10-megohm VTVM via thermocouple.	Accuracy: ±5% on E_t; E_n also measured.
C. Davisson J. Weeks.	Platinum	0.005-in. wire	25–1200	Specimen ρ	Battery	10^{-7}	Platinum wire, 0.001 in	$E_t=f(\rho T)$; power loss via voltage taps, 20%.
D. Bradley A. G. Entwistle.	90% Platium–10% rhodium.	2 wires, 0.00057 in	600–1450	Specimen ρ by Wheatstone bridge.	110-v d-c	10^{-4}	Specimen ρ vs temperature independent determination.	Accuracy: 1.5% at 1450.
W. E. Forsythe E. M. Watson.	Tungsten	0.010-in. wire 110-cm long.	0–2700	Disappearing filament optical; previous E_λ of tungsten.	Battery	Not stated.	0.02-mm tungsten leads	Approx 1%.

The $Pt_{90}Rh_{10}$ wires also serve as voltage taps on the specimen, so their position on the specimen determines the length of the test section. Their locations were accurately determined by means of a calibrated filar eyepiece. The point of contact of a wire on the specimen was arbitrarily assigned as the center of each wire. Measurements on a given specimen by different persons gave length variations of less than ± 10 filar units (± 0.002 in.), which corresponds to about $\pm \frac{1}{2}$ of a wire diameter. Assignment of the center of a flattened 0.005-in. wire is responsible for this variation. A four-pronged knifeblade resistance calibration measurement could reduce this error.

Specimen Power System

The specimen was directly heated by direct-current power from a magnetic-regulated, transistorized direct-current power supply (Electronics Research Associates, Inc., model 36–12M) which has $\pm 0.05\%$ load regulation and $\pm 0.005\%$ rms ripple. The specimen current was determined from the voltage drop across a 0.01-ohm L & N standard resistor, model 4222, in series with the specimen. The voltage drop along the specimen was determined by means of the five 0.005-in. $Pt_{90}Rh_{10}$ wires. All measurements were made using the K–3 potentiometer. The specimen power input electrodes were two $\frac{1}{2}$-in.-diameter copper rods, Aquadag-coated, which were sealed by O-rings to the chamber base plate. A weighted, flexible cable served as the bottom and top connections to the specimen. This allowed for expansion and contraction of the specimen on heating and cooling. A special four-pole mercury-contact switch allowed the current direction in the specimen to be reversed.

Specimen Chamber

The specimen chamber was a 14-in.-ID, 30-in.-tall brass cylinder which was sealed by an O-ring to a 20-in.-diameter, $\frac{3}{4}$-in.-thick, stainless steel base plate. The cylinder and base plate were covered with $\frac{3}{8}$-in.-OD copper tubing with a maximum center-line separation of 1 in. The outside of the chamber was insulated with 1 in. of Fiberglas, covered by aluminum foil. A coating of Aquadag was applied to all surfaces inside the chamber.

A baffled 4-in. oil diffusion pump and a mechanical pump maintained a pressure of 5×10^{-6} torr in this chamber as measured with an ionization gage located in a cylinder connecting the diffusion pump to the base plate. It is probable that the pressure at the specimen was slightly higher.

A pressure thermostat was used to circulate water through the above-mentioned copper tubing and to control the wall temperature of the chamber. A thermocouple attached to the wall of the chamber was used to monitor this temperature and during a typical run this remained constant at $30 \pm 0.05°$ C. Flexible leads allowed the chamber to be opened without affecting the chamber-temperature control system.

Alternative Specimen Design

A modified specimen design was tested which involved the replacement of the strip specimen with a hollow cylinder. This cylinder was $1\frac{3}{16}$-in.-OD, 3-in. long, and had a $\frac{1}{32}$-in.-wall thickness. The specimen was polished and thermocouples were welded to its top, bottom, and sides. A $Pt_{90}Rh_{10}$ wire-wound axial heater was totally enclosed in the cylinder but electrically insulated from it. Voltage taps were placed on the heater at the top of the cylinder. The same equation was used to calculate E_t. This specimen design has the distinct added advantage of insulating the direct-current power system from the thermocouple system.

SYSTEM OPERATION AND ERRORS

Operation

A typical determination of $E_t:T$ was made in the following manner. After the specimen was machined and polished, the thermocouples were welded and their location determined. This assembly was bolted in place in the apparatus and the attached thermocouples were welded to the appropriate $Pt_{90}Rh_{10}$ and Pt leads. The system was evacuated to 5×10^{-6} torr and the direct-current power applied to the specimen. Thirty minutes were allowed for equilibration and readings were made of the five specimen thermocouples, the four voltage drops, the current, and the chamber thermocouples. The direct current was reversed, a second set of data was taken after 15 min, and the specimen

power was changed for the next data point. The forward and reverse EMF values were averaged to remove the effects of direct-current pickup by the thermocouples. Equation (2) was used to calculate E_t.

Errors

An analysis of the errors in an E_t determination can be divided into two groups: the errors associated with the measurement of the terms appearing in equation (2), and the errors associated with certain phenomena neglected in deriving equation (2). The former errors were assessed from the estimated uncertainty of each term in the equation. The latter errors can be calculated or measured by adept testing and a correction applied therefor.

Determinate Errors

Based on the stated accuracy of the L & N type K–3 potentiometer of 0.018%, the error in the product $V{\cdot}I$ is $\pm 0.036\%$. However, associated with the measurement of $V{\cdot}I$ is a $\pm 0.015\%$ error in the standard resistor. The total $V{\cdot}I$ error thus becomes $\pm 0.05\%$. The length, and width plus thickness are respectively known to: 1.6 ± 0.008 in., $\pm 0.50\%$; 0.210 ± 0.0002 in., $\pm 0.095\%$. This gives a cumulative error in the determination of the area of $\pm 0.595\%$. The temperature is obtained by measuring the thermal EMF with the L & N type K–3 potentiometer. From consideration of all of the factors affecting the thermocouple EMF, it is reasonable to state that the $Pt_{90}Rh_{10}/Pt$ thermocouple is accurate to at least $\pm 0.5\%$. However, this error enters the equation as the fourth power and so yields an absolute error of approximately $\pm 2\%$. A summation of these determinate errors yields a total absolute error in the apparent value of E_t of $\pm 2.7\%$. It is interesting that repeat runs on a given specimen are reproducible to $\pm 0.5\%$ and for different specimens prepared by the described procedure, a reproducibility of better than $\pm 2\%$ is observed.

Systematic Errors

The systematic errors neglected in deriving equation (2) were treated in the following manner. A correction was applied for the heat loss from the measuring section due to thermal conduction within the specimen because of a temperature gradient, if this heat loss exceeded 0.4% of the measured power input. A correction was applied for the heat adsorbed by the specimen strip from its surroundings by using equation (2) to calculate E_t. This presumes the first-order approximation of Abbott, Alvares, and Parker (ref. 3) is valid. A correction was applied for heat loss from the measuring section of the specimen due to thermal conduction within the thermocouples. This heat loss was measured experimentally and is described in the platinum measurements section. Finally, a correction was applied to the radiating area due to thermal expansion of the specimen.

MEASUREMENTS

This measurement program was initiated to obtain engineering data on the temperature dependence of E_t of Inor–8. Inor–8 is a nickel-molybdenum-chromium-iron alloy which is corrosion-resistant to molten fluoride salts and is the construction material for the Molten Salt Reactor Experiment, as well as being used in other high-temperature applications, such as heat exchangers.

The development of the apparatus was made using specimens of Inor–8. Refinements in the techniques were subsequently accomplished using specimens of Pt and Cb–1% Zr, and the data on Inor–8 specimens redetermined. Thus, some of the results reported in the following sections are considered tentative at best in view of the technique refinements which were developed during testing. This section will attempt to show how certain variables affect the values of E_t:

In Pt

(1) the need for knowing precisely the thermocouple positions
(2) the heat loss caused by the thermocouple wires

In Cb–1% Zr

(1) the effect of a specimen reaction with its measuring environment
(2) the effect of surface roughening

In Inor–8

(1) the effect of surface finish and air oxidation
(2) the corresponding changes of E_t and electrical resistivity

(3) an alternative method of measurement
(4) the effect of oxide reduction.

Measurements on Platinum

Platinum was studied in order to standardize the apparatus and to perfect the special instrumentation technique. The results obtained indicated the need for precise control of the specimen dimensions, of the thermocouple positions, and the manner of thermocouple attachment. In addition, a platinum specimen was used to quantitatively determine the heat loss from the measuring section by conduction through the thermocouples.

Specimen 1 was machined from a platinum sheet[2] and polished; three thermocouples tweezer-welded to the specimen, and their separation measured to the nearest 1/64 in. Later this procedure was found to be inadequate. The E_t values for this crudely prepared sample are shown in figure 38–1, and exhibited a minimum at 350° C before rising monotonically with temperature to 860° C. At 860° C a thermocouple opened; it was rewelded and the length remeasured; and it was designated specimen 2. This crude length measurement caused the E_t results for specimen 2 to be below those of specimen 1 to 1000° C. However, the results were reproducible to ±0.5% upon cooling from 1000° to 550° C. Specimen 3 was produced from specimen 2 using the precision techniques previously described. The E_t values for specimen 3 were near those of specimen 2, but this is probably because of a fortuitous 1/64-in. meas-

[2] Platinum sheet composition: 99.50% Pt–0.20% Ir–0.20% Pd–0.05% Rh–0.03% Fe–0.02% Cu.

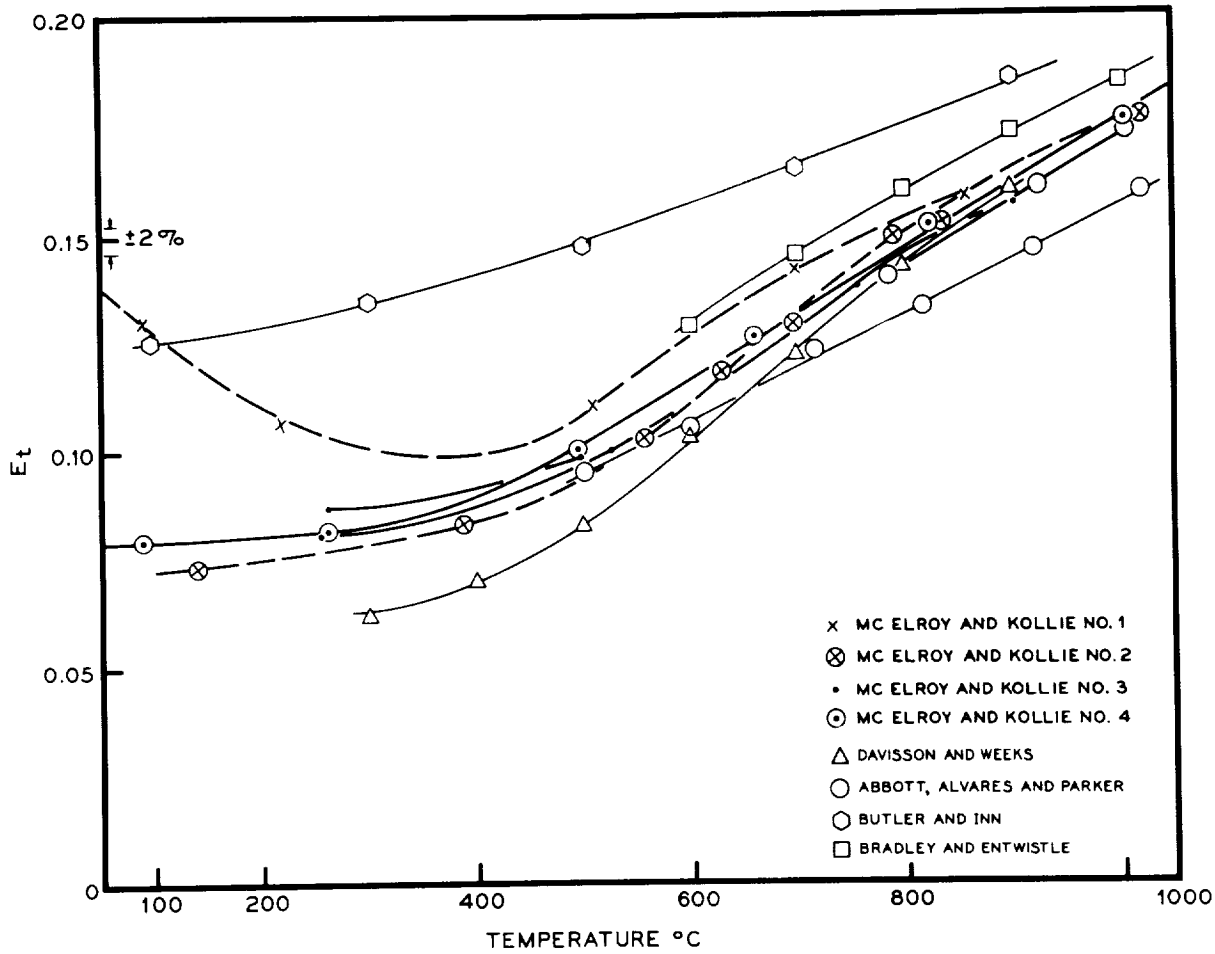

FIGURE 38–1.—E_t:T for platinum. Specimens 1 and 2 show the effect of length measurement errors. Specimens 3 and 4 reflect improved measuring technique on machined specimens and illustrate the reproducibility (±0.5%) and the accuracy (±2.7%). Bradley and Entwistle data are for Pt–10 Rh.

urement on specimen 2. The new fabrication technique appeared successful because specimen 4 was prepared by the same method and confirmed the E_t values of specimen 3 to 900° C to better than ±2%. The agreement of these data with other literature values is shown on this plot. The E_t: T of these runs is similar to but higher than that reported by Davisson and Weeks (ref. 6), and is nearly parallel to that of Abbott, Alvares, and Parker (ref. 3). The data are also definitely lower than those reported by Butler and Inn (ref. 8), or Bradley and Entwistle (ref. 5) for $Pt_{90}Rh_{10}$.

The E_t values reported for all specimens were corrected for heat loss by thermal conduction within the thermocouples. The correction was obtained by direct measurement on a platinum specimen instrumented by the precision technique. A set of runs was made in which one wire of a measuring thermocouple was removed after each run. The difference in power required to attain a given temperature was determined and the actual power loss for two thermocouples based on removal of one and two wires is shown in figure 38–2. Although the data are not as precise as desired, a conclusive trend is shown, i.e., more heat loss at higher temperatures, but a greater percentage of heat loss at the lower temperatures. The fractional correction for this loss on several specimens is shown in the top of figure 38–2. For the particular specimen sizes studied, this correction can be as large as 20% at low temperatures.

Measurement on Columbium—1% Zirconium Alloy

A Cb–1% Zr alloy[3] was tested to 1200° C in the apparatus using only three measuring thermocouples. Specimens 1 and 2 were hand polished and specimen 3 was roughened to a 45-μin. surface finish. The data on these specimens are plotted in figure 38–3.

Specimen 1 was heated in steps to 790° C and E_t was independent of temperature to 400° C, but then increased sharply with temperature to 790° C. After a 15-hr anneal in situ at 790° C, a stepwise cooling gave E_t values which were 70% higher than values obtained on heating. Furthermore, continued annealing for 21 hr at 770° C caused a 2% decrease in E_t values. Examination of the specimen surface revealed a thin white film, presumably an oxide which had formed during these thermal treatments in an indicated vacuum of 5×10^{-6} torr. Electrical resistivity values obtained during these cycles were temperature dependent but insensitive to thermal history, as shown in figure 38–3.

Specimen 2 was heated directly to 770° C and an attempt was made to follow the increase in E_t with time due to oxidation. The E_t at 770° C agreed with that of specimen 1, but a 3% rise in E_t was noted during a 10-hr period. A subsequent 75-hr soak at 760° C of this specimen did not change E_t. Thermal cycling confirmed (±2%) that the same E_t observed for specimen 1 on cooling had been achieved in specimen 2. A stepwise heating of specimen 2 was extended to 1200° C. The E_t values obtained below 760° C agreed with the previous E_t values. However upon exceeding 760° C, E_t exhibited a temperature dependence which was parallel but displaced about 200° C to the E_t values of specimen 1 on first heating. The E_t values obtained on cooling from 1200° C were 10% higher but parallel to the stable E_t values produced at 770° C. Thus, the E_t value for a polished Cb–1% Zr alloy heated in a vacuum of 5×10^{-6} torr depends on the temperature to which the specimen is heated and is stable if this temperature is not exceeded on repeated heating. The final appearance of specimen 2 was very similar to that of specimen 1. The electrical resistivity values for specimen 2 were insensitive to thermal treatment but were about 2% higher than those of specimen 1, which was probably due to a measurement error in the thickness.

Specimen 3, which was roughened to a 45-microinch surface finish, gave E_t values which were approximately 60% higher than the original E_t values of specimen 1 but exhibited the same general temperature dependence. The electrical resistivity values were 2–3% higher than either specimen 1 or 2, probably because of the surface roughness effect on the measured specimen cross section. The electrical resistivity of all specimens was above that for pure columbium and distinctly higher than the results of Dotson (ref. 4).

[3] Original minor impurities: 100 ppm O_2, 120 ppm N_2, 120 ppm C, and 1 ppm H_2.

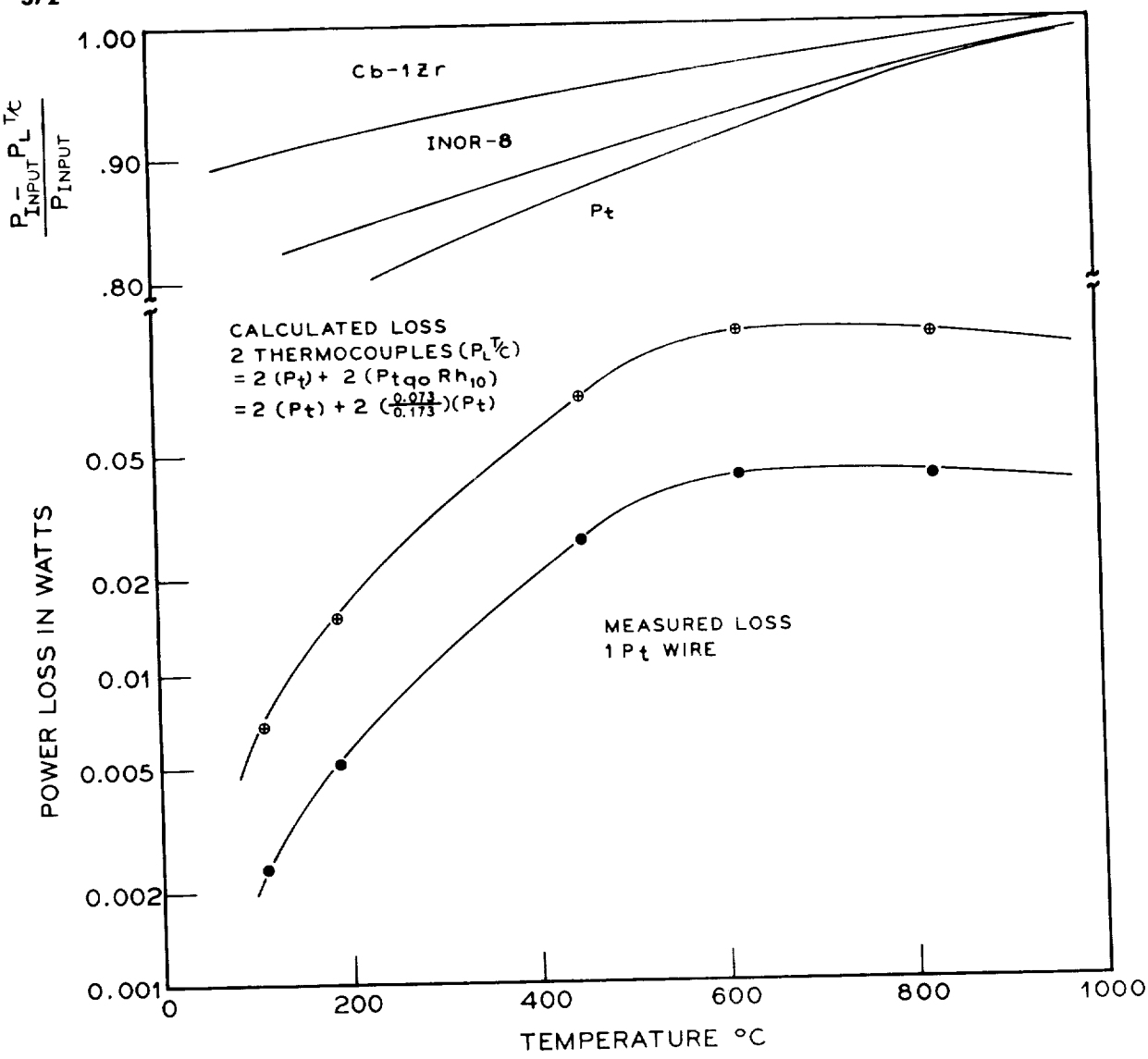

FIGURE 38-2.—Heat loss from the specimen measuring section caused by thermal conduction in the thermocouples. Measured on one platinum wire and on one 90% platinum-10% rhodium wire and calculated for two thermocouples. Temperature gradients in 0.005-in. platinum wire calculated for k = 0.72 w/cm-°C. Insert shows the fractional power correction based on these heat losses for platinum, Inor-8, and columbium-1% zirconium specimens.

Measurements on Inor-8

Three Inor-8 specimens were fabricated by stamping tensile-test specimens from 0.020-in. sheet and cold rolling this form to 0.009-in. thick. This material was clamped between two ¼-in. steel bars and filed to a uniform web thickness. Three thermocouple wires were attached to specimen 1, which had a matte (as-received) finish, and their separation measured to the nearest 1/64 in. This specimen yielded E_t values to 700° C which were on the top boundary of region I in figure 38-4. A slight minimum was observed in E_t at 200° C. This specimen was then oxidized in air at 830° C for 1 hr and gave results which form the bottom boundary of region III in figure 38-4.

FIGURE 38-3.—Columbium-1% zirconium E_t: T and electrical resistivity: T. E_t of specimens 1 and 2 shows effects of reaction with 6×10^{-6}-torr environment. E_t of specimen 3 shows the effect of surface finish. Electrical resistivity: T was insensitive to environment reaction and above that of pure columbium.

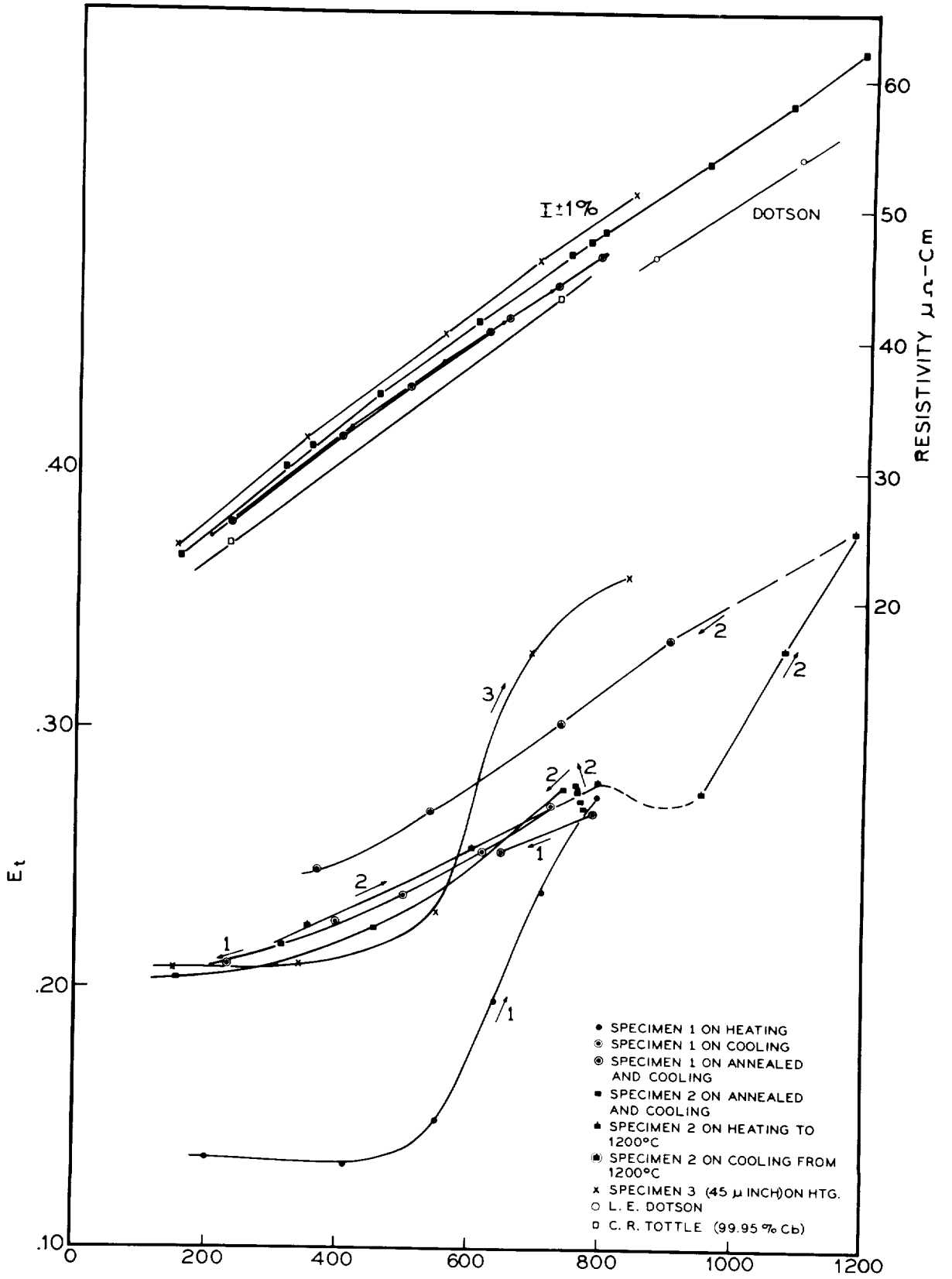
I±1%
DOTSON
RESISTIVITY μΩ-CM
60
50
40
30
20
.40
.30
.20
.10
E_t
0
200
400
600
800
1000
1200
1
2
3
SPECIMEN 1 ON HEATING
SPECIMEN 1 ON COOLING
SPECIMEN 1 ON ANNEALED AND COOLING
SPECIMEN 2 ON ANNEALED AND COOLING
SPECIMEN 2 ON HEATING TO 1200°C
SPECIMEN 2 ON COOLING FROM 1200°C
SPECIMEN 3 (45 μ INCH) ON HTG.
L. E. DOTSON
C. R. TOTTLE (99.95 % Cb)

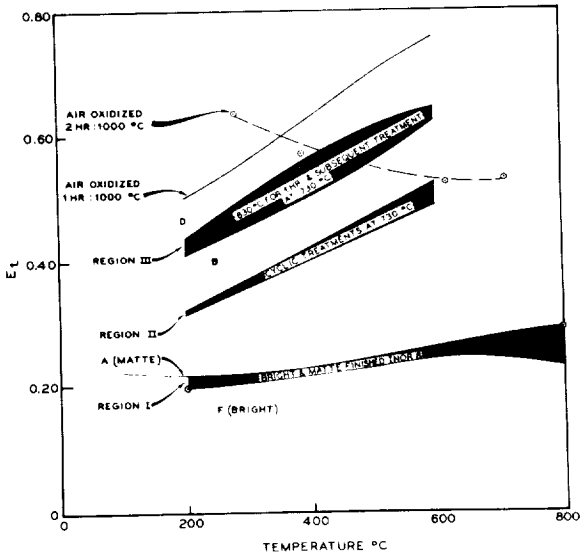

FIGURE 38–4.—E_t:T for Inor–8. Exploratory measurements to show effects of intentional oxidation of the specimen. E_t values were not corrected for conduction heat losses.

Subsequent specimen treatments at 730° C in air included holding for 1 hr, five thermal cycles to room temperature, and 9 hr of further holding. After each treatment an E_t:T run was made and all results were within region III. Thus, E_t was increased 2.5 times by air oxidation at 830° C after which it was relatively insensitive to thermal cycles to 730° C or to prolonged exposure at 730° C.

Specimen 2 was hand polished to a bright finish, three thermocouples were tweezer-welded to its surface, and their separation measured to the nearest $\frac{1}{64}$ in. This specimen yielded E_t:T values which form the bottom boundary of region I in figure 38–4. Thus, the smooth surface existing on specimen 2 caused a reduction in E_t compared to the matte finish of specimen 1. This specimen was then given 100 1-min thermal cycles in air to 730° C. After each 25 cycles an E_t:T measurement was made, and the values obtained lie totally in region II, although the value increased slightly with increasing number of cycles.

Specimen 3 was identical to specimen 2 and gave E_t:T values which were within 5% of those of specimen 2, and consistently lower than specimen 1. Specimen 3 was then oxidized 1 hr at 1000° C in air and gave the E_t values indicated in figure 38–4. This oxide caused a three-fold increase of E_t at 600° C. Because of the crude length measurements on specimens 1–3, all of the E_t results reported in figure 38–4 were calculated by equation (1) without corrections for heat losses. These values are presented only to indicate approximate magnitude of effects.

Specimen 4 was prepared by machining a sheet of Inor-8 with Micarta backup plates, and this reduced the specimen dimensional variations. This specimen was hand polished, the thermocouples were attached, and the thermocouple separation was measured using a Filar eyepiece. Data on heating to 830° C were below region I of figure 38–4 and are plotted in figure 38–5. A reproducibility of better than 0.5% was obtained on cooling. An interesting increase in E_t was found near 740° C and was reproduced on cooling. It is known that the specific heat [4] and thermal conductivity (ref. 9) of Inor-8 increase near this temperature. Although the exact cause for this is unknown, such increases are normally associated with the temperature dependence of short range order effects. This specimen was then oxidized in air for 2 hr at 1000° C and E_t:T determined. It was expected that the E_t values would lie totally above those of the 1 hr at 1000° C treatment of specimen 3, and this was the case at low temperatures. But, as indicated in figure 38–4, the E_t values decreased with increasing temperature and were quite erratic. Inspection of the specimen showed the surface not to be covered with oxide, as in the previous specimens, but to be covered with a flaky metallic-appearing film. A photograph of this specimen is shown in figure 38–6. The exact cause for this phenomenon is unknown; however, the oxidized specimen received several heatings to at least 600° C in vacuum prior to data collection. This may have been sufficient to allow the carbon contained in the alloy to

[4] Private communication from E. E. Stansbury and C. R. Brooks, Dept. of Chem. and Met. Eng., U. of Tenn., Mar 1, 1961.

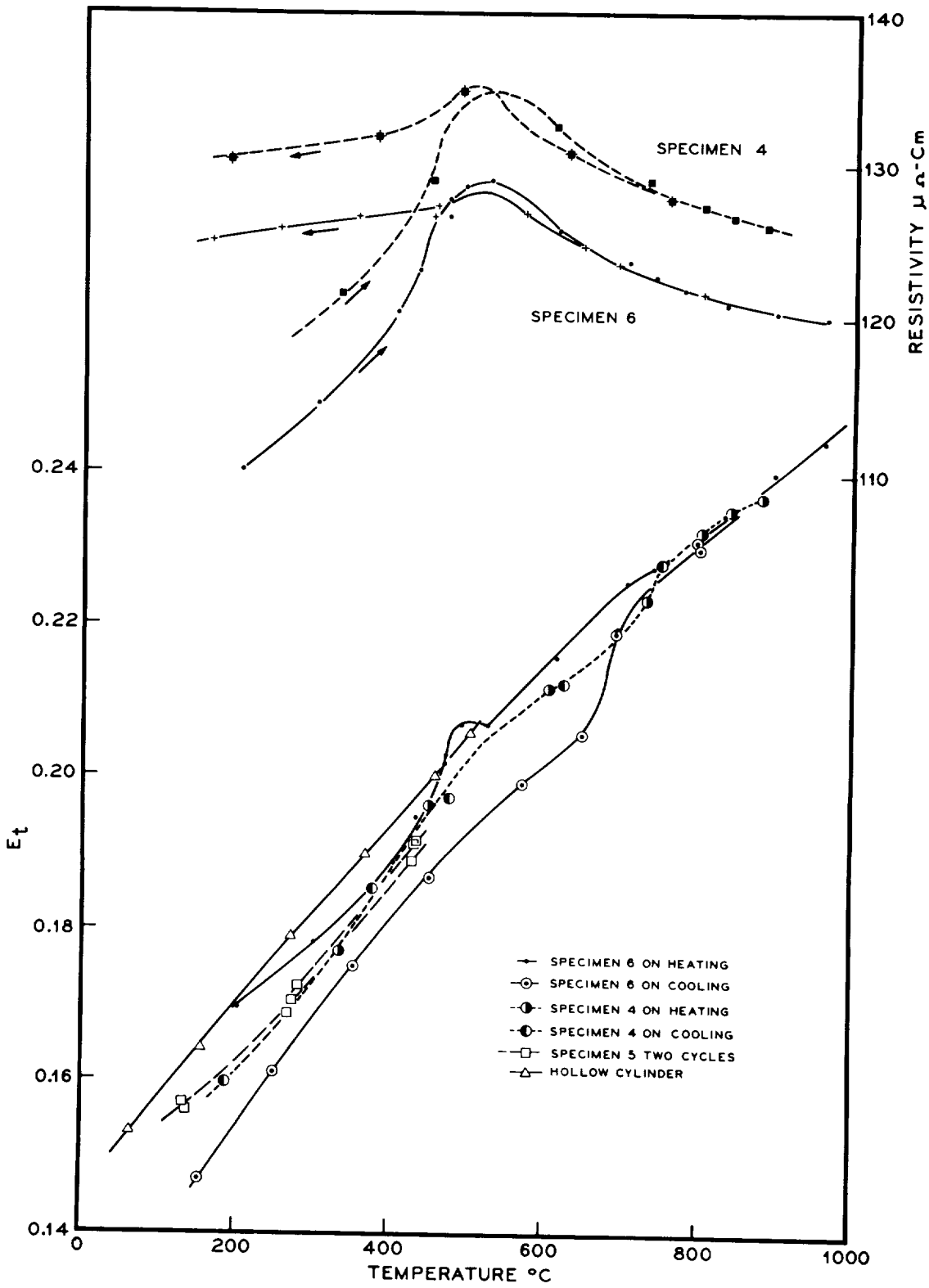

FIGURE 38–5.—Polished Inor–8 E_t:T and electrical resistivity:T. Note change in E_t at 440° C and near 700° C. E_t for hollow cylinder is shown.

692–146 O—63——25

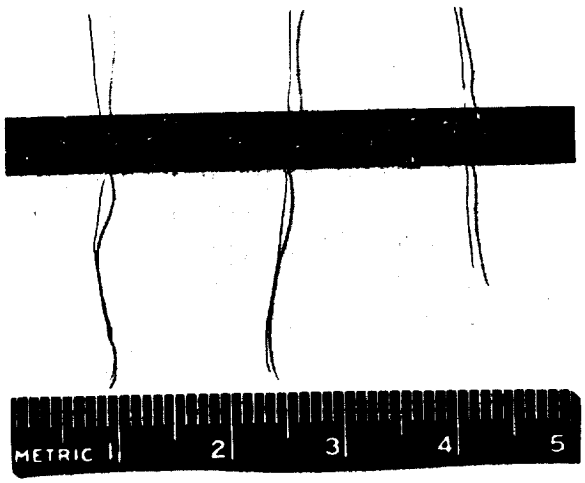

FIGURE 38–6.—Photograph of Inor–8 specimen oxidized at 1000° C and vacuum tested. See figure 38–4 for E_t:T for this specimen.

diffuse into and reduce the oxide, or spontaneous oxide decomposition may have occurred.

Specimens 5 and 6 were machined to 0.0001-in. tolerances and finished to better than 1-microinch and five thermocouples were attached and located by the technique used on speciment 4. Specimen 5 was tested only to 450° C but gave reproducible E_t values quite close to those of specimen 4, as shown in figure 38–5. Speciment 6 was used to study E_t to 1000° C on heating and cooling with small temperature intervals between data points. These values are shown in figure 38–5. Electrical resistivity (ρ) values were calculated and are shown in the upper portion of figure 38–5. The electrical resistivity of specimens 4 and 6 exhibited the same general temperature dependence. The values obtained on heating the cold-worked Inor–8 specimens differed by 4% because of a thickness measurement error and reflect cold-working, recovery, and recrystallization effects. The values obtained on cooling below 400° C are higher than those obtained on heating; this was due to the thermal treatment given the Inor–8 and not to a changed specimen size. The E_t values of specimen 6 on heating exhibited a distinct change near 450° C where the electrical resistivity undergoes the maximum change on heating. The E_t increase observed at 740° C for specimen 4 was missing on heating but was apparent on cooling. The E_t values above 750° C increased linearly with temperature and were reproduced on cooling. The E_t values obtained below 600° C were 6% below those obtained on heating, which is associated with the order-disorder phenomenon caused by the thermal treatment given to the specimen and is reflected in the electrical resistivity. Thus, E_t values are sensitive to internal specimen changes just as are electrical resistivity, specific heat, and thermal conductivity.

Finally, a hollow cylinder of Inor–8 was used to measure E_t:T. This can was manually polished to a bright finish. The results, shown in figure 38–5, agree ($\pm 2\%$) with corrected strip specimen 6 on heating to 500° C. This approach offers the advantages of a means for separating the direct-current power system and the thermocouple system, removal of the need for accurate measurement of thermocouple position, and reduced effects of thermocouple heat leakage.

SUMMARY

The experimental details of a method for determining the temperature dependence of the total hemispherical emittance (E_t:T) using a hot-filament strip in a constant-temperature, blackbody vacuum chamber were described. It was shown that precise specimen dimensions and thermocouple positioning are requisite to the method and the techniques used to accomplish these were described. From the data taken in an E_t measurement, it is possible to calculate the specimen electrical resistivity at temperature.

Corrections for systematic errors were applied to the E_t:T data. One of these errors, the heat loss due to thermal conduction through the thermocouples, dominates the particular strip specimen design used, and measurements of this heat loss revealed at least a 20% correction was necessary at low temperatures. However, if the systematic errors can be evaluated, then the accuracy of the E_t measurement is limited by the determinate error, which was shown to be $\pm 2.7\%$. The E_t:T results proved to be reproducible to $\pm 0.5\%$. Experimental measurements were made on Pt, Cb–1% Zr, and Inor–8 and illustrated how certain variables affect the values of E_t.

The platinum results illustrated the precision needed on thermocouple positioning and the heat loss which accompanies thermocouples. The corrected results were in agreement with literature values for E_t:T to 1000° C.

The Cb–1% Zr results illustrated how E_t is increased by surface roughness and by specimen reaction with a 5×10^{-6}-torr environment. The electrical resistivity of Cb–1% Zr was temperature dependent, above that reported for pure columbium, and insensitive to the specimen environment reaction.

The Inor–8 E_t:T results increased with increasing surface roughness and were increased threefold at 600° C by air oxidation. The E_t:T of an Inor–8 oxide formed at 830° or 730° C was insensitive to thermal cycling in air. However, an oxide formed by a 2-hr air exposure at 1000° C decomposed during the E_t:T determination in a vacuum and gave very erratic results. A detailed study of E_t:T for cold-worked and polished Inor–8 showed a distinct break at 440° C on heating and this was accompanied by a large change in the electrical resistivity. On cooling, the 440° C change was absent, but a change was noted near 700° C, where corresponding changes have been noted in the specific heat and the thermal conductivity of Inor–8.

Finally, the applicability of the method on a hollow cylinder specimen of Inor–8 was demonstrated and the resulting E_t:T values were within ±2% of the strip data. This offers a means of E_t:T determinations by this method on insulators.

ACKNOWLEDGMENT

The authors would like to acknowledge the work of Ralph H. Jones, who was responsible for machining the specimens; William A. Laing and William P. Murray, University of Cincinnati cooperative students, and Ronald S. Graves, who were responsible for several equipment modifications and who made a number of the measurements.

APPENDIX—COMMENTS ON PAPER 33, "A MULTICHAMBER CALORIMETER FOR HIGH-TEMPERATURE EMITTANCE STUDIES"

The paper by A. I. Funai (page 317) presents a technique for the measurement of total hemispherical emittance E_t similar to one of the techniques in use at the Oak Ridge National Laboratory (ORNL). The majority of the ORNL measurements, however, were made by a modification of the hot-filament technique in which an instrumented strip-type specimen is directly heated by an external power source.

The following comparison can be made of the two methods.

ADVANTAGES OF THE ENCLOSED-HEATER TECHNIQUE

The power and thermocouple circuitry are separated in the internal-heater method. This allows the use of a direct-current power supply, which affords simpler and more accurate power measurements than does an alternating-current power supply commonly used with strip-type specimens. If direct current is used in the directly heated strip technique, it is necessary to reverse the current to correct for any pickup by the thermocouples.

The enclosed-heater method necessitates more power to produce a given specimen temperature than does the strip technique. Consequently, the percentage power loss by heat leakage through the termocouples and through the input electrodes is less. This is vividly illustrated by figure 2 of reference 1 which shows the power loss of two 5-mil Pt–$Pt_{90}Rh_{10}$ thermocouples spot welded 0.5 in. apart on a 0.200-in.-wide, 0.008-in.-thich platinum strip specimen. The percentage power loss to these thermocouples for the alloys Cb–1 Zr and Inor–8 is also shown. This power loss is negligible in the internal-heater technique.

The strip technique requires precise thermocouple placement, whereas the internal-heater method does not.

The strip technique requires more precise machining. For example, it was found necessary to machine strip specimens to ±0.0001-in. tolerances to produce acceptable temperature profiles.

The enclosed-heater method allows the measurement of E_t of insulators which cannot be heated directly.

Disadvantages of the Enclosed-Heater Technique

Severe temperature variations can occur along the specimen in the internal-heater technique. For example, at 477° C using a 1¾₆-in.-OD, 3-in.-tall cylindrical specimen, 60° C temperature differences from the bottom to the top of the specimen were measured. This may be due to the heater design.

The maximum temperature of the internally enclosed heater method is probably 1800° C for a reasonable heater life, whereas the strip technique is limited only by the melting point of the specimen and the power supply available.

The electrical resistivity of the specimen can be calculated from the data collected in the strip technique. This affords additional information related to metallurgical changes occurring in the specimen. For example, Worthing (fig. 3 of ref. 1) shows the effect of the cold work-anneal cycle and a short-range order reaction on E_t and electrical resistivity of Inor–8, a nickel-molybdenum-chromium-iron alloy which is the containment material for the Molten Salt Nuclear Reactor.

COMPARISON OF LMSC AND ORNL TECHNIQUES

A direct experimental comparison of the LMSC and ORNL techniques is shown in figure 38–5. This figure shows the results for Inor–8 obtained by using these two techniques. It can be seen that the corrected results agree to within ±3%. The instability of surfaces of metals or coatings on metals in hard vacuums is likely to cause changes in E_t. For example, a strip of Inor–8 was oxidized in air at 1000° C for 2 hr. It was then placed in a vacuum of 5×10^{-6} torr and the results shown in figure 38–4 were obtained. It was expected that the E_t values would lie above those for the specimen oxidized for 1 hr in air. But E_t decreased with increasing temperature and was erratic. Inspection of the surface showed the surface not to be covered with oxide but to be covered with a flaky metallic-looking film (shown in fig. 38–6). The exact cause for this phenomenon is unknown; however, the oxidized specimen received several heatings to at least 600° C in vacuo prior to data collection. This may have been sufficient to allow the carbon contained in the alloy to diffuse into and react with the oxide, or spontaneous oxide decomposition in this vacuum may have occurred. Figure 38–3 shows the effect of the oxidation of Co–1% Zr occurring above 400° C in a vacuum of 5×10^{-6} torr.

QUESTIONS

Finally, comment on the following is requested.

(1) Is correction for the thermal expansion of the specimen desirable? For example, at 1100° C (2000° F) a first-order expansion correction for Inor–8 is 2%.

(2) The onset of complications incurred by appreciable infrared transmission of the very thin coatings on the metal specimens could affect the measured "emittance" of the system. In addition, estimation of the surface temperature of the coating requires knowledge of its thermal conductivity. Are independent measurements of such coating properties being made?

REFERENCES

1. Worthing, A. G.: Temperature, Its Measurement and Control in Science and Industry, pp. 1164–87, American Institute of Physics, Reinhold Publishing Corp, New York, 1941.
2. Richmond, J. C.; and W. N. Harrison: "Equipment and Procedures for Evaluation of Total Hemispherical Emittance," J. Am. Ceram. Soc. 39(11), 668–73 (1960).
3. Abbott, G. L.; N. J. Alvares; and W. J. Parker: Total Normal and Total Hemispherical Emittance of Polished Metals, WADD Tech. Rept. 61–94 (April, 1961).
4. Dotson, L. E.: Emittance Coating Studies on Cb 1 Zr Alloy, General Electric Rept. R61FPD571 (Mar. 15, 1962).
5. Bradley, D.; and A. G. Entwistle: Determination of the Emissivity for Total Radiation, of Small Diameter Platinum-10% Rhodium Wires in the Temperature Range 600–1450° C, Brit. J. Appl. Phys. 12(2), 708–11 (Dec., 1961).

6. Davisson, C.; and J. R. Weeks: "The Relation Between the Total Thermal Emissive Power of a Metal and Its Electrical Resistivity, J. Opt. Soc. Am. 8, 585 (1924).
7. Forsythe, W. E.; and E. M. Watson: Resistance and Radiation of Tungsten as a Function of Temperature, *J. Opt. Soc. Am. 24*, 114–18 (1934).
8. Butler, C. P.; and E. C. Y. Inn: A Method for Measuring Total Hemispherical Emissivity of Metals, First Symposium Surface Effects on Spacecraft Materials, John Wiley and Sons, Inc., New York, 1960.
9. McElroy, D. L.; T. G. Godfrey; and T. G. Kollie: The Thermal Conductivity of INOR–8 Between 100 and 800° C, ASM Trans. Quart. (pending publication).

39—MEASUREMENT OF TOTAL HEMISPHERICAL EMITTANCE OF STRUCTURAL MATERIALS AND COATINGS UNDER SIMULATED SPACECRAFT CONDITIONS

BY G. MIKK AND W. H. ASKWYTH

PRATT & WHITNEY AIRCRAFT DIVISION, UNITED AIRCRAFT CORPORATION, EAST HARTFORD, CONNECTICUT

Several test rigs were designed and constructed to measure total hemispherical emittance, over a wide range of temperatures, under conditions which simulate the vacuum of space. The method used in all of the rigs is to compare the electrical power dissipated from an isothermal test section of a resistance-heated specimen to the total emissive power of a blackbody operating at the specimen temperature. Two types of tests are conducted in these rigs—determination of total hemispherical emittance as a function of temperature from approximately 200° F to 2200° F and determination of total hemispherical emittance as a function of time at fixed elevated temperatures (endurance tests). Specimens used for these tests were usually in the form of coated metal strips or coated thin-walled metal tubes. Some typical data presented are comparisons of results of various investigators and of results obtained in the various rigs used in these tests.

Studies of space propulsion systems have indicated the importance of radiant heat transfer in the design of such systems. Achievement of a proper design requires a knowledge of the emittance, absorptance, and reflectance of the materials of some components at conditions similar to those encountered in space, particularly the high vacuum.

Studies of the literature indicated that the published data on thermal radiation properties were not sufficient to design optimum space propulsion systems. It was found that information was lacking for many materials of interest at the desired temperatures of application and that most of the information available had not been obtained in a vacuum environment. Furthermore, little information was found on the change of emittance of materials due to prolonged periods in a high vacuum at representative temperatures. This information is necessary since chemical changes and phenomena such as sublimation may limit the application of otherwise desirable materials. For example, oxidized Inconel has high emittance, but, at high temperature and in a vacuum, the oxygen leaves, and the result is a bright surface of low emittance.

To provide information necessary for space radiator design, various rigs were built at Pratt & Whitney Aircraft to determine total emittance. Three of these rigs are discussed in detail in this paper: the original rig used to measure total hemispherical emittance under high vacuum conditions and over the approximate temperature range of 200° F to 2000° F; a new, larger total hemispherical emittance rig constructed in the early part of 1962; and an endurance rig in which emittance is measured as a function of time at constant temperature. A brief discussion of a fourth rig, one ordinarily used for spectral normal emittance measurements but which may also be used for total hemispherical emittance measurement, is also included.

The method used for measuring total hemispherical emittance involves determination of the temperature of and the power dissipation per unit surface area in the central portion of an electrically heated tube or strip specimen. If heat conduction and convection from this central portion or test section of the specimen as well as radiation returning to the test section from its surroundings are negligible, the total hemispherical emittance may be computed as

the power dissipation per unit surface area divided by the emissive power of a blackbody at the test section temperature. Radiation returning to and absorbed by the specimen is minimized by blackening and cooling the chamber walls. At the lower specimen temperatures, conduction of heat to the electrodes at each end of the specimen poses a problem, but this conduction heat loss is minimized in these tests by the use of controlled auxiliary electrical heating of the ends of the specimen. Since these tests are conducted in a high-vacuum environment, convection of heat from the specimen surface is not a problem.

All specimens for these tests involved a metal strip or tube as a base or substrate material. All nonmetal materials tested were thin coatings on the metal base. The emittances reported are based on the temperature of the metal substrate or the essentially black radiation from a cavity at the metal substrate temperature. This procedure has an engineering advantage for the intended application of the data, in that the questions of how much temperature drop there is through the coating layer and how opaque the coating layer is do not require separate answers. The data, as reported, give a direct measure of the emissive power of the surface as a function of the substrate metal temperature.

APPARATUS AND TEST PROCEDURE

Original Total Emittance Rig

The original total emittance rig consisted of a vacuum chamber, instrumentation flange, evacuating equipment, power supplies for sample heating and instruments for measuring power and temperature. A photograph of the test setup is shown in figure 39–1.

The test chamber was an 8-in. long, 3-in. internal diameter windowless chamber made of type 304 stainless steel. The inner walls were grooved and blackened with cupric oxide, to produce a low-reflectance surface. This minimized the reflection of energy, which originated from the sample surface, by the walls of the chamber. The chamber walls were also water-cooled to minimize the energy

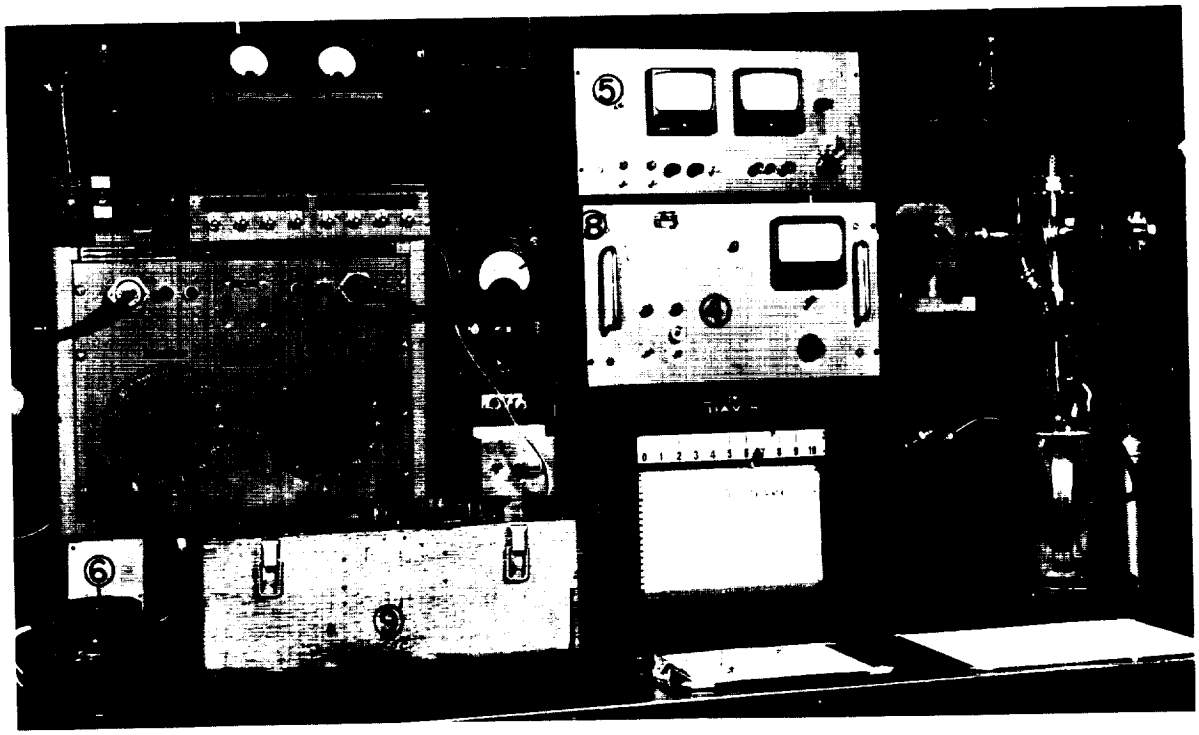

FIGURE 39–1.—Total emittance rig and associated equipment: (1) vacuum chamber and cooling bath, (2) ion gettering pump, (3) ionization gage, (4) pump power supply, (5) ionization gage power supply, (6) power supply for heating specimen, (7) end heater power supplies, (8) potential and current meter, and (9) potentiometer.

directly radiated from the chamber to the specimen.

The instrumentation flange, or chamber-top cover plate, contained the vacuum connection, power feed-throughs, thermocouple feed-throughs, and the specimen-support assembly. The vacuum connection was a 1-in. outside diameter tube leading to a "cross" where provisions were made through high-vacuum valves for the roughing and ion-gettering pumps. The remaining outlet of the cross was used for attaching a Bayard-Alpert ionization gage. The power feed-throughs for specimen heating, and end heating, were water-cooled copper leads which were soldered to the inside of type 410 stainless steel tubes. These were installed into the flange with "Pyroceram"—a form of solder glass manufactured by the Corning Glass Company. The thermocouple feed-throughs were similarly installed but were not water cooled. This method of installation of the feed-throughs provided a high vacuum seal and electrical insulation between the wires and the chamber components. The specimen-support assembly, consisting of the sample holder, fastening clamps, and thermocouple wire supports, was oriented so as to place the specimen away from the centerline of the chamber to minimize the effect of specularly reflected radiation from the chamber as discussed in appendix A of reference 1. A beryllium-copper leaf spring holding the lower specimen clamp was used to compensate for specimen thermal expansion. These details of chamber construction and specimen installation are shown in figure 39–2.

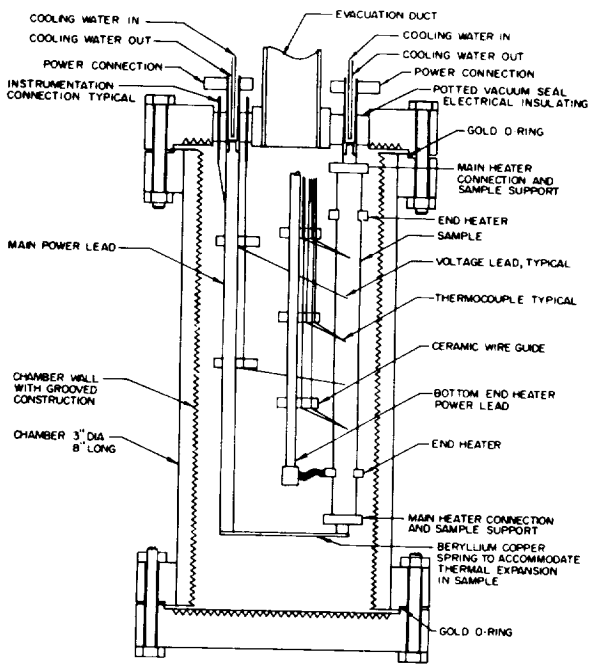

FIGURE 39–2.—Cutaway sketch of the total emittance rig showing the relative location of specimen and rig detail.

The evacuation equipment consisted of an oil-sealed mechanical roughing pump, and a 5-liters/sec ion-gettering pump. The mechanical pump was used in conjunction with a cryogenic trap to remove condensable materials from the system during pretest bakeout. Pressures of the order of 10^{-4} mm Hg were attainable with this pump. At the conclusion of bakeout, the ion-gettering pump, capable of 10^{-9}mm Hg, was valved in. Vacuum was measured by means of a Bayard-Alpert type ionization gage, and by noting the current in the ion-gettering pump which is calibrated to indicate the vacuum in the pump itself.

The specimens were heated by a-c power to simplify control and to eliminate thermocouple error caused by misalignment of thermocouple wires on the specimen which would result if heating was done by d-c power. Misalignment would introduce a portion of the specimen voltage drop into the thermocouple circuit. The power was obtained from a 7.5-kva transformer whose primary voltage was varied to provide an output ranging from 0 to 32 volts. The power input to the transformer was regulated to provide constant voltage at any desired level. A block diagram showing the vacuum and power system for this rig is shown in figure 39–3.

The test specimens were in the form of metal strips (usually stainless steel, molybdenum or aluminum) approximately 6 inches long, 0.40 in. wide and 2 or 5 mils thick. During the early part of the program some testing was done with uncoated strips to compare the results of this testing to those of other investigators and to establish emittance base-lines for some of the metals. Most tests were conducted on strips coated on both sides with selected coating materials. A few tests were conducted in which the strips were coated on one side only. The specimens were resistance-heated with the

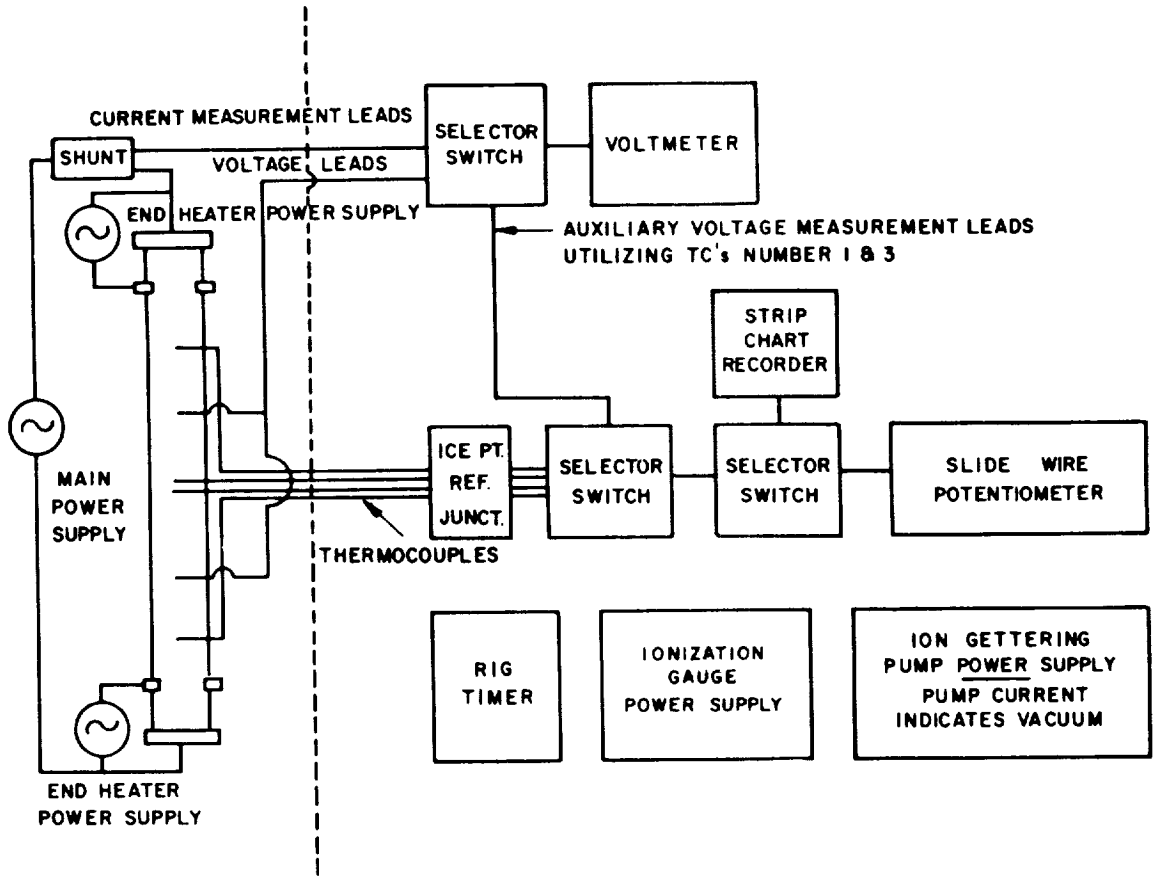

FIGURE 39–3.—Block diagram of total emittance rig instrumentation.

base, or substrate material of the strips, used as the resistance element.

Each specimen was instrumented with four surface thermocouples and a pair of voltage leads as shown in figure 39–4. A 1-mil Chromel-Alumel or platinum-platinum, 10% rhodium thermocouple wire was used throughout the tests. The wires were resistance welded to the specimen substrate except when aluminum specimens were used in which case the wires were buried in the substrate. Each pair of thermocouple wires was located on a line perpendicular to the axis of the strip so that errors due to axial temperature gradients were eliminated. When strips coated on one side were tested, the thermocouple and voltage leads were applied to the uncoated side of the strip to minimize possible thermocouple contamination by the coating material. However, the testing of strips coated on only one side was abandoned after a few tests. (For these specimens the emittance of the uncoated side had to be known for each test point. Testing of uncoated metals showed that changes in emittance due to "cleanup" were temperature-time phenomena which could not be easily repeated.) When strips coated on both sides were tested, scratches were made through the coating to the base metal so that the thermocouples and voltage leads could be attached. A schematic drawing of a typical thermocouple installation is shown in figure 39–5.

Additional heat was supplied at the ends of the specimen making it possible to obtain essentially uniform temperature for the specimen test section. This was done to minimize thermal conduction to cooled power leads and specimen supports. The end-heating was accomplished using separate variable a-c power supplies connected across ¾-in. segments at the ends of the specimen. These supplementary heaters were electrically phased to aid the main heating current and were controlled to achieve equal temperatures at thermocouples 1, 2, and 3.

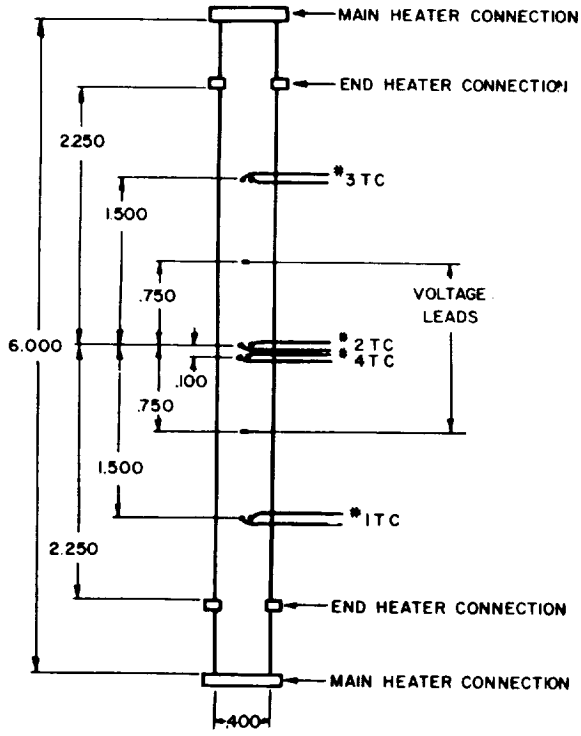

FIGURE 39–4.—Test specimen geometry and instrumentation arrangement for total emittance and endurance rigs.

The end heaters were usually not used for test points higher than 1000° F.

The test section of the specimen was a centrally located segment, approximately 1½ in. long. Its actual length and location were determined by the axial location of the voltage leads on the specimen. The test section temperature was measured by central thermocouples 2 and 4.

Specimen width, thickness, and distance between voltage leads were measured with a traveling microscope. The measurements as determined by this instrument can be considered to be accurate within ±0.0005 in. A vacuum-tube voltmeter was used to measure the voltage drop across the test section. The same instrument was used to measure the specimen current by measuring the voltage drop across a 50 mv-50 amp shunt. The measurements determined by this instrument are accurate to within ±1%. The outputs of the thermocouples were measured by a slide-wire millivolt potentiometer. The possible errors associated with these temperature readings are estimated to be ±0.5%. Therefore, it is estimated that errors in the total emittance values—due to voltage, current, dimension, and temperature measurement—are no greater than ±2.5% (rms).

Upon completion of each specimen installation, the chamber was baked out for 4 hr at 400°–450° F to remove contaminants. During this bake-out period, the system was pumped with the mechanical roughing pump in conjunction with the cryogenic trap. When bake-out was completed, the roughing pump was valved out of the system and the ion-gettering pump valved in. The rig was then left to cool to near-ambient temperature before cooling water was applied to the chamber walls. When the chamber had been pumped down to pressures in the 10^{-7} mm Hg range the emittance test was started. Pumping was continued throughout the test to maintain the lowest possible pressure. Emittance measurements were never made when pressures were sufficiently high to permit a significant amount of energy transfer by residual gas conduction.

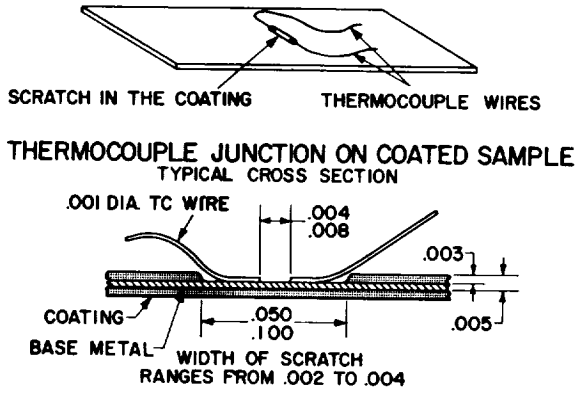

FIGURE 39–5.—Typical segment of coated sample with thermocouple and thermocouple junction on coated sample.

The following data are taken, from which the total hemispherical emittance of the specimen is determined:

V_{ts} the voltage drop across the test section of the specimen,

I the current through the specimen

T_m the measured temperature near the center of the test section.

The total hemispherical emittance can then be determined from the approximate relationship

$$\epsilon_{th}=\frac{I V_{ts}}{A_{ts}\sigma(T_m^4-T_w^4)} \qquad (1)$$

where A_{ts} is the surface area radiating the power (IV_{ts}), T_w is the temperature of the chamber wall, and σ is the Stefan-Boltzmann constant.

Emittance was determined at temperatures ranging from 200° F to 2000° F. For points below 1000° F supplemental heat was usually applied to the ends of the specimen to maintain a uniform temperature over the test segment. At each test point, data were taken when steady-state conditions had been established. In many cases, the specimens were maintained at 1450° F for approximately 17 hr (overnight) to get some indication of the stability of the coating when exposed to high temperature and high vacuum. Emittance was measured immediately before and after the overnight endurance period. When this procedure was followed, any data obtained at temperatures higher than 1450° F were taken after the overnight endurance period. As the specimen temperature was reduced, more emittance measurements were made to determine changes in the emittance vs. temperature curve due to exposure of the coating to high temperature and vacuum. When a preliminary evaluation of the data indicated that the test results were reliable, the specimen power was shut off, the rig was vented to the atmosphere, and the specimen was removed for further inspection and evaluation. When coatings were tested on aluminum substrates, the test procedure was essentially the same as above except that specimen temperatures were necessarily limited to 900° F and no overnight endurance tests were conducted.

Spectral Emittance Rig

A rig which is ordinarily used for spectral normal emittance measurements is also used occasionally for direct total hemispherical emittance measurements at high temperatures.[1] This rig is described fully in reference 1 and Paper 36 presented at this symposium by R. House, et al.

[1] In a few cases, both spectral normal and total hemispherical emittance measurements were made in this rig during the same tests. When this was done, the spectral normal emittance values were used to obtain total normal emittance by integration. The total normal and total hemispherical emittance values were then compared to each other and were usually in close agreement.

The test procedure for measuring total hemispherical emittance in this rig is essentially the same as discussed above except that ¼-in.-diameter thin-walled tubular specimens are used instead of strips. The specimens were heated by d-c power which necessitates voltage reversal to eliminate errors in indicated thermocouple output due to misalignment of thermocouple wires. Voltage and current measurements are made by a millivolt slidewire potentiometer in conjunction with appropriate auxiliary range resistors. Thermocouples were used for temperature up to 1400° F. At higher temperatures, an optical pyrometer was used to measure the temperature of a small blackbody hole drilled in the wall of the specimen. It is believed that these measurements are more reliable, at these high temperatures, than those obtained with thermocouples, since thermocouples may becomes contaminated by the specimen.

Endurance Rig

A total emittance endurance rig was built to provide a means of carrying out endurance tests to determine changes in emittance due to prolonged exposure to high temperature and high vacuum. This rig also yielded valuable qualitative information concerning the ability of the various coatings to adhere to the substrates for long periods of time under these conditions.

The rig is similar to the total hemispherical emittance rig. The chamber is slightly longer and is equipped with a window to allow the use of an optical pyrometer. End heaters were not included in the rig, since endurance tests are always conducted at temperatures sufficiently high for end conduction losses to be negligible.

Each endurance specimen is a coated ¼-in. diameter by 9-in. long thin-walled metal tube, and is provided with a small blackbody hole for temperature measurement by optical means. The specimens are instrumented in the standard manner with voltage leads and thermocouples to provide total emittance data as the specimens are heated from approximately 200° F to the endurance temperature and as they are cooled to approximately 200° F after the endurance test.

A few strip specimens were also endurance tested in this rig. In these tests, thermocouples were used to measure temperature during endurance, since the optical pyrometer could only be used to measure the surface brightness temperature of the strip specimens.

The endurance tests were usually conducted for periods of approximately 300 hours or until the emittance value stabilized. However, some samples were tested for longer periods of time. A few were tested for as long as 800 hours. Emittance data were usually taken several times during each working day. When the data indicated that changes in emittance were taking place, the data taking schedule was revised to obtain sufficient data to describe the test.

The test procedure for these tests was essentially the same as in ordinary total emittance tests until the point at which the endurance test was started. End conduction loss corrections, based on an analysis in reference 1, were made, when necessary, for total emittance data obtained at low temperatures.

New Total Emittance Rig

A new total emittance rig was designed and built during the early part of 1962. Several improvements which past testing indicated were necessary or desirable were incorporated into this rig. A major consideration in the design of the rig was that it be adaptable for use in other investigations relating to space radiator operation.

The rig consists of a 20-in. high, 15½-in. internal diameter vacuum chamber which is evacuated by a 400-liter/sec oil diffusion pump. Pressures of less than 1×10^{-7} mm Hg are attainable with this system. The rig can also be operated with an ion-gettering pump when higher vacuums are desired High-vacuum seals and bakeout heaters have been incorporated into the rig for this purpose. For routine operation, the large oil diffusion pump will be used so that rapid data taking can be accomplished.

The design of the rig is based on the bell jar type of system, as shown in figure 39–6, to simplify operating procedures. The chamber is fabricated from type 304 stainless steel and is coated on the inside with an aluminum phosphate bonded mixture of silicon carbide and

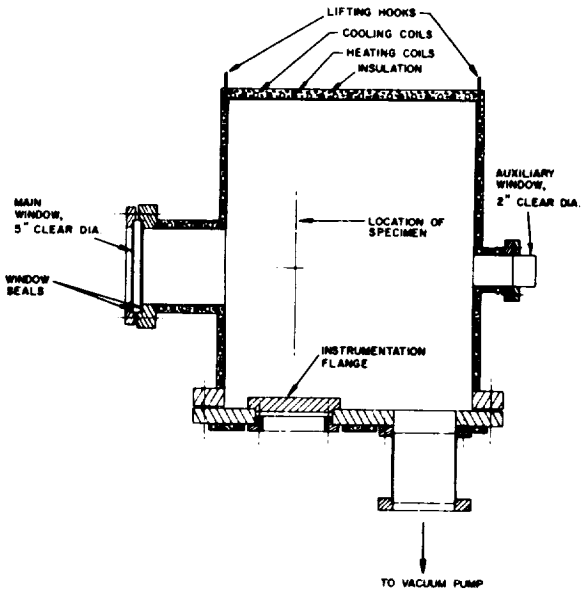

FIGURE 39–6.—Vacuum chamber for new total emittance rig.

silicon dioxide. This permanent high-emittance (low-reflectance) surface and the large diameter of the chamber satisfy the requirement that the reradiation from the chamber to the specimen be negligible. Permanent bakeout heaters and cooling coils are incorporated into the rig to allow the chamber to be baked out prior to test when necessary and to be cooled to any desired level during test. Water is the normal cooling fluid. However, with appropriate accessory systems any coolant, including liquid nitrogen, may be used.

Two windows, of 5.4- and 2.0-in. clear diameters, are located 180° apart to provide for visual inspection of the specimen and to permit temperature measurement by optical means during test. When the windows are not in use, magnetically-operated shutters reflect the radiation originating from the specimen onto nearby cooled walls. This eliminates heating of the windows and consequent reradiation of energy from the window to the specimen.

The rig is usually assembled with "Viton" O-rings, but O-rings of other materials, including soft metals such as annealed gold, can be used.

A removable instrumentation flange holds the specimen during test and provides all the thermocouple and power terminals and accessory systems—such as end heaters and the ex-

pansion take-up device. The flange is removable so that the rig can be conveniently converted to use for other purposes. The specimens are installed under tension by compressing the expansion take-up coil to prevent buckling due to thermal expansion. All power leads are cooled and coated with a high-emittance material to minimize reflection and reradiation of energy back to the specimen. Figure 39–7 is a sketch of the instrumentation flange showing the relative location of the components.

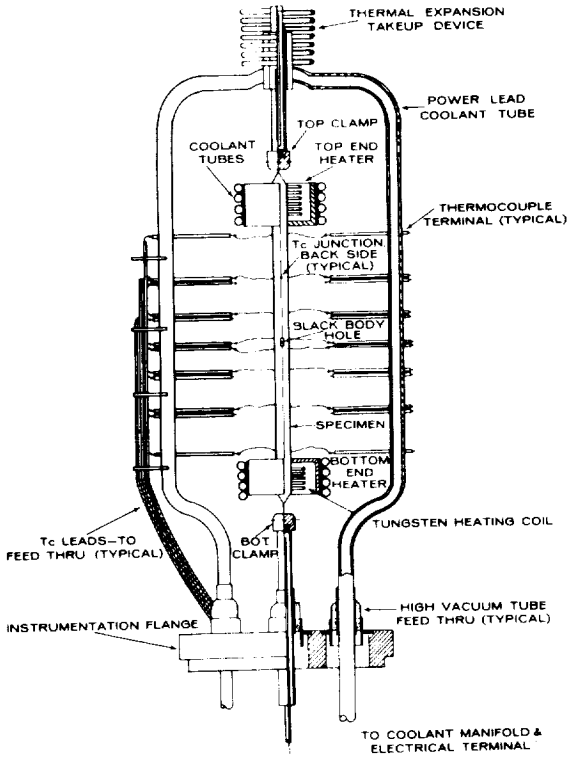

FIGURE 39–7.—Instrumentation flange for new total emittance rig.

The specimens are in the form of coated or uncoated ¼-inch-diameter, 9-inch-long thin-walled metal tubes. As in the previous rig, they are electrically resistance heated by a-c power. End heating, to minimize thermal conduction to cooled electrical connections and specimen clamps, is accomplished by means of radiation end heaters. These end heaters consist of tungsten wire coils which heat a small segment of the specimen near each end by radiation only. The coils are oriented and shielded so the radiation from them does not strike the centrally located test segment.

Power for specimen heating and end heating is provided by a Superior Electric voltage regulator capable of 0.25% regulation. Control is by variable voltage output transformers in the primary circuits of the rig power transformers. Current as high as 550 amp can be provided for specimen heating and an additional 100 amp are available for each end heater. This large current capacity permits greater flexibility of operation such as the use of thicker specimens or very high operating temperatures.

The instrumentation flange, which provides for seven platinum-platinum, 10% rhodium and five Chromel-Alumel thermocouple terminals, allows specimens to be instrumented with either, or both, of these types of thermocouples. Normally, 3-mil-diameter reference-grade wire is used, but wires as small as 1 mil have been used. The thermocouples are installed on the specimen either by resistance welding or by burying in the substrate metal. As in previous total emittance tests, scratches are made through the coatings to the base metal so that the thermocouples can be installed. The specimens are usually instrumented with seven platinum-platinum, 10% rhodium and one Chromel-Alumel thermocouple, as shown in figure 39–8. Thermocouples 1 and 7 are used for end heater control. All thermocouples are available to determine the temperature profile of the specimen so that end conduction losses may be calculated accurately when end heating is not used.

In addition to temperature measurements by thermocouples, measurements are also made by an optical pyrometer and an infrared pyrometer. These instruments are used to measure the temperature of a blackbody hole drilled through the specimen wall. As the specimens are heated to 1400° F the No. 4 thermocouple reading is used as the primary temperature measurement. For data taken at temperatures of 1400° F, or higher, the optical pyrometer reading is used as the primary temperature measurement and the rest of the measurements provide reliability data.

Voltage measurements for power dissipation are made by selecting any desired set of thermocouple leads and measuring the voltage drop over the segment defined by the location of the leads. Thermocouples 3 and 5 are used to define the standard test section but any other

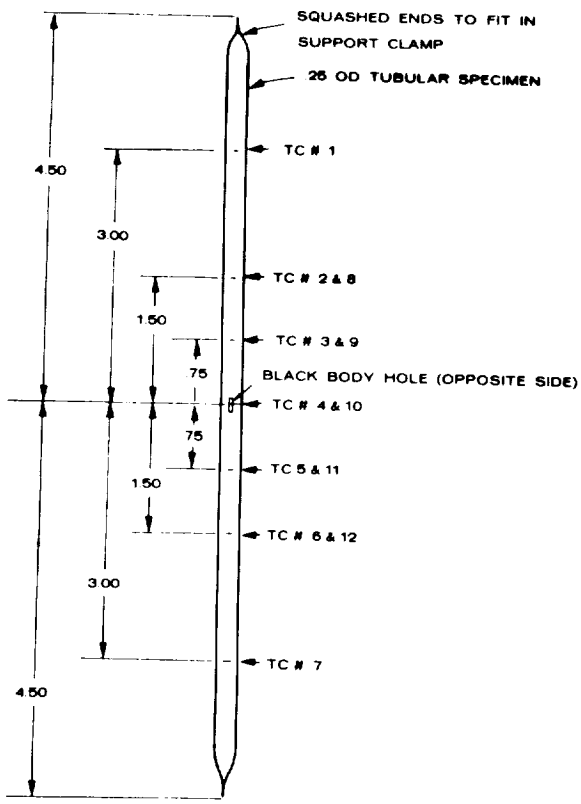

FIGURE 39-8.—Schematic drawing of tubular emittance test specimen showing thermocouple locations.

pair can be used by turning the voltage lead selector switch to the appropriate set. The distances between the thermocouple wires are measured with the traveling microscope and are accurate to ± 0.0005 in.

Voltage across the specimen test section is measured by a model 803 differential a-c, d-c voltmeter produced by John Fluke Manufacturing Company. This instrument is also used to determine specimen heating current by measuring the voltage across a selected shunt. The instrument provides $\pm 0.2\%$ accuracy for each of these two measurements as compared to $\pm 1\%$ accuracy for the same measurements made in the previously used total emittance rig.

Thermocouple output is measured with a Leeds and Northrup millivolt potentiometer in conjunction with an ice-bath reference junction. It is estimated that thermocouple error remains at $\pm 0.5\%$.

A RG-3A Veeco ionization gage is used to measure the vacuum level in the system.

As with testing in the previously used total emittance rig, the specimen is installed in the rig and clamped under tension to compensate for thermal expansion upon heating. The chamber is assembled and pumped down to a pressure of less than 1×10^{-6} mm Hg before the emittance test is started. In cases where the system has become contaminated the chamber is baked out at 350° F to remove the contaminating material before the test is begun.

Total emittance of each sample is usually measured at temperatures from 200° F to 2200° F with at least one measurement for every 100° F interval. Testing is usually completed in a single day, and no overnight endurance test is included as part of the standard testing procedure.

ACCURACY

The errors introduced by the measuring apparatus are discussed with the description of each rig. The root-mean-square values of these errors are:

	%
old total hemispherical rig	2.5
new total hemispherical rig	2.0
emittance endurance rig	2.5
spectral emittance rig—when used for total hemispherical emittance measurements	1.6

In addition to the correction for instrument precision, various other corrections have been considered. A brief discussion of each of these corrections follows. A complete analysis of each may be found in the designated appendix to reference 1.

The correction for chamber wall reflection, as discussed in appendix B of reference 1, is estimated to be less than 1% even for the highest emittance materials. Application of this correction would give a higher value of emittance than calculated directly from equation (1).

In some instances, drift in the calibration of the thermocouples was encountered. One of these instances, described in appendix N of reference 1, involved the use of a Chromel-Alumel thermocouple welded to a molybdenum specimen. This instance led to the use of platinum-platinum, 10% rhodium thermocouples in all other tests involving molybdenum as the substrate material. Another instance occurred

using a platinum-platinum, 10% rhodium thermocouple welded to a stainless steel (substrate) tube with a chromium-black coating. While data have not been reported in any case where more than $\pm\frac{1}{2}\%$ drift was detected, this effect has not been checked in every test. Spot checks were made, however, by reinstrumenting the sample and comparing emittance values before and after the change. On the total emittance rig, the standard deviation (rms value) of the total emittance data, based on the test on crystalline boron coated on one side of a vapor blasted molybdenum strip, was 0.7%. On the endurance rig, the standard deviation (rms value) of the total emittance data based on the test on boron carbide was 0.9%.

Corrections were also considered for the effect of temperature differences between the coated and the uncoated side of a one-side-coated strip specimen, and the effect of specimen "flickering" due to the use of 60-cps heating current (for tests in the total emittance and endurance rigs, only).

The magnitude of these corrections was found to be negligible. Temperature difference between the coated and the uncoated face of a specimen is evaluated and discussed in appendix J of reference 1, and the effect of the increase and decrease in specimen temperature due to the 120-cps fluctuation in heat generation rate (for the total emittance and the endurance rigs, which use a-c heating) is evaluated in appendix K of reference 1 and is negligible for these tests.

The effect of heat conduction losses at the extremities of the test section is analyzed in appendix G, of reference 1. The results of this analysis indicate that the correction for heat conduction loss is generally negligible for these tests, even without compensating end heat applied, when the temperature at the center of the specimen is above 1000° F. For the test of a molybdenum strip coated on both sides with boron carbide and tested without end heating, this correction was applied, giving lower emittance values than computed from equation (1) by the amounts shown in Figure 39–9.

In tests where emittance was measured with compensating end heat applied, error on the order of $\pm 5\%$ from this source alone is difficult to avoid as the temperature level is reduced below about 350° F, because of the inability of

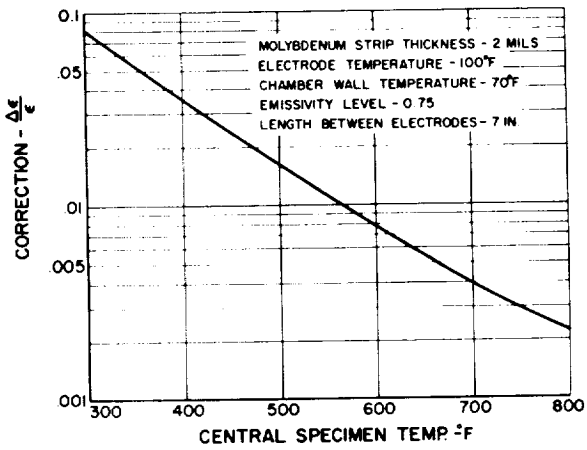

FIGURE 39–9.—Correction for heat conduction losses.

setting indicated end and central temperatures precisely equal and because of the error in measuring these temperatures. This effect may also be readily seen from the results of appendix G, of reference 1. More accurate measurements of emittance at the lower temperatures could be achieved by using longer chambers and specimen strips. The new total emittance rig permits the use of longer specimens to improve the accuracy of data taken at low temperatures.

RESULTS

A large number (approximately 100) of specimens has been tested in the rigs described, and new total emittance data are being generated continuously. Examples of some of the data obtained are shown in figures 39–10, –11, and –12. Figure 39–10 compares total hemispheri-

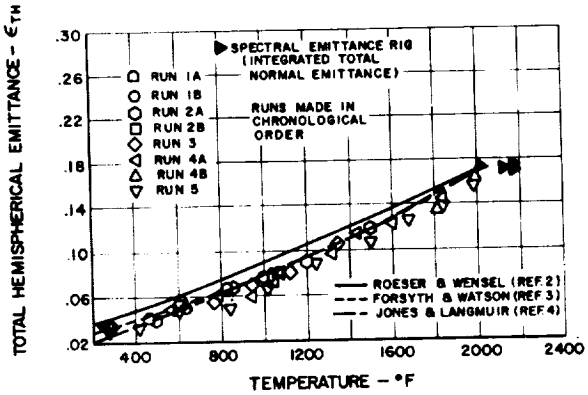

FIGURE 39–10.—Total hemispherical emittance of tungsten.

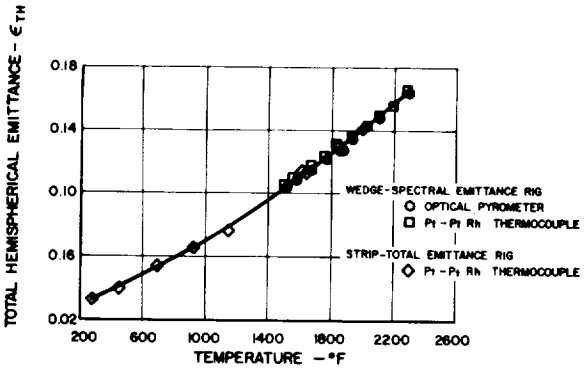

FIGURE 39–11.—Total hemispherical emittance of molybdenum.

cal emittance data obtained with a tungsten strip specimen to those of other investigators (ref. 2, 3, and 4). Figure 39–11 compares data obtained with molybdenum samples, fabricated from the same sheet of stock, in the small total hemispherical rig and the spectral emittance rig when used as a total hemispherical emittance rig. Figure 39–12 compares typical total emittance data obtained in the small total emittance rig and in the endurance rig.

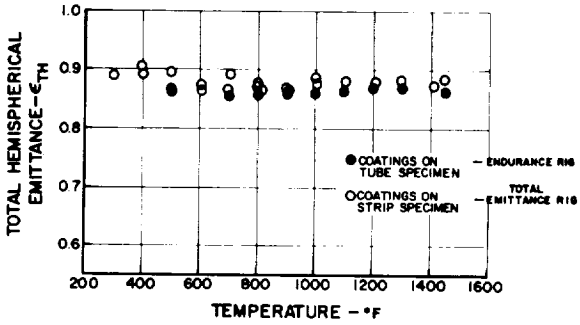

FIGURE 39–12.—Effect of temperature on total hemispherical emittance of aluminum phosphate bonded mixture of nickel-chrome spinel and silicon dioxide on type 310 stainless steel.

REFERENCES

1. Anon.: Measurement of Spectral and Total Emittance of Materials and Surfaces Under Simulated Space Conditions. PWA–1863, Pratt & Whitney Aircraft Co., 1960.
2. ROESER and WENSEL (National Bureau of Standards): Table of Properties of Tungsten in Handbook of Chemistry and Physics (C. D. Hodgman, ed.), Chemical Rubber Publishing Co., Cleveland, 40th ed., p. 2955.
3. FORSYTHE, W. E., and WATSON, E. M.: Resistance and Radiation of Tungsten as a Function of Temperature. Jour. of Opt. Soc. of Am., vol. XXIV, Apr. 1934, pp. 114–118.
4. JONES, H. A., and LANGMUIR, I.: The Characteristics of Tungsten Filaments as Functions of Temperature. Gen. Elec. Rev., vol. XXX, June 1927, pp. 310–319; July 1927, pp. 354–361.

40—APPARATUS FOR THE MEASUREMENT OF HEMISPHERICAL EMITTANCE AND SOLAR ABSORPTANCE FROM 270° TO 650° K

BY T. W. NYLAND

NASA LEWIS RESEARCH CENTER, CLEVELAND, OHIO

A steady-state heat-balance method is used in making measurements of total hemispherical emittance, solar absorptance, and the ratio of solar absorptance to emittance. Equations are developed that relate the radiant properties to the test procedure and apparatus. The system utilizes 1-inch-square test samples, which are mounted on an electrically heated, temperature controlled plate. Automatic temperature control is employed to increase accuracy in maintaining temperatures. An evacuated low-temperature radiation receiver is used for the test environment, and a carbon arc is utilized as the source of solar simulation. An error analysis of the system predicts a nominal accuracy of ±5%.

The prediction and control of temperature in space systems requires knowledge of the radiation properties of vehicle surfaces. In both active and passive satellite temperature-control systems, coatings with particular emittance and/or absorptance properties are selected to obtain desired thermal equilibrium conditions. For many space power systems, radiators comprise a large percentage of system weight, and the emittance properties of the radiator surface influence the weight to a large degree. For radiators operating at 650° K or less, the radiated power is sufficiently low that the absorbed incident solar flux must also be considered in thermal analysis of such systems. Thus, the measurement of the emittance and absorptance of surfaces and coatings are important in the development of space systems.

Many problems involving coatings for space systems have been encountered in various projects undertaken at the Lewis Research Center. Equipment for measuring spectral emittance and reflectance of materials has been available at the Center for some time, but not equipment for making easy and accurate measurements of total hemispherical emittance and normal solar absorptance. Since the latter measurements would be useful for preliminary screening of various test samples, suitable equipment has recently been developed. (Total hemispherical emittance and normal solar absorptance are hereinafter referred to as emittance and solar absorptance, respectively.)

An energy-balance method is used in making the measurements on 1-inch-square test samples at temperatures from 270° to 650° K. An evacuated liquid-nitrogen-cooled radiation receiver and a high-current-density carbon arc are used to obtain the required test conditions. Temperature-control equipment is utilized to simplify the test procedure. Similar measurement techniques are described in references 1 to 4.

SYMBOLS

A	exposed surface area, cm²
c	sample specific heat, (watt-sec)/(gram)(° K)
m	sample mass, grams
Q	power absorbed by specimen from external source, watts
Q_{gen}	internal heat generation, watts
Q_l	unknown energy losses, watts
Q_{mc}	power stored by specimen thermal mass due to non-steady-state condition
$Q_{rad\ in}$	power radiated from receiver to specimen, watts
$Q_{rad\ out}$	power radiated from specimen to receiver, watts
q	external incident flux, watts/cm²
q_{ei}	electrical internal power input per unit area, watts/cm²
t	time, sec
α_{rs}	effective absorptance of receiver for sample radiation

α_{sr} absorptance of sample surface for receiver radiation
α_{ss} absorptance of sample surface for solar radiation
ϵ_r effective receiver emittance
ϵ_s sample emittance
θ_r radiation receiver temperature, ° K
θ_s sample temperature, ° K
σ Stefan-Boltzmann constant, watts/(cm²)(° K⁴)

HEAT-TRANSFER ANALYSIS

The equations relating the radiation parameters to the temperature of a surface in a space environment can be derived by applying an energy balance to a test specimen. The resulting equations can be transformed under various assumptions to a form from which the emittance, solar absorptance, and/or the ratio of solar absorptance to emittance can be calculated from measurements of temperature and power.

Figure 40–1 illustrates a test specimen with a coated test surface suspended in a vacuum surrounded by a radiation receiver. The test specimen has a source of internal heat generation, and is mounted in a system such that the coated test surface can be irradiated with an external source of simulated solar radiation.

Applying an energy balance to the test specimen results in the following general equation:

$$Q+Q_{gen}+Q_{rad\ in}=Q_{rad\ out}+Q_{mc}+Q_L \qquad (1)$$

The terms $Q_{rad\ in}$, $Q_{rad\ out}$, and Q apply only to energy emitted or absorbed by the test surface. Q_L includes all other energy exchange terms applicable to an energy balance on the test specimen. Each of these terms can be expressed

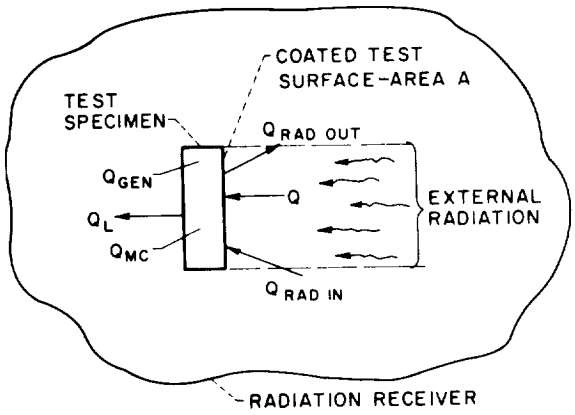

FIGURE 40–1.—Schematic diagram of heat balance.

in fundamental heat-transfer parameters as follows:

$$Q=\alpha_{ss}qA$$

$$Q_{gen}=q_{ei}A$$

$$Q_{rad\ in}=\alpha_{sr}\epsilon_r\sigma A\theta_r^4$$

$$Q_{rad\ out}=\alpha_{rs}\epsilon_s\sigma A\theta_s^4$$

$$Q_{mc}=mc\frac{d\theta_s}{dt}$$

$$Q_L=f(\theta_s, \theta_r)$$

Substituting these terms into equation (1) results in

$$\alpha_{ss}qA+Aq_{ei}+\alpha_{sr}\epsilon_r\sigma A\theta_r^4 = \alpha_{rs}\epsilon_s\sigma A\theta_s^4+mc\frac{d\theta_s}{dt}+f(\theta_s, \theta_r) \qquad (2)$$

Equation (2) can be simplified by making four basic assumptions:

(1) The receiver has the properties of a blackbody cavity

$$\epsilon_r=\alpha_{rs}=1$$

(2) The ratio

$$\frac{\alpha_{sr}}{\epsilon_s}=1$$

(3) Steady-state conditions exist during tests

$$\frac{d\theta_s}{dt}=0$$

(4) No external energy loss occurs in the mounting arrangement

$$f(\theta_s, \theta_r)=0$$

The resulting equation is

$$\alpha_{ss}q+q_{ei}=\epsilon_s\sigma(\theta_s^4-\theta_r^4) \qquad (3)$$

Setting various test conditions on the system, the parameters α_{ss}, ϵ_s, and the ratio α_{ss}/ϵ_s can be found:
Conditions for the emittance test:

$$q=0 \therefore \epsilon_s=\frac{q_{ei}}{\sigma(\theta_s^4-\theta_r^4)} \qquad (4)$$

Conditions for the $\alpha/_{ss}\epsilon_s$ test:

$$q_{ss}=0 \qquad \theta_r^4 << \theta_s^4$$

$$\frac{\alpha_s S}{\epsilon}=\frac{\sigma\theta_s^4}{q} \qquad (5)$$

Conditions for the solar-absorptance test:

$$q=0$$

and thus,

$$q_{et_1}=\epsilon_s\sigma(\theta_{s_1}^4-\theta_{r_1}^4) \tag{6}$$

$q=SC$ or a solar constant

$$q\alpha_{sS}+q_{et_2}=\epsilon_s\sigma(\theta_{s_2}^4-\theta_{r_2}^4) \tag{7}$$

Subtracting equation (6) from (7) with $\theta_{s1}=\theta_{s2}$ and $\theta_{r1}=\theta_{r2}$ gives

$$\alpha_{sS}=\frac{q_{et_1}-q_{et_2}}{q} \tag{8}$$

Equations (4), (5), and (8) indicate that the emittance, the ratio of absorptance to emittance, and the solar absorptance can be measured by using an evacuated blackbody low-temperature receiver, a source of solar energy, a test specimen capable of internal heat generation, and a support or mounting assembly that eliminates external energy losses from the specimen.

TEST APPARATUS

The test equipment consists of the following components: the test specimen, the test chamber and associated vacuum system, the test specimen mounting assembly, the carbon-arc solar simulator, and two automatic temperature controllers.

Test Specimen

The test apparatus is designed to use 1-inch-square test samples. The test sample is applied or bonded to a back-up plate shown in figure 40–2. Aluminum, 0.060 inch thick, is preferred as the back-up plate material because of thermal-conductivity considerations. The back-up plate and test specimen are hereafter referred to as the test specimen. Two 0–80 tapped holes are used to attach the test specimen to the heater plate, which is described later.

Test Chamber

A schematic diagram of the test chamber and vacuum system for the emittance test is shown in figure 40–3A. The outer chamber consists of a 25-inch-long, 8-inch-diameter stainless steel cylinder with bolt-on end flanges using neoprene O-ring seals. The radiation

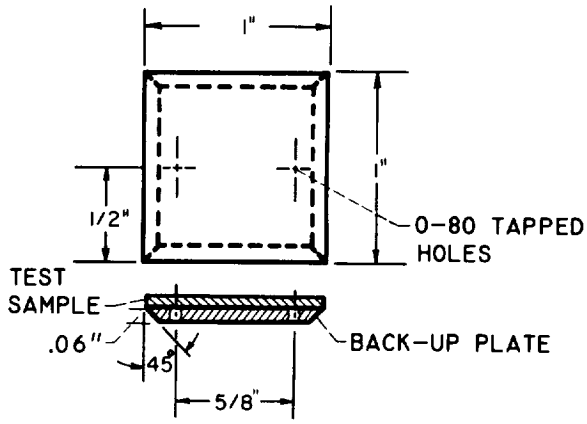

FIGURE 40–2.—Test specimen and back-up plate.

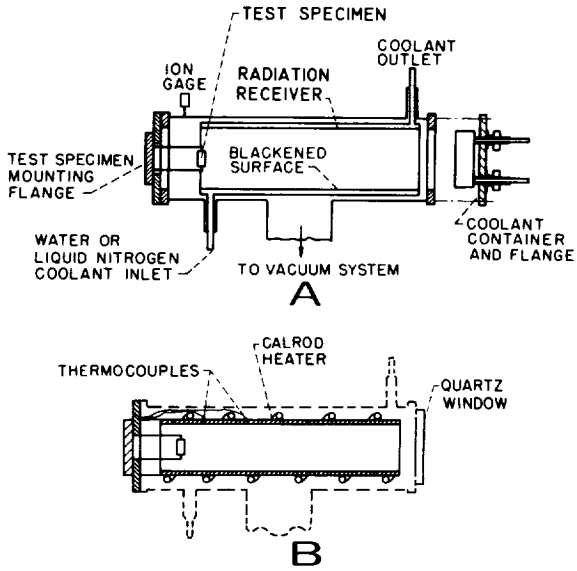

FIGURE 40–3.—Test chamber. A—Test chamber setup for emittance tests and low-temperature absorptance tests. B—Test chamber insert for high-temperature absorptance tests.

receiver consists of a hollow cylinder 22 inches long and 6 inches in diameter and is located concentrically inside the outer chamber. The inside surface of the radiation receiver is blackened with carbon soot and is cooled with either liquid nitrogen or water. The test-specimen mounting assembly is supported from a flange on the left end of the chamber. The emittance tests are made with the right flange fitted with a coolant container in which either liquid nitrogen or water can be circulated. A quartz window replaces this assembly when the absorptance or ratio tests are run.

For absorptance tests at 450° K or above, a heated tube is positioned inside the radiation receiver as shown in figure 40–3B. The purpose of the tube is to reduce the net steady-state emitted power from the test specimen so that the difference in power measured with and without irradiance is large in comparison to the net power rediated from specimen to receiver. This in effect increases the sensitivity of the power measurement.

The tube is supported from an end flange, which is bolted to the outer chamber. The test-specimen mounting assembly is inserted into the center of the tube. The tube is 3 inches in diameter and 16 inches long and is made from ¼-inch-thick copper blackened on the inner surface. A Calrod type heater is silver-soldered to the outside surface of the tube. Iron-constantan thermocouples are peened into the outside surface and spaced so that the temperature is measured at distances covering constant hemispherical angles as seen from the test-specimen plane. The temperature of the tube is controlled manually.

A line diagram of the vacuum system is shown in figure 40–4. The pumping system can evacuate the test chamber to 10^{-5} torr in 15 min and 10^{-6} torr in 30 min with liquid nitrogen in the 3-inch baffle and water in the radiation receiver. The ultimate pressure of the system is less than 10^{-7} torr with liquid nitrogen in the receiver. Pressure measurements are made with two ion gages, one located near the test specimen, and the second in the area above the ion pump. Normal working pressures are 10^{-6} torr, where heat transfer by molecular conduction compared to heat transfer by radiation is small.

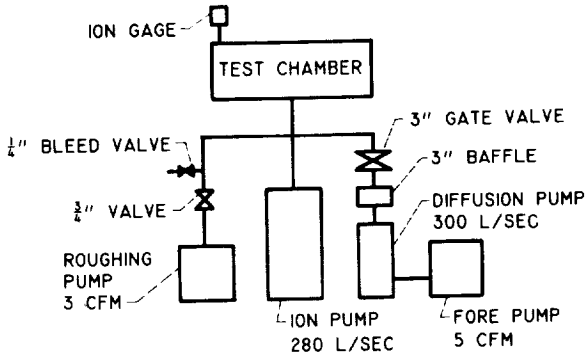

FIGURE 40–4.—Vacuum system.

Test-Specimen Mounting Assembly

A cutaway drawing of the test-specimen mounting assembly is shown in figure 40–5. The test specimen is held with two 0–80 cap screws to a 0.96- by 0.96- by 0.120-inch aluminum heater plate. A series of grooves is milled part way through the plate, and a length of 36-gage glass-coated Chromel wire is cemented into each groove. This wire provides the resistive heating element required for the internal-energy generation in the test specimen. The heater wire is terminated on a glass-to-metal feedthrough, peened into the back surface of the aluminum plate. A 36-gage iron-constantan thermocouple is peened into the top surface of the plate and is used to measure the temperature of the test specimen.

The heater plate is centered inside a temperature-controlled heat shield as shown in figure 40–5. The heat shield is made of aluminum and is in the form of a square cup having outside dimensions of 1½ by 1½ by ¾ inch and inside dimensions of 1⅛ by 1⅛ by ½ inch. A 32-gage glass-coated iron wire is cemented in a series of grooves milled on the outside surface and is used as the heating element for the shield. A 36-gage iron-constantan thermocouple is peened into an inside surface of the shield and used for temperature-measurement and control. The inside surfaces of the shield are blackened with carbon soot.

For the purpose of reducing heat losses from the edge of the test specimen, a mask is placed on the outside surface of the heat shield and is adjusted so that the slot width between the test-specimen surface and heat shield is minimized.

Four thermally-insulated screws are used to center the heater plate in the shield. 32-gage

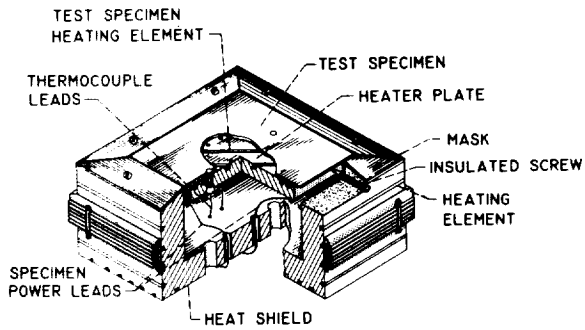

FIGURE 40–5.—Test specimen mounting assembly.

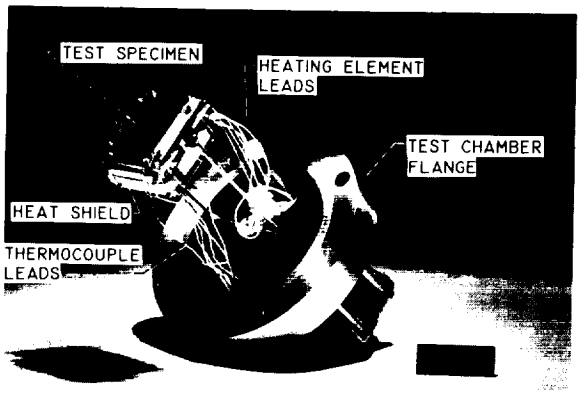

FIGURE 40-6.—Test specimen mounting assembly with flange.

copper wire is used to extend the power leads from the heater plate through two electrically insulated holes in the bottom of the shield. These wires terminate on two standoffs located on the back surface of the shield. Pairs of potential leads and power leads are then wrapped twice around the shield for temperature stabilization (about 15 inches of wire) and brought out through the mounting flange. The power leads for the shield are also wrapped in a similar manner.

The heater plate and shield assembly are supported from a stainless steel flange by stainless steel tubing. Two glass-to-metal seals are used to bring the power and thermocouple leads through the flange. Figure 40-6 shows some of the detail.

The test specimen can be mounted to the heater plate without removing the heater plate from the cup assembly. The 0-80 cap screws are inserted through two holes in the bottom of the heat shield and into the test specimen. In this manner, the need for instrumenting each individual test specimen is eliminated, since the same heater plate and thermocouple are used for all test specimens.

Solar Simulator

The solar simulator, consisting of a modified carbon arc source and an optical system, is an in-house development of the Lewis Research Center. A commercial carbon arc source has been modified to burn 10-mm diameter positive carbons at 150 amp. A fused-quartz refractive condensing system is used to form a $\times 3$ magnified image of the arc. This image is located at the focus of a spherical mirror that forms a collimated beam of radiation. To maximize the uniformity in the target plane, one of the condensing lenses is imaged in the target plane. By use of suitable optics, a portion of the beam

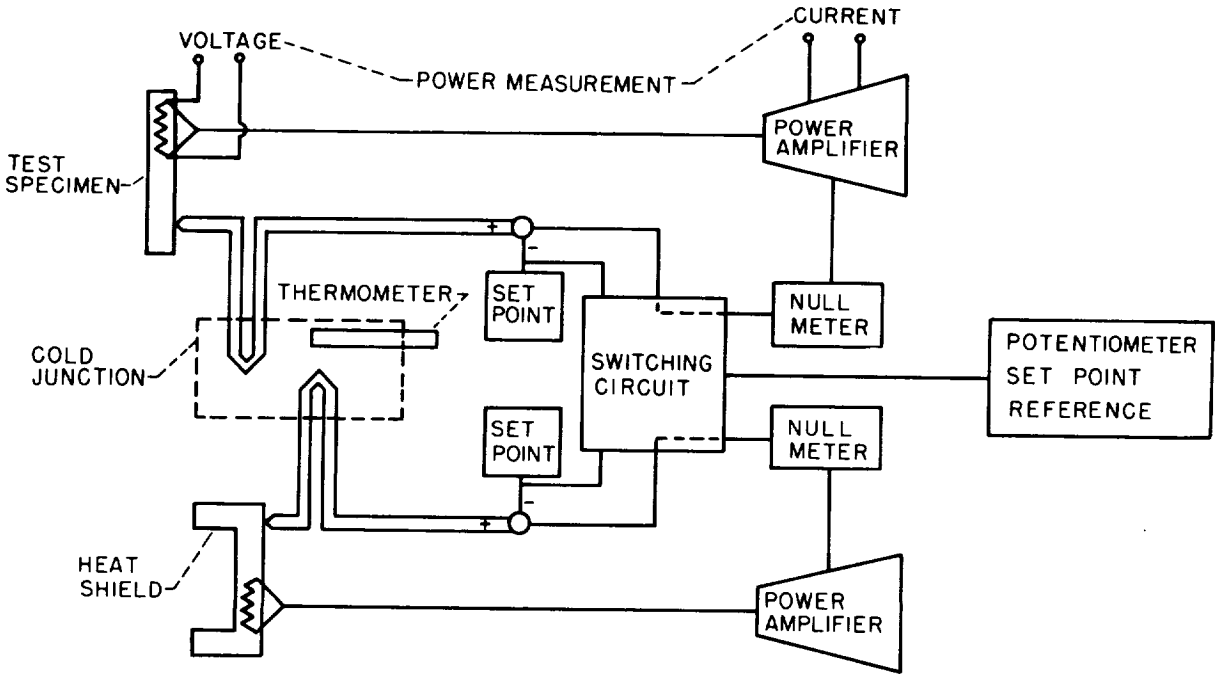

FIGURE 40-7.—Temperature control system.

is directed toward a photovoltaic cell, which acts as a radiation monitor and sensor for an automatic intensity-control system. The plane of the photocell is conjugate to the target plane in the system. A movable lens in the condensing system is automatically positioned to compensate for variation of the source irradiance.

Initial calibration of the system for one solar constant of irradiance is accomplished by placing a calibrated narrow-angle pyroheliometer in the target plane. The irradiance in the collimated beam has been measured to 2% and is controlled to within ½% of a constant value. Variation of the irradiance over the 6-inch-diameter beam in the vicinity of the test plane is 2% when measured with a sensor whose sampling diameter is 2% of the beam diameter. More details of a similar source are given in reference 5.

Automatic Temperature Control

A diagram of the temperature measurement and control system is shown in figure 40–7. The purpose of the control system is to make the temperature of the test specimen and the heat shield the same so as to eliminate extraneous heat losses from the test-specimens assembly. A null method is used for control employing two similar control systems for the test specimen and heat shield. A switching circuit provides a means to measure the temperature set-point voltages externally with a potentiometer and balance the heat-shield set point against the test-specimen set point.

The iron-constantan thermocouples from the test specimen and shield are referenced to cold junctions and applied to the set-point voltages. The differences between the thermocouple EMF and the set-point voltages are detected with commercial null meters built into the control system. The voltage supplies for the set points are stabilized with temperature-compensated Zener diodes.

A power amplifier, similar to that used in reference 6, is placed across the indicator circuit of the null meter. A differential amplifier drives a two-stage transistorized power amplifier to provide the controlled current to heat the test specimen or heat shield. The current in the test-specimen heater is measured in the form of a voltage drop across a calibrated series resistor. The voltage is measured with potentiometer leads brought out from the heater plate. A potentiometer is used to make these measurements.

ERROR ANALYSIS

An error analysis has been made to determine the accuracy of the measurements and the magnitude of error inherent in the measurement technique. A discussion of a number of systematic and random errors associated with the test apparatus along with the general procedure used to determine the relative magnitudes of error follows.

SYSTEMATIC ERRORS

Blackbody Assumption

A source of systematic error is introduced in the measurements because of the design of the radiation receiver. Values for the effective radiant emission from the open end of a closed cylinder were found in reference 7 and given as a function of the length-to-diameter ratio and actual surface emittance. The values were obtained from equations derived under the assumption that the surfaces emit in a gray diffuse manner. The emittance of the cylinder surface was assumed to be 0.95 or higher, and it was estimated from the tables that the effective emittance of the cavity is no less than 0.99. In neglecting a receiver emittance of 0.99, an error of less than 1.5% is introduced into the measurement and results in a lower emittance or ratio when not considered.

Test-Specimen Edge Loss

Radiant-energy exchange between the test-specimen edges and the enclosure creates a second source of systematic error. Calculations were made to determine the relative amount of flux emitted from the test-specimen edges through the space between the heat shield and the specimen surface. A configuration factor of less than 0.075 was estimated from computations made using an equation given in reference 8. (The relative amount of heat lost can be determined by multiplying this factor by the area and emittance ratios of edge to specimen.) For a specimen with emittances greater than 0.3 (estimated edge emittance), the error is less than 1.8%. The calculated emittance is higher when this factor is neglected.

Test Specimen Nonuniformity

A third source of systematic error is introduced because of the nonuniformity of the test-specimen surface caused by the presence of the mounting screws. These screws are normally set flush with the test-specimen surface and have a low emissivity. The ratio of the screw to test specimen area is approximately 0.005 and thus the maximum error is estimated to be less than ½%, the calculated emittance being smaller when the term is neglected.

Thermocouple Placement

Placement on the heater plate of the thermocouple used to measure test-specimen temperature introduces a fourth source of systematic error. Since reliance is placed on conductive heat transfer between the heater plate and the test specimen, a high termal resistance due to a small contact area between the two pieces can produce large temperature errors if warped test specimens and/or heater plates are used. Both heater plates and test specimens are lapped to ensure a high degree of flatness. Tests have also been run with a number of thermocouples placed on the front surface for the purpose of comparing average surface temperatures with those measured with the heat plate thermocouple. Differences of 1.5° K at a specimen temperature of 500° K have been found between various readings and would result in a 1.2% error in emittance measurement. The emittance is lower when this error is neglected.

α_{sr}/ϵ_s Assumption

The assumption that $\alpha_{sr}/\epsilon_s=1$ introduces another source of systematic error, because the real-temperature difference term in equation (3) becomes $(\theta_s^4-(\alpha_{sr}/\epsilon_s)\theta_r^4)$ when this ratio is considered. The ratio α_{sr}/ϵ_s for small temperature differences is normally considered equal to 1. At large temperature differences, $\theta_s^4 >> (\alpha_{sr}/\epsilon_s)\,\theta_r^4$ and $(\alpha_{sr}/\epsilon_s)\,\theta_r^4$ can be neglected. It is of interest, however, to determine the magnitude of error associated with this assumption. For purposes of calculation, it was estimated that the ratio could range between 0.5 and 2. The calculated emittance is found to be in error from 0.3 to −0.6% when values for α_{sr}/ϵ_s of this order are not considered (at $\theta_s=270°$ K, $\theta_r=77°$ K).

Gas Conduction

Free molecular gas conduction was considered as another source of systematic error. By Knudsen's theory of gas conductivity and equation (1.138) in reference 9, the amount of heat conducted from a test specimen at temperatures and pressures encountered in the experiments was computed and found to be of the order of 0.9 mw at a test-specimen temperature of 650° K. For comparison purposes a 1-inch-square black surface would emit 6.5 watts at 650° K and 0.2 at 270° K. Thus, for low emittance, heat losses of the order of milliwatts will produce sizeable errors in the emittance calculations.

RANDOM ERRORS

Instrumentation Accuracy

An analysis of the system components indicates that a probable error of the order of 1.5% is introduced because of the limitation of the instrumentation. The major portion of this error is associated with the temperature measurement, whose estimated accuracy is ±1° K. As the emittance and the ratio of solar absorptance to emittance is a function of the fourth power of the temperature, the ±1° K uncertainty in temperature causes a 1.5% uncertainty in the calculated emittance or ratio when measurements are made with the test specimen at 270° K and the receiver at 77° K. It should be pointed out that this error does not exist in the absorptance measurements because the equation is independent of temperature.

The power measurement is estimated to have an inaccuracy of less than ¼%. Potentiometers with suitable voltage dividers are used to make the measurements of voltage and current in the test specimen.

Measurement of the area of the test specimen is considered accurate to ¼%. The specimen dimensions are measured with a micrometer.

Test-Specimen and Heat-Shield Power Losses

Random errors are introduced into the system depending on the degree to which the test-specimen and heat-shield temperature can be maintained equal. Since heat is transferred between the two components by radiation, gaseous conduction, and conduction through the

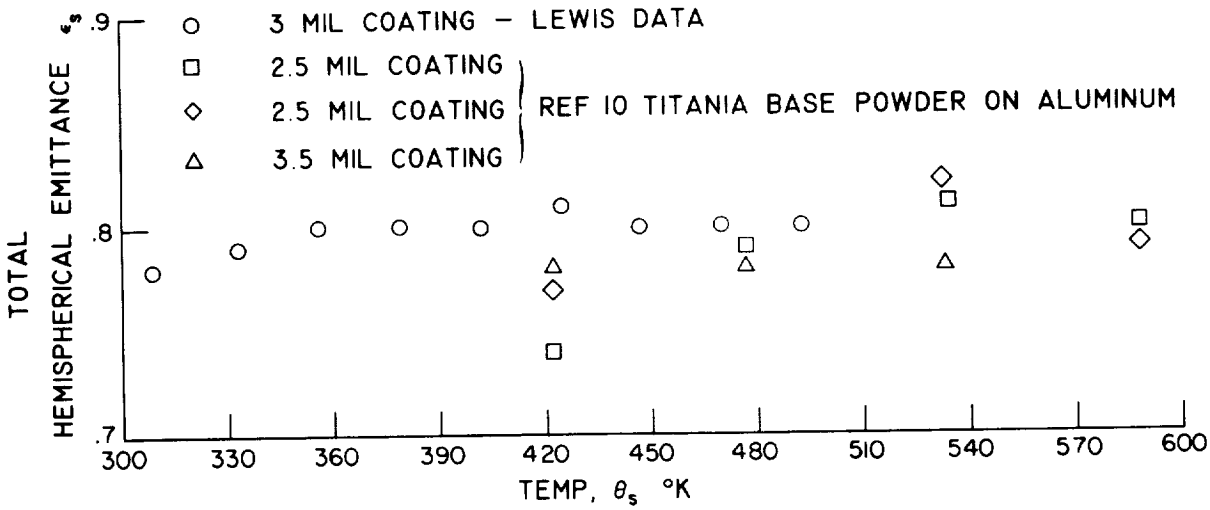

FIGURE 40–8.—Total hemispherical emittance versus temperature.

power leads and spacing screws, a calculation with any degree of accuracy is difficult. Therefore, tests were conducted to determine the degree of thermal coupling between the two components. The test procedure involved measuring the amount of power required to hold the test specimen at a constant temperature (θ_s=450° K) while varying the heat-shield temperature. The differences in power were then determined and a plot of the change in power against temperature difference was obtained. From the slope of this curve at the origin, an overall heat-transfer coefficient of 5 mw/° K was found to exist between shield and test specimen. Under normal operation the heat shield and specimen are controlled to within ¼° K of each other, which is sufficient to eliminate this source of error from all but low temperature low-emittance tests.

Another source of random error considered in the system would occur if temperature gradients existed on the inside surface of the heat shield. The heat shield was designed to eliminate this source of error by making use of large thicknesses of aluminum and applying the heating power throughout the entire shield assembly.

SUMMARY OF ERRORS

The error analysis indicates that a number of the errors investigated are functions of the emitted power and absolute temperature at the measurement point. The largest uncertainty in an emittance measurement will occur at the lowest temperature and with specimens of low emittance. In summing the positive and negative uncertainties and estimating the extraneous heat losses, the actual emittance will range between 2.1% higher to 4.0% lower than the measured emittance with a variation of less than ±0.01.

PRELIMINARY RESULTS AND CONCLUDING REMARKS

Preliminary tests have been conducted to determine the operating characteristics of the system. Measurements of emittance and solar absorptance have been made in the 270° to 500° K temperature range. In figure 40–8, results of a preliminary emittance test for a titania base powder are presented. Also plotted are emittance values for a similar powder obtained from reference 10. Repeatibility of the emittance measurements have been better than 2%. Other measurements have been made on samples ranging 0.15 to 0.92 in emittance.

Measurements are presently being made of the emittance and absorptance of thin films for use in a satellite system. Future tests will involve measurements of the absorptance of ceramics to be used in low-temperature space radiators.

REFERENCES

1. Campbell, D. A.; and Schulte, H. A.: Measurement of Emissivity at Low Temperatures. Tech. Rep. MT–R2J, Missile Operations, Chrysler Corp.
2. Butler, C. P.: Solar Absorptance and Emittance of Real Surfaces at High Temperatures. Pt. I, Polished Metals. Tech. Rep. USNRDL–TR–483, Research and Development.
3. Gordon, G. D.: Measurement of Ratio of Absorptivity of Sunlight to Thermal Emissivity. Rev. Sci. Instr., vol. 31, no. 11, Nov. 1960, p. 1204.
4. Measurement of Spectral and Total Emittance of Materials and Surfaces Under Simulated Space Conditions. PWA–1863, Pratt and Whitney Aircraft Co., 1960.
5. Pollack, John: Development of a Solar Simulator. Paper presented at NASA Conf. on Thermal Radiation Problems in Space Technology, Sept. 12 to 13, 1960.
6. Rachal, L. H.: Fast Response, Low Inertia Vacuum Furnace. Rev. Sci. Instr., vol. 32, no. 8, Aug. 1961, pp. 940–942.
7. Sparrow, E. M.; Albers, L. V.; and Eckert, E. R. G.: Thermal Radiation Characteristics of Cylindrical Enclosures. Jour. Heat Transfer, ser. C, vol. 84, no. 1, Feb. 1962.
8. Hamilton, D. C.; and Morgan, W. R.: Radiant-Interchange Configuration Factors. NACA TN 2836, 1952.
9. Dushman, S., and Lafferty, J. M.: Scientific Foundations of Vacuum Technique. John Wiley & Sons, Inc., 1949.
10. Anon.: Progress Report: Determination of the Emissivity of Materials. Rep. PWO–2043, Pratt and Whitney Aircraft Corp.

DISCUSSION

J. Allyn, Sandia Corporation: In reading the preprint of this paper, I was interested in the ratio, sample-to-receiver absorptance over emittance of the sample, and the demonstration that for reasonable assumptions this ratio can be neglected. The paper quoted sample temperatures—one sample temperature of 270° K, a receiver temperature of 77° K— and showed that this assumption caused no difficulty. I wonder whether you checked this assumption for some of your higher sample temperatures and, presumably, for different receiver temperatures.

Nyland: We use liquid nitrogen for the low-temperature receiver for all the emittance tests. When we made the calculation it was assumed that the low temperature 270° K would be the worst case. We have not made any calculations, but I thought it was apparent that the low temperature end is the one to worry about.

Allyn: Could you, just for the record, give us the point in your experiment at which the chamber temperature was cooled with water? Did this start at, say, a specimen temperature of 300° K on up or what?

Nyland: We have not used the water very often on the emittance measurements. It would be used at the high temperatures where the fourth power of the chamber was small in comparison to that of the specimen.

Allyn: At the high end, say, starting at 500° K?

Nyland: Possibly. Yes. And if the sample were clean and there was no requirement for cryopumping.

Drummeter, U.S. Naval Research Laboratory: Did I understand your curve to indicate that you found a marked difference in absorption, that is solar absorptance, with a difference in thickness of aluminum from 0.1–1μ?

Nyland: Yes.

Drummeter: How do you account for this? Is the surface of a 1-μ coating severely degraded? I had in mind that 1000 Å, which is what your 0.1 μ is, is essentially already opaque.

Nyland: On those specimens for which we have data the 0.1 μ thickness of aluminum was beginning to be transparent. Absorption was taking place in the mylar film beneath it.

Drummeter: The ratio still surprises me. Do you see cracks at all in this film? I mean, is this an integral film?

Nyland: No. There were no visible cracks in this specimen.

41—AN APPROACH TO THERMAL EMITTANCE STANDARDS

BY JOSEPH C. RICHMOND, WILLIAM N. HARRISON, AND FREDERICK J. SHORTEN

NATIONAL BUREAU OF STANDARDS, WASHINGTON, D.C.

A double-beam ratio-recording infrared spectrometer was modified to record directly the normal spectral emittance of strip specimens that are heated by passing a current through them. A laboratory blackbody furnace and a hot specimen at the same temperature serve as sources for the respective beams. Temperature equalization is achieved by means of a differential thermocouple. Automatic data-processing equipment corrects for "zero-line" and "100%-line" errors on the basis of previously-recorded calibrations, and also computes from the spectral data, as the measurement progresses, total emittance or absorptance for radiant energy having any known spectral distribution of flux.

This paper describes the development of equipment and procedures [1] for the measurement of normal spectral emittance of metals and other materials that can be heated by passing a current through them, at temperatures in the range of 800° to 1400° K, and over the wavelength range of approximately 1 to 15 μ. The equipment includes a data-processing attachment to automatically correct for calibration errors of the spectroradiometer, to record the corrected spectral emittance on punched paper tape in a form suitable for direct entry into an electronic digital computer, and to compute a single value for total emittance from the recorded spectral emittance.

In only a limited sense does the report cover the development of thermal emittance standards as such, although the selection and calibration of working standards of normal spectral emittance was included among the objectives. In a broader sense, it points out the need for standardization in the entire field of thermal emittance measurements, and in the field of terminology it makes several definite recommendations.

This paper is intended to be an elementary treatise covering the many elements involved in the production of thermal emittance standards.

[1] The work was done under the sponsorship and with the financial assistance of the Aeronautical Systems Division, U.S. Air Force.

DEFINITIONS

Several important items of nomenclature in the field of electromagnetic radiation have not been firmly established. Different meanings are ascribed to the same words by different individuals, and some of the conflicting definitions have been adopted by different technical and scientific organizations of national scope. The terminology used in this investigation follows that of Worthing (ref. 1) in that the word-ending "ivity" is reserved for the properties of materials, and "ance" for the properties of specimens. The word-ending "ion," as in reflection, absorption, and transmission, is applied to acts or processes, rather than properties.

All bodies are constantly emitting electromagnetic radiation as a result of the thermal vibration of the particles, atoms and molecules comprising the body; this process is known as thermal emission, and the rate of such emission per unit area is often referred to as thermal emissive power.

Radiant flux is the rate of flow of radiant energy.

Emittance is a property of a specimen; it is the ratio of the emitted radiant flux per unit area to that of a blackbody radiator at the same temperature and under the same conditions.

A blackbody absorbs all radiation incident upon it and at any given temperature has the maximum possible rate of thermal emission.

An ideal blackbody is a complete enclosure with opaque walls at a uniform temperature. The amount, and also the geometric and spectral (or wavelength) distribution of radiant flux emitted, per unit area, by a blackbody at a given temperature can be computed from the Stefan-Boltzmann relationship, Lambert's cosine law and the Planck radiation law, respectively. Laboratory blackbody furnaces which radiate energy are approximate blackbodies, because the opening through which the radiant energy is emitted destroys the ideal character. The extent to which they deviate from the ideal depends upon such factors as the relative size of the opening, the emittance of the inside surface, and the thermal gradients that may be present in the cavity. The rate of thermal emission of any real specimen is less than that of the blackbody at the same temperature.

Emissivity is a special case of emittance; it is a fundamental property of a material, and is measured as the emittance of a specimen of the material which has an optically smooth surface,[2] and is sufficiently thick to be opaque.

Reflectance is a property of a specimen; it is the ratio of reflected radiant flux to incident radiant flux.

Reflectivity is a special case of reflectance; it is a fundamental property of a material, and is measured as the reflectance of a specimen of the material that has an optically smooth surface, and is sufficiently thick to be opaque.

Transmittance is a property of a specimen; it is the ratio of transmitted radiant flux to incident radiant flux.

Absorptance is a property of a specimen; it is the ratio of absorbed radiant flux to incident radiant flux.

Absorptivity is a special case of absorptance; it is a fundamental property of a material and is measured as the absorptance of a specimen of the material that has an optically smooth surface and is sufficiently thick to be opaque.

A specimen is opaque when none of the radiant energy incident upon it is transmitted through it. All materials theoretically require infinite thickness to become opaque. In practice, a specimen is considered to be opaque when the transmitted radiant flux is too small to be detected, a condition which occurs at a very small thickness for some materials, and at great thicknesses for others. The thickness required for a specimen to be opaque also varies with the wavelength of the incident flux, for any one material.

All of the properties that are defined above vary with the spectral (or wavelength) distribution of the radiant flux. All are temperature dependent, some strongly so, and others only moderately. All of the properties are influenced by the angular distribution of flux in the radiant energy. All of the properties that pertain to specimens are influenced by the surface texture of the specimen, and by the thickness, unless the specimen is opaque.

Since the emission, reflection and absorption characteristics of a specimen are influenced by the direction of propagation, relative to the surface, of the emitted, incident, or reflected energy, and by the spectral distribution of radiant flux, most of the terms defined above must be qualified in order to convey precise meanings. For reflection, the direction of propagation of both the incident and reflected radiation must be specified. Specular, referring to reflection, means in the direction of mirror reflection. Diffuse, referring to reflection, means in all possible directions. Emission in all possible directions is referred to as hemispherical. When limited directions of propagation are involved, the word directional may be used. Normal is a special case of directional, and means in a direction normal to the surface. For other directions, the angle of deviation from the normal is stated. The terms normal and directional apply strictly to beams of parallel radiation, but are also used for beams contained within a small solid angle, in which case the direction of propagation is taken as that of the axial ray. Since all laboratory sources, specimens and receptors are of finite size, significant deviations from parallelism exist in all laboratory instruments. Hence the source and field apertures should be specified to define the extent of such deviations from parallelism.

Radiant energy having a stated wavelength, or more precisely, that is within a narrow

[2] Any surface contamination may alter the thermal radiation properties, hence a contamination-free surface is also essential.

wavelength interval centered on a specified wavelength, is referred to as spectral. Spectral emittance at a stated temperature is frequently plotted as a function of wavelength to produce a spectral emittance curve. The word total as used to modify terms describing thermal emission characteristics, means that the modified term pertains to the integral of rates of spectral emission at all wavelengths.

Some examples of the qualified expressions that are required to convey precise meanings are: "total hemispherical emittance at 500° K," "normal spectral emittance at 1400° K in the wavelength interval 1 to 15 μ," and "spectral diffuse reflectance from normal illumination over the wave-length interval 0.3 to 3.0 μ."

CONSIDERATIONS IN SELECTION OF EQUIPMENT AND PROCEDURE

In general, accurate absolute measurements of radiant energy are not easy to make. Comparative measurements of radiant energy can be made more readily. For this reason it appears logical to base emittance determinations on direct comparison of the radiant flux from a specimen at a given temperature to that from a comparison standard.

Since any comparison standard other than a blackbody furnace must be calibrated against a blackbody furnace at each temperature of test, and even then may change with continued use, it is desirable to use a blackbody furnace as the comparison standard.

The total radiant flux density of a blackbody varies as the fourth power of its absolute temperature. Thus, even a small error in temperature measurement could lead to a large error in emittance. Emittance, however, and particularly spectral emittance, varies only slightly with small changes in temperature. The critical requirements with respect to temperature control in the determination of emittance are (a) that the thermal gradients over the surface of the specimen and comparison standard be reduced as far as praticable, and (b) that the standard and specimen be kept at the same temperature within acceptable tolerances. A thermocouple produces an EMF that is a function of the temperature difference between the hot and cold junctions. Thus, small temperature differences can be measured more accurately by a single direct measurement by means of different thermocouple systems. Thus, it is desirable to use a differential thermocouple with suitable instrumentation to maintain the specimen and the comparison standard at the same temperature.

The spectral emittance curve of a solid material heated to a temperature below its melting point does not show the sharp peaks and valleys that are characteristics of the emission and absorption curves of solutions and gaseous materials. Hence, prism monochromators with relatively wide slits are suitable for use in spectral emittance determinations, in spite of their rather poor wavelength resolution, because they pass relatively large amounts of radiant flux for measurement over a side spectral range. The use of a variable-width slit is desirable so that in wavelength regions of low radiant flux the amount passed can be increased by broadening the wavelength band accepted for measurement. Thus, the available radiant flux in the comparison beam can be maintained at a level commensurate with the sensitivity of the detector.

DEVELOPMENT OF EQUIPMENT FOR NORMAL SPECTRAL EMITTANCE MEASUREMENTS

The general plan that was followed in developing equipment for determination of normal spectral emittance was to use a double-beam ratio-recording infrared spectrometer with a laboratory blackbody furnace and a heated specimen as the respective sources for the two beams. With this arrangement the instrument will record directly the normal sprectral emittance of the specimen, if the following conditions are met within acceptable tolerances: (1) the temperature of the specimen must be the same as that of the blackbody furnace; (2) the optical path length in the two beams must be equal or, preferably, the instrument must operate in a nonabsorbing atmosphere or a vacuum, in order to minimize the effects of differential atmospheric absorption in the two beams; (3) front-surface mirror optics must be used throughout, except for the prism, and equivalent optical elements must be used in the two beams in order to minimize attenuation of the beams by absorption in the optical elements; and (4) the source and field apertures of the two beams must be equal in order to ensure that radiant flux in the two beams compared by the apparatus will pertain to

equal areas of the sources and equal solid angles of emission.

It soon became apparent that the conditions specified under 2, 3, and 4 were not met within sufficiently close tolerances to permit direct recording of normal spectral emittance with the equipment described. It was necessary to use a second, or reference, laboratory blackbody furnace, identical to the first, or comparison, blackbody furnace, in order to correct for these errors.

Description of Spectrometer

The Perkin-Elmer model 13 spectrometer used for the measurements is equipped with a wavelength drive that provides automatic scanning of the spectrum of radiant flux, and a slit servomechanism that automatically opens and closes the slits to minimize the variations of radiant flux in the comparison beam. Three prisms were available: (1) fused silica, to cover the spectral range of 0.25 to 3.5 μ, (2) sodium chloride to cover the spectral range 0.7 to 15 μ, and (3) cesium bromide to cover the spectral range of 15 to 38 μ. Several photomultiplier detectors were available for use in the spectral range of 0.25 to 1.0 μ, a lead sulfide detector for use in the spectral range 1.0 to 2.0 μ, a vacuum thermocouple with sodium chloride window for use in the spectral range 1 to 15 μ, and a vacuum thermocouple with cesium bromide window for use in the spectral range 1 to 40 μ.

The source optics of the instrument were modified by incorporation of an external optical system, which is the standard Perkin-Elmer transfer optical system, used with the hohlraum reflectrometer. Two 90° folds in a vertical plane were introduced in the specimen beam, to raise the axial ray of the beam 9 inches above the optical plane of the spectrometer. The comparison blackbody furnace was mounted in a fixed position to act as the source of the comparison beam, and the specimen furnace and reference blackbody furnace were mounted side by side on a movable plate attached to a slide, in positions such that they could be brought alternately into position to serve as source for the specimen beam, by sliding the plate against fixed stops on the lathe bed. A sketch of the complete optical path is shown in figure 41–1, and a photograph of the external optical system with furnaces in place and cover removed is shown in figure 41–2.

It was found by experience that when the

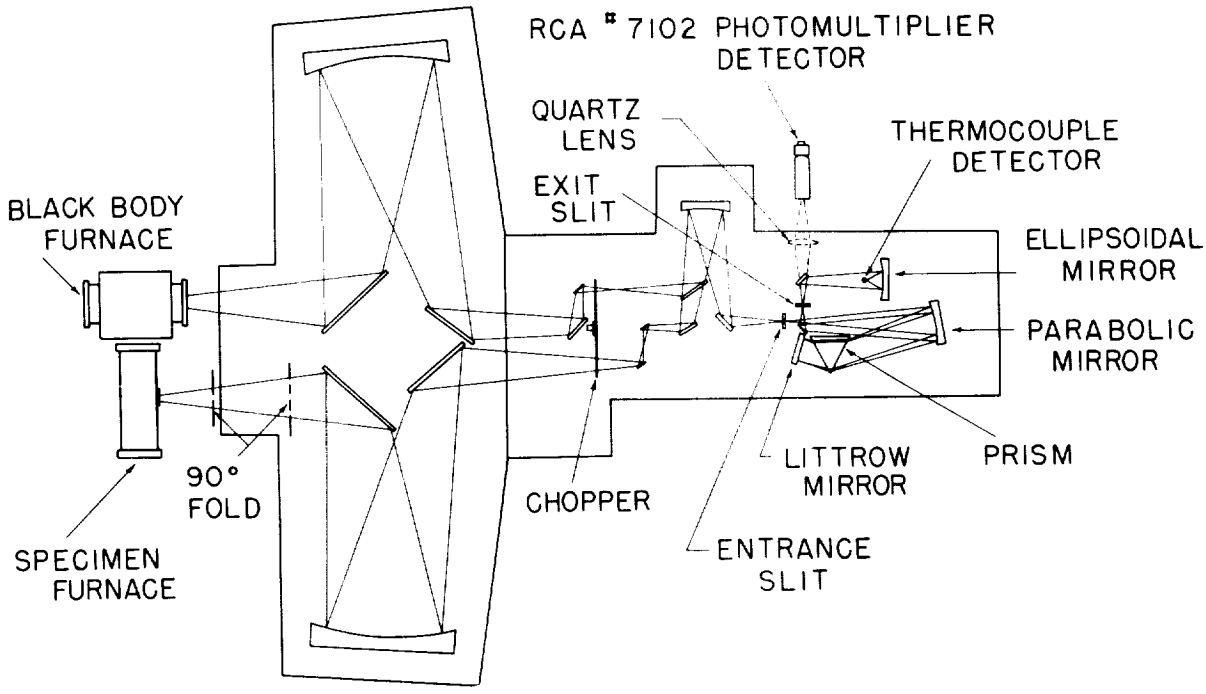

FIGURE 41–1.—Optical paths of the spectrophotometer.

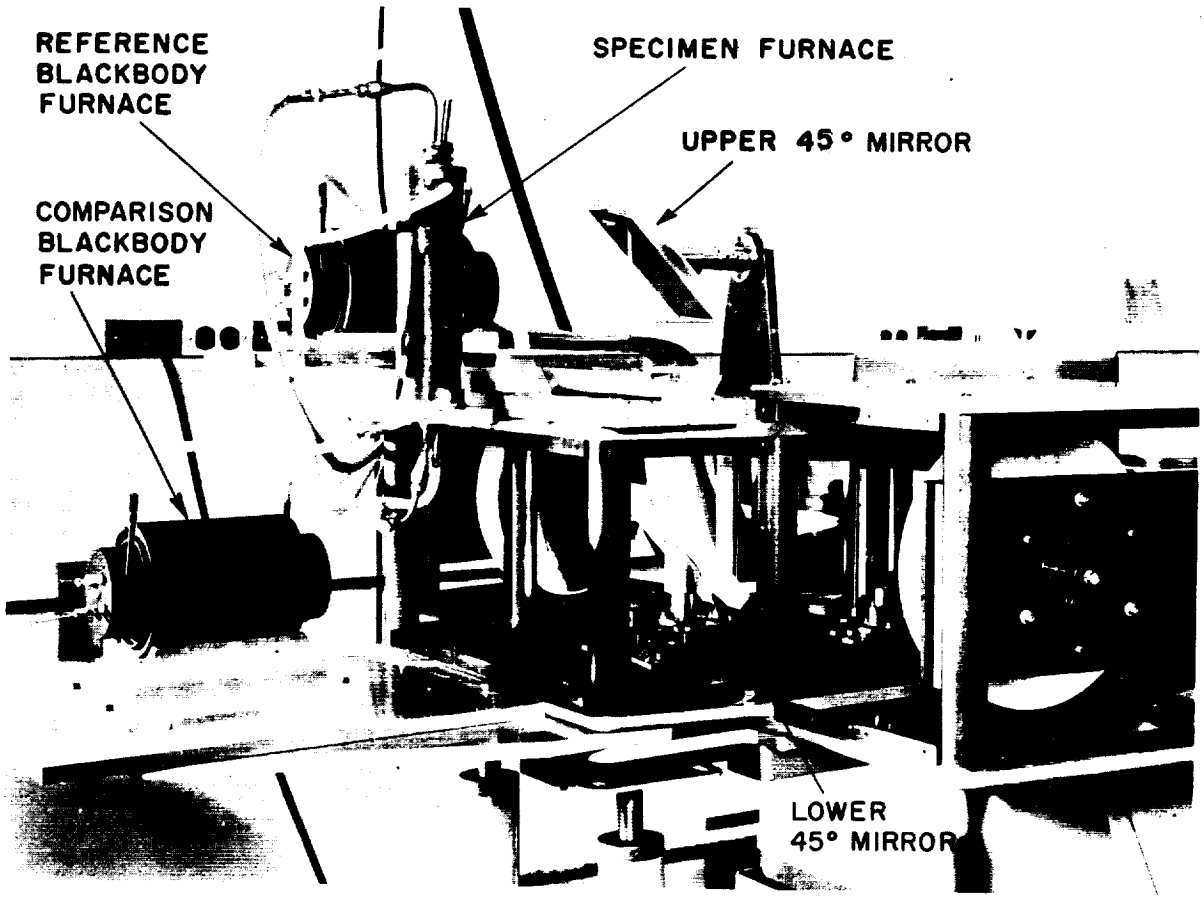

FIGURE 41–2.—External optical system of the spectroradiometer. The comparison blackbody furnace remains in position to act as the source for the comparison beam. The specimen is in position to act as source for the specimen beam, but can be replaced by the reference blackbody furnace by shifting the movable table on the slide.

two blackbody furnaces were used as sources for the respective beams of the spectrometer, deviations of the recorded "100% curve" occurred at the wavelength intervals within which there is significant absorption of radiant energy by water vapor and carbon dioxide in the atmosphere. Such absorption should be identical in both beams if the spectral distribution of flux and path lengths are identical. However, the two beams are separated in time, passing through the monochromator alternately at a frequency of 13 cps. Since the spectrum is being traversed continuously, one energy pulse is displaced relative to the other on the wavelength scale, by a very small amount. The effect of this displacement is negligible over most of the range, where the slope of the energy-wavelength curve is not large. But at the wavelengths near those of maximum absorption, the energy-wavelength curves become very steep, and the slight spectral displacement of the successive energy pulses can produce significant deviations in the ratios which are continuously recorded on the instrument.

In order to reduce the effects of absorption by atmospheric water vapor and carbon dioxide, the entire external optical system of the normal spectral emittance equipment, including the blackbody furnaces and specimen furnace, was enclosed in a Lucite box. Gas-tight connecting passages were designed to join (1) the Lucite box enclosing the external optics, (2) the metal cover for the chopper assembly, (3) the metal cover for the combining optics, and (4) the metal cover for the monochromator. Thus, the entire length of both optical paths in the instrument was enclosed in a single system of interconnecting housings that was nearly

692–146 O—63——27

gas-tight. Humidity in the enclosure was monitored and recorded by means of a humidigraph which records temperature and humidity. Immediately before a test the enclosure was purged with "super-dry" nitrogen, free from carbon dioxide, which was fed into the enclosure through several inlets, at a slow, constant rate, so that the enclosure was maintained at a slight positive pressure relative to the surrounding atmosphere. Tests were not started until the recorded humidity was less than 5%.

Blackbody and Specimen Furnaces

Two small laboratory blackbody furnaces were designed and built. Figure 41–3 is a sectional drawing of a furnace. The core was a Nichrome V casting, $1\frac{3}{16}$ inches in diameter and 4 inches long. The cavity was $\frac{3}{4}$ inch in diameter and $3\frac{3}{8}$ inches deep, threaded with 13 threads to the inch. The threads were cast in place. The Nichrome V oxidizes to produce a high-emittance surface in the cavity. The furnace was heated by means of a platinum–20% rhodium winding. There were two taps on the heating coil approximately one inch from each end. Shunts across the taps and leads were used to reduce thermal gradients in the cavity. The aperture in the cavity was reduced to a slit approximately $\frac{1}{4}$ by $\frac{3}{4}$ inches in size by means of a Nichrome cover plate.

The temperature of the blackbody furnace was measured by means of a platinum, platinum–10% rhodium thermocouple, the bare bead of which extended about $\frac{1}{4}$ inch into the cavity from the rear. The thermocouple leads were insulated from the core by high-alumina refractory tubing, which was surrounded by a platinum tube that was grounded, in order to prevent pickup by the thermocouple of spurious signals due to electrical leakage from the winding.

The efficiency of the blackbody furnace, computed from the Gouffé (ref. 2) equation, and assuming that the interior of the cavity is at uniform temperature, and is a completely diffuse reflector, was better than 0.999. Both of these assumptions are known to be only approximations, so that the actual efficiency was somewhat less than the computed value. The thermocouple bead in the back of the cavity cannot be seen, even with an optical pyrometer, when the furnace is in operation, which indicates that the efficiency is very high.

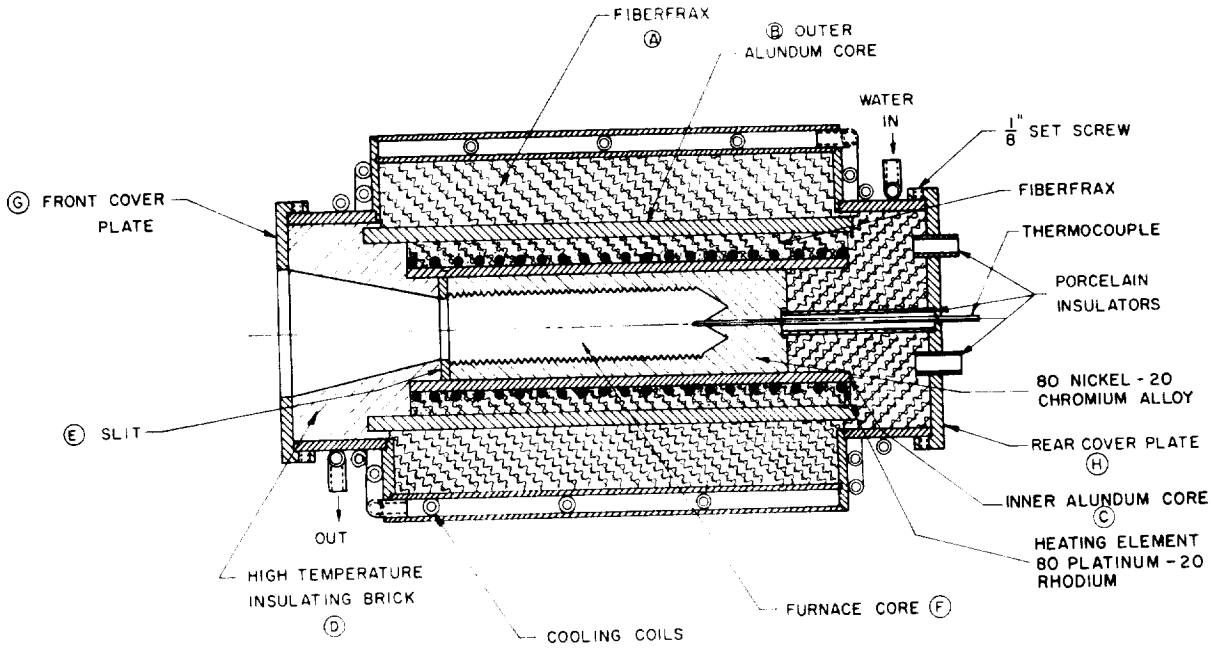

FIGURE 41–3.—Sectional drawing of blackbody furnace.

The specimens were strips of metal, ¼ inch wide by 8 inches long, of any convenient thickness in the range of approximately 0.010 to 0.060 inch. A sketch of the specimen furnace is shown in figure 41–4. The outer shell was water cooled, and its inner surface was of Inconel that had been threaded with a No. 80 thread and then oxidized in air at a temperature above 1350° K for 6 hours to produce a surface having a reflectance of less than 0.05 at the operating temperature of the water-cooled walls. The specimen was positioned off-center in the cylindrical enclosure, so that any radiant flux reflected from the walls would be reflected twice before hitting the specimen.

The electrodes were of water-cooled copper and were insulated from the brass end caps of the furnace by means of bakelite sleeves. The lower electrode fitted loosely in the hole through the end cap to permit the specimen to expand without buckling when heated. The specimen was viewed through a window about ¾ by 1 inch in size. A viewing window insert reduced the opening to about ¼ by ¾ inch.

Adjustable baffles above and below the viewing window were used to reduce convection and the resulting temperature fluctuations and thermal gradients. Adjustable telescoping cylindrical platinum reflectors surround the specimen at each end. These were used to reduce heat loss at the ends of the specimen, and hence the thermal gradient along the specimen.

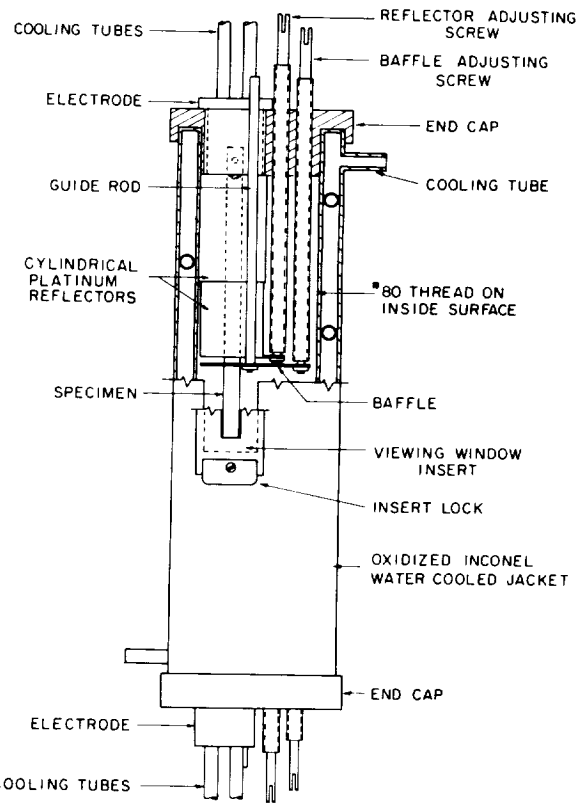

FIGURE 41–4.—Specimen enclosure.

Temperature Control Equipment

The power input to the comparison blackbody furnace was adjusted manually by means of an autotransformer. The heater winding of the furnace had two taps, located approximately one inch from each end of the winding. Variable resistors were connected as shunts across the taps and from the taps to the input leads, as indicated in the wiring diagram, figure 41–5. Adjustment of these resistors permitted variation of the power distribution along the cavity of the furnace, by means of which thermal gradients in the cavity could be reduced as far as practicable. It was found by experience that the heat capacity of the blackbody furnace was large enough to practically eliminate temperature fluctuations due to momentary voltage fluctuations in the power supply. A cold furnace could be brought to 1400° K and stabilized at that temperature in about 6 hours, and only about 30 min was required to achieve stability after a temperature change of up to about 30° K. Normally the blackbody furnaces were heated overnight before use.

The power supply for the reference blackbody furnace was identical to that shown in figure 41–5, except that when the temperature was to be controlled a saturable core reactor was substituted for the autotransformer, as is described below.

The temperature of the specimen (or reference blackbody furnace) was controlled to that of the comparison blackbody furnace, within narrow limits, by means of a differential thermocouple. One bead of the differential thermocouple was in the cavity of the comparison blackbody furnace, and the other was attached to the back of the specimen, in the center of the area being viewed, as described later in this report. The signal from the differential thermocouple was amplified by a d-c amplifier and fed to a center-zero recorder-controller. The output of the recorder-

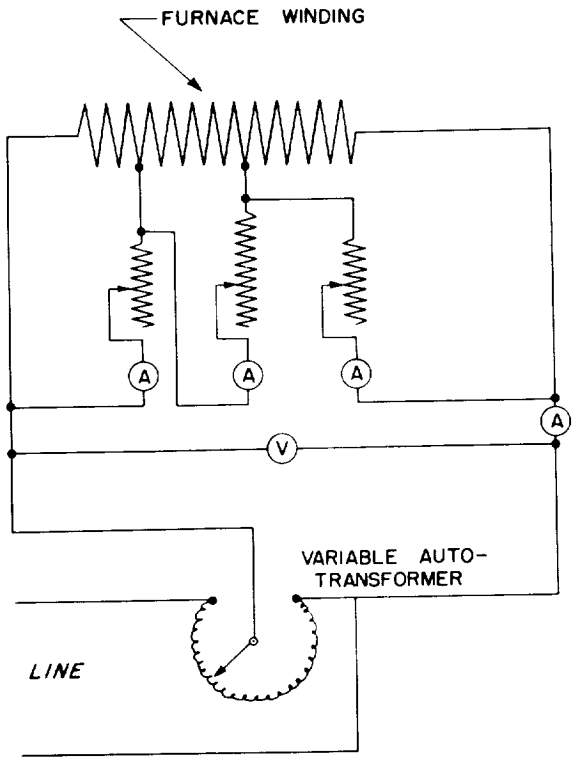

FIGURE 41–5.—Wiring diagram for power supply to comparison blackbody furnace.

controller is proportional to the distance between the control pointer and the recorder pointer on the scale, which is in turn proportional to the temperature difference between blackbody furnace and specimen. The output of the recorder-controller was fed to a current-actuating-type controller, the output of which was separated into three portions, each of which could be varied as desired. One portion was proportional to the input signal, one was proportional to the first time derivative of the input signal, and one was proportional to the second time derivative of the input signal. The output of the current-actuating-type control was fed to the coil of a saturable core reactor which varied the power input to the specimen. It was possible to reduce undershoot and overshoot of the controlled temperature by proper adjustment of the three components in the output of the current-actuating-type control. A block diagram of the temperature control equipment is shown in figure 41–6.

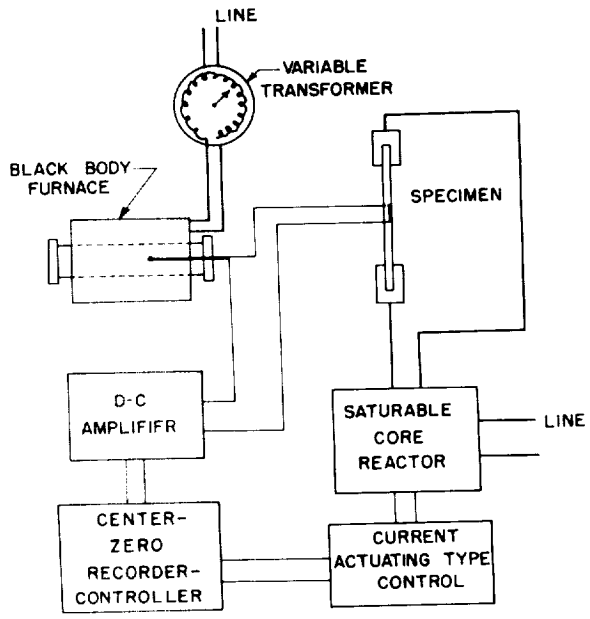

FIGURE 41–6.—Block diagram of temperature control equipment. The controller operates from a signal produced from a differential thermocouple.

With the described control equipment it has been possible to hold the temperature of a specimen as indicated by the welded thermocouple to well within $\pm 1°$ K of that of the comparison blackbody furnace, and the temperature of the reference blackbody furnace to within $\pm 0.5°$ K of that of the comparison blackbody furnace.

CALIBRATION OF EMITTANCE EQUIPMENT

Wavelength Calibration of Monochromator

A complete wavelength calibration was made of the spectrometer with the fused silica and sodium chloride prisms, respectively, mounted in the monochromator. In calibrating the equipment with the fused silica prism, emission spectra of a helium arc and a mercury arc, and absorption spectra of a didymium glass and a polystyrene film were recorded. The emission and absorption peaks having known wavelengths were identified in the respective curves, and for each peak the observed wavelength drum position at which the peak occurred was plotted as a function of the known wavelength of the peak (ref. 3). A total of 66 such points, at wavelengths in the range 0.24 to 2.2μ, was plotted, and a smooth curve was drawn between the points to produce the calibration curve.

A similar procedure was followed in calibrating the equipment with the sodium chloride prism mounted in the monochromator. In this case, the atmospheric absorption curve replaced the absorption curve for didymium glass. A total of 52 points, at wavelengths from 0.4 to 15 μ, was plotted to produce the calibration curve.

Calibration for Linearity of Response

All of the work done with the spectrometer had been based on the assumption that the response of the instrument (the height of the recorded emittance curve above the recorded "zero curve") was linear with (1) the radiant flux (within the varying wavelength interval encompassed by the exit slit) passing through the monochromator, when the instrument is operated in single-beam mode, or (2) the ratio of the fluxes (within the varying wavelength interval encompassed by the exit slit) in the respective beams that pass through the monochromator when the instrument is operated double-beam in ratio mode. This assumption had not been checked, and a confirmation of (1) and (2) above was considered desirable.

Slit Linearity Calibration

The entrance and exit slits of the monochromator open and close simultaneously, and both are controlled at the same width by the slit micrometer. Because of this construction, when a true image of a source is formed at the entrance slit of the monochromator, somewhat larger than the slit at its maximum width, the radiant flux reaching the detector from the monochromator varies as the square of the slit width. This relationship was used to check the linearity of detector response when the instrument is used single-beam in direct mode (item (1) above). A single blackbody furnace, at 1400° K, was used as a source, and each series of measurements was made at a number of central wavelengths throughout the sensitive range of the thermocouple detector. Experimental results were in conformity with the theoretical relationship. In every case, when the height of the recorder curve was plotted against the square of the slit width, the points obtained with the sodium chloride prism and thermocouple detector fell on a straight line intersecting the origin, within the error of measurement.

Similar measurements were also made at several wavelengths when the spectrometer was operated with the fused silica prism and the lead sulfide detector. Again, experimental results were in conformity with the theoretical relationship.

When the spectrometer was used with the fused silica prism and 1P21 detector, appreciable deviations from the theoretical relationship were found at first, but after careful realignment of the monochromator optics, all of the points again fell on a straight line, within experimental error.

Calibrations With Sector-Disk Attenuator

A sector-disk attenuator for use in calibrating the normal spectral emittance equipment was designed and built. The attenuator consists of a variable speed motor, 0 to 4000 rpm, with an attenuator disk mounted on its shaft.

Five interchangeable attenuator disks were prepared, having nominal transmissions of 75, 50, 25, 12.5 and 5.0%, respectively. The disks were machined from sheet aluminum, 0.065 inch thick. The 5% disk is 10 inches in diameter, and has four equally spaced radial notches, each 4.5° wide, extending inward from the rim for 3 inches. The other disks are 9 inches in diameter, and have eight notches each, extending inward from the rim for 2½ inches. The notches are 33¾° wide in the 75% disk 22½° wide for the 50% disk, 11¼° wide for the 25% disk, and 5¾° wide for the 12.5% disk.

The attenuator is normally operated at about 1300 rpm, and the direction of rotation is opposite to that of the chopper of the spectrometer. At this speed the beam is interrupted at a frequency of more than 85 cps by the 5% disk, and more than 170 cps by the other disks. The chopper in the spectrometer interrupts the beam at a frequency of 13 cps. No coupling has been observed between the attenuator and chopper frequencies.

The attenuator disks were calibrated in the Engineering Meteorology Section of NBS by measuring the angular width of the notches and blades on each disk, at two positions corresponding to the radial positions at which the top and bottom, respectively, of the interrupted beam strike the disks when in use. The unobstructed area of the disk between the two circles was

computed as a percentage of the total area between the circles, with the results shown below:

Nominal Transmittance, %	*Measured Unobstructed Area, %*
75	75.10±0.22
50	50.00±0.02
25	25.28±0.14
12.5	12.73±0.14
5	5.07±0.03

The measured values were assigned to the respective sector-disk attenuators.

In the next group of experiments, made for additional checking of item (1) above, the sector-disk attenuator was introduced into the beam near the blackbody furnace. Each series of measurements was made at a single wavelength, a single slit width, and a single gain setting. In each case the gain was adjusted to give a reading of slightly less than 100 units on the strip chart without the attenuator. The attenuator was then introduced into the beam, and operated with each of the disks in turn. The height of the recorder curve was plotted against the previously measured fraction of the beam passed by the attenuator. In every case the points fell on a straight line passing through the origin, indicating linear detector response for every combination of slit width and wavelength tested, with both the sodium chloride and fused silica prisms, and with the thermocouple, as well as the lead sulfide and photomultiplier detectors.

In the preceding experiments for which the instrument was being used in direct mode, with single beam, the height of the recorder curve varied linearly with the signal produced by the detector. This signal was proportional to the radiant flux passing through the monochromator. Normally, however, the instrument is used in ratio mode, with double beam. In this case, the height of the recorder curve should vary linearly with the ratio of the two signals produced by the detector when it is receiving flux alternately from the respective beams.

In order to check item (2) above, the two blackbody furnaces, controlled very closely to the same temperature (about 1400° K), were used as sourses for the two beams. The instrument was adjusted so that the "100% curve" would actually fall between 90 and 100 on the chart, after which such a curve was obtained over the wavelength range of interest. The sector-disk attenuator was then introduced into the specimen beam near the blackbody furnace, and operated with each of the disks in turn, to obtain "75%, 50%, 25%, 12.5% and 5% curves", each over the wavelength range of interest. The heights of the respective curves were then measured at 100 selected wavelengths, and the height of each curve above the experimentally obtained zero for the pertinent wavelength was plotted against the percentage of the flux in the specimen beam that was passed by the attenuator. In every case the points fell on a straight line intersecting the origin, within the error of measurement. No significant departures from linearity of response were detected for any combination of prism and detector, at any point within the wavelength range at which they could be used.

The data for the thermocouple detector and and sodium chloride prism are shown in figure 41–7. In this case, the "apparent emittance" of the combination of the reference blackbody furnace and each attenuator disk is plotted as a function of wavelength. Every value of apparent emittance was within ±0.01 of the measured transmittance of the respective disk.

EXPERIMENTAL PROCEDURE

It was found by experience that the 100% curve, obtained when the two blackbody fur-

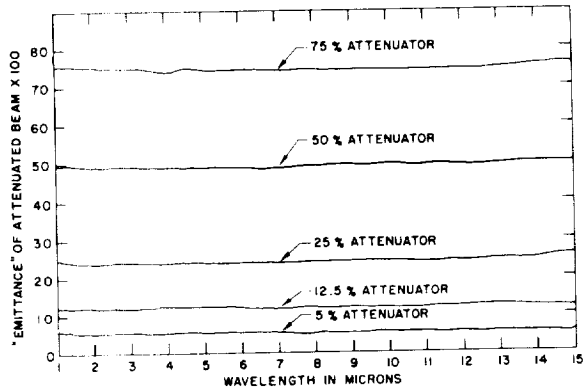

FIGURE 41-7. Spectral "emittance" of the combination of the reference blackbody furnace and sector-disk attenuator when using the 75%, 50%, 25%, 12.5% and 5% attenuator disks. Data are for the spectrometer with the sodium chloride prism and thermocouple detector.

naces at the same temperature served as sources for the respective beams of the spectrometer, deviated appreciably from flatness. These deviations may be due to either (1) variations in spectral absorption or other losses along the respective optical paths from source to detector, or (2) variations in spectral sensitivity of the detector to radiant flux from the two beams. There are two more mirrors in the specimen beam than in the comparison beam, as is shown in figure 41–1. The two beams follow different paths from the sources to the spherical mirror in the combining optics, and are reflected by different mirrors in this portion of the path. From the spherical mirror in the combining optics to the detector, the two beams follow the same general path and are reflected by the same mirrors. However, the paths are not identical, and the beams are reflected by slightly different areas of each mirror, and are transmitted by different areas of the prism and the detector window. These differences could account for spectral differences in losses in the two beams, due to absorption, and to scattering, for instance, by dust particles on the mirrors. The two beams are also focused on slightly different areas of the sensitive surface of the detector. No detector is completely black, and variations in spectral absorptance over the sensitive surface of the detector could be responsible for part of the observed effect.

It was also found by experience that the zero curve, obtained when the specimen beam was blocked near the specimen furnace, deviated from flatness. These deviations are undoubtedly due to stray radiation in the monochromator, which produces a spurious signal when there is in fact no radiant energy being supplied by the specimen.

A test procedure was developed to correct for the errors which result in the deviations of the "100% line" and zero line referred to above. The procedure is as follows:

(1) The two blackbody furnaces are placed in position to act as sources for the respective beams of the spectrometer, and are brought to the same temperature. The "Full Scale" control of the spectrometer is adjusted to bring the 100% line to a position between 90 and 100 on the chart. The specimen beam is blocked, and the "Ratio Zero" control on the spectrometer is adjusted to bring the zero line to a position between 1 and 3 on the chart. The specimen beam is unblocked, and the position of the 100% line is checked. These instrument settings then remain fixed throughout the emittance determinations on the specimen being tested.

(2) The 100% line, over the wavelength range of interest, is obtained by automatic recording on the strip chart, after which the chart paper is rerolled.

(3) The specimen beam is blocked near the source, and the zero line is similarly obtained over the wavelength range of interest, after which the chart paper is again rerolled.

(4) The specimen enclosure is next substituted for the reference blackbody furnace, in position to act as source for the specimen beam of the spectrometer. The temperature of the specimen is brought to and held at the temperature of the comparison blackbody furnace. The specimen beam is unblocked, and the "specimen line" is obtained over the wavelength range of interest.

The heights of the respective curves are measured at preselected positions of the wavelength drum (corresponding to known wavelengths), as indicated in figure 41–8, and the normal spectral emittance is computed for each such wavelength. If Z_λ is the height of the zero line, S_λ the height of the specimen line, and H_λ the height of the 100% line, at some wavelength λ, the normal spectral emittance, E_λ is given by

$$E_\lambda = \frac{S_\lambda - Z_\lambda}{H_\lambda - Z_\lambda} \qquad (2)$$

Values of E_λ are computed for each of 100 wavelengths in the range of 1 to 15 μ, and E_λ is plotted as a function of wavelength. A curve is drawn through the plotted points to represent the spectral emittance curve of the specimen.

SELECTION AND CALIBRATION OF WORKING STANDARDS

The selection and calibration of suitable working standards of normal spectral emittance, to be used for the comparison of results in several different laboratories, was one of the objectives of this program.

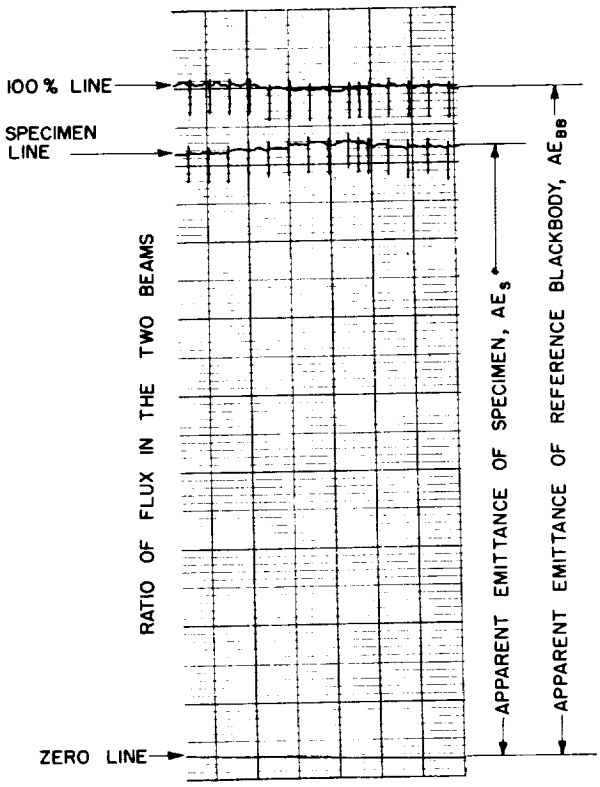

FIGURE 41-8.—Section of recorder chart, showing sections of a 100% line, specimen line, and zero line. The normal spectral emittance is the ratio AE_s/AE_{BB}.

Working standards having high, intermediate, and low emittance were desired. In addition to having the desired normal spectral emittances, the working standards, to be useful, should be stable on heating in air at temperatures up to the maximum temperature at which they can be used, for times of several hundred hours. They should also be of a material that is not easily damaged in use. In order to be suitable for measurement with the equipment described in this report, the specimens are required to have electrical properties that will permit them to be heated by passing a current through them.

Specimens machined from sheet material of uniform thickness, three of each material in each of several different sizes and shapes were desired, suitable for measurement in the equipment used by different laboratories, as follows:

strips, ¼ x 8, ¾ x 10 and 1 x 10 inches in size
squares, 2 x 2 inches in size
disks, ⅞, 1, 1⅛, and 1¼ inches in diameter.

Because it was not possible to measure the normal spectral emittance of specimens of all of the above shapes and sizes with the equipment described in this report, it was decided that the measurements would be confined to six ¼-x-8-inch strip specimens of each material. All of the specimens of a single material were cut from a single sheet of metal, and all were treated as nearly alike as possible during surface preparation.

After an extensive series of tests, the following materials were selected on the basis of the above criteria, for use in preparing the working standards:

1. for standards of low normal spectral emittance, 0.035-inch platinum sheet that had been polished and then annealed
2. for standards of intermediate normal spectral emittance, 0.043-inch Kanthal sheet that had been sandblasted and then oxidized
3. for standards of high normal spectral emittance, 0.053-inch Inconel sheet that had been sandblasted and then oxidized.

The tests indicated that specimens of these three materials, when prepared as outlined below, were stable in total hemispherical emittance to better than 0.02 on heating in air at the maximum temperature at which they were calibrated for periods of 200 hours.

Platinum Working Standards

The platinum specimens were received from the fabricator as 0.035-inch sheet, six ¼-x-8-inch strips and three each in the following shapes and sizes: ⅞-, 1-, 1⅛- and 1¼-inch diameter disks, 2-x-2-inch squares, and 1-x-10- and ¾-x-10-inch strips. It had been specified that the specimens were to be supplied with highly polished surfaces. The finish actually supplied was not as smooth as had been desired, but it was decided to use the finish supplied, rather than send the specimens back for reworking. A ⅛-inch hole was drilled in one end of each strip specimen, to facilitate hanging during annealing.

Each specimen was washed in hot tap water to which a commercial detergent had been added, rinsed in running hot tap water, then in distilled water, and finally in ethyl alcohol. Rubber surgical gloves were worn at all times while handling the specimens, and the central

portion, observed for emittance determinations, was not touched after cleaning. The specimens were dried in air and placed in a closed container, supported by the ends or edges only, for storage prior to annealing.

All specimens were annealed in an electrically-heated, silicon carbide element furnace. The strip specimens were hung by means of platinum hooks suspended from aluminum oxide rods in the furnace; the square and disk specimens were supported by the edges only on ceramic forms resting on a flat ceramic slab. All of the specimens were then enclosed in a ceramic muffle. Starting with a cold furnace the temperature of the furnace was raised to 1523° K (1250° C) over a period of 6 hours, and held at that temperature for 1 hour. The power was then turned off, and the specimens were allowed to cool in the furnace, which required 2 days.

The specimens were removed from the furnace by means of cleaned platinum-tipped tongs and were placed in individual plastic holders, in which they were supported only by the ends or edges. Each plastic holder, containing a specimen, was then placed in an individual cardboard box, to protect it from contamination.

The six ¼-x-8-inch strips were prepared for measurement by welding a platinum-platinum, 10% rhodium thermocouple to each specimen. A shallow groove was scratched in each specimen, normal to its axis and located at the mid-length. The 10-mil thermocouple wires were separately welded to the specimen by means of a condenser-discharge type of electronic spot welder. Each wire was laid in the shallow groove to position it for welding, and the welding operation was observed through a low-power microscope.

Precautions were taken at all times to avoid contamination of the specimens. They were handled as little as possible, and when handling was unavoidable the use of rubber gloves was continued, and even then the center portion of the specimen was not touched.

Three sets of curves were made for each strip specimen at each of three temperatures: 800° K, 1100° K, and 1400° K. Each set of curves consisted of (1) a 100% curve, obtained when the two blackbody furnaces at the test temperature were the sources for the respective beams; (2) a zero curve, obtained when the specimen beam was blocked near the specimen furnace; and (3) a specimen curve, obtained with the comparison blackbody at the test temperature as one source and the specimen at the same temperature, as the other. Each curve was recorded over the range of wavelength drum settings corresponding to a wavelength range of approximately 1.0 to 15.0 μ.

The normal spectral emittance was computed at a total of 100 wavelengths, approximately uniformly spaced from 1 to 15 μ.

The 18 values (3 each on 6 specimens) at each temperature and wavelength drum setting were tabulated, and the following values were computed: (1) E, the arithmetic average of the 18 measured values, (2) σ_t, the total standard deviation [3] of the 18 values about the average of the 18 values, (3) e, the 95% confidence error of E, (4) σ_m, the average of six standard deviations, each computed from the three measured values on one of the six specimens, and (5) σ_s, the standard deviation of the six average values, one for each of the six specimens, about the grand average for all six.

The average normal spectral emittance, E, of the six platinum specimens at 1100° K is plotted as a function of wavelength in figure 41–9. The 95% confidence errors [4] associated with the plotted average emittance values are also plotted in the same figure.

The value σ_m is a measure of the overall reproducibility of the test procedure or the precision of measurement. The average value of σ_m for all of the 100 wavelengths, is 0.45 at 1100° K. Thus the overall precision of measurement on platinum is better than 0.005,

[3] All standard deviations computed in this study are precisely defined as "estimates of the standard deviation of the parent population from which the measurements were drawn." This quantity is assigned the symbol σ, to distinguish it from the root-mean-square standard deviation, S. D., of individual values from the mean of a given sample.

[4] The 95% confidence error has the following statistical significance. If the measurements were repeated a large number of times, say 1000 times, and the average and 95% confidence error was computed for each group of 18 measurements, then the limits of the group average ± the 95% confidence error would bracket the overall average of the 1000 groups of measurements about 19 times out of 20.

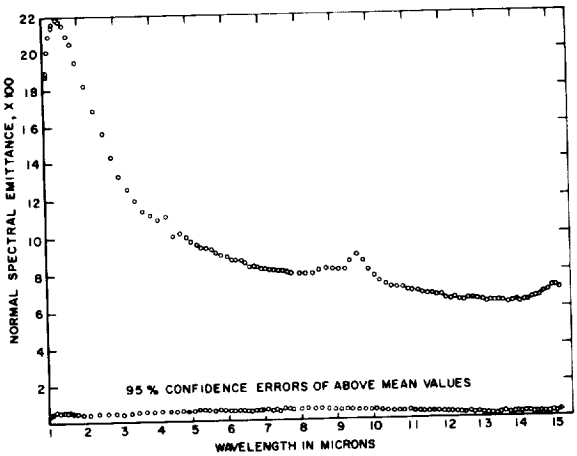

FIGURE 41–9.—Normal spectral emittance at 1100° K of platinum working standards. The points in the upper curve represent averages of 18 measurements, 3 each on 6 specimens. The points in the lower curve represent the 95% confidence errors of the average values in the upper curve.

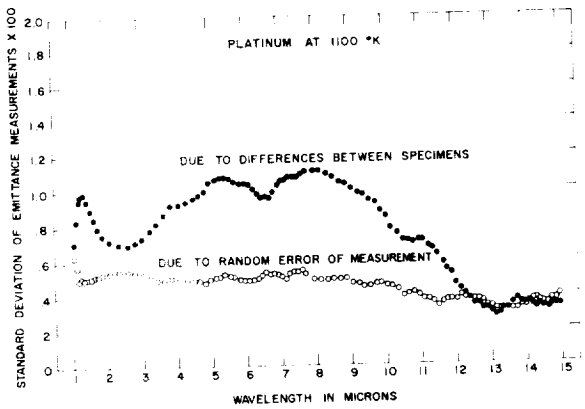

FIGURE 41–10.—Spectral distribution of two categories of standard deviations, each computed from 18 measured emittance values obtained at 1100° K, 3 each on 6 platinum working standards. The upper curve represents standard deviations due to real differences in emittance between specimens, identified as σ_s in the text. The lower curve represents standard deviations due to random error, identified as σ_m in the text. In both curves each point represents the moving average of five adjacent values.

expressed as a standard deviation in units of emittance. In order to show any trend of σ_m with wavelength, the moving average of 5 values at adjacent wavelengths was computed, and plotted as a function of wavelength as the lower curve in figure 41–10. The scatter due to errors of measurement, σ_m, shows significantly less variation than σ_s.

The value σ_s indicates actual differences in emittance of the specimens that were measured. The average value of σ_s for all of the 100 wavelengths was 0.74. In order to show any trend of σ_s with wavelength, the moving average of five values at adjacent wavelengths was computed and plotted as a function of wavelength to form the upper curve in figure 41–10. There appears to be a significant variation in σ_s with wavelength.

The values of σ_s are larger than the corresponding values of σ_m by an amount sufficient to demonstrate statistically that the observed differences between specimens are real, and could not occur due to chance fluctuations of the error of measurement.

Curves similar to those shown in figures 41–9 and 41–10 were prepared from the data obtained at 800° K and 1400° K. In general the curves of data obtained at 800° K and 1400° K were similar in shape to the corresponding curves at 1100° K. The normal spectral emittance at each wavelength increased with an increase in temperature, as would be predicted by the Hagen-Rubens equation. No significant change in σ_m or σ_s with temperature was noted.

Oxidized Kanthal Working Standards

Specimens of the same sizes and shapes as those referred to above were machined from 0.043-inch Kanthal sheet and were cleaned with acetone to remove any oil or grease from the machine operation. They were then marked for identification, and sandblasted with 60-mesh fused aluminum grit at an air pressure of approximately 70 psi. The sandblasted specimens were cleaned ultrasonically in acetone, passivated for one minute in 10% nitric acid at 316° K (43° C), rinsed in distilled water and then acetone. They were placed in a cold furnace, which was brought to 1340° K and held for 400 hours, after which they were allowed to cool in the furnace.

The normal spectral emittance of the six ¼-x-8-inch oxidized Kanthal specimens was measured, following the procedure outlined above for platinum specimens, except that the measurements were made at temperatures of 800°, 1100° and 1300° K. The normal spectral

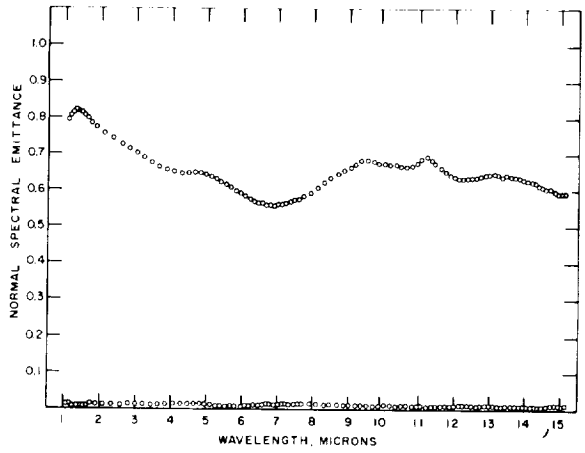

FIGURE 41–11.—Normal spectral emittance at 1100° K of oxidized Kanthal working standards. The points in the upper curve represent averages of 18 measurements, 3 each on 6 specimens. The points in the lower curve represent the 95% confidence errors of the average values in the upper curve.

emittances and 95% confidence errors were computed as before and plotted to produce curves of the type shown in figure 41–11 for measurements at 1100° K and the standard deviations due to differences in specimens and random error of measurement were computed as before and plotted to produce curves of the type shown in figure 41–12 for measurements at 1100° K.

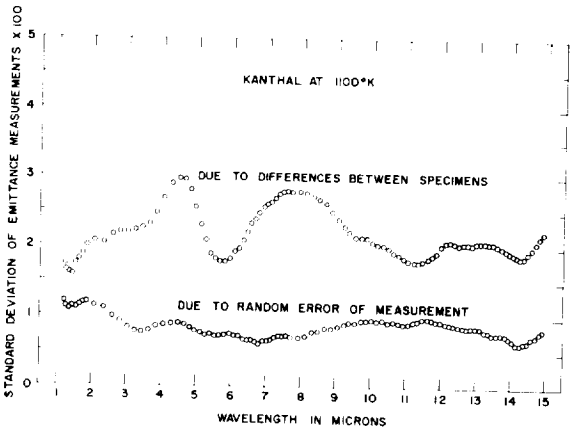

FIGURE 41–12.—Spectral distribution of 2 categories of standard deviations, each computed from 18 measured emittance values obtained at 1100° K, 3 each on 6 oxidized Kanthal working standards. The upper curve represents standard deviations due to real differences in emittance between specimens, identified as σ_s in the text. The lower curve represents standard deviations due to random error of measurement, identified as σ_m in the text. In both curves each point represents the moving average of 5 adjacent values.

Oxidized Inconel Working Standards

Specimens of the same sizes and shapes referred to above were machined from 0.053-inch Inconel sheet, and were cleaned and sandblasted as outlined above for the Kanthal specimens. The cleaned specimens were placed in a cold furnace, which was brought to 1340° K (1067° C) and held for 24 hours; the temperature was then reduced to 1100° K and held for an additional 24 hours, after which the specimens were allowed to cool in the furnace.

The normal spectral emittance of the six ¼-x-8-inch oxidized Inconel specimens was measured, following the procedure outlined above for platinum specimens, except that the measurements were made at temperatures of 800°, 1100°, and 1300° K. The normal spectral emittances and 95% confidence errors were computed as before, and plotted to produce curves of the type shown in figure 41–13 for measurements at 1100° K. The standard deviations due to differences in specimens and to random error of measurement were also computed as before, and plotted to produce curves of the type shown in figure 41–14 for measurements at 1100° K.

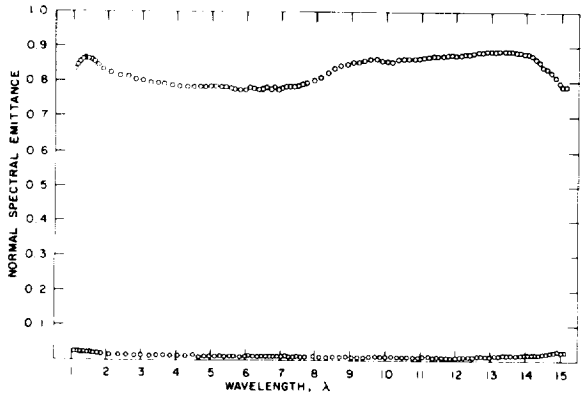

FIGURE 41–13.—Normal spectral emittance at 1100° K of oxidized Inconel working standards. The points in the upper curve represent averages of 18 measurements, 3 each on 6 specimens. The points in the lower curve represent the 95% confidence errors of the average values in the upper curve.

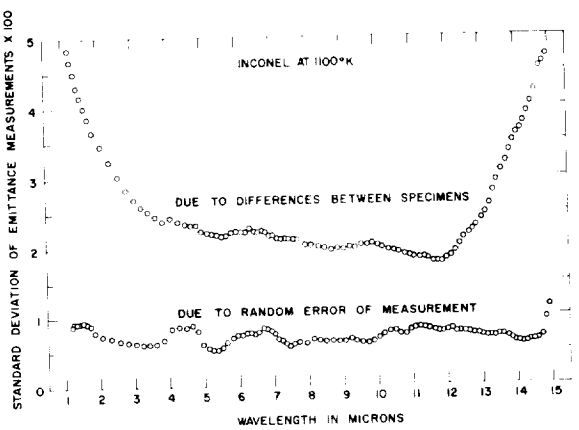

FIGURE 41-14.—Spectral distribution of 2 categories of standard deviations, each computed from 18 measured emittance values obtained at 1100° K, 3 each on 6 oxidized Inconel working standards. The upper curve represents standard deviations due to real differences in emittance between specimens, identified as σ_s in the text. The lower curve represents standard deviations due to random error of measurement, identified as σ_m in the text. In both curves each point represents the moving average of 5 adjacent values.

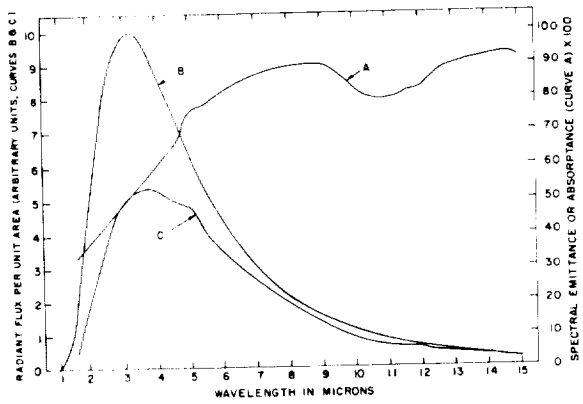

FIGURE 41-15.—Graphical form of data and derived values used in computing from the spectral emittance of a specimen its total emittance, its total absorptance, or its total emissive power. Curve A represents spectral emittance values obtained on a specimen at 650° K (about 1200° F). Curve B represents the spectral distribution of radiant flux from a blackbody at the same temperature. The ordinates of curve C are in each case the product of the ordinates of curves A and B at the same wavelength. Curve C represents the spectral distribution of flux emitted by the specimen having the spectral emittance indicated by curve A.

PRINCIPLES OF DATA REDUCTION

Computation by the Weighted-Ordinate Method

Two main steps are necessary in order to compute the total normal emittance or absorptance of a specimen for radiant flux having a specified spectral distribution from its spectral emittance curve. These steps are described in relation to figure 41-15, which represents an actual case.

The first step is to weight a series of ordinates chosen at uniform intervals along the emittance-wavelength curve for the specimen (curve A) according to the spectral distribution of radiant flux from the source under consideration, which can be represented graphically by a second curve, B. The weighted ordinates, which are the products of ordinates at identical wavelengths for curves A and B, provide points for a third curve, C, which indicates the spectral distribution of the energy that would be absorbed in unit time by the specimen, from the specified source. For the special case in which the designated source of radiation, represented by curve B, is a blackbody (as it is in figure 41-15) at the temperature of the specimen (which is in thermal equilibrium), curve C represents, also, the spectral distribution of the energy emitted in unit time by the specimen at the temperature under consideration, since under these specific conditions the rate at which energy is absorbed by the specimen at each wavelength is exactly equal to that at which it is emitted at the same wavelength.

The second step in computing the total emittance or absorptance of the specimen consists of determining the ratio of the area under curve C to that under curve B. A rigorous mathematical expression of the quantity sought is as follows:

$$E_{ts}=\frac{\int_0^\infty \epsilon_{b\lambda}E_{s\lambda}d\lambda}{\int_0^\infty \epsilon_{b\lambda}d\lambda} \qquad (3)$$

where:

E_{ts} = total Emittance of specimen

$\epsilon_{b\lambda}$ = rate of energy emission per unit wavelength interval, of a blackbody, for the increment λ to $(\lambda+d\lambda)$

$E_{s\lambda}$ = Emittance of the specimen, between λ and $(\lambda+d\lambda)$.

In practice, with a sufficient number of uniformly spaced ordinates (which are taken at

the same set of wavelengths for all the curves) this ratio of areas is approximated with the required precision by dividing the sum of the ordinates for curve C by the sum of the ordinates for curve B. The mathematical expression of this operation is

$$E_{ts}=\frac{\sum_{\lambda_1}^{\lambda_2}\epsilon_{b\lambda}E_{s\lambda}\Delta\lambda}{\sum_{\lambda_1}^{\lambda_2}\epsilon_{b\lambda}\Delta\lambda} \tag{4}$$

Since all values of $\Delta\lambda$ are equal, they cancel out numerically as well as dimensionally.

The units in which the ordinates of curve A are expressed are pure numbers, representing spectral-emittance values. The units in which the ordinates for curve B are expressed occur in both the numerator and denominator of the final ratio; hence it is of no consequence what units are used, provided they are the same for the numerator and denominator, or whether the ordinates for curve B are expressed simply as numbers of the correct relative magnitudes. The final answer in either case is a number signifying the total absorptance of the specimen for radiant flux of the specified spectral distribution.

The procedure is identical for computing either the total emittance of the specimen or its total absorptance for energy from the sun, the earth, or any other source, because the total absorptance for blackbody radiation at the temperature of the specimen is equal to the total emittance of the specimen. Hence to compute total emittance or total solar absorptance as desired, one merely modifies the procedure by selecting for curve B either the spectral distribution of radiant flux for a blackbody at the temperature of the specimen, (which was done for fig. 41–15) or the spectral distribution of radiant flux for solar radiation, or radiation from the earth or any other source.

When it is desired to compute the total amount of radiant energy, for unit time and area, emitted by the specimen at a given temperature, curve B will represent blackbody radiation and its ordinates will be expressed in energy per unit time and area; hence, those of curve C will also. In this case, the quantity sought is represented by the area under curve C, which can be obtained by integration. The equation that rigorously describes this relationship for all possible wavelengths is:

$$\epsilon_{ts}=\int_0^\infty E_{s\lambda}\epsilon_{b\lambda}d\lambda \tag{5}$$

where ϵ_{ts} is the total radiant flux density of the specimen.

In practice the value can be computed with the required precision by the following approximation:

$$\epsilon_{ts}=\sum_{\lambda_1}^{\lambda_2}E_{s\lambda}\epsilon_{b\lambda}\Delta\lambda \tag{6}$$

Since $E_{s\lambda}$ is a ratio, and $\epsilon_{b\lambda}$ represents radiant flux per unit area and wavelength interval, the λ cancels out dimensionally. Numerically, the fraction of the span between λ_1 and λ_2, that is occupied by a single interval, $\Delta\lambda$ is the reciprocal of the number of ordinates, n, (each ordinate representing one interval); hence equation (6) may be written:

$$\frac{\epsilon_{ts}=\sum_{\lambda_1}^{\lambda_2}E_{s\lambda}\epsilon_{b\lambda}}{n} \tag{7}$$

This equation states that the total radiant flux per unit area is obtained by simply adding all the ordinates of the points from which curve C was constructed (each of which represents radiant flux per unit area), and dividing by the number of such ordinates. Any required precision of the approximation can be attained by using a sufficient number of ordinates.

As in the case of emittance and absorptance, the procedure is the same whether the object is to compute the total radiant flux emitted by unit area of the specimen or the total radiant flux absorbed upon exposure to a specified source. In the former instance, curve B represents blackbody radiation; in the latter case, it represents radiant flux from the specified source that is incident upon the specimen.

Computation By the Selected Ordinate Method

Regardless of what method of computation is chosen, the objects remain (1) to obtain the ratio of areas under two curves, B and C, for total emittance or total absorptance, and (2) to evaluate the area under one curve, C, for total radiant flux per unit area of the specimen, absorbed from a specified source, or emitted.

Ordinarily it is preferable to use no more ordinates for the calculations than are needed to give the required precision. The optimum number of ordinates can be chosen by spacing them to represent equal areas under curve B, a device which results in unequal values of $\Delta\lambda$. When this method is used, the first step is to choose ordinates for curve B at increments of λ such that the areas between all adjacent pairs of these ordinates correspond to a constant amount, k, of radiant flux per unit area. Then the median wavelengths within the respective intervals between these adjacent pairs of ordinates determine the locations of the selected ordinates. When the ordinates of curve A are read at these specified values of λ, the rate at which energy is emitted per unit area of the specimen can be obtained with the required accuracy simply by adding up these ordinates and multiplying the sum by the constant, k. The basic equation is:

$$\epsilon_{ts}=\sum_{\lambda_1}^{\lambda_2} E_{s\lambda}(\epsilon_{b\lambda}\Delta\lambda) \tag{8}$$

But since $(\epsilon_{b\lambda}\Delta\lambda)$ has the constant value k, independent of wavelength, the equation becomes:

$$\epsilon_{ts}\cong k\sum_{\lambda_1}^{\lambda_2} E_{s\lambda} \tag{9}$$

Often, for convenience, ordinates are selected at intervals such that $k=1$.

The economy in number of ordinates required for a given precision makes this method especially advantageous in the absence of electronic computers. Like the weighted-ordinate method, it is applicable to calculation of total emittance or total absorptance from the spectral data, as well as to calculation of rate of emission or absorption of energy by unit area of the specimen.

DESIGN AND INSTALLATION OF DATA-PROCESSING EQUIPMENT

A photograph of the spectrophotometer with data-processing equipment installed is shown in figure 41 16. This equipment was designed to perform the following functions: (1) to produce a corrected graphical record of the normal spectral emittance of a specimen as a function of wavelength, (2) to record in digital form on punched paper tape the corrected spectral emittance values, for possible use in a separate electronic digital computer, and (3) to accumulate the digitalized emittances at wavelengths which have been pre-selected to yield specific information as described farther in this report.

The output of the spectrometer is digitized by two shaft encoders, one mounted on the

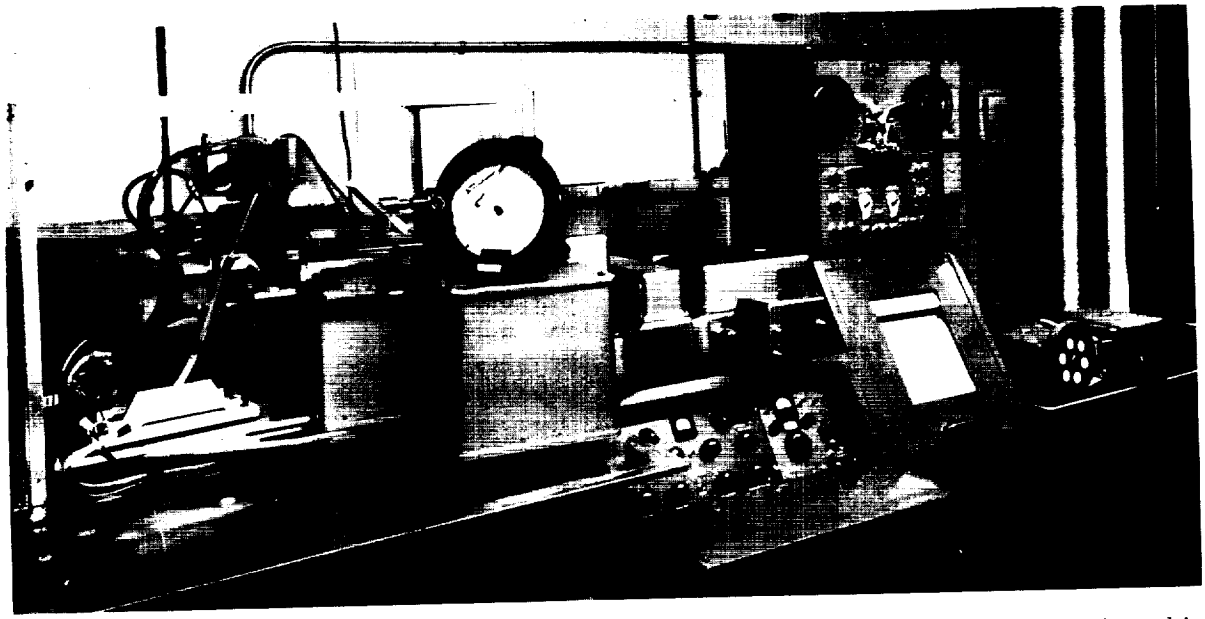

FIGURE 41–16.—Data-processing equipment attached to the spectrometer. The electronic circuits are housed in the chassis above the recorder at the right, and the paper tape punch and punched paper tape reader are on the table at the extreme right.

wavelength drive shaft, and the other on the recorder pen shaft. Each encoder produces a pulse for each 0.001 revolution of the shaft, and the pulse also contains a signal indicating direction of rotation. These pulses are counted in the data-processing attachment, by reversible counters which increase in count for pulses in the forward direction, and decrease in count for pulses in the backward direction.

During calibration, the pulses from the recorder shaft encoder are recorded on four-channel magnetic tape. During measurement of a specimen, the magnetic tape is played back synchronously with the automatic wavelength scanning, and the data-processing attachment automatically corrects for the 100% line and zero line errors, as is described in more detail in a paper by Horace M. Joseph (to be published). The corrected normal spectral emittance of the specimen appears as the curve drawn by the recording potentiometer. The output of the potentiometer is digitized, as before.

The wavelength drum position and recorder pen position can be automatically recorded on punched paper tape at preselected increments of wavelength drum position. The spectral emittance values can be accumulated at the same or other preselected increments of wavelength drum position.

In order to compute total emittance or absorptance for radiant energy having known spectral distribution of flux, the accumulation must be performed at unequal increments of wavelength drum position, at the selected ordinates which represent equal areas under the spectral energy distribution curve for the blackbody or source as previously described. These unequal increments are prepunched into paper tape, which automatically controls the accumulation process. The sum on the accumulator is then n times the total emittance or absorptance, where n is the number of selected ordinates.

SUMMARY

Test equipment and procedures were developed to measure normal spectral emittance of strip metal specimens that can be heated by passing a current through them, at temperatures from about 800° K to above 1400° K, and over the wavelength range of 1 to 15μ.

The equipment consisted essentially of a double-beam, ratio-recording infrared spectrometer, in which the source optics were modified to include a blackbody furnace in a fixed position as the source for the comparison beam, and a second blackbody furnace and a specimen furnace mounted on a movable plate attached to a slide so that either could be positioned to serve as the source for the specimen beam. Special control equipment maintained the two sources at the same temperature.

The test procedure corrected for zero line and 100% line errors in the measured emittance. The zero line error arises as a result of a spurious signal produced in the specimen beam when the beam is blocked near the source. The 100% line error results from differences in the ratio of the signal produced to radiant flux entering the instrument along the two beams of the spectrometer.

An electronic data-processing attachment was designed and built to (1) automatically correct for "zero line" and "100% line" errors, (2) record the corrected data in digital form on punched paper tape, suitable for direct entry into an off-line electronic digital computer and (3) compute, from the spectral data as obtained, a single value of total emittance, or absorptance for radiant energy having any known spectral distribution of flux.

Three types of specimens for use as working standards in other laboratories were prepared and calibrated. These specimens had high, intermediate and low spectral emittance, respectively. Tests of these standards indicated that the overall reproducibility of the method is on the order of 0.005 in emittance, expressed as a standard deviation.

REFERENCES

1. Worthing, A. G.: Temperature Radiation Emissivities and Emittances, Temperature—its Measurement and Control in Science and Industry. American Institute of Physics. Reinhold Publishing Corp., New York, 1941, pp 1164–1187.
2. Gouffé, André: Corrections des Corps Noires Artificiel Compete Teun des Diffusions Multiples Internes, Revue d'Optique *24* [1–3], Jan. to March 1945, pp 1–8.
3. Butterworth, ed.: Table of Wavenumbers. Int. Union of Pure and Applied Chemistry. 1961.

DISCUSSION

G. J. Zissis, Institute for Defense Analyses: One thing that worries me a bit is the effect of the corrugations on the walls of the cylinder of the cavity. In the De Vos treatment of a cavity, the first-order correction term gives the equivalent of the Gouffé theory, but the second-order corrections are quite dependent on the amount of radiation coming in through the opening and reflecting off of the walls. I have a feeling that with corrugations a direct return from the sides of the walls through the opening might be larger than it would be if you had, say, a flat wall with a Lambertian distribution. As long as you do not see the walls when you are operating I would imagine this would make only a very small difference, but it might be worth while carrying out the calculation of the emissivity by the De Vos method just to compare.

Richmond: The walls of the cavity were of 80 nickel-20 chromium alloy which had been oxidized for many hours at temperatures up to 1400 °K so that there was a rather thick oxide layer which was quite rough. Also, this was a sand casting which had not been smoothed; so the walls were quite rough inside. Under these conditions I believe that the De Vos analysis would not apply. I think the Gouffé analysis would be more nearly correct.

S. Sklarew, The Marquardt Corporation: What is the availability of this type of emittance standard, and are these standards reliable in the visible portion of the spectrum?

Richmond: I am going to ask Bob Winn to answer the first part of that question.

Winn: The standards themselves have been received at ASD; however, the program has been transferred from the Physics Laboratory to the Applications Laboratory, and I would suggest that you contact Mr. Don Stevinson (ASRCEE-2) who will be responsible for making arrangements to lend these standards.

Richmond: The other part of the question was with regard to the reliability of the standards in the visible. So far they have not been calibrated below one micron. We hope to do that eventually. We do not have any information on the reliability in that range. However, we do have some experimental evidence to indicate that these specimens will probably be relatively stable in emittance as long as they are heated in air at temperatures no higher than 1400° K for the platinum, 1300° K for the other standards, for periods up to at least 200 hours. We have run some of them for periods up to 1,000 hours, and we find probably not over 2 or 3% change in emittance as a result of this continued heating. However, they should be handled with care to avoid contamination of the surface because that can really change emittance.

Abbott, Naval Radiological Defense Laboratory: You mentioned integration of the spectral curve to obtain total normal emittance. Have you done any of this?

Richmond: We have done some of it. The automatic data processing equipment is not yet in operation so what we have done has been done by longhand methods, which is quite tedious as you probably know.

Abbott: You seem to be making the measurements from 1 to 15 μ.

Richmond: 1 to 15.

Abbott: How do you account for the range below and above?

Richmond: At the temperatures at which we are working there is only a small percentage of the energy below and above, and we assume that the emittance curve is flat below and above the ranges on which we have actual data.

Abbott: Do these agree reasonably well with measurements of direct total normal emittance?

Richmond: We do not have any data on the same specimens for direct measurement of normal total, but they agree within 1 or 2% with direct measurements of total hemispherical when you make a correction for the difference between normal and hemispherical according to the equations given in Jakob.

I. J. Barsy, Armstrong Cork Company: In describing the threaded alloy liner you made the statement that the reflectance is less than 0.05. How did you determine this?

Richmond: That was determined first from measured values on flat specimens that had been subjected to the same treatment and then making the correction for the effect of the threading.

I. J. Spiro, The Aerospace Corporation: Mine is not a question but a comment to you on your definitions. In your discussion on emissivity you call attention to the fact that you must have an optically smooth surface. I would like to caution your committee to consider wavelengths when you describe optically smooth surfaces. As you change in wavelengths to 50 and 100 μ, what was optically smooth at one place is no longer, and what was an "emittance" may now become an "emissivity".

Richmond: That is very definitely true, but as you go up in wavelength a rough surface tends to appear to be smoother. There has been some data published

not too long ago (Bennet, I believe was the author), in which it was shown that you can have effects from surface roughness on the order of a hundredth of a wavelength of the light involved. The major effects, however, do not begin to appear until you get up to something on the order of a tenth of the wavelength involved. That is peak-to-valley distance.

SHOULDERS, General Technology Corporation: When you were showing the curve on platinum you implied that you did not understand why you had a peak at the longer wavelengths around the 15-μ region. Did you mean to imply that you understood why you had the other peaks? I would like to have a little bit of an explanation on that.

RICHMOND: Suppose I see you after the meeting to talk about that. It gets quite involved. I think briefly that the one around 9½ or close to 10 μ is probably due to contamination in the specimen, but we are not sure. The one down around 1 μ we believe is due to resonance effects.

WILLIAM CLAYTON, Boeing Company: I think it might be useful if you were able to state what you believe to be the accuracy of your method, divorced from material changes, of course. Your method is probably two or three times as accurate as anybody else's, at least mine. It might give us all a good target.

RICHMOND: That is a rather difficult question to answer. I think that the precision of our measurements is certainly on the order of 0.01 in emittance. If you wanted it in a percentage, that would depend on the emittance value that you are measuring. The only data we have on the accuracy is what we obtained by use of a sector-disk attenuator; we find that our entire system gives linear response to better than 0.01. On that basis, assuming that errors are additive, conservatively any value should be good to about 0.02. I don't have any rigid analytical basis for stating that; that is just my own feeling.

STREED, Lockheed Missiles and Space: Is it possible to clean these standards, and do you have any recommendations in handling them?

RICHMOND: As far as handling them is concerned, the specimens are mounted in plastic holders so that the central area, the area on which you would be making measurements on all specimens, is not touching anything. Our recommendation would be to avoid touching the portion where you would be looking at the specimen. In fact, you would probably be better off if you were to wear surgical gloves at any time when handling the specimen, to avoid fingerprints. Fingerprints can be very very bad, and they are very difficult to remove, particularly if the specimen has been heated before you attempt to remove them. Other than that, I would say avoid letting anything come in contact with that central portion of the specimen. I think probably the specimens could be cleaned if they should become contaminated, but it might be a considerable job. The oxidized Inconel specimens tend to be self-cleaning, because a type of oxide forms on them that gradually spalls away as a very fine powder so that you get a self-renewing surface. I would expect that all you would have to do on those specimens would be to heat them for a few hours, at a high temperature in air. They would probably come back pretty close to what they were originally. That same treatment would not apply to the oxidized Kanthal however, because a very stable oxide film is formed on them.

J. I. WITTEBORT, ASD: The problem of thermal etching on the surfaces comes up at high temperatures. Have you noticed much difference in the emittance, at say, 1500° to 1800° F at the beginning of the test and later on after thermal etching has occurred?

RICHMOND: We did notice that on unannealed platinum specimens. I am not sure that the effect is due to thermal etching, I think it is due to recrystallization, but the specimens had been annealed above the recrystallization temperature before we made any determinations. I think that you have to take the platinum up to temperatures above those at which we have made any measurements in order to get appreciable thermal etching. I am not positive but that is my impression.

KOSTKOWSKI, NBS: I would like to make a comment here that when one begins to get into accuracies of a few percent, one factor that should be taken into account in any type of radiance measurements is the relative size of the two samples one is comparing. For example, in your case, the specimen is of the order of ¼-inch wide, and the blackbodies, at least the effective size of the blackbody is probably an inch in diameter or greater. Is that right?

RICHMOND: I did not mention this, but the blackbody has an opening approximately ¼-inch wide by ¾-inch long.

KOSTKOWSKI: But how about the area adjacent to the cavity hole? It is probably still bright, is it not?

RICHMOND: No, it is not. When the blackbody furnace is at a temperature of 1400° K that area adjacent to the opening is not incandescent.

KOSTKOWSKI: The problem I am referring to does not apply in this case, but I still think I should mention it. When the relative sizes of the two sources one is comparing are very different, the apparent brightness or radiance of the two can differ by several percent due to diffraction effects alone.

RICHMOND: We are very much aware of that in some of the work Dwight Moore has been doing, which he will describe tomorrow; there we are using an extremely small area of the specimen.

42 — SYSTEM FOR THE MEASUREMENT OF SPECTRAL EMITTANCE IN AN INERT ATMOSPHERE

BY R. A. SEBAN

UNIVERSITY OF CALIFORNIA, BERKELEY, CALIFORNIA

There is described a system for the measurement of spectral emittance, certain operating difficulties are considered, and results for a metal and for a ceramic coating are presented to reveal satisfactory operation at temperatures from 1500° F to 2000° F.

In the design of a system for the measurement of spectral emittance in an inert atmosphere, considerable choice is available with respect to the position of the sample and of the reference and to the degree that the system is enclosed in the inert atmosphere. A number of examples of such systems are available (ref. 1 and 2) and each one represents certain compromises in the accuracy of the determination of the emittance, in the nature of the sample that can be accommodated, and in the mechanical complexity of the system. The system that is described here is no exception, and this system was designed to accommodate metallic or coated metallic samples in the form of disks 0.87 inches in diameter, to produce values of the normal spectral emittance with sample temperatures between 1300° F and 3000° F, to operate with a single beam through identical optics for both sample and reference observations, and to have an inert gas enclosure of minimum size. In addition to the description of the system and the method of observation, certain difficulties in operation are described as these have so far occurred, and these have essentially limited the operation to the lower part of the temperature range. Thus this presentation is in the nature of a progress report, and the results for the emittance that are presented support the view that adequate operation will be achieved ultimately in the whole range of temperatures and wave-lengths.

SYSTEM

The reference cavity and the sample furnace are mounted on horizontal rails within a tank which is 16 inches in diameter and 36 inches long, as shown schematically on figure 42–1. A mirror, positioned against stops by a selsyn motor, serves to direct radiation from either the sample or from the cavity through the window in the tank wall, to a Perkin-Elmer Model 98 monochromator, via an external optical system. In the initial arrangement, the definition of the observed area, at the cavity and at the sample, is by horizontal slits at the chopper location and by the monochrometer inlet slits. The magnification is nearly unity, so that the observed area was estimated to be in height the 3-mm opening of the horizontal slits and in width of the order of the opening of the monochrometer inlet slits. Later consideration, particularly of the results that have been obtained, implies that this method of image definition may be partially inadequate because of the astigmatic effects of the off-axis spherical mirrors and that image definition may be needed at the location of the focal lines.

Figure 42–1 also indicates a system for the appraisal of total emittance that has not yet been installed. It consists of a detector which is irradiated by further rotation of the movable mirror, so that radiation from either the cavity or the sample would be focused on a thermopile detector.

A mechanical vacuum pump provides a pressure of 1 μ in the tank and this is maintained, with a temperature of about 500° F in the cavity and sample holder, for about four hours or longer before argon is introduced, through a drier, into the system. The argon pressure is maintained at slightly above atmospheric pressure.

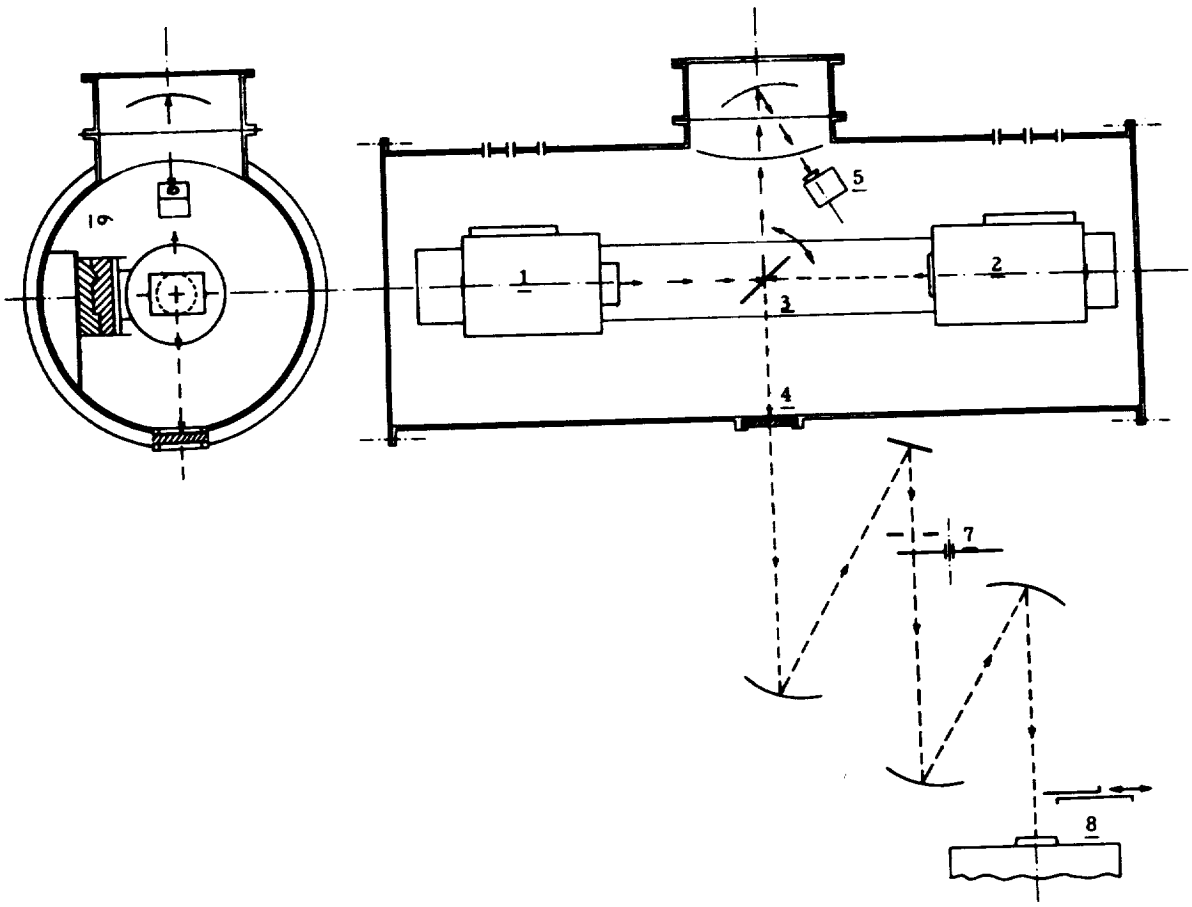

FIGURE 42–1.—System for emittance determination: (1) sample heater, (2) cavity, (3) moveable mirror, (4) window, (5) total detector, (6) mounting rails (7) chopper horizontal slits, (8) monochromator inlet slits.

Both the cavity and the sample furnace are heated electrically by tungsten wire coiled on Alundum tubes, fixed with refractory cement and covered externally with other Alundum sections to provide high-temperature insulation. Fiberfrax is employed as the insulation between these elements and the water-cooled external jacket; as noted later, the operating experience has indicated undesirability in this application of this material.

Figure 42–2 shows some details of the cavity furnace and indicates the position of the graphite tube which forms the cavity itself. This hole, ½-inch inside diameter and 2.75 inches long, is bored to leave a plug in which a thermocouple is mounted and from which plug originates most of the radiation which enters the optical system. A front orifice with a 0.30-inch diameter aperture reduces the radiation loss from the open end of the cavity. Three separately-controlled heaters are provided for the control of cavity temperature.

Figure 42–3 shows some details of the sample furnace and sample mounting arrangement. The sample, contained in a holder made of molybdenum sheet, is positioned in the opening of a ceramic ring and introduced therein by opening the door in the furnace; this door is shown partly open in figure 42–3. The sample thermocouple, welded to the back of the sample, leaves the interior through an insulator also held by the sample holder. The front of the holder extends over the area defined by the ceramic ring that provides insulation in the door, and the center of the molybdenum sheet contains a 0.30-inch diameter

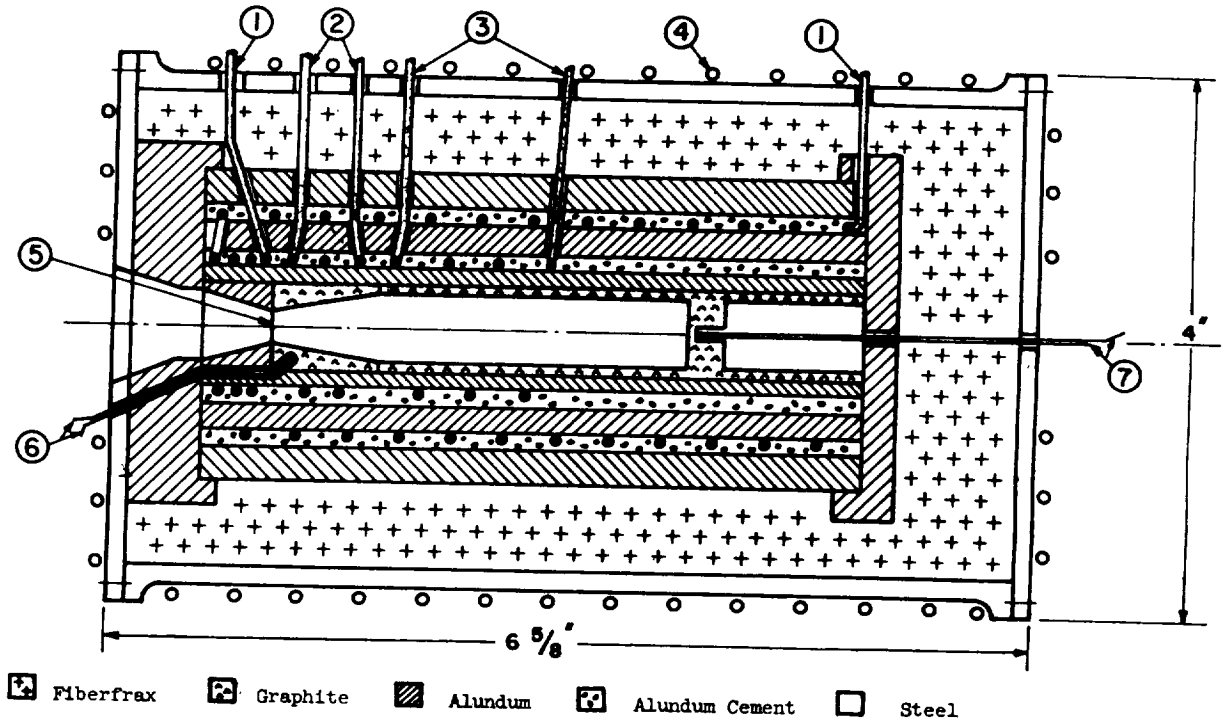

FIGURE 42-2.—Reference cavity: (1, 2, and 3) heater wires, (4) jacket water tubes, (5) orifice, (6) front thermocouple and (7) rear thermocouple.

hole through which the sample is viewed. This view is through the water-cooled shield in the door of the sample furnace, the inside of the shield being honed smooth to achieve specular reflection, out of the hole, of radiation incident on the walls from the sample and shield. In addition to the shield and the external region viewed through the shield opening, the sample also "sees" the edge of the aperture in the sample holder and also a small part of the ceramic door insulating ring, through the gap between the radiation shield and the sample holder. The aggregate angle factor of this view is about 0.017, and the radiation from it is at a lower temperature than that emitted by the sample. With a diffuse reflector, having an emittance of 0.30, the reflection would be 0.017/0.20 of the radiosity if the radiation from the surfaces concerned were black at the temperature of the sample. Actually, the materials which are poor emitters tend to be specular reflectors and, if specular, none of this radiation is reflected into the cone of observation.

A small component of irradiation of the sample arises from reflection from the window, via the internal mirror. The first reflection therefrom is equivalent to the radiation from the image of the source and this radiation being diffuse, only a negligible portion (1/1000) thereof, would again impinge on the sample even if the window were a perfect reflector. Thus, because of the small lateral extent of the heated surface, the interreflection contribution is negligible compared to what it would be for a heated surface of large lateral extent.

EVALUATION OF EMITTANCE

The detector output datum is established by sighting on a black shutter located near the monochrometer inlet. If the remainder of the system is at a temperature near that of the shutter, then the output of sights on the cavity and on the sample will be zero. Outputs above this are produced by emissive powers exceeding the datum value in any of the components beyond the chopper. In addition to the emission from the sample or from the cavity such additional emission may be produced by the internal mirror or by the window, if the equilibrium temperature of these elements exceeds substantially the datum value. Analysis indicates that with an argon atmosphere the loss of heat by

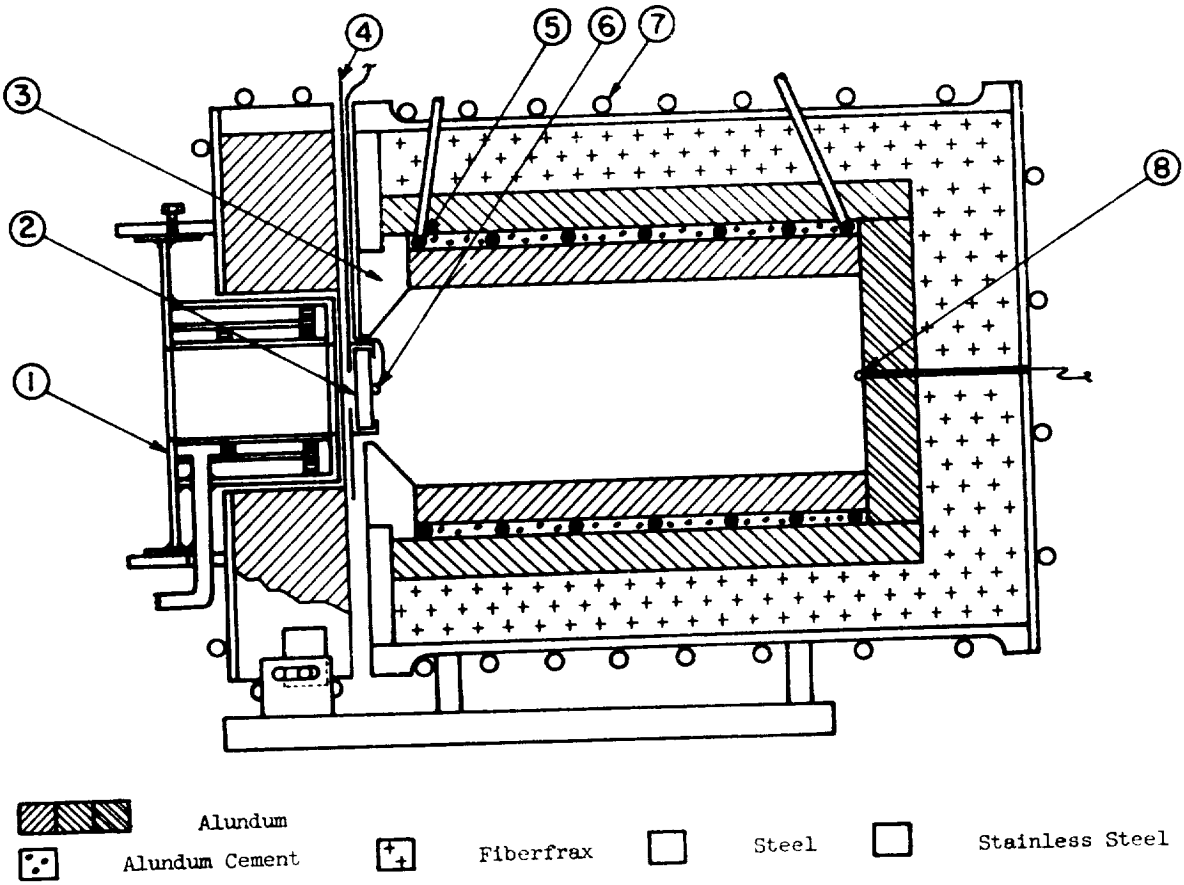

FIGURE 42-3.—Sample heater: (1) water-cooled front shield, (2) sample, (3) ceramic ring, (4) sample holder, (5) heater, (6) sample thermocouple, (7) water tube jacket, and (8) thermocouple.

free convection is sufficient to prevent excessive temperatures in the mirror and in the window but that with a vacuum the mirror, in particular, may attain temperatures which would affect the accuracy of the measured emittance.

The response of the monochromator detector is proportional to the energy above the datum level that emerges from the window, and the ratio of the responses that is obtained for a sight on the sample and on the cavity is then specified in terms of the reflectances, r_s and r_m, of sample and internal mirror, and the reflectance, R, of the window.

$$\frac{S_s}{S_c}=\frac{\epsilon_s\,[E_s-E_o]+(1+r_s r_m)\,\frac{\epsilon_m}{r_m}\,(E_m-E_o)+[r_m^2 r_s+1-r_m^2 r_s R]\,\frac{\epsilon_w}{r_m}\,[E_w-E_o]}{\left[(E_c-E_o)+\frac{\epsilon_m}{r_m}\,(E_m-E_o)+\frac{\epsilon_w}{r_m}\,(E_w-E_o)\right]}, \tag{1}$$

and if the emissive powers of the mirror, E_m, and of the window, E_w, are at the datum level, E_o, then the ratio of responses is

$$\frac{S_s}{S_c}=\frac{\epsilon_s[E_s-E_o]}{[E_c-E_o]} \tag{2}$$

Equation (2) has been used to evaluate the results so far obtained, on the assumption that the temperatures of the mirror and of the window were low enough to make negligible the contributions of the radiation from those components as they appear in equation (1). This,

of course, is also based on the assumption that the radiosity of the sample is due to its emission alone.

OPERATING EXPERIENCE

In initial trials, the front heater of the cavity was not used, and the temperatures within the cavity were nonuniform to such a degree that optical pyrometer indications (corrected separately for the transmittance of the window, internal mirror, and additional external mirror) revealed that the temperature indicated by the thermocouple at the back of the cavity was, at 1500° F, lower by 50° F than the indication of the pyrometer. A correction deduced from this kind of observation was then applied to the thermocouple indication. Optical pyrometer observations were always made, but their interpretations is affected by fogging of the sodium chloride window after the initial calibration.

When the front heater was made operative, temperatures inferred from the pyrometer indication differed by about 5° F from those indicated by the thermocouple. While this indicates satisfactory performance, a new cavity system with an improved heating arrangement has been produced; its installation was delayed because of the other difficulties that are next indicated.

Early in the history of operation, indications of chemical reaction in the heating system were given by deposits on cold surfaces, particularly on the water-cooled radiation shield of the sample furnace. Also, at 2300° F, there was evidence of chemical reaction with a coated sample. Finally, in an error in operation, the temperatures, in vacuum, attained levels above 3000° F. Then the cavity orifice was closed by a deposit and subsequent inspection revealed a heavy deposit on the cold surfaces of the cavity jacket near the cavity opening. The external deposit appeared to be tungsten oxide, and a green deposit in the cavity opening and within the cavity appeared to be aluminum carbide. The source of the oxygen for the production of oxide was not clear, but there was visual alteration of the nature of the Fiberfrax external insulation and this element of the system is suspect. To allow continued operation a new orifice and carbon tube were installed and the use of the cavity was continued, while the installation of the new cavity was delayed to permit the replacement of the Fiberfrax insulation with bubbled zirconia.

RESULTS

Despite the indicated operating difficulties a considerable number of results have been obtained, on nickel, the coated material XP–6789, a Chance-Vought coated material, and oxidized Inconel, at operating temperatures as high as 2300° F, but with the majority of the results secured at about 1500° F. These results serve to appraise the operation of the system but they do so somewhat indirectly through a comparison to the reflectance measured at room temperature on the same sample, and the comparison is affected by the relatively unknown dependence of the emittance on temperature that the system is intended to discover. Some of the results for nickel and for XP–6789 are presented here to indicate this type of comparison and to provide at least a partial basis for an appraisal of the accuracy of the results.

Figure 42–4 contains results for the emittance of mechanically-polished nickel, and these results are identified in the order in which they were obtained. The increase in emittance which occurs after successive determinations thereof is attributed to an effect of aging, which at least visibly changes the surface structure and apparently does so sufficiently to alter

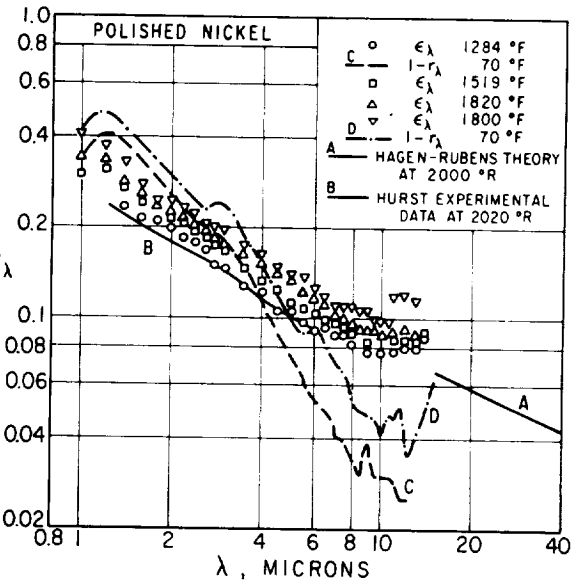

FIGURE 42–4.—Emittance of polished nickel sample.

its properties. Such effects have been observed in total and spectral determinations of the emittance of platinum (ref. 3 and 4). The values of the reflectance at room temperature indicate a permanent effect which would require such a change.

The initial values of the emittance of the nickel sample are only slightly above the values found by Hurst (ref. 5), at a similar temperature, and this lends confidence to the magnitude achieved for the initial results, at least to a wavelength of about 9μ. At greater wavelengths the emittances tend to either remain constant or to rise, and in this spectral region current expectation would be for a trend like that of the Hagen-Rubens law, illustrated on figure 42–4 by its value for the electrical resistivity of nickel at 2000° R. Yet, it is also known that the Drude theory, of which the Hagen-Rubens expression is an asymptotic form, requires a smaller electrical conductivity than the d–c value, so that it is equally reasonable to expect an asymptotic trend of the actual emittances to a Hagen-Rubens line having a magnitude greater than that shown on figure 42–4. But the trend of the data still arouses uncertainty and the optical system has been checked repeatedly in an effort to locate error; it is quite conclusive that, for instance, the unexpected trend of the results is not due to light scattering in the monochromator. It may be due to improper image definition in the system, but it is not yet clear why such an effect, which would, for example, include some radiation from the edge of the orifice in the observed beam, should produce an effect more important at long wavelengths.

Because of the difficulties cited previously, there is also the possibility of some chemical reaction, and the irregular nature of the reflectance results near 10μ suggests that some surface film may have been present, though the results at lower wavelengths do correspond well with other information on this material.

A second set of results is shown on figure 42–5 for a coated molybdenum sample, XP–6789, and again the tabulation of results is in chronological order. Compared to the presentation of the results for nickel, there is now no comparison available, either theoretical or experimental, so that these results for XP–6789 can be considered

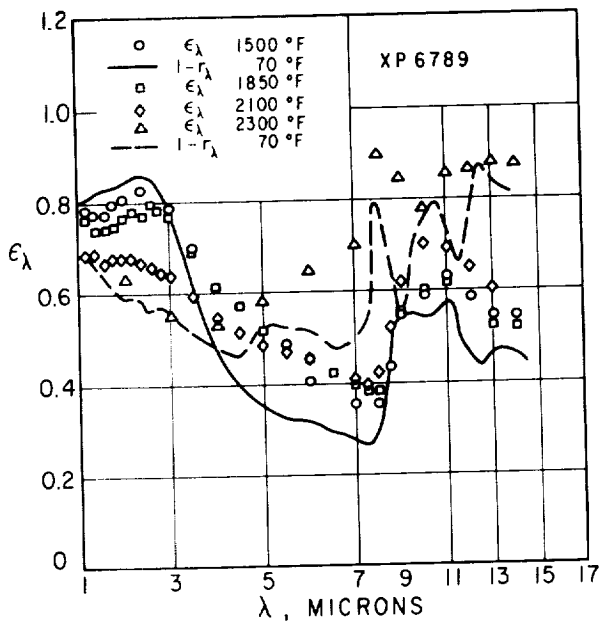

FIGURE 42–5.—Emittance of coated molybdenum sample.

only as representative of this material and the difficulties associated with it, and not in the aspect of verification of the operation of the system.

Below 2000° F the measured emittances correspond well and they do not depart too greatly from the reflectance at room temperature as measured between the two emittance determinations. It is not clear, however, that the difference in the emittances at room temperature and 1800° F is exclusively a temperature effect.

Significant differences in the emittance occurred at higher temperature, first apparent in the emittances for 2100° F. Those at 2300° F changed radically, and the altered appearance of the sample after this operation supported the assumption of change due to chemical reaction. The reflectance results obtained thereafter support the change in the nature of the surface, but the emittance deduced from these results, while of the correct magnitude, does not correspond well in detail with that measured at high temperature.

CONCLUSIONS

The system described, intended for the determination of normal spectral emittance in the temperature range from 1300° F to 3000° F,

has, despite certain operating difficulties associated with the thermal insulation and possibly with image definition, yielded satisfactory results for the emittance at temperatures below 2000° F. Improvements in the cavity and a resolution of the problem that has arisen in connection with thermal insulation should allow the use of the system for measuring emittance in the entire design range.

ACKNOWLEDGMENT

The development, construction, and operation of the system described was accomplished with the support of the U.S. Air Force under Contracts AF 33(616)-6630 and AF 33(657)-7793.

REFERENCES

1. Gravina, A.; and Katz, M.: Investigation of High Emittance Coatings to Extend Mach Number Range of Application of Structural Materials, WADD Tech. Rep. 60-102, Mar. 1961.
2. Blau, H., et al.: High Temperature Thermal Radiation Properties of Solid Materials. AFCRC Tech. Notes 60-165, Mar. 1960.
3. Abbott, G.; Alvares, N.; and Parker, W.: Total Normal and Total Hemispherical Emittance of Polished Metals. WADD Tech. Rep. 61-94, Apr. 1961.
4. Seban, R. A.: Thermal Radiation Properties of Materials. WADD Tech Rep. 60-370, pt. II, Jan. 1962.
5. Hurst, C.: The Emission Constants of Metals in the Near Infra-Red. Proc. Royal Society, Sec. A., Vol. 142, p. 466-490.

DISCUSSION

E. Schatz, American Machine and Foundry: I get the impression that you are sighting on the back of the blackbody. Shouldn't you be sighting on the front of the blackbody where the radiation originates?

R. A. Seban, University of California: The focus is actually made at the sample position which is about 6 inches from the mirror. When the mirror is turned that point is just about in the throat of the open part of the cavity where it necks down. Ray tracing from there on would indicate that most of the radiation passing through that section originates at the back of the cavity. Thus, the plane that you are looking at is about at the minimum opening of the cavity, but the radiation which passes through that point comes mostly from the back.

Richmond: Theoretically, I can see no reason why it should make any difference whether you are focused on the opening or the back. Presumably, any gas that is within the cavity will be at the same temperature as the walls, and there will be essentially no absorptance within the hot gas.

Seban: That is substantially correct. There is a slightly longer optical path length because of the greater distance, but it will not make any difference.

43—A METHOD FOR MEASURING THE SPECTRAL NORMAL EMITTANCE IN AIR OF A VARIETY OF MATERIALS HAVING STABLE EMITTANCE CHARACTERISTICS

BY WAYNE S. SLEMP AND WILLIAM R. WADE

NASA LANGLEY RESEARCH CENTER, HAMPTON, VIRGINIA

A method and apparatus is described for the measurement of spectral normal emittance in air of a variety of materials. The system permits measurements to be performed over a wavelength region of 1.0 through 15.0 microns and over a temperature range of 600° F to 1800° F with an accuracy of ±5.0%. The advantages of this system are described. Results obtained by this system are compared with results reported by another observer using a different technique.

In order that the proper selection of materials for the design of space radiators, heat rejection systems, and power plants for use in space can be made, accurate heat-transfer calculations must be performed. Since the spectral emittance of these materials plays an extremely important part in these calculations, a program has been initiated at the Langley Research Center of NASA for the investigation of these properties. One phase of the spectral emittance program is the measurement of spectral normal emittance in air of a variety of materials with stable emittance properties. These materials include ceramics, cermets, stably oxidized metals, and coatings on metallic substrates.

In efforts to provide an improved system for obtaining these measurements, a technique together with necessary apparatus was developed which has proved to be relatively simple, fast, and reliable. The apparatus utilized in this system consisted of a modified commercially-available recording spectrophotometer and a blackbody furnace similar to that used by McMahon in his investigation of glasses in reference 1. This system permits measurements of spectral normal emittance to be made over a temperature range from 600° F to 1800° F. Since the primary use of the data obtained by this system will be for heat-transfer calculations, the near infrared region form 1.0 through 15.0μ was chosen. This region, according to Planck's spectral energy distribution law, contains a minimum of 90% of the energy in the 600° F to 1800° F temperature range.

The description of this system and the procedure used to obtain these measurements is the subject of this paper.

APPARATUS

The apparatus under consideration can be divided into two main parts. A spectrophotometer with its detector and recorder is one part. A furnace, which contains the test specimen and a blackbody cavity, and an associated temperature monitoring system and power supply comprise the second part. These two parts of the apparatus are described in detail in the following sections.

Spectrophotometer and Associated Apparatus

A commercially-available spectrophotometer is used in this investigation. A minor modification was made to the optical system to allow the use of an external source. These modifications together with the original optical path are shown schematically in figure 43–1. Mirrors M_1 and M_2, as well as the internal source of the standard instrument, were removed. Mirrors, M_3, a 6-inch focal length parabolic

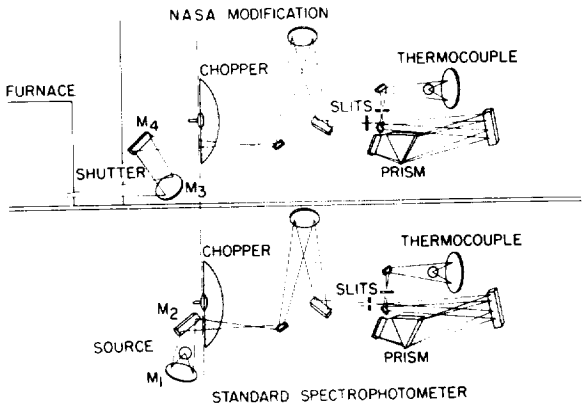

FIGURE 43–1.—Optical schematic of spectrophotometer.

mirror, and M_4, a plane-surface mirror, were positioned to transmit radiation from the external source and to focus this radiation at the same point as the original instrument optics. A new cover for this portion of the instrument was designed with an aperture and watercooled shutter so that the radiation from the external source could be prevented from passing into the instrument when so desired.

Since this spectrophotometer has several interchangeable prisms and detectors available for use in various regions of the spectrum, the sodium chloride prism and the high-speed evacuated thermocouple detector with a potassium bromide window were chosen to cover this spectral region, from 1.0 through 15.0 μ.

Furnace and Associated Apparatus

The furnace, shown in figure 43–2, is designed similarly to the furnace used by McMahon (ref. 1) in his investigation of glasses. It is constructed essentially of three cubes. The inner cube, called the liner, serves as the blackbody cavity. It is composed of heavily oxidized Inconel approximately $\frac{1}{16}$ inch thick and 6 inches on each side. This liner fits inside a cube of silicon carbide which serves as the furnace core. The silicon carbide is wound with 17-gage (AWG) Nichrome V resistance wire that serves as the heating element. The core is well insulated by an outer cube of high-temperature refractory firebrick. All these cubes are fabricated in two halves to facilitate specimen placement. The lower half of the furnace contains a blackened, tapered, watercooled viewport, as well as provisions for rotating the test specimen within $\frac{1}{16}$ inch of

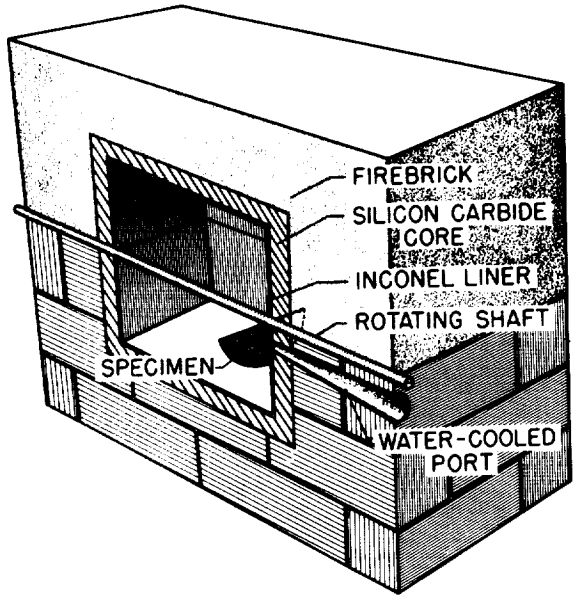

FIGURE 43–2.—Cross section of blackbody furnace.

the Inconel liner by an external 15-rpm motor.

Since the furnace is divided into two halves and the Nichrome V windings are separated, the power is supplied and controlled by two continously variable autotransformers.

In operation 30-gage (AWG) Chromel-Alumel thermocouples are spotwelded to the outer surface of the Inconel liner. These thermocouples are constantly monitored to adjust and hold the temperature of the cavity (and thus the temperature of the test specimen) at the desired value.

TEST PROCEDURES

Specimens used for this investigation were cut from $\frac{1}{8}$-inch stock in the form of a 4-inch-diameter semicircle. These specimens were positioned on the rotating shaft in the furnace normal to the axis of the viewport and passing within $\frac{1}{16}$ inch of the viewport for each cycle of rotation. By manual control of the autotransformers, the furnace cavity is brought to equilibrium at the desired temperature, and emittance measurements are begun.

An example of a typical recorder trace showing the measuring technique is shown in figure 43–3 for a particular temperature and wavelength. The recorder zero V_o is displaced up-scale to allow the complete monitoring of any change in this setting. The monochro-

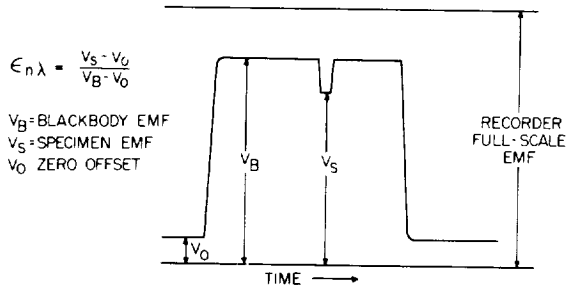

FIGURE 43-3.—Typical data trace.

mator is then set at the desired wavelength and the water-cooled shutter is opened. The radiant flux intensities from the blackbody reference V_B and from the test specimen V_S are then recorded and the water-cooled shutter is closed. This procedure is repeated at 0.5 μ intervals from 1.0 through 15.0 μ. The monochromator slits are held constant and the instrument amplifier gain is adjusted at each reading in order that a maximum recorder deflection can be obtained. The large recorder deflection minimizes the error in calculating emittance values from recorder charts. The calculation of the spectral normal emittance $E_{n\lambda}$ is then obtained by the ratio:

$$E_{n\lambda}=\frac{V_S-V_O}{V_B-V_O}$$

CALIBRATION

Spectrophotometer

Since several prisms are interchangeable for this spectrophotometer, the wavelength indicator is divided in arbitrary units. Each prism used in this instrument must, therefore, be calibrated through the wavelength region covered by this prism. Since the infrared region from 1.0 through 15.0 μ is of interest in this study, the sodium chloride prism was chosen. This prism was then calibrated through this region by the use of absorption and emission spectra of known compounds and elements and a calibration curve of wavelength indicator number as a function of wavelength was constructed.

Furnace

In order to determine whether any possible temperature differential exists between a test specimen and the cavity, an Iconel specimen with three thermocouples attached, as shown in figure 43–4, was placed in the furnace out of view of the port. The temperature of the cavity was measured by thermocouples attached at eight points on the Inconel cavity. The placement of these eight thermocouples is also shown in figure 43–4.

The temperatures of the specimen and of the cavity were measured over the temperature range from 600° F to 1800° F and were found to be in close agreement as shown in figure 43–5.

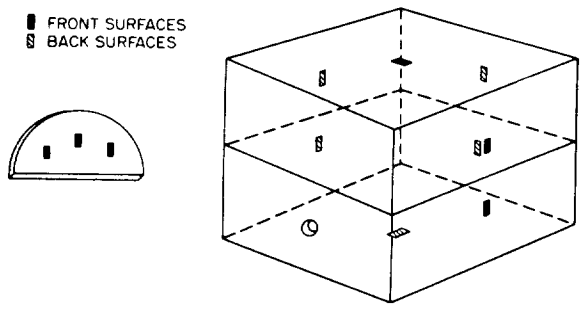

FIGURE 43-4.—Thermocouple placement on specimen and cavity.

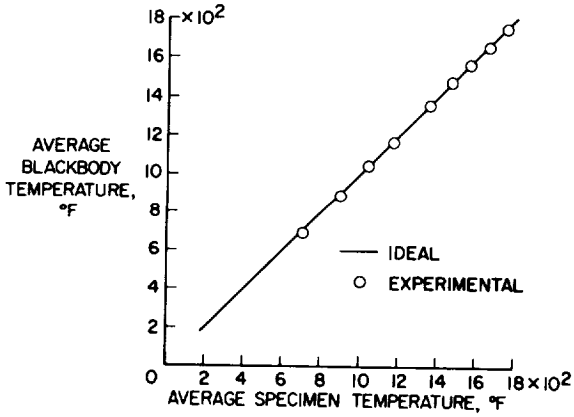

FIGURE 43-5.—Deviation of specimen temperature from blackbody temperature.

Although these temperatures are averages of all thermocouples on the specimen or cavity, the actual differences are less than 1.0%. The specimen temperature was lower than the cavity temperature over the entire temperature range, but the maximum deviation was only 0.87% of the absolute temperature. These measurements indicate that the assumption of thermal equilibrium between specimen and

cavity is valid for the nonmeasuring portion of the specimen cycle. Thus, the measurement of cavity temperature may be taken also as specimen temperature with a possible total emittance error of less than 3.50%. The spectral emittance error at 600° F would vary from 11.0% at 1.0 μ to 1.2% at 15 μ, and at 1800° F would vary from 3.5% at 1.0 μ to 0.4% at 15 μ.

When the specimen is rotated in front of the viewing port it radiates to the cooler surroundings and obviously must cool. The rate of cooling is determined by many factors, one of which is the emittance of the specimen. To determine the effects of this cooling on emittance measurements the following procedure was used. An Inconel specimen was placed in the furnace, out of view of the port, and heated to 1800° F. After the furnace temperature was stabilized, measurements of radiant flux intensity were obtained by use of a total radiation bolometer. With the specimen out of view of the port, the bolometer was focused into the cavity, and a measurement of the blackbody flux intensity was recorded. The specimen was then rotated past the viewport, and a measurement of the specimen flux intensity was recorded. This procedure of obtaining measurements for the blackbody and specimen alternately was continued for 12 cycles. The results are shown in figure 43–6 where

f_S radiometer output for specimen, rms volts
f_B radiometer output for blackbody, rms volts

From a comparison of the ratio of the radiant flux intensities of specimen and blackbody, an indication of the cooling effect is obtained. The specimen emittance measured for the ½ cycle (the first viewing cycle) was 0.95, and that measured for the ½ cycle was 0.94. This difference is about 1.00%, which indicates that the specimen cooling from rotating past the viewport is negligible for most materials.

The reproducibility of this system as measured during these tests is within 0.5%.

The total error possible in considering all these factors cannot exceed 5.0% for total emittance and 12.5% at 1 μ and 600° F to 1.9% at 15 μ and 1800° F for spectral emittance.

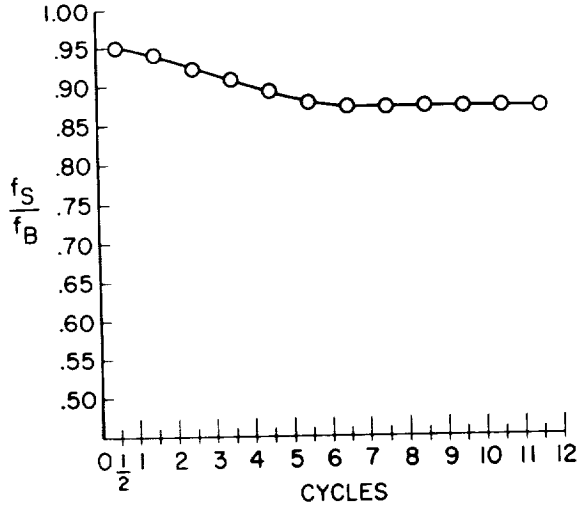

FIGURE 43–6.—Decrease of radiant intensity ratio for specimen of gritblasted Inconel X at a furnace temperature of 1800° F.

ADVANTAGES OF SYSTEM

This system for the measurement of normal spectral emittance in air of materials with stable emittance properties at moderately high temperatures has several distinct advantages over many other systems used in these studies.

One advantage is the elimination of attached thermocouples on the surface of the specimen or use of other temperature measuring devices, such as optical pyrometers, to obtain the temperature of the test specimen. The temperature of the cavity is measured by thermocouples spotwelded to the outer surface of the cavity and the specimen temperature can be maintained to within 1.00% of the cavity temperature, which makes the system practical for use with a large variety of materials. These include ceramics, cermets, thick coatings on metallic substrates, and other materials to which it is difficult or impossible to attach a thermocouple.

Methods utilizing a dual-beam spectrophotometer for these measurements are complicated by the cost and time involved in equalizing the path lengths and absorption of mirrors in each beam. Since a separated specimen and black-body reference is used in that type of operation, a problem of maintaining them at equal temperatures is present. On the other hand, methods favoring single-beam

operation and separated reference and specimen are confronted with the same problem of temperature control or the problem of absorbing gases in the optical path.

The use of the blackbody-cavity method requires only one path, so that the problem of equalizing the beams, as in dual-beam operation, is avoided. The blackbody reference and test specimen are kept at approximately equal temperatures, with differences of less than 1.00%, by control of the furnance temperature alone; thus, the need for elaborate temperature regulating devices is eliminated. The reference and test specimen are viewed within 2 sec, so that the effects of changes in composition and quantity of absorbing gases in the optical path are canceled out.

TYPICAL RESULTS

Measurements of normal spectral emittance using this method have been performed on several high-temperature materials including boron nitride, Inconel, Inconel-X, alumina, and zirconia as well as several other refractory metals. The apparatus is currently being used to study flame-sprayed ceramics on refractory metals.

Figures 43–7, –8, and –9 present comparisons of the results obtained by this system and those obtained by Henry H. Blau, Jr. and associates using a different technique, as reported in reference 2. The NASA data shown in figure 43–7 were taken from reference 3.

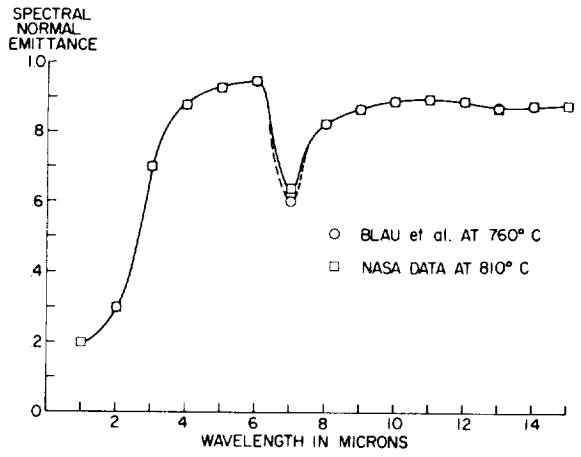

FIGURE 43–7.—Spectral normal emittance data for boron nitride

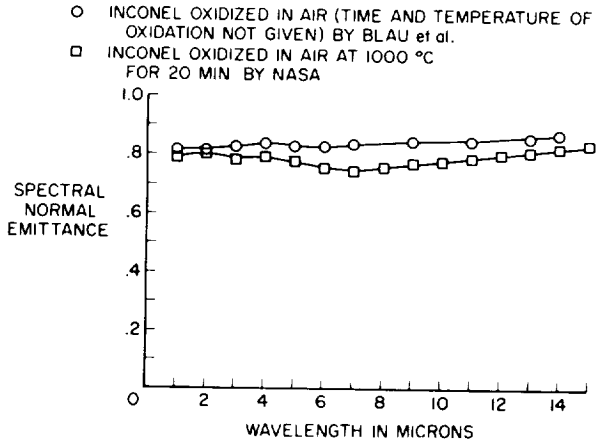

FIGURE 43–8.—Spectral normal emittance data for oxidized Inconel at 1000° C.

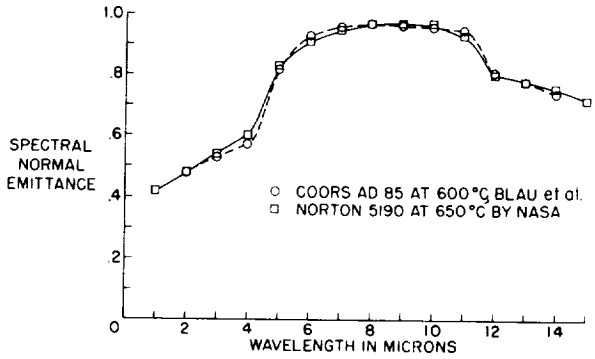

FIGURE 43–9.—Spectral normal emittance data for alumina.

The measurements reported by Dr. Blau and associates were made on test specimens heated in air at temperatures from 600° C to 1000° C and over a wavelength region from 2.0 to 15.0μ, with a reported accuracy of $\pm 4\%$. The procedures used differed from those described in this paper in that temperatures of both specimen and blackbody were measured by embedded thermocouples and values of radiant intensity from the specimen and blackbody reference were measured independently. Although the specimen and blackbody heat source varied from those used in this investigation, almost all other apparatus and techniques were very similar to those reported in this paper.

One main problem discussed in reference 2 is that of determining the temperature lag of

the thermocouples used to obtain the temperature of the blackbody and specimen.

Another problem, although not discussed in reference 2, is the control of absorbing gases in the optical path due to the time interval necessary between measurements of specimen and blackbody radiation. The temperature and humidity of the room were closely controlled so that the errors caused by these absorbed gases would be extremely small.

As illustrated in figures 43-7, -8, and -9, agreement in the results obtained by the two systems is extremely close, and the error in each system is approximately the same. Therefore, the choice between these two systems depends on such other factors as the ease of specimen preparation and of operation of the apparatus.

CONCLUDING REMARKS

A system has been developed for the measurement of spectral normal emittance in air of materials with stable emittance properties. The variety of materials which can be tested, the simple method of specimen and blackbody temperature control, and the elimination of problems associated with absorbing gases in the optical path are some of the advantages of this system over others now in use.

Both consideration of possible errors and comparison of results with those of a prior investigator indicate that the results are accurate and reliable.

REFERENCES

1. McMahon, Howard O.: Thermal Radiation Characteristics of Some Glasses. Journal American Ceramic Soc., vol. 34, no. 3, 1951, p. 91.
2. Blau, Henry H., Jr.; Marsh, John B.; Martin, William S.; Jasperse, John R.; and Chaffee, Eleanor: Infrared Spectral Emittance Properties of Solid Materials. AFCRL-TR-60-416. Geophys. Res. Directorate, Air Force Res. Div., Oct. 1960.
3. Walker, Gilbert H.; and Casey, Francis W., Jr.: Measurement of Total Normal Emittance of Boron Nitride From 1200° F to 1900° F With Normal Spectral Emittance Data at 1400° F. NASA TN D-1268, 1961.

DISCUSSION

Richmond: This paper is now open for discussion, and I would like to start the discussion by asking what is the time required to make a complete wavelength scan from, say, 1 to 15μ?

W. S. Slemp, NASA-Langley Research Center: This scan can be measured in from 45 min to 1 hour. We are taking measurements at 600°, 900°, 1200°, 1500°, and 1800° F, and with this particular furnace, we can go from one temperature to another in approximately 30 min.

Richmond: How many points do you get in that wavelength range?

Slemp: We obtain a reading at 1 μ and then proceed each 0.5μ through the 15-μ reading, which would be approximately 30 points.

Dwight Moore, National Bureau of Standards: I don't believe you told us either in your paper or in your talk whether the specimen was driven automatically or whether you just turned it by hand.

Slemp: It is driven automatically. We rotate the specimen at 15 rpm by an external motor mounted at the end of the rotating shaft.

Moore: One of the other papers in this symposium, which is not being presented, by Mr. Peavy and Mr. Eubanks of the National Bureau of Standards gives periodic heat flow analysis of a rotating cylinder method which is comparable in many respects to what you have here. In that study we got very sizable temperature drops as the point on the surface passed the viewing port, unless we were operating at speeds considerably above 15 rpm. Of course, our geometry was somewhat different. I believe you said your temperature drop was 1%. Is that correct?

Slemp: Yes.

Moore: At the temperatures you were using it would be of approximately what magnitude?

Slemp: At 1800° F it was something in the neighborhood of 7°.

Moore: It may be just a difference in geometry, but our temperature drops were greater than that.

Slemp: We have tested this system by attaching thermocouples of Chromel-Alumel as well as platinum-platinum rhodium to the surface of the specimen and rotating it past the viewport. Whenever we take these readings we allow approximately 60 sec, while the specimen is in the top of the furnace, for it to obtain an equilibrium temperature before the rotation. At the temperature of 1800° F our temperature variation for three continuous rotations was only 35°.

Richmond: This is in further elaboration of Dwight Moore's comment. I think the conditions are somewhat different because the specimens that were used in the Peavy-Eubanks experiments were ceramic specimens where the thermal diffusivity and thermal con-

ductivity were much lower than for the metal specimens used in this particular investigation.

S. SKLAREW, The Marquardt Corporation: Does the viewing port arrangement modify the apparent emittance characteristics of the specimen? Also, did Blau use a similar arrangement for viewing his specimen?

SLEMP: Blau did use a similar arrangement. I do not think that it would change the apparent emittance of the specimen. It is a straight viewport, although it is tapered. It is less than ¼ inch in diameter on the inside, and larger than ⅜ inch on the outside. It is also blackened and tapered.

RICHMOND: Two questions: First, what was the spacing between your specimen and the viewing port? Second, what investigation did you make of the effects of multiple reflection between the specimen and the viewing port?

SLEMP: First the Inconel liner is 1/16 inch thick. This fits against the furnace wall with the viewport protruding into the cavity to be even with the inside of the liner. Then we rotate the specimen to within 1/16 inch of this so there is, at a maximum, 3/32-inch space between viewport and the sample.

RICHMOND: I would still be afraid of multiple reflections if you are 3/16 inch away from the specimen, or even 3/32 inch away. I think it would be worth while for you to try to get your specimen up within one or two thousandths if you could, and see if you find any difference between results with that spacing and with the 3/32-inch spacing.

SLEMP: This particular furnace is being replaced with another one where we can have this arrangement. As a passing comment, the new furnace is platinum-wound so that it will be able to go on up to 2700° F. Using an arrangement similar to this and mounting the specimen on top of a ceramic rod will allow us to come to within, say, a few thousandths of an inch of the viewport. With the present furnace there is a little slack in the rod, due to thermal expansion, which does not allow us to come this close without danger of marring the surfaces of the specimens to be tested.

HERMAN SCHWARTZ, NASA Lewis: Basically, my question is on this rotating specimen technique. This is an ideal type of experiment in that there is not an appreciable thermal gradient through the specimen. However, where there is net heat transfer, a thermal gradient does exist. Therefore, how is the isothermal emittance data transformed to the situation in which there is net heat transfer? This is a question I would like to address to the people who are using the rotating specimen technique.

W. CLAYTON, Boeing Company: We also use the rotating specimen technique. In answer to Mr. Schwartz's question I believe that you obtain a better approximation when a value obtained on a relatively isothermal specimen is used in heat transfer analysis than you do when using values obtained from specimens which may be translucent and not isothermal; where you do not know the temperatures at the points of origin of the radiation and therefore, cannot specify what the emittance really is. At least with an isothermal specimen we can get a property that has some meaning. It is possible that as we understand the mechanisms better we can use this and work back to the gradient cases. We cannot make a measurement on a translucent material under conditions where a temperature gradient exists and make any sense out of the measurement, because we would have to know the complete temperature distribution and where the energy was coming from. Usually we do not know even how it is being transported within the material.

R. L. COX, Chance-Vought Astronautics: First, I'd like to comment on Mr. Schwartz's question. I believe that to resolve the emittance of a translucent material under the cases of heat transfer and to do it exactly, you will have to evaluate the optical constants, the absorption, and scattering coefficients, which could be done if you measure transmittance as well as emittance. I also want to comment on temperature drop across the viewing port. We have done an analysis studying this method, and we have calculated for aluminum oxide at a rotational speed of 100 rpm a temperature drop across the viewing port at 2000° F of roughly 8° F. Now, if you increase the specimen temperature to 3000° F this temperature drop jumps up to about 36° F. It is very dependent on the material under test. At 3000° F for zirconium oxide, the temperature drop at 100 rpm is roughly 80° F. This is all for a viewing to heating ratio of about 8%.

SLEMP: This is similar to what we have experienced. A 7° F temperature drop at 1800° F and 15 rpm, for the metallic specimens which have higher thermal conductivity and diffusivity than the ceramics you have tested, will probably result in an error of the same magnitude.

692-146 O—63——29

SESSION V

MEASUREMENTS AT HIGH TEMPERATURES (ABOVE 1400° K)

Chairman: HYMAN MARCUS

44—PRESENT AND FUTURE REQUIREMENTS FOR HIGH-TEMPERATURE MEASURMENTS

BY HYMAN MARCUS

AERONAUTICAL SYSTEMS DIVISION, WRIGHT-PATTERSON AIR FORCE BASE, OHIO

Previous papers in this symposium have been part of an evolutionary process, leading through an entire temperature spectrum from extremely low temperatures, cryogenic temperatures, to the moderately high temperature regime characterized by a peak temperature of about 1500° K. The next papers are primarily concerned with an area of the temperature spectrum which transcends the state-of-the-art and extends into the very high temperature regimes. It is an area which has created new technological problems in temperature measurement, in designating precise measurement equipment, and in providing natural and simulated environments to study the behavior of materials at very high temperatures. It is an area which has increased in popularity and in population many-fold in the past few years. Many investigators are beginning to appreciate the inherent problems posed by high-temperature research and development. It is an area which has taken on increased stature and import in light of current weapons systems (Dyna-Soar, RS–70) and future weapons systems which, in some instances, are still in pre-preplanning stages. However, without imaginative and visionary scientific individuals, technological progress would not be as far as it is today. Of particular concern is the requirement for and the measurement of the thermal radiation properties of solids in the temperature range from 1400° K to as high as it is experimentally feasible.

The design and performance of advanced weapons systems and space vehicles depend to a great extent upon the thermal radiant energy characteristics of surfaces exposed to this energy from sources such as high-energy rocket propellant exhausts, high-velocity shock waves (orbital and superorbital re-entry), special weapons effects, and solar radiation. These characteristics are emittance, absorptance, reflectance, and transmittance, and all are dependent upon the temperature and condition of the surface under consideration. (Emittance is a measure of the ability of a surface to emit radiant energy, and absorptance is a measure of the fraction of incident radiation absorbed by a surface.) Information on these characteristics is obviously required to utilize properly available materials and/or coatings in the design and construction of hypersonic and space vehicles, among others, to obtain optimum control of thermal energy entering and leaving the vehicle.

Although much information on the thermal radiation characteristics of the surfaces of materials is available in the literature, the data, in general, are not reproducible from specimen to specimen nor from source to source for the same material and/or coating. This, coupled with the fact that high-temperature techniques and high-temperature measurements have not as yet reached a satisfactory level of accuracy and reliability, describes a rather unhealthy technical situation with respect to proper choice of materials and/or coatings for advanced weapons systems.

The problems associated with temperature measurement, particularly in the transition regime—where thermocouples are being extended beyond their useful limitations and where optical pyrometry leaves a great deal to be desired as far as accuracy is concerned—are quite well defined. The solutions are not so well defined, although a considerable amount of research effort is being expended in this area. Some of this effort is being directed toward the

development of new thermocouples which can operate with reasonable accuracy up to about 2300° K. These are the relatively new refractory and refractory metal combinations such as tungsten-tungsten : rhenium pairs and molybdenum-molydenum : tungsten pairs. Considerable care must be exercised in the use of these refractory thermocouples—to provide suitable atmospheres to prevent oxidation of the elements, to eliminate the possibility of chemical interaction between elements and/or specimen materials and construction materials, and to preclude deposition of contaminating materials on the elements under certain conditions of vacuum. A great deal of work still remains to be done in this area.

Progress is being made in experimental techniques. The state-of-the-art has been reached for the moderate-temperature regions but not so for the high-temperature regions. Many techniques have been advanced for high-temperature measurements but none have been proven satisfactory. Although it may be argued that any data are better than none at all, in the long run such data are useless to the design engineer who is faced with the responsibility of selecting the proper material for a particular application. Efforts are being increased in the development and perfection of high-temperature techniques to achieve greater accuracy and reproducibility of data.

The materials problem is illustrated by figure 44–1, a plot of the total normal emittance versus temperature for coated molybdenum from six different sources. It is quite evident that it is impossible to derive any information from this plot. The data are inconsistent and vary too greatly to establish a pattern or a trend. The graph is presented on a more or less prejudicious point of view because it indicates a need for better and/or improved materials and closer quality control on the materials and their coatings and not just for improved techniques of temperature measurement and control. All three are intimately enmeshed with each other, and all are equally vital in our scheme of things. In the quest for techniques of measurement and temperature control the critical need for better materials (and more information about them) must not be overlooked.

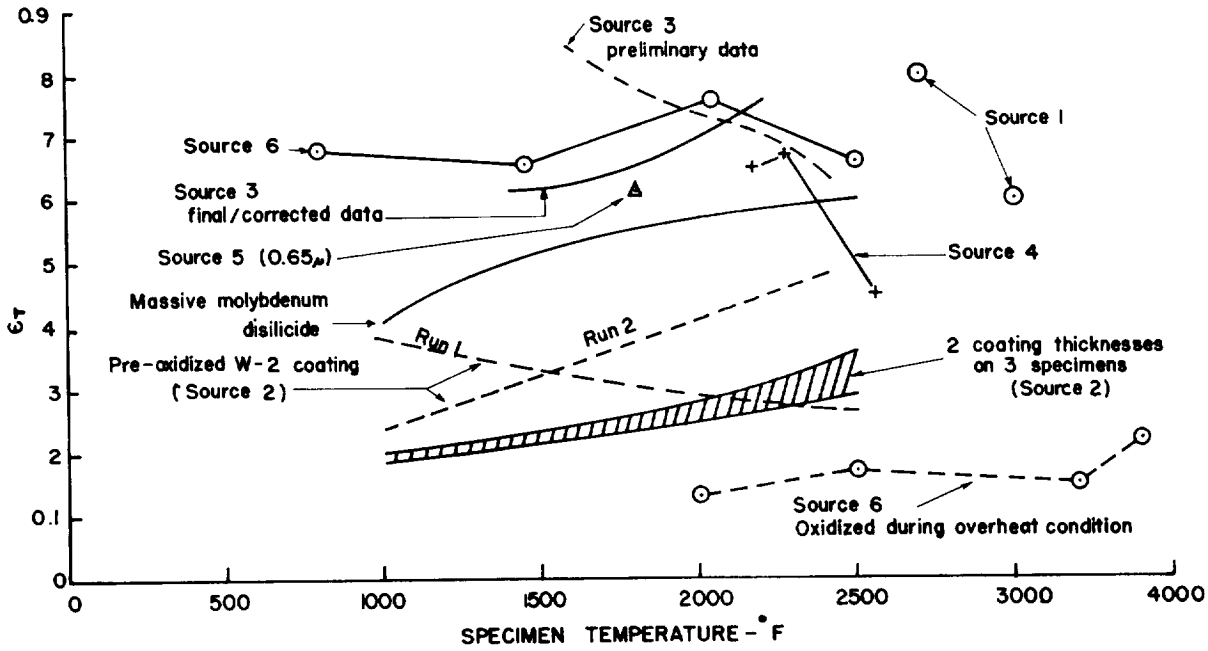

FIGURE 44–1.—Total normal emissivity of W–2 coated molybdenum.

45—A 500° TO 4500° F THERMAL RADIATION TEST FACILITY FOR TRANSPARENT MATERIALS

BY W. A. CLAYTON

THE BOEING COMPANY, SEATTLE, WASHINGTON

This paper describes a new method designed for very high temperature measurements on the general case of transparent materials, which automatically provides for measurements on semitransparent or opaque materials. Total normal emittance and total normal apparent transmittance are measured. The corresponding spectral properties can be measured with the addition of a monochromator and collecting optics. Lack of a suitable technique has previously limited the collection of emittance and transmittance data to about 1800° F on optical and infrared transmitting materials and the bulk of the dense ceramic bodies. Previous methods of other investigators are briefly reviewed.

An error analysis from a 500° to 3000° F prototype thermal radiation test facility is emphasized in this paper. Some comparative data are shown. The absence of any temperature limitation in the experimental approach other than material reaction is demonstrated. Accuracy that can be expected in any measurement is apparent. Overall, the method described in this paper is shown as superior for the determination of accurate, analytically defined high temperature thermal radiation properties on any solid material.

Lack of ability to measure thermal radiation properties at high temperatures on the general case of transparent materials has prevented the collection of reliable data on important classes of solid materials, particularly ceramics for high-temperature applications. The method presented in this paper offers capability for simultaneous measurements of emittance and high values of apparent transmittance to above 4000° F. The method is believed to meet basic requirements for a standard method since it provides capability for accurate, analytically defined measurements on any solid material.

The nomenclature and experimental methods of McMahon (ref. 1), with McMahon's theoretical work expanded and generalized to the three dimensional case by Gardon (ref. 2), provide the basis for the method described here. Disadvantages of previous methods developed on the same basis are eliminated in the present facility. McMahon's furnace could not be used with the relatively slow response times of the more rugged and reliable thermal radiation detectors, and his mechanisms for viewing a rotating, semicircular specimen inside a furnace and alternately viewing the furnace as the reference blackbody cavity could not be used above 1800° F. Moreover, the accuracy of McMahon's method was limited by the difficulty in verifying the assumptions on the relationship of the specimen temperature to the measured furnace temperature. Armour Research Foundation (ref. 3) later developed another device which presented a series of specimens on a reciprocating rack at a view port in a very long tube furnace surrounding the rack, enabling measurements to 2800° F on several specimens at a time. This approach, however, did not eliminate the limitations of the earlier McMahon furnace. The new facility to be described was designed to provide more accurate measurements over an unlimited temperature range with standard instrumentation.

NOMENCLATURE

ϵ_{TH} Total hemispherical emittance: the fraction of the theoretical maximum (blackbody) thermal radiation actually emitted over all wavelengths and angles by a material as a consequence of its temperature

ϵ_{TN} Total normal emittance: emittance over all wavelengths in a small solid angle about the normal to the specimen surface

τ_{TN} Total normal apparent transmittance: the fraction of radiation incident on a flat specimen from all angles and wavelengths which is

transmitted to emerge in a small solid angle about the normal to the surface, regardless of the path through the material.

ρ_{TN} Total normal apparent reflectance: the fraction of radiation incident on a flat specimen from all angles and wavelengths which is reflected in a small solid angle about the normal to the surface, regardless of where in the material reflections occured

T temperature, ° F or ° R

T_s Specimen temperature (true), ° R

T_t Apparent specimen temperature: blackbody temperature which would give a radiant heat flux equivalent to the total radiation flux emitted from the specimen, ° R

$T_{t\tau}$ Apparent specimen temperature: blackbody temperature which would give a radiant heat flux equivalent to the total radiation flux emitted and transmitted by the specimen, ° R.

T_{BB} Blackbody reference temperature, ° R

T_{tBB} Blackbody transmittance source, temperature, ° R

C_r Reflection correction, fraction of measured radiation not due to included reflection errors.

APPARATUS AND TEST METHOD

This method is designed for use on transparent, as well as opaque materials, and simultaneously measures both emittance and apparent transmittance. Figures 45–1 and 45–2 are a sketch and photograph of the overall facility, which in its present prototype form is designed to operate in inert atmosphere. An induction heated furnace is used to obtain a combination of isothermal specimen and high temperature. The specimen and its support, which incorporates a 3:1 depth to diameter blackbody reference, rotate inside the induction-heated furnace. The rotating blackbody is sighted through a water-cooled tube inserted in the side of the furnace. Since the blackbody rotates with the specimen and is heated to approximately the same temperature as a function of constant geometrical conditions, the true temperature of the specimen can be easily and accurately deduced from temperature measurements on the rotating blackbody reference. In addition, when a thermocouple is installed at the base of the rotating blackbody, it provides radiometer calibrations for use in the calculation of emittance and apparent transmittance.

Emission from and transmission through the rotating specimen is measured through the water-cooled sighting tube at the top of the furnace, which is mounted in an eccentric that can be indexed so that the specimen sighting tube sees the specimen in two ways. It is shown at the inside position in the sketch, where the radiometer sees the energy from the specimen plus the energy transmitted through the specimen. Taking its effective opening as the area under the sighting tube, the source of the transmitted energy is already calibrated since it is a 3:1 blackbody at the same temperature as the reference blackbody. At the outside position the radiometer sees energy emitted from the specimen only. The radiation trap blocks transmittance through the specimen and prevents reflection upward of energy emitted in the downward direction. A 7.5-inch-diameter specimen is required for measurement of both emittance and apparent transmittance in this prototype facility. Variable specimen thickness is provided for by raising and lowering the top sighting tube with the ratchet device shown in figure 45–2.

About 3 hours are required to obtain equilibrium throughout the present furnace, at which time total radiation readings are recorded with calibrated Brown Instrument Company model RL–2 miniature radiamatic radiometers which cover the wavelengths 0.2 to 9.6 μ (ref. 4). About 20 min must be allowed between readings at the two sighting tube positions. Spectral properties could be obtained with the addition of a monochromator and collecting optics. All data taken through the specimen sighting tube are functions of the temperature of the isothermal specimen which is related to the temperature of the geometric blackbody reference rotating with the specimen. In this manner, the measurement of temperature can be accomplished by radiation pyrometry on the blackbody alone, avoiding problems associated with the unreliability of thermocouples capable of operating to 4000° F, the difficulties in attaching such thermocouples, and their tendency to react with specimens at such temperatures.

OPERATING EQUATIONS

All measurements of the total normal radiated energy can be expressed in terms of the fourth power of the temperature of a blackbody that would be radiating the same energy through the same view factor (ref. 5). This apparent black-

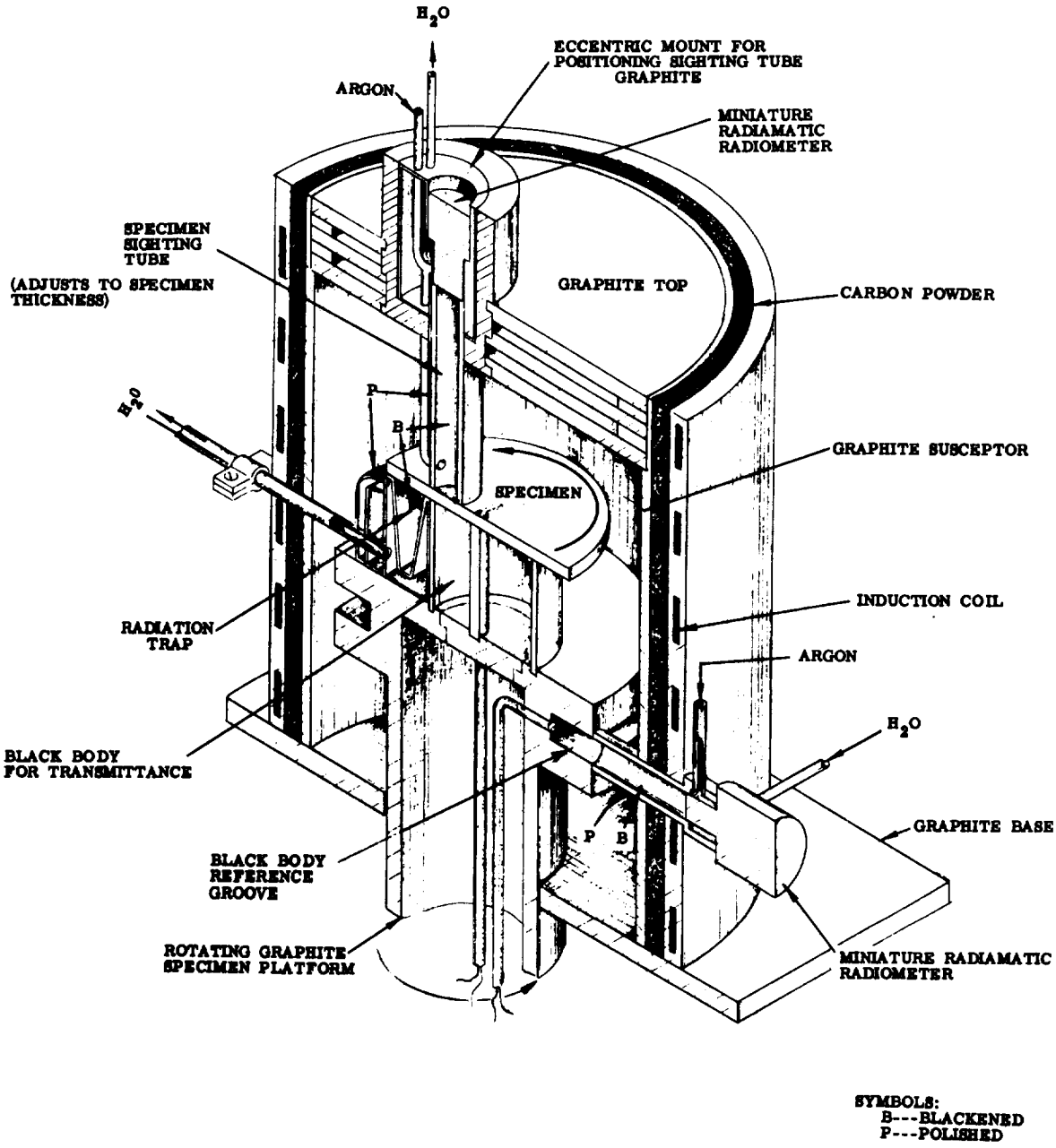

FIGURE 45–1.—500° to 4500° F thermal radiation test facility.

body temperature can be obtained in any measurement directly from the radiometer millivolt output by use of the radiometer blackbody calibration curve. In this manner, all characteristics of the particular radiation detector in use are accounted for in its blackbody calibration. Total normal emittance is then expressed as below. (All terms are defined in the Nomenclature section.)

$$\epsilon_{TN}=\frac{T_c^4}{T_s^4} \tag{1}$$

The measurement of the emitted plus the transmitted energy taken with the sample over a

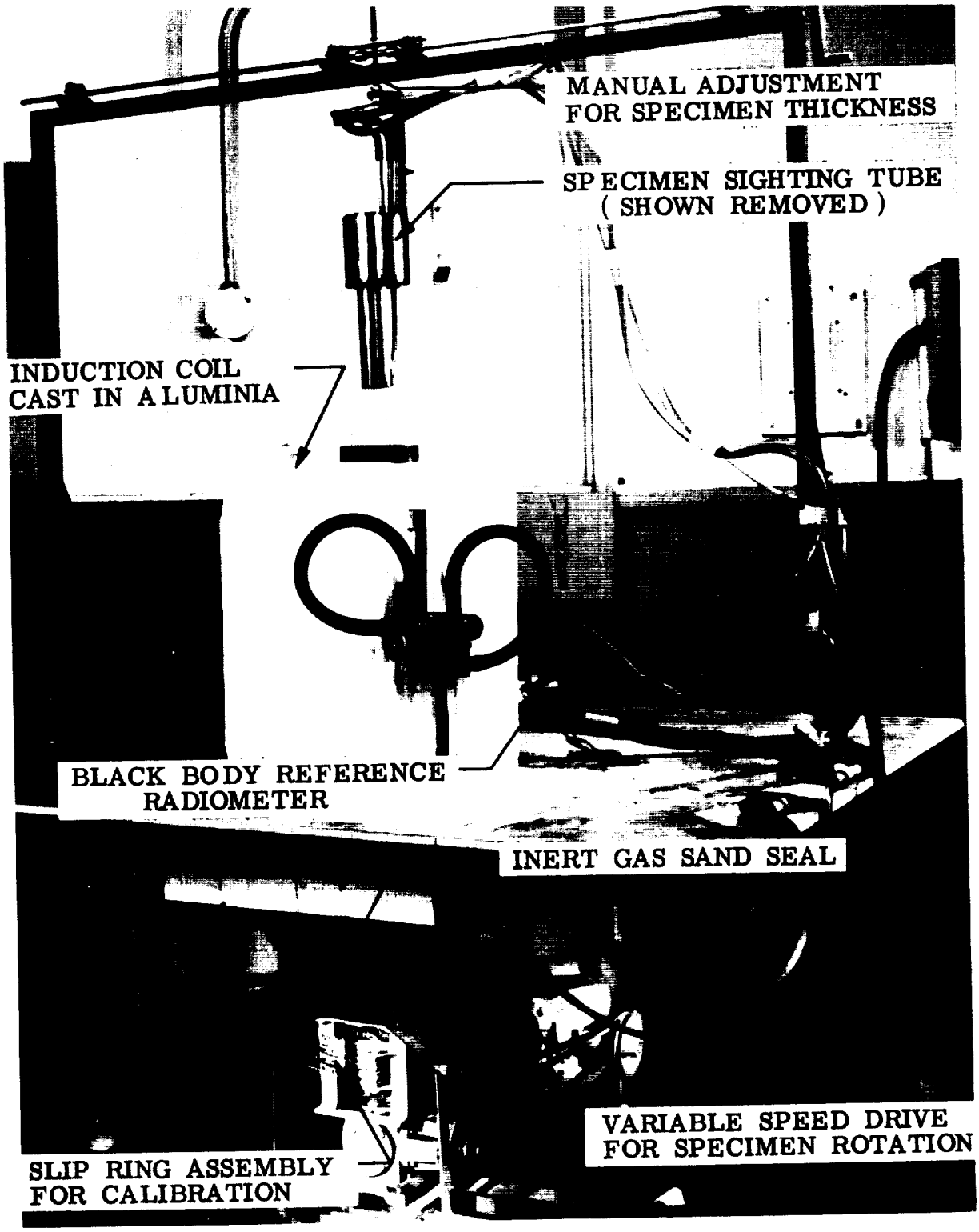

FIGURE 45-2.—Thermal radiation test facility—front view.

blackbody transmittance source at the same temperature is also expressed in terms of an apparent blackbody temperature.

$$\epsilon_{TN}+\tau_{TN}=\frac{T_{\epsilon\tau}^4}{T_s^4} \tag{2}$$

Total normal transmittance may then be obtained from equations (1) and (2) by subtraction.

$$\tau_{TN}=\frac{T_{\epsilon\tau}^4}{T_s^4}-\frac{T_\epsilon^4}{T_s^4} \tag{3}$$

These equations are analytically exact only for the case where no corrections for reflection errors or temperature gradients in the furnace are required.

Actual values and theory for any correction terms which must be added to the above basic equations are derived from the laboratory analysis discussed in the following section. Equations (1) and (3) are rewritten to include all the terms which may be required in actual measurements.

$$\epsilon_{TN}=\frac{T_\epsilon^4}{T_{BB}^4}\cdot C_R\cdot\frac{T_{BB}^4}{T_s^4} \tag{4}$$

$$\tau_{TN}=\left[C_R \text{ inside}\cdot\frac{T_{\epsilon\tau}^4}{T_{BB}^4}-\frac{T_\epsilon^4}{T_{BB}^4}\cdot\frac{T_s^4 \text{ inside}}{T_s^4 \text{ outside}}\cdot C_R \text{ outside}\right]\frac{T_{BB}^4}{T_{\epsilon BB}^4} \tag{5}$$

In general, the uncertainty in final results obtained by using equations (4) and (5) increases as the thermocouples installed for direct measurement of the temperature correction factors are removed.

In equation (5) the transmittance is based on the transmittance blackbody temperature rather than on the sample temperature because the measured transmittance will be more sensitive to the incident radiation level than to the shift in spectral distribution over a small temperature range. Another available operating equation is the familiar equation relating apparent reflectance to emittance and apparent transmittance.

$$\rho_{TN}=1-\epsilon_{TN}-\tau_{TN} \tag{6}$$

ERROR ANALYSIS

Evaluation of a facility on the basis of a detailed analysis of all conceivable errors provides the best description of the operating characteristics of the facility. It also makes possible a valid prediction of the errors involved in measurements, and provides a guide for improvement or extension of the capabilities of the technique. For these reasons, this paper is devoted to, and its conclusions are based on the detailed error analysis conducted on the prototype thermal radiation test facility.

First it was determined that the furnace was sufficiently isothermal for the success of the concept. Thermocouples installed on the furnace walls after initial assembly showed that at 2000° F the vertical walls and inside top of the furnace were isothermal within ±1% except within a 1½ inch radius of the sighting tube entrances to the furnace.

The remaining analysis of the facility involved the determination and qualification of all factors required for operation according to equations (4) and (5). The experimental procedure for the evaluation of these factors was simply the determination of temperature distribution within the operating facility on the basis of platinum–platinum 13% rhodium (Pt–Pt, 13% Rh) thermocouples installed on the furnace walls and on the rotating elements inside the furnace. Thermocouples installed on the rotating elements were read-out through the slip ring assembly shown in figure 45–2.

CORRECT DETERMINATION OF SAMPLE RADIATION T_ϵ AND $T_{\epsilon\tau}$

Accuracy of Radiometer Blackbody Calibrations

All radiometers were calibrated against a Pt–Pt, 13% Rh thermocouple installed in the rotating blackbody reference sighted through the side of the furnace. A thermocouple is in continuous use at this blackbody position when temperatures over 2500° F are not required. All temperature calibration points obtained on any of these radiometers have fallen within ±½% of a mean line through all the points. Calibration points have been obtained in reference to 10 different Pt–Pt, 13% Rh thermocouples installed in the rotating blackbody. At least 30 calibration points have been obtained on each radiometer.

Since at least 8 inches of the referenced thermocouple is heated to within ±1% of the junction temperature, errors in the thermocouple reading due to conduction losses are eliminated. There is no fluctuation in the

thermocouple reading or the radiometer output at any temperature due to the rotation of the blackbody.

Since it had been demonstrated that the radiometer calibrations are stable and that the temperature of the blackbody was adequately known, the only remaining question was that of the blackness of the blackbody reference. A major criterion for a successful geometric blackbody is that its surfaces be isothermal. The isothermal characteristics of the furnace itself and the constant temperature obtained from the thermocouple installed in the blackbody, no matter what its position during rotation, were indications of the isothermal characteristics of the blackbody. Additional experimental proof of the isothermal character of this rotating blackbody was the fact that optical pyrometer readings on holes in the blackbody base or on any portion of the cavity walls or adjacent furnace wall were identical and within 10° F of the installed thermocouple. In addition, it was impossible to distinguish corners or edges in the blackbody. Rotation of the blackbody within the isothermal furnace makes possible its excellent isothermal characteristics.

The theoretical emittance of an isothermal cavity can be determined from one of several theories (ref. 7). The theory of Gouffé is most easily applied to an unusual shaped cavity (ref. 6). From the Gouffé theory, an emittance of 0.996 is obtained for this cavity. The large inside surface area of this unusually shaped cavity gives it an effective emittance higher than could be obtained with a cylinder or cone of the same depth to radius ratio.

It has been shown that the cavity is black and that ideal conditions for temperature measurement exist, so the radiometer calibration accuracy limits are the same as the precision obtained against several calibrated thermocouples over many measurements, i.e. ± ½% of the blackbody temperatures from a line fitted to all data points.

Reflection Error

In the measurement of the energy emitted or emitted plus transmitted by the sample, there are potential reflection errors of two different types. These errors arise because there must be a clearance between the end of the sighting tube and the rotating specimen which allows furnace energy to inpinge on the specimen target area at grazing angles, and because the specimen sighting tube does not absorb 100% of the energy impinging upon it. The effect of the errors was calculated, and methods were devised for experimental determination of the error on samples for which the calculated corrections might not apply.

About 90% of the total potential reflection error is a result of furnace energy passing through the necessary clearance space between the specimen sighting tube and the rotating specimen and diffusely reflecting from the specimen target area directly to the total radiation detector. The remaining reflection error results from the fact that a small portion of the radiant energy striking the blackened interior of the water cooled specimen sighting tube can be diffusely reflected back to the specimen target area where it is again diffusely reflected to the total radiation detector.

Figure 45–3 is a plot of the calculated total potential reflection error. The error for a diffusely-reflecting specimen is the maximum possible error. A specimen with combined diffuse and specular reflecting characteristics will cause a reflection error less than the perfectly diffuse reflecting specimen, since that part which is specularly reflected cannot cause an error. DeVos (ref. 8) has given the reflecting characteristics of clean metals of various roughness in a form that is easily applied to a calculation of the effect of partially diffuse reflectance on emittance measurements. The lower two curves in figure 45–3 are for clean metal on the basis of the DeVos data. While it is true that almost no low-emittance surface will have highly diffuse total reflection characteristics which give the maximum error, the error for smooth metals can be as high as 15%.

It was necessary to develop a method for the experimental determination of the reflectance error on smooth specimens for the purpose of correcting the measured emittance and to check the validity of the calculated reflection errors. The method developed was suggested by the fact that most of the error is caused by direct sample reflection of furnace energy. If there

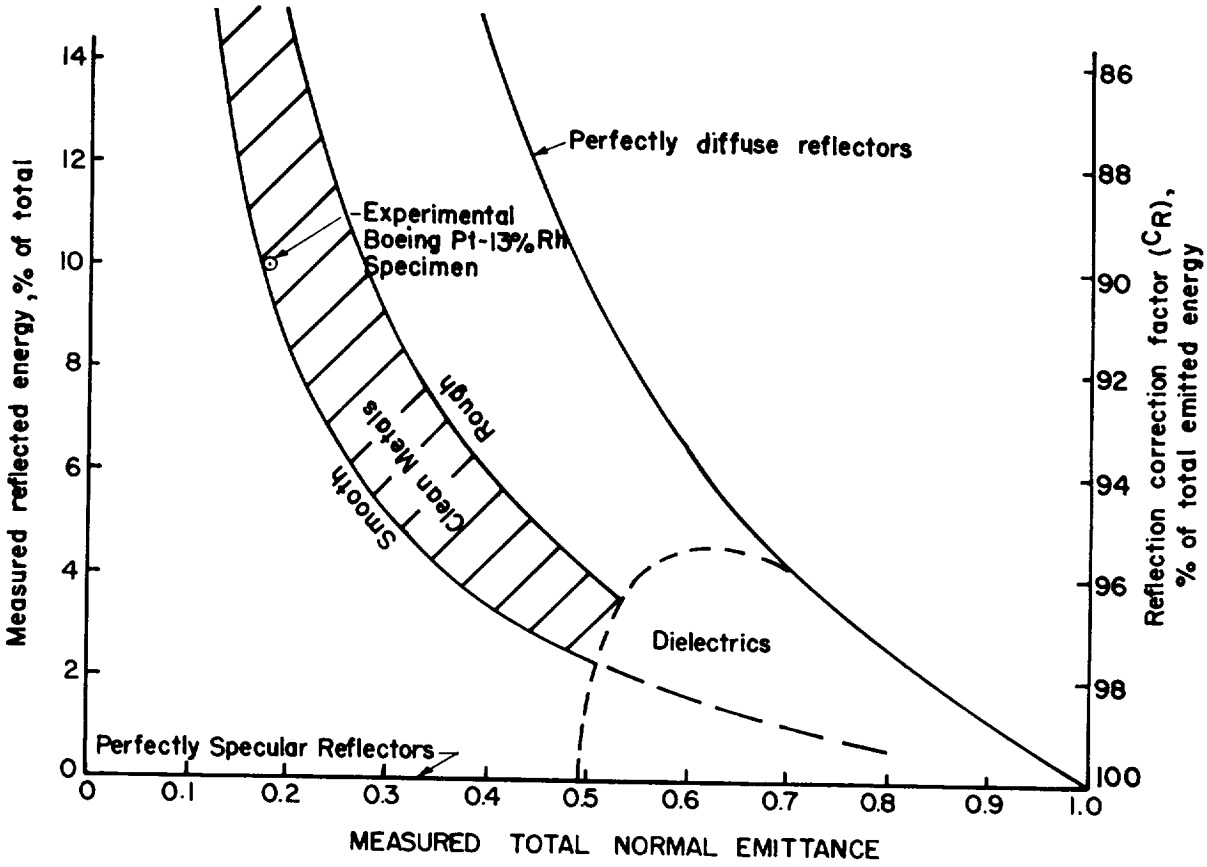

FIGURE 45–3.—Total reflection error versus measured emittance values.

could be no gap between the sighting tube and the specimen, the reflection error could be neglected.

A Pt–Pt, 13% Rh thermocouple was spotwelded to the surface of a polished Pt–Pt, 13% Rh specimen for specimen temperature measurement. After equilibrium was reached and the regular emittance measurement was made, the distance between the sample and the sighting tube was varied between ⅛ in. and 1 in. For each distance setting, a new emittance was measured. The emittance values obtained at each sighting tube distance from the sample were expressed as a percentage of the emittance value obtained at a distance of ¼ in., the regular sighting tube distance, and plotted against sighting tube distance from the sample. Extrapolation of this plot to zero distance gave the correct percentage of a reading at ¼ in. distance which was due to emitted energy only.

This procedure was carried out at several temperatures, and it was found that the error was independent of temperature, as expected. The experimental correction point for the polished Pt–Pt, 13% Rh specimen is shown on figure 45–3, after adding the small reflection error which still remained. Good agreement with the calculated error and its independence of temperature corroborates the calculated error. It is estimated from the results of this experimental test that the reflection error can always be corrected to cause less than 3% uncertainty on the measured emittance value for the worst case of a very low emittance specimen, with the uncertainty decreasing linearly as the specimen emittance approaches unity.

Transmission Error in the Emittance Measurement

The effectiveness of the blackbody radiation trap in preventing transmission during measurement of the sample emittance depends upon the scattering characteristics of the semitransparent sample. As in the case of the specimen sighting

tube, furnace energy can impinge on the specimen through the necessary gap between the radiation trap and the sample. The possible error due to the transmission of this energy is difficult to evaluate for any real case, but a combination of worst conditions will give an estimate of its importance.

The worst case that can be visualized is a very transparent specimen with a rough, diffuse reflecting surface and a characteristic of complete scattering of transmitted energy. Without offering any detailed proofs, it can be seen that for a thin sample of this type, the view factors involved are essentially the same as for the first surface reflection errors previously evaluated, and that the total error due to furnace energy is essentially the same as for the case of the opaque materials. Errors not a result of apparent first surface reflection will be a result of apparent transmission of furnace energy, making the total error the same for any emittance whether or not the specimen is transparent.

Therefore, the reflection error given in figure 45–3 can be used as an indication of the magnitude of reflection plus transmission error on transparent specimens during the emittance measurement. During the transmission measurement, there is no transmission error so the maximum reflection error alone can be obtained from figure 45–3 by using values of emittance plus apparent transmittance in place of emittance alone. For any case in which the specular characteristics of the specimen are in doubt, actual errors can be determined by varying the distance from the sample of both the specimen sighting tube and the radiation trap, and extrapolating the variance in measured values to zero distance to obtain the correction.

Quality of Transmittance Blackbody

The blackbody for transmittance measurements is the graphite hollow cylinder upon which the specimen rests. Its isothermal character is shown by the fact that thermocouples pressed into the base of the blackbody and placed between the specimen and the top edge of the cylinder during emittance tests always read within 1% of each other, the one under the specimen reading lower. The theory of Gouffé applied to this cavity yields a theoretical emittance of 0.996. It is important to note that the high efficiency obtained with Gouffé's equation is for hemispherical radiation. Richmond (ref. 9) has made it clear that for measurements of total normal transmittance, energy incident on the specimen must be hemispherical. The large diameter of the cylinder with respect to its effective opening, which is the area under the specimen sighting tube, together with the high emittance of its graphite walls, assures that the incident radiation to be transmitted is representative of a hemispherical source.

Thermocouple measurements have shown that the transmittance blackbody temperature is always within ½% of the reference blackbody temperature. Transmission calculations are therefore based on the blackbody reference temperature except in cases where thermocouples are installed. Then a correction is made for the ½% or less temperature difference.

CORRECT DETERMINATION OF SAMPLE TEMPERATURE, T_s

To calculate the specimen emittance and transmittance on the basis of the measured T_e and T_{er} evaluated in the previous section, the true specimen temperature, T_s, is needed for equations (4) and (5). A major advantage of the thermal radiation test facility is that the sample temperature can be obtained indirectly from the accurate temperature measurements possible on the rotating blackbody.

To evaluate the relationship of the specimen temperature to the temperature at the blackbody reference, thermocouple temperature measurements were taken at both positions during tests on Pt–Pt, 13% Rh and oxidized Unitemp 41 samples, as shown in figure 45–1. The sample thermocouple wires were independently spotwelded to the test surface and ran parallel to and just above the surface to a two-hole alumina insulator protruding through a hole at the center of the specimen.

For a sample rotating at constant speed, the greatest transient and lowest average sample temperature will be obtained on any point which inscribes the circle whose arc under the sighting tube spans the maximum angle. The specimen thermocouple was spotwelded at a position to evaluate the worst case defined above. Temperatures for points on the speci-

men which spend a lower proportion of time under the sighting tube were obtained by rotating the sighting tube toward the outside position. Transient temperatures were recorded on a special, Boeing modified, Brown strip chart recorder, and fine-wire thermocouples were used to cut thermal lag as much as possible.

The maximum transient range for the specimens was 0.5% of the temperature at temperatures from 800° to 1200° F. The specimen was rotating at the slowest speed provided by the belt drive pulleys installed (16 rpm), avoiding problems of alignment and of holding the specimen in place at higher speeds. Transients with the sighting tube moved toward the outside position were somewhat less, but the average temperature was very nearly the same. On this basis, it was concluded that the transient specimen temperature conditions were negligible, and that the average thermocouple reading at the position corresponding to the worst case could be taken as representative of the sample temperature at the inside sighting tube position.

The average sample temperature at the inside sighting tube position is plotted against the temperature of the blackbody reference in figure 45–4. It can be seen that the relationship of the sample temperature to temperature at the blackbody is essentially the same for both the high emittance oxidized Unitemp–41 and the low emittance Pt–Pt, 13% Rh.

It is believed that the thermocouple readings were accurate, since the wires were heated to nearly the same temperature as the hot junction. The points given in figure 45–4 are for two thermocouple installations on each specimen, or a total of four different thermocouple installations, so that any random errors in the thermocouple calibrations are included. The temperature correction is independent of temperature because it is primarily a function of the radiant heat exchange view factors, and they are constant.

Some additional considerations are involved in extending the temperature correction obtained from thermocouple measurements on metal specimens to the case of dielectric specimens, particularly thick, highly transparent

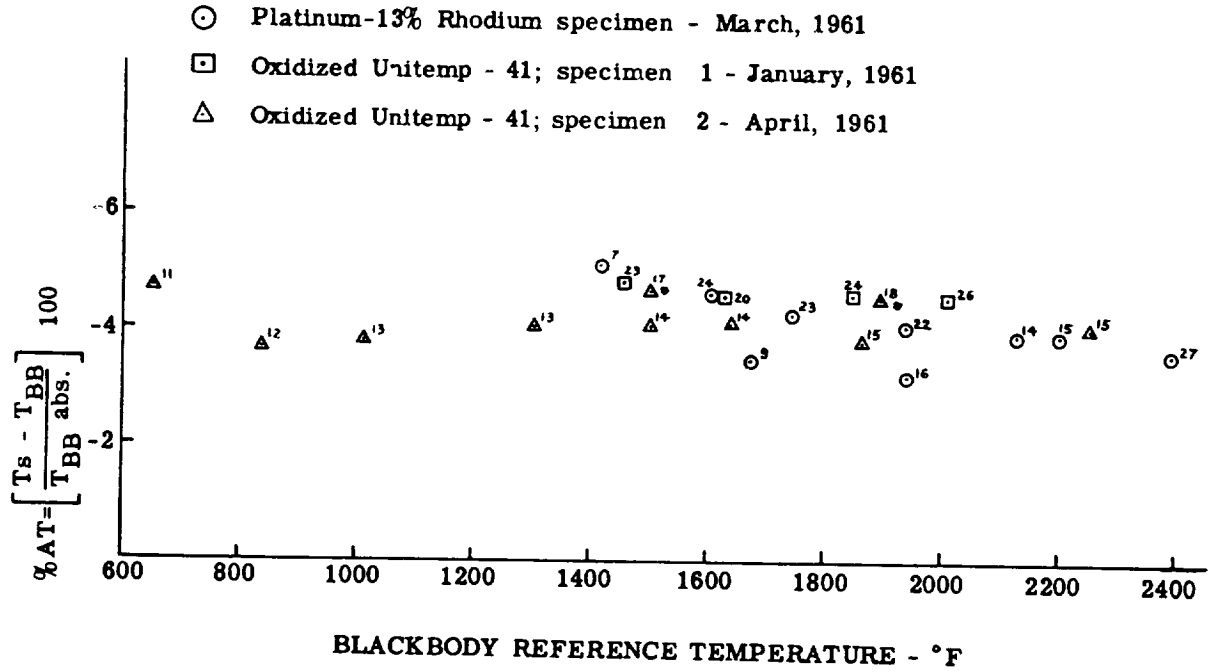

FIGURE 45–4.—Relationship between sample temperature and blackbody reference temperature (thermal radiation test facility platinum–platinum, 13% rhodium thermocouple temperature measurements). Numbers indicate day of month that point was obtained. *Equilibrium approached from higher temperature; approached from lower temperature on all others.

specimens. The maximum gradient possible through a specimen normal to its surfaces is the difference between the specimen temperature measured on metals and the temperature of the blackbody reference. For a specimen emitting from throughout its volume the emission will be from the total range of temperature included in the gradient. However, the gradient is a small percentage of the higher temperature; is independent of emittance, and the total emittance will be largely from the volume near the surface under the sighting tube. Hence, the temperature relationship measured for metals should hold reasonably well for dielectric materials when the sighting tube is at the inside position over the transmittance blackbody.

Since the radiation trap is required for emittance measurements on transparent materials the relationship between the sample temperature with the specimen sighting tube at the outside over the radiation trap and the temperature at the inside position over the transmittance blackbody was determined for stannic oxide-coated Corning 7923 alumina-silicate glass at low temperature. Stannic oxide-coated alumina silicate glass was chosen because it has practically no transmission for energy from temperatures below 700° F. Since the average specimen temperature is a function of constant geometrical factors, the temperature relationship for temperatures below 700° F holds for all other temperatures.

The measured ratio of emitted energy at the inside sighting tube position to that at the outside sighting tube position was 1/1.24 This means that the temperature at the outside position was $\sqrt[4]{1.24}$ or about 5.5% greater than the temperature at the inside position, so the temperature at the outside position was higher than the blackbody referense temperature. The apparent inconsistency here is explained by the fact that the furnace was designed to limit heat losses at the top end as compensation for the presence of the water cooled heat sinks in that position. This is demonstrated by the fact that during heat up periods, rotating elements near the top of the furnace are heated faster than those near the bottom of the furnace.

The error in indirect sample temperature measurements on the basis of the blackbody reference temperature is believed to be represented by the scatter in measured values shown in figure 45-4. For measurements at the inside sighting tube position, a conservative estimate of the resultant error on measured values of emittance plus transmittance is ±3%. For indirect temperature measurements at the outside position, the error in the radiant energy measurements on which the temperature relationship to the inside position is based must be added, making an effective error of ±6% on the final emittance value.

TOTAL MEASUREMENT ERRORS

Rather than attempting to present a statistical interpretation of the accuracy of thermal property measurements made in this facility, percentage limits of error have been determined. This approach has been selected for several reasons:

(1) Statistical analysis of the results of any experiment includes a variance due to the instability of the material measured, and will rarely give a true picture of the precision of the test method alone.

(2) Statistical analysis of the results of any measurement gives no information on any deviations from the true value of the measured property.

(3) Statistical analysis of measured factors which are used to obtain the final results, including any correction terms, might yield a statistical expression for the final result expressed as a product of the measured factors. However, results from this kind of combination cannot be rigorously obtained unless the error distribution of each of the experimental factors can be analytically expressed. Adequate expressions for the error distribution of every factor in the measurement is usually not possible, at least not without considerable data on each factor.

At such time as sufficient volumes of operating data are obtained, a statistical description of the validity of results from the facility will be attempted by the approach in (3). Since the facility described in this paper is relatively new, it is most useful at this time to obtain the best estimate possible of the maximum deviation of experimental results from the true values of the property under the condition of the test.

Percent accuracy as reported herein means that the true value will not vary from any experimental value by more than the stated percentage accuracy, i.e., accuracy limits of +9% −11% mean that the true value is on more than the 9% above or 11% below the measured value; percentages are based on the measured value.

Percentage accuracies reported in this manner are obtained from an analysis of the measurement techniques employed. They represent the accumulated inaccuracies contributed by all conceivable factors in the measurement when all portions of the test equipment are operating according to the normal fashion determined in the laboratory analysis of the measurement technique. Limits of accuracy determined in this manner are not final, but may be narrowed any time the uncertainty in any factor in the measurement can be reduced by technique improvement, etc.

Figure 45–5A shows the breakdown of the total error for the various ways in which the thermal radiation test facility may be instrumented for emittance measurements on opaque materials, where the specimen sighting tube is at the inside position. Figure 45–5B shows the error breakdown on the emittance measured on transparent materials, where the specimen sighting tube is at the outside position over the radiation trap. There is greater uncertainty in the specimen temperature with the sighting tube at the outside position, as previously discussed. It is apparent from figure 45–5 that the use of thermocouples, when possible, decreases the uncertainty in the results.

For opaque materials such as metals, where emittance measurements can be made with the sighting tube at the inside position, the incremental uncertainty in the calculated reflectance value is the same as in the measured emittance value, and the percentage error in reflectance is easily calculated. Obviously, high percentage error in reflectance will be obtained when the emittance is high. For transparent materials, the error in the apparent transmittance and apparent reflectance values is dependent on all three thermal radiation properties, hence is not so simply illustrated. The error in apparent transmittance is a function of the error in the two measured values, transmittance plus emittance and emittance alone, used according to equation (5). The error in apparent reflectance is a function of the errors in the final apparent emittance value and the final apparent transmittance value used in equation (6).

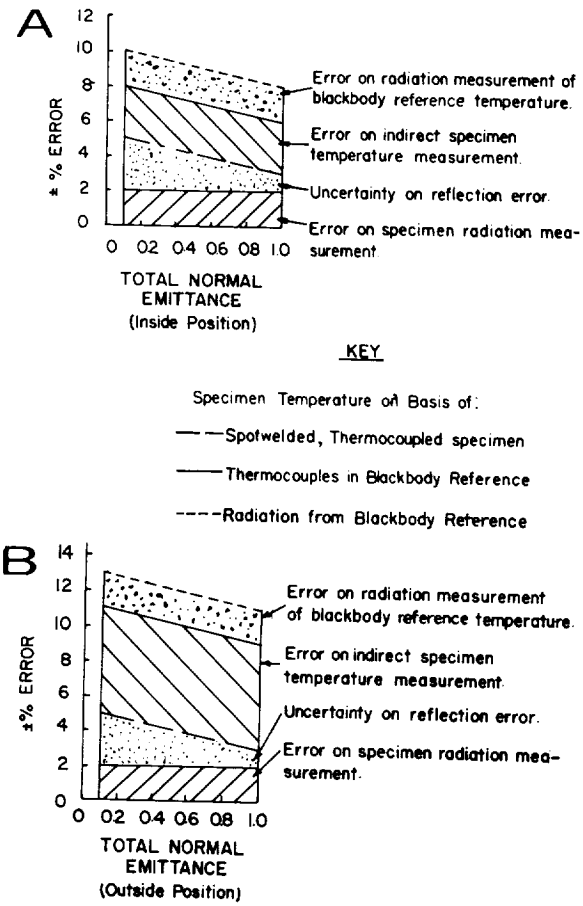

FIGURE 45–5.—Total error on emittance of opaque materials (A) and of transparent materials (B). Based on average error involved in measurements without thermocouples—least error possible with thermocouple installed is above one-half that shown.

Figure 45–6 presents nomographs for determining the potential error in the apparent transmittance and apparent reflectance values resulting from any measurement. The high percentage errors in low values of measured apparent transmittance and apparent reflectance values are a consequence of the lack of practical general relationships other than the differences between large, nearly equal measured values. For the limited special cases where adequate expressions for the transmission and reflection mechansims can be written, values calculated from optical constants may be of

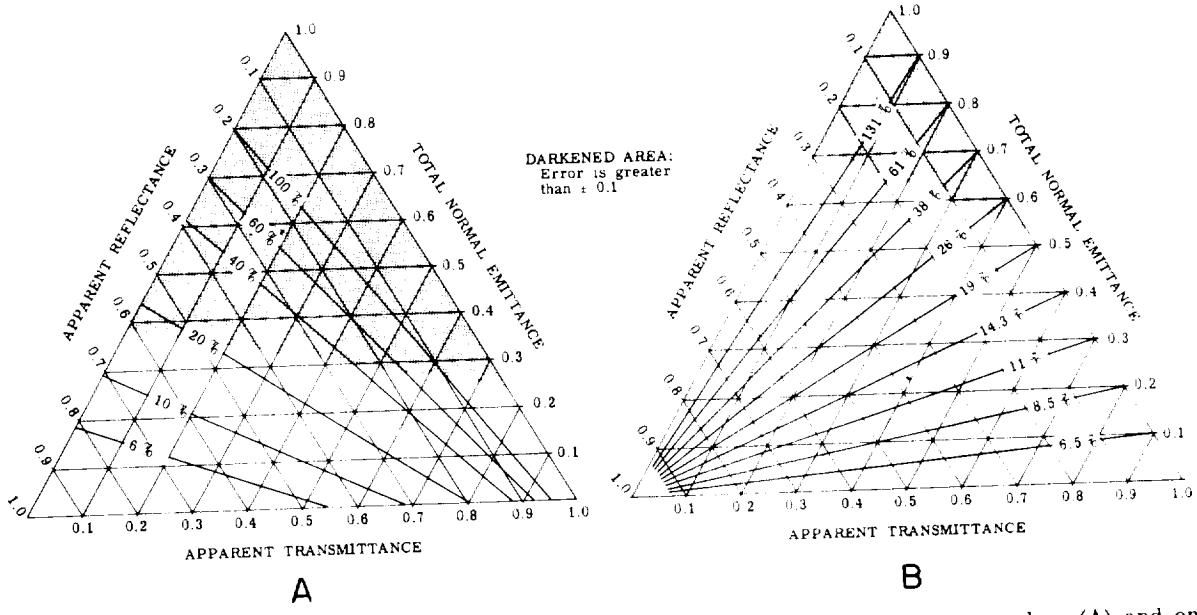

FIGURE 45–6.—Percentage error obtained for transparent materials on apparent reflectance values (A) and on apparent transmittance values (B).

greater accuracy when transmittance and reflectance are low.

The limits of accuracy obtained by this method are by nature conservative, since the limits depend upon all factors in any measurement being in error by the maximum amount in the worst combination of plus or minus sign. A mean value from several measurements will always lie well inside the limits of accuracy indicated.

COMPARISON OF MEASURED VALUES

Comparison of emittance measuring methods on the basis of the respective experimental values obtained is usually difficult due to variations in samples tested and in their behavior under differing test environments. It is unusually fortunate that three valid bases are available for the comparison of measured values obtained on the thermal radiation test facility; high and low emittance metal standards prepared by the National Bureau of Standards, high and low emittance controlled specimens distributed to several investigators through the Aeronautical Systems Division, and the relatively inert and reproducible high-temperature transparent glass materials.

Figure 45–7 presents data obtained by Boeing and the National Bureau of Standards (ref. 10) on duplicate specimens prepared at NBS and

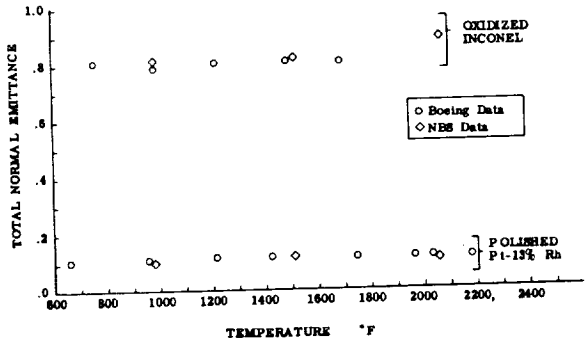

FIGURE 45–7.—National Bureau of Standards calibration thermal radiation test facility.

provided by Aeronautical Systems Division. Boeing and NBS results were compared after completion of the testing in both laboratories. As can be seen from figure 45–7, the Boeing emittance values agree with the NBS values for the emittance standards well within the experimental accuracy of the Boeing results. The Boeing results are on the basis of the sample temperature obtained indirectly from a thermocouple installed in the blackbody reference rotating with the sample, giving a potential error of $\pm 6\%$ on the oxidized Inconel standard and $+9\%$, -11% on the Pt–Pt, 13% Rh standard. The higher negative limit on accuracy of the Pt–Pt, 13% Rh results is to include the effect of a small area that was accidently scratched. The

NBS reported average standard deviations for their values, in order of increasing temperatures, of 0.0103, 0.0160, and 0.0074 on the oxidized Inconel and 0.0065, 0.0070, and 0.0074 on the Pt–Pt, 13% Rh. The NBS results were independently substantiated by their relationship to the very accurate (±0.02) measurements of total hemispherical emittance made at NBS.

Results of an emittance "round robin" conducted through the cooperation of the Aeronautical Systems Division are shown in figure 45–8. These results indicate that the Boeing and WADD contractor facilities compared can be expected to give equivalent measured values on materials unaffected by test conditions such as heating time and test atmosphere. All specimens of oxidized Universal Cyclop Unitemp–41 and of Pt–13% Rh used in these tests were cut from a single sheet of each material at the Boeing Company. The rather large scatter in the data is due in part to some instability in the emittance values of these materials under the various test conditions used, and is an indication of the extreme difficulty of the task of providing a material standard of emittance. The NBS standards furnished to Boeing were superior to the round robin samples, a result of an extensive emittance material standards program conducted by NBS, and it would be desirable if NBS control samples were used in any future emittance round robin on opaque materials.

The chemical stability and reproducibility of high-temperature glasses make them a good basis for data comparison at the present time. Figure 45–9 presents data from the Boeing thermal radiation test facility on one available transparent material. Comparison values are available only at the lower temperatures (ref. 3), but the Boeing values appear to substantiate previous values in the literature as well as extending the temperature range of the previous data.

CONCLUSIONS

Evaluation of a facility on the basis of a detailed analysis of all conceivable errors provides the best description of the operating characteristics of the facility, a valid basis for predicting errors involved in measurements,

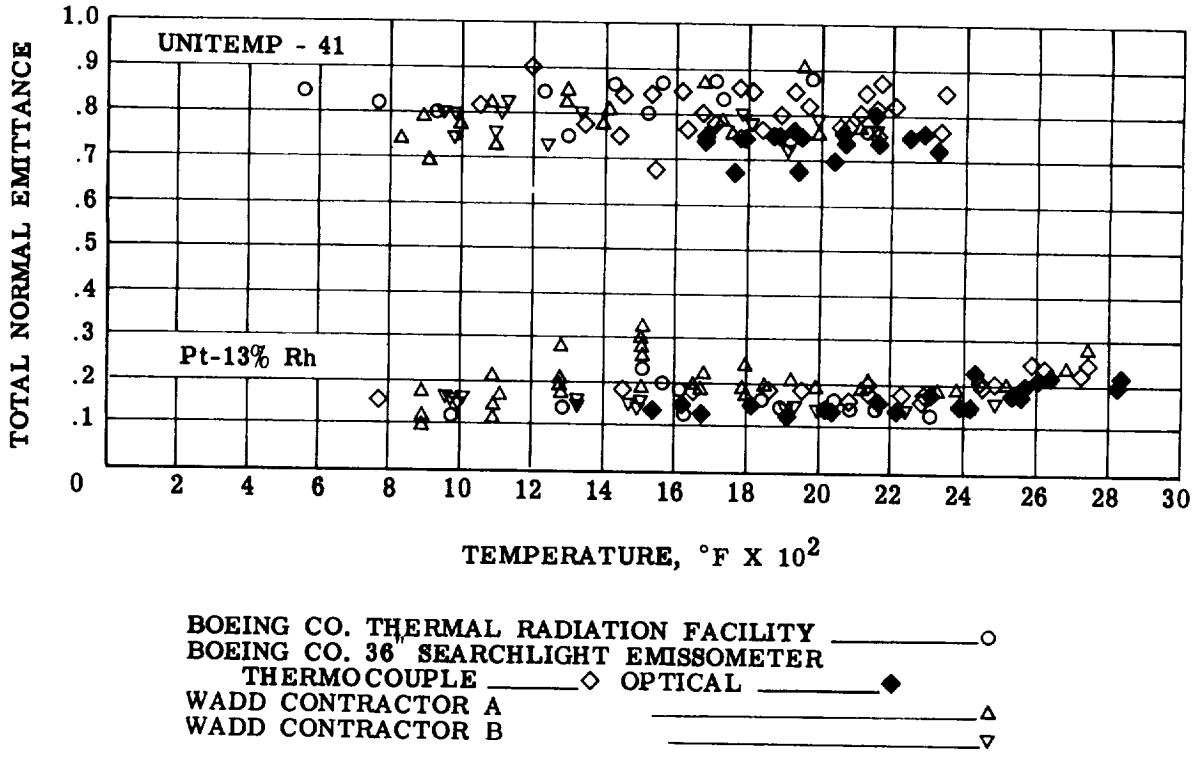

FIGURE 45–8.—Emittance data comparison for Boeing-prepared samples.

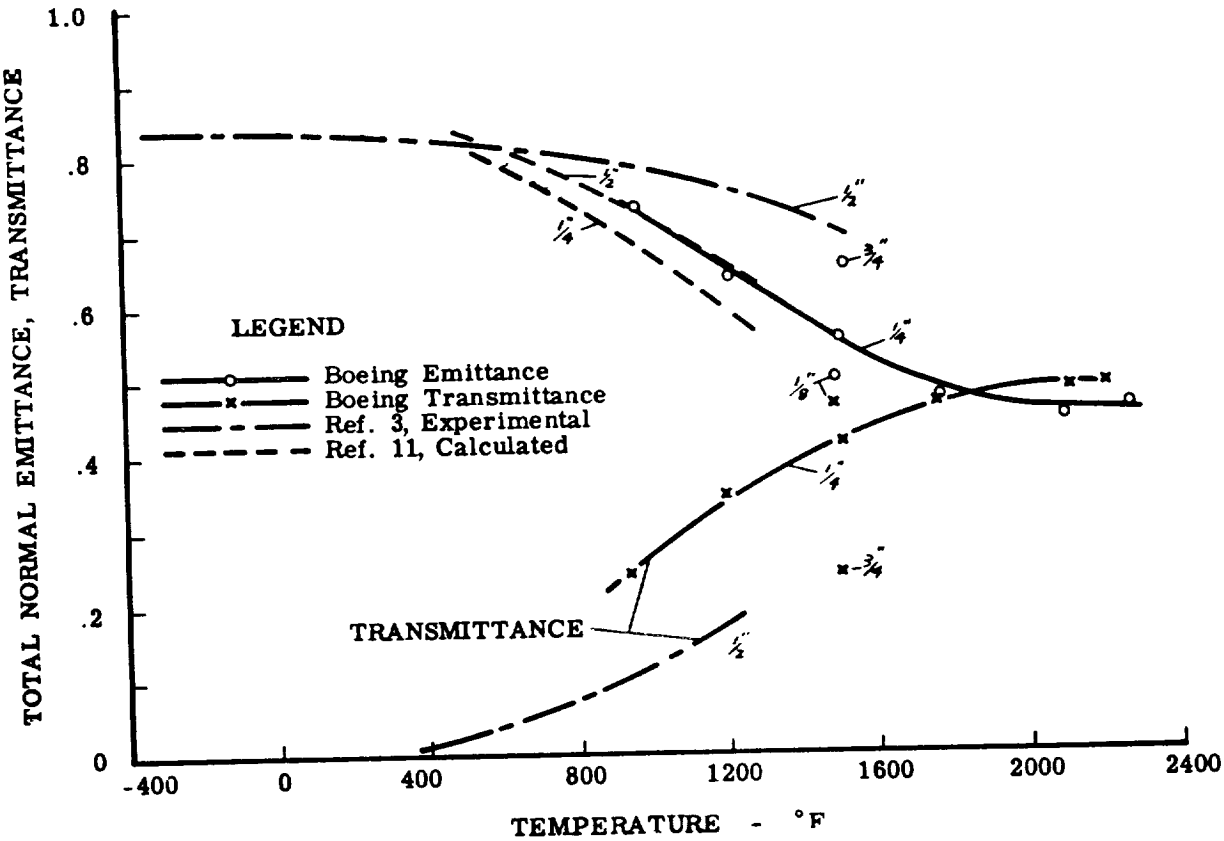

FIGURE 45-9.—Total normal emittance and apparent transmittance data comparison on Corning 7940 fused silica. Specimen thickness (inches) indicated.

and a basis for improvement or extension of the capabilities of the technique. The close agreement with NBS values for emittance standards is an indication that the Boeing thermal radiation test facility has been adequately evaluated, potential errors successfully corrected or eliminated, and that results from this facility can be expected to be accurate within the limits of error given.

The method presented in this paper offers above-average accuracy and higher temperature capability for general case measurements on either transparent or opaque materials than any other existing technique. The techniques utilized in the described facility are subject to only the material limitations to furnace temperature capability and the necessity to maintain the desired specimen condition. For example, the practical limit of the prototype facility described in this paper is 3000° F due to contamination of specimens by products of the graphite furnace components. For unstable specimen materials intended for short time applications, faster techniques, if available, may be required.

While total normal emittance and apparent transmittance are measured in the Boeing prototype facility, the corresponding spectral properties could be measured with the addition of a monochromator and collecting optics. The Boeing thermal radiation test facility is considered to meet basic requirements for a standard method, since it has proven itself superior for the determination, on any solid material, of high temperature radiation properties which are analytically exact according to the presently available general theoretical relationships.

REFERENCES

1. McMahon, H. O.: Thermal Radiation From Partially Transparent Reflecting Bodies. Jour. Optical Soc. of America, vol. 90, no. 6, June 1950, p. 376.
2. Gardon, Robert: The Emissivity of Transparent Materials. Jour. Opt. Soc. of America, vol. 39, no. 8, Aug. 1956, p. 278.
3. Betz, Howard T.; Olson, O. Harry; Schurin, Bert D.; and Morris, James C.: Determination of Emissivity and Reflectivity Data on Aircraft Structural Materials. Part II: Techniques for Measurement of Total Normal Emissivity, Normal Spectral Emissivity, Solar Absorptivity, and Presentation of Results. WADC TR 56-222, Oct. 1958.
4. Harrison, Thomas R.: Radiation Pyrometer and its Underlying Principles of Radiant Heat Transfer. John Wiley & Sons, Inc.
5. Kingery, W. D.: Property Measurements at High Temperatures. John Wiley & Sons, Inc.,1959.
6. Gouffé, André: Corrections d'overture des Corps-noirs Artificiels Compte Tenu des Diffusions Multiples Internes. Rev. d'Optique, vol. 24, nos. 1-3, 1945, p. 1.
7. Williams, Charles S.: Discussion of the Theories of Cavity-Type Sources of Radiant Energy. Jour. Optical Soc. of America, vol. 51, no. 5, May 1961, p. 564.
8. De Vos, J. C.: Evaluation of the Quality of a Blackbody. Physics, vol. 20, 1954, p. 669.
9. Harrison, William N.; and Richmond, Joseph C., et al.: Standardization of Thermal Emittance Measurements. WADC TR 59-510, Aug. 1959.
10. NBS Letter to Boeing—Joseph C. Richmond to F. T. Gustafson, No. 9.4/09441, July 14, 1961, Emittance Values for the NBS Standards Used by the Boeing Company.
11. Anon.: Materials Handbook. Corning Glass Works, New Products Division, Corning, New York.

DISCUSSION

Eubanks, NASA Goddard Space Flight Center: Please draw on the black board the temperature transient curve for one cycle, and make some comments about how this curve might change for a material such as alumina.

Clayton: I have drawn both a top and side view of the specimen and specimen-sighting tube, showing the relative locations and areas of each, including the radiometer target area on the specimen. Now the worst case for the specimen temperature transient is the case in which the water-cooled specimen-sighting tube is closest to the center of the specimen because the highest proportion of time is spent in the cooling portion of a cycle of one specimen revolution. For this case, temperature transients measured on the surface of both high- and low-emittance metal specimens with spotwelded, finewire thermocouples give identical results. The total amplitude of the transient is ½% of the temperature, which is considered a negligible percentage. The transient in the radiometer target area is much narrower than ½% because the target area is only a portion of the cooled area under the specimen sighting tube. The average sample temperature is depressed 4% below the temperature of the furnace as measured at the blackbody reference. These results are independent of both emittance and temperature level.

Eubanks: Did the minimum in the curve occur after the thermocouple was outside the viewing port?

Clayton: No, it occurred just before because the thermocouple is starting to see energy from the furnace when it gets close to the edge.

Eubanks: Would the maximum and minimum points in the curve go up or down in the case of alumina rather than a metal?

Clayton: They would not shift very much. If we look at this thing in the side view, what we have is the same as in any overall radiant-heat-exchange situation. Whether the radiant fluxes are acting throughout a volume or mostly at a surface is probably not very important to what the effective temperature is on a sample in a furnace. The 4% gradient from the sample to the blackbody reference where I am measuring my temperature is, I feel, the maximum possible gradient I could have through this sample. I think it is a fair bound. It certainly is conservative.

Moore, NBS: What about the calibration of your thermocouples? In a carbon furnace of this type, with platinum-platinum rhodium thermocouples, one would expect some rather large changes in thermocouple calibration with time at the temperature that you were using in your measurements.

Clayton: The calibration holds throughout a normal 4-hour run, but not for more than that, unless the temperature never gets over about 2000° F. These thermocouples are good to only about 2000° F in this atmosphere. Part of this due to contamination of the insulator. We found that we could not use them all the way up to their supposed limit.

Cox, Chance Vought Astronautics: I am sure you had a good reason for it, but I would like to know why you did not design your viewing port so that you could adjust it closer to the specimen and avoid having to make a correction for the reflected energy.

CLAYTON: I could not visualize starting with a few mils clearance at room temperature and maintaining it at 3000° F. That is the main reason; it is just a practical problem. This prototype is overly large and crude in some respects. The sight tube represents more area than is absolutely necessary, which causes a higher cooling load. However, it does work quite well, and it does indicate that the technique could be utilized to any temperature for which you can build a furnace, providing you can build a furnace that is compatible with the specimen. This is the major consideration.

COX: I would like to ask one more question. Have you had the opportunity to compare your measured temperature transients across the viewing port with analysis?

CLAYTON: No. I am not worried about it because I do not think there is much I can do about it except to design for as low a cooling load as possible within optical and specimen size limitations. I am mostly concerned that the average stays about the same for any material. I believe I set enough bounds on the transient that it is not a big factor. That has been my approach.

46—A RADIATION TECHNIQUE FOR DETERMINING THE EMITTANCE OF REFRACTORY OXIDES

BY DANIEL F. COMSTOCK, JR.

ARTHUR D. LITTLE, INCORPORATED, CAMBRIDGE, MASSACHUSETTS

Devices which concentrate and reflect heat from the sun or from other sources, such as an arc, appear to offer great potential as a means of investigating certain properties of high-melting-point solids. Among these properties is the emittance of a material, defined as the ratio of the radiation emitted by a sample to that emitted by a blackbody at the same temperature. Emittance varies from zero to one (0–1). The hemispherical spectral emittance of a material, the emittance at a particular wavelength averaged over a hemisphere, is the subject of this paper. For some materials, such as diffuse reflectors, the normal spectral emittance is approximated by the hemispherical spectral emittance. The normal spectral emittance of a sample is significant because, once it is known, the experimenter, using laboratory optical pyrometers, can determine the true temperature of the sample under other circumstances (ref. 1 and 2). In this paper, hemispherical spectral emittance will be considered throughout, but the word hemispherical will be omitted.

In 1954, Conn and Braught (ref. 3) suggested a technique for measuring the temperature of samples in a solar furnace. In their technique, which was later adapted (ref. 2 and 4) by Arthur D. Little, Incorporated, for a materials study, the light source is briefly interrupted while the radiation from the sample alone is being measured. At other times, while the full radiation is falling on the sample, the sum of the sample radiation and reflected radiation is recorded. From these two measurements, one can deduce both the value of the spectral emittance of the sample at one wavelength and its true temperature.

The purpose of this paper is to describe a method by which the spectral emittance of a sample may be determined conveniently over a wide temperature range by use of an arc-imaging furnace (ref. 5 and 6).

The author wishes to express his thanks to his colleagues of Arthur D. Little, Incorporated: to Armand Camus for his invaluable help in carrying out this work and to Peter Glaser and Jack Jasperse for their helpful suggestions.

PRINCIPLE

In the method described in this paper, the arc radiation is used for two purposes: (1) to heat the sample and (2) to provide a means for measuring the hemispherical spectral reflectance of the surface of the sample. By measuring the radiation at a chosen wavelength incident on the sample and measuring the same radiation reflected from the sample, we may determine their ratio, and thus obtain the reflectance of the sample. From the value of reflectance so determined, we may now deduce the spectral emittance.

To determine emittance from reflectance, we use Kirchhoff's law that the spectral absorptance of a body at a given wavelength and temperature is always equal to its spectral emittance at the same wavelength and temperature (ref. 7). According to the law of conservation of energy, (in this case the conservation of power) the sum of the spectral reflectance and spectral absorption of an opaque body must always equal one, and thus, by Kirchhoff's law, the sum of the spectral reflectance and spectral emittance of an opaque body must also equal one. In practice, by measuring what percentage of the incident arc light falling on the sample

is reflected, we may determine the spectral emittance of the sample at a given wavelength.

Formally stated:

$\epsilon_\lambda = 1 - \text{hemispherical spectral reflectance} =$

$$1 - \frac{r_\lambda}{i_\lambda} = 1 - \frac{(r_\lambda + e_\lambda) - e_\lambda}{i_\lambda} \tag{1}$$

where

- r_λ the reflected light from the sample
- e_λ the emitted light from the sample
- i_λ the incident light on the sample
- ϵ_λ the hemispherical spectral emittance of the sample

The quantities needed to solve equation (1) may be measured if a means is provided for separating reflected and emitted light from the hot sample. In the present apparatus, a fast shutter briefly and periodically interrupts the incident arc light so that the radiation emitted by the sample can be measured. This emitted light measurement, subtracted from the measurement of all radiation leaving the sample face, gives the reflected radiation measurement alone. Thus, the statement of equation (1) at the right-hand side of the page is in the form in which the experimental readings are obtained.

In practice, the experimental equipment may be arranged to measure the quantities of equation (1), or, what is simpler, their ratios. The equipment is described later. By measuring ratios, one eliminates the necessity of determining constants of the apparatus, such as losses in the optics and sensitivities of the measuring and recording equipment. Thus, one can measure the incident and reflected light ratio by measuring the ratio of these signals, which are indicated as amplitude readings in arbitrary units on a permanent racord, such as the output oscillogram from a galvanometer recorder.

The measuring apparatus has two sets of optics, one for measuring the arc or incident radiation, and one for measuring the sample emitted and reflected radiation. Though the optics are constructed similarly, they may be assumed to have different losses.

Therefore, we may write

$$r_\lambda = k_1 R_\lambda,\ e_\lambda = k_1 E_\lambda, \text{ and } i_\lambda = k_2 k_3 A_\lambda$$

Where

- R_λ the oscillogram amplitude of the reflected light
- E_λ the oscillogram amplitude of the emitted light
- A_λ the oscillogram amplitude of the arc light
- k_1 the pyrometer sensitivity through the sample viewing optics
- k_2 the pyrometer sensitivity through the arc viewing optics
- k_3 that fraction of light from the arc image which reaches the sample as incident light

Now equation (1) may be written as

$$\epsilon_\lambda = 1 - k_1 \frac{(R_\lambda + E_\lambda) - E_\lambda}{k_2 k_3 A_\lambda} = 1 - K \frac{(R_\lambda + E_\lambda) - E_\lambda}{A_\lambda} \tag{2}$$

where K is a combined constant of the arc furnace and pyrometer apparatus.

Thus, the spectral emittance of a sample may be determined from equation (2) from relative amplitudes R_λ, E_λ, and A_λ all read from the same oscillogram. The combined constant K of the apparatus is determined by a calibration procedure described later.

It is desirable to know not just the emittance of the sample, but the emittance as a function of temperature (ref. 8). Therefore, we must determine the temperature. If a standard lamp is added to the present apparatus, the temperature of the sample can be determined from the same oscillogram readings used to determine emittance. A comparison is made between the radiation from a standard lamp and the radiation from the unknown sample. Wien's law may be written for the sample and for the standard lamp. By taking the ratio of the two expressions, we may specify the constants or eliminate them, obtaining the expression

$$T = \frac{T_L}{1 - \frac{\lambda}{C_2} T_L \frac{E_\lambda}{E_L \epsilon_\lambda}} \tag{3}$$

where

- λ the wavelength under consideration
- C_2 the second constant of Planck's equation
- T the true absolute temperature of the sample
- ϵ_λ the spectral emittance of the sample

E_λ the sample oscillogram amplitude in arbitrary units

E_L the standard-lamp oscillogram amplitude in the same arbitrary units

T_L the equivalent blackbody, lamp-filament temperature observed with a laboratory spectral radiation pyrometer

In practice, therefore, the oscillogram traces, E_λ and E_L, of sample and standard lamp radiation, together with the emittance, ϵ_λ, previously determined from equation (2), can be combined in equation (3) to give the absolute temperature, T, of the sample.

EXPERIMENTAL APPARATUS

The equipment consists of two major components: an imaging system and an arc source for heating the sample; and an optical measuring and recording system for making measurements on the sample.

The sample is heated in an ADL-Strong arc-imaging furnace. In this furnace, an arc is imaged by two identical elliptical optical collecting mirrors onto a sample seven feet away (ref. 9). The image is the same size as the arc, and, if all radiation were collected and transmitted, the temperature at the sample would be the same as that in the arc (about 7500° C). However, because optical losses are substantial, the sample temperature is usually limited to approximately 3700° C.

The basic configuration of the imaging furnace is shown in figure 46–1. Radiation from the arc is collected by a 21-inch ellipsoidal reflecting dish and cast onto a similar ellipsoid that refocuses radiant energy onto a 1-cm-diameter spot on the face of the sample. Approximately 11,000 electrical watts of power are supplied to the arc, but the thermal power arriving at the sample is about 650 watts at maximum. About 60% of the radiation from the arc is in the visible spectrum, with its peak in the visible blue region.

The measuring apparatus takes advantage of the fact that in the arc imaging furnace used, two enlarged images are formed at an intermediate image plane of the optical system. One image is of the sample, seen by looking to the right, and the other image is of the arc, seen by looking to the left. A scanning detector mounted at this common plane is arranged to scan both the sample and arc images by viewing alternately in one direction and then in the other.[1]

The scanning detector consists of two platinum hypodermic needles, each encasing a quartz light pipe and mounted on a rotating drum (fig. 46–2.) It may be set either to scan across the sample or to give a continuous history of sample radiation. Each pipe sheath contains a single aperture, and the two face in opposite directions. As the drum rotates, one aperture is exposed to radiation from the arc source, while the other is exposed to radiation emitted and reflected by the sample. A chopper synchronized with the rotating drum periodically blanks out the arc radiation im-

[1] C. P. Butler, Naval Radiological Defense Laboratory, San Francisco, has pointed out that the so-called "cross-over point" in the center of a two-ellipsoid arc furnace is in fact a bundle of rays that do not converge entirely, resembling more a sheaf of wheat in their geometry.

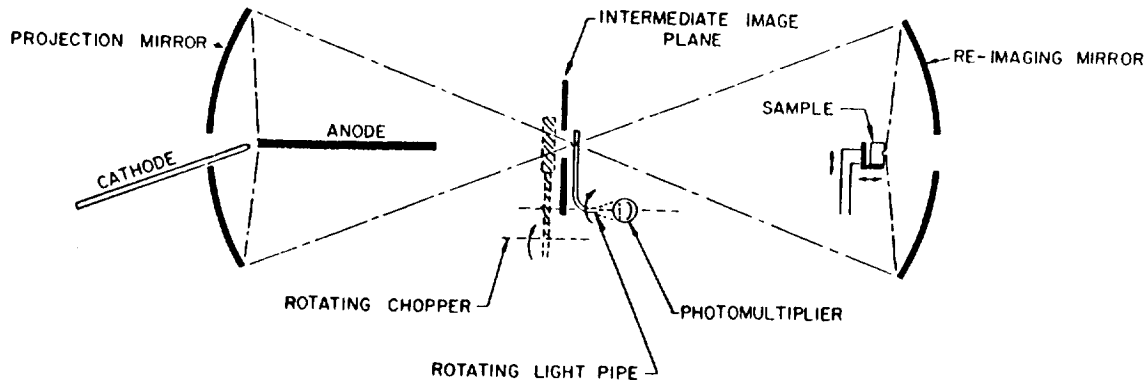

FIGURE 46–1.—Schematic of arc furnace and pyrometer.

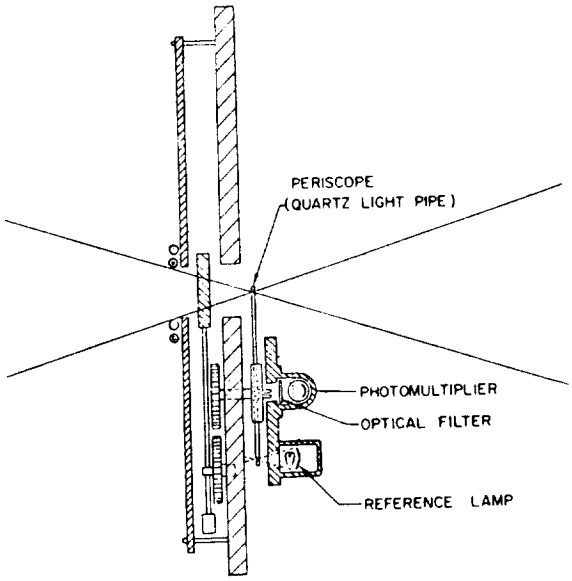

FIGURE 46–2.—Detail of light pipe assembly.

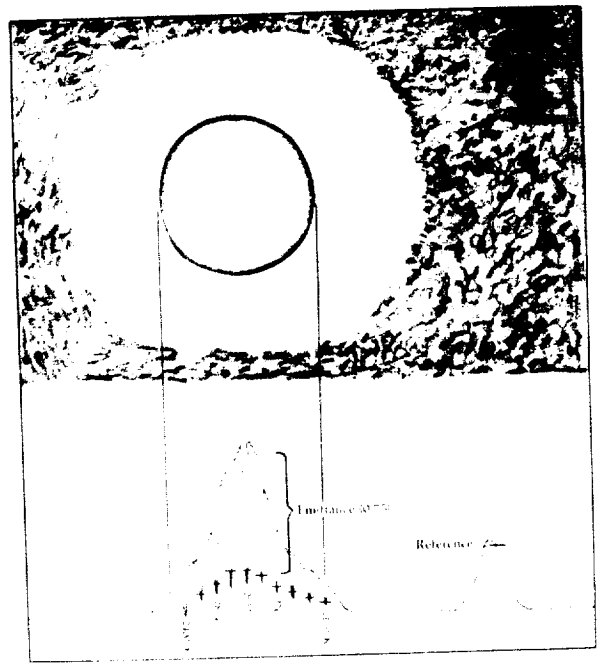

FIGURE 46–3. Trace taken of molten puddle in an alumina brick, showing calculated temperature profile and emittance.

pinging on the sample for brief intervals so that only radiation from the sample is measured.

There are two modes of operation of the detector, slow and fast. In the slow mode, the sample aperture scans across the sample in one-half second and repeats the scan every three seconds. The arc is scanned similarly every ½ sec during another part of the cycle. The output, while operating in the slow mode, is a profile of the radiation emitted by points across the sample. The result is an output oscillogram, as shown in figure 46–3.

As the light pipe passes through the sample image, radiation is conducted along the quartz rod and through a filter to a photomultiplier tube. The level of radiation passed by the filter at a single wavelength produces a signal related to the temperature and emittance of the sample. The signal is amplified and transmitted to a high-speed recorder, where a standardizing signal produced by an auxiliary light source is also recorded. From these recorded values, the sample emittance and temperature can be calculated.

From the oscillogram (e.g., fig. 46–3) an emittance and temperature profile across the sample can be calculated from one cold edge of the sample, through the molten spot at the center, and to the other cold edge. These calculations are carried out using equations (2) and (3), as indicated previously.

The time interval during which the chopper interrupts the heating radiation reaching the sample is made brief (5 msec) and widely spaced (every 30 msec) in order to avoid too much cooling of the sample during the interrupted interval. Unless care is taken, the sample will cool so rapidly that a false determination of temperature results. For example, the center of the molten alumina brick illustrated in figure 46–3 cooled 20° during the 5-msec interval that the light was obscured from the brick. This cooling effect can be seen on the record of sample radiation shown in the lower half of the figure. The bottom of each recorded dip represents light emitted from the sample alone; the slanted line at the bottom of each dip indicates cooling of the sample during a reading. The obvious solution to the problem of cooling was to make the interruption as brief as possible and to take the readings rapidly.

The fast mode of scanning is used for taking a time history of the sample as it heats up. In this mode, the same apertures used for slow scanning scan the sample image and the arc image once every 16 msec. Instead of a radiation profile of the sample, the output oscillogram indicates the radiation intensity

from that portion of the sample emitting the most radiation, usually the center of the sample. A typical fast scan oscillogram of zirconia is shown in figure 46–4.

RESULTS

While we were developing a working unit, we gathered data on several high-melting-point materials. Because this information was incidental to our program, the data are incomplete. However, to indicate what information might be obtained, we have shown in figure 3 a sample slow-scan mode profile of an alumina brick that has been heated at its center to above the melting point. The emittance of the molten alumina at a temperature of 2950° K is found to be 0.75 at a wavelength of 0.7μ.

In a second determination taken in the fast mode to obtain a time history of the sample, a zirconia brick was heated from room temperature to above its melting point. The record obtained is shown in figure 46–4. The total time of heating, from the time the arc light was first applied to the sample to the time it was removed and allowed to cool, was 6 sec.

Figure 46–5, which is an ink tracing of the original oscillogram of figure 46–4, shows the variation with time of: the arc radiation, the emitted plus reflected radiation, and the emitted radiation alone. From the three traces of figure 46–5, the emittance and the temperature can be calculated by using equations (2) and (3).

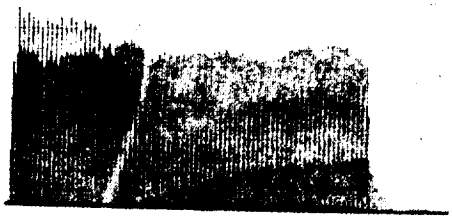

FIGURE 46–4.—Typical fast scan oscillogram of zirconia.

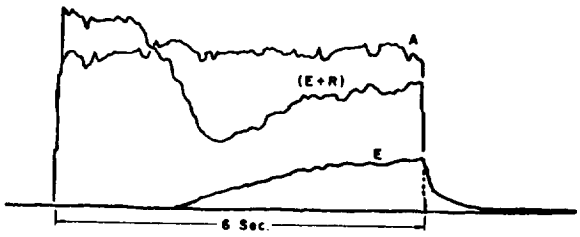

FIGURE 46–5.—Typical record of zirconia sample (fast mode)—ink tracing of original oscillogram of figure 46–4.

At room temperature, the spectral emittance of the zirconia sample (at a wavelength of 0.7μ) was found to be 0.34. As the heating progressed, the emittance rose, reaching a value of 0.82 in 2.75 sec. Its temperature at that point was 2440° K. In 6 sec, the sample temperature had reached 3200° K, and the sample had an emittance of 0.73. When the sample reached 3200° K, we cut off the arc radiation and allowed the sample to cool; its cooling curve is quite apparent in figure 46–5.

DETAILS OF CONSTRUCTION AND TECHNIQUE

The pyrometer frame, which consists of a square plate about 1½ feet on edge, is inserted vertically at the crossover point of the arc furnace. A hole 2½ inches in diameter at the plate's center allows for transmission of the arc light to the re-imaging mirror; the edges of the hole are water-cooled. Attached to this plate are two bearings and two positive-grip belts connected to a gear box driven by a synchronous motor. The two belts drive two wheels: one is the light chopper, and the other is a small rotating hub holding the two small optical light pipes that scan the arc and sample images. This hub rotates below the hole in the plate in such a way that the ends of the light pipes (apertures) pass briefly and periodically through the arc and sample images. (Figure 46–6 shows a light pipe at the cross-over point.) The light pipe consists of platinum hypodermic needles (0.030-inch OD) with monofilament quartz light pipes inside. The light from each aperture is conducted to the center of the hub and then out through its axis via the quartz monofilament through a red glass filter to a photomultiplier tube.

The pyrometer system presently consists of: the pyrometer frame, a 1P22 photomultiplier with a 900-volt regulated power supply, a 50-k helipot on the output of the photomultiplier (with which the gain of the system is adjusted), a solid-state current amplifier that amplifies the output signal and transmits it to a galvanometer, and, finally, a galvanometer oscillograph (the Heiland Visicorder) capable of recording oscillations at frequencies to 3000 cps. Incidental equipment includes two Variacs (one for driving the reference lamp and one for driving the standard lamp), a precision

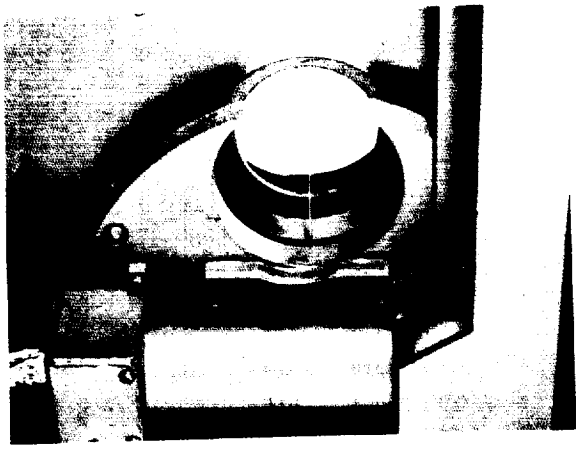

FIGURE 46-6.—Light pipe and photocell housing.

laboratory optical pyrometer, a standard lamp, and a water-cooled copper block.

A reference lamp (not the same as the standard lamp) is included in the apparatus for the purpose of normalizing all radiation readings so that they may be independent of drifts in the electronic and recording equipment. The reference lamp in the main body of the pyrometer is sampled by the sample light pipe once each cycle. It is not essential that the reference lamp provide a known amount of radiation; its function is to provide reproducible, though arbitrary, amounts of radiation. A reference "blip" appears on the oscillograms at all times; the height of this blip is the value against which all readings except ratios are normalized. The reference lamp is a Sylvania TruFlector type operated below its rated voltage to imporve stability. The voltage supply feeding the lamp is 60 cycles, adjustable by a Variac, and regulated to better than 1%. Powerline ripple in the output of this lamp does not appear to be a noticeable problem.

The duty cycle for both the slow and the fast scans has been chosen with some care. If the light pipe is made too long, the scan will be linear across the sample—which is advantageous—but the total duty cycle of scan time versus entire-cycle duration will be so small that the chart will be difficult to read. If the light pipe is too short, the chart becomes much easier to read, but the scan becomes semicircular rather than linear and, thus, is difficult to interpret. The best compromise is to make the length of the light pipe roughly equal to the diameter of the field stop hole.

Two constants of the apparatus, K and λ, must be determined. K relates to the optical losses and electronic sensitivities of the apparatus, and λ is the effective wavelength at which the emittance is measured.

We may evaluate the K in equation (2) by replacing the sample with a material of known emittance and taking measurements with the arc light on. Under these conditions, a known fraction of the arc light falling on the sample will be reflected back through the re-imaging mirror to the sample light pipe. Thus, R_λ, E_λ, and A_λ may be determined, and equation (2) may be solved for K. Once this value of K has been determined, it may be used in the determination of unknown emittances.

In the determination of K it is convenient to use a cooled sample of known emittance as the "white block", because a cool sample emits no radiation ($E_\lambda=0$), and because its surface state is stable. For example, in these experiments a water-cooled copper block coated with magnesia-ribbon smoke was used as an emittance standard; its surface is believed to have a reflectance between 0.95 and 0.97. It is coated with magnesia by burning a magnesium ribbon near and underneath the copper surface. The resulting deposit is clean, uniform, and white. The surface may be wiped off the copper and redeposited for each new determination.

The effective wavelength of the operation of the pyrometer is determined by the cutoff properties of a red glass filter and the wavelength response of the photomultiplier.

The exact value of λ may be determined by operating the arc-furnace pyrometer with the standard lamp set successively at two different temperatures, T_1 and T_2. Under these conditions,

$$\lambda = C_2 \frac{T_1 - T_2}{T_1 T_2 \ln \frac{E_1}{E_2}} \qquad (4)$$

In the present apparatus λ is found to be 0.7 μ.

In running a temperature determination on an unknown sample, we have found it convient to follow this procedure: First, we align and focus the furnace. For this, we use a

flashlight bulb in place of the arc and the standard lamp in place of the sample. The sample, the standard lamp, and the water-cooled white block can be mounted so that the front surface of each successively occupies the same point in space. We then position the water-cooled white block, and with the arc on, determine a K value by using amplitudes taken from the oscillogram substituted in equation (2). For this determination, an assumed value (such as 0 or 0.03) for the emittance of the magnesia-smoke surface is used. With the arc off, we operate the standard lamp in place of the sample, at a known blackbody temperature, and take an oscillogram. We then mount and heat the sample.

From the sample record, the standard lamp record, and the K value determined above, the emittance is determined from equation (2), and the temperature is determined from equation (3).

ACCURACY

The absolute temperature accuracy of the device has not been established, because of the lack of high-temperature reference points. The accuracy, when a standard lamp is used in place of the sample, is $\pm 15°$ C, and the reproducibility for reflectance determination of zirconia and alumina samples is $\pm 4\%$.

CONCLUSIONS

A convenient and useful method has been developed for measuring the spectral emittance in the visible red (0.7 μ) of refractory oxides. The method, based on the Kirchhoff law and using the reflectance technique, appears to be applicable to sample materials in the solid or molten state at temperatures of 2000° C and up. The equipment measures and records spectral emittance as a function of time as the sample is heated.

The accuracy of the method is at present not known, but the reproducibility between emittance determinations on similar aluminum samples is estimated to be $\pm 4\%$.

REFERENCES

1. Kingery, W. D.: Property Measurements at High Temperatures. Ch. 4, sec. 4, John Wiley & Sons, Inc., 1959.
2. Blau, H. H., Jr.: Measurement of Flux, Emittance and Related Properties. Proceedings of an International Symposium on High Temperature Technology, Copyright Stanford Research Institute, 1960, distributed by McGraw-Hill Book Co., Inc.
3. Conn, W. M., and Braught, G.: Separation of Incident and Emitted Radiations in a Solar Furnace by Means of Rotating Sectors. Jour. Optical Soc. of America, vol. 44, no. 1, Jan. 1954.
4. Laszlo, T. S.: Temperature and Flux vs. Geometrical Perfection. Jour. Solar Energy Sci. and Eng., vol. 1, 1957, p. 78.
5. Comstock, D. F., Jr.: Method for Temperature and Reflectance Determination in an Arc Imaging Furnace. Temperature Its Measurement and Control, vol. III, pt. II, Reinhold Pub. Co., 1962.
6. Cook, J. C.: A Scanning Radiation Sampler for Imaging Furnaces. Temperature Its Measurement and Control, vol. III, pt. II, Reinhold Pub. Co., 1962.
7. Weinstein, M. A.: On the Validity of Kirchhoff's Law for a Freely Radiating Body. Am. Jour. Physics, vol. 28, 1960, pp. 123–125.
8. Emslie, A. G., and Blau, H. H., Jr.: Journal of Electrochemical Soc., vol. 106, no. 6, June 1960, pp. 579–580.
9. Glaser, P. E.: Imaging-Furnace Developments for High-Temperature Research. Journal of Electrochemical Soc., vol. 107, no. 3, March 1960, pp. 226–231.

DISCUSSION

Clayton, Boeing Company: You mentioned that you had an instrument calibration factor which accounted for the difference in optical paths and so forth. I was curious what this was and whether you found it was stable.

Comstock: There are two factors. One relates to the wavelength response of the instrument and the other relates to the losses in the optical system. The constant relating to the losses should be determined every day, at the beginning of the day's run. The wave-

length response constant need be determined only every two weeks or so. The need for these constants is second order since the instrument takes ratio measurements.

LOZIER, National Carbon Company: I have one question on molten samples. How can you be sure that all the non-reflected light is absorbed? This is necessary in order to equate the emittance to one minus the reflectance.

COMSTOCK: I was hoping that this question either wouldn't come up or that we would have half an hour to discuss it. One of the advantages for the wide angle optics (170° optics), is that the illumination of the sample and the viewing of the sample are almost hemispherical. Thus all radiation to or from the sample is either absorbed or reflected and collected. There is not much else it can do except be transmitted by the sample. This method obviously will not work for translucent samples. The optical depth of the sample we're using is of the order of a 16th of an inch or less and is considered opaque. I'm not sure I have answered the question. The Kirchhoff law is a reasonable assumption to make for these samples.

SKLAREW, The Marquardt Corporation: With regard to a non-polished specimen, is the normal spectral reflectance of the surface necessarily equal to one minus the normal spectral absorption? If so, can this be shown theoretically?

COMSTOCK: We are dealing with 170° hemispherical illumination, reflectance, absorptance and emittance. I believe that under these conditions the emittance equals one minus the reflectance whether the sample is a diffuse or specular reflector providing that it does not transmit.

RICHMOND, National Bureau of Standards: I think I can answer that last question, at least to some extent. The reflectance that is the counterpart of the normal emittance, regardless of the surface contour of the specimen, is going to be the reflectance that is measured under conditions of normal illumination and hemispherical viewing or the optical equivalent of that, which is completely diffuse illumination and normal viewing. In order for these relationships to be valid you have to have consistent geometry of the radiant energy being measured. These are the conditions that apply to the comparability of normal emittance and reflectance.

47—A TECHNIQUE FOR MEASURING THERMAL RADIATION PROPERTIES OF TRANSLUCENT MATERIALS AT HIGH TEMPERATURE

BY R. L. COX

VOUGHT ASTRONAUTICS DIVISION, CHANCE-VOUGHT CORPORATION, DALLAS, TEXAS

A method is described for measuring total emittance of translucent materials in such a manner that any effect of subsurface temperature gradients can be observed. The axial temperature distribution of a disk-shaped specimen is controlled by relative positioning of a plasma torch heating the front face and a propane torch heating the rear face. Total radiation leaving the front face is measured with a thermopile detector, and corrections are applied to account for the reflection of plasma emission. Temperatures are measured internally on the specimen axis by utilizing small blackbody cavities drilled radially to the centerline. The entire specimen temperature distribution is then determined by use of standard heat transfer means employing a measured external temperature profile and independently measured thermal conductivity values as the required boundary conditions.

Results with this technique to 4600° F are presented for zirconium oxide and indicate a measurable effect of subsurface temperature gradients on emittance. Methods of improving accuracy are discussed briefly, and an extension of the present technique to allow thermal conductivity measurements is suggested.

With the advent of re-entry aerospace craft, a challenge has been posed to engineers in the design of heat shields and nose cones. Material systems capable of withstanding extreme heat flux and temperature environments are being developed. Radiative cooling constitutes an important portion of the overall heat balance on these systems. For this reason an accurate knowledge of the emittance of materials under consideration is imperative.

Refractory oxides constitute a promising class of candidate materials for radiatively cooled components. Many refractory oxides are translucent in wavelength bands important to radiant heat transfer at high temperatures. This is demonstrated at low temperature by a high reflectance and low emittance at the wavelengths where transmission is high for single crystals or fused nonporous bodies. A moderate thickness is required for opacity; for instance, about 0.16 inch for visible light for a typical polycrystalline stabilized zirconia formulation. As temperature is increased, the two basic factors affecting translucency, the scattering coefficient and the absorption coefficient, are changed. The absorption bands of materials broaden, tending to reduce transmission, while, in regions remote from the absorption bands, the index of refraction (which affects the scattering coefficient) is predicted to decrease, increasing transmission. These opposing effects can cause an overall increase or decrease in translucency. Tests on zirconia during the present study indicated a mild decrease in its translucency when taken from room temperature to melting. Observations of total emission from various thickness disks at melting indicated that about 0.05 inch is required for opacity at this temperature.

Since materials that are translucent necessarily emit from the same depth that is required for opacity, their emittance based on surface temperature is dependent on subsurface structure and temperature distribution. Either emittance must be measured under the same conditions that occur in the application, or determinations must be made in such a way as to allow a theoretical or empirical correlation between test and design conditions. As it is often impractical to duplicate conditions occur-

ring in the application, means of implementing the latter approach must then be devised.

Emittance measurements on translucent materials at high temperature involve several difficulties. Heating must be accomplished in such a way as to control temperature gradients, avoid unwanted chemical reactions, and assure no transmission of radiation from the heater itself. A means of varying suitable parameters to isolate the effect of subsurface emission must be provided. Temperature must be measured in a way not adversely affected by subsurface emission or otherwise subject to large errors. The objective of the present investigation was to accomplish these goals with a reasonable degree of accuracy while using simple and readily available instrumentation. An experimental technique has been developed, and a mildly translucent formulation of zirconia has been studied. Present results can be correlated with the design conditions by empirical means. Refinements should allow the scattering and absorption coefficients to be inferred. The radiative transfer equations can then be used to specify emittance under any set of boundary conditions.

DESCRIPTION OF EXPERIMENTAL APPARATUS

The basic system of measurement employed is the remote energy comparison technique, which has been used by numerous investigators in the past. In this technique, the specimen is heated in such a way that its emission alone can be observed, with radiated energy detected by some remote sensing device. Specimen temperature is measured, and emittance is determined by comparing the detected radiant energy to that radiated from a blackbody at the same temperature. In the present application, temperature is measured in a new way so that both the value at the surface and the internal distribution can be defined, while heating is accomplished in such a manner as to allow control of the internal temperature distribution. These modifications allow translucent materials to be studied. Temperature and temperature distribution are derived by heat transfer analysis from measured internal temperatures and a survey of the external temperature profile. Total radiation is detected with a calibrated thermopile, and corrections are applied to account for energy originating in the heat source which is reflected from the specimen.

Experimental Arrangement

Figure 47–1 illustrates the basic elements of the experimental system. The disk-shaped specimen, about 1½ inches in diameter and ¾ inch thick, was tapered to allow secure mounting in machined zirconia bricks. A plasma torch was used to heat the specimen front face, while the rear face was heated with a propane torch. Total radiation leaving the center of the front face was detected at an angle of about 44° to the normal with a thermopile. An optical pyrometer is shown in position to measure temperature at the bottom of one of three cylindrical blackbody cavities drilled radially into the specimen to its axis. These cavities were viewed through a port cut in the supporting bricks. The pyrometer was mounted on a movable and adjustable stand and used to measure the brightness temperature profile of the specimen front face, rear face, and outside diameter (through the port). Figure 47–2 is a photograph of the apparatus inserted into an exhaust hood.

Heating System

The specimen temperature and temperature distribution were controlled by relative positioning of the plasma and propane torches. Temperature along the specimen axis could be varied from a gradient of about 3000° F to a condition of equal front and rear face temperatures. Zirconia could be melted with either torch. A 40-kw plasma torch, operating on

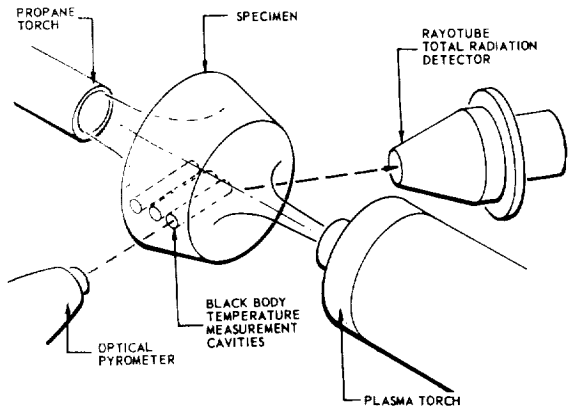

FIGURE 47–1.—Schematic arrangement for measuring total emittance.

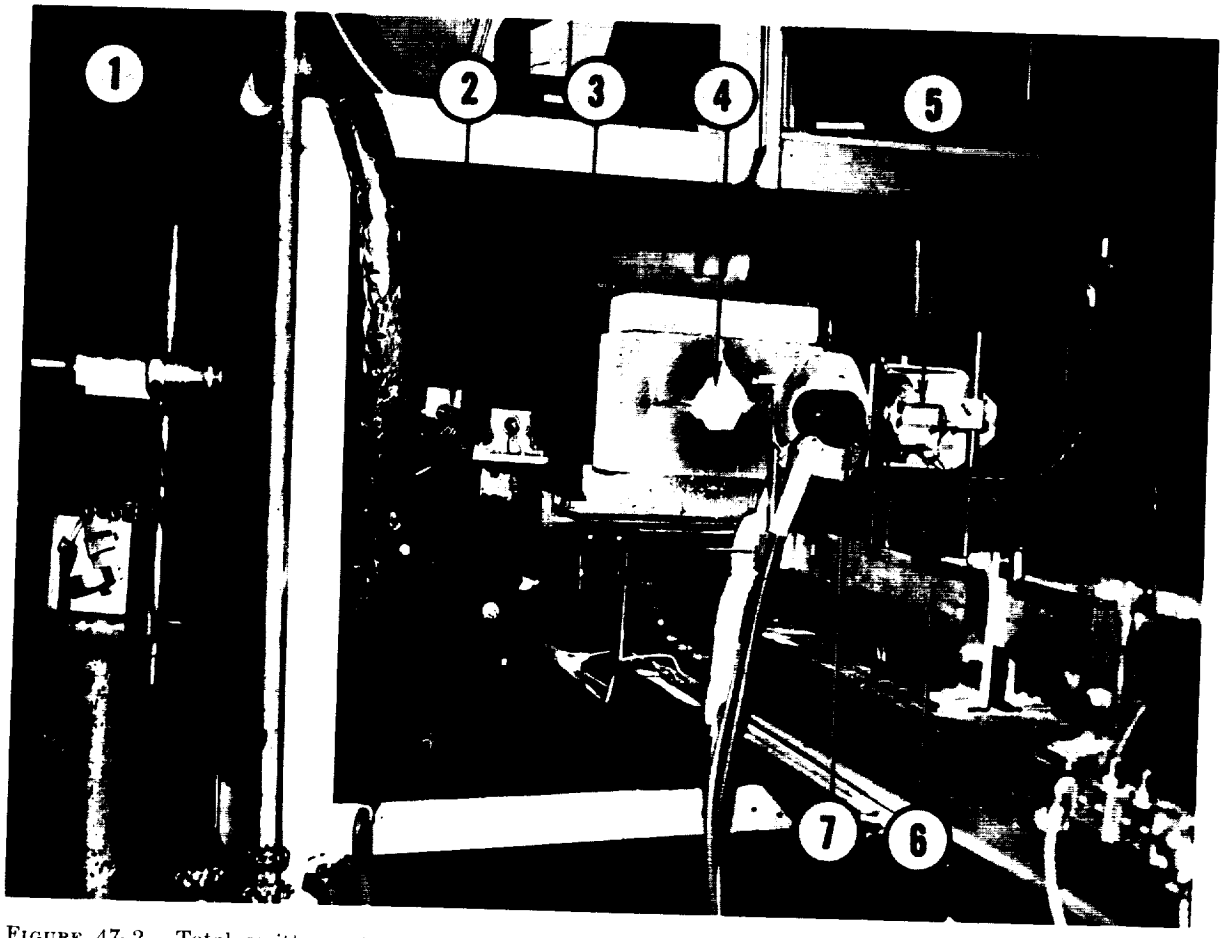

FIGURE 47–2.—Total emittance test apparatus: (1) optical pyrometer, (2) propane torch positioning screw, (3) propane torch tube, (4) zirconia specimen, (5) Rayotube mounted in water-cooled sight tube, (6) plasma torch positioning arm, and (7) plasma torch.

either nitrogen or a mixture of nitrogen and oxygen, was used. The estimated plasma temperature is 7500° F. A specimen environment closely approximating air resulted as the plasma gases mixed with the room atmosphere. The plasma torch provided a moderately steady source, with a flux deterioration on the order of 5–10% per hour. A symmetrical temperature distribution across the specimen front face was produced, as shown by the brightness temperature plots of figure 47–3. The plasma torch was positioned relative to the specimen by an electrically driven lead screw. With a zirconia specimen, a temperature of about 1800° F was attained at a distance of 7 inches from the specimen to the plasma nozzle face, while a distance of 2 inches was required to reach 4300° F. The nozzle front face was blackened to avoid the possibility of multiple reflections.

A single propane torch heating head provided a steady convective source to produce relatively uniform rear face temperatures, as shown in figure 47–3. Three propane cylinders and eight oxygen cylinders were manifolded to provide the required gas generation rate and allow a 2-hour run. The torch distance from the specimen was manually positioned by cranking a lead screw.

Temperature Measurement

Temperature determination was based on the measurement of internal temperatures and sufficient boundary conditions to allow the temperature distribution and surface temperature to be calculated. By careful selection of the location of internal measurement points, the effect of any uncertainty in the calculated temperature distribution could be minimized. In

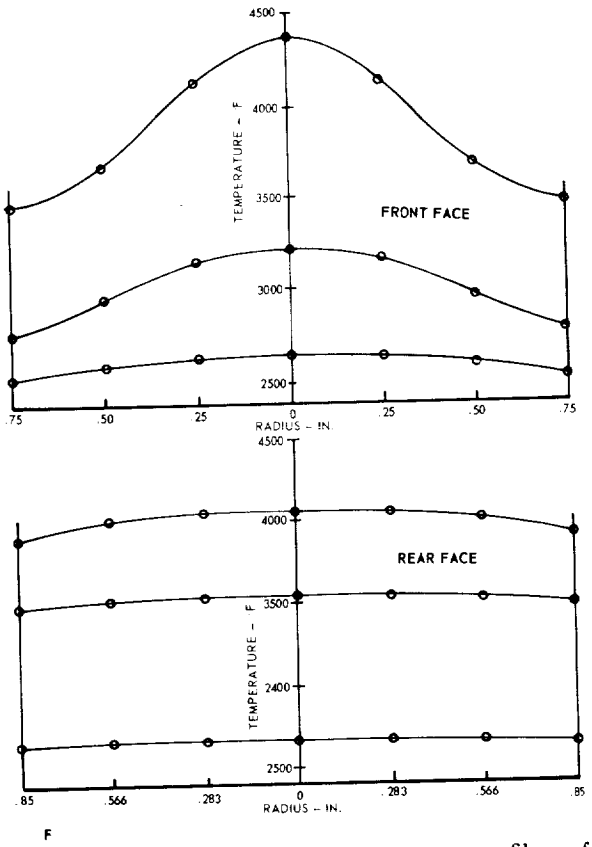

FIGURE 47-3.—Brightness temperature profiles of zirconia specimen faces.

the present tests, three temperatures along the specimen axis at varying depths below the surface were measured, as indicated by figure 47–1.

A steady-state finite-difference heat transfer analysis, using the method described by Schneider (ref. 1), was conducted to calculate the temperature distribution, and the resulting simultaneous equations were solved by using an IBM 7090 digital computer. Since the specimen and its external temperature profile were axially symmetric, heat flow occurred only in the axial and radial directions, and the analysis could be reduced to two-dimensional by using polar coordinates. In present results, a grid system composed of seven slices at various axial depths and five slices at various radii was used. Unequal slice thicknesses were chosen to place the smaller slices in regions of maximum temperature gradient. Inputs required for the analysis were the specimen external temperature profile, specimen geometry, and the variation of thermal conductivity with temperature. No knowledge of heat flow rates across the boundaries was required. Figure 47–4 shows a typical plot of calculated specimen isotherms. By cross-plotting isotherms, temperature versus depth along the axis was obtained, and these cross-plots were applied to measured internal points to specify surface temperature as shown in figure 47–5.

The specimen external temperature profile was obtained from optical pyrometer surveys like those presented in figure 47–3, plus values on the outside diameter measured through the viewing port. External optical temperatures were corrected for plasma reflections and for spectral emittance values from preliminary data analysis. (Temperature was estimated in preliminary analysis by extrapolating internal measured values to the surface. The resulting emittance values were found in the final analysis to be very little in error.) Since the shape of the internal axial temperature profile is a mild function of temperature level, errors in preliminary analysis had little effect on final re-

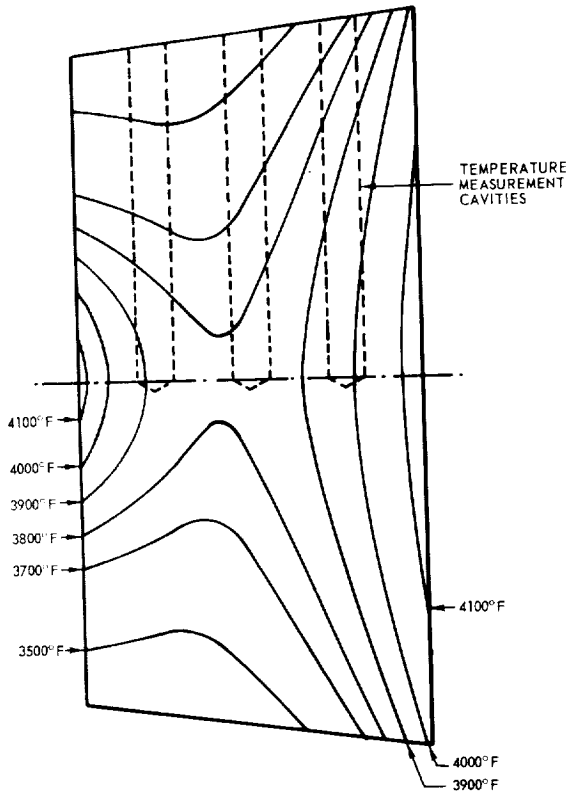

FIGURE 47-4.—Isotherms in zirconia specimen.

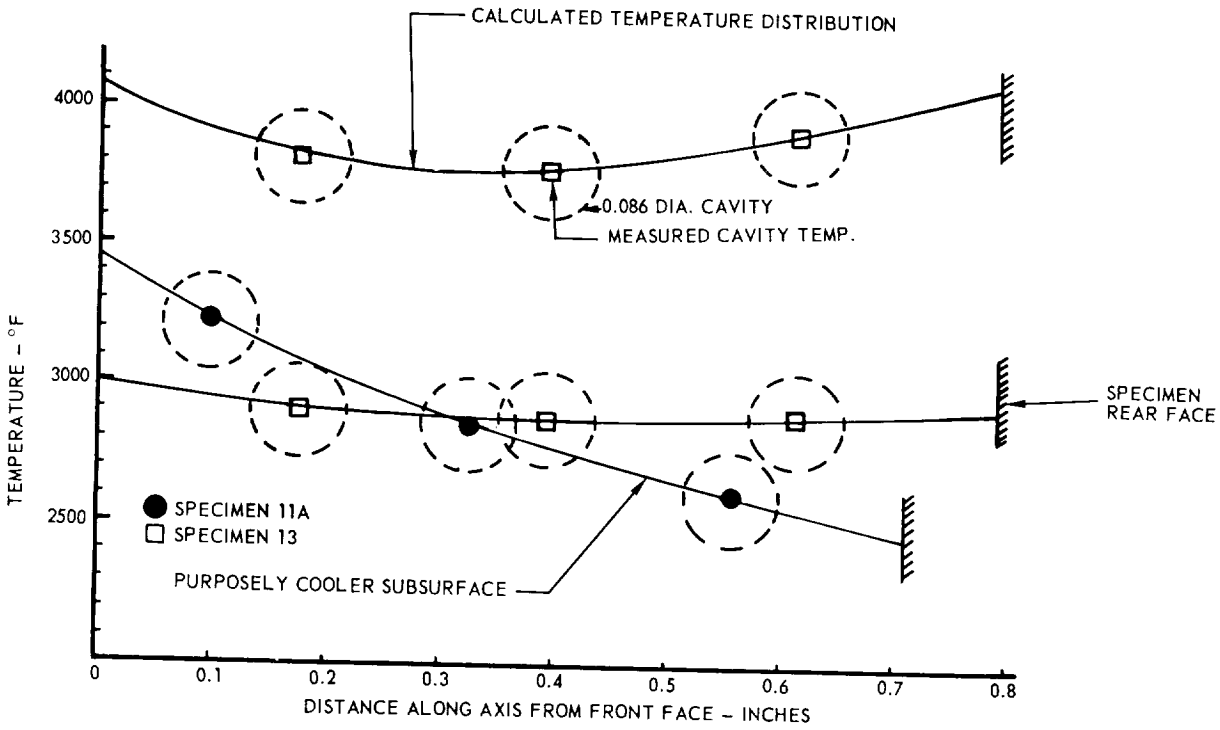

FIGURE 47-5.—Axial temperature distribution in zirconia specimen.

sults. Thermal conductivity, required only to account for the variation of this property with temperature, was obtained from independent tests on the same material.

The temperature measurement blackbody cavities presently used have been 0.086 inch in diameter and approximately 0.8 inch deep. This length-to-diameter ratio is in excess of that required to provide an apparent emittance of essential unity for an isothermal hole, but in practice a temperature gradient down the hole existed. A correction for the nonisothermal walls in the cavities was conservatively calculated using an approximate incremental analysis, and found to be on the order of 5° F under the worst conditions (maximum temperature). Temperature was measured using a Leeds & Northrup model 8622 optical pyrometer, whose calibration was verified with a National Bureau of Standards lamp.

The temperature measurement system restricts the experimental technique to moderately translucent materials. One obvious requirement is that the presence of the blackbody cavities does not affect emission from the front face. A second consideration is that the blackness of the cavities must not be destroyed by the unavailability of a sufficient emitting volume below the hole base or around its walls. Similarly, large temperature gradients cannot be tolerated within the emitting volume which affects the cavities. Corrections can be applied to cavity emission, however, if the optical constants (absorption and scattering coefficients) are determined. A tedious iterative data reduction procedure would be required.

Translucency imposes another restriction to the temperature measurement system by the radiative redistribution of gradients. This effect is basically due to an alteration of the ratio of radiation to overall (radiation plus lattice) thermal conductivity near the surface. A temperature gradient different from that calculated using the present "opaque" heat transfer analysis results. The effect can be defined mathematically, and has been discussed at some length by Klein (ref. 2). If the optical constants of the material are measured, the magnitude of the redistribution can be determined. An iterative analysis is again implied to include this effect in data reduction. In present results redistribution was calculated

to raise surface temperature approximately 30° F at the worst condition (maximum temperature). A scattering coefficient from room temperature data and an absorption coefficient inferred from the measured thickness required for opacity at melting were employed in this calculation.

Detection System

A special Leeds & Northrup model 8891–C–S Rayotube pyrometer was used to detect total radiation. The sensing element is a single-junction chromel,constantan thermopile, blackened for high and uniform spectral absorptance, and thermally shunted to allow for ambient temperature compensation up to 350° F. Energy is focused on the thermopile through a system of two front-surfaced spherical mirrors and a diaphragm after passing through a calcium-fluoride window. This instrument was focused for a window-to-target distance of 12 inches, and the diaphragm was designed to allow a ⅛-inch-diameter area to be viewed. The entire unit is sealed to achieve a stable calibration, and, as reported by the manufacturer, a long-term stability with a degradation in radiation temperature on the order of 2° F in 10 years can be expected. The thermopile response time is 0.6 sec. Output was recorded on a Leeds & Northrup Speedomax–G single-pen strip-chart amplifier-recorder with a response time of 1.0 sec. The Rayotube was mounted in a water-cooled conical viewing tube to avoid excessive heating. The tube was made from brass, wrapped with copper cooling coils, and painted flat black on the inside to avoid stray radiation.

A blackbody calibration curve was supplied with the Rayotube. The instrument was adjusted for an output of 4 mv at 5000° F by moving an attenuating arm across the window. The blackbody calibration was accomplished at 2700° F by the application of a predetermined variation of output with temperature. This temperature variation of output was established from a knowledge of the spectral selectivity of the optical components of the Rayotube and experimental results up to 3500° F obtained on a similar instrument at Leeds & Northrup and the National Bureau of Standards.

Reflection of Plasma Radiation

Flux emitted by the plasma torch had to be considered since it was, in part, reflected from the specimen and added to that emitted by the specimen. Measurements were made to isolate reflected energy, and these quantities were subtracted from total observed energy in calculating emittance. It was found that plasma radiation is strong at the optical pyrometer wavelength. Reflected energy from the zirconia specimen at this wavelength varied from very much larger than emitted energy below 2000° F to about 80% of emitted energy at 3000° F, and 10% at the melting point. Total plasma radiation reflected from the specimen was much smaller compared to specimen emission. Total reflected energy varied from 3 5% of emitted energy below 2000° F to 1.5 3% of emitted energy above 2000° F.

The plasma torch emits energy from two sources the hot rear electrode and the heated gases. The tungsten rear electrode is located at the back of the cylindrical nozzle exit flow passage and operates at a temperature near melting. The plasma flame itself emits detectable flux. At a head-on view (flame plus electrode radiation) a brightness temperature of 6675° F was measured by using a special high-temperature filter for the optical pyrometer, and a radiation temperature of 5800° F was measured with a water-cooled polished copper mirror. At a side view of the flame, brightness temperatures of about 3600° F at the nozzle exit plane and 2730° F at the tip of the hot zone (about 1 inch from the exit) were measured. Similar radiation temperatures were about 2000° F at the exit plane and 400° F at the hot-zone tip.

Several procedures were used in calibrating reflected plasma radiation. Irradiating intensity was determined both analytically and experimentally. Measurements of reflected intensity were made to account for nondiffuseness of energy reflected from the specimen. Figures 47–6 and –7 show the various quantities determined.

Spectral and total irradiance were calculated by using plasma torch brightness and total radiation temperatures and assuming complete nozzle filling. Dashed curves, appearing as

straight lines on the log-log plots, display these results. Irradiance was measured by employing diffuse reflectors. Both a magnesium carbonate block and a water-cooled polished copper plate smoked with magnesium oxide were placed in the specimen position, and reflected energy was observed with the Rayotube and optical pyrometer. Reflections from the magnesium carbonate are not shown in figure 47–7 as this material overheated prior to the detection of any reflected total radiation.

Reflected flux from the specimen was evaluated by direct measurement with a movable water-cooled shutter, and indirectly by comparing the difference in specimen front face and rear face true minus brightness temperatures. The movable shutter allowed a curve of reflected energy versus torch-to-specimen distance to be determined at distances where specimen heating occurred. By first measuring specimen emission plus reflection, then inserting the shutter between the torch and specimen, and measuring emission alone, an increment in energy due to reflection could be observed. By a procedure of presetting the optical pyrometer, fair accuracy could be achieved until extremely rapid specimen cooling was encountered. At distances where rapid cooling occurred, the direction of error placed measured values of reflected intensity too high. Due to the slow Rayotube response, its usefulness was limited in this determination. In addition to the reflected energy points, limited data obtained with flame-sprayed zirconia on a water-cooled copper plate is presented in figure 47–7. Spectral reflected intensity calculated from the difference between true minus brightness temperatures is shown as a dashed curve. The configuration of zirconia bricks surrounding the specimen rear face caused a slight cavity effect, producing a value for reflected plasma radiation which was too low. The solid curve, used in correcting emittance data, was estimated between these measured extremes of spectral radiation. The same relationship between reflected intensity and calculated plasma emission was assigned total energy as was determined for spectral energy in areas where total reflected energy could not be measured.

The magnitude of the reflected energy compared to irradiance indicated that a small

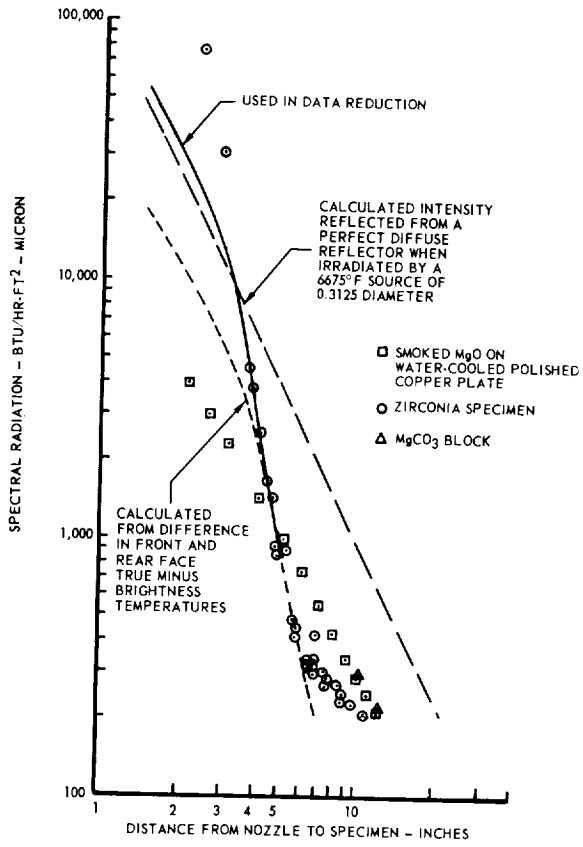

FIGURE 47–6.—Reflected spectral radiation due to plasma emission.

specular component of reflected plasma radiation existed at elevated temperature with the zirconia specimen. A further indication that the specular component existed was an observed angular dependence of brightness temperature of about 40° F at 3700° F. From a knowledge of plasma irradiance and by assuming that zirconia approximates a diffuse emitter, a specular component of reflectance of 0.002 due to the angular dependence was calculated. The energy involved in this specular component is of the same order of magnitude as that of the specular component inferred by the calibration procedure.

Discussion of Errors

Errors can be grouped into basically three classifications for the present experimental system: temperature measurement inaccuracies, errors in the detection of radiant energy, and uncertainties in the calibration of reflected plasma radiation. An overall accuracy can

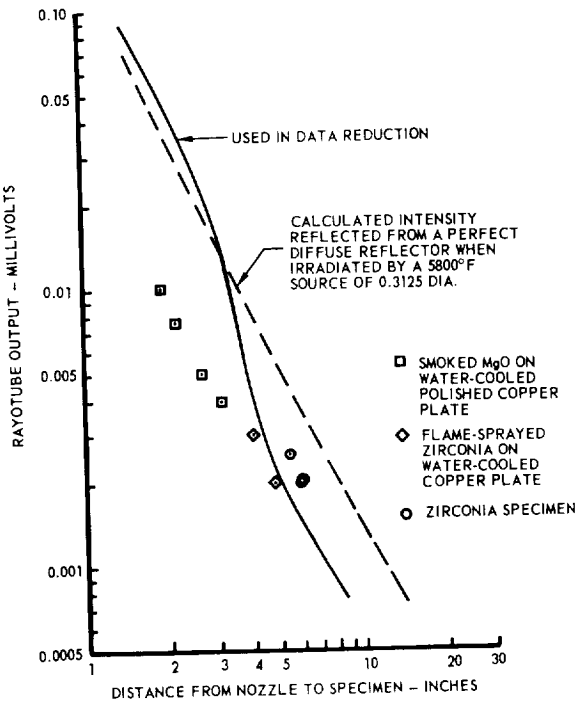

FIGURE 47-7.—Reflected total radiation due to plasma emission.

only be estimated from a consideration of error sources since no absolute high-temperature values of total emittance of translucent materials exist.

TEMPERATURE MEASUREMENT

Contributing errors were those in the optical pyrometer readings, those present in corrections applied to optical values, and those due to approximations and uncertainties in the calculation of temperature distribution.

Sources of error in optical pyrometer readings included instrument calibration, human error, high-frequency fluctuations in the plasma torch, and long-period decay of temperature. Human, fluctuation, and decay errors were minimized by repeated readings during runs. It is estimated that the overall error in optical values read at 4000° F is ±30° F for the cavities, and ±35° F for the faces.

Corrections were applied to optical readings for nonisothermal cavities (conservatively calculated using an incremental analysis), and for plasma reflections from the front face. Corrections were not applied to account for a nonisothermal emitting volume in cavities, and for a small cavity effect on observed rear face optical temperatures due to surrounding brick supports. Including the errors in these corrections, or lack of corrections, it is estimated that face brightness temperatures were measured to ±65° F, and absolute cavity temperature to ±40° F, both at 4000° F.

The calculation of true temperature from the measured temperatures presented the largest source of error, and included several contributing factors. Uncertainties in the temperature variation of thermal conductivity contributed an error proportional to the temperature gradients in the specimen. The use of finite-sized increments in the heat transfer analysis resulted in an error believed to be small. The measurement of actual specimen dimensions contributed a source of error. A small error exists in present results due to the difference in subsurface gradients at the various surface locations measured optically during profile surveys, and the subsurface gradient at the point of spectral emittance measurement. (This affects the accuracy of the true temperature profile obtained when correcting brightness temperatures for emittance). Uncertainties in the knowledge of spectral emittance slightly affected the results. An error proportional to cavity size and axial temperature gradient existed due to an uncertainty in the exact location that was characteristic of the temperature measured in the cavities. Present results also neglected the radiant redistribution of temperature near the surface, incurring an error proportional to the specimen temperature gradient and the ratio of radiation to lattice conductivity As stated previously, this effect probably contributed an error of less than 30° F. In present results, the overall error in surface temperature measurement at 4000° F is estimated to be within ±120° F. A melting point of 4740° F measured on calcia-stabilized zirconia during checkout indicates a better accuracy when compared to reported data on essentially the same composition. Duwez, Odell, and Brown (ref. 3) reported a value of 4710° F, while Yavorsky [1] reported a value of somewhat above 4800° F.

[1] Personal communication from P. J. Yavorsky, Zirconium Corp. of America, Solon, Ohio, Nov. 1961.

Detection of Radiant Energy

The detector viewed a projected specimen area of elliptical shape with a major axis of 0.174 inch. The error due to temperature gradients across the viewed area was calculated to be less than $\pm 0.5\%$.

The Leeds & Northrup Research Division conducted a special error analysis for the Rayotube used and estimate a calibration accuracy of $\pm 3\%$ at 4000° F. At the conclusion of present tests, the calibration curve was verified at Vought by using a blackbody below 2500° F. Spectral selectivity of the detector optical components produces negligible error at 4000° F, while at lower temperatures it must be considered. (At 1800° F, approximately 5% of the blackbody radiation falls outside the window transmission band.)

Other inaccuracies were due to high-frequency plasma fluctuations, recorder errors, and reading errors. These are estimated to not exceed $\pm 1.5\%$, resulting in an overall detection accuracy within $\pm 5\%$ at 4000° F.

Plasma Reflections

Uncertainties in the calibration of energy emitted by the plasma and reflected from the specimen caused errors in the correction of optical readings, and in the measurement of spectral and total emission.

Contributing factors to errors in the calibration are plasma fluctuations and irreproducibility, measurement of distance to the specimen, and human error (especially in reaction time). Human error is by far the greatest. The magnitude of the spectral reflection error is estimated to be within $\pm 7\%$ of spectral emission, and total reflection error within $\pm 1\%$ of total emission, all at 4000° F.

Overall Accuracy

At 4000° F, the estimated error of the mean total emittance curve is $\pm 15\%$, and the spectral emittance curve $\pm 20\%$, both for the condition of equal face temperatures. At lower temperatures, errors in total emittance are reduced, and errors in spectral emittance are increased (due to plasma reflections).

RESULTS

Data reported are for the Zirconium Corporation of America (Zircoa) Y–542 formulation of zirconia. According to Zircoa analysis, this material is 97.1% zirconia and 2.17% calcia. It is a mixture of 70% fines of 10-μ top particle size and 30% fused grog of 48–mesh top particle size, pressed with Methocel and Dextrine organic binders at 5000 psia and fired at 3250° F. The end product has an apparent density of 290 lb/ft^3 and an apparent porosity (open pores) of 18.6%.

Figure 47–8 shows total emittance results. A gradual increase in emittance with temperature above 2000° F is exhibited, and measured values are lower for runs with a cooler specimen subsurface. Both the expected increase in the absorption coefficient and decrease in the scattering coefficient predict this observed increase in emittance. The measurably lower emittance for the cooler subsurface is consistent with the thickness required for opacity of this zirconia formulation. Of additional interest, the effect of surface roughness over the range 100 to 400 microinches rms was not measurable. These roughness values would not be expected to greatly affect emittance, as the size of the irregularities is fairly small compared to the depth required for opacity.

A permanent increase in emittance was observed on a specimen whose surface was partially vitrified by an excursion to 4650° F–4700° F. A closing of pores by vitrification, reducing scattering, would be expected to produce this increase. (Scattering is detrimental to emittance, as it increases attenuation but does not contribute to emission.) Cycling below the temperature of rapid vitrification did not measurably alter emittance.

Figure 47–9 shows spectral emittance results which follow a pattern similar to total emittance. Data below 3000° F are not presented due to large errors at lower temperature in the spectral plasma reflection calibration.

RECOMMENDATIONS FOR EXTENDING USEFULNESS

Several refinements can be incorporated in the present experimental approach to improve accuracy and reduce uncertainties. These refinements would then justify more sophisticated analytical techniques, allowing the optical constants to be inferred. With a knowledge of optical constants, the radiative transfer equations can be applied to calculate emittance under any set of boundary conditions. In

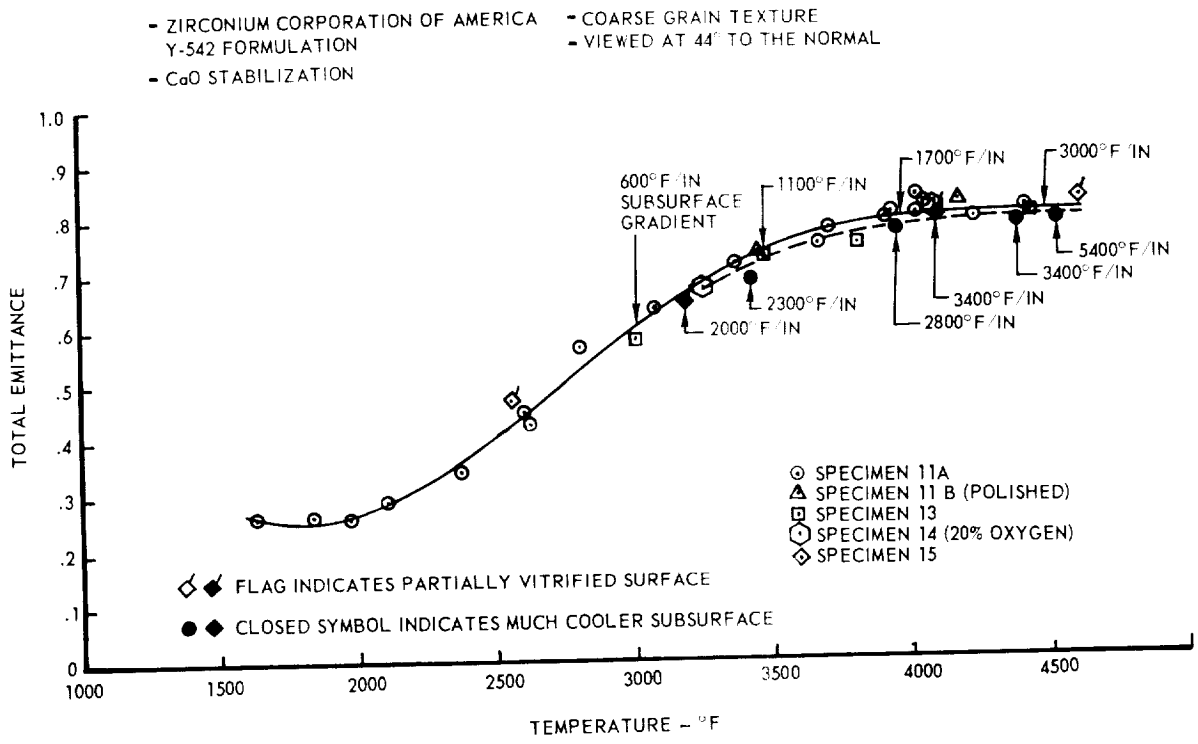

FIGURE 47-8.—Total emittance of zirconia.

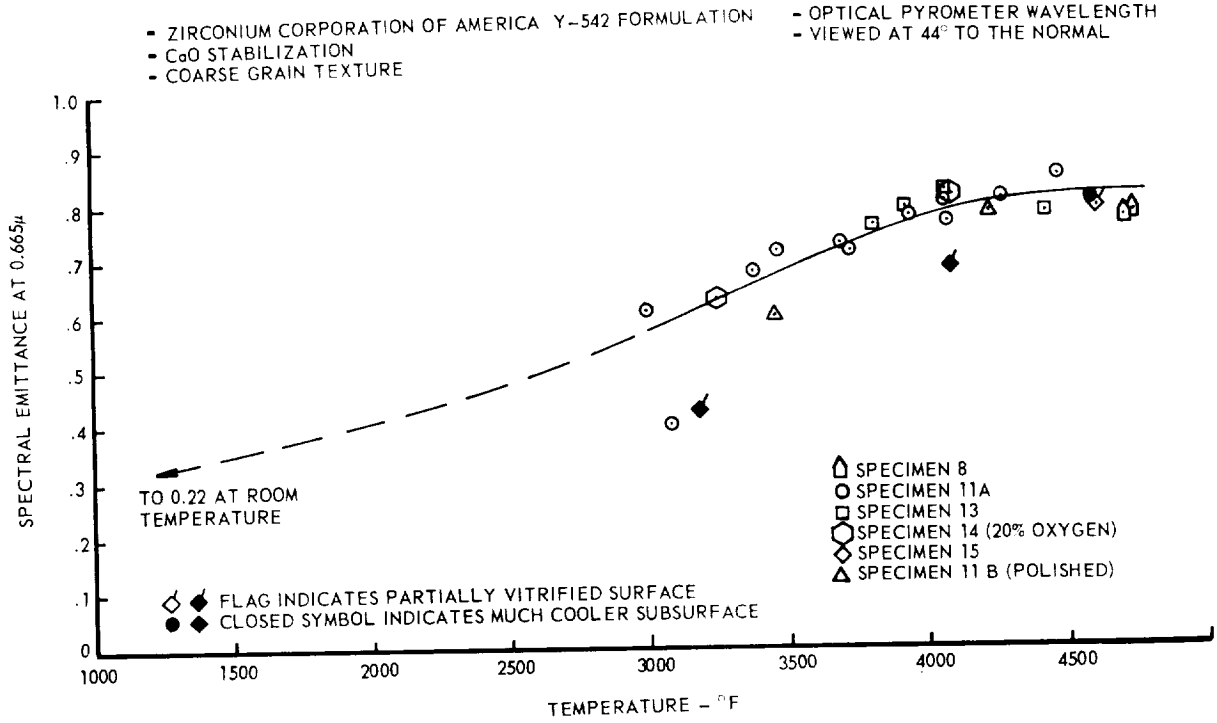

FIGURE 47-9.—Spectral emittance of zirconia.

addition, the possibility of extending the approach to also measure thermal conductivity is mentioned since this would render the technique completely self-sufficient.

Experimental Refinements

Temperature measurement accuracy can be improved by using smaller diameter blackbody cavities and employing a microoptical pyrometer, thus precisely defining the location of measured internal temperatures and eliminating the need for any correction for nonisothermal cavity walls. A further improvement in temperature measurement accuracy can be obtained by producing a more nearly linear axial temperature gradient in the specimen. Incorporation of a larger-diameter plasma flame would achieve this effect. Uncertainties due to plasma reflections can be completely eliminated by designing a system of rotating shutters to provide alternate heating and viewing of the specimen. A transient analysis shows that a seven-bladed water-cooled shutter about 10 inches in diameter and rotating at 6000 rpm in the plasma flame will reduce cooling during viewing to an acceptable level. Sectored disks placed in the Rayotube and optical pyrometer viewing paths and rotating synchronously with the plasma shutter would allow viewing while plasma heating is blocked, thus eliminating reflected radiation. Measured energy would be merely attenuated since the human eye and Rayotube response rates are significantly below the resultant 700-cps pulse rate.

An improvement in the accuracy of total radiation detection can be achieved by a more complete blackbody calibration. This should be accomplished with the rotating shutter in place. Due to the attenuation by the shutter, a higher thermopile output will be needed at the lower temperatures. This can be accomplished with a second instrument with a larger target area, used below about 3000° F where the front face gradients are less severe. The above incorporation of a larger plasma nozzle will reduce these gradients.

A somewhat thinner specimen can be used with the smaller blackbody cavities. This will provide a wider range of axial temperature gradients, allowing the effect of subsurface emission to be more precisely determined.

Analytical Refinements

With more precise inputs of raw experimental data, the calculation of the radiant redistribution of specimen temperature can be accomplished with sufficient accuracy to warrant its inclusion in data reduction. This would involve the inference of the optical constants (absorption and scattering coefficients) with the radiative transfer equations.

Hamaker (ref. 4) defined emission from a light-scattering material mathematically in terms of its scattering coefficient, absorption coefficient, and temperature distribution. Then if total emission at a given surface temperature can be measured under two known conditions of subsurface temperature distribution, sufficient information is provided to infer the two unknown coefficients. Probably the most practical analytical procedure to employ would be first, the calculated "opaque" specimen temperature distributions, would be used to determine the absorption coefficient and scattering coefficient values that produce the measured increment in emission. Next, these coefficients would be used to calculate a radiant redistribution of the gradients, and a new set of coefficients would be determined from the new temperature distribution. This technique would be repeated until the solution converged. In materials similar to the present zirconia formulation, where the radiative redistribution is small, such an iterative process should converge fairly rapidly.

Any errors in the specimen external temperature profile due to variations in the subsurface temperature distribution can be corrected for, if warranted, by an extra step in the iterative procedure to determine the optical constants. Errors due to the choice of increment size in the finite-difference heat transfer analysis can be eliminated by a series of calculations to select the maximum allowable increment size.

Measurement of Thermal Conductivity

Slight modification to the existing experimental technique can also allow thermal conductivity to be determined. By using rear face heating only, energy crossing the front face is then due entirely to heat conducted through the specimen. This energy transfer rate can be determined from a measurement

of total emission using a thermopile, and a calculation of convection losses (which are relatively small) from established heat-transfer coefficients. The heat flow paths through the specimen would be defined, as before, by a finite-difference heat transfer analysis using a measured external temperature profile. It would be necessary now, however, to first neglect the temperature variation of thermal conductivity through the specimen. After determinations at several temperature levels, a curve of conductivity versus temperature would be indicated, and values from this curve could be used to recalculate conductivity. The process would be repeated until further calculation did not alter results.

An order-of-magnitude determination of conductivity of zirconia using this method, but only estimating the specimen axial temperature distribution, yielded values in fair agreement with independently determined data on the same material.

REFERENCES

1. Schneider, P. J.: Conduction Heat Transfer. Addison-Wesley Publishing Company, Inc., Reading, Mass., 1955.
2. Klein, J. D.: Radiation Heat Transfer to and From Ceramic Coatings on Metals, Am. Ceram. Soc. Bull., 40, No. 6, June 1961, pp. 366–370.
3. Duwez, P.; Odell, F.; and Brown, F. H., Jr.: Stabilization of Zirconia with Calcia and Magnesia. J. Am. Ceram. Soc., 35, No. 5, 1952, pp. 107–113.
4. Hamaker, H. C.: Radiation and Heat Conduction in Light-Scattering Material, Parts I–IV, Philips Res. Rep., 2 (1947), pp. 55–67, 103–111, 112–125, 420–425.

DISCUSSION

Moore, NBS: I am a bit concerned about your temperature coefficient. As you know, most of these ceramic oxides have spectral curves that start out low at the low wavelengths and then gradually come up to high values as the wavelengths increase. This tends to give a negative temperature coefficient for the total normal emittance. You find a positive temperature coefficient for zirconia. Of course, your temperatures do not go down too far, and I grant you that there are no spectral data on any of the oxides at very high temperatures. But it does make me wonder because the positive temperature coefficient is really not what I would expect.

Cox: I am glad you asked that. We demonstrated at low temperatures a negative coefficient which is in agreement with other reported data. At high temperatures the energy is in the wavelength bands where existing low-temperature spectral emittance data show low emittance values. There are some theoretical reasons why you would expect the spectral emittance at these wavelengths to increase with temperature. These are based on two factors: there is evidence that as temperature increases absorption bands broaden, and, also, electromagnetic theory predicts that in regions remote from the absorption bands the index of refraction decreases with temperature. Both of these would produce an increase in spectral emittance with temperature at the wavelengths of interest. Olson and Morris in their work at Armour Research Foundation demonstrated an increasing spectral emittance with temperature at the optical pyrometer wavelength at moderate temperatures. I believe another paper on this program also shows an increasing spectral emittance at higher temperature So, if the spectral emittance is increasing in these bands, total emittance would also be expected to increase.

Dr. Riethof: I was sort of agreeing with you up to the last sentence. I agree that you will get an increase in spectral emittance but I do not think this in any sense necessarily implies that the total emittance will go up. You are still shifting a tremendous fraction of your energy into the shorter wavelength where, true, spectral emittance goes up, but the spectral emittance there is still less than it is at long wavelengths.

Cox: In the temperature regions we are talking about, the bulk of the total energy is concentrated around approximately 1 μ; in these bands you would expect to have a correlation with the spectral emittance curves mentioned. Our high-temperature total emittance results are of comparable magnitude to our present spectral emittance results, and to the previously mentioned spectral emittance results of other investigators.

In summary, the negative coefficient below 2000° F results from the shifting of total energy from wavelength regions of high spectral emittance to those of low spectral emittance. Here the emittance decrease with wavelength dominates over the monochromatic emittance increase with temperature. Above 2000° F, the energy still shifts, but remains within the wavelength bounds of what was a spectral emittance valley. As the monochromatic emittance in this valley continues to rise, total emittance also increases.

Metcalf, Solar Aircraft: Is it not a fact that you are getting radiation emitted from greater depths of the material at high temperatures, because of the increased transparency? May I ask a supplementary

question? I wonder whether this is a factor in the interpretation of the shallow-hole experiments, in that the difference of temperature may not be between the surface and the bottom of the hole, but should take into account the effects of transparency.

Cox: In answer to your first question, some data exist as to the change in transparency or translucency with temperature. We have generated a little bit, and some have been generated by Dr. Klein. At low temperature or room temperature, some of the measured data indicate the depth required for opacity to be on the order of 0.1–0.2 inch on this material in the visible and near infrared. We did some work at melting temperature; the results are shown in figure 47–10. The data are rather crude, but might shed some light on this question.

The data in this figure were obtained on various thicknesses of zirconia disks. These disks were melted and total radiation was detected at melting, and you can see that we did measure in a somewhat crude fashion a dependency of emission at melting on thickness. Now this might lead you to estimate that a depth of about 0.05 inch is required for opacity at melting, which does not seem unreasonable, based on the room-temperature data. You would expect, due to the changes in the scattering and absorption coefficients, some change in opacity with temperature, but it is hard to make quantitative predictions.

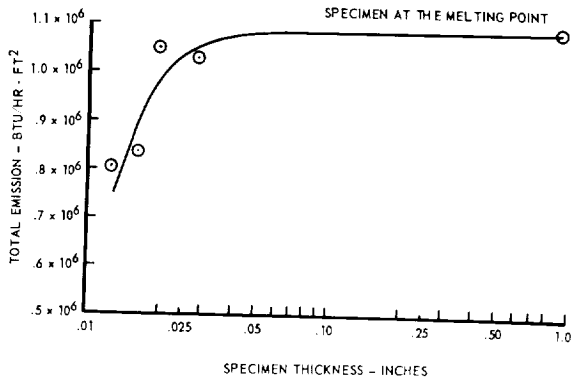

FIGURE 47–10.—Effect of specimen thickness on total emission.

I will comment on the second question, whether this affects the shallow-hole technique. I think it will affect it if the translucency of the particular material under test is appreciable. I believe it will affect the validity of the analysis as to the effective emittance of the cavity. Also, it will affect the results because the emission is no longer uniquely from the surface.

48—A VERY RAPID 3000° F TECHNIQUE FOR MEASURING EMITTANCE OF OPAQUE SOLID MATERIALS

BY R. J. EVANS, W. A. CLAYTON, AND M. FRIES

THE BOEING COMPANY, SEATTLE, WASHINGTON

This paper presents a rapid, total normal emittance measurement technique useful for comparative tests. The heat source is a 10-kw tungsten-filament lamp whose energy is focused on the specimens with two 36-inch parabolic mirrors. The method described is useful between 1000°–3000° F with all tests conducted in air. Accuracy depends on surface temperature measurements, with an accuracy of +5% and −10% when the thermocouples are used and an accuracy which depends on the deviation of the specimen from a gray body when an optical pyrometer is used.

INTRODUCTION

The radiative efficiency of any specimen may be controlled by its chemical stability in the environment to which it is exposed. For engineering applications it is quite necessary to know the magnitude of change in radiative efficiency with time at temperature in a given atmosphere. It is often necessary to screen a multitude of specimens to obtain the most efficient radiator for a particular environment. This paper presents a very rapid technique for emittance screening and for measurement of emittance changes vs. times in an atmosphere uncontaminated by the heat source.

EQUIPMENT AND MEASUREMENT TECHNIQUE

The equipment consists basically of a heat source, temperature-sensing device, and thermal radiation detector. Energy from a 10-kw General Electric G96K lamp located at the focal zone of a 36-inch parabolic reflector is collimated onto a second 36-inch reflector located in optical alignment with the source mirror. This energy is then focused on the back of the test specimen located at the focal zone of the second mirror. To increase the energy received at the test specimen, approximately one half of the lamp envelope located on the side opposite the source mirror is silvered. With this arrangement, thermal fluxes up to 75 Btu/ft^2-sec on a 1-inch square area can be obtained.

Figure 48–1 is a schematic, and figure 48–2 is a photograph of the test apparatus. The thermal flux from the lamp is controlled by a venetian-blind-type louver system and by a step-wise voltage control in the lamp circuit.

The specimens can be any configuration between ¾- x ¾-inch and 1- x 1½-inch. This method, utilizing standard available lamps, is capable of heating the cold face of thin metals (to 75 mils) to 3000° F and opaque ceramics and/or non-conductors (to ⅛-inch thick) to 2700° F, depending on the absorption characteristics of the body for the lamp radiation. With this heat source and these specimens, equilibrium is quickly reached, within 2–3 min, at any temperature.

The specimens are mounted in holders cut from commercially-available aluminum-silicate insulating board (Fiberfrax). These holders serve to insulate the specimen from the metal mounting, and minimize thermal gradients across the specimen due to conduction losses.

A Brown Instrument Company model RL2 miniature radiamatic radiometer is used to measure the energy emitted from the specimen. This radiometer has a calcium fluoride lens which passes energy between 0.2 and 9.6 μ from a target area ½ inch in diameter at 6 inches from the specimen. It sights on the specimen through a water-colled sighting tube blackened to absorb extraneous radiation. The optical

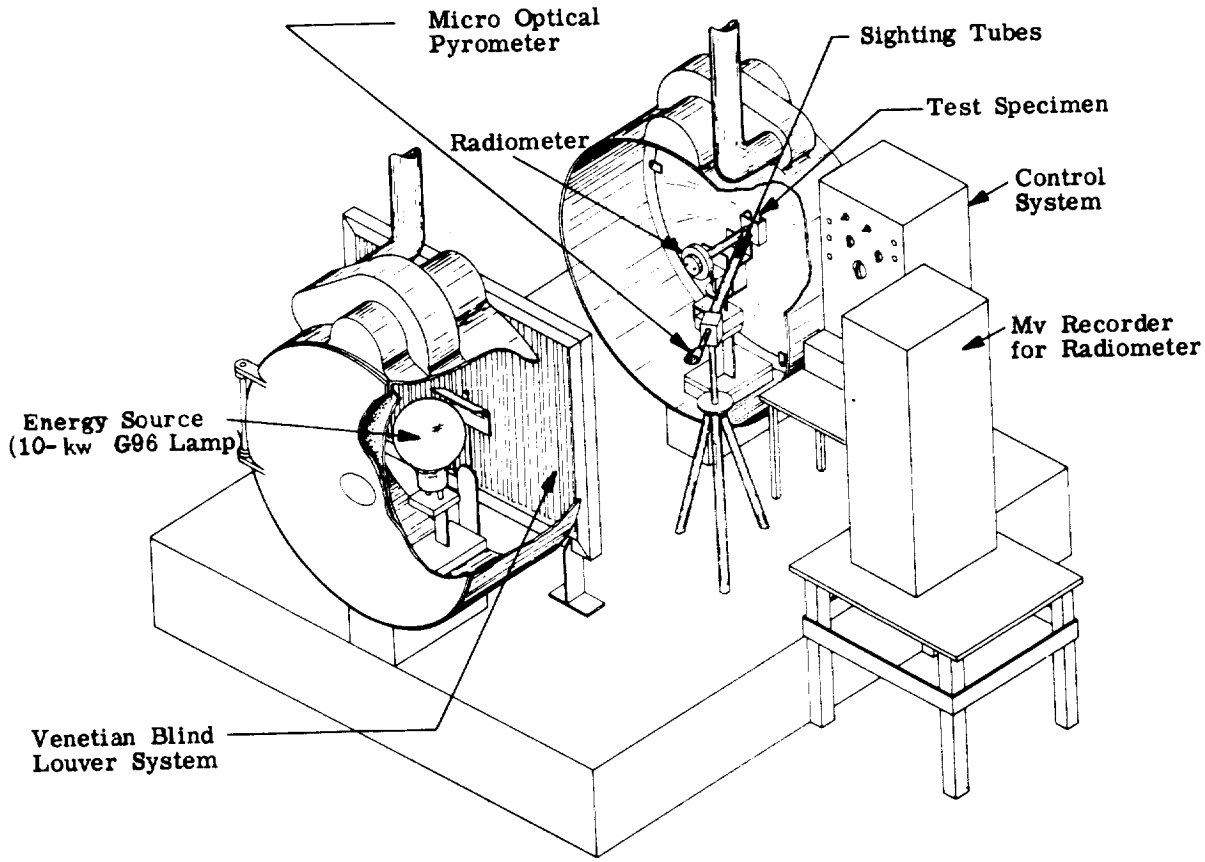

FIGURE 48-1.—Searchlight emittance test apparatus.

pyrometer used for measuring temperature is a model 95 pyro-micro-optical pyrometer with a sighting area just slightly smaller than that of the radiometer. If thermocouples can be attached, 2.5-mil platinum-platinum–13% rhodium wires are used so that conduction losses along the wire are minimized. Thermocouples are spotwelded to the surface of the specimen in the middle of the radiometer target area.

Two readings are required to calculate emittance from the following relationship which is derived from the Stefan-Boltzmann total radiation equation.

$$\epsilon_{TN}=\frac{T_a^4}{T_t^4} \tag{1}$$

where T_a output of radiometer converted to an apparent blackbody temperature, obtained from the radiometer blackbody calibration

T_t true specimen temperature.

True temperature is measured directly for materials to which thermocouples can be attached. If they cannot be attached, as on ceramics and coated refractory alloys, an optical pyrometer reading must be used with the radiometer reading to calculate both the emittance and true temperature by the method outlined below.

An optical pyrometer, which passes only radiation in a narrow band around 0.665 μ, reads a brightness temperature lower than true for any radiator less efficient than a blackbody. The true and brightness temperatures are related by the expression:

$$\frac{1}{T_t}-\frac{1}{T_b}=\frac{\lambda \ln \epsilon_\lambda}{C_2} \tag{2}$$

where:

T_t true temperature, ° R

T_b brightness temperature, °R

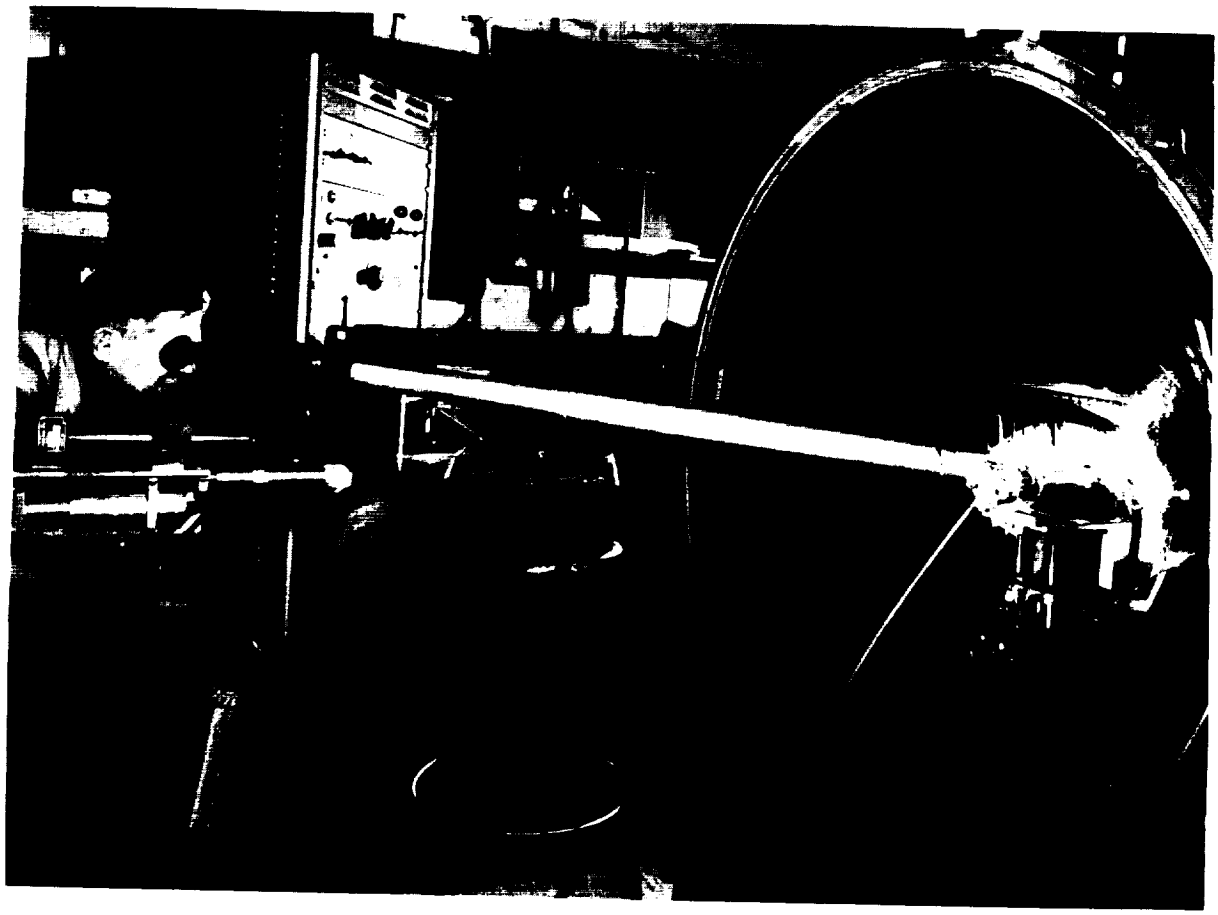

FIGURE 48-2.—Searchlight facility, 36-inch.

λ Mean effective wavelength of the optical pyrometer (0.665 μ for red filter)
C_2 second radiation constant=25,896 μ-°R
ϵ_λ spectral emittance at 0.665 microns

Then the emittance and true temperature of a specimen can be calculated by assuming a gray-body, $\epsilon_{TN}=\epsilon_{0.665}$, and solving equations (1) and (2) for ϵ_{TN} and T_t. This solution can be found by a method of successive approximations which for a large number of calculations is eliminated by construction of a working nomograph. The solution given by the nomograph in figure 48-3 represents the emittance value which will approximately satisfy the two equations. The accuracy of the nomograph is better than 0.01 on the emittance value. The radiometer is calibrated against a blackbody reference groove, in this case a 6:1 depth to radius blackbody cavity. The micro-optical pyrometer is calibrated against an NBS certified Leeds and Northrup optical pyrometer and an NBS standard lamp.

ERROR ANALYSIS

The errors in measuring emittance arise from the following sources:

1. Error in apparent total radiation temperature due to uncertainty in radiometer calibration. This has been determined to have $\pm\frac{1}{2}\%$ uncertainty or a total of $\pm 2\%$ on the final emittance calculation for calibrations obtained from the blackbody in the Boeing thermal radiation test facility.
2. Error caused by reflected energy which is emitted from the specimen other than normal to the target area and is diffusely reflected from the sighting tube back to the target area and to the radiometer. Calculations show this to be a maximum

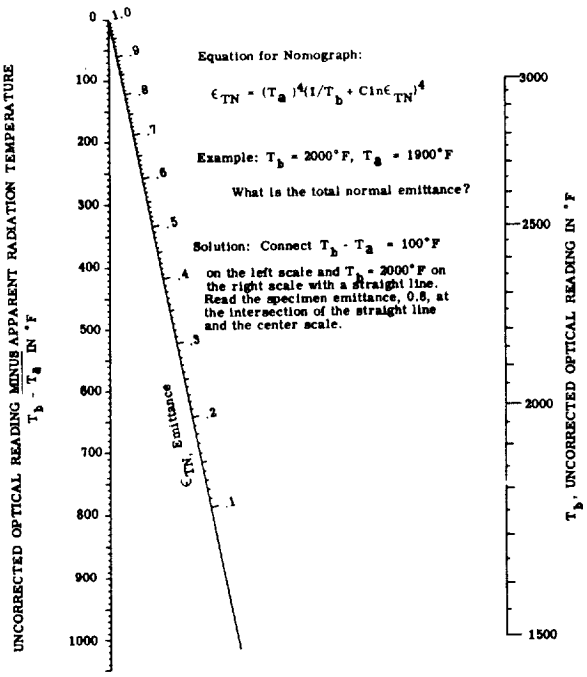

FIGURE 48-3.—Nomograph for calculation of total normal emittance (from optical and total radiation pyrometer readings).

of +1% for a distance of ¼ inch between the specimen and the sighting tube.

3. Error caused by ±½% uncertainty in the optical pyrometer reading; the acknowledged accuracy of this instrument. Boeing optical pyrometers consistently show less than ½% error when compared to NBS standard lamps. Because of the simultaneous solution required for equations (1) and (2), this error ranges from ±3.5% at 2800° F to ±2.5% at 1600° F.
4. Error due to nonisothermal conditions, if they exist, would be of the same magnitude as Error 3.
5. The error caused by using an optical pyrometer and the graybody assumption arises because the spectral emittance at 0.665 μ, the wavelength band pass of the pyrometer, may differ from the total normal emittance. When these two emittance values differ, solving equations (1) and (2) will give a specimen temperature different from true specimen temperature, causing an error in the measured emittance. This error is a function of the ratio of spectral to total normal emittance. Figure 48-4 is a plot of this error as a function of the variables. The appendix includes a development of the error.
6. Error caused by uncertainty in thermocouple measurement. Because of conduction up the wires, thermocouples tend to read lower than true temperature, causing the measured emittance to be higher than true. A total accuracy of +5% −10% on measurements with thermocouples is believed to be realistic for this case.

Figure 48-5 is a plot of data obtained on platinum-13% rhodium and oxidized Inconel X. Each set of data represents 4 or 5 repetitions on the standard over the entire temperature range and was obtained during a calendar month. The data were obtained with an optical pyrometer. All the Inconel X data fall in a band of 0.066 unit, and the platinum-13% rhodium in a band of 0.02 to 0.03 unit. This is quite close to the scatter predicted by the uncertainties assigned to the optical pyrometer readings and the radiometer measurements.

The error due to the graybody assumption is constant for any temperature, so it should not affect scatter. The platinum-13% rhodium

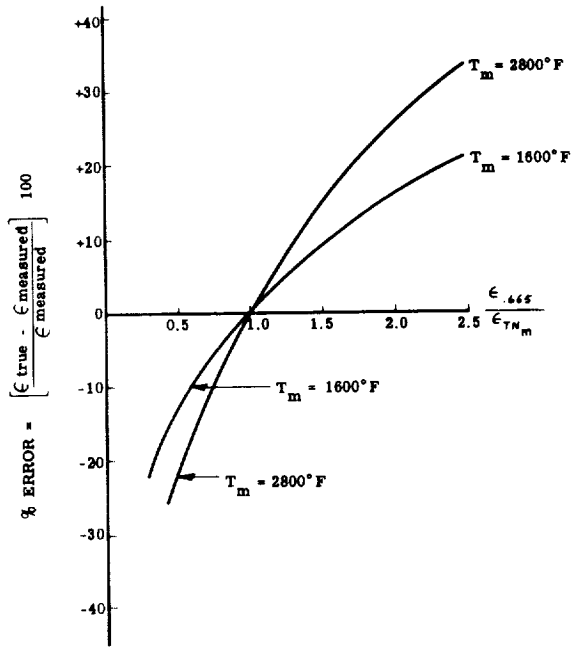

FIGURE 48-4.—Error on emittance from 36-inch searchlight emissometer due to specimen departure from the graybody condition.

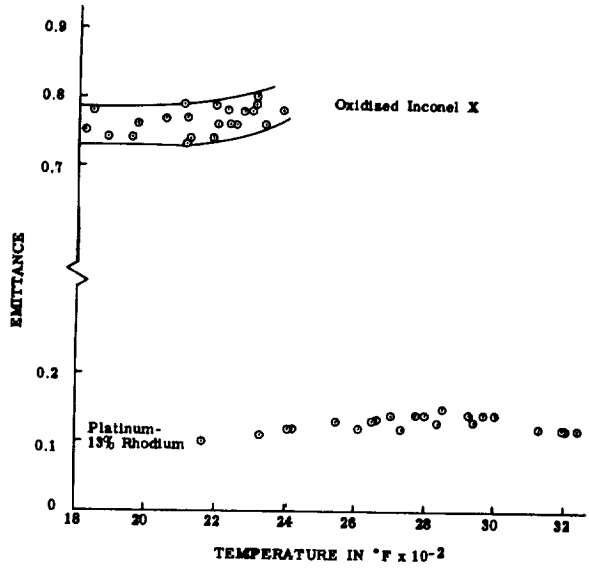

FIGURE 48-5.—Emittance plotted against temperature for oxidized Inconel X and platinum-13% rhodium.

scatter may be slightly exaggerated because the final numbers are always rounded off to the nearest 0.01. It is believed that the Inconel X data represent an upper limit in the scatter band in this emittance range. It includes scatter due to surface changes, which were visually noticeable during the several runs.

CONCLUSIONS

This technique is valuable where a rapid test and good reproducibility are important. The technique is particularly adaptable to programs where a large number of specimens must be evaluated. Small specimen size and simple configuration greatly reduce program costs. The accuracy of the emittance values obtained is comparable to classic techniques which employ the same temperature measurement method; +5%, −10% using thermocouples, and ±10% for most measurements based on optical and total radiation pyrometer readings alone.

APPENDIX—ERROR INVOLVED IN THE GRAYBODY ASSUMPTION WHEN AN OPTICAL PYROMETER IS USED TO MEASURE TEMPERATURE

The two equations involved are:

$$\epsilon_{TN}=\frac{T_a^4}{T_t^4} \tag{1}$$

where

T_a apparent blackbody temperature as determined by the radiometer
T_t true specimen temperature
ϵ_{TN} total normal emittance

$$\frac{1}{T_c}-\frac{1}{T_b}=C \ln \epsilon_{0.665} \tag{2}$$

where

T_c corrected optical pyrometer temperature
T_b brightness or observed optical pyrometer temperature

$$C\frac{0.665}{C_2}=(2.57\times 10^{-5})^\circ R$$

$\epsilon_{0.665}$ spectral emittance at the band pass of the pyrometer, 0.665 μ

If we assume a graybody, we assume

$$\epsilon_{TN}=\epsilon_{0.665}$$

If this assumption is true, the corrected optical temperature in equation (2) is the same as the true specimen temperature. If the assumption is not true then the corrected temperature will not be the true specimen temperature and will be equal to some final calculated temperature defined as T_m.

where

$$\epsilon_{TN_{(t)}}=\frac{T_a^4}{T_t^4} \tag{4}$$

$$\epsilon_{TN_{(m)}}=\frac{T_a^4}{T_m^4} \tag{5}$$

Substituting into the error expression

$$\%\ \text{Error}=\left[\frac{(T_m)^4}{(T_t)^4}-1\right]100 \tag{6}$$

T_t and T_m differ from each other because the assumed spectral emittance (which is also the measured ϵ_{TN}) differs from the true spectral emittance, that is;

$$\frac{1}{T_m}-\frac{1}{T_b}=C \ln \epsilon_{0.665}\ (\text{assumed})=C \ln \epsilon_{TN_{(m)}} \tag{7}$$

and

$$\frac{1}{T_t}-\frac{1}{T_b}=C \ln \epsilon 0.665\ (\text{true}) \tag{8}$$

Subtracting equation (7) from equation (8):

$$\frac{1}{T_t}-\frac{1}{T_m}=C\ln\frac{\epsilon_{0.665}}{\epsilon_{TN_m}} \tag{9}$$

As the ratio of spectral to total emittance increases or decreases from 1.00, the difference in these temperatures increases, thus increasing the difference between measured and true values. A plot of the error as a function of various ratios of $\epsilon_{0.665}/\epsilon_{TN_m}$ for two different temperatures is presented in figure 48–4. For example, if the measured total normal emittance ϵ_{TN_m} of platinum–13% rhodium is 0.15 at 2800° F and the spectral emittance $\epsilon_{0.665}$ is actually 0.3, then the ratio $\epsilon_{0.665}/\epsilon_{TN_m}=2$. From figure 48–4 for $T_m=2800°$ F the error is +25%. This shows that the true emittance is greater than the measured value by this percentage.

49—MEASUREMENT OF NORMAL AND DIRECTIONAL HIGH-TEMPERATURE TOTAL AND SPECTRAL EMITTANCE

BY J. R. GRAMMER AND E. R. STREED

LOCKHEED MISSILES & SPACE COMPANY, PALO ALTO, CALIFORNIA

Apparatus to measure the total hemispherical and directional total and spectral emittance in the temperature range of 400° to 2000° C is described. The device consists of a water-cooled evacuated chamber in which a sample formed into a modified Mendenhall wedge enclosure is heated electrically by its own resistance. The sample can be rotated in azimuth while viewed externally through a double-slit collimating optical system. Total or spectral emittance is determined by comparing emitted radiation from the surface to radiation emitted from the enclosure as detected by a vacuum thermocouple used with or without a monochromator.

The spectral and directional emission characteristics of materials as a function of composition, temperature, and surface condition are becoming increasingly important in space-age technology. The departure of practical, available materials from the ideal blackbody radiator demands that experimental measurements be performed on most materials to determine their optical characteristics. In addition, spectral and/or directional data are needed during material development programs or for vehicle design purposes. High-temperature measurements are best accomplished by radiometric methods. A radiometric method usually implies direct comparison of the radiant flux emitted from the material under investigation to the radiant flux of an ideal radiator, both at identical temperature and with the same measuring instrument field of view.

Advantages of a radiometric system are: (1) measurement of the desired quantity, emittance; (2) sample temperature and vacuum conditions readily achieved during measurement; (3) sample surface condition generally typical of actual available material; and (4) measurements rapidly performed after apparatus has been proven adequate. Some of the problems inherent in direct emittance determinations are: (1) reducing or correcting for background radiation; (2) achieving a blackbody reference source; (3) attaining and maintaining a constant and uniform sample temperature during the measurement period; and (4) design and alignment of identical transfer optical paths for blackbody and sample radiation.

A measure of the departure from Lambert's law (cosine distribution) can be expressed as the ratio of the total hemispherical to the total normal emittance when measured under the same conditions. The theoretical deviation of this ratio has been presented by Jacob (ref. 1) and by Eckert and Drake (ref. 2). The ratio as a function of emittance and deviations obtained from experimental data are shown in figure 49–1. It is the intent of this paper to describe apparatus, procedures, and results pertinent to the obtaining of actual values of spectral, total, hemispherical, and directional emittance in the temperature range of 400° to 2000° C.

NOMENCLATURE

$\epsilon_\phi(\lambda, T)$	directional spectral emittance
$J_\phi(\lambda, T)$	monochromatic power radiated per unit surface area in direction making an angle ϕ with the normal to the surface element of a material at a temperature T
$J_{\phi b}(\lambda, T)$	monochromatic power radiated per unit surface in direction making an angle ϕ with the normal to the surface element of a blackbody of the temperature T

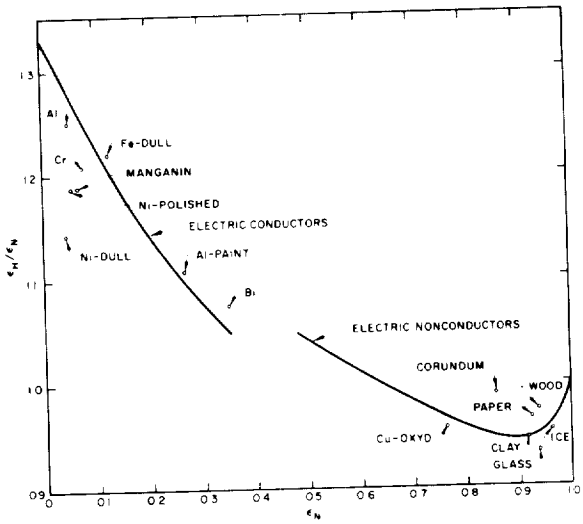

FIGURE 49-1.—Theoretical and experimental values for the ratio of hemispherical to total normal emittance.

$J(\lambda,T)$	monochromatic power radiated per unit surface area of a material at temperature T
T	temperature
λ	wavelength
c_1 and c_2	Planck's radiation constants
v	alternating voltage developed by the detector
k	responsivity (volts/watt) of the detection
P_s	radiant power received by the detector from the source
P_0	radiant power received by the detector from the chopper blade
w	solid angle
h	slit height
t	transmissivity of optical system
σ	Stefan-Boltzmann constant
$\epsilon_\phi(T)$	total directional emittance
$J_\phi(T)$	power radiated per unit surface area and unit solid angle in direction making an angle ϕ with the normal to the surface of a material at a temperature T
$J_{\phi b}(T)$	power radiated per unit surface area and unit solid angle in the direction making an angle ϕ with the normal to the surface of a blackbody at a temperature T
I	current through sample
V	voltage drop across the element in direction of current flow
$\epsilon_H(T)$	total hemispherical emittance
A_s	area of surface
T_s	temperature of surface
T_w	temperature of chamber walls
q_c	thermal conduction loss from radiating element to colder electrodes
l	thickness of window
r_s	reflectance of sample surfaces
K_1	thermal conductivity of sample
ρ	resistivity
x_1	thickness of sample
x_2	thickness of coating
K_2	thermal conductivity of coating
i	current density

METHOD

Direct emittance measurements must be of a directional nature; consequently, the direction at which the sample is viewed and the solid angle viewed must be specified. In general, only simple modifications of a system are required to convert from spectral normal to total normal; therefore, no distinction between the two will be made.

The directional spectral emittance $\epsilon_\phi(\lambda, T)$ is defined as the ratio of $J_\phi(\lambda, T)$, the monochromatic power radiated per unit surface area, unit wavelength interval, and unit solid angle, in the direction making an angle ϕ with the normal to the surface element of a material at a temperature T, to $J_{\phi b}(\lambda, T)$, the monochromatic power radiated per unit surface area, unit wavelength interval, and unit solid angle, in the direction making an angle ϕ with the normal to the surface element of a blackbody at the same temperature T,

$$\epsilon_\phi(\lambda,T)=\frac{J_\phi(\lambda,T)}{J_{\phi b}(\lambda,T)} \tag{1}$$

where

$$J_{\phi b}(\lambda,T)=\frac{J_b(\lambda,T)}{\pi} \tag{2}$$

and by Planck's radiative law

$$J_b(\lambda,T)=\frac{c_1\lambda^{-5}}{e^{c_2/\lambda T}-1}, \tag{3}$$

in units of power per unit wavelength interval and unit surface area, as shown by Bell (ref. 3) and Blau (ref. 4).

The alternating voltage v, developed by the detector of a mechanical chopping radiation measuring system, is proportional to the difference in radiant power (P_s-P_o) received by the detector when it views first the source and then the chopper blade,

$$v=k(P_s-P_o) \tag{4}$$

where k is the responsivity (volts/watt) of the detector.

The radiant power incident on the detector from a source at a temperature T is given by

$$P_s=J_\phi(\lambda,T)whst\Delta\lambda \tag{5}$$

where w is the solid angle, h is the slit height, s is the slit width, t is the transmissivity of the optical system, $\Delta\lambda$ is the wavelength interval, and $J_\phi(\lambda, T)$ is the spectral emissive power of the source. Combining equations (4) and (5) gives

$$v=[J_\phi(\lambda,T)-J_{o\phi}(\lambda,T)]kwhst\Delta\lambda \quad (6)$$

where $J_{o\phi}(\lambda, T)$ is the spectral emissive power of the chopper blade. For source temperatures above about 400° C, $J \gg J_o$, and thus

$$v=J_\phi(\lambda,T)kwhst\Delta\lambda \quad (7)$$

if v_s is the voltage response of the system to sample radiation and v_b is the response to blackbody radiation.

$$\frac{v_s}{v_b}=\frac{J_\phi(\lambda,T)}{J_{\phi b}(\lambda,T)}=\epsilon_\phi(\lambda,T) \quad (8)$$

The spectral emittance from 1 to 15μ has been determined by a similar method for temperatures above approximately 400° C by Richmond (ref. 5) by matching the sample and blackbody temperatures and measuring the ratio of the emitted radiation with a double-beam spectrophotometer. A variation of this method was devised by Weber (ref. 6) to obtain normal spectral data at sample temperatures approaching room conditions.

Similarly, the directional total emittance can be expressed as

$$\epsilon_\phi(T)=\frac{J_\phi(T)}{J_{\phi b}(T)} \quad (9)$$

where

$$J_{\phi b}(T)=\frac{J_b(T)}{\pi}$$

and by Stefan's law

$$J_b(T)=\sigma T^4 \quad (10)$$

and accordingly,

$$\frac{v_s}{v_b}=\frac{J_\phi(T)}{J_{\phi b}(T)}=\epsilon_\phi(T) \quad (11)$$

Somewhat lower sample temperatures can be utilized for total energy measurements.

The total hemispherical emittance $\epsilon_H(T)$ is defined as the ratio of $J_H(T)$, the power radiated per unit surface area into a hemisphere by a material at a temperature T, to $J_b(T)$, the power radiated per unit surface area into a hemisphere by a blackbody at the same temperature T, or

$$\epsilon_H(T)=\frac{J_H(T)}{J_b(T)} \quad (12)$$

A steady-state power technique of measuring $\epsilon_H(T)$ of electrical conductors has been described by Worthing and Halliday (ref. 7) and also by Abbott, Alvares, and Parker (ref. 8). The value $\epsilon_H(T)$ is determined from the equilibrium temperature of the sample with a known electrical power input in a vacuum environment to an enclosure temperature different from its own. Assuming that the current density is isotropic through the sample, then the heat generated per unit cross section of volume element is given by

$$Q=IV$$

where I is the current through the sample, and V is the voltage drop across the element in the direction of flow of the current. In the steady-state condition, the heat energy generated per volume element must equal the heat radiated by the surface of that volume element plus that which is conducted away from the element, or

$$\epsilon_H(T)A_s\sigma T_s^4+q_c=IV+\alpha_H(T)A_s\sigma T_w^4 \quad (13)$$

$\epsilon_H(T)$ total hemispherical emittance of surface
A_s area of surface under consideration
σ Stefan-Boltzmann constant
T_s temperature of surface
T_w temperature of chamber walls
q_c thermal conduction loss from radiating element to colder electrodes
$\alpha_H(T)$ total hemispherical absorptance of surface

As T_s approaches T_w, the absorptance of the sample for radiation from the chamber walls, $\alpha_H(T)$, becomes approximately equal to the sample emittance ϵ_s. For $T_s >> T_w$, the emission of the chamber walls becomes negligible with respect to that of the sample. Thus, one

may assume $\alpha_H(T)=\epsilon_H(T)$, and rewriting the equation gives

$$\epsilon_H(T)A_s\sigma(T_s^4-T_w^4)=VI-q_c \qquad (14)$$

$$\epsilon_H(T)=\frac{VI-q_c}{A_s\sigma(T_s^4-T_w^4)}$$

The voltage drop across a length of the uniformly heated control portion of a strip sample is measured by a high impedance a-c VTVM. The current is measured by the use of a 0–5 amp ammeter with an external transformer. The temperature range of determination is approximately 400° to 2000° C.

APPARATUS

The apparatus consists, in general, of a water-cooled evacuated chamber in which a sample formed into a modified wedge enclosure is heated electrically by its own resistance. The sample can be rotated in azimuth while viewed externally through a double-slit collimating optical system. Signals are obtained with a vacuum thermocouple operated in a-c or d-c mode. A detailed description of the major components shown in figures 49–2 and –3 follows. Items are keyed by number to figure 49–3.

1. Vacuum System—The vacuum chamber (shown in cross section in fig. 49–2, –3) consists of a stainless steel ball jar (1) which is 12 in. in diameter by 14 in. in height and rests on a 1-in.-thick stainless steel baseplate (2). The bell jar is cooled by circulating water through tubing brazed to the exterior (3). The inner surface of the bell jar is coated with Parson's optical black lacquer, which has a diffuse reflectance of about 3% to minimize reflected radiations entering the optical system. Pressures of the order of 1×10^{-5} mm of Hg or less are maintained within the chamber to minimize the thermal conduction loss by air molecules and minimize degradation of sample surfaces. Vacuum pumping is accomplished by a 2-in. diffusion pump (4) and a 5-cfm mechanical pump. A liquid nitrogen trap and baffle are mounted between the diffusion pump and the base plate to prevent back-streaming of oil into the chamber. Removable vacuum feed-throughs are incorporated in the base plate for passage of the thermocouple leads. These units consist of glass-to-metal feed-throughs which are soft-soldered to a copper tube and vacuum sealed with a Swagelok fitting.

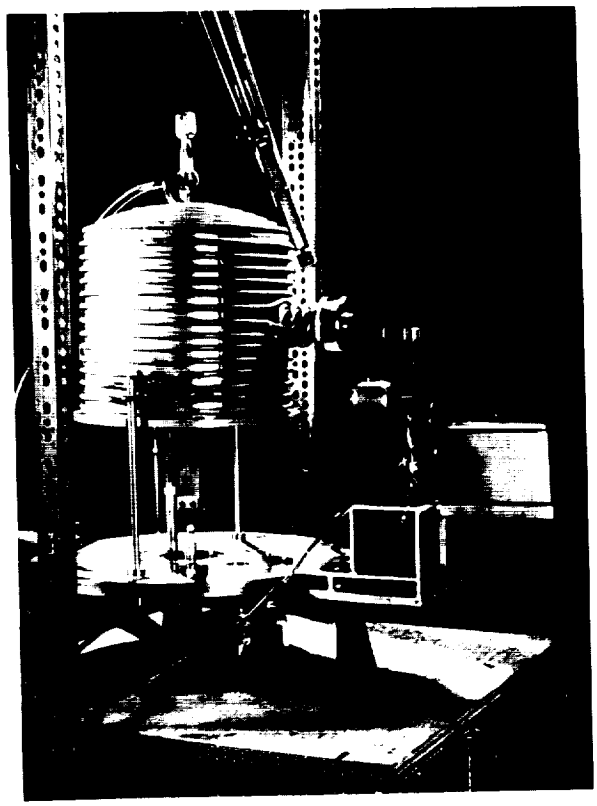

FIGURE 49–2.—High-temperature angular dependence apparatus.

2. Dynamic Seal—The dynamic seal (4) which permits the azimuthal rotation of the sample is shown in detail in figure 49–4. The flange rotates in an O-ring for vacuum sealing. Electrode feed-throughs also utilize Swagelok vacuum seals to permit vertical and horizontal adjustment of the electrodes. Clamps are provided to lock the electrodes in position with respect to the flange. Weights, suspended from the lower electrode, keep the sample under a slight tension to compensate for linear expansion. The electrodes are water cooled (6) as shown in figure 49–3. They consist of concentric copper tubing of 5/16-in. and 3/4-in. outside diameter, with the conductor on the inside. The water flows up through the 5/16-in. tubing and out through the separation of the two tubes. Four ceramic insulators (7) electrically isolate the portion of the electrode in contact with the base plate. Electrical power for heating the sample is supplied by a Variac-

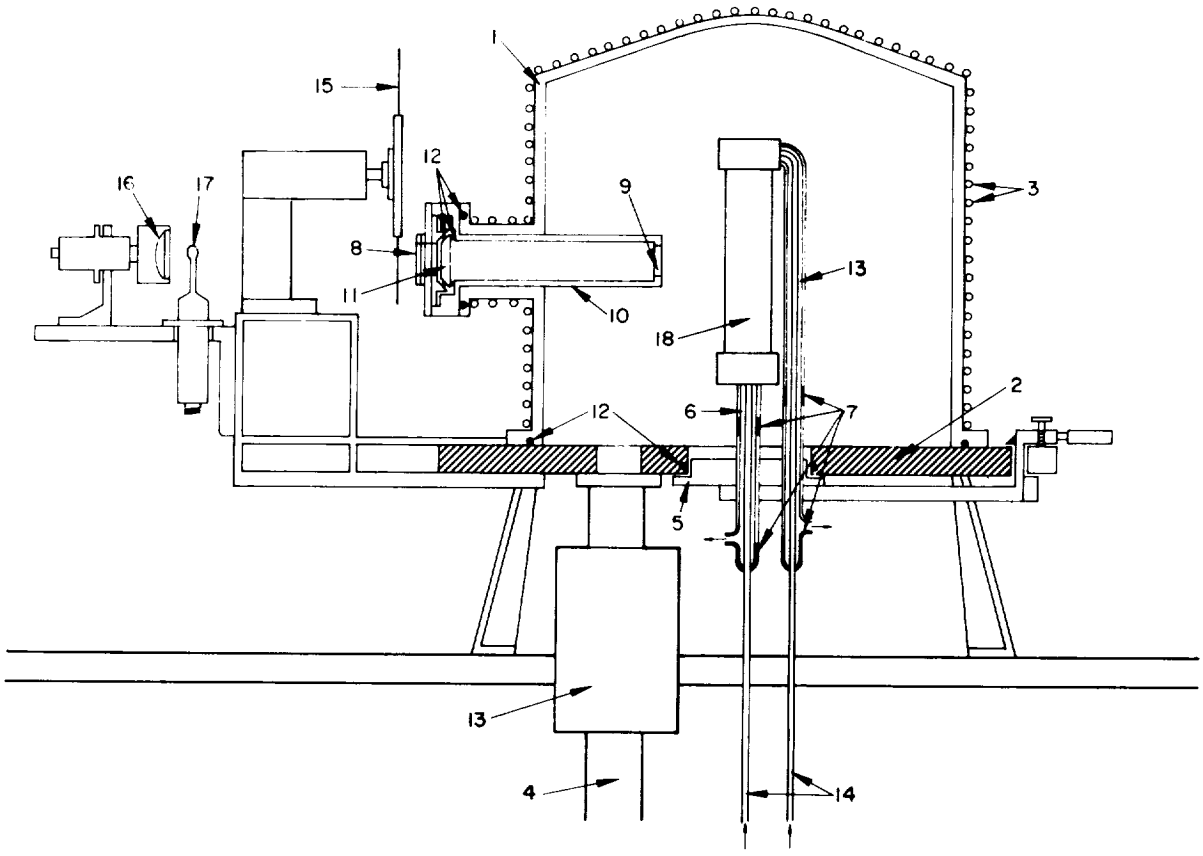

1. Vacuum chamber bell jar
2. Base plate
3. Cooling coils on bell jar
4. Diffusion pump
5. Dynamic seal
6. Water coolant
7. Ceramic insulators
8. Slit
9. Slit
10. Slit housing
11. Potassium bromide window
12. "O" ring vacuum seals
13. Cold trap
14. Electrodes
15. Chopper
16. Collector mirror
17. Vacuum thermocouple
18. Sample

FIGURE 49-3.—Cross-sectional view of emittance device in total normal emittance operation.

controlled 10-kva stepdown transformer with a rated output of 1,000 amp at 10 v.

3. Collimating Slits and Windows—The sample and blackbody are viewed externally through a double-slit collimating optical system (8 through 12). The two slits (8 and 9) are separated by 8.5 in. and are mounted in a 1.5-in. stainless steel tube (10). The tube has internal threads and is coated with Parson's optical black lacquer to minimize internal reflections. A potassium bromide window (11) is used with O-rings (12) for a vacuum seal. Slit widths of the order of 0.020 in. define very effectively the area and position on the sample surface and the direction from which the sample is viewed by the external detection system. The slit widths are not small enough to cause loss of energy by diffraction effects of single slits.

4. Radiation Detection System—The energy which emerges from the exit slit is collected and focused upon a vacuum thermocouple by an elliptical mirror. For total radiation data, the EMF output of the thermocouple is measured with a micro-millivoltmeter. The background radiation is measured initially with a water-cooled baffle placed in front of the entrance slit, and the entire exit optical path is enclosed in a black box to eliminate spurious reflections.

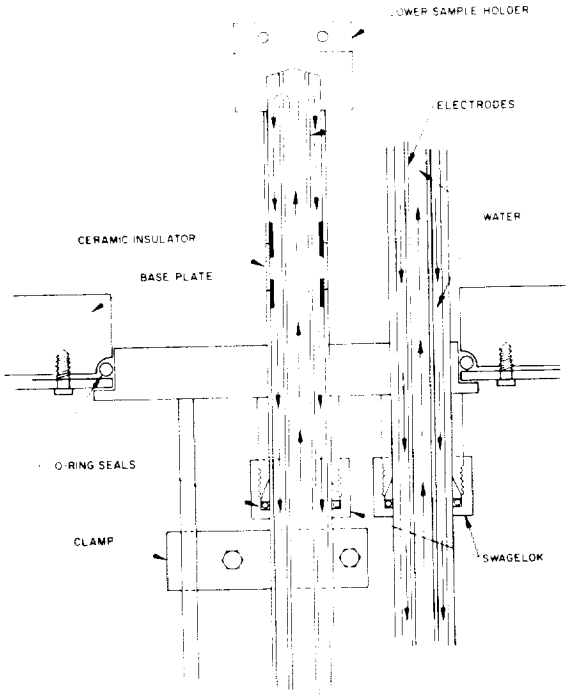

FIGURE 49–4.—Dynamic seal and water-cooled electrodes.

Spectral measurements are performed by installing the 13-cps synchronous chopper and rectifier directly behind the exit aperture. The radiation is then directed to the spectrophotometer transfer optics, and the normal spectrophotometer amplifier and recorder systems are used. The monochromator is equipped with a sodium chloride prism to provide maximum spectral resolution in the 1- to 10-μ region (fig. 49–5).

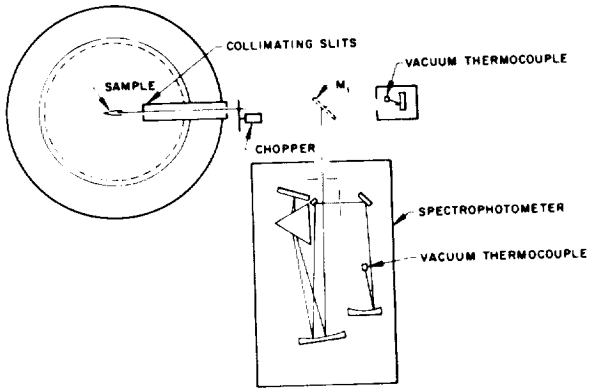

FIGURE 49–5.—The radiation detection system for spectral and total normal operation.

5. Sample Construction—The sample is constructed from sheet stock which is 0.003 to 0.010 in. thick, 6 in. long, 1½ in. deep, and ⅛ in. wide, with a cross section as shown in figure 49–6B. The sample forms an enclosure with open ends and a 1-in. by ⅛-in. opening in the central portion of the ⅛-in. side. Baffles are spot-welded above and below the opening, forming a cavity in the center portion of the sample, to eliminate radiation losses to the water-cooled electrodes. Sample surfaces are limited to materials which can be heated by their resistance or to very thin opaque coatings which can be applied to resistance-heated substrates. The coating thermal conductivity must be high

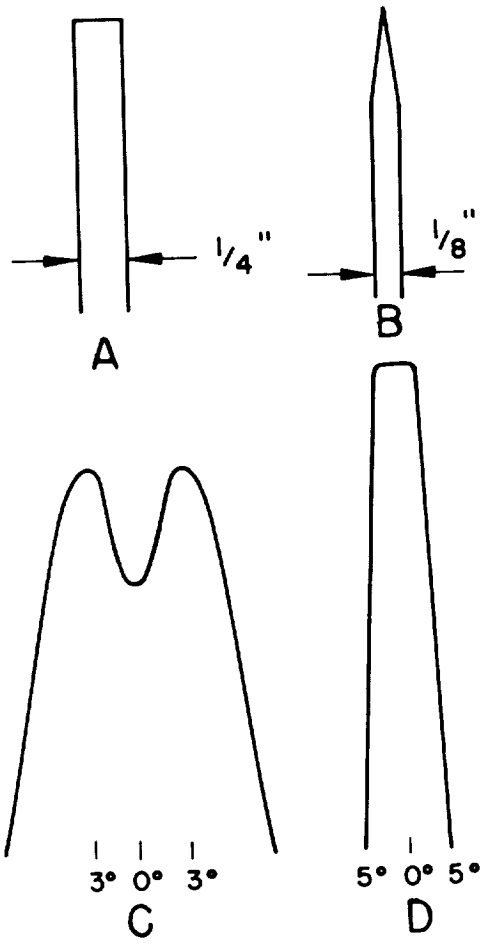

FIGURE 49–6.—Angular distribution of the radiation from a blackbody cavity for a rectangular and wedge-shaped cavity: A—rectangular cavity, B—modified wedge cavity, C—angular distribution of radiation from rectangular cavity, and D—angular distribution of radiation from modified wedge cavity.

enough to minimize temperature gradients from the inside of the enclosure to the outside.

6. Temperature Measurements—Temperatures of the sample surface up to 1500° C are measured with 0.003-in.-diameter platinum/platinum–13% rhodium thermocouples. A 1-in.-diameter window mounted in the bell jar permits visual observations of the sample and optical pyrometer temperature measurements. By observation of the blackbody cavity, the temperature of the sample is obtained directly by the pyrometer reading, since the temperature gradient through the wall in most cases is negligible. For optical pyrometer temperature determinations of samples which do not have a blackbody cavity enclosed, the observed apparent temperatures are corrected in accordance with the relationship (ref. 10):

$$\frac{1}{T}-\frac{1}{T_{app}}=\frac{\lambda}{c_2}\ln \epsilon_\lambda e^{-\mu l}$$

where

T	actual temperature
T_{app}	apparent temperature
λ	wavelength of operation of pyrometer
c_2	Planck's second radiation constant
ϵ_λ	emittance of sample at wavelength λ
μ	absorption coefficient of window
l	thickness of window

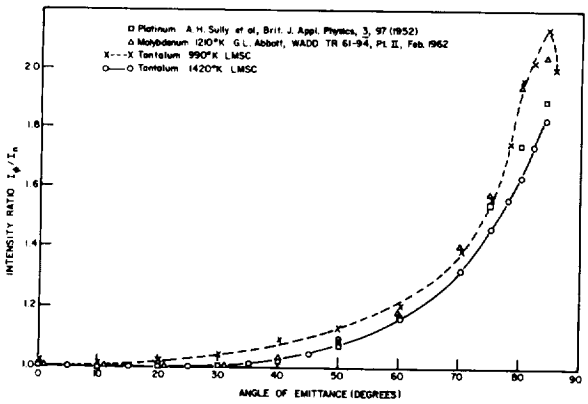

FIGURE 49–7.—Relative directional total radiance of tantalum.

Figure 49–7 is typical of the data obtained with the equipment.

EVALUATION

Blackbody Efficiency

The accuracy of the determination of the directional spectral and total emittance is dependent upon the efficiency of the reference blackbody cavity. The spectral distribution and density of the theoretical radiation is given by the radiation laws of Planck and Stefan.

The radiation characteristics of practical blackbody cavities deviate from the theoretical blackbody because of the necessity for one or more holes in the cavity walls and because of the inhomogeneities in the temperature of the walls. As shown in reference 11, the degree of the deviation will depend upon:

ratio of the area of the opening to that of the internal dimensions
position of the surface element observed through the hole
dimensions and positions of any additional holes
temperature distribution over the walls

In addition, the apparatus described in this paper requires a blackbody cavity enclosed within a sample which has a planar surface that can be viewed externally. These restrictions limit the possible sample configurations to the two investigated below.

The angular distribution of the radiant intensity of the rectangular cavity is shown in figure 49–6. It is seen that a maximum is reached when viewing either corner of the rectangular cavity. Each corner in itself forms an approximation to a Mendenhall wedge (ref. 12), increasing the efficiency of the cavity when viewed at a small angle. The modified-wedge cavity shown in figure 49–6C provides the maximum blackbody efficiency which can be utilized in this application. It consists of a Mendenhall wedge with extended parallel sides. The angular distribution of the modified wedge, shown in figure 49–6D, indicates that the intensity of the radiation is constant across the aperture port.

Considering the absorption of the cavity to be equal to its emittance, the departure of the cavity from the theoretical blackbody can be determined. The number of reflections which occur before a ray entering the cavity is reversed in direction is given by $n=180/\alpha$ where α is the apex angle of the wedge. The effective emittance (ϵ_w) of the cavity (ref. 14) is given by

$$\epsilon_w=\epsilon_s\left(1+\sum_{i=1}^{n} r_s^{\,n}\right)$$

where

ϵ_s emittance of sample surface
r, reflectance of sample surface

The deficiency of the cavity is then given by

$$\frac{\Delta\epsilon}{\epsilon}=\frac{\epsilon_b-\epsilon_w}{\epsilon_b}=1-\epsilon_w$$

For an apex angle of 15° and considering only 10 reflections, the departures of the cavity from a blackbody are as follows:

ϵ_s	$\frac{\Delta\epsilon_b}{\epsilon_b}$
0.4	0.004
0.3	.030
0.2	.097
0.1	.314

Temperature Gradient Through the Wall of the Blackbody Cavity

If the interior of the blackbody cavity is at a greater temperature than the outside surface, then the determined emittance will be less than the true emittance of the surface.

Consider a cross-sectional volume element of the sample when heated electrically by its own resistance. The heat energy transferred in unit time in a plate of thickness dx (ref. 13) is given by

$$Q_1=K_1A dx\,\frac{\partial^2T}{\partial x^2}$$

where Adx is volume element and K_t is thermal conductivity. If Δq is the rate of heat generation per volume element, then an amount

$$Q_2=Adx\Delta q$$

will be generated. Under a steady-state condition, the sum of Q_1+Q_2 must equal zero. Thus,

$$K_1A dx\,\frac{\partial^2T}{\partial x^2}+Adx\Delta q=0$$

or

$$\frac{d^2T}{dx^2}=-\frac{\Delta q}{K_1}$$

Integration yields

$$\frac{dT}{dx}=-\frac{\Delta qx}{K_1}+C_1$$

Measuring x from the inside of the cavity at $x=0$, we have $T=T_1$ and $dT/dx=0$; thus $C_1=0$

Integration again yields

$$T=-\frac{\Delta qx^2}{2K_1}+C_2$$

at

$$x=0,\ T=T_1,\ \therefore C_2=0$$

and

$$T-T_1=-\frac{\Delta qx^2}{2K_1}$$

If Δx is the thickness of the sample material and T_2 is the temperature of the surface, then

$$T_1-T_2=\frac{\Delta q(\Delta x)^2}{2K_1}$$

or

$$\Delta T=\frac{\Delta q(\Delta x)^2}{2K_1}$$

The heat energy generated per volume element is given by

$$\Delta q=i^2\,\rho_t$$

where i is current density and ρ_t is resistivity of the material

Thus,

$$\Delta T=\frac{i^2\rho_t(\Delta x)^2}{2K_1}$$

In the steady-state condition, the heat energy generated per volume element must equal the heat radiated by the exterior surface of that volume element. Thus,

$$\epsilon_sA_s\sigma T_s^4=i^2\rho_t\Delta xA$$

and

$$i^2\rho_t\,\Delta x=\epsilon_s\sigma T_s^4$$

where ϵ_s is emittance of surface and T_s is temperature of surface.

Substitution in the equation for T yields

$$\Delta T=\frac{\epsilon_s\sigma T_s^4}{2K_1}\,\Delta x$$

For a compound sample where a substrate of thickness x_1 has been coated with a material of thickness x_2 and emittance ϵ, the temperature gradient ΔT_{12} across the substrate is given, as before, by

$$\Delta T_{12}=\frac{i^2\rho_t x_1^2}{2K_1}$$

Under steady-state conditions, the heat energy radiated by the exterior surface at a tem-

perature T_3 must be equal to that conducted across the coating. Thus,

$$\frac{K_2 A \Delta T_{23}}{x_2} = \epsilon_3 A \sigma T_3^4$$

and

$$\Delta T_{23} = \epsilon_3 \sigma T_3^4 \frac{x_2}{K_2}$$

The total gradient T_{13} is then given by

$$\Delta T_{13} = \Delta T_{12} + \Delta T_{23} = \frac{i^2 \rho x_1^2}{2K_1} + \epsilon_3 \sigma T_3^4 \frac{x_2}{K_2}$$

At steady state, the heat radiated must equal the heat generated within the element. Thus,

$$i^2 \rho x_1 A = \epsilon_3 \sigma A T_3^4$$

and

$$\Delta T_{13} = \epsilon_3 \sigma T_3^4 \left(\frac{x_1}{2K_1} + \frac{x_2}{K_2} \right)$$

Some typical temperature gradients are given in the following tabulation:

Material	*Temperature*	x_1, *mil*	x_2, *mil*	ΔT, °C	$\Delta\epsilon$, %
Tungsten	1000	10	------	0. 024	------
	2000	10	------	. 19	------
Titanium	1000	10	------	. 10	------
	2000	10	------	. 80	0. 4
Rokide "C" on titanium	1000	10	5	2. 75	1. 5
	2000	10	5	22. 0	5. 3

$\Delta\epsilon$ is the error correction in the determined emittance for the temperature gradient described. As shown, for most materials it is negligible and need be considered only for coated materials.

Error Analysis for Directional Spectral and Total Emittance Data

The error associated with a particular determination for the directional spectral and the directional total emittance will be the same, since the same type of measurement is utilized in both cases. The expression derived for the emittance in the discussion was

$$\epsilon(T) = \frac{v_s}{v_b}$$

and it was assumed that

$$\frac{v_s}{v_b} = \frac{J_s(T)}{J_b(T)}$$

Actually, the voltage v_s, corresponds to

$$v_s = \epsilon_s A_s \sigma T_s^4 + r_s A_s \sigma T_w^4 + B_g$$

where

$\epsilon_s A_s \sigma T_w^4$ power radiated by sample surface

$r_s A_s \sigma T_w^4$ power radiated by chamber walls and reflected into optical system

B_g = background signal

and the voltage v_b, corresponds to

$$v_b = \epsilon_b A_s \sigma T_b^4 + B_g$$

where $\epsilon_b A_s \sigma T_b^4$ is the power radiated by blackbody cavity.

The factor B_g is determined before the actual measurement and is a zero correction. From the temperature gradient determinations we have $T_s = T_b$ and thus

$$\epsilon_m = \frac{v_s}{v_b} = \frac{\epsilon_s A_s \sigma T_s^4 + r_s A_s \sigma T_w^4}{\epsilon_b A_s \sigma T_s^4}$$

or

$$\epsilon_m = \frac{\epsilon_s}{\epsilon_b} + \frac{r_s T_w^4}{\epsilon_b T_s^4}$$

Where ϵ_m is the measured emittance, for $T_s > 400°C$, we have $T_s^4 >> T_w^4$ where $T_w^4 \sim 25°C$, and we have

$$\epsilon_m = \frac{\epsilon_s}{\epsilon_b} = \frac{v_s}{v_b}$$

The probable error is then given by

$$\frac{\Delta\epsilon_m}{\epsilon_m} = \left[\left(\frac{\Delta\epsilon_s}{\epsilon_s} \right)^2 + \left(\frac{\Delta\epsilon_b}{\epsilon_b} \right)^2 \right]^{1/2}$$

The uncertainty in ϵ_s is given by the instrument uncertainty. And, thus,

$$\frac{\Delta\epsilon_s}{\epsilon_s} = 0.03$$

Thus, the probable error in the determined emittance is given by the following tabulation:

ϵ_s	$\frac{\Delta\epsilon_m}{\epsilon_m}$
0.4	0. 03
0.3	. 034
0.2	. 109
0.1	. 314

REFERENCES

1. Jacob, Max: Heat Transfer. John Wiley & Sons, Inc., 1957.
2. Eckert, E. R. G.; and Drake, R. M. Jr.: Heat and Mass. Transfer. McGraw-Hill Book Co., 1959.
3. Rome Air Development Center, Final Report, Part 1, by Bell Contract AF30(602)-1047.
4. Blau; Marsh; Martin; Jasperse; and Chaffe: Infrared Spectral Emittance Properties of Solid Materials. AFCRL-TR-60-416, Oct. 1960.
5. Richmond, J.: First Symposium—Surface Effects on Spacecraft Materials. (F. J. Clauss, ed.,) John Wiley & Sons, Inc., 1960, pp. 182-192.
6. Weber, D.: Low Temperature Directional, Spectral Emissivity of Translucent Solids. Jour. Opt. Soc. Am., vol. 50, no. 8, Aug. 1960, pp. 808-810.
7. Worthing, R. G.; and Halliday, D.: Heat. John Wiley & Sons, Inc., 1948.
8. Abbott, G. L.; Alvares, H. J.; and Parker, W. J.: Total Normal and Total Hemispherical Emittance of Polished Metals. WADD Tech. Rep. 61-94, Nov. 1961, pp. 61-94.
9. Price, D. J.: The Emissivity of Hot Metals in the Infra-Red. Proc. Phy. Soc., vol. 59, 1947, pp. 118-131.
10. Wood, W. P.; and Cork, J. M.: and Pyrometry. McGraw-Hill Book Co., 1941.
11. De Vos, J. C.: Evaluation of the Quality of a Blackbody. Physica, vol. XX, 1954, pp. 669-689.
12. Mendenhall: Astrophys., vol. 33, 1911, 1. 91.
13. Jacob, M.; and Hawkins, G.: Elements of Heat Transfer. John Wiley & Sons, Inc., 1957.
14. Worthing, A. G.: Temperature Radiation Emissivities and Emittances. Jour. Appl. Phys., vol. 11, p. 421, June 1940.
15. Sully, A. H.; Brandes, E. A.; and Waterhouse, R. B.: Some Measurements of the Total Emissivity of Metals and Pure Refractory Oxides and theVariation of Emissivity with Temperature. Brit. Jour. of Appl. Phys., vol. 3, no. 3, Mar. 1952, pp. 97-101.
16. Abbott, G. L.; Alvares, H. J.; Parker, W. J.: Total Normal and Total Hemispherical Emittance of Polished Metals. WADD-TR-61-94, Part II, Feb. 1962.
17. Rutgers, G. A. W.: Temperature Radiation of Solids. *in* Handbuck der Physik, vol. 26, Berlin, Springer-Verlag, 1958.

50—EMITTANCE MEASUREMENT CAPABILITY FOR TEMPERATURES UP TO 3000° F

BY A. S. KJELBY

AERONCA MANUFACTURING CORPORATION, MIDDLETOWN, OHIO

The emittance of a re-entry vehicle heat shield plays an important role in maintaining low substructure temperatures. State-of-the-art literature does not furnish sufficient data for the radiation properties of ceramics in the temperature range realized during re-entry. In order to provide these data it was necessary to design and construct a special apparatus capable of measuring emittances up to to 3000° F.

The method of determination of the total hemispherical emittance by comparison with a blackbody is the basis of the technique herein employed. If the temperatures and the areas of the unknown surface and the blackbody are made equal, the method becomes simply the determination of the ratio of the rates of emission.

Developments in our space programs have brought us to the point where re-entry vehicles are now within the state-of-the-art. Intensive studies are being conducted on re-entry vehicles for both circular and super-circular orbits. Many of these vehicle concepts are of the lifting body type.

It is well known that re-entry vehicles, in general, and lifting body types, in particular, will be subjected to extremely high surface temperatures for appreciable periods of time during the re-entry flight. Materials and structures development lags behind the requirements in that the temperatures to be encountered exceed the capabilities of the present structural materials. The designer must, therefore, protect his structure from these extreme temperature environments.

Among the many methods of protection are active cooling systems, insulation systems, ablation systems, and re-radiation systems. In February 1960, the Aeronautical Systems Division of the U.S. Air Force awarded contract AF 33-(616)-7050 to Aeronca Manufacturing Corporation to establish the feasibility of the re-radiation structural concept shown in figure 50-1. The results of this work are reported in ASD-TR-61-706 Volume II.

In this concept, a foamed ceramic heat shield material with high emittance characteristics is used for the outer surface of the structure. A reinforcement honeycomb core is used to break up the monolithic effect in the ceramic body and to attach the ceramic to the structure. The fibrous insulation provides the high-efficiency insulative capacity for further protection of the load-bearing metallic structure. The optional cooling manifolding can be used for extremely high heat flux environments.

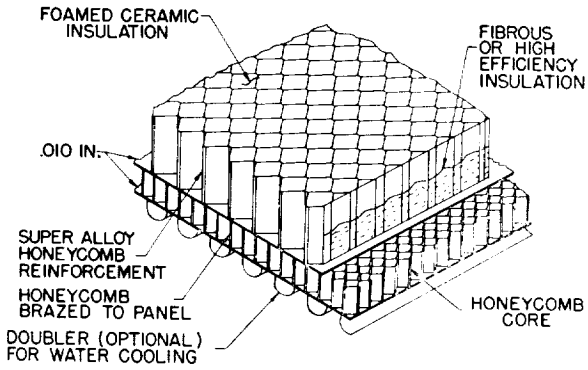

FIGURE 50-1.—Aeronca Thermantic construction.

The emittance characteristics of the heat shield play an important role in maintaining low substructure temperatures. It is desired that in excess of 98% of the incident heat to this surface be re-radiated back into space rather than allowed to penetrate into the structure. Therefore, an integral part of the materials development and the ceramic foam

investigations was the raising of the emittance characteristics to as high a level as possible.

The state-of-the-art of such ceramic development work does not furnish sufficient data for the radiation properties of the ceramic in the temperature range realized during re-entry. In addition, the then current equipment for measuring emittance characteristics was not suitable for use with large composite materials and structures as was shown in figure 50–1. In order to obtain these data, it was, therefore, necessary to design and construct a special apparatus capable of measuring emittance at temperatures up to 3000° F.

Using the Stefan-Boltzmann law, we find that the total hemispherical emittance may be experimentally evaluated if the rate of emission, absolute temperature, and area of the test surface can be measured. It is not difficult to measure the absolute temperature or the area of the radiating surface. However, it is difficult to devise an apparatus capable of measuring the absolute value of the rate of emission. It is considerably easier to obtain comparative readings of rates of emission.

Theoretically, a cavity having a small opening emits blackbody radiation through its opening when the inner surfaces of the cavity are at uniform temperature. Such a blackbody radiation source affords a standard of comparison against which the rate of emission of a surface of unknown emittance may be measured.

With the comparison blackbody denoted by the subscript b, and the surface of the unknown emittance by the subscript u, the ratio of their emissions is obtained from equation (1).

$$\frac{\epsilon_u}{\epsilon_b}=\frac{R_u T_b^4 A_b}{R_b T_u^4 A_u} \tag{1}$$

Because the emissivity of a blackbody is unity, this equation reduces to equation 2:

$$\epsilon_u=\frac{R_u T_b^4 A_b}{R_b T_u^4 A_u} \tag{2}$$

If the temperature and the areas of the unknown surface and the blackbody surface are made equal, equation (2) further reduces to equation (3):

$$\epsilon_u=\frac{R_u}{R_b} \tag{3}$$

Under these conditions, the method becomes simply the determination of the ratio of the rates of emission R_u over R_b.

On this basis, the test apparatus was designed to measure the radiation intensity of a sample and compare it with that of a blackbody surface.

A general view of the complete apparatus is shown in figure 50–2. The complete apparatus consists of two groups of components. First, the test furnace and its accompanying temperature controller; second, the total radiation detector for comparing the intensity of radiation emitted by the test specimen with that emitted by the blackbody.

Figure 50–3 gives two schematic views of the test furnace, the original device (A) and a modification (B). The test chamber is completely surrounded by a ceramic muffle, behind which are suitable heating elements. By this arrangement, the interior of the furnace, the test sample, and all other components in the chamber can be brought to test temperature and allowed to stabilize so that all elements in the furnace reach the same temperature. Sufficient insulation of suitable type is provided to minimize the heat losses through the furnace walls.

The test furnace as seen in figure 50–3A and 50–3B consists of two areas. The upper portion contains two sight tubes. One tube permits measurement of the intensity of the blackbody radiation, the other allows measurement of the intensity of radiation from the specimen surface.

The uncooled sight tube tapers from the outside to the inside of the furnace wall to prevent excessive heat loss and stray radiations from the sides of the sight tube from entering the radiation detector. This sight tube is located in such a manner as to allow viewing of the specimen face by the radiation detector. Under the conditions of the specimen and furnace interior being at the same temperature, the radiation viewed at this location is blackbody radiation.

A water-cooled sight tube is extended to the sample surface to permit measurement of the sample's radiation intensity exclusive of the surrounding environment. The tube is water cooled to prevent its becoming a source of radiation and introducing extraneous energy

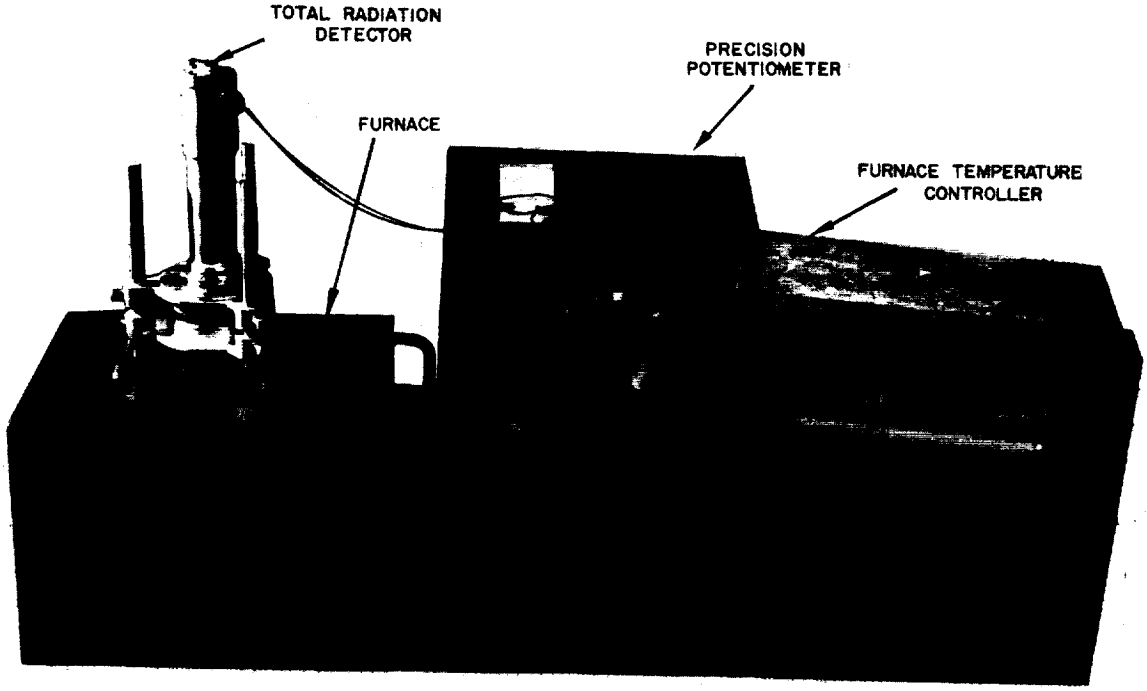

FIGURE 50-2.—Emissivity comparator setup.

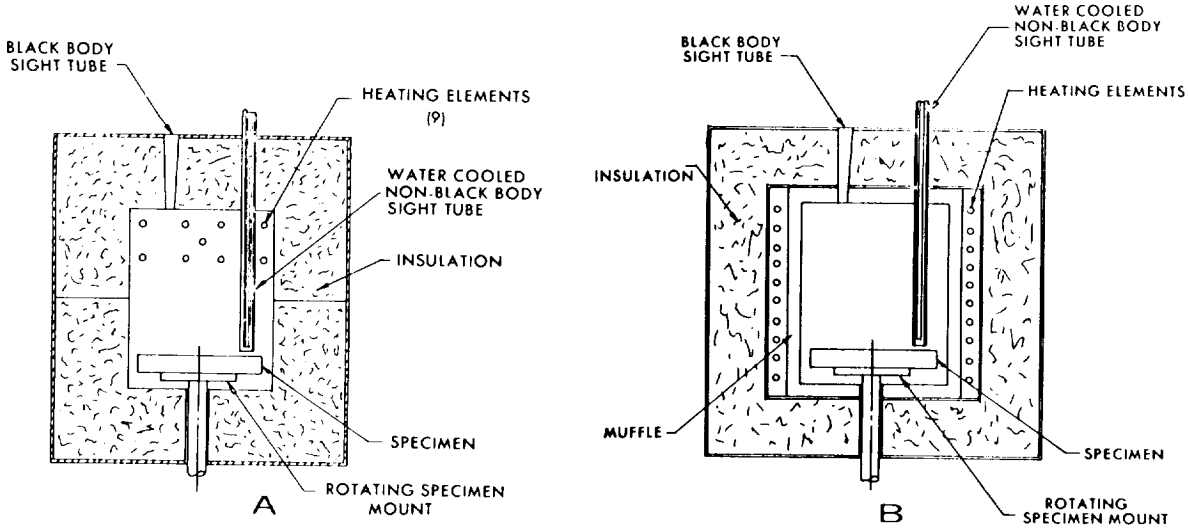

FIGURE 50-3.—Schematic cross section of emittance test furnace. A—original design, and B—modification.

into the reading of the radiation detector. The lower end of this tube is approximately 1/16 inch above the surface of the specimen to prevent reflections and stray radiations from other areas of the furnace cavity entering into the tube. Such reflections and stray radiations would cause an error in the reading through this sight tube. The interior of the sight tube was blackened to minimize reflections which would cause erroneous observations. It is from this sight tube that we obtain the readings of the emittance characteristics of the sample, itself, for comparison with the blackbody readings previously taken.

The lower portion of the furnace contains the specimen mount. This consists of a cooled stainless-steel shaft. A 1-inch refractory spacer was placed between the shaft and sample. This spacer served to bring the test specimen to the proper height. It also insulated the test specimen from the shaft, thus insuring the uniform temperature distribution within the specimen. The test specimen was rotated at approximately 20 rpm to present a uniform freshly heated surface to the sample sight tube for radiation measurements.

An additional feature was that slip rings were mounted on the shaft of the rotating specimen mount. With this arrangement, thermocouples could be placed within the specimen, brought down through the hollow mounting shaft, and, through the slip rings, connected to suitable recording or controlling devices. In practice, it was found that this was not required for test work, as accurate temperature measurements could be taken by sighting an optical pyrometer through the blackbody sight tube.

The radiation detection instrument used was a Minneapolis Honeywell radiation detector with a calcite lens and a thermopile of ten chromel-constantan thermocouples. The effective target diameter was 0.5-inch. The calcite lens was used because of its ability to transmit a wide frequency range necessary for measurement of total radiation on the surface. Electrical potentials generated by the radiation detector were read on a precision potentiometer accurate to 0.001 millivolt.

In order to establish the accuracy of this system, calibration tests were made. Inconel X was chosen for the standard on the basis of the information published in NACA TN 4121 which deals with the emittance of Inconel X at temperatures up to 2000° F. The test specimens were prepared in the same manner as stated in the report. They were thoroughly cleaned, polished, and then oxidized at 2000° F for 30 minutes. At 2000° F, an averge of the calibration data indicated an emittance of 0.91. This was within 3% of the published value of 0.93. The calibration was limited to a maximum of 2000° F, as this was the highest temperature for which data were found.

The procedure used in testing was very straight forward. With the sample in position and rotating, the furnace was heated to test temperature and allowed to stabilize so that all elements of the furnace chamber and contents reached the same temperature. Readings were taken with the radiation detector alternately through the blackbody and sample sight tubes. These readings were millivolt outputs of the radiation detector as read on a potentiometer. The temperature was read before and after each set of readings with an optical pyrometer sighted through the blackbody sight tube. Since the potential developed by the thermopile in the radiation detector is proportional to the intensity of the radiation incident upon it, the emittance of the specimen may be calculated from the ratio of the potential developed by the radiation detector viewing the specimen over that developed by the detector viewing the blackbody.

The emittance characteristics of several ceramics have been determined by this procedure. Among these were compositions with different coloring oxides in an attempt to raise the ceramic's emittance to the highest possible value. As shown in figure 50–4, the emittance of the plain alumina and zirconia foams were below that which was desired to take full advantage of the radiation cooling during re-entry. The alumina foam with a 15% addition of 80–20 nickel oxide-chrome oxide exhibited an appreciable increase over the plain alumina. The alumina foam with a coating of oxidized Inconel X powder possessed the highest emittance. The test data ranged from 0.87 at 1600° F to 0.82 at 2600° F, which was well above emittance of the plain alumina and also

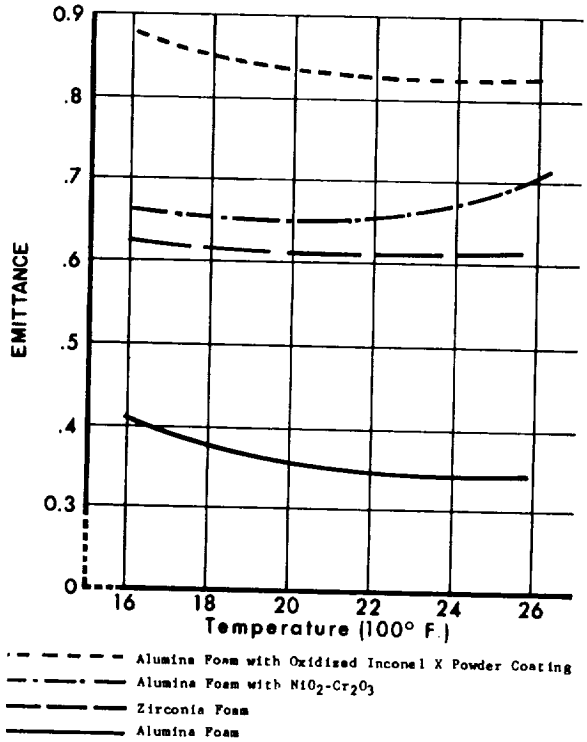

FIGURE 50–4.—Results of emittance tests for various oxides.

the alumina with the nickel oxide-chrome oxide addition.

Some of the many advantages to a device of this nature, are:

1. Separate blackbody and nonblackbody units are noted required. The specimen and furnace cavity serve as sources for both data conditions by taking readings at each of the two positions in the apparatus.
2. High test temperatures can be achieved in the equipment as now used in our laboratory. Test temperatures up to 3000° F can be achieved. The upper limit is dictated only by the material capability for the heating element and furnace cavity.
3. Nonhomogeneous and composite specimens can be tested. Coatings and base material combinations can readily be be tested. Both metals and nonmetals can be used for the specimen. As seen in figure 50–1, porous, composite, or laminar materials may be tested to determine the total effect rather than trying to calculate for the individual effect of each component.
4. Large specimens can be tested. This is a distinct advantage for porous, composite or nonhomogeneous specimens.
5. Extreme care and high precision of specimen manufacture is not required to achieve a high degree of accuracy in the test results. Also, extreme care and precision in setup and alignment are not required.
6. Uniformity and equilibrium of test temperature are easily achieved by use of optical pyrometers and/or thermocouples and can be easily verified.
7. The apparatus is simple, inexpensive, easy to maintain and repair, and made from readily obtainable materials. High precision of manufacture, hence high costs, is not required to construct such an apparatus.

51—EVALUATION OF THERMAL RADIATION AT HIGH TEMPERATURES

BY S. KONOPKEN AND R. KLEMM

NORTH AMERICAN AVIATION, INCORPORATED, LOS ANGELES, CALIFORNIA

Because many materials change in radiation characteristics with increasing temperature, it has become increasingly important to determine emittance values directly instead of by the comparatively easier method of computing emittance values from reflectance data. This is particularly true if the material is partially transparent to radiation. A new apparatus is being built to extend the capability for evaluating emittance from the currently available 1500° F to at least 4000° F. The technique being applied is to rotate specimens in a high-temperature furnace which is also utilized as a blackbody radiation source. The analytical techniques used to establish speed of rotation, field of view, and other design problems are discussed.

A review of other radiation test equipment is also presented.

The two most important passive means by which heat energy can be dissipated from air vehicle surfaces are convection and radiation. Which of these two is more important depends, of course, on many factors, such as geometry, rate of air circulation, temperature, characteristics of the surfaces across which heat transfer occurs, and so forth. While the importance of radiative transfer is universally recognized, historically, serious consideration of this phenomenon in system design is relatively recent. At North American Aviation, Incorporated (NAA), for example, the study of radiative heat transfer was given its first important impetus during the design of the F–86 Sabrejet, in which it was essential to analyze the radiative exchange across a 1-foot gap between a 400° F compressor case and the fuselage. Since then, radiative heat transfer has become an increasingly important factor in thermodynamic analysis for air vehicular design.

Over the years, considerable progress has occurred in the analysis and use of radiation phenomena. Today, designers, research people, and other investigators know that if, in addition to the value of total radiant emission, the specific frequencies emitted are known, a very useful tool is available, not only for thermal control purposes per se, but also for application to such diverse problem areas as air and space detection, IR countermeasures, missile discrimination, space powerplants, re-entry structure, and so forth. By the judicious selection and modification of materials, the development of surfaces having predetermined spectral radiation characteristics becomes feasible. The need to utilize data on radiation phenomena—in all of its manifestations—generated the requirement at NAA to obtain the test apparatus to be described.

TOTAL EMITTANCE VALUES

The first technique used for evaluating the emittance characteristics of materials at NAA was a pyrometric technique in which a specimen is heated in a temperature-controlled housing. The emittance, ϵ, was calculated by,

$$\epsilon=\left(\frac{T_A}{T_R}\right)^4$$

Where T values are apparent and real temperatures as determined with a radiation pyrometer and thermocouple, respectively. Emittance values obtained by this simple means are often quite close to true values. However, there are some complicating factors, including detector response, temperature of the detector and housing, mirror characteristics, and so forth. The treatment of this subject can become quite involved. A general solution used in our labora-

tory was derived by Dobbins (ref. 1):

$$\epsilon=\left(\frac{T_A}{T_R}\right)^4-r\left(\frac{T_O}{T_R}\right)^4$$

Where r is the reflectance of the heating source and T_O is the temperature of detector housing. When very accurate results are desired, a correction factor for mirror reflectivity and changes in thermocouple cold junction temperatures can also be applied (ref. 1).

In practice, the utilization of the pyrometric technique is somewhat cumbersome and time-consuming. For routine, day-to-day problems, the piece of equipment shown in figure 51–1 was built. In this apparatus, the specimen is attached to a movable rod and placed deep inside a sufficiently long susceptor (the susceptor is graphite or coated tantalum, depending upon whether tests are to be made in an inert or an oxidizing atmosphere). Induction coils are spaced to avoid thermal gradients within the cavity. A radiometer is optically aligned to the susceptor axis in such position that the field of view is less than the angular subtense of the specimen. With the specimen deep in the cavity, the radiometer indicates blackbody radiation (the top line in figure 51–2). When the specimen is moved towards the aperture, the indicated radiation drops in value. The arrival of the specimen at the aperture is signaled by an abrupt change of slope in the trace. The ratio of ordinates at the knee of the curve and blackbody radiation is a measure of the emittance of the specimen. It is possible with this equipment to vary the angle of view up to 45° for evaluating the directional characteristics of emittance.

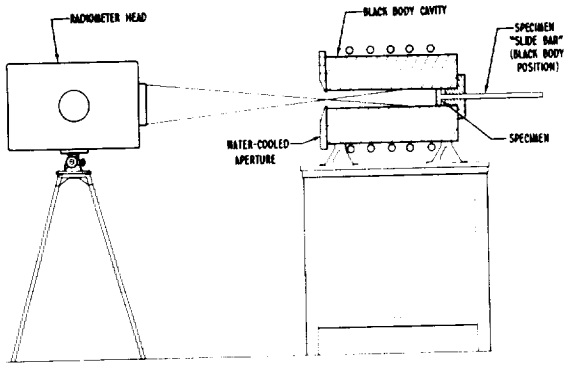

FIGURE 51–1.—Schematic of emittance apparatus.

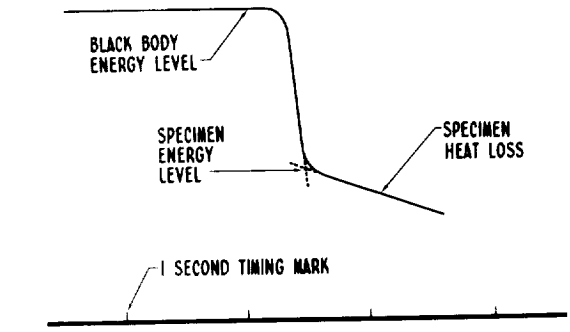

FIGURE 51–2.—Sample of stripchart data.

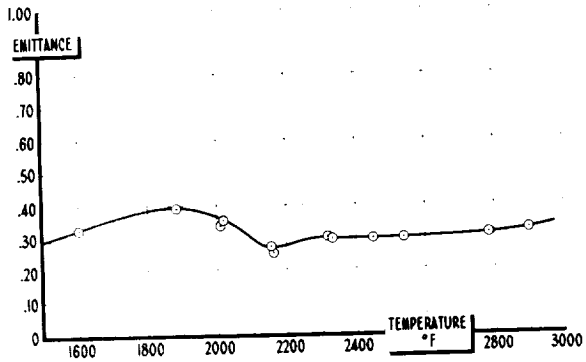

FIGURE 51–3.—Normal emittance of zirconium as received.

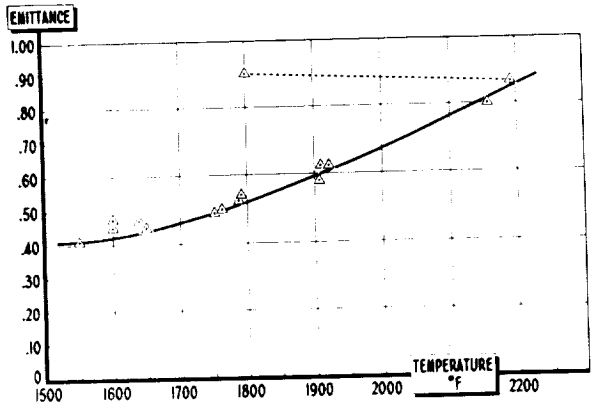

FIGURE 51–4.—Normal emittance of beryllium.

This apparatus has been used to test a wide variety of materials at rather high temperatures. Some representative data curves are shown in figures 51–3, 51–4, and 51–5. Runs are normally completed in less than an 8-hour day. Both pieces of equipment previously described determine normal emittance.

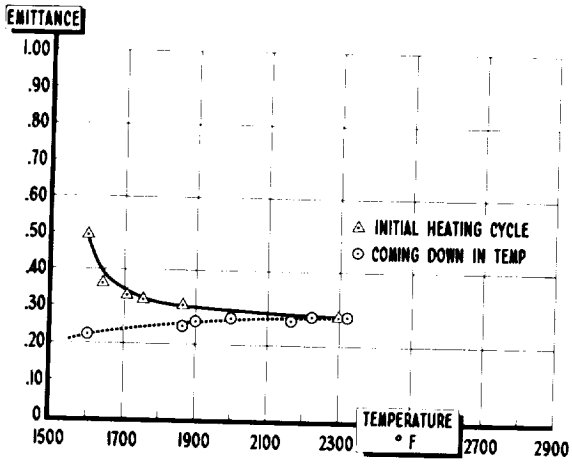

FIGURE 51–5.—Total normal emittance of A–316 steel.

For accurate system analysis, however, thermodynamicists prefer hemispherical emittance. For this purpose, the equipment shown in figure 51–6 was built. This system works on the "power loss" principle, in which hemispherical emittance is a function of the relative power required to keep a specimen and a perfect emitter (of identical geometry) at a given temperature. The North American equipment uses strip specimens measuring 0.040 by ½ by 18 inches. Voltage leads are attached 4 inches from each end (3 inches from each bus bar). Specimen temperature is monitored by thermocouples. The chamber walls are painted black and are kept at 40° F. While the method is simple, a little patience

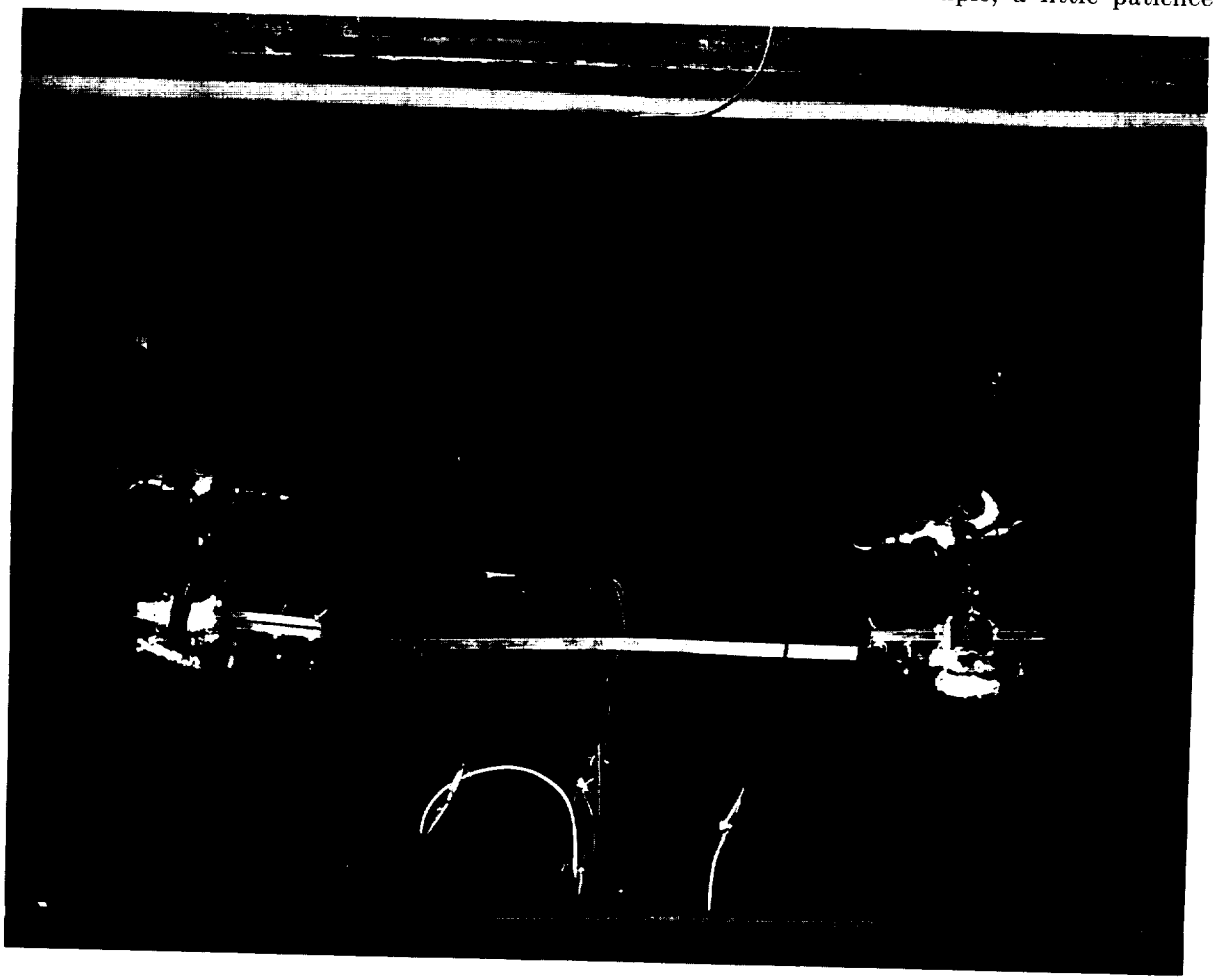

FIGURE 51–6.—Hemispherical emittance apparatus.

and care is required for accurate results. We find that it takes about one hour per data point to get reliable results.

SPECTRAL EMITTANCE VALUES

The equipment used for spectral emittance determinations at temperatures up to 1800° F, is an adaptation of a Perkin-Elmer 13–U spectrophotometer. In the original 13–U instrument, figure 51–7, radiant energy from a Nernst glower is intercepted by a spherical mirror. The optical path is such that the flux is directed along two separate routes. Nominally, there is equal flux in the two beams. For ordinary transmittance (or reflectance) evaluations, a sample is placed in one of the beams and the instrument automatically records the relative flux in sample and reference beams. For emittance tests, it is necessary to replace the original source with two new sources: (1) a heated specimen and (2) a blackbody reference. Radiant energy from each new source must then be directed to intercept the original path at some convenient point, so that the flux in the two beams can be compared as before. The new optical arrangement is shown in figure 51–8. The actual equipment is shown in figure 51–9. Warm-up time from room temperature to test temperature is about 2 hours. A complete test run takes 6 to 8 hours. This lengthy time is caused chiefly by the difficulty in balancing specimen and blackbody temperatures. The spectral range covered is 0.2 to 28μ. A Gier-type reflectometer is also used with this equipment. The optical arrangement is shown in figure 51–10.

The equipment just described was designed and built to handle materials at temperatures associated with Mach 3 flight conditions. Today, the problems associated with re-entry structures—winged vehicles entering the atmosphere, being subjected to extremely high heating rates—reaching temperatures of 3000° F, 4000° F, or even higher, must be considered. One approach for such structures is to utilize ablative materials (e.g., Mercury capsules). Another approach, promising greater operational freedom to maneuver, is so-called "hot" or "heat shielding" structure. Exemplifying the "hot" or "heat shielding" structure concept is figure 51–11, which shows a plausable

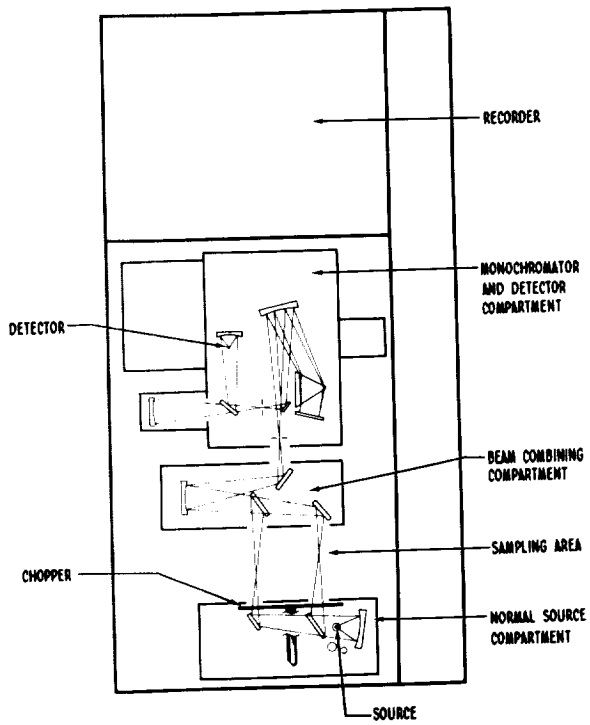

FIGURE 51–7.—Schematic of Perkin-Elmer model 13–U spectrophotometer.

wing leading edge consisting of hot-pressed beryllium oxide segments, mounted on a siliconized graphite support. This model was tested in a plasma tunnel under conditions which kept the tip at 4000° F for nearly 30 min (fig. 51–12). To gain maximum design freedom in either the ablative or hot structure system, it is necessary to know the total radiation efficiency of candidate materials at operating temperatures. To gain maximum operational efficiency, it appears desirable and possibly essential to know also the spectral emittance and absorptance characteristics. Such data, for example, may be used for calculating the radiant exchange between re-entering leading surfaces and the gas cap and with other nearby structures. If such spectral data were available, it is possible to believe that something can be done to favorably alter the radiation characteristics of applied materials by the use of additives or other means. For these and other purposes, NAA has undertaken the task of designing and building an emittance apparatus capable of evaluating specimens at temperatures at least to 4000° F.

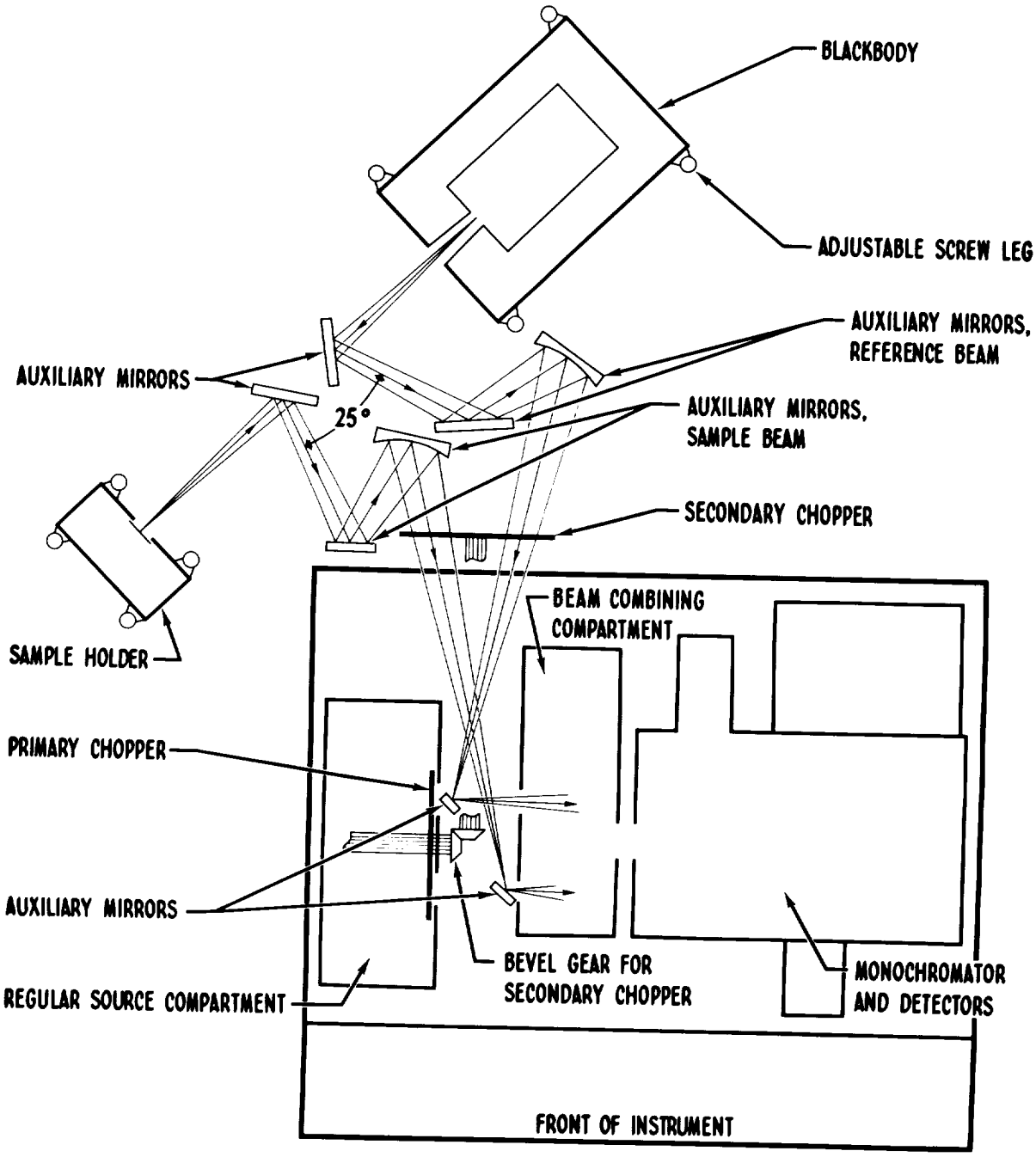

FIGURE 51-8.—Typical layout of reflectometer and emissivity apparatus.

A schematic of the equipment being built is shown in figure 51-13. The specimen is mounted on a shaft and rotated in front of a black-body cavity. Both specimen and cavity are heated in a Curtiss-Wright heating chamber, which is capable of over 5000° F operating temperatures. A single optical system alternately transfers specimen and reference radiation to the spectrophotometer for processing, as before. A single optical path is a highly-desirable feature, since it avoids the problems of matching the optical geometries and reflectances of optical components when two optical paths are utilized. The arrangement shown,

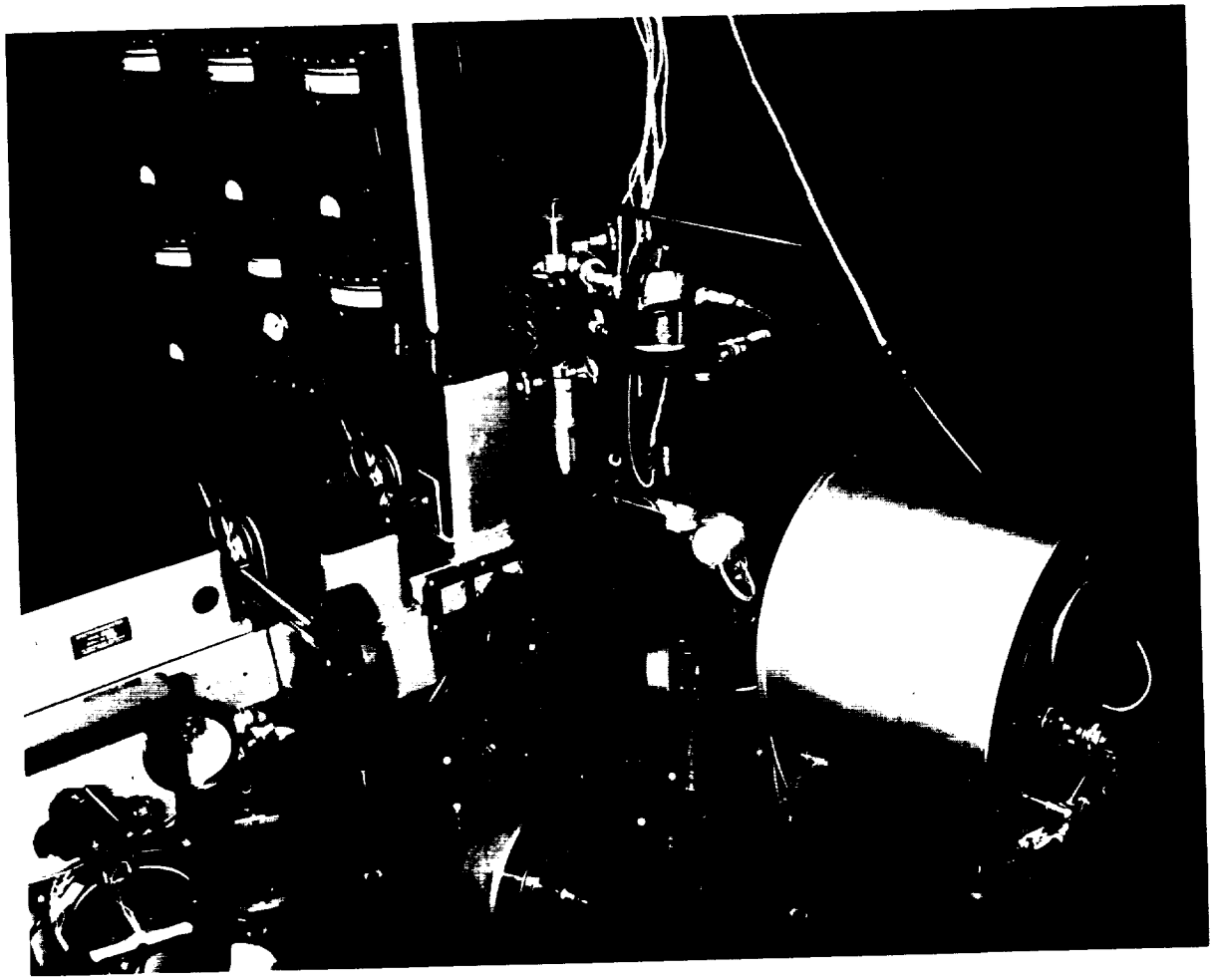

FIGURE 51-9.—Spectral emittance apparatus at North American Aviation Incorporated.

however, is the optical equivalent of a double-beam system.

The complete design of this equipment is a rather involved affair and is more completely covered in reference 2. Just a few of its design problems are discussed here. One problem is that of eliminating stray radiation. This is handled with cooled aperture stops and an internally placed radiation shield (fig. 51-13). The radiation issuing from this shield is, of course, a function of its temperature. Design complexity is minimized, however, if the shield is operated at the highest temperature compatible with desired accuracy. For NAA purposes, the worst case would involve a specimen of emittance equal to 0.1 and heated to 4000° F; the assumed shield emittance is 1.0. A 1% tolerance was assigned for allowable shield radiation in comparison to specimen radiation. Arranged analytically,

$$A_1\epsilon_1 T_1^4 = (0.01)\, A_2\epsilon_2 T_2^4$$

where A is effective radiation area, ϵ is emittance, T is absolute temperature, and subscripts refer to shield and specimen, respectively. For the system shown, the effective radiation areas are essentially the same. Solving for T_2 shows that the shields can be operated at 715° F at 4000° F test temperatures. Lower test temperatures require, of course lower shield temperatures.

Another factor affecting the accuracy of results is specimen cooling during the time it is exposed to the system aperture. The permissible reduction of temperature caused by this "radiation leak" can be calculated, and this

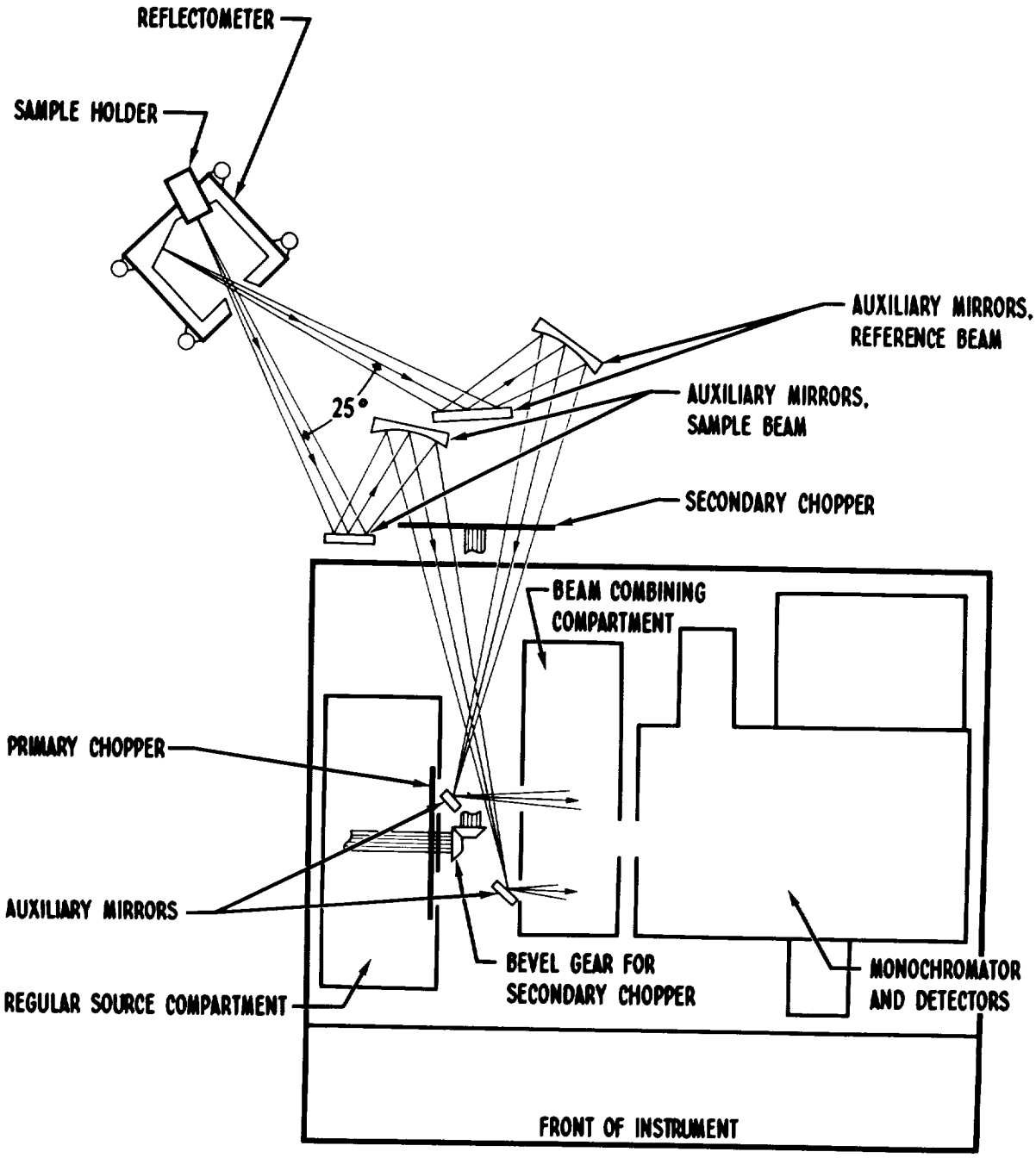

FIGURE 51-10.—Typical layout of reflectometer and emissivity apparatus.

information, in turn, can be used to establish size and shape of the specimen and the rate of shaft rotation. If it is assumed that the cooling effect will be small, the emittance will be essentially equal at actual and test temperature. The apparent emittance, ϵ_A, however, will vary.

By utilizing the Stefan-Boltzmann relationship and setting $\epsilon_A/\epsilon=0.99$, an expression can be set up by which means a value for allowable cooling can be established:

$$\frac{(T-\Delta T)^4}{T^4}=0.99$$

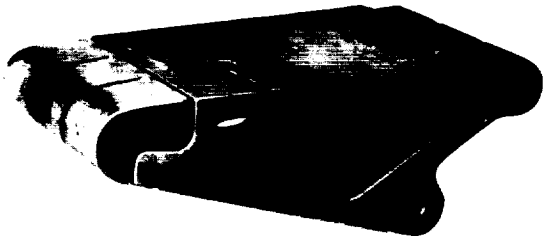

FIGURE 51-11.—Prototype composite leading edge structure.

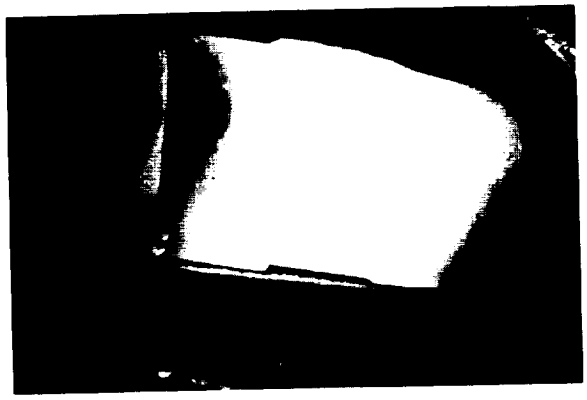

FIGURE 51-12.—Hot structure plasma tunnel tests.

Representative values which have been calculated with this expression are:

T, ° F	2000	3000	4000	5000
ΔT, ° F	7	9	11	13

The next step is to calculate specimen exposure time with the help of an expression found in reference 3,

$$e^{-t/z}=1-\frac{\Delta T}{T-T_0}$$

- e base, natural logarithms
- t time of specimen exposure
- z ratio of thermal capacity to thermal conductance.
- T specimen temperature
- T_0 detector temperature
- ΔT temperature tolerance

The values for z are derived from handbook values and vary from 2 to 6 for specimens ½-inch square by 0.05-inch thick. Representative values thus calculated are tabulated as follows:

T, ° F	2000	3000	4000	5000
ΔT, ° F	7	9	11	13
Low z	2	2	2	2
High z	6	6	6	6
Low t, sec	0. 0073	0. 0062	0. 0056	0. 0053
High t, sec	0. 0218	0. 0186	0. 0168	0. 0159

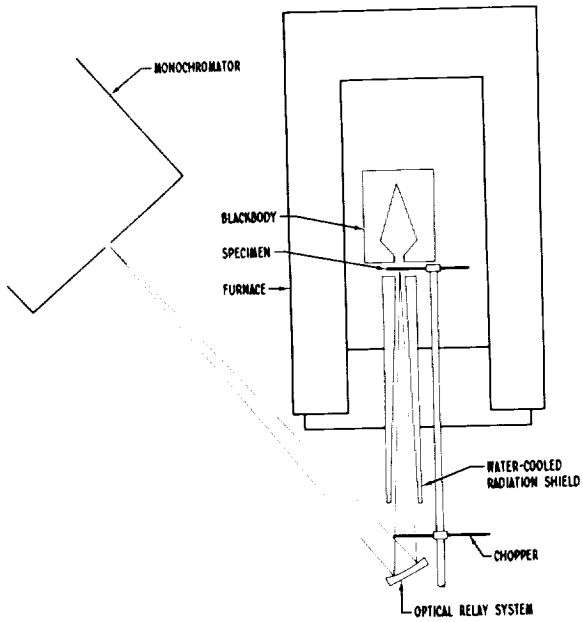

FIGURE 51-13.—Single path, double-beam configuration.

It can be seen that the smallest t is 0.0053 sec. Chopper speed, aperture size, and radial distance of the specimen from the chopper shaft must be selected to be compatible with this value. For example, in the NAA equipment, the specimen occupies $\frac{1}{25}$ of the area swept out by a chopper rotating at 19 cps. The specimen, therefore, is exposed for 0.004 sec., well below the 0.0053-sec. limiting value.

The detectors used in this apparatus require high sensitivity in the wavelengths of interest and must have a fast response time (0.004 sec). For the intended application, the performance of thermocouples appeared marginal. Pneumatic cell-type detectors are suitable concerning wavelength range, but cells with sufficiently fast response time are relatively expensive. The NAA decision was to use two detectors; a phototube in visible regions and a bolometer for longer wavelengths. This, of course, required a mid-run interruption while detectors are changed. Optical components required are dispersing elements, windows, and focusing devices. For dispersing elements, our system utilizes two prisms, a fused quartz prism for use with the phototube, and a calcium fluoride

prism for use with the bolometer. Windows are of potassium bromide and appear to have sufficiently high transmittance over most of the wavelength region of interest (0.35 to 15 μ). For focusing devices, aluminum-coated mirrors are used throughout.

The operational results obtained with this equipment were expected to be available at the time this report was presented. Delays in the procurement of some equipment items, however, require postponement of this information Such data will be available through the Los Angeles Division's Technical Data Section in the near future.

CONCLUDING REMARKS

The design, construction, and use of high-temperature spectral emittance apparatus are relatively recent developments. Preliminary results and data appearing from various laboratories often show significantly different values for ostensibly identical materials. Examination of the methods and equipment indicate that the basic techniques being utilized are essentially the same. It seems that the establishment of a working group (evolved, perhaps, from this symposium) could do much to identify the cause of and resolve discrepancies in data.

The results achieved thus far in the utilization of spectral emittance data for the design of and application to aerospace systems is very encouraging. In our view, developments such as antidetection coatings for military air vehicles, low-absorptance–high-emittance coatings for space radiators, and other spectrally tailored coatings are highly dependent on the availability of such data. Even greater problems lie in future efforts. These problems will be challenging, and their solutions will be limited only by the availability of suitable test equipment and by the human capability to apply obtained data in an imaginative manner.

REFERENCES

1. North American Aviation, Inc.: Emittance Measurement Methods. Report NA–49–1, Jan. 1949.
2. North American Aviation, Inc.: High Temperature Spectral Emittance Feasibility Study. Report NA–60–1064, Jan. 1961.
3. Smith; Hones; and Chasmar: The Detection and Measurement of Infrared Radiation. Clarendon Press, 1958.

52—INVESTIGATION OF SHALLOW REFERENCE CAVITIES FOR HIGH-TEMPERATURE EMITTANCE MEASUREMENTS

BY DWIGHT G. MOORE

NATIONAL BUREAU OF STANDARDS, WASHINGTON, D.C.

Total normal emittance measurements were made on small specimens with shallow reference holes of circular cross section. The ratio of the radiant flux density from the surface to the flux density from the hole was measured and this value then converted to emittance by a theoretical expression based on hole dimensions. The expression applies only to diffusely reflecting materials.

Measurements were made on four different diffusely reflecting materials. Specimens of oxidized nickel that had reference holes with depth-to-radius ratios of 1.7 to 3.7 gave corrected total normal emittance values at 1350° K in the range 0.85 to 0.87. The emittance of oxidized Inconel, when determined for a specimen with a reference hole having a depth-to-radius ratio of 1.7, was found to be in good agreement with values obtained by a heated strip method. The emittance measurements on four sintered alumina specimens varied from 0.43 to 0.47 when measured in air at 1375° K.

The determined emittance for a polished specimen of high-purity graphite with a shallow reference hole increased with temperature linearly from 0.59 at 1100° K to 0.74 at 2150° K. These values were in good agreement with those reported for polished graphite when measured by the rotating specimen method.

Large errors in emittance measurements may arise when a supposed temperature equality between the specimen surface and the reference-blackbody is not closely approximated. At moderate temperatures close equivalence can be achieved through proper use of differential thermocouples. At temperatures above 1800° K, however, thermocouples are not always reliable, and some other method is needed to maintain the necessary temperature balance.

Several investigators (ref. 1, 2, and 3) have incorporated a reference blackbody cavity into either a tubular or spiral-wound specimen in such a way as to insure that the cavity walls and test surface are at the same temperature when the specimen is heated, usually by internal resistance. This approach is satisfactory for metals than can be fabricated as thin sheets or foils; however, it is obviously unsuited for the brittle nonmetals such as carbides, nitrides and oxides. For materials of this type Blair (ref. 4) and Reithof and coworkers (ref. 5) have used a method in which small cylindrical specimens with deep circular reference cavities were heated to high temperatures by high-frequency induction. The ratio of the radiant-flux density from the surface to that from the reference hole was then taken as the emittance of the specimen.

This deep-hole method when properly used may be suitable for metals and for some of the intermetallics, but for materials of low thermal conductivity, such as most nonmetals, a sizeable temperature difference between the hole bottom and the specimen surface is often difficult to avoid. Under most conditions of heating, the magnitude of the difference will increase with hole depth; therefore, if the hole is made shallow, the temperature difference between the hole bottom and test surface will be reduced. While a shallow hole will have an emittance appreciably less than that of a blackbody, it is nevertheless possible to compute its emittance

from theoretically derived expressions. Further, if the specimen material is a diffuse reflector, as are most nonmetals, it has been shown by Gouffé (ref. 6) that under conditions of temperature equilibrium the specimen emittance can be computed from the following expression:

$$\epsilon=\frac{E(1+R-R_0)-R}{1-R+E(R-R_0)} \qquad (1)$$

where:

ϵ emittance of specimen

E ratio of radiant flux density from the surface to the flux density from the hole

R $\frac{1}{2(1+h/r)}$ for a cylindrical cavity and

R_0 $\frac{1}{1+(h/r)^2}$

where:

h hole depth and r=hole radius.

The purpose of the present investigation which is still in progress, is first to test the validity of equation (1) for several diffusely reflecting specimens with shallow reference cavities, and second, in the event that an experimental confirmation is achieved, to measure the total normal emittance of a number of refractory nonmetals by the shallow-hole approach at temperatures as high as 3000° K.

The present paper is a progress report of the investigation. It describes equipment and test procedures, discusses measurement errors that have been encountered and gives the results of preliminary measurements on several different materials. Although additional work is needed, these preliminary results indicate that the shallow-hole approach has considerable promise as a method for the measurement of the emittance of nonmetals.

The author gratefully acknowledges the assistance of Alfred W. Crigler of the NBS staff, who not only constructed much of the equipment but also made many of the measurements.

The investigation is being conducted for the NASA Marshall Space Flight Center, under Contract H-22727.

EQUIPMENT

Figure 52–1 is a schematic drawing and figure 52–2 is a photograph of the furnace equipment which is similar in many respects to that used by Blair (ref. 4). Two types of specimen are used as indicated in figure 52–3. Susceptors for type 1 specimens have been prepared of platinum, iridium, tungsten, and graphite.

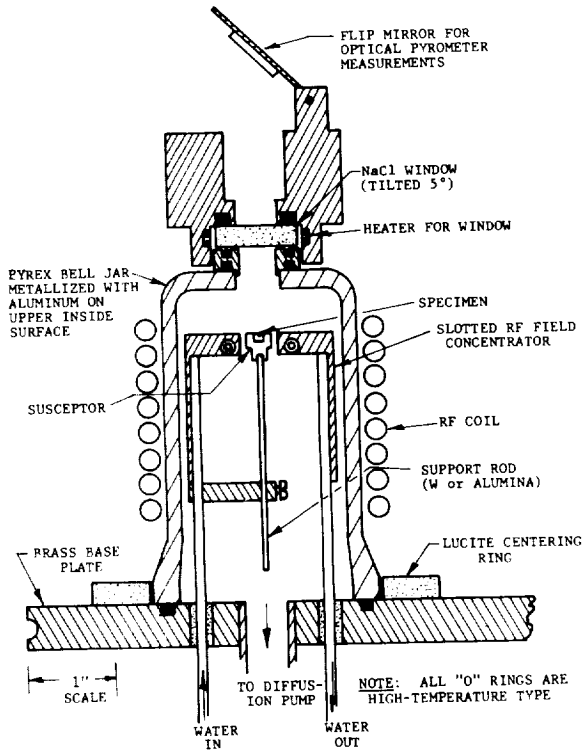

FIGURE 52–1.—Schematic of furnace.

The induced field for heating is supplied by a 10-kw, 30-mc, radio frequency generator with a controlled power output. A water-cooled field concentrator with a longitudinal slot concentrates the energy from the field into the volume occupied by the specimen. The concentrator is fabricated of copper and has a bright plating of silver.

The bell jar consists of a Pyrex glass pipe cap with both ends ground and polished. A ½-in.-diameter hole at the top permits viewing of the specimen through a sodium chloride window.

The vacuum system consists of mechanical pump, oil diffusion pump, and liquid-nitrogen cold trap. A needle valve above the cold trap permits argon to be let into the system. A titanium wire filament is positioned inside the bell jar below the concentrator to purify the

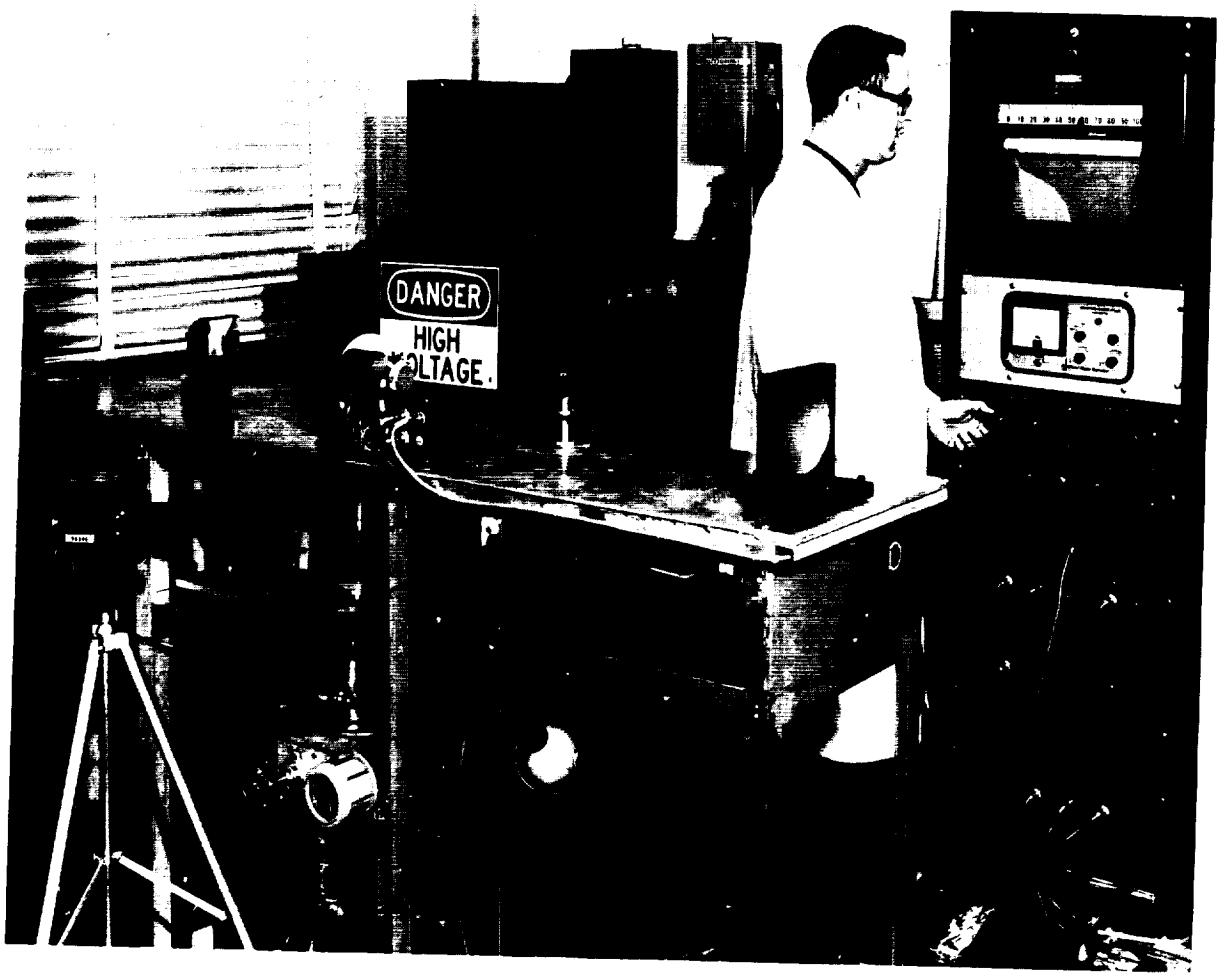

FIGURE 52–2.—Photograph of equipment.

argon. This filament is heated to a bright red heat both before and during test by an auxiliary power supply.

The flip mirror mounted at the top of the bell jar permits the specimen temperature to be measured with a micro optical pyrometer. The pyrometer was calibrated by the Temperature Physics Laboratory of the National Bureau of Standards with both the window and flip mirror in the optical path. The brightness temperature of the test surface was measured at the start and finish of each emittance determination and this temperature was converted to "true" temperature through use of $\epsilon_{0.65}$ values given in the literature. This meant that the specimen temperature was not known with high accuracy; however, because of the relatively minor effect of temperature on thermal emittance, the error from this source was small.

As shown in figure 52–4 radiant energy from the specimen is directed by a 45° mirror (90° fold in fig. 52–4) through a 13-cps chopper, after which it is collected by a 5-in.-diameter spherical mirror and brought to a focus on a thermocouple detector. The path length from the specimen to the mirror is fixed so as to give an image that is twice the size of the specimen.

The detector, which is a commercial vacuum-thermocouple type, is mounted on a base plate that can be moved either vertically or horizontally by means of micrometer screws. These screws permit the detector to be centered at any point on the image within 0.1 mm. A small sheet of platinum foil with 0.5-mm-

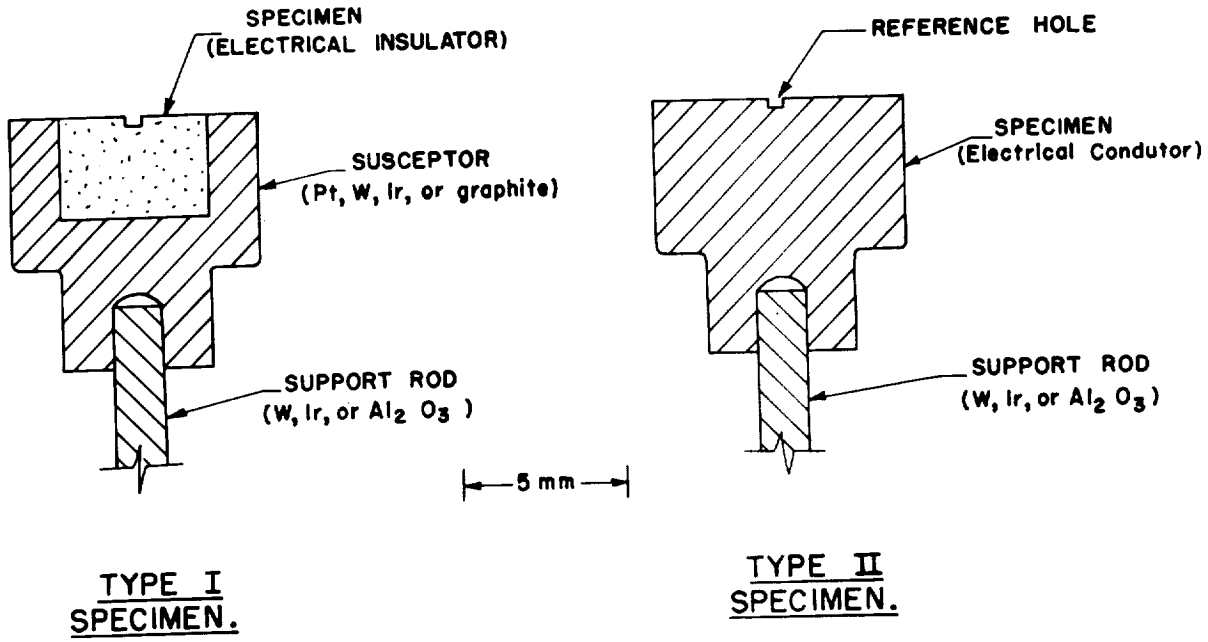

FIGURE 52-3.—Two types of specimens.

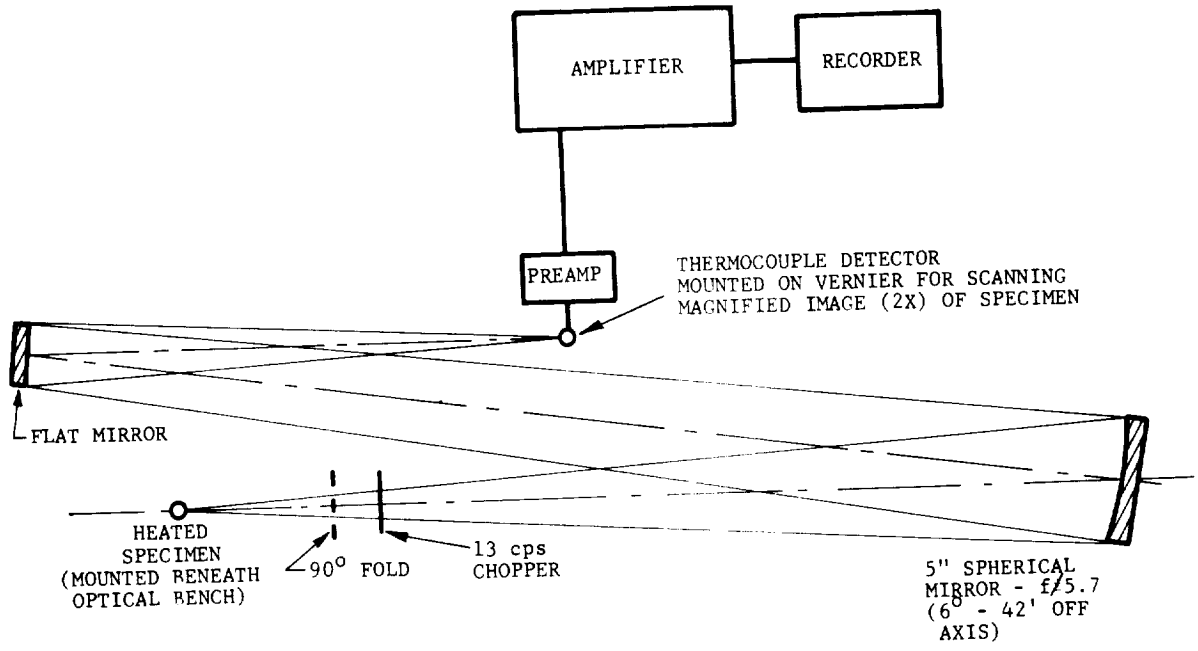

FIGURE 52-4.—Schematic diagram of optics and radiation detection system.

diameter center hole is placed over the front of the detector to serve as a limiting aperture Because of the 2:1 magnification, this means that the detector sees an area of the specimen that is only 0.25 mm in diameter

The equipment for amplifying the detector signal was obtained commercially, as was the electronic high-speed potentiometer. The linearity of response from the detector-amplifier system was tested by placing high-speed sector-

disk attenuators in the beam near the chopper. The attenuator blades reduced the radiant flux reaching the detector by 25, 50, 75, 87.5, and 95%. The response was found to be linear within the limit of error of the measurements.

The optics were aligned visually with a heated specimen as a radiation source. To obtain a satisfactorily uniform detector response from the image of the specimen, it was found that the optical elements had to be accurately aligned so that the radiant flux filled the spherical mirror symmetrically. When this was done, the response from a grit-blasted platinum specimen was found to be uniform to $\pm 1\%$ over a center area of the image which was 3 mm in diameter, and to $\pm 3\%$ over an image area 7-mm diameter.

PREPARATION OF TEST SPECIMENS

Type II specimens (fig. 52–3) were prepared by standard machining practices. The ceramic oxide specimens (type I) were formed by grinding bar specimens into 4.7-mm diameter cylindrical rods on a diamond grinder. These rods were then cut into sections about 3.5 mm long and each section was then ground and polished with No. 14 diamond powder (average particle diameter 14 μ) to give a length of 3.20 ± 0.02 mm. Epoxy resin was then bonded to the face surface and a center hole, approximately 0.5-mm diameter, was formed at the center point with an ultrasonic drill with the No. 14 diamond powder as the cutting medium. The epoxy resin was found to be necessary in order to prevent chipping back of the material from the hole edge. The remaining resin was removed prior to testing by heating the specimen to about 200° C which destroyed the bond between the resin and the specimen. Hole dimensions were measured with a microscope. Care was taken with both metals and nonmetals to insure that the bottoms of the holes were flat.

Each specimen was cleaned ultrasonically in benzene prior to testing. In all tests the top of the type I specimens was flush with the top of the susceptor; also, both types of specimen were positioned so as to be flush with the top surface of the field concentrator.

TEST PROCEDURE

In making a test, the specimen was first centered in the field concentrator and the desired atmosphere achieved. The specimen was then heated to the test temperature as determined with the optical pyrometer sighted on the specimen surface. Once thermal equilibrium was established this temperature was found to remain constant to within about 4° K. No temperature gradients over the 2-mm-diameter test area of the surface were detected with the micro optical pyrometer for any of the specimens tested. Temperature differences as small as 2° K could be detected with the pyrometer.

Prior to making relative flux measurements, the specimen image was scanned with the detector to determine the position of the reference hole. The detector was then positioned over the center of the hole image and the amplifier gain adjusted to give a high reading on the recorder. The detector was next moved to several positions centered on a circle of 1.5-mm radius around the image of the hole center, a reading being obtained at each position. The number of readings varied with specimen uniformity. For most of the porous specimens, eight to twelve readings were required to obtain an average with a satisfactorily low standard deviation, while for polished nonporous specimens, four readings were usually sufficient.

Figure 52–5 is typical of the readings obtained from the two types of specimen. For both types, the ratio, E, in equation (1) was obtained by dividing the average reading from the surface by the reading from the hole center.

RESULTS

Oxidized Nickel in Air

Two type II specimens were prepared of high-purity nickel, each of which contained five 1.25-mm-diameter holes of different depths. Four of the holes were equally spaced on a 4-mm-diameter center line; the fifth was drilled at the center. After oxidation for 1 hour at 1400° K, measurements were made at 1350° K, in air without a sodium chloride window. The purpose of the test was to determine the effect of hole depth on the emittance of a specimen as computed from the flux ratios by the Gouffé expression; the purpose was not to measure the emittance of a well characterized specimen of oxidized nickel.

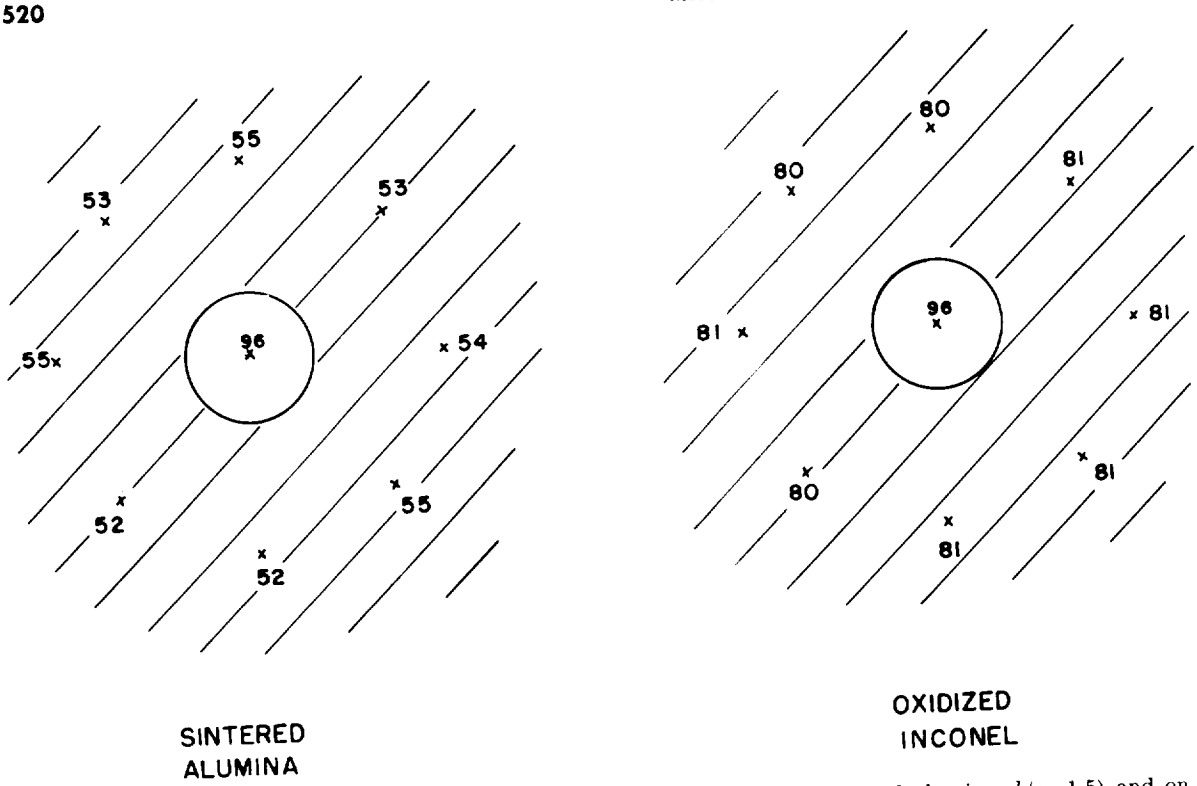

FIGURE 52-5.—Relative flux density measurements on a porous specimen (sintered alumina, $h/r=1.5$) and on a nonporous specimen (oxidized Inconel, $h/r=1.7$). Center circle represents edge of reference hole.

Table 52–I lists the results. Agreement between specimens is good; also the emittances as computed from equation (1) from holes with depth-to-radius ratios of 1.7 to 3.7 all fall within the range 0.86 ± 0.01. The emittances computed from the two most shallow holes (h/r of 0.9 and 0.6) are significantly lower. This indicates that equation (1) is not valid at h/r ratios below 1.0.

TABLE 52–I.—*Total Normal Emittance of Oxidized Nickel at 1350° K*

(Hole diameter = 1.25 mm)

Spec. No.	Hole No.	Hole Depth, mm	h/r [a]	E [b]	ϵ_{tn} [c]
N–1	1	0. 54	0. 9	0. 913	0. 81
	2	1. 13	1. 8	. 895	. 86
	3	1. 77	2. 8	. 872	. 86
	4	2. 16	3. 5	. 874	. 86
	5	2. 32	3. 7	. 862	. 85
N–2	1	. 40	. 6	. 923	. 76
	2	1. 06	1. 7	. 897	. 87
	3	1. 71	2. 7	. 887	. 87
	4	2. 32	3. 7	. 862	. 85
	5	2. 25	3. 6	. 868	. 86

[a] Depth-to-radius ratio.

[b] Ratio of radiant flux from surface adjacent to reference hole to the flux from the hole.

[c] ϵ_{tn} = total normal emittance, computed from equation (1).

Oxidized Inconel in Air

One type II Inconel specimen was prepared in which a single hole, 0.576 mm diameter by 0.486 mm deep, was drilled at the center of the face surface. The specimen was mechanically polished, etched and then oxidized by procedures that were given in detail in a recent report by O'Sullivan and Wade (ref. 7). The radiant flux density from the surface and from the hole was measured at three temperatures and the resulting flux ratios converted to total normal emittance by equation (1). No viewing window was used.

Table 52–II compares the results with those obtained by O'Sullivan and Wade. Agreement is good except for a somewhat lower temperature coefficient for the measurements with the shallow-hole method.

High-Purity Graphite in Vacuum

A small block of graphite was machined into several type II specimens. Principal impurities

TABLE 52–II.—*Total Normal Emittance of Oxidized Inconel*

Temperature		Total Normal Emittance	
° K	° F	O'Sullivan and Wade [a]	NBS Shallow Hole [b]
1033	1400	0. 78	0. 79
1144	1600	. 80	. 80
1255	1800	. 82	. 81

[a] From ref. 7.
[b] Depth-to-radius ratio of reference hole, 1.7.

in the material were, in ppm, 100–200 calcium, < 100 titanium, < 100 iron and < 100 vanadium. The porosity was approximately 25 percent.

The results of measurements made with a highly polished specimen with a depth-to-radius ratio of 2.8 are plotted in figure 52–6. The measurements were made in a vacuum of 5×10^{-6}mm of Hg. As shown in the figure, the values for the polished graphite with filled pores are in good agreement with those reported by Plunkett and Kingery (ref. 8) for a polished commercial-grade graphite as measured by the rotating cylinder method.

The polished graphite used by Plunkett and Kingery contained a small number of pits, caused probably by open pores at the surface. Open pores of this type were filled for the present measurements by first polishing with 3/0 paper that had been wetted with carbon tetrachloride and then heating the specimen in vacuum to 2350° K for 15 min to consolidate the graphite that had entered the pores during the polishing operation. Although the walls of the reference hole were polished, the polish was not equal to that of the specimen surface.

The sizeable increase in emittance caused by presence of a large number of open pores is illustrated in figure 52–6. The specimen used for this test had a depth-to-radius ratio of 2.5. It was dry polished with 3/0 paper and then cleaned ultrasonically to remove the graphite that had entered the pores during polishing.

Sintered Alumina in Air

Type I specimens of alumina were prepared from bars fabricated from 99.9+ alumina that had been cold-pressed and then heat treated at 2075° K to give a porosity of 15.6% (Code 15

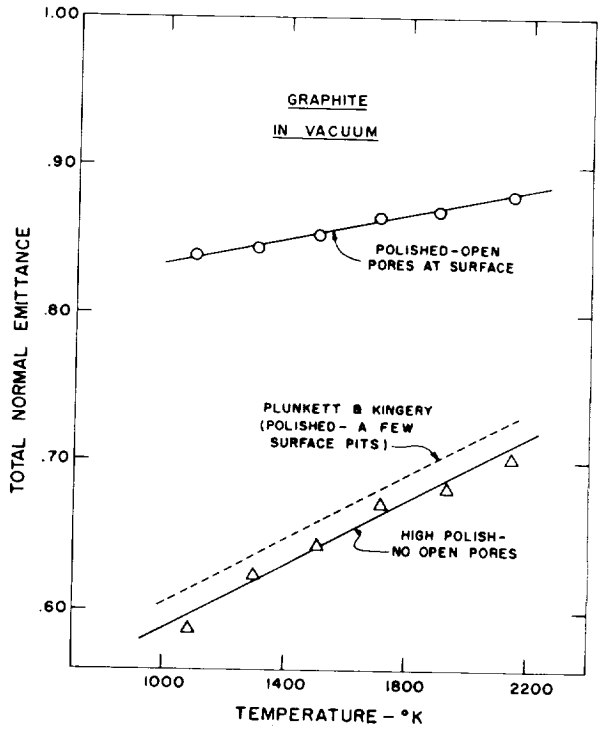

FIGURE 52–6.—Total normal emittance of graphite.

in ref. 9). Tests were made in air in a platinum susceptor at temperatures in the range 1200–1600° K.

The results at a single temperature (1375° K) for the four specimens tested are listed in table 52–III. The variation between specimens is fairly high. This could be caused by real differences in emittances.

A specimen of commercially sintered alumina was also tested. This material when examined with a microscope appeared to have a glass phase with corundum crystals in the matrix. There were very few open pores. Figure 52–7 shows the emittance-temperature curves for the two types of alumina.

MEASUREMENT ERRORS

Precision of Measurement

Repeated determinations on the same specimen with a fixed hole depth at a single temperature showed that the precision of measurement was within ±0.005 emittance unit. This was true even when specimens were removed from the equipment and then repositioned in the field concentrator in a different radial orientation. The same measurement precision was observed for type I and type II specimens.

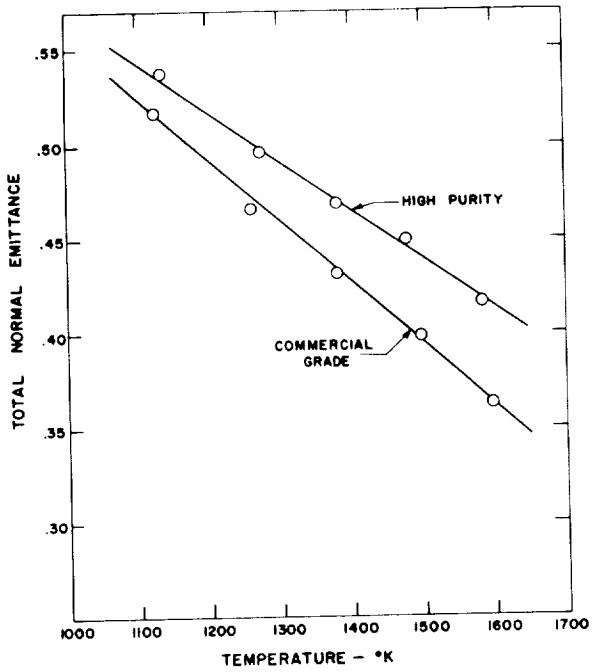

FIGURE 52–7.—Total normal emittance of two sintered alumina specimens.

Table 52–III is a report of some typical data.

TABLE 52–III.—*Total Normal Emittance of High-Purity Alumina Specimens at 1375° K.*

Spec. No.	Hole diam., mm	Hole depth, mm	h/r [a]	E [b]	ϵ_n [c]
A–1	0. 580	0. 433	1. 5	0. 575	0. 43
A–2	. 562	. 510	1. 8	. 580	. 47
A–3	. 550	. 530	1. 9	. 553	. 45
A–4	. 554	. 544	2. 0	. 536	. 43
Average					0. 445

[a] Depth-to-radius ratio.
[b] Ratio of radiant flux from surface adjacent to hole to flux from hole.
[c] Total normal emittance as computed from equation (1).

Back Reflection from Bell Jar

Early in the testing a thin layer of aluminum was vapor deposited on the inside top of the bell jar to serve as a radiation shield and thereby reduce the temperature that the window O-rings would attain during testing. Although no appreciable error from this source was anticipated, recent tests in which measurements were made in air both with and without the bell jar indicated that back reflections from the top of the bell jar caused the emittances as herein reported to be high by about 3%. Future measurements will be made without this reflecting film

Error from Viewing Window

When a sodium chloride window is used in emittance equipment, about 10% of the radiant flux reaching the window is reflected back toward the source. If the window is parallel with the specimen surface, this back reflected energy will reinforce the flux from the surface to a greater extent than it will that from the reference cavity which, in turn, will cause the emittance readings to be high. Tilting of the window at a small angle to the specimen surface should have prevented this window error in the present design. However, it was found late in the testing that the emittance was from 10 to 20% higher with either a flat or tilted window in the beam than when no window was present. Numerous tests have indicated that some of the energy that is back reflected from the viewing window eventually reaches the detector because of multiple reflections within the bell jar. This has necessitated a redesign of the furnace chamber with a radiation trap containing an aperture immediately below the window. The data for graphite in vacuum, as shown in figure 52–6, however, were obtained before the design was changed. The data for oxidized nickel, oxidized Inconel, and sintered alumina were obtained with no window in the system; hence, the data for these materials are free of window error.

CONCLUDING REMARKS

The Gouffé expression is based on two main assumptions; first, that the specimen is a perfectly diffuse reflector and, second, that no temperature differences exist between hole and surface. Neither of these conditions can be achieved in a real specimen, but they can be approached. It follows that errors will always be present in measurements made by the shallow-hole method based on the Gouffé equation. The measurements completed up to the present time suggest that these errors will not be excessive for oxidized metals. They also suggest that the Gouffé expression is valid to within a few percent if (a) the specimens are diffusely reflecting and of relatively high thermal conductivity, and (b) the reference hole

has a depth-to-radius ratio in the range of about 1.5 to 3.7.

The good agreement obtained between measurements on similarly prepared oxidized Inconel made by the shallow-hole approach and those made by O'Sullivan and Wade, who used the heated strip method, can be considered as a confirmation of the Gouffé expression. The agreement observed for graphite with the rotating cylinder measurements of Plunkett and Kingery, however, may be mostly fortuitous, not only because of differences in the two graphites, but also because of the window error. Although this same type of error may have been present from the calcium fluoride window used in the rotating cylinder measurements of Plunkett and Kingery, it seems safe to assume that its magnitude would have been smaller because of their use of a blackened, water-cooled viewing port.

It is believed that the shallow-hole method would find its greatest usefulness in measuring the emittance of polycrystalline ceramics. Because of the low thermal conductivity of such materials, sizeable temperature differences between hole and surface would be expected if deep reference cavities were used. In the case of the alumina specimens, holes approximately 0.5-mm diameter by 0.5 mm deep were employed as reference cavities. While only small temperature differences should be present between holes of this type and the specimen surface, these differences cannot, a priori, be assumed to be negligible. Before the accuracy of the shallow-hole method can be accepted, these differences need to be investigated. Possible approaches include (a) theoretical heat-transfer calculations, (b) temperature measurements made with microsize thermocouples, and (c) comparison of the emittance of an oxide material as determined by the shallow-hole method with the emittance of the same material determined by the rotating specimen method. Because of the importance of temperature equivalence between hole and surface to the reliability of the measurements, it may be necessary to use all three of these approaches. Until this is done, the results reported for sintered alumina should be considered as preliminary and, hence, of questionable accuracy.

APPENDIX—DERIVATION OF GOUFFÉ EXPRESSION FOR COMPUTING EMITTANCE

The original article by Gouffé appeared in Revue d'Optique in 1945. Because it was written in French and also because volumes of this journal may not be readily available, Gouffé's derivation of Equation (1) is given in detail.

CORRECTION FOR EMITTANCE OF A CAVITY

Consider an enclosure of any form (fig. 52–8) at uniform temperature in whose wall is bored an opening of area s, small relative to the total surface area S (opening included) of the wall. This chamber very roughly constitutes a blackbody, whose emittance is, however, not strictly equal to unity.

If ρ denotes the factor of diffused reflection of the material of which the chamber is formed, and Ω, the solid angle in which the radiation of the blackbody is emitted to the outside, the general formula that is often used to express

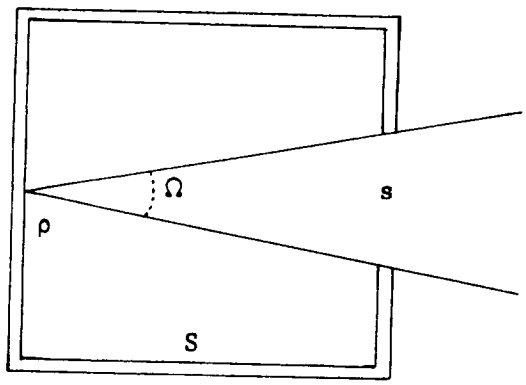

FIGURE 52–8.—Blackbody enclosure.

the effective emittance, ϵ_0, of such a radiator is (ref. 10):

$$\epsilon_0 = 1 - \rho\frac{\Omega}{\pi} \qquad (1a)$$

This equation has been derived by supposing

that a unit incident flux, penetrating into the blackbody through the opening s, is diffusely reflected by the portion of the wall opposite this opening according to Lambert's Law and supposing that only the fraction $\rho(\Omega/\pi)$ of this flux goes out again from the chamber diffused into the solid angle Ω in which the cavity can radiate. One assumes that the portion of incident flux diffusely reflected toward the wall of the chamber is completely absorbed by the latter, which is manifestly inexact, since this wall reflects it diffusely in turn in all directions, particularly toward the opening. The emerging flux therefore must be appreciably larger than $\rho(\Omega/\pi)$.

In order to obtain its exact value, it is necessary to take into account the multiple diffuse reflections which are produced in the interior of the chamber.

If we consider an element dS of the internal wall of the radiator, the total flux which it emits includes:

1. the flux dF due to its own radiation.
2. the flux $\rho d\phi$ diffusely reflected by the element and proceeding from the flux $d\varphi$ emitted by the other parts of the internal surface of the blackbody and incident on dS.

Since the element dS can be compared in rough approximation to a perfect blackbody of uniform radiance as defined, the total flux which it emits is proportional to its area dS. As the flux, dF, due to the natural radiation of the element is also proportional to dS, the result is that the flux $d\varphi$ is in turn proportional to dS. This means that after multiple reflections in the interior of the chamber, the emitted flux φ distributes itself uniformly over the internal surface of the radiator and, for present purposes, it will be assumed that this uniform distribution of emitted flux is brought about as early as the second reflection.

Now return again to the case of a unit incident flux penetrating into the blackbody through the opening, s, and consider the fraction of that flux which after an infinite number of diffuse reflections, will be absorbed by the wall. This fraction will be equal to the sought-for emittance of the cavity.

The fraction of the flux leaving through the opening, s, after the first reflection has the value $\rho(\Omega/\pi)$,[1] just as we have already shown at the beginning, and there is left in the chamber, a flux, $1-\rho(\Omega/\pi)$, which undergoes a second reflection after that; conforming to the above-mentioned hypothesis we assume that it is uniformly distributed.

Under these conditions, the fraction of the flux twice reflected which leaves through s will have for its value:

$\rho^2(1-\Omega/\pi)s/S$ and there will remain in the interior $\rho^2(1-\Omega/\pi)(1-s/S)$ which will be reflected again.

The fraction of flux reflected 3 times leaving through the opening will be:

$$\rho^3\left(1-\frac{\Omega}{\pi}\right)\left(1-\frac{s}{S}\right)\frac{s}{S}$$

and

$$\rho^3\left(1-\frac{\Omega}{\pi}\right)\left(1-\frac{s}{S}\right)^2,$$

will remain.

On the whole, a total flux:

$$\rho\frac{\Omega}{\pi}+\rho^2\left(1-\frac{\Omega}{\pi}\right)\frac{s}{S}\left[1+\rho\left(1-\frac{s}{S}\right)+\rho^2\left(1-\frac{s}{S}\right)^2+\rho^3\left(1-\frac{s}{S}\right)^3+\cdots\right]=\rho\frac{\Omega}{\pi}+\frac{\rho^2\left(1-\frac{\Omega}{\pi}\right)\frac{s}{S}}{1-\rho\left(1-\frac{s}{S}\right)}$$

will be leaving through the opening s.

The total emittance of the cavity is then:

$$\epsilon_0=1-\rho\frac{\Omega}{\pi}-\frac{\rho^2\left(1-\frac{\Omega}{\pi}\right)\frac{s}{S}}{1-\rho\left(1-\frac{s}{S}\right)}=\frac{(1-\rho)\left[1+\rho\left(\frac{s}{S}-\frac{\Omega}{\pi}\right)\right]}{1-\rho\left(1-\frac{s}{S}\right)}$$

But $1-\rho$ is the emittance, ϵ, of the material which constitutes the wall (supposedly opaque) of the cavity, hence:

$$\epsilon_0=\frac{\epsilon\left[1+(1-\epsilon)\left(\frac{s}{S}-\frac{\Omega}{\pi}\right)\right]}{\epsilon\left(1-\frac{s}{S}\right)+\frac{s}{S}} \qquad (2)$$

[1] This assumes that the material constituting the chamber is a perfectly diffuse reflector, and that Ω is a small fraction of π.

This expression of total emittance of the cavity, although more complex than that which provided equation (1*a*), is much more satisfactory because it includes factors for the shape of the chamber in the form of the ratio s/S in addition to the aperture, Ω, of the radiator and its natural emittance, ϵ.

In the general case of a chamber, of any shape, equation (2) can be written in the form [2]

$$\epsilon_0=\frac{\epsilon\left[1+(1-\epsilon)\left(\frac{s}{S}-\frac{s}{S_0}\right)\right]}{\epsilon\left(1-\frac{s}{S}\right)+s/S} \qquad (3)$$

S_0 representing the surface of a sphere of the same depth as the cavity in the direction normal to the opening, s.

In equation (3), ϵ_0=emittance of cavity, ϵ=emittance of material, s/S=ratio of area of opening to area of cavity (opening included)= $1/2(1+h/r)$ for a cylindrical cavity of depth, h, and radius, r, and $s/S_o=1/1+(h/r)^2=\Omega/\pi$ for $(r/h)\rightarrow 0$.

[2] Equation (3) is a combined form of Gouffé's equations (2*b*) and (4).

Equation for the Emittance of a Material

If E is the ratio of the flux density from the surface to that from the bottom of the hole, ϵ is the emittance of the specimen, and ϵ_0 is the emittance of the hole, then
$\epsilon=E\epsilon_0$, or when equation (3) is substituted for ϵ_0,

$$\epsilon=\frac{E\left(1+\frac{s}{S}-\frac{s}{S_0}\right)-\frac{s}{S}}{1-\frac{s}{S}+E\left(\frac{s}{S}-\frac{s}{S_0}\right)} \qquad (4)^3$$

and, if $s/S=R$ and $s/S_0=R_0$ as in equation (1) in the main body of the report, then

$$\epsilon=\frac{E(1+R-R_0)-R}{1-R+E(R-R_0)}$$

[3] Gouffé equation (5).

REFERENCES

1. De Vos J. C.: Evaluation of the Quality of a Blackbody. Physica, vol. 20, no. 10, Oct. 1954, pp. 669–689.
2. Ornstein, L. S. (Communicated by): Tables of the Emissivity of Tungsten as a Function of Wavelength From 0.23 μ —2.0 μ in the Region of Temperature 1600°–3000° K. Physica, vol. 3, no. 6, June 1936, pp. 561–562.
3. Forsythe, W. E.; and Adams, E. Q.: Radiating Characteristics of Tungsten and Tungsten Lamps. Jour. Opt. Soc. Am., vol. 35, no. 2, Feb. 1945, pp. 108–113.
4. Blair, G. R.: Determination of Spectral Emissivity of Ceramic Bodies at Elevated Temperatures. Jour. Am. Cer. Soc., vol. 43, no. 4, Apr. 1960, pp. 197–203.
5. Reithof, T. R.; Achione, B. D.; and Branyau, E. R.: High Temperature Spectral Emissivity Studies on Some Refractory Metals and Carbides. Symp. on Temperature—Its Measurement and Control in Science and Industry. Columbus, March 1961, Preprint no. B. 10. 2.
6. Gouffé, A.: Temperature Corrections of Artificial Black Bodies, Taking Multiple Internal Diffusion into Consideration. NRL Trans. 429, translated from Revue d'Opt. 24, Jan.–Mar. 1945, pp. 1–10.
7. O'Sullivan, William J., Jr.; and Wade, William R.: Theory and Apparatus for Measurement of Emissivity for Radiative Cooling of Hypersonic Aircraft with Data for Inconel, Inconel X, Stainless Steel 303, and Titanium Alloy RS–120. NASA TR R–90, 1961.
8. Plunkett, J. D.; and Kingery, W. D.: The Spectral and Integrated Emissivity of Carbon and Graphite. Proc. of the Fourth Conf. on Carbon, Pergaman Press, N.Y., 1959, pp. 457–472.
9. Lang, S. M.: Properties of High-Temperature Ceramics and Cermets; Elasticity and Density at Room Temperature. Nat. Bur. Standards Monograph No. 6, Mar. 1960.
10. Ribaud, G.: Traite de Pyrometric Optique, p. 232.

DISCUSSION

SKLAREW, The Marquardt Corp.: Have you determined the effect of the hole shape on the accuracy of they system?

MOORE: No we haven't. We decided to use a cylindrical hole because holes of this type can be drilled into a ceramic specimen fairly easily with a Cavitron. Also, if we are using metal or some of the non-metals we can drill holes of this type with an ordinary drill. The expression can also be used for holes with a conical bottom, although we haven't tried them. I think you would have more difficulty in forming such holes. The holes that we use are very small; they are only ½ mm in diameter.

SCHATZ, American Machine and Foundry: What would be the calculated emittance of the shallow blackbody cavities having different depth-to-radius ratios, such as 1.5, and 1.8.

MOORE: If a material is a diffuse reflector the efficiency can be computed. You have to assume an emittance of your specimen material in order to calculate the emittance of the cavity. I don't know that we have ever done that on a cavity with a depth-to-radius ratio of 1.5. In the case of alumina specimen, I think the emittance of the cavity would be about 0.8.

SCHATZ: Isn't that far from what it should be?

MOORE: In this method we know that we are not looking at a blackbody cavity, but if the theory is correct, and we think it is, and if we have a diffuse reflector, it all balances out in the Gouffé expression. The nice part of using this expression is that you do not have to know the emittance of the specimen material. The shallow hole method is based on the use of a reference hole of fixed geometry; the emittance of this hole need not be known.

SCHATZ: I am not sure I understand. Assuming the Gouffé expression for a blackbody with the depth-to-radius ratio of 1.5, would you have a cavity with an emittance approximating 1.0?

MOORE: No, the blackbody does not approximate 1.0.

RICHMOND, National Bureau of Standards: I think that I can clear up the misunderstanding. The point is that we do not have a very good blackbody, but since we know how bad it is, we can make corrections for it.

MOORE: That is one way of saying it.

LEE, Avco Corporation: You stated, at the beginning of the paper, that you made some assumptions. One was that you should have a perfectly diffuse cavity and that the cavity walls should have the same emittance as the surface. Now, in some of these ceramic materials, sintered materials, or pressed materials, the surface has a very much different character than the substrate material, and the hole is so shallow that you may not be able to realize these assumption. Could you perhaps discuss this a little more?

MOORE: Of course, all of these specimens that we prepared were machined specimens. In other words, we were not using the original surface of the ceramic after firing. The test surface was first ground with diamond powder and then we drilled our hole with the same diamond powder using a Cavitron so that the two surfaces in that respect were comparable. Granted there are certain assumptions in use of this shallow hole method. At the moment, we are just interested in seeing what kind of accuracy we can obtain through its use. The method is intended for very high temperature measurements and I know there is much more work needed on it. For one thing, we need a good heat-transfer analysis, which is very difficult with the type of specimens that we are using. But we hope to make such an analysis before too long, and again I would like to say that this is a progress report. We are not, as yet, ready to recommend it as an accurate method of emittance measurement.

ZISSIS, Institute for Defense Analyses: As far as I know the De Vos treatment is more accurate than the Gouffé treatment and is superior to it in every way except in simplicity. If you take the DeVos calculations, assume a perfectly diffuse wall and no temperature gradient, you get the generalized Gouffé expression, $1-\rho/(\Omega/\pi)$. Using the De Vos expressions, you have a chance to evaluate the effects of different characteristics of the walls of your shallow cavity and also to consider how big a difference would be introduced by a temperature gradient. I wonder if more theoretical work of this type is being planned, or whether you feel that this is beyond the precision of the experiment.

MOORE: Well, we certainly have studied the De Vos expression, as well as some of the others that have been developed. As you say, most of them are much more complex in nature than the Gouffé equation. We plan to investigate some of these other expressions to determine if they will bring the data into better agreement, but right at the moment our problems are not so much in the use of the expressions for calculation of the emittance as they are in the elimination of temperature differences between hole and surface. Large errors will be introduced unless we can reduce this temperature difference to a small value.

R. L. COX, Chance Vought Astronautics: I would like to compliment Mr. Moore on his very interesting and excellent paper. Some work has been done by Dr. Sparrow at the University of Minnesota on the emission from holes with temperature gradients down the cavity. I believe it might help resolve your temperature gradient problem if such an analysis were performed.

MOORE: I must admit that I had not seen this recent publication by Professor Sparrow, but I have made a note to look that up just as soon as I get back. Of course, one nice thing about the Gouffé expression is that the emittance term is eliminated from the equation that we use. I doubt that this would be possible with some of the other expressions.

53—EMITTANCE MEASUREMENTS OF REFRACTORY OXIDE COATINGS UP TO 2900° K

BY V. S. MOORE, A. R. STETSON, AND A. G. METCALFE

SOLAR, A SUBSIDIARY OF INTERNATIONAL HARVESTER, SAN DIEGO, CALIFORNIA

The hot-filament method for the measurement of total hemispherical emittance has been adapted for ceramic coatings. The radiated energy per unit area is measured simply and accurately by potential probes in the uniform temperature region of the filament. Several methods have been examined to determine the true surface temperature. An approximate solution has been used in which it has been assumed that the coating is a gray body. In this case, the true surface temperature and emittance are determined from the solution of simultaneous equations derived from the Wien and Stefan-Boltzmann Laws. A more accurate method is based on the use of the hot filament as a resistance thermometer. For opaque, non-conductive, uniform coatings, it can be shown that extrapolation of this resistance temperature to zero thickness coatings for constant energy radiated per unit area gives the true surface temperature for this density of radiation.

An analysis of the sources of error shows that this method is capable of high accuracy if suitable filaments can be found for the ceramic coating under study.

The need for emittance data has increased markedly in the last few years. This need is particularly true of space applications where radiation is the principal means of heat transfer. In the development of radiation-cooled structures for superorbital re-entries,[1] coatings of the highest emittance are required to operate at temperatures up to 2900° K. Solar has adapted the well-known hot-filament method to such measurements.

The principle of the hot-filament method is that the energy radiated per unit area, E/A, is determined from the electrical power dissipated over a known length in a constant temperature region (ref. 1). From the surface temperature (T_F), usually determined with very fine thermocouples attached to the surface, the emittance can be calculated from the Stefan-Boltzmann radiation equation $E/A = \sigma\epsilon(T_F^4 - T_S^4)$, where

σ Stefan-Boltzmann constant
ϵ total hemispherical emittance
T_S temperature of absorber (usually negligible at high T_F)
A Radiating surface area

Errors in the method are almost all related to the accuracy with which surface temperatures can be measured (ref. 1). On highly conductive metals and coatings to which the thermocouples can be metallurgically bonded, errors can be minimized. With ceramic coatings, large errors in surface temperature measurement occur. For example, at 2500° K thermocouples of tungsten −25% rhenium vs. tungsten (0.005-in. diameter wires) may read as much as 500° K lower than the true temperature. Such differences are not surprising in view of the high thermal gradients in coatings of low thermal conductivity. These may reach 30,000° C per inch.

In the method described, these problems are avoided by measuring the filament temperature. Tungsten filaments have a high temperature coefficient of resistivity so that simple measurements permit the temperature to be calculated to an accuracy of approximately 3° K. The true surface temperature is obtained from measurements with different coating thicknesses followed by the extrapolation to zero coating thickness for constant energy radiated per unit area.

[1] The work described was performed on U.S. Air Force contract AF33(616)8497 under the technical direction of Jesse Ingram M/Sgt., USAF.

EXPERIMENTAL METHOD

Apparatus

The apparatus is shown in figures 53–1 and –2. The water-cooled bell-jar is blackened inside so that essentially complete absorption of all incident radiation occurs. The tungsten filament is ⅛-inch diameter by 9½ inches long and is heated by a 500-amp d-c source. The chamber can be pumped down to 10^{-5} torr, although many measurements are made at 10^{-4} torr because it has been found that volatilization of materials at 2900° K is reduced somewhat at the higher pressure.

The base plate is water cooled and has provision for the introduction of thermocouple wires and potential leads. The potential leads are 0.005-inch diameter tungsten wires to avoid thermoelectric effects. Preliminary surveys by optical pyrometer have shown that 1½-inches on either side of the center of the rod is at uniform temperature. Potential leads are spaced 2 inches apart within this zone (fig. 53–3). The tungsten filaments or rods are ground to an accuracy of 0.001 inch and the potential leads are located with an accuracy of 0.010 inch. The potential drop is measured by a high-input-impedance vacuum tube voltmeter with an accuracy of ±½ percent. The current is measured by means of a precision current shunt (±½ percent

FIGURE 53–1.—Total hemispherical emittance test chamber and instrumentation.

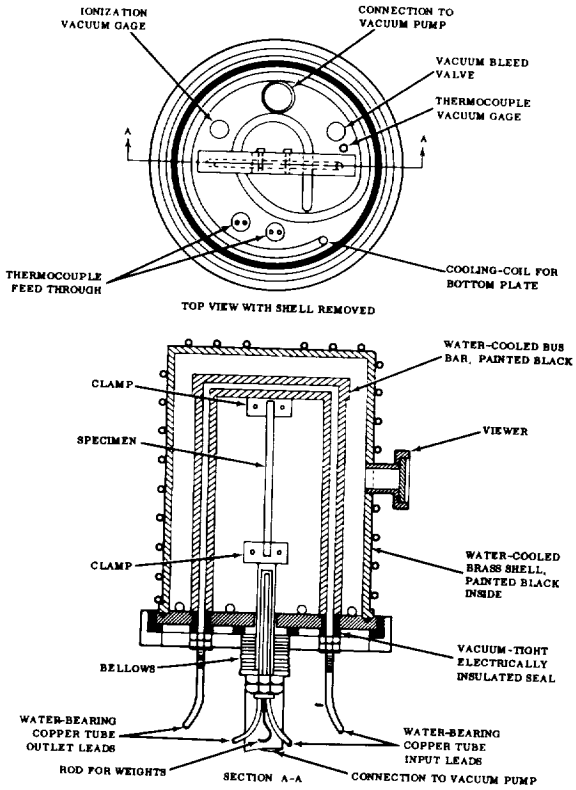

FIGURE 53–2.—Schematic drawing of emittance test apparatus.

accuracy) using a Leeds & Northrup K2 potentiometer.

Test Method

The resistivity of the tungsten filaments was determined as a function of temperature in preliminary work. The temperature was determined by melting points and by optical pyrometry. Short lengths of fine wires were spot welded to the tungsten and the temperature of melting observed. Gold (1336° K), platinum (2042° K), and molybdenum (2893° K) were used in this calibration. These determinations showed that optical pyrometer readings on the tungsten surface could be corrected by published spectral emittance data (ref. 2) to give results in agreement with the melting points. It was found that rods from one vendor gave reproducible resistivity-temperature curves with an average scatter of data points within 6° K of the curve. Rods from a second vendor gave slightly different results with a maximum separation of the curves of 12° K. The resistivity-temperature curves determined in this way agreed within the same accuracy with the best available data for tungsten (ref. 2).

A series of these tungsten rods was coated with ceramic by plasma-arc spraying to produce coatings varying in thickness from 0.0025 inch to 0.012 inch (0.06 to 0.30 mm). Yttria-stabilized hafnia gave excellent coatings on tungsten rods and this combination will be used to discuss the test procedure and results. It is necessary that the rod-coating combination be compatible in both physical and chemical properties.

The coating is removed by grinding small "windows" approximately 2 inches apart and attaching the 0.005-inch tungsten leads by spot welding. These wires can be seen in figure 53–3 The separation distance of these leads is measured by vernier calipers.

Experimental measurements are made in the following sequence:

1. The calumber is evacuated and the tungsten rod heated to 1650° K.
2. The potential drop across the current shunt is measured to determine the current I.

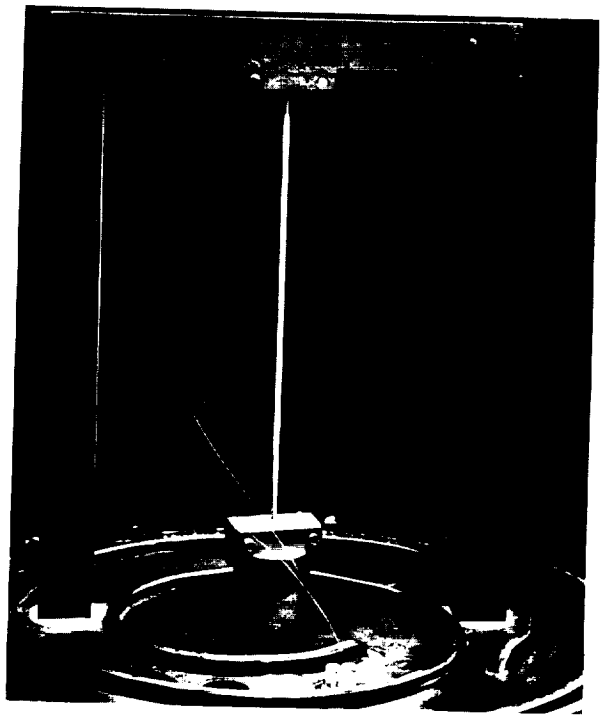

FIGURE 53–3.—Emittance test chamber showing specimen and voltage measurement leads.

3. The potential drop, V, along the tungsten rod is determined over the 2-inch length.
4. From the potential drop, the current and the known dimensions, the resistivity of the tungsten is determined and hence the tungsten temperature, T_W.
5. The energy radiated per unit area of the coating is calculated and plotted against T_W as shown in figure 53–4.
6. Measurements are repeated at higher temperatures up to a maximum of 2900° K tungsten temperature.

The following assumptions are made to complete this analysis:

1. Heating is solely in the tungsten, i.e., the coating is nonconductive.
2. Coatings are applied uniformly and consistently in different thicknesses.
3. At the same level of energy radiated per unit area, the surface temperatures of the coatings are equal.
4. The coating is opaque to radiation.

On the basis of these assumptions, both the true surface temperature and energy radiated can be corrected for the effect of the thermal gradient in the coating by an extrapolation to zero thickness. A plot for constant tungsten temperature is shown in figure 53–5. Extrapolation to zero thickness gives the energy radiated for a ceramic surface temperature equal to the tungsten temperature. From these data, the emittance is calculated using the Stefan-Boltzmann equation. The results of measurements on hafnia are shown in figure 53–6.

DISCUSSION OF METHOD

Three assumptions are made in the analysis of results. These assumptions are that the coatings are non-conductive, opaque, and uniform. Each of these assumptions has been investigated. Conduction in the coating will cause errors because of heating within the coating and of a reduction in the resistance that will be attributed to a lower tungsten temperature. Both errors will decrease to zero as the thickness of the coating decreases so that they will be eliminated by the method of extrapolation. The effect is small, in any case: for a coating with a resistivity of 10^{-1} ohm-cm, the

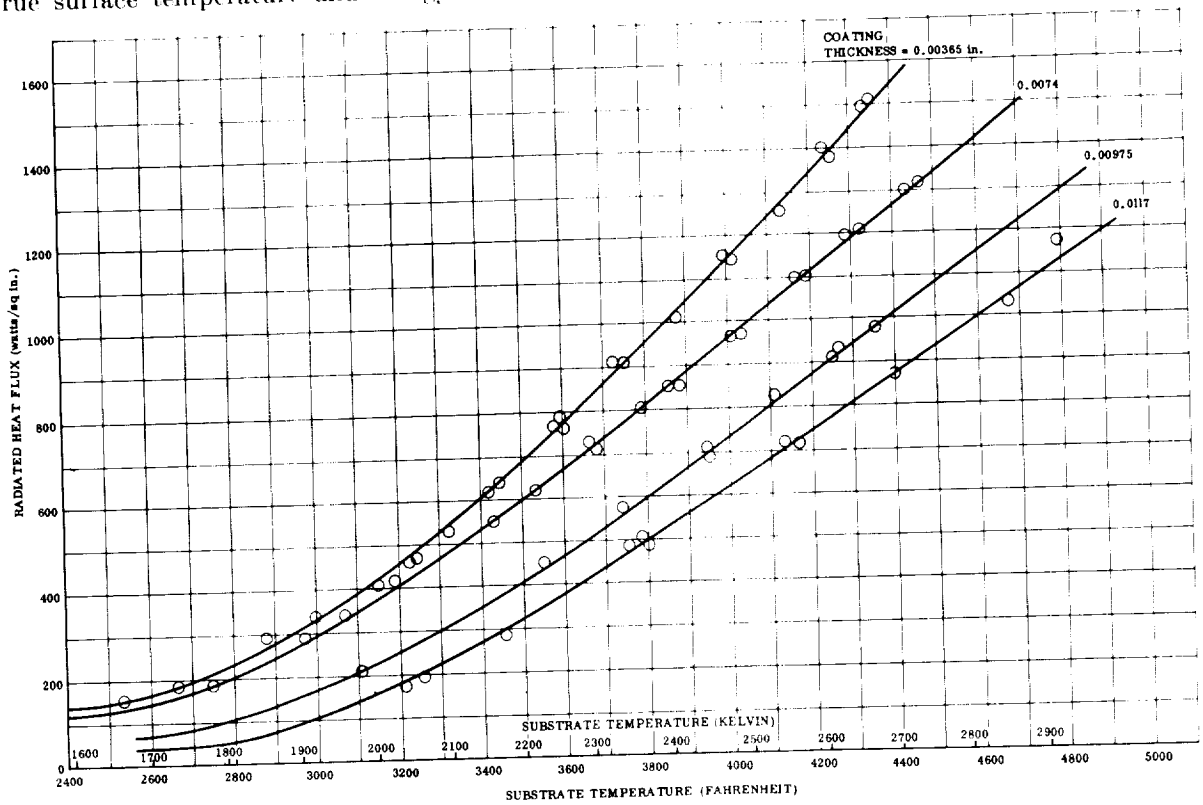

FIGURE 53–4.— Radiated heat flux for plasma-arc sprayed hafnia (yttria-stabilized) vs tungsten temperature.

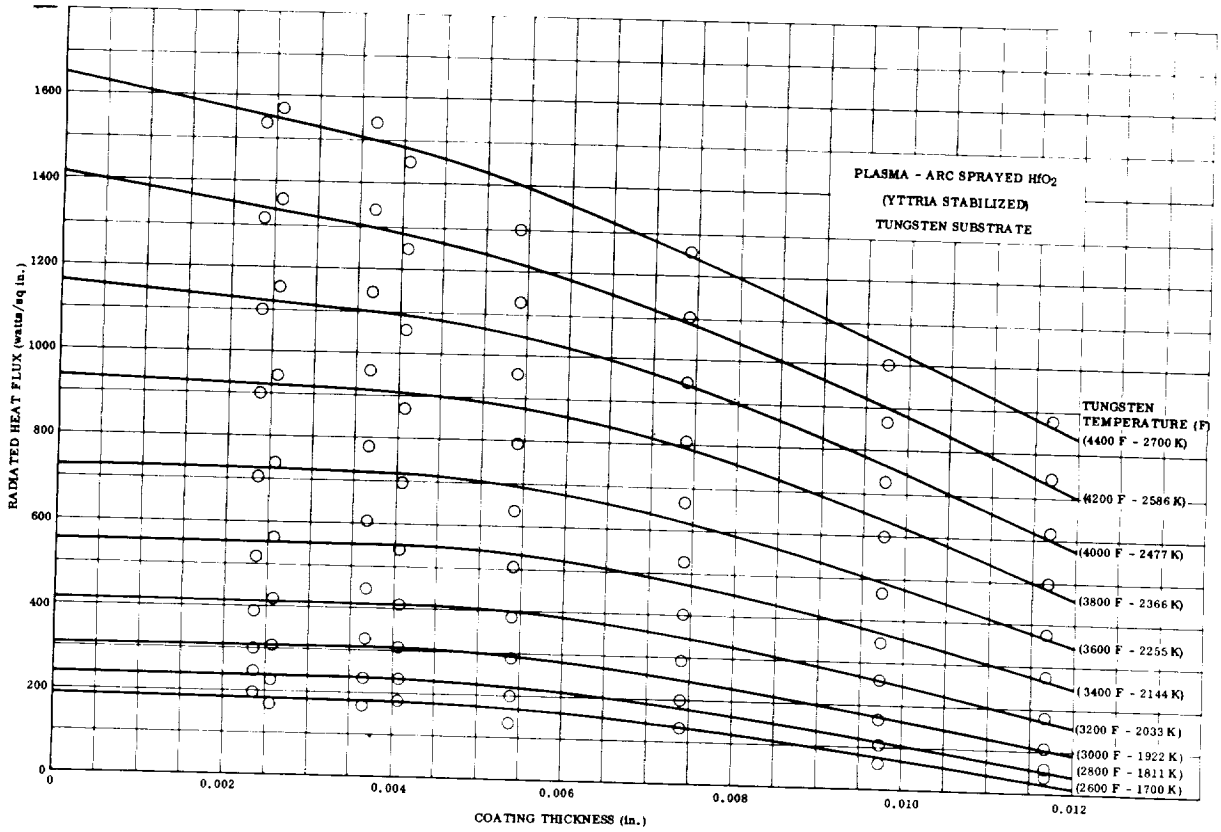

FIGURE 53–5.—Radiated heat flux vs coating thickness at constant substrate temperature of hafnia (yttria-stabilized).

tungsten temperature will never be in error by more than 0.04%. This error increases to 4% for a resistivity of 10^{-3} ohm-cm so that complete elimination of the error by extrapolation is no longer certain.

Opacity of the coatings is essential if a single surface temperature can be used to represent the temperature of the emitter. This has been tested in a simple manner by plotting the brightness temperature measured by optical pyrometer against the energy radiated from the coating. If the thin coatings become sufficiently transparent to permit energy to be radiated directly from the tungsten rod, then the optical pyrometer readings will no longer vary as the radiated heat flux. Figure 53–7 shows that the coatings appear to remain opaque at thicknesses as low as 0.0025 inch. The true surface temperature has been determined previously (fig. 53–5) so that these optical pyrometer readings allow the spectral emittance to be calculated and plotted in figure 53–6. These values are for a wavelength of 6500 Å for the microoptical pyrometer.

Uniformity of the coatings is the final assumption. It has to be assumed that all coatings are alike so that the thermal conductivity is reproducible and hence the temperature gradient in the coating. The scatter in figure 53–5 is believed to be attributable mainly to differences in the coatings rather than differences in measurement. Sections of coatings have been examined, and these show that the surface irregularity is such that the average radiating surface is approximately 0.0005 inch below the surface measured by a micrometer. Figure 53–5 shows that this correction can be applied readily by extrapolation to a thickness of 0.0005 inch rather than zero thickness. The effect of this correction is very small because the area is also reduced so that the radiated energy per unit area is changed in opposite directions. Sections of coatings show that some tungsten is also transferred to the lower

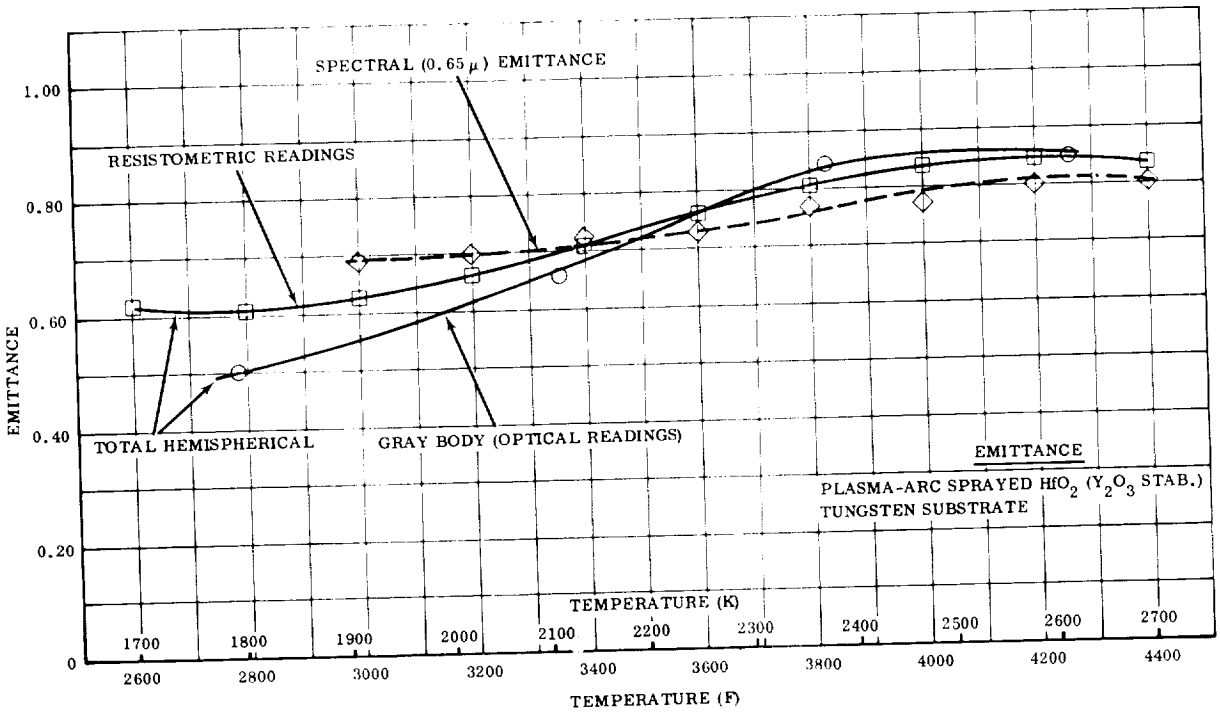

FIGURE 53-6.—Spectral and total emittance of plasma sprayed hafnia (yttria-stabilized).

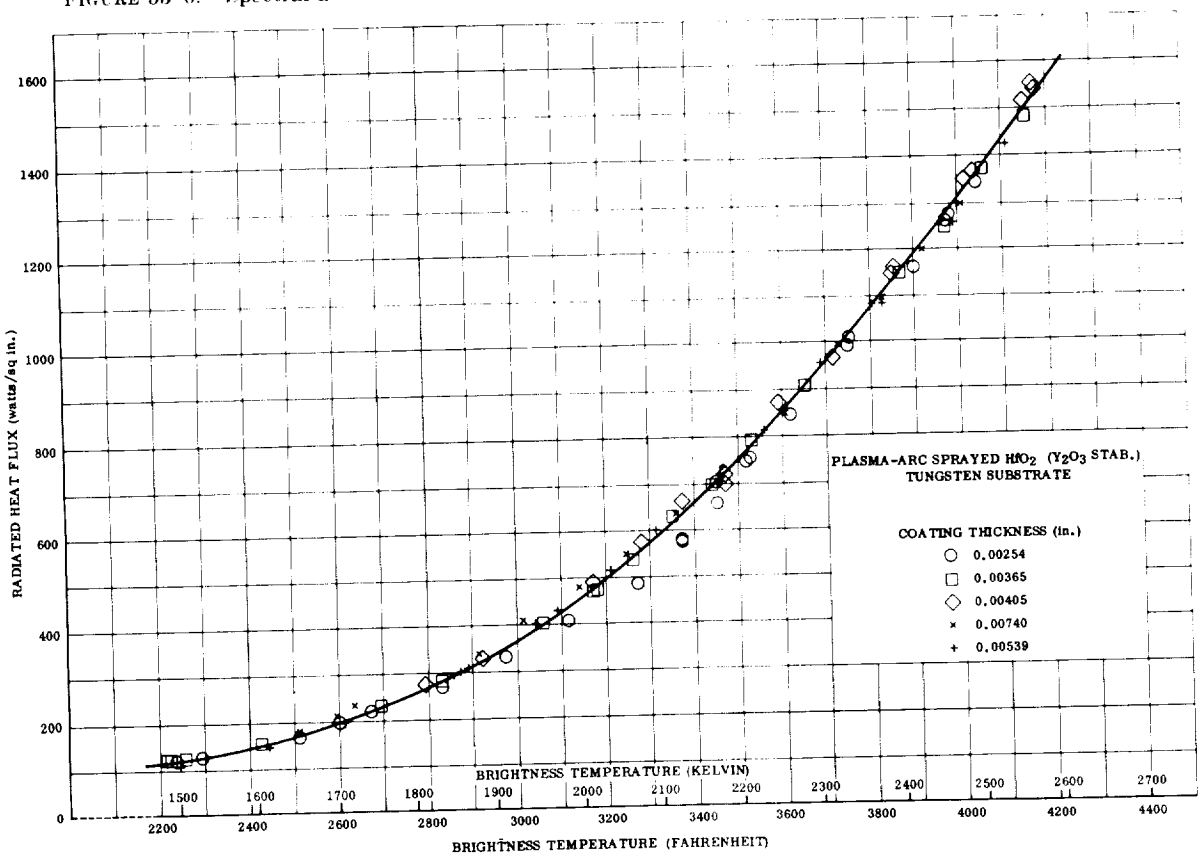

FIGURE 53-7.—Brightness temperature vs radiated heat flux for various thicknesses of hafnia.

layers of the coating by an unknown mechanism. It is believed that this is responsible for the flattening of the curves in figure 53–5 below 0.004 inch. The higher thermal conductivity of the lower layers would cause the thermal gradient to be smaller in this region and hence the energy radiated will not change as rapidly with thickness.

Other work has shown that the hafnium oxide is not completely stable in high vacuum at high temperatures. Some dissociation to HfO_n occurs where a typical value of n might be between 1.98 and 2.00, depending on temperature and pressure. Subsequent work in a reducing atmosphere (carbonaceous) gave consistently high values for emittance between 0.90 and 0.88, confirming that a more defective lattice has higher emittance. One limitation of the filament method is, therefore, that the specimen must be stable in vacuum (or sufficiently low pressure of neutral or reducing gas to avoid convection heat losses), unless measurements are desired on the partially defective oxide. Another limitation of the method became apparent when attempts were made to measure the emittance of thoria. On a tungsten filament, thoria tends to crack because of its high expansivity and direct radiation from the hotter tungsten filament interferes with results. On a tantalum filament, thoria is partially dissociated with a change in the resistivity of the tantalum by dissolved oxygen. In both cases, the method is applicable, but the error will be much higher than for the system tungsten-hafnia. In conclusion, the method can be recommended in those cases where a compatible system is possible.

REFERENCES

1. Richmond, J. C.; and Harrison, W. N.: Equipment and Procedures for Evaluation of Total Hemispherical Emittance. Bulletin of Am. Ceramic Soc., vol. 39, 1960, pp. 608–673.
2. Barth, V. D.: Physical and Mechanical Properties of Tungsten and Tungsten-Base Alloys, DMIC Report 127, March 1960, pp. 44–45.

54—MEASUREMENT OF REFLECTANCE AND EMITTANCE AT HIGH TEMPERATURES WITH A CARBON ARC IMAGE FURNACE[1]

BY M. R. NULL AND W. W. LOZIER

RESEARCH LABORATORY OF NATIONAL CARBON COMPANY, DIVISION OF UNION CARBIDE CORPORATION, PARMA, OHIO

A technique is described for the determination of the spectral reflectance and emittance of carbon and graphite at the sublimation temperature using a carbon-arc-image furnace. Sublimation was produced by an electric arc at the surface of the positive electrode. Rapid heating effects have been observed due to the radiation from the image furnace used for the reflectance measurement. These heating effects have been minimized and measured to permit determination of a correct value for the reflectance. The spectral reflectance at a 45° angle in the visible part of the spectrum falls in the range 0.011 to 0.024 and shows a weak wavelength dependence, with the reflectance at 5010 Å being about 10 to 20% lower than at 4305 Å and 6080 Å.

The application of a carbon-arc-image furnace to the measurement of spectral emittance has previously been described (ref. 1, 2, and 3). The carbon-arc-image furnace employed in these studies has an optical system consisting of a pair of elliptical mirrors (ref. 4) and the measurement of reflectance involves the use of suitably placed synchronous shutters for separation of the emitted from the reflected radiation. The application of this method to the study of graphite at the sublimation temperature posed special problems for which new procedures are described below.

APPARATUS AND METHODS OF MEASUREMENT

The arrangement of the apparatus is shown in figure 54–1. The graphite surface to be studied was the hot crater face of the positive electrode of an electric arc. This is the so-called "pyrometric arc" recently described by the authors (ref. 5) and operated in a fashion to maintain the crater face of the positive electrode consistently at a temperature of 3800° K. The crater face was placed at the sample heating position E in the carbon-arc-image furnace which provided radiation for determination of the reflectance of the electrode surface.

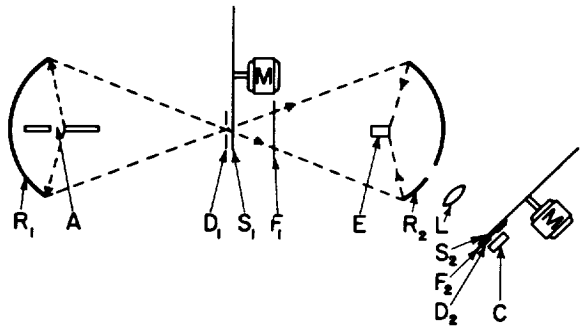

FIGURE 54–1.—Arrangement of arc image furnace for reflectance measurement: A—image furnace arc, D_1 and D_2—diaphragms, S_1 and S_2—synchronous shutters, L—lens, C—photocell, F_1 and F_2—filters, E—exposed sample (positive electrode of pyrometric arc), M—motor, and R_1 and R_2—furnace reflectors.

The emitted and reflected radiation from the electrode surface was measured with an RCA type 929 vacuum phototube connected across a 4700-ohm load resistor to a Tektronix model 502 cathode-ray oscilloscope. Traces were photographed with a Polaroid camera and measured with a traveling microscope print reader. Lens L and diaphragm D_2 limited the view of the photocell C to an area of 1.15-mm diameter at

[1] This research was sponsored by the Air Research and Development Command and the Air Material Command, United States Air Force.

692–146 O—63——35

the crater position. Narrow-band interference filters F_2 were used to limit the response of the photocell to the desired spectral range.

The measurement of reflectance in these tests with the arc-image furnace depends on the separation of reflected from emitted radiation by a rapidly rotating shutter, S^1, which alternately interrupts and transmits the radiation from the image furnace for 5/360- and 1/360-sec intervals (1800-rpm shutter, 2°–30° openings). If the emitted radiation remains unchanged during the short interval (less than 1 msec) required to close or open the shutter, then one can measure the reflected component of the sample by measurement of the radiance immediately before and after closing or opening the shutter. However, any change in the temperature and emitted radiance of the surface which is rapid enough to occur during the time required for the edge of the shutter to traverse the beam would erroneously be classed as "reflected" radiation. The following experiments have shown the existence of such rapid heating effects and the means of correcting for them to obtain the true reflectance.

The image furnace radiation was passed through a "stock thickness" Corning H.R. 2–58 red glass filter placed at F_1 which removed all visible radiation within the responsive wavelength range of the photocell but transmitted longer wavelength red and infrared radiation sufficient to produce an irradiance on the crater face amounting to a little more than half of the unfiltered value. Separate tests performed by reflecting this filtered radiation from magnesium oxide deposited on the surface of a water-cooled copper disk confirmed that the photocell indeed was not affected. Nevertheless, when this radiation was allowed to pass through the 30° openings of shutter S_1 and fall on the hot arc electrode surface at E, it produced an increase in spectral radiance measured by the photocell C which must have been due to an increase in temperature of the crater surface. A sample oscillograph trace for the heating of a graphite electrode is shown in figure 54–2. The profile of the oscillograph traces generally showed the increases in temperature to be essentially completed during the less than 1 msec time required to open or close the shutter and showed little evidence of any

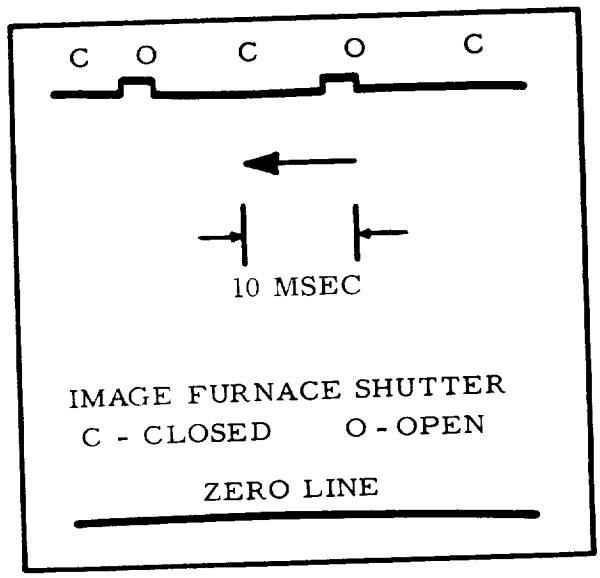

FIGURE 54–2.—Oscillograph trace of crater radiance at 4305 Å for AGKSP graphite electrode irradiated by arc image furnace through Corning H.R. 2–58 red glass filter.

subsequent heating or cooling during the completely open or closed portions of the shutter cycle.

The increase in spectral radiance was measured relative to that of the background of emitted radiation from the crater. The results are plotted in figure 54–3 for three different wavelengths and for three different types of "National" spectroscopic electrode materials with the properties shown in table 54–I. The solid lines show the increases in spectral radiance expected for 18° K and 48° K temperature increases at 3800° K, the known radiance temperature of the crater. Within the accuracy

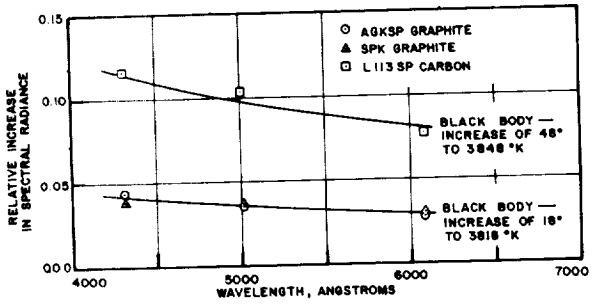

FIGURE 54–3. Increase in spectral radiance of pyrometric arc crater produced by carbon arc image furnace radiation filtered through H.R. 2–58 red filter (4.7 watts/mm). Instantaneous value through shutter with 0.167 transmission.

TABLE 54–I.—*Typical Physical Properties of "National" Spectroscopic Electrodes* Used in Reflectance Measurements*

Grade	Type	Bulk Density, g/cc	Resistivity, ohm-inch	Maximum Ash, ppm
AGKSP	Graphite	1. 61	0. 00025	10
SPK	Graphite	1. 90	. 00045	10
L113SP	Carbon	1. 45	. 0025	10

*All electrodes ¼-inch diameter.

of the measurements, the data fit blackbody radiance increases of 18° K for the AGKSP and SPK graphite electrodes and 48° K for the L113SP carbon electrodes. The greater temperature increase for the carbon electrode is no doubt related to its lower conductivity.

The radiant flux transmitted by the red filter was further attenuated by passage through one and two Nichrome wire screens. The solid line in figure 54–4 shows that the magnitude of the increase of spectral radiance at 5010 Å, measuring the heating of the crater surface, was nearly linearly dependent on the total irradiance incident on the crater. Total irradiance of the image-furnace radiation was measured by viewing a magnesium oxide coated, water-cooled disk through a small diaphragm with a calibrated thermopile. From the reflectance of the magnesium oxide, the dimensions of the diaphragm and the calibration of the thermopile, the level of irradiance of the magnesium oxide disk may be determined. The calibration of the thermopile was done by means of an NBS carbon-filament radiation standard.

The following procedure was adopted to measure the spectral reflectance of the crater, corrected for the rapid heating described above. The radiation from the image furnace was filtered at F_1 to reduce greatly the quantity outside the wavelength sensitive range of the photocell-filter combination. It was passed through a Pittsburgh Plate Glass Company 2043 phosphate infrared absorbing filter of 2-mm thickness and through a "stock thickness" of either a Corning H.R. 3–66 orange glass filter for measurements at 6080 Å or a Corning H.R. 4–74 blue-green filter for measurements at 4305 Å and 5010 Å. The oscilloscope deflection included the effects of both reflectance from

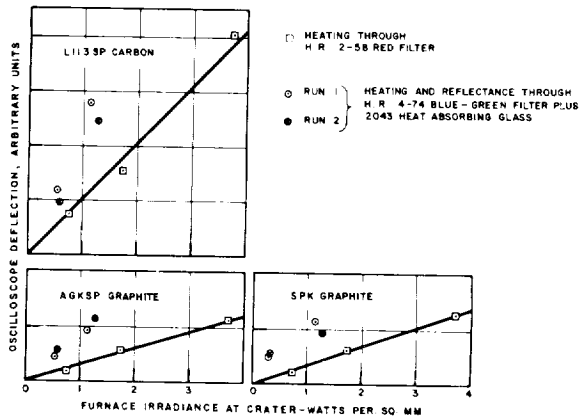

FIGURE 54–4.—Reflectance and heating of carbon and graphite craters at 5010 Å wavelength.

and heating of the sample, but measurement of the total radiant flux incident on the sample permitted a correction for the heating effect of the furnace radiation. Figure 54–4 shows the oscilloscope deflections plotted at the correct flux values. The excess deflection above the heating curve represents the component due to reflection. Two levels of radiation were used, the lower of which represents interposition of a single Nichrome wire screen, and the results of two independent runs are shown in figure 54–4. Calibration of the reflectance measurement was accomplished using a water-cooled, magnesium-oxide smoked surface as a reflectance standard.

DISCUSSION OF RESULTS

The results of figure 54–4 and similar measurements at the other wavelengths are listed in table 54–II and plotted in figure 54–5.

Figure 54–5 shows that the reflectance at the 5010–Å wavelength (green) is approximately 10 to 20% lower than that at the 4305-Å (blue) or 6080-Å (red) wavelengths. This is believed to

TABLE 54–II.—*Spectral Reflectance* and Emittance of Carbon and Graphite at the Sublimation Temperature*

Grade	4305 Å		5010 Å		6080 Å	
	Reflectance	Emittance	Reflectance	Emittance	Reflectance	Emittance
AGKSP	0. 013	0. 987	0. 012	0. 988	0. 014	0. 986
SPK	. 014	. 986	. 011	. 989	. 012	. 988
L113SP	. 024	. 976	. 020	. 980	. 024	. 976

*Measured at 45° from normal to surface.

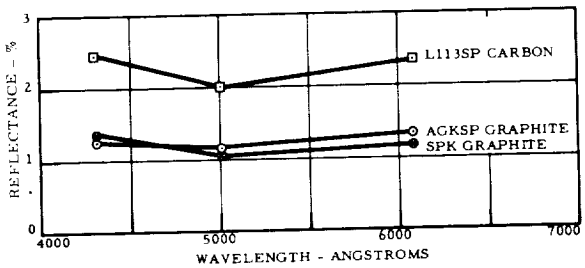

FIGURE 54–5.—Spectral reflectance of spectroscopic graphite and carbon electrodes at 45° angle and a surface temperature of 3800° K.

be real since it has been observed repeatedly in these tests and since some similar indications were obtained several years ago (ref. 2).

The AGKSP and SPK graphite electrodes both show a reflectance just a little above 1%. The reflectance of the L113SP carbon electrode is 2% or a little higher. The graphite materials are more crystalline and more highly oriented than the carbon. The orientation present in the graphite electrodes exposes predominantly low-reflectance edges of the graphite crystals compared to a more random orientation with the carbon electrode.

From the reproducibility of the reflectance data, it is believed that they are generally precise to ± 0.002 and at worst no more than ± 0.004. The emittance values in Table 54–II were obtained by subtraction of the reflectance from unity and have the same precision as the reflectance. The errors result from the fact that the reflection and heating signals were no more than 5% of the emitted light signal, the noise of which constituted a limiting factor.

The graphite craters with their emittance near 0.99 are a close approximation to a blackbody radiator in the visible region. This confirms radiation measurements recently reported on these same sources (ref. 5). This high emittance is due in large measure to the roughened surface produced by the sublimation. Measurement of the reflectances of these craters at lower temperatures show little change from the values measured at the sublimation temperature.

The only similar measurements of the reflectance and emittance of graphite at the arc temperature are those reported by Euler in Germany (ref. 6–9). However, Euler's values for the reflectance have been shown (ref. 2) to be approximately ten times too high.

The methods described in this paper possess wider utility than the examples presented and promise to clarify effects of surface structure on emittance. They can be extended to other methods of heating. For example, heating can be accomplished resistively or inductively and the image furnace, as here, be used to measure reflectance.

The extremely rapid response of the crater surface to incident radiation bespeaks an exceptionally low thermal conductivity or thermal inertia which is under continuing investigation.

REFERENCES

1. NULL, M. R.; and LOZIER, W. W.: Measurement of Reflectance and Emissivity of Graphite at Arc Temperature with a Carbon Arc Image Furnace. Jour. Appl. Phys., vol. 29, no. 11, Nov. 1958, p. 1605.
2. LOZIER, W. W.: Development of Graphite and Graphite Base Multi-component Materials for High Temperature Service. WADD TR 59 789, Apr. 1960.

3. Anon: Research and Development on Advanced Graphite Materials. WADD Technical Note 61-18, Apr. 1961.
4. Null, M. R.; and Lozier, W. W.: Carbon Arc Image Furnaces. Rev. Sci. Instr., vol. 29, no. 2, Feb. 1958, pp. 163-170.
5. Null, M. R.; and Lozier, W. W.: Carbon Arc as a Radiation Standard (Abstract) of Paper. Jour. Opt. Soc. Am., vol. 51, no. 120, 1961, p. 1470.
6. Euler, J.: The Graphite Arc as a Spectrophotometric Standard of Radiation Density in the Range from 0.25 to 1.8 μ. NRL Transl. no. 894, 1962, pp. 1-28 *from* Ann. Physik, series 6, vol. 11, 1953, pp. 203-224.
7. Euler, J.: Über den vergleich zivishchen graphitbogen und UV-standard. Ann. Physik, series 6, vol. 14, no. 3/5, Feb. 1954, pp. 145-173.
8. Euler, J.: Die axiale temperaturver—teiling im inneren der anode des kohlebogens und das waermeleitvermoe—gen von graphit bei hohen temperaturen. (In German.) Ann. Physik, series 6, vol. 18, no. 5/8, Nov. 1956, pp. 345-369.
9. Euler, J.: Sitzber. Heidelberg. Akad. Wiss. 1956/57, 4 Abh, p. 418.

DISCUSSION

Jerry Allyn, Sandia Corporation: Perhaps I do not understand, but it appear from your description that you have assumed that the absorption of your crater in the infrared is the same as the absorption in the visible. In regard to the way in which you calibrated your heating effect, is this true and is this generally a good assumption?

Lozier: It is true for this type of material. It would not be generally true, and, possibly, allowance should be made for it in cases where filters are used to isolate different regions. We have shown in our radiation measurements that this electrode crater approaches the blackbody all the way from about 3000 Å to about 40,000 Å within 1 or 2%, except at a few wavelengths where there is a little radiation from the gas. We were fortunate in this regard with this particular source.

55—SOME PROBLEMS IN EMMITTANCE MEASUREMENTS AT THE HIGHER TEMPERATURES AND SURFACE CHARACTERIZATION

BY C. D. PEARS

SOUTHERN RESEARCH INSTITUTE, BIRMINGHAM, ALABAMA

The emittances of several refractory materials were determined at temperatures from 800° F to 5000° F with an instrument in which the radiance of a specimen was compared with the radiance of a blackbody cavity at the same temperature. A thermopile type of detector was used. The emittance was found to be related to the structure of the material at the higher temperatures.

Small disk-shaped specimens were placed on similar disks of tantalum or tungsten and heated inductively to a steady-state temperature. The surface temperature of the specimen was determined by thermocouples to 2500° F and by optical pyrometry to 5000° F assuming gray body distribution at the wavelength of the optical pyrometer (0.665μ). For the thermocouples, several methods of attachment were used depending on the nature of the structure of the specimen. For the temperature determinations by optical pyrometry, a method of iterating between the readings of the optical pyrometer and the total radiation detector was developed for the computer to permit the solution of true temperature.

The calibration of this instrument, an error analysis, and the general data have been presented in another paper and will be discussed here only briefly. In this paper, the major emphasis is directed to a requirement of "instrument and techniques" that must assume greater attention at the higher temperatures. Specifically, the emittance must be related to the structure of the surface of the specimen as a function of temperature and time. Surface characterization is mandatory. The analysis of the data must include photomicrographs which will reveal the topographical conditions, the chemistry of the surface with the high-temperature migration of contaminants of small quantity (ppm), and the structure which may alter considerably with temperature.

The emittance of a surface may be defined as the ratio of the radiance of that surface and the radiance of a blackbody at the same temperature. As a means of measuring the emittance of various refractory materials, a thermopile was used to measure the normal radiance at a fixed distance from the material. Emittance was calculated by dividing the millivolt output of the thermopile viewing the material by the millivolt output of the thermopile when viewing a blackbody at the same temperature. Most of this work was performed under Contract No. AF33(616)-7319 for Aeronautical Systems Division, under industrial contract, and in-house at Southern Research Institute.

SPECIMENS

The dimensions of the test specimens varied from ½ inch to 1½ inches in diameter and from 1/16 inch to ¼ inch thick. Uncoated materials were generally ground to a smooth finish, with the finish defined by the method used to produce it. Although this method of defining the finish is not precise, it is probably adequate within the engineering stringency of the data application and certainly seems more definitive than RMS measurements of the surface of most of these kinds of materials, which contained numerous macro voids. Of course, all material conditions of composition, surface finish, thermal history, and environment should be very carefully delineated in all emittance determinations.

EQUIPMENT ARRANGEMENT

A cross-sectional view of the apparatus is given in figure 55-1. The specimen was housed in the lower section in which a specially designed flat induction coil was used to bring the target surface to temperature. A water-cooled circular tube extended from the top plate of the lower housing up to the radiometer housing.

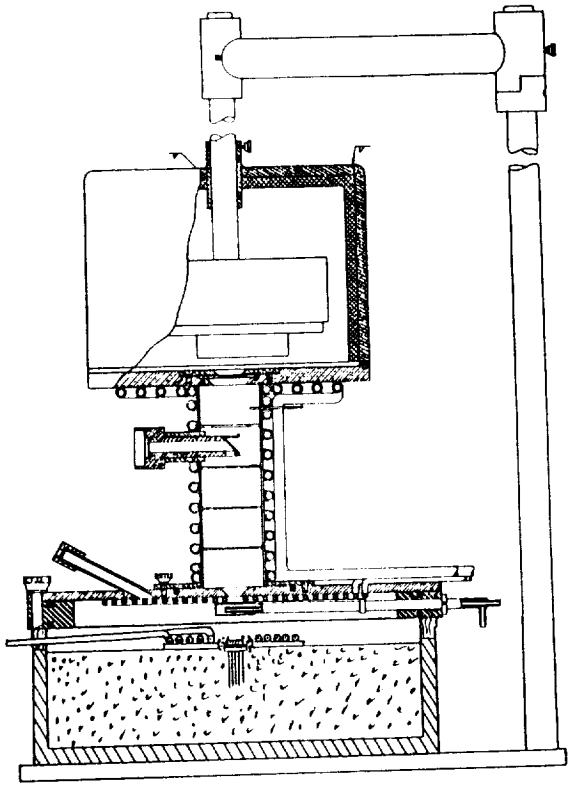

FIGURE 55–1.—Cross section of emittance apparatus.

FIGURE 55–2.—Apparatus for measuring total normal emittance.

Within this upper housing, the multijunction thermopile and optical stops were mounted. Purge lines were attached to both the upper and lower housings. To evacuate the housings, a mechanical vacuum pump inlet was provided on the top flange of the lower section. The thermocouple leads and the power leads from the 25-kw induction furnace also entered this lower section. Optical sight ports viewing the target surface were provided in the circular tube as well as through the top of the lower section. O-ring seals were provided at all joints so that the entire system could be evacuated to 2 mm Hg preparatory to operation. After evacuation, dried argon or helium was admitted to provide an inert environment. A picture of the equipment is shown in figure 55–2.

SPECIMEN HEATING

The specimens were heated by a flat induction-heating coil, which concentrated the magnetic field at the specimen in a small hole in the center of the coil. If the specimen was an electrical conductor, it was used as the susceptor. If not, the specimen rested on a tungsten or tantalum disk 0.010 inch thick serving as the susceptor and was heated by conduction and radiation from the disk. The susceptor was supported by tungsten wires, which in turn were supported vertically by zirconia grog. Fine zirconia sand separated the susceptor and specimen from the copper plate secondary of the induction heating coil. The plate, and consequently the zirconia sand, were protected by the cooling water in the induction heating coil.

For heating the blackbody cavity, a helical induction coil was used in place of the flat coil. Since the blackbody had a greater length-to-diameter ratio than the specimen, a better distribution of power input to the load was necessary.

RADIOMETER

The radiance of either the specimen or the blackbody was measured by a 160-junction thermopile constructed according to Snyder (ref. 2) and Gier (ref. 3) with some modifications.

The radiometer housing prevented ambient temperature changes from adversely affecting the thermopile. Water maintained at a constant temperature was circulated through all parts of the apparatus viewed by the themo-

pile. Also, blackened copper baffles were provided to prevent spurious reflections from reaching the thermopile. The water-cooled shut-off valve was provided to obtain a stable zero reading.

During operation, argon gas was passed into the radiometer housing and down the support tube to prevent smoke and fumes from contaminating the radiometer. No windows were used between the specimen and the thermopile. In order to calibrate the thermopile, a graphite blackbody with a ½ inch diameter cavity, 6 inches deep, was positioned below the radiometer.

TEMPERATURE MEASUREMENT

Since the blackbody had an emissivity of unity, all blackbody temperatures over 1400° F were easily and accurately measured with an optical pyrometer. For temperatures below 1400° F, and as a check at temperatures up to 2500° F, a platinum-platinum, 10% rhodium thermocouple was placed in the blackbody cavity. Tungsten-rhenium thermocouples were used to extend the temperature check to 4600° F; however, the variation between different wires, and even for a single couple on subsequent runs, was as high as 200° F at 4000° F so that the precision of these exotic couples is somewhat limited.

A major problem of the work was the measurement of the surface temperature of each specimen. Several different means of attaching thermocouples to the surface were employed. In some cases, the thermocouple was cemented in a small hole in the top side of the specimen; for obvious reasons, this technique is no more than adequate. Some materials permit peening the thermocouples in small holes or grooves in the surface; this technique provides good readout for homogeneous specimens. For some specimens, the couples were inserted in holes drilled radially in the specimen. For others the thermocouple was formed by welding the ends of the dissimilar thermocouple wires to the surface of the specimen. This technique is good if the wires leading away from the weldments are kept close to the specimens to minimize their heat loss. The most satisfactory method for a specimen in which the wires could not be welded to the specimen proved to be pressing the welded thermocouple junction to the surface with a zirconia pad about ⅛ x ¼ x 1/16 inch thick. A thin layer of Fiberfrax under the pad provided for more even contact. The top pad was held in place by a tungsten wire cantilevered off the side of the furnace and bearing on the pad.

Temperatures above 1400° F were also measured with an optical pyrometer with a filter of 0.665μ wavelength. The sapphire window and front-surface mirror used in the optical ports were calibrated by viewing the blackbody through these ports and directly through the top of the furnace. This correction was about 150° F at 5000° F, decreasing with decreasing temperature. The two great advantages of the optical method of measuring temperature are: (1) the target surface is not distorted thermally, and (2) devices need not be extended into a hot zone in which available materials have a limited life. Temperatures of a gray body can be measured optically without knowing the emittance by measuring the spectral and total irradiances separately and combining the principles of the Stefan-Boltzmann and Wein laws. The analysis is valid because there is only one set of conditions of spectral radiance, total radiance, and surface emittance that will satisfy the spectral and total radiation laws for a single true temperature. There can be fairly large deviations in the spectral emittance within the wavelength range of the total energy spectrum and still not introduce a particularly large error since the true temperature is a function of the quarter power of the total radiance.

This procedure gives correct values for all materials that radiate as "gray" bodies. The error in the values for nongray bodies varies, depending on the difference between the 0.665μ spectral and total emittances and the distribution of radiant energy within the particular spectrum. If deviation from gray body became very great at temperatures up to 2500° F, it was indicated by the thermocouple measurements. At 4850° F, a temperature check was obtained from the melting of the zirconia grog around the specimen.

INFLUENCE OF SURFACE CAVITIES ON SURFACE TEMPERATURE AND RADIANCE

The radiance of a flat opaque surface is defined by the Stefan-Boltzmann law in which $Q=$

ECT^4, in which Q is the radiance, E the emittance, C the constant, and T the absolute temperature. This equation assumes that the entire surface is at the same temperature.

Many of the ceramic materials, and some of the nitrides, borides, and carbides, contain surface cavities at least 0.005 inch deep. Further, some investigators drill small holes in the surface to measure surface temperature. It is doubtful if the temperature at the bottom of the cavities is the same as at the top surface; further, a few degrees difference can cause a large difference in the radiance. For example, the temperature drop through a material with a relatively low thermal conductivity (zirconia, char, ceria, thoria, or 'c' direction pyrolytic graphite) will be about 150° F per 0.005 inch at 4000° F. If the specimen is heated from the back side, the radiance of the nominal surface (the peaks) will be 12% less than the radiance of the bottoms of cavities 0.005 inch deep. Conversely, temperatures measured at the bottoms of the cavities, to permit the assumption of blackbody, will contain similar error in addition to the false assumption of a blackbody cavity.

For materials with a higher thermal conductivity such as tungsten, graphite, and several of the carbides, the temperature drop through a specimen heated from the back side falls to 5° to 15° F per 0.005 inch or an error in radiance of only about 1%. However, for deeper holes, this error could become more significant.

SOME CALIBRATION "STANDARDS" AND SUMMARY OF AN ERROR ANALYSIS

In calibrating emittance equipment, some reference specimens, or "standards," are mandatory to establish the operating procedures and the different techniques that can be employed in heating, measuring temperature, and controlling the variation from prescribed conditions. Several standards have been used.

The results for Unitemp 41 and platinum are shown in figure 55-3. These specimens were selected by Aeronautical Systems Division and distributed to several investigators. Although all of the data are not in, it appears that the Southern Research Institute data are in good agreement with the literature data furnished by Aeronautical Systems Division. For the platinum, the thermocouples were welded directly to the target surface; whereas, for the Unitemp 41, the thermocouples were held in place by the spring-loaded zirconia pad.

A statistical analysis of the data accuracy is of interest. Generally, the probable error in each blackbody reading is about 4%, and the probable error in each specimen reading is about 8%. If the data points are used to calculate emittance, the maximum probable error would then be about 12%. The curve-fitting approach undoubtedly reduces this maximum to about 5%. As a general conclusion, the accuracy of the measuring system is usually well within the range of variation as is experienced by different surface conditions on the same material.

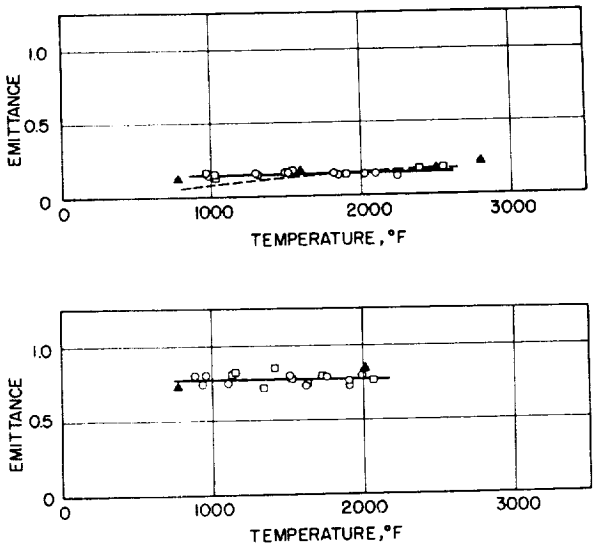

FIGURE 55-3.—Calibration standards for total normal emittance of 87% platinum-13% rhodium (top curve) run in nitrogen with specimen annealed in air 1 hour at 2900 °F, and Universal Cyclops Unitemp No. 41 (bottom curve) run in air with specimen preoxidized in air at 2000 °F. Δ designates data from *ASD* 58-476.

THE EMITTANCE OF SOME REFRACTORIES

Over the past several years, the emittances of several hundred specimens have been determined. Generally, the values increase with temperature for metals and decrease with temperature for ceramics; however, there are notable exceptions to each of these general observations so that precise theoretical relations cannot be developed for the field of engineering materials. Occasionally, some very

sharp inflections have been found in the emittance-temperature curves that are unrelated with known stress or structure changes. These inflections may be reversible or irreversible.

The emittances of several materials are shown in figure 55–4. These data are included to show the general values that can be expected and, as shown, should not be used in any precise engineering design but only as a guide for initiating a preliminary material selection. For precise data, more information is necessary concerning detailed composition, surface finish, environment, and other parameters.

SURFACE CHARACTERIZATION AND INFLUENCE ON EMITTANCE

An analysis of the influence of the character of the surface on the emittance is extremely difficult and can induce conflicting opinions between cause and effect. A direct review of some of the specific results should provide a basis for understanding.

Pyrolytic graphite is a rather well ordered structure of the hexagonal crystal of carbon with the 'a' and 'c' directions being very anisotropic both thermally and mechanically. For thermal conductivity, the ratio is about 40 to 1. For tensile strength, the ratio is about 30 to 1. Observe the well ordered columns (in the 'c' direction) in figure 55–5. The emittance for this structure, shown in figure 55–6, was fairly high and constant when viewing either side of the columns; however, the emittance was con-

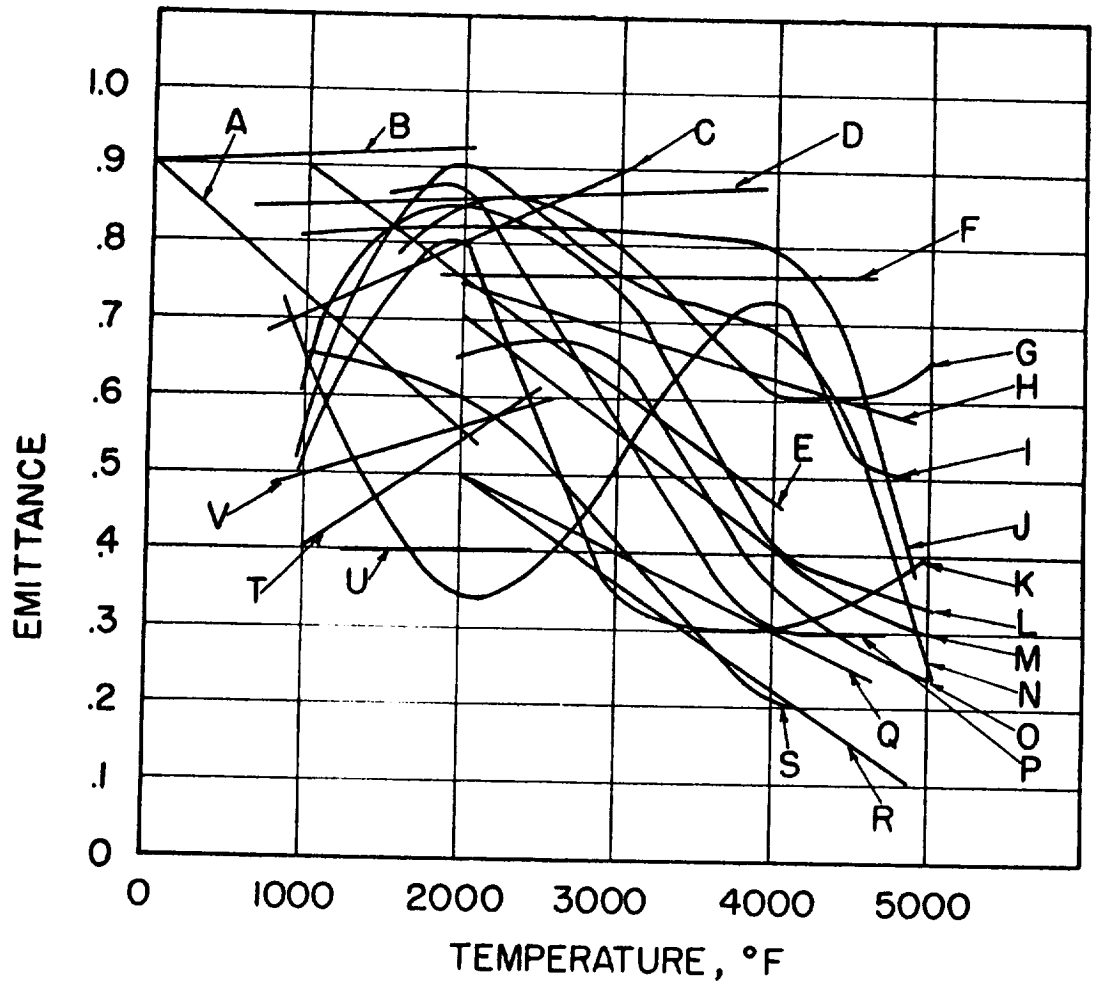

FIGURE 55–4.—Total normal emittance of the following materials: *A*—asbestos-phenolic in air; *B*—asbestos-phenolic in helium; *C*—*KT SiC*; *D*—*ATJ* graphite; *E*—*BN*; *F*—HfB_2; *G*—*HfC*; *H*—*HfN*; *I*—ZrO_2; *J*—*ZrC*; *K*—*WC*; *L*—*TiC*; *M*—*TiN*; *N*—*TaC*; *O*—*VC*; *P*—*CbC*; *Q*—*Cb*+½*Zr*; *R*—*Mo*+½ *Ti*; *S*—Mo_2C; *T*—MoS_2; *U*—SiO_2; and *V*—*SiC* bonded graphite.

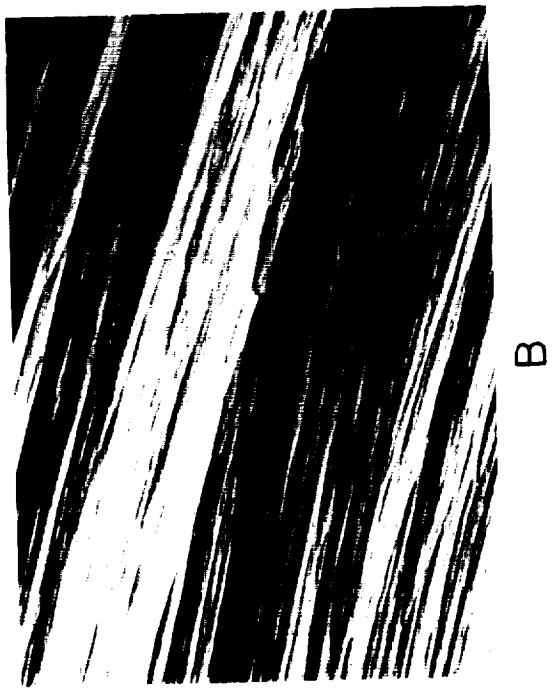

B

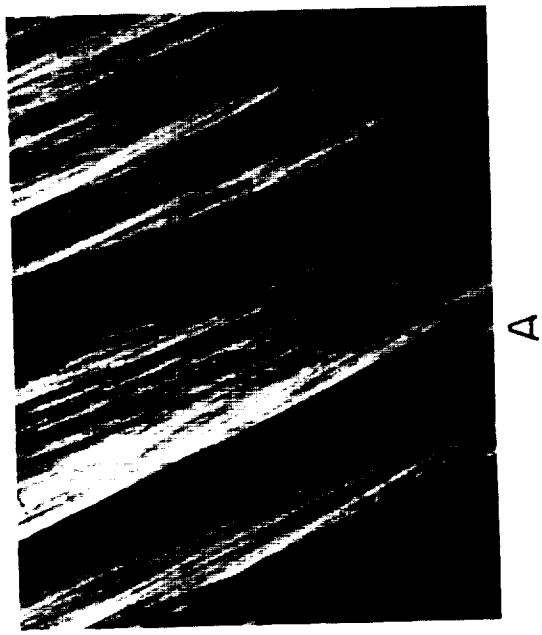

A

C

FIGURE 55-5.—Picture of pyrolytic graphite at 150× showing columnar structure: A—unexposed, B—first exposure, C—second exposure.

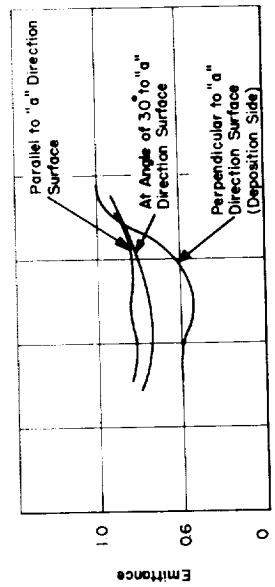

FIGURE 55-6.—Emittance of pyrolytic graphite at different orientation with the columnar structure.

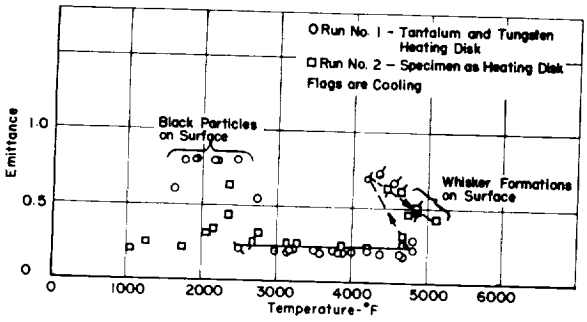

FIGURE 55–7.—Emittance of tungsten showing the influence of surface contaminants.

siderably less below 3000° F when viewing the ends of the columns. At a selected angle off of the columns, the emittance was about equal to the geometric distribution between the two orientations. Above 3000° F, the emittances were about the same at any orientation. For this material, the emittance was dependent on the orientation of the grains. For regular polycrystalline graphites that are less anisotropic, this variation of emittance was not found. Perhaps a similar influence does exist, but cannot be detected. Many of the refractory materials are pressed or extruded and contain a marked grain alignment that may or may not influence emittance.

The chemistry of a surface may change at temperature as components boil out, migrate out, or even diffuse out. The data shown in figure 55–7 for tungsten are indicative of a transient surface that was observed visually. At the lower temperatures and at the higher temperatures, a dark deposit showed on the surface and caused a high emittance. After blowing off the deposit or permitting it to "dissolve" into the specimen, the emittance returned to the normal low value. This dark phase would probably develop in most commercial applications unless blown off.

The zirconium diboride shown in figure 55–8 developed a phase at the surface, after temperature exposure, that had not been present before exposure. Different specimens provided data with fair agreement on subsequent runs. The chemistry of the surface apparently changed, as well as the macro structure, inducing a different emittance. In application, this material would have an emittance depending on the temperature-time environment of the structure.

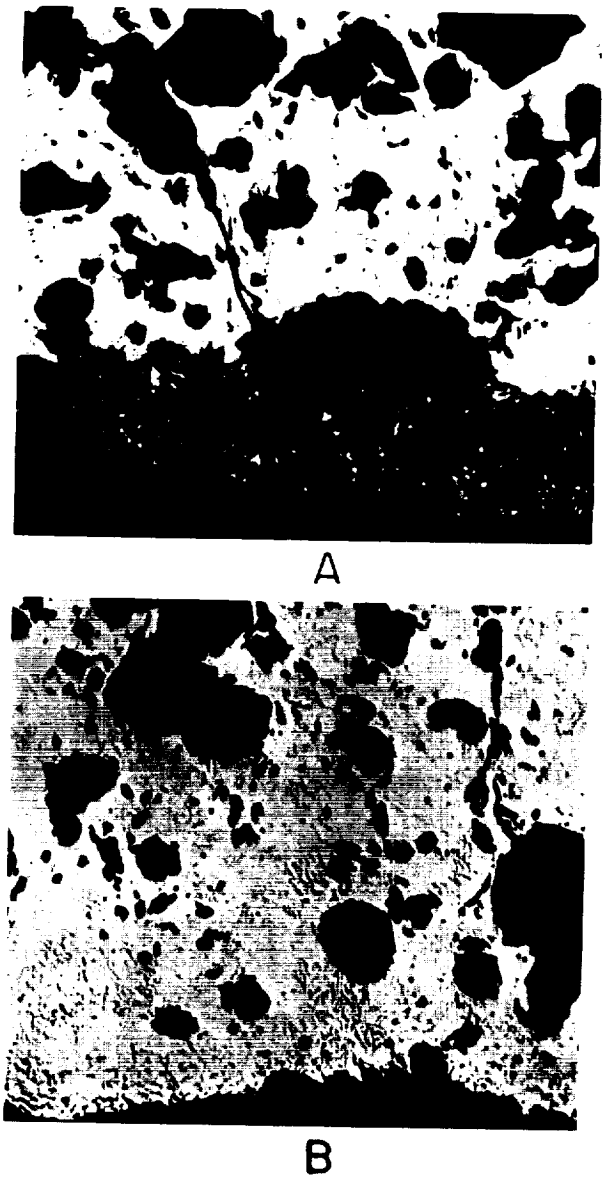

FIGURE 55–8.—Zirconium diboride (emittance material 6) at 150 × before and after exposure to temperature showing unidentified phase at the surface. A—oxidized at 1850° F, unexposed at *SRI*, bottom edge; observe absence of small crystallites and the gray phase on the edge. B—oxidized, exposed at *SRI* to +4000°F in argon, bottom edge; observe absence of small crystallites and the scattered phase.

Further evidence of change in structure and chemistry of the surface can be seen in the pictures of a silica-coated graphite in figure 55–9. The exposure disrupted the continuity of the

silica coating and undoubtedly introduced silicon carbide at the surface. Both changes would be temperature-time-environment sensitive and would change the emittance.

The emittances of some oxidized coatings are extremely dependent on temperature-time-environment. The data for W–2 in figure 55–10 indicate that the emittance ranged from 0.3 to 0.7 depending on many variables; specifically, an oxidizing environment increased the emittance. However, heating the specimen in either a reducing environment or helium apparently deoxidized the surface and dropped the emittance values. Obviously, the data would depend on and vary with the history of the specimen.

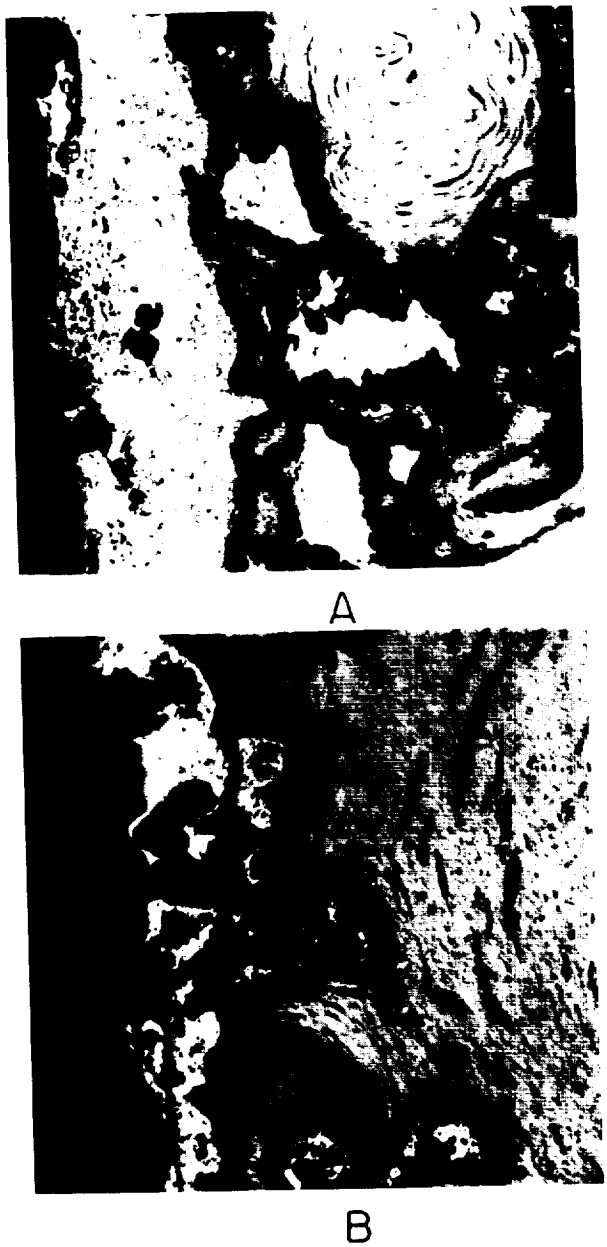

FIGURE 55–9.—Silica-coated graphite at 150× before (A) and after (B) exposure showing changes in the coating structure and chemistry.

In some cases, gross changes in the flour size, as in the different zirconias in figure 55–11, have not had a big influence on emittance, at least over the full temperature range. For these different surface conditions, the emittances varied less for topography than for other parameters, such as additives, since the existence of cavities did not explain the differences theoretically.

On this same type of zirconia, gross changes in emittance at about 3000° F were obtained by exposing the surface to either helium or air. In helium, the emittance at temperature was high (0.85) and, after quench, the surface was gray. In air, the emittance was lower (0.5) and, after quench, the surface was the typical yellow color. Apparently the zirconia surface either formed a suboxide in helium or was contaminated by the boil out of some contaminant, such as iron oxide, which was burned off in air. The emittance data for these runs are shown in figure 55–12.

Many aerospace applications require a knowledge of the emittance of chars and other materials that have both continuous and discontinuous voids. The char shown in figure 55–13 was about 75% voids. The thermal conductivity was low at up to 2500° F and then increased drastically in a character similar to a plot of the Stefan-Boltzmann radiation law. Even though the material appeared to conduct heat primarily by radiation internally, the emittance was fairly constant at a high value. If there had been much subsurface radiance reaching the

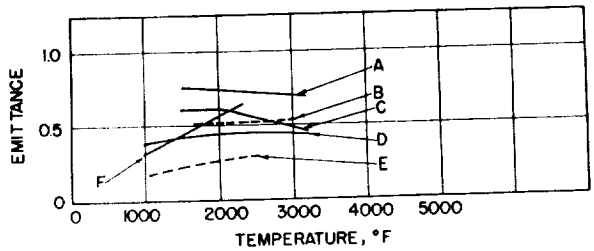

FIGURE 55–10.—Emittance of W–2 coated molybdenum with different exposures.

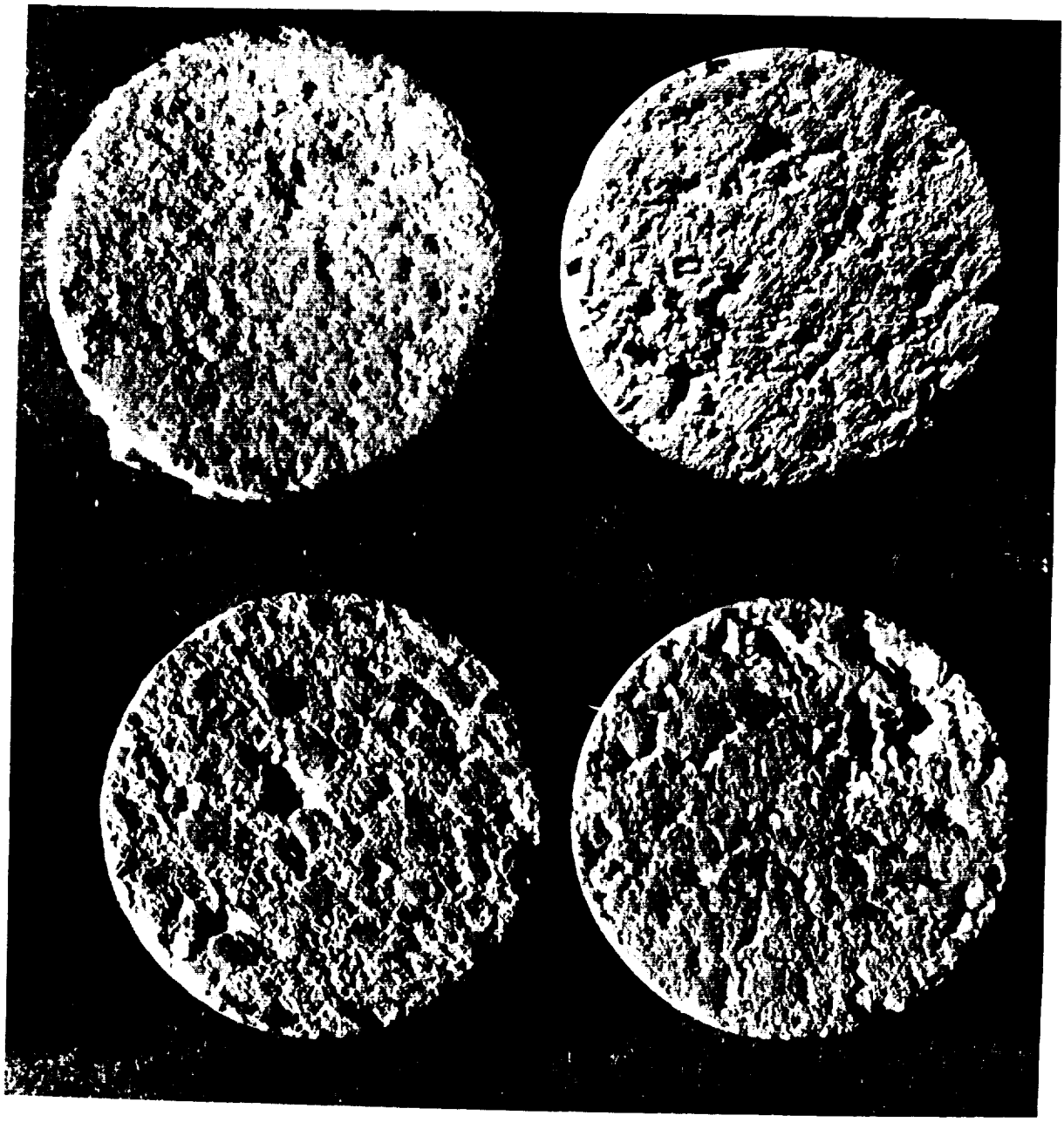

FIGURE 55-11.—Zirconias at 15× with different surface roughness.

detector, the "indicated" emittance should have been greater than unity. It seems improbable that the surface temperature measurements were an accurate "mean" temperature of the radiating volume of the specimen material; however, that conclusion must be made or else completely reject the data as coincidental.

The change in structure at the surface of a tantalum-10 tungsten is shown in figure 55–14. The gray phase in the grain boundaries near the surface became practically continuous at the surface. The tantalum-10 tungsten was actually the white phase, and the data were about double the anticipated values. Obviously, the emittance of the gray phase was being measured.

All of these specific examples demonstrate that precise information is needed on the specimen materials both before and after the temperature-time-environment exposures. The information includes (1) topographical, (2) chemical to parts per million, and (3) structural at the surface. For all three phases, photomicrographs are required to supplement other analytical tools.

CONCLUSIONS

The measurement of emittance of refractory materials at the higher temperatures requires a knowledge of the experimental art, the theory, and the behavior of materials at these temperatures. There does not seem to be a safe experimental procedure that will guarantee good results. The investigator must be alert to the different arts and observe, visually, the phenomena at the surface as the temperature is increased and upon quench. Also, specimens must be quenched from intermediate temperature levels to provide some information on the surface condition as the exposure proceeds. A careful analysis of the specimen after the exposure often assists in understanding and analyzing the data. This post-mortem should include chemical, spectrographic, and photomicrographic studies of the surface material.

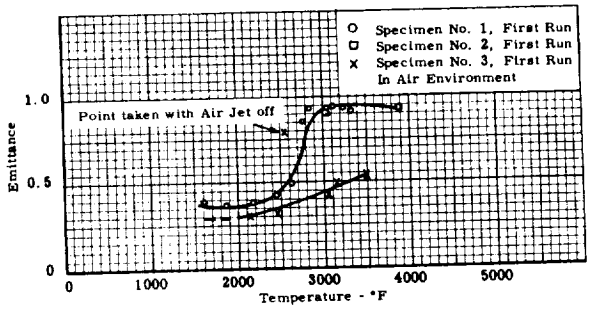

FIGURE 55–12. Influence of argon and air on the emittance of a zirconia.

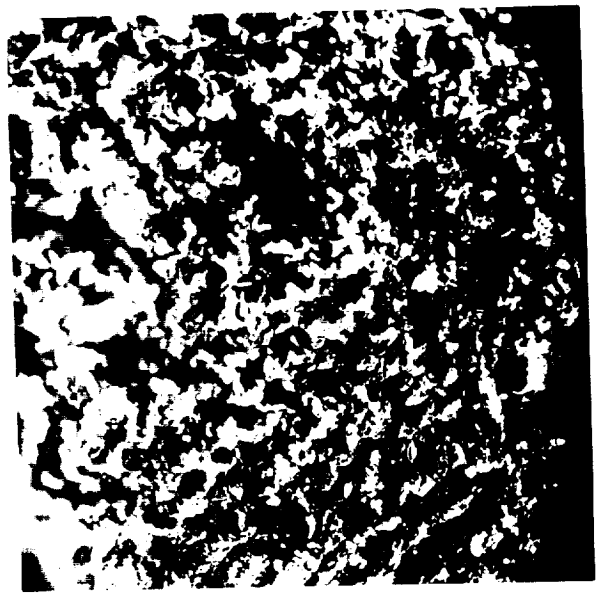

FIGURE 55–13.—Porous char at 7.5×.

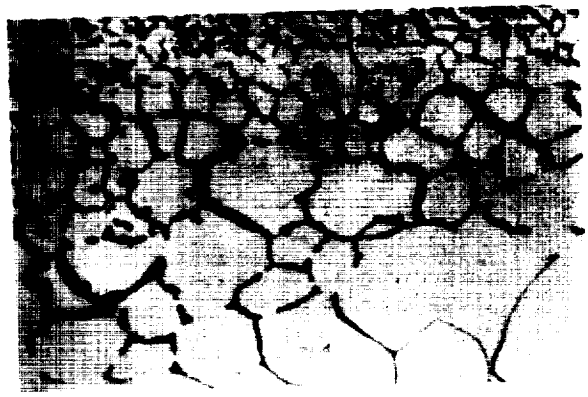

FIGURE 55–14. Tantalum-tungsten at 150× showing unidentified phase at the surface.

REFERENCES

1. PEARS, C. D.: The Determination of the Emittance of Refractory Materials to 5000° F. Second Symposium on Thermophysical Properties, Jan. 1962.
2. SNYDER, N. W.; GIER, J. T.; and DUNKLE, R. V.: Total Normal Emissivity Measurements on Aircraft Materials Between 100° and 1000° F. Trans. of the A.S.M.E., vol. 77, p. 1011, 1955.
3. GIER, J. T., and BOELTER, L. M. K.: The Silver-Constantan Plated Thermopile, in Temperature—Its Measurement and Control in Science and Industry. American Institute of Physics, 1941, p. 1284.

692-146 O—63——36

56—PERIODIC HEAT FLOW IN A HOLLOW CYLINDER ROTATING IN A FURNACE WITH A VIEWING PORT

BY B. A. PEAVY AND A. G. EUBANKS

NATIONAL BUREAU OF STANDARDS, WASHINGTON, D.C.

A rotating-specimen furnace has been designed and constructed for use in determining the thermal emittance, both spectral and total, of materials in the temperature range 1300° to 1800° K. In this apparatus, a hollow cylindrical specimen is rotated at constant speed in a concentric cylindrical furnace with heated walls, and the radiant flux from the specimen surface is measured as it passes a small viewing port.

An analytical method is given for estimating the surface temperature of the specimen as a function of rotation speed, thermal properties of the specimen material, and system geometry.

The apparatus is described, and data obtained with the specimen rotating at slow speeds are compared with values predicted by the analytical method.

A rotating-specimen furnace has been designed and constructed at the National Bureau of Standards for measuring the thermal emittance (both spectral and total) of nonmetallic solids in the temperature range from 1300° to 1800° K. In this apparatus, a hollow cylindrical specimen is rotated continuously in a concentric cylindrical furnace with heated walls, and the radiant flux from the specimen surface as it passes a small viewing port is measured with a suitable radiometer. In passing the viewing port, the surface is lowered in temperature by heat transfer to surfaces at or near room temperature and the magnitude of this reduction is dependent upon both the speed of rotation and the thermal properties of the specimen. Previous investigations (ref.1, 2, 3, 4, and 5) employing the principles of the rotating specimen furnace did not present an analysis of this temperature variation.

The present paper gives an analytical method for estimating the surface temperature of the specimen as a function of angular velocity and thermal properties of the specimen material. The purpose of this investigation was to determine reasonable speeds of rotation at which surface temperature changes become negligible. The surface temperature must be determined quite accurately for computing emittances and consideration must be given principally to radial temperature gradients in the specimen, especially if the specimen material is of low thermal conductivity or diffusivity.

As the specimen rotates in the furnace (fig. 56–1), an area of its surface gains heat principally by radiation from the furnace walls, and loses heat at the viewing port during the portions of the cycle when the respective surfaces are seen. Because this is a continuous operation, a steady periodic heat flux boundary condition, as illustrated in figure 56–2, is assumed at the outer surface of the hollow cylindrical specimen. A zero heat flux is assumed at its inner surface.

Concurrently with the analytical treatment, experiments were conducted with the specimen rotating at slow speeds, and the temperature changes thus obtained were compared with the values predicted by the analytical method.

MATHEMATICAL DEVELOPMENT

General Analysis

For conduction heat transfer in the hollow cylindrical specimen it is assumed that there is no flow of heat at the inner radius $r=a$, and that the heat flux at the outer radius $r=b$ is a

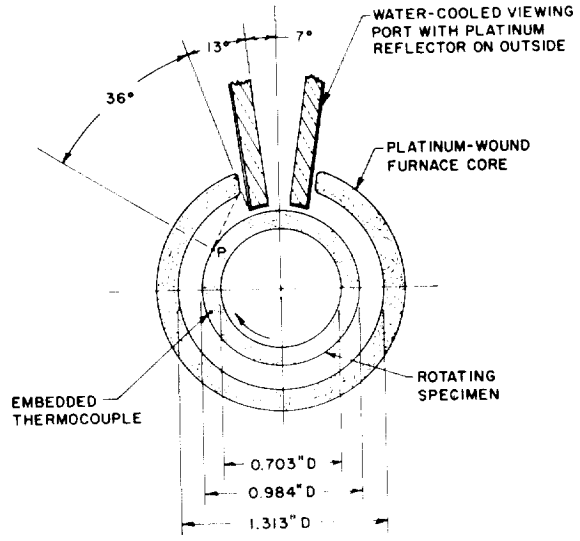

FIGURE 56-1.—Cross section through rotating specimen furnace and viewing port with dimensions and angular positions.

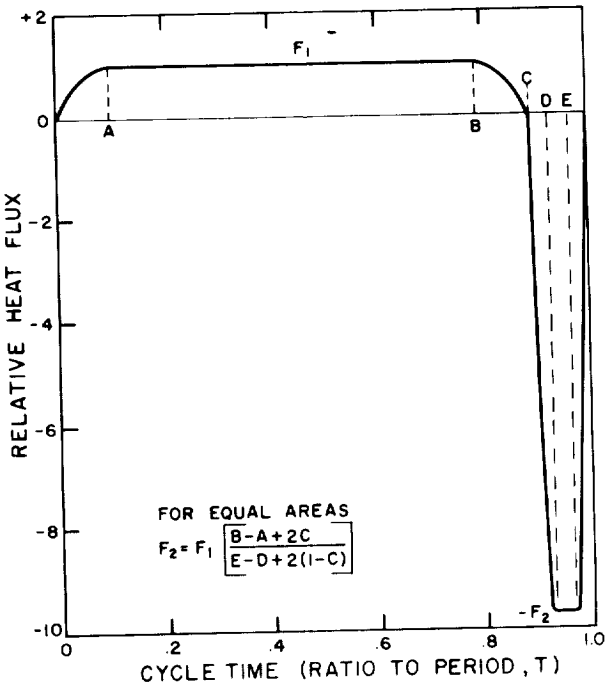

FIGURE 56-2.—Assumed heat flux history of a point on the surface of the rotating specimen.

periodic function of time. As shown in general terms in figure 56-2, F_1 represents the average heat flux radiated to the specimen surface from the furnace walls during the time period A to B, and F_2 is that radiated from the specimen as it passes the viewing port from D to E. The times A, B, C, D, and E, are arbitrary and are proportioned to the period T of one revolution of the specimen.

The curved lines between O and A, B and C, C' and D, and E and 1.0 are quadratic curves chosen to give heat flux continuity throughout, and slope continuity at A, B, C, and E. By selecting the designated times, changes in the contour can be made, and the continuity conditions used give faster convergence of the Fourier series involved in the analysis. The amplitudes of the positive and negative fluxes are adjusted so that the summation over the cycle of the areas above and below the zero flux line is zero. By this adjustment, a steady periodic condition is assured.

As the cylinder rotates, a point P $(r=b, \varphi=\varphi_1)$ on the surface experiences a flux cycle. Assuming the cylinder stationary and the furnace rotating with a period T, a complex form of a Fourier series

$$k\left(\frac{\partial\theta}{\partial r}\right)_{r=b} = F_1\left\{\sum_{n=1}^{\infty}(P_n+iQ_n)\mathrm{Exp}\left[i\left(\varphi+\frac{2n\pi t}{T}\right)\right] + \text{conjugate}\right\} \quad (1)$$

can be used to describe the arbitrary periodic flux function which serves as a boundary condition. k is the thermal conductivity of the specimen, θ is the temperature departure from the mean temperature of the system, φ is an arbitrary angular position within the specimen and

$$P_n = \frac{2}{(2n\pi)^2}\left[\frac{\psi}{1-E}-\frac{1}{A}+\left(\frac{\psi}{D-C}-\frac{1}{C-B}\right)\cos 2n\pi C\right]+\frac{2}{(2n\pi)^3}\left[\frac{\sin 2n\pi A}{A^2}-\frac{\sin 2n\pi B}{(C-B)^2}+\left\{\frac{\psi}{(D-C)^2}+\frac{1}{(C-B)^2}\right\}\sin 2n\pi C+\psi\left\{\frac{\sin 2n\pi E}{(1-E)^2}-\frac{\sin 2n\pi D}{(E-D)^2}\right\}\right],$$

$$Q_n = \frac{2\sin 2n\pi C}{(2n\pi)^2}\left[\frac{1}{C-B}-\frac{M}{D-C}\right]-\frac{2}{(2n\pi)^3}\left[\frac{1-\cos 2n\pi A}{A^2}+\frac{\cos 2n\pi B}{(C-B)^2}-\left\{\frac{\psi}{(D-C)^2}+\frac{1}{(C-B)^2}\right\}\cos 2n\pi C+\psi\frac{\cos 2n\pi D}{(E-D)^2}-\frac{1-\cos 2n\pi E}{(1-e)^2}\right\}\right].$$

To yield a zero net flux over the cycle, $F_2=\psi F_1$ where

$$\psi=\frac{B-A+2C}{E-D+2(1-C)}.$$

The partial differential equation for conduction heat transfer in a homogeneous material, where heat flow in the axial direction is neglected, is for polar coordinates (r, φ)

$$\frac{\partial^2\theta}{\partial r^2}+\frac{1}{r}\frac{\partial\theta}{\partial r}+\frac{1}{r^2}\frac{\partial^2\theta}{\partial\varphi^2}-\frac{1}{\alpha}\frac{\partial\theta}{\partial t}=0 \qquad (2)$$

where α is the thermal diffusivity. Substituting

$$\theta=f_{\pm n}(r)\ \mathrm{Exp}\left[\pm i\left(\varphi+\frac{2n\pi t}{T}\right)\right],\ n=1,\ 2,\ 3\ ,\ \ldots\ . \qquad (3)$$

in equation (2) gives

$$f''_{\pm}+\frac{1}{r}f'_{\pm n}-f_{\pm n}\left[\frac{1}{r^2}\pm\frac{2n\pi i}{\alpha T}\right]=0. \qquad (4)$$

Equation (4) is a first order modified Bessel equation and its general solution is

$$f_{\pm n}=M_{\pm n}I_1\left(\frac{rz}{a}\,i^{\pm\frac{1}{2}}\right)+N_{\pm n}K_1\left(\frac{rz}{a}\,i^{\pm\frac{1}{2}}\right) \qquad (5)$$

where $z^2=2n\pi/(\alpha T/a^2)$, and I_1 and K_1 are first order modified Bessel functions of the first and second kind, respectively. Substitution of boundary conditions $d\theta/dr=0$ at $r=a$, and equation (1) at $r=b$, in the first derivative of equation (3) gives a solution for M and N, and yields

$$\frac{\theta k}{F_1 a}=\sum_{n=1}^{\infty}\left\{\frac{(P_n+iQ_n)}{z}L_n\ \mathrm{Exp}\left[i\left(\varphi+\frac{2n\pi t}{T}\right)\right]+\frac{[P_n-iQ]}{z}L_n\ \mathrm{Exp}\left[-i\left(\varphi+\frac{2n\pi t}{T}\right)\right]\right\} \qquad (6)$$

$$L_{\pm n}=\frac{I_1\left(\frac{rz}{a}\sqrt{\pm i}\right)K_1'(z\sqrt{\pm i})-K_1\left(\frac{rz}{a}\sqrt{\pm i}\right)I_1'(z\sqrt{\pm i})}{\sqrt{\pm i}\left[I_1'\left(\frac{bz}{a}\sqrt{\pm i}\right)K_1'(z\sqrt{\pm i})-K_1'\left(\frac{bz}{a}\sqrt{\pm i}\right)I_1'z\sqrt{\pm i})\right]}$$

$$=\frac{R_n\left(\frac{rz}{a};\,z\right)\pm iS_n\left(\frac{rz}{a};\,z\right)}{X_n\left(\frac{bz}{a};\,z\right)\pm iY_n\left(\frac{bz}{a};\,z\right)}$$

where

$$X_n(x;\,y)=ber_1'x\ ker_1'y-bei_1'x\ kei_1'y-ber_1'y\ ker_1'x+bei_1'y\ kei_1'x$$

$$Y_n(x;\,y)=ber_1'x\ kei_1'y+bei_1'x\ ker_1'y-ber_1'y\ kei_1'x-bei_1'y\ ker_1'x$$

$$R_n(x;\,y)=ber_1x\ ker_1'y-bei_1x\ kei_1'y-ker_1x\ ber_1'y+kei_1x\ bei_1'y$$

$$S_n(x;\,y)=ber_1x\ kei_1'y+bei_1x\ ker_1'y-ker_1x\ bei_1'y-kei_1x\ ber_1'y$$

which are obtained from the identities (6):

$$i^{\pm1}I_1(x\sqrt{\pm i})=ber_1x\pm i\ bei_1x$$

$$i^{\pm3/2}I_1'(x\sqrt{\pm i})=ber_1'x\pm i\ bei_1'x$$

$$i^{\pm1}K_1(x\sqrt{\pm i})=ker_1x\pm i\ kei_1x$$

$$i^{\pm1/2}K_1'(x\sqrt{\pm i})=ker_1'x\pm i\ kei_1'x$$

Rationalizing the denominators of L, equation (6) becomes

$$\frac{\theta k}{F_1 a}=2\sum_{n=1}^{\infty}\frac{U_n\cos\left(\frac{2n\pi t}{T}+\varphi\right)-V_n\sin\left(\frac{2n\pi t}{T}+\varphi\right)}{z(X_n^2+Y_n^2)} \qquad (7)$$

where

$$U_n=R_n(X_nP_n+Q_nY_n)-S_n(Q_nX_n-Y_nP_n)$$

$$V_n=R_n(Q_nX_n-Y_nP_n)+S_n(X_nP_n+Q_nY_n)$$

The expressions for P_n and Q_n contain, and their values are fixed by, the arbitrary values chosen for A, B, C, D, and E (fig. 56–2). Accordingly, equation (7) can be represented using dimensionless parameters in the following functional form,

$$\frac{\theta k}{F_1 a}=g\left(\frac{\mathrm{A}T}{a^2},\frac{b}{a},\frac{r}{a},\frac{t}{T}\right) \qquad (7a)$$

assuming the angular position $\varphi=0$.

Radiation Geometry Considerations

The convection and conduction heat transfer across the air space between the specimen and furnace surfaces is assumed to be negligible, and heat transfer by radiation only is considered in the determination of F_1 for use in equation (7).

Referring to figure 56–1, a point P on the rotating specimen surface will see the walls of the water-cooled viewing port when within an angular displacement of about 36° before and after passing these walls. The geometry of the arrangement and the different emittances of the surfaces involved make an exact analysis of this problem virtually impossible; so it is assumed that F_1 is equal to the average heat flux between the two surfaces when the point P of the cycle sees only the furnace walls, involving a total angle of about 248° of the cycle. The net heat flux to the specimen within the two 36° angles will be somewhat less due to radiation to the colder veiwing port walls. The time dimensions as shown on figure 56–2 are assumed from the above consideration to be: $A=0.1$, $B=0.79$, $C=0.89$, $D=0.927$, $E=0.963$, and $\Psi=9.65$.

The computation for F_1 then becomes

$$F_1=\frac{\sigma}{\frac{1}{\epsilon_1}+\left(\frac{1}{\epsilon_2}-1\right)\frac{A_1}{A_2}}\left[T_2^4-\frac{\sum_{n=1}^{p}T_{1,n}^4}{p}\right] \qquad (8)$$

σ is the Stefan-Boltzmann constant, 5.67×10^{-12} w/cm^2 K^4, ϵ is the emittance, T is absolute temperature, A is the surface area, and subscripts 1 and 2 refer to properties of the specimen and furnace surfaces, respectively. The summation is taken from temperature determinations for p intervals in the region where a point on the specimen sees only the furnace wall. The temperature of the furnace wall is assumed to remain constant.

Numerical Solutions

Numerical solutions to equation (7a), with the time dimensions as given above and with ap-

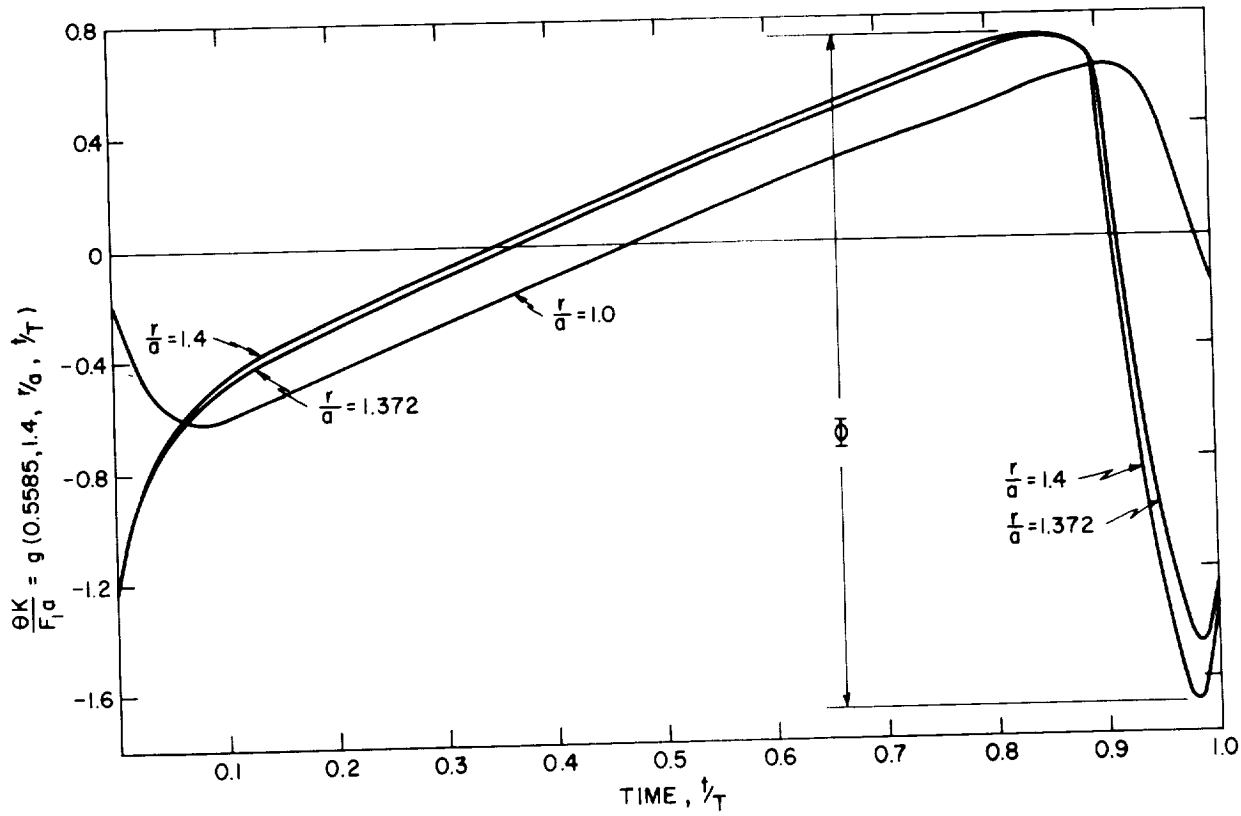

FIGURE 56–3.—Plot of $\Theta k/F_1 a$ versus time for $\alpha T/a^2=0.5585$ and $r/a=1.4$, 1.372, and 1.0.

propriate experimental dimensions, were computed by a digital computer. Figure 56–3 is a plot of $\theta k/F_1 a$ against t/T for $\alpha T/a^2=0.5885$ (corresponding to the experimental speed of 1 rpm), and for $r/a=1.4$ (specimen outer surface), 1.372 (an embedded thermocouple), and 1.0 (specimen inner surface). For a particular specimen with k, a, and F_1 remaining constant, the temperature difference θ varies above and below the mean temperature of the cycle represented by $\theta=0$.

The maximum change in $\theta k/F_1 a$ during a cycle of period T is denoted by $\Phi[=f(\alpha T/a^2, b/a, r/a)]$, illustrated on figure 56–3. Figure 56–4 shows Φ versus $\alpha T/a^2$ for $b/a=1.4$ and various values of r/a. Figure 56–4 shows that a reduction of the temperature fluctuation occurs with distance into the specimen, and with an increase in the rotational speed, which is inversely proportional to the period T.

EXPERIMENTAL APPARATUS AND PROCEDURE

Figure 56–5 is a vertical cross section of the rotating-specimen furnace, and figure 56–6 is a photograph of the furnace and accessory parts. The 1⅝-inch ID alumina tube surrounding the specimen is wound with platinum-20% rhodium wire, with taps to adjust power input into the center and end sections. The center winding is continuous to the edges of the hole that is cut into the tube to permit entrance of the viewing port. An outer "booster coil" is provided, as shown in the figure, to supply additional heat to the central portion of the furnace. The temperature of the furnace is thermostatically controlled by a recorder-controller actuated by a platinum:platinum-10% rhodium (Pt:Pt-10% Rh) thermocouple embedded in the wall of the furnace tube. The heater and apparatus were designed to operate in the temperature range from 1300° to 1800° K.

The viewing port was machined from solid copper. A radiation shield of platinum foil surrounds the outside surfaces of the viewing port, including the edges that face the specimen. The inside surfaces are coated with a black heat-resistant paint. The inner face of the port was machined to a cylindrical surface of 0.503-inch radius.

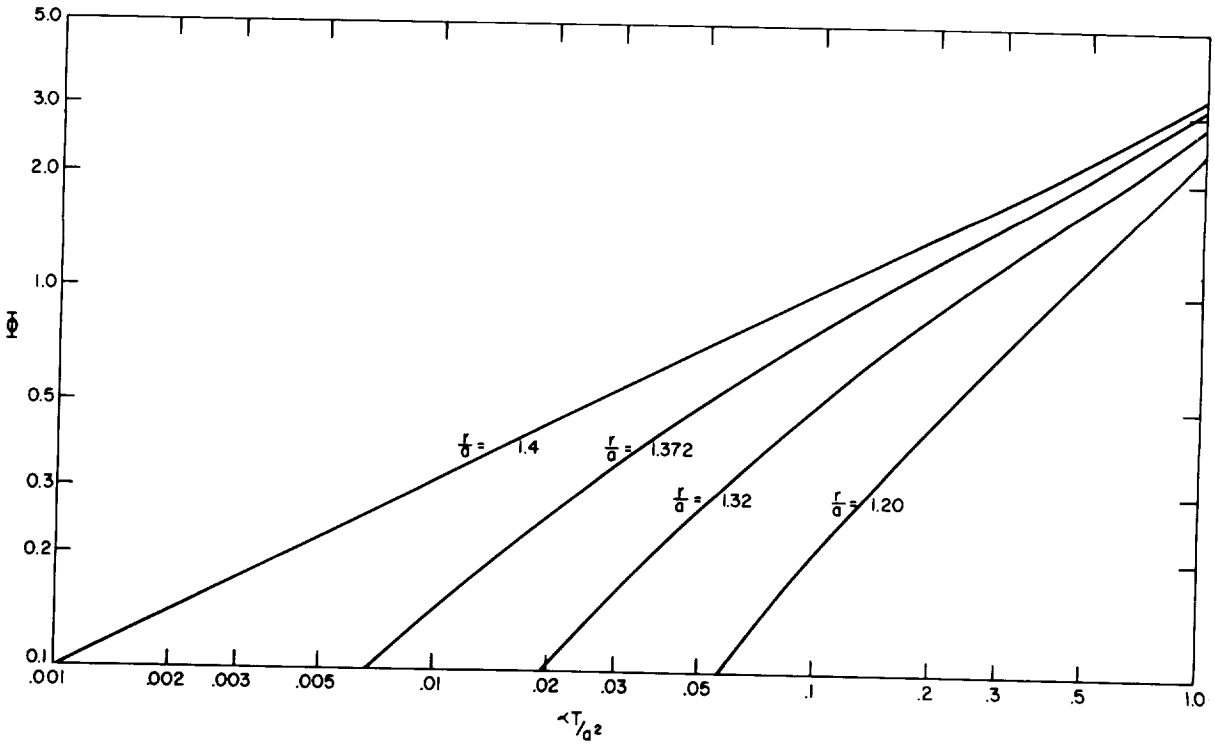

FIGURE 56–4.—Plot of Φ versus $\alpha T/a^2$ for $r/a=1.4$, 1.372, 1.32, and 1.2.

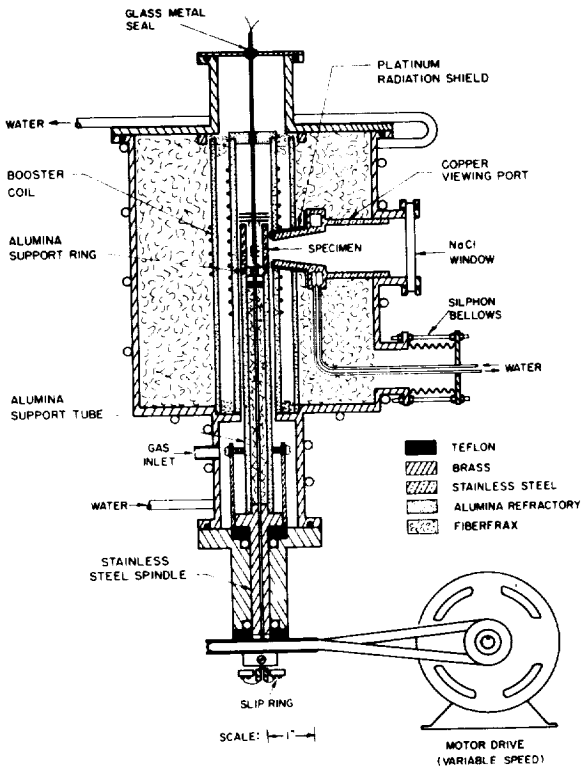

FIGURE 56–5.—Vertical section through rotating specimen furnace with viewing port.

The furnace shell is sealed so that the specimen may be heated in an inert atmosphere, as well as in air. Power leads and thermocouple leads are brought out through glass-metal seals, while O-ring seals are used for the shell ends, as well as the viewing window. The Teflon thrust bearings provide a gas-tight seal at the point where the spindle shaft which supports the specimen enters the shell. The entire furnace shell is water cooled.

The spindle is driven through a gear reducer by a ⅛-hp motor. The rotation of the specimen can be adjusted to any speed in the range from 1 to 300 rpm.

The specimen is a hollow cylinder with nominal dimensions of 1-inch outer dimeter by 1 inch high, with ⅛-inch walls. Prior to test, each specimen is surface ground so as to be cylindrical to ±0.002 inch. The alumina support tube, or pedestal, was surface-ground to the same tolerance. The inner surfaces of this tube are surface-ground near both ends so that the alumina support plug can be inserted with a slip fit in the top and the stainless steel spindle could be inserted into the support tube with close tolerances at the bottom. Three stainless steel strips, spaced 120° apart, project up from the spindle outside the alumina support tube. Each has a steel centering screw at the upper end that bears against a strip of stainless steel foil attached to the tube. These three screws are used for the final centering of the specimen. The temperature in the center cavity of the hollow specimen is observed by means of a calibrated thermocouple suspended from above and shielded from extraneous radiation.

Experiments were carried out to determine how the temperature near the surface of a non-metallic specimen fluctuated as the specimen rotated in the furnace and also to determine the rotational speed that was required to virtually eliminate temperature differences from the inner wall of the specimen and at a point near the outer wall.

A coarse-grained alumina refractory was selected for this investigation as a suitable non-metallic material. A specimen was prepared of this material by first forming a cylinder and then firing it to about 1250° K to give a soft machinable structure. After finishing to the desired size and shape, as specified above, a small groove was machined circumferentially in the outer wall surface midway between the two ends. A butt-welded Pt:Pt−10%Rh thermocouple made of calibrated wire, 0.005 inch in diameter, was placed in this groove, with the leads passing through two holes that had been drilled through the specimen wall at points nearly diametrically opposite to the bead position. The leads from the thermocouple were then brought down through the support tube and spindle assembly to a slip ring with silver-to-sliver contacts at the bottom of the spindle.

The depth of the thermocouple bead was measured and the center-line of the bead was found to be 0.010 inch below the outer wall surface of the specimen. Next, the groove with the thermocouple wire in position was filled with an excess of the alumina refractory and the specimen fired at 1800° K. The final operation consisted of surface grinding the outside of the specimen until the excess material had been ground flush with the original surface.

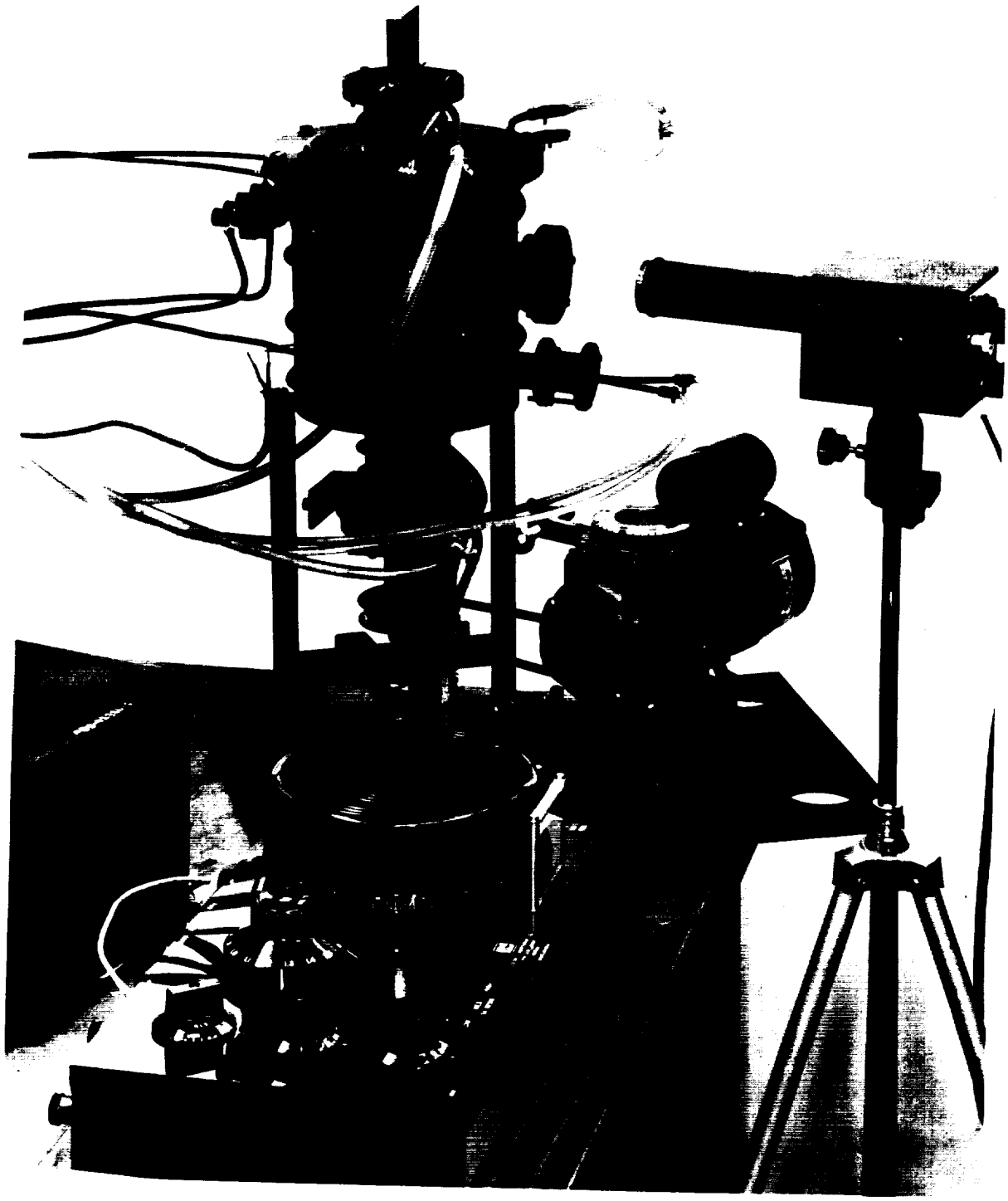

FIGURE 56-6.—Rotating specimen furnace and accessory equipment.

The finished specimen was uniform in appearance and free from surface cracks.

Data with the alumina specimen were obtained at various speeds of rotation. The temperature of the embedded thermocouple changed as the specimen rotated through 360°. The termperatures were obtained with a Leeds & Northrup type K potentiometer by observing the deflection of the galvanometer spot as a function of the angular position of the thermocouple and converting these readings to temperature.

RESULTS

The average observed temperature variation of the embedded thermocouple as a function of angle is shown in figure 56–7 for speeds of 1, 1.5, 2, and 2.5 rpm, with the furnace wall temperature maintained at 1430° K. The dotted vertical lines show the angular positions of the outside edges of the viewing port. The maximum temperature change of the thermocouple as a result of passing the viewing port decreased systematically from 100° K at 1.0 rpm to 64° K at 2.5 rpm, which was the maximum speed at which measurements of this type could be made by the galvanometer method.

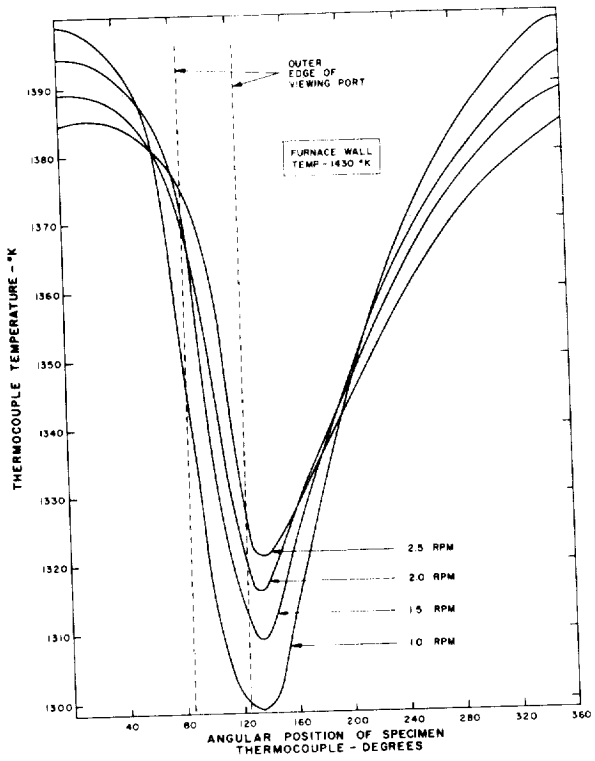

FIGURE 56 7. Temperature of embedded thermocouple versus angular position of thermocouple.

The maximum temperature reached by the embedded thermocouple while it was in the hot zone of the furnace decreased as the rotation speed was increased, but the mean temperature during a cycle remained constant within ±1° K for all rotation speeds, at approximately 1362° K. The mean temperature during a cycle was above the minimum temperature by approximately 63% of the maximum temperature change.

Other tests were performed on this specimen over a wide range of rotational speeds and at different furnace temperatures where temperatures of the embedded thermocouple and shielded thermocouple in the center cavity of the hollow specimen were observed. For rotational speeds from 10 to 360 rpm, the mean temperature of the embedded thermocouple was within ±1° K of the temperature of the shielded thermocouple. These results indicated that the shielded thermocouple will give the mean temperature of the specimen within reasonable limits of speeds. Below 10 rpm, the temperature of the shielded thermocouple was 3–5° K above the mean temperature of the embedded thermocouple, the latter computed by adding 63% of the maximum temperature change to the minimum temperature.

ANALYSIS

For the purpose of the mathematical analysis the pertinent properties of the alumina test specimen were determined, or estimated from the literature, as follows:

thickness, b-a	=0.357 cm (0.141 in.)
density, ρ	=2.16 g/cm^3
porosity	=38%
specific heat eq. (7), c	=1.3 w-sec/g.°K
thermal conductivity eq. (8), k	=0.0208 w/cm°K
thermal diffusivity, α	=0.0074 cm^2/sec
emittance, ϵ_1 (estimated)	=0.4
outside radius, b	=1.25 cm (0.492 in.)
inside radius, a	=0.893 cm (0.352 in.)
radius at thermocouple	=1.225 cm (0.482 in.)

From these data, $\Phi=(0.00931T, 1.4, 1.372)$ at the position of the embedded thermocouple. Values of Φ are shown in figure 56–4, and the maximum change in temperature at any radial position during any cycle is $\Delta\theta=42.92\,\Phi F_1$.

F_1 was computed using equation (8), in which the emittance of the furnace wall was assumed to be the same as that of the specimen. The temperatures $T_{1,n}$ used in the summation of equation (8) were the observed temperatures of the embedded thermocouple. Actually, the temperature of the surface in passing through the heating part of the cycle should slightly exceed the embedded thermocouple temperature, as can be seen in figure 56–3. The slight difference between these two temperatures can be calculated using the value of F_1 obtained above, and applied as a correction to $T_{1,n}$ for computation of a better value of F_1. This correction was not considered for this paper. This is shown in the following table, in which parameters for the four tests are given, and also the analytically calculated, and the experimental, values of $\Delta\theta$.

Rotation Speed, rpm	F_1 (eq. (8)) w/cm²	$\alpha T/a^2$	Φ, (fig. 56-4)	$\Delta\theta$, °K(r/a = 1.372) Analysis	Experiment
1.0	1.084	0.558	2.18	101	101
1.5	1.087	.372	1.70	79	85
2.0	1.081	.279	1.46	68	73
2.5	1.108	.223	1.27	61	64

Figures 56–8 and 56–9 were plotted from the analytical solution assuming F_1 was constant irrespective of rotational speed. Curves A and B of figure 56–8 show the maximum temperature change, $\Delta\theta$, at the surface and the position of the embedded thermocouple, respectively, versus the rotation speed. Curve C of figure 56–8 shows the temperature change of the specimen surface in passing from one edge of the viewing port to the other edge. An optical pyrometer focused on the specimen at the two edges of the viewing port opening should see the temperature difference indicated by curve C, if the specimen surface is opaque to radiation. The temperature difference across the viewing port, when determined from measurements made with an optical pyrometer, was found to be approximately 32° K at 2 rpm and 2° K at 50 rpm.

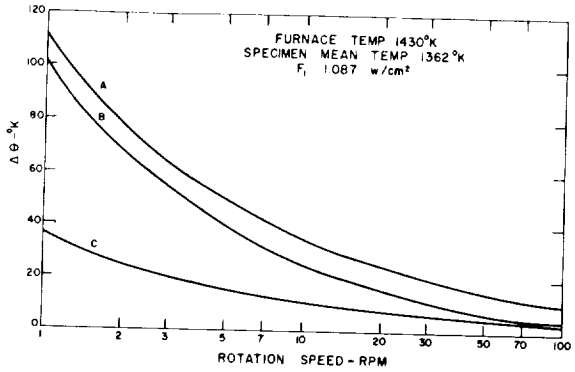

FIGURE 56–8.—Temperature departure versus rotation speed: A—Maximum temperature change in one revolution at specimen surface, $r/a=1.4$; B—maximum temperature change in one revolution at position of embedded thermocouple, $r/a=1.372$; and C—temperature change at specimen surface from inside edge of viewing port to other inside edge.

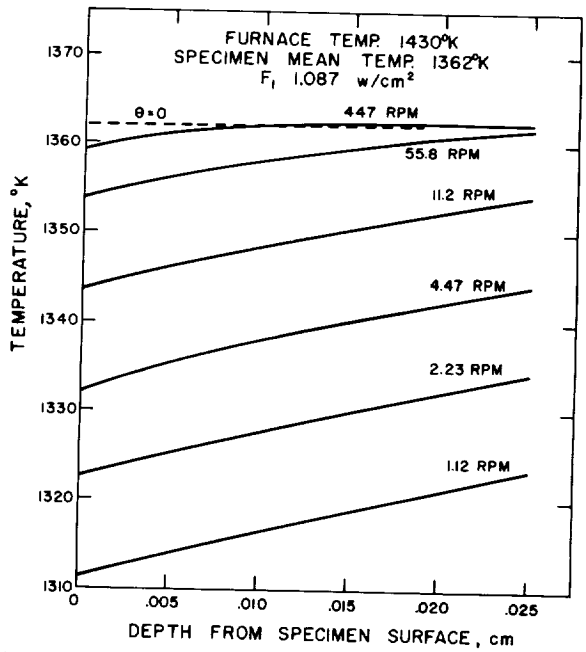

FIGURE 56–9.—Specimen temperature at center of viewing port opening versus depth from specimen surface for various rotation speeds.

Figure 56–9 shows the specimen temperature as a function of depth from the surface for six rotation speeds for a position at the center of the viewing port, assuming a mean temperature ($\theta=0$) of 1362° K. According to this analysis, fairly high rotation speeds are required for the porous alumina specimen before the temperature of the shielded cavity thermocouple can be accepted as a good approximation to the true temperature at or near the specimen surface.

The factor, F_1, of equation (7a) was computed from equation (8), where the summation term was determined from experimental temperatures of a thermocouple embedded in the specimen. For the emittance tests to be conducted in this apparatus there will not be an embedded thermocouple. The experimental data seem to show that the summation term can be approxi-

mated, for this apparatus, by

$$\frac{\sum_{n=1}^{p} T_{1,n}^4}{p} = (T_m + T_d)^4$$

where T_m is the mean temperature, approximated by the temperature of the shielded cavity thermocouple, and $T_d = 4.0$, for experiments with speeds from 1 to 2.5 rpm. With F_1 computed from this approximation, the temperature at the center of the viewing port opening, $T_c = T_m - gF_1a/k$, can be computed from figure 56–10 for a specimen whose thermal properties are known and which has a rotation speed of period T.

SUMMARY

Equations were developed analytically for computing cyclic temperatures of a hollow cylindrical specimen rotating in a furnace with a viewing port as a function of system geometry, rotational speed, thermal properties of the specimen material, and a derived average heat flux for the portion of the cycle when the specimen is being heated by the furnace. Simplifying assumptions were that (1) the heat flux history at the outside surface of the specimen for one cycle is as shown in figure 56–2, (2) there is no heat flow at the inside surface of the specimen, and (3) there is no longitudinal heat flow in the specimen.

A comparison was made between specimen temperatures computed analytically and those obtained experimentally at low speeds of specimen rotation. Agreement within 6% was obtained, at rotational speeds from 1 to 2.5 rpm, in regard to the maximum temperature change occurring at the position of an embedded thermocouple 0.01 inch under the surface. This agreement seems well within possible experimental error and uncertainty as to the thermal properties of the specimen material.

The analysis showed that the surface temperature of the specimen, at the center of the viewing port opening, was substantially lower than the mean temperature of the specimen at low rotational speeds, but the departure was reduced to within 3° K at about 450 rpm for this case. Because the error in surface temperature acceptable for emittance determinations is less than 1° K, a function is given graphically (figure 56–10) with which the departure can be estimated for various speeds in this apparatus.

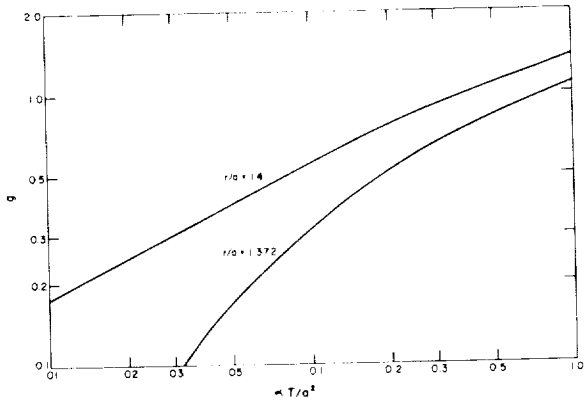

FIGURE 56–10.—Plot of $\Theta k/F_1 a = g(\alpha T/a^2, 1.4, r/a, 0.945)$—eq. (7a)—versus $\alpha T/a^2$ for $r/a = 1.4$ and 1.372, where $t/T = 0.945$ is the center of the viewing port opening.

REFERENCES

1. FERY, C.: Rayonnement Calorifique et Lumineux de Quelques Oxydes, Ann. Chim. de Phys., *27*, 1902, p. 433.
2. KINGERY, W. D.: Property Measurements at High Temperatures, John Wiley & Sons, Inc., New York, N.Y., pp. 119–120 (1959).
3. PLUNKETT, J. D.; and KINGERY, W. D.: The Spectral and Integrated Emissivity of Carbon and Graphite, Proc. of Fourth Conf. on Carbon, Pergamon Press, Belfast, England, pp. 457–472 (1960).
4. OLSEN, H. O.; and MORRIS, J. C.: Determination of Emissivity and Reflectivity Data on Aircraft Structural Materials: Part III, Techniques of Measurement. WADC Tech. Rpt. 56–222, Jan. 1959.
5. CLAYTON, W. A.: Thermal Property Measurement Techniques, Boeing Co. (Seattle Div.) Report No. DZ–80281 to Wright Air Dev. Div., on Contract AF33(600)–41517, Dec. 1961.

6. Dwight, H. B.: Tables of Integrals and Other Mathematical Data. The Macmillan Co., 1934.
7. Russell, A. S.: Alumina Properties. Tech. Paper 10, Aluminum Company of America, Pittsburgh, Pa., 1953.
8. Goldsmith, A.; and Waterman, T. E.: Thermophysical Properties of Solid Materials, Section VII–M–1. Armour Research Foundation, WADC Tech. Rpt. 58–476, Wright Air Dev. Center, Wright-Patterson Air Force Base, Ohio, 1959.

57—TECHNIQUES OF MEASURING NORMAL SPECTRAL EMISSIVITY OF CONDUCTIVE REFRACTORY COMPOUNDS AT HIGH TEMPERATURES

BY T. R. RIETHOF AND V. J. DeSANTIS

GENERAL ELECTRIC COMPANY, PHILADELPHIA, PENNSYLVANIA

Techniques for measuring the spectral distribution of normal emittance over a wavelength bandwidth of from 0.4 to 5μ and up to temperatures of 3000° K is described. Special design features of the apparatus for heating the specimen, controlling specimen cavity atmosphere and semi-automatic recording of emittance are discussed. An approach to specimen characterization is proposed and the emittance of the borides of niobium, zirconium, and titanium are presented. In addition, the normal spectral emittances of zirconium, hafnium, and tantalum nitrides are described.

In recent years the use of materials at very high temperatures has become very important, and as a result interest in the high-temperature physical properties has also increased. One physical property that increases in importance as the temperature increases is the thermal radiation of solid materials.

The thermal radiation of a unit area of an opaque solid may be expressed as a function of its temperature and its emissivity (ϵ). Emissivity is the dimensionless ratio which compares the radiation from the material under consideration with that from an ideal radiator (or blackbody) at the same temperature. Emissivity may be considered total or spectral, depending on whether one compares the radiation over all or over just a narrow portion of the entire spectral region. Geometrically the radiation may be characterized as normal or hemispherical, and consequently one can consider either normal or hemispherical emissivity. In the remainder of this paper the term emissivity will refer to the spectral normal emissivity.

In an opaque solid, light penetrates only a short distance into the material and, as a result, thermal radiation characteristics are strongly influenced by surface inhomogeneities which are large compared to the wavelength of the radiation under consideration. Worthing (ref. 1) has used the term emittance as the ratio of the emitted radiant flux per unit of area of a specimen to that of a blackbody at the same temperature and under the same conditions, and has defined emissivity as the emittance of a material that has an optically smooth surface and a thickness sufficient to be opaque. In all measurements that will be discussed at least an attempt has been made to produce "optically smooth" surfaces, and hence the term emissivity will be used. Kirchhoff's law relates the reflectivity to the emissivity, and for an opaque body it indicates that the sum of the two dimensionless quantities is unity. Careful examination indicates that the complement to the normal emissivity is the hemispherical (i.e., diffuse plus specular) reflectivity.

The authors gratefully acknowledge the helpful contributions of P. Gorsuch, D. A. Donatelli who performed the experimental work, and the U.S. Air Force who sponsored this work under Contract AF 33(616)-6841.

APPARATUS

General

By definition, the spectral emissivity of an opaque solid is the ratio of radiation from an area of its surface to the radiation from the

same area of a blackbody radiator at the same temperature and over the same narrow wavelength interval.

In principle then, an apparatus for measuring emissivity, that is, an "emissometer," will consist of a specimen, a comparison blackbody or secondary standard, a means of heating both specimen surface and reference to the same (or known) temperatures, a device for dispersing radiation spectrally, and a detector to measure the intensity of the radiation. Auxiliary equipment must include an optical system to transfer radiation from specimen and reference through the monochromator to the detector, and electronic devices to permit the measurement of the detector output as a function of wavelength. It is also necessary to have a device to measure the surface temperature of both the specimen and the references, and to be able to control the environment in which both are heated, to reduce undesired surface effects.

Since it was desired to study the spectral emissivity of refractories at temperatures up to 3500° K or higher, it seemed advisable to consider RF induction heating. This has been used successfully by Marple (ref. 2) and Blau (ref. 3), among others. An alternate method would have been to use radiative heating, using a solar or arc-image furnace. Previous difficulties encountered by Metzger (ref. 4) with the latter method confirmed the decision in favor of induction heating. These difficulties included lack of source constancy, lack of sufficient heat fluxes to attain desired temperatures, and inability to separate emitted and reflected radiation adequately. It should be pointed out, however, that the advent of more compact and powerful image furnaces, such as the one now available from Arthur D. Little, Incorporated, which use stabilized high-temperature arcs and elliptical mirrors, makes this technique definitely useful as a source for the study of spectral emissivity, particularly in the case of nonconductors, which are difficult to heat by RF fields.

The other choice is in the technique used to determine the emissivity itself. It is possible to measure the flux from the specimen and from the reference separately, using the monochromator-detector combination to measure relative flux. This permits using separate, accurate, blackbody cavities, and also permits separate environments for the specimen and reference, if this should be desirable. On the other hand, it requires either maintaining the reference and specimen at the same temperature, or knowing accurately the temperature of both specimen and reference. A slight modification of this method involves using the blackbody to calibrate the monochromator-detector combination as an absolute intensity measuring device, and then measuring the actual radiated flux from the specimen at a later time. (ref. 3) All of these methods suffer from the common difficulty of determining the temperature of the specimen surface. Once one passes the upper limit of usefulness for thermocouples, temperature is measured from the thermal radiation characteristics of the source. Measurements can either make use of brightness temperature, which requires a knowledge of the emissivity of the specimen at the wavelength under consideration (usually 0.65 μ) as a function of temperature, or of the variation of spectral radiant flux with wavelength, which requires a knowledge of the variation of spectral emissivity with wavelength.

One method which avoids all of these difficulties is to have the blackbody reference incorporated in the specimen being investigated. Under these circumstances only two conditions must be fulfilled: namely, that the reference is an adequate blackbody, and that the temperature of the cavity is the same as that of the surface. To some degree, the errors in these two conditions tend to compensate each other, for if the cavity is not quite "black," it radiates less and tends to get to a higher temperature, since cooling is mostly by radiation and the inside of the cavity can radiate only through a small solid angle. This technique has successfully been used by De Vos (ref. 5) and Marple (ref. 4), and was also employed in the present system.

As indicated above, the emissometer consists of a source unit, external optics, a monochromator, a detector, and electronics. Important auxiliaries are the specimen chamber and the optical pyrometer. Figure 57–1 is an over-all view of the emissometer. It shows the specimen chamber (1) with the primary coil of the induction heater (2). The external optics are

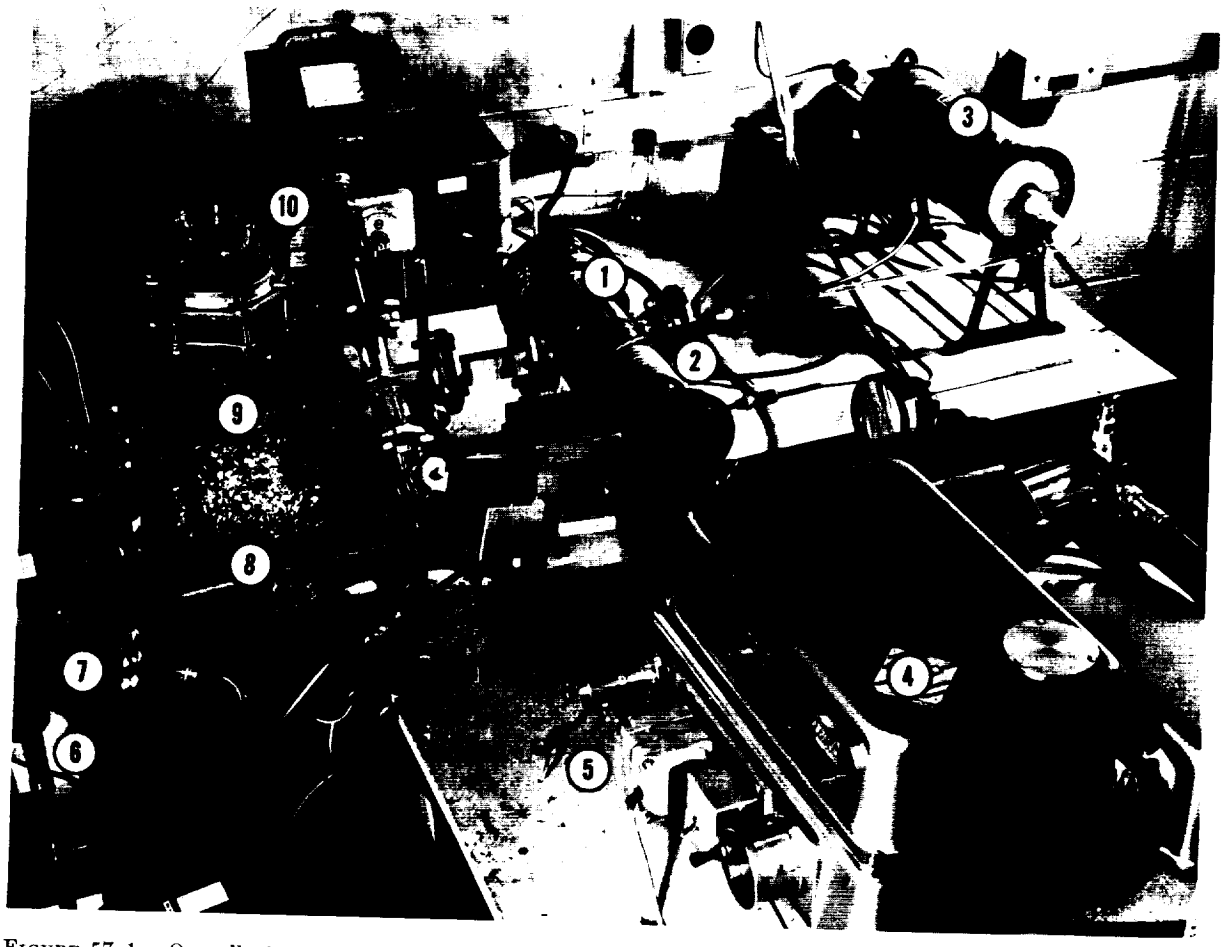

FIGURE 57–1.—Overall view of emissometer: (1) specimen chamber, (2) induction heater coil, (3) muffle furnace for purifying argon, (4) Perkin-Elmer model 112 monochromator, (5) constant energy slit servomechanism, (6) three-stage metal oil diffusion pump, (7) 2-inch vacuum gate valve, (8) micro-optical pyrometer, (9) cold trap, and (10) Phillips gage.

between the specimen chamber and the monochromator (4). One detector is inside the monochromator, and the other can be seen at its left rear. The electronics and recording system are out of the photograph at the right front, and the induction heater is located beneath the table surface, underneath the specimen chamber and monochromator.

Operationally, the emissometer consists of a source unit for heating the specimen, external transfer optics to provide alternately an image of the blackbody reference cavity and an equivalent area of specimen surface, the monochromator, detector, sorting cams and choppers, and electronics.

Each of the emissometer components will now be considered in some detail.

692-146 O—63——37

Source Unit

The source unit must produce uniform, constant, high temperatures in both the specimen surface and the reference blackbody in such a manner that only radiation by these two objects can be observed. Ideally, the sample alone would be heated to an appreciable degree. A high-intensity induction light source that is manufactured by the Sylvania Electric Company (model RFS–4) very nearly satisfies these conditions. This is the same unit used by Blau (ref. 3), and this description is patterned after his.

Figure 57–2 is a diagram showing both the source unit, as modified for the present study, and the specimen chamber.

The induction source consists of three coaxial

elements: the primary induction coil (item 2 in figure 57–1), a water-cooled concentrator, and a specimen and a specimen support. All of these elements were used as supplied with the light source. A Pyrex cylinder—part of the specimen chamber—separates the primary coil and the concentrator. The sample (figure 57–3) consists of a small rod, ¼ in. in diameter and ½ in. long, which is mounted in a hollow zirconia rod. The specimen is so located in the concentrator that only the ⅛ in. back from the surface portion is in the main RF field, the remaining length being heated by conduction only. The zirconia rod serves to reduce heat loss to the remainder of the system. The concentrator, which serves to increase the electromagnetic coupling between the primary coil and the sample, is a water-cooled cylindrical metal shell open on the lower end. A circular opening slightly wider than the sample is centered at the upper end. The hole connects with a narrow slot (not shown in figure 57–2) running across the upper face and down the side wall. The hole-slot geometry acts to increase the density of the current induced in the sample in the immediate vicinity of the front surface of the concentrator. Electrically the concentrator may be considered a two-turn loop that acts as an impedance match between the specimen and the primary induction coil. Blau (ref. 3) indicates that the

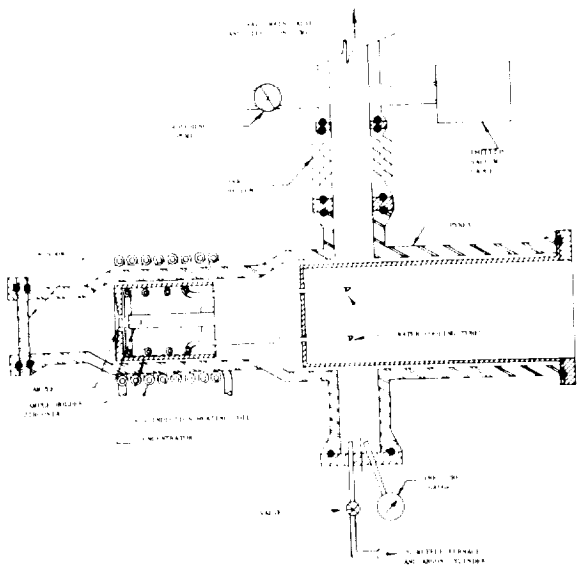

FIGURE 57-2.– Induction furnace emissometer source unit and specimen chamber.

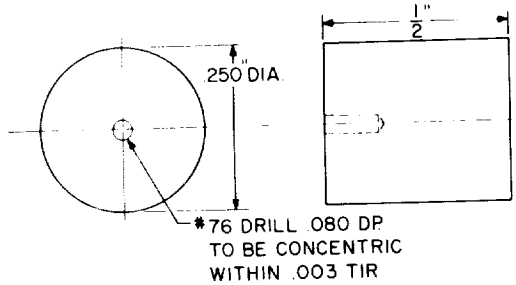

FIGURE 57-3.– Emissivity specimen design.

coupling is so efficient that temperatures in excess of 4000° K can be obtained with a 7-kva input to the power supply. In the present study, temperatures of about 3200° K have reached by operating the RF power supply at about 75% of capacity.

The concentrator is inside the glass specimen chamber, and it is supported by the copper water-cooled tubes that are attached to a metal plate and tubing assembly, which in turn is held by flanges to the far end of the specimen chamber. The specimen is supported in the zirconia tube inside the concentrator. It may be removed by either removing the entire concentrator assembly, or by removing the window at the other end. The entire specimen chamber and auxiliary glass systems were built with standard Pyrex pipe and fittings. The chamber itself is a Pyrex cross, the long section being 3 in. in diameter, and the short section 1 in. in diameter. Standard Pyrex tubing is used between the concentrator and primary coil, and the tubing diameter is then further reduced to the next smaller size of standard glass pipe. The 2 in. window, either quartz or calcium fluoride, is actually held by flanges to a water-cooled copper ring, which in turn is held to the glass pipe. All seals use O-rings to insure a vacuum-tight system. One side arm (left in fig. 57–1, top in fig. 57–2) of the specimen chamber leads to a junction, cold trap, valve, and vacuum system. It was necessary to insert brass, vacuum-tight bellows between the specimen chamber and the remainder of the vacuum system, in order to prevent leaks due to the stresses produced during the replacement of specimens. Both the cold trap and the cross used to attach the Phillips, cold cathode, vacuum gage and rough pumping line, are standard Pyrex pipe components. To insure maximum

pumping speed, all components between the chamber and diffusion pump are large diameter, and vacuums of 10^{-7} mm Hg (indicated on the Phillips gage) are obtained when the trap is filled with liquid nitrogen. Compressed air is used to cool the hot portion of the specimen chamber walls.

The other side-arm of the specimen chamber leads to a pressure gage and to a purifying train and argon cylinder. While the system is designed to operate with any desired environment, the present procedure has been to operate either in vacuum or in an argon environment. The argon (99.996%) is prepurified by passing over titanium chips heated to about 1000° C in the muffle furnace (item 3 in fig. 57–1).

The reference source is a blackbody cavity drilled in the specimen. As indicated in fig. 57–3, the hole is about 0.02 in. in diameter and 0.08 in. deep, giving a depth to aperture ratio of 4. The dimensions are a compromise between a large diameter, which is needed to obtain an adequate signal since the hole diameter determines the size of the (slightly smaller) mask over the monochromator and hence the radiating area and energy, and a small diameter that is required for a high depth to width ratio and hence a "blacker" cavity. The depth of the cavity is limited by the thickness of the specimen disk, and the thickness over which the RF field produces approximately uniform heating. While the 4:1 ratio may at first be considered marginal, the situation is improved somewhat by the rough sidewalls (and hence higher effective emissivity) produced in drilling small holes in rather hard materials. The results for tungsten indicate that even in the case of a material with quite low emissivity, the reference is an adequate blackbody. Because of the proximity of the surface and blackbody there is good assurance that both are at the same temperature.

External Transfer Optics

The purpose of the transfer optics is two fold: they must produce a sharp image of the specimen on the spectrometer slit, and they must alternate images from the specimen surface and the blackbody cavity.

The transfer optics are indicated in diagram form in figure 57–4. It is seen that radiation from the specimen is deflected by mirror M_1

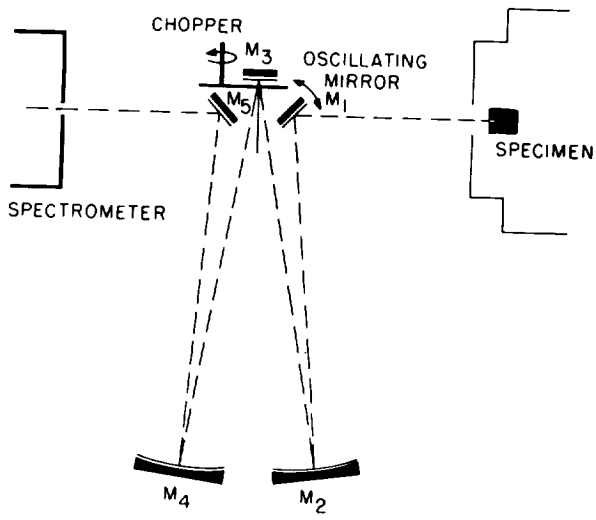

FIGURE 57–4.—Optical path of induction furnace emissometer.

onto the spherical mirror M_2, which brings it to a focus on mirror M_3. The radiation is then reflected onto M_4 (identical to M_3) and refocused onto the spectrometer slit mask, after being deflected by M_5. The use of two spherical mirrors in this arrangement tends to cancel out the slight astigmatism due to the off-axis arrangement, and also provides an intermediate focus at M_3. A chopper is located immediately in front of M_3 to produce a 14-cycle alternating signal suitable for amplifying in the standard Perkin-Elmer amplifier system (ref. 6). Mirror M_1 is oscillated at a frequency half that of the chopper, that is 7 cps. In one position it images the blackbody cavity on the spectrometer slit mask, and in the other position it images the specimen surface onto the slit mask.

In operation, the transfer optics are covered by a metal box which not only serves to exclude stray light, but also supports a mirror which can be inserted between the specimen and mirror M_1, in order to permit seeing the specimen surface with the micro-optical pyrometer (No. 8 in fig. 57–1).

Monochromator and Detectors

The monochromator is the standard unit supplied with the Perkin-Elmer model 112 spectrometer. This monochromator is double-pass, the radiation usually being chopped by the (indicated) internal chopper between the first and second pass. In this manner, the synchronous rectifying system of the electronics

system serves to amplify the desired, chopped, second-pass radiation impinging on the detector, while ignoring the first-pass radiation (of different wavelength) which simultaneously arrives at the detector. In the present system it is necessary to chop ahead of the monochromator, since the chopper also drives various sorting cams (see below) and the monochromator had to be masked so that only second-pass radiation can arrive at the detectors. This was accomplished by masking the lower half of the entrance slit, and the upper half of the exit slit. The entrance slit was further reduced by a mask, centered on the upper half of the slit, and slightly smaller in diameter than the diameter of the blackbody cavity. The entire system can be aligned easily by placing a mercury arc lamp behind the slit and inside the monochromator, and by adjusting the optics to image the source in the blackbody cavity.

The thermocouple detector is housed inside the monochromator. A photomultiplier detector located along the same axis as the exit slit can be utilized by flipping the intervening plane mirror out of the light path. Figure 57–5 shows an RCA type 7160, experimental, infrared, end-window photomultiplier in position. The size of the active surface of this photomultiplier is sufficient that it is not necessary to re-focus the divergent radiation from the exit slit. The tube is usable out to 1.5 μ. In most cases a 1P21 photomultiplier has been used, in conjunction with a standard Perkin-Elmer housing, and a lens to reimage the exit slit on the active surface. This tube provides much more sensitivity at the shorter wavelengths but its response decreases rapidly at wavelengths longer than 0.8 μ. There is adequate energy to use the thermocouple at wavelengths longer than 0.8 μ, particularly at the higher specimen temperatures.

Electronics and Sorting System

The block diagram (figure 57–6) serves to explain the operation of the amplifying and sorting system. The key to the system is the chopper and its associated cams. The chopper motor turns at 7 cps, but since the chopper has two blades, the effective chopping speed is 14 cps, which is selected to be compatible with the normal 13 cps chopping speed of the Perkin-Elmer system. The chopper shaft carries three

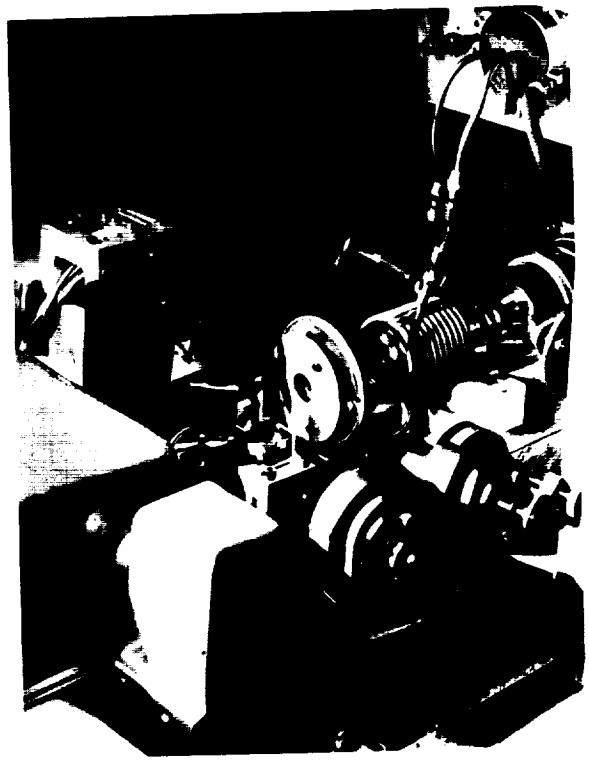

FIGURE 57–5. Induction furnace emissometer.

cams which operate the microswitches. Two of the switches operate at 7 cps (SW_1 and SW_2) and the other operates at 14 cps (SW_3).

The radiation is originally converted to 14 cps chopped radiation by the chopper, and is rectified by the switch SW_3. In addition, however, the oscillating mirror (M_1 in figure 57–4) is moved at 7 cps by SW_1, which operates a solenoid coil. Switch SW_2 serves to separate radiation from the blackbody cavity, that is collected when the solenoid activating M_1 is off, from that due to the specimen surface, that is collected when the solenoid is activated and M_1 is in a different position.

M_1 moves only about 2° under the influence of the solenoid and is returned by the action of a permanent magnet on the iron core of the solenoid.

The actual sorting system is considerably more elaborate, in that the microswitches actually operate mercury relays which in turn bias various tubes in the circuitry to cut-off.

The output of the sorting circuit may be used to record each channel (surface or blackbody) individually using a standard recorder.

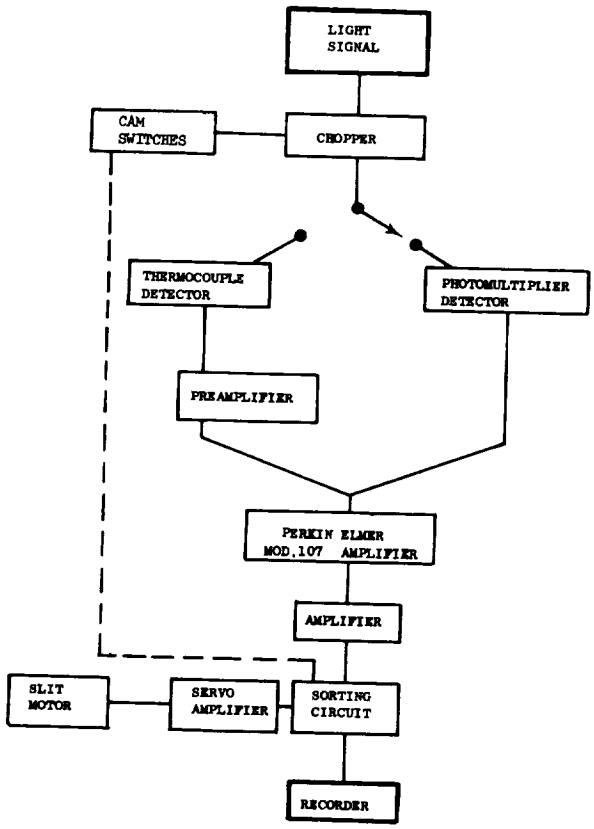

FIGURE 57-6.--Emissometer electronics.

Alternatively, it is possible to amplify the "blackbody" signal and apply it instead of the battery voltage across the entire recorder slide-wire. At the same time the "surface" signal is fed into the recorder the normal way, and thus the recorder reads the ratio (ref. 7) directly, which is the spectral emissivity.

The principal advantage of this system is that the emissivity is independent of fluctuating specimen temperature or amplifier gain. To insure that the system is operating at all times at an optimum signal level, the signal from the "blackbody" is monitored through a servo system, which in turn operates the spectrometer slit control to maintain this energy constant while scanning the spectrum.

SPECIMEN PREPARATION

Specimens of all materials employed in this study were procured from the Carborundum Company and were prepared by starting with micronized powders of the compound having a particle size less than 1 μ. These powders were hot-pressed in an oversized graphite mold at temperatures in excess of 2000° C. After sintering they were ground to size in order to remove traces of diffused carbon and any carbides that may form on the surface.

SPECIMEN CHARACTERIZATION

It is well known that the value of spectral emissivity is intimately associated with the chemical and physical properties of a given material. Worthing (ref. 1), for example, in his definition of emissivity limits its application to polished surfaces. Because experimental results depend in a large measure on this and other specimen properties at the time its emissivity is being measured, a substantial amount of study was devoted to systematic characterization of the various specimen materials. In applying the system it was found that the characterizing parameters did not, in all cases, admit of rigorous interpretation because of other factors that influenced their validity.

These factors are a direct result of the high temperatures at which measurements were made. In some instances their dynamic nature could be observed when the specimen was being viewed through the optical pyrometer during measurement of specimen temperature. Included in these observations were slow changes in surface texture from polished to an etched or matt structure, the formation of micropores that gave the appearance of a multiplicity of microscopic blackbody cavities, and apparent changes in surface grain size. Other changes that are believed to occur while the specimen is standing at high temperatures in vacuum and inert atmospheres are those involving surface composition, bulk densification, evaporation, interaction of the specimen with its holder, and reaction with trace contaminants in the specimen chamber.

PROCEDURES OF SPECIMEN CHARACTERIZATION

In order to differentiate between perturbations in specimen emissivity and its true variation with wavelength and temperature the following characterizing steps were carried out on each material.

Chemical composition was first established by running wet chemical analysis to determine major elemental components and spectrochemi-

cal analysis to determine the trace elements present in the specimen. In addition, those elements looked for and not found were recorded.

Each specimen was then polished, etched, and photomicrographed to determine grain size, boundary distribution, pore distribution and microinclusion content. Microscope optics were standardized as to objectives, oculars, bellows setting, angle of polarized light, and light intensity. Filters were not used. In addition, an effort was made to maintain standard photographic procedures.

Next the etched specimen surface was replicated and electron micrographs of crystalline structure recorded.

The surface was again polished and slow-scan x-ray diffraction patterns were run. In this step "d" spacings were measured, line intensity recorded and related to inclusion concentrations, and miller indices measured. These x-ray observations were carried out after polishing to establish whether or not the polishing operation had caused the surface to possess an amorphous structure indicative of multiple layers of free atoms on the surface. It is believed that such layers are unstable and would undergo evaporation and crystallization during emissivity measurements. Therefore, when this was observed, the specimens were repolished in a manner that removed the amorphous layer.

Specimen weight and density measurements were then made for the purpose of comparing possible changes in these properties during emissivity measurement. In several cases weight and density changes could not be attributed entirely to evaporation, densification, and modifications in composition because there occurred an interchange of material due to interaction of the specimen and its zircon holder.

Normal spectral emissivity measurements were then made over a temperature range understood to be compatible with thermal stability of the specimen. As a further measure of relating changes in emissivity induced by thermal and or environmental conditions, a steady-state low temperature was selected at which emissivity determinations were made. These determinations then served as a benchmark against which to measure changes in emissivity as a result of making measurements at higher temperatures.

Following emissivity measurements the specimens were again weighed, density measurements made, photomicrographs, x-ray diffraction and electron microscope studies run and compared with previous measurements and observations.

EXPERIMENTAL PROCEDURE

In making emissivity measurements, the following procedure was carried out. The specimen chamber was first pumped to pressures below 5×10^{-5} torr, and by manipulating the appropriate valves the system was checked for leaks. Following this, the specimen was heated to about 700° C in order to degas it and liberate residual moisture from associated surfaces. The chamber was then flushed several times with prepurified argon and finally filled with argon to a pressure of about 1.5 to 2 atmospheres.

Specimen temperature, as measured by means of a calibrated optical pyrometer, was then raised to the intended temperature at which emissivity values were measured. Both blackbody and surface temperatures were measured to an accuracy of 5° and again checked at the end of each emissivity run. Observed pyrometer temperatures were corrected for absorption of the calcium fluoride infrared transmitting window of the specimen chamber and incomplete reflections from the front-surface mirror.

EXPERIMENTAL RESULTS

In this work normal spectral emissivity measurements were determined over a wavelength bandwidth starting at 0.4 μ in the visible out to 5 μ in the infrared, and involved the following refractory compounds:

1. niobium diboride—NbB_2
2. zirconium diboride—ZrB_2
3. titanium diboride—TiB_2
4. zirconium nitride—ZrN
5. hafnium nitride—HfN
6. tantalum nitride—TaN

The various temperatures at which measurements were made ranged from 1500° K to 3000° K. Total normal emissivity was computed from spectral emissivity data.

Calculation of Total Normal Emissivity

The measurement of normal spectral emissivity at a given temperature, combined with the blackbody distribution of radiation at that temperature, can be used to calculate the total normal emissivity.

Table 57–I lists the blackbody functions required for the calculation of total normal emissivity from measured normal spectral emissivity. The data were obtained from the General Electric "Radiation Calculator" slide rule. The calculation is estimated to introduce no more than 5% error in the value of total emissivity. To obtain total normal emissivity for a particular substance at a given temperature, one simply reads the spectral emissivity from the measured data and multiplies it by the fraction of energy radiated by a blackbody corresponding to that wavelength internal and temperature. The total emissivity is simply the sum of the products of "energy fraction" and spectral emissivity and can be expressed as follows:

$$\epsilon_{n t(T)} = \Sigma \epsilon_{n d\lambda(T)} \cdot I_{b b d\lambda(T)}$$

Where $\epsilon_{n t(T)}$ is total normal emissivity at temperature T, $\epsilon_{n d\lambda(T)}$ is normal sprectal emissivity at temperature T. $I_{b b d\lambda}$ is the fraction of energy radiated from a blackbody in the wave length internal d_λ at temperature T.

Chemical Analysis

Table 57–II presents the results of chemical analysis of niobium diboride on which spectral emissivity measurements were made. Similar detailed composition determinations were made on the compounds of ZrB_2, TiB_2, ZrN, TaN, and HfN.

The theoretical composition of NbB_2 is 81.11% niobium and 18.89% boron. Actual specimen composition is close to theoretical being 79.07% and 19.09%, respectively. The presence of 0.26% iron is believed to have very little effect on emissivity at high temperatures. Iron has a vapor pressure of 10^{-6} torr at 1273° K and most likely evaporates from the surface at temperatures in excess of 1600° K. In fact, all trace elements in the specimen except hafnium, molybdenum, titanium, tantalum, tungsten and zirconium have vapor pressures greater than 10^{-6} torr below 1473° K.

Surface Characterization

Figure 57–7 shows light photomicrographs at 300× of NbB_2 surface, (A) after polishing, (B)

TABLE 57–I. *Conversion of spectral emissivity to total emissivity*

Mean wavelength [a] or wavelength interval, μ	Fraction of total energy at effective mean wavelength at temperature (° K) indicated								
	1400	1600	1800	2000	2200	2400	2600	2800	3000
0.5 [b]	----	----	----	----	----	----	0. 01	0. 01	0. 01
0.6 [b]	----	----	----	----	0. 006	0. 01	. 01	. 02	. 03
0.7 [b]	----	----	----	0. 01	. 014	. 02	. 025	. 03	. 04
0.8 [b]	0. 001	0. 004	0. 01	. 01	. 02	. 03	. 035	. 05	. 06
0.9	. 002	. 006	. 01	. 02	. 03	. 04	. 05	. 06	. 07
1.0	. 007	. 01	. 02	. 03	. 03	. 04	. 06	. 06	. 06
1.1	. 02	. 04	. 06	. 07	. 09	. 11	. 11	. 13	. 13
1.3	. 03	. 05	. 07	. 07	. 10	. 09	. 12	. 11	. 12
1.5	. 05	. 07	. 08	. 09	. 10	. 09	. 10	. 09	. 09
1.7	. 06	. 07	. 08	. 09	. 08	. 09	. 08	. 08	. 07
1.9	. 035	. 08	. 08	. 08	. 08	. 07	. 06	. 06	. 06
2.2	. 155	. 13	. 13	. 12	. 12	. 11	. 10	. 09	. 08
2.6	. 11	. 10	. 10	. 10	. 08	. 07	. 07	. 06	. 05
3.0	. 10	. 09	. 08	. 08	. 06	. 05	. 04	. 04	. 04
3.4	. 07	. 07	. 06	. 05	. 04	. 04	. 03	. 03	. 02
3.8	. 06	. 05	. 04	. 04	. 04	. 03	. 02	. 04	. 02
4.5	. 11	. 09	. 07	. 06	. 04	. 04	. 04	. 02	. 02
Above 5.0 [c]	. 19	. 14	. 11	. 08	. 07	. 05	. 04	. 04	. 03
All wavelengths	1. 01	1. 00	1. 00	1. 00	1. 00	1. 00	1. 00	1. 00	1. 00

[a] Mean wavelengths are not spaced equally but rather are spaced to adequately reflect rate of emissivity variation with wavelength for many opaque solid materials.

[b] Shortest wavelength used is a function of temperature and includes all radiation below that wavelength.

[c] Spectral emissivity varies slowly at the long-wavelength end of the spectrum where only a small fraction of the energy remains—particularly at the higher temperatures.

NOTE. All data taken from Radiation Calculator.

TABLE 57–II.—*Chemical Analysis of Niobium Diboride*

	ppm[a]	%
Niobium	----	79.07
Boron	----	19.09
Silver	[b] 5	
Aluminum	70	
Arsenic	[b] 100	
Barium	[b] 10	
Beryllium	[b] 10	
Bismuth	[b] 10	
Calcium	100	
Cadmium	[b] 10	
Cobalt	[b] 10	
Chromium	150	
Copper	[b] 10	
Iron	2600	
Germanium	[b] 10	
Hafnium	[b] 100	
Indium	[b] 10	
Lithium	[b] 10	
Magnesium	[b] 5	
Manganese	30	
Molybdenum	[b] 10	
Sodium	10	
Nickel	150	
Lead	[b] 10	
Antimony	[b] 50	
Silicon	30	
Tin	[b] 10	
Strontium	[b] 10	
Tantalum	700	
Tellurium	[b] 100	
Thallium	[b] 10	
Titanium	50	
Vanadium	30	
Tungsten	[b] 500	
Zinc	[b] 50	
Zirconium	[b] 50	
Potassium	10	

[a] ppm—parts per million.
[b] Not detected in concentration indicated.

after etching, and (C) after heating to 2415° K. Similar observations were made on the other borides and nitrides on which spectral emissivity measurements were made. The procedure for etching consisted of swabbing the polished surface with 48% hydrofluoric acid followed by immersion in concentrated orthophosphoric acid at 100° C for 30 min. No well-defined crystal structure is observable at this magnification, but rather a structure typical of refracting materials consolidated by sintering at high temperatures from micronized powders.

X-Ray Diffraction Studies

X-ray diffraction measurements provide an opportunity to examine crystal character, orientation, phase changes and surface composition of each specimen. The x-ray data for NbB_2 is shown in Table 57–III giving the relative intensities of reflected rays I/I_1, d^2-spacing in Angstrom units and Miller indices, *hkl*.

From the indices given in Table 57–III, a hexagonal structure is indicated having the following cell parameters; a=3.1, c=3.3, and

TABLE 57–III.—*X-Ray Diffraction Pattern of Niobium Diboride*

I/I_1	d, Å	hkl
30	3.30	001
50	2.69	100
100	2.08	101
5	1.65	002
15	1.55	110
20	1.40	111
10	1.34	200
15	1.24	201
10	1.13	112
5	1.04	202
5	1.02	210
5	.972	211
5	.896	113

TABLE 57–IV.—*Weight and Density Changes*

Material	NbB_2	ZrB_2		TiB_2	ZrN	TaN		HfN
Specimen No.	1	1	2	1	1	1	2	1
Temperature, °K*	2415	2389	2480	2022	2287	2860	2070	2192
Weight, g	−0.0305	−0.0270	−0.0341	−0.0045	+0.0073	−0.0026	−0.0235	+0.0014
Density, g/cc	−0.30	−0.38	+0.17	+0.20	−0.45	0	−0.19	0

*Time at temperature ranged from 8 to 16 hrs.

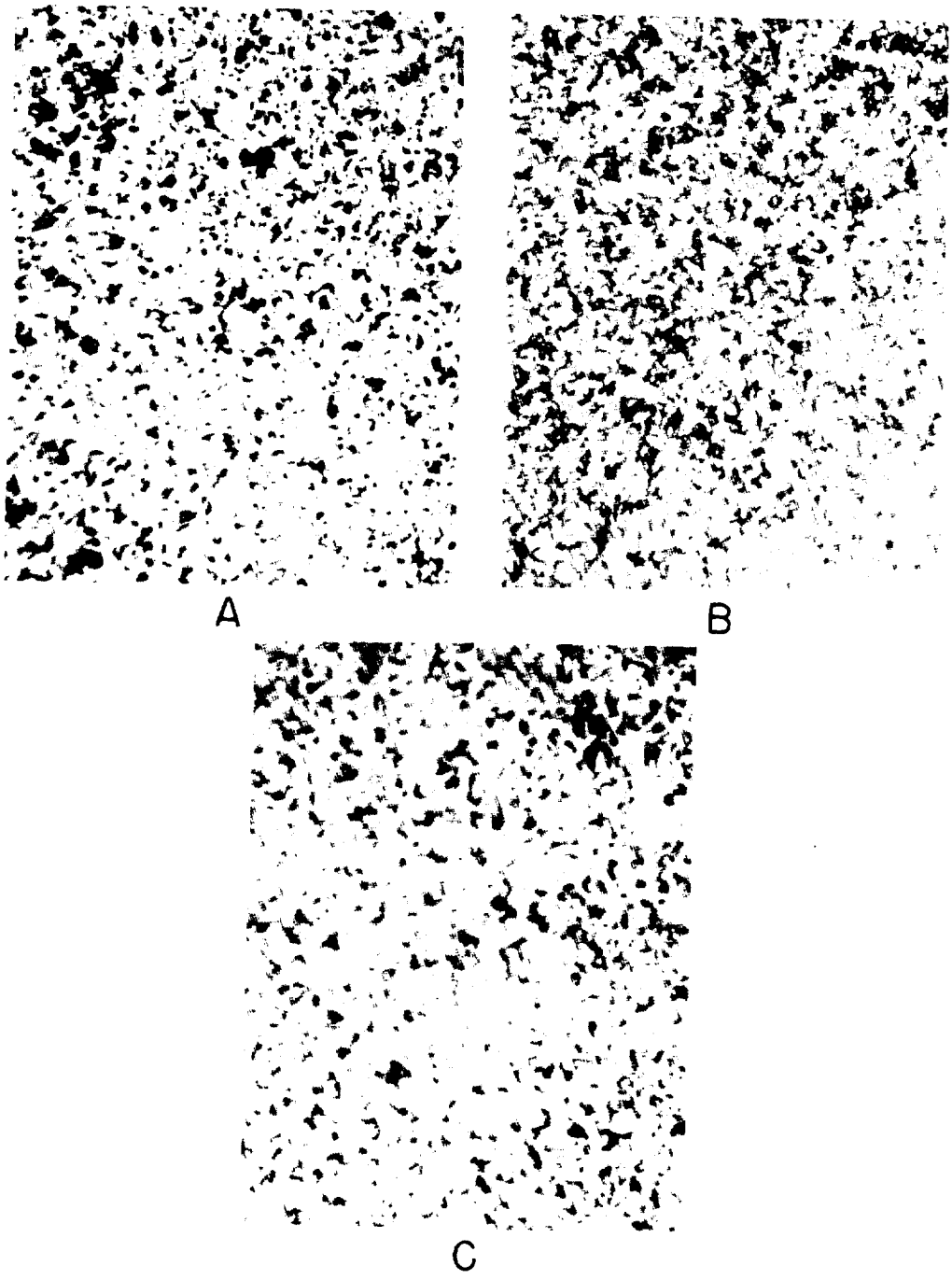

FIGURE 57-7.—Niobium diboride, 300×: A—polished, B—etched, C—after heating to 2415° K.

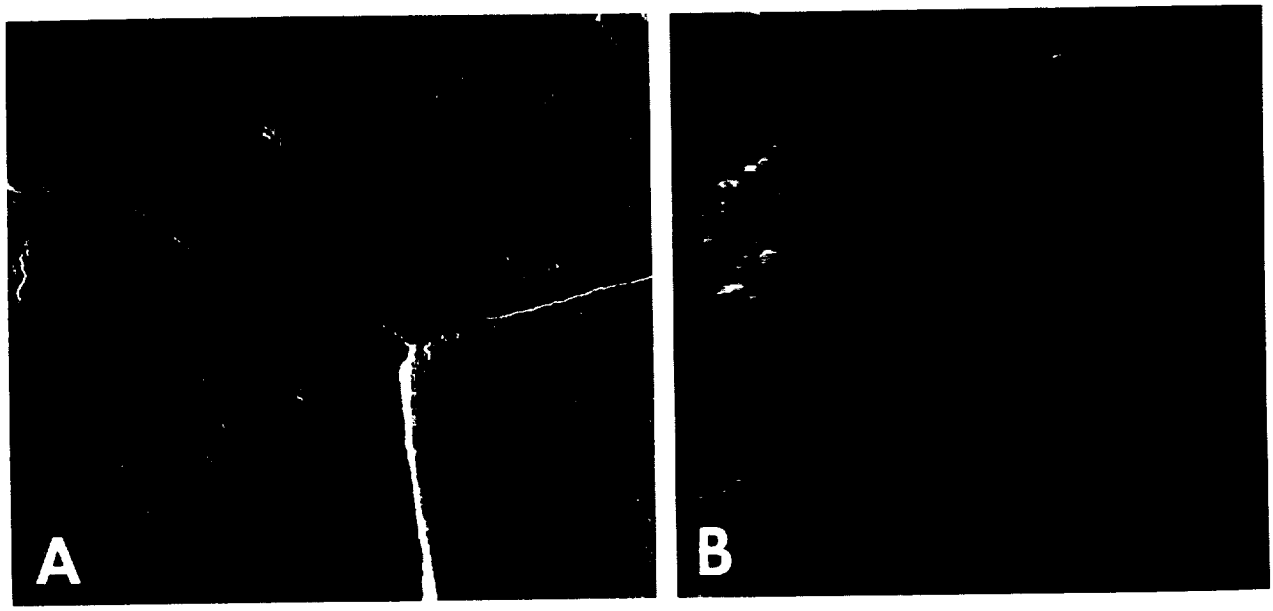

FIGURE 57-8.—Electron micrograph of etched niobium diboride, 42000×: A—before emissivity measurement, B—after emissivity measurement.

c/a ratio=1.06. The same x-ray values were measured after the NbB_2 had been heated to 2415° K during emissivity measurement. It, therefore, could be concluded that no basic changes, such as transformation and composition, took place in the specimen during measurement. Similar x-ray analyses were run on other compounds discussed in this report.

Weight and Density

Weight and density measurements were made before and after measuring emissivity. Table 57–IV tabulates the change in weight and density that took place after heating the various specimens to the stated maximum temperature. The time at temperature was different for each specimen and ranged from 8 to 16 hr.

Normal Spectral Emissivity

Before measuring spectral emissivity, replicas were made of each etched specimen surface and electron micrographs were taken. Figure 57–8A shows the surface of NbB_2 before heating at 42000×. Here the hexagonal crystal structure characteristic of NbB_2 is well defined in comparison to that which was seen at 300× under a light microscope. Figure 57–8B shows the same surface after heating to 2415° K in an argon atmosphere. Here, what is believed to be grain boundaries can be seen. In addition,

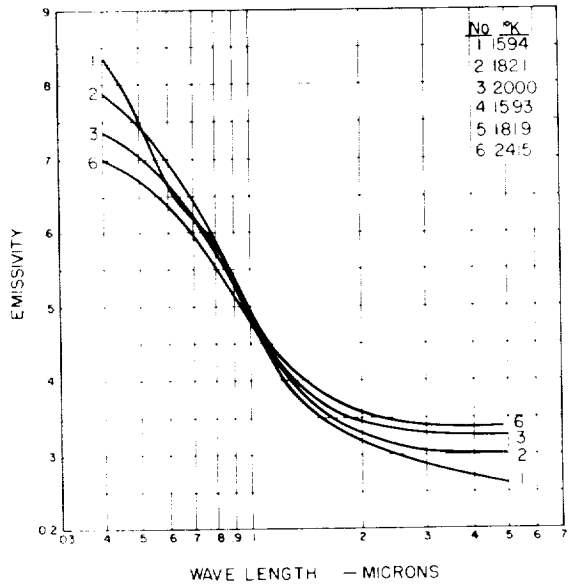

FIGURE 57-9.—Normal spectral emissivity of niobium diboride, argon atmosphere.

thermal evaporation has etched the surface in a manner that discloses random non-oriented dislocations and slip plane structure. The observed change in surface structure is believed to contribute, in part, to the slight attenuation of normal spectral emissivity at 1594° K below 1 μ wavelength, curve 1, figure 57-9. Also

shown is spectral emissivity at temperatures of 1821° K, 2000° K, and 2415° K. Figure 57–10 shows emissivity of NbB_2 at 2415° K, 1819° K and 1593° K. Spectral data for this latter temperature, curve 4, were determined after the 2415° K measurements, giving spectral emissivity values that are in good agreement with those first determined at 1594° K, curve 1 in figure 57–9, thus leading to the conclusions that NbB_2 remains stable at least to 2415° K. The crossover point at which emissivity is independent of temperature occurs at 1 μ.

Figure 57–11 shows the spectral emissivity of ZrB_2, specimen 1, at temperatures of 1704° K, 2032° K, and 2389° K. Because emissivity at 2389° K did not follow a characteristic decrease with increasing wavelength that would be predicted from the 1704° K and 2032° K determinations, the specimen was removed from the specimen chamber. When X-rayed it was found to have converted to ZrN. Figure 57–12 is a plot of spectral emissivity of ZrB_2, specimen 2, at 1604° K, 1702° K, 2000° K, 2330° K and 2480° K, after stabilizing at 2000° K for 8 hr. Emissivity is independent of temperature at wavelength of 0.55 μ and has a value of 0.85.

Figures 57–13 and 57–14 are electron micrographs at 36000× of ZrB_2 before and after

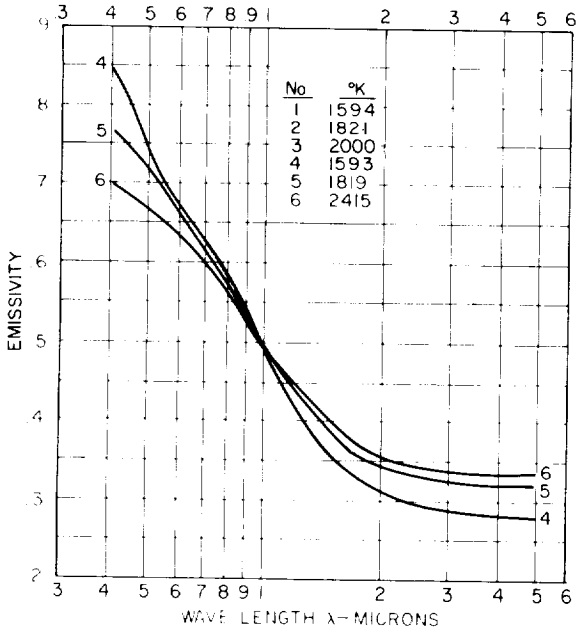

FIGURE 57–10.—Normal spectral emissivity of niobium diboride, argon atmosphere.

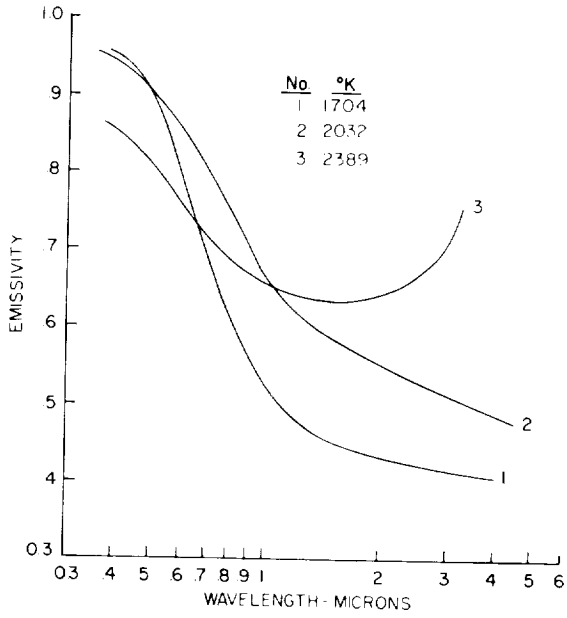

FIGURE 57–11.—Normal spectral emissivity of zirconium diboride, 1.5 atmospheres argon, specimen 1.

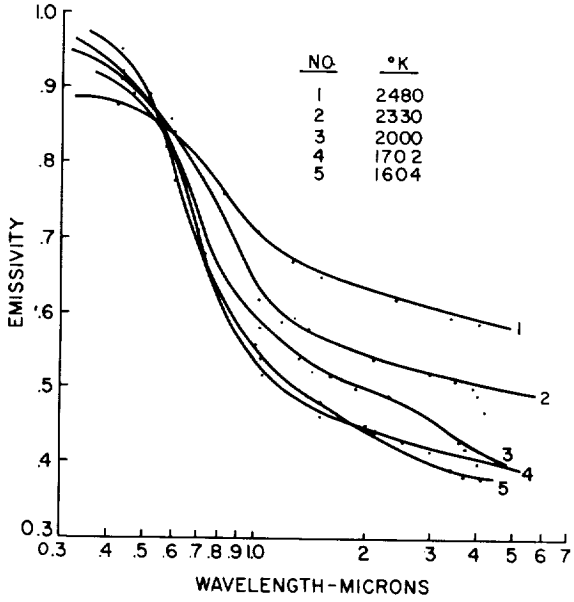

FIGURE 57–12.—Normal spectral emissivity of zirconium diboride, argon atmosphere.

making emissivity measurements up to 2480° K. It can be observed that changes in surface structure take place where pitting and thermal etching are evident. Possibly the observed attenuation of emissivity at 1702° K and 2000° K, beyond 0.8 μ, is caused by dynamic surface structure modifications taking place at these

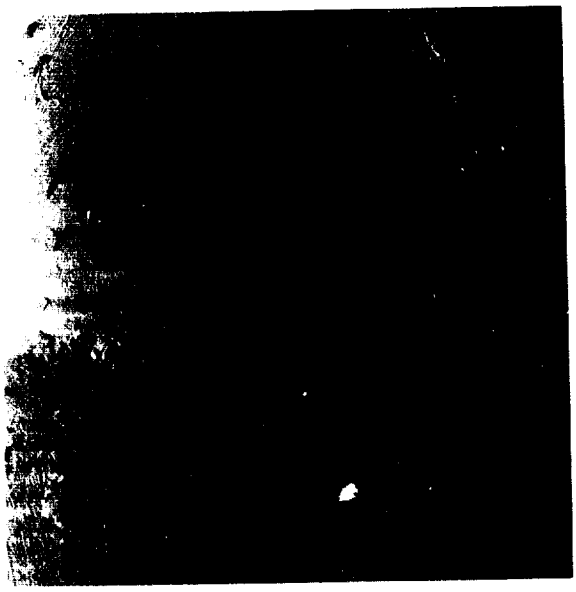

FIGURE 57-13.—Electron micrograph of zirconium diboride before emissivity measurement, specimen 2, 36000×.

FIGURE 57-15.—Electron micrograph of titanium diboride before emissivity measurement, 8100×.

FIGURE 57-14.—Electron micrograph of zirconium diboride after emissivity measurement, specimen 2, 36000×.

FIGURE 57-16.—Electron micrograph of titanium diboride after emissivity measurement, 10,300×.

temperatures. The x-ray diffraction examination showed that no basic changes in composition took place.

It should be mentioned that chemical analysis of ZrB_2 disclosed the presence of 3% tungsten and 8% oxygen in the as-received material.

Figures 57-15 and 57-16 are electron micrographs of TiB_2 before and after making emissivity measurements up to 2022° K. Substantial surface structural changes take place as a result of continued heating at high tempratures. There is a definite rounding and thermal polishing of surface grains.

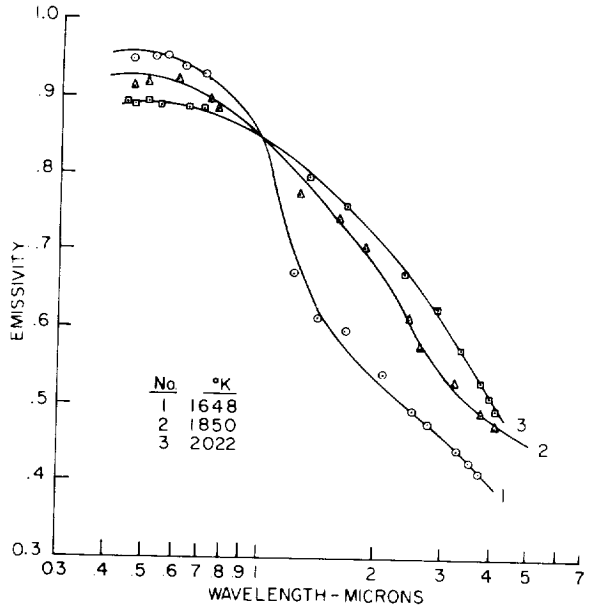

FIGURE 57–17.—Normal spectral emissivity of titanium diboride, 1.5 atmospheres argon.

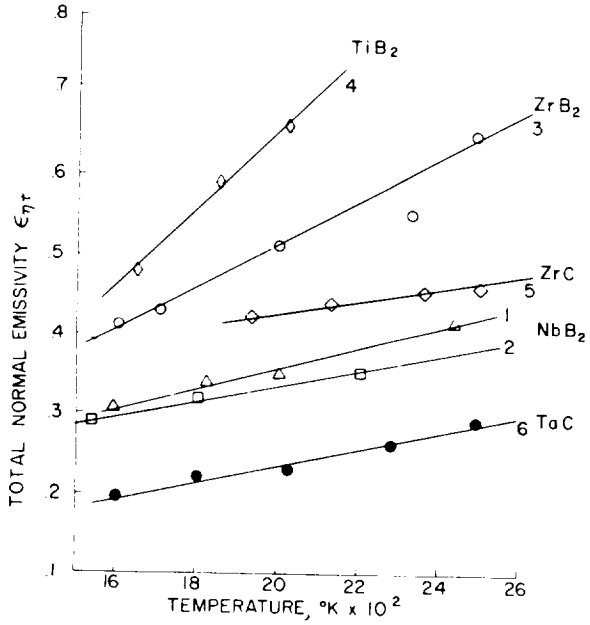

FIGURE 57–18.—Total normal emissivity of borides of titanium, zirconium, and niobium and of carbides of zirconium and tantalum.

Figure 57–17 shows the spectral emissivity properties of TiB_2 at 1648° K, 1850° K, and 2022° K between 0.4 μ and 5 μ. It is very similar to the spectral radiance properties of ZrB_2.

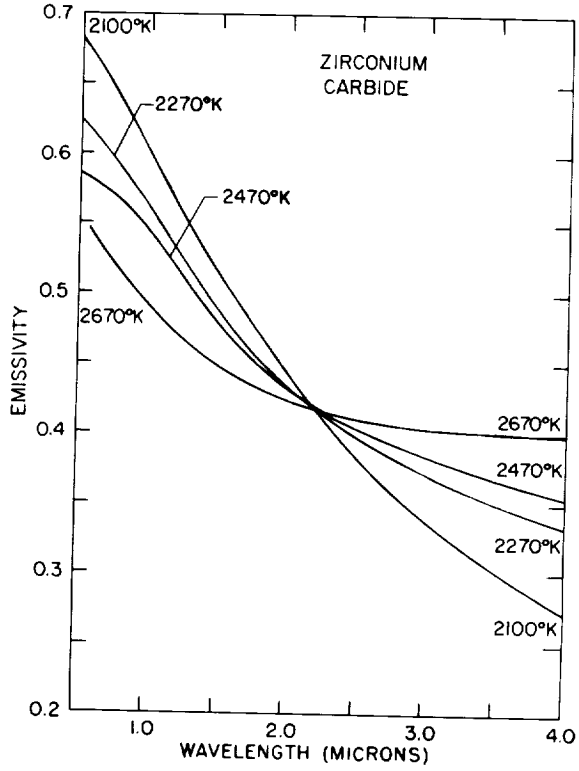

FIGURE 57–19.—Normal emissivity of zirconium carbide.

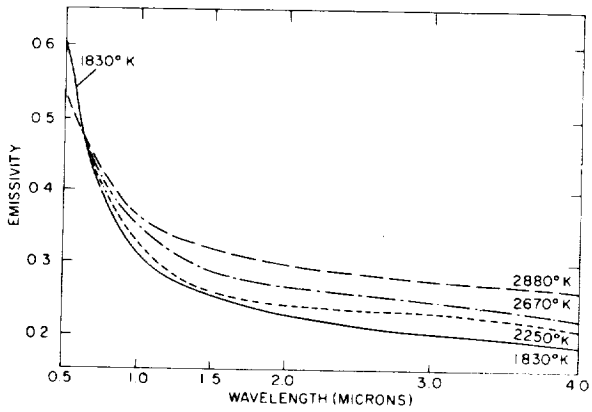

FIGURE 57–20.—Normal emissivity of tantalum carbide.

Figure 57–18 is a plot of total normal emissivity as a function of temperature for the borides of niobium, zirconium, and titanium calculated from measured spectral emissivity data.

Also shown are plots of total normal emissivity of zirconium and tantalum carbides for which spectral emissivity is shown plotted in figures 57–19 and 57–20, respectively.

FIGURE 57-21.—Electron micrograph of zirconium nitride before emissivity measurement, 36000×.

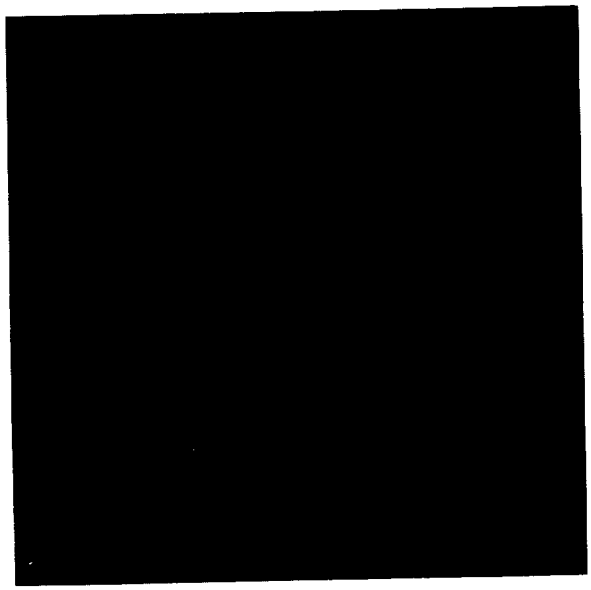

FIGURE 57-22.—Electron micrograph of zirconium nitride after emissivity measurement, 36000×.

Spectral emissivity measurements were also made on characterized nitrides of zirconium, tantalum, and hafnium. Chemical analysis showed that these compounds contained less than one atom of nitrogen per atom of metal. However, x-ray diffraction observations showed

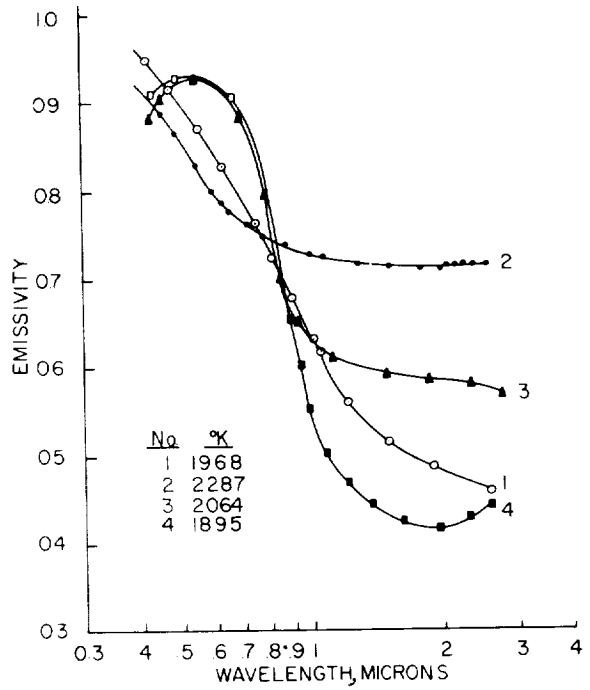

FIGURE 57-23.—Normal spectral emissivity of zirconium nitride.

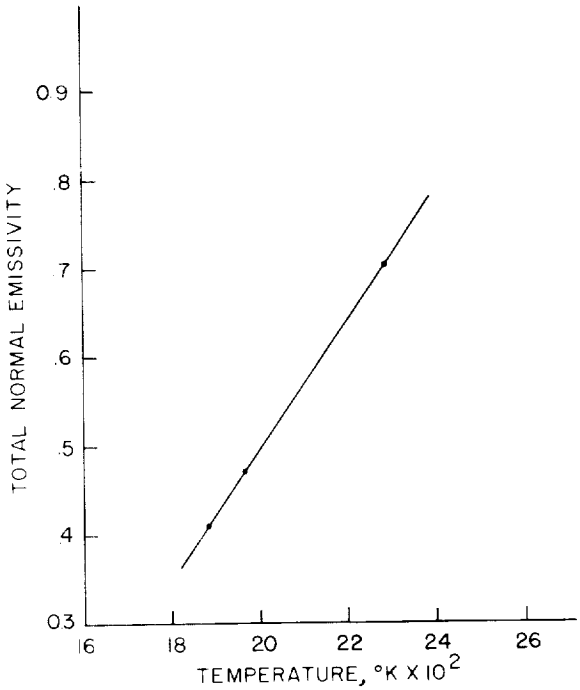

FIGURE 57-24.—Total normal emissivity of zirconium nitride.

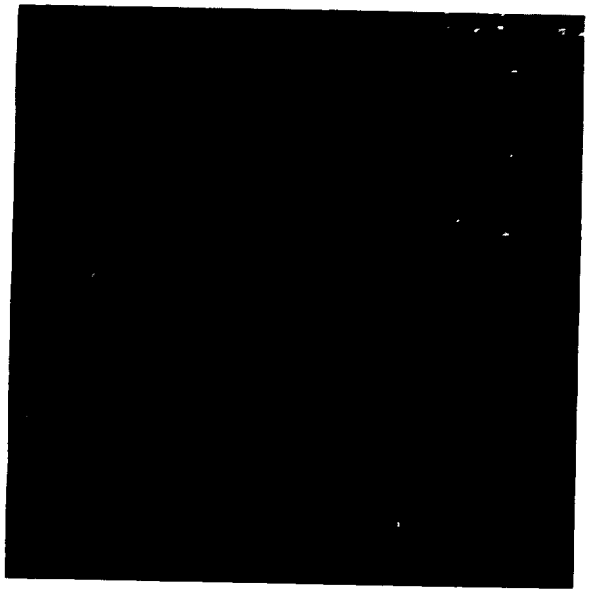

FIGURE 57–25.—Electron micrograph of tantalum nitride before emissivity measurement, 36000×.

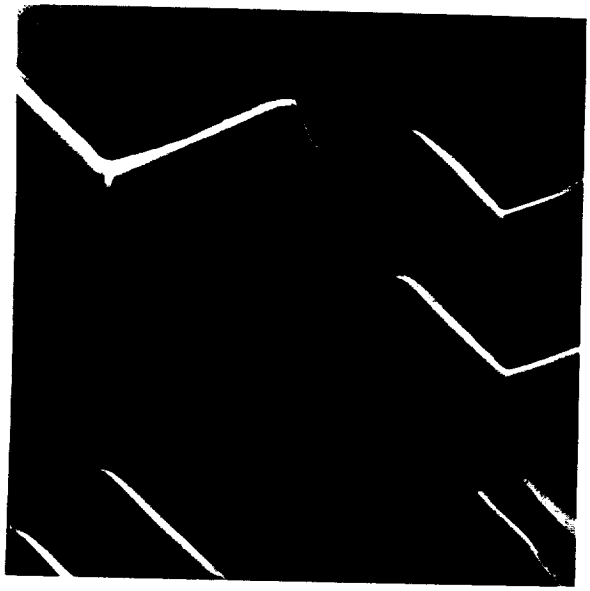

FIGURE 57–26.—Electron micrograph of tantalum nitride after emissivity measurement, 36000X.

only the metal nitride crystal phase present in the specimens. After emissivity measurements were made there was x-ray evidence of slight surface oxidation of the zirconium and hafnium nitrides. A loss of nitrogen takes place when TaN is heated above 2000° K in vacuum, and nitriding was evident when the sample was heated in a purified nitrogen atmosphere.

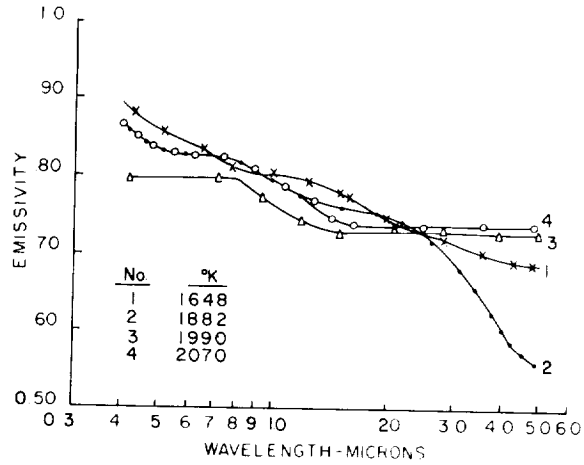

FIGURE 57–27.—Normal spectral emissivity of tantalum nitride, 2 atmospheres nitrogen.

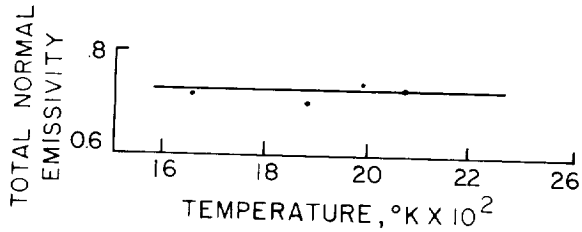

FIGURE 57–28.—Total normal emissivity of tantalum nitride.

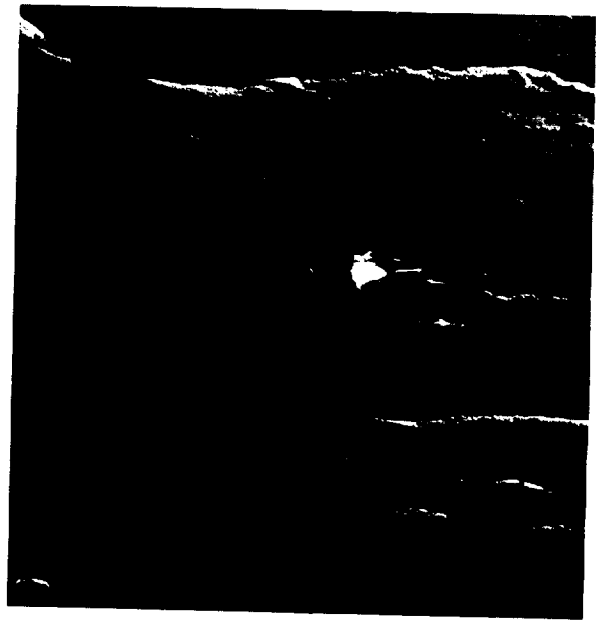

FIGURE 57–29.—Electron micrograph of hafnium nitride before emissivity measurement, 36000×.

These changes were substantiated in the observed changes in specimen weight and density.

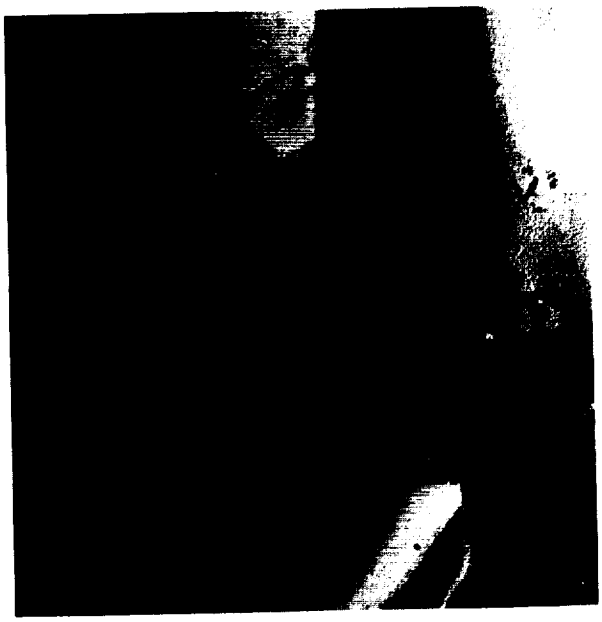

FIGURE 57-30.—Electron micrograph of hafnium nitride after emissivity measurement, 36000×.

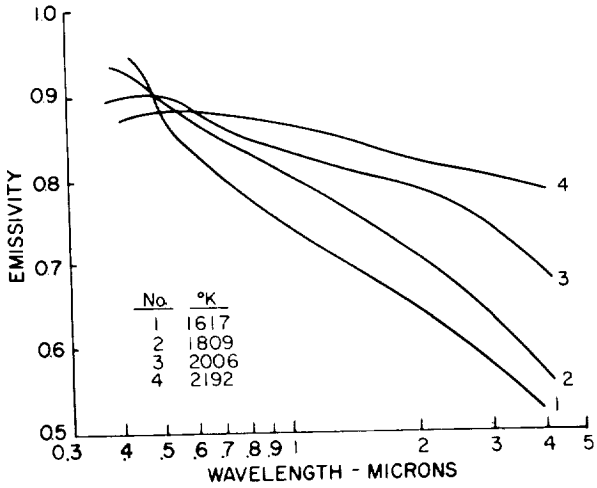

FIGURE 57-31.—Normal spectral emissivity of hafnium nitride, 2 atmospheres argon.

Figure 57-21 is an electron micrograph of ZrN at 72000× showing a surface characterized by a multiplicity of random dislocations. Figure 57-22 is a 36000× electron micrograph after heating ZrN to temperatures up to 2287° K. Here again is seen intense surface structure modifications showing the appearance of discrete crystals possessing slip plane dislocations.

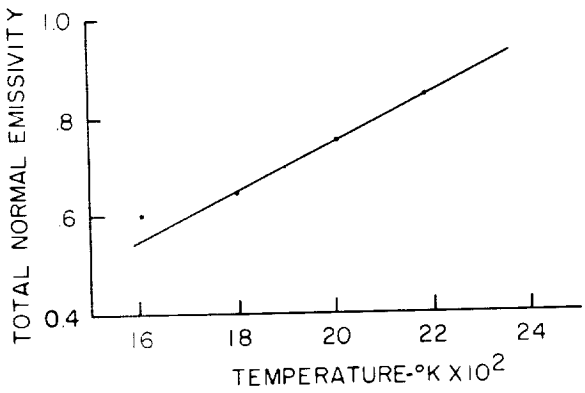

FIGURE 57-32.—Total normal emissivity of hafnium nitride computed from spectral data.

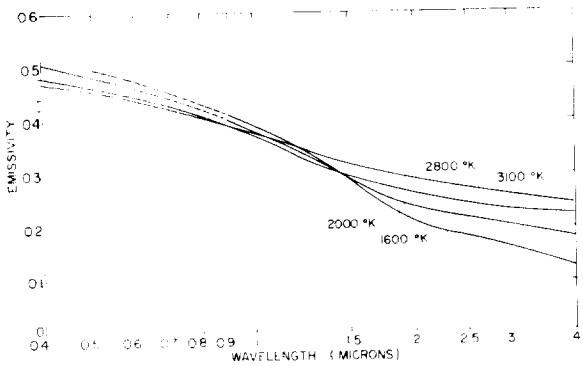

FIGURE 57-33.—Normal emissivity of tungsten.

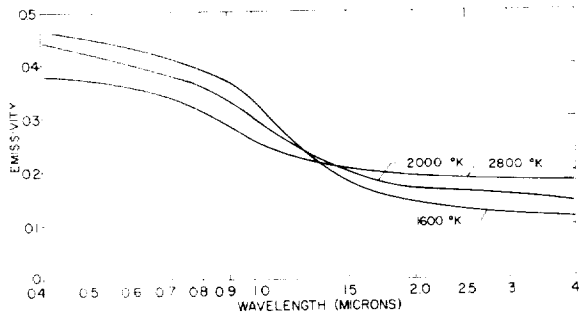

FIGURE 57-34.—Normal emissivity of molybdenum.

Figure 57-23 is a plot of emissivity of ZrN as a function of wavelength at 1895° K, 1968° K, 2064° K, and 2287° K. The numbers refer to the order in which measurements were made. Figure 57-24 is a plot of total normal emissivity calculated from spectral data for ZrN.

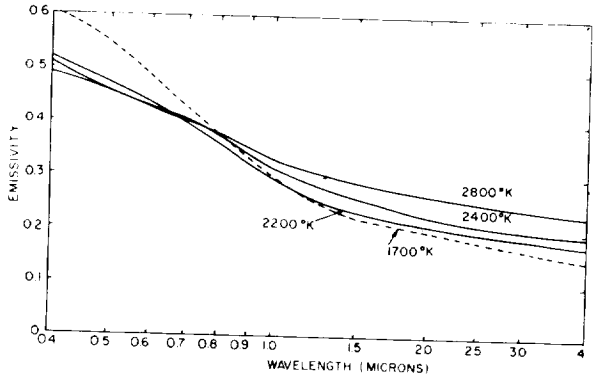

FIGURE 57-35.—Normal emissivity of tantalum.

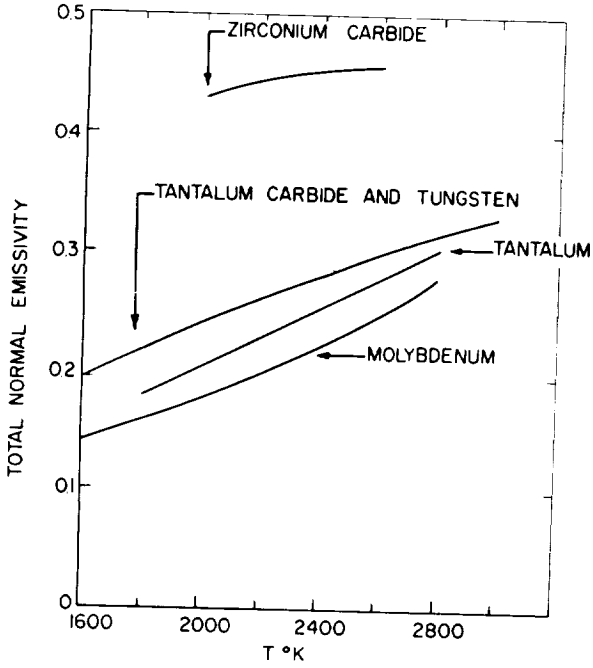

FIGURE 57-36.—Total normal emissivity of zirconium carbide, tantalum carbide, tungsten, tantalum, and molybdenum.

Figures 57-25 and 57-26 are electron micrographs of the surface of tantalum nitride at 36000× before and after measurement of emissivity up to temperatures of 2070° K in an atmosphere of purified nitrogen. In figure 57-25 a well-defined hexagonal crystal structure, with grain boundaries intersecting at 120°, can be observed. During the measuring of emissivity the surface of the specimen converted to a polycrystalline powder layer which could be readily removed with lens paper. X-ray disclosed this to be TaN. Figure 57-26 shows the structure of the surface beneath this layer. Shown in sharp contrast are etch pits along the grain boundaries. These intersect at 120° indicating the retention of an hexagonal structure characteristic of TaN.

Figure 57-27 is a plot of spectral emissivity of TaN at 1648° K, 1882° K, 1990° K, and 2070° K. Emissivity becomes independent of wavelength beyond 1.5 microns and above 1882° K. Figure 57-28 is a plot of total normal emissivity as a function of temperature calculated from spectral data presented in figure 57-27. It shows virtually no temperature dependence over the range of measurement.

Figures 57-29 and 57-30 are electron micrographs of the surface of HfN before and after making emissivity measurements respectively. As a result of heating the specimen to 2192° K its surface develops a thermally etched crystal structure displaying uniformly oriented slip planes. Figure 57-31 is a plot of spectral emissivity of HfN at temperatures of 1617° K, 1809° K, 2006° K, and 2192° K. Figure 57-32 shows total normal emissivity of HfN computed from spectral data. Figures 57-33, -34, and -35 show the spectral emissivity of tungsten, molybdenum and tantalum. The data for tungsten is in good agreement with the data of De Vos (ref. 5) who also found the emissivity of tungsten at 1.3 μ to be 0.33. Figure 57-36 is a plot of total normal emissivity as a function of temperature. Even though the spectral emissivity of tungsten and tantalum are quite different their total normal emissivity is the same over the temperature range of 1600° K to 2000° K.

REFERENCES

1. Worthing, A. G.: Temperature Radiation Emissivities and Emittances, p. 1164 *in* Temperature, Its Measurement and Control in Science and Industry. Reinhold Publishing Corp., 1941.
2. Marple, D. T. F.: Spectral Emissivity of Rhenium. J. Opt. Soc. Am., 46, 1956, p. 490.
3. Blau, H. H., Jr.; Chaffee, Eleanor; Jasperse, J. R.; and Martin, W. S.: High Temperature Thermal Radiation Properties of Solid Materials, AFCRC-TN-60-165, March 31, 1960.
4. Metzger, J. W.: The Measurements of Infrared Emissivities of Metals at Elevated Temperatures. M. S. Thesis, Drexel Institute of Technology, June, 1959.
5. De Vos, J. C.: A New Determination of the Emissivity of Tungsten Ribbon. Physica 20, 1954, p. 690.
6. Perkin-Elmer Corp.: Infrared Reflectivity Attachments, Instruction Manual, Norwalk, Conn., p. 990-9188.
7. Horning, D. F.; Hyde, G. E.; and Adcock, W. A.: A Ratio Recording Double Beam Infrared Spectrophotometer with Automatic Slit Control. J. Opt. Soc. Am., vol. 40, 1953, p. 497.

DISCUSSION

Richmond: Have you had any trouble with fogging a window, and, if so, how did you eliminate it?

Riethof: We have had trouble with fogging, if you want to call it that, only once and that was a case with zirconium carbide. I hate to call it fogging because it was actually decomposition of the specimen and we were depositing carbon on the window. Originally we maintained a static atmosphere of argon in the chamber. Lately we have been flushing continuously with argon, partially to reduce the possibility of deposition. We have never observed fogging due to moisture.

Comstock, Arthur D. Little Company: If you heat the sample a second time having previously allowed it to cool, how does the sample's emittance change?

Riethof: This is best shown by referring to figure 57-10. When we talk about operating times of 8, 16 or 20 hr on a given specimen, we are not doing it continuously.

Butler, U.S. Naval Radiological Defense Lab.: Would you comment on the very remarkable agreement of the X-point? Your data on tungsten agrees with De Vos in which the X-point occurs at 1.2 μ. I notice some of these other ones go clear down to 0.5 μ, and yesterday I noticed in Professor Seban's paper that the X-point for platinum from his slide occurs beyond 2 μ. Would you comment on this very large change in wavelength with that X-point?

Riethof: I'm sorry, I unfortunately was not here yesterday. Were all these papers dealing with tungsten specifically?

Butler: No, Professor Seban's paper was on platinum. He gave the spectral emittance of platinum as a function of temperature.

Riethof: Well, as I think we all know, there is no theoretical reason for an X-point, except that if you have a temperature coefficient that is positive in one spectral range and negative in another one it must be zero somewhere. The X-point is a well-observed phenomenon and I have used it many times to check operation of my equipment. I wish I had some explanation for it. In tungsten specifically the intersections of some of the curves are so flat that you can shift the X-point better than 0.1 μ by just deciding on how your curves intersect (see fig. 57-33). I don't think there is any specific reason why X-points for different materials should be in the same spectral region.

Gravina, Republic Aviation: Dr. Kostkowski of NBS showed a plate indicating the errors which are introduced when imaging very small objects into these spectrometers. Now, each of these last two papers has featured this idea of imaging a very small source, essentially a point source, in the spectrometer systems. Would Dr. Kostkowski or any of the investigators care to discuss this as a source of error? Have they considered this as a source of error?

Riethof: I don't think that is for me to answer.

Gravina: Well, I was going to address it to Dr. Kostkowski since he brought out this point yesterday. I believe it was during Mr. Richmond's presentation.

Kostkowski: In my particular group, we have not been making any spectral or total emittance measurements, so I cannot speak about corrections in that respect. However, in looking at sources of different sizes and determining the spectral radiance of these sources, when a source varies in size from about 1 mm to, say, 10-15 mm in diameter, maintaining the same surface properties and temperature, the apparent spectral radiance may change by as much as several per cent, depending on the aperture of the optical system. This is due to diffraction and the magnitude may be computed for any optical system.

Riethof: I think we ought to point out that this set of mirrors we are using was actually designed to be used with slits down to considerably smaller dimension than my hole sizes. I would be more worried about a fact that Richmond and I have shown several times. We see that the area we look at is so small that at times it may be a nonrepresentative portion of the specimen, and, hence, the data may also be nonrepresentative.

INDEX*

*Paper numbers are given in italics; D following paper number indicates discussion of the paper

L

M

N

O

P

R

S

U.S. GOVERNMENT PRINTING OFFICE: 1963 O—692-146